Mechanical, Industrial, and Manufacturing Engineering

Selected, peer reviewed paper from 2011 International Conference on Mechanical, Industrial, and Manufacturing Engineering (MIME 2011)

Australia, Melbourne, 15-16 January, 2011

Edited by

Ming Ma

INFORMATION ENGINEERING RESEARCH INSTITUTE, USA

Information Engineering Research Institute
100 Continental Dr, Newark, DELAWARE 19713, Unite State, USA
http://www.ier-institute.org

Volume 1~2
ISBN: 978-0-9831693-1-4
Lecture Notes in Information Technology
ISSN: 2070-1918

Distributed worldwide by

Information Engineering Research Institute
100 Continental Dr, Newark, DELAWARE 19713, Unite State, USA

E-mail: admin@ier-institute.org

Preface

We are delighted to announce that 2011 International Conference on Mechanical, Industrial, and Manufacturing Engineering (MIME2011) will be held in Australia, Melbourne, from 15 to 16 January, 2011.

The goal of MIME 2011 is to bring together the researchers from academia and industry as well as practitioners to share ideas, problems and solutions relating to the multifaceted aspects of Mechanical, Industrial, and Manufacturing Engineering. We are pleased to invite authors to submit their papers to MIME 2011, addressing issues that serve present and future development of the field.

2011 International Conference on Mechanical, Industrial, and Manufacturing Engineering (MIME2011) offers a wide variety of technical targeted at Mechanical, Industrial, and Manufacturing Engineering theoreticians and practitioners, including: formal paper sessions, tutorials, panel sessions, case studies, and a lecture series. Authors are invited to submit original, unpublished papers describing recent work in the field of test and design. In addition, authors are invited to submit practical, industry best practices to be included in application/lecture series sessions. Submissions simultaneously under review or accepted by another conference, symposium or journal, will be rejected. This year, we received about 420 submissions. Every paper was reviewed by three program committee members and about 140 were selected as regular papers for MIME 2011, representing a 33% percent acceptance rate for regular papers.

2011 International Conference on Mechanical, Industrial, and Manufacturing Engineering (MIME2011) is co-sponsored by Singapore Management University, Huazhong Normal University, Wuhan Institute of Technology and Information Engineering Research Institute.

We would like to thank the program chairs, organization staff, and the members of the program committees for their hard work. Special thanks go to IERI Publisher.

We hope that MIME 2011 will be successful and enjoyable to all participants. We look forward to seeing all of you next year at the MIME 2012.

January, 2011
Ming Ma, Singapore Management University, Singapore

Organization

Honorary Chairs

IEEE Fellow Prof. Chin-Chen Chang, Feng Chia University, Taiwan
IEEE Fellow Prof. Jun Wang, Chinese University of Hong Kong, Hong Kong
IEEE Fellow Prof. Chris Price, Aberystwyth University, United Kingdom

Organizing Chairs

Yijin Wu, Huazhong Normal University, China
Qihai Zhou, Southwestern University of Finance and Economics, China

Program Chairs

Xu Gang, Shenzhen Univerisity, China
Daviad Zhongh, University of Kentucky Lexington, USA

Publication Chair

Ming Ma, Singapore Management University, Singapore
Honghua Tan, Wuhan Institute of Technology, China

International Committees

Ying Zhang, Wuhan University, China
Jia Luo, International Communication Sciences Association, Hong Kong
Peide Liu, Shandong Economic University, China
Dariusz Krol, Wroclaw University of Technology, Poland
Dehuai Zeng, Shenzhen Univerisity, China
Jason J. Jung,Yeungnam University, Republic of Korea
Xiaochun Cheng, Middlesex University, UK
Honghua Tan, Wuhan Institute of Technology, China
Paul Davidsson, Blekinge Institute of Technology, Sweden
Cao Longbing,University of Technology Sydney, Australia
Huaifeng Zhang, University of Technology Sydney, Australia
Qian Yin, Beijing Normal University, China

MIME 2011 Contents

2011 International Conference on Mechanical, Industrial, and Manufacturing Engineering
Lecture Notes in Information Technology Vols. 1-2

Spares Demand System with Consideration of Integration Management and Optimization

Jing Lin
Department of Computer Science and Electrical Engineering
Luleå University of Technology
Luleå, SE97187, Sweden
janet.lin@ltu.se

Magnus L.Nordenvaad
Department of Computer Science and Electrical Engineering
Luleå University of Technology
Luleå, SE97187, Sweden
magnus.lundberg@foi.se

***Abstract* - Spares inventory management differs from other manufacturing inventory managements, mainly due to its specialists in function with maintenance. So far, enormous attention has been paid by standing on spares' manufacturing factories, sales companies, end users' purchasing departments, or maintenance engineers, separately. However, not only "bullwhip effect" in forecasting spares demands, but also deteriorated relationships among the spares supply chains have shown that, spares optimization strategies with isolated consideration could only bring short-term or partial improvements. In this paper, the spares demand system with consideration of integration management is promoted, the new Solid-Net relationships among four main components are elaborated. Then, the root causes of ineffective in spares demand system are analyzed. Also, distinct optimization policies are illustrated. What's more, successful stories in practice are cited.**

Index Terms* - *Systems Engineering；Maintenance; Spares parts；Inventory Optimization Management

I. INTRODUCTION

Spares inventory management differs from both work-in-process (WIP) inventory management and finished product inventories, mainly due to its unique aspects in function with maintenance (see [1]-[3]). Recent researchers (see [4]-[8], and references therein) have shown that relative achievements regarding spares optimization mainly focus on three aspects: 1) spares classification optimization; 2) spares forecasting optimization; 3) spares inventory strategies optimization.

During the above studies, two standing points are identified: one is the *end users*, where spare parts are consumed (including maintenance departments or purchase departments in the factories); the other is *suppliers*, from where spares are supplied (including the sales companies or spares' manufacture factories). Regarding the former, research achievements are mainly focusing on that how to get balance between losses of stock-out and costs of keeping stock. For the latter, how to enhance spares supply chains' effectiveness is followed with great interest.

However, in practice, the most common situations are: 1) when end users optimize their own spares' demanding forecasting results, pressures often come out from not only the uncertainty regarding the equipments' running situations, but also suppliers' capability to supply the "right item" at "right place" and "right time"; 2) when suppliers optimize their spares supply chains separately, "fire-fighting" orders or "bullwhip effect" may also made it hard to reach their business goals. In another words, any isolated optimization will be easily influenced by "stakeholders".

To deal with above problems, end users begin to show emphasis on their ERP or CMMS systems. Meanwhile, innovative inventory management patterns come up for suppliers, including Zero Inventories, Joint Management Inventory (JMI), Vendor Management Inventory (VMI), Collaborative Planning Forecasting and Replenishment (CPFR), and the like. Although such efforts sometime seem to be effective, seen from more and more spares in warehouses and the more and more deteriorated relationships among suppliers, inspections have shown that, spares optimization strategies with isolated consideration could only bring short-term or partial improvements. After all, each one's business goals are different and they primarily prefer to fit for their own goal. Additionally, sometimes the root causes are more complex than one can imagine. Integrated ideas should be paid attention to in the future whatever in theatrical researches or in practices. Those are also the reasons why the authors promote spares integrated demand system here.

The paper is organized as follows: first, the spares demand system with consideration of integration management is promoted; second, relationships among four main components are elaborated; then, the root causes of ineffective in such systems are analysed; finally, distinct optimization policies are illustrated for integrated spares demand system. Also, successful stories in practice are cited.

II. SPARES DEMAND SYSTEM

A. Components in Concept Model

During spare parts' lifetime cycles, they will experience several stages, e.g.: manufactured, for sale, stocked, in use, maintenance, obsolescence. In fig1, the traditional and the simplest relationships are high lightly , there are four main components in spares demand systems: 1) manufacturing factories ("M"); 2) sales companies (including distributors, "S"); 3) end users' purchasing departments ("P"); 4) maintenance engineers (equipment departments of end users, "E"). Their connections can be shown from the perspective of a "pull process" and a "push process" in the spares demand system.

- Seen from a simplified "pull process": To ensure the running of equipments, E submit spares applications to P through work orders or other purchasing lists; After surmising applications from different maintenance

departments, P organize purchasing and buy spares from S; Then, S purchases spares from M and M produce spares based on orders and forecasting at markets. In such a process, the ideal situation is: there are only WIP or spares on the way, where the costs of keeping stock are low. However, due to uncertainty and also very long lead times, the spares waiting time in the whole system may be very long, and the risk for stock-out is very high. So, such a pull process usually fit spares whose criticality is relative low on site.

- Contrary by considering a simplified "push process": M produce spares based on forecasting of markets' demand. In case of stock-out, and considering the uncertainty of lead time, the forecasting results are often exaggerated, and spares inventory formed in M's warehouse. At the same time, S often buys spares from M ahead of time, in order to achieve quick response to customer's needs, by which to enhance competitive power. For end users, no body knows the exact time of when and how many spares are needed, and no body would like to be responsible for the loss caused by spares stock-out, especially for critical spares, which have verified the spares' specialists. So, P purchases spares from S ahead of time. Also, for most situations, M will apply their needs ahead of time from P in case of stock-out, where the spares inventory may also be formed on site. At such a process, we can also say that, spares inventory exists naturally mainly because of spares' uncertain forecasting quality as well as uncertain purchasing lead times. Due to multiple channels which M, S, P and E all have to face to, the situations are more complex in practice. Those can be also viewed as the root causes of the whole spares demand systems' un-robustness, and the root causes of wasting in system.

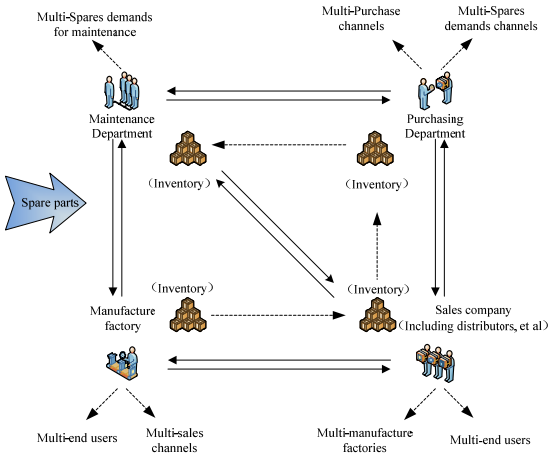

Fig. 1 Components for Spares Demand System

B. The Solid-Net Relationships

In the above spares demand system, the components' connections should not solely be described as "chains". The first reason is that, those components compose the nets structure by many chains (shown in Fig.1). The second reason is that, those nets are not only plain but also solid (shown in Fig.2).

- **Relationships between sales company and Maintenance Department**—— Nowadays, more and more end users transfer partial or full risk to sales company through different kinds of purchase contracts such as "long-time service", "Zero Inventory", VMI, or CPFR. Due to high competing pressures, most sales companies have to accept such inventory risks. In this situation, more exact forecasting render lower capital occupied risk. On the other hand, many sales companies with competence may often supply back-market services for maintenance department, such as spare parts' choosing, quality tracking, and condition monitor service and other relative maintenance services. Such services have influences on maintenance engineers' suggestions submitted to purchase departments regarding on purchase decisions, such as which suppliers to choose.
- **Relationships between Manufacturing factory and Maintenance Department**—— Spares manufacturing factories need to improve its products, based on end users' feedback. This means that, maintenance engineers should reflect the spares performance information to both manufacturing factories and sales companies, to support spares decision making. Additionally, the manufacturing factories have responsibility for conducting end users' spares usage.
- **Net Relationships in spares demand system ——** Although for some spares manufacturing factories (such as SKF, ABB, GE), communicating with end users (including maintenance engineers and purchase departments) are common, different departments have different work scopes and power styles. However, it is very common to view the existence at two basic demand chains in such spares demand systems. One is E-P-S; the other is E-S-M. Moreover, these two chains form the demand closed loop system E-P-S-M-E.
- **Solid Relationships in spares demand system ——** In real world, the complexity situation is far more than imagination. Usually, for one kind of spares, the manufacturing factory serves several sales companies and several end users. One Sales Company has to face several manufacturing factories and several end users. What's more, for spares with the same functionality, purchasing departments have to choose suppliers through several channels and consider several equipments' maintenance needs. At the same time, maintenance departments achieve their forecasting results based on several equipments' needs. Nowadays, advanced spares strategies, such as VMI, JMI, and CPFR, become more and more popular. So, solid relationships exist in spares demand system. For instance, as seen in Fig.2, sales company A, under the VMI strategy for example, may serve end user B and have relationships with B's maintenance department and purchase department. Under the CPFR strategy, sales company A may form a union

with sales company B and several other sales companies. Under the JMI strategy, end user A may also have relationship with end user B. Too many to be listed here; however, it is easy to find solid relationships in spares demand system.

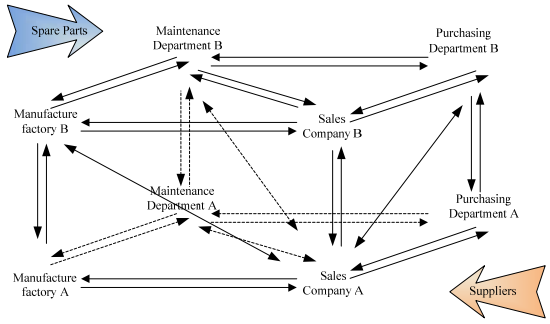

Fig. 2 Solid-Net Relationships among components in spares demand system * *Note: the solid-net shown here is just a part for the whole system, as well as the relationships shown here are also a part.

II. Ineffectiveness In Spares Demand System

A. *"Bullwhip effect" in Spares Demand System*

As shown above, spares inventories exist widely in manufacturing factories, sales companies, end users' purchasing departments and maintenance departments. Meanwhile spares inventory exist with different considerations. The root cause is to reduce spares stock-out risk. As an example, manufacturing factory wants to avoid stock-out for market's needs, the sales company wants to avoid stock-out for end user's needs, purchase department wants to avoid stock-out for maintenance, and the maintenance department wants to avoid stock-out for maintenance tasks.

In order to reduce the loss caused by stock-out, demand information is naturally exaggerated from one level to another, and that is how the "bullwhip effect" occurs. In correspondence, asset efficiency is low in spares demand system. From the point view of maintenance engineers, they hope to keep their spares with enough categories and quantities. In contrast, purchase department hope to reduce the cost of keeping spares. From the sales company's point view, they hope to enhance circulation rate. In a contrary manner, the manufacturing factories hope to sell more to sales company, especially for those with slow moving speed. The true example is that, some manufacturing factories will ask their distributors to buy more spares violently, to reduce its own stock level. To avoid the loss due to "bullwhip effect", components in spares demand system may consider many strategies to reduce others' influences, which may lead relationships becoming continually worse and worse. For example, one end user's equipment department may deliver spares from purchase department before some account time, in case that the budget will be reduced in the next account period. Commercial bribery may occur to enhance end users' purchase quantities. Also manufacturing factories may ask sales companies (their distributors, et. al) unfairly to stock more than needed. It is a vicious cycle.

B. *CRM in Spares Demand System*

From the customer relationship management (CRM)'s view point, all components may be viewed as customers of each other. It means that, as soon as all components are being satisfied with each other, good relationships value will be enhanced in such a system. Unless the enhanced relationships are achieved, the whole system will become more and more stable. In another words, unless all components' spares inventory is optimized, the whole demand system can get stable.

From the view point of spares inventory management, any kind of inventory problem, for any component, may lead to dissatisfaction in itself. So, everyone aims to optimize it own spare inventory. For example, maintenance department hope to ensure the spares' maintenance needs, and avoid stocking useless spares or lead to budget's constricts. The purchase department hopes their money will be used to do the best shot with best gun, promote the inventory cycle rate, and avoid money kept in inventory. The sales company hopes that their inventory structure become logical, in case they have to care much on unfair competition and even clearing stocks. The manufacturing factory hope to get more exact forecasting, in case of oversupply. Whichever unexpected thing happens, the relationships among components will become worse, and the relationships' value will be reduced step by step. Above things support again that, any isolated optimization has only short-term or partial effectiveness.

III. Integrated Optimization Policies In Spares Demand System

Due to the components' solid-net relationships, all optimization policies should be considered with integration thinking. In another word, the focus is, how to optimize spares inventory for all components in the whole system with consideration of integration management, by utilizing associations. In this section, the authors try to promote four main ways.

A. *Integrated Classification Optimization*

Scientific classification at spare parts is the first key point for optimization. One problem which may be easily neglected is the insufficient consideration for influence factors, which should be considered. In traditional classification methods, for example, sales companies may divide spares into different categories only by inspecting the profits that can be brought to them, or ordered frequency. Few one know the spares maintenance strategies when they are used on site. For instance, the spares life times can be enormously different under different maintenance strategies, which means, the consuming rate is different even for the same spares equipped on the same equipments. Another example is, for end users, besides spares' costs and critical aspects, characters regarding on purchasing and maintenance should also be considered. Sometimes, spares' lead time may be as long as 24 months, even longer, which should be paid much attention to (if that, it should be viewed as critical spares even if the loss of stock-out will be not that high). Spares with different classifications

should be set up with different strategies. The earlier an integrated point is considered, the more likely scientific spares inventory strategies can be made.

B. Integrated Demand Forecasting Optimization

To reduce the "bullwhip effect", one of the most important things is to improve the forecasting ability for all components.

- Spares have connections with equipments. To improve forecasting ability, maintenance departments should control comprehensive running information of all equipment. The forecasting results should include max/min quantities, safe quantities, order quantities per time, and the like.
- Work emphasis for purchasing department is to integrate spares demand information that become available from different sources. To choose suitable suppliers and to achieve best order strategies for all kinds of spares are also important.
- The sales company has to effectively forecast its orders from the market, and integrate the demand information for each kind of spare.
- The manufacturing factory should know the true needs of the end users' in order to arrange production.

Know yourself and know your enemy, victory is assured. Obviously, improving only each component's own forecasting ability is not enough. All should understand the root cause of spares inventory, and then, exact forecasting results will be got step by step.

C. Management Pattern Optimization Based On Integrated Information

Information sharing is another important factor. Based on information sharing, maintenance department have to monitor the running conditions of spares and equipments. Based on information sharing, purchasing department have to get feedback on spares usage information, lead time for suppliers, price discount information, purchasing channels information, and the like. With integrated information, sales companies have to control feedback from end users, lead time for produce and price discount information from manufacture factories. Especially, for those end users with whom "Zero Inventory" agreements are signed, information sharing is a key. With the help of information sharing, manufacturing factories can get both feedbacks from both end users and market. This in turn will enhance the integrated ability for multi-end users and multi-sales companies. In spares demand system, management information systems (MIS)' utilization is very important. Some successfully implemented MIS, including EAM and ERP, have already proved their tremendous value. Such information systems' successful running will set up the base for the whole spares demand systems' optimization.

D. Integrated Supply Chain Optimization

The supply chains' optimization can not be neglected neither. From the integrated view point: how to make spares safe inventory? Which kind of spares fit for VMI or JMI strategies? How to choose different suppliers for different kinds of spares? For all components in spares demand system, how to make scientific supply chain strategies with consideration of integration management is another pivotal thing for achieving the whole system's optimization.

IV. Example

Fortunately, for some famous manufacturing factories, decision makers begin to realize the importance of considering integration in spares decision making. Successful stories in real world are not alone. For example, for some novel traditional manufacture factories (such as SKF, ABB, et al), special asset management service departments have been set up, to help their end users and sales companies to improve spares management level. The service businesses usually include helping them manage spares data, teaching them how to use scientific forecasting methods, as well as how to make strategies for different spares, even how to set up inspection routines. On the other hand, many manufacturing factories begin to implement uniform inventory systems with their distributors. By above ways, information could be shared among all components. As discussed above, the efficiency of the whole spares demand system can be enhanced.

V. Conclusions

In spares demand system, there are four main components: manufacturing factories, sales companies, end users' purchasing departments, and maintenance departments. In this system, isolated spares optimization strategies could only bring short-term or partial improvements for each component. In future studies, all optimization strategies should be made with consideration of integration management.

References

[1] J Huiskonen, "Maintenance spare parts logistics: Special characteristics and strategic choices," *International journal of Production Economics*, vol.71, pp.125–133,2001

[2] W J Kennedy, J Wayne Patterson, Lawrence D, Fredendall, "An overview of recent literature on spare parts inventories," *International journal of Production Economics*,vol. 76, pp:201–215,2002

[3] B Ghodrati, et.al. "Spare parts estimation and risk assessment conducted at choghart iron ore mine," *Journal of Quality in Maintenance Engineering.* Vol.13,pp:353-363,2007

[4] J E Boylan1, AA Syntetos,GC Karakostas, "Classification for forecasting and stock control: a case stu*dy,"Journal of the Operational Research Society.* Vol.59,pp:473 -481,2008

[5] A A. Syntetos, J E Boylan, J D Croston. "On the Categorization of Demand Patterns," *Journal of the Operational Research Society,* vol.56, no.5,pp: 495- 503,2005

[6] A H C Eaves, B G Kingsman. "Forecasting for the Ordering and Stock-Holding of Spare Parts ,"*Journal of the Operational Research Society*, vol.55, no.4,pp: 431-437,2004

[7] A A. Syntetos, et al."The effects of integrating management judgment into intermittent demand forecasts,"*International journal of Production Economics*. Vol.118, pp:72–81,2009

[8] T M Mccarthy. "The Evolution of Sales Forecasting Management: A 20-Year Longitudinal Study of Forecasting Practices," *Journal of Forecasting*. Vol.25,pp:303-324,2005

2011 International Conference on Mechanical, Industrial, and Manufacturing Engineering
Lecture Notes in Information Technology Vols. 1-2

Experimental study on the atlanto-axial joint and related structures with regional anatomy and medical imaging

Shaomao Lv, Hongwei He, Lie yang, Qingchi Lin, Shaoyin Duan
Medical imaging Department,
Zhongshan Hospital of Xiamen University,
Xiamen 361004, China
Corresponding author:Shaoyin Duan, xmdsy@xmzsh.com

Abstract - **Objective: To evaluate the application and characteristics of anatomy and medical imaging in observing atlanto-axial joint (AAJ) and related structures. Methods: Eight cadaveric specimens of AAJ segment were studied with both anatomical and imaging methods. Vertebral arteries of AAJ segment (VA-A) , the first, second cervical nerve (CN1, CN2) and synovial fold (SF) of AAJ were observed and measured. Results: After extending from vertebral canal, CN1 goes between the posterior arch of atlas and VA-A, and CN2 passes between the posterior arch of the atlas and axis, and is posterior to VA-A. Among the 8 cases, 6 were found the SF in central anterior AAJ and 5 in lateral. VA-A goes along the AAJ with 4 curves, of which the second and fourth are away from the bone structure. The distance from CN1, CN2 to VA-A and that from the second, fourth curve of VA-A to AAJ is 0.0-2.2mm, 0.0-3.6mm and 0.0-4.8mm, 2.0-7.9mm respectively. There is no significant difference between the measurements of anatomical and imaging method (P ＞ 0.05). Conclusion: Anatomical method has advantages in obseving the CN and SF, while imaging method shows clearly and directly the VA-A and AAJ. Both are mutually complementary with consistent measurements. The combined use of the two provides a new way to study the complicated anatomy.**

Keywords –Atlanto-axial joint; Relational structure; Medical imaging; Anatomy

I. INTRODUCTION

Atlanto-axial joints (AAJ) and related structures connect the head and neck with important functions and complicated anatomy. Recently there are lots of literatures studying about atlanto-axial joint (AAJ) and vertebral artery at the AAJ (VA-A) [1-5]. To our knowledge, combination of anatomical and imaging method to study the anatomy of AAJ, VA-A, the first and second cervical nerve (CN1, CN2), synovial fold (SF) and their relations has not been reported. In this study, we combine the both methods to observe those structures on the specimens of cadaveric AAJ segmental and hope to provide an detailed anatomy for clinical diagnosis and surgery.

II. MATERIAL AND METHODS

A. Ascertaining the sample number

According to the principle of reproducibility, researchers set the probability of type I error with the $\alpha = 0.05$, type II error with the $\beta = 0.1$, the differentiating measurement with 0.5 mm, the standard deviation with 0.25 mm- 0.5 mm and have the paired t test. Calculating the experimental sample numbers or looking for the T table, 5-13 cases of sample are demanded. In our study, 8 cases cadaveric specimens of AAJ were used.

B. Marking and preparing specimen

Eight cadaveric specimens of AAJ with the surrounding ligaments, VA-A, CN1 and CN2 were chosen. Firstly, the VA was marked using interventional guide wires or red latex liquid containing 30% Urografin, then holes were drilled respectively from the medial aspect of occipital bone to bilateral atlanto-occipital joint, and from the centrum, spinous process of 3 or 4 cervical vertebrae to that of the second cervical vertebrae. Non-metallic materials and epoxy resin (for avoiding artifacts of CT and MRI scan) were used to fix the specimens. Measurement tools include the vernier caliper, compass, dissecting instrument and so on.

C. Examination methods

CT scan with 64-multi-detector row spiral CT (64-MSCT, Light Speed VCT, GE Corporation, USA) was performed. Scanning parameters were thickness of 0.625 mm, increment of 0.3mm and of pitch 0.984. Scanning area covered the whole specimen. MRI scan with 1.5T MRI (HD propeller, GE Corporation, USA) was performed when AAJ specimen box was put along with water model (available weight) for scan and cardiac coil was chosen. parameters include the checking sequences of FIESTA, FOV of 14 cm × 14 cm, reverse angle of 73 degrees, TR = 4, TE = 1, FL=60, NEX = 4, BW= 41.67, THK / SP = 2.0/-1.0; or the checking sequences of 3DSPGRE, FOV of 14 cm × 14 cm, TR = 10, TE = 5, NEC = 1, FL: 20, TI = 350, THK / SP = 1.4/-0.7, BW = 15.63.

D. Imaging process and structures observation or measurement

Three-dimensional (3D) imaging with image data of CT or MRI was performed on the workstation (Advantage workstation 4.2, GE Corporation, USA). Imaging methods were volume rendering (VR), maximum density projection (MIP) and multi-planar reformation (MPR). On these images, the AAJ and related structures were observed and measured with anatomy and medical imaging respectively. The contents

* This work is supported by National Natural Science Foundation (30870690), China.

include the size of SF, the features of VA and the distance between CN1, CN2, AAJ to VA-A. Statistical comparisons were made with paired t test on the measurements between anatomy and medical imaging, the t and P values were calculated.

III. RESULTS

Anatomical method clearly demonstrated that the CN1 goes between posterior arch of atlas and VA-A, CN2 between the posterior arch of the atlas and axis, behind the VA (Fig.1, 2). In the course of VA-A with 4 curves, there were two apparent curves away from the AAJ, one (VA-AC2) is on the side of AAJ space, the other (VA-AC4) on the posterior arch of the atlas. In the 8 specimens, there were 6 cases with SF in central anterior AAJ, 5 in lateral AAJ (Fig.3) and none in posterior AAJ. Imaging method clearly and globally showed the course of VA-A, adjacent ligaments, CN2 and the relations between AAJ and VA-A (Fig. 4-6), whereas it can not clearly show the CN1 and SF. Anatomical and imaging observations or measurements were listed (Table 1,2). The distance from CN2 to VA-AC2 is 0.0-3.6 mm, from AAJ to VA-AC2, VA-AC4 is 0.0-4.8 mm and 2.0-7.9 mm respectively. There is no significant difference between the measurements of anatomical and imaging method ($P > 0.05$).

IV. DISCUSSION

A. Studying significance

Observing the AAJ, VA-A and relational structures is important for the surgery. Anatomical and imaging methods have own advantages respectively. Anatomical method is propitious to observe the detailed anatomy of CN and SF, while imaging method has advantages on displaying the structure of AAJ, VA-A and their spatial loction [5-8]. The combined use of the two can provides reliable anatomical basis and found a new study method, which can judge the abnormal structures and functions of AAJ and VA. It helps discuss the pathogenesis of related diseases and look for the new methods of treatment. In additional, to clarify the 3D-relations between AAJ and VA or adjacent structures can enrich the contents of the regional anatomy, and improve the accuracy or safety of surgery [9-13].

B. Advantages of imaging methods

Medical imaging can show the VA, atlas, axis and other structures respectively. MRI can show the ligaments, CN and joint capsule. CT 3D-imaging can show the course of VA as clearly as DSA does and the bone structures of atlas or axis as vividly as the bone specimens. In the 3D-imaging, VR technique is common use and have been widely used in imaging diagnosis, it can show independently or jointly the AAJ, VA-A or the atlas, epistropheus with different color or transparency based on the techniques of separating, fusing, opacifying and false-coloring, and displayed the relations between superficial and deep structures [8]. At the same time, 3D imaging with combining the technologies of cutting, adding or deleting structure can ensure to show clearly the observing objects. In addition, imaging data can be used repeatedly and observed or analyzed by other doctors. All these will improve the diagnosis accuracy of the variations or lesions of AAJ and VA [7-9].

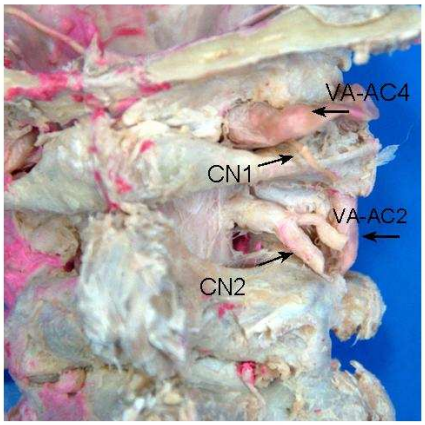

Fig.1 The posterior view observing the relations between VA-AC4 and CN1,VA-AC2 and CN2（the black arrow and labels）.

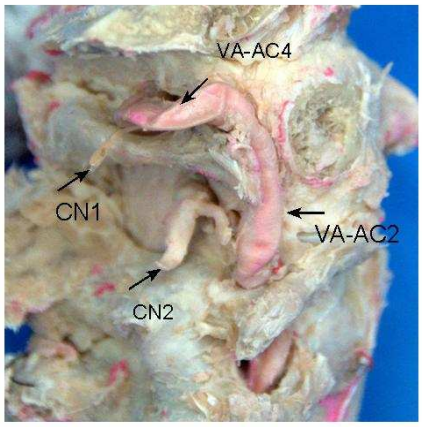

Fig.2 The lateral view observing the relations between VA-AC4 and CN1,VA-AC2 and CN2（the black arrow and labels）.

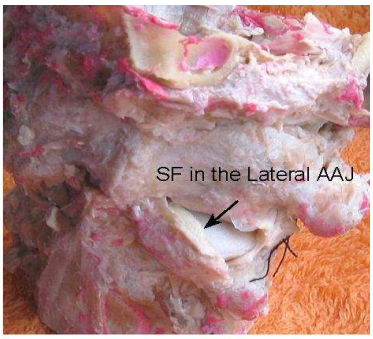

Fig.3 SF in lateral AAJ (the white arrow and labels).

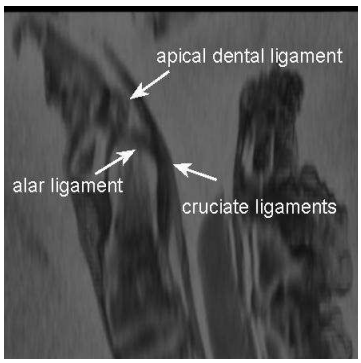

Fig.4 MRI image showing the adjacent ligaments in AAJ (the white arrow and labels).

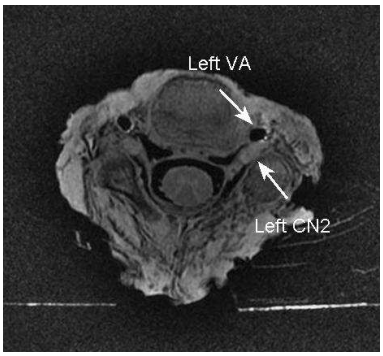

Fig.5 MRI image showing the relation between VA and CN2 (the white arrow and labels).

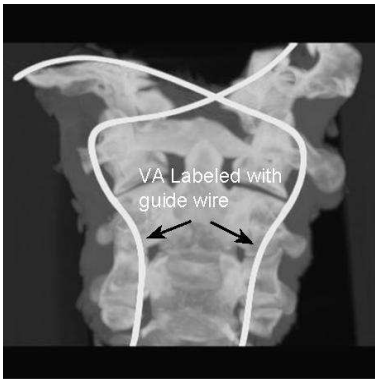

Fig.6 CT 3D-image showing the course of VA marked by interventional guide wires (the white arrow and labels).

TABLE Ⅰ. MEASUREMENTS OF 8 SPECIMENS WITH IMAGING AND ANATOMICAL METHODS

Measurement methods	Imaging (mm)	Anatomical (mm)	t	P
Distance of CN1-VA-AC4	—	0.0-2.2	—	—
Distance of CN2-VA-AC2	0.0-3.5 (1.46±1.22)	0.0-3.6 (1.56±1.16)	0.442	0.665*
Distance of VAC4-AAJ	2.1-7.8 (4.56±2.08)	2.0-7.9 (4.51±2.06)	0.230	0.821*
Distance of VAC2-AAJ	0.0-4.8 (2.83±1.34)	0.0-4.7 (2.83±1.32)	0.000	1.000*
Size of SF in lateral AAJ	—	2.2-5.5	—	—
Size of SF in anterior AAJ	—	1.5-4.3	—	—

Note: "—" represent no measurement because of displaying unclear; * P > 0.05.

TABLE Ⅱ. COMPARISON OF SHOWING THE STRUCTURES WITH IMAGING AND ANATOMICAL METHODS.

Observation methods	Imaging		Anatomical
	CT	MRI	
DISTANCE OF CN1-VA	UNCLEAR	LESS CLEAR	MORE CLEAR
DISTANCE OF CN -VA	LESS CLEAR	CLEAR	MORE CLEAR
DISTANCE OF VAC1-AAJ	MORE CLEAR	CLEAR	CLEAR
DISTANCE OF VAC2-AAJ	MORE CLEAR	CLEAR	CLEAR
SIZE OF SF IN AAJ	UNCLEAR	LESS CLEAR	MORE CLEAR
JOINT SPACES OF AAJ	MORE CLEAR	CLEAR	CLEAR

C. Comparison of anatomical and imaging methods

Anatomical method was superior to the imaging on observing the detailed anatomy of AAJ, such as the size and shape of SF, ligaments, CN and so on. However, it was less clear to show the whole course of VA and the relations to AAJ. Its measurement accuracy is subject to other factors, which is not only form the subjective of researcher, but also from the objective of measuring instruments. Imaging method was superior to the anatomical on showing the bony structure, the course of VA-A and their correlation due to three-dimensional views, and without the shelter from the other structures. However, it distinguishes some detailed anatomy less clearly. Of course, the combination of two methods was used, it will increase the contents of the regional anatomy, as well as extend the baisc study ranges of medical imaging.

D. New exploration of anatomical research

Combining both anatomical and imaging methods will improve to study ability of AAJ and adjacent structures due to their mutual complementary in displaying related structures or functions. Regional anatomy can observe the tiny structures, while imaging method with 2D- or 3D-imaging of CT or MRI can show not only their sectional anatomy, but also the whole and relations of the complex structures. 3D-imaging can overcome drawbacks of structures overlapping and realizeb individually "non-invasive anatomy in vivo" for surgery. To our knowledge, combining both anatomical and imaging methods in studying AAJ and adjacent structure has not been reported, it will promote the anatomical studies and provide a new approach on the basic research of medical imaging. Comparing with regional anatomy, it has following advantages: ① displaying accurately the tiny anatomy and the whole relation between the deep and shallow structures. ② Observing the sectional anatomy and 3D anatomy in vivo. ③ providing detailed preoperative anatomy for interventional radiology or surgery [12,13].

E. Clinical value

Anatomical and imaging methods can clearly show AAJ and adjacent structures, they give a anatomical basis for diagnosing and treating related the diseases of AAJ and VA. Anatomical research about the SF may provide an anatomical basis for the pathogenesis of atlanto-axial dislocation [14]. 3D-imaging show the course of VA and related variation can give a solid support for the choice of treating methods and safety of operation, it has important studing significance on the clinical medicine. There are lots of treatment way for vertebro-basilar artery stenosis and occlusion, but it is very important to know the detailed anatomy of VA and the relationship with adjacent structures before operation. This study clarified the values of anatomical and imaging methods in showing AAJ and adjacent structures with accurate measurements. Combination of two research methods will have important value of studying on the applied anatomy, and form a new study method on the the complex anthropotomy [9-15].

ACKNOWLEDGMENT

We would like to express our thanks for the support of Xiamen Board of Health's Medical Research Program (WSK 0622), China.

REFERENCES

[1] RS. Tubbs, NA. Shah and BP. Sullivan, "Surgical anatomy and quantitation of the branches of the V2 and V3 segments of the vertebral artery," Laboratory investigation. J Neurosurg Spine, vol. 11, pp. 84-87, January 2009.

[2] T. Gupta, "Quantitative anatomy of vertebral artery groove on the posterior arch of atlas in relation to spinal surgical procedures," Surg Radiol Anat, vol. 30, pp. 239-242, March 2008.

[3] F. Cacciola, U. Phalke and A. Goel, "Vertebral artery in relationship to C1-C2 vertebrae: an anatomical study," Neurol India, vol. 52, pp. 178-184, February 2004.

[4] SY. Duan, SM. Lv and F. Ye, "Three-dimensional CT angiography study on the relations between the vertebral artery and atlantoaxial joint," Chin Med J, vol. 122, pp. 917-920, August 2009.

[5] F. Siclari, IM. Burger and JH. Fasel, "Developmental anatomy of the distal vertebral artery in relationship to variants of the posterior and lateral spinal arterial systems," AJNR Am J Neuroradiol, vol. 28, pp. 1185-1190, June-July 2007.

[6] CW. Pfirrmann, CA. Binkert and M. Zanetti, "MR Morphology of Alar Ligaments and Occipitoatlantoaxial Joints: Study in 50 Asymptomatic Subjects," Radiology, vol. 218, pp. 133-137, January 2001.

[7] JT. Hong, SW. Lee and BC. Son, "Analysis of anatomical variations of bone and vascular structures around the posterior atlantal arch using three-dimensional computed tomography angiography," J Neurosurg Spine, vol. 8, pp. 230-236, March 2008.

[8] SY. Duan, SM. Lv, F. Ye and QC. Lin, "Imaging anatomy and variation of vertebral artery and bone structure at craniocervical junction," European Spine Journal, vol. 18, pp. 1102-1108, August 2009.

[9] PN. Sylaja, V. Puetz and I. Dzialowski, "Prognostic value of CT angiography in patients with suspected vertebrobasilar ischemia," J Neuroimaging, vol. 18, pp. 46-49, January 2008.

[10] JM. Hong, CS. Chung and OY. Bang, "Vertebral artery dominance contributes to basilar artery curvature and pri-vertebrobasilar junctional infarcts," J Neurol. Neurosurg. Psychiatry, vol. 80, pp. 1087-1092, October 2009.

[11] JM. Provenzale and B. Sarikaya, "Comparison of Test Performance Characteristics of MRI, MR Angiography, and CT Angiography in the Diagnosis of Carotid and Vertebral Artery Dissection: A Review of the Medical Literature," Am. J. Roentgenol, vol. 193, pp. 1167 – 1174, April 2009.

[12] LJ. Coward, DJ. McCabe and J. Ederle, "Long-Term Outcome After Angioplasty and Stenting for Symptomatic Vertebral Artery Stenosis Compared With Medical Treatment in the Carotid And Vertebral Artery Transluminal Angioplasty Study (CAVATAS)," Stroke, vol. 38, pp. 1526 – 1530, May 2007.

[13] M. Yamazaki, A. Okawa and M. Hashimoto, "Abnormal course of the vertebral artery at the craniovertebral junction in patients with Down syndrome visualized by three-dimensional CT angiography," Neuroradiology, vol. 50, pp. 485–490, March 2008.

[14] S. Inami, K. Kaneoka and K. Hayashi, "Types of synovial fold in the cervical facet joint," J Orthop Sci, vol. 5, pp. 475 ~ 480, May 2000.

[15] G. Sparacia, F. Bencivinni and A. Banco, "Imaging processing for CT angiography of the cervicocranial arteries: evaluation of reformatting technique," Radiol Med (Torino), vol. 112, pp. 224-238, March 2007.

2011 International Conference on Mechanical, Industrial, and Manufacturing Engineering
Lecture Notes in Information Technology Vols. 1-2

Composition Principle of Internet of Things Architecture

LIU Pu
Shandong University of Technology
Zibo, Shandong Province, P.R.China
liupu@sdut.edu.cn

LI CHao
Dep. of Clothing Engineering
Shandong Silk Textile Vocational College
Zibo, Shandong, P.R.China

Abstract: As an emerging technology, Internet of Things has been caused attention by domestic academia and industry. This paper introduces the basic concepts and development process of Internet of Things; then introduces its architecture, focuses on the features dissertation of each network layer; in this paper, the key technologies of Internet of Things are studied and discussed; finally, the development of its future prospects.

Keywords: Internet of Things; Network Architecture; Sensor Technology; Nanotechnology; RFID; Tag

I. INTRODUCTION

The concept "Internet of Things (IOT)" war proposed in 1999 by EPCglobal, EPCglobal Joint more than l00 organizations and companies to establish alliances for the research and development IOT. Once been put forth, this concept got great concern by the United States. Since then, researchers around the world expand research gather around the theme of IOT, and IOT was hailed as a new opportunity with historical development of the times given.

IOT is a network concept for the purpose of perception of the physical world; it is a dynamic distributed intelligent multi-sensor collaborative awareness system which integrated communication networks, sensors, microelectronics, micro-nano technology and other fields. Through RFID, infrared sensors, GPS, laser scanners and other information sensing device, IOT enables interconnection, information exchange and data communications between any item according to protocol agreed. IOT is designed to meet the intelligent positioning, tracking, monitoring and management needs.

Using RFID, data communications and other technologies, Internet-based IOT forms a network covering the integration of everything in the world; all things in the network can automatically identify and information enable share to achieve mutual "exchange" without human intervention. Compared with the Internet, IOT expands client to any goods and articles. It is connected to the reality of the physical world, through integrated the "real things in the world" and "virtual Internet" into a same network, to achieve "Internet of Things".

II. HISTORY OF INTERNET OF THINGS

General definition of IOT is that, through RFID technology, sensors, GPS, laser scanners and other equipment, according to the agreed protocol, after connected to the wireless network through interfaces, items can communicate and exchange information with each other. IOT is a large network with intelligent identification, location, tracking, monitoring and management needs.

From August 2009 that "Experience China" concept, to clear the sensor network, the Internet of Things into the range of strategic and emerging industries, within a few months, Premier Wen Jiabao has three times to make the development of IOT instructions, indicating that Internet of Things technology and information network industry in the emerging industries of strategic importance which occupies a key place. November 2005, World Summit of Information Society (WSIS) held in Tunis and issued a "ITU Internet Reports 2005: Internet of Things", the report pointed out that "Internet of Things" communication era coming; The end of 2008, IBM CEO Sam Palmisano for the first time proposed "the wisdom of the Earth" concept, that is, embedded sensors and equipment to all corners of the world's power grids, railways and other objects, and with the idea of "cloud computing" integration, formatted "Internet of Things "; January 2009, U.S. President Barack Obama make the IBM "wisdom of the Earth" concept rose to U.S. national strategy (he proposed new government invest in new generation of intelligent infrastructure); August 2009, Premier Wen Jiabao visited Wuxi R & D sub-centers, Wireless sensor engineering center in Jiaxing, Chinese Academy of Sciences, he made earnest hope for the breakthrough of IOT core technologies and on the "Feel China" put forward ideas; The end of October 2009, domestic scientists in the sensing technology and representatives of Mobile, China Unicom, Telecom, Huawei, ZTE, Datang, Lenovo and other related industries gathered in Wuxi, announced the establishment of Sensor Network Industry Alliance of China (SNIAC); March 2010, Hainan, Guangdong, Wuhan and other cities have been carrying out applied research and practice of IOT,

978-0-9831693-1-4/10/$25.00 ©2011 IERI

Hainan planed to combine IOT applications with international tourism, and Guangdong promoted commercial IOT through the integration of scattered IOT applications. China's IOT industry is entering "hundred flowers flourishing" and "application launch" stage.

III. Internet of Things Architecture and its Core Technology

Integration of sensors, computers, communication networks, semiconductor technology, IOT realizes the interconnection communication between items. As a large-scale self-organizing network, its features include: sensor node layout-intensive, collaborative, self-organizing, wireless communications. According to the flow direction and processing methods of data within the network, IOT can be bottom-up divided into three levels: perception layer, transport layer and application layer. IOT's core is "self-networking, collaborative awareness"; To have functions of fully aware, reliable transmission, intelligent processing of information, and so on, the critical application technologies IOT involved include radio frequency identification technology, sensor technology, nanotechnology, smart materials embedded networking technology, etc.

To achieve communication of items, IOT should consider three basic elements: the real-time information gathering, effective transmission of information, and intelligence processing of information. Problems of any essential element in the process would lead network terminal not collect information accurate and reliable, and as a result, communication between items could not be achieved. A primary aspect of IOT communications is the timeliness of data collection. This requires the collection devices such as sensors or RFID, embedded in the location, objects and systems which need to focus on or collect information. Through appropriate technology and methods, the collection devices can real-time and efficient collect the changing information of objects, and the information obtained will be processed and integrated; To ensure the effective transfer of information, the collected data need security encryption, and uses efficient routing protocol, communication protocols and network security protocols to ensure high reliability and accuracy of data; Through the ubiquitous wireless communications network, the collected information is transferred out, and to achieve effective transfer of information; Throughout the whole process from being collected, being transmitted and being received, the information needed for processing.

A. Perception Layer

Perception Layer that is, information recognition layer, which implements the monitoring object identification and perception based on two-dimensional codes, RFID, and sensors. Perception layer is to be solved perception and acquisition of information, This layer mainly includes the reading and writing RFID technology, sensors and sensor networks, robotics intelligent sensing technology, remote sensing technology, IC card and bar code technology, etc.

RFID is an important technology of IOT. RFID is the abbreviation for Radio Frequency Identification technology, which is an automatic identification technology raised on 90 years of the 20th century; and it is a more advanced non-contact identification technology. Based on a simple RFID system, combined with existing network technology, database technology, middleware technology, a large IOT is composed of a large number of readers and numerous mobile label which more massive than the Internet. It is the development trend of RFID technology. RFID is a technology that can make objects "speak". In the conception of "IOT", RFID tags stored in specification and interoperability information. Information is automatically collected to the central information system through wireless data communication network, and thus achieving aim of recognition items. And then through open computer networks for information exchange and sharing, IOT achieve transparent management of goods.

Sensing technology is known as the three pillars of information technology along with computer technology and communication technology. Sensing technology is a modern interdisciplinary engineering science which major research on access to information from the natural source, and processing (transformation) and recognition. The core of sensing technology is the sensor, which is the necessary component responsible for the realization of the things and objects, things and people information exchange in IOT. Most of the current applications of wireless sensor networks focused on simple, low complexity, access to information, and can only obtain and process information about the physical world scalar. However, this scalar information can not describe the variety of the physical world; it is difficult to achieve real communication between people and the physical world. To overcome this deficiency, both for scalar information and for vector information such as accessing video, audio and images, wireless multimedia sensor networks have emerged. As a new information acquisition and processing technology, wireless multimedia sensor network is more focus on information collection and processing. It uses compression, recognition, integration, reconstruction and other methods to process information in order to meet the diversity applications of wireless multimedia sensor networks.

Manufacture of intelligent sensors is based on micromachining technology, the silicon mechanical, chemical, welding process, and then use different packaging technology to package. In recent years, LIGA processing (Lithography, Galvanoformung and

Abformung), deep into the sensitive X-ray lithography electroplating film, has developed for the manufacture of sensors. Smart sensors generally have very strong real-time features, in particular, often requires dynamic measurements in a few microseconds to complete data acquisition, computing, processing and output. Functions of smart sensors are carried out under the program supports; many parameters to some extent depend on the software design and its quality, such as the number of functions, basic performance, easy to use, reliable. These software are five categories, including the scale conversion, digital-zero, nonlinear compensation, temperature compensation, digital filtering technology.

B. Transport Layer

Transport layer, also known as network communication layer, mainly including the bearer network composed by various communication networks and the Internet of Things. Through the existing Internet, satellite, mobile communication network, enterprise network, etc., the transport layer access to the IOT communication network, achieves further data processing and transmission, and completes information communication and data transmission between the perception layer and the application layer. Data security protection is the core issue for transport layer to resolve. During transmission, the data is fragile and vulnerable to be attack, change, conflict, congestion and retransmission. Because of this, the transport layer needs to use data fusion and security controlling technology to improve the fault tolerance of network and ensure data reliability. Transport layer mainly includes wireless sensor technology, intelligent embedded technology, etc.

The basic function of Wireless Sensor Networks (referred to as WSN) is to connect a series of space distributed self-organizing sensor unit through a wireless network, which will summary the own data collected and transmitted through the wireless network, in order to achieve within the space of physical dispersion or collaborative environment monitoring, and appropriate based on these information analysis and processing. Running through three levels of IOT, WSN technology is an emerging technology combination of computing, communication and sensor technology. It has advantages of wide range, low-cost, high-density, flexible layout, real-time acquisition, work around the clock, and so on. WSN has a significant leading role for other industries of IOT.

Embedded technology is a technology that treated the computer as an information processing component and embedded it into the application systems, i.e., it solidified software into hardware system what the hardware system and software system were integrated. Micro Controller Unit (MCU), known as embedded systems because computer chips are embedded in the device, and not have their own separate enclosure, has been applied in various fields include the family and the industry. Most embedded systems are still in the independent application stage, the MCU as the core, with some monitoring, server, indicates the device with the realization of certain functions. Internet has become one of important basic information facilities; it is an important channel for the flow of information. If the embedded system can connect to the Internet, you can easily and cheaply transfer the information to virtually any place in the world.

C. Application Layer

Application layer, i.e. the terminal processing layer, is the input and output control terminal (including computers, mobile phones and other terminal server), mainly composed by a variety of applications; its` functions include aggregation, conversion, analysis and sharing of the acquired data, as well as corresponding support platform for user applications to achieve storage, mining, processing and application of information send from the transport layer. The application layer provides users with IOT application interface, and provides application services for varieties of user equipment and terminal.

Core purpose of IOT is to enhance the central processing capacity. IOT intelligent processing needs M2M systems through the different functions of information between the link-sharing, the central processing unit in collaboration with co-operation of the system, the smart sensor integrated into the functioning of the whole society. Central processing unit should be established on the basis of a distributed cloud computing to provide high-speed computing and disaster recovery capabilities and protect the normal operation of the network of IOT. Operators should start from building cloud computing-based M2M support operations center, play BI data analysis advantages associated with the establishment of the M2M system coordination mechanism, and gradually enhance the data analysis and processing capabilities of the operations center, and ultimately form the "brain" with intelligent processing function.

IV. PROSPECT OF INTERNET OF THINGS

Although the application of IOT on the whole is still in its infancy, its application in some areas has achieved initial success. Currently, the application of IOT is mainly in logistics, military, monitoring and management, medical care and other fields. Through the use of IOT technology in the military, it can reduce the attack time, expand the detection range, improve tracking accuracy and continuity, and enhance capacities of target detection and identification, which effectively improve the operational effectiveness. In other areas, it can better grasp the dynamic information about the object, so as to target

identification, diagnosis, emergency treatment and other applications to provide basis for decision making.

As technologies (sensing, monitoring and control, communications, networking, computer, etc.) have developed, the IOT would show a stronger vitality, its application would permeate all sectors and across every aspect of people's lives. Future IOT applications, mainly in the following areas: urban management, such as environmental monitoring, vehicle tracking and positioning, interactive car navigation, etc.; home health care, such as smart home, bio-pharmaceuticals, remote meter reading and so on; mobile e-commerce, such as mobile payment, mobile ticketing, mobile card, etc.; other applications: green agriculture, public safety, intelligent transportation, community integrated services. As a cutting-edge technology with strong demand for traction, IOT will continue to promote the computer, Internet, sensors and other industries, and will enable a revolutionary turn for the better in accessing information, leading to a new level of information technology; and also, IOT would drive the micro-system and sensor industry rapid development, which set of sensing, collecting, processing, sending and receiving, network in one. Internet and its related technologies and industries are difficult to estimate the market value and development prospects.

V. CONCLUSION

The IOT is an advanced system that contains many complex and huge technologies, and its flexible application in the form will involve in all aspects of human social life. This paper introduced, analyzed and discussed the concept, structure and key technologies of IOT, focusing on the network architecture. For each level, the paper analyzed information on the IOT in all aspects of real-time acquisition, security and effective transmission, and intelligent processing, etc. Finally, author makes exploration and prospect for the application and development of IOT.

REFERENCES

[1] Luigi Atzori, Antonio Iera, and Giacomo Morabito, The Internet of Things: A survey, Computer Networks [M], Vol. 54, pp. 2787-2805, Oct 2010

[2] Geng Xiaochuan, Applications prospect of RFID technology in the future of Internet of Things, China Quality Supervision [M], Aug 2010

[3] Song Junde, Discussion on the Present and Future of Internet of Things, Mobile Communications [M], Jan 2010

[4] Rolf H. Weber, Internet of Things – New security and privacy challenges, Computer Law & Security Review [M], Vol. 26, pp. 23-30, Jan 2010

[5] Zhang Jian, The Next Step: Internet of Things, China Logistics & Purchasing [M], Jul 2010

[6] Zhang Yunyong, Fang Bingyi, Technology Standardization and Development Suggestions for Smart Home Based on the Internet of Things, Mobile Communications [M], Jan 2010

[7] Rolf H. Weber, Internet of things – Need for a new legal environment? Computer Law & Security Review[M], Vol. 25, pp. 522-527, Nov 2009

[8] Wang Jiajia, What Border Does the Internet of Things needs to break? Software Engineer [M], Apr 2010

[9] Dimitris Kiritsis, Closed-loop PLM for intelligent products in the era of the internet of things, Computer-Aided Design [M], Available online, Mar 2010

[10] Luo hang, Internet of Things: the future direction of technology development in logistics industry, Maritime China [M], Aug 2010

[11] Li ye, Wang Jingbo, etc., Aplication Resaerch of Internet of Things in the Intelligent Transportation, Mobile Communications [M], Jan 2010

[12] Jiang Hongmin, Wireless City: Better Thoroughfare Pointed to the Development of Internet of Tthings, Information Network [M], Jul 2010

2011 International Conference on Mechanical, Industrial, and Manufacturing Engineering
Lecture Notes in Information Technology Vols. 1-2

Research on Tag Chips of RFID Technology

LIU Pu
Shandong University of Technology
Zibo, Shandong Province, P.R.China
liupu@sdut.edu.cn

LI CHao
Dep. of Clothing Engineering
Shandong Silk Textile Vocational College
Zibo, Shandong, P.R.China

***Abstract*—** Barcode recognition technology is not new for people, and radio frequency identification technology may be unfamiliar to most people, although its application in some areas is now taking shape. Tags are the data carrier of RFID technology, which is a non-contact automatic identification technology. This article describes the principles of RFID technology and Tags, summarizes the advantages of Tags, analyzes several factors restricting the popularity of Tags, briefly describes the status of domestic RFID applications and presents recommendations for its development.

Keywords- RFID; Tag; Non-contact; Technical standards; Encryption; reliability

I. INTRODUCTION

From August 2009 that "Experience China" concept, to clear the sensor network, the Internet of Things (IOT) into the range of strategic and emerging industries, within a few months, Premier Wen Jiabao has three times to make the development of IOT instructions, indicating that Internet of Things technology and information network industry in the emerging industries of strategic importance which occupies a key place. China's IOT industry is entering "hundred flowers flourishing" and "application launch" stage.

The concept "Internet of Things" was proposed in 1999 by EPCglobal, EPCglobal Joint more than l00 organizations and companies to establish alliances for the research and development IOT. Once been put forth, this concept got great concern by the United States. Since then, researchers around the world expand research gather around the theme of IOT, and IOT was hailed as a new opportunity with historical development of the times given.

IOT is a network concept for the purpose of perception of the physical world; it is a dynamic distributed intelligent multi-sensor collaborative awareness system which integrated communication networks, sensors, microelectronics, micro-nano technology and other fields. Through RFID, infrared sensors, GPS, laser scanners and other information sensing device, IOT enables interconnection, information exchange and data communications between any item according to protocol agreed. IOT is designed to meet the intelligent positioning, tracking, monitoring and management needs.

As a key technology of the Internet of Things, RFID (abbreviation of Radio Frequency Identification) technology is developing rapidly, it is widely used in industrial automation, business automation, transportation control and management and other fields. Although RFID technology in China started late, it is gradually extended to related areas and narrowing the distance and abroad. Tags are the information carriers of RFID, and this article will briefly describe them, hoping to help those who are interested.

II. RFID AND TAGS

RFID is a non-contact automatic identification technology, which uses radio signals through space coupling (alternating magnetic field or electromagnetic field) to achieve non-contact transmission of information, and it achieves identification purposes through the message. It uses radio frequency to non-contact two-way communication, automatic target recognition and access to relevant data, the recognition process without human intervention, in a variety of harsh environments. The technology can identify the high-speed moving objects and also it can identify multiple tags at the same time, the operation is quickly and conveniently.

General RFID system consists of three parts, i.e., smart cards, readers and back-end data management system (BEDMS), shown in Figure 1. Smart cards, also known as radio frequency card or Tags, have the smart ability to read and write, and encrypted communication; it is the real data carrier of radio frequency identification system. Generally, Tags are composed by the tag antenna and tag-specific chip. Each tag has a unique electronic code, which attached to the target object. Tag is equivalent to the barcode in bar code system; it is used to store the information necessary to identify and transmission. Reader, also known as read-writer, which consists of wireless transceiver modules, antenna, control module, the interface circuit and other components, is the equipment responsible for reading or writing tag information. Reader can not only have read and write, display, data processing and other functions alone, but also combined computers or other systems , to complete the operation of Tag. Back-end data management system is mainly for data storage, information management, Tags read and write control.

978-0-9831693-1-4/10/$25.00 ©2011 IERI

In applications, Tags attached to the items to be identified; when the item goes by the reading range, Reader automatically non-contact identifies the agreed information in order to achieve functions of automatic identifies items or automatically collected identification information. Typically Reader contains the high-frequency module (transmitter and receiver), the control unit and the Reader antenna. In addition, many Readers have additional interfaces (RS232, RS485, Ethernet interface, etc.) in order to transfer the obtained data to the application system or receive commands from the system. Tag and Reader achieve the space (no contact) coupling of RF signal by coupling device; in the coupling channel, according to the timing relationship, they achieve the goals of energy transmission and data exchange.

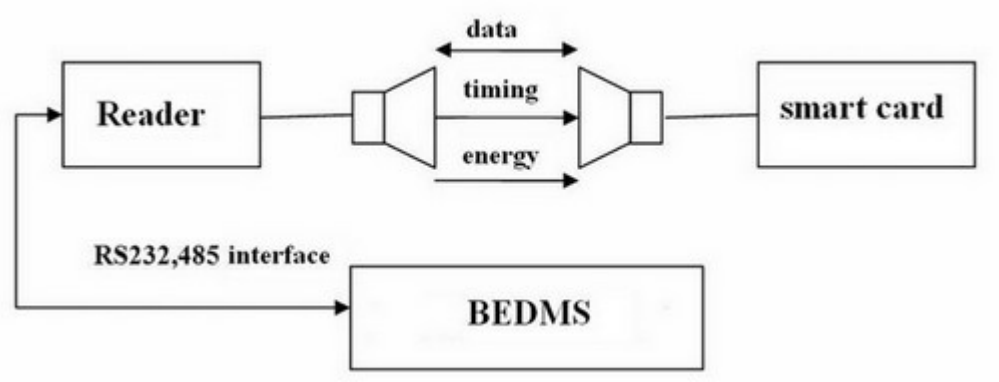

Figure 1. Basically consists of RFID system

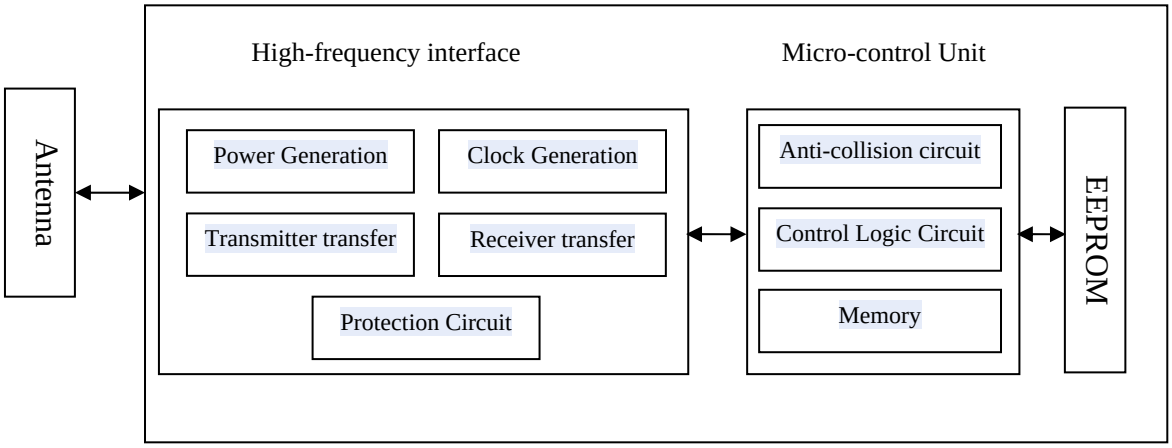

Figure 2. Tag's internal structure

Tag's circuit mainly composed of four parts by the antenna, high-frequency interface, the micro control unit and the EEPROM, shown in Figure 2. High-frequency interface consists of five modules: Power generation module generates working voltage for circuit from the RF wave; Clock generation module provides the stable and adjustable system clock; Transmitter and receiver circuit module complete the two-way half-duplex communication links of instructions response and signal receiving and transmitting between the Reader and the Tag; Protection circuit module can prevent Tag damage due to the excessive antenna voltage or power supply voltage when it is close to the reader; Micro control unit completes the Tag identification and implements the Reader's instructions, it mainly consists of three parts by the anti-collision circuit, control logic and memory interface. EEPROM unit is mainly used for storing data; data users to store are stored in the EEPROM and they would be maintained when the card loses power or beyond the effective work scope of Reader antenna.

Tags are the true data carrier of RFID system. Generally, Tag consists of the antenna and chips (Recently proposed non-chip tags and surface acoustic wave (SAW) tags may have greater development in the future, they are still the early embryonic products now), it has become the main development direction of global automatic identification technology in the 21st century. According to the different power supply, Tags can be divided into Active Tag and Passive Tag. Active Tag builds a battery while Passive Tag does not. For the Active Tag, according to the different built-in battery-powered, the Tags can be subdivided into Active Tag and Semi-passive Tag.

III. ADVANTAGES OF TAGS

Compared with other automatic identification technologies such as bar code identification technology, RFID has the following characteristics:

Tag achieves a "free access" without aiming line scan, its read and writes speed is high and read range is great. Therefore, RFID technology can identify the high-speed moving objects and also can identify multiple tags at the same time, the operation is quickly and conveniently, for example, used to track parts or products in the factory's assembly line; Long-range RF products can be used to automatic fare collection and automatically identify the vehicle or other transportation, its identify distance may achieve tens of meters; Tag readers can read tags through non-metallic materials (mud, dirt, paint, oil, timber, cement, plastics, water and steam, etc.), it is not necessarily in direct contact with the Tags, which makes Tags become ideal choice for reading under the harsh environment such as dirty, wet and harsh, etc.

Tags have a large data storage capacity and the data can be encrypted and updated at any time, which particularly suited to store large amounts of data or be used in the required situation where stored data needs to be changed frequently; Tags are small, easy packaging, diverse shape (e.g., card-shaped, circular-shaped, button-shaped, pencil-shaped, etc.), which can be hidden or embedded in most of the materials or products, so that the goods were marked more beautiful. Tags can be used in different occasions and it is very easy to use; Its life is up to ten years and can be read and write hundreds of thousands of times with no mechanical wear or mechanical failures, it can be used in harsh environments and the working temperature is within -25℃ ~ +70℃;

The main difference of Tags and barcode is that Tags data is stored in the electronic storage unit. Using a dedicated chip, according to a unique serial identification number, the Reader can identify each piece of cargo and make key authentication to protect data security; Tag number is unique and can add security identifiers (e.g., the last one can be set as the digital security encoding, it needs to use the preceding code numbers obtained through an encryption algorithm); through networking anti-theft identification device scanning, we can immediately identify the authenticity of the product.

Tags have high read and write speed, long reading distance, large data capacity and other characteristics; application of this technology in the logistics process and supply chain management, would lead to the reduction of distribution and transaction costs and the increase of management levels.

IV. PROBLEMS FACED BY TAGS

Although Tag has these advantages, it also faces many problems in the actual production application. According to the survey, the several prominent factors which affect RFID implementations in abroad are the implementation costs, technical standards, market demands, the reliability of systems and Tags. Among them, the cost factor is considered to be the greatest resistance; technical standards factors followed.

If we want to label each piece of merchandise, the price of Tags should be reduced to very low. The current market price of tag is about 50 cents, and it is likely to exceed the value of the goods themselves when used in the small objects like toothpaste, razor blades, chewing gum. In contrast, Barcode can be printed on the product packaging as long as the application complete, so its cost is close to zero;

Technical standard is another key factor restricting the development of Tag. The current national standards of the frequency standards, coding standards and application standards are inconsistent. Only in the coding standards field, there are three separate categories as Japan's UID, Europe and America's EPC and China's GB18937-2003 (NPC) systems. Also in the frequency standards field, at 850 ~ 910MHz UHF band frequency allocation, national frequency allocation is not the same;

Market demand is the third resistance factor restricting the development of Tags. Many scholars believe that the uncertainty demand is the impact factor for RFID applications. China Federation of Logistics and Purchasing said that this factor is more obvious in China. The awareness needs of RFID applications in domestic enterprises is far less then in foreign enterprises, this will become a key obstruct factors to the development of domestic Tags.

Reliability refers to the ability of product to complete the function under the provided conditions and within the specified time. According to this definition, RFID system reliability can be defined as: under the provided conditions and within the specified time, the ability of reader to successful recognizes tags. Due to the characteristic of radio frequency identification and the impact of complexity application environmental, RFID systems may occur abnormal reading phenomenon, which affecting the reliability of RFID system applications. RFID abnormal reading include: Leakage Reading (Tag is not recognized when it pass by the Reader; this is the main reason for not reliable RFID applications); Read more (when Tag is out of reading range, Reader still recognizes it); Rereading (Tag is identified repeatedly when it pass by the reading range).

Tag itself is a Very Large Scale Integration (VLSI), major failure modes affecting its reliability are: open circuit, leakage or short circuit, parameter drift. Open circuit mainly refers that the metal wire or interconnects open, the main failure mechanism have: over point damage (including CMOS circuit latch), electrostatic discharge damage, metal electro migration, stress migration and metal corrosion. The main leakage or short circuit failure mechanisms are: electrostatic discharge damage, had electrical injury, PN junction defects, and dielectric breakdown under normal voltage. The main electrical parameter drift failure mechanisms

are: sodium ion contamination, water vapor condensation within packages and hot carrier effect, metal electro migration, dielectric breakdown and hot carrier effect. In EEPROM using floating gate technology, the data retention characteristics and non-degraded write/erase cycles (durability) are the most critical reliability problems. Floating gate memory device with erase and programming-related stress can cause changes in device characteristics. Repeated erase/program cycles would make the memory transistor oxide layer vulnerable to the stress and cause failure, such as the tunnel oxide breakdown in the EEPROM.

V. Domestic Developing Situation and Prospects of Tags

Although RFID technology in China started relatively late, Tags have been launched the application pilot projects in electronic ID card, urban public transport payment, licenses and commodity security, special equipment mandatory testing, safety management, electronic identification of animals and plants, modern logistics management and other fields, which have made some progress. China's RFID industry has made real progress in the chip design and manufacturing, Tags packaging, Readers design and manufacture, and other aspects; it has a certain system integration capabilities and has developed related application systems in several specific areas, providing a complete solution of Tags application. Ministry of Information Industry has implemented the RFID technology, standards and R&D and demonstration of RFID products, and carried out industrial deployment in this year's Electronic Development Fund.

The primary reason Chinese enterprises are not active for the application of RFID is that companies can not get many benefits from the application, while multinational corporations consider that the main benefits of RFID applications is to improve the entire supply chain management and reduce costs; we can see the main differences between the two are the base of supply chain and the management concepts.

VI. Conclusions

Tags can not replace barcodes and other automatic identification technologies in the short period, but with the development of market economy, as Tags manufacturing and identification technologies mature, Tags production costs reduce, and distribution companies improve awareness on the demand for RFID, we are confident looking forward to in the near future, RFID would replace barcodes and other automatic identification technologies, widely used into logistics, transport, health, mining and other industries.

References:

[1] ZHU Xiao-jun, A Brief Analysis of the Application of RFID in China, Computer Knowledge and Technology, Vol 23, 2010

[2] Zhang Guang-li, A Brief Analysis of Radio Frequency Identification (Tag), China Anti-Counterfeiting Report, Vol 10, 2010

[3] Jordan J. Lichty, Joshua L. Malecki, Heather D. Agnew, Daniel J. Michelson-Horowitz, Song Tan, Comparison of affinity tags for protein purification, Protein Expression and Purification, Vol 41, May 2005

[4] Liesbeth De Mol, Tag systems and Collatz-like functions, Theoretical Computer Science, Vol 390, Jan 2008

[5] V. Sarangan, M.R. Devarapalli, S. Radhakrishnan, A framework for fast RFID tag reading in static and mobile environments, Computer Networks, Vol 52, Apr 2008

[6] Won-Ju Yoon, Sang-Hwa Chung, Seong-Joon Lee, Implementation and performance evaluation of an active RFID system for fast tag collection, Computer Communications, Vol 31, Nov 2008

[7] Ahmed Ashry, Khaled Sharaf, Magdi Ibrahim, A compact low-power UHF RFID tag, Microelectronics Journal, Vo 40, Nov 2009

[8] Matthew J.B. Robshaw, An overview of RFID tags and new cryptographic developments, Information Security Technical Report, Vol 11, 2006

2011 International Conference on Mechanical, Industrial, and Manufacturing Engineering
Lecture Notes in Information Technology Vols. 1-2

Research on distributions of stress and strain during spinning of quadrilateral arc-typed cross-section hollow part

Qinxiang Xia, Peng Zhang and Xiaoyu Wu
School of Mechanical and Automotive Engineering
South China University of Technology
Guangzhou, Guangdong Province, China
meqxxia@scut.edu.cn

Xiuquan Cheng
Department of Airplane Maintenance Engineering
Guangdong Civil Aviation College
Guangzhou, Guangdong Province, China
chengxiuquan@yahoo.com.cn

***Abstract* – In recent years, a new spinning technology of hollow part with non-circular cross-section is developed. It has the characteristics of high flexibility, high productivity and lost productive cost, and can be used to produce various parts with complex shapes and sizes. The software MSC.MARC was adopted to simulate the spinning process of quadrilateral arc-typed cross-section hollow part. The distributions of stress and strain during different stages of spinning were obtained. It shows that during the spinning process of quadrilateral arc-typed cross-section hollow part, defects such as local thinning at the areas of bottom corner and side wall of the workpiece, and local thickening at the opening-end of workpiece occur easily.**

Index Terms - Spinning; Quadrilateral arc-typed hollow part; Numerical simu1ation; Stress and strain

I. INTRODUCTION

A new spinning technology for hollow parts with non-circular cross-section is developed in recent years. It has the characteristics of high flexibility, high productivity and lost productive cost, and can be used to produce various parts with complex shapes and sizes [1]. Many researches have been carried out on the spinning technology with non-circular cross-section parts in Japan, Germany and other countries. The feasibility of the hollow part with similar triangle cross-section can be produced by spinning was proved by B. Awiszus etc. in which the spinning forming occurred under a constant radial force provided by a simple spring tension device [2]. A hybrid force/position control system was adopted by Arai, H etc. to produce the hollow cone with quadrilateral non-circular cross-section, in which the roller moves along the mandrel with the variable radius[3]. The synchronous movement of the mandrel rotation, mandrel feed, and roller feed controlling by the pulse controller and stepper motor was put forward by Ichiro Shimizu etc., to form the box-shaped hollow parts with quadrilateral side non-circular cross-section [4]. To solve the problem of using expensive numerical system to control the movement of mandrel and roller, and keep a constant clearance between mandrel and roller, a profiling spinning method was developed by XIA Qinxiang, etc., in which the movements of the mandrel rotation and roller feed were controlled by the special profiling devices to form the non-circular cross-section parts with the triangle and quadrilateral arc-typed hollow part [5, 6]. Some theoretical analysis also carried out by means of finite element method to explore the complex space tracks of roller, and the distributions of stress and strain during spinning of the hollow parts with non-circular cross-section [7, 8].

The spinning of quadrilateral arc-typed cross-section hollow part belongs to complex metal plastic deformation process. The software MSC.ADAMS was used to analyze the non-linear track of the roller due to the complex motion among the roller and mandrel. The finite element analysis software MSC.MARC was used to establish a reasonable finite element model of spinning, and the distributions of stress and strain during the spinning of the quadrilateral arc-typed cross-section hollow part were obtained by numerical simu1ation.

II. ESTABLISH OF FINITE ELEMENT MODEL

A. Spinning Process of Quadrialateral Arc-typed Cross-section Hollow Part

The conical quadrilateral arc-typed cross-section hollow part with quadrilateral arc-typed and equidistant curved arc-typed cross-section was researched (as shown in Fig. 1), where a_i was the half-cone angle corresponding to a random generatric AA'. During shear spinning, the wall thicknesses of workpiece and blank meets the sine law $t = t_0 \times \sin a_i$, where t is the workpiece thickness, t_0 is the blank thickness, a_i is the half-cone angle of workpiece. The phenomenon of uneven workpiece thickness by shear spinning is inevitable due to the half-cone angles corresponding to different gyniatrics during spinning of the hollow part with non-circular cross-section are not equal. To obtain the even workpiece thickness of hollow part with non-circular cross-section, conventional deep drawing spinning was adopted to form the part and the clearance between the spinning mandrel and roller was equal to the blank thickness [9].

The spinning process of quadrilateral arc-typed cross-section hollow part is as follows (as shown in Fig. 2): a)install the quadrilateral arc-typed conical mandrel on the main spindle of spinning machine; b) clamp the quadrilateral arc-typed blank between the mandrel and the tailstock; c) the plastic deformation occurs under the action of the roller. As the roller moves along the generatrix direction of workpiece, the radial feed of roller varies with the distance between the workpiece edge and the mandrel centre. The clearance between mandrel and roller is equal to the thickness of blank during spinning to obtain the even thickness of workpiece.

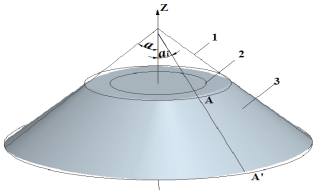

Fig. 1 Schematic diagram of quadrilateral arc-typed cross-section hollow part

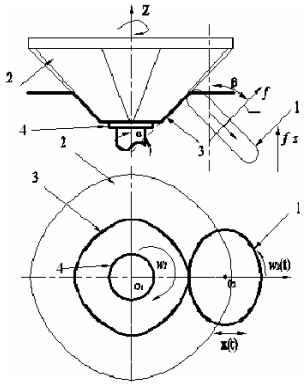

Fig. 2 Schematic diagram of spinning process of quadrilateral arc-typed cross-section hollow part
1-Spinning roller 2-Mandrel
3-Workpiece 4-Tailstock

B. *Track of Roller*

For obtaining the required clearance between the roller and mandrel in the spinning process of quadrilateral arc-typed cross-section hollow part, how to establish the corresponding relationship among the roller track and spindle speed and time has become one of the key technologies in the numerical simulation. It is very difficult to derivate the roller track by geometric method due to the complex movement relationship between spinning mandrel and roller during the quadrilateral arc-typed cross-section hollow part spinning [7]. The roller track is obtained by means of the software MSC.ADAMS, which has the powerful model building tools and kinematics, dynamics analysis functions [8]. Fig. 3 shows the mechanical simulation model established by MSC.ADAMS; Fig. 4 shows the roller track obtained by mechanical movement simulation.

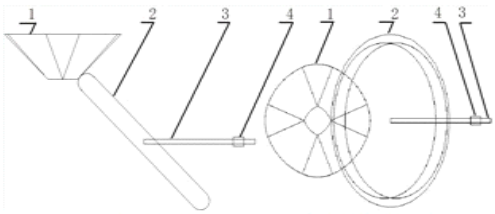

a) Front view b) Top view

Fig. 3 Mechanical simulation model by MSC.ADAMS
1-Outline of ideal model of workpiece 2-Roller
3-Virtual axle 4-Virtual shaft sleeve

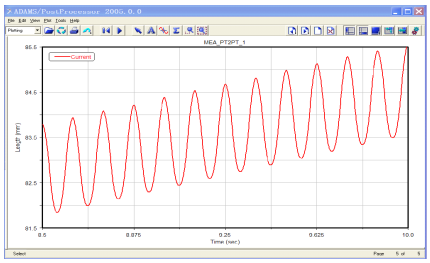

Fig. 4 Roller track obtained by MSC.ADAMS

C. *Establishment of FEA Model*

1）Shape of blank： The shape of blank was obtained by software Pro/e and Dynaform. Firstly, establish the solid model of workpiece by software Pro/e; then, extract the neutral surface of workpiece and save as IGES format; finally, input the neutral surface to the software Dynaform and carried out the following steps.

a) Mesh the workpiece automatically;

b) Check out and modify the quality of mesh and the consistency of unit normal;

c) Define the blank type, material thickness, etc.;

d) Submit and run. The obtained blank shape was shown in Fig. 5.

2）Establishment of geometrical mode: The software Msc. MARC was used to simulate the spinning process of the conical quadrilateral arc-typed cross-section hollow part. The blank is defined as the elastic-plastic body in simulation due to a certain amount of elastic deformation occurs during spinning process besides plastic deformation. The hexahedral element with eight nodes was adopted for the blank meshing by the advantages of high precision, less element numbers, easy deformation analysis, etc [10, 11]. The No.7 element used for large metal deformation was adopted, which is the default element type of software MSC.MARC. Mesh subdivision was used in the small arc area of blank (as shown in Fig. 5). The mesh of blank is discretized into double layers along the thickness direction. The total number of elements is 12800 and the total number of nodes is 19800 in the established FEA model. The spinning mandrel, tailstock and roller were defined as rigid bodies due to no deformation (as shown in Fig. 6). The Coulomb friction model is used for the contact between the roller and the blank, the friction coefficient is 0.1. The blank material is SPCC. The mechanical properties listed in Table 1 were obtained by the uniaxial tensile test.

Fig. 5 Mesh model of blank

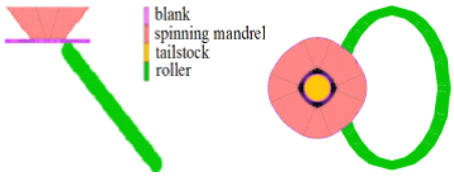

Fig. 6 FEA model of the quadrilateral arc-typed cross-section hollow part spinning

Table 1 Mechanical properties of blank

Young's modulus E (GPa)	Poisson's rate μ	Stress yield σ_s (MPa)	Tensile strength σ_b (MPa)	Hardening index n	Strengthening coefficient K
182.9	0.26	218	327	0.22	571.8

III. Analysis and Comparison Result

To analyze the distributions of stress and strain during the spinning process of quadrilateral arc-typed cross-section hollow part, the spinning process is divided into three stages, the initial, middle and final stage. The shape and size of blank, roller and mandrel used in numerical simu1ation are shown in Fig. 7. The relevant geometric and processing parameters are listed in Table 2 and Table 3, respectively.

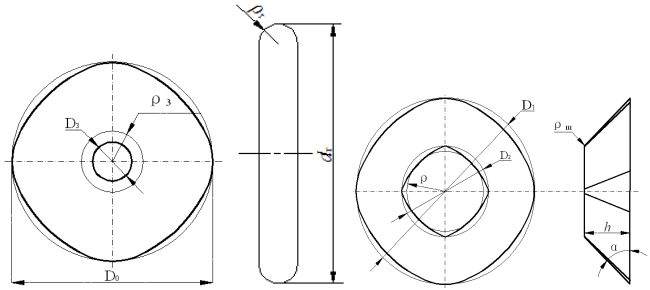

a) Blank b) Roller c) Mandrel

Fig. 7 Diagram of blank, roller and mandrel

Table 2 Geometric parameters of blank, rollers, mandrel

Blank			Roller	
Circumscribed circle diameter×thickness	Generating radius	Hole diameter	Diameter	Roundness radius
$D_0 \times t_0$ (mm)	ρ_3 (mm)	D_3 (mm)	d_r (mm)	ρ_r (mm)
96×2	13.14	28	240	4，6，8
Mandrel				
Circumscribed circle diameter	Generating radius	Roundness radius	Height	Half cone angle
d_1，d_2 (mm)	ρ(mm)	ρ_m (mm)	h (mm)	a (°)
40，100	13.14	5	30	45

Table 3 Processing parameters

No.	Rotational speed of main spindle n (r/min)	Axial feed rate of roller f_z(mm/r)
1	120	0.6
2	120	0.8
3	120	1.0

For convenient the analysis and discussion, the deformation area of quadrilateral arc-typed cross-section hollow part is divided into four areas along the generatrix direction, the areas of the bottom, fillet, side wall and opening-end; and divided into two arc areas along the tangential direction, the areas of large arc and small arc (as shown in Fig. 8). The area of roller contact with blank is defined as the contact area (as shown in Fig. 9).

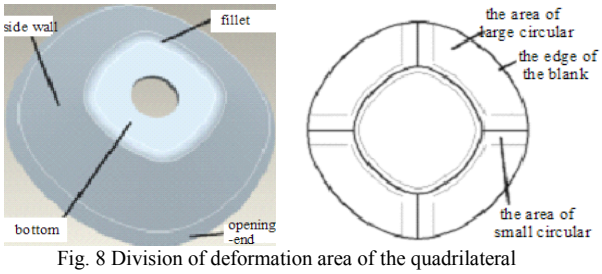

Fig. 8 Division of deformation area of the quadrilateral arc-typed cross-section hollow part

A. *Initial spinning stage*

In The initial spinning stage is defined as the stage form the moment as soon as the roller contact with the blank to the end of the bottom corner of workpiece, that is the stage of roller moving pass through the workpiece bottom corner area. The distributions of the equivalent stress, and strain, and the three principal strains at the contact area are shown in Fig. 10 and Fig. 11, respectively.

During the initial spinning stage, the flat blank was formed into the shell with small curvature. Fig. 10 shows that both the maximum equivalent strain and stress exists near the bottom corner area of blank. The equivalent strain and stress decreases gradually from the bottom to the edge of blank. Fig. 11 shows that the strain of deformation zone is in the state of compression along the radial direction, and in the state of elongation along the tangential and axial direction, so both diameter and wall thickness decrease and depth increases. When the technical parameters are unreasonable, e.g. the feed rate or the roundness radius of roller is too small, the crack occurs easily at the bottom corner of workpiece.

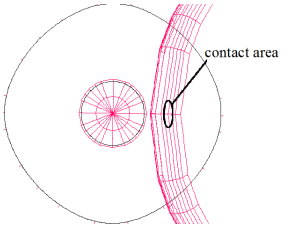

Fig. 9 Schematic diagram of contact area

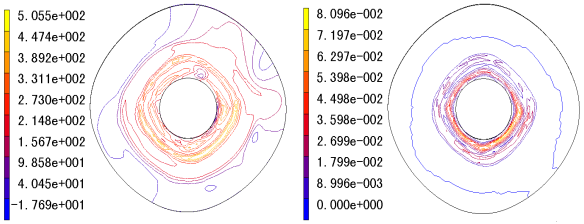

a)Equivalent stress b)Equivalent strain

Fig. 10 Contour of effective stress and strain during initial spinning stage

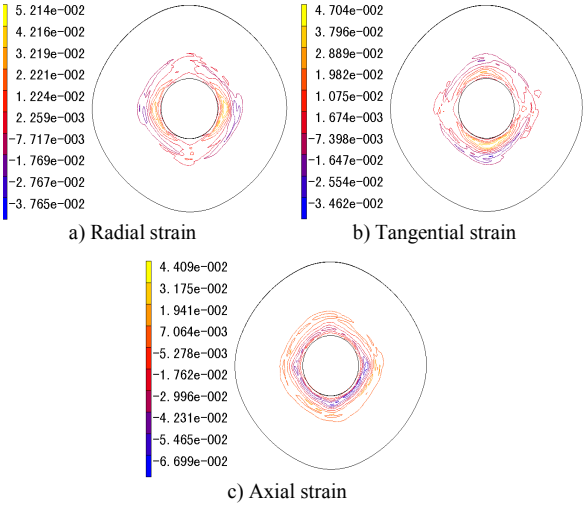

a) Radial strain b) Tangential strain

c) Axial strain

Fig. 11 Contour of three principal strains during initial spinning stage

B. *Middle spinning stage*

The middle spinning stage is defined as the stage of roller moving pass through the area of side wall of the workpiece, the unformed area height from the opening-end to the side wall of workpiece is about 5 mm. The distributions of three principal strains at the contact area are shown in Fig. 12. It shows that the strain of deformation zone is in the state of compression along radial direction, and in the state of elongation along tangential and axial direction, local thinning occurs easily in the side wall of workpiece. Therefore, the accuracy of roller

track must be controlled strictly to avoid shear spinning caused by too small clearance between the spinning mandrel and roller.

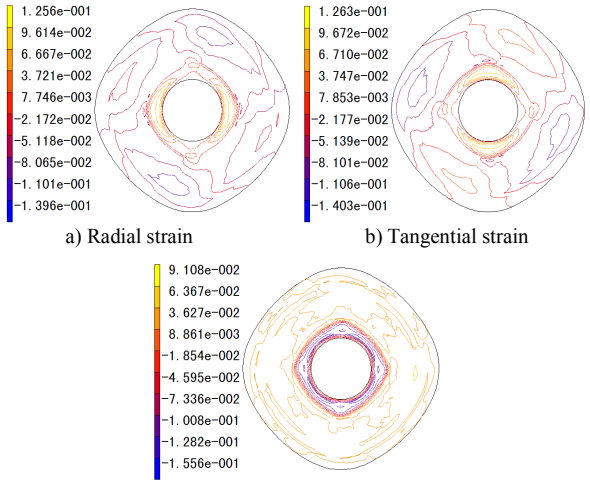

a) Radial strain b) Tangential strain

c) Axial strain

Fig. 12 Contour of three principal strains during middle spinning stage

C. *Final spinning stage*

The final spinning stage is defined as the stage of roller moving pass through the area of opening-end of workpiece. The distributions of three principal strains are shown in Fig.13. In this stage, the meterial at the undeformed zone flows easily into the deformation zone because the constraint decreases with decreasing in the blank dimension. The strain of deformation zone is in the state of compression along radial and tangential direction, and in the state of elongation along axial direction. Local thickening occurs at the opening-end of workpiece. When the technical parameters are unreasonable, e.g. the feed rate or the roundness radius of roller is too large, wrinkling occurs easily at the opening-end of workpiece.

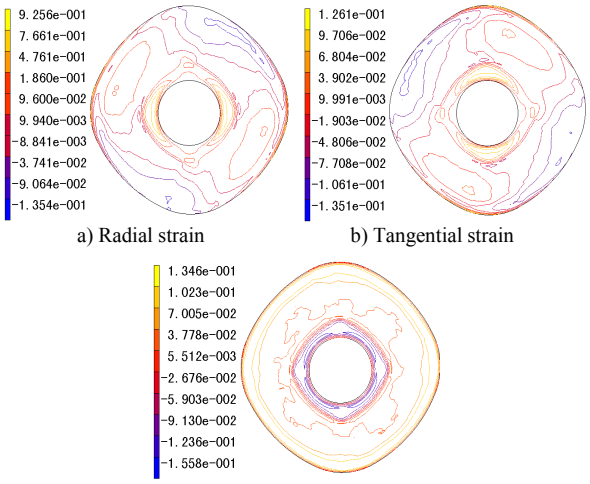

a) Radial strain b) Tangential strain

c) Axial strain

Fig. 13 Contour of three principal strains during final spinning stage

IV. CONCLUTINS

1) During the spinning process of the quadrilateral arc-typed cross-section hollow part, local thinning occurs at the area of the bottom corner of workpiece, crack occurs easily if the feed rate or the roundness radius of roller is too small. Local thickening occurs at the opening-end of workpiece, wrinkling occurs easily if the feed rate or the roundness radius of roller is too large.

2) In the initial spinning stage, the strain of deformation zone is in the state of compression along the radial direction, and in the state of elongation along both tangential and axial directions, the diameter and wall thickness of workpiece decreases, and the depth of workpiece increases.

3) In the middle spinning stage, the strain of deformation zone is in the state of compression along radial direction, and in the state of elongation along both tangential and axial directions, local thinning occurs in the side wall of workpiece.

4) In the final spinning stage, the strain of deformation zone is in the state of compression along both the radial and tangential directions, and in the state of elongation along the axial direction, local thickening occurs at the opening-end of workpiece.

ACKNOWLEDGMENT

This research is financially supported by National Natural Science Foundation of China (No.50775076).

REFERENCES

[1] Qin-xiang Xia, Shuai-bin Zhang, Xin-xi Zhan and Xiu-quan Cheng, “Linear motor and its application in the manufacture of parts with non-circle section,” Modern Manufacturing Engineering, 2008, Vol.6, pp.8-11.

[2] B. Awiszus, F. Meyer, “Metal spinning of non-circular hollow parts. Proceedings of the 8th International Conference on Technology of Plasticity,” Verona, Italy, pp. 353-355, 2005.

[3] Arai, H, “Robotic Metal Spinning Forming Non-axisymmetric Products Using Force Control. Proceedings of the 2005 IEEE International Conference on Robotics and Automation,” Barcelona, Spain, pp. 2691-2696, April 2005.

[4] Ichiro Shimizu, “Asymmetric forming of aluminum sheets by synchronous spinning,” Journal of Materials Processing Technology 210 (2010), pp. 585-592.

[5] Qinxiang Xia, Zhouyi Lai, Xinxi Zhan, Xiuquan Cheng, “Research on spinning method of hollow part with triangle arc-type cross section based on profiling driving,” Journal of Iron and Steel Research International, Vol. 81(9) , pp. 994-997, 2010.

[6] Qinxiang XIA, Xinxi ZHAN, ZHANG Shuaibin, CHENG Xiuquan, “Movement Locus Design of the Roller in Spinning the Hollow Part with Isometric Cross Section of Three Arcs,” Metalforming Equipment & Manufacturing Technology, 2008, Vol. 6 , pp. 77-82.

[7] Qinxiang Xia, Yingpin Wang, Ning Yuan, Xiuquan Cheng, “Parameters Analysis of Solving Complex Space Tracks Based on ADAMS,” The International Conference on Electrical and Control Engineering (ICECE), Wuhan, 2010, China, pp. 143-147.

[8] Qin-xiang Xia, Xiao-yu Wu, Shuai-bin Zhang, Xiu-quan Cheng, “Numercal Simulation and Experimental Investigation of Hollow Part with Triangular Arc Section,” Journal of South China University of Technolory, 2010, Vol.38, No.6 , pp.100-106.

[9] Cheng QIN, “Study on Virtual Prototype of Cam Mechanism Based on Pro/E and ADAMS,” Mechanical Engineering & Automation, 2008, Vol. 17 , pp. 35-36.

[10] Jian-sheng Liu, Hui-qin Chen, Xiao-xia Guo, “The Technology and Application of Finite Element Simulation of Metal Plastic Procession,” edited by Liu Jian-sheng, BeiJing Metallurgical Industry Press, 2003.

[11] Shang-jian Li, “The Simulation of Metal Plastic Forming Process,” edited by Li Shang-jian, BeiJing China Machine Press, 1999.

2011 International Conference on Mechanical, Industrial, and Manufacturing Engineering
Lecture Notes in Information Technology Vols. 1-2

E-Group Collaboration Learning Tools in Higher Education Systems

Adam Marks, PhD
Department of Business Administration – World Wide
Embry-Riddle Aeronautical University
Daytona Beach, FL, 3211, USA
marksa@erau.edu

Kees Rietsema, PhD
Department of Business Administration – World Wide
Embry-Riddle Aeronautical University
Daytona Beach, FL, 3211, USA
Rietsd37@erau.edu

***Abstract* –Online students in higher education are increasingly using Electronic Group Collaboration learning tools such as Discussion Forums, Blogs, Wikis, and Journals within their course environment. This study discusses some of these new online group-collaborative tools, and the extent to which they are being used. This study also investigates the level of acceptance of learners of these tools. The findings of this study describe the number and type of Electronic Group Collaboration tools most preferred by online student, and the reasons behind that preference.**

Index Terms – Electronic Learning, Higher Education, Group Collaboration Tools.

I. INTRODUCTION

The past few years have witnessed a significant increase of network-based technologies that enable students to work collaboratively online [11], and [5]. Electronic Learning (e-Learning) facilitates the sharing of costs, sharing of information and expertise among multiple sites and different constituencies, while providing additional educational opportunities [9], [14], and [21]. Web 2.0 applications, particularly wikis and blogs, have been adopted increasingly because of their ease of use, rapidity of deployment, and their ability to facilitate information sharing and collaboration. The fact that there are many free and open source versions of these tools may also be responsible for their explosive growth [5].

As e-learning continues to grow in popularity with both traditional and non-traditional students, educational institutions are now utilizing collaborative group e-learning to improve the learning experience of their students. According to the theory of Social Facilitation, working in groups significantly increases learning perceptions, problem solving skills, and helps students achieve a higher level of learning than individuals learning alone [10]. Group learning can offer valuable lessons regarding group communication and problem solving, which are easily transferable to the work environment [2]. This is particularly important given the fact that virtual work groups are a common component of today's corporate structure [3].

Collaborative group learning exercises are student centered, and enable students to share authority and empower themselves with the responsibility of building on their foundational knowledge [16]. However, these group activities are not always enthusiastically accepted by students. Previous studies into the impact of e-learning highlight a number of quality concerns [7]. The efficiency and effectiveness of group e-learning may be affected by any the following factors: non-contributing group members, unequal workload, scheduling, personal/social conflicts between group members, computer self-efficacy, surrounding technological factors, or instructional design issues [2], and [1].

As research has shown, technology is neutral until it delivers content [6] and may lose its effectiveness if it is not applied in a planned and systematic manner [12]. Empirical research is still needed to fully understand the different aspects of electronic group collaboration tools in the context of higher education, and to assist practitioners to effectively and successfully deploy them. For example, the mere availability of such tools does not necessarily mean that they should always be enabled. Instructors and system administrators should keep the learning objectives of each course in mind and how they could be best served. Some courses may be best served with a single tool such as group discussion forums, while other courses may be best served with several group collaboration tools. Student acceptance of these collaborative tools directly influences their motivation and creativity in meeting associated learning objectives.. This study contributes to the body of knowledge by conducting an exploratory study in students' acceptance of the number and types of Electronic Group Collaborative Tools within the context of Higher Education learning systems.

The primary objective of this study is to determine potential ways to integrate E-Group Collaborative Tools into existing e-learning systems

by identifying the most preferred E-Group Collaborative Tools, and the number of tools students expect/accept to see in one class.

II. Related work

According to [11], collaborative systems can be classified into three types; the first category includes systems collect raw data and make it available for display to collaborators, such as systems that reflect the number of students in a chat room, or that display the login information for students in a class to all other users; the second category of collaborative systems includes those which monitor and model the state of interaction and provide collaborators with visualizations that can be used to analyze the interaction, an example of which is the number of posts by a specific user to a specific discussion board. The third category of systems guides the collaborators by recommending actions students might take to improve their interaction. This category may include systems that allow group discussion rooms, or group project assignments, where interaction/evaluation among students and between the group and the instructor is conducted within the system [11].

While most higher education learning systems contain functions from all three listed categories, this paper is mainly concerned with the third category of systems, where interaction/evaluation among students and between the group and the instructor is conducted within the learning system. More specifically this paper is concerned with the use of discussion forums, blogs, wikis, and journals to facilitate Electronic Group Learning in the higher education online environment.

Group Collaboration e-Systems provide students with a forum to meet and connect with their peers. They allow students to communicate and collaborate effectively. They also provide instructors with more insight into individual student participation within group activities. Instructors can easily create and enroll students into multiple groups and allow students to create their own groups. Instructors can provide default settings and descriptions for each groupwhile managing them collectively or individually.

Group material can be saved and authored collectively from this location. Group members can create their own discussion forums that allow them to conduct ongoing conversations, or use blogs to blog thoughts and ideas for the rest of the course to comment on, or add journal entries for private reflection within the group. They can also create tasks to track the progress of their deliverables. These tasks can be conducted and completed by any of the members in the group. [4]

Discussion Boards allow members of the class to communicate with one another asynchronously. Discussions on the Discussion Board are logged, organized, and viewable by all class members. Conversations are grouped into threads that contain a main posting heading and all related replies. A course may have one or more discussion board linked to one or more topic. Discussion boards may also be created and assigned to several groups within a class. This structure is usually used with group projects. Instructors can email, provide feedback, and grade the assignment of each group individually [4].

Blogs are online web journals that can offer a resource-rich multimedia environment. They contain dated entries in reverse chronological order (most recent first) about a particular topic. Blogs and journals provide students and instructors with a social learning tool for expressing their thoughts and reflecting on their learning, either privately (with the Instructor) or publicly (with others in the Course). Blogs are an effective means of sharing knowledge and materials created and collected by the group with the rest of the course members. These tools empower all Course users to create and share ideas, while instructors maintain the ability to edit or remove any inappropriate material. Multiple blog types, including course, group and individual blogs are available. Instructors can assign a journal to each user in a course or course group that is accessible by only the user and the instructor. Group Blogs allow groups of students to collaboratively post thoughts and comment on each others' work while all other users in the course can view and comment on their entries. Journal entries can also be made available to the rest of the users in a course. Individual journals allow students to record their course experiences and what they are learning. Group journals allow groups of Students to reflect collaboratively on their course work and comment on their fellow group members' findings [4], and [5].

Wikis allows instructors to create places for courses, organizations, and groups to host collaborative content and group projects. Course and organization wikis allow the entire course or organization to participate. Group wikis allow a subset of the course or organization members to work on collaborative projects. Instructors specify whether and when students are allowed to view or edit a

particular wiki. Both Students and instructors can easily create content within the wiki such as study guides and shared notes. Wikis provide organizations with a powerful collaborative editing tool that can be used for any content that requires collaboration and change tracking, such as meeting minutes, by-laws, or simple pieces of content. Instructors can also use the wiki for collaborative group projects where the wiki's history and participation summary tools give the instructor greater insight when assessing individual contributions as well as throughout the collaborative process. Students can use the wiki to collaborate on content for the course as well as for group projects. The wiki's collaborative capabilities and history features help students see what others s have contributed and help avoid redundancy of effort [4], and [5].

Although the advantages of Electronic Group Collaboration tools are obvious, their implementation does not ensure a high-quality education. Wikis and blogs are prone to possible to serious quality issues, because of their free form nature and the (relative/potential) lack of control over their content. In an open and collaborative web environment, anyone can easily post copyrighted material without the permission of copyright holders, post unsuitable or misleading content, or edit existing content in a way that reduces its quality/accuracy. Students may encounter many problems commonly related to technological factors, including issues of access, connection, internet familiarity, etc. Students may also feel isolated and unmotivated [20]. Researchers argue there is a relationship between the instructional design of these tools and the perceived ease of use and perceived usefulness by students [15]. During the online collaborative learning experience, strategies that promote students' feelings of connectedness and belonging appear to be critical to successful learning [22]. Research [8] shows that student retention and satisfaction rely heavily on the ability of the online system's medium, materials, and services to make students feel socially present and connected to the instructor and other students. Online learning environments intended to support collaborative learning should be designed in a way that considers the social nature of the learning process [18]. Thus, student acceptance of these technologies is one of the critical factors that should be evaluated in order to adequately assess whether the successful implementation of these tools can support teaching-learning activities and the student experience [13].

III. METHODOLOGY

The proliferation of courses offered online and the way in which technology is used in their delivery has an effect on the quality of learning [19]. Students' acceptance of Electronic Group Collaboration Technologies is one of the critical factors that should be evaluated in order to adequately assess whether the successful implementation of these tools can support teaching-learning activities and the student experience [13].

This research conducts an exploratory study in students' acceptance of Electronic Group Collaboration Tools within the context of higher education learning software systems. This study seeks to answer the following research questions:

1. How many Electronic Group Collaborative Tools do students prefer to use in one class?
2. What Electronic Group Collaborative Tools are most preferred by students?

This study used a descriptive quantitative research design. The population of the study consisted of Online learning students from 8 different programs in 4 different universities. Data were obtained through convenience sampling of the respondents. A questionnaire was designed to capture data on the following variables: discussion boards (DB), blogs (BL), journals (JR), and wikis (WK). The questionnaire was composed of three sections. The first section consisted of personal demographic questions (i.e., age, sex, GPA, and declared major). The second section consisted of questions that examined the students' familiarity with computer technology. The third section was comprised of questions that explored students' acceptance toward Electronic Group Collaboration Tools. A total of 30 questions were developed to capture information on all variables. Each statement on the questionnaire was based on the Likert scale, and each answer was assigned weights to establish normally distributed scores. The weights of the responses from the questionnaire were assigned as follows:

1. Refers to "Strongly Agree"
2. Refers to "Agree"
3. Refers to "Neutral"
4. Refers to "Disagree"
5. Refers to "Strongly Disagree"

In total, 410 questionnaires were randomly distributed. All of the survey responses were successfully received, and only 11 were incomplete. The online surveys were conducted and collected between August 09, 2010 and August 16, 2010. In order to ensure the reliability of the test

measurement, Cronbach's alpha was computed and reported for each scale that measured the concepts being examined. The overall alpha score for the pilot data was 0.975, which indicated high reliability of the instrument.

IV. Findings

Table (1) displays students' acceptance of the number of Electronic Collaboration Group in one class.

TABLE I

APPROPRIATE NUMBER OF E-GROUP COLLABORATION TOOLS USED IN ONE COURSE

Priority	Number of Collaboration Tools in One Course	Percentage
1	1 E- Group Collaboration Tool	47%
2	2 E- Group Collaboration Tools	32%
3	3 E-Group Collaboration Tools	17%
4	More than 3E-Group Collaboration Tools	4%

The majority of students examined (47%) believed that a course should have only one E-Group Collaboration Tool. 32% of the respondents indicated that two E-Group Collaboration Tools are more appropriate per course. 17% of the respondents chose three E-Group Collaboration Tools per course, and 4% of the respondents chose more than three E-Group Collaboration Tools per course.

Table (2) displays students' acceptance of the importance of Electronic Group Collaboration Tools used in higher education software systems.

TABLE 2

PREFERRED ELECTRONIC GROUP COLLABORATION TOOL

Priority	Group Collaboration Tool	Percentage
1	Discussion Boards	72%
2	Blogs	13%
3	Wikis	9%
4	Journals	6%

The majority of students (72%) viewed Discussion Forums as the most preferred Electronic Group Collaboration Tools used in the courses they've taken. 13% of the respondents viewed Blogs were the most preferred choice. 9% of the respondents chose Wikis, and 6% of the respondents chose Journals as the most preferred E-Group Collaboration Tools.

V. Discussion

Understanding students' perceptions regarding the E-Group Collaboration Tools used in Higher Education Learning Systems is the first step in developing and implementing a successful online learning environment. It is necessary for institutions of higher education to focus on learners' satisfaction in order to continuously improve online learning programs. Such careful monitoring will ensure the success and viability of online learning programs. Group learning is a good way of encouraging learning interaction. A good e-learning system should do well in promoting the use of group learning styles [17]. If effectively deployed, discussion boards, blogs, wikis, and journals could offer a way to enhance students' learning experiences, and deepen levels of learners' engagement and collaboration within the higher education e-learning environments. The primary objective of this study was to determine the best ways to integrate E-Group Collaborative Tools into existing e-Learning systems by identifying the most preferred E-Group Collaborative Tools, and the number of tools students expect/accept to see in one class.

In reference to the first question of this study, the findings suggest that the majority of the examined students (47%) prefer to have only one E-Group Collaborative Tool per class. Almost 80% of the examined students indicated that two E-Group collaborative tools per class is the maximum number they prefer to see in one class. Many students indicated that the majority of class activities in e-learning environments are individual-related activities, and that the number of group-related activities that require the use of group collaboration is usually 1-2 per class. The majority of students also indicated that they prefer to use the same type of technology in one class, and that the use of more than one technology could add more work load if students are not familiar with the use of that technology. Twenty one (21%) of the examined students indicated that they prefer the use of 3 or more E-Group Collaboration Tools per class. Most of these students indicated that they were more technology-oriented and that the availability of 3 or more tools would diversify the technology used and expose them to a variety of learning methods. Juniors were more open to trying new technologies than seniors. Given how recently blogs, wikis, and journals have been added to higher education E-Learning systems, the preference of most seniors is understandable, as they were exposed to only one tool (Discussion Boards) in the past few years. Many of the students that did not choose several E-Group Collaboration Tool

expressed concern over their level of computer competency, and factors including issues of access, connection, internet familiarity, that could affect their use of more technologies, which is also supported by the findings of [1].

The second question of this study is concerned with the most preferred E-Group Collaboration Tool by students. The overwhelming majority of examined students (72%) chose discussion boards. The remaining 28% were divided among blogs (13%), wikis (9%), and journals (6%). Students' answers clearly indicated that the majority of students did not understand the key features of these tools, or the main differences among these tools with the exception of discussion boards. Most examined students indicated that they did not see a need for an additional tool since discussion boards offered many of the functions required for their group assignment work. Discussion boards can be assigned at the class level or at the group level. They can be classified by topic or by time. Students are able to post entries viewable by all class members, or specific group. They are able to attach text and media files if needed, and most importantly most students are familiar with them. Most students also indicated that Discussion Boards are usually used either for discussion activities, or as a group area to discuss work related to class project. The remaining 28% of examined students indicated that discussion boards should not be used in place of blogs, wikis, and journals, and that the nature of the group assignment should be the catalyst in deciding the type of E-Group Collaborative Tool used.

VI. CONCLUSION

The number and quality of Electronic Group Collaboration tools in higher education learning systems have been on the rise. Similar to email, discussion boards, blogs, wikis, and journals will increasingly be among the key modes of interaction that students can be expected to use in their university education learning processes [1], [4], and [22]. Understanding students' perceptions regarding these tools is the first step in developing and implementing a successful online learning environment.

The findings of this study suggest that the majority of online students in higher education prefer only one E-Group Collaboration Tool per class. Two types of E-Group Collaboration Tools is the maximum number expected by the great majority of students. Many students preferred consistency on the type of E-Group Collaboration tools being used, and did not want to spend additional time learning how to use the tool. Many of the examined students preferred the use of discussion boards over blogs, wikis, and journals, mainly because many of them have been using discussion boards for years, or because they did not see the additional benefits involved in using blogs, wikis, and journals over discussion boards.

The findings also suggest that in order to enhance the learning experience of online students, higher education institutions need to address the issues of computer competency, and technological factors including issues of access, connection, and internet familiarity, as they have direct impact on students' acceptance of the utilized E-Group Collaboration Tools. Universities should dedicate areas within each online course, and within the orientation process of both students and instructors to educate them about the available E-Group Collaboration Tools, and how to use them. Universities should also make available training and help materials to explain the features and the associated benefits of using such tools. More importantly, instructors and course administrators should be educated, not only on the technical aspects of these tools, but also on the proper use of these tools. Instructors and course administrators should be able to judge what E-Group Collaboration tool would best serve a specific group exercise, and how to decide on the number and the type of E-Group Collaborative Tools to be used in class.

Research into the use Electronic Group Collaboration Learning Tools in higher education is still in its infancy. We would therefore like to invite educators/researchers to examine the use of these tools in a formal way and report back their results to the higher education community, so that we may start building a proper evidence base about best practices and uses in higher education Electronic learning.

REFERENCES

[1] S. Al-Fadhli, "Factors Influencing the Acceptance of Distance Learning: A Case Study of Arab Open University in Kuwait", *Online Journal of Distance Learning Education*. Vol 13-3, 2010.

[2] D. Becker, and M. Dwyer, "The impact of student verbal/visual learning style preference on implementing groupware in the classroom". *Journal of Asynchronous Learning Networks* , 2(2), 61-69. 1998

[3] G. Black, "Student assessment of virtual teams in an online management course". *Journal of Business Administration Online* , 1(2). 2002

[4] Blackboard Manual, “Blackboard Learn Manual V9.1. 2010

[5] M. Boulos, I. Marambe, and S. Wheeler, “Wikis, blogs and podcasts: a new generation of Web-based tools for virtual collaborative clinical practice and education”. *BMC Medical Education Vol, 6:41*, 2006

[6] R.E. Clark, “Media will never influence learning’. *Education Technology Research and Development* , 37(1):57-66. 1994

[7] L. Cuban, “Oversold and underused: computers in the classroom Cambridge’, *MA: Harvard University Press*; 2003.

[8] C. Gunawardena, and M. clsaac, “Distance education. In D. Jonassen (Ed.), *Handbook of research for educational communications and technology (2nd ed.) (pp. 355–395). Bloomington, IN: Association for Educational Communications & Technology*. 2004

[9] P. Hackley and J. Webster “Teaching Effectiveness in Technology-Mediated Distance Learning”. *Academy of Management Journal, 40 (6), 1282 - 1309*. 1997

[10] S.R Hiltz, N. Coppola, N. Rotter, and M. Turoff, “Measuring the importance of collaborative learning for the effectiveness of ALN: A multi-measure, multi-method approach”. *Journal of A synchronous Learning Networks* , 4(2), 103-125. 1999

[11] P. Jermann, A. Soller, and M. Muehlenbrock, “From Mirroring to Guiding: A Review of State of the Art Technology for Supporting Collaborative Learning”, *International Journal of Artificial Intelligence in Education archive Volume 15 Issue 4, December* 2005.

[12] D. Laurillard, “Rethinking University Teaching”, *London: Routledge Falmer*; 2002.

[13] L. Martins, and F. Kellermans, “A Model of Business School Student’s Acceptance of a Web- Based Course Management System”. *Academy of Management Learning and Education, 3(1), 7-28*. 2004

[14] P. Meier and B. Simon. “Reengineering Undergraduate Teaching by Introducing Internet-based Learning Information Systems”. Springer, Vienna. 2000

[15] L. Muilenburg, and Z. Berge, “Student barriers to online learning: A factor analytic study”. *Distance Education, 26(1), 29-48.*2005

[16] J. Myers, “Cooperative learning in heterogeneous classes”. *Cooperative Learning, 11(4).* 1991

[17] D. R. Newman, B. Webb, and C. Cochrane, “A content analysis method to measure critical thinking in face-to-face and computer supported group learning”, *Queens University Belfast, Information Management Dept.*2008

[18] J. Richardson, and K. Swan, “Examining Social Presence in Online Courses in Relation to Students’ Perceived Learning and Satisfaction”. *Journal of Asynchronous Learning Networks, 7(1), 68-88.* 2003

[19] AP. Rovai, and KT. Barnum, “On-Line Course Effectiveness: An Analysis of Student Interactions and Perceptions of Learning”. *Journal of Distance Education, 18(1), 57-73.*2003

[20] R. Saade, and B. Bahli, “The Impact of Cognitive Absorption on Perceived Usefulness and Perceived Ease of Use in On-line Learning: an Extension of the Technology Acceptance Model”. *Information and Management, 42, 317-327.*2005

[21] B. Simon, P. Haghirian, and P. Schlegelmilch, “Case Study Teaching via Collaborative Inormation Technology”. *Proceedings of ECIS (European Conference on Information Systems.)* Gdansk, Poland, 2002

[22] H. So, and B. Kim, “Instructional methods for computer supported collaborative learning (CSCL): A review of case studies”. *Paper presented at the 10th CSCL Conference, Taipei, Taiwan*. 2005

2011 International Conference on Mechanical, Industrial, and Manufacturing Engineering
Lecture Notes in Information Technology Vols. 1-2

Stock Decision Method based on Storage Capacity Limited

Li Qu
Beijing Information Science and Technology University
Beijing, China
Email: qulisohu@sohu.com

Ying Shi
Beijing Information Science and Technology University
Beijing, China
Email: shiyingshuijing@sina.com

Abstract: This paper analyses three inventory control programs of limited storage capacity to be selected: to store goods according to the stock capacity, to rent warehouse to store the goods and to invest to extend a warehouse. Then this paper analyzes to determine the most economical order quantity, ordering cycle and the daily average ordering cost of the various options, making the optimal inventory decision by comparing the daily average cost, and an example is analyzed.

Index Terms: Ordering cycle; Ordering quantity; Inventory

Note: Funding by discipline and Graduate Education - key disciplines - management science and engineering（PXM2010_014224_096205）and key project of Beijing Municipal Education Commission (SZ201010772022).

1. INTRODOUCTION

The researchs of decision-making of inventory related to limited storage space are mainly three aspects about these problems:

(1) Whether stock-out is allowable. Here are researches under this assumption: Such as Dequan Liu (2002) studied a model of allowed goods shortage storage due to limited-space storehouse, Chenyou Lu and Qiulan Luo (2004) studied the storage model under the condition of limited-space storehousel, Feng Sha and Yimin Yang (2006) studied the two type storage models about limited-space storehouse, zhenggeng Qu (2006) studied the optimal inventory model based on shortage characteristic, Weiqi Zhou, Nianwen Xue and Zhongxing Li (2007) studied order and selling inventory model with shortage not allowed under the condition of limited-space warehouse and lot-size discount, Lina Huo (2010) studied the random storage model with allowing goods shortage under the condition of limited-space storehouse.

(2) Inventory decision of stochastic demand. Such as Hongjian Wang and Guoxing Fang (2005) studied the random storage model under the condition of limited-space storehouse. Zhenfei Zhang and Peng Zhao (2006) studied decision model analysis of random storage management under the condition of limited warehouse capacity, Xin Xie, Yufeng Wei, and Damin Liu (2008) studied application of the random storage model to the case of a limited-space storehouse, Zonghong Cao and Yongwu Zhou (2008) studied supply chain coordination model with limited warehouse and inventory-dependent demand.

(3) Inventory decision for Multi-merchandise. Such as AMIYA (1981,1986) studied sequential and multi-merchandise inventory decision of limited storage space and with price discounts. The book "Inventory Control and Management" written by Donald (2003) proposed intuitive algorithm of inventory decision for multi-merchandise under the condition of limited-space storehouse and inventory decisions under the condition of limited inventory investment. Such as Dan Shao, Yeming Zhou, Haitao Hu and Xiaoyong Liu studied (2007) studied stochastic storage policy for multi-merchandise under the condition of limited-space storehouse, Yunguo Lin (2007) studied random inventory model of perishable items in a limited storage capacity.

In fact, when the enterprise making the stock decision of limited storage capacity, it should choose the optimal option by comparing the economy of different options. Discussion of the current literature is limited to a situation of order quantity and the order cycle, lack of comparison of different options. So this paper discusses the stock decision of limited storage

capacity under deterministic demand, by comparing the economy of different options choose the optimal option.

2. Problem Description

In order to simplify the study, the demand and ordering lead time are certain. Typically, companies use EOQ model to determine the most economical order quantity to replenish storage. There are three options when economic order quantity exceed storage space: (1) order by storage capacity, allowing the stockout; (2) when the demand exceeds inventory storage capacity, considering the rental of warehouses; (3) expansion of the warehouse. Then calculate the daily average cost of three options and select the minimum cost option as optimal decision.

To calculate the economic order quantity and average cost under the various options, this paper makes the following assumptions:

(1) Demand on the inventory system is a constant rate r;

(2) Known lead time, and is constant LT, order the quantity of Q every T;

(3) No price discounts at procurement and transport;

(4) Order cost is R and unrelated to the order quantity.

3. The average daily cost under the allowable stock-out circumstances

Allowing the out of stock under the above assumptions, and let Clost be unit shortage loss of unit time. Let M be storage capacity, To be order cycle time. When the damand rTo>M, the order quantity will be M according to the storage and it can only meet the damands of T time segment, that is tr=M, and shortage loss is $\frac{1}{2}$ Clost（To-t）（rTo-M）, the total cost of every order cycle is

$$R+H_l\int_0^{\frac{M}{r}}(M-rt)dt+\frac{1}{2}C_{lost}(\mathrm{T_o}r-M)(T_o-t)=R+\frac{H_lM^2}{2r}+\frac{1}{2}C_{lost}(\mathrm{T_o}r-M)(T_o-t)$$

The average daily cost is

$$C_{day}(T_o)=\frac{R}{T_o}+\frac{H_lM^2}{2rT_o}+\frac{C_{lost}(\mathrm{T_o}r-M)(T_o-t)}{2T_o}$$
$$=\frac{R}{T_o}+\frac{H_lM^2}{2rT_o}+\frac{C_{lost}(\mathrm{T_o}r-M)(T_o-\frac{M}{r})}{2T_o}$$

Formula 1

Applying the method of doing the first-order derivation $\frac{dC_{day}(T_o)}{dT_o}=0$ over the formula 1, let , and get

$$T_o^*=\sqrt{\frac{2rR+H_lM^2+C_{lost}M^2}{2r^2C_{lost}}}$$

Formula 2

T_o^* is the most economical order cycle according to the circumstance of the first option. And at last, the minimum average daily cost can be obtained by substitution of the T_o^* into formula 1.

4. The average daily cost and order quantity under the rental of warehouses circumstance

At this point, stock-out is not allowable. By rental of warehouses we can solve the problem of storage capacity shortage. Then calculate the most economical order quantity and order cycle. On the basis of the assumptions in part 2, let Ht be storage fee of unit items per unit time by using their own warehouse and let Hl be storage fee of unit items per unit time by using leased warehouse, in general H1> Ht. Therefore, the first consumption of inventory will be the rented warehouse inventory, maintaining inventory cost is linear function of stock.

Let CL be the unit costs for warehouse, M be the storage capacity and （Ql-M） be the storage quantity of the rented warehouse. To make them general, let rt be consumption quantity and r be random variable. This model can solve similar stochastic inventory problems.

The storage cost of a rented warehouse for an order cycle is

$$H_l\int_0^{\frac{(Q_l-M)}{r}}(Q_l-M-rt)dt=\frac{H_l}{2r}(Q_l-M)^2$$

M is the storage quantity of own warehouse and storage does not change during time （Ql-M） /r before every ordering cycle. This makes the storage cost of own warehouse for an order cycle is

$$H_t M\frac{Q_l-M}{r}+H_t\int_{\frac{(Q_l-M)}{r}}^{\frac{Q_l}{r}}(M-r(t-\frac{Q_l-M}{r})dt=\frac{H_t M}{2r}(2Q_l-M)$$

Considering ordering cost R, the total cost of every order cycle under this circumstance is

$$R+\frac{H_t M}{2r}(2Q_l-M)+\frac{H_l}{2r}(Q_l-M)^2$$

The average daily cost is

$$C_{day}(T_l)=\frac{R}{T_l}+\frac{M^2}{2rT_l}(H_l-H_t)-(H_l-H_t)M+\frac{H_l r T_l}{2}$$ Formula 3

Applying the method of doing the first-order derivation $\frac{dC_{day}(T_l)}{dT_l}=0$ over the formula 3, let , and get

$$T_l^*=\sqrt{\frac{2R}{rH_l}+(1-\frac{H_t}{H_l})\frac{M^2}{r^2}}$$ Formula 4

$$Q_l^*=\sqrt{\frac{2Rr}{H_l}+(1-\frac{H_t}{H_l})M^2}$$ Formula 5

T_l^* is the optimum economical order cycle according to the circumstance of the second option, Q_l^* is the optimum economical order quantity. And at last, the minimum average daily cost can be obtained by substitution of the T_l^* into formula 3.

5.THE AVERAGE DAILY COST AND ORDER QUANTITY UNDER THE EXPANSION OF WAREHOUSES CIRCUMSTANCE

At this point, stock-out is also not allowable and we choose expanding warehouse to solve the storage capacity insufficient problem. Similarly , on the basis of the assumptions in part 2, let TI=QI/r be ordering cycle, CI be the unit cost of investment to expand the warehouse. The investment cost of building warehouses is CI（QI－M）by taking no account of time value of capital. The total storage cost of an order cycle is

$$R+H_t\int_0^{\frac{Q_l}{r}}(Q_l-rt)dt+C_l(Q_l-M)=R+\frac{H_t Q_l^{\ 2}}{2r}+C_l(Q_l-M)$$

The average daily cost is

$$C_{day}(T_l)=\frac{R}{T_l}+\frac{H_t r T_l}{2}+C_l r-\frac{C_l M}{T_l}$$ Formula 6

Applying the method of doing the first-order derivation $\frac{dC_{day}(T_l)}{dT_l}=0$ over the formula 6, let , and get

$$T_l^*=\sqrt{\frac{2(R-C_l M)}{rH_t}}$$ Formula 7

$$Q_l^*=\sqrt{\frac{2r(R-C_l M)}{H_t}}$$ Formula 8

T_l^* is the most economical order cycle according to the circumstance of the third option, Q_l^* is the most economical order quantity. And at last, the minimum average daily cost can be obtained by substitution of the T_l^* into formula 6.

6. EXAMPLES OF APPLICATION

An enterprise for a certain material warehouse capacity M is 400 pieces, rate of day demand r is 100 pieces, ordering cost R is 3500 yuan per time, the fee of using own warehouse Ht is 2.8yuan per unit per time, the fee of renting warehouse Hl is 3yuan per unit per time, the unit costs of expanding warehouse CI is 2 yuan, the unit shortage loss in unit time Clost is 4 yuan. The enterprise have three choices: (1) ordering according to the storage capacity (400 pieces); (2) unallowed stock-out, can rent warehouse; (3) unallowed stock-out, can expand warehouse. We need to analyze the economical efficiency of three kinds of options, select the lowes expenses of the option.

Option 1: ordering according to the storage capacity. Using the formula 1 and 2 ,get daily average expenses and the most economical ordering cycle in this option:

$$C_{day}(T_o) = 1242(yuan)$$
$$T_o^* = 4.7(days)$$
$$Q = M = 400(pieces)$$

Option 2: renting warehouse. According to the fomula3、4 and 5 ， get the average daily expenses, the most economical order quantity and cycle in this option:

$$C_{day}(T_l) = 1377(yuan)$$
$$Q_l^* = 494(pieces)$$
$$T_l^* = 4.9(days)$$

Option 3:expanding warehouse. According to the fomula6、7 and 8， get the average daily expense, order quantity and cycle in this option:

$$C_{day}(T_l) = 1430(yuan)$$
$$Q_l^* = 439(pieces)$$
$$T_l^* = 4.4(days)$$

The lowest average daily expense is the best, so choose ordering as the storage capacity ,ordering quantity be 400 pieces, ordering cycle be 4.7 days.

7. CONCLUSION

Through the above analysis, when the enterprise making the actual decision of storage, it should not only consider the optimum order quantity and ordering cycle in one specific order scheme, but also should analyze the existing proposed schemes for economical comparison to determine the most economical storage solution.

This paper studies the certain demand and ordering cycle schemes comparison, in fact, to demand and ordering cycle under uncertainty, can use the same ideas to solve. Also, in this paper, There is no consideration of the time value of fund, during the practice, short-term projects don't need to consider, or need to consider the time value of fund.

REFERENCES

[1] [1] Dequan Liu. A model of allowed goods shortage storage due to limited-space storehouse[J]. Journal of Air Force Radar Academy, 2002, 16(1):22-23

[2] [2] Chenyou Lu and Qiulan Luo. The storage model under the condition of limited-space storehousel[J]. Mathematics In Practice and Theory, 2004, 34(6):1-5

[3] [3] Feng Sha and Yimin Yang. The two type storage models about limited-space storehouse[J]. Mathematics In Practice And Theory, 2006, 36(4):67-71

[4] [4] Weiqi Zhou, Nianwen Xue and Zhongxing Li. Order and selling inventory model with shortage not allowed under the condition of limited-space warehouse and lot-size discount[J]. Logistics Sci- Tech, 2007, 3:107-111

[5] [5] Lina Huo. The random storage model with allowing goods shortage under the condition of limited-space storehouse[J]. Journal of Chifeng University（Natural Science Edition）, 2010, 26(3):8-10

[6] [6] Hongjian Wang and Guoxing Fang. The random storage model under the condition of limited-space storehouse[J]. Journal of Fuzhou University(Natural Sciences Edtion), 2005, 33(06):711-715

[7] [7] Zhenfei Zhang and Peng Zhao. Decision model analysis of random storage management under the condition of limited warehouse capacity[J]. Journal of Beijing Jiaotong University(Social Sciences Edition), 2006,5(1):32-37

[8] [8] Xin Xie, Yufeng Wei, and Damin Liu. Application of the random storage model to the case of a limited-space storehouse[J]. Journal Of Beijing University Of Chemical Technology, 2008,35(1):104-108

[9] [9] Zonghong Cao and Yongwu Zhou. Supply chain coordination model with limited warehouse and inventory-dependent deman[J]. Chinese Journal of Management Science, 2008, 16(1):66-73

[10] [10] Donald Waters. Inventory Control and Management. John Wiley&Sons, 2ed 2003

[11] [11] Dan Shao, Yeming Zhou, Haitao Hu and Xiaoyong Liu. stochastic storage policy for multi-merchandise under the condition of limited-space storehouse[J]. Science Technology and Engineering, 2007,7(9):2003-2008

[12] [12] Yunguo Lin. Random inventory model of perishable items in a limited storage capacity[J]. Journal Of Fuqing Branch Of Fujian Normal University, 2007, 79(2):6-11

2011 International Conference on Mechanical, Industrial, and Manufacturing Engineering
Lecture Notes in Information Technology Vols. 1-2

Effects of the mass fraction of graphite flake on the microstructure and properties of SiC-B_4C-TiB_2 composites*

Liang Yu, Yanli Jiang, and Kun Luo
Key laboratory of new processing technology for nonferrous metals & Materials, Ministry of Education
College of Materials Science and Engineering Guilin University of Technology
Guilin City Guangxi Zhuang Autonomous Region ,541004, China
syyuliang@163.com jiangyanli024@163.com
luokun@glite.edu.cn

Hongqiang Ru, Jidong Cai
Key Laboratory for Anisotropy and Texture of Materials (Ministry of Education),
Northeastern University,
Shenyang City Liaoning Province, 110004 China
ruhq@smm.neu.edu.cn caijidong024@163.com

***Abstract* - SiC-B_4C-TiB_2-G composites were prepared with graphite flake, SiC, B_4C and TiO_2 powders by in situ synthesis and hot-pressed at 2000 ℃, and effect of graphite flakes mass fraction on the microstructure, mechanical properties of the composites were investigated. It was shown that the fracture toughness was improved due to the introduction of graphite flake, whereas the flexure strength and hardness decreased. The density and flexure strength decreased, however, fracture toughness increases with graphite flake mass fraction increasing. The density, flexure strength and fracture toughness of the composite was 2.81 g/cm^3, 276±4 MPa, 5.5±0.4 MPa·m$^{1/2}$, respectively, with the graphite flake of mass fraction 20 wt.%. However, The density, flexure strength and fracture toughness of the composite was 2.81 g/cm^3, 276±4 MPa, 5.5±0.4 MPa·m$^{1/2}$, respectively, with the graphite flake of mass fraction 65 wt.%. The toughening mechanisms are crack deflection and branching as well as stress relaxation near the crack tip. Although graphite flake can reduce flexural strength compared to SiC-B_4C based ceramics, but newly created TiB_2 particles, which were initially very fine and active, both provide additional driving force for sintering and increases flexural strength of the composite for TiB_2 particle of smaller sizes led to improved densification. The results here pointed to a potential method for improving fracture toughness of SiC-B_4C based ceramics.**

Keywords: SiC-B_4C-TiB_2-G; graphite flake; microstructure; mechanical property;

Index Terms

I. INTRODUCTION

SiC possesses unique combination of thermo-mechanical properties which makes it one of the most suitable structural ceramics for both high- and low- temperature applications [1]. However, wider application of SiC as structural material is limited by relatively low fracture toughness and service reliability [2, 3]. One of the methods of improving fracture toughness of SiC is the reinforcement with particles having different elastic and thermal properties such as B_4C [4], ZrB_2 [5] and TiB_2 [6].

Furthermore, it is well known that lamellar domain type of microstructure contribute to the fracture toughness of materials. Recent studies have demonstrated that the inclusion of lamellar graphitic phases as inter layers in carbon, metal matrix or ceramic matrix can drastically increase the damage tolerance of the material, imparting a large increase to the fracture toughness of the carbon or metal body [7]. The graphite flake is an attractive material for high temperature applications due to its high strength, high modulus, layered structure that allows for self-lubrication, excellent thermal shock resistance, and high fracture toughness [8]. X. H. Zhang et al, fabricated graphite flake-ZrB_2-SiC by hot pressing, and found the fracture toughness was improved due to the introduction of graphite flake [9]. A. R. Mirhabibi et al showed that the apparent work of fracture could be increased by a factor of more than 5 times with 10-15 vol.% graphite flakes of various dimensions [10]. Y. F. Sun et al, found the mechanisms for improving the toughness is to incorporate weak interfaces into the material which act to deflect propagating cracks and promote crack bridging [11]. Nevertheless, up to date, there are only a few papers devoted to the study on SiC matrix composites toughened by the graphite flake.In this paper, we have prepared SiC-B_4C-TiB_2 composite toughened by the mass fraction 20 wt. %~65 wt. % graphite flake (SiC-B_4C-TiB_2-G) by hot pressing. The TiB_2 particles were created by the internal synthesis involving TiO_2, B_4C and graphite as raw materials [12, 13]. Newly created TiB_2 particles, which are initially very fine and active, both provide additional driving force for sintering and increases fracture toughness of the SiC-B_4C-TiB_2-G

* This work was supported by the Natural Science Foundation of Liaoning, China #20072026; Supported by the Basic Research Fund for the Northeastern University #N090302005; Supported by the China Postdoctoral Science Foundation #20090451271; Supported by the National Natural Science Foundation of China #50872018, and the Program for Chang Jiang Scholars and Innovative Research Team in University #IRT0713.

composite. As well as, the effect of graphite flake on the microstructure and mechanical properties was analysed.

II. EXPERIMENTAL

The raw materials used are graphite flake (ρ=2.20 g/cm^3, purity > 95%, mean diameter d_{50} = 5~10 μm , thickness 1.0~1.5 μm, Huasheng graphite factory, Jixi city, Heilongjiang province, China), α-SiC (ρ=3.20 g/cm^3, purity > 98%, mean diameter d_{50} = 1.5~2.1 μm, Tangshan Hexagon Co., Ltd , Tangshan city, Hebei province, China), B_4C (ρ=2.50 g/cm^3, purity > 95%, mean diameter d_{50} = 1.3 μm, Juxin Superhard Materilal Co., Ltd, Dalian city , Liaoning province, China.) and TiO_2 (ρ=3.90 g/cm^3, purity > 99.99%, mean diameter d_{50} = 0.1~0.3 μm, Baotou rare earth institute, Baotou city, Inner Mongolian Autonomous Region, China) powders. The compositions of raw materials of SiC-B_4C-TiB_2-G composites (mass fraction %) was listed in Table I, phenol formaldehyde resin was used as the binding agent.

TABLE I COMPOSITIONS OF RAW MATERIALS OF SiC-B_4C-TiB_2-G COMPOSITES (MASS FRACTION %)

Sample	*w*(graphite flake)/%	*w*(SiC) /%	*w*(B_4C) /%	*w*(TiO_2) /%
SBTG20	20	61.7	12.3	6
SBTG35	35	49.2	9.8	6
SBTG50	50	36.7	7.3	6
SBTG65	65	24.2	4.8	6

The composites were prepared as described as follow. Firstly, the powder mixtures were ball-mixed for 24 h in a plastic container using high purity Al_2O_3 balls and ethanol as a mixing media. After mixing, the obtained slurry was dried and screened. The resulting powder mixtures were compacted under a uniaxial load of 15 MPa in a graphite mould. The SiC-B_4C-TiB_2-G composites were in situ synthesized using hot pressing, first heated at 1450 ℃ for 3.6 ks and then at 2000 ℃ for 2.7 ks under a uniaxial load of 30 MPa in a vacuum of 30 Pa, using the impulsion hot pressing furnace (Jinxing Co., Ltd , Jinzhou city Liaoning province, China). The heating rate was 5 ℃/min. The relative density of the composite was investigated using the Archimedes' method. The phases of the composite were identified by X-ray diffraction using Cu Kα radiation (λ=0.154178 nm). (XRD, X'Pert Pro MRD, Panalytical B.V., Holland). The microstructures were observed by optical microscope (GX71, Olympus Optical Co. Ltd., Japan), scanning electron microscope (SEM, SSX-550, Shimadzu Corporation, Japan). The phase compositions were identified by energy dispersive spectroscopy (EDS) analysis. The flexural strength and the fracture toughness were evaluated using hydraulic universal testing machine (WE-10A, Mts Systems (China) Co. Ltd., China), respectively. The flexural strength was measured by three point bending tests (specimen size = 40 mm × 4 mm × 3 mm, bend span = 20 mm, load speed = 0.05 mm/min). The fracture toughness was measured by single edge notched beam method (specimen size=30 mm × 5 mm × 5 mm, notch width = 0.2 mm, notch depth = 3 mm, bend span = 20 mm, load speed = 0.05 mm/min). All flexural and fracture bars were cut with the tensile surface perpendicular to the hot pressing direction. A minimum number of six specimens were tested for each experimental condition

III. RESULTS AND DISCUSSION

A. *Phase analysis*

The X-ray diffraction patterns (XRD) obtained from the polished surface of the hot pressed SiC-B_4C-TiB_2-G composites with 20 wt. %~50 wt. % graphite flake sintered at 2000 ℃ for 2.7 ks were shown in Fig.1. Apparently, the phase analysis indicated the predominant phases for the as-sintered composite were graphite, B_4C, SiC. It was shown that there is no TiO_2 in SiC-B_4C-TiB_2-G composites, which indicates that the formation of TiB_2 process was basically complete. We can see that the TiB_2 phase was present at 2000 °C, the formation of TiB_2 was attributed to the reaction of graphite, B_4C with TiO_2. The internal synthesis of TiB_2 was based on the following reaction (1) which takes place at temperature lower than the sintering temperature [14].

XRD patterns of SiC-B_4C-TiB_2-G composites with 20 wt. %~50 wt. % graphite flake showed no significant change. The peak intensities of graphite flake increase as he content of graphite flake increasing.

$$B_4C+2TiO_2+3C=2TiB_2+4CO\uparrow \quad (1)$$

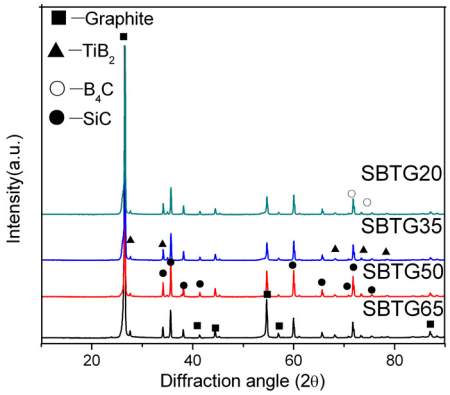

Fig. 1 XRD pattern of the hot pressed SiC-B_4C-TiB_2-G composites with mass fraction 20 wt. %~65 wt. % graphite flake sintered at 2000 ℃ for 2.7 ks

B. *Microstructure*

The SEM polished cross-sectional imagines of the hot pressed SiC-B_4C-TiB_2-G composites with different mass fraction of graphite flake were shown in Fig.2. It was found that the microstructure of SiC-B_4C-TiB_2-G composite was characterized by grey TiB_2, dark SiC and B_4C, as well as the long and narrow dark graphite flake, with the EDS analysis [15]. However, it was difficult to distinguish the difference between B_4C and SiC. Furthermore, the hot pressed SiC-B_4C-TiB_2-G composites had shown a preferred orientation of the

lamellar microstructure graphite flake, with its basal planes perpendicular to the hot pressing direction [7]. The mass fraction of graphite flake had effected on the densification of the composites obviously. The density decreased with the content of graphite flake increasing, and the highest density was obtained with the graphite flake 20wt. %, as shown in Fig.2a. We can see main lamellar graphite flake inlays in the SiC, B_4C and TiB_2 ceramic phase mixture. The composite had low residual porosity, and the interface of graphite and ceramic tightly combined, which can improve the mechanical properties of composites notably. The SiC particles located the lamellar graphite flake was decomposed to Si atoms and C atoms under the hot pressing condition, and the decomposed production Si and C atoms should diffuse to the outside of lamellar graphite flake and generated SiC particles located at the graphite and ceramic interface again, as shown in Fig.2a. The relative density of the composite SBTG35 was still considerably high in Fig.2b, however, the slots on the polished surface of the composite SBTG35 were the graphite, which revealed that obviously pull-out of graphite occurred during the polishing process, indicating the weaker bonding within composite due to the presence of soft graphite. We can see that the densification of SBTG50 and SBTG65 decreased, it indicates that the graphite flake has not good sinterability. As shown in Fig.2a, Fig.2b, Fig.2c and Fig2d, the thickness of lamellar graphite flake increased with the increasing of mass fraction of graphite flake. The thickness of lamellar graphite flake of SBTG20 was 3~5μm, SBTG35 was 5 μm, SBTG50 was 10 μm, SBTG65 increased to 15~20 μm, respectively.

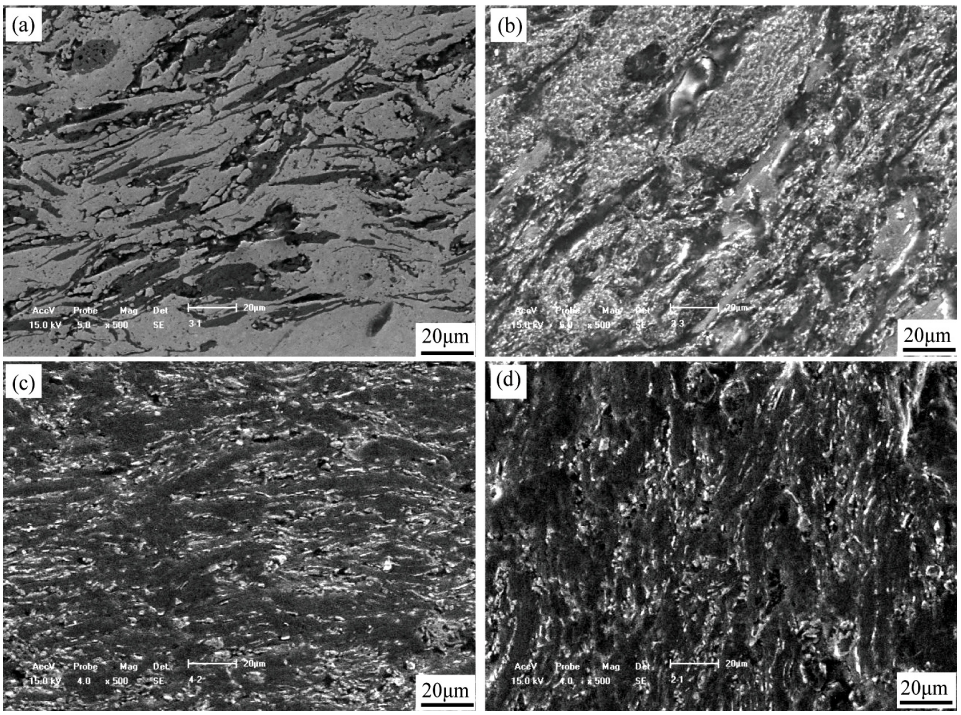

Fig. 2 The SEM imagines of polished surface of the hot pressed SiC-B_4C-TiB_2-G composites with mass fraction 20 wt. %~65 wt. % of graphite flake (A)SBTG20 ,(B) SBTG35, (C) SBTG50, (D)SBTG65.

The fractured surface imagines of composites with different mass fraction of graphite flake were showed in Fig.3. It was found that the feature of composites was trans-crystalline fracture and inter-crystalline cracking. As shown in Fig.3a and Fig.3b, the deflection and branching of crack were observed near the interface of the graphite flake and ceramic phases. In addition, the crack propagation through the graphite flake was clearly observed for SBTG20 and SBTG35. These were presumably attributed to both of the weaker bonding between graphite and other ceramic phases and the weaker lamination of graphite [9]. It was believed that such interaction absorbs the energy of crack propagation during fracture and leads to the improved toughness [15]. The main reason of the improved toughness is that the crack deflection and branching as well as stress relaxation near the crack tip. The black traces in Fig.3c and Fig.3d were the flaws of graphite flakes after being pulled out of the composite, and the pulled out graphite flakes were found as well. It was believed that the second reason of the improved toughness is the factor of the work of pulling out of graphite flake increased with the increasing of mass fraction of graphite flake. A. V. Polotai et al demonstrated the formation of submicron scale B_4C-TiB_2 eutectic surface layers via laser processing of ceramic powders [13]. Their research showed that the B_4C-TiB_2 system (75mol% B_4C) which displays a lamellar-type eutectic microstructure is a candidate for armor and tribological coatings where low density and high hardness are stringent requirements [9, 16].

Our research showed that the mass fraction of graphite flakes effect on the significantly increase the work of fracture of the composite. The graphite flake incorporated weak interfaces of graphite and ceramic into the composites which act to deflect propagating cracks and promote crack bridging, which can increase the toughness of brittle ceramic materials as results listed in Table II. Thus, the incorporation of flakes should modify the fracture behaviours by incorporating cracks into the structure.

The SiC-B_4C-TiB_2-G composites with the lamellar-type microstructure should be a new candidate for armor and tribological material.

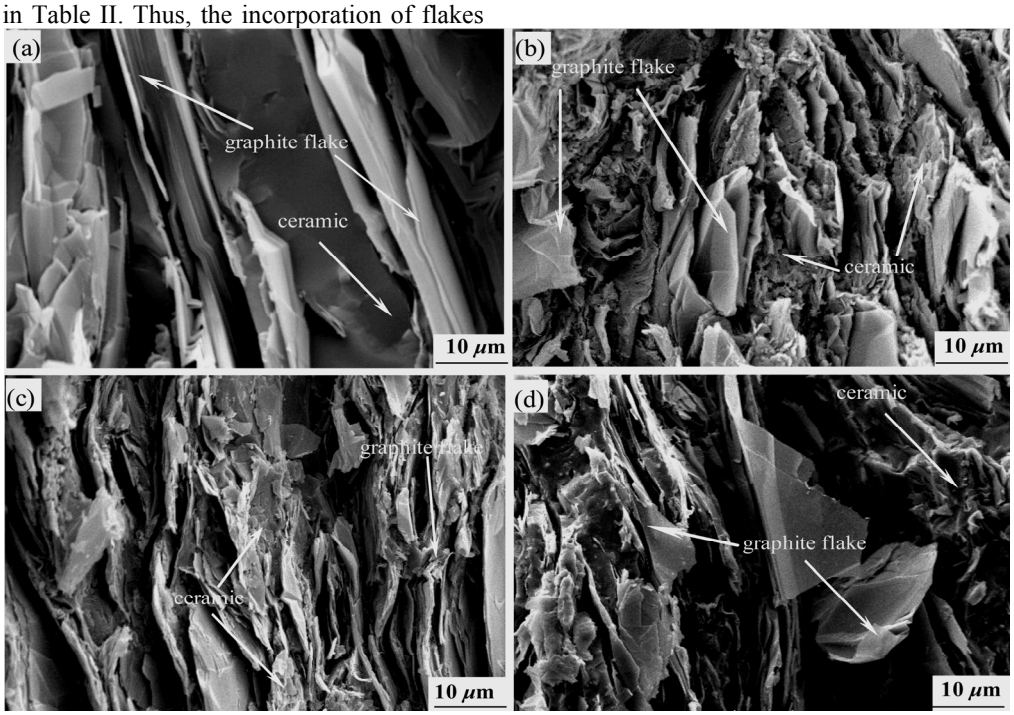

Fig.3 The fractured surfaces imagine of composites with mass fraction 20 wt. %~65 wt. % of graphite flake
(A) SBTG20; (B) SBTG35; (C) SBTG50; (D) SBTG65

C. Mechanical properties

The properties (apparent porosity, bulk density, flexural strength σ_b fracture toughness K_{IC},) of SiC-B_4C-TiB_2-G composites with mass fraction 20 wt. %~65 wt. % of graphite flake were shown in table 2. It was shown that the density and flexure strength decrease with increasing graphite flake content, however, the fracture toughness increased with increasing graphite flake content. The density, apparent porosity, flexure strength and fracture toughness of the composite was 2.81 g/cm^3, 2.4 %, 276±4 MPa, 5.5±0.4 MPa·m$^{1/2}$, respectively, with graphite flake content 20 wt. % at 2000 ℃. When the mass fraction of graphite flake was approached 65 wt. %, the flexural strength decreased to 118±3 MPa, however, fracture toughness rapidly increased to 8.1±0.5 MPa·m$^{1/2}$, respectively. The reason of density decrease while apparent porosity increased with the increasing of mass fraction of graphite flake was that the graphite flake eliminates follow the grain boundary of graphite flake and ceramic phase in the sintering process. Although it was well known that density (porosity) strongly affects strength, it was reasonable to assume that in compositions in which the length of graphite flake size was much larger than the pore size, the effect of graphite flake length on strength was more pronounced than the effects of porosity, As Fig. 3c and Fig. 3d showed. Although the introduction of graphite flake can increase fracture toughness, it can reduce flexural strength compared to TiB_2-SiC. The highest strength of 485 MPa was measured in samples containing 12vol% TiB_2 reported by D. Bucevac et al [2, 3]. Accordingly, the reduction in flexural strength could be attributed to the weaker bonding within SiC-B_4C-TiB_2-G composite and lower load transfer due to the lower strength of the graphite flake as well as the flake acting as flaw in composite. Furthermore, the strength of SiC-B_4C-based ceramics is reported to be strongly dependent upon grain size [13, 17]. Therefore, the character and size of graphite flake (especially in the diameter direction, 10~20 μm) in our work limited the flexural strength, comparing to SiC-B_4C composites. In our work, the TiB_2 particles were created by the internal synthesis involving TiO_2, B_4C and graphite flake as raw materials, and the presence of TiB_2 particles suppressed the grain growth of SiC and facilitated to increase flexure strength of the SiC-TiB_2 composite.

Additional, newly created TiB_2 particles, which were initially very fine and active, both provide additional driving force for sintering and increases flexural strength of the SiC-B_4C-TiB_2-G composite. Thus, a fine grain size and a uniform distribution of TiB_2 particles played an important role in the sintering and mechanical properties of the SiC-B_4C based

ceramics, comparing to G. Magnani et al [18] reported flexure strength and fracture toughness of α-SiC-B_4C are 400~420 MPa，4.19~4.25 MPa·$m^{1/2}$, respectively. It was shown that the TiB_2 particle of smaller sizes led to improved densification, finer grain sizes, and higher strength of SiC-B_4C-TiB_2-G composites.

TABLE2 PROPERTIES OF SiC-B_4C-TiB_2-G COMPOSITES SINTERED AT 2000 °C FOR FOR 2.7 ks

Sample	Bulk density ($g·cm^{-3}$)	Apparent porosity (%)	Flexural strength, σ_b(MPa)	Fracture toughness, K_{Ic}(MPa·$m^{1/2}$)
SBTG20	2.81	2.4	276±4	5.5±0.4
SBTG35	2.64	3.2	215±5	6.1±0.2
SBTG50	2.51	5.4	164±3	6.8±0.5
SBTG65	2.43	8.2	118±3	8.1±0.5

IV. CONCLUSIONS

SiC-B_4C-TiB_2-G composites were prepared with graphite flake, SiC,B_4C and TiO_2 powders by in situ synthesis and hot pressing at 2000 ℃.The results showed that the flexure strength of the composites decreases while fracture toughness increases, with the increasing of graphite flake mass fraction. The effect of graphite flake length on strength is more pronounced than the effect of porosity and the ceramic grains. The density, flexure strength and fracture toughness of the composite is 2.81 g/cm^3, 276±4 MPa, 5.5±0.4 MPa·$m^{1/2}$, respectively, with the mass fraction 20 wt.% graphite flake. However, The density, flexure strength and fracture toughness of the composite is 2.43 g/cm^3, 118±3 MPa, 8.1±0.5 MPa·$m^{1/2}$, respectively, with the mass fraction 65 wt.% graphite flake.

The graphite flakes lamellar structure of the composites is formed clearly with mass fraction carbon increasing.

The toughening mechanisms are crack deflection and branching as well as stress relaxation near the crack tip. The introduction of graphite flake can increase fracture toughness. Although graphite flake can reduce flexural strength compared to SiC-B_4C based ceramics, but newly created TiB_2 particles, which were initially very fine and active, both provide additional driving force for sintering and increases flexural strength of the SiC-B_4C-TiB_2-G composite for TiB_2 particle of smaller sizes led to improved densification. The results here pointed to a potential method for improving fracture toughness of SiC-B_4C or TiB_2-SiC based ceramics.

ACKNOWLEDGMENT

This work was supported by the Natural Science Foundation of Liaoning, China (No. 20072026), the Besic Research Fund for the Northeastern University (N090302005), the China Postdoctoral Science Foundation (No. 20090451271), the National Natural Science Foundation of China (No. 50872018) and the Program for Chang Jiang Scholars and Innovative Research Team in University (IRT0713).

REFERENCES

[1] N. Frage, M.P. Dariel, and E. Zaretsky, “Divergent Impact Study Of The Compressive Failure Threshold In SiC And B_4C”, *International Journal of Impact Engineering*, In Press.

[2] D. Bucevac, B. Matovic, S. Boskovic, S. Zec, V. Krstic, “Pressureless sintering of internally synthesized SiC-TiB2 composites with improved fracture strength”, *Journal of Alloys and Compounds*, In Press.

[3] D. Bucevac, Snezana Boskovic, Branko Matovic, Vladimir Krstic, “Toughening of SiC matrix with in-situ created TiB2 particles”, *Ceramics International*, Vol. 36, no.7, pp. 2181-2188, September 2010.

[4] A. J. Li, Y. H. Zhen, Q. Yin, L. P. Ma, Y. S. Yin, “Microstructure and properties of (SiC, TiB2)/B4C composites by reaction hot pressing” *Ceramics International*, Vol. 32, no. 8, pp. 849-856, December 2006.

[5] S. H. Meng, F. Qi, H. B. Chen, Z. Wang, G.H. Bai, “The repeated thermal shock behaviors of a ZrB_2–SiC composite heated by electric resistance method International”, *Journal of Refractory Metals and Hard Materials*, Vol.29, no.1, pp. 44-48, January 2011.

[6] J. J. Kim, S. K. Park, “Solid-particle erosion of hot-pressed silicon carbide and SiC-TiB_2 composite”, *Journal of Materials Science Letters*, Vol.16, No.10, pp.821-823, 1997.

[7] X. H. Zhang, Z. Wang, P. Hu, W. B. Han, C.Q. Hong, “Mechanical properties and thermal shock resistance of ZrB_2–SiC ceramic toughened with graphite flake and SiC whiskers” ,*Scripta Materialia*, Vol. 61, no. 8, pp. 809-812, October 2009.

[8] Z. Wang, S. Wang, X. H. Zhang, P. Hu, W. B. Han, C. Q. Hong , “Effect of graphite flake on microstructure as well as mechanical properties and thermal shock resistance of ZrB_2–SiC matrix ultrahigh temperature ceramics”, *Journal of Alloys and Compounds*, Volume 484, no. 1-2, 18 ,pp. 390-394 ,September 2009.

[9] X. H. Zhang, Z. Wang, X. Sun, W. B. Han, C. Q. Hong, “Effect of graphite flake on the mechanical properties of hot pressed ZrB_2–SiC ceramics”, *Materials Letters*, Vol. 62, no. 28, 15, pp. 4360-4362, November 2008.

[10] A.R. Mirhabibi, B. Rand, “Graphite flake-carbon composites. II: Fracture behaviour, toughness, notch insensitivity and Weibull modulus”, *Carbon*, Vol. 45, no. 5, pp. 991-997, April 2007.

[11] Y. F. Sun, C. H. Shek, S. K. Guan, B. C. Wei, J. Y. Geng, “Formation, thermal stability and deformation behaviour of graphite-flakes reinforced Cu-based bulk metallic glass matrix composites”, *Materials Science and Engineering: A*, Vol. 435-436, no. 5 pp. 132-138, November 2006.

[12] I. Gunjishima, T. Akashi, T. Goto. Characterization of directionally solidi-fied B_4C–TiB_2 composites prepared by a floating zone method. Materials Transactions 43:712–20. 2002;

[13] A. V. Polotai, J. F.Foreman, E. C. Dickey, K.Meinert, “Laser surface processing of B_4C–TiB_2 eutectic”. *International Journal of Applied Ceramic Technology*, Vol. 5, no. 6, pp. 610–617, November 2008.

[14] I. Bogomol, T. Nishimura, O. Vasylkiv, Y. Sakka, P. Loboda, “Microstructure and high-temperature strength of B_4C-TiB_2 composite prepared by a crucibleless zone melting method”. *Journal of Alloys and Compound*, Vol. 485, no.1-2, pp.677–681, October 2009.

[15] S. B. Zhou, Z. Wang, W. Zhang, “Effect of graphite flake orientation on micr”ostructure and mechanical properties of ZrB_2-SiC-graphite composite *Journal of Alloys and Compounds*, Vol. 485, no. 1-2, pp. 181-185 , October 2 009.

[16] A.V. Mirhabibi, B. Rand, S. Baghshahi, R. Agha Baba Zadeh, “Graphite flake carbon composites with a ‘sinterable’ microbead matrix: I. mechanical properties”, *Carbon*, Vol. 41, no. 8, pp. 1593-1603, 2003.

[17] Y. Yan, H. Zhang, Z. Huang, J. Liu, D. Jiang, “In Situ Synthesis of Ultrafine TiB_2-SiC Composite Powders and the Pressureless Sintering Behaviors”, *Journal of the American Ceramic Society* ,Vol. 91, no. 4, pp. 1372-1376, April 2008.

[18] G. Magnani, G. Beltrami, G. L. Minoccari , L. Pilotti, “Pressureless sintering and properties of αSiC–B_4C composite”, *Journal of the European Ceramic Society*, Vol. 21, no. 5, pp. 633-638,May 2001.

2011 International Conference on Mechanical, Industrial, and Manufacturing Engineering
Lecture Notes in Information Technology Vols. 1-2

Simulation Analysis on Impact Location Detection for Piezoelectric Smart Structures

Jianhong Xie
School of Software and Communication Engineering,
Jiangxi University of Finance and Economics, Nanchang 330013, China
jhxie2006@126.com

***Abstract*—Based on the first-order shear deformation theory and finite element method, the piezoelectric smart composite laminated plates is simulated, and its piezoelectric transient responsive signals are obtained and analyzed under the low-velocity impact load. Then, Least Square Support Vector Machine (LS-SVM) is applied to detect the impact locations for the piezoelectric smart composite laminated plates based on the features of piezoelectric sensors' transient responsive signals. The results show that, the accuracy of impact location detection based on piezoelectric transient responses combined with LS-SVM method is much higher. In addition, the simulation method can give a certain of guidance for the practical structural impact damage locations self-diagnosing.**

***Keywords* —piezoelectric smart structures; piezoelectric transient response; LS-SVM; impact location detection**

I. INTRODUCTION

As a new materials, composite materials has become widely used in many important areas of engineering applications such as aerospace, energy sources, transportation, due to their advantages of low density, high intensity and so on. However, the damage mechanism of composite materials is different from that of the common metals, because composite materials is a kind of anisotropic and complicated multiphase architecture. Especially, composite materials is very sensitive to impact loads. In order to avoid the severe loss coming of damages in composite materials, the piezoelectric smart composite materials and structures is constructed, which mainly includes the integration of piezoelectric sensors into or onto the structural materials combined with advanced signal processing and possibly even control, and can provide an interesting platform to monitor continuously the structural damages [1]. During the present research, a general formulation for composite laminated plates as the principal part of piezoelectric smart composite materials has been developed. These formulations include classical laminated plate theory, shear deformation (first-order and third-order) theory, layer laminated theory, and 3-dimensional elasticity theory [2].

In this paper, based on the first-order shear deformation theory and finite element method, the piezoelectric smart composite laminated plates is simulated, and its piezoelectric transient responsive signals are obtained and analyzed under the low-velocity impact load. Then, Least Square Support Vector Machine (LS-SVM) is applied to detect the impact locations for the piezoelectric smart composite laminated plates based on the features of piezoelectric sensors' transient responsive signals.

II. SIMULATION ANALYSIS ON IMPACT PIEZOELECTRIC RESPONSES

The mechanics of piezoelectric smart composite materials involves the coupling between electric, thermal, and mechanical effects. In addition to this coupling, it may be necessary to account for geometric and material nonlinearities, and other factors. Therefore, the perfect method used to analyze the above coupling problem is the numerical simulation method rather than the resolution method. In all numerical methods, the finite element method is an important, effective, and widely used method. In this paper, the finite element method is applied to analyze the impact piezoelectric responses for piezoelectric smart composite laminated plates.

The simulation example adopts the fiber-reinforced carbon/epoxy composite laminated plates (Gr70%-Epoxy30%, Orthotropic, stacking sequence (0/90)s) shown in Fig. 1. The composite laminated plates has the geometrical dimension of Lx=400mm, Ly=320mm, Lz=0.5mm×4, and its material property parameters are the followings [3],

E_{11}=108GPa E_{22}=E_{33}=10.3GPa $\mu = 0.28$

G_{12}=G_{13}= G_{23}=7.17Gpa $\rho = 1389.2\ \mathrm{Kg/m^3}$

The composite laminated plates is simply supported on four sides, and instrumented with 9 piezoelectric patches as sensors affixed on the surface of the laminated plates. Fig. 1 shows the total distribution of piezoelectric patches used. The piezoelectric patch has the geometrical dimension of 25mm×20mm×0.25mm, and its material is PZT-5 with the following property parameters [4],

E_{11}=E_{22}=62GPa G_{12}=G_{13}=23.6GPa G_{23}=18GPa

$\mu = 0.31$ e_{31}=e_{32}=19.678C·m^{-2} $\rho = 7400\ \mathrm{Kg/m^3}$

$\xi_{11} / \xi_0 = \xi_{22} / \xi_0 = \xi_{33} / \xi_0 = 2598$

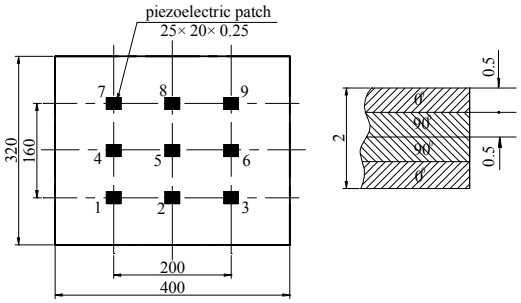

Fig. 1 Piezoelectric composite laminated plates

The composite laminated plates is subjected to a semi-sine low-velocity impact load formulated as the following,

$$q_t = q_0 \cdot \sin\left(\frac{\pi}{\tau} \cdot t\right) \tag{1}$$

where q_0=1N, $\tau = 1\,\text{ms}$, $0 \le t \le \tau$.

For the piezoelectric smart composite laminated plates shown in Fig. 1, the ANSYS finite element method is applied to establish its geometry solid model, and define elements' properties for different parts of the model. Namely, the composite laminated plates adopts the 3-dimensional solid layer element SOLID46 with 8 nodes based on the first-order shear deformation theory, and the piezoelectric patches adopt the 3-dimensional solid coupled element SOLID5 to couple with the element SOLID46. Moreover, the SOLID46 element is polarized at Z-direction. Through meshing and imposing the simply boundary constraint condition for the above geometry solid model, the finite element model for the piezoelectric composite laminated plates can be established as shown in Fig. 2.

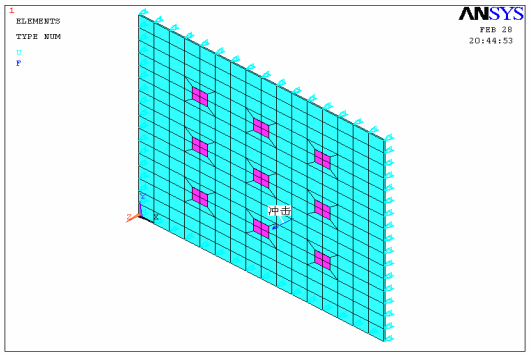

Fig. 2 Finite element model for piezoelectric composite laminated plates

Then, the simulation analysis on impact piezoelectric transient responses for the piezoelectric composite laminated plates can be carried out under the above semi-sine low-velocity impact load. For example, if the load is exerted at the location shown in Fig. 2, the responsive signals of each of piezoelectric sensors can be obtained as shown in Fig. 3. Fig. 3 shows that the respective signals' characteristics of different piezoelectric sensors are closely related to the factors such as sensor placement locations, impact load locations, and boundary conditions of plates. Moreover, the signals' characteristics mainly include signal peak values (maximum and minimum), time corresponding to peak values, signal mean and variance. To differentiate largely the responsive signals of different sensors, and decrease the computation of feature extracting, by comprehensively analyzing the respective signals' characteristics of different piezoelectric sensors, the maximum and minimum of signals are extracted as features. Through compiling and implementing the post-processing program of finite element, the signals' features of different piezoelectric sensors can be obtained as shown Table 1. Table 1 indicates that, because the times corresponding to peak values (maximum and minimum) for different sensors' responsive signals are much more constant, the times are not appropriate as features to be extracted, but the maximum and minimum are appropriate as features to be extracted.

Adopting the above scheme, the low-velocity impact simulation tests at 85 different locations on the surface of laminated plates shown in Fig. 1 are carried out respectively, and the transient responsive signals of piezoelectric sensors and their features (maximum and minimum) are obtained under the different locations' impact.

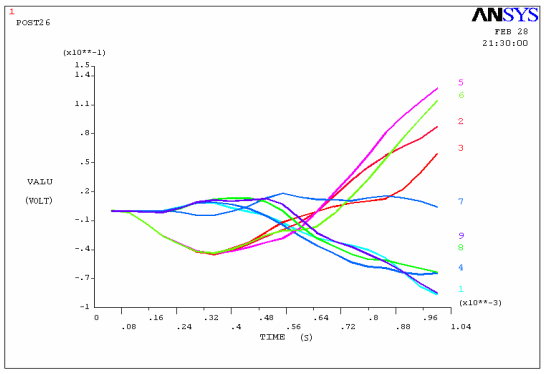

Fig. 3 Impact transient responses for different piezoelectric sensors

Table 1 Features extracted from different piezoelectric responsive signals

Sensor Number	Minimum (v)	Time corresponding to minimum (s)	Maximum (v)	Time corresponding to maximum (s)
1	-0.8638E-01	0.1000E-02	0.8955E-02	0.3000E-03
2	-0.4481E-01	0.3500E-03	0.8718E-01	0.1000E-02
3	-0.4431E-01	0.3500E-03	0.5928E-01	0.1000E-02
4	-0.6577E-01	0.9500E-03	0.9027E-02	0.3500E-03
5	-0.4391E-01	0.3500E-03	0.1271	0.1000E-02
6	-0.4366E-01	0.3500E-03	0.1142	0.1000E-02
7	-0.4539E-02	0.3500E-03	0.1843E-01	0.5500E-03
8	-0.6333E-01	0.1000E-02	0.1347E-01	0.4000E-03
9	-0.8500E-01	0.1000E-02	0.1282E-01	0.5000E-03

III. IMPACT LOCATION DETECTION BASED ON LS-SVM

As a new learning machine, Support Vector Machine based on Statistical Learning Theory has various types. Among these types, Least Square Support Vector Machine (LS-SVM) with the advantages of simpler algorithm, faster operation speed, etc., is widely applied to pattern recognition and nonlinear regression [5]. The regression principle of LS-SVM can be explained as follows:

Consider first a model in the primal weight space of the following form,

$$y(x) = \omega^T \varphi(x) + b \tag{2}$$

where $x \in R^n$, $y \in R$ and $\varphi(\cdot) : R^n \to R^{nh}$ is the mapping to the high dimensional and potentially infinite dimensional feature space. Given a sample set $\{(x_i, y_i),\ i = 1,2,\cdots,l\}$ that needs to regress, we can formulate the following optimization problem in the primal weight space,

$$\begin{aligned} &\min_{\omega,b,\xi} \ J(\omega,\xi) = \frac{1}{2}\omega^T\omega + \gamma\frac{1}{2}\sum_{i=1}^{l}\xi_i^2 \\ &s.t. \ \ y_i = \omega^T\varphi(x_i) + b + \xi_i \end{aligned} \tag{3}$$

where $\gamma > 0$ denotes a real constant used to control the punishment degree for misclassification. Because ω becomes infinite dimensional, this primal problem cannot directly be solved. Therefore, let us proceed by constructing the following Lagrangian,

$$L(\omega,b,\xi;\alpha) = J(\omega,\xi) - \sum_{i=1}^{l}\alpha_i\left\{\omega^T\varphi(x_i) + b + \xi_i - y_i\right\} \tag{4}$$

where α_i are Lagrange multipliers. The conditions for optimality are given by

$$\frac{\partial L}{\partial \omega} = 0,\ \frac{\partial L}{\partial b} = 0,\ \frac{\partial L}{\partial \xi_i} = 0,\ \frac{\partial L}{\partial \alpha_i} = 0 \tag{5}$$

After elimination of the variables ω and ξ, a set of linear equations can be obtained,

$$\begin{bmatrix} 0 & 1_v^T \\ 1_v & \Omega + I/\gamma \end{bmatrix}\begin{bmatrix} b \\ \alpha \end{bmatrix} = \begin{bmatrix} 0 \\ y \end{bmatrix} \tag{6}$$

where $1_v = [1;1;\cdots;1] \in R^l$, $I \in R^{l\times l}$ denotes a unit matrix, $\alpha = [\alpha_1;\alpha_2;\cdots;\alpha_l]$, $y = [y_1;y_2;\cdots;y_l]$, $\Omega_{ij} = \varphi(x_i)^T\varphi(x_j) = K(x_i,x_j),\ i,j = 1,2,\cdots,l$.

Solving the above equations, then the resulting LS-SVM model for regression becomes,

$$y(x) = \sum_{i=1}^{l}\alpha_i K(x,x_i) + b \tag{7}$$

Based on the above regression model, the unknown data can be gotten to predict and estimate. Note that in the case of RBF kernel $K(x,x_i) = \exp(-\|x - x_i\|^2/2\sigma^2)$, LS-SVM has only two additional tuning parameters, one is the punishment factor $\gamma > 0$, the other is the width of RBF $\sigma > 0$. And these two parameters can be optimized by Genetic Algorithm (GA).

Setting the signals' features of above different sensors as the input of LS-SVM, and the corresponding impact locations as the output of LS-SVM, then the nonlinear relationship between the sensors' responses and impact locations can be established to realize the structural impact damage locations self-diagnosing. Because two features (maximum and minimum) are extracted from each sensor, 9 sensors have 18 features under each impact location, namely (s(1), s(2), …, s(18)). Therefore, the input layer of LS-SVM has 18 dimensions, and the output layer has 2 dimensions which denote the values of horizontal coordinate and vertical coordinate of impact location. Set 49 sets of the above 85 sets of test data as training samples of LS-SVM, and the other 36 sets as testing samples of LS-SVM. The test data as training samples and testing samples of LS-SVM are shown in Table 2 and Table 3.

Considering the above problem's property, RBF kernel is adopted as kernel function of LS-SVM. In order to optimize the tuning parameters (γ,σ^2) of LS-SVM, let us establish the following error function of impact location detection for the composite laminated plates,

$$g(x,y) = \frac{\frac{1}{p_0}\sum_{p=1}^{p_0}\left|x_p - \bar{x}_p\right| \cdot \frac{1}{p_0}\sum_{p=1}^{p_0}\left|y_p - \bar{y}_p\right|}{A} \tag{8}$$

where x_p and y_p denote the network actual outputs, $\bar{x}_p$ and $\bar{y}_p$ denote the network desired outputs, p_0=36 denotes the number of testing samples, the plate's area A=400mm×320mm.

Set the inverse of above error function as the fitness function of GA, namely $f(x,y) = 1/g(x,y)$. Based on the fitness function $f(x,y)$, GA is applied to optimize the above LS-SVM parameters (γ,σ^2) according to the training samples and testing samples. Then the resulting optimum parameters are $(\gamma,\sigma^2) = (4,13)$, under which, the fitness value is maximum $f(x,y) = 2608.4$, and the corresponding error of impact location detection is minimum $g(x,y) = 0.038\%$. Under the optimum parameters $(\gamma,\sigma^2) = (4,13)$, the testing results of LS-SVM are shown in Table 3. The results show that, the accuracy of impact location detection based on piezoelectric transient responses combined with LS-SVM method is much higher. In addition, the simulation method can give a certain of guidance for the practical structural impact damage locations self-diagnosing.

Table 2 LS-SVM training samples

Samples number	Input samples					Output samples	
	Sensor 1		…	Sensor 9			
p	$s_p(1)$	$s_p(2)$	…	$s_p(17)$	$s_p(18)$	$\bar{x}_p$	y_p
1	-7.255e-2	2.746e-1	…	-2.173e-2	1.452e-2	50	40
2	-3.728e-2	3.371e-1	…	-1.727e-2	6.319e-3	100	40
…	…	…	…	…	…	…	…
48	-1.727e-2	6.319e-3	…	-3.728e-2	3.371e-1	300	280
49	-2.173e-2	1.452e-2	…	-7.255e-2	2.746e-1	350	280

Table 3 LS-SVM testing samples and testing results

Samples number	Model inputs					Actual outputs		Desired outputs	
	Sensor 1		…	Sensor 9					
p	$s_p(1)$	$s_p(2)$	…	$s_p(17)$	$s_p(18)$	x_p	y_p	$\bar{x}_p$	$\bar{y}_p$
1	-1.17e-2	3.96e-1	…	-1.34e-2	2.75e-3	76.4	59.7	75	60
2	-1.17e-2	3.29e-1	…	-6.19e-3	4.27e-3	129.4	56.9	125	60
…	…	…	…	…	…	…	…	…	…
35	-6.19e-3	4.27e-3	…	-1.17e-2	3.29e-1	270.6	263.1	275	260
36	-1.34e-2	2.75e-3	…	-1.17e-2	3.96e-1	323.6	263.3	325	260

IV. CONCLUSION

As a new materials, composite materials has become widely used in many important areas of engineering applications due to their advantages of low density, high intensity and so on. However, the damage mechanism of composite materials is complex, and especially sensitive to the impact loads. In this paper, based on the first-order shear deformation theory and finite element method, the piezoelectric smart composite laminated plates is simulated, and its piezoelectric transient responsive signals are obtained and analyzed under the low-velocity impact load. Then, Least Square Support Vector Machine (LS-SVM) is applied to detect the impact locations for the piezoelectric smart composite laminated plates based on the features of piezoelectric sensors' transient responsive signals. The results show that, the accuracy of impact location detection based on piezoelectric transient responses combined with LS-SVM method is much higher. In addition, the simulation method can give a certain of guidance for the practical structural impact damage locations self-diagnosing.

ACKNOWLEDGEMENTS

The authors gratefully acknowledge the support of the science and technology research program of Jiangxi Provincial Department of Education, China (Project No. GJJ10437).

REFERENCES

[1] Xie Jianhong, Zhang Weigong, Liang Dakai. Smart Materials and Structures: Research Status and Future Development. Materials Review, 2006, 20(11): 6-9.

[2] Reddy J. N. On Laminated Composite Plates with Integrated Sensors and Actuators. Engineering Structures, 1999, 21: 568-593.

[3] Hong Zhangqing, Liu Qingji, Guo Jiayuan. ANSYS7.0 Teaching Examples. Beijing: China Railway Publishing House, 2003.

[4] Dimitris Varelis, Dimitris A. S. Nonlinear Coupled Mechanics and Initial Bucking of Comosite Plates with Piezoelectric Actuators and Sensors. Smart Material and Structure, 2002(11): 330-336.

[5] Johan A. K. Suykens, Tony Van Gestel, etc. Least Squares Support Vector Machine[M]. Singapore: World Scientific Publishing Co. Pte. Ltd. 2002.

2011 International Conference on Mechanical, Industrial, and Manufacturing Engineering
Lecture Notes in Information Technology Vols. 1-2

The Effect of Combined Cold Air and Minimum Liquid Cooling on End Milling

Dr Brian Boswell and Erika Voges
Department of Mechanical Engineering
University of Curtin
Bentley, Perth 6845, WA
b.boswell@curtin.edu.au

***Abstract* - Modern machining companies constantly face the challenges of quality and cost pressures as well as the ever increasing global awareness of social and environmental issues that affect the manufacturing of machined parts. For companies to remain competitive and sustainable in the future they need to develop new techniques which reduce the environmental impact of manufacturing. Conventional wisdom [1] states that it is essential to use flood coolant to reduce thermal shock on the tool tip during end milling, as intermittent cooling increases this effect. End milling dry is preferred to milling with too little cutting fluid for this reason, especially for carbide tool tips. Previous experimental evaluation of Minimal Quantities of Lubrication (MQL) when applied to an end milling operation has proved to be inconclusive as to the effectiveness. The cause is believed to be ineffective heat removal from the cutting zone. The research presented in this paper represents the initial experimentation involved in developing a suitable alternative approach to using copious amounts of cutting fluid during end milling. It has been found from cutting tests that eliminating the cutting fluid entirely has not been practical: the most promising results have been derived from a combination of air cooling with the addition of small amounts of vegetable oil**.

***Index Terms* – environmental issues, flood coolant, thermal shock, Minimal Quantities of Lubrication, air cooling.**

I. INTRODUCTION

The machining process involves removing unwanted material from the workpiece in the form of chips, and is one of the principle methods of manufacturing. According to Childs *et. al*. [2] the wealth of nations can be judged by their investment in machining. However, the high reliance on traditional liquid cutting fluid to prolong the tool life has resulted in environmental, ecological, health and cost issues. It is known that traditional liquid coolants employed in metal cutting processes accounts for up to 17% of the cost of machining due to the initial cost of the fluid and the eventual disposal cost of the fluid. This demonstrates the urgency for the manufacturing industry to seek machining techniques that reduce the amount of coolants used, or eliminate them altogether. The machining parameters selected to determine the effectiveness of the cooling methods are based on the tool tip manufacturer recommendations. This study uses a single point milling cutter to aid with the analysis of the cutting action due to the combined intermediate cutting action of a multi tool tip.

The customary end milling process uses copious amounts of liquid coolant, with the liquid coolant being used to increase the tool life and to improve the workpiece surface finish. Unfortunately, even with the recognition of the aforementioned benefits a more environmental tool cooling method is sought. Simply reducing the amount of coolant used is not a viable solution for end milling due to the intermittent nature of cutting action at the tool tip, as thermal shock at the tool tip would increase. In order to minimise the consequences of thermal shock a cooling method that can remove the generated heat during the entire cutting cycle is required.

A number of alternative cooling methods have been trialled to help improve the machining performance, resulting in some success. One such method is called minimal quantities of lubrication (MQL) [3]. This is where an extremely small amount of lubricant is blasted by air onto the tool. There have been very few articles published which use MQL in end milling compared to that of turning. The challenge for MQL has been to show that tool life is compatible with that of traditional flood cooling. The cold air (vortex tube) and MQL have shown to have improved tool life, cutting force, surface finish and chip shape during turning machining tests. A novel cooling approach is examined in this paper where the cutting tool is continually surrounded by cold air with the addition of MQL to reduce the cutting friction. Very few papers are available on cold air assisted end milling or MQL. A research paper by M. Rahman *et. al.* [4] examined the design of a new cooling system which used liquid mist and air. The results showed that the performance of this cooling system was better than that of traditional flood coolant under certain cutting conditions. For example the tool wear obtained by this new cooling method was found to be lower than that for flood coolant at low feed rates and low cutting speeds. The average surface roughness of the workpiece is lower at higher feed rates, and at higher cutting speeds the average surface roughness of the workpiece was compatible to that of flood coolant. Previous research [5] has shown that the dry cutting force is greater than flood coolant or chilled air cooling methods. This research endeavours to show the effectiveness and suitability of different methods of prolonging tool life during the high-speed end milling of 1040 steel. The Taguchi method [6] was used to strategize the experimental procedure and optimized the experimental parameters. This was completed by using an orthogonal array of the cutting parameters used in the cutting tests.

978-0-9831693-1-4/10/$25.00 ©2011 IERI

II. CUTTING TESTS AND SET-UP

The metal cutting tests consisted of a Leadwell vertical machining centre (V-30), a Kistler three component dynamometer (Type 9257BA) and a Yokogawa CW140 clamp on power analyser. An Airtx vortex tube (Model 20008) with an inlet pressure of 85 psi supplied chilled air at a temperature of -5^{o}. The compressed air used was supplied from the workshop air line. The MQL was delivered from a Uni-max cutting tool lubrication system which distributed atomised coolube metalwork lubricant to the cutting zone. This system operates on the same principle as a Serv-O-Spray allowing the lubricant to be sprayed from a single air source, which allows adjustment to the amount of lubricant delivered to the cutting zone. A traditional emulsified cutting fluid (Cocol ultra cut) was used for wet machining, and the cutting tool selected for all of the tests was a Sandvik single tip tool (R390-012A16-1L) with a coated tungsten carbide insert (R390-11 T3 08M-PL 1030). All cooling nozzles used during the tests were kept at approximately 25 mm from the tool during all tests. A single tooth cutter was selected to avoid the influence of tool run out on the flank wear, and to simplify the analysis of the tests. The workpiece was clamped onto the dynamometer that in turn was secured onto the machine table of the vertical milling centre. Cutting forces were then recorded onto the computer's hard disk for later analysis. Fig. 1 shows the cutting test set-up.

Fig. 1 Machining set-up.

Metal cutting tests were carried out using three cooling conditions; cooled air (CA), minimal quantities of lubrication (MQL), and cooled air combined with minimal quantities of lubrication (CA+MQL). The best practice cutting path was used to produce the machined face ensuring that the tool tip was constantly removing 70% of the material along the tool path. The cutting forces and power were measured for each face machined with the cutting power being recorded at the positions shown in Fig. 2.

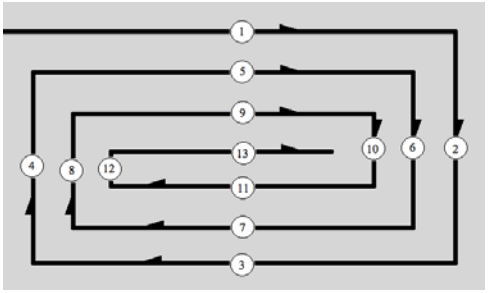

Fig. 2 Tool path

In this research the tool failure criteria applied to the cutting edges were:

1. Catastrophic failure or localised chipping.
2. Flank-wear greater than 0.4 or total edge fracture.
3. Dramatic change in tool forces and cutting power.

All tool tips were examined for wear after the machining of each test sample by using a tool maker microscope, and the surface roughness of the work-pieces were measured by a Mitutoyo portable stylus type surface roughness tester.

III. RESULTS AND DISCUSSIONS

The cutting conditions used (see Table I) in this research were selected to reflect typical working environments, in order to determine the effectiveness of the cooling parameters in production.

TABLE I
Cutting Test Settings

Cutting Speed m/min	DOC mm	Feed Rate mm/min	Cooling Parameter
220	3	480	Cold air (CA)
235	3	480	Minimal quantities of lubrication (MQL)
250	3	480	Cooled air combined with minimal quantities of lubrication (CA+MQL)

In an attempt to prove the success of cold air combined with MQL in production it is first necessary to measure the wear at the extreme operating cutting conditions. Conventional dry milling and flood milling is used to set the bench mark for the cooling processes as they are the two extreme positions. Previous research conducted by M. Rahman *et. al.* [7] has shown MQL to be compatible to that of flood coolant for cutting conditions within the following range: cutting speed 75 to 125 m/min, feed rate 0.01 to 0.03 mm/tooth, and a depth of cut (DOC) of 0.35 to 0.7 mm. Fig. 3 shows the flank wear and surface roughness recorded for a feed rate of 0.015 mm/tooth, and depth of cut (DOC) of 0.35 mm. When contrasted with the production cutting conditions it found that the flank wear had increased as expected, and that MQL was not as effective due to the higher cutting temperatures.

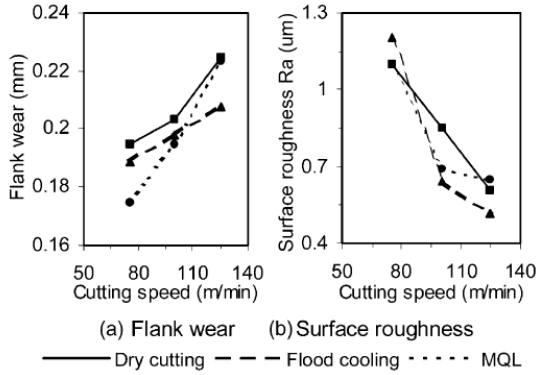

Fig. 3 Effect of cutting speed on tool wear and surface roughness by M. Rahman [4]

Using Taguchi's experiment design method [8] reduces the cutting tests to nine conditions while not compromising the robustness of the cutting test results. The combination of cutting test conditions and cooling parameters (are shown in Table II) for each experimental cutting test. Column A represents the cooling parameters with 0 representing air cooled, 1 represents MQL and 2 represents MQL+AC. Column B represents the cutting speed with 0 representing a lower cutting speed, 1 represents the recommended tool tip cutting speed and 2 represents a higher cutting speed.

Table II
Orthogonal Test Array

Cutting Test No.	A	B
1	0	0
2	0	1
3	0	2
4	1	0
5	1	1
6	1	2
7	2	0
8	2	1
9	2	2

All cutting tests had their cutting force and power recorded for each test sample twice, producing copious amounts of data. An extract of this data is used in this paper to demonstrate the effectiveness of each of the cooling parameters.

(a) VT+MQL (b) Four cooling nozzle+MQL

Fig. 4 Cooling Parameters

From previous research [9] it was found that the one cold air nozzle Fig. 4(a) combined with MQL produced improvements in the machining operations but was still subject to thermal cracking reducing the tool life. The additional air cooled nozzles reduced the thermal cracking substantially as the tool tip was now being cooled in all cutting directions.

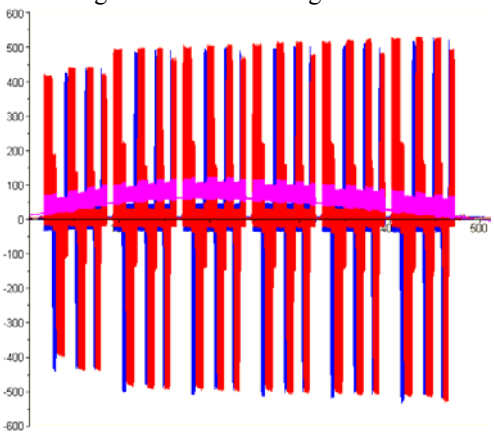

Fig. 5 Typical Forces Output From Dynamometer

The dynamometer allows the cutting forces to be analysed for each of the cooling parameters as shown in Fig. 5, where the X (blue), Y (red) and Z (pink) axis shows the magnitude of the forces, with corresponding increases identifying tool wear. Fig. 6 shows the average force for one test condition (1) over the range of cooling parameters (0, 1&2). A dry and flood cutting sample is included for reference purposes in Fig. 6 and 7.

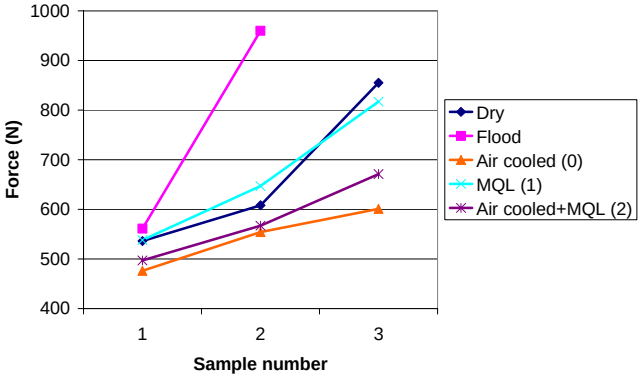

Fig. 6 Cutting forces

Fig. 6 shows that the cutting forces for the cold air cooling are the lowest for the three cooling parameters used over the three samples. This however was not demonstrated by a similar reduction in the cutting power as shown in Fig. 7. This apparent difference between measured force and power is due to the power being the cutting power and the force being one vector of the cutting force. The most inclusive illustration of which cooling parameter is the most effective is shown by which one gives the most reduction in tool wear. All the tool tips were examined under the microscope after machining of each sample, and a picture was taken to record the wear before continuing to machine. Typical wear of the tool tip is shown in Fig. 9. The cutting power gives a good indication of the cutting performance as the power rises with respect to the wear on the tool. However, determining the effectiveness of

the cooling parameters cannot be judged simply by considering one function only e.g. cutting forces, as metal cutting is a very complex system to analyse. Therefore, it is necessary to include all important tool parameters when specifying the best cooling method.

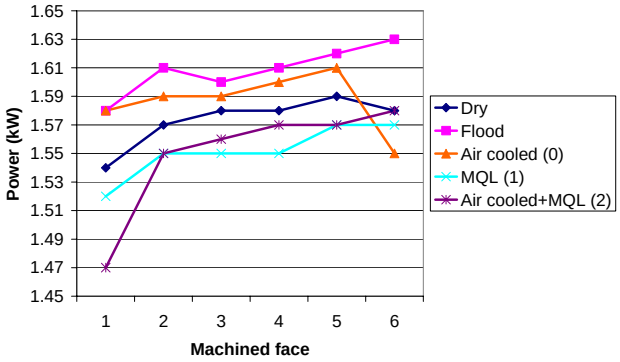

Fig.7 Cutting power for sample 1 at position 5

Finally the surface finish was examined for all samples, which showed that all samples were in the limits for semi-finishing operations. The wear mechanism for each sample correlated well with the surface roughness data as shown in Fig. 8.

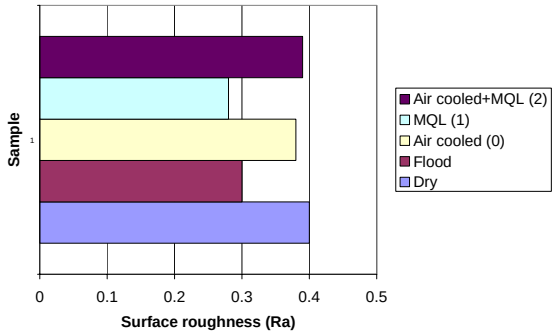

Fig. 8 Cooling parameters surface roughness (µm)

(a) Cold air (0) (b) Cold air + MQL (2)

Fig. 9 Tool tip wear

IV. CONCLUSIONS

End milling is a machining process that has proven to be extremely difficult to eliminate traditional cutting fluid because of the intermittent cutting action leading to thermal cracking. To reduce this effect the tool tip was constantly surrounded with cold air as well as a small quantity of vegetable oil to reduce the cutting friction. The nature of the heat generating process makes it impossible to eliminate thermal stress within the tool tip. The goal of this research is to prolong the tool life for dry machining. Although air cooling with the use of a small amount of vegetable oil is not a totally dry process it is quite close. It is interesting to note that M. Rahman *et.al.* [5] found that dry cutting produced the highest cutting force with a depth of cut of 0.35 mm and cutting speed of 75 m/min, whereas in this research dry cutting was close to air cooling. The power used during each of the cutting operations gives a better direct indication of the effectiveness of the cutting process than can be obtained by analysing the dynamometer force readings. The results have shown that Cold air+MQL can be used to increase the tool life even with normal production cutting speeds, feed rates and depths of cut are used. Using this method of machining helps make metal cutting more sustainable. Further work is necessary to examine how efficient air cooling is with other milling tools and materials.

REFERENCES

[1] T. J. Drozda, "Machining," in *Tool and Manufacturing Engineers Handbook*, fourth ed. vol. volume 1, T. J. Drozda, Ed. Dearborn Michigan: Mc Graw-Hill Book Co, 1976, p. 1484.

[2] T. H. C. Childs, K. Maekawa, T. Obikawa, and Y. Â Â. Â Yamane, "Metal Machining - Theory and Applications," Elsevier, 2000.

[3] K. Weinert, I. Inasaki, J. W. Sutherland, and T. Wakabayashi, "Dry Machining and Minimum Quantity Lubrication," *CIRP Annals - Manufacturing Technology,* vol. 53, pp. 511-537, 2004.

[4] M. Rahman, A. Senthil Kumar, and M. U. Salam, "Experimental evaluation on the effect of minimal quantities of lubricant in milling," *International Journal of Machine Tools and Manufacture,* vol. 42, pp. 539-547, 2002.

[5] M. Rahman, A. S. Kumar, M.-U. Salam, and M. S. Ling, "Effect of Chilled Air on Machining Performance in End Milling," *The International Journal of Advanced Manufacturing Technology,* vol. 21, pp. 787-795, 2003.

[6] R. Roy, *A Primer on the Taguchi Method*: Society of Manufacturing Engineers, 1990.

[7] M. Rahman, A. Senthil Kumar, U. I. S. Manzoor, and U. I. S. Manzoor, "Evaluation of Minimal of Lubricant in End Milling," *The International Journal of Advanced Manufacturing Technology,* vol. 18, pp. 235-241, 2001.

[8] Y.-K. Hwang, C.-M. Lee, and S.-H. Park, "Evaluation of machinability according to the changes in machine tools and cooling lubrication environments and optimization of cutting conditions using Taguchi method," *International Journal of Precision Engineering and Manufacturing,* vol. 10, pp. 65-73, 2009.

[9] B. Boswell, "An experimental approach to determining the effectiveness of minimum liquid cooling for end milling 1040 steel," in *6th Australasian Congress on Applied Mechanics, ACAM 6* Perth: Mechanical Institution of Australia, 2010.

2011 International Conference on Mechanical, Industrial, and Manufacturing Engineering
Lecture Notes in Information Technology Vols. 1-2

Study on the law of the soil water infiltration with two-point-source

Jing Du, Shumei Ren*, Peiling Yang, Xianyue Li, Jun Du
College of Water Conservancy & Civil Engineering, China Agricultural University
dujing861011@163.com renshumei@126.com

Abstract: **On the base of the laboratory experiment, in conditions of different drip irrigation flow and spacing, the infiltration of soil water with two-point-source is measured. The researchers studies the drip irrigation flow and spacing have effects on the shape of the interference infiltration wetting soil、the water distribution and the law of its movement of wetting soil. The result indicates that at the beginning of the settlement, the wetting soil shape is close to W-shaped. As time goes on, the shape turns into a semi-elliptic and circular; The horizontal and vertical movement distance of soil wetting front accords the quadratic polynomial function well with infiltration time on the intersection side; As infiltration time prolonging, the horizontal and vertical movement velocity decreases; When the time of irrigation is long enough, vertical distance in the interference interface is greater than that in the center of emitter; Soil moisture content of convergence in the interface is greater than that at the same soil depth. The result of study has certain guidance functions to the systematic design theory of different roots drip irrigation.**

Key word: two-point-source infiltration, interference infiltration, Emitter flow, Emitter spacing.

I. INTRODUCTION

Drip irrigation technology has been recognized as a water-saving technology, many scholars have paid much attention on theoretical and experimental research of point-source free infiltration [1-5]. But many studies found that the fine roots of deep root plant distributed between 0-60cm in depth and within 250cm in horizontal direction [6-12]. Generally the space between fruit trees is 3-4 meters, and the roots of fruit trees are deeper. Sokalska found that the yield of fruit tree was 23% higher in two-point source drip irrigation than in single point source drip irrigation [6]. Gerstl study the distribution of herbicides in Soil in a simulated drip irrigation system, through analyzing the concentration of herbicide in the wet body, the distribution of soil moisture and herbicides [13]; Pascual Romero studied under subsurface drip irrigation, water stress had effect on root density, fruit growth and fruit abscission [14]; Fernandz found comparing dry land conditions and drip system, the roots within the wet soil zones near the drippers. The highest root densities occur in wet zones, down to 0.6m depth, the most abundant being the <0.5mm diameter roots. The most intensive root activity was also found in wet zone [15]. Therefore, it is necessary to study the regularity of water flow in two-point source drip irrigation system with different flow and drip emitter space, which can provide a theoretical basis for drip irrigation system designing for plants with different roots.

Ⅱ. TEST MATERIALS AND METHOD

A. Test materials

This experiment was carried in the experimental hall of China Agricultural University from March to June, 2009. Soil samples were taken from Beijing's holly orchard. Dried and crushed before trial, after over 2mm sieves, the center of emitter, the soil texture has been classified by international standard, the composition of soil particles was shown in Table Ⅰ.

TABLE Ⅰ Basic physical parameters of soil

soil type (mm)	0.05-1	0.002-0.02	
sandy loam soil (%)		29.2	6

B. Test System and Methods

Experimental system contained water supply systems and soil box. The rectangular soil box was made by transparent organic glass (120cm × 80cm × 60cm); water was provided by the Mariotte bottle; the dripper discharge was controlled by adjusting knob or changing the needle size under the constant water head.10cm thick gravels were put(with a diameter of 0.5-2cm) at the bottom of the soil box, the treated soil was put into the box by bulk density 1.4g/cm, the thickness of each layer was 10cm, five layers, soil was loaded as even as possible. To

*Corresponding author
E-mail address: renshumei@126.com; Supported by State Natural Science Fund: 50779068

prevent the effects of evaporation, temperature and other factors on the readings of first layer sensor, soil moisture sensors in the first layer were placed 5cm below the soil surface, experimental installation was shown in Fig.1. When irrigation started, the two drippers discharged at the same speed. The horizontal and vertical migration distances of wetting front during different duration of irrigation were recorded; wetting front was drawn from the side of the box. When the two wetting fronts were confluence, the case of wetting front (confluent time, confluent depth and water content) were recorded. Beginning dipping, the movement law of wetting fronts and the distribution of water content were observed. According to the distribution of plant roots in the horizontal direction, the experiment contained the following four treatments, as shown in Table II.

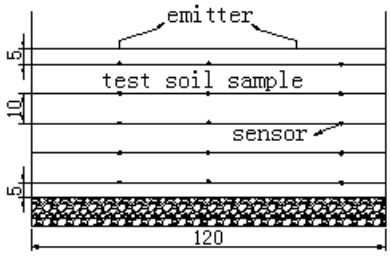

Fig.1 Experimental Installation Picture

Table Ⅱ Multi-source drip irrigation treatments

Emitter spacing (cm)	Emitter flow(L/h)
40	2
40	4
60	2
60	4

Ⅲ RESULTS AND ANALYSIS

The process of two-point source drip irrigation infiltration was divided into two stages: the first stage was before the intersection of the two wetting fronts; the second stage was after the intersection of the two wetting fronts.

A. the shape of wetting soil

Fig.2 was the profile chart of wetting soil near the intersection along drip tape, with a space of 40cm, and a flow of 2L/h and 4L/h. this chart was one-fourth of the entire profile, the figures on the curves were wetting front migration time (min).

The wetting front shape near the intersection was approximated to two discrete half-oval or semicircular (Fig.2), which was related to the flow. When flow did not exceed the soil infiltration capacity, only matric potential gradient acted in the horizontal direction; in the vertical direction, not only matric potential gradient, but also the role of gravity gradient acted. Because very little water infiltrated in the initial stage, the function of gravity was not significant, the infiltration rates in both directions were very similar, the shape of wetting front was semi-circular (Fig.2a); When flow was larger than the soil infiltration capacity, surface water occurred, the migration velocity in the horizontal direction increased, but the depth of water in vertical decreased, the shape of wetting front was semi-elliptical (fig.2b).

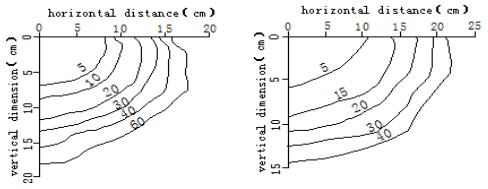

（a）flow 2L/h （b）flow 4L/h

Fig.2 Wetted front shape

Figure 3 was the profile chart of wetting soil after the intersection along drip tape, with a space of 40cm and 60cm, and a flow of 2L/h and 4L/h. Fig.3 was half of the whole profile, vertical axis was the interface between the two wetting fronts, the figures on the curves were wetting front migration time (min).

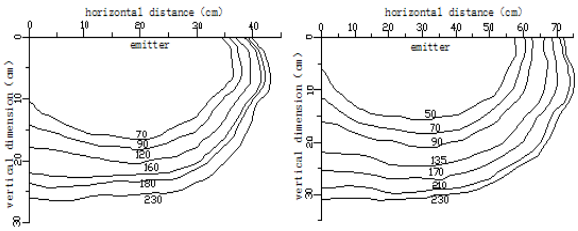

（a）Spacing 40cm, flow 2L/h (b) Spacing 40cm, flow 4L/h

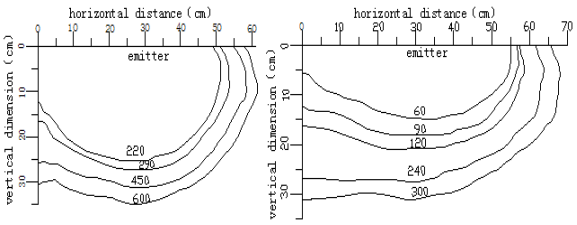

(c) Spacing 60cm, flow 2L/h (d) Spacing 60cm, flow 4L/h

Fig.3 wetting front migration process after convergence

As shown in Fig.3, the first intersecting point was at a certain depth below the surface. The greater the flow was, the smaller the space would be, the shorter the time required for intersection, the smaller the distance to the surface would be. Fig.3a showed that the convergence

*Corresponding author
E-mail address: renshumei@126.com; Supported by State Natural Science Fund: 50779068

time was 220min, the convergent point was 13.5cm below the surface; Compared with Fig.3b, if the flow rate doubled, the convergent time was reduced by 20min, the distance was reduced by 2.9cm; when the intersection occurred, the vertical distance between the center of emitters and convergent interface were respectively 7.4cm and 9.7cm larger than the situation in Fig.3b. When the emitters dropped for 320min, the differences were 0cm and-0.4cm. We could conclude from the above analysis that when the spaces were the same, large flow made the root system absorb water earlier, and wetting front in the vertical direction was larger, which was advantageous for the roots to absorb water. When the intersection occurred, the wetting front shaped like the letter W- meaning the wetting front of intersection interface bent significantly. The differences became smaller and smaller through time, which was because the water near intersection interface did not infiltrate to other side in the horizontal direction. Accelerating the migration of wetting front in the vertical direction and reducing the distance between them made the wetting fronts which between the two emitter into a zonal distribution; In Fig.3, under the condition of large spacing and small flow, the degree of wetting fronts intersection was low and the bending was obvious. It could also be obtained from Fig.3 that the flow and emitter spacing both had great influence on the bending of wetting front. The greater the flow and the smaller the spacing were, the lesser obvious the bending would be.

It could be concluded that the two-point source drip irrigation system with a space of 60cm and a flow of 4L/h was suitable for fruit trees and other deep-rooted plants. By analyzing experimental data, we could obtain that flow and emitter spacing had great influence on soil moisture at the intersection interface. For example, when Stopping irrigating over 24 hours, comparing soil moisture between spacing 60cm, flow 2L/h and 4L/h, It showed that in the center of emitter, the latter one was 0.82% more than the former one; in intersection interface, the latter one was 6.27% more than the former.

Therefore, the flow could be increased to meet water demand of deep-root plants.

B. The movement law of wetting front of two-point source drip

Fig.4 is the wetting front migration law graphs with the spacing 60cm, flow 2L/h and 4L/h, before stopping dripping below the emitters.

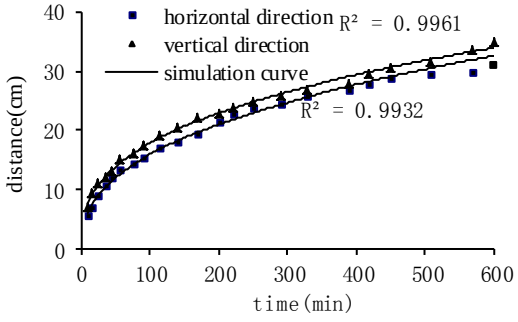

(a) flow 2L/h

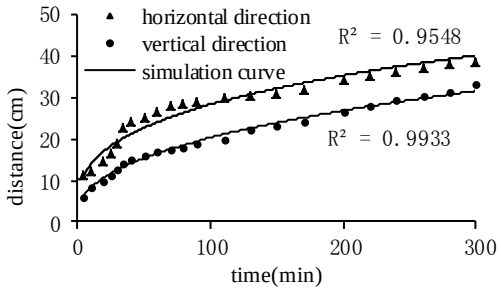

(b) flow 4L/h

Fig.4 the wetting front migration process in center of emitter

In Fig.4: with the increase of dripping time, both horizontal and vertical infiltrating distances of wetting fronts increased, the speeds decreased, which was due to the bulk of the wetted soil was small in the initial phase of infiltration, forming high matrix potential gradient at the front of wetting fronts, the rate of wetting front was quicker, With the increase of wetting body bulk, the matrix potential gradient was smaller, resulting in the decreasing of wetting front moving rate as the time went by [12].The measured data of various combinations were fitted, which showed that the mean square deviation of the power function relationship of the horizontal, vertical moving distance and infiltration time were larger than 0.95.

Through analyzing, the wetting front movement law of one-point source was not the same with the law of two-point-source, this was because the water at the intersection interface of two-point-source formed two wetted soils. Fig.5 shows the relation of the horizontal and vertical infiltrating distance and time, with a space of 40cm and a flow of 4 L/h. The figure showed that after convergence, as the time went on, the horizontal and vertical distance at the convergent interface increased, the rate decreased

*Corresponding author
E-mail address: renshumei@126.com; Supported by State Natural Science Fund: 50779068

gradually, which was the same with the law of one-point source. The linear function between the infiltrating distance (horizontal and vertical) and time existed by fitting the data, which was different from the results that the relation between the infiltrating distance (horizontal and vertical) and time was power function [16-17], was the same to the result of Sun Hainan's [18], this difference might be caused by different soil properties, flow rate, and spacing.

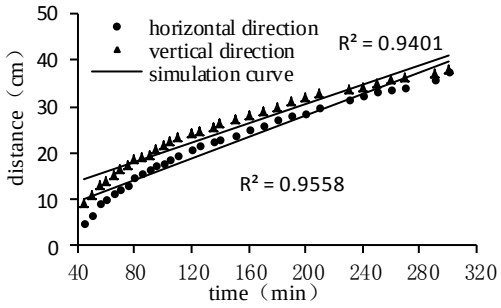

Fig.5 the interface migration process of interface

As the plants such as corn, wheat and cotton plants, the roots distribution of which are shallow, the depth of the roots are mostly no more than 40cm, and in the horizontal direction, As the plants such as corn, wheat and cotton plants, the roots distribution of which are shallow, the depth of the roots are mostly no more than 40cm, and in the horizontal direction, they mainly distribute in the cylinder with a radius within 20cm [19-22]. Using these four combinations of irrigation system to irrigate, when irrigation depth was 40cm, the time required were 724min, 545min, 625min and 378min, the horizontal distance calculated by the fitting equation were 30cm, 47cm, 34cm and 39cm. Using the equation to calculate the vertical distance at interface, the results of which were 45cm, 61cm, 72cm and 49cm. Considering root respiration and root distribution, the drip emitters spacing 40cm, flow of 4L/h could be selected for the irrigation system of shallow root plants, and the drip emitters spacing 60cm, flow of 4L/h could be selected for the irrigation system of deeper roots plants. The deep-rooted plants should be planted at the intersection interface of the two emitters, because the maximum moisture in vertical distance was at interference interface.

After stopping dripping, the water more than the field capacity still migrated, and water in wetting soil redistributed. Fig.6 shows the relation between the distance (vertical and horizontal) and time after dipping, with a space of 40cm, and a flow of 4L/h. The figure shows that both at the center of emitters and the intersection interface, the wetting front migration speed had undergone great changes after dripping. Especially in the horizontal direction, after stopping dripping, the speed became almost zero in a short time. This was due to deficiency of outside water source as driving forces; because of the gravity in the vertical direction, the wetting front was still migrating, infiltration water met the demand of deeper roots. At the intersection interface and the center of emitter, the wetting front migration distance and time after dripping water accorded with power function by analyzing experimental data, the fitting effect was shown in Fig.6.

When stopping irrigating over 24 hours, comparing the shape of spacing 60cm, flow 2L/h and 4L/h; as to flow 2L/h, the maximum length of wetting soil was 138.94cm, the vertical distance of emitter center was 43.5cm, the vertical intersection interface distance was 37.2cm; as to flow 4L/h, the corresponding length was 146.2cm, 40.1cm and 40.1cm. By comparing the two sets of measured data, It could been seem that the larger the flow was, the more uniform wetting front at bottom would be, and the larger the ratio of width to depth of wetted soil, which was according with the distribution of plant roots.

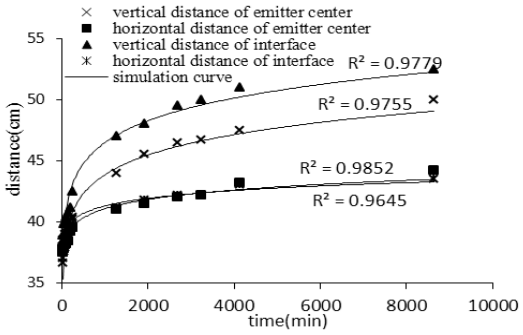

Fig.6 wetting front migration process after stopping dripping

C. The water distribution of wetting soil after intersection

It can be found from Comparing of test data that flow and distance have great influence on moisture at the interface. For example, when stopping dripping, comparing the spacing 60cm, flow 2L/h and 4L/h wet body moisture, at the central of emitter, the latter was 0.82% more than the former, at the interface the latter was6.27% more than the former. Therefore, the flow can be adjusted to meet the deep-root plant.

*Corresponding author
E-mail address: renshumei@126.com; Supported by State Natural Science Fund: 50779068

It was found that at the same depth, the maximum water content was at the interface, which could meet the needs of fine roots-fine roots were near to main root [6-8, 11]. Fig.7 shows the relation of the moisture content and time at the center of emitter and intersection interface, 25cm below the surface, emitters with a space of 40cm, and flow 4L/h. When irrigating 150min, the moisture was 11.8% at the interface, the emitter center was 22.21%, with the irrigation time, the more the intersection confluence, the larger the moisture at the interface. When irrigating 300min, the moisture reach 29.86% at the interface, the center emitter only 23.96%, the former was 5.9% more than the latter, This is one of the reason why planting the deep roots of plants at the interface.

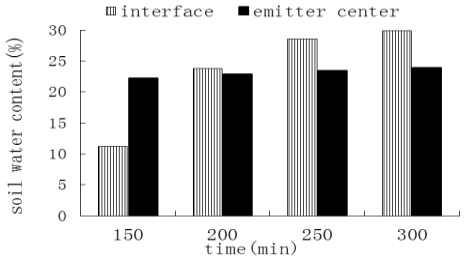

Fig.7 time and moisture content relationship(after convergence)

After stopping irrigating, the water in the wet body still migrating, but the migration law has been great changed, the wet body which was closer to surface, the moisture was larger than that in field, the water still moving as gravity action, so the moisture was decreasing and wetting front edge moisture content was increasing. Fig.8 shows the change of the soil moisture at the center of emitter, with a space of 40cm, and a flow of 4L/h, 15cm and 45cm below the intersection interface. Just when stopping dripping, the moisture was 23.24% in central emitter and 26.77% at the interface 15cm below the surface, after 4140min, corresponding moisture were 16.86% and 19.97%, which were smaller than the former and the larger drop at the interface as gravity action. When just stop irrigating, 15cm below the surface, the moisture was 18.26% at the interface and 9.5% in central emitter which was near to initial water content, after 4140min, corresponding moisture were 16.28% and 14.79%. Therefore, when using the drip irrigation system to irrigate, there was no need to continue supplying water until it reached the roots at the bottom, this might result in deep percolation and water waste, there were few roots exceeded a certain depth, and there was no need to irrigate too much water. So when the water infiltrates to a certain depth, stop irrigating, and make the infiltrated water of the wet body meet the water demand of deep roots.

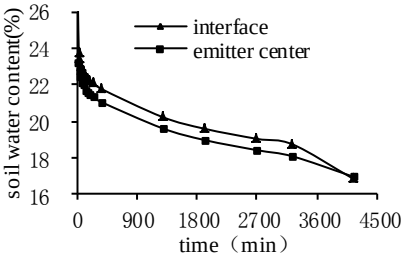

(a) underground 15cm

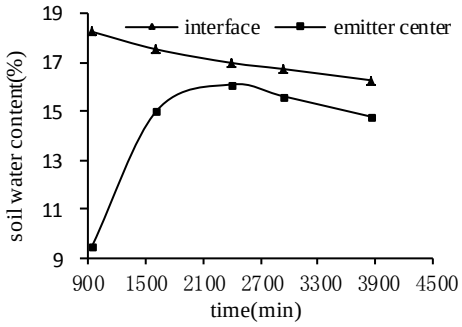

(b) underground 45cm

Fig.8 time and moisture content relationship

III. CONCLUSION

(1) Wetting front shape before intersection was two discrete half-oval or semi-circular, which was related to the flow. When the intersection occurred, the wetting front shaped like the letter “W”. After a certain time, the wetting soil between the two emitters was in a zonal distribution. Though analyzing, the greater the spacing and the greater the flow were, the more flat the wetting front would be; the smaller the spacing and the smaller the flow were, the more narrow and deeper the wetting fronts would be. Therefore, it could be designed different drip irrigation systems according to the distribution of plant roots, which could save water.

(2) Wetting front migration law: in the center of emitter, the distance (horizontal and vertical) and time accorded with power function; at the intersection interface after intersection, they accorded with linear relationship; after stopping dripping water, the distance (horizontal and vertical) and time accorded with the power function; at the interface after intersection, the wetting front migration rate at the interface was greater than the center of emitters. When the flow and spacing were appropriate, the

*Corresponding author
E-mail address: renshumei@126.com; Supported by State Natural Science Fund: 50779068

infiltrating distance at the interface in vertical direction was greater than that at the center of emitter. For deep-rooted plants, they should be planted at the interface of the two sub-interfaces.

(3) Distribution of soil moisture: the soil moisture at wetting front edge was close to initial soil water content; after intersection, the maximum water content at the same depth was at the interface; after stopping dripping, the wetting front continued to spread around; the soil water content near emitter decreased; while soil water content at the edge of wetting front increased; combining this law with the distribution of plant roots, stopping irrigating when the water reached a certain depth, infiltration water met the needs of deep root water requirements, which could prevent the phenomenon of deep leakage.

This experiment showed that the emitters with a space of 40cm and a flow rate of 4L/h drip irrigation systems could be used to irrigate shallow root plants, the emitters with a spacing of 60cm and a flow rate of 4L/h drip irrigation systems could be used to irrigate deep root plants such as fruit trees. By doing this, water could be saved and the water need of roots could be met.

REFERENCES

[1] Khan A A, Yitayew M, and W arrick A W, "Field evaluation of water and solute distribution from a points source," Irr and Drain Eng ,vol. 122, no. 4, pp. 221- 227,1996.

[2] Sun Haiyan, Li Mingsi, Wang Zhenhua and Xu Yonglin, "Influence factors on soil wetting front under point drip irrigation," Journal of Irrigation and Drainage, vol. 23, no. 3, pp. 15-17,2004.

[3] Fei Liangjun, Tan Qilin, and Wang Wenyan, "Infiltration Character and Influential Factor of Point Source Under Adequate Water Supply," Journal of Soil Erosion and Soil and Water Conservation, vol. 5, no. 2, pp. 71-74, 1999.

[4] Wang Zhirong, Wang Wenyan, Wang Quanjiu, and Zhang Jianfeng. "Experimental study on soil water movement from a point source," Journal of Hydraulic Engineering, no. 6, pp. 41-43, 2000.

[5] Li Xiaobin, and Sun Haiyan, "Experimental Research about Point Source Drip Irrigation Infiltration under Different Soil Texture," Science Technology and Engineering. vol. 8, no. 15, pp. 4293-4294, 2008.

[6] D.I.Sokalska, D.Z.Haman, A.Szewczuk, J.Sobota, and D.Deren, "Spatial root distribution of mature apple trees under drip irrigation system," Agricultural Water Management, no. 96, pp. 221- 227, 2009.

[7] Zhang Runfang, Zhang Aijun, Wang Hong, Zhang Haitao, and Zhou Damai. "Study on the law of pear root distribution in river ancient channel," Chinese Agricultural Science Bulletin, vol. 22, no. 4, pp. 383-384,2006.

[8] Zhou Zhenmin, "Drip irrigation test for apple trees in hilly and gully region and study on the water-saving irrigation system," Journal of Anhui Agricultural Sciences, vol. 36, no. 7, pp. 2722-2725, 2008.

[9] Yang Shengli, Liu Honglu, Hao Zhongyong, and Wu Wenyong, "Spatial distribution characteristics of cherry tree roots under border irrigation condition," Agricultural Engineering, vol. 25, no. 1, pp. 34-37, 2009.

[10] Zhang Miaoxian, "Optimum matching between soil infiltration body and crop root system under trickle irrigation," Chinese Journal of Eco-Agriculture, vol. 1, no. 13, pp. 103-104, 2005..

[11] Zhang Jinsong, Meng Ping, and Yin Changjun, "Spatial distribution characteristics of apple tree roots in the apple-wheat intercropping, "Scientia Silvae Sinicae, no. 4, pp. 31-33, 2002

[12] Wang Chengzhi, Yang Peiling, Ren Shumei, and Yang Linlin, "Laboratory experiment on the effects of super absorbent polymer on wetting front of drip irrigation," Agricultural Engineering, vol. 22, no. 12, pp. 3-5, 2006.

[13] Z. Gerstl, et al, "Distribution of Herbicides in Soil in a Simulated Drip Irrigation System," Irrigation Science, no. 2, pp. 157-164, 1981.

[14] Pascual Romero, Pablo Botia, and Francisco Garcia, "Effects of regulated deficit irrigation under subsurface drip irrigation conditions on vegetative development and yield of mature almond trees, "Plant and Soil, no. 260, pp. 172-177, 2004.

[15] J.E. FERNANDEZ, et al, "Drip irrigation soil characteristics and the root distribution and root activity of live trees," Plant and Soil, no. 133, pp. 240-250, 1991.

[16] Cheng Dongjuan. Fei Liangjun. and Yin Juan, "Reduction volume and interference interface area under film hole unilateral interference infiltration," Agricultural Engineering, vol. 23, no. 6, pp. 105-108, 2007.

[17] Liu Shijun, "Test and Study on Characteristics of Wetted Body of Bilateral Interference Infiltration of Film Hole," Underground Water, vol. 26, no. 1, pp. 65-68,2004.

[18] Sun Haiyan, and Wang Quanjiu. "Research for Soil Water Movement from Drip Irrigation Interference Infiltration," Journal of Soil and Water Conservation, vol 21. no. 2, pp. 117-118,2007.

[19] Wang Yan, Guo Huami, Fan Junchen, and Zhang Fusuo, "Genetic difference on Root Morphology under different Light Intensity and N Levels of Maize," Soils and Fertilizers Sciences in China, no. 3.pp 12-17.2001.

*Corresponding author
E-mail address: renshumei@126.com;

Supported by State Natural Science Fund: 50779068

[20] Yang Qinghua, et al, “Effect of Different Textural Soils on Root Dynamic Growth in Corn,” Acta Agriculturae Boreali-Sinica,vol 15. no. 3, pp. 89-92, 2000.

[21] SunHao,Li Mingsi,Ding Hao, Wang Chunxi, and Cui Weimin, “Experiments on effect of dripper dischargeon cotton-rootdistribution,” Agricultural Engineering, vol 25. no. 11, pp. 14-16, 2009.

[22] Mao Zhenqiang, Yu Zhenrong, Liu Yunhui, and Zhang Kefeng, “Comparative Study on Two Root Sampling Methods and Winter Wheat Root Distribution in Soil Profile,” Chinese Agricultural Science Bulletin, vol. 21. no. 5, pp. 265, 2005.

*Corresponding author
E-mail address: renshumei@126.com; Supported by State Natural Science Fund: 50779068

2011 International Conference on Mechanical, Industrial, and Manufacturing Engineering
Lecture Notes in Information Technology Vols. 1-2

Improving organizational resilience by applying information and communication technology: A case study

PhD student Aleksandar Aleksic, PhD Slavko Arsovski, PhD Miladin Stefanovic

Department of Industrial Engineering
Faculty of Mechanical Engineering,
University of Kragujevc
Sestre Janjic 6, Kragujevac, Serbia
{aaleksic & cqm & miladin}@kg.ac.rs

PhD Zora Arsovski

Department of Statistics and Informatics
Faculty of Economics,
University of Kragujevc
Đure Pucara Starog 3, Kragujevac, Serbia
zora@kg.ac.rs

***Abstract* - In the business conditions of today, many organizations experience a stressed need for rapid organizational response to changes, especially in crisis situations that can cause a significant loss of performance and competitiveness, and even work termination or a business crash. One way for organizations worldwide to deal with changes in business can be presented as organizational resilience. This paper emphasizes the importance of improving management of keystone vulnerabilities including connectivity and propose new model for that which consider information and communication technology (ICT). Through the case study are presented interconnections between organizational resilience indicators and ICT impact on them. The organizational resilience values are quantified which is base for calculations of further resilience improvement.**

Index Terms - ICT, resilience, keystone vulnerabilities

I. INTRODUCTION

The latest changes on the world market such as new trends and global crisis have a great impact on positioning organizations on the market. These new conditions caused many changes in the society and make very strong influence on the sustainability of many organizations. In order to overcome current challenges, many organizations based their business on the concept of organizational resilience [1]. It originated in the study of ecosystems [2], and later it was the subject of study in biological, economic, organizational and information systems.

In the literature that treats resilience, there are more ideas that identify concept of resilience from another point of view. In that way, the ecological resilience, engineering resilience, social resilience, and organizational resilience can be distinguished [3]. The history was dominated by empirical observations of ecosystem dynamics interpreted in mathematical models, developing into the adaptive management approach for responding to ecosystem change [4].

These concepts are developed in different scientific areas and have their own structure but their laws are increasingly common to the all concepts. Gallopin [5] proposed a conceptual model of vulnerability, resilience and the capacity of response. According this author, resilience is addressed to the capacity of response and system vulnerability. The significance of resilience is recognized worldwide, and its directions and advices are presented in many guidelines and standards [6].

The concept of the organizational resilience is given by McManus [7]. In her PhD thesis, organizational resilience is presented as a function of an organization's situation awareness, identification and management of keystone vulnerabilities and adaptive capacity in a complex, dynamic and interconnected environment. In this research, the quantification of organizational resilience is given through the three group indicators - Situation Awareness, Management of Keystone Vulnerabilities and Adaptive Capacity.

The contribution of this paper is developing the new model for improving connectivity through information and communication technology (ICT) in organizations. Connectivity is identified as indicator of the keystone vulnerabilities which is part of the overall resilience of the organization.

II. PROBLEM DESCRIPTION

Improved hardware and software solutions are becoming easy available and that is the reason of their relatively fast implementation in different segments of organizations. These solutions are usually computers with high performances, communication hardware and software, database systems and database management systems, etc., where the improvements are related to speed, capacity, security, accuracy, reliability, etc.

These new solutions can represent improvement and risk in the same time from the aspect of resilience. Researchers are making everyday effort in order to shed light on this scientific field.

Pham and Jordan [8] emphasize the importance of information technology (IT) capability, organizational capability and core capabilities from the resilience perspective. Also, they discuss about improvisation concept, especially in crisis situations. The positive result of improvisation is learning: (1) how to improve, (2) through the re-utilization of improvisation, (3) through the action component of improvisation. On the example of IT use in an insurance company, they analyzed the various situations and actions taken in the process of IT solutions improvisation. Also, they analyzed the necessary competencies at the level of the company for successful improvisation.

Scott et al [9] discuss the aspect of enabling technology for organizational resilience through the development of virtual teams using enabling technologies such as video - conferencing. They investigated supporting innovation in the virtual teams, video - conferencing with the influence on resilience. The examples of implementing XP in the multicultural conference, collaborative problem - based learning environment were found to be extremely important.

Consideration of the expansion of the resilience concept on the entire economy is generally given by Opstal [10]. In this report, Council on Competitiveness for corporate executives, the top 10 risk priorities are presented: (1) Reputation, (2) Business interruption, (3) Third party liability, (4) Supply chain failure, (5) Market environment, (6) Regulation / legislation, (7) Talent (8) Market risk, (9) Physical damage (10) Merger acquisition.

In many cases organizations integrate key business processes through the appropriate individual software solutions and thus enable complete flow of information in the organization. They are primarily focused on internal processes, but may include transactions with the environment (customers, suppliers). When this situation is analyzed from the resilience perspective it can be concluded that information and organization systems have much in common.

The basis for this is the fact that information system is model of a real system and therefore it reflects the structure and workflow of a real system business organization [11]. Relations among resilience components of organization (SAo – Situation Awareness of organization, KVo – Management of Keystone Vulnerabilities of organization and ACo – Adaptive Capacity of organization) and IS (SAi – Situation Awareness of IS, KVi – Management of Keystone Vulnerabilities of IS and ACi – Adaptive Capacity of IS) could be recognized as interconnected (figure 1).

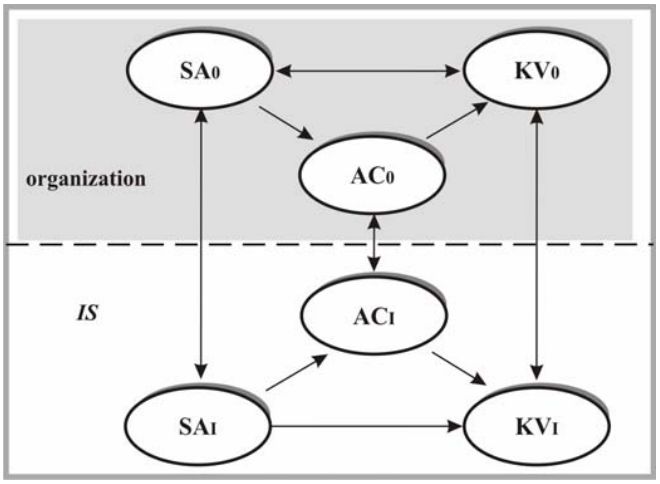

Fig. 1 Relations among resilience components of organization (O) and information system (I)

Resilience indicators are divided in three large groups and they have strong interdependence which is presented in the table 1.

TABLE I
INTERDEPENDANCE OF ORGANIZATIONAL RESILIENCE INDICATORS [5]

	SA1	SA2	SA3	SA4	SA5	KV1	KV2	KV3	KV4	KV5	AC1	AC2	AC3	AC4	AC5
SA1	+			+				+	+	+	+	+		+	+
SA2		+		+	+	+	+	+	+						+
SA3			+		+		+	+	+	+	+	+		+	
SA4				+	+	+		+	+	+			+		
SA5					+	+	+	+	+			+	+	+	+
KV1						+	+	+	+	+		+	+	+	+
KV2							+	+	+	+		+	+	+	+
KV3								+		+	+	+			+
KV4									+	+	+	+		+	
KV5										+	+	+		+	
AC1											+	+		+	+
AC2												+	+	+	+
AC3													+	+	+
AC4														+	+
AC5															+

From the perspective of improving resilience, there is a need for increasing knowledge and transparency of business processes in order to quickly detect a significant disturbance of the system, which can increase vulnerability of the system. The model which is going to be presented in this paper has intention to improve Management of Keystone vulnerabilities and indirectly Adaptive Capacity of organization.

III. THE MODEL FOR IMPROVING CONNECTIVITY IN ORGANIZATIONS

In accordance with the increased competition on the global level, organizations need to learn and quickly adapt to the new technologies such as the group of information and communication technology.

Favorable conditions of procurement and maintenance of ICT equipment affect the possibility of faster replacement of the old ICT equipment in the long run. Globalization has shorted the time of procurement of ICT equipment as well as time needed for installation and trial run. Maintenance of ICT equipment is increasing in the perspective of quality because of the wider service network, the speed of eliminating conflicts of ICT equipment and this all improve the reliability and effectiveness of organizations.

This creates the conditions for changing the nature of work, which is becoming less direct and more indirect because of increasing levels of automation. Also, the share of outsourcing in the realization of products has increasing nature. Application of ICT impacts on redefining of the organization in a way of [12]: new and improved product capabilities, new industry order and business models, improving the supply chain, impact on Manufacturing (WCM, LEAN, virtual manufacturing), impact on finance and accounting, impact on human resources management and training.

Better communication is a requirement when creation of relationships with external stakeholders (customers, suppliers, state, etc.) is the goal. This is typical of the role of ICT, which is provided by modern extranet solutions such as B2B, B2C, B2E, B2G, etc. In this case the integration is done at the level of data and information. Increased level of resilience can be obtained through the improved Management of Keystone Vul-

nerabilities. Model for improving connectivity which is one of identified vulnerability sources of every modern organization is presented on the figure 2.

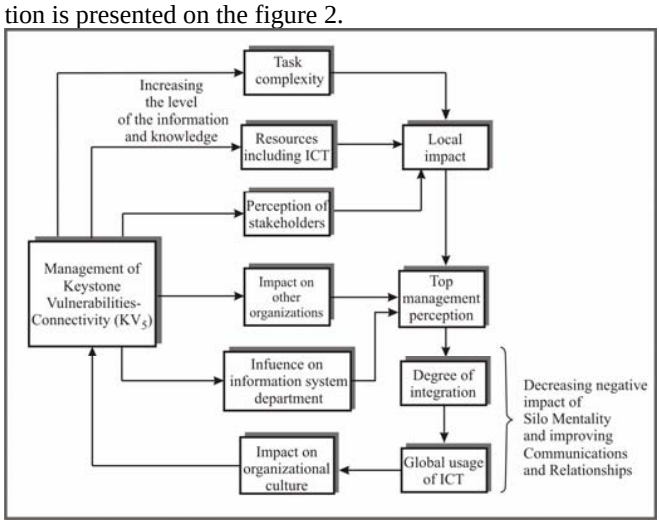

Fig. 2 The model for improving ICT impact on organizational culture

In this way organizational culture becomes more based on lateral relationships: Direct contacts, Task forces, Teams, Integrating roles, Managerial linking roles, Matrix organization.

With increased usage of ICT, the degree of process control is increased which is associated with a large number of organizational units (departments).

ICT impact on increasing awareness of the vulnerability and resilience through:

- the feeling of helplessness of employees in the event of failure or component of ICT fraying around ICT (ICT solutions must be reliable),
- trust in the fast recovery of organizational system that provides ICT solutions based on: built-in communication with stakeholders, use of specific procedures supported by ICT, confidence in technological improvements and"technological wizards".

Both characteristics of awareness of the vulnerability and resilience of ICT are present in every enterprise. Which of these is dominant depends on the degree of impact of ICT on the performance, sustainability and the concept of ICT in terms of organizational resilience.

IV. The Case Study in Serbia

The proposed model with reliable ICT solutions are applied to business processes in 12 organizations in Serbia. The organizations belong to the same economy branch and they match as small and medium organizations. They are selected in a random manner. Before that, the level of organizational resilience is obtained by using the model of McManus [5]. This quantification is based on the data collected during 2010. On the figures 3, 4 and 5 are presented obtained results before implementation of the model.

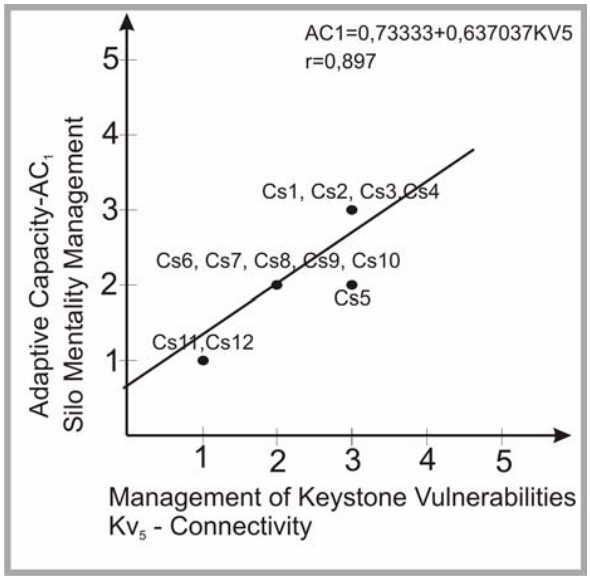

Fig. 3 The relationship between measured indicator of the Management of Keystone vulnerability (Connectivity) and indicators of Adaptive capacity (Silo Mentality Management)

On the figure 3 is presented relationship between Connectivity and Silo Mentality Management. The correlation between these indicators is very high and has the value 0.897. The analysis shows that dependence between these two indicators can be presented as linear. The dpt`shnmthat describes this relationship is: y = 0,73333 + 0,637037x.

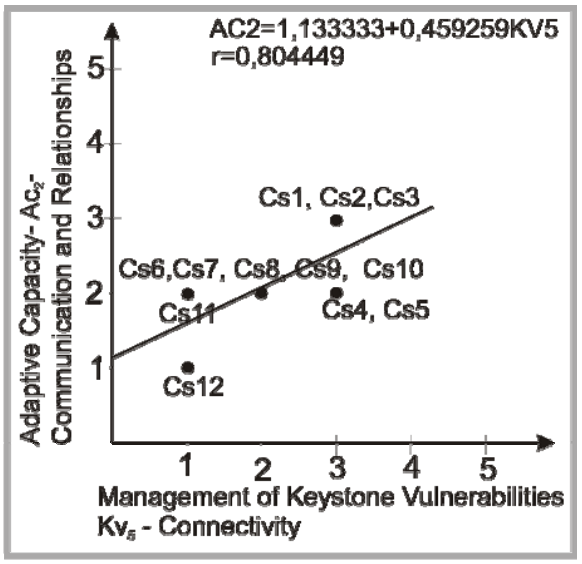

Fig. 4 The relationship between measured indicator of the Management of Keystone vulnerability (Connectivity) and indicators of Adaptive capacity (Communications and Relationships)

On the figure 4 is presented relationship between Connectivity and Communication and Relationships. The correlation between these indicators is very high and has the value 0.804449. The dpt`shnmthat describes this relationship is: y = 1,133333 + 0,459259x.

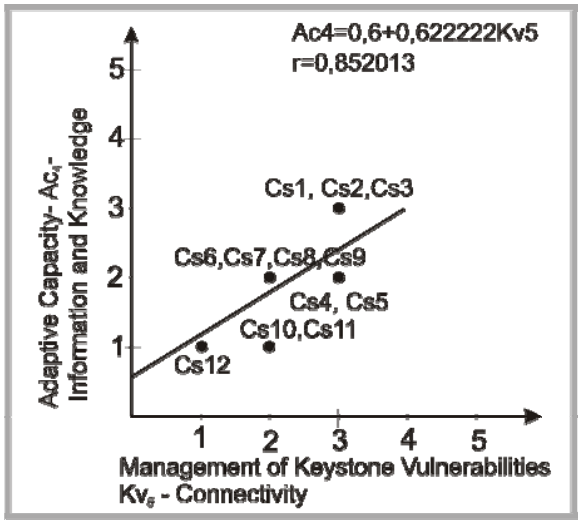

Fig. 5 The relationship between measured indicator of the Management of Keystone vulnerability (Connectivity) and indicator of Adaptive capacity (Information and knowledge)

On the figure 5 is presented relationship between Connectivity and Information and knowledge. The correlation between these indicators is very high and has the value 0.852013. The dpt `shmmthat describes this relationship is: y = 0,6 + 0,622222x.

According the calculated correlations and derived equations, improving of organizational resilience is going to be significant. For example, if improvement of Connectivity is 20%, indicators of Adaptive Capacity – Silo Mentality and Management, Communications and relationships, Information and Knowledge might increase from 5 to 20 %.

V. Conclusions

In the past few years the ICT sector are mainly developed on the basis of the process requests, although there were situations when offered ICT solutions exceeded the needs and requirements of the process. That was initial base for information systems designers to propose new ICT solutions for the development of certain processes.

In this research, the resilience of information systems in organizations wasn't the subject of analysis. Further research will be directed in that way.

This paper investigated the relations between Connectivity on the one side (which is identified as one of the organization's Keystone Vulnerability) and Silo Mentality Management, Communications and Relationships, Information and Knowledge on the other side (which are indicators of Adaptive Capacity). Since there is the strong impact between these resilience indicators, the new model for improvement is proposed. Expected improvements can be described in percents. It cannot be present as determined values because every organization may experience some difficulties during implementation of proposed model. In some cases, improvement of KV5 indicator – 10 % will impact on AC1 with increasing of minimum 10 % and in the other organization this expected ratio will be 10% - 20% but in some organizations it may happen that new model will not have so significant impact of AC indicators. Confirmation of expected results will be obtained in the next survey in the studied organizations. Further research will cover bigger example in order to acquire more precise and reliable data.

References

[1] McManus, S., T., Seville, E., Brunsdon, D., Vargo, J., Resilience Management: A Framework for Assessing and Improving the Resilience of Organisations, Resilient Organisations, Research Report 2007/01

[2] Folke, C., Resilience: The emergence of a perspective for social–ecological systems analyses, Global Environmental Change 16 (2006) 253–267

[3] Wang, C., H., Blackmore, J., Wang, X., Yum, K., K., Zhou, M., Diaper, C., McGregor, G. and Anticev J., Overview of resilience concepts, with application to water resource systems, eWater Cooperative Research Centre Technical Report 2009

[4] Folke, C., Carpenter, S., Walker, B., Scheffer, M., Elmqvist, T., Gunderson, L., & Holling, C.S. (2004). Regime shifts, resilience and biodiversity in ecosystem management. Annual Review of Ecology and Systematics, 35, 557-581.

[5] Gallopın, G., Linkages between vulnerability, resilience, and adaptive capacity, Global Environmental Change 16 (2006) 293–303.

[6] Organizational Resilience: Security, Preparedness, and Continuity Management Systems – Requirements with Guidance for Use, ASIS SPC.1 – 2009, American National Standard

[7] McManus. S. T., Organisational Resilience in New Zealand. PhD thesis, Department of Civil Engineering, University of Canterbury, New Zealand, 2007

[8] Pham, T., L., Jordan, E.: International Federation for Information Processing (IFIP), Volume 206, The Transfer and Diffusion of Information Technology for Organizational Resilience, eds. B. Donnellan, Larsen T., Levine L., DeGross J. (Boston: Springer), (2006) pp. 139-156.

[9] Scott, M., Sorcinelli, G., Gutierrez, P., Moffatt, C., DesAutels, P., The Transfer and Diffusion of Information Technology for Organizational Resilience, International Federation for Information Processing (IFIP), Volume 206, pp. 219-227, 2006.

[10] Opstal, D., (ed), Workshop on risk intelligence and resilience, Deloitte, Council of competitiveness, 2008.

[11] Arsovski, S., Arsovski, Z., Andre, P., Relation Between Organizational – And Information Resilience: A Way For Improvement of System Capacity, Proceedings 4th International Quality Conference, May 19th 2010, ISBN: 978-86-86663-49-8

[12] Arsovski, Z., Informacioni sistemi, Univerzitet u Kragujevcu, Ekonomski Fakultet, 2008., ISBN: 978-86-82203-85-8.

2011 International Conference on Mechanical, Industrial, and Manufacturing Engineering
Lecture Notes in Information Technology Vols. 1-2

Analysis of Multi Object Selection and Multi Resource Pool Task Assignment in Cloud Computing*

Jianming Yao
School of Business
Renmin University of China
Beijing 100872, China
jmyao@163.com

***Abstract* – Under the circumstance of cloud computing network, there is a higher flexibility of resource pool task flows needed for the diversity and stochastic character of service objects' demand and there is also a big challenge of the flexibility of resource pool task distribution needed for them. It is one of important ways to satisfy this demand by distributing multi resource pools to realize service task assignment at the same time. In order to settle the problems of the multi service object selection and its task assignment of multi resource pools flexibly from the systemic angle to build the rational computing network and improve the operational efficiency of cloud computing system, based on the analysis of the multi service object selection and assignment, a method by using decomposing algorithm to select the multi service objects and assign the service tasks among them are put forward in this paper in order to realize the comprehensive optimization object. Finally, the validity and feasibility of the method are tested by a decision case and there is a satisfaction result.**

Index Terms - Cloud computing. Multiple service object selection. Multiple task assignment. Decomposing algorithm.

I. INTRODUCTION

Cloud Computing is a new computing mode for business. Its character is to distribute the complicated computing tasks into the resource pool composed of lots of computers in order to make every application systems obtain their essential computing ability, the related memory room and software service [1]. The concept of Cloud Computing springs up in 2007 which is the development of Parallel Computing, Distributed Computing and Grid Computing. It is a business development and implement of these computing science concepts [1].

Comparing with the traditional computing science methods, Cloud Computing has obvious virtues. For example, it is a super computing mode based on internet and can integrate lots of data and processor resource of lots of distributed computers to work together. As a burgeoning method of sharing basic frame, it can provide every kind of IT service by linking huge system resource pools. This character warrants that enterprise can switch resources into the required application and visit the computer and memory system on demand [2].

The reason of people taking care of Cloud Computing is that its process power can compete with the super computer and it can provide huge data memory room based on little customer expenditure. Cloud Computing can help users not to worry about their IT cost will be washed out and can reduce the total energy sources consumption [2]. For all of these advantageous of Cloud Computing, we can see that this concept has been made attention by enterprises and scholars [1-5]. For example, reference [2] summarized six factors for promoting the development of Cloud Computing which are user-centered, task-centered, powerful, intelligent, the feasibility of infrastructure and the program ability of parallel software and so on. Reference [3] discussed the concept and characteristics of Cloud Computing from the perspective of building IT platform. Reference [4] and [5] give interpretation and analysis of Cloud Computing still from the perspective of basic concept.

Although more research discussed for the concept and characteristics of Cloud Computing, but still need the in-depth analysis of operational and implementation method for this computing model. In this regard, an important question is how to determine reasonably the dynamics task allocation among multiple users and multiple resource pool and this is a classic optimization problem of many to many options and task allocation. In order to explore an effective way to optimize, this paper proposes a modelling method and using decomposed arithmetic [6] to solve the problem based on the analysis of the task distribution in resource pool.

II. ANALYSIS OF TASK DISTRIBUTION IN RESOURCE POOL

In Cloud Computing, in a given period of time, for more specific service objects, selecting more than one resource pool to achieve the decomposition and allocation of service tasks is an effective means to enhance operational efficiency. This is determined by the complexity deployment and distribution caused by the diversified needs of Cloud Computing. As a specific period of time until, the required target of service objects to resource characteristics of Cloud Computing and to the operational efficiency of service are different so that different resource pool in different service objects, its comprehensive service cost, comprehensive service efficiency and other evaluation for both supply and demand yield are

* This work is partially supported by the national natural science foundation of China under Grant #71072148, the national natural science foundation of Beijing, China under Grant #9102011 and the national social science foundation of China under Grant #08BJY078.

different. In this case, selecting rationally multi service objects to make task coordination and distribution of resource pool dynamically from the prepared service objects can not only reduce the total cost of the cloud computing operating system, improve system efficiency, but also improve the flexibility of service flow of Cloud Computing.

To make comprehensive analysis on resource allocation in multi resource pools and makes full optimization have more important characters. The following will establish an allocation optimization model and validated algorithm to describe and analyze this multi-target selection and resource allocation optimization process in task pool.

III. OPTIMIZATION MODEL

We suppose that in Cloud Computing, the number of every kinds of resource pools can be integrated that provided by service main body in some special period is n, we record them as (1, 2, ..., n). The number of the prepared service objects is w. As the comprehensive service cost, comprehensive service efficiency and other characters reflecting the service demand of different service set composed dynamically of different resource pools are different, so, how to select and make decision to the styles and amount and to make rational task scheduling and distribution are most important. Suppose that in this decision process, we will choose m prepared service objects to meet their service demands of the comprehensive service characters of n resource pool.

Let eij denote the comprehensive indexes of the service object i(i=1,2,…,w) to different resource pool j(j=1,2,…,n) in Cloud Computing system. They are including several indexes such as the comprehensive service cost, comprehensive service efficiency and other needed indexes. The smaller the better its value is. We introduce two groups of 0-1 variables:

$$y_i = \begin{cases} 1, & \text{selecting } i \text{ as service object} \\ 0, & \text{not} - \text{selseting } i \end{cases}$$

$$x_{ij} = \begin{cases} 1, & \text{the service of } i \text{ is provided by } j \\ 0, & \text{orherwise} \end{cases}$$

Then the above problem can be described as:

$$\min \sum_{i=1}^{w}\sum_{j=1}^{n} e_{ij}x_{ij} \tag{1}$$

$$s.t. \quad \sum_{i=1}^{w} x_{ij} = 1, \tag{2}$$

$$\sum_{i=1}^{w} y_i = m, \tag{3}$$

$$x_{ij} \le y_i, \tag{4}$$

$$x_{ij}, y_i \in \{0,1\} \tag{5}$$

$$i = 1,2,\cdots,w;\ j = 1,2,\cdots,n$$

Equation 1 is the objective function that selecting m service objects (see the constraint 3) to complete the dynamic task allocation and make the comprehensive index minimum. Constraint 2 ensures that every prepared service object should be served by a particular resource pool; Constraint 4 ensures that if we not choose service object i, there would be not j serve to i. We introduce the following solution method [6] to solve this problem.

IV. SOLUTION

A. Solution process

We make the constraint (2) as a complex restriction. To every $\pi_0 = (\pi_{01},\cdots,\pi_{0n})$, we can define problem $R(\pi_0)$ as follows:

$$\min \sum_{i=1}^{w}\sum_{j=1}^{n} c_{ij}x_{ij} + \sum_{i=1}^{w}\sum_{j=1}^{n} \pi_{0j}x_{ij} - \sum_{j=1}^{n} \pi_{0j}$$

$$\text{s.t.} \quad \sum_{i=1}^{w} y_i = m,$$

$$x_{ij} \le y_i,$$

$$x_{ij}, y_i \in \{0,1\};\ i = 1,2,\cdots,w;\ j = 1,2,\cdots,n$$

We know that the best solution of $R(\pi_0)$ meet the following relationship:

$$x_{ij} = \begin{cases} y_i, & c_{ij} + \pi_{0j} \le 0, \\ 0, & \text{otherwise} \end{cases} \tag{6}$$

Therefore, if we define:

$$\bar{c}_{ij} = \min\{c_{ij} + \pi_{0j}, 0\},\quad \bar{c}_i = \sum_{j=1}^{n} \bar{c}_{ij},$$

Then $R(\pi_0)$ can be written as:

$$\min \sum_i \bar{c}_i y_i, \tag{7}$$

$$s.t. \quad \sum_{i=1}^{w} y_i = m, \tag{8}$$

$$y_i \in \{0,1\};\ i = 1,2,\cdots,w \tag{9}$$

If we find the best solutions of the Equations (7) to (9), we can determine the value of the x_{ij} by equation (6). Then if we assume that $\bar{c}_i$ has be arranged as:

$$\bar{c}_1 \le \bar{c}_2 \le \cdots \le \bar{c}_w,$$

We can prove that the best solution y_0 of $R(\pi_0)$ is

$$y_{01} = y_{02} = \cdots = y_{0m} = 1,$$

$$y_{0j} = 0, \quad j = m+1,\cdots,n.$$

We can determine the best solution $\{y_{0i}, x_{0ij}\}$ of $R(\pi_0)$ through this and equation (6).

We define the sub-program $P(y)$ to every 0-1 vector $y = (y_1,\cdots y_n)$ which meets the equation (3) as:

$$x_0(y) = \min \sum_{i=1}^{w}\sum_{j=1}^{n} c_{ij}x_{ij} \tag{10}$$

$$s.t. \quad \sum_{i=1}^{w} x_{ij} = 1, \tag{11}$$

$$0 \le x_{ij} \le y_i,\ i = 1,2,\cdots,w;\ j = 1,2,\cdots,n \tag{12}$$

Define the spouse program $D(y)$ of $P(y)$ as:

$$\max \sum_{j=1}^{n} \pi_j - \sum_{i=1}^{w}\sum_{j=1}^{n} \pi_{ij}y_i$$

$$s.t. \quad \pi_j - \pi_{ij} \le c_{ij},$$

$$\pi_{ij} \ge 0, \quad i = 1,2,\cdots,w;\ j = 1,2,\cdots,n$$

We can write the best solutions of $P(y)$ and $D(y)$ as to $R(\pi_0)$. That is we suppose y meet:

$$y_1 = y_2 = \cdots = y_m = 1,$$

$$y_{m+1} = y_{m+2} = \cdots = y_n = 0.$$

Define $c_{i,s} = \min_{1 \le i \le m} c_{is}, s = 1,2,\cdots,n$, then the best solution of $P(y)$ is:

$$i = 1,2,\cdots,w;\ \ j = 1,2,\cdots,n$$

We can determine the best solution of $D(y)$ as:

$$\pi_j = c_{i_j j},\ \ j = 1,2,\cdots,n \ ,$$

$$\pi_{ij} = 0, \quad i = 1,2,\cdots,m;\ \ j = 1,2,\cdots,n$$

$$\pi_{ij} = \max\{0, c_{i,j} - c_{ij}\},$$

$$i = m+1,\cdots,w,\ \ j = 1,2,\cdots,n$$

Set all the acmes of the polyhedron

$$U = \left\{\pi = (\pi_j, \pi_{ij}) \middle| \pi_j - \pi_{ij} \le c_{ij}, \pi_{ij} \ge 0, \right\}$$

$$i = 1,2,\cdots,w;\ \ j = 1,2,\cdots,n$$

are π^t , $t \in T_U$, then the problems (1) to (5) can be transformed to a equivalent IP:

$$\min_y \quad x_0(y)$$

$$= \min_y \min\left\{\sum_{i=1}^{w}\sum_{j=1}^{n} c_{ij}x_{ij} \middle| x_{ij} \quad \text{meet} \quad \text{equation1}1,12\right\}$$

$$= \min_y \max\left\{\sum_{j=1}^{n}\pi_j - \sum_{i=1}^{w}\sum_{j=1}^{n}\pi_{ij}y_i \middle| (\pi_j, \pi_{ij}) \in U\right\}$$

$$= \min\left\{x_0 \middle| \sum_{j=1}^{n}\pi_j - \sum_{i=1}^{w}\sum_{j=1}^{n}\pi_{ij}y_i \le x_0, (\pi_j, \pi_{ij}) \in U,\right.$$

$$\left.\sum_{i=1}^{w} y_i = m, y_i \in \{0,1\}\ \right\}$$

$$= \min\left\{x_0 \middle| \sum_{j=1}^{n}\pi^t_j - \sum_{i=1}^{w}\sum_{j=1}^{n}\pi^t_{ij}y_i \le x_0, t \in T_U,\right.$$

$$\left.\sum_{i=1}^{w} y_i = m, y_i \in \{0,1\}\ \right\}$$

To every $Q \subseteq T_U$, we define the relaxation problem $P(Q)$ of (IP) as:

$$x_0(Q) = \min\left\{x_0 \middle| \sum_{j=1}^{n}\pi^t_j - \sum_{i=1}^{w}\sum_{j=1}^{n}\pi^t_{ij}y_i \le x_0, t \in Q,\right.$$

$$\left.\sum_{i=1}^{w} y_i = m, y_i \in \{0,1\}\ \right\}$$

B. Steps of Solution

Based on the above analysis, we give the steps of decompose algorithm as follows:

Step 1: take a y and let it meet

$$\sum_{i=1}^{w} y_i = m, y_i \in \{0,1\}$$

Solve $P(y)$ and $D(y)$, let (π^1_j, π^1_{ij}) the best solution of $D(y)$, let $Q = \{1\}, i = 1$.

Step 2: Solve $R(\pi^i)$, let its best solution be (x^*_{ij}, y^*_i).

Step 3: Solve $P(y^*)$ and $D(y^*)$, let their best solutions be $\left(\bar{x}_{ij}, y^*_i\right)$. and (π^*_j, π^*_{ij}), let their objective functions be $x_0(y^*)$.

Step 4: if $j = 1,2,\cdots,n$, we have $\pi^*_j = \pi^i_j$, then stop the algorithm. $\left(\bar{x}_{ij}, y^*_i\right)$. is its best solution. Otherwise, solve $R(\pi^*_j)$, let its best solution be $\left(\bar{x}^*_{ij}, \bar{y}^*_i\right)$.

Step 5: if $i = 1,2,\cdots,w$, we have $\bar{y}^*_i = y^*_i$, then stop the algorithm. $\left(\bar{x}_{ij}, y^*_i\right)$. is the best solution. Other wise turn to Step 6.

Step 6: we select one from Step 6.1 and Step 6.2.

Step 6.1: let $\pi^{i+1}_j = \pi^*_j$, $Q = Q \cup \{i+1\}$, $i = i+1$, turn to Step 2.

Step 6.2: solve $P(Q)$, let its best solution be $\bar{y}$, its best value be $x_0(Q)$.

Step 7: solve $P\left(\bar{y}\right)$ and $D\left(\bar{y}\right)$, let their best solutions be $\left(x'_{ij}, \bar{y}_i\right)$ and $\left(\bar{\pi}_i, \bar{\pi}_{ij}\right)$

Step 8: if $x_0\left(\bar{y}\right) = x_0(Q)$, then stop. $\left(x'_{ij}, \bar{y}_i\right)$ is the best solution of the multi-supplier selection problem in multi-material. Otherwise, let $\pi^{i+1}_j = \bar{\pi}_j$, $Q = Q \cup \{i+1\}$, $i = i+1$, turn to Step 2.

We can see from the two selections in Step 6 that we can solve the problem through different ways.

V. Application and Case Analysis

To test the effectiveness and feasibility of the method, here give a simple example to verify. In a specific period of time, there are 10 enterprises need to obtain information resource services via Cloud Computing. Main service suppliers provide dynamically 15 kinds of resource pools for its use based on different characteristics of every enterprise and their service demand. First, we need to select four resource pools to allocate the tasks of 15 enterprises based on the character of the resource pool dynamic set. To facilitate resource management, improve operational efficiency, we make decision that each resource pool will serve one enterprise for the time being, but the same enterprise can also obtain service from multi resource pools. Let the comprehensive index e_{ij} (this value has been normalized) denote different enterprise obtaining different service from different resource pool as shown in Table 1 and 2.

At the same time, let w =10; m =4; n =15 by analyzing from the above data.

We take the beginning value $y = (y_1, y_2, \cdots, y_{10}) = (0,1,1,0,0,0,1,0,1,0)$ according to the solving steps.

TABLE I

VALUE OF THE COMPREHENSIVE INDEX e_{ij}

Resource pool / Enterprise	1	2	3	4	5	6	7	8
P_1	0.909	0.447	0.291	0.712	0.383	0.810	0.643	0.804
P_2	0.885	0.357	0.233	0.373	0.597	0.737	0.969	0.292
P_3	0.748	0.221	0.897	0.082	0.012	0.542	0.749	0.248
P_4	0.718	0.528	0.157	0.632	0.545	0.675	0.799	0.797
P_5	0.678	0.453	0.232	0.675	0.655	0.565	0.500	0.876
P_6	0.535	0.315	0.266	0.999	0.987	0.876	0.453	0.234
P_7	0.134	0.509	0.731	0.414	0.543	0.456	0.678	0.789
P_8	0.925	0.295	0.795	0.290	0.680	0.672	0.454	0.458
P_9	0.413	0.515	0.876	0.961	0.113	0.304	0.931	0.777
P_{10}	0.491	0.309	0.129	0.988	0.711	0.388	0.246	0.675

TABLE II

VALUE OF THE COMPREHENSIVE INDEX e_{ij}

Resource pool / Enterprise	9	10	11	12	13	14	15
P_1	0.493	0.346	0.961	0.103	0.389	0.974	0.793
P_2	0.730	0.821	0.680	0.650	0.965	0.206	0.748
P_3	0.710	0.339	0.810	0.423	0.876	0.543	0.987
P_4	0.336	0.748	0.231	0.667	0.455	0.617	0.567
P_5	0.987	0.676	0.343	0.234	0.123	0.676	0.650
P_6	0.987	0.234	0.400	0.876	0.500	0.560	0.346
P_7	0.686	0.992	0.673	0.490	0.278	0.413	0.569
P_8	0.555	0.808	0.453	0.667	0.342	0.104	0.432
P_9	0.492	0.533	0.258	0.952	0.901	0.734	0.890

We select the 2, 3, 7, 9 enterprises to obtain the services, by calculate $P(y)$ and $D(y)$, through the Step 2 to 8, the best solution is:

$$\begin{bmatrix}
0,0 & 0,0 & 0,0 & 0,0 & 0,0 & 0,0 & 0,0 & 0,0 & 0,0 & 0,0 & 0,0 & 0,0 & 0,0 & 0,0 & 0,0 \\
0,0 & 0,0 & 0,0 & 0,0 & 0,0 & 0,0 & 0,0 & 0,0 & 0,0 & 0,0 & 0,0 & 0,0 & 0,0 & 0,0 & 0,0 \\
0,1 & 1,1 & 0,1 & 1,1 & 1,1 & 0,1 & 0,1 & 1,1 & 0,1 & 1,1 & 0,1 & 0,1 & 0,1 & 0,1 & 0,1 \\
0,1 & 0,1 & 0,1 & 0,1 & 0,1 & 0,1 & 0,1 & 0,1 & 1,1 & 0,1 & 1,1 & 0,1 & 0,1 & 0,1 & 0,1 \\
0,0 & 0,0 & 0,0 & 0,0 & 0,0 & 0,0 & 0,0 & 0,0 & 0,0 & 0,0 & 0,0 & 0,0 & 0,0 & 0,0 & 0,0 \\
0,0 & 0,0 & 0,0 & 0,0 & 0,0 & 0,0 & 0,0 & 0,0 & 0,0 & 0,0 & 0,0 & 0,0 & 0,0 & 0,0 & 0,0 \\
0,0 & 0,0 & 0,0 & 0,0 & 0,0 & 0,0 & 0,0 & 0,0 & 0,0 & 0,0 & 0,0 & 0,0 & 0,0 & 0,0 & 0,0 \\
0,1 & 0,1 & 0,1 & 0,1 & 0,1 & 0,1 & 0,1 & 0,1 & 0,1 & 0,1 & 0,1 & 0,1 & 1,1 & 1,1 & 1,1 \\
0,0 & 0,0 & 0,0 & 0,0 & 0,0 & 0,0 & 0,0 & 0,0 & 0,0 & 0,0 & 0,0 & 0,0 & 0,0 & 0,0 & 0,0 \\
1,1 & 0,1 & 1,1 & 0,1 & 0,1 & 1,1 & 1,1 & 0,1 & 0,1 & 0,1 & 0,1 & 1,1 & 0,1 & 0,1 & 0,1
\end{bmatrix}$$

That is we select the enterprise 3,4,8,9 to provide service and the total index is 3.861. The task distribution is shown in Table 3.

TABLE III

THE TASK DISTRIBUTION

	1	2	3	4	5	6	7	8	9	10	11	12	13	14	15
P_3		√		√	√			√		√					
P_4									√		√				
P_8													√	√	√
P_9	√		√			√	√					√			

Note: '√' is the distribution of the service tasks.

VI. CONCLUSION

Cloud computing is not only a product of the development of modern computer science, but also an effective mean for enterprise obtain complex market information and make scientific decision. How to give a dynamic allocation scientific and rational decision of dynamically distributing multi resource pools to multi users is of great significance in achieving the task decomposition, avoiding information congestion and improving the computational efficiency. This paper presents an adaptive multi-target strong resource pool selection and multi-task allocation decomposition algorithm. From the application results, this method has the advantage of global optimization from a systemic point of view. It can facilitate comprehensive evaluation of multi-object selection and service needs of the task allocation decision-making, can improve the selection efficiency of the process of rationing and can enhance the reliability of decision-making results. In the analysis based on the ideas and methods, we can deploy in-depth analysis and research around Cloud Computing.

REFERENCES

[1] P. Wang, and J. Zhang, "Cloud Computing and Network Study", *Modern Educational Technology*, vol. 18, no. 11, pp. 81-84, November 2008.

[2] K. Li, "Cloud Computing", *China Education Network*, no. 6, p. 34, June 2008.

[3] B. Rajkumar, S. Chee, V. Srikumar, B. James, and B. Ivona, "Cloud Computing and Emerging IT Platforms: Vision, Hype, and Reality for Delivering Computing as the 5th Utility", *Future Generation Computer Systems*, vol. 25, no. 6, pp. 599-616, June 2009.

[4] B. Hayes, "Cloud Computing", *Communications of the ACM*, vol. 51, no. 7, pp. 9-11, July 2008.

[5] B. Guptill, W. McNee, "SETS THE STAGE FOR 'Cloud Computing'", *Financial Executive*, vol. 24, no. 5, pp. 37-44, May 2008.

[6] Z. Chen, Z. Xu "Computer Mathematics-Computational Complexity Theory and NPC, NP Hard Problem Solving", Beijing: Science Press, 2001, pp. 221-234.

2011 International Conference on Mechanical, Industrial, and Manufacturing Engineering
Lecture Notes in Information Technology Vols. 1-2

Determination of Step-Over in Magnetic Abrasive Polishing of AZ31B to Get the High Precision Surface

Jae-Seob Kwak
Department of Mechanical Engineering
Pukyong National University
San 100, Yongdang-Dong, Nam-Gu, Busan, South Korea
jskwak5@pknu.ac.kr

Tae-Hui Kim
Graduate School of Mechanical Engineering
Pukyong National University
San 100, Yongdang-Dong, Nam-Gu, Busan, South Korea
thkin@naver.com

***Abstract* - This study focuses on determination of the optimal step-over value in MAP of AZ31B magnesium alloy. Since the different magnetic flux density and tangential force are generated according to distance from the center of magnetic tool, improved surface roughness is different. Therefore, to get the uniform surface roughness on workpiece, it is necessary to determine the optimal value of step-over. In this study, the second order response surface models for surface roughness according to distance from tool center were developed, and then optimal parameters with the maximum improved surface roughness for each radius were determined by the genetic algorithm and simulated annealing. To get the uniform surface roughness, the best step-over was calculated using improved surface roughness curve. As a result, it was found that step-over value of 6.6mm was suitable for MAP of magnesium alloy.**

Index Terms - Genetic algorithm, Simulated annealing, Magnetic abrasive polishing, Step-over

I. INTRODUCTION

Magnetic abrasive polishing(MAP) is a relatively new super finishing technique primarily used for producing nanometric level of surface finish especially on the non-magnetic material and hard material. MAP is a process in which workpiece surface is smoothened by removing the material in the form of micro chips by abrasive particles in the presence of magnetic field in the finishing zone [1-2]. The working gap between workpiece and inductor is filled with mixture of ferromagnetic particles and abrasive powder well known as magnetic abrasive particles. These particles form a flexible magnetic abrasive brush which does not require dressing. This flexible tool can remove a very small amount of materials from a workpiece and then a better surface can be produced after polishing the workpiece without damages on the surface [3-4]. Nevertheless, it is very difficult to adopt MAP for polishing of non-magnetic materials because magnetic force on the working field determines the efficiency of this process. Therefore, it is necessary to increase magnetic force on the surface of non-magnetic material during MAP process. Kwak [5] showed that improving strategy of magnetic force using permanent magnet, which installed in the opposite side of non-magnetic material, was very effective for the better surface roughness. Moreover, in previous study, it was obvious that the magnetic flux density was different in accordance with distance from center of tool and the location of the maximum value was verified as a diameter/4 distance from the center. These results bring out the difference of surface roughness on the working area after MAP. Therefore, to resolve this problem, proper step-over of tool path for MAP of plate workpiece have to be determined.

In this study, to determine the optimal step-over value in MAP of AZ31B magnesium alloy as one of non-magnetic materials, the second order response surface models for surface roughness according to distance from tool center were developed, and then optimal parameters with the maximum improved surface roughness for each radius were determined by the genetic algorithm and simulated annealing. And then, to get the uniform surface roughness, the best step-over was calculated using improved surface roughness and the radial distance-surface roughness curve based on the optimal process condition was developed.

II. CORRELATION BETWEEN MAGNETIC FORCE AND SURFACE ROUGHNESS IN MAP PROCESS

Magnetic abrasive polishing process has total cutting force (F) that consists of normal force (F_n) by magnetic flux density and tangential force (F_h) by rotation force of inductor.

Material removal in the MAP process as a function of the number of cycle is as follows:

$$M = C\frac{\Delta fnN}{H_{mt}\pi\tan\theta}\sum_{i=1}^{2n}(1-\frac{R_a^i}{R_a^0})l_\omega \tag{1}$$

According to surface profile, the relationship between the surface roughness and the stock removal after *n* number of cycle is expressed as

$$R_a^i = R_a^{i-1} - \frac{1}{l_\omega}\sqrt{R_a^{i-1}M} \tag{2}$$

$$R_a^i = R_a^{i-1} - \frac{1}{l_\omega}\left(R_a^{i-1}\right)^{1/2}C'\sqrt{\frac{\Delta fnN}{H_{mt}\pi\tan\theta}\sum_{i=1}^{2n}(1-\frac{R_a^i}{R_a^0})l_\omega} \tag{3}$$

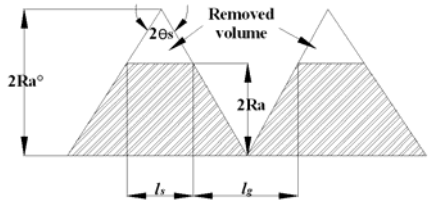

Fig. 1 Shape of scratch machined

Eq. (3) is a combination of the Eqs. (1) and (2) that mean the average surface roughness.

Where, $C' = C^{1/2}$, l_w is the total length of the workpiece, H_{mt} is the hardness of workpiece and N is the number of magnetic abrasives that are participated in machining. And the force acting on a cutting edge is given as

$$\Delta f = \frac{f}{n} = \frac{D^2\pi}{4n} P \tag{4}$$

Where n is the number of cutting edges participating in the machining for a magnetic abrasive. And P is machining pressure. Eq. (4) can be rearranged for the force acting on a cutting edge as follows [6]:

$$\Delta f = \frac{D^2\pi}{4n}(\mu_0 \frac{H_a^2}{4} \frac{3\pi(\mu_m - 1)\omega}{3(2+\mu_m) + \pi(\mu_m - 1)\omega}) \tag{5}$$

Where, D is diameter of abrasive particle, μ_m is relative permeability, ω is volume ratio of magnetic abrasive particle and H_a is the force of magnetic flux in air gap.

III. Characteristic of MAP for AZ31B Magnesium Alloy According to Radial Distances

In MAP of plate surface, the magnetic flux density occurs differently on the surface of workpiece because the magnetic flux density on the surface of inductor has different value according to radial distance from the center of tool. Fig. 2 shows the magnetic flux density and tangential force according to the change of radial distance in MAP of non-magnetic materials. Thus, because of that result, the efficiency of MAP is changed according to radial distance.

In this study, to evaluate the properties of MAP according to radial distance of inductor, MAP of AZ31B plate was performed under the experimental conditions listed in Table I. Fixed experimental conditions for evaluation of MAP parameters were indicated as shown in Table II. Magnetic abrasives mixed with ferromagnetic particles and abrasives in silicone gel were used in this experiment as a tool for polishing. The ferromagnetic particle was iron powder of 150 ㎛, and the green carbide(GC) of 8.5㎛ was chosen as abrasives. The silicone gel could efficiently constrain iron powder and GC grain on the surface of non-magnetic material because of high viscosity of silicone gel medium. Given that the shorter working gap can identify the larger magnetic force in MAP process, the working gap between the magnetic tool and work material was set to 1.5mm. The diameter of inductor tool was 20mm. In the result of experiment, it indicated that the surface roughness was clearly different in accordance with the change of radial distance. Fig. 3 shows the micrograph of surface at a point of each radial distance after MAP. As shown in Fig. 4, it was obvious that the surface roughness was clearly different in accordance with the change of radial distance.

IV. Development of RSM and Parameter Optimization using GA and SA

A. *Parameter design and response surface model*

For evaluating that which parameter has most effect on surface roughness according to radial distance, and developing the second order response surface model at each radial distance, Taguchi's design method was used in this study. The fixed experimental condition was listed in Table II.

A current of table, a current of tool, a spindle speed and weight of magnetic abrasive were considered as experimental factors which would influence the surface roughness on the second generation MAP of AZ31B. All selected experimental factors were changed at three levels as listed in Table III. The factor of the current of table means amount of a current supplied into electro-magnet arranged in electro-magnet array table. The magnetic flux density was about 45mT when the supplied current was 0.8A. On the other hand, when a current of tool which means amount of a current supplied into the inductor was 2.5A, the maximum magnetic flux density was about 100mT. The spindle speed was used in the range of 900 to 1,500rpm since most abrasive particles could easily fly from working area in high rotational speed over 1,600rpm. The weight of abrasive is represented as total amount of magnetic abrasives including iron powder, abrasive and silicone gel medium. A Taguchi's L_{27} (3^4) orthogonal array that includes the four factors and three levels was applied. In this study, two-factor interaction was concerned with effectiveness factor on the second generation MAP of AZ31B.

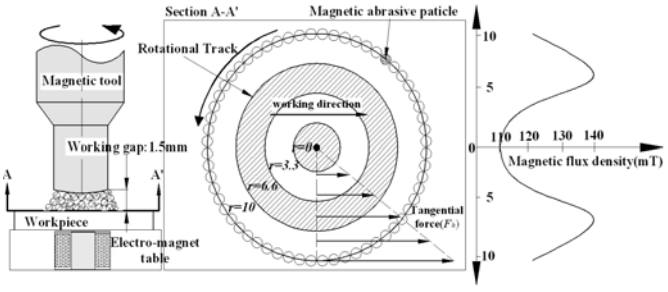

Fig. 2 Rotational track and magnetic flux density

TABLE I
Experimental Conditions Used in This Experiment

Items	Conditions
Workpiece	AZ31B(80mm×60mm×2mm)
Current of tool	2.5A-120mT
Current of magnet table	0.8A-20mT
Spindle speed	1200rpm
Working time	5min

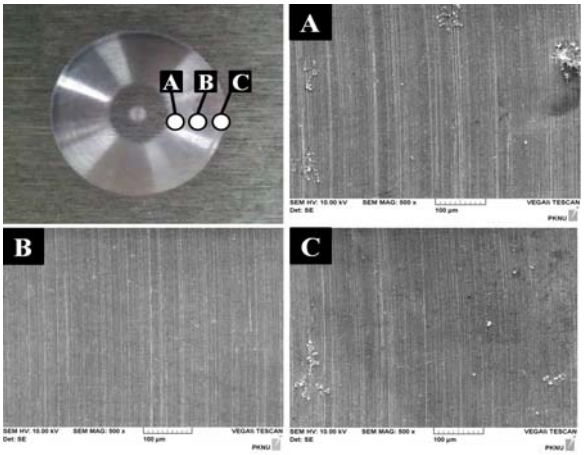

Fig. 3 SEM images according to radial distance after MAP

Experimental results were obtained in each experiment according to radial distance. To evaluate the effect of process factors on the surface roughness, ANOVA was conducted and results are listed in Table IV and Table V. When the radial distance was 0~3.3mm, the spindle speed had a dominant effect on the improvement of surface roughness. On the other hand, at radial distance of 6.6~10mm, the current of electro-magnet table had a dominant effect on the improvement of surface roughness.

Thus, based on the experimental results obtained in this study, the more tangential force is required near the center of inductor to improve the surface roughness efficiently. However, at the edge of tool, the more magnetic force is demanded because of the larger tangential force.

For predicting surface roughness at each radial distance, the second-older response surface models using the current of table, the current of tool, spindle speed and abrasive weight were developed.

B. Parameter optimization using GA and SA

In this study, an integration of GA, SA and RSM is applied to find the optimal polishing parameters in a magnetic abrasive polishing using commercial software MATLAB [7]. The RSM is used to establish the linear and nonlinear relationships between the MAP parameters and the responses. The GA and SA approach are then applied to find the optimal polishing parameters using the RSM models as the fitness function to measure the fitness value for the polishing parameters. GA was used with following parameters: Population size is 20, reproduction operator is roulette wheel method, and crossover and mutation probability is 0.8 and 0.05, respectively. And SA with following parameters was used: Initial temperature is 100. Table VI shows the results of the optimal values from GA. Although similar optimal factors were applied in the MAP process, the surface roughness was different according to radial distance. After the optimization, the highest surface roughness is in the center and the lowest surface roughness is in the r=6.6. Table VII shows the results of the optimal values determined by SA. These results are also similar to a case of GA.

TABLE II
FIXED EXPERIMENTAL CONDITIONS

Items	Conditions
Workpiece	AZ31B(80mm×60mm×2mm)
Magnetic abrasive	GC grain(8.5㎛)+Iron powder(150㎛)+Silicone gel(300,000cs)
Working gap	1.5mm
Working time	5min
Tool diameter	20mm

TABLE III
FACTORS AND LEVELS USED IN EXPERIMENTS

Factors	Levels		
	1	2	3
Current of table, A(A)	0.2	0.5	0.8
Current of tool, B(A)	1.5	2.0	2.5
Spindle speed, C(rpm)	900	1200	1500
Weight of abrasive, D(g)	1.5	2.0	2.5

TABLE IV
ANOVA FOR EACH FACTOR AT POINT OF *R=0*

	SS	DOF	V	F_0	$F_{0.01}$
A	3.832	2	1.916	3.946	10.9
B	1.695	2	0.847	1.745	10.9
C	10.602	2	5.301	10.915**	10.9
D	0.029	2	0.014	0.03	10.9
AxB	11.803	4	2.95	6.076	9.15
AxC	11.517	4	2.879	5.929	9.15
BxC	2.38	4	0.595	1.225	9.15
Error	2.913	6	0.485		
Total	44.775	26			

TABLE V
ANOVA FOR EACH FACTOR AT POINT OF *R=6.6*

	SS	DOF	V	F_0	$F_{0.01}$
A	26.015	2	13.007	13.249**	10.9
B	3.709	2	1.854	1.889	10.9
C	19.674	2	9.837	10.019*	10.9
D	2.103	2	1.051	1.071	10.9
AxB	9.617	4	2.404	2.449	9.15
AxC	9.662	4	2.415	2.46	9.15
BxC	12.513	4	3.128	3.186	9.15
Error	5.89	6	0.981		
Total	89.186	26			

TABLE VI
OPTIMAL VALUES AND FACTORS CALCULATED BY GA

Parameter	*r=0*	*r=3.3*	*r=6.6*	*r=10*
A	0.792	0.799	0.799	0.798
B	1.515	1.5	1.91	1.5
C	1232.8	1127	1340	1004.3
D	1.5	1.5	1.5	1.501
Ra(Op)	0.39	0.354	0.181	0.239

TABLE VII
OPTIMAL VALUES FACTORS CALCULATED BY SA

Parameter	*r=0*	*r=3.3*	*r=6.6*	*r=10*
A	0.201	0.8	0.798	0.749
B	2.49	1.5	1.823	1.927
C	1040	1120.1	1354.6	1129.7
D	2.489	1.5	1.5	1.517
Ra(Op)	0.389	0.354	0.180	0.211

V. DETERMINATION OF STEP-OVER ON MAP OF AZ31B

To reduce the deviation of surface roughness according to radial distance from center of tool, the radial distance-surface roughness curve was developed by calculated value of optimal surface roughness using GA and SA. Fig. 4 shows the radial

distance-surface roughness curve, which indicates the predicted improvement of surface roughness. The step-over, as shown in Fig. 5, was determined by distance from peak value of improvement of surface roughness to lowest value, and the optimal step-over was 6.61mm.

To verify the proposed step-over, the MAP of magnesium alloy plate with calculated step-over was performed. As shown in Fig. 6, it indicated that predicted surface roughness well coincided with experimental results, and the deviation of surface roughness was reduced after the optimized MAP with step-over of 6.61mm. The experimental conditions were determined by GA approach (*r=6.6*).

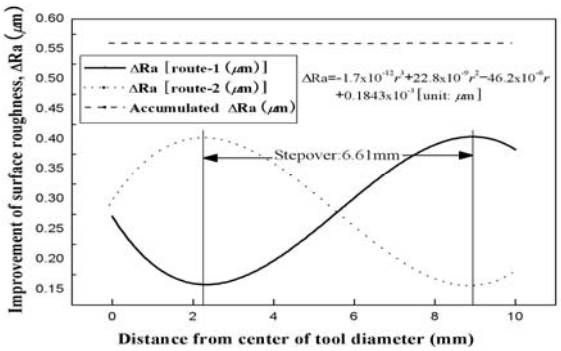

Fig. 4 Determination of step-over value on MAP

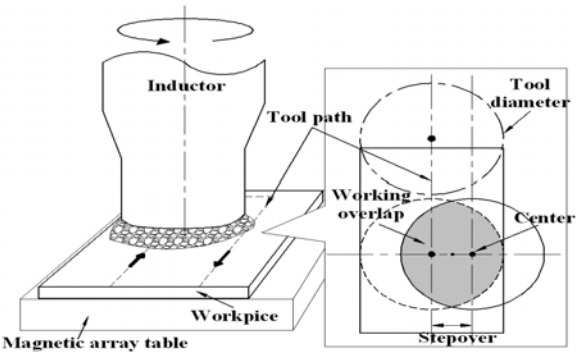

Fig. 5 Schematic diagram of working overlap and step-over

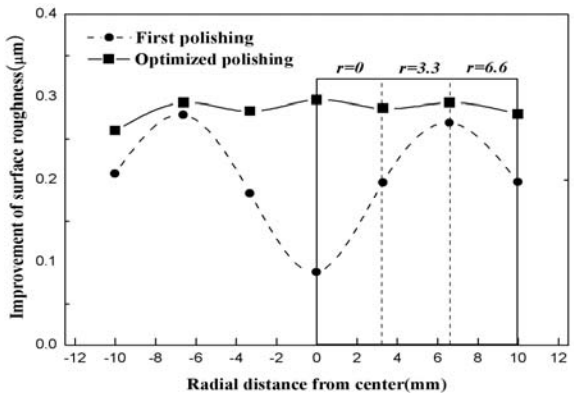

Fig. 6 Results of experimental verification for optimized MAP with step-over of 6.61mm

VI. CONCLUSIONS

In this study, to determine the optimal step-over in MAP of AZ31B magnesium alloy, an integration of GA, SA and RSM is applied to find the optimal polishing parameters in a magnetic abrasive polishing, and then the radial distance-surface roughness curve was developed by calculated value of optimal surface roughness using GA and SA. The obtained conclusions are as follow.

1. In the MAP of plate surface, the surface roughness was clearly different in accordance with change of radial distance, since the magnetic flux density occurs differently on the surface of workpiece.
2. When the radial distance was 0~3.3mm, the spindle speed had a dominant effect on the improvement of surface roughness. On the other hand, at radial distance of 6.6~10mm, the current of electro-magnet table had a dominant effect on the improvement of surface roughness.
3. To reduce the deviation of surface roughness according to radial distance from center of tool, the radial distance-surface roughness curve was developed using GA and SA. As a result, the optimal step-over was 6.61mm.

ACKNOWLEDGMENT

This work is the result of the "Human Resource Development Center for Economic Region Leading Industry" Project, supported by the Ministry of Education, Science & Technology(MEST) and the National Research Foundation of Korea(NRF).

REFERENCES

[1] Y. Shaohui and S. Takeo, "A Comparative Study: Polishing Characteristics and its Mechanisms of Three Vibration Modes in Vibration-assisted Magnetic Abrasive Polishing," *International Journal of Machine Tools and Manufacture*, vol. 44, no. 4, pp.383-390, March 2004.

[2] G. Kumar and V. Yadav, "Temperature distribution in the workpiece due to plane magnetic abrasive finishing using FEM," *International Journal of Advanced Manufacturing Technology*," vol. 41, no. 11-12, pp.1051-1058, 2009.

[3] S. O. Kim and J. S. Kwak, "Magnetic Force Improvement and Parameter Optimization for Magnetic Abrasive Polishing of AZ31 Magnesium alloy," *Transactions of Nonferrous Metals Society of China*, vol. 18, no. 1, pp. 369-373, December 2008.

[4] V. K. Jain, "Magnetic field assisted abrasive based micro-/nano-finishing," *Journal of Material Processing Technology*, vol. 209, no. 20, pp. 6022-6038, November 2009.

[5] J. S. Kwak, "Enhanced Magnetic Abrasive Polishing of Non-ferrous Metals Utilizing A Permanent Magnet," *International Journal of Machine Tools and Manufacture*, vol. 49, no. 7-8, pp. 613-618, June 2009.

[6] A. M. Wani, V. Yadava and A. Khatri, "Simulation for the prediction of surface roughness in magnetic abrasive flow finishing (MAFF)," *Journal of Materials Processing Technology*, vol. 190, no. 1-3, pp. 282-290, July 2007.

[7] E. W. Mcgookin and D. J. Murray-Smith, "Submarine manoeuvring controllers' optimization using simulated annealing and genetic algorithms," *Control Engineering Practice*, vol.14, no. 1, pp. 1-15, January 2006.

2011 International Conference on Mechanical, Industrial, and Manufacturing Engineering
Lecture Notes in Information Technology Vols. 1-2

Evaluation of Magnetic Abrasive Polishing for Non-Magnetic Materials with CNT Particle

Jae-Seob Kwak
Department of Mechanical Engineering
Pukyong National University
San 100, Yongdang-Dong, Nam-Gu, Busan, South Korea
jskwak5@pknu.ac.kr

Sang-Oh Kim
Graduated School of Mechanical Engineering
Pukyong National University
San 100, Yongdang-Dong, Nam-Gu, Busan, South Korea
kso6260@pknu.ac.kr

***Abstract* - This study focuses on the characteristic of MAP with CNT particle. Since the CNT particle is very small and high strength, it is suitable for precision surface polishing. However, the properties of MAP with CNT were changed according to the kind of magnetic particle and amount of CNT particle. In this study, to improve the capacity of MAP with CNT, cobalt powder was used as magnetic particle instead of iron powder. Moreover, by design of experiment, it revealed that amount of CNT had a dominant effect on the improvement of surface roughness in MAP, and optimal conditions were an applied current of electro-magnet of 0.8A, spindle speed of 900rpm, weight of CNT particle of 0.26g and weight of cobalt of 3.9g.**

Index Terms - Carbon nanotube, Magnetic abrasive polishing, Surface roughness, Non-magnetic materials

I. INTRODUCTION

Recently demand for parts of high quality and precision is rapidly increasing with the development of electronics and optical products. It is required that the parts used in manufacturing semiconductors, atomic energy parts, medical instruments and aerospace components have a very precise surface roughness. The new finishing method, magnetic abrasive polishing(MAP) is one of advanced machining processes in which cutting force is primarily controlled by the magnetic field. This process can be used to produce efficiently good surface quality of the few nanometer-scale finishing on surfaces. This method has applied to machining of not only ferromagnetic materials such as steel, but also non-ferromagnetic materials such as stainless steel and brass [1].

In this study, to estimate the polishing properties of CNT particle as abrasives mixed with the magnetic abrasive, surface topography and surface roughness were measured using AFM after MAP of stainless steel. In addition, to improve the polishing efficiency of CNT particle, the cobalt powder was used in instead of iron power that is magnetic particle in MAP, because cobalt of 1μm has the larger magnetic force and much smaller than iron particles of 150μm. Moreover, for polishing a thin magnesium alloy plate by CNT particle, the optimal conditions were determined by the design of experimental method.

II. CARBON NANOTUBE

Carbon nanotubes are hexagonally shaped arrangements of carbon atoms that have been rolled into tubes. These tiny straw-like cylinders of pure carbon have useful electrical properties. Carbon nanotubes are allotropes of carbon with a cylindrical nanostructure. These cylindrical carbon molecules have novel properties, making them potentially useful in many applications in nanotechnology, electronics, optics, and other fields of materials science, as well as potential uses in architectural fields. Nanotubes can be selectively produced with properties ranging from 1 to 15 micrometers in length and diameters from 2 to 100 nanometers. These nanotube powders come in agglomerate and aligned bundles and can be put into dispersion using ultrasonic process. They may also have applications in the construction of body armor. They exhibit extraordinary strength and unique electrical properties, and are efficient thermal conductors. There are two main types of nanotubes: single-walled nanotubes(SWNTs) and multi-walled nanotubes(MWNTs) [2-4].

Table I shows the several characteristics of abrasives that used in MAP. Carbon nanotube has very tiny diameter, high strength and low density as compared with other abrasives. Fig. 1 shows the SEM images of multi-walled nanotubes(CM-95) used in this study that was produced by a type of chemical vapor deposition(CVD) method of HANWA .

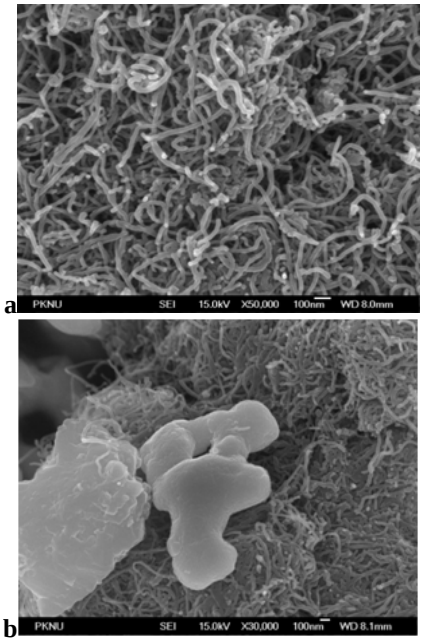

Fig. 1 SEM image of CNT used in this study, (a) CNT particle, (b) Cobalt powder and CNT

TABLE I

PROPERTIES OF ABRASIVE USED IN MAGNETIC ABRASIVE POLISHING

	Diameter(μm)	Strength(GPa)	Density(g/cm^3)
Boron nitride	140	3.3~4.0	2.3~2.5
SiC	15~145	2.9~4.0	2.5~3.5
Al_2O_3	20	1.5	3.9
CNT	0.01~0.04	20~50	1.6

TABLE II
TYPE OF MAGNETIC ABRASIVE USED IN EACH EXPERIMENT

Items	Ferrous particle	Abrasive	Medium
EXP.1	Fe(2.5g)	-	Oil(2.5g)
EXP.2	Fe(1.7g)	CBN(0.85g)	Oil(2.5g)
EXP.3	Fe(2.0g)	CNT(0.2g)	Oil(2.5g)
EXP.4	Co(2.0g)	CNT(0.2g)	Oil(2.5g)

TABLE III
PARTICLE SIZE OF MAGNETIC ABRASIVES

	Fe	Co	CBN	CNT
Size(μm)	150	3	1~2	0.003~0.005

TABLE IV
EXPERIMENTAL CONDITIONS

Items	Conditions
Current of inductor	2.5A
Current of electro-magnet	0.12A
Working gap	1.5mm
Spindle speed	900rpm
Traverse speed	20mm/min
Working time	40min
Workpiece	AISI316(60mmx40mmx3mm)

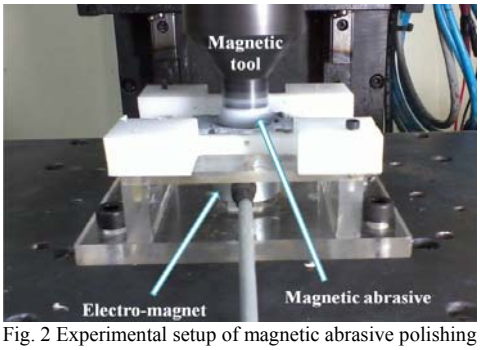

Fig. 2 Experimental setup of magnetic abrasive polishing

III. PROPERTIES OF CNT PARTICLE IN MAP PROCESS

A. *Experimental setup and procedure*

To evaluate the characteristic of MAP with CNT, a series of experiments were conducted in this study. The experimental setup for MAP with CNT was constituted as shown in Fig 2. It consists of the inductor of magnetic tool, power supply and DC motor. To overcome disadvantage of MAP for non-magnetic materials, electro-magnet was installed under the workpiece. This improving strategy of magnetic force is very effective on producing better surface roughness during MAP of non-magnetic materials. Moreover, the jig for fixing workpiece was made of plastic material to prevent the distribution of magnetic intensity.

Table II shows the composition of magnetic abrasive used in each experiment. First experiment was performed using just iron powder without abrasives. In the second experiment, CBN abrasive of 3μm was used as abrasives. On the other hand, in the third experiment, CNT particle was used instead of CBN abrasive to confirm the effectiveness of CNT in MAP. The properties of cobalt powder were estimated in the last experiment. Table III listed the particle size of magnetic abrasive. As listed in Table 3, size of Fe powder is the biggest one, but the cobalt powder is smaller about 50 times than Fe powder. In this experiment, CNT particle was dispersed in the magnetic abrasive by means of ultrasonic vibration.

The fixed experimental conditions that optimized in preliminary study were chosen as listed in Table IV. The workpiece was AISI316 stainless steel to evaluate the polishing properties of CNT particles. Therefore, for estimating the nano-scale polishing, pre-processing was performed during 5 minutes using CBN of 3.15μm as abrasives in the magnetic abrasive. The current supplied into electro-magnet was set to 0.12A and current of inductor was 2.5A. Because the shorter working gap can identify the larger magnetic force in MAP process, the working gap between the magnetic tool and work material was set to 1.5mm. Since magnetic abrasive easily breaks away from the working field, spindle speed of 900rpm ensured the stable polishing condition. All of experiments were carried out for 40 minutes.

B. *Experimental results and analysis*

In this study, a series of experiments were performed for evaluating the machinability of CNT particle mixed with magnetic abrasive. Fig. 3 shows the change of the surface roughness according to experimental conditions. In this result, amplitude of output was expressed as the average surface roughness and RMS roughness which was done by connecting an AC voltmeter to measure the electric signal.

As shown in results, when the CNT particle was mixed with cobalt powder, the RMS was the lowest among the results of experiments. Therefore, in a case that CNT was mixed with Fe powder, the improvement of surface roughness was similar with a case that CBN was mixed with Fe powder. These results indicated that CNT particle is very suitable to magnetic abrasive in precision MAP process and the smaller size of particle in magnetic abrasive is effective to improve the surface roughness in MAP with CNT.

Fig. 4 shows the measured results of surface topography after MAP. In the results of experiments, Fig. 4 (a) shows the surface of workpiece in a case of MAP with only Fe powder. It indicated that the Fe particles plough the surface of workpiece, thus, surface roughness is the largest in this experiment. Fig. 4 (b), (c) and (d) show that the better precision surface was observed as compared with using only Fe particle.

However, Fig. 4 (b) is seen that larger amplitude of vertical distance between highest peak and lowest valley more than in a case of using CNT, shown in Fig. 4 (c) and (d), was observed.

As comparing with Fig. 4 (c) and (d), a CNT abrasive mixed with cobalt powder used as magnetic particle, the average gap between highest peak and lowest valley was lower than in a case of using Fe powder.

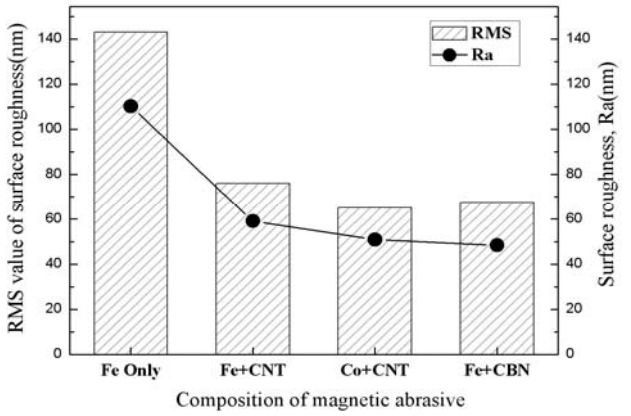

Fig. 3 Comparing to surface roughness according to experimental conditions

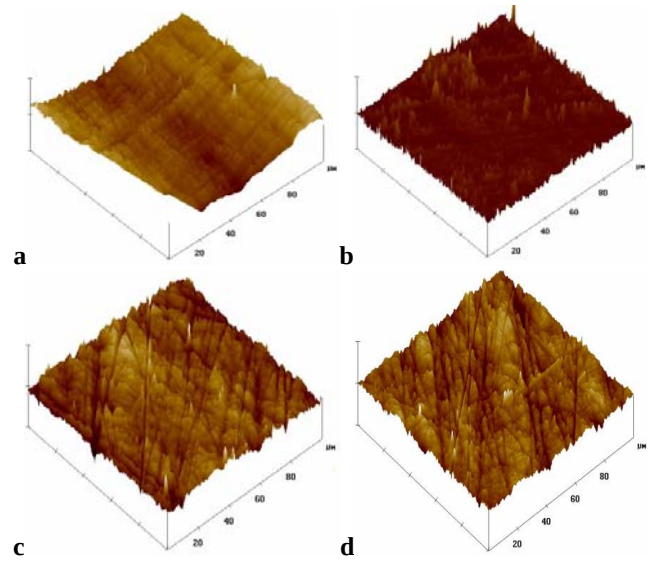

Fig. 4 Comparing to surface topography using AFM (a) only Fe-powder, (b) Fe-powder + CBN, (c) Fe-powder + CNT, (d) Co-powder + CNT

Moreover, the RMS roughness with CNT was lower than Fe powder and CBN particle. These results are explained that the smaller size of the ferrous particle increases the cohesion of magnetic abrasive in the magnetic field because of increasing the viscosity of magnetic abrasive. Thus, it is estimated that the growing of viscosity is related with the increasing of the number of abrasive contacted with surface of workpiece.

IV. MAP WITH CNT FOR MAGNESIUM ALLOY

A. *Design of experiments*

For evaluating that which parameter has most effect on improvement of the surface roughness and finding optimal process condition for MAP using CNT particle, Taguchi's design method was performed in this study. Fixed experimental conditions for evaluation of MAP parameters were indicated as shown in Table V. The work material used was AZ31 magnesium alloy which is length of 80mm, width of 65mm and thickness of 0.65mm. The working gap between the magnetic tool and workpiece was set to 1.0mm. The diameter of inductor tool was 20mm and a current supplied into the magnetic tool was 2.5A. For improving the viscosity and lubrication effect, olive oil was mixed with abrasives. The MAP process had performed for 5minutes.

In this study, a current of electro-magnet, a spindle speed, weight of CNT particles and a weight of cobalt powder were considered as experimental factors which would influence the surface roughness on MAP of AZ31 with CNT particle. All selected experimental factors were changed at three levels as listed in Table VI. The factor of the current of electro-magnet means amount of a current supplied into electro-magnet installed on the opposite side of workpiece. The maximum magnetic flux density on the surface of workpiece was about 20mT when the supplied current was 0.8A. The spindle speed was used in the range of 900 to 1,300rpm since most abrasive particles could easily fly from the working area in high rotational speed over 1,500rpm. The weight of CNT and cobalt powder expresses the amount of abrasives used as magnetic abrasives at one time. As listed in Table VII, a Taguchi's $L_9(3^4)$ orthogonal array that includes the four factors and three levels was applied.

B. *Parameter effect and optimal conditions*

Experiments were conducted according to the Table VII and then the measured results were evaluated with the help of the signal-to-noise ratio and the ANOVA. Experimental results indicate the improvement of the surface roughness after the MAP. Generally, the signal-to-noise ratio is used to quantify the present variation in the Taguchi method. In this study, the-larger-is-the-better type of the signal-to-noise ratio was selected as the quality characteristic, since the more change in the surface roughness means the better efficiency of the MAP. The S/N ratio (η) is calculated as follows.

$$\eta = -10\log(\frac{1}{n}\sum\frac{1}{y_i^2}) \quad (1)$$

Where n represents the number of measurements and y_i is the measured values.

Both the measured experimental results and calculated S/N ratios were listed in Table VII. To evaluate the effect of process parameters on the enhanced the surface roughness, ANOVA(analysis of variance) was conducted and results are listed in Table VIII.

According to the Table VIII, the weight of CNT particle had a dominant effect on the improvement of surface roughness in the case of the MAP for AZ31 magnesium alloy. The spindle speed was a process parameter considered in this study that had the least influence on the surface roughness. Thus, that parameter was pooled as an error in ANOVA. Based on the experimental results obtained in this study, the amount of CNT particles played an important role in producing better surface than other process parameters. It means that the larger amount of CNT particle in magnetic abrasives has the larger improvement of the efficiency of MAP because the cohesion between magnetic particle and abrasives is increased.

In the Taguchi method, the highest S/N ratio for the result is desirable. As shown in Fig. 5, the levels corresponding to the highest S/N ratio in each parameter were chosen as the optimum conditions. The selected optimal conditions were $A_3B_1C_3D_3$ (current of electro-magnet of 0.8A, spindle speed of 900rpm, weight of CNT particle of 0.26g and weight of cobalt of 3.9g). These optimal conditions can minimize the process variation and produce the better surface roughness.

TABLE V
FIXED EXPERIMENTAL CONDITIONS

Items	Conditions
Current of inductor	2.5A
Medium of abrasive	Oil(168cs)
Working gap	1.5mm
Working time	40min
Workpiece	AZ31(80mmx65mmx0.65mm)

TABLE VI
PARAMETERS AND LEVELS USED IN EXPERIMENTS

parameters	Levels		
	1	2	3
Current of electro-magnet, A(A)	0.2	0.5	0.8
Spindle speed, B(rpm)	900	1100	1300
Weight of CNT, C(g)	0.14	0.2	0.26
Weight of cobalt, D(g)	2.1	3.0	3.9

TABLE VII
ORTHOGONAL ARRAY $L_9(3^4)$ AND RESULTS OF EXPERIMENT

No	A	B	C	D	Improvement of surface roughness(μm)	S/N ratio
1	0.2	900	0.14	2.1	0.009	-40.915
2	0.2	1100	0.20	3.0	0.016	-35.917
3	0.2	1300	0.26	3.9	0.036	-28.873
4	0.5	900	0.20	3.9	0.028	-31.056
5	0.5	1100	0.26	2.1	0.02	-33.979
6	0.5	1300	0.14	2.0	0.013	-37.721
7	0.8	900	0.26	2.0	0.048	-26.375
8	0.8	1100	0.14	3.9	0.026	-31.700
9	0.8	1300	0.20	2.1	0.022	-33.151

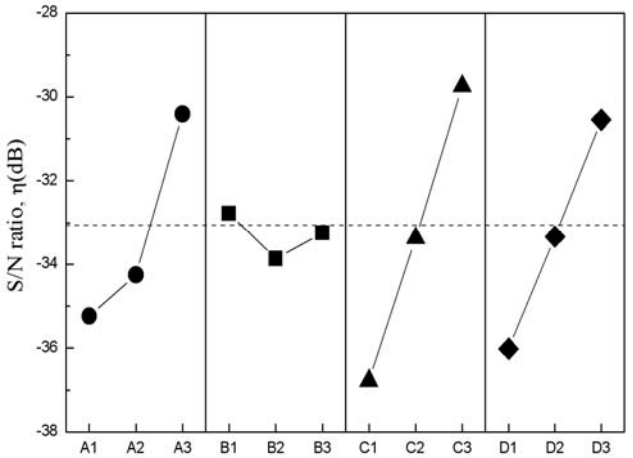

Fig. 5 Influence of parameters on MAP with CNT particle

TABLE VIII
ANOVA FOR EACH PARAMETER

	SS	DOF	V	F	$F_{0.05}$
A	39.032	2	19.516	22.025*	19.0
B	(1.772)	(2)	(0.886)		
C	74.286	2	37.143	41.918*	19.0
D	44.914	2	22.457	25.344*	19.0
Error	5.057	2	0.886		
Total	160.005	8			

V. CONCLUSIONS

To evaluate the characteristic of MAP with CNT particle, a series of experiments were conducted and to estimate the results of experiments, surface morphology was measured by means of AFM. Moreover, the evaluation of process parameter was performed by Taguchi's design method. The obtained conclusions are as follow.

1. The RMS roughness was the lowest among the results of experiments when the CNT was mixed with cobalt powder. So, CNT particle is appropriate to magnetic abrasive in precision MAP process.
2. The smaller size of the ferrous particle increases the cohesion of magnetic abrasives in the magnetic field due to increase the viscosity of magnetic abrasive. Thus, it is estimated that the growing of viscosity is related with the increasing of the number of abrasive contacted with surface of workpiece.
3. The weight of CNT particle had a dominant effect on the improvement of surface roughness in the case of the MAP with CNT particle. On the other hand, the spindle speed had the least influence on the surface roughness.
4. The optimal conditions for the MAP with CNT particle were an applied current of electro-magnet of 0.8A, spindle speed of 900rpm, weight of CNT particle of 0.26g and weight of cobalt of 3.9g.

ACKNOWLEDGMENT

This study was supported by Basic Science Research Program through the National Research Foundation of Korea (NRF) funded by the Ministry of Education, Science and Technology (Grant No. 2010-0007932).

REFERENCES

[1] J. S. Kwak, "Enhanced Magnetic Abrasive Polishing of Non-ferrous Metals Utilizing A Permanent Magnet," *International Journal of Machine Tool and Manufacture*, vol. 49, no. 7-8, pp. 613-618, Jun 2009.
[2] A. Pantano, D. M. Parks, and M. C. Boyce "Mechanics of deformation of single- and multi-wall carbon nanotubes," *Journal of the Mechanics and Physics of Solids*, vol. 52, no.4, pp.789-821, April 2004.
[3] B. S. Jung, K. I. Jang, B. K. Min, S. J. Lee , and J. W. Seok , "Magneto-rheological finishing process for hard materials using sintered iron-CNT compound abrasives," *International Journal of Machine Tools and Manufacture*, vol. 49, no. 52, 2, pp407-418, April 2009.
[4] Y .Y. Tsai, J. S. Su, and C.Y. Su, "A novel method to produce carbon nanotubes using EDM process" *International Journal of Machine Tools and Manufacture*, vol. 48, no.15, pp1653-1657, Dec 2008.

2011 International Conference on Mechanical, Industrial, and Manufacturing Engineering
Lecture Notes in Information Technology Vols. 1-2

Research on lending rate of Chinese commercial banks

Xinyao Shan
School of Management
Tianjin University
Tianjin, China
Sxy19860621@126.com

Qing Li
School of Management
Tianjin University
Tianjin, China
lovelyqq@yahoo.cn

Abstract - In the context of lending rate market, the research on the pricing model of lending rate is currently a major challenge for commercial banks. State-owned commercial banks and joint-stock commercial banks are two representative types of banks in China, and its asset size and market share are top two in the industry. Therefore, the study of commercial bank loan interest rate pricing mechanism is of great significance. This paper selects some listed companies' loan data in the state-owned commercial banks and joint-stock commercial bank, and makes empirical analysis. Research shows that the pricing behavior feature of state-owned commercial banks' and joint-stock commercial banks' lending rates are significantly different and joint-stock commercial banks in determining lending rates has a higher operating efficiency.

Index Terms - lending rates, commercial banks, listed companies

I. INTRODUCTION

The determination of lending rate is a process that the commercial Banks provide their loan service. Because the process in the competition is directly related to whether banks could achieve business objectives or not, it is so significant that commercial banks should pay a lot of attention on it. However, because of long-term control of interest rate, Chinese commercial Banks often executed strictly central bank's interest rate policy. Although the central bank had increased their lending rate's fluctuation space, commercial banks have a certain amount of autonomy, in fact, the influence factors of loan interest rate is also usually depended on the competition between commercial Banks and their customer. The pricing of Chinese commercial banks' lending rate is lack of practical experience, and the loan pricing management is very weak.

Generally speaking, Berger & Udell[1]divided commercial bank loans into four categories by lending technology: (1)financial statements type loans,(2)the asset-backed type loans, (3)credit scoring and (4)relational loans. They states that the first three kinds of them are usually market transactional lending technology. The credit decision of the bank is based on the easily openly obtained and relatively objective hard information, such as financial ratios, credit scoring. But relational loan decision depends largely on the soft information which is not easily obtained and hard to measured and transferred such as the enterprise owners' quality and ability. Peterson & Rajan [2]demonstrate that the relationship between banks and enterprise is the longer and loans accessibility is the taller, loan interest rate and security requirements also can be reduced. In their view, the possibility of small and medium-sized enterprises to obtain low-interest loans is positively related to the length of time of the relationship. Blackwell & Winters and Cole [3] made different conclusions. Blackwell & Winters argue that the length of time of lending relationship have no effect to interest rates by analyzing American's two bank holding assertion companies. In china, B.Li[4] calculates the weighted average cost rate(WACC) by the banks' historical financial data and then plus commercial banks' target profit margins, average risk compensation ,average loan cost and constitutes an average loan interest rate (also known as the benchmark lending rate) . Z.Li[5]believes that the small and medium enterprises' heterogeneity, mortgage and transaction cost are three main factors to influence small and medium-sized enterprises to obtain credit from Banks, alleviate information asymmetry problem[6], increase the mortgage[7], reduce transaction costs will make small and medium-sized enterprises get more credit[8].

II. MODEL

A. *Sample Selection and Data Collection*

The sample was selected the loan data in the part of listed company from the end of 1998 to the end of 2008 in state-owned commercial Banks and joint-equity commercial Banks. Total sample size is 339. Data include: current benchmark lending rates, lending rates, loan type, loan bank, loan term, and the number of bank exists lending relationship with enterprise and the listed company financial data and asset scale.

B. *Research Model*

In this study, we use multivariate linear regression model to analyze the factors which influence on lending rates.

$$Y = \alpha_0 + \alpha_1 FIN + \alpha_2 SC + \alpha_3 GUA + \alpha_4 NUM + \alpha_5 FIR + \varepsilon$$

FIN: enterprise financial index (Z score)

SC:enterprise asset scale

GUA: whether the enterprise could provide guarantee

NUM: number of enterprise exist relationship with bank

FIR: whether the enterprise does the first time apply loan

Y: the ratio of lending rates over the same period benchmark lending rate

C. *The description of main variables*

1) Benchmark interest rate

Benchmark interest rate is very important rate in the financial markets and play decisive role in the interest rate system. With Chinese market-oriented interest rate mechanism is arriving, the people's bank of China adjusted the benchmark lending rate several times to Control investment and market liquidity from 1998 to 2002.

Table 1

	6 months	From 6 months to 1 year	1year to 3years	3years to 5years	More than five years
1998.12.07	6.12	6.39	6.66	7.20	7.56
1999.06.10	5.58	5.85	5.94	6.03	6.21
2002.02.21	5.04	5.31	5.49	5.58	5.76
2004.10.29	5.22	5.58	5.76	5.85	6.12
2006.04.28	5.40	5.85	6.03	6.12	6.39
2006.08.19	5.58	6.12	6.30	6.48	6.84
2007.03.18	5.67	6.39	6.57	6.75	7.11
2007.05.19	5.85	6.57	6.75	6.93	7.20
2007.07.21	6.03	6.84	7.02	7.20	7.38
2007.08.22	6.21	7.02	7.20	7.38	7.56
2007.09.15	6.48	7.29	7.47	7.65	7.83
2007.12.21	6.57	7.47	7.56	7.74	7.83
2008.09.16	6.21	7.20	7.29	7.56	7.74
2008.10.09	6.12	6.93	7.02	7.29	7.47
2008.10.30	6.03	6.66	6.75	7.02	7.20
2008.11.27	5.04	5.58	5.67	5.94	6.12
2008.12.23	4.86	5.31	5.40	5.76	5.94

In different economic development period, loan interest rate is great difference. Especially the sample data from the end of 1998 to the end of 2008 had a larger time span, and each phase of economic background is also different. Therefore, absolutely lending rates cannot accurately measure actual levels. This paper chooses the ratio of lending rates over the same period benchmark lending rate to measure Chinese commercial banks' lending rate level.

2) Z score model

The original Z-score formula was as follows:

$Z = 0.012T_1 + 0.014T_2 + 0.033T_3 + 0.006T_4 + 0.999T_5$.

T_1 = Working Capital / Total Assets.

Measures liquid assets in relation to the size of the company.

T_2 = Retained Earnings / Total Assets.

Measures profitability that reflects the company's age and earning power.

T_3 = Earnings Before Interest and Taxes / Total Assets.

Measures operating efficiency apart from tax and leveraging factors. It recognizes operating earnings as being important to long-term viability.

T_4 = Market Value of Equity / Book Value of Total Liabilities.

Measures company's capital structure and solvency

T_5 = Sales/ Total Assets. Standard measure for sales turnover

Measures the ability of sales income brings asset.

$Z > 2.99$ -"Safe" Zones

$1.8 < Z < 2.99$ -"Grey" Zones

$Z < 1.80$ -"Distress" Zones

That means when the Z score is less than 1.81, the company will soon in the few years go towards bankruptcy. And if the Z score greater than 2.99, it indicates that the operation of the company is very normal, would not have financial difficulties, If the company Z score is between 1.81 to 2.99 between, in this section, the future of the company is very hard to speculated through Z score. It might bankrupt and probably keep the normal working. Generally, if Z-score falls into grey zone, and accompanied with the downtrend or obvious fluctuation, it should be taken care.

This paper choose to use Z - score model because firstly, Z-score model is multivariate difference analysis and its forecast effect is pretty good and not easily interfered .Secondly, Z-score model is a linear model. Compared with the LOGIT model and PORBIT model, it does not involve complex professional knowledge, more easily to be accepted, and has good practical value.

3) GUA: whether the enterprise could provide guarantee

If the enterprise could provide guarantee, its value is "1",

If the enterprise could not provide guarantee, its value is "0"

4) FIR: whether the enterprise does the first time apply loan

If it is the first time that the enterprise apply loan in the bank ,its value is "1".

If it is not the first time that the enterprise apply loan in the bank ,its value is "0".

5) NUM: number of enterprise exist relationship with bank

D. Variable statistical properties

Table 2

variables	(Mean)	(Median)	(Std.Dev)
Y	0.964866	-3.013183	12.11331
FIN-Z score	31.14111	24.61564	20.90245
SC	44.70336	41.78352	19.91008
GUA	0.516224	1.000000	0.500475
NUM	4.053097	3.000000	2.360326
FIR	0.351032	0.000000	0.477999

E. Result

Included observations: 203 after adjustments

Variable	Coefficient	Std. Error	t-Statistic	Prob.
C	4.351698	1.541829	2.822426	0.0053
Z-0.508614*Z(-1)	-0.057719	0.038627	-1.494265	0.1367
SC-0.508614*SC(-1)	-0.023258	0.041757	-0.556985	0.5782
GUA-0.508614*GUA(-1)	7.319871	1.526310	4.795794	0.0000
NUM-0.508614*NUM(-1)	-1.868872	0.471919	-3.960151	0.0001
FIR-0.508614*FIR(-1)	-1.505237	1.264317	-1.190553	0.2353

R-squared	0.172169	Mean dependent var	1.078332
Adjusted R-squared	0.151158	S.D. dependent var	9.371130
S.E. of regression	8.633866	Akaike info criterion	7.178373
Sum squared resid	14685.10	Schwarz criterion	7.276300
Log likelihood	-722.6048	F-statistic	8.194266
Durbin-Watson stat	2.145020	Prob(F-statistic)	0.000000

Figure 1: state-owned commercial Banks' the regression results (10% of significant level)

Included observations: 134 after adjustments

Variable	Coefficient	Std. Error	t-Statistic	Prob.
C	0.773392	2.410132	0.320892	0.7488
Z-0.461787*Z(-1)	-0.097671	0.053138	-1.838071	0.0684
SC-0.461787*SC(-1)	0.142300	0.047471	2.997640	0.0033
GUA-0.461787*GUA(-1)	1.833483	2.193460	0.835886	0.4048
NUM-0.461787*NUM(-1)	-1.155124	0.589144	-1.960684	0.0521
FIR-0.461787*FIR(-1)	-2.382797	2.001544	-1.190479	0.2361

R-squared	0.114131	Mean dependent var	-0.406047
Adjusted R-squared	0.079527	S.D. dependent var	11.29340
S.E. of regression	10.83503	Akaike info criterion	7.647189
Sum squared resid	15026.94	Schwarz criterion	7.776943
Log likelihood	-506.3617	F-statistic	3.298182
Durbin-Watson stat	2.033905	Prob(F-statistic)	0.007784

Figure 2: joint-stock Banks' the regression results (10% of significant level)

As is shown in Fig. 1, to state-owned Banks, Z score, enterprise asset scale was not significant influence on lending rates. But to the same customer's competition between banks, it has the significant effects. Enterprise applying for credit has more loan relationship with the banks, the state-owned commercial bank more probably provide lower lending rates because of competition between them. If the enterprise could provide guaranty, the state-owned commercial bank will give higher mortgage rates, because provide guarantee for the enterprise make the credibility lower and has more potentially risk. According to the benefits and risks proportional principles, the bank should charge higher interest rates. Z score and enterprise asset scale of loan interest rate is not significant, which shows that Chinese state-owned bank pay not so much attention on financial statements and asset scale.

As is shown in Fig.2, to joint-stock Banks, guarantee was not significant. But the Z score, enterprise asset scale have significant influences on lending rates. Consistent with state-owned commercial Banks, both joint-stock banks and state-owned commercial show the "relationship features". Enterprise applying for credit has more loan relationship with the banks; the two kinds of bank will more probably provide lower lending rates. However, compared with the state-owned commercial bank, joint-stock banks pay more attention to enterprise financial value. The higher Z score is, enterprise has a better financial situation, and the joint-stock bank more probably provides lower lending rates. This phenomenon is easily to demonstrated. Because joint-stock banks differ from state-owned commercial banks, their customers were mainly in small and medium enterprises and these enterprises assets scale and profit space are not so abundant. They could not bear too high lending rates. It is unrealistic that they burden high lending rates. Therefore, compared with the large enterprises, the phenomenon appeared that if the greater asset scale is, the lending rates are higher.

III. CONCLUSION

This paper selects some listed companies' loan data in the state-owned commercial banks and joint-stock commercial bank, and makes empirical analysis. Research shows that the pricing behavior feature of state-owned commercial banks' and joint-stock commercial banks' lending rates are significantly different. Joint-stock commercial bank in the field of determining lending rates has a higher operating efficiency. State-owned commercial Banks in the field of determining the loan interest rate show obvious "relationship features".The competition between Banks have significant influences on lending rates. It is consistent with Berger & Udell, Blackwell & Winters. Enterprise applying for credit has more loan relationship with the banks, the state-owned commercial bank more probably provide lower lending rates because of competition between them. However, compared with the state-owned commercial bank, joint-stock banks pay more attention to enterprise financial value.

REFERENCES

[1] Berger, A.N,Udell,G.F.Relationship,Lending and lines of credit in small Firm Finance.Journal of Business,vol 3,pp.351-382. 1995.

[2] Peterson, M. and R. Rajan,The Effect of Credit Market Competition on Lending Relationships.Quarterly.Journal of Economics, vol 110,pp 407-443. 1995.

[3] David W.Blackwell, Thomas R.Noland, Drew B.Winters, The Value of Auditor Assurance: Evidence from Loan Pricing .Journal of Accounting Research,vol 1,pp57-70, 1998.

[4] B.Li,,Pricing management of lending rates in Interest rate marketization. Journal of Jinan Financial.vol 9, pp16-19. 2002.

[5] Z.Li ,Bank structure and small financing.Journal of economic research. Vol 6,pp 27-31, 2002.

[6] G.Zhang,Discuss our country commercial bank's loan pricing method.Journal of finance and economy. vol 8 ,pp 47-49,2005.

[7] J.Zhang,Relationship lending and bank organizational structure.Journal of Economic Research, vol 6,pp 52-53,2008.

[8] X.Jin, M.Fu,Personal relationship problems of lending.commercial economy and management, vol 3,pp17-18. 2005.

2011 International Conference on Mechanical, Industrial, and Manufacturing Engineering
Lecture Notes in Information Technology Vols. 1-2

Integrated Production-and-Delivery Cycle Model for a Three-Echelon Supply Chain System*

Hari Prasetyo, Lee Luong and Sang-Heon Lee
School of Adv. Manufacturing and Mechanical Engineering
University of South Australia
Mawson Lakes, Mawson Boulevard, Australia
prahy001@mymail.unisa.edu.au

***Abstract* – This paper presents a model to determine the number of manufacturer's and buyers' shipments, production cycle length and production sequence simultaneously in a three-level supply chain system. The system comprises of a number of distributors, single manufacturer/ assembler and multiple part suppliers. The objective of the model is to find a set of the decision variables which minimize the average total relevant costs of the entire system.**

Index Terms – production cycle, sequencing, inventory system.

I. Introduction

A significant saving could be gained when operational decisions along a supply chain are simultaneously determined instead of being decided independently. Reference [1] initially proposed a collaborative decision approach in determining the lot size for a buyer and a vendor. The lot size was jointly set to minimize the total cost of the whole system. It was assumed that the vendor supplies the buyer's demand instantaneously. This circumstance was then revisited in [2] by considering a finite vendor's replenishment rate. In subsequent works, for instance in [3], [4] and [5], a single-setup multi-delivery (SSMD) policy was introduced and adopted to reduce the inventory handling cost. A comprehensive review on types of SSMD policy and the extension can be found in [6]. The works mentioned above deal with a simple supply chain system, i.e. the supply chain comprises of a manufacturer and a distributor handling single item.

A number of works addressing the coordination of production and delivery decisions for single-vendor multi-buyer (SVMB) problems include [7], [8] and [9]. Under SVMB environment, the vendor should synchronize the delivery time for each buyer to avoid demand shortage. The number of delivery cycle for each buyer and the vendor's production cycle are concurrently decided. The majority works addressing SVMB problems cover only single item cases. Reference [7] discussed multiple buyers each of whom ordered a unique product. This research was then extended by Kim et al. as in [10] by incorporating the vendor's procurement policy. Kim et al. confirmed that the average inventory at the vendor could be further reduced if the production sequence is also properly determined. Hence, the vendor's production sequence emerged as one decision variable. However, in their model they assumed that all products were made from a common raw material. In addition, the raw material needed during one production cycle had to be available at the beginning of the cycle. Under this arrangement, a substantial warehouse capacity might be required.

Acknowledging those circumstances in [10], this research contributes to improving Kim's model in several ways. Firstly, it proposes a multi-delivery procurement policy during one production cycle. This procedure is expected to improve operational performances in dealing with Kim's system. Secondly, this research generalizes the model by considering a number of raw materials required for each product. Finally, the suppliers are also incorporated in the system, thus we deal with a three-echelon supply chain system. The rest of this paper is organized as follows. In Section 2, the problem is further elaborated. The model development is presented in Section 3, while preliminary results and upcoming works are given in Section 4. Finally, Section 5 provides concluding remarks.

II. Problem Description

The supply chain system considered in this research comprises of multiple distributors, an assembler/ manufacturer and a number of part suppliers, as depicted in Fig. 1. Reference [1] studied similar structure, yet they dealt with a single-item problem. Hence, the production sequencing was an insignificant issue to deal with.

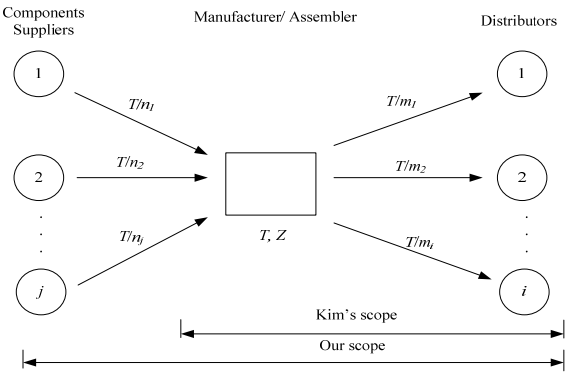

Fig. 1 The supply chain structure of the problem

Each distributor places an order of a unique product to the manufacturer. The demand is assumed to be known and

* This work is partially supported by Indonesian Government funding through Muhammadiyah University of Surakarta.

constant. In response to the order, the manufacturer produces all products every T and has to deliver them to the corresponding distributors every $T/\mathbf{m}$, where $\mathbf{m}$ is a vector containing m_i representing the number of deliveries (integer values) for the i-th distributor during T. Every product requires a similar type of parts with certain quantity, which can be observed from the Bill of Material (BOM) profiles. The manufacturer procures parts to support the production from the suppliers. It is assumed that each supplier produces a particular part. They are required to deliver the part $\mathbf{n}$ times (equal size) during T, where $\mathbf{n}$ is a vector containing integer values corresponding to number of deliveries for the j-th supplier. In this circumstance, manufacture's production sequence (Z) needs to be properly determined to ensure the average part inventory at the manufacturer is maintained at a minimum level.

All those operational decisions ($\mathbf{n}$, Z, T, $\mathbf{m}$) should be simultaneously decided to ensure the average total relevant costs of the entire system is minimized. The main aim of this research is to develop a mathematical representation for the described problem. The following section provides step-by-step of the formula development.

III. Model Formulation

A. Manufacturer-Distributor Interface

Fig. 2 shows the inventory trajectory for manufacture-distributor linkage for three distributors (M=3) and a given production sequence (Z=1-3-2). The relevant costs at the distributors include the ordering cost and inventory holding cost, whereas those at the manufacturer consist of production setup cost and inventory holding cost.

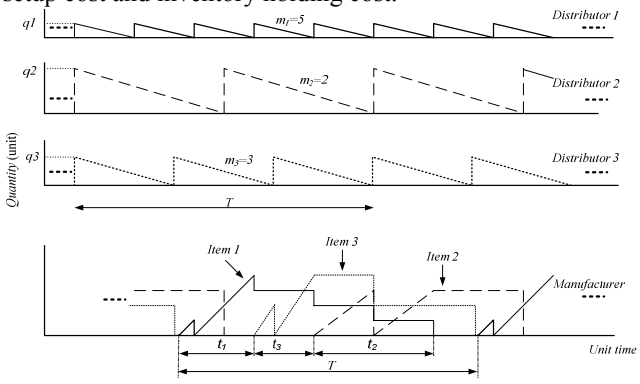

Fig. 2 The manufacturer-distributor inventory profile

Recalling formula in [10], the average total cost for this interface (ATC_{MD}) is given as in (1).

$$\mathbf{ATC_{MD}}(\mathbf{m},T)=\left(\sum_{i=1}^{M}A_i m_i+S_i\right)/T+Ty \quad (1)$$

Where $y=\sum_{i=1}^{M}0.5D_i/m_i\left(H_i\left(m_i\left(1-D_i/P_i\right)-\left(1-2D_i/P_i\right)\right)+h_i\right)$.

D and P are distributors' demand rate and manufacturer's production rate, respectively. H[h] is holding cost for manufacturer [distributor] while A and S represent distributor's ordering cost and manufacturer's setup cost, respectively. Subscript i indicates the product index.

B. Supplier-Manufacturer Interface

The pattern of part demand ($Dp(t)$) and the average part demand, ($\overline{Dp}$), depends on the production sequence (Z), production time (t_i) and BOM profiles, see Fig. 3(a). The manufacturer receives the required parts in an equal delivery cycle during α (n=3 in Fig. 3(a)). Under this circumstance, the shortage may occur when $\overline{Dp} < Dp(t)$. Therefore, a buffer mechanism is introduced. The inventory trajectory for the buffer part is shown in Fig. 3(b). The buffer builds up when $\overline{Dp} > Dp(t)$ and decreases for otherwise conditions. The average total part inventory status at the manufacturer (Ip) is obtained by summing the shaded areas in Fig. 3(a) and Fig. 3(b), dividing the result by T, and subtracting final result with IC, where IC=IB-IA as shown in Fig. 3(c).

The relevant costs in procurement activities consist of the ordering cost and part inventory holding cost. Then, the average total cost (ATC_M) for N number of suppliers/parts can be represented as in (2).

$$\mathbf{ATC_M}(\mathbf{n},T,Z)=\sum_{j=1}^{N}Ar_j n_j/T+Hr_j Ip_j(\mathbf{n},T,Z) \quad (2)$$

Where Ar and Hr represent the manufacturer's ordering cost and inventory holding cost per unit/time, respectively. Subscript j denotes the part/ supplier index.

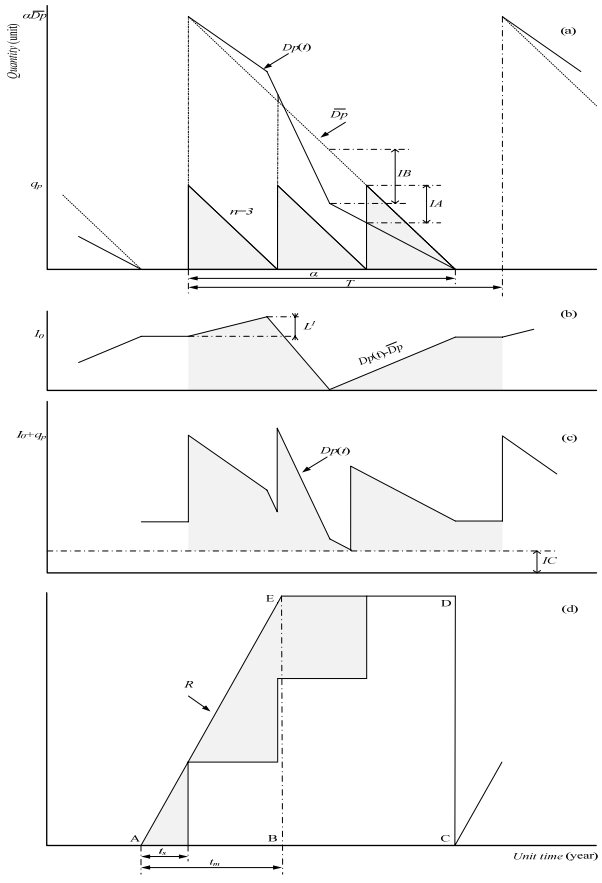

Fig. 3 The supplier-manufacturer inventory profile

Let $\rho_i = D_i/P_i$; a_{ij} denotes the number of part j required for producing one unit item i, then Ip is as in (3), see Appendix A for the procedures of acquiring Ip in details.

$$Ip_j(\mathbf{n},T,Z) = 0.5T\sum_{i=1}^{M} a_{ij}D_i\sum_{i=1}^{M}\rho_i / n_j + W \quad (3)$$

Where

$$W = I_{0j}(1-\sum_{i=1}^{M}\rho_i) + \sum_{k=1}^{M}\rho^k(I_{0j} + 0.5L_j^k + \sum_{l=1}^{k-1}L_j^l) - IC_j(\mathbf{n},Z) \quad (4)$$

The relevant costs for suppliers include the production setup cost and inventory holding cost. Here, it is assumed that all the delivery related costs are inclusive in manufacturer's ordering cost. Furthermore, the suppliers' production cycles are equal to the manufacturer's. Given R is the supplier's replenishment rate, the shaded area in Fig. 3(d) can be obtained by subtracting area ABCDE with area under step-like pattern. Dividing the result by the cycle time (T) will obtain the average inventory at suppliers (Is) and can be expressed as in (5), see Appendix B for the detailed procedures.

$$Is_j(\mathbf{n},T) = T\sum_{i=1}^{N} a_{ij}D_i\sum_{i=1}^{M}\rho_i((\overline{Dp}_j / R_j - 0.5)/n_j + 0.5(1-\overline{Dp}_j / R_j)) \quad (5)$$

The average total cost at suppliers (ATC_s) then can be written as in (6). The supplier's setup cost is denoted with K.

$$\mathbf{ATC_s}(\mathbf{n},T) = \sum_{j=1}^{N} K_j / T + Hs_j Is_j \quad (6)$$

Summing Eq.(1), (2) and (6) returns the average total cost of entire system (ATC) as a function of **m**, T, Z and **n** and is given in (7).

$$\mathbf{ATC}(\mathbf{m},T,Z,\mathbf{n}) = ((\sum_{i=1}^{M} A_i m_i + S_i) + (\sum_{j=1}^{N} Ar_j n_j + K_j))/T + Ty + \sum_{j=1}^{N} Hr_j Ip_j(\mathbf{n},T,Z) + Hs_j Is_j(\mathbf{n},T) \quad (7)$$

Here, the objective is to find a set of decision variables, which contain the number of the ordering deliveries for each distributor, the common production cycle for each item, the production sequence and the number of part shipments of each part, that minimize Eq. (7). Vectors **n** and **m** have integer values, a real value for T, while Z contains the best sequence.

IV. Upcoming Works

Formula in Eq. (7) has been manually verified. Observing that to solve the problem analytically is almost intractable, we performed extensive numerical experimentations using guided looping procedures to confirm our model. It is important to note that Kim's model is a special case of our model. By setting the values N=1, a_{i1}=1 for all i, n_1=1 and all other suppliers' parameters to zero our model then should behave as Kim's. Based on the numerical experimentations for such problems, our model returned the same results as in Kim's [10]. Further, Table I presents the performance of our model in dealing with more general problems for five cases with three products and one part in comparison to Kim's. The parameters are randomly generated. The results confirmed that adopting the SSMD policy provides better outcomes in dealing with three-echelon problems.

As the number of parts and items increase, the looping procedure becomes hardly implemented. The existence of Z inevitably leads the problem to fall into combinatorial categories. The solution space explodes exponentially along with the number of products. Consequently, solving such a problem using the procedures consume a considerable computation time. For instance, finding solution for a problem with two products and three components requires approximately 45 minutes.

Acknowledging this issue, we are currently working on developing a genetic algorithm to find the best solution for the problem in (7). The genetic algorithm is utilized as this algorithm has an excellent performance on handling combinatorial optimization. It offers an "optimal" or close to the best solution with a reasonable computation time provided it is appropriately designed. In addition, an extensive numerical experimentation will also be carried out to investigate the performance of the developed model and algorithm.

TABLE I
NUMERICAL RESULTS COMPARISON

	Parameters input a=[2 1 2]	*ATC* ($)		Saving (%)
		Kim's	Ours	
1	*D*=[2706;2377;2880], *h*=[8;6;8], *A*=[13;15;23], *P*=[10320;11108;11611], *H*=[5;5;4], *S*=[219;325;319], *Hr*=3, *Ar*=182, *R*=15139; *Hs*=3, *K*=391	18061	14856	17.74
2	*D*=[2420;3315;3204], *h*=[6;9;8], *A*=[18;24;15], *P*=[10889;11479;11392], *H*=[5;4;5], *S*=[387;228;212], *Hr*=3, *Ar*=170 *R*=17109; *Hs*=3, *K*=315	18342	15941	13.10
3	*D*=[2864;2325;2870], *h*=[6;7;8], *A*=[13;24;15], *P*=[10715;10122;10011], *H*=[5;5;5], *S*=[466;386;381], *Hr*=2, *Ar*=218 *R*=14121; Hs=2, *K*=579	19320	16484	14.68
4	*D*=[2857;2856; 2277], *h*=[9;7;7], *A*=[21;11;18], *P*=[11126;11018;11070], *H*=[5;5;5], *S*=[418;202;370], *Hr*=4, *Ar*=180 *R*=15749; Hs=3, *K*=409	19376	16537	14.65
5	*D*=[3770;3426;3053], *h*=[6;7;7] *A*=[14;14;13], *P*=[11563;11766;11878], *H*=[4;5;5], *S*=[399;274;266], *Hr*=4, *Ar*=248 *R*=18792; *Hs*=3, *K*=525	23228	19990	13.94

V. Conclusions

This paper extends Kim's model (10) by covering a three echelon problem comprising of a number of distributors, single manufacturer/ assembler and several part suppliers. The manufacturer and suppliers agree to adopt SSMD policy in handling the fluctuating part demand. A mathematical model representing the considered problem has been successfully formulated and verified. The numerical experimentation results show that our model outperforms to Kim's. However, a considerable computation time is required to find the optimal solution. It emerges as one main drawback to address in the upcoming works. For that reason, the authors are currently working on developing genetic algorithms to find an effective and efficient solution search.

References

[1] Goyal, S. K., "An integrated inventory model for a single supplier-single customer problem," *International Journal of Production Research,* Vol.15, pp. 107 – 111, 1977.
[2] Banerjee, A., "A joint economic-lot-size model for purchaser and vendor," *Decision Sciences*, Vol.17, pp. 292–311, 1986.
[3] Goyal, S. K., "A joint economic-lot-size model for purchaser and vendor: A comment," *Decision Sciences*, Vol.19, pp. 236–241, 1988.
[4] Hill, R. M., "The single-vendor single-buyer integrated production–inventory model with a generalized policy," *European Journal of Operational Research*, Vol. 97, pp. 493–499, 1997.
[5] Kim, S.-L. & Ha, D., "A JIT lot-splitting model for supply chain management: Enhancing buyer–supplier linkage," *Int. J. Production Economics*, Vol. 86, pp. 1–10, 2003.
[6] Ben-Daya, M., Darwis, M. & Ertogral, K., "The joint economic lot sizing problem: Review and extensions," *European Journal of Operational Research*, Vol. 185, pp. 726–742, 2008.
[7] Lu, L., "A one-vendor multi-buyer integrated inventory model," *European Journal of Operational Research*, Vol. 81, pp. 312-323, 1995.
[8] Siajadi, H., Ibrahim, R. N. & Lochert, P. B., "A single-vendor multiple-buyer inventory model with a multiple-shipment policy," *Int J Adv Manuf Technol*, Vol. 27, pp. 1030–1037, 2006.
[9] Hoque, M. A., "Synchronization in the single-manufacturer multi-buyer integrated inventory supply chain," *European Journal of Operational Research*, Vol. 188, pp. 811–825, 2008.
[10]Kim, T., Hong, Y. & Chang, S. Y., "Joint economic procurement--production-delivery policy for multiple items in a single-manufacturer, multiple-retailer system," *Int. J. Production Economics*, Vol.103, pp. 199-208, 2006.
[11]Jaber, M. Y. & Goyal, S. K., "Coordinating a three-level supply chain with multiple suppliers, a vendor and multiple buyers," *Int. J. Production Economics*, Vol. 116, pp. 95-103, 2008.

APPENDIXES

Appendix A. The average total part inventory at the manufacturer (Ip)

Inventory at the manufacturer comprises of regular (Fig. 3(a) and buffer inventories Fig. 3 (b)). The average of the shaded area in Fig. 3(a) is equal to

$$0.5\alpha^2 \overline{Dp}_j /(Tn_j)\,. \quad (8)$$

Since $\overline{Dp}_j = \sum_{i=1}^{M} a_{ij} D_i / \sum_{i=1}^{M} \rho_i$ then

$$0.5T\sum_{i=1}^{M} a_{ij} D_i \sum_{i=1}^{M} \rho_i / n_j\,. \quad (9)$$

For given Z, the buffer inventory area for part j, Fig. 3(b), can be calculated as

$$0.5t^1(I_{0j} + I_{0j} + L^1_{.j}) + 0.5t^2(I_{0j} + L^1_{.j} + I_{0j} + L^1_{.j} + L^2_{.j}) + ... +$$
$$0.5t^M(I_{0j} + L^1_{.j} + ... + L^{M-1}_{.j} + I_{0j} + L^1_{.j} + ... + L^M_{.j}) + I_{0j}(T-\alpha)\,. \quad (10)$$

Where

$I_{oj} = \left|\min \sum_{k=1}^{l} L^k_{.j}\right|, \forall l \in 1,2,...,M_i$ and $L^k_{.j} = T\rho^k(\overline{Dp}_j - a^k_{.j}P^k)$.

Note, a superscript indicates the order number in sequence Z. Employing algebraic manipulation then we acquire Eq. (11).

$$I_{0j}(T-\alpha) + \sum_{k=1}^{M} t^k (I_{0j} + 0.5L^k_{.j} + \sum_{l=1}^{k-1} L^l_{.j}) \quad (11)$$

Replacing t_i and α with $\rho_i T$ and Σt_i, respectively and divide the result by T to obtain the average inventory of Fig. 3(b) yields Eq. (12).

$$I_{0j}(1-\sum_{i-1}^{M}\rho_i) + \sum_{k=1}^{M}\rho^k (I_{0j} + 0.5L^k_{.j} + \sum_{l=1}^{k-1} L^l_{.j}) \quad (12)$$

Given Z, then part demand pattern as function of t is

$$Dp_j(t \mid Z) = \begin{cases} a^k_{.j} P^k \text{ for } \alpha_{k-1} < t < \alpha_k \\ 0 \quad \text{for } \alpha_M < t < T \end{cases}; k = 1, 2, ..., M\text{-}1 \quad (13)$$

Where $\alpha_k = \sum_{i=1}^{k} t^i; \alpha_0 = 0; \alpha_M = \alpha$

Based on Fig. 3(a), the values of *IB* and *IA* are as in Eq. (14) and (15), respectively.

$$IB_j(Z) = \left|\min(\overline{Dp}_j t - Dp_j(t \mid Z)t)\right|, \forall t \in \sum_1^k t^k; k = 1,2,...,M \quad (14)$$

$$IA_j(n,Z) = \left|\min(\overline{Dp}_j t - Dp_j(t \mid Z)t)\right|, \forall t \in \sum_{b=1}^{n_j} b\alpha / n_j \quad (15)$$

Summing Eq. (9) and (12), then subtracting the result with IC_j yields the average total part inventory at the manufacturer (*Ip*), as in Eq. (16).

$$\mathbf{Ip}_j(\mathbf{n}, T, Z) = 0.5T\sum_{i=1}^{M} a_{ij} D_i \sum_{i=1}^{M} \rho_i / n_j +$$
$$I_{0j}(1-\sum_{i=1}^{M}\rho_i) + \sum_{k=1}^{M}\rho^k (I_{0j} + 0.5L^k_{.j} + \sum_{l=1}^{k-1} L^l_{.j}) - IC_j(n,Z) \quad (16)$$

Where $IC_j(\mathbf{n},Z) = IB_j(Z) - IA_j(\mathbf{n},Z)$

Appendix B. The average inventory for suppliers (Is)

The shaded area in Fig. 3(d) is calculated by summing the area of triangle ABE and rectangular BCDE and subtracted by area under the step-like trajectory.

The area of triangle ABE is

$$0.5tm_j \overline{Dp}_j \alpha\,. \quad (17)$$

The area of triangle BCDE is

$$(T - tm_j)\overline{Dp}_j \alpha\,. \quad (18)$$

The area under step-like pattern is

$$1/n_j((\overline{Dp}_j \alpha(T - ts_j) + \overline{Dp}_j \alpha(T - ts_j - \alpha/n_j) + ... +$$
$$\overline{Dp}_j \alpha(T - ts_j - (n-1)\alpha/n_j)) \quad (19)$$

Simplifying Eq. (19) returns Eq. (20).

$$\overline{Dp}_j \alpha(n_j(T - ts_j) - 0.5\alpha(n-1))/n_j \quad (20)$$

Summing Eq. (17) and (18) then deducted by Eq. (20) to acquire the total shaded area in Fig. 3(d) and expressed as

$$\overline{Dp}_j \alpha(ts_j + 0.5\alpha(n-1))/n_j - 0.5tm_j)\,. \quad (21)$$

The average inventory is then given by

$$\overline{Dp}_j \alpha(ts_j + 0.5\alpha(n-1))/n_j - 0.5tm_j)/T\,. \quad (22)$$

From Fig. 3(d), we have

$$ts_j = \overline{Dp}_j \alpha/(n_j R_j) \quad (23)$$

$$tm_j = \overline{Dp}_j \alpha / R_j \quad (24)$$

Substituting α, Eq. (23) and (24) to the formula in (22) and after simplifications return *Is* as in (25).

$$Is_j(\mathbf{n}, T) = T\sum_{i=1}^{N} a_{ij} D_i \sum_{i=1}^{M} \rho_i((\overline{Dp}_j / R_j - 0.5)/n_j + 0.5(1 - \overline{Dp}_j / R_j)) \quad (25)$$

2011 International Conference on Mechanical, Industrial, and Manufacturing Engineering
Lecture Notes in Information Technology Vols. 1-2

Quantum-behaved Particle Swarm Optimization Algorithm for Dynamic Parameters Optimization of Electromechanical Coupling System

LI Qiang
College of Electromechanical Engineering
North China University of Technology
Beijing 100144, China
liqiang@ncut.edu.cn

Zheng Xin
College of mechanical Engineering
Inner Mongolia University of Technology
Hohhot, Inner Mongolia,010051, China
sunday5921@yahoo.cn

Abstract - **Dynamic optimization of electromechanical system is a multi-subject problem .The modeling method and optimization of such kind of problem is studied in the paper. A kind of new exponential inertia weight quantum-behaved particle swarm algorithm is presented. The results of application example proved that practical optimization parameters can be obtained in limited time by the method, and it is an effective way to solve such kind of problem .**

Keywords: electromechanical system. quantum-behaved particle swarm optimization. Dynamic parameters optimization.

I. INTRODUCTION

Complex electromechanical system occupies an important position in people's actual production and daily life. The traditional design will show some of the features of the defect because the design process does not take into account the coupling system of multi-disciplinary relationships in design tasks. Electromechanical analysis of dynamics is an effective way in studying in most of the mechanical and electrical coupling system of Dynamics which studies the interaction of mechanical and electrical coupling rule by means of energy coupling to establish electrical and mechanical systems of the mathematical model.

This algorithm has lots of merits such as less control parameters, a strong global optimization capability and so on. In practice, QPSO is a effectively global convergence optimization algorithm much better than the traditional algorithm in convergence, stability and so on.Based on the study of particle swarm optimization(PSO) algorithm and quartum-behaved particle swarm optimization, this paper proposed an exponential inertia weight quantum-behaved particle swarm optimization algorithm (EQPSO). Using the energy method , the electrical and mechanical parameters of the electromechanical coupling is designed in the movement and the dynamics of complex partial differential equations are trial and error solution in several different ways. At last the exponential inertia weight quantum-behaved particle swarm optimization algorithm is useful in finding the right solution in time. Through the theoretical analysis of the exponential inertia weight convergence, the superiority of the exponential inertia weight quantum-behaved particle swarm optimization algorithm is given.

II. PSO AND QUANTUM DESCRIPTION

Most of the optimization problem can be viewed as m-dimensional space of the point or vector in the m-dimensional space optimization problem . And the optimization problem can be described as:

$$\left.\begin{array}{ll} \min & f(x)= \quad f(x_1,x_2,\cdots,x_m) \\ s.t. & a_i \le x_i \le b_i; \quad i=1,2,\cdots,m. \end{array}\right\}$$

Here:

M is the number of variables to be optimized;

$[a_i\, b_i]$ is the definition demain of the variable x_i;

f is the objective function, making its value as the particle fitness.

Particle swarm optimization(PSO) is a population-based optimization strategy introduced by Kennedy and Eberhart[17]

In recent years it shows huge advantages in many complex optimization problems . It is initialized using a group of random particles and updating its velocities and positions with the following equation:

$$v_{id}^{k+1} = w \times v_{id}^{k} + c_1 \times r_1 \times (P_{id} - x_{id}^{k}) + c_2 \times r_2 \times (P_{gd} - x_{id}^{k})$$

$$x_{id}^{k+1} = x_{id}^{k} + v_{id}^{k+1}$$

Quantum computation is a novel multidiscipline that includes quantum mechanics and information science. In quantum computing, the smallest unit of information is called a Q-bit, which is defined as

$$|\phi\rangle = \alpha|0\rangle + \beta|1\rangle$$

in the other form could be expressed as $\begin{bmatrix}\alpha \\ \beta\end{bmatrix}$. Where α and β are complex numbers that specify the probability amplitudes of the corresponding states. The moduli $|\alpha|^2$ and $|\beta|^2$ are the probabilities that the Q-bit exists in state "0" and state "1", respectively, which satisfy

$$|\alpha|^2 + |\beta|^2 = 1$$

an m-Q-bit is defined as $\begin{bmatrix}\alpha_1 & \alpha_2 & \cdots & \alpha_m \\ \beta_1 & \beta_2 & \cdots & \beta_m\end{bmatrix}$,

where $|\alpha_i|^2 + |\beta_i|^2 = 1 \ (i=1,2,\cdots,m)$,and m is the number of Q-bits. A quantum also could be defined as $\begin{bmatrix}\sin(\theta) \\ \cos(\theta)\end{bmatrix}$ and it

is satisfies that $|\sin(\theta)|^2 + |\cos(\theta)|^2 = 1$ spontaneously. So an m-Q-bits could be the same form $\begin{bmatrix} \cos(\theta_1) & \cos(\theta_2) & \cdots & \cos(\theta_m) \\ \sin(\theta_1) & \sin(\theta_2) & \cdots & \sin(\theta_m) \end{bmatrix}$. Then an m-Q-bits could be replaced by the form $\left[\theta_1 \middle| \theta_2 \middle| \cdots \middle| \theta_m\right]$ and it is the same form as an particle in the PSO.

Besides, a Q-gate was introduced as a variation operator to promote the optimization of the individuals Q-bit.

$$\begin{bmatrix} \cos(\Delta\theta) & -\sin(\Delta\theta) \\ \sin(\Delta\theta) & \cos(\Delta\theta) \end{bmatrix}$$

In the iteration it works with following equation:

$$\begin{bmatrix} \cos(\theta_{ij}^{(k+1)}) \\ \sin(\theta_{ij}^{(k+1)}) \end{bmatrix} = \begin{bmatrix} \cos(\Delta\theta_{ij}^{(k+1)}) & -\sin(\Delta\theta_{ij}^{(k+1)}) \\ \sin(\Delta\theta_{ij}^{(k+1)}) & \cos(\Delta\theta_{ij}^{(k+1)}) \end{bmatrix} \begin{bmatrix} \cos(\theta_{ij}^{(k)}) \\ \sin(\theta_{ij}^{(k)}) \end{bmatrix}$$
$$= \begin{bmatrix} \cos(\theta_{ij}^{(k)} + \Delta\theta_{ij}^{(k+1)}) \\ \sin(\theta_{ij}^{(k)} + \Delta\theta_{ij}^{(k+1)}) \end{bmatrix}$$

III. EQPSO ALGORITHM

The exponential inertia weight quantum-behaved particle swarm optimization algorithm updates its velocities and positions with the following equation:

$$\Delta\theta_{ij}^{(k+1)} = e^{-(ak)}\Delta\theta_{ij}^{(k)} + c_1 r_1(\theta_{ij}(Pbest) - \theta_{ij}^{(k)}) + c_2 r_2(\theta_{ij}(Gbest) - \theta_{ij}^{(k)}) \quad (1)$$

$$\theta_{ij}^{(k+1)} = \theta_{ij}^{(k)} + \Delta\theta_{ij}^{(k+1)} \quad (2)$$

$(i = 1,2,\cdots,n;\ j = 1,2,\cdots m;\ k = 1,2,\cdots d)$

Where, i is a particle in population, j is the number of dimensions, a, c_1, c_2 are the selected positive real numbers; r_1, r_2 are random numbers in the field of [0,1].

The Procedure of EQPSO is shown in the following:

Do

$k \leftarrow 0$

Initialize $Q^k(\theta_{ij}) = (\theta_{i1}^k, \theta_{i2}^k, \cdots, \theta_{im}^k)$,

Initialize $Pbest(\theta_{ij}) = (\theta_{P-i1}, \theta_{P-i2}, \cdots, \theta_{P-im})$,

for max-iteration $k \leftarrow k+1$

Solution space transforming:

$Q(\theta_{ij}) \rightarrow X(\theta_{ij})$ and $Pbest(\theta_{ij}) \rightarrow X(\theta_{P-ij})$,

mapping transformation from [-1 1] to $[a_i\ b_i]$

Evaluate $f(X(\theta_{ij}))$ and $f(X(\theta_{P-ij}))$,

save the value of

$f(X(\theta_{P-ij}))$ and $Pbest(\theta_{ij})$,

If $f(X(\theta_{ij})) < f(X(\theta_{P-ij}))$

$f(X(\theta_{P-ij})) = f(X(\theta_{ij}))$

$\theta_{P-ij} = \theta_{ij}$

End if

get the Gbest's value and θ_{best} save in Gbest

if termination condition

break

end if

Update $\Delta\theta_{ij}^{(k+1)}$ using (1)

Update $\theta_{ij}^{(k+1)}$ using (2)

End for

Output Gbest

To induce (2) with (1), we can deduce the following equation:

$$\theta_{ij}^{(k+1)} = \theta_{ij}^{(k)} + e^{(-ak)}\Delta\theta_{ij}^{(k)} + c_1 r_1(\theta_{ij}(Pbest) - \theta_{ij}^{(k)}) + c_2 r_2(\theta_{ij}(Gbest) - \theta_{ij}^{(k)}) \quad (3)$$

From (2), we get

$$\Delta\theta_{ij}^{(k)} = \theta_{ij}^{(k)} - \theta_{ij}^{(k-1)} \quad (4)$$

To combine (4) and (3), we get

$$\theta_{ij}^{(k+1)} = \theta_{ij}^{(k)} + e^{-ak}(\theta_{ij}^{(k)} - \theta_{ij}^{(k-1)}) + c_1 r_1(\theta_{ij}(Pbest) - \theta_{ij}^{(k)}) + c_2 r_2(\theta_{ij}(Gbest) - \theta_{ij}^{(k)}) \quad (5)$$

With the increase of generation number k, e^{-ak} gradually tends to zero, (5) is changed to the following:

$$\theta_{ij}^{(k+1)} = \theta_{ij}^{(k)} + c_1 r_1(\theta_{ij}(Pbest) - \theta_{ij}^{(k)}) + c_2 r_2(\theta_{ij}(Gbest) - \theta_{ij}^{(k)}) \quad (6)$$

According to (6), it is obvious to know that $\theta_{ij}^{(k)}$ is operated in iterative way by Pbest and Gbest, which is acted by random disturbance r_1 and r_2.Inertia weight factor w which controlling the the global searching ability and local searching capabilities is a key influencing factor in algorithm performance. Large inertia weight factor could increase the ability in the global best result searching and help the particles to rush out of local minimum points, but making the algorithm working too slow; smaller inertia weight factor is much better for the local search ability, making the algorithm to be conducive to quick results, but easy to falling into the local optimum . So in the experiments, the valuation of the w should be taken a large number to strengthen the global search ability at first, decreasing the valuation of the w gradually to accelerating convergence. The value of the w in the standard quantum-behaved particle swarm optimization algorithm is between 0 and 1.

IV. Dynamic Optimization Method of lectromechanical System

The swing spindle system of machine tool for solid rocket is taken as the application example. In the spindle system shown as Fig. 1, the rise of speed in spindle motor will cause tool vibration in the actual machining. So, dynamic optimization on electromechanical parameters of spindle system is necessary in order to meet the needs of dynamics performance. Servomotor dynamics modeling is the key issue of electromechanical coupling dynamics analysis. Based on electromechanical energy equations, Lagrange-Maxwell equation and Park transform are adopted to construct the dynamic equations.

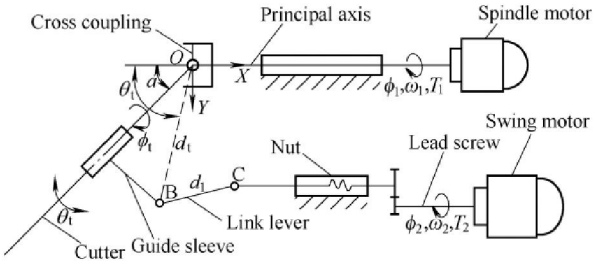

Fig.1. Swing spindle system of machine sketch

by permanent magnet synchronous servomotor, dynamic differential equations of 2DOF spindle system have been deduced. The dynamic differential equation is expressed as follows:

$$\begin{cases} L_{d1}\dfrac{d(i_{d1})}{dt}+r_1 i_{d1}-L_{q1}i_{q1}\dot{\varphi}_1=U_{d1} \\ L_{q1}\dfrac{d(i_{q1})}{dt}+r_1 i_{q1}+P_1 L_{d1} i_{d1}\dot{\varphi}_1+P_1\psi_{f1}\dot{\varphi}_1=U_{q1} \\ L_{d2}\dfrac{d(i_{d2})}{dt}+r_2 i_{d2}-L_{q2}i_{q2}\dot{\varphi}_2=U_{d2} \\ L_{q2}\dfrac{d(i_{q2})}{dt}+r_2 i_{q2}+P_2 L_{d2} i_{d2}\dot{\varphi}_2+P_2\Psi_{f2}\dot{\varphi}_2=U_{q2} \\ J_{11}\ddot{\varphi}_1+J_{12}\ddot{\varphi}_2+\dfrac{1}{2}\dfrac{\partial J_{11}}{\partial\varphi_1}\dot{\varphi}_1^2+\dfrac{\partial J_{11}}{\partial\varphi_2}\dot{\varphi}_1\dot{\varphi}_2+ \\ \left(\dfrac{\partial J_{12}}{\partial\varphi_2}-\dfrac{1}{2}\dfrac{\partial J_{22}}{\partial\varphi_1}\right)\dot{\varphi}_2^2-\dfrac{3}{2}\left[i_{q1}\psi_{f1}+\right. \\ \left.(L_{d1}-L_{q1})i_{d1}i_{q1}\right]+B_1\dot{\varphi}_1=T_1 \\ J_{22}\ddot{\varphi}_2+J_{12}\ddot{\varphi}_1+\dfrac{1}{2}\dfrac{\partial J_{22}}{\partial\varphi_2}\dot{\varphi}_2^2+\dfrac{\partial J_{22}}{\partial\varphi_1}\dot{\varphi}_1\dot{\varphi}_2+ \\ \left(\dfrac{\partial J_{12}}{\partial\varphi_1}-\dfrac{1}{2}\dfrac{\partial J_{11}}{\partial\varphi_2}\right)\dot{\varphi}_1^2-\dfrac{\partial\theta_t}{\partial\varphi_2}\left[m_t g(l\cos\alpha)+\right. \\ \left.m_t g\left(\dfrac{d_t\cos\theta_t}{2}\right)\right]-\dfrac{3}{2}\left[i_{q2}\psi_{f2}+(L_{d2}-L_{q2})i_{d2}i_{q2}\right]+B_2\dot{\varphi}_2=T_2 \end{cases} \quad (7)$$

In (7),l_{d1},l_{q1} and l_{d2},l_{q2} are the inductances of the servomotor in coordinate axes; i_{d1}, i_{q1} and i_{d2}, i_{q2} are the currents of the servomotor; r_1, r_2 are the equivalent electricity resistances; P_1, P_2 are the magnet pole numbers; U_{d1}, U_{q1} and U_{d2}, U_{q2} are the voltages of the servomotor; ψ_{f1}、ψ_{f2} are the magnet chains of the servomotor; B_1,B_2 are the viscidity stagnant resistances; T_1,T_2 are the moment loads of the servomotor; g is gravitation acceleration; J_{11},J_{22},J_{12} are the machine equivalent moment of inertia.

The dynamic optimization problem of the swing spindle system is how to choose the dynamics parameters of the electromechanical system, in order that the turning and deflexion vibration acceleration of tool A_1 and A_2 can become minimum:

$$A_1=\max_{0\le t\le 3}\left|\ddot{\varphi}_1(t)\right|$$

$$A_2=\max_{0\le t\le 3}\left|\ddot{\varphi}_2(t)\right|$$

Because the tool turning acceleration direction and the deflexion acceleration direction are kept perpendicularity with each other, the adaptation function can be constructed as follows:

$$G(x)=\sqrt{A_1^2+A_2^2} \quad (8)$$

The EQPSA optimization method is adopted to implement optimization calculation. Compared with different kinds of numerical solution methods of nonlinear and variable coefficient ordinary differential equation, Hamming method is adopted to solve the dynamic differential equations. Flow chart of spindle system optimization is shown as Fig. 3. The design variables are listed in Table. B_x is the abscissa value of B; B_y is the vertical coordinate value of point B; C_x is the abscissa value of C; C_y is the vertical coordinate value of point C; R is the rolling resistance of the servomotor; L is the inductance; Ψ is the magnetic flux. The mechanical parameters of the swing spindle system, such as mass and inertia moment of tool, guiding knot, connecting rod and leading screw, are decided by the coordinate values of points B and C.

The population scale of the EQPSO is 100. The largest iterative number is 100. After 34.3 hours calculation on Dell Optiplex 330 computer, the results of the dynamic optimization of the swing spindle system are obtained as in Table

TABLE I
OPTIMIZED RESULTS OF SWING SPINDLE ELECTROMECHANICAL PARAMETERS

parameter		Optimized value
Adaptation	$G(x)/(rad\cdot s^{-2})$	5.97398
Coordinate	B_x/m	-0.0776
Coordinate	B_y/m	0.0516
Coordinate	C_x/m	0.0478
Coordinate	C_y/m	0.06154
Resistance	R/Ω	1.583268
Inductance	L/H	0.005702
Flux	Ψ/Wb	0.111142

The optimized design variables are applied to the dynamic differential equations of the swing spindle system. Then we solve the equations again, and obtain the optimization results. The curves in Fig. 2 and Fig. 3 are the solution of speed and

acceleration separately. The optimized vibration curve is very similar to the original curve, but the amplitude of vibration is decreased obviously.

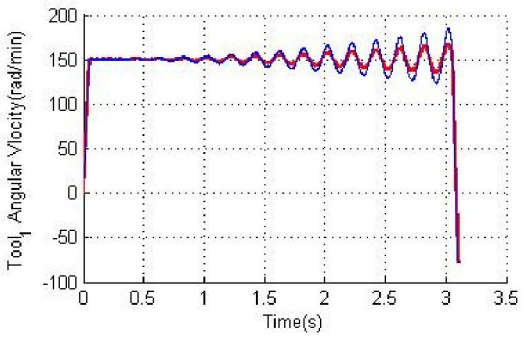

Fig. 2.Rotational speed of tool1 before-and-after optimization

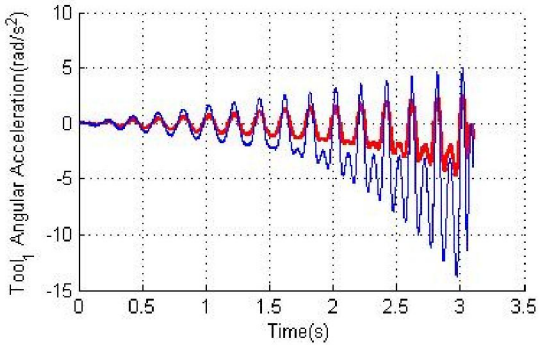

Fig. 3.Rotational acceleration of tool1 before-and-after optimization

The tool maximum speed is 185.0806rad/min before optimization, after the optimization the tool maximum speed is 168.0864rad/min. The decrease of angular velocity improves the stability of the machine cutting process. The Tool rotation angular acceleration is 13.8058rad/s^2 and after optimization it is reduced to 4.7155 rad/s^2. Because the rotational acceleration of tool's amplitude of vibration is reduced significantly, the impact effect of the rotating tool is reduced as expected. The Swing tool's deflection angular velocity decreased significantly making the swing tool working more smoothly.

V. CONCLUSIONS

(1) The novel quantum-behaved particle swarm optimization algorithm is a high efficiency global optimization capability algorithm.

(2) The problem of dynamic optimization of electromechanical system can be solved with the combining of dynamic analysis of electromechanical system and EQPSA.

(3) For the high dimensional complex problem on dynamics optimization of electromechanical system, if the weight value of the swarm particle algorithm can be changed with special exponential function, the global optimization efficiency can be enhanced greatly.

(4) The results of application example prove that the acceleration of the tool and the torque vibration of deflexion servomotor are decreased by the optimized electromechanical system parameters. The dynamics optimization of electromechanical coupling system is feasible. The presented method can be applied to the design of robots and other mechatronics equipments.

REFERENCES

[1] Samin J C,Bruls O,Collard J F. Sass L. Fisett.P Multiphysics modeling and optimization of mechatronics multibody systems[J]. Multibody System Dynamics, 2007, 18: 345~373

[2] Shoemaker A C,Tsui K L. Jeffwu C F, Economical experimentation methods for robust design [J]. Technometrics, 1991, 33: 415~427

[3] SUNDARESAN S. A robust optimization procedure with variations on design variables and constrains [J]. Journal Mechanical Design, 1993, 115:379~386

[4] Su J, Renaud J E Automatic differentiantion in robust optimization [J]. AIAA Journal, 1997, 35(6): 1072~1079

[5] Chen W. Qualityutility—a compromise programming approach to robust design [J]. Journal Mechanical Design, 1999,121:178~187

[6] PARK F C. Quality utility – a compromise programming approach to robust design [J]. AIAA Journal, 1997, 35 (6): 1072~1079

[7] SASS L, MCPHEE J. A comparison of different methods formodelling electromchanical multibody systems [J]. Multibody System Dynamics, 2004, 12: 209~250

[8] ANUKAL C, SANKARAN M. Decoupled approach to multidisciplinary design optimization under uncertainty[J]. Optimization Engineering, 2007, 8: 21~24

[9] SIRISHA R, ANOOP M, ACHILLE M. The challenge of equality constaints in robust design optimization: examination and new approach[J]. Struct Multidisc Optim, 2007,34:381~401

[10] GUNAWAN S, AZARM S. Multi-objective robust optimization using a sensitivity region concept[J]. Struct Multidisc Optim, 2005,29:50-60.

[11] AXEL S, CHRISTIAN O. Robust design considering highly nonlinear structural behavior[J]. Struct Multidisc Optim, 2008,35:263-272

[12] HYUNGSUK H, TAEWON P. Robust optimal design of multi-body systems[J]. Multibody System Dynamics, 2004,11:167-183.

[13] NGUYEN CC, POORAN F J. Dynamic analysis of 6 DOF robust end-dffector for dual-arm telerobot systems[J]. Robotics and Autonomous Systems, 1989,5:37-39

[14] SASS L, MCPHEE J, SCHMITKE C,et al. A comparison of different methods for modelling electronmechanical multibody systems[J]. Multibody System Dynamics,2004,12:209-250.

[15] SELIM D, OLIVIER V. Application of evolutionary strategies to optimal design of multibody system[J]. Multibody System Dynamics 2002,8:393-408.

[16] WEN Xisen, QIU Jing, TAO Junyong. Analytic dynamics and application of electromechanical system[M]. Beijing: Science Press 2003.(in Chinese).

[17] J .Kennedy , R C. Eberthart , Particle swarm optimization , in: Proceeding of IEEE International Conference on Neural Networks, vol . IV , Perth , Australia, 1995, pp . 1942-1948 .

[18] Yan Wang, et al A novel quantum swarm evolutionary algorithm and its applications. Neurocomputing 70 (2007) 633-640

[19] K.H.Han, J.H.Kim, Quantum-inspired evolutionary algorithm for a class of combinatorial optimization, IEEE Trans. Evolut. Comput,6(6)(2002)580-593.

[20] Li Shiyong, Li Panchi, Quantum particle swarms algorithm for continous space optimization[J] Chinese Journal of Quantum electronics 2007, 9: 569-574

[21] K.H.Han, J.H.Kim, Quantum-inspired evolutionary algorithm for a class of combinatorial optimization, IEEE Trans. Evolut. Comput,6(6)(2002)580-593

2011 International Conference on Mechanical, Industrial, and Manufacturing Engineering
Lecture Notes in Information Technology Vols. 1-2

Discrete Exterior Calculus implementation in MATHEMATICA: preliminary results

Giancarlo Zaccone
C.N.R. Istituto di Cibernetica 'E. Caianiello'
Via Campi Flegrei 34, 80078 Pozzuoli (Na), Italy
g.zaccone@cib.na.cnr.it

Mario Mango Furnari
C.N.R. Istituto di Cibernetica 'E. Caianiello'
Via Campi Flegrei 34, 80078 Pozzuoli (Na), Italy
mf@cib.na.cnr.it

Abstract –*Discrete Exterior Calculus* (DEC) [8] is a discrete version of the *Smooth Exterior Calculus* [2]. Exterior calculus is calculus on smooth manifolds, and DEC is a calculus for discrete manifolds, the logical connection is obtained through the algebraic topology methods applied to simplicial meshes. The main application area of DEC, is the creation of discrete operators (e.g Divergence, Gradient, Curl) to be used in numerical methods for Partial Differential Equations. Important fields of application of DEC algorithms are computational – mechanic [11], fluid dynamic, electromagnetism [4] and computer graphics. We describe the implementation of *Discrete Exterior Derivative* and *Discrete Hodge Star*, that act on discrete differential forms in a way that faithfully mirrors the behavior of the smooth operators [3], [9]. The implementation of this calculus requires an appropriate data structure to represent the *primal mesh* and its *dual* (*circumcentric dual*), because it needs to support local traversal of elements, adjacency and orientation information for the simplices of any dimension. In this paper, after a brief introduction on DEC theory, we will describe our implementation of the Discrete Exterior Derivative [8] and Discrete Hodge Star [8]. The paper end with a short description of the DEC application implement the mathematical problem of *decomposition of vector field*.

Index Terms – Discrete Exterior Calculus, Discrete Exterior Derivative, Discrete Hodge Star, Discrete Differential Forms

I. A very short introduction to DEC theory

Vector Calculus consists of operations on vectors, *primal* objects, while the Exterior Calculus [2] consists of operations on *forms, dual* objects. This duality makes possible to define differential operators algebra on smooth manifolds starting from vector calculus and using, in a very simple manner, the formalism of Exterior Calculus. It is possible since the Exterior Calculus has basically two differential operators, the *Exterior Derivative*, ***d***, and the *Hodge Star*, *******. Using these operators we express the following differential operators:

$$\begin{aligned} \nabla f &= df \\ \nabla \times F &= *dF \\ \nabla \cdot F &= *d*F \end{aligned} \qquad (1)$$

In the discrete setting, here considered, the *discrete differential forms* are defined as discrete mathematical objects using simplicial complexes (meshes). We both defined data structures to represent simplicial complexes and the implementation of the *Discrete Exterior Derivative D*, and the *Discrete Hodge Star* ♿, that act on these forms like smooth operators.

I.1 Discrete Differential Forms

Discrete differential forms [5] have a very simple representation: a *k*-form by a single scalar quantity at each *k*-dimensional simplex of the mesh. A *0*-form stores a scalar value at each vertex, a *1*-form stores a scalar value at each edge, while a *2*-form stores a scalar value at each face of the simplex.

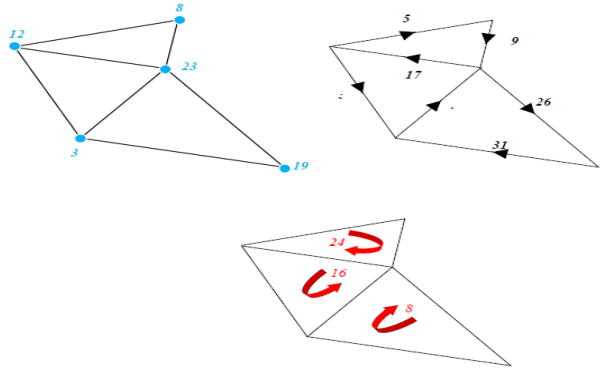

Figure 1 : Representation of 0- 1- 2- discrete differential forms

For *0*-forms, we think of this scalar as simply a point sample of a scalar-valued function, for *1*-forms, we think of this scalar as total circulation along that edge, in general we think of a discrete *k*-form as the integral of the evaluation of a smooth *k*-form over each *k*-simplex.
In addition to knowing how much stuff is moving through each simplex we also know in *which direction* the stuff is moving, if we have an edge between the vertices *a* and *b*, we need to know whether the stuff is flowing from *a* to *b* or from *b* to *a*. Hence we give an orientation that gives us a canonical direction along which the stuff flows. A positive scalar on this edge indicates that stuff is flowing in the canonical direction, and a negative scalar indicates that stuff is flowing in the opposite direction. See [1] and [6] for more references.

I.2 Discrete Exterior Derivative

Le be a discrete *k*-form. The k^{th} Discrete Exterior Derivative D_K, of is the transpose of the $(k + 1)$-st *boundary operator* [7], denoted by $\partial : D_K = (\partial_{k+1})^T$. The action

of D_K on a *k*-discrete form ω is the matrix multiplication : $D_K = (\partial_{k+1})^T$.

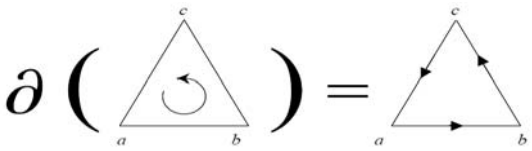

Figure 2 : the boundary ∂ operator applied to a *2*-simplex is equal to the signed sum of the edges (1-faces of the 2-simplex)

To get the scalar value for a particular (*k* + *1*)-simplex, we basically just add up the values stored on all the *k*-simplices along its boundary, but we need to be careful about orientation. Since the sign of the scalar value changes depending on the orientation of each simplex (and since this choice is arbitrary), we must take the orientation into account in our sum. This means that if the orientation of a simplex and one of the simplices on its boundary are opposite, we subtract the value stored on the boundary simplex from our sum; otherwise, we add this value. The first order exterior derivative evaluated at the edge (*1*-form) of the triangle in the figure is : *3 - 1 - 0.5 = 1.5* (the *2*-form in red). We also recall that the *smooth* exterior derivative ***d*** , maps a *k*-form to a (*k* + *1*)-form. In the discrete framework, this means we want an operator that maps a scalar quantity stored on *k*-dimensional simplices to a scalar quantity on (*k* + *1*)-dimensional simplices.

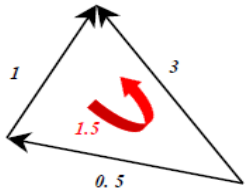

Figure 3 : Discrete Exterior Derivative

I.3 Circumcentric Dual

DEC require that we define a dual mesh or dual complex. In general, the dual of an *n*-dimensional simplicial complex identifies every *k*-simplex in the primal (i.e., original) complex with a unique (*n* - *k*)-cell in the dual complex. In a two dimensional simplicial complex, for instance, primal vertices are identified with dual faces, primal edges are identified with dual edges, and primal faces are identified with dual vertices. The combinatorial relationship between the two meshes is often not sufficient, however. We may also need to know where the vertices of our dual mesh are located. In the case of a simplicial *n*-complex embedded in $\Re^n$, dual vertices are often placed at the circumcenter of the corresponding primal simplex. The circumcenter of a *k*-simplex is the center of the unique (*k -1*)-sphere containing all of its vertices; equivalently, it is the unique point equidistant from all vertices of the simplex (this latter definition is perhaps more useful in the case of a 0- simplex). This particular dual is known as the *circumcentric dual* [8]. We also refer a discrete differential form defined on dual mesh as dual forms.

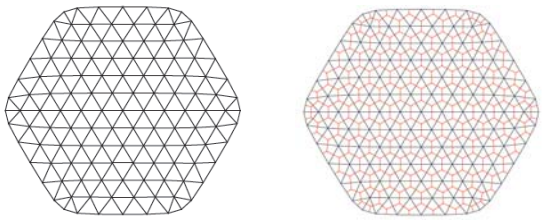

Figure 4 :Primal and Circumcentric Dual Mesh

I.4 Discrete Hodge Star

In Smooth Exterior Calculus, the Hodge Star, * [8] [5], identifies an operator that transforms a primal *k*-form into a dual *(n-k)*- form. In [8] is defined the *Discrete Hodge Star* ♁ as the discrete exterior calculus analogous of the smooth one: i.e., a discrete *k*-form on the primal mesh is an (*n* - *k*)-form on the dual mesh. Similarly, for a *k*-form Hodge Star on the dual mesh is a *k*-form on the primal mesh. Given a discrete form (whether primal or dual), its Hodge star is typically written as ♁ . The star is sometimes used to denote a dual cell as well. For instance, if is a simplex in a primal complex, ♁ is the corresponding cell in the dual complex. Unlike smooth forms, discrete primal and dual forms live in different spaces (for instance, discrete primal *k*-forms and dual *k*-forms cannot be added to each other). In fact, primal and dual forms often have different (but related) physical interpretations [6]. For instance, a primal *1*-form might represent the total circulation along edges of the primal mesh, whereas in the same context a dual *1*-form might represent the total flux through the corresponding dual edges.

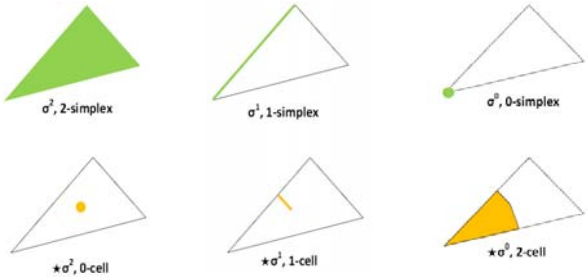

Figure 5 : *K*-Primal and (*n-k*)-Dual Form

II. Implementation

Exploiting the MATHEMATICA [12] graphical and computing capabilities, we implement these discrete objects and the *Discrete Exterior Derivative* and the *Discrete Hodge Star* operators. A simplicial complex is represented with the triple (Vertex , Edges , Faces), where Vertex is the list of simplicial complex vertex coordinates, while each row of Edges gives a pair of vertex indices defining an edge, and each row of Faces gives a triple of edge indices defining a face. In the figure 6 an example of a very simple simplicial complex is shown (it's like the OBJ representation):

```
Vertex = {{0 , 1 , 1 , 0 },{0 , 0 , 1 ,1}};
Edges = ({{1 , 3}, {3 , 4} , {1 , 4} , {1 , 2} , {2 , 3}});
Faces = ({{1 , 2 , -3} , {4 , 5 , 1}});
```

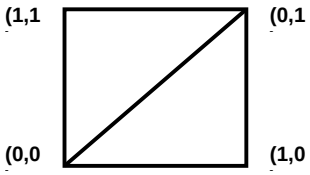

Figure 6 : simplicial complex triple and its representation

The *Discrete Exterior Derivative* on *k*-forms is represented by a matrix $D_K \in \Re^{m \times n}$ where *n* is the number of *k*-simplices into the complex, *m* is the number of $(k + 1)$ - simplices. Entry (i,j) of D_K equals ± 1 if the i^{th} $(k+1)$-simplex contains the j^{th} *k*-simplex, where the sign is positive if the orientation of the two simplices agree and negative otherwise: all other matrix entries are zero.

```
For[i = 1, i <= EdgeNumber, i++, Edge = Edges[[i]];
   vstart = Min[Edge];
   vend = Max[Edge];
   Do[[I,vend]] = 1;
   Do[[I,vstart]] = -1;
]
```

Figure 7 : source code for the primal exterior derivative

There are several ways to define the *Discrete Hodge Star*, but the most common is the diagonal Hodge Star. Consider a primal *k*-form defined on a complex *K* and let *K*' be the corresponding dual complex. If α_i is the value of α on the *k*-simplex *i*, then the diagonal Hodge star is defined by :

$$\hbar \alpha_i = (|\hbar \quad_i| / |\sigma_i|) \alpha_i \qquad (2)$$

where $|\ \ |$ indicates the volume of (note that if is a 0-cell then $|\ _i| = 1$) and $\hbar \quad \in K'$.

To compute the dual form we simply multiply the scalar value, stored on each cell, by the ratio of corresponding dual and primal volumes. This particular Hodge Star is called *diagonal* since the i^{th} element of the dual form depends only on the i^{th} element of the primal form. Hence the Hodge Star can be implemented as multiplication with a diagonal matrix whose entries are simply the ratios above described. Our procedure builds diagonal matrices representing the diagonal Hodge Star operators on primal *0*- *1*- and *2*-forms.

II.1 An application example

The *Hodge Decomposition Theorem* [5] states that:

Any vector field, $X : \Re^3 \to \Re^3$*, with compact support can be written as a unique sum of a divergence free component* ∇f *a curl free component* $\nabla \times A$ *and a harmonic part* $H : X = \nabla f + \nabla \times A + H$,

where *f* is called *scalar potential* and **A** *vector potential*, **H** is a *harmonic vector field*, i.e., a vector field such that both $\nabla \cdot H = 0$ and $\nabla \times A = 0$. Intuitively, ∇f accounts for *sources and sinks* in $X, \nabla \times A$ for *vortices*, and **H** for *any constant motion*.

The Hodge decomposition theorem also applies to two-dimensional vector fields $X : \Re^2 \to \Re^2$, but in this case **A** is a *scalar field* interpreted as the signed magnitude of a vector potential sticking out of the plane. Since vector and exterior calculus are dual, we can translate the Hodge Decomposition Theorem into the language of exterior calculus:

$$\omega \qquad = D\alpha + \hbar D \hbar \beta + \gamma \qquad (3)$$

where ω is a *1*-form input field, α is a *0*-form for the scalar potential, β is a *2*-form for the vector potential and γ is the harmonic *1*-form. On doing so, we will be able to easily compute the Hodge Decomposition of a vector field using our DEC framework. To compute the Hodge decomposition (3) we use this new version of theorem and the following system of equations:

$$\begin{aligned} D\hbar\omega &= D\hbar D\ \alpha \\ D\omega &= D\hbar\ D\hbar\ \beta \\ \gamma &= \omega - D\alpha - \hbar D\ \hbar\ \beta \end{aligned} \qquad (4)$$

In our implementation we consider the *1*-form $\omega \in \Re^2$, $\omega(x,y) = 2e^{-(x^2+y^2)}((x+y)dx + (y-x))dy)$ given on the Primal Mesh of Figure 4. To do this we discretize the *1*-form, using *one-point Gaussian quadrature*, evaluating the *1*-form over each edge with a single quadrature point located at the edge midpoint:

```
Omega = Table[0,{i,EdgeNumber},{j,1}];
For[s=1, s<=EdgeNumber,s++,indices = Edges[[s,All]] ;
      w1 = Vertex[[All,indices[[1]]]]; w2 = Vertex[[All,indices[[2]]]];
      edg = w2 - w1;
      midpoint = 0.5 (w1 + w2);
      x = midpoint[[1]]; y = midpoint[[2]];
      W = 2 Exp[-(x^2+y^2)]((x + y){1,0} + (y - x) {0,1});
      Omega[[s]] = W .edg;
]
```

Figure 8 : source code for the discretization of the ω *1*-form

After the *1*-form discretization, in order to compute and visualize the *vector field* generated by we need to interpolate the corresponding values. Since, the *Whitney bases* [4] [11] provide a set of smooth forms, that interpolate discrete forms defined on a simplicial complex, we used them to build a smooth form corresponding to a discrete form. A similar procedure have been implemented for divergence free vector field, for curl-free and harmonic field. The final results of our implementation are represented in the in figure 7.

III. Conclusions

In this paper we synthesized the main ideas underlying the DEC. Using some concepts of differential geometry and algebraic Topology we gave a simple discrete characterization of the major mathematical operators (*Divergence*, *Curl*, *Gradient*). The main DEC applications are the definition of discrete operators to be used in Partial Differential Equations numerical methods. With these goal in mind a software implementation using the MATHEMATICA framework was proposed. The symbolic manipulation approach fostered by MATHEMATICA environment simplify the programming efforts and enabled us to build the Discrete Exterior Derivative and Discrete Hodge Star operators which underpin the entire

calculation scheme. Finally, this implementation allowed us to develop the *Decomposition of Vector Fields*.

From the computational point view, few DEC-based solvers have been implemented and convergence and error analysis estimates remains to be studied. Since an increase number of PDE problems are considered in a DEC framework, further issues will undoubtedly arise.

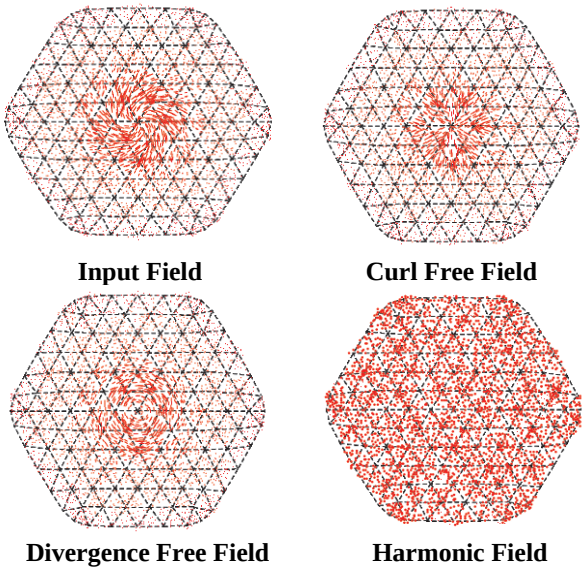

Figure 7 : Computing the decomposition of vector fields

REFERENCES

[1] R. Abraham, J. E. Marsden, and T. Ratiu. Manifolds, tensor analysis, and applications, volume 75 of Applied Mathematical Sciences. Springer-Verlag, New York, second edition, 1988.

[2] E.Cartan . Les Systemes Differentiels Exterieurs et leurs Applications Geometriques. Hermann, Paris. 1945

[3] P. Bochev and J. Hyman. Principles of mimetic discretizations of differential operators. In Compatible Spatial Discretizations, pages 89-119. Springer, 2006.

[4] A. Bossavit. Whitney forms: a class of finite elements for three-dimensional computations in electromagnetism. Proc. Of the IEEE, 135(8):493-500, 1988.

[5] M. Desbrun, E. Kanso, and Y. Tong. Discrete differential forms for computational modeling. In SIGGRAPH '06: ACM SIGGRAPH 2006 Courses, pages 39 - 54, New York, NY, USA, 2006. ACM.

[6] T. Fraenkel. 2004. The Geometry of Physics. Second Edition.Cambridge University Press, United Kingdom.

[7] A. Hatcher. Algebraic topology. Cambridge University Press, Cambridge, 2002.

[8] A. N. Hirani. Discrete exterior calculus (dissertation). Technical report, California Institute of Technology, 2003.

[9] J.M. Hyman, and M . Shashkov, M. 1997. Natural Discretizations for the Divergence, Gradient, and Curl. International Journal of Computers and Mathematics with Applications 33.

[10] E. Kanso, M. Arroyo, M. Desburn., J.E. Marsden and Y.Tong 2004. On the geometric character of continuum mechanics.

[11]H. Whitney. Geometric Integration Theory. Princeton Press, Princeton 1957.

[12] S. Wolfram . The Mathematica book. Cambridge University press 2004.

2011 International Conference on Mechanical, Industrial, and Manufacturing Engineering
Lecture Notes in Information Technology Vols. 1-2

Geotechnical Engineering Problems of Highway Project in West China

Sheng Liu
School of Science , Chang'an University
Xi'an, Shanxi Province, 710064,China
86128875@163.com

Guanglong Zhang;Xiaowei Liu
School of Highway, Chang'an University
Xi'an, Shanxi Province, 710064,China
373159626@qq.com

***Abstract* -In the past geotechnical engineering workers paid more attention on water conservancy,railway and mine construction;In recent years, along with the development of highway,geotechnical engineering problems are increasingly outstanding in the highway construction,and some of them have become the key factors of construction highway investment and engineering success or failure. Geotechnical engineering is regarded and developed in highway construction with the development of highway, which plays a tremendous role and achieves remarkable economic and social benefits.In spite of this,owing to the limit of engineering qualities,many geotechnical engineering problems of highway construction should be studied in depth,therefore some geotechnical engineering common problems of highway construction are discussed and the solutions of such problems solution are provided.**

Keywords:highway project; slope; tunnel; geotechnical engineering;groundsill; surrounding rock

I. INTRODUCTION

As we all know, the development of highway construction is the necessary condition of the coorld economic booming during the material preparation. Such as America after the World War, Europe in 1960s, Japan in 1970s, south-east Asia in 1980s, which all have proved this. No matter how perfect the basic traffic facilities except highway in these countries, or whatever geotechnical properties they have, the development of highway project, especially the development of freeway is the decision condition of its economic development.

After the reform and opening up, highway construction in China also has a rapid development. By the end of 2001, the total highway in used has been up to 1,400,000 kilometers, and the freeway has been amounted to 16,000 kilometres. According to the general plan of the highway development in China, the total highway in used will be up to 1600,000 kilometres and the freeway will amount to 80,000 kilometres after the next ten years construction. So the next ten years is still the important stage of the freeway construction in China.

Geotechnical problems met in highway construction were paying much attention to is begun with the development of the freeway. Because the grade of the highway in the past was very low, wherever we met the geotechnical problems, we avoided it. But with the construction of the freeway, to deal with the related geotechnical problems has become a very important condition to make sure that the highways in constructing will have good quality in the future. According to the usage classification, the geotechnical problems met in the highway construction can be summarized as follow aspects:

(1)Ground Engineering : mainly points to the soft ground treatment in different areas.

(2)Subgrade Engineering: mainly concludes the deformation and stability of the high-stacked embankment, the subgrade engineering with special stacked materials, the construction techniques at the bridge abutment, the culver under the high-stacked embankment, the protection and retaining wall engineering of the subgrade and the illness treatment of the subgrade, etc.

(3)high slope engineering-with the construction of the freeway in mountain terrain, more and more high slope engineers are met, and the evaluation of its stability and the relevant treatment method not only relates to the invest, but also becomes a important factor for the safe usage of the freeway.

(4)Foundation Engineering : highway bridges have many forms and its own properties, thus, its foundation should also has different forms and properties.

(5)Tunnel Engineering :highway tunnel usually has a big span, especially when short tunnel is adopted in the freeway at mountainous areas, consider with the highway alignment, will be selected, and all these will result in many related problems to be solved.

II. PROBLEMS AND DEVELOPMENT

A Ground Engineering

(1) The treatment of the soft ground under the high-stacked embankment.

Because the freeway in east China began earlier and developed more rapidly than the other areas in China, the first difficult problem met in the freeway construction is the soft ground treatment. There are two problems need to be solved in soft ground treatment in the freeway construction: ①to promote the ground strength so as to make the ground keep stability during the stacked progress; ②to control the ground deformation to satisfy the settlement of the subgrade of the freeway.

In fact, during the construction of the freeway, almost all the ground treatment methods have been used. Through many years practice and sum up, two methods are widely used in the soft ground treatment in the

freeway project: ①drainage consolidation method; ②composite foundation. In the drainage consolidation method, sand drain (or plastic drain) ground with surcharge preloading and sand drain ground with vacuum preloading have been widely used. In the composite foundation, powder deep mixing method is mainly used.

(2) The treatment technique of the loess ground

Loess have a widely distribution in China, and the construction of the high-grade highway cannot avoided from the loess area. The loess problems need to be solved in the construction of the high-grade highway includes two aspects: ①collapsible loess treatment; ② investigation and treatment of the cell under the loess area.

The study of the collapsible loess began at the beginning of 1900s, but the real study work was acted with many projects after the establishment of People's Republic of China, and the main results can be seen from the four revision of the build standard in the collapsible loess area. But the freeway is strip engineering and always longer than 100 kilometers, if all the classification and treatment methods obey the existed standard, the highway construction investment will not be accepted. Thus, relevant classification criterion and treatment rules should be built combined with the highway load properties, which is very important in the highway construction in the west part of China.

In the past, the affection from the collapsible of the loess during the freeway construction was not pay attention to and thus brought many problems, which was not only a waste of money, but also undermining the social affection of highway and its usage. In recent years, the serious affection of the collapsible loess met in the highway construction have been, realized and much attention have been pay to its investigation and study, which is good for the highway construction in the loess area.

The cell under the loess area is another ground illness in the highway construction in this area. Some of the cells are formed from the big void structure of the loess and its moistening, some others are formed from the excavation of the sand, gravel and other human actions. The distributions of the cells don't have any rules, and its depth are not fixed, which all bring great affection to the construction quality of the high-grade highway. So, how to efficiently investigate the distribution range and size of the cells, how to evaluate its affection degree, how to select a treatment method and detect its treatment effect is a difficult task.

(3) Other ground problems

Except the soft ground and the loess ground, other special soil also has a widely distribution in other arrears in China, such as expansive soil, salty soil, permafrost, etc. The highway construction in these areas also can meet many difficulties and its ground treatments are also a problem need to be studied. And, the highway construction in the karst area also has the ground treatment problems, which has been pay attention to now.

B Subgrade Engineering

(1) The stability and deformation of high-stacked embankment and dam embankment.

Because of its special topography, high stacked embankment and dam embankment are widely used in the loess area, and there are many problems during its usage, the first is the stability problem and the second is the deformation problem.

The stability of the embankment concludes the decision of the proper slope ratio, the reasonable across section and the affection of the water to the subgrade stability in the dam embankment, ect. Compaction standard also has a bad affection to the stability of high-stacked embankment.

The settlement of the high-stacked embankment is another more difficult problem than its stability in the high grade highway engineering. How to calculate its settlement and control settlement are always according to the experience, especially the evaluation and control of the settlement at the fill and cut transition pant is another problem has not been solved.

(2) The subgrade with the soil-stone mixture or big size gravel

The west part of China is a mountainous and hilly terrain, and the south west area has abundant gravel materials. In the real project, the deep cutting and tunnel construction also makes out many big size gravel. But according to the relevant standard now in use in China, soil stone mixture and big size gravel are not fit for the fill material of the subgrade But, take into account the economic, social and environment factors, the construction department has tried to use the soil-stone mixture and big size gravel as the fit material of the subgrade. Most of the projects are successful, although there are still many problems.

For a long term, compaction properties of the fit material and the test of detection standard are all built on the basis of the fine-grained soil. How to select the construction machines, select the relevant compact method, quality detect and evaluate method of the soil-stone mixture and big size gravel subgrade is still in study now.

(3)The subgrade construction technique at the bridge abutment.

Bridge abutment is a place with many highway illnesses. Jump at bridge abutment is the most common form of the illness. Jump at bridge abutment of the freeway makes people feel uncomfortable and unsafe. The construction technique of the bridge abutment relates to the structure, material, etc. The settlement of the subgrade concludes the embankment settlement and the ground settlement.

(4)The culvert under the high-stacked embankment.

The culvert under the high-stacked embankment is widely used in the highway construction in the west China. Because its function just likes the small bridge, but its investment and construction condition requiment is much lower than the small bridges, the culvert is always as the first selected measurement. But the actuality of it at present is that almost all the constructed culverts have illness. And the mainly reasons of the illness are as follow:

(1) The calculation of the earth pressure on the culvert is incorrect

(2) The realization of the mutual work mechanics for the culvert, the fill soil and the ground are not clear.

(3) The calculation method of the culvert structure is not reasonable.

(4) The design and investigation standard of the culvert is low.

(5) The construction procedure and method of the culvert is not reasonable, the detection standard and control method of the construction quality is not satisfied.

The usage of the culvert under the high-stacked highway in the engineering should be considered as an engineering problem with Chinese characteristic. The highway mountainous also has culverts, but the high-stacked embankments and deep excavations are always substitute by the viaduct in other countries. And domestic mountainous highway often use high-stacked embankment and deep excavation with culverts under them, and its design standard is low, so the problems of the culvert under the high stacked embankment is very outstanding.

The theory study of the culvert under the high-stacked highway mainly concludes the study of the earth pressure out on the culvert and the mutual work mechanics of the culvert with the soil. As for the earth pressure of the culvert, we all know it is bigger than its own gravity load, but its quantity is affected by the construction method, classification of the fill and the geologic and topographic feature.

(5) subgrade protection and retaining wall engineering

The protection and retaining wall engineering of the subgrade have to a big ratio in the highway project, especially, the highway in the mountainous terrain, Retaining wall engineering is one of the important aspects to make sure that the highways have a good quality. In the recent highway development, there are more and more new forms of the walls, such as reinforced soil wall, geocell biological wall, geotexitile wall, etc. There are many successful projects, but also has some failure projects.

(6) The treatment of the subgrade illness

Because of the unreasonable design and construction quality problems, there are always many kinds of illnesses of the subgrade engineering after the highway is in use. The problems are more serious in the earlier constructed highways. These illnesses affect the usage of the highway and traffic safety and should be treated in time. Directed against these, proper treatment method and construction procedure should be found out.

C high slope engineering

There are many high slopes in the mountainous freeway, especially in China. Because of the limitation of the investment, the high slope engineering is very common. It will directly affect the project investment and bring many unsafely problems if the high slope engineering is designed unreasonably. In the highway high slope engineering, the following problems should be studied:

(1) The reasonable slope ratio and the slope form of the high slope.

(2) The biological protection of the soil high slope.

(3) The biological protection of the rock high slope.

(4) The disaster monitors and forecast technique of the high slope engineering in the mountainous terrain.

D Foundation Engineering

Pile foundation can be said as the most common foundation form in the highway bridge. Directed against its different use areas, it has many new forms, which can be concluded as the following aspects:

(1)The usage of the excavated and cast-in-place pile.

(2) The usage of the big diameter pile foundation.

(3) The reasonable depth of the pile foundation in the loess area.

(4)The usage of the low strength pile of the composite ground in the loess area.

E Tunnel Engineering

In 1960s to 1970s, the railway department studied the distribution rules of the surrounding rock pressure and the construction method of the small span (<8m) loess tunnel and had some results, which efficiently guided the design and construction of the single-line railway tunnel at the loess area. But, as the freeway tunnel usually has a big span (>13m), and its force, deformation and environment conditions all has its own properties, the existed results can't satisfy the requirement of highway construction. So,combined the freeway construction with the properties of the loess area in China, studies the surrounding rock pressure of the big span loess tunnel and the movement of the water in the soil; decides the design parameters, and makes out relevant construction procedure will promote the construction level of the highway tunnel in the loess area, decrease the tunnel illness and guide its design and construction.

III. SUMMARY

(1)Pay much more attention to the basic theory study of the Geotechnical. Engineering Problems in the highway project.

(2)Widely borrow and adopt the advanced techniques and experiences of the other industrial and other countries.

(3) Perfect the industrial standard.

(4)Adopt new thoughts, new techniques and new materials,promote the level of the Geotechnical Engineering in the highway project.

ACKNOWLEDGEMENTS

I would like to thank very much the chairman of highway school of chang'an university(Prof. Y.L.Xie)whose constructive comments are helpful for this paper revision.

REFERENCE

[1]Yang She-qiang, Geotechnical Engineering Problems in Highway Construction,Coal Geology of China,2008,V20, No11,pp:47-49

[2]Huang Ming-qiang,Research and Development of Geotechnical Engineering Discipline,Modern urban transit,2010,4,pp16-21

2011 International Conference on Mechanical, Industrial, and Manufacturing Engineering
Lecture Notes in Information Technology Vols. 1-2

Finite Element Simulation of Cyclic Load Test of Precast Segmental Bridge Columns

Bu Zhan-Yu
Faculty of Architecture, Civil Engineering and Environment
Ningbo University
Ningbo City, China
buzhanyu@nbu.edu.cn

Tang Guang-Wu and Zheng Wan-Shan
State Key Laboratory of Bridge Engineering Structural Dynamics
Chongqing Communication Research & Design Institute Co. Ltd., China Merchants Group
Chongqing, China
tangguangwu@cmhk.com, zhengwanshan@cmhk.com

***Abstract* - This paper investigated the finite element simulation for cyclic load test of precast segmental bridge columns. The simulation utilized fiber model beam column element and was proved valid by comparing the simulation results with the test results. The influences of prestressing tendon ratio and mild reinforcement bar ratio were studied with two additional assumed specimens. The simulation results show that unbonded prestressing tendon has good self-centering ability and bring little residual displacement in segmental bridge columns. Increasing the area of mild reinforcement bar leads to the increment of hysteresis cycle area, residual displacement, yield strength and ultimate strength. The base joint opening size of pure prestressing column is the biggest, while that of pure mild reinforcement column is the smallest under the same lateral drift. The column with pure mild reinforcement dissipates the most energy and the column with pure prestressing tendon fails at about 4% drift. The proportion of the two kinds of reinforcement needs careful consideration to fulfill the stiffness and residual displacement requirement of specifications.**

Index Terms - precast concrete; segmental construction; bridge columns; fiber model; finite element simulation

I. INTRODUCTION

In the last decade, more and more scholars began to pay attention to the research, development and application of precast segmental components and systems in highway bridges. Conventional cast in place construction method of bridges needs formworks, usually causing traffic jam, which influences the progress of cross-river or cross-sea project, or leads to a waste of time for passing vehicles in busy urban areas. Precast segmental construction of bridges provides a solution to this problem by transferring most of work from construction site to precast factories and makes the quality easily controlled. Precast construction also produces less waste and reduces environmental pollution.

Wang Z.Q. et al[1] studied the seismic resistant design of precast segmental bridge columns in the approach span of East Sea Bridge in Shanghai China, and concluded that the arrangement of prestressing tendons caused strong influence to initial stiffness, but little to ultimate strength, and the bonded prestressing tendons caused large residual displacement in cyclic loading test. Ge J.P. [2] studied precast segmental bridge columns by cyclic load test and shaking table test, considering segmental or cast in place, bonded or unbonded, prestressing tendon or mild reinforcement bar. But there are significant differences between simulation results and test results. The reason is that the concrete damage and deactivating after crushed is not considered. Zhao N. [3] et al carried out precast segmental bridge column cyclic load test, and the results show prestressing tendon increases the self-centering ability and decreases energy dissipation of components. The damage of precast segmental bridge columns concentrates in joint region, and the residual displacement was less than that of socket joint specimen.

Billington S. L. [4]studied the cyclic test of precast bridge columns, in which the first segment is made of high performance composite fiber concrete. The results show the system can dissipate more energy than conventional concrete precast segmental bridge columns, the lateral drift can reach 3%~6%, the depth of column base embedded in pile cap has much influence to the development of column base micro crack and the ability of hysteresis energy dissipation. Hewes J. T. et al[5]studied unbonded prestressing precast segmental concrete bridge columns by cyclic load test and theoretical analysis. The specimen base was strengthened by steel tube. Test results indicates that column shear is transferred by friction between segments in the high axial compression ratio, but structural details such as shear key are needed in the low axial compression ratio. Adequate ductility of the column can be ensured when the volume reinforcement ratio of steel tube is no less than 2%. Ou Y. C. et al[6] made an improvement by placing additional bonded energy dissipation reinforcing bars in segmental column besides the unbonded prestressing tendon. The energy dissipation bars are unbonded some length in pile cap below column-base joint to make the stress distribution of reinforcing bar uniform, and to delay the fracture of ED bars. The bridge aseismic specification of Japan requires the residual displacement of bridge after earthquake not larger than 1% to be repaired easily [7]. Ou Y. C. et al[8] has verified through test that the residual displacement will not larger than 1% if the shear resistance provided by energy dissipation bar is below 35% in segmental bridge columns.

The specimen in literature [6] was studied utilizing fiber model method to find the influence of prestressing tendon and mild reinforcement ratio to the force-displacement curve, joint opening, equivalent damping and energy dissipation of unbonded prestressing precast segmental bridge columns.

II. CYCLIC LOAD TEST

The test was carried out in Taiwan by Ou Y. C. et al[6].Test specimen C5C-UB was shown in Fig. 1.The component has a height of 5700mm, with a cap beam and base cap. The column height is 3600mm, which consists of four 900mm high segments. The column cross section is rectangle with a middle hollow area, the outer rectangle is 860×860mm, while the inner side length is 430×430mm. Four unbonded prestressing tendons were placed in the inner hollow area of column. The prestressing tendon each has an area of 281.6mm^2, and the initial prestress is 55% yield strength corresponding to the total prestressing force of 1042kN. Twelve energy dissipation reinforcement bars were placed inside the concrete section and grouted. For the flexural moment of the 3rd and 4th segment is low, the reinforcement bars were cut off in the middle of the 3rd segment. Each of the energy dissipation bars has an area of 220 mm^2, and the corresponding ratio to the total reinforcement is 0.5%.The energy dissipation(ED) reinforcement bars were unbonded in the range of 400mm in the base cap to make the stress distribution of reinforcing bar uniform, and to delay the fracture of ED bars. The gravity load was applied to the cap beam by two hydraulic actuators and remained constant throughout the testing. The displacement-controlled lateral cyclic loading was applied by a hydraulic actuator with one end anchored to the reaction wall and the other end to the cap beam. The drift levels 0.25, 0.375, 0.5, 0.75, 1.0, 1.5, 2.0, 3.0, 4.0, 5, and 6% are included with each drift level repeated twice. The material property is shown in Tab. I. In order to study the influence of prestressing and reinforcement bar ratio to seismic response, two additional specimens were assumed and calculated. Specimen C5C-C only has prestressing tendons obtained by transforming the mild reinforcement bars in C5C-UB to prestressing tendons according to the principle of equal yield strength. Specimen C5C-E only has mild reinforcement bars obtained by transforming the prestressing tendons in C5C-UB to reinforcement bars as well. Dead Load Axial Compression Ratio was 10% for all specimens. The parameters of the three specimens were given in Tab. II.

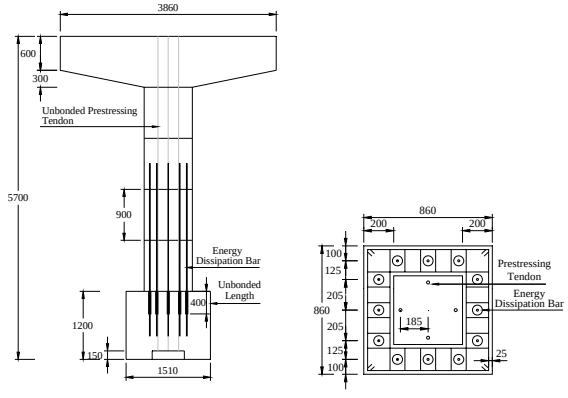

(a)Elevation (b) Section

Fig. 1 Test specimen elevation and section arrangement (Unit:mm)

TABLE I
MATERIAL PROPERTY

Grout	Concrete	Reinforcing Bar		Prestressing Tendon	
Compressing Strength (MPa)	*Compressing Strength (MPa)*	*Yield Strength (MPa)*	*Ultimate Strength (MPa)*	*Yield Strength (MPa)*	*Ultimate Strength (MPa)*
49	45	454	665	1682	1852

TABLE II
SPECIMEN PARAMETERS

Specimen	Prestressing Level (%)	Dead Load Axial Compression Ratio (%)	Prestressing Tendon Ratio (%)	Reinforcement Ratio (%)
C5C- UB	55	10	0.21	0.50
C5C-C	55	10	0.35	0.00
C5C-E	-	10	0.00	1.29

III. COMPARISON OF TEST AND SIMULATION RESULTS

The cyclic load test of precast segmental bridge column was simulated by fiber model. The finite element model was shown in Fig. 2. The column and conventional ED bars were modeled by fibers of beam column element. The prestressing tendons were modeled by truss element. The initial prestressing was simulated by initial strain.

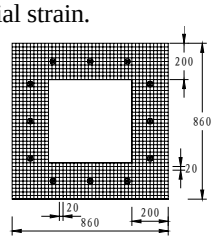

(a)FE model section

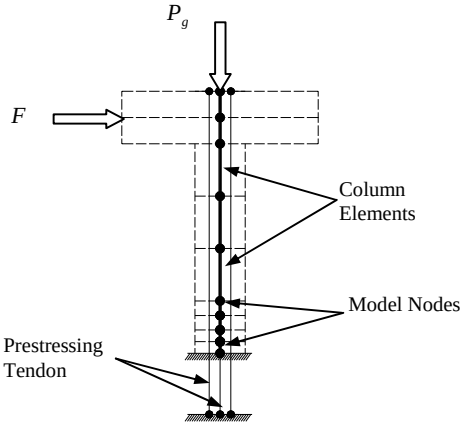

(b) Elevation of FE model

Fig. 2 Sketch map of FE model (Unit:mm)

To verify the validity of the simulation method, the results of test and simulation of C5C-UB were compared as shown in Fig. 3. Fig.3(a) is the test and simulated force-displacement curves, which shows although the results of simulation have some error compared with test results but can present most of

response property of the column. Fig.3(b) is the comparison of prestressing tendon force versus lateral drift, which shows good agreement between test and simulation. Fig.3(c) is column base joint opening, test and simulation results agree well. Fig.3(d) is the comparison of equivalent damping ratios of test and simulation, which shows good agreement at beginning, but the damping ratios of simulation became smaller at about 2% drift because of the bond-slip effect of ED bars can't be modeled in the fiber model. The results comparison shows the simulation is correct and can be used to study the response property of segmental columns.

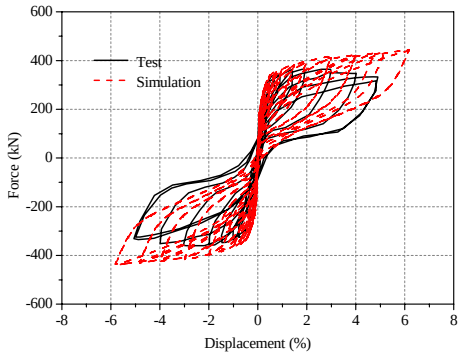

(a) Force-displacement curve

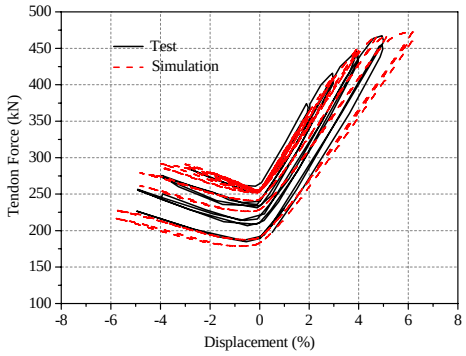

(b) Prestressing tendon force-displacement curve

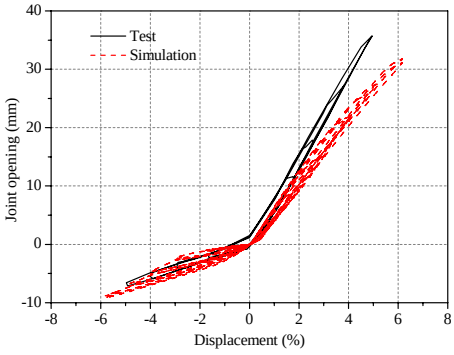

(c) Column base joint opening-displacement curve

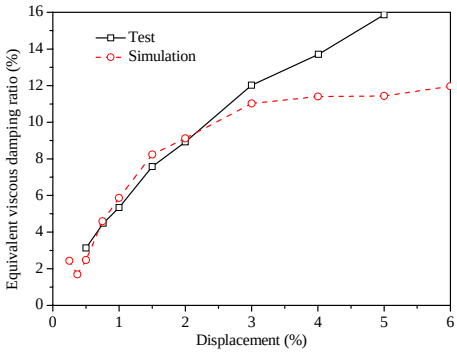

(d) Equivalent viscous damping ratio

Fig. 3 Comparison of test and simulation results of C5C-UB

IV. Parameter Analysis

The response of specimen C5C-C and C5C-E listed in Tab. II were also simulated and compared with simulation results of C5C-UB to study the influence of prestressing tendon and reinforcement bar ratio to response of segmental column. Fig. 4(a) is the force displacement relation of the three specimen calculation results. It shows that C5C-E has the highest strength and biggest hysteresis cycle area, while C5C-C has the lowest strength and smallest hysteresis cycle area. This is because of the tendon of opposite side is loosed by compression during displacement. It also shows C5C-E has the biggest residual displacement nearly reaching 4%. Fig. 4(b) shows the comparison of base joint opening. The specimen C5C-C has the biggest opening but fails near 4% drift. The specimen C5C-E has the smallest opening. Fig. 4(c) shows the equivalent damping ratio. The specimen C5C-E has a very high damping ratio of about 0.20, while C5C-C only has a damping ratio of about 0.025. The equivalent stiffness is shown in Fig. 4(d), the specimen C5C-C has the highest stiffness at beginning, but has the lowest stiffness at last and fails at about 4% drift.Fig.4(e) is the energy dissipation which shows specimen C5C-E is highest and specimen C5C-C is lowest.

V. Conclusions

The unbonded precast prestressing segmental bridge columns were studied in this paper. The comparison between the test results and simulation results verified the validity of the simulation method utilized in this paper. From the parameter analysis it can be concluded as below,

1) Unbonded prestressing tendon can reduce residual drift of segmental bridge columns.

2) Mild reinforcement bar can increase hysteresis cycle area and residual displacement, also provides higher yield and ultimate strength.

3) The base joint opening of pure prestressing column is biggest, while that of pure mild reinforcement column is smallest.

4) Column with pure mild reinforcement dissipates the most energy and the column with pure prestressing tendon fails at about 4% drift.

5) The proportion of these two kinds of reinforcement needs careful consideration to fulfill the stiffness and residual displacement requirement of specification.

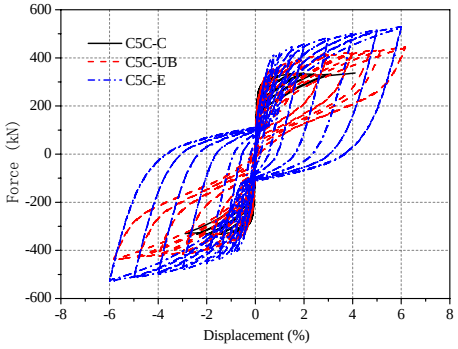

(a) Force-displacement curve

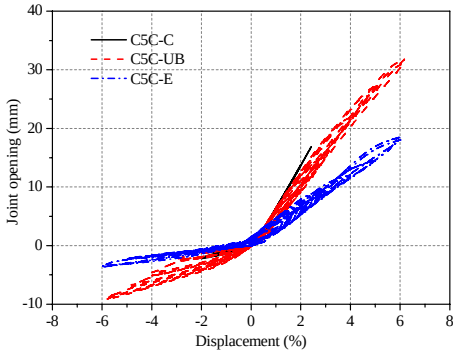

(b) Column base joint opening-displacement curve

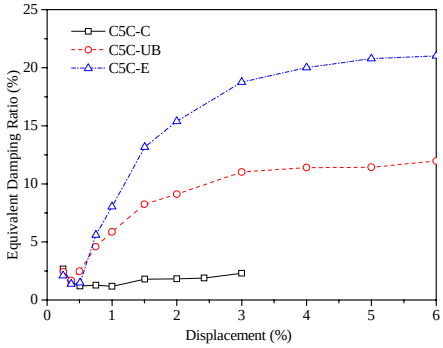

(c) Equivalent viscous damping ratio

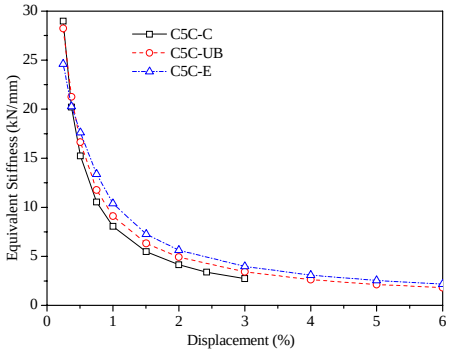

(d) Equivalent stiffness

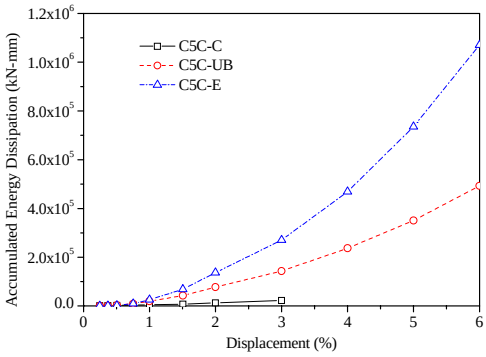

(e) Accumulated energy dissipation

Fig. 4 Comparison of simulation results of three specimens

ACKNOWLEDGMENT

This paper is sponsored by the Fund of State Key Laboratory of Bridge Engineering Structural Dynamics, China (The project No. is 201002); This work is also supported by the Scientific Research Fund of Zhejiang Provincial Education Department, China (The project No. is Y201017490), Startup Found of Ningbo University, China (No. 2010148) .

REFERENCES

[1] Wang Z. Q. , Ge J. P. and Wei H. Y.. "Seismic performance of pre stressed concrete bridge column of East Sea Bridge".*Journal of Tongji University(Natural Science)*, vol. 36, no. 11, pp. 1462-1466, Nov. 2008.

[2] Ge J. P., Wang Z. Q., Wei H. Y.. "Seismic performance analysis of segmental bridge columns with match-cast dry joints using fiber beam-column element method".*Journal of Vibration and Shock*, vol. 29, no. 3,pp. 52-57, 2010.

[3] Zhao N. and Wei H. Y.. "Pseudo static test investigation on segmental precast erected prestressed columns".*Shanghai Highways*,no. 4,pp. 24-28, 2008.

[4] Billington S. L. and Yoon J. K.. "Cyclic response of unbounded posttenioned precast columns with ductile fiber-reinforced concrete".*Journal of Bridge Engineering*,ASCE,vol.9,no.4, pp. 353-363, 2004.

[5] Hewes J. T. and Priestley M. J. N.. "Seismic design and performance of precast concrete segmental bridge columns". Technical Report, Department of Structural Engineering, School of Engineering, University of California, San Diego,2002.

[6] Ou Y. C., Tsai M. S., Chang K. C. and George C. Lee. "Cyclic behavior of precast segmental concrete bridge columns with high performance or conventional steel reinforcing bars as energy dissipation bars".*Earthquake Engineering and Structural Dynamics*.2010, DOI:10.1002/eqe, in press.

[7] Kawashima K. "Seismic performance of RC bridge piers in Japan: an evaluation after the 1995 Hyogo-ken nanbu earthquake". *Progress in Structural Engineering and Materials*, vol. 2, no.1, pp. 82-91,2000.

[8] Ou Y. C., Wang P. H., Tsai M. S., Chang K. C. and George C. Lee. "Large-Scale Experimental Study of Precast Segmental Unbonded Posttensioned Concrete Bridge Columns for Seismic Regions". *Journal of Structural Engineering*, vol. 136,no.3, pp. 255-264,2010.

2011 International Conference on Mechanical, Industrial, and Manufacturing Engineering
Lecture Notes in Information Technology Vols. 1-2

An improved data structure for seeking capacity and saving memory

Li Xiaotang and Zhan Feng
Department of Computer Application
Shenzhen Institute of Information Technology
Shenzhen 518029,China
{lixt & zhanf}@sziit.com.cn

Abstract - Hash map is a kind of very useful data structure in huge data project; it is often used in cache, row weight, seek and so on. Based on stl (standard template library) hash map data structure, this article aims to improve it in some particular application occasion, in order to save memory greatly, and enhance seeking capacity at the same time.

Index Terms - Hash map, improvement，seeking，memory

I. INTRODUCTION

Hash map <key, value, hash, compare> in stl uses a separate chaining (separate chaining) method, it supports user-defined hash function and comparison function. Its data structure described as below

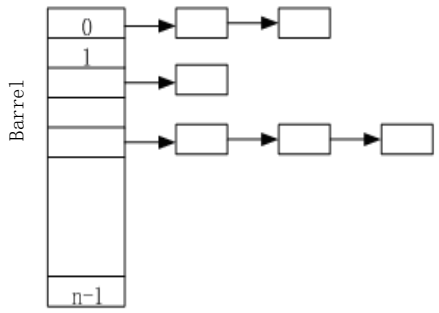

Fig.1 Description of stl data structure

It uses vector to realize a barrel with size n, subscript is from 0 to n-1. In order to ensure elements evenly distributed in each barrel, it uses the user-supplied hash function to calculate a hash value of the key, and get the barrel number of the key with the hash value modular n. This makes it possible to create hash conflict: many elements fall into the same barrel. In order to solve the conflict, hash map uses linked list to connect elements in the same barrel and save key value on the linked list nodes. In locating an element, locate to a specific barrel according to key value and then seek the entire list and compare key value of every node with comparison function.

Although the operation to the list can only be linear, but as long as hash function is not too bad, and the number of barrels are close to the number of elements, the number of corresponded elements in the list are very few (often 1-2). Therefore, the computational complexity is O in the insert, seek, modify, and delete operations of hash map (1).

When hash map is constructing, it can specify the size of the barrel in advance, it can also be automatically increased as the data insert. It uses a set of prime numbers (53, 97, 193, 389, ..., 50331653, 100663319, ..., 4294967291) to determine the need for reconstruction of the barrel. When the hash map is reconstructed, it will cause all data relocation and replication with low efficiency. So, when the total number of elements is known, if specify the size of barrel when it is constructing, it can improve efficiency.

II. PRINCIPLE OF IMPROVEMENT

In this article, we can improve hash map against the following situations: elements in hash map are relatively stable (for example, the cache system), it only loads all the data at the initialization, after that, it is mainly used for seek or modify and rarely do insertion and deletion operation. Meanwhile, hash function can guarantee that it does no create conflict or conflict can be tolerated (for example, the use of md5 algorithm).

At this point, we can optimize for the following three points:

A. Do not save the key values on nodes

We know that each element node is stored key value (used to compare when seeking) in stl's hash map. Usually, the key length is large. Such as in search engine project, it often uses url as key, which greatly limits the number of total elements hash map can load for each process.

In general, the length of hash value is less than the key. If hash function can guarantee that it does no create conflict or conflict can be tolerated, we do not need to save the key values on nodes, it only need to preserve hash value on it.

B. Only save part of hash value on nodes

In most cases, the number of hash map barrel are very large, it often reaches tens of millions. If we are able to skillfully use subscripts of these barrels, we can save a considerable portion of memory. Specifically, if we modify the method of locating barrel according to hash value: use some bytes of hash value to indicate barrel number, then it is not necessary to save the complete key values on each element node, it only needs to preserve the rest bytes of hash value.

Take 64-bit md5 hash value as an example, if we set the number of barrels as 16777216 (2^24), barrel number can represent 24 bits of hash value; it only needs to save the rest 40 bits on nodes. For example, hash (key) = 0x0123456789abcdef, if we use lower 24 bits as barrel number, then barrel number is 0xabcdef (decimal 11,259,375), it only needs to save the higher 40 bits 0x0123456789 on nodes. When seek, it gets the barrel number by acquire lower 24 bits of key and find nodes equal to lowers 40 bits in linked list of the barrel.

In above example, we have save three bytes for each node. If the hash map needs to load 50 million, we can save 150M memory.

C. Revise the corresponding linked list of each barrel to array

We know that in hash map, the elements in same barrel are managed by linked list. As each node of the list occupy four bytes pointer. If the numbers of elements in hash map do not often change, we can use fixed-size array or dynamic array. On one hand, it can reduce memory occupation; on the other hand, it can improve locating speed.

In above example, if the hash map needs to load 50 million, we can save 200M memory. Thus, through 2 and 3, a total of 350M memory can be saved.

III. CODE REALIZATION

GetFist3Bytes（）Function obtains the first three bytes of hash value.
GetLast5Bytes（）Function obtains the last five bytes of hash value.
m_pData is barrel array.
CHashMapNodeVector is self realized dynamic array.
Major add and seek code are as follows:

```
// Add function
void CHashMap::Add(unsigned long long ullHash, unsigned long long ullValue)
{unsigned int dwIndex = GetFist3Bytes(ullHash);
 assert(dwIndex < 16777216);
 char pszTmp[5];
 unsigned long long ullTmp = GetLast5Bytes(ullHash);
 memcpy(pszTmp, &ullTmp, 5);
 CHashMapNodeVector& vec = m_pData[dwIndex];
 for (unsigned int i = 0; i < vec.m_dwSize; i++)
 { const CHashMapNode& oNode = vec.m_pHead[i];
 if (memcmp(pszTmp, oNode.pszData, 5) == 0)
 { return;
  }
  }
 CHashMapNode oNode;
 memcpy(oNode.pszData, pszTmp, 5);
 oNode.ullValue = ullValue;
 m_pData[dwIndex].Add(oNode);
}
// Seek function
bool CHashMap::Find(unsigned long long ullHash, unsigned long long& ullValue)
{
 unsigned int dwIndex = GetFist3Bytes(ullHash);
 assert(dwIndex < 16777216);
unsigned long long ullTmp = GetLast5Bytes(ullHash);
CHashMapNodeVector& vec = m_pData[dwIndex];
for (unsigned int i = 0; i < vec.m_dwSize; i++)
{const CHashMapNode& oNode = vec.m_pHead[i];
if (memcmp(&ullTmp, oNode.pszData, 5) == 0)
{ ullValue = oNode.ullValue;
return true;
}
}
 return false;
}
```

IV. EXPERIMENT COMPARISON

In order to facilitate calculation and comparison, we make all key and value are eight bytes long integer. Prepared five sets of data, the number is 10 million, 20 million, 30 million, 40 million and 50 million. Respectively load these five sets of data with old hash map and improved one, use them to perform 50 million randomized seeking respectively and observe their memory occupation and per second seeking speed. To make the test of seeking speed more accurate, randomized 50 million data is loaded into memory, and it will occupy an extra 400M memory.

Test environment:
Intel (R) Xeon (R) CPU 5130@2.00GHz
8G RAM
suse linux 10.0
g + + 4.1.2
The results are as follows:

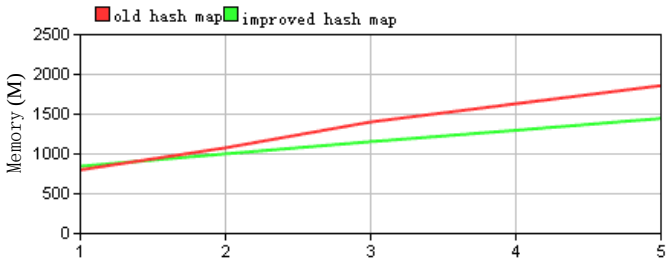

The number of hash map elements (10million)
Fig.2 Changes in memory occupation

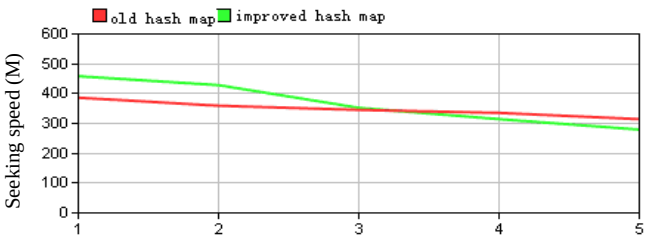

The number of hash map elements (10million)
Fig.3 Changes in seeking speed

From above figures we can find that with the number of elements increases, improved hash map significantly reduces

memory occupation. At the same time, when the numbers of elements are less than 30 million, the seeking speed of improved hash map has significantly improved. When the numbers of elements are more than 30 million, due to the number of old hash map barrel has reached 50,331,563, the average number of elements of each barrel is less than one, but the number of improved hash map barrel fixes at 16777216, the average number of elements of each barrel are three-four, the seeking speed has spent on elements comparison in the same barrel, so the speed decreased.

V. Conclusion

We can improve hash map according to its characteristics and applications. Through the experiment comparison we can find that in most cases, it saves memory and improve the seeking speed at the same time.

Acknowledgment

The research was sponsored by the Natural Science Foundation of Guangdong Province (9151014002000002)and (9151008004000027).

References

[1] Hou Jie. Stl Source Code Analysis [M]. Wuhan: Huazhong University of Science and Technology Press, 2002.

[2] Yan Weimin. Data Structures [M]. Beijing: Tsinghua University Press, 1999.

[3] Zhu Hong, etc. Algorithm Design and Analysis [M]. Shanghai: Shanghai Science and Technology Literature Publishing House, 1989.

[4] Niu Mu,etc.Using hasp Map For simple ORM[J]. Computer Development & Applications2007.12.

[5] Patrick Hagerty Anthony M. Bloch Michael I. Weinstein Radiation Induced Instability in Interconnected Systems,2001

[6] P. R. Herwig M. J. H. Heule P. M. Van Lambalgen H. Van Maaren A new method to construct lower bounds for van der Waerden numbers,2002.9.

2011 International Conference on Mechanical, Industrial, and Manufacturing Engineering
Lecture Notes in Information Technology Vols. 1-2

Study of the mechanical properties of surface nanostructure using nanoindentation and FEM simulation

F.C.Lang, *Y.M.Xing, A.F.Jiang
School of Science, Inner Mongolia University of Technology, Hohhot,010051

Abstract- A nanostructured surface layer about 10 μm was formed on 316L stainless steel plate using technology of Surface nanocrystallization(SNC). Grain of the surface layer of the sample was refined into nanometer after SNC treatment. The microstructural and mechanical properties of nanostructured surface layer are analyzed using by transmission electron microscope (TEM), nanoindentation, and FEM simulation.

Key words: Metallic Mmaterials; 316L Stainless Steel; Surface Nanocrystallization; Mechanical Properties;

1. Introduction

Surface mechanical attrition treatment is a developed technique that can induced grain refinement into the nonascale regime on the surface layer of metal materials[1]. Nanocrystalline materials have been found to exhibit novel properties over their coarse grained polycrystalline counterparts[2]. The majority of failures of engineering materials are very sensitive to the structure and properties of the material surface, and most of failures of material begin from surface. Therefore, Optimization of the surface structure and properties may enhance the global behavior of materials. Surface nano-crystallization(SNC) [3] can improve overall properties and behaviors of materials through the surface modification by generation of a nanocrystallization surface layer, and has been regarded as one of the most prosperous surface technologies. Most of surface treatments can used for SNC, among them ultrasonic shot peening (USP) is simple and flexible,and therefore low-cost,this technique is very useful in industrial application. Over the past years, many researches have been actively carried out. The nanocrystallization mechanism was analyzed in terms of the deformation behavior and TEM observations of the microstructural evolution of the 316L stainless steel after SNC treatment in reference [4]. The residual stresses induced by ultrasonic shot peening had been studied by moiré interferometery method, X-ray techniques and the finite element method [5-7]. Some researchers[8-10] have developed simple theoretical analysis of the shot peenig process. Wang [11] studied the effect of SNC on the fraction and wear properties in low carbon steel. And it had reported that the thermal stability of structure and hardness of the surface layer of 316L stainless steel after surface mechanical attrition treatment by reference [12].

In this paper, a 316L stainless steel was selected to be treated by USP, a nanostructured surface layer was formed on 316L stainless steel plate about 10 μm thick. The microstructural and mechanical properties of nanostructured surface layer were analyzed by using TEM and nanoinedtation. And the process of nanoindentation has been numerically simulated employing the finite element software (MSC. Marc). The distribution of the deformation, the relation between the stress and strain, and the Mises equivalent stress for the nanostructur layer and the matrix were extracted from the simulation process.

2. Experiment procedure

2.1 Sample preparation

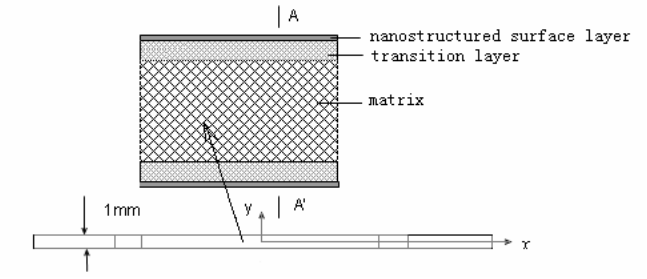

Fig. 1 Diagrammatic sample structure after SNC treatment with nanostructured surface layer about 10 microns thick

The material used in this work is 316L stainless steel plate of 1 mm thick, its chemical compositions contain(mass%) 0.019C,17.07Cr,11.95Ni,2.04Mo, 1.68Mn,

0.04Cu, and 0.007S. Sample were treatmented using USP, as the image shown in Fig.1.

The principle of the USP is based on the vibration of spherical shots using a high power ultrasound. Because of the high frequency of the system, the entire surface of the component to be treated is peened with a very high number of impacts in a shot period of time. Each peening of the ball to the surface will result in plastic deformation in the surface layer of the treated sample. As a consequence, repeated multidirectional peening at high strain rates onto the sample surface layer leads severe plastic deformation that makes the microstructure of the surface layer of the sample was refined into nanoscale. The transition layer of about 90 μm thick were formed underneath the nanostructured surface layer during the USP processing, and there is no distinctness interface beween the nanostructured surface layer and the transition layer. The main parameters of the USP process in this work were chosen as follows: the vibration frequency of the chamber driven by ultrasonic generator is 20KHz; the shot diameter is 2 mm; and the processing durations is 960s, respectively.

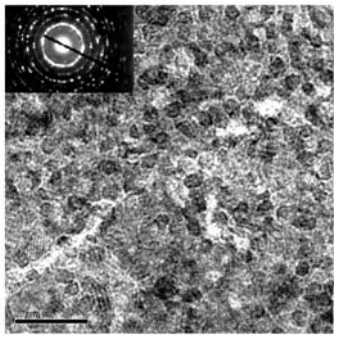

Fig.2 TEM images and SAED patters of nanostructured surface layer

Transmission electron microscopy(TEM) obervations were carried out on a JEM-2010 transmission electron microscope with operating voltage of 200KV. Fig.2 show the TEM observation of the top nanostructured surface layer at the amplificatory of 200K.The microstructure of the nanostructured surface layer is charactered by uniformly distributed nanoscale grains of about 8nm. The corresponed electron diffraction pattern illustrates that these grains are matensites with random orientation and roughly equiaxed shap.

3. Results and discussion

3.1 Nanoindentation

The nanonoindentation method was introduced in 1992 for measuring hardness and elastic modulus by indentation techniques has widely been adopted and used in the small scales [13,14]. The method was developed to measure the mechanical properties of a material (the hardness and elastic modulus etc) from indentation load-displacement data obtained during one cycle of loading and unloading. There are three important quantities that must be measured from load-depth curves: the maximum load, $P_{\max}$, the maximum displacement, $h_{\max}$, and the elastic unloading stiffness, $S = dP/dh$,(also called the contact stiffness), defined as the slope of the upper portion of the unloading curve during the initial stage of unloading. For a body of the revolution, related the contact stiffness S to the effective elastic modulus E_r and to the projected contact area A:

$$E_r = \frac{\sqrt{\pi}}{2\beta}\frac{S}{\sqrt{A}} \qquad (1)$$

Where β is a constant that depends on the geometry of the indenter Where E_r is defined by :

$$\frac{1}{E_r} = \frac{1-\nu^2}{E} + \frac{1-\nu_i^2}{E_i} \qquad (2)$$

Where E_i and ν_i are the elastic modulus and Poisson's ratio of the diamond indenter, E and ν are the elastic modulus and Poisson's ratio of the specimen.

the nanohardness H is estimated from:

$$H = \frac{P}{A} \qquad (3)$$

In this work, experiment nanoindentation tests were made using a nano indenter®XP (MTS Nano Innovation Center))with a sharp diamond Berkovich tip by CSM technique. To measure the hardness and elastic modulus of nanostructured surface layer and matrix, nanonoindentation Continuous Stiffness Measuremen was introduced .

The curves were obtained from nanoindentation tests as shown in Fig.3.It can be seen that the maximum loads and the residual deepth for nanostructured layer were 7.09mN and 140nm, however, the value of them are 5.52mN and 164nm for the matrix under the same maximum indentation depth 200nm. And the nanohardness and the elastic modulus of the nanostructure surface layers are about

6.05GPa and 227GPa, respectively, and are 1.4 times and 1.2 times than those of the matrix. So the nanostructured layer performed high strength for the load of indentation.

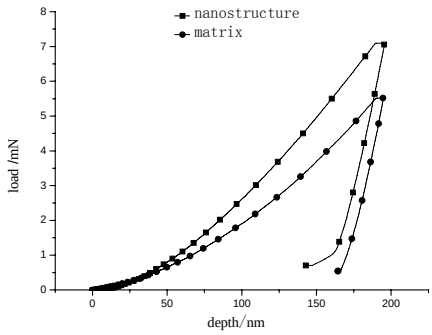

Fig.3 The load-depth curves of nanostructured layer

3.2 Finite elements simulation

The nanoindentation process involves material indented by a rigid indenter under the condition of frictionless contact. To simplify the analysis to a two-dimensional axisymmetric problem, an ideally axisymmetric conical indenter of the same area-depth function as the Berkovich indenter, therefore, an equivalent perfect conical indenter with a semi-apical angle of $\theta = 70.3°$ was used.

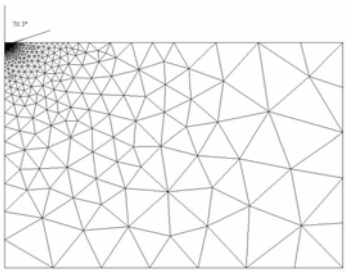

Fig.4 The finite element mesh of the model

No discernable differences in the result have been shown by simulation when varying the friction coefficient [15, 16], therefore, the contact between the indenter and the specimen surface is also assumed to be frictionless.The elements near the region of contact to improve the numerical stability of the finite element calculations were refined. The size of the third elements just under the indenter is less than 10 nm to ensure convergence and to perform an accurate model of contact. To avoid edge effects, the total width is $300\ \mu m$ and height is $200\ \mu m$ of the mesh are greater than that of the indent, and the total number of 3-node triangle elements is 4616.

The parameter of FEM model needed input for nanostuctured surface layer derived from above nanoindentation experiment.For indentation process simulation, a 200 nm downward displace was imposed on the indenter which is agrenment with the experimental. Note that because the contact area was small, the indented material may be assumed uniform and homogeneous. The indentation process can be simulated with the finite element mesh shown in Fig.4

For the curve of the load-deepth determined by simulatioan of FEM is comparable to the date from the nanoindentational experiment,as shown in fig.6,7. The FEM results of the load-deepth was agreement with the experimental.

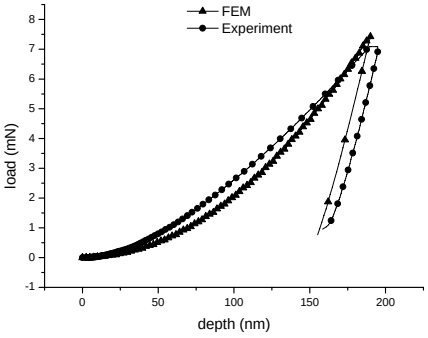

Fig.5 Curves of the FEM and experiment for nanostructured layer

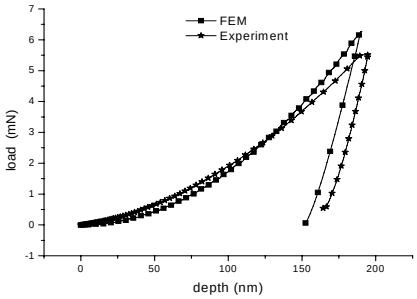

Fig.6 Curves of the FEM and experiment for matrix

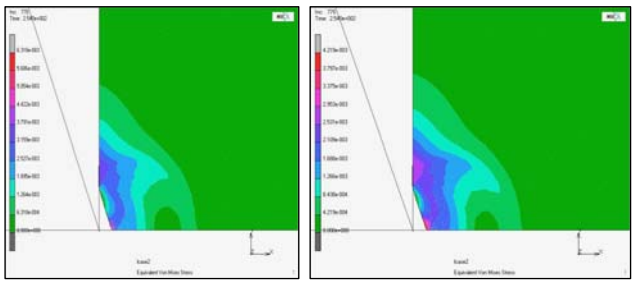

Fig.7 Mises equivalent stress filed pattern of nanostructured layer and matrix under the unloaded

The Mises equivalent stress filed pattern of nanostructured layer and matrix under the unloaded as shown in Fig.7. it can be seen that the yield region of the

matrix is larger than the nanostructured layer under the unloading completely.

3 conclusion

A nanostructured surface layer ,at which the grian were refined to nanoscale, was formed on 316L stainless steel plate by using SNC treatment. The microstructural and mechanical properties of nanostructured surface layer are analyzed using transmission electron microscope (TEM) nanoindentation,and FEM method. The research findings may be summarized as fellow.

1.The TEM results show that the grains size are 8nm in the nanostructured surface layer and these nanocrystalline grains possess random crystallographic orientation form and roughly equiaxed shape.

2. the nanoindentation tests show that the hardness and the modulus of the nanostructured surface layer are larger than the matrix.

3. The process of the nanoindentation was developed by FEM showed that the the Mises equivalent stress filed pattern of nanostructured layer and matrix under the unloaded were different.

Ackonledgements

This research is supported by the Basica Research of Inner Mongolia University of Technology No. X200830.

Reference

[1] Gleiter H. Nanocrystalline materials. Prog Mater Sci 1988;33: 223-35.

[2] Lu K.Nanocrystalline metals crystallized from amorphous solids: nanocrystallization, structure, and properties. Mater Sci R 1996; 16:161-21.

[3] Lu K, Lu J. Surface nanocrystallization of metallic materials presentation of the concept behind a new approach. J Mater Sci Tech 1999;15:193-7.

[4] Liu G, Lu J, Lu K. Surface nanocrystallization of 316L stainless steel induced by ultrasonic shot peening. Mater Sci Eng 2000;1:91-5.

[5] Xing Y M, Lu J. An experimental study of residual stress induced by ultrasonic shot peening. J Mater Pro Tech 2004;152:56-61.

[6] Menig R, Pintschovius et al. Depth profiles of macro residual stresses in thin shot peened steel plates determined by X-ray and neutron diffiraction. Scipta Mater 2001; 45:977-3.

[7] Meguid S A, Shagal G, Stranart J C. Finite element modelling of shot peening residual stresses. J Mater Pro Tech. 1999;92:401-4.

[8] [6] Al-Obaid YF. Shot peening mechancs: experimental and theoretical analysis. Mech Mater 1955;19:251-260.

[9] Kobayashi M, M Matsui T, Murakami Y. Mechanics of creation of compressive residual stress by shot peening. Int J Fatigue1998;20:351-7.

[10] Meguid S A. Mechnics of shot peening. Ph.D.thesis, MIIST,UK:1975.

[11] Wang Z B, Tao N R, Li S, wang W, Liu G, Lu J, Lu K. Effect of surface nanocrystallization on friction and wear properties in the low carbon steel. Mater Sci Eng.2003;1:144-9.

[12] Wang A et al. Thermal stability of structure and hardness of the surface layer of 316L stainless steel after surface mechanical attrition treatment. Acta Metallurgica Sinica 2005;41:577-82.

[13] Oliver W C et al. An improved technique for determing hardness ans elastical-modulus uisng load and displacement sening indentation experiments.J Mater Res 1992;7:1564-83.

[14] Oliver W C et al. Measurement of hardness and elastic modulus by instrument indentation: Advance in understanding and refinements to methodology.J Mater Res 2004;19:1-20.

[15] Lichinchi M et al.Simulation of Berkovich nanoindentation experiments on thin films using finite element method. Thin Solid Films 1998;312:240-8.

[16] Sun Y, Bell T , Zheng S. Finite element analysis of the critical ratio of coating thickness to indentation depth for coating property measurement by nanoindentation. Thin Solid Film 1995;258:198-4.

2011 International Conference on Mechanical, Industrial, and Manufacturing Engineering
Lecture Notes in Information Technology Vols. 1-2

The Actualities and Prospects of Ultrasound-based Pattern Recognition in Crop Feature Extraction

Shanshan Yu, Chongyou Wu, Suzhen Wang and Minjuan Hu
Engineering Technology Center of Modern Agricultural Machinery and Equipment for Staple Crops
Nanjing Research Institute for Agriculture Mechanization, Ministry of Agriculture
Nanjing, Jiangsu Province, China
yushanshan1109@sohu.com

Abstract – With the advances in information technology and electronics, various intelligent agricultural machines and equipments have been developed for crop production during pre-harvest, harvest and post-harvest stages, respectively. Accurate information about the crop feature parameters is very important for precision agriculture in crop production. Sensing techniques and systems for measuring crop parameters with an acceptable accuracy and high reliability at a reasonable price are essential prerequisite for obtaining this information. Ultrasound, as a nondestructive, fast and reliable technique, can be used to measure the parameters of crop. Utilizing the pattern recognition technique, canopy volume, crop biomass and fruit maturity state can be determined based on these parameters. This paper reviewed the developments in ultrasound-based pattern recognition system for extracting feature of crop over the past decades up to 2010. The current status of ultrasonic systems was described in the context of commercial application. Some of the challenges and considerations on the use of the sensor and technology for specialty crop production are also discussed. Emphases are placed on the technology that have been proven effective or have shown great potential for crop feature extraction.

Index Terms - Ultrasound technology; Pattern recognition; Feature extraction; Canopy volume; Tissue parameters.

I. Introduction

In crop production, degree of coverage, crop height, canopy volume and biomass density are important parameters for precise fertilizer application, irrigation, chemical application, as well as health assessment [1-3]. Based on these parameters, expected crop yields can be appraised and the amount of fertilizers and pesticides for the site-specific crop management can be optimized. Smart et al. (1990) described the relationship between canopy management and yield for grape [1]. Furthermore, in harvesting combines parameters as the height above ground or the rotation speed of units can be specifically adapted to site crop conditions [4]. Meanwhile, tissue texture is a very important parameter, which reflects the changes in tissue during the course of growth, maturation, storage and shelf-life. The degree of firmness is usually associated with ripeness, freshness, retention of good quality and, therefore, with sale-ability. Furthermore, when acoustical measurements are used in conjunction with other physiochemical measurements, such as firmness, dry weight content (DW), oil content, total soluble solids (TSS), and acidity, a link between acoustical parameters and physio-chemical indices enables the indirect assessment of proper harvesting time, storage period or shelf-life [5-8].

The texture analysis can be considered as one of applicable techniques for extracting textural features of crop and also for pattern recognition. Pattern recognition is the research field that studies the operation and design of systems that recognize patterns in data. It encloses subdisciplines like discriminant analysis, feature extraction, error estimation, cluster analysis (together sometimes called statistical pattern recognition), grammatical inference and parsing (sometimes called syntactical pattern recognition). There have been several attempts for extracting crop and products textural parameters, utilizing different methods such as ultrasonic, laser scanning, aerial sensing, and light penetration measurement of the parameters. Pattern recognition discussed here is limited to Ultrasound-based Pattern Recognition.

II. Fundamental of ultrasound technology

Ultrasound technology has been known for many years, its main application areas being ultrasonic biophysics, and industrial processes and inspections. At high frequencies and low power it can be used as an analytical and diagnostic tool, and at a very high power it can assist processing. Throughout the scope of its applications, ultrasound is generated in the same way: a device known as a transducer contains a ceramic crystal which is excited by a short electrical pulse that has a typical form of several sine cycles. Through the piezoelectric effect, this electrical energy is converted to a mechanical wave that is propagated as a short sonic pulse at the fundamental frequency of the transducer. This energy is transferred into the material or body under analysis and propagated through it [9]. The ultrasonic signal emerging from the test specimen is sensed by a piezoelectric element that acts as a receiver, converting any ultrasound impinging on it back to electrical energy. When the system operates in 'pulse-echo' mode, the same piezoelectric element acts as a transmitter and a receiver alternately; when a 'through-transmission' mode is used, a second piezoelectric element acts as a receiver.

Ultrasonic energy will propagate through a material until the sound wave encounters an impedance change, which means that there are some changes in the material density or/and the velocity of the sound wave [10]. This can occur inside the material, when the nature of the tissue changes or a

void or reflector is present. Some of the sound energy is reflected, and the amount reflected depends on the impedance change and/or the size of the reflector. If there are no internal reflectors, the wave will continue until it reaches the far side of the test object, or until the energy is totally attenuated. The energy attenuation of the ultrasound beam and the speed of wave propagation depend on the nature of the material and its structure [10]. Most physical or chemical changes in the material, cause changes in the attenuation and velocity of the propagated beam. In most solids and liquid industrial materials, as well as in most biological tissues, such as in the human body, ultrasound energy is easily propagated, which facilitates diagnostic or detection procedures [11].

III. Applications of ultrasound-based pattern recognition in crop feature extraction

A. Canopy volume/crop biomass detection

As the earlier work, Turrell et al. (1969) studied the changes in feature data of citrus trees over period of time. They discussed establishing growth equations for different variables for the citrus varieties using above-ground tree parameters including tree height, branch size and number, leaf surface area, number of leaves, and many others (truck diameter, fruit yield, fruit size, fruit diameter, fruit weight, woody frame, branch number, root density, and yield). Results showed that citrus trees and tree parts followed growth curves similar to non-woody plants [12]. A significant amount of the physic-chemical processes that underlie tree growth were found to be linear semi-log or log-log functions [13]. In the 1970s, Albrigo et al. (1975) evaluated various tree measurements (canopy fruit bearing densities, tree height, canopy skirt height, canopy max diameter in horizontal plane, and vertical height to max diameter) to determine reliable yield and reported that the R^2 between canopy volume and fruit weight ranged from 0.24 to 0.85 using multiple stepwise regression and correlation to yield, and that no other combination of the variable predicted accurate yields. This information was all measured manually[14].

Ultrasonic sensors were used in crop production starting the late 1980s. Giles et al. (1988) used commercial ultrasonic range transducers to measure tree canopy volume. The system was mounted and tested with an air blast sprayer and the results showed an error rate of less than 2% on calibration targets and an average error of 10% for apple and peach orchards applications. They reported that the results could be used as a means of sprayer control in the future [15]. Then, Giles et al. (1989) investigated spray volume savings using an ultrasonic measurement which ranged between 28 and 52%, and varied greatly depending on target crop structure [16]. Molt ó et al. (2001) also investigated the possibility of saving the chemicals by measuring the distance between the sprayer and tree canopy using ultrasonic sensors and reported savings of spraying products up to 37% [17]. Other similar studies also reported chemical saving in spraying operations. Solanelles et al. (2006) tested a prototype sprayer with an electronic control system containing ultrasonic sensors in olive, pear and apple orchards, and reported 28-70% spray product saving when comparing spray deposits to a conventional application [18]. Gil et al. (2007) also reported an average of 58% less liquid applied using ultrasonic sensors when comparing a uniform application rate with variable rate of a sprayer based on vineyard structure variations [19].

Other groups of researchers conducted studies in different aspects of ultrasonic sensor application. Zaman and Salyani (2004) investigated the effect of travel speed on ultrasonic measurement of citrus tree canopy by a Durand-Wayland ultrasonic system. For dense foliage, the travel speed did not affect much to canopy measurement, yielding standard errors of 1.0-1.1% compared to manual measurements, while light foliage measurements were affected more by the travel speed with 1.5-3.0% standard error in canopy and light density of foliage might reduce the ultrasonic signal to result in poor performance in light foliage measurements. However, the ground speed did not produce any significant effect on canopy volume measurements [20]. Schumann and Zaman (2005) developed a real-time software system to map citrus tree canopy volume and height using ultrasonic sensors and a DGPS receiver (Fig. 1). The system continuously monitored the ultrasonic sensors and the DGPS receiver, and measured the tree size and canopy volume. They reported high accuracies between manual and the automated measurements with R^2 values of 0.94 for tree height and canopy volume [21]. Balsari et al. (2002) developed a prototype sprayer which could measure target size and density of apple trees using ultrasonic sensors and found that travel speed did not significantly affect the vegetation measurement using the sensor, and suggested that an average of at least 10 measurements in every meter of travel distance would be needed for proper adjustment of the sprayer [22]. Scotford et al. (2003) developed a radiometer and ultrasonic sensing system which could measure the normalized difference vegetation index and height respectively of three varieties of winter wheat (Claire, Consort and Riband) (Fig. 2) [23].

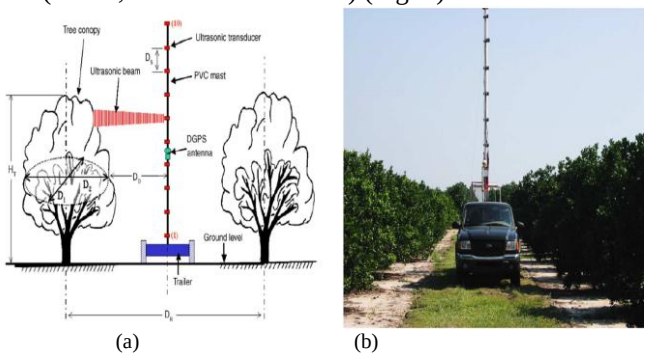

(a) (b)

Fig. 1 Schematic layout of ultrasonic transducer system and manually measured tree dimensions used for calculation of tree canopy sizes in a citrus grove.

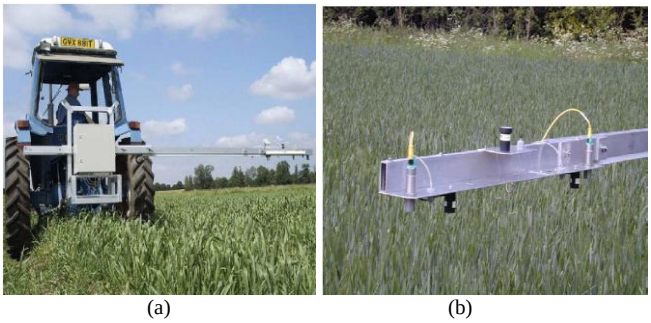

(a) (b)

Fig. 2 Radiometer and ultrasonic sensing system in operation

One of the ultimate goals of estimating canopy volume is site-specific variable rate application of fertilizer and pesticides. Zaman et al. (2005) generated a prescription map for variable nitrogen application to citrus trees from the measurements of tree sizes by the ultrasonic system, and reported that 38-40% of granular fertilizers were saved when variable nitrogen applications were implemented on a single-tree basis [24]. As described previously, other researchers also reported savings in chemical application based on canopy volume measurements [16-19]. Further, Zaman et al. (2006) mapped a citrus grove with an automated ultrasonic system and a sensor-based automatic yield monitoring system. They found that ultrasonically-sensed tree sizes were linearly correlated with fruit yield (R^2=0.80) [25].

B. Fruit maturity state detection and classification

For fruit and vegetable tissues, changes in these properties from part of the natural processes that occur during growth and maturation, and in the course of the harvest period, storage and shelf-life. Various physiological and physiochemical changes occurred during these processes, and each change is specifically determined by one or more factors, characteristic of the pre-harvest, harvest, and postharvest periods. The changes are expressed differently in the course of the various periods, and are mostly reflected in the quality of the final produce. Textural attributes are among the factors considered in quality assessment, and are regularly used for determination of the stage of maturity and its changes during the ripening and softening process start on the tree and continue during harvesting, handling and storage [26]. Chemical contents and concentration in fresh tissues are also important factors in determining maturity of fruit and vegetables.

The ultrasonic properties of fruit and vegetables have been studied in tissue segments and in whole fruit. Tissue specimens in cylindrical or other shapes have been studied to assess their acoustical parameters in conjunction with their physiochemical properties such as firmness, sugar content, and dry weight percentage [5, 27, 28], cut halves of fruit were used for studying of ultrasonic wave paths within fruit tissues and for directional model development [29], and whole fruit were used for non-destructive determination of their physio-chemical properties, and storage and shelf-life [30-33].

Avocado fruit have been measured in the practice by using ultrasonic systems during the pre-and postharvest stages, including growth, maturation, storage, marketing and shelf-life. The physiochemical changes in whole avocado during growth and maturation, and determination of the appropriate harvest time were studied with continuous-touch ultrasound systems (Fig.3) [34]. Attenuation of 50kHz ultrasonic waves was measured during the pre-harvest stage. Changes in the physiochemical and chemical parameters of the fruit were correlated with the changes in ultrasonic attenuation. Mizrach et al. (1997) measured the attenuation of the ultrasonic signal of mango fruit during 10 days of shelf-life at room temperature, and found an increase in attenuation from 2.7dB/mm on the first day to 4.16dB/mm at the end of the test. The trends were numerically and graphically analyzed by means of statistical and curve fitting procedures, and a quadratic expression was found to be a good fit to the changes in attenuation (R^2=0.99) [35]. A study of the ultrasonic determination of the internal physicochemical parameters of ripe autumn-grown and winter-grown melons was carried out by [36]. They found that the modulus of elasticity and the tangent modulus of the sample tissues decreased drastically, from 644 to 209kPa, and the attenuation of a transmitted ultrasonic pulse decreased from 3.17 to 1.1dB/mm, as the sampling depth increased from 10 to 30mm. when the authors correlated these results they found a strong dependence between attenuation measurements in the tissue sectors, and their physiochemical parameters, firmness and sugar contents. They concluded that this strong dependence on depth indicated a potential for using the attenuation coefficient for the determination of internal fruit quality. Ki-Bok Kim et al. determined the firmness (apparent elastic modulus and rupture point) of apples as a function of ultrasonic velocity and attenuation of the received ultrasonic signal through the whole fruit using a multiple linear regression method. They found that the correlation coefficients between apparent elastic modulus and ultrasonic velocity and attenuation were 0.884 and -0.867, respectively, and those between rupture and ultrasonic velocity and attenuation were 0.803 and -0.798, respectively (Fig. 4) [37].

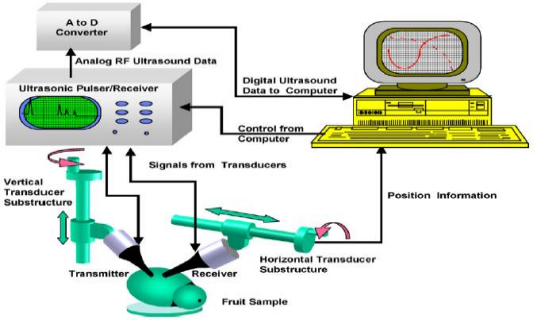

Fig.3. Schematic diagram of the set-up for ultrasonic testing of avocado fruit.

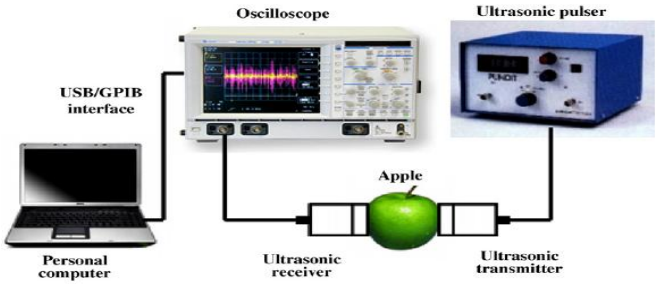

Fig.4. Ultrasonic measurement setup for measuring velocity and attenuation for the whole fruit

IV. Obstacles

This review presented the concepts, technologies, developments and applications associated with the use of ultra- sound-based pattern recognition technique for crop growth and quality assessment. It surveyed various ultrasound measurement methods and how they have been adopted for measuring canopy volume of trees and physiochemical changes and quality indices of various tissues, specimens and whole fresh fruit. This survey confirmed that, in the decades of attempts to apply ultrasound technique to crop feature extraction, the technique is feasible now.

There has been considerable progress since the early studies that were undertaken several years ago. These studies were hampered by limited knowledge of the responses of crop to ultrasonic waves, the lack of suitable equipment or components, the inappropriate frequency ranges of the transducers, or lack of power. In fact, most of the ultrasound techniques still remain as an efficient research tool not yet applicable in actual use. This suggests that the technology is not yet ripe for commercial use and there are many things to be done.

V. Future prospects

Robotic harvesting still poses a great challenge. Improved feature extraction algorithms are needed for yield estimation, maturity detection, coordination of robotic arms for harvesting and adjustment of harvesting combines parameters such as the height above ground or the rotation speed of units. Main prospects may including:

(1). A new ultrasonic-based pattern recognition system may be used for detecting missing seedlings and the ratios of missing plant, and navigating rice transplanter. Since it is difficult to determine whether the pixel of interest belongs to plant or background because of the dense canopy of rice seedlings, and the sun, clouds, blue sky, and other objects outside the paddy field (building, trees and mountains) are strongly reflected on the water surface in flooded paddy fields.

(2). Automatic feed-rate control systems have recently been introduced to lighten the job of combine harvester operators by adjusting the driving speed according to the amount of biomass entering the straw elevator. This means that the feed-rate is measured when the crop material is already cut and transported into the machine. Consequently, automatic control systems always operate fractionally too late and this can lead to suboptimal performance. With the aim of providing increased performance and comfort, it is expected to adjust the driving speed, the position of the header and reel relative to the crop, and the rotation speed of the reel according to the information of the height, frame, and density of crop a few meters ahead of the header, which can be obtained by the ultrasonic-based pattern recognition system.

Acknowledgments

The authors wish to acknowledge the financial support provided by the Nanjing Research Institute for Agriculture Mechanization, Ministry of Agriculture (NRIAM). We want to thank Dr. Haibin Li for proofreading the manuscript.

References

[1] Smart, R.E., Dick, J.K., Gravett, I.M., Fisher, B.M., 1990. Canopy management to improve grape yield and wine quality-principles and practices. S. Aft. J. Enol. Vitiv. 11 (1), 3-7.
[2] Haselgrove, L., Botting, D., van Heeswijck, R., Høj, P.B., Dry, P.R., Ford, C., Iland, P.G., 2000. Canopy microclimate and berry composition: The effect of bunch exposure on the phenolic composition of Vitis vinifera L cv. Shiraz grape berries. Aust. J. Grape Wine Res. 6, 141-149.
[3] Wood, B.W., Conner, P.J., Worley, R.E., 2003. Relationship of alternate bearing intensity in pecan to fruit and canopy characteristics. HortScience 38 (3), 361-366.
[4] Detlef Ehlert, Hans-Jürgen Horn, Rolf Adamek, 2008. Measuring crop biomass density by laser triangulation. Comput. Electron. Agric. 61, 117-125.
[5] Mizrach, A., Galili, N., Rosenhouse, G.., 1989. Determination of fruit and vegetable properties by ultrasonic excitation. Trans. ASAE 32, 2053-2058.
[6] Mizrach, A., 2008. Ultrasonic technology for quality evaluation of fresh fruit and vegetables in pre- and postharvest processes. Postharvest Biol. Technol. 48, 315-330.
[7] Abbott, J.A., 1999. Quality measurement of fruit and vegetables. Postharvest Biol. Technol. 15, 207-225.
[8] Butz, P., Hofmann, C., Tauscher, B., 2005. Recent developments in noninvasive techniques for fresh fruit and vegetable internal quality analysis. J. Food Sci. 70, R131-R141.
[9] William D., O'Brien Jr., 2007. Ultrasound-biophysics mechanisms. Progress in Biophysics and Molecular Biology 93, 212-255.
[10] Kuttruff, H., 1991. Ultrasonics: Fundamentals and Applications. Elsevier, New York, NY.
[11] Walls, P.N.T., 1969. Physical principles of Ultrasonic Diagnosis. Academic Press, New York.
[12] Turrell, F.M., Garber, M.J., Jones, W.W., Cooper, W.C., Young, R.H., 1969. Growth equations and curves for citrus trees. Hilgardia 39 (16), 429-445.
[13] Lee, W.S., Alchanatis, V., Yang, C. Hirafuji, M., Moshou D., Li, C., 2010. Sensing technologies for precision specialty crop production. Comput. Electron. Agric. 74, 2-33.
[14] Albrigo, L.G., Anderson, C.A., Edwards, G.J., Bistline, F.W., Hepburn, W.J., Cary, T., 1975. Yield estimation of 'Valencia' orange research plots and groves. Proc. Fla. State Hort. Soc. 88, 44-49.
[15] Giles, D.K., Delwiche, M.J., Dodd, R.B., 1988. Electronic measurement of tree canopy volume. Trans. ASAE 31 (1), 264-272.
[16] Giles, D.K., Delwiche, M.J., Dodd, R.B., 1989. Sprayer control by sensing orchard crop characteristics: orchard architecture and spray liquid savings. J.Agric. Eng. Res. 43, 271-289.
[17] Moltó, E., Martin, B., Gutierréz, A., 2001. Pesticide loss reduction by automatic adaptation of spraying on globular trees. J. Agric. Eng. Res 78 (1), 35-41.
[18] Solanelles, F., Escolà, A., Planas, S., Rosell, J., Camp, F., Gracia, F., 2006. An electronic control system for pesticide application proportional to the canopy width of the treecrops. Biosyst. Eng. 95, 473-481.
[19] Gil, E., Escolà, A., Rosell, J.R., Planas, S., Val, L., 2007. Variable rate application of plant protection products in vineyard using ultrasonic sensors. Crop Protect. 26 (8), 1287-1297.
[20] Zaman, Q., Salyani, M., 2004. Effects of foliage density and ground speed on ultrasonic measurement of citrus tree volume. Appl. Eng. Agric. 20 (2), 173-178.

[21]Schumann, A.W., Zaman, Q.U., 2005. Software development for real-time ultrasonic mapping of tree canopy size. Comput. Electron. Agric. 47 (1), 25-40.
[22]Balsari, P., Doruchowski, G., Marucco, P., Tamagnone, M., Van de Zande, J., Wenneker, M., 2002. A System for Adjusting the Spray Application to the Target Characteristics. Agricultural Engineering International: the CIGR Ejournal. Manuscript ALNARP 08 002 Vol. X.
[23]Scotford, I.M., Miller P.C.H., 2004. Combination of Spectral Reflectance and Ultrasonic Sensing to monitor the Growth of Winter Wheat. Biosystems Engineering 87 (1), 27-38.
[24]Zaman, Q.U., Schumann, A.W., Miller, W.M., 2005. Variable rate nitrogen application in Florida citrus based on ultrasonically-sensed tree size. Appl. Eng. Agric. 21 (3), 331-335.
[25]Zaman, Q.U., Schumann, A.W., Hostler, H.K., 2006. Estimation of citrus yield using ultrasonically-sensed tree size. Appl. Eng. Agric. 22 (1), 39-44.
[26]Peacock, B.C., Murray, C., Kosiyachinda, S., Kosittrakul, M., Tansiriyakul, S., 1986. Influence of harvest maturity of mangoes on storage potential and ripe fruit quality. ASEAN Food J., 99.
[27]De-Smedt, V., 2000. Measurement and modeling of mealiness in apples. Unpublished Phd, Katholieke University of Lenven, Belgium.
[28]Gaete-Garrenton, L., Vargas-Hernandez, Y., Leon-Vidal, C., Pettorino-Besnier, A., 2005. A novel noninvasive ultrasonic method to assess avocado ripening. J. Food Sci. 70, E187-E191.
[29]Mizrach, A., Galili, N., Rosenhouse, G.., 1992. Half-cut fruit response to ultrasonic excitation., ASAE Paper No. 923017. Amer. Soc. Agric. Eng., St. Joseph, MI, USA.
[30]Galili, N., Mizrach, A., Rosenhouse, G., 1993. Ultrasonic testing of whole fruit for nondestructive quality evaluation. ASAE Paper No. 936026.
[31]Mizrach, A., 2000. Determination of avocado and mango fruit properties by ultrasonic technique. Ultrasonics 38, 717-722.
[32]Self, G.K., Ordozgoiti, E., Povey, M.J.W., Wainwright, H., 1994. Ultrasonic evaluation of ripening avocado flesh. Postharvest Biol. Technol. 4, 111.
[33]Nielsen, M., Martens, H.J., Kaack, K., 1998. Low frequency ultrasonics for texture measurements in carrots (Daucus carota L.) in relation to water loss and storage. Postharvest Biol. Technol. 14, 297-308.
[34]Mizrach, A., Flitsanov, U., El-Batsri, R., Degani, C., 1999. Determination of avocado maturity by ultrasonic attenuation measurements. Sci. Hortic. 80, 173-180.
[35]Mizrach, A., Flitsanov, U., Fuchs, Y., 1997. An ultrasonic nondestructive method for measuring maturity of mango fruit. Trans. ASAE 40, 1107-1111.
[36]Mizrach, A., Galili, N., Rosenhouse, G.., 1994. Ultrasonic evaluation of some ripening parameters of autumn and winter-grown galia melons. Sci. Hortic. 56, 291-297.
[37]Ki-Bok Kim, Sangdae lee, Man-Soo Kim, Byoung-Kwan Cho, 2009. Determination of apple firmness by nondestructive ultrasonic measurement. Postharvest Biol. Technol. 52, 44-48.

2011 International Conference on Mechanical, Industrial, and Manufacturing Engineering
Lecture Notes in Information Technology Vols. 1-2

A Research of University-Industry Cooperative Education Mode for Cultivating Innovative Talents in Universities

Ying Ma
School of Management
Wuhan University of Technology
Wuhan, Hubei, P.R.C 430070
mying331@163.com

Jie Liu
School of Management
Wuhan University of Technology
Wuhan, Hubei, P.R.C 430070

Atract -University-industry cooperative education is an effective approach to cultivate innovative talents in universities. This paper analyses the purpose of innovative talents cultivating of cooperative education, and discusses four operating mechanisms of innovative talents cultivating by the cooperative education mode. Then it puts forward operating patterns of cooperative education for innovative talents cultivating. Finally the paper proposes safeguard measures to provide reference for practices of University-Industry Ccooperative Research.

Index Terms - Innovative talents, University-Industry cooperation， University education

I. INTRODUCTION

Laws of education development and talent development have both showed that talent cultivating is a tough and complicated system project which consists of education environment, education resource, education process and method. Cooperative education aims at cultivating students' comprehensive qualities and abilities, and employment competitive power through taking advantages of resources and environment of universities, enterprises and scientific research institutions and their experience in talents cultivating. Then combine the university education of initiating knowledge with the practice education of obtaining experience directly and practice ability to cultivate talents.

II. PURPOSES OF UNIVERSTIY-INDUSTRY COOPERATIVE EDUCATION FOR CULTIVATING INNOVATIVE TALENTS IN UNIVERSITIES

A. To Promote the Transformation of Talents Cultivating.

The macro system reformation of economy, technology and education has greatly promoted the incorporation process of cooperative research in China. There are already thousands of colleges, enterprises and research institutions which have preceded a number of different cooperation types. The cooperative education centering on talents cultivating is an important program which have been extensive practiced and got great effect. The practical effect is not only to establish a cooperation relationship to some extend, but also to promote the transformation of talents cultivation on the hand of education model and operation system.

B. To Be Good for Revolution of Education system

It can create consistently various education advantages to make a qualitative change of the whole system of education. Objectively speaking, the cooperation and practice pattern are corresponding to the thinking of "applied talents". Obviously, this is necessary, but not enough for innovative talent cultivating[1], it doesn't meet the demand of establishing national innovation system and strengthening national comprehension power. This means both the practice and theory facet of cooperative research should get promotion and development

C. To Gestate Huge Potential Power of Education.

Through the cooperative education, we could take the advantages of universities and society together, and by arranging correctly courses and social practice, to make university activities closer to the demand of society development, such as the major set, initial preparation and education content. At the same time, it could enhance the construction of teaching team, develop the practice ability and entire quality of teachers, and stimulate the cooperation in researches and strengthen teaching vitality. All these are to make students master knowledge, realize society, develop ability and polish quality.

III. RUNNING MECHANISM OF UNIVERSITY-INDUSTRY COOPERATIVE EDUCATION FOR CULTIVATING INNOVATIVE TALENTS IN UNIVERSITIES

The cooperation of University-Industry should make a resultant force. It must centre on the urgent demand of industry and enterprises to gather talents, and stimulate independence innovation, thus enhance talents cultivating of enterprises. The running mechanisms are as following.

A. United Cultivating Mechanism

By selecting a sort of powerful enterprises as the cooperative units for students practice education, colleges and enterprises establish united fostering base together. It is certainly a great reforming action for universities facing social economy market to practice the two strategies, those are "prosper market through science and education, strengthen market by talents".

B. Construction Mechanism of "Base"

"Base" is a platform of talent cultivating in colleges which is established by universities with authorities to give master's degree and doctor's degree, and some the first-rate large scale enterprises and high-tech enterprises. It aims at putting the University-Industry Strategy Union in practice, putting the common policy of talents training into effect, supervising the quality of talents training and promoting information exchange and communication and so on. Through

establishing "base", we could further universities' revolution of models and mechanisms of talents training, make universities go deep into the market economic battlefield and strengthen the teaching team; meanwhile, we could also raise students' comprehensive qualities and innovation abilities by carrying out some practical research programs, which are beneficial to the economy construction , science progress and society development. It also could improve the enterprises' social reputation, strengthen talents gathering and reserving power and enhance research and innovation abilities[2].

C. Evaluation and Appointment Mechanism of Enterprises' Part-time Tutor

For evaluation and appointment part-time tutors, we should hold a high-level standard[3]. We should free our mind and make some breakthrough in idea and conception to adjust the old evaluation and appointment mechanism; at the same time, the standard and request should be strictly hold by the degree evaluating committee of universities. Generally speaking, the part-time tutors should have following qualities: ability of realizing the technique demands of enterprises, ability of solving practical problem, as well as deep theory basic. Only those with the above qualities can instruct students to solve technique problems for enterprises with theory knowledge meanwhile [4].

D. Property Right Mechanism.

In the process of cooperative education of University-Industry, we should be clear about the belonging of intellectual property right. Students must participate in the products development. Now all technique staff who gets in the process of products development should sign an agreement with company to keep the intellectual property right which belongs to the company. However the company will give award for some important researches, especially for some bringing economic benefit for enterprises. So the united trained students must also sign an agreement with company [5]. In the study process, all the research production, no matter independent research or cooperative research, should belong to company. Otherwise enterprises won't permit students to contact the important technique content and students will learn nothing. But in the case of theoretic research paper, the property should be considered to give to students for universities paying attention to this.

IV. OPERATION MODES OF UNIVERSITIES-INDUSTRY COOPERATIVE EDUCATION FOR CULTIVATING INNOVATIVE TALENTS IN UNIVERSITIES

The key of combination of University-Industry is to promote a real fusion between universities and enterprises. Its goal is to accelerate technique innovation by assembling "three kinds of talents" (colleges teaching team, students talents team and enterprises technique professor team) enclosing the important core technique. Thus, Colleges can take full advantages of social resources to overflow their resources of teachers, talents and achievements, in order to realize the seamless connection with enterprises and to provide more expansive space for innovative talents cultivating. The models are as the following:

A. Pattern I:" Introduced coming and introduced going out".

Universities can introduce famous industrial professors, research talents and high-level managers to be part-time tutors. They would bring the industrial frontier theories, the key techniques which directly affect industry development and urgent demand for national economy development into colleges, so students could contact with the advanced techniques and participate in significant scientific research projects which would broaden their horizon greatly[6]. In the other hand, colleges should insist the principle of "introduced going out", and let students get training directly from enterprises bases, in order to make relationships tighter between colleges and enterprises.

B. Pattern II: "Two tutors" training pattern.

This pattern is to take the enterprise tutor as the primary tutor and the university tutor as the secondary. Under their direction, the research projects and thesis should be some problems and techniques urgent to be solved for enterprises. Meanwhile, united contract of University-Industry must be signed, and excellent students should be constantly sent to enterprises to study and research.

C. Pattern III*: Joint of subject cluster and industry cluster.*

This is a perfect model for universities to cultivate talents. The old model is mostly the one of "point to point" which is hard to take the advantage of cluster and hard to gain huge achievements. Now some colleges combine their core competitive subjects which can form subjects cluster with local industries cluster of pillar industries to construct a core competitive technique cluster. For example, Shanghai University of Transportation recently cooperated with CHINA SPRING FACTORY, Shanghai Electric, Shanghai Media Group, Shanghai Maple Automobile Company and East Shipyard of Shanghai to apply for important projects. Since 2004, it positively research and develop the automobile electric research platform which will face to the whole automobile industry. Surrounding the significant programs, the university breaks down the administration obstacle among schools and assembles teachers and students resource to joint with industry cluster. At the same time, the university can take it as the students cultivating platform and carrier, and make students participate in the technology innovation which will lead to industry core competition power, these will strengthen social sense of responsibility and sense of historical mission for students.

D. Pattern IV: *Co-construction of research center.*

Co-construct of research center can promote innovative talents cultivating. Innovative platform construction has always been the "soft rib" of universities, it demands the breakthrough of innovation mechanism for solving the existing problems of "small scale, decentralize, spontaneity, and repeat" phenomenon. We should tie up the talents, bases and projects, take interdisciplinary advantages to establish technology innovation platform and make research be done in

an organized way[7]. We should strive for constructing the platform and make it become the scientific innovation entity to serve national strategy and local economic demand and bring great influence to our country. It also makes students strengthen their ability by participation.

V. BASIC GUARANTEES OF UNIVERSITY-INDUSTRY COOPERATIVE EDUCATION FOR CULTIVATING INNOVATIVE TALENTS IN UNIVERSITIES

To ensure the cooperative education model of University-Industry to play a role in talent cultivating process, some guarantee measures are necessary.

A. Cultivation of high quality teacher team.

Colleges could retain talents to be teachers from other institutions, such as scientific research institution and industry department. Meanwhile industry department could invite teachers as projects' principals from colleges and scientific research institutions. Through this bidirectional teachers exchange mechanism, we could integrate the talents resource of industry, university and scientific research department. At the same time, teachers could enhance their theory level and professional ability through taking scientific research, and then enrich the teaching content. The scientific research achievements could get test in practice and quickly be transferred into productivity, and the updated technique and theory could soon become teachers' scientific research task. This platform requests that teachers can farther develop in longitude, as well as extend in latitude, and teachers are not only steady, but also opening and innovative, and they are good at both theoretic research and practical operation, thus, they can cultivate high quality and compound talents who will undertake national and local great scientific research independently. They should grasp mainstream of social development and transfer scientific achievements into practice productivities [9].

B. *Set the "wide-caliber and deep foundation" scientific course system.*

It's good for students to form reasonable knowledge structure by establishing expansive adaptation, reasonable structure and high level subject and optimized course system. The process of university-industry cooperative education could tightly connect colleges with society and make subjects in universities more suited to the demand of social economy development. Through constantly adjusting and optimizing, it can promote subjects and majors cross, percolation and fuse. Then we could establish scientific, reasonable talents cultivate subjects and major structures which provide more innovation opportunities for students in the cross subjects. Colleges could bring the development frontier of economy and the new technique of production into courses and adjust the current course system in order to make it more scientific, more perfect to satisfy the demand of social development and talent cultivating. These scientific course systems not only make students master the massy theory foundation and systemic specialized knowledge, but also master relevant subject frontier knowledge to broaden their horizon for interdisciplinary research.

C. *Expansion of education network***.**

The social and economic development is the constant resource of teaching content. Traditional teaching network is just restricted to course and campus which lay particular stress on theory teaching and indirection knowledge passing on. Although colleges are equipped with lab and experimental facilities which is limited, they are still not as good as practical producing environment. University-industry cooperative education could conformity colleges and society's education environment and resource, make up the shortage of talent cultivating in colleges and enrich teaching content, and finally establish a complete and open teaching process and construct thorough education network.

D. *Establishment of united cultivation organization***.**

University-industry cooperative education is based on the principle of "equal, voluntary, respect and mutual benefit". It is important for efficient and smooth operation to keep coordinate relationship among each department and strengthen organization management of cooperative education. This organization of broad is a typical form of cooperative education for internal management in China. The broad is mainly based on universities, at the same time uniting enterprises and leading departments which have relationship with universities, and is consists of the leaders of colleges and enterprises. The broad supervise, instruct, consult and considerate colleges' education direction, university scale, recruiting students, graduation distribution, scientific research and technique development. This kind of organization form comes from the horizontal alliance between colleges and industry departments, which are different from the vertical leading relationship in administration. The competent department instructs indirectly, colleges and enterprises, as the legal entity, normalizes the equal negotiation principle and procedure through legal procedure, thus stable management system and model can be established. It is beneficial to promote cooperative education's smooth development for the broad with authority[9].

ACKNOWLEDGMENT

The paper is supported by Social Science Foundation of Wuhan City(No. 20092s0080); Supported by Independent Innovation Fund of WUT(N0:2010-Ib-030); Supported by Technology Bureau of Wuhan City(No. 200940833375-10)

REFERENCES

[1] Wang Shengyu, Liu Qiaoyun, Ding Jingmin. Research of the Existing Problems of University-Industry Cooperative Education. Education Exploration and Practice. 2006(6)

[2] Zhang Xisheng, Bai Qinghua. Research of High-level Talent Cultivating Mechanism of University-Industry Cooperative Alliance---Take Shanghai as an Example. Journal of Handan College. 2007(1)

[3] Ding Kun. Research of Motive Mechanism of University-Industry cooperation[J]. Scientific Management Research. 2006.06

[4] Ma Hui. Research of Partner Selection of Cooperation and Operation Mechanism[D], Xidian University, 2006

[5] Xie Wei, Luo Li. Motive Mechanism of University-Industry Cooperation[J]. Research and Development Management, 1997 03
[6] Ma Dexiu. How to Promote High-level Innovative Talents Cultivating in University-Industry Cooperative Education[N]. Wen Hui News, 2005 (03)
[7] Wang Xiaojian, Wang Zhenhua, Li Yushen. Empirical Study of Interaction Model of University-Industry cooperative education. Journal of Chang'an University(Natural Science Edition), 2009(3)
[8] Song Yan. Research of Model of University-Industry Cooperative Education. Northern Economy Trade, 2008(2)
[9] Wu Yandeng. The Necessary Way: Operation Instruction of University-Industry Cooperative Education for High Vocational Education[M]. Beijing: Higher Education Press

2011 International Conference on Mechanical, Industrial, and Manufacturing Engineering
Lecture Notes in Information Technology Vols. 1-2

Thermal Design of Satellite Electronic Equipment Based on MSC/NASTRAN

Shi Yunxu, Fang Shijie
School of Mechatronic and automobile Engineering
Yantai University
Yantai, Shandong *Province*, China
shiyunxu@126.com

***Abstract* - In this paper, the thermal analysis model of satellite electronic equipment has been established using the software MSC.PATRAN, and the key technologies in the process of establishing the finite element thermal model of temperature field has been discussed. The steady-state thermal analysis has been done in the thermal module of MSC.NASTRAN, and the results show that the operating temperature of components can meet the requirements, and the thermal design is reasonable and feasible.**

Index Terms - thermal analysis; temperature field; electronic equipment

I. INTRODUCTION

When electronic devices work, the output power devices are often only part of the input power, the power loss are generally distributed in the form of heat out, along with electronic components and electronic equipment, the increasing power density, temperature has an impact on the reliability of the one of the key factors[1][2].

The relationship between the accelerated coefficient of the function degradation of electronic components and temperature can be obtained by the Arrhenius model:

$$\tau = \frac{t_1}{t_2} = \exp\left[\frac{E_a}{K_b}\left(\frac{1}{T_1} - \frac{1}{T_2}\right)\right] \quad (1)$$

Where, τ is the accelerated coefficients of the function degradation of electronic components; t_1 is the function degradation time of electronic components at the temperature T_1 ; t_2 is the function degradation time of electronic components at the temperature T_2 ; E_a is the activation energy of electronic components; K_b is the Boltzmann constant; T_1 and T_2 are the component junction temperature.

We can see in (1), the relationship between the function accelerated degradation coefficient of components and the junction temperature is exponential, and the reliability decreases along with the junction temperature increasing.
Therefore, heat from the components of electronic equipment reliability issues brought to the attention caused by the designer in the design process needs to take full account of PCB thermal design and thermal analysis problems.

Satellite electronic equipment is very poor working conditions, relatively large changes in ambient temperature, and the components within the equipment has high temperature sensitivity. So, in the process of equipment design needs to take full account of the temperature of components inside the equipment requirements. In order to ensure the reliability of equipment operation and must be reasonable thermal design.

Electronic equipment for early detection of problems in thermal design, shorten the design cycle, the introduction of the design process in the thermal finite element thermal analysis to determine the prototype design before production.

In this paper, the design of the satellite thermal design of electronic equipment using the software MSC.PATRAN /NASTRAN, and gradually found design deficiencies, and make relevant improvements. After the implementation of the new thermal design, the device operating temperature within the various components can meet the requirements.

II. THERMAL DESIGN

A. Equipment's Working Temperature

Equipment's working environment temperature is 0-40 ℃ , requires the ability to ensure the environmental temperature is 40℃, the device operating temperature of each component to meet the temperature derating requirements (components of the junction temperature must not exceed 85 ℃)[3].

B. Chassis Thermal Design

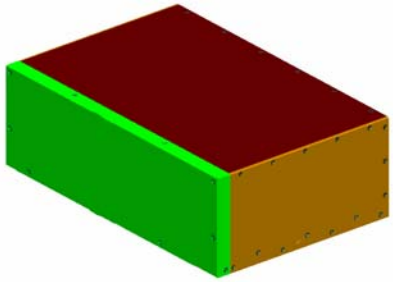

Fig.1 Equipment structure model

In order to heat dissipation, in the design process of the onboard electronic equipment chassis we give the following considerations: a) the design of the chassis components as conducive to heat, weight reduction measures can not cut off the path or the component cooling heat resistance become larger; b) to ensure the PCB between the plug and the chassis has a good thermal connection between the two fill the contact surface layer of thermal conductive filler; c)the installation of

the chassis have enough contact area, surface roughness and flatness of installation comply with the relevant regulatory requirements; d) chassis with good thermal conductivity of aluminium, the surface (except mounting surfaces) black anodized, the radiation rate is not less than 0.85.

The equipment used plug-in structure, just as shown in Fig.1.

C. PCB Thermal Design and Thermal Conductivity Coefficient Calculation

a) PCB thermal design

There is a PCB in chassis. In the design process, we take the following measures in order to enhance heat dissipation:

1) the equipment within the PCB material is FR4, but the thermal conductivity of FR4 is low which can not be good. So cover the copper on the PCB in the corresponding layer. The heat transfer directly to the boards through most of the copper layer and the heat dispel through the copper foil.

2) to ensure that printed border in close contact with the chassis, PCB locking wedge is installed on both sides of the border agencies, boards and chassis frame between the contact surface is coated with thermal grease.

3) In order to enhance the PCB heat transfer between the border and panel capacity, the two are closely connected by screws.

b) The calculation of effective thermal conductivity of PCB

To simplify the PCB multi-layer structure after copper clad, equivalent to anisotropic material will be printed, in which direction along the PCB plane thermal conductivity is k_x , thickness of the thermal conductivity of k_y.

PCB plane along the direction of the equivalent thermal conductivity is [1]:

$$k_x = k_{Cu} \times V_{Cu} + k_{FR4} \times (1 - V_{Cu}) \quad (2)$$

Where, k_{Cu} is Thermal conductivity of copper, V_{Cu} is the copper content in the volume of PCB, k_{FR4} is the thermal conductivity of FR4.

PCB thickness direction in a small proportion of copper, much of the material is FR4, the direction of the thermal conductivity can be simplified as:

$$k_y = k_{FR4} \quad (3)$$

c) Thermal design of components

Spacecraft electronics components within the chassis for heat dissipation in two ways:

1) Components and PCB soldering, the heat passes through the solder to the PCB.

2) The components of their own heat radiation.

PCB heating components on the main installation is divided into: components covered aluminium heat sink top surface, heat sink and component thermal pad placed between the top surfaces; aluminium heat sink screws through the frame with the PCB connection, contact Thermal grease between the coated surfaces.

III. THERMAL ANALYSIS

Thermal analysis thermal model is the basis and core of the analysis. And the model is good or bad largely determines the accuracy of analytical results. Therefore, thermal analysis modelling is the key issue.

Finite element method is a numerical approximation of the true situation. We solve a finite number of numerical simulations of the multiple unknowns' real environment through the mesh of the object.

Node of the grid by finite element analysis is the cornerstone, but the more the number of nodes does not mean more accurate thermal analysis. Thermal model from the point of view, the nature of the node the more the results reflect the model was more accurate.

The starting point is the numerical analysis and thermal analysis of discrete nodes in the network equation, so the finite element modeling of the basic requirements is:

1) Finite element model must be adapted to the characteristics of thermal analysis;

2) Finite element modeling of thermal boundary conditions must be conducive to attach;

3) Finite element modeling and mesh nodes throughout the division of the thermal model must be consistent with the physical properties, such as: whether the insulation board, the board whether the installation of equipment such as surface or cooling surface;

4) Heat transfer characteristics of a geometry node must be unified interface.

Several aspects of the above described only from the finite element modeling of a number of considerations. The most critical requirements of the physical model from the hot start, analyze specific issues, a clear physical meaning of each node of the heat in order to build the finite element model of thermal analysis. In this article the finished product suing the software MSC.PATRAN thermal analysis model. In the modeling process, first create the various components of the finite element model, and then the finite element model of these independent assembled into machine model. Whole model is completed, then one by one definition of boundary conditions, radiation conditions and the thermal coupling, and ultimately complete the thermal model of the set.

A. Geometric Simplification

Cell types according to structure and shape, and analysis software to determine the heating conditions, the main applications include the shell per unit type, body cells and so on. The device geometry is very complex, in order to facilitate the finite element analysis, in the process of modelling its appropriate simplified. The finite element thermal model is shown in Fig.2.

In the choice of unit, made the following considerations:

1) The chassis and printed are sheet structure, which are used 4-node plate elements (Quad4) simulation;

2) Printed border and the parts of the aluminium heat sink can be reduced to sheet structure, with 4-node plate element (Quad4) simulation;

3) PCB heating components are the major 8-node solid elements (Hex8) simulation;

4) Do not separate components of small heat loss model.

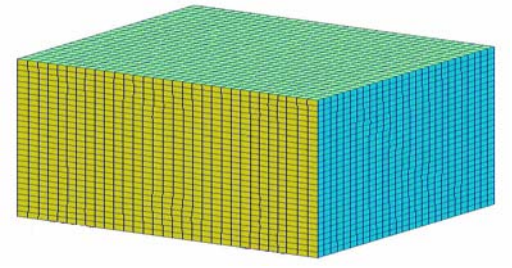

Fig.2 Machine thermal model

B. Define Material Properties

The major components of the thermal performance parameters are shown in Table 1.

Table I

Thermal property of materials

component	Material	Thermal conductivity W/(m·℃)	Hemispherical emissive
Enclosure surface	Aluminum	117	0.85
Chassis mounting plate Heat sink Printed Box	Aluminum	117	0.2
PCB	FR4	Plane direction: 48.77 Thickness:0.3	0.02
Shell components	Plastic	0.8	0.5

C. Loading Boundary Conditions and Constraints

1) equipment chassis mounting plate as the temperature is 40 ℃ heat sink surface, the surface of the chassis as the rest of the adiabatic boundary treatment.

2) In all major components of the top surface of heat load the appropriate heat flux (heat flux = heat loss / component top surface area).

3) PCB processing components on a small heat consumption for the uniform heat source.

4) Consider the components, chassis and radiation heat transfer between the PCB. Ignore the thermal radiation component pin.

5) Printed on both sides of the chassis frame housing the contact between the heat transfer coefficient determined based on experience 1500W / (m^2 • ℃). Printed border between the chassis panel contact heat transfer coefficient is 150W / (m^2 • ℃).

6) aluminium heat sink and PCB border between the aluminium heat sinks (or printed box) and the components of the contact surface between the various pieces of PCB thermal contact between the heat transfer coefficients obtained 1500W / (m^2 • ℃).

D. Thermal Analysis

By thermal analysis, we can calculate the components of the shell temperature (heat sink surface temperature components), components of the junction temperature is using the following formula:

$$T_j = T_c + Q \cdot R_{j\text{-}c} \qquad (4)$$

Where, T_j is the Components of the junction temperature, T_c is the components of the shell temperature, Q is the heat Components costs, $R_{j\text{-}c}$ is the components of the crust thermal resistance.

The main cloud temperature heating components is shown in Fig.3.

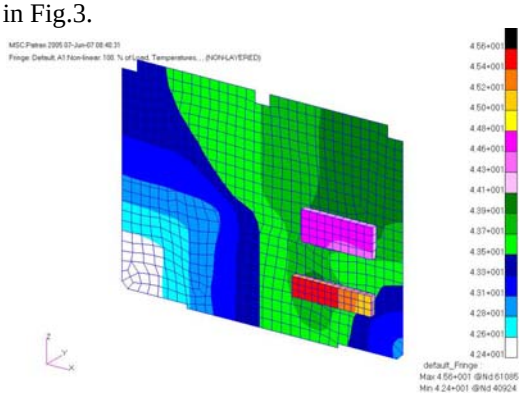

Fig.3 Temperature distribution of the components on the PCB

IV. CONCLUSIONS

We can draw the following conclusions through the thermal analysis and thermal balance test:

1) High heat consumption of the device operating junction temperature of components below the steady-state temperature derating, thermal design to meet the temperature derating requirements, which is reasonable and feasible.

2) The thermal analysis model of the chassis, PCB and components is basically in accordance with the actual structure of the heat transfer device, which can simulate the situation.

REFERENCES

[1] Renyuan Jiang, Xingtang Zhang, et al. The temperature stress under function degradation of type of accelerated life testing problem(in chinese). Journal of Nanjing University of Science and Technology, vol.24,no.6,pp.523-527,2000.

[2] Guijie Yang, Yintang Yang, et al. Research on Multichip module thermal analysis technology(in chinese). Journal of Microelectronics and computer, no.7, pp.78-80,2003.

[3] Hai Jiang, et al. Research on Thermal analysis integration technology(in chinese). Proceedings of The fifth spatial thermal physical ,pp.151-157,2000

2011 International Conference on Mechanical, Industrial, and Manufacturing Engineering
Lecture Notes in Information Technology Vols. 1-2

The Application of Queue in Binary Tree Layer Order Traversal

Min Wang
Department of Computer Science
Weinan Teachers University
Weinan, Shanxi Province, China
wntcwm@126.com

Zhibin Ren
Department of Computer Science
Weinan Teachers University
Weinan, Shanxi Province, China
wnrenzb@163.com

***Abstract* - Detailed analyzes and introduces the design ideas of the binary tree layer order traversing algorithm with the usage of auxiliary queue space, gives the algorithm description in C, and evaluates the algorithm from two aspects of the time complexity and the space complexity, so as to provide a specific example of the applications of the queue.**

Index Terms – Queue, Binary tree, Binary tree layer order traversal, Time complexity, Space complexity

I. INTRODUCTION

Queue is known as FIFO(First In First Out) linear list[1,2]. Binary tree has the tree logical structure. The so-called binary tree traversal is a process accessing all nodes on a binary tree, and each node only once, according to a certain rule[3,4]. The meaning of "access" is very wide, it can be various operations such as outputting the information of the node[1].

This paper will introduce the application of queue in binary tree layer order traversal, analyze detailedly the algorithm design ideas, give the algorithm description in C, and analyze two aspects of time complexity and space complexity of the algorithm, so as to provide a specific example of the applications of the queue.

II. QUEUE STORAGE STRUCTURE

The logical structure of queue only allow of insertion in the rear and deletion from the head, so it requires the head location and the tail location of the queue. Similar to the linear list, the structure of queue can be both the sequential storage structure (called sequential queue) and the linked storage structure (called linked queue). The operations of linked queue are actually the same as the single linked list, but the insertion is only allowed at the rear and the deletion is only at the front[1]. Binary tree layer order traversal uses only the FIFO property of auxiliary queue space to achieve traversing all nodes, and the linked storage structure will reduce the utilization of the auxiliary space, so we choose the sequential storage structure for the queue.

The type of sequence queue can be defined in C as follows:

```
typedef struct{
    ElemType queue[MAX];
    int front,rear;
}SeqQueue[1-3];
```

The member *queue* is the vector space of the queue, which is used to store the elements. The members *front* and *rear* are vector subscript indicators. The former indicates the previous element location before the first element, while the latter indicates the last one.

III. BINARY TREE STORAGE STRUCTURE

If the binary tree has the form similar to the complete binary tree, you'd better choose the static vector storage, so that the parent-children relationship of nodes can be specified according to the property 5 of the complete binary tree[4]. But for the non-complete binary tree, you'd better choose the binary linked storage structure instead.

The binary linked storage structure is shown as Fig.1.

Lchild	*data*	*Rchild*

Fig. 1 The node type of the binary linked storage structure

The type of binary linked storage structure can be defined in C as follows:

```
typedef struct Node{
    DataType data;
    struct Node *Lchild,*Rchild;
} Node, *BTree[3,4];
```

The member *data* is used to store the value of a node, and the members *Lchild* and *Rchild* are two pointers that point respectively to the left and right children of the node.

Without loss of generality, we use the binary linked storage structure to store the binary tree in this algorithm.

IV. BINARY TREE LAYER ORDER TRAVERSING ALGORITHM

The binary tree layer order traversal accesses all the nodes from top to bottom, left to right in each layer, so the algorithm design and implementation can use an auxiliary queue space.

A. Algorithm Design Ideas

The key of designing the binary tree layer order traversing algorithm using auxiliary queue space is how to store and access the node pointers according to the order of layers[2]. You can define the elements of the queue to be pointers pointing to the node addresses on a binary tree, so the algorithm can be carried out as follow:

(1) The root pointer enter the queue;
(2) Remove an element from the head of the queue(delete from the queue), and perform the following steps:
① Visit the data value of the deleted node;

② If the *Lchild* pointer of the node is not NULL, then the left child node enter the queue;

③ If the *Rchild* pointer of the node is not NULL, then the right child node enter the queue;

(3) Repeat *step(2)* until the queue is empty, and then terminate the algorithm[2].

In order to avoid "false overflow", and economize as far as possible the auxiliary queue space, we use the circular queue, so that the size of the auxiliary space is 2^{h-1} at most, where *h* is the depth of the binary tree.

B. Algorithm Description in C

Firstly, We need some assumptions below for the algorithm to be introduced later.

- The value type of node on the tree is character, that is the foregoing abstract data type *DataType* is *char*.
- The proccess of accessing the binary tree nodes is just outputting the node values.
- The binary tree is stored using a binary linked storage structure (*BTree*), and the auxiliary queue space is stored using a sequential structure(*SeqQueue*).
- The abstract data type *ElemType* of member *queue* of the queue is *Node**.

Then the algorithm can be described below in C:

```
void LevelOrderTranverse(BTree root)
{  SeqQueue Q;  Node *p;
   Q.front=Q.rear=0;          //Initializes an empty queue.
   if(!root)  return;  //Terminates in case of an empty tree.
   Q.rear=(Q.rear+1)%MAX;
   Q.queue[Q.rear]=root;  //Root pointer enters the queue.
   while(Q.front!=Q.rear)
   {  Q.front=(Q.front+1)%MAX;
                    //Deletes the first element of the queue.
      p=Q.queue[Q.front];
      printf("%c",p->data);  //Outputs the deleted element.
      if(p->Lchild)
 //If the left child exist, the Lchild pointer enter the queue.
       {  Q.rear=(Q.rear+1)%MAX;
          Q.queue[Q.rear]=p->Lchild;   }
       if(p->Rchild)
  //If the right child exist, the Rchild pointer enter the queue.
       {  Q.rear=(Q.rear+1)%MAX;
          Q.queue[Q.rear]=p->Rchild;   }
   }// End_while
}
```

C. Algorithm Performance Evaluation

The core statement of function *LevelOrderTranverse( )* is the *while* loop statement, so the implementing frequency of the basic statements depends on whether the condition of *while* is satisfied, that is the total number of elements into the queue. Obviously, the number of elements into the queue equals to that of the binary tree nodes. Regarding *n*, the total number of nodes on binary tree, as the scale of the problem, the algorithm average time complexity is linear order, that is *T(n)=O(n)*.

In addition to the binary linked storage space used by the binary tree nodes, this function also introduces an auxiliary queue space, so the algorithm space complexity depends on the size of it's vector member *queue*. Since the size of member *queue* is 2^{h-1} at most, we can deduce that $h=[\log_2 n]+1$ according to the property 4 of the complete binary tree, and then the algorithm space complexity is linear order, that is *S(n)=O(n)*.

V. CONCLUSION

To verify the correctness of function *LevelOrderTranverse()*, we add two functions *CreateBTree ()* and *main()* to ensure the integrity of the procedure. Function *CreateBTree ()* creates a binary linked storage structure for the nodes of a binary tree in the form of generalized list, and uses a *root* pointer pointing to the root. Function *main()* is a calling function that calls functions *CreateBTree ()* and *LevelOrderTranverse()*. Also, to simplify the input and output, this program set the abstract data type *DataType* for *char*.

In this paper, the algorithm descriptions in C has passed through VC++ 6.0 environment to test their accuracy.

Binary linked list is non-linear structure, and each node structure has a pointer pointing to its successor, but the address of the next node to be visited can not be obtained directly from the current node during the binary tree layer order traversal. The sequential queue is used to store the node pointers on the binary linked list, and since its FIFO characteristics, the deleting sequence and the entering sequence have the same order, thus we get the node visited sequence[2].

This paper provides a specific example of the applications of the queue, and plays a guiding role in teaching the relevant chapters in "Data Structure" curriculum.

ACKNOWLEDGMENT

This work is supported by Research Fund of Weinan Teachers University (No. 11YKS002).

REFERENCES

[1] Yan Weimin, Wu Weimin, *Data Structures(C language edition)*, Beijing: Tsinghua University Press, 2002.

[2] Wang Zhongyi, *Data Structure*, Xi'an:Xi'an Jiaotong University Press, 2003.

[3] Geng Guohua, *Data Structure—C Language description*, Xi'an:Xi'an Electronic Science and Technology University Press, 2006.

[4] Wang Min, "Research on Searching the Longest Path in Binary Tree Based on Traversing Algorithm," *Modern Electronics Technique*, vol. 33, no. 4, pp. 54-55,58, Feb. 2010.

2011 International Conference on Mechanical, Industrial, and Manufacturing Engineering
Lecture Notes in Information Technology Vols. 1-2

A Time Series Analysis Method for Regional Foundation Education Planning Prediction

Wen-liang Gao,Wan-zhi Chen
College of Business Administration
Liaoning Technical University
HuLuDao, Liaoning Province 125105, China
e-mail: ltuchenwanzhi@gmail.com

Lei-fu Gao
College of Science
Liaoning Technical University
FuXin, Liaoning Province 125105, China
e-mail: gaoleifu@yahoo.com.cn

***Abstract*—In order to regional foundation education development, following "The national education reform and development medium to long-term program (2010-2020)", a city as the foundation education object in this paper, based on the theory and empirical analysis of the statistical data for foundation education financial investment, expenditure structure, urban and rural area education condition and balanced etc. from 1997 to 2009, combining time series analysis method, to established regional basis education structure optimization and planning of regional prediction model, providing strong support to data analysis of education the optimal financial investment and resource allocation, adjust the structure of fiscal expenditure etc., in the end, to the benefit of science education plan of education cost accounting, overall supervision mechanism, control the school education foundation moderate scale, promote the balanced development.**

Keywords-time series analysis; foundation education; education planning; prediction

I. INTRODUCTION

The foundation education is the elementary living and development education of people's basic knowledge and ability in China at present, which including preschool, elementary and secondary education (senior and junior high school). And the expenditure is refers to the national budget directly to the various levels school education expenditure and investment in infrastructure, which is the main part of the funds, which is realized over the distribution of the national budget based on the country's the first distribution and redistribution of fiscal revenue for the gross social product and national income. "The national education reform and development medium to long-term program (2010-2020)" is the programmatic document to guide future education reform and development, including explicitly pointed out that education must be correspondent with the social and economic development planning, embody the strategic, self-evidence, overall and long-term. Formulate education program is a wide range of social systems engineering, difficult task, including overall planning and classification of planning. Therefore, as to local foundation education development, must to seize opportunities, optimize structure for the foundation education, planning of regional classification, rational configuration of education resources, improve the efficiency of education expenditure, and the use of education foundation funds more rational, the limited education resource configuration optimization to realize benefit maximization, further promoting education compulsory education reform and development, realize the balance, healthy and sustainable development, but also provide a good foundation for the modernization education and quality education.

II. THE TECHNICAL ROUTE FOR TIME SERIES ANALYSIS MODEL

The technical route as shown in Fig.1. With time series analysis method, and the theoretical study and empirical analysis combination way, establishes the foundation education major statistical data of time series model by Excel and EViews software based on regional actual education statistical manual data, and then analyzes its inherent characteristics and compares the exponent model and time series model, in the end forecast regional education development planning that provides the basis of foundation education structure optimization decision.

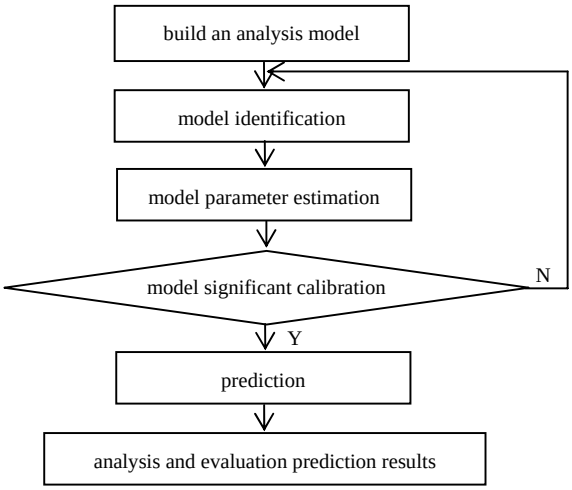

Figure 1. The schematic diagram of technical route

III. BULIDING THE ARIMA MODEL OF REGIONAL EDUCATION APPROPRIATION EXPENDITURE

A. Time Series Analysis of Regional Education Appropriation Expenditure

The time series data come from the statistical handbook for education appropriation expenditure of a city's education and other departments from 1997 to 2009.

1) Stationarity test

Import Education Appropriation Expenditure (EAE) to EViews software come into being the scatter diagram as shown in Fig.2, which approximate to exponential growth trend, thus non-stationary.

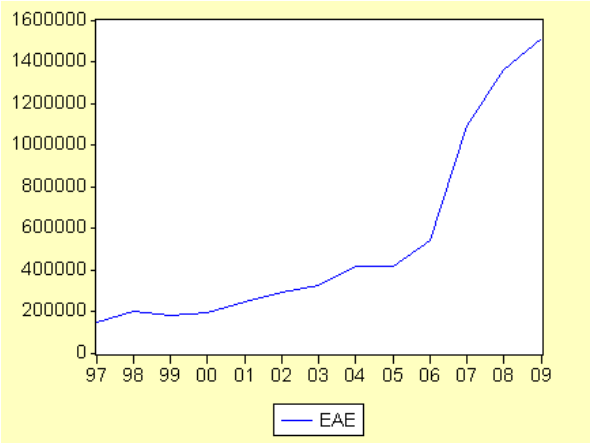

Figure 2. The time series for EAE of a city's education and other departments

2) Tranquilization and white noise test

At first should differential transform the non-stationary time series into stationary time series and then establish model. So input the command line in EViews:

Genr y = EAE - EAE(-1)

The result as shown in Fig.3.

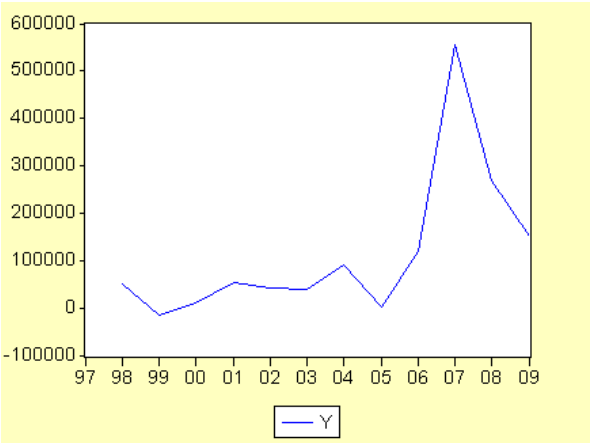

Figure 3. The time series for EAE after first difference

And then stationarity test again by DF test, the result as shown in Fig.4.

Augmented Dickey-Fuller Unit Root Test on Y

Null Hypothesis: Y has a unit root
Exogenous: Constant
Lag Length: 2 (Automatic based on SIC, MAXLAG=2)

		t-Statistic	Prob.*
Augmented Dickey-Fuller test statistic		1.794360	0.9983
Test critical values:	1% level	-4.420595	
	5% level	-3.259808	
	10% level	-2.771129	

Figure 4. Augmented Dickey-Fuller Unit Root Test of the time series for EAE after first difference

But after first difference the EAE series non-stationary also, So do the second difference, input the command line in EViews:

Genr dy = y - y(-1).

And the second difference of EAE defined as *dy*. And then stationarity test again by DF test, the result as shown in Fig.5.

Augmented Dickey-Fuller Unit Root Test on DY

Null Hypothesis: DY has a unit root
Exogenous: Constant
Lag Length: 1 (Automatic based on SIC, MAXLAG=1)

		t-Statistic	Prob.*
Augmented Dickey-Fuller test statistic		-4.039482	0.0168
Test critical values:	1% level	-4.420595	
	5% level	-3.259808	
	10% level	-2.771129	

Figure 5. Augmented Dickey-Fuller Unit Root Test of the time series for EAE after second difference

Correlogram of DY

Date: 10/27/10 Time: 09:40
Sample: 1997 2009
Included observations: 11

Autocorrelation	Partial Correlation		AC	PAC	Q-Stat	Prob
		1	-0.302	-0.302	1.3031	0.254
		2	-0.126	-0.239	1.5566	0.459
		3	0.010	-0.128	1.5584	0.669
		4	-0.005	-0.090	1.5589	0.816
		5	-0.010	-0.068	1.5613	0.906
		6	0.000	-0.047	1.5613	0.955
		7	0.000	-0.034	1.5613	0.980
		8	0.000	-0.024	1.5613	0.992
		9	0.000	-0.017	1.5613	0.997

Figure 6. Correlogram of the time series for EAE after second difference

After the second difference, *dy* don't exist unit root under 1% and 5% by DF test stationarity test, the series is stationary series.

Then the stationary series should passed pure random inspection (white noise test), only the stationary non-white noise series could undertake ARMA model fitting. Observe

correlogram of the time series for EAE after second difference as shown in Fig.6, *dy* series passed.

B. ARIMA Model Fitting

According to the determining order the basic principle for ARMA model as shown in Tab.1. Because the subjectivity judgment from autocorrelation coefficient and partial correlation coefficient's trailing or truncated, only roughly judgment series should choose the model of concrete form. Take advantage of AIC and SBC rule and calculate repeatedly in EViews software, select the optimalizing *dy* model ARIMA(2,2,1)

TABLE I. THE BASIC PRINCIPLE TABLE OF DETERMINING ORDER FOR ARMA MODEL

Autocorrelation Coefficient	**Partial Correlation Coefficient**	**Determining Order For Model**
trailing	*p* order truncated	AR(*p*) model
q order truncated	truncated	MA(*q*) model
trailing	trailing	ARMA(*p*,*q*) model

So the command line in EViews:

Ls dy dy(-1) dy(-2) ma(1)

The result as shown in Fig.7. So the second difference model of EAE is:

$$dy_t = -0.395086dy_{t-1} - 0.740974dy_{t-2} + u_t + 4.941541u_{t-1}$$

Variable	Coefficient	Std. Error	t-Statistic	Prob.
DY(-1)	-0.395086	0.345341	-1.144047	0.2962
DY(-2)	-0.740974	0.087776	-8.441664	0.0002
MA(1)	4.941541	1.972418	2.505322	0.0462

Figure 7. Calculate of factor for ARIMA model

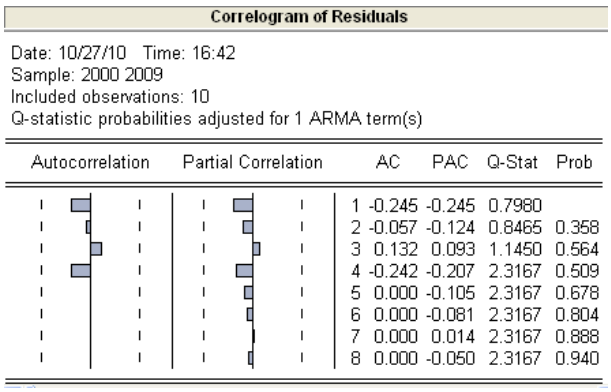

Figure 8. Correlogram of residuals

C. The Model Test

After the model identification and parameter estimation, should test the evaluation result to make sure of the model correct. Judgment model fitting quality and residual series randomness by Q-Statistic as shown in Fig.8. The right Prob column of figures show the probability that the under the corresponding DOF conditions Chi-Square statistics values greater than the corresponding Q value. And the probability value greater than 0.05, that means the random error series of model is a white noise series, and further declare the fitting model is appropriate.

D. The Model Prediction

The model prediction based on the ARIMA model following:

$$dy_t = -0.395086dy_{t-1} - 0.740974dy_{t-2} + u_t + 4.941541u_{t-1}$$

$$dy_{2010} = -0.395086dy_{2009} - 0.740974dy_{2008}$$
$$= 0.395086 \times 119108 + 0.740974 \times 28485 = 258125.1$$

$$y_{2010} = y_{2009} + dy_{2010} = 150249.0 + 258125.1 = 408374.1$$

$$EAE_{2010} = EAE_{2009} + y_{2010} = 1511785 + 408374.1 = 1920159$$

$$\eta = \frac{1980500 - 1920159}{1920159} = 0.03$$

The fact value of the city's EAE is 1980500, so the prediction relative error is 0.03. The model and actual fitting degree is high, could well predict the development trend of the decisive role elements for education program.

IV. CONCLUSION

Although the model in the short-term prediction relatively correct, but with the predictive period growth prediction error will appear gradually increasing trend. Some outside uncontrolled factor affecting the accuracy of model prediction too, and the influence of regional foundation education planning have many factors Which the data of utmost relevance, different perspectives prediction should choose different elements to constructing model, even some subject study is required to apply multiple linear regression to determine the correlation coefficient between the various factors. But time series analysis method for basic education structure optimization and prediction to a certain extent could realize the target of optimized foundation education structure, so to the benefit of local making reasonable and scientific development strategy combined specific situations.

REFERENCES

[1] HE Zheng-dao and HE Rui-yin. "Analysis on the relationship between gross power of agriculturalmachinery and key influencing factors based on time series analysis," Chinese Agricultural Mechanization, 2010, (1): 20~24

[2] Laurie J. Bates and Rexford E. Santerre. "A Time Series Analysis of Private College Closures and Mergers," Review of Industrial Organization,2000(3), pp. 267-276.

[3] Cui Jing and Zhang Ke, "Application of ARIMA Model in Forecasting China's Investment in Education," Statistical Thinktank, 2009(2), pp.43-46.

[4] Last M,Klein Y, Kandel A. "Knowledge Discovery in Time Series Databases," Systems and Cybernetics,Part B,IEEE Transactions on ,Vol.31, Feb 2001.

2011 International Conference on Mechanical, Industrial, and Manufacturing Engineering
Lecture Notes in Information Technology Vols. 1-2

Influence of nano-clay addition on porosity of cement paste at early age*

Yingfang Fan, Shiyi Zhang and Haiyang Luan
Department of Civil Engineering
Dalian Maritime University
Dalian, Liaoning 116026, CHINA
fanyf72@yahoo.com.cn

***Abstract* – Effect of Kaolinite nano-caly to the porosity of cement paste at early age is examined. Cement paste samples with 3 kinds of additives dispersed by 2 methods are prepared. Mercury propsimetry technique was employed to investigate the porosity characteristics in different sample. Scanning electron microscopy (SEM) and energy dispersive spectra (EDS) were applied to investigate the morphology and chemical element distribution inside the matrix. The results show that the addition of well dispersed nanocly can reduce the pore diameter in the cement paste at early age, and the porosity properties of the matrix can be enhanced with suitable additives.**

Index Terms – Kaolinite, nano-caly, dispersion, porosity, cement, SEM/EDS.

I. INTRODUCTION

It is well known that concrete is a kind of porous materials. Various kinds of aggressive agents exist in the environment will get through the pores and capillaries inside the structure, which will generate the destruction of the materials starting from the surface. With the inclusion of the aggressive agents continues, the concrete will be damaged. Therefore, the durability of the concrete has a close relation to porosity, which determines the intensity of interactions of the material with aggressive agents.

Kaolinite is a clay mineral; it has a crystalline structure and contains silicon. The theoretical formula for kaolinite is $Al_2Si_2O_5(OH)_4$, and the other formulas are $Al_2O_3{\cdot}2SiO_2{\cdot}2H_2O$ and $Al_2O_7Si_2.2H_2O$ (Varga, 2007). It has been reported that the structure of Kaolinite includes two layers. The upper layer is the gibbsite layer, which composed of aluminum oxide (Al_2O_3), while the lower layer is composed of silica (SiO_2). Since the layers are close to each other, it is difficult for the water molecules to go through the sheets. Therefore the permeability of the cement paste with the addition of Kaolinite nanoclay will be improved (Tregger, 2010; Morsy, 2010).

In this study, influence of nanocaly addition on the porosity characteristics of cement pastes is investigated. A kind of Kaolinite nanocaly was used in this study. The microstructure of the nanoclay was observed by Scanning and Electron Microscope (SEM) techniques. Effects of the additive amount, dispersing methods on the porosity characteristics of cement paste are studied respectively. 3 kinds of additive amounts, 2 kinds of dispersing methods are considered herein. Mercury intrusion test, Scanning Electron Microscope (SEM) and Energy Dispersive Spectra (EDS) test are fulfilled on the cement samples. The changes of porosity characteristics for the cement paste with Kaolinite nanocly additions are discussed.

II. MATERIALS USED AND SAMPLE PREPARATION

A. Cement:

Ordinary Portland cement of type 42.5R was used in this study. The specification of Chinese standard JTGE30-2005 was followed during the mixing of the cement pastes.

B. Nano clay:

A kind of commercially available powder Kaolinite nanoclay was used in this study. The details of the Kaolinite nanoclay are as follows, particle size, 370nm; composition contents, is listed in Table.1. To clarify the microstructure of the Kaolinite nanoclay studied in this paper, SEM and EDS test are executed on the neat caly powder. The resulting SEM image and EDS of Kaolinite nanoclay powder sample is shown in Figure 1.

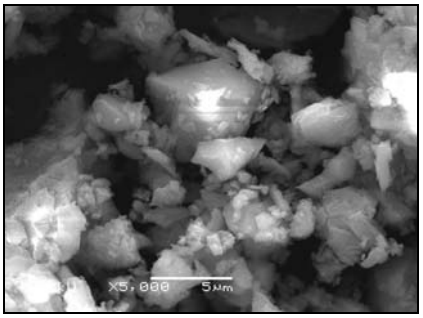

a. SEM morphology of Kaolinite clay (5000×)

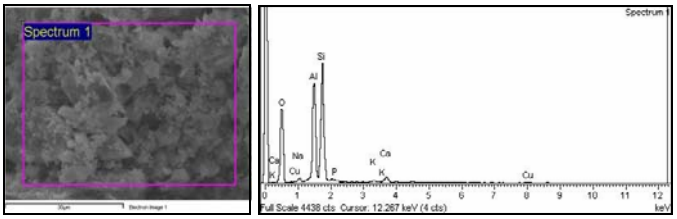

b. EDS spectrum of neat clay powder

Fig. 1 Micrograph and EDS spectra of neat clay powder.

* This work is partially supported by NSF Grant #50708010 and LNSF Grant #20092149 to Y.F. Fan.

TABLE I
CHEMICAL COMPOSITION OF KAOLINITE NANOCLAY (WEIGHT%)

Chemical composition	Content / %
SiO_2	47.8
CaO	0.28
Al_2O_3	41.8
Fe_2O_3	0.30
MgO	0.03
K_2O	0.58
TiO_2	0.02
Na_2O	0.06

Figure 1a. shows SEM image of the kaolinite. With magnifications of 5,000 or more, a considerable amount of fine platy material is visible. From the EDS spectra shown in Figure 1b., the chemical element contents of the 3 Kaolinite clay power samples are achieved, which are listed in Table.2 respectively.

TABLE 2
CHEMICAL ELEMENT AMOUNT IN KAOLINITE NANOCLAY

Element	Weight /%		
	Sample No.1	Sample No.2	Sample No.3
O K	**44.35**	**48.36**	**43.40**
Si K	**32.11**	**27.85**	**35.04**
Al K	16.93	18.25	16.51
Na K	3.37	1.24	2.82
Ca K	0.69	1.78	
Cu K	1.34	1.49	1.62
K K	0.52	0.44	0.61
Fe K	1.96		
S K	1.00		
Mg K	0.84		
Ti K	0.69		
P K		0.57	

C. Specimen preparation:

To prepare the paste samples, 0.75wt%, 1wt%, and 1.5wt% of cement by weight was replaced by nanoclay. An effective water-to-binder (cement + nanoclay) ratio of 0.5 was maintained. Since the properties of the nanoparticle modified cement are depended on the dispersion of nanoparticle in cement, how to disperse the nanoparticle in the cement paste averagely is very important. To achieve a good dispersion of nanoclay in cement paste, nanoclay was dispersed in water by hand and machine for 5 minutes, respectively. Then, the dispersed nanclay will be mixed with the cement by mixing machine for 7 minutes. The samples were kept in molds at 95% relative humidity for 24 hours, and then cured in the standard curing condition for 3 days at 20°C. The sample conditions are given in Table.3.

TABLE 3
TESTING SAMPLES

Sample No.	Content of nanoclay / %	Dispersion method
NC0	0	N
NCH1	0.75 wt	Disperse in water for 2 minutes by hand
NCH2	1.0 wt	
NCH3	1.5 wt	
NCM1	0.75 wt	Disperse in water for 2 minutes by mixing machine
NCM2	1 wt	
NCM3	1.5 wt	

D. Testing:

Mercury propsimetry:

The porosity of hardened cement paste was measured by the method of mercury porosimetry using high-pressure porosimeter Micrometrics Auto-Pore Ⅱ 9200 (with pressure range up to 400 MPa).

Microstructure:

SEM was applied for identification of the changes occurred in the microstructure of the cement paste with different amount of nanoclay addition. The chemical elements contents were analyzed by the EDS results as well.

III. RESULTS AND DISCUSSIONS

A. Porosity characteristics:

From the Mercury propsimetry test executed on the cement paste with nanocaly added by two dispersion methods, the porosity characteristics, such as total mercury volume, total specific surface area in hole, medium hole diameter volume, medium hole diameter areas, skeleton density, apparent density at 0.52psia, porosity ratio and average pore diameter, are achieved. The testing results are listed in Table.4.

TABLE 4
CHEMICAL COMPOSITION OF CEMENT

No.	medium hole diameter volume /nm	medium hole diameter areas / nm	skeleton density / g/ml	porosity ratio / %	average pore diameter /nm
NC0	**121.6**	**13.8**	**40.7**	**2.3294**	**28.4163**
NCH1	179.5	13.3	44.4	2.3758	32.1085
NCH2	98.8	12.8	34.2	2.3472	29.4309
NCH3	138.6	13.9	39.7	2.3636	30.5988
NCM1	**92.9**	**13.0**	**35.7**	**2.3170**	**26.4681**
NCM2	**69**	**14.4**	**32.3**	**2.3174**	**23.1658**
NCM3	108.0	13.5	38.3	2.3426	28.7818

Figure 2 shows the relation between the nanoclay additions with the porosity characteristics under the two dispersing methods. From the development of pore diameter with nanoclay additions, it is clear that both the medium hole diameter volume and the average pore diameter will decrease for the cement pasted with 0.75 wt% and 1.0 wt% machine-dispersed nanoclay additives. Compared with the neat cement paste, the average pore diameter of cement paste with 0.75 wt% and 1.0 wt% additive achieved a reduction of 6.9% and 18.5% respectively. The pore diameter has an increase for the cement paste with 1.5% machine-dispersed nanoclay, which may be caused by the dispersion condition of nanoclay. That is, the dispersing time of 2 seconds may be too short for 1.5 wt% additive; it should be longer if the amount of clay additives is increased. However, the average pore diameter has a slight increase for the cement paste with hand-dispersed nanoclay. Simultaneously, the porosity ratio of cement paste with 0.75 wt% and 1.0 wt% additive achieved a slight reduction of 0.5%. The porosity ratios of the cement pastes with 1.5 wt% machine-dispersed and hand-dispersed nanoclay have a slight increase.

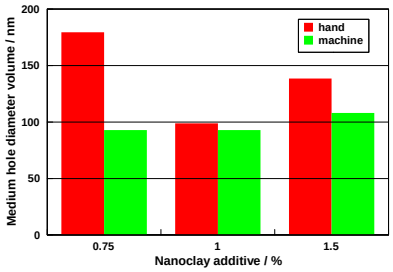

a. medium hole diameter volume

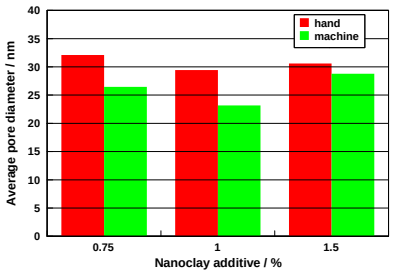

b. average pore diameter

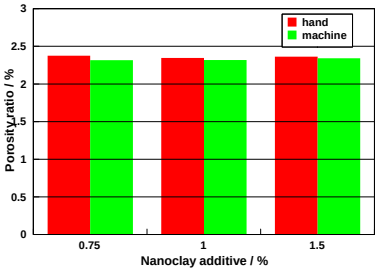

c. porosity ratio

Fig.2.Relation between the nanoclay additions with the porosity characteristics under the two dispersing methods

B. Microstructure of nanoclay modified cement paste:

Figure 3 shows the SEM micrographs of cement paste with different machine-dispersed nanoclay additions. Figure 4 shows the SEM micrographs of cement paste with different hand-dispersed nanoclay additions. The test samples for microstructures were obtained from the central part of mortar specimens. It is obvious the microstructure is quite different for the cement pastes with two dispersion methods. From the SEM images of the cement paste with machine dispersed nanoclay, it can be seen that the microstructure is average for 0.75 wt% and 1.0 wt% additives, plate structure can be observed once the additive increased to 1.5 wt%. This result can well explain why the porosity characteristics of the cement paste with 1.5 wt% nanoclay additive decrease from the micro-scale level.

In morphology properties, it can be seen that the effect of dispersing methods of clay on the microstructure of the cement pastes. It can be achieved that, the porosity can be improved if the nanocly is well dispersed.

C. Element distribution in nanoclay modified cement paste:

From the energy dispersive spectra, the chemical element distribution in the cement paste samples are achieved, which is listed in Table.5. Relations between nanoclay additives and the amount of chemical elements in the cement are shown in Figure 5.

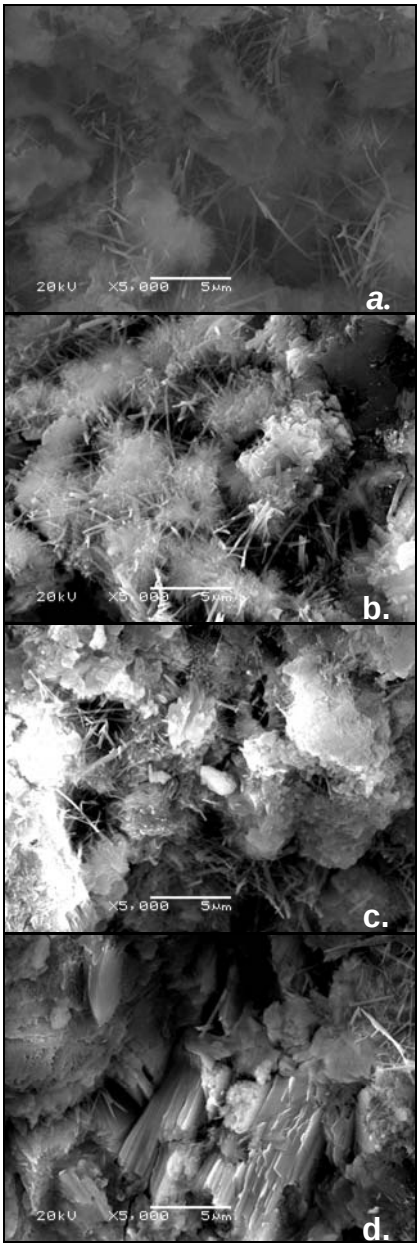

Fig.3. SEM micrograph of cement paste with additive of (a) 0 wt% clay (b) 0.75 wt% clay (c) 1.0 wt% clay (d) 1.5 wt% clay dispersed by mixing machine (5000×)

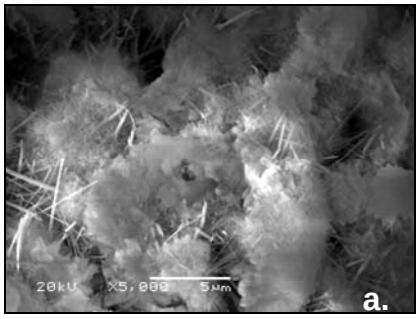

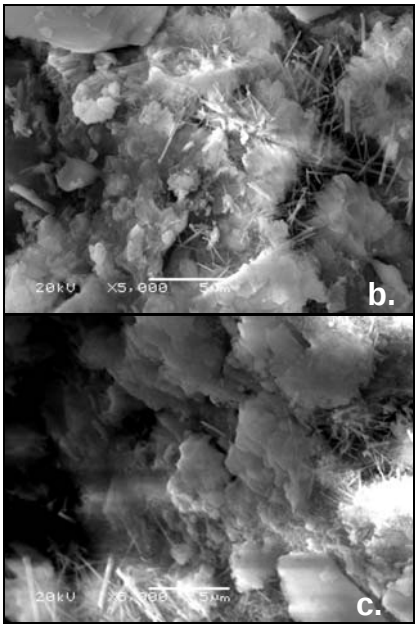

Fig.4. SEM micrograph of cement paste with additive of (a) 0.75 wt% clay (b) 1.0 wt% clay (c) 1.5 wt% clay dispersed by hand (5000×).

TABLE 5
CHEMICAL ELEMENT DISTRIBUTION OF NANOCLAY ADDED CEMENT

Element	Weight%						
	0	dispersing by machine			dispersing by hand(y)		
		0.75	1.0	1.5	0.75	1.0	1.5
Ca K	**46.14**	**49.61**	**45.97**	**63.45**	**40.51**	**43.64**	**55.00**
O K	**31.11**	27.08	33.58	23.80	38.28	33.27	23.34
Si K	**13.94**	14.02	12.02	6.85	13.26	14.54	11.08
Al K	**2.52**	3.15	2.80	1.21	2.42	2.48	1.85
K K	**2.30**	2.34	1.62	1.83	1.98	1.45	2.80
Fe K	**1.98**	1.96	1.88	2.87	1.20	1.93	1.41
S K	**1.09**	1.00	0.96		1.21	1.12	
Mg K	**0.92**	0.84	1.17		1.15	1.57	0.73

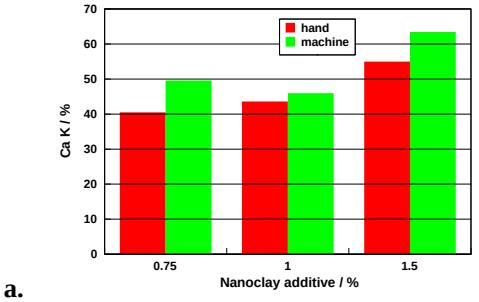

a.

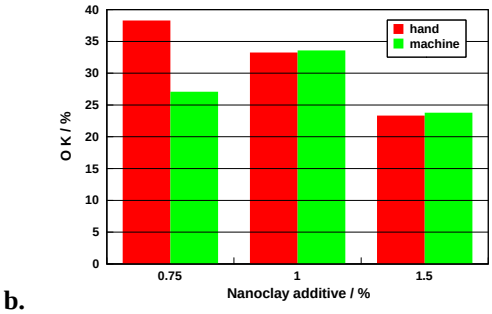

b.

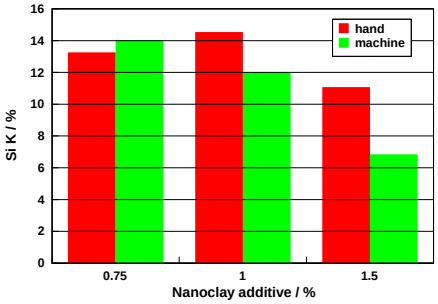

c.

Fig. 5. Relations between nanoclay additives with the amount of chemical elements in the cement (a)Ca (b)O (c)Si under the different dispersing methods.

IV. CONCLUSIONS

This study is focused on the influence of Kaolinite nanocly on the porosity of cement pastes. Cement paste samples with 0 wt%, 0.75 wt%, 1.0 wt% and 1.5 wt% additives are prepared. Nanoclay is dispersed by hand and mixing machine, respectively. Mercury injection apparatus was applied to determine porosity and pore diameter of the concrete sample. SEM/EDS tests were then executed on the cement paste samples as well. Micrographs and energy dispersive spectra are achieved. The porosity characters for the nanoclay added cement paste are discussed. The following conclusions can be drawn: (1)it is better to disperse nanoclay by mixing machine than disperse by hand; (2) compared with the neat cement paste, the average pore diameter of cement paste with 0.75 wt% and 1.0 wt% additive achieve a reduction of 6.9% and 18.5% respectively; and the reduction of the diameter will limit the introduction of the aggressive agents; (3)with the small amount of clay additives(no more than 1.5 wt%), the addition of nanoclay just has a slight effect on the porosity ratio of the cement paste.

ACKNOWLEDGMENT

The authors gratefully acknowledge the financial support of National Natural Science Foundation of PR China (Grant No.50708010), Liaoning Provincial Funded project (Grant No.20092149) and a Foundation for Youth Key Teacher in Dalian Maritime University (Grant No.2009QN045).

REFERENCES

[1] N. Tregger, M. Pakula, and S. P. Shah. “Influence of Micro- and Nanoclays on Fresh State of Concrete”. *Transportation Research Record* Vol. 2141, pp.68-74, 2010.
[2] M. S. Morsy, S. H. Alsayed and M. Aqel. “Effect of Nano-clay on Mechanical Properties and Microstructure of Ordinary Portland Cement Mortar”. *International Journal of Civil & Environmental Engineering*, Vol.10, no. 1, pp. 23-27, February, 2010.
[3] JTGE30-2005. *Test methods of cement and concrete for highway engineering*. Beijing: China Communications Press, 2005.
[4] G. Varga. "The structure of kaolinite and metakaolinite". *Építoanyag*, Vol.59, no.1, pp.6-9, 2007.
[5] http://www.doctorspiller.com/ceramics_1.htm

2011 International Conference on Mechanical, Industrial, and Manufacturing Engineering
Lecture Notes in Information Technology Vols. 1-2

Approximated Two Dimensional Daubechies Wavelets

Gao Zhongshe
School of Mathematics and Statistics
Tianshui Normal College
Tianshui, Gansu Province, P.R. China
gaozhongshe@hotmail.com

Wang Sanfu
School of Mathematics and Statistics
Tianshui Normal College
Tianshui, Gansu Province, P.R. China
wsf5435@hotmail.com

***Abstract* - With Legendre orthogonal polynomial to approximate scale function and wavelet function, approximate representation of Daubechies wavelet function was obtained, and we give the figures of approximate wavelets.**

***Index Terms* – wavelet, polynomial, approximate.**

I. INTRODUCTION

Daubechies wavelets have nice properties, such as compactly supported, orthogonal, regularity and vanish moment and so on [2],[3],[4],[6]. But Daubechies wavelets have not analytic expression general which made some difficulties for their application in the differential equation numerical solution. So it is approximated by Legendre orthogonal polynomial attempted to get the approximate expression of it. According to the relation of scale function and wavelet function, scale function was approximated by Legendre orthogonal polynomial at first, after the approximate expression of scale function was obtained, thus the approximate expression of wavelet function could be attained by the refine equation of scale function and wavelet function.

II. LEGENDRE ORTHOGONAL POLYNOMIAL APPROXIMATE TO SCALE FUNCTION AND WAVELET FUNCTION

The refine equation of Daubechies wavelet scale function $\phi(x)$ and wavelet function $\psi(x)$ are differently

$$\varphi(\tfrac{x}{2}) = 2\sum_{n\in Z} h_n \varphi(x-n)\,,\ h_n \in \mathrm{R}\,, \tag{1}$$

$$\psi(\tfrac{x}{2}) = 2\sum_{n\in Z} g_n \varphi(x-n)\,,\ g_n \in \mathrm{R}\,. \tag{2}$$

where

$$h_k = 2^{-\frac{1}{2}}\int_{\mathrm{R}} \phi(\tfrac{x}{2})\cdot\phi(x-k)\mathrm{d}x,\ g_n(x) = 2^{-\frac{1}{2}}\int_{-\infty}^{+\infty}\psi(\tfrac{x}{2})\phi(x-n)\mathrm{d}x$$

By reference [2],[4], the relation of g_n and h_n is

$$g_n = (-1)^n h_{1-n}\,. \tag{3}$$

From reference [2],[7], Suppose the sequence $\{h_n\}$ is finite, then corresponding scale function $\varphi(x)$ and wavelet function $\psi(x)$ are all have compactly supported set.

$$\mathrm{supp}\varphi = [0, 2N-1],\ \mathrm{supp}\,\psi = [-(N-1),\ N].$$

in reference[4],[6],[7], when $N=5$,then

$$\mathrm{supp}\varphi = [0,9],\ \mathrm{supp}\psi = [-4,5].$$

And corresponded frequency response $\{h_0, h_1, \cdots, h_9\}$

The following we discuss how to approximate scale function $\varphi(x)$ and wavelet function $\psi(x)$ by Legendre orthogonal polynomial, let $h = \frac{b-a}{M}$, $x_0 = a, x_i = x_0 + ih$, $i = 0, \cdots, M$, $x_M = b$, and apart prolong one node on the two side of nodes, coordinate is $x_{-1} = a-h$, $x_{M+1} = a+(M+1)h$, and let $x = a + th$, express the continuous function $f(x)$ on [*a*, *b*] by the linear combination of $\{\varphi(\frac{x-x_i}{h})\}_{i=-1,0,\cdots,M+1}$, thus[8]

$$f(x) \approx \sum_{i=-1}^{M+1} C_i \varphi(\frac{x-x_i}{h})\,.$$

So

$$\int_a^b f(x)dx \approx \int_a^b \sum_{i=-1}^{M+1} C_i \varphi(\frac{x-x_i}{h})\mathrm{d}x = \sum_{i=-1}^{M+1} C_i \int_a^b \varphi(\frac{x-x_i}{h})\mathrm{d}x$$

$$= h\sum_{i=-1}^{M+1} C_i \int_0^M \phi(\tau - i)\mathrm{d}\tau = h\sum_{i=-1}^{M+1} C_i \int_{-1}^{+1} \phi_i^*(\bar{x})\mathrm{d}\bar{x}. \tag{4}$$

where

$$\varphi_i^*(\bar{x}) = \tfrac{M}{2}\varphi(\tfrac{M}{2}\bar{x} + \tfrac{M-2i}{2})\,, \tag{5}$$

$$\varphi_i^*(\bar{x}) = 2\sum_{k=-i}^{M-i} h_k \varphi_i^*(2\bar{x} - \tfrac{2}{M}k + \tfrac{M-2i}{M})\,. \tag{6}$$

$\varphi_i^*(x)$ can be expanded by Legendre orthogonal polynomial $\{P_n(x)\}_{n=0,1,\cdots}$, then

$$\varphi_i^*(\bar{x}) = \sum_n a_n^{(i)} P_n(\bar{x})\,. \tag{7}$$

If the coefficients $a_n^{(i)}$ can be get, by (7), the approximation expression of $\varphi_i^*(\bar{x})$ can be obtain too. For getting the value of $a_n^{(i)}$, define inner product $(f, g) = \int_{-1}^{+1} f(\bar{x})g(\bar{x})\mathrm{d}\bar{x}$. According to the orthogonal of Legendre orthogonal Polynomials, there is

$$a_n^{(i)} = (\varphi_i^*(\bar{x}),\ P_n(\bar{x}))/(P_n(\bar{x}), P_n(\bar{x})) = \frac{2n+1}{2}(\varphi_i^*(\bar{x}),\ P_n(\bar{x}))\,. \tag{8}$$

Let

$$\tilde{a}_n^{(i)} = (\varphi_i^*(\bar{x}),\ P_n(\bar{x})) = \int_{-1}^{1} \varphi_i^*(\bar{x})\ P_n(\bar{x})\mathrm{d}\bar{x}\,,$$

From the equation (6) we have

$$\tilde{a}_n^{(i)} = \int_{-1}^{+1} 2 \sum_{k=-i}^{M-i} h_k \varphi_i^*(2\bar{x} - \tfrac{2}{M}k + \tfrac{M-2i}{M})\, P_n(\bar{x}) \mathrm{d}\bar{x}$$

$$= \sum_{k=-i}^{M-i} h_k \int_{-1}^{+1} \varphi_i^*(u) P_n(\frac{u + \frac{2}{M}k - \frac{M-2i}{M}}{2}) \mathrm{d}u \quad .$$

Thus

$$\tilde{a}_n^{(i)} = \frac{1}{2^n - 1} \sum_{j=0}^{n-1} (\sum_{k=-i}^{M-i} h_k w_j^{(i)(k)}) \tilde{a}_j^{(i)} . \tag{9}$$

In the deduce process of former formula using equation

$$P_n(\frac{u + \frac{2}{M}k - \frac{M-2i}{M}}{2}) = 2^{-n} \sum_{j=0}^{n} w_j^{(i)(n)} P_j(u) . \tag{10}$$

In order to express convenience, also let $\xi = \frac{2}{M}k - \frac{M-2i}{M}$, $i = 0$, let $a_n^{(0)} = a_n, \tilde{a}_n^{(0)} = \tilde{a}_n, w_j^{(0)(k)} = w_j^{(k)}, \varphi_0^*(\bar{x}) = \varphi^*(\bar{x})$, then

$$P_{k+1}(\frac{u + \frac{2}{M}k - \frac{M-2i}{M}}{2}) = P_{k+1}(\frac{u+\xi}{2}) = 2^{-(k+1)} \sum_{j=0}^{k+1} w_j^{(k+1)} P_j(u) , \tag{11}$$

By reference [8], the calculating method of $w_j^{(k+1)}$ are

$$\begin{cases} d_1 = \dfrac{2k+1}{k+1};\ d_2 = \dfrac{4k}{k+1}, \\ w_0^{(k+1)} = \frac{1}{3} d_1 w_1^{(k)} + \xi d_1 w_0^{(k)} - d_2 w_0^{(k-1)}, \\ w_1^{(k+1)} = d_1 w_0^{(k)} + \frac{2}{5} d_1 w_2^{(k)} + \xi d_1 w_1^{(k)} - d_2 w_1^{(k-1)}, \\ w_j^{(k+1)} = \frac{j}{2j-1} d_1 w_{j-1}^{(k)} + \frac{j+1}{2j+3} d_1 w_{j+1}^{(k)} + \xi d_1 w_j^{(k)} - d_2 w_j^{(k-1)}, \\ w_k^{(k+1)} = \frac{k}{2k-1} d_1 w_{k-1}^{(k)} + \xi d_1 w_k^{(k)}, \qquad 2 \le j \le k-1, \\ w_{k+1}^{(k+1)} = 1, \end{cases} \tag{12}$$

By (12), the expression of $w_j^{(k+1)}$ with ξ are obtained. When M and k $(k = 0,1,2,\cdots)$ are given, the value of $w_j^{(k+1)}$ can be get, take it into (9), get the value of $\tilde{a}_n$, by (8) can get the value of a_n, that is the approximation expression of $\varphi^*(\bar{x})$ can be obtained. According (4), (5) the approximation expression of $\varphi(x)$ can be obtained, the figures is following in Fig1 and Fig2.

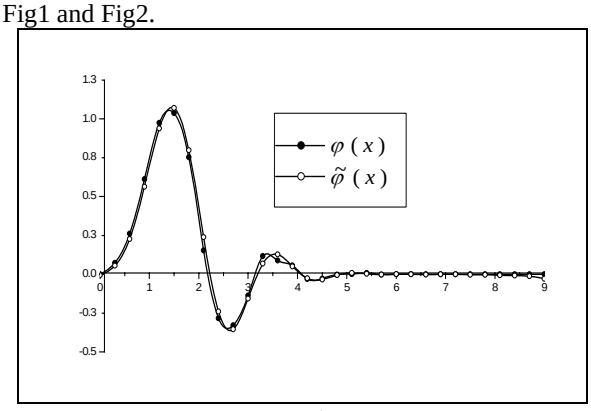

Fig. 1. Figure of $\tilde{\phi}(x)$ and $\varphi(x)$

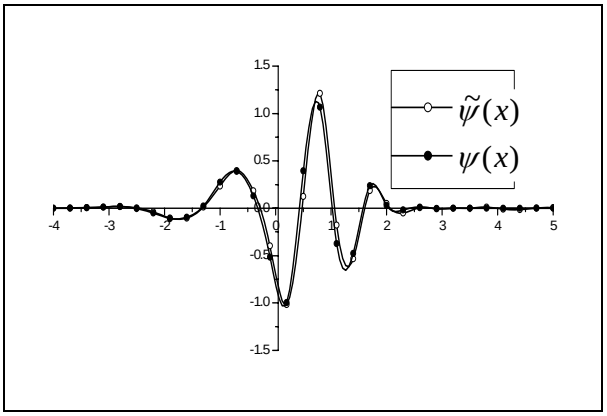

Fig. 1 Figure of $\tilde{\psi}(x)$ and $\psi(x)$

III. TENOR FORM TWO DIMENSION DAUBECHIES WAVELET

According the front discusses, $\{V_j\}_{j \in Z}$ is a multiresolution analysis which is constructed by scale function $\varphi(x)$, correspond Daubechies wavelets function is $\psi(x)$, then two dimension tenor spaces sequence $\{V_j^2\}_{j \in Z}$ construct two dimension multiresolution of $L^2(\mathrm{R}^2)$, where two dimension multiresolution space is $V_j^2 = V_j \otimes V_j$, two dimension scale function is

$$\varphi(x, y) = \varphi(x) \cdot \varphi(y) . \tag{13}$$

Then V_j^2 can be expressed

$$V_j^2 = \overline{\mathrm{span}\{\varphi_{j,k} \mid k \in \mathrm{Z}^2\}} , \tag{14}$$

Where

$$\varphi_{j,k}(x, y) = 2^{-j} \varphi(2^{-j} x - k_1) \varphi(2^{-j} y - k_2) . \tag{15}$$

Correspond two dimension wavelet space is

$$W_j^2 = (V_j \otimes W_j) \oplus (W_j \otimes V_j) \oplus (W_j \otimes W_j) . \tag{16}$$

Thus there have three two dimension wavelets function, these are

$$\begin{cases} \psi_1(x, y) = \varphi(x)\psi(y) \\ \psi_2(x, y) = \psi(x)\varphi(y) \\ \psi_3(x, y) = \psi(x)\psi(y) \end{cases} . \tag{17}$$

Where

$$V_j \otimes W_j = \overline{\mathrm{span}\{\psi_{1,j,k} | k \in Z^2\}};$$
$$W_j \otimes V_j = \overline{\mathrm{span}\{\psi_{2,j,k} | k \in Z^2\}};$$
$$W_j \otimes W_j = \mathrm{span}\{\psi_{3,j,k} | k \in Z^2\} .$$

$$\psi_{1,j,k}(x, y) = 2^{-j} \varphi(2^{-j} x - k_1) \psi(2^{-j} y - k_2) , \tag{18}$$

$$\psi_{2,j,k}(x, y) = 2^{-j} \psi(2^{-j} x - k_1) \varphi(2^{-j} y - k_2) , \tag{19}$$

$$\psi_{3,j,k}(x, y) = 2^{-j} \psi(2^{-j} x - k_1) \psi(2^{-j} y - k_2) . \tag{20}$$

Then we obtain figure of $\tilde{\phi}(x)\tilde{\phi}(y)$, $\tilde{\phi}(x)\tilde{\psi}(y)$, $\tilde{\psi}(x)\tilde{\phi}(y)$, $\tilde{\psi}(x)\tilde{\psi}(y)$ are follow.

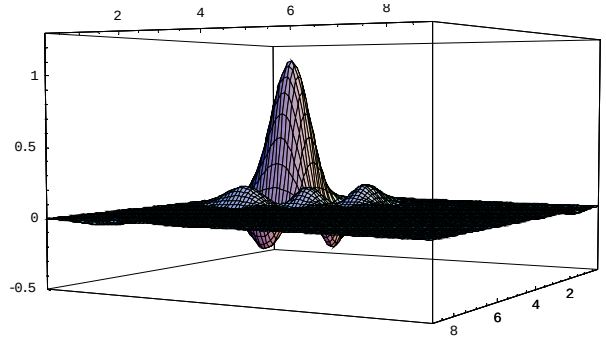

Fig. 3 Figure of $\tilde{\varphi}(x)\tilde{\varphi}(y)$

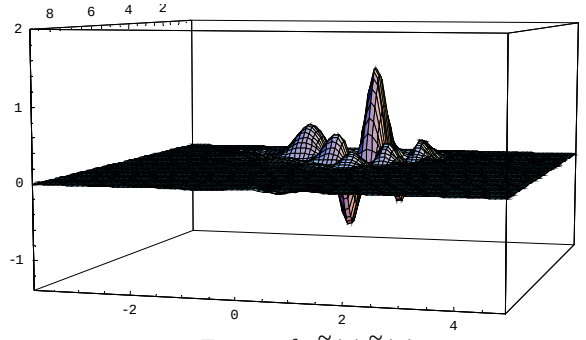

Fig. 4 Figure of $\tilde{\varphi}(x)\tilde{\psi}(y)$

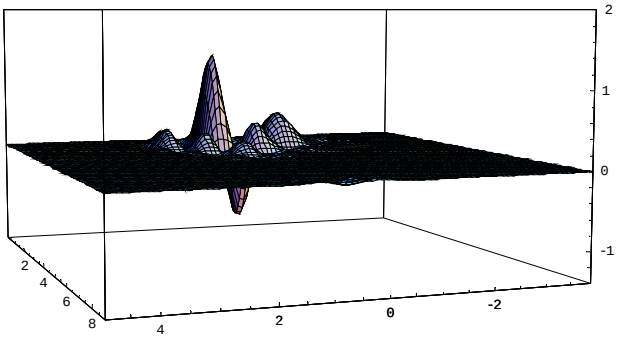

Fig. 5 Figure of $\tilde{\psi}(x)\tilde{\varphi}(y)$

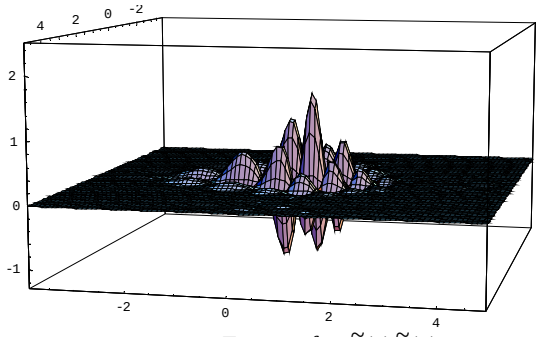

Fig. 6 Figure of $\tilde{\psi}(x)\tilde{\psi}(y)$

ACKNOWLEDGMENT

I am particularly grateful to my teachers, friends and my parents give me various help on this way.

REFERENCES

[1] Daubechies, "Orthogonal Bases of Compactly Supported Wavelets," *Pure&Appl.Math*, vol. 41, pp.909-996, 1988.

[2] Daubechies, "Ten Lectures on Wavelets". *SIAM Philadephia*, 1992.

[3] Jianzhong Wang, "On compactly supported spline wavelet and a duality principle," *Applied and Computional Harmonic Analysis*, vol.12. no.2, pp154-163, 1996

[4] C. K. Chui, J. Z. Wang, "On compactly supported spline wavelet and a duality principle," *Trans. Amert. Math. Soc*. Vol.330, no.4, pp. 903-916, 1992.

[5] S. Mallat, "Multiresolution approximations and wavelet orthonormal bases of L2(R)," *Trans. Amer. Math. Soc*. Vol.315, pp.69-87, 1989.

[6] Liang Xuezhang.He Jiaxing.Wang Xinmin,Li Qiang, "Wavelet analysis," *National Defence Industry Press*. 2005.

[7] Albert Cohen, *Numerical analysis of wavelet methods*, North-Holland, 2003.

[8] Xu Changfa, Yao Yifeng, calculation for Cauthy principle integral with scaling functions, *Numerical Mathematics a journal of Chinese University*, vol.20. no.2, pp94-105, 1998.

2011 International Conference on Mechanical, Industrial, and Manufacturing Engineering
Lecture Notes in Information Technology Vols. 1-2

[1]Research on Realizing a Shelf of Production Planning System Based on Wagner-Whitin Algorithm*

Kun Zhang
College of Electronics and Information Engineering
Qiongzhou University
Sanya, Hainan, China
zk0588@163.com

***Abstract*-MRP (Material Requirements Planning) is mainly applied in the stock control of dependence requirement i.e. relevant requirement which can decrease the stock level significantly. This paper designs a kind of MRP system that can concerns the production with guarantee period by using Wagner-Whitin Algorithm.**

Keywords-MRP; Production with guarantee period; Wagner-Whitin Algorithm

Ⅰ.INTRODUCTION

MRP (Material Requirements Planning) is a system based on material planning staff or stock management staff which mainly applied in the stock control of dependence requirement (relevant requirement). MRP suggests that the required quantities and when the manufacturer plans to make and apply them. The using of this tool would decrease the stock level significantly in terms of material management. At the same time it also can increases productivity. It has been payed more and more attention to the topic of MRP for more than 20 years. However, the problem of the management of stock with guarantee period was always ignored in the MRP system. In this paper, the MRP system of the sole problem has taken the constant deterioration of the products into consideration. The system designed by this article has an eye to the deterioration problem in the production system to calculate the expense of stock's productions, including deterioration exhaustion and storage charges with Wagner-Whitin algorithm and to find out the minimum cost.

Ⅱ.FUNCTIONAL REQUIREMENT

The functions that this system needs to complete are generally through the demand of products in each period of time that input in the MRP and the parameter (the cost of each order C, the holding cost of each period h, unit cost of purchase P, the rate of deterioration t)get through the Wagner-Whitin is to calculate the optimal jobshop order and the best order time of the deteriorated stock.

In this system, the demand and input parameter are kept in the database, where you can retrieve the data whenever you need, and the result will be kept in the database too. Therefore, the connection between the program and database must be completed. This system adopts a graphical interface to make the management more convenient for the administrator's managing data. The several fundamental functions that the system must complete are: the input, save, read and delete of the demand and parameter, and the calculate, display, save and delete of the result.

Ⅲ. SYSTEM ANALYSIS

A. Describe the demand of system by using case diagram with UML

The only one ID allowed in the planning system of production with guarantee period is administrator. After login system, the administrator can add, save and delete the demand and the parameter, and also calculate and save the result. That is the administrator 's management to the demand data, the parameter and the result.

Use case diagram for this system as the following:

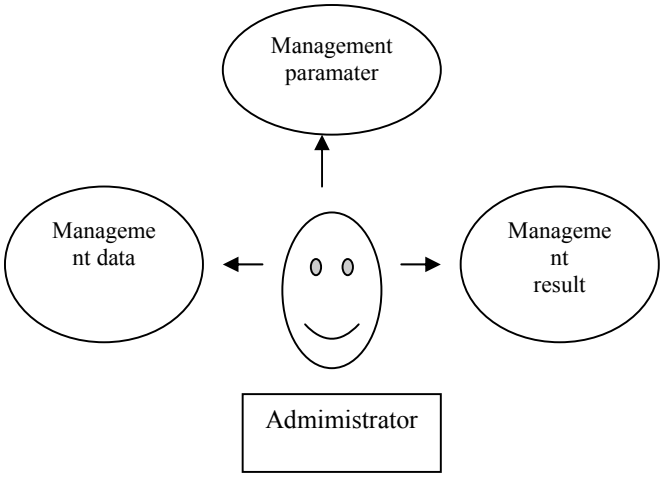

Figure1. The diagram of the planning system of production with Guarantee Period

* The work was supported by the research foundation for outstanding Young Teachers of Qiongzhou university (QY200920); The scientific and technological cooperative project for college and region of Sanya (2010YD49, 2010YD32,YD09074); Hainan Provincial Natural Science Fund(610225, 609006); Social development special fund of science and technology for Hainan province (2010SF004); Key Laboratory of Tropical Crops of Hainan Province Information Technology Application Research Fund Open Project(rdzwkfjj001).

1)Management Data: Refers to the administrator's management to the demand data of each period. When new data appears, the administrator can save the new data into the database, and also can read the data from the database to calculate, and delete the unnecessary data.

2)Management Parameter: Refers to the administrator's management to the parameter information of each group. When new parameter groups appear, the administrator can save the new into the database, and also can read the parameter groups from the database to calculate, and delete the unnecessary parameter groups.

3)Management Result: Refers to the administrator's management to the result. It includes the result calculate of the data and parameter that has been read, and the presentation in the way of form, and saving the data into the database.

4) Operating Process: The operating process of the planning system of production with guarantee period is very simple. After the administrator logs in the system, he can get the result directly through the calculate of these two kinds of information that have been read, if the demand data information and the parameter information have been saved in the database already. If you need to save the result, you can save the result into the database directly. If there is no necessary data in the database after logging in the system, you can input the new data or parameter, then save them in the database and then read and calculate them.

As the analysis above, we can draw the operating process as Fig 2 and Fig 3.

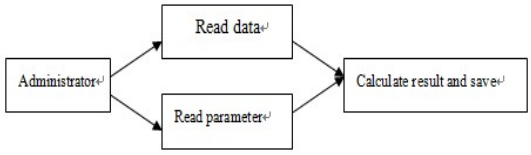

Figure2.Operating process of database with data after login

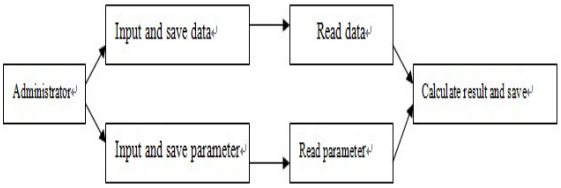

Figure3. Operating process of database without necessary data after login

B. Aims of System

Refers to calculate the deteriorated stock management through Wagner-Whitin order to get the exact demand of material. It's convenient for the administrator to manage the purchase of material. After the administrator logs in the system, he can manage the database, and manage the demand data and parameter information. The administrator can calculate the result and present it in the way of form. And save the necessary result. The administrator can delete the information that is out of date.

C. Analysis of Functions

We can draw the Functional Structure as Fig 4 based on the analysis of the planning system of production with guarantee period above.

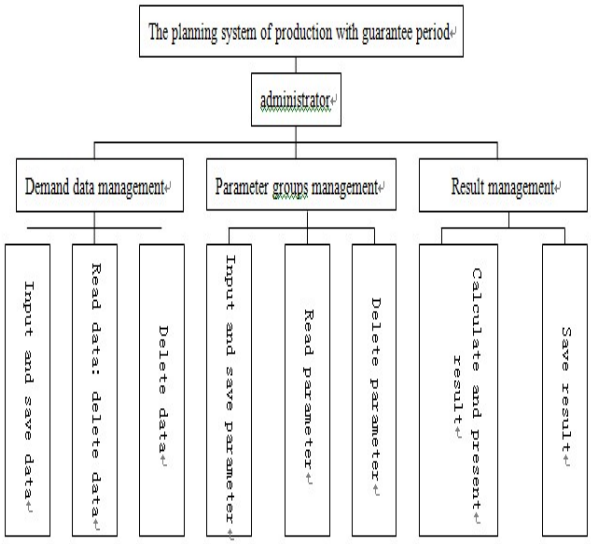

Figure4. Functional structure of the system

The administrator manages the whole system, such as the management to the demand data, the management to the parameter groups data and the management to the structure. And each function has several subfunctions. Through implementing these functions, the design of the whole system has been completed.

D. Deteriorated stock management model

1) Wagner— Whitin Algorithm: WW is used in a limited range about searching for a best solution for discrete orders of the deteriorated stock management. It is similar to the dynamic program. The following is this model's development sequence: Qce the order quantity in the deteriorated stock from period c to period e, the order must be received in the initial period c, and the amounts must meet the demand from period c to period e. The meaning of the Qce described with formula is :

$$Q_{ce} = \sum_{k=c}^{e} R_k /(1-\theta)^{k-c} \quad (1)$$

Combining the ordering cost, inventory cost and consumption costs is the total relevant cost Zce

$$Z_{ce} = C + hP\sum_{i=c}^{e}(Q_{ce} - Q_{ci})(1-\theta)^{i-c} + P\left(Q_{ce} - \sum_{k=c}^{e} R_k\right) \quad (2)$$

Multiply (1-θ)i-c by the holding cost apart from the depletion cost .

The most probable minimum cost from period 1 to period e :

$$fe = \mathrm{Min}(Z_{ce} + f_{c-1}) \quad (3)$$

E. Heuristic algorithm

1) Silver-Meal: Based on the average cost Silver and Meal of each period, a kind of heuristic batch algorithm has been developed. When the average cost of each period begins to grow, the order quantity is designed for the ordering demand of previous period. The original SM was modified for the constant deteriorated stock management. When the ordering of the first period arrive, and also meet the last ordering demand of the period T, the total storage expenses and cost of wear and tear in the last of period T are described with formula (4) and (5). As the amount of depleted productions, the cost of carry is divided by (1-θ)i

$$HC = hP\sum_{k=2}^{T}\sum_{i=1}^{k-1} R_k /(1-\theta)^i \qquad T>1, \qquad (4)$$

HC=0， T=1

$$DC = P_x\left\{\sum_{k=1}^{T} R_k /(1-\theta)^{k-1} - \sum_{k=1}^{T} R_k\right\} \qquad (5)$$

The total relevant cost TRC(T) is expressed by the ordering cost, stock cost and depletion cost

$$TRC(T)=C+HC+DC \qquad (6)$$

The total relevant cost TRC(T)/T of each period is

$$TRC(T)/T=(C+HC+DC)/T \qquad (7)$$

This heuristic model can compare the value of TRC(T)/T, follow T's growing until

$$TRC(T+1)/(T+1) > TRC(T)/T \qquad (8)$$

When the total relevant cost of each period begins to grow by (T+1), and the T that associated with it is chosen as the order point of the order quantity. Then the total amount of the order that related to T's particular value is

$$Q = \sum_{k=1}^{T} R_k /(1-\theta)^{k-1} \qquad (9)$$

2) The Heuristic Least Unit Cost: The Heuristic Least Unit Cost is similar to the SM. Except that it calculates the total relevant cost of each unit, but not of each period. This heuristic method is trying to find out the value of T. When the total relevant cost of each unit comes out with growing for the first time, the total relevant cost of each unit is

$$TRC(T)/\sum_{k=1}^{T} R_k = (C+HC+DC)/\sum_{k=1}^{T} R_k \qquad (10)$$

The heuristic method is to increase the value of T. The value of T starts from 1,and when it meets the conditions below:

$$TRC(T)/\sum_{k=1}^{T+1} R_k > TRC(T)/\sum_{k=1}^{T} R_k \qquad (11)$$

When the ordering demand of period T is satisfied, the amount of orders can be get from Eq (10).

ACKNOWLEDGMENT

The work was supported by the research foundation for outstanding Young Teachers of Qiongzhou university (QY200920); The scientific and technological cooperative project for college and region of Sanya (2010YD49, 2010YD32,YD09074); Hainan Provincial Natural Science Fund(610225, 609006); Social development special fund of science and technology for Hainan province (2010SF004); Key Laboratory of Tropical Crops of Hainan Province Information Technology Application Research Fund Open Project(rdzwkfjj001).

REFERENCES

[1] Spethen R.Schach. Sofware Engineering [M], Beijing University Press, 2000, 125-128

[2] Yin Ren-kun, C++ OOP Object Oriented Programming techniques[M], Tsinghua University Press 2000,93-185

[3] MA Shi-hua, Operation Management [M], Higher Education Press, 2002, 70-149.

2011 International Conference on Mechanical, Industrial, and Manufacturing Engineering
Lecture Notes in Information Technology Vols. 1-2

Opportunities and Challenges Education Technology is Confronted with in Network Times*

Kun Zhang
College of Electronics and Information Engineering
Qiongzhou University
Sanya, Hainan, China
zk0588@163.com

***Abstract* - This paper mainly discusses opportunities and challenges in the modernization construction of education technology, which are brought by the development and popularity of computer network, as well as brings forward how the education technology adapt to the development of network times.**

Index Terms -Network;Education Technology; Opportunities.

I. INTRODUCTION

The 21st century is the information age, computer technology, communication technology and multimedia technology, exchange of information to the human way of bringing about a profound change. The computer network technology into all aspects of teaching will inevitably lead to teaching, teaching methods, teaching methods and teaching tools, a major innovation, and to achieve a "student-centered, teacher-led" modern educational thinking provides an effective of education. But our schools for teaching computer network efficiency is generally low, not fully play its due role. The new techniques of teaching law in the context of an urgent research and teaching only built on the basis of the latest technology, can achieve real breakthroughs in order to integrate with the world of education.

II. NETWORK OF OPPORTUNITIES FOR EDUCATION

A. On a fundamental change in student learning

Through the computer teaching to enable students to learn knowledge in addition to the teacher, according to their needs, from the Internet to obtain the necessary knowledge and information, and to cultivate students to collect, collate and use of various information habits and ability to train students to learn, to theoretical consideration, comments and conduct communication capabilities and personality of students into full play. Computer network computer and communications combined, significantly broadening the function of stand-alone computer, making the computer does not only deal with text and data, and communicate with a communication function. Researchers around the world can e-mail capabilities through computer networks together with like-minded text stream. In schools, teachers and students can use the information network contacts, networking, online all the users can share information and technology. Computer networks are also breaking the traditional concepts of classrooms, schools and even the boundaries of the constraints, through the network to communicate with other peers, thus sharing resources and improve efficiency.

B. On a fundamental change in classroom teaching methods

Teaching through the use of computers and the Internet has totally changed in the past to textbook-centered teaching methods, the students into the virtual environment, to arouse their interest in learning and lead to active learning and reflection, so that fundamental change in methodology of classroom teaching, and received to good teaching. Teaching multimedia computer network may not be limited to a network can be achieved through networking online communications. Online communication to further exclude the time, place and human factors and other restrictions, teachers, students can use computers anytime, anywhere, collect information on the network, retrieving a school district or other school district in the lectures. This paradox, in remote areas of the students can hear and see the famous cities of teachers lecturing; are not subject to radio or television co-curriculum requirements limit the right time in their demand at any time they want to learn the course.

C. On the fundamental changes in school management

Will promote the development of computer education to improve school management, to promote school, family and close contact with the local community, will make a fundamental change in the management of the school. Such as: you can close links between schools and parents. In the past, contact the school and parents of students, mainly through the year, several parents and teachers to the school visits conducted home visits to students, the students when problems arise mostly through telephone contact with parents. With the popularity of the Internet family, school and parents of students in more detail through the Internet connection will be possible, especially teachers and parents can e-mail at any time by two-way communication and contact. Teachers can e-mail problems for students, targeted education to carry out detailed guidance. This will reduce the large workload of the affairs of the school, enable teachers to devote more time with

* The work was supported by the research foundation for outstanding Young Teachers of Qiongzhou university (QY200920); The scientific and technological cooperative project for college and region of Sanya (2010YD49, 2010YD32,YD09074); Hainan Provincial Natural Science Fund(610225, 609006); Social development special fund of science and technology for Hainan province (2010SF004); Key Laboratory of Tropical Crops of Hainan Province Information Technology Application Research Fund Open Project(rdzwkfjj001).

students or to carry out teaching activities. Meanwhile, to facilitate schools and local education administrative departments to contact. School and working contacts between the Board of Education via the Internet, can reduce the number of missions, save time and money expenditures. There are also beneficial to the teachers and improve education. Teachers via the Internet to participate in national and local Board of Education held an annual seminar for teachers in various forms, can solve the first line of school teachers for teaching shortage of teachers can not go out further studies to improve the problem.

III. NETWORK TO THE CHALLENGES OF EDUCATION

A. Teaching content

The use of computer networks, especially in networking, the sharing of resources in schools, teaching rich in content, it is in the number of school education has gone far beyond the information provided. Computer networking, enrich the teaching content for students to choose teaching content meet their needs provided for convenience. Students can choose different modules to build their own knowledge structure, to form the individual's unique knowledge. At that time, a student can choose a different computer networks courses, choose a different country of the same course, choose the same course in different units. Courses may be the smallest unit modules, each module supporting a certain credit requirements.

B. The impact of teaching methods

The use of computer networks and multimedia technology to produce educational software, able to achieve individualized. Teachers can allow students from the network, according to their level and needs of the random extraction of a large number of software to learn. Also according to the teaching needs of teachers and computer feedback for each student learning, to take measures to modify the course content at any time, curriculum software changes to improve teaching. Computer network, can make the school and outside educational institutions, organizations and individuals to work together to engage in educational activities. Schools regardless of time constraints, to grasp the necessary information, used in teaching practice. This will give students more learning materials to enrich their interests, broaden their horizons.

C. Role of Education

Multimedia and online teaching staff can not replace teachers, but it can greatly reduce the burden on teachers can be teaching them from the enclosed space, freeing more time for individual guidance for students to propose solutions to educational problems of students the task of guide their absorption from the computer network of educational resources. In this way, teachers will no longer be the main source of knowledge in the classroom, and will be the students in the learning and application of information problem-solving process of counselors. That self-education students who, given the form of modern teaching technology students during the full autonomy, they use the computer network can own choice, to choose courses, self-teaching time and grasp the progress of teaching, self-evaluation. This will enable students to become creators of their own learning progress and evaluators, and change "by the people of education" as "personal self-education." This self-learning approach will help students to self-discovery and self-binding potential enhancements to help develop the tendency of the Personality of the students, helping to develop creative talents.

IV. HOW TO DEAL WITH THE NETWORK TO THE OPPORTUNITIES AND CHALLENGES OF EDUCATION

A. Information Resources and Development

Information Resources and Development is a multimedia information network core. To build the best schools, training first-class talents, we must have first-class information resources and the environment. The development and delivery of information resources will be directly related to the quality of school education. Schools should gradually improve the information infrastructure, but also to great efforts to build information resources (especially Web information resources), including a variety of excellent educational software, multimedia educational database. To build the campus network based on-line information resource sharing system for faculty and students to provide information retrieval, reading, information presentation, software, browse, download and other services for the school to create a teaching and research with the international information network environment.

Multimedia Schools Network to promote the work of the rapid development of construction and for strengthening curriculum development and promote educational reform, school construction should be strengthened curriculum and teaching reform project inputs, especially network technology based on the campus online computer assisted instruction, counseling, training software Development. Construction of the school curriculum to enhance and promote education reform, to encourage teachers to develop a network of multimedia courseware development measures, through the courseware appraised incentives to mobilize teachers to participate in the school of information resources development and utilization of enthusiasm, gradually built multi-media teaching courseware library. Through self-control, outsourcing and other means to build a certain amount of CD-ROM databases, Online Multimedia Library, a rich network of information resources in schools.

B. Strengthening the network of multimedia in teaching Teachers

Information infrastructure, construction and information resources development and utilization of multimedia teaching only improve one aspect of the network (ie, material conditions), the network multimedia multimedia Teachers are doing a good job teaching. Teachers are the most important producers of information resources and users. To do a good job in network multimedia teaching of teachers, step by step through the training so that teachers learn to education, modern information technology, learn how to use networked multimedia devices, instructional design and web master of

multimedia teaching methods. Schools should pay attention to the information in the network based multimedia teaching teachers, teacher organizations, the ongoing training of modern educational technology and learning, including computer network technology, multimedia technology and office information technology, computer network based on universal knowledge and basic skills, master production multimedia courseware technology and methods to improve the network of teachers teaching the theory and practice of multimedia standards.

Network brings the campus educational technology, the means of progress, and educational needs of the community to expand the scope, time, location uncertainty, will make the network technology in education means the application of information technology play a greater role.

ACKNOWLEDGMENT

The work was supported by the research foundation for outstanding Young Teachers of Qiongzhou university (QY200920); The scientific and technological cooperative project for college and region of Sanya (2010YD49, 2010YD32,YD09074); Hainan Provincial Natural Science Fund(610225, 609006); Social development special fund of science and technology for Hainan province (2010SF004); Key Laboratory of Tropical Crops of Hainan Province Information Technology Application Research Fund Open Project(rdzwkfjj001).

REFERENCES

[1] Sakamoto teach all. The Japanese primary and secondary schools computer education[J]. Elementary & Secondary Schooling Abroad. 2001,(1):26-30.

[2] Chen Xiaofang. Information Age Education in China[J]. Fujian Computer .2002,(2):22-25.

[3] Yu May, Cao Shi-hua. Journal of Shaoxing University(Philosophy and Social Sciences Edition).2003,(23):13-17.

2011 International Conference on Mechanical, Industrial, and Manufacturing Engineering
Lecture Notes in Information Technology Vols. 1-2

[1]Mobile Learning Applied Research Based on 3G Technology *

Kun Zhang
College of Electronics and Information Engineering
Qiongzhou University
Sanya, Hainan, China
zk0588@163.com

Zhuang Li , Xiao-yan Chen
College of Electronics and Information Engineering
Qiongzhou University
Sanya, Hainan, China
hitlz@163.com, xiaoyan0205@126.com

***Abstract*-China has entered the 3G era, this paper introduces the concept and function of 3G technology, analysis the characteristics of mobile learning. 3G technology has rich characteristics, which can be used for M-learning. When the 3G technology are applied in mobile learning, mobile learning will have new identities.**

Keywords-3G, M-learning, study mode

Ⅰ. INTRODUCTION

3G is the third generation mobile communication. The third generation mobile communication system can provide a variety of broadband services, comparing to previous two generations, the main difference is data transmission speed, the data transmission speed of the third generation is upgraded greatly. 3G has a higher transmission speed, fast image processing and audio-visual and multimedia forms. User can hear voice more clearly, see image more fluent and browse the Web more conveniently and quickly. In mobile learning, the broadband information provided by 3G main in the following areas:

1)Mobile Internet: 3G technology integrate wired Internet with mobile communication network, wired Internet can not mobile, mobile Internet make up the disadvantage of wired Internet, which break the space limitations to the learners, as long as there is signal coverage area, learners will be able to learn through the 3G network. Making use of 3G technology, regardless of where the learners are, they can access mobile Internet, using the mass of educational resources in Internet.

2)Audio and video teaching: The development of mobile teaching can not be separated from the real-time teaching and real-time interaction. In 2G era, real-time teaching and using wireless to transmit a large number of audio and video are impossible, which brings a lot of constraints for real-time teaching. Between students and teachers are usually only can hear the sound of a person, but can not see the person, real-time teaching at a low level, it has become the bottleneck of the development of mobile learning. 3G technology provides voice and video services, the learner can watch lectures in real-time online classroom, teachers can teach online and through the way of video-conferencing and image to exchange, which enhanced the interaction of teaching and learning greatly.

3) Multimedia services: Multimedia services include short message service, multimedia message service, wireless video-on-demand business, wap browser and interactive games and so on, which provide wireless mobile devices for learners, and allow learners accessing a wide range of learning resources and learning services.

Ⅱ. M-LEARNING AND CHARACTERISTICS

A.The concept of M-learning

Mobile learning (M-learning) is a new mode of learning, it emerges after e-learning. Mobile learning depends on mobile communication technology and mobile communication terminal, as long as learners access wireless network, learners can study at anytime and anywhere. Mobile learning has the characteristic of interactive, convenient, and real-time, so M-learning has a wide range of applications. M-learning integrates mobile communication with education, it breaks the shackles of wired connection, learners can study according to their needs, anytime, anywhere access to any network of educational resources, enhance the efficiency of learning and working, mobilize the learner's interests in learning. There are several M-learning devices, figure1 shows the basic devices of M-learning.

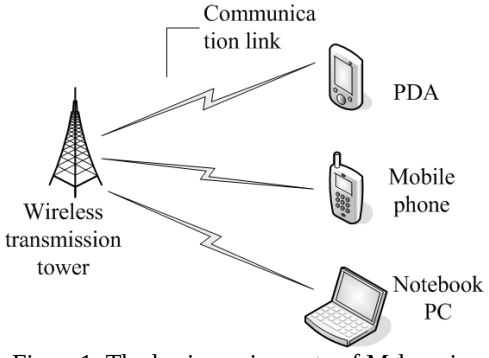

Figure1. The basic equipments of M-learning

* The work was supported by the research foundation for outstanding Young Teachers of Qiongzhou university (QY200920); The scientific and technological cooperative project for college and region of Sanya (2010YD49, 2010YD32,YD09074); Hainan Provincial Natural Science Fund(610225, 609006); Social development special fund of science and technology for Hainan province (2010SF004); Key Laboratory of Tropical Crops of Hainan Province Information Technology Application Research Fund Open Project(rdzwkfjj001).

B .The characteristics of M-learning at this stage

1）Local resources are limited: Learners are affected by factors, for example: mobile device storage capacity, price, network bandwidth. At the same time, the resources on mobile devices are limited, early storage capacity is only between128 MB ~ 512 MB, can only store a small amount of text messaging and video and audio information. But the study resources download from network are text form, video and audio stream can not be uploaded and downloaded fluently, which impact the abundance of local study resources. The development of multimedia digital resources, learners need mass storage devices and high-speed download network.

2）Learning content based on text: In M-learning process, learners study through receiving SMS, visting website. The performances of the teaching contents are very single, some study contents can not be presented well, and mobile study contents are limited. If we can overcome the limitations of the speed of network transmission, transmit video and audio stream fluently, enrich the way of study contents, the scope of M-learning will be enlarged greatly, at the same time, the learning outcomes will be improved.

3）The separation of teachers and students in mobile environment: Make use of mobile devices, people can access wireless network to study in any environment, people can begin to study in Subway, the bus station, and even before they go to bed, as long as they have a short time, they can study. This approach of learning causes the separation between teachers and students. Therefore, how to ensure the quality of communication in different environment, avoid communication barriers caused by environment factors, so that mobile learning can be fluently in different environment, which has becoming the most pressing problem.

4）The interactive way of teacher-student affects study effects: In mobile learning, the teachers and students are in different environment, they are unable to communicate face to face. How to ensure the quality of communication between teachers and students, convey feedback to learners in a short time, improve the effects of study, which become the important problems in the process of mobile learning. Seeing from domestic research status, mobile learning is limited by the network bandwidth, the main ways of study are SMS、mobile instant messaging tool, e-mail, BBS and other forms of communication. The way of communication is single, learners are unable to see and hear each other, which affect the effects of communication. Therefore, improving the network bandwidth, enriching the way of communication between teachers and students has become very necessary.

Ⅲ. M-LEARNING BASED ON 3G TECHNOLOGY

3G technology has rich characteristics, which can be used for M-learning. When the 3G technology are applied in mobile learning, mobile learning will have new identities. At present, the M-learning models based on 3G network have three kinds: M-learning model based on 3G multimedia short message services, the model based on the 3G mobile video service, the model based on the 3G wireless network services, such as WAP browser for mobile learning. In these learning models, the new changes brought by 3G technology are incarnated, at the same time, brought the new function modules for M-learning.

A. The application of 3G technology in M-learning

3G is used for mobile learning, it can as a tool to improve the attention to education, assigning more resource for education, cultivating more talented person. 3 G provides various broadband information businesses will make mobile education system to provide more convenient service for a user, its application shows as follow:

1) Mobile resource: Teachers can collect the experiment, plotting, sound, portrait and large amount of data from Internet, searches out required material, making use of again, process to required class of teaching resource, build the various data base on the school education platform. Because of 3 G data transmission rates are very high, students can collect required contents by mobile network, such as the emphases, difficulties and general problems of course. Students can query various problems and not be restricted by time and place.

2) Mobile discussion and bbs: The BBS users can query the title and content of bbs by mobile telephone, can publish papers by mobile telephone, can make use of hyper text connection way to make users discuss the problems they are interested in. This discussion can be celebrated at anytime, anywhere, the exchanges between teacher and teacher, teacher and student, student and student have increased greatly. Students not only can communicate with teachers in school, but also can communicate with famous expert of home and abroad.

3) Providing mobile net: Mobile Internet is a network that integrate wired Internet ,mobile communication net , it include wired Internet , wireless connection and nimble terminal mainly. Wired Internet is Internet; Wireless connection is the network being composed of wireless module; The nimble terminal points to the end instrument having terminal treatment ability. Compared with wired Internet, mobile Internet has made up the shortcoming that wired Internet not able to move. Mobile Internet being able to contact every person in school ,it has broken close learning space, making students get a space that can develop their individuality, classroom has been expanded by boundless field in theory. As long as places are coveraged by the communicating signal, can actualize mobile teaching. Mobile users use wireless terminal to connect Internet, visit teaching server and browse, query, real time alternation, similar to general Internet users.

4) Mobile multimedia: Multimedia has gathered two kinds or more than two kinds mediums module, such as voice, data, image, video. In 3 G system, can actualize data, video multimedia communication between end users, which make "face-to-face" communication at mobile telephone, teacher can guide them to study. In addition to watch the lecture, students are able to use 3G mobile telephone to handle equipment, use mobile telephone to carry out surveillance and control.

B. The mode of M-learning based on 3G technology

3G technology brings the new function modules for M-learning, enriching the functionality of M-learning. These modules include the communities of mobile exchange, mobile video and audio course room, mobile mass resource storeroom.

1) Mobile interactive video platform: Make use of 3G video services, we can achieve video conference, video blog, video communities. Video conferencing can be used for the group discussion in mobile learning, when the study group or class of virtual exchange activities, the adoption of mobile video will be meeting to see and hear all of the real-time situation to express their views. When Video blog for mobile learning, learners will learn not only through text study and experience of the virtual partners, but also through visual content, understanding the virtual partners profoundly. The emergence of mobile video community, the learners can make use of 3G network to create a virtual forum, to share information and to discuss issues.

2) Mobile video and audio rooms: With the development of 3G technology, download video and audio streaming have become easy in mobile environment, the phenomena of transmission delay has disappeared. Mobile learners can play the video and audio streaming fluently even in the high-speed train. Mobile video and audio classroom will become an important part of mobile learning. Anytime, anywhere becoming possibility. Supposed that student can see teacher's course not in classroom, can carry out exchange through their computer or PDA.

3) Mobile mass resource storeroom: As the capacity of M-learning devices are increased, lower prices, and the 3G networks of the substantial increase in speed, mobile learners will carry massive resources at any time, they can view multimedia resources at any time, and search the vast resources of the required material from the Internet, they can become knowledgeable person easily.

Ⅳ. CONCLUSION

3G technology brings a lot of convenience for people's lives, applying 3G technology to mobile learning, which avoid the disadvantage of traditional study way, enhance the efficiency of learning greatly. M-learning based on 3G technology has becoming a convenient rapid study way, Its advantages, becoming an important study way, and it has broad application prospect. Therefore, M-learning based on 3G technology is very meaningful and necessary.

ACKNOWLEDGMENT

The work was supported by the research foundation for outstanding Young Teachers of Qiongzhou university (QY200920); The scientific and technological cooperative project for college and region of Sanya (2010YD49, 2010YD32,YD09074); Hainan Provincial Natural Science Fund(610225, 609006); Social development special fund of science and technology for Hainan province (2010SF004); Key Laboratory of Tropical Crops of Hainan Province Information Technology Application Research Fund Open Project(rdzwkfjj001).

REFERENCES

[1] Rung-Ching Chen, Ya-Ching Lee and Ren-Hao Pan"ADDING NEW CONCEPTS ON THE DOMAIN ONTOLOGY BASED ON SEMANTIC SIMILARITY", Department of Information Management, Chaoyang University of Technology168, Jifong East Road, Wufong Township, Taichung County 41349, Taiwan ROC, 2006.

[2] Aleksander Dyeet al."Mobile_Education- A Glance at The Future"[EB/OL], http://www.nettskolen.com/ forskning/ mobile_education.pdf.

[3]Keegan D.:The future of learning:From eLearning to M-learning[EB/OL] ,http://learning.ericsson.net/leonardo/thebook/book.html. PP. 569 – 572.

[4] C. Y Chang, Sheu, J. P., and Chan, T. W" Concept and design of Ad Hoc and mobile classrooms", computer assisted Learning, vol.19, pp.336-346,2003.

[5]ben_kasim.3G[EB/OL].[2009-3- 10].http://baike.baidu.com/view/808.html.

2011 International Conference on Mechanical, Industrial, and Manufacturing Engineering
Lecture Notes in Information Technology Vols. 1-2

Study on Method to Determine the Weight of each factor in Automobile Dashboard

ZHANG Xian-kui, YANG Jing
School of Mechanical and Electrical Engineering
Harbin Institute of Technology
NO.92, Xidazhi Street , Nangang District , Harbin City, Heilongjiang Province, China
zhangxk@hit.edu.cn

***Abstract* – Automobile dashboard is one of the most important Human-Machine Interfaces in cars, unreasonable ergonomics relations in design may lead to many potential safety problems. Take the drivers reading rate and reaction time for automobile dashboard as the evaluation goals, with the help of fuzzy mathematics and ergonomics knowledge to solve the various factors' membership which relative to the decision-making language set in the fuzzy evaluation of automobile dashboard, then establish the membership function of each basal factor, and determine the each factor's weight at last. According to basal factors' membership functions and weights, do the fuzzy computing in accordance with the method of multi-plate fuzzy evaluation to determine the membership of the top element.**

Index Terms –Automobile Dashboard, Weight, Fuzzy Evaluation , Membership

I. INTRODUCTION

Study on automotive human - machine interface making a major role in automotive ergonomic evaluation, it does have far-reaching practical significance. In the human - machine interaction study, determining the weight of each factor is particular important, it is directly related to product evaluation and improvement measures, good and bad choices.

Ergonomics is a subject that studying the interaction among people, equipment and work environment. It has become a new technology power to promote the development of industrial production, and has already got general attention by developed countries. But this subject emerged late in China, the studying on the comprehensive fuzzy evaluation system of product human-machine interface has just begun, especially the work on car human - machine interface comprehensive assessment is almost blank in Chine. Furthermore, many related research only stay on the establishment of a framework overall system, but no more in-depth discussions for a part [1]. It is for this phenomenon, selecting automobile dashboard as object to study the method of how to determine the weight of each factor. By the fuzzy evaluation system and experimental analysis, focused on studying relationship between factors set and membership set and weight distribution of factors [2]. This can be a subsystem and the preliminary work of comprehensive evaluation system of the whole automobile human – machine interface, it also stimulates public discussion on product fuzzy evaluation system, has a very important and long-term significance.

II. THE EVALUATION SYSTEM OF AUTOMOBILE DASHBOARD

A. Establish Framework of Evaluation System

Evaluation system is the systematic and formal description of design object's external characteristics, it can feedback the overall performance of the design object as well as the relationship between subsystems [3]. Take multi-level model to evaluate the automobile dashboard [4], the overall framework of the evaluation system is shown in Fig.1.

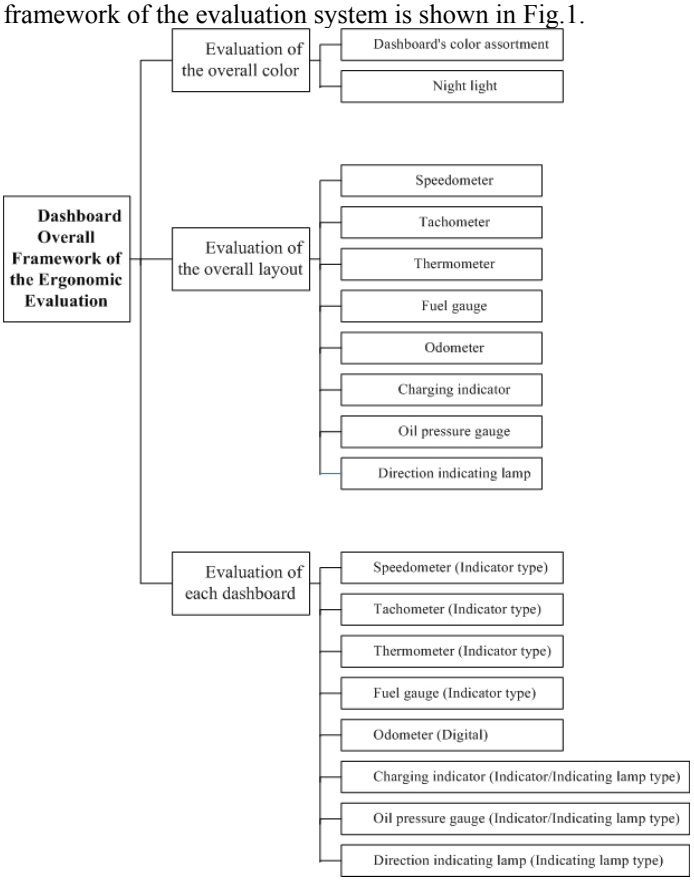

Fig.1. The overall framework of the evaluation system

To simplify the processing, evaluation of the decision-making language set is:

$$V = \{v_1, v_2\} = \{Good, Bad\}$$

By the overall framework of the evaluation system to determine its first-level factor set and the corresponding weight vector:

U = {U1, U2, U3} = *{Evaluation of the overall color, Evaluation of the overall layout, Evaluation of each dashboard}*

$$A=\left(A_1,A_2,A_3\right)$$

Second-level factor set of the evaluation system and its corresponding weight vector:

1) Evaluation of the overall color:

$U_1=\{u_{11},u_{12}\}=$ *{Dashboard's color assortment, Night light}*

$$A_1=\left(a_{11},a_{12}\right)$$

2) Evaluation of the overall layout:

$U_2=\{u_{21},u_{22},u_{23},u_{24},u_{25},u_{26},u_{27},u_{28}\}$ = *{Speedometer, Tachometer, Thermometer, Fuel gauge, Odometer, Charging indicator, Oil pressure gauge, Direction indicating lamp }*

$A_2=\left(a_{21},a_{22},a_{23},a_{24},a_{25},a_{26},a_{27},a_{28}\right)$ 3)

Evaluation of each dashboard:

$U_3=\{u_{31},u_{32},u_{33},u_{34},u_{35},u_{36},u_{37},u_{38}\}$ = *{Speedometer, Tachometer, Thermometer, Fuel gauge, Odometer, Charging indicator, Oil pressure gauge, Direction indicating lamp }*

$$A_3=\left(a_{31},a_{32},a_{33},a_{34},a_{35},a_{36},a_{37},a_{38}\right)$$

Considering the identical type instrument's appraisal factors are the same, to simplify processing, the indicator type instrument, the digital instrument and the indicating lamp type instrument distinction comes out to carry on the appraisal abstractly. The indicator type instrument's evaluation module is shown in Fig.2.

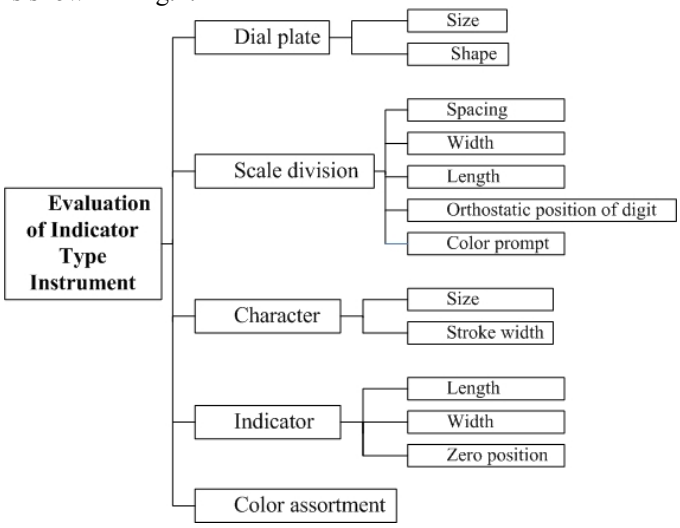

Fig.2.The indicator type instrument's evaluation module

According to the above module, the indicator type instrument's first level factor set and correspond the weight vector respectively is:

$$U=\{U_1,U_2,U_3,U_4,U_5\}$$

= *{Dial plate, Scale division, Character, Indicator, Color assortment}*

$$A=\{A_1,A_2,A_3,A_4,A_5\}$$

Second-level factor set of the indicator type instrument's evaluation module and its corresponding weight vector:

1) Dial plate：

$U_1=\{u_{11},u_{12}\}=$ *{Size, Shape}*

$$A_1=\left(a_{11},a_{12}\right)$$

2) Scale division：

$$U_2=\{u_{21},u_{22},u_{23},u_{24},u_{25}\}$$

= *{Spacing, Width, Length, Orthostatic position of digit, Color prompt}*

$$A_2=\left(a_{21},a_{22},a_{23},a_{24},a_{25}\right)$$

3) Character:

$U_3=\{u_{31},u_{32}\}$ = *{Size，Stroke width }*

$$A_3=\left(a_{31},a_{32}\right)$$

4) Indicator：

$U_4=\{u_{41},u_{42},u_{43}\}=$ *{Length, Width, Zero position}*

$$A_4=\left(a_{41},a_{42},a_{43}\right)$$

In order to simplify processing, two level of factor merge into one level factor, the new set of factor is:

$$U'=\{u_1',u_2',u_3',u_4',u_5',u_6',u_7',u_8',u_9',u_{10}',u_{11}',u_{12}',u_{13}'\}$$

= *{ Dial size, Dial shape, Scale space, Scale width, Scale length, Orthostatic position of digit, Color prompt, Character size, Stroke width, Indicator length, Indicator width, Zero position, Color assortment}*

According to the second-level fuzzy synthesis principle, may get basal factors' total weight vector based on the weighted average computation in the indicator type instrument:

$$A'=\{d_1,d_2,d_3,d_4,d_5,d_6,d_7,d_8,d_9,d_{10},d_{11},d_{12},d_{13}\}$$

B. Method to Determine the Weights of Evaluation Factor

When evaluating a product, the influence of each factor is different to the product, therefore, we must give various factors assignment inevitably. Now there is no unified theory to determine the weights of factors that at the same level. Generally uses the expert determination method, the dual correlation method, the fuzzy method of average and borrows the existing experience and so on to determine the weight. This research is mainly investigate expert and the person who has the automobile driving experience, as well as the experiment analyzes, and further uses the weight analytic method in the dual correlation method to determine some results. Below mainly the weight analytic method:

In order to carry sort of the elements of $U=\{u_1,u_2,...,u_n\}$, if each u_i has weight $w_i=w(u_i)$ objectively, $W=(w_1,w_2,...,w_n)$ is called the weight vector. Then can obtain the U sorting according to

the weight, the weight ratio of two elements u_i , u_j is w_i / w_j , may construct the weight ratio matrix M [5].

May know according to the matrix theory, exists $M \cdot X = \lambda \cdot X$, λ is the maximum non-vanishing solid characteristic value of matrix M . X is the correspond eigenvector of λ . Because we did not know weight vector W beforehand (this is precisely we must look for), we also did not know matrix M , but we can obtain $f_{u_j}(u_i)$ and $f_{u_i}(u_j)$ through two-two comparisons, command[6]:

$$t_{ij} = f_{u_j}(u_i) / f_{u_i}(u_j)$$

May compare t_{ij} as the weight ratio w_i / w_j the estimated value, matrix $T = T(t_{ij})$ may take matrix M an estimate matrix. We can obtain the maximum characteristic value and corresponding eigenvector of matrix T through the method of linear algebra, this eigenvector as the estimate of the weight vector $W = (w_1, w_2, ..., w_n)$, thus can obtain the sort of U .

A characteristic value correspondence's eigenvector is not generally only, but the various sets of factors' sum of weight component is 1, therefore takes normalized vector $W' = (w'_1, w'_2, ..., w'_n)$ as the estimated weight vector , This can determine the weight of each factor set. And

$$W' = \left(\frac{w_1}{\sum_i w_i}, \frac{w_2}{\sum_i w_i}, ..., \frac{w_n}{\sum_i w_i} \right)$$

III. EXAMPLE: INDICATOR TYPE INSTRUMENT VARIOUS FACTORS WEIGHT DETERMINATION

In order to study each factor to indictor type instrument reading recognition time influence, giving the corresponding factor's degree of membership or membership function through the experimental analysis, then to determine the assignment of each factor's weight.

Uses the HSV color system to express the color, in the HSV color system, the H value represents the color appearance, the S value represents the saturation of color, and the V value represents the color brightness. H value expression color on a hue circle's angle number, scope between 0-360; S and V values were between 0-1. For expressing easily, the following S and V values are used to remove percent sign (that is 100 times the numerical expansion). The specific value of some main colors in HSV color system is shown in Tab.1.

TABLE I
THE MAIN COLORS' SPECIFIC VALUE IN HSV COLOR SYSTEM

Color	H	S	V	Color	H	S	V
B	0	0	0	Green(1)	120	100	50
W	0	0	100	Green(2)	120	100	100
R	0	100	100	Blue	240	100	100
Y	60	100	100	Purple	300	100	100

The experiment is carried out by PC machine graph programming, and laboratory equipment is also PC machine itself. The main interface of experimental procedure is shown in Fig.3.

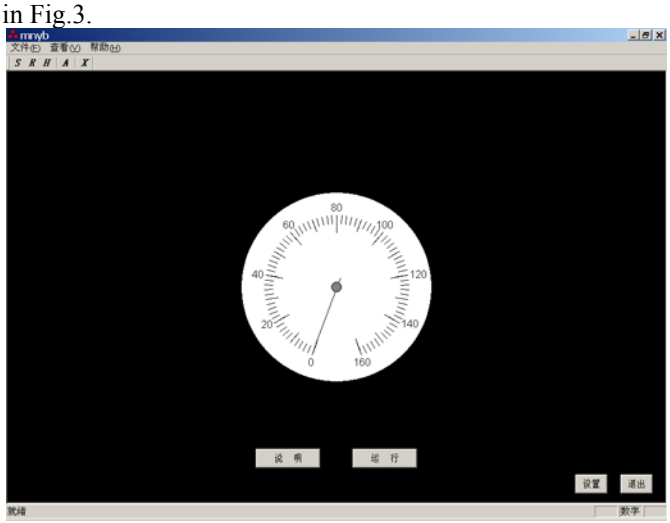

Fig.3. The main interface of experimental procedure

A. *Determine the Indicator Type Instrument's Color Assortment Membership Function*

The indicator type instrument color assortment experiment needs to change the dial plate color, and change scale division and indicator's color. Considering actual use situation, the colors which the experiment used are matching quite clearly, easily for reading.

Experiment goal: This experiment's goal is to study the dial plate, the scale division, indicator's color assortment influence to instrument's recognition time and the accuracy.

Experiment sample: 20 subjects, 17 men and 3 women who are college students and graduate students, aged between 20-26 years of age, vision or corrected visual acuity of 1.0 or above, normal color vision.

Experiment content: Through changes the dial plate, the scale division and the indicator color combination to determine that the color influence to recognition time and accuracy. Each color combination appears twice, specific HSV color values shown in Tab.1. The default setting for other programs: the dial plate shaped circular, dial size 70mm, scale spacing 3mm, scale length is 4.3mm, scale width of 0.3mm, The scale division does not have the color, orthostatic position of the scale division digit select 0, that is, the sign number in the outside of dial plate and Vertical display, the character size (height) is 4.3mm, character thickness is 400 degrees (that is in a normal stroke width), the indicator needle-tip according to the short scale division line terminal's distance is 1.6mm, the indicator needle-tip width is 0.4mm, and position the indicator at the bottom left of zero.

Experimental data statistics: Statistical analysis of experiments of various color combinations available, the average response time and error rate are shown in Fig.4 and Fig.5 respectively.

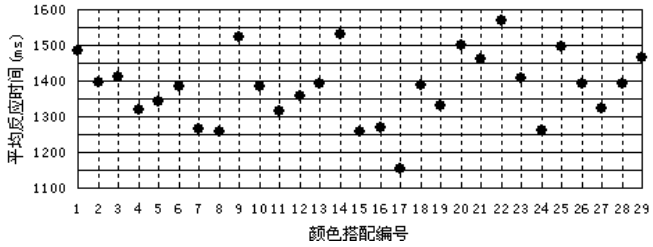

Fig.4. Average response time distribution

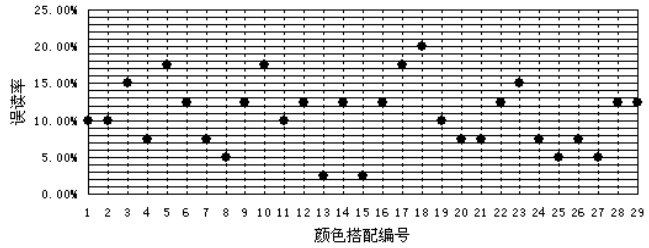

Fig.5. Error ratio distribution

Supposes r_{31} and r_{32} respectively to be the membership of a variety of colors that opposed to "good" and "bad". From Fig.4 may know that the average reaction time of all kinds of color combination is between 1100-1600(ms). Average response time for each case relative to the decision on the phrase "good" assessment of the situation. Set t to be the average response time. The evaluation criteria decide as [7]:

$$r_{31} = \begin{cases} 1, & t < 1300 \\ 0.75, & 1300 \le t < 1450 \\ 0.5, & 1450 \le t < 1600 \end{cases}$$

$$r_{32} = 1 - r_{31}$$

According to Fig.5 may know that misreading of various colors within the 25% rate. The various combinations according to the error rate on words relative to the decision-making "good" evaluation of the situation. Set x is the error ratio, the evaluation criteria decided as:

$$r_{31} = \begin{cases} 1, & x < 10\% \\ 0.75, & 10\% \le x < 15\% \\ 0.5, & 15\% \le x < 25\% \end{cases}$$

$$r_{32} = 1 - r_{31}$$

Considering the membership in the above two kind of standard condition, particularly to carry r_{31} , which is the degree of membership of various colors opposed to "good" in the two standards, on the fuzzy computation, then take kinds of fuzzy computation to obtain the corresponding average value.

B. Determining the weight set of each factor in indicator type instrument

Determining the weight set of each factor in indicator type instrument through the experimental method, studying various factors influence to recognition time, thus determination weight assignment of indicator type instrument factors. Carry on the fuzzy analysis computation to the instrument basic factor weight value, as shown in Tab.2 [8].

TABLE Ⅱ

THE FUZZY ANALYSIS COMPUTATION TO THE INSTRUMENT BASIC FACTOR WEIGHT VALUE

Factors	Chad And	Chad Or	Product And	Product Or	Bounde And	Bounded Or	Einstein And	Einstein Or	Jarger And (p=2)	Jarger Or (p=2)	Mean Value
u'_1	0.172	0.1974	0.034	0.3355	0	0.3694	0.0204	0.3573	0	0.2618	0.1748
u'_2	0.0685	0.1138	0.0078	0.1745	0	0.1823	0.0043	0.1809	0	0.1328	0.0865
u'_3	0.083	0.1053	0.0087	0.1796	0	0.1883	0.0048	0.1867	0	0.1341	0.0891
u'_4	0.0426	0.083	0.0035	0.122	0	0.1256	0.0019	0.1251	0	0.0933	0.0597
u'_5	0.0439	0.0685	0.003	0.1094	0	0.1124	0.0016	0.1121	0	0.0814	0.0532
u'_6	0.0232	0.0338	0.0008	0.0562	0	0.057	0.0004	0.0569	0	0.041	0.0269
u'_7	0.0338	0.0685	0.0023	0.1	0	0.1023	0.0012	0.102	0	0.0764	0.0486
u'_8	0.0685	0.0917	0.0063	0.1539	0	0.1602	0.0034	0.1592	0	0.1144	0.0758
u'_9	0.0426	0.0492	0.0021	0.0897	0	0.0918	0.0011	0.0926	0	0.0651	0.0433
u'_{10}	0.0619	0.083	0.0051	0.1398	0	0.1449	0.0028	0.1442	0	0.1036	0.0685
u'_{11}	0.0259	0.083	0.0022	0.1068	0	0.1089	0.0011	0.1087	0	0.087	0.0524
u'_{12}	0.1182	0.1222	0.0144	0.2259	0	0.2404	0.0081	0.2369	0	0.17	0.1136
u'_{13}	0.0315	0.0851	0.0027	0.1139	0	0.1166	0.0014	0.1163	0	0.0908	0.0558

Change the combination of basic factors, through changing the basic factors' value to determine the influence to recognition time and the error ratio. Extract the total weight of each basic factor according to average reaction time and the error ratio that get from experiment, carrying on the fuzzy computation to the obtained weight, then goes to the mean value, finally normalized processing. Normalized values are correspondence total weights of factors. The final weight value of basic factor is the vector which composed of normalized average value vector, so:

A'=(0.1843,0.0912,0.0939,0.0630,0.0561,0.0284,0.0513,0.0799,0.0457,0.0723,0.0552,0.1198,0.0589)

We can find the second-level factors weight of the original indicator type instrument at the same time.

$$A = (0.2755, 0.2927, 0.1256, 0.2473, 0.0589)$$

$$A_1 = (0.0310, 0.6690)$$

$$A_2 = (0.3209, 0.1917, 0.2151, 0.0970, 0.1753)$$

$$A_3 = (0.6363, 0.3637)$$

$$A_4 = (0.2922, 0.2233, 0.4845)$$

REFERENCES

[1] Toru Nakata, Altion Simo, Koji Kitamura, Takeo Kanade. Human Operational Errors in a Virtual Driver Simulation. National Institution of Advanced Industrial Science and Technology. Digital Human Research Cetner.2004

[2] LIN Yi, ZHANG Xin, SHI GuoObiao, XING HongObin. Subjective Evaluation Method Study on Vehicle Steering Feeling. Journal of Highway and Transportation Research and Development. 2007, 24(2): 130-134

[3] Hanson Lars, Wienholt Willfried, Sperling Lena. A control handling comfort model based on fuzzy logics.International Journal of Industrial Ergonomics. 2003,31(2): 87-100

[4] Dweiri F, Meier F.A. Application of fuzzy decision-making in facilitieds layout planning. International of Production Research.1996,34(11):3207-3225

[5] Zhang Hui, Zhu Yu-Ran,Wang Pei-Feng. Multi-model fuzzy weight control based on prediction. Light Industry Machinery. 2008,26(4): 73-75

[6] MA Guozhong, MI Wenyong, LIU Xiaodong. Multi-level Fuzzy Evaluation Method for Civil Aviation System Safety. JOURNAL OF SOUTHWEST J IAOTONG UN IVERSITY. 2007,42(1): 104-109

[7] Vilém Novák,Irina Perfilieva,Jiří Močkoř. Mathematical principles of fuzzy logic. Kluwer Academic Publishers.1999: 6-14

[8] Ntuen Celestine A. Application of fuzzy set theory to cognitive workload evalution of electronic circuit board inspectors. Human factors and Ergonomics In Manufacturing. 1999,9(3):291-301

2011 International Conference on Mechanical, Industrial, and Manufacturing Engineering
Lecture Notes in Information Technology Vols. 1-2

Optimal Transient Disturbances Preceding Vortex Shedding in Magneto-Hydrodynamic Flow past a Circular Cylinder in a Duct

Wisam K. Hussam, Mark C. Thompson, and Gregory J. Sheard

Department of Mechanical and Aerospace Engineering, Monash University, Clayton, Victoria 3800, Australia

{wisam.alsaadi, mark.thompson, and greg.sheard}@monash.edu

***Abstract* – Flow of liquid metal in an electrically insulated rectangular duct past a circular cylinder under a strong axial magnetic field is investigated in the subcritical regime, below the onset of von Kármán vortex shedding. In this configuration, the flow is quasi-two-dimensional and can be solved over a two-dimensional domain. A transient energy growth analysis of optimal linear perturbations is carried out. Parameters are considered for Reynolds numbers $50 \le Re \le 2500$, Hartmann numbers $500 \le Ha \le 1200$, and blockage ratios $0.1 \le \beta \le 0.4$. Transient growth is determined as a function of the evolution time of disturbances. For all β, the energy amplification of the disturbances was found to decrease significantly with increasing *Ha* and the peak growths shift towards smaller times. The nature of the disturbance does not vary with the blockage ratios.**

Index Terms – transient growth, magnetohydrodynamic, quasi-two-dimensional, circular cylinder.

I. INTRODUCTION

The study of flows of electrically conducting fluids in ducts in the presence of a transverse magnetic field is important because of its practical applications in magnetohydrodynamic generators, pump, and metallurgical processing. The primary application motivating this study is magnetic confinement fusion reactors, where liquid metal is used as a coolant and as a breeder material [1]. In most fusion reactor blankets, the liquid metal circulates in an electrically insulated duct perpendicular to the applied magnetic field. The motion of liquid metal in a strong magnetic field induces electric currents, which in turn interact with the magnetic field resulting in a Lorentz force. This has a significant effect on the velocity distribution and turbulence characteristics, and exerts a retarding force on the flow.

The flow under a strong magnetic field is characterized by a laminar structure because the velocity fluctuations in the direction of the magnetic field are strongly damped. Therefore, the heat transfer in the ducts of the blanket where a large amount of heat must be removed is dramatically decreased [2]. However, two-dimensional turbulence that consists of vortices with axes parallel to the magnetic field are not significantly damped [3]. This turbulence could be used to enhance the heat and mass transfer by using turbulence promoters such as a circular cylinder placed inside the duct of a blanket.

The concept of using internal obstacles to induce vortices and enhance the heat transfer rate has been investigated experimentally by [4, 5] and numerically by [6]. The results reveal that the heat transfer rate under a strong axial magnetic field in insulated ducts was improved by a factor of more than 2 times that of laminar flow.

Stable flow may be sensitive to transient growth of disturbances for some time before decaying to zero [7]. In purely hydrodynamic parallel shear flows (*Ha* = 0), transient growth has been demonstrated for the plane channel [8], pipe [9], rectangular duct [10], and abrupt geometrical expansion flows [11, 12]. This growth can be attributed to the non-normality of the eigenmodes associated with many shear flows [7, 8]. For the cylinder wake without magnetic field (*Ha* = 0), the adjoint and direct eigenmodes in the region of primary instability has been investigated numerically by [13, 14] to understand the sensitivity of the flow. More recently, the transient response of the subcritical and supercritical flow has been investigated by [15] and [12], respectively. The transient growth in supercritical and subcritical flow of the circular cylinder wake in an open flow has been studied by [16].

The effect of an applied magnetic field on the transient growth for the case of steady Hartmann flow (channel flow of an electrically conducting fluid in presence of uniform magnetic field) has been analyzed by [17-19]. The optimal modes were found to have the form of streamwise rolls confined to the Hartmann layers. In addition it was found that energy gains of the optimal perturbation are proportional to $(Re/Ha)^2$, and the critical Reynolds number was much higher than for Poiseuille flow.

More recently, [20] analyzed the optimal linear growth of perturbations in a rectangular duct with different aspect ratio subjected to a uniform transverse magnetic field. The disturbances of optimal growth are confined to the Shercliff layers. The optimal perturbations are significantly damped by the magnetic field irrespective of the duct aspect ratio. They conclude that the Hartmann boundary layers perpendicular to the magnetic field is not contribute to the transient growth.

The aim of this paper is to quantify and analyze the transient growth of infinitesimal perturbations in a quasi-two-dimensional MHD flow past a confined circular cylinder exposed to a strong magnetic field in the subcritical regime prior to the onset of vortex shedding. This research may lead to improved mechanisms for enhancing heat transfer in strongly magneto-hydrodynamically damped duct flows.

Parameter ranges to be considered are $50 \le Re \le 2500$, $500 \le Ha \le 1200$, and $0.1 \le \beta \le 0.4$. In particular, the effect of Hartmann number and blockage ratio on the transient growth will be investigated.

II. Mathematical Formulation

The system under investigation is a rectangular duct confining a circular cylinder placed at the center of the duct parallel to the transverse direction and perpendicular to the flow direction. The duct walls and the object are assumed to be electrically insulated. A homogeneous vertical magnetic field with a strength *Bo* of up to 2 Tesla is imposed along the cylinder axis. For a high Hartmann number, the magnetic Reynolds number Re_m, which represents the ratio between the induced and the applied magnetic field, is very small that the induced magnetic field is negligible and the resulting magnetic field is imposed in the *z*-direction only. Under these conditions the flow is quasi two-dimensional and consists of a core region, where the velocity is invariant along the direction of the magnetic field, and thin Hartmann layer at the wall perpendicular to the magnetic field. The quasi two-dimensional model has been derived by [21, 22], by integrating the flow quantities along the magnetic field direction as shown in Fig. 1.

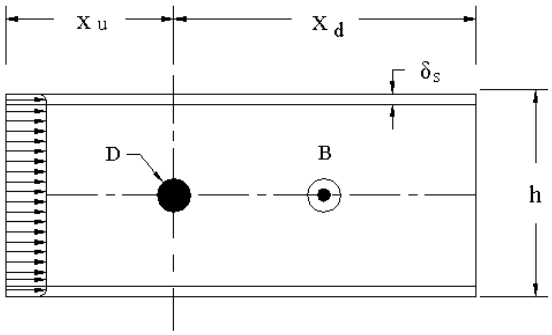

Fig. 1: Schematic representation of the computational domain for the flow past a confined circular cylinder in the average plane

In this case the non-dimensional magnetohydrodynamic equations of continuity and momentum [22, 23] are

$$\nabla_\perp \cdot \mathbf{u}_\perp = 0 \tag{1}$$

$$\frac{\partial \mathbf{u}_\perp}{\partial t} + (\mathbf{u}_\perp \cdot \nabla_\perp)\mathbf{u}_\perp + \nabla p_\perp = \frac{1}{\mathrm{Re}}\nabla_\perp^2 \mathbf{u}_\perp + \frac{d}{a}\frac{Ha}{\mathrm{Re}}\mathbf{u}_\perp, \tag{2}$$

where the variables are scaled by taking d, ρU_0^2, and d/U_0 as a respective length, pressure, and time. The dimensionless parameters *Re* and *Ha* are the Reynolds number and Hartmann number, respectively. They are defined as

$$Re = \frac{U_0 d}{\nu} \tag{3}$$

$$Ha = \sqrt{\frac{\sigma}{\rho \nu}} \tag{4}$$

The linearised Navier-Stokes equations are derived by substituting velocity and pressure fields decomposed into a two-dimensional base flow and an infinitesimal fluctuating components $\mathbf{u}'(x,y,t)$ and $p'(x,y,t)$. The linearised expansion is based on a steady two-dimensional base flow.
The maximum energy growth of initial perturbations for a given time period can be expressed as an eignvalue problem in which the perturbation can be expressed in terms of a set of optimal modes which grow at different amplitudes over the chosen time interval. The relative energy amplification (*G*) of an optimal mode is written as

$$G(\tau) = \frac{E(t=\tau)}{E(t=0)}, \tag{5}$$

where $E(t)$ is the energy of the disturbance at time *t*. $G(\tau)$ is the leading eigenvalue obtained after integrating a disturbance field forward in time using the linearized Navier-Stokes equations, and backwards in time using the adjoint linearlized Navier-Stokes equations. For the linearized and adjoint equations, it has been determined that the Hartmann friction term (the last term in equation 2) appears as $+\frac{d}{a}\frac{Ha}{\mathrm{Re}}\mathbf{u}'_\perp$ and $+\frac{d}{a}\frac{Ha}{\mathrm{Re}}\mathbf{u}^*_\perp$, respectively, where $\mathbf{u}^*_\perp$ denotes the adjoint disturbance velocity field. In all other respects, the direct transient growth technique applied here is identical to that described in [11], and the linearized eigenmode solver has been validated in [23, 24].

III. Numerical Methodology

A spectral-element method is used to discretise the governing flow equations [22]. The chosen scheme employs a Galerkin finite element method in two dimensions with high order Lagrangian interpolants used within each element. The nodes points within each element correspond to the Gauss-Legendre-Labatto quadrature points.

A no-slip boundary conditions for velocity is imposed on all solid walls. At the channel inlet, a normal component of velocity is assumed to be zero, and a Hartmann velocity profile for the axial velocity is applied. At the exit, a constant reference pressure is imposed and a zero streamwise gradient of velocity is weakly imposed through the Galerkin treatment of the diffusion term of the momentum equation. A constant reference pressure is imposed at the outlet, and a high order Neumann condition for the pressure gradient is imposed on the Dirichlet velocity boundaries to preserve the third-order time accuracy of the scheme [25].

The computational domain is divided into a grid of macro-elements. Elements are concentrated in areas of the domain that undergo high gradients. A grid resolution study determined the domain size, the number of mesh elements,

and the required number of nodes per element to resolve the flow features to within 1%. The meshes typically comprise 1052 to 1484 macro elements with 49 (7×7) nodes per element. The inlet length and outlet length were 8*D* and 25*D*, respectively.

IV. RESULTS AND DISCUSSION

The base flow

The base flow is characterized by a steady recirculation region of a pair of symmetric counter-rotating vortices on either side of the wake centreline. In Fig. 2, the effect of Hartmann number and blockage ratio on the flow is presented. It can be seen that an increase in the Hartmann number acts on the wake by decreasing the length of the recirculation bubble. This is due to the domination by the Lorentz force which produces a convective motion in a direction opposite the flow, resulting in the decrease of the wake length. For β = 0.1 the recirculation bubble does not completely vanish up to Ha = 1200, but for β = 0.4, though, it is suppressed completely at Ha = 1000 (not shown).

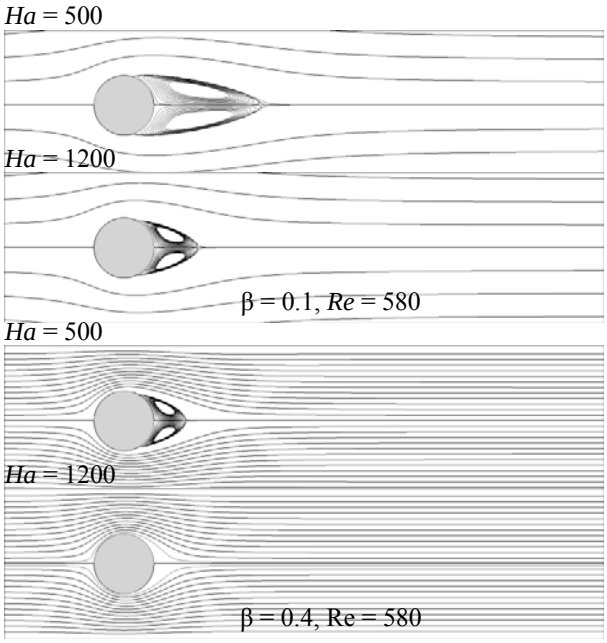

Fig. 2: Streamlines of the steady base flow at Re = 580 for blockage ratio and different Hartmann numbers as shown. Flow is left to right.

Transient growth analysis

Fig. 3 show the base-10 logarithm of the transient energy growth *G* of optimal disturbances as a function of evolution time τ for the steady base flow for blockage ratio β = 0.1 at different Hartmann numbers Ha. The initial observation on these data is, though the chosen *Re* for the analysis is well below the critical Reynolds number Re_c at the lowest Hartmann number *Ha* = 500, there exist perturbations which grow in energy by a factor of thousands. For example, for β = 0.1, the energy grows by a factor of 3.5×10^3 and 1.3×10^3 at *Ha* = 500 and *Ha* = 1200, respectively. For β = 0.4 (not shown), there is a growth of energy by a factor of 4.55×10^3 and 1.47×10^3, respectively. For all β, it is found that increasing *Ha* leads to a significant reduction of the energy amplification of the disturbances and to shift of the peak growth towards smaller times. In fact, the interpretation of such suppression is the reduction of perturbation kinetic energy by the Hartmann damping. Remarkably, the global maxima of energy vary significantly with the blockage ratio.

β = 0.1, *Re* = 580

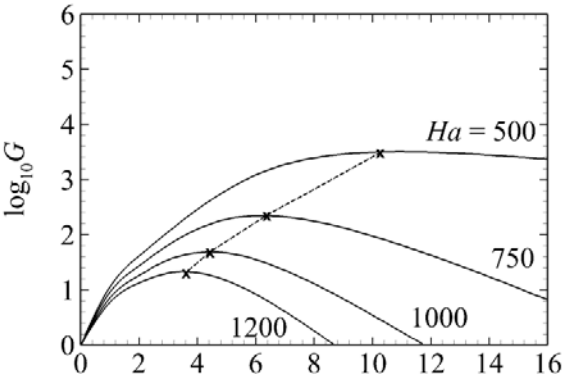

Fig. 3: Plots of $\log_{10}G$ against τ at β = 0.1, *Re* = 580, and Hartmann numbers as shown. The dashed curve shows the locus of maximum growth as a function of τ.

Fig. 4 plots the streamwise vorticity field of the optimal initial perturbations for the blockages β = 0.4 at low and high Hartmann numbers, i.e., *Ha* = 500 and *Ha* = 1200, respectively. In each, the perturbation maximum is located in the region of the boundary layer separation around the cylinder near the wake. The perturbation travels along the separating region as long as possible, hence providing the optimal growth. Remarkably, the nature of the disturbance does not vary with the blockage ratios. Fig. 5 (a, c) shows the streamwise vorticity of initial perturbation for β = 0.4, *Re* = 1160 and *Ha* = 500 and *Ha* = 1200, for which τ_{max} = 7 and 2, respectively. It is clear to see that by increasing Hartmann number, the optimal perturbations are more concentrated around the boundary layer separation. In Fig. 4 (b, d), the evolution from this initial disturbance is plotted. The flow structures are a series of counter-rotating spanwise rollers, which are similar to structures seen in transient growth analysis of a cylinder in an open flow [13, 14]. Over time, vorticity detaches from the aft of the cylinder and travels downstream along the wake centreline, and a region of opposite sign voricity forms at the aft of the cylinder. In addition, boundary layer detachment from the duct side wall occurs downstream of the cylinder. Vorticity is drawn into the channel and interacts with that detached from the rear of the cylinder. The boundary layer detachment from the walls was observed to change significantly as β is further increased.

(a)

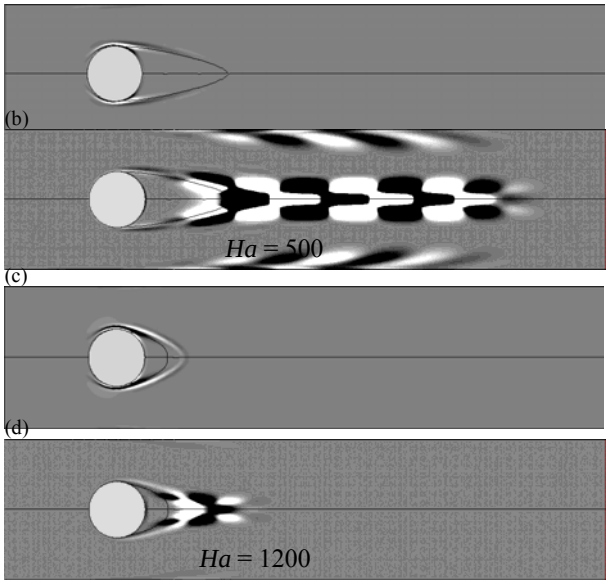

Fig. 4: Plots of stream-wise vorticity for β = 0.4 (a, c) optimal initial perturbation at *Re* = 1160 at *Ha* = 500 and 1200, respectively. (b, d) the corresponding linear growth evolved at τ_{max} for the same Reynolds numbers and Hartmann numbers of (a, c). The streamlines of the stable base flow is overlaid in each case

V. CONCLUSIONS

An investigation has been carried out into the transient growth of optimal linear perturbations of a liquid metal magneto-hydrodynamic flow past a confined cylinder in a duct under a strong magnetic field in the subcritical regime prior the onset of oscillations. Under these conditions, the flow is quasi-two-dimensional.

For all blockage ratios, very significant transient energy growth was found in this regime, which suggests a potential for the design of actuation mechanisms to promote vortex shedding and thus enhance heat transfer in these ducts. The energy amplification of the disturbances was found to decrease significantly with increasing Hartmann number, where the growth peaks at shorter time intervals. The nature of the disturbance does not vary with blockage ratio.

ACKNOWLEDGMENT

This research was supported by a Monash University Faculty of Engineering Small Grant. Computations were supported by Monash the e-Research Centre and ITS-Research Support Services through the use of Monash Sun Grid cluster, and the NCI National Facility in Canberra, Australia. NCI is supported by the Australian Commonwealth Government. W.K.H. is supported by the Ministry of Higher Education and scientific Research from the Iraqi Government.

References

[1] S. Münevver, Magnetohydrodynamic flow in a rectangular duct. *International Journal for Numerical Methods in Fluids*, 1987. **7**(7): p. 697-718.

[2] I. R. Kirillov, C. B. Reed, L. Barleon, K. Miyazaki, Present understanding of MHD and heat transfer phenomena for liquid metal blankets. *Fusion Engineering and Design*, 1995. **27**: p. 553-569.

[3] O. Lielausis, Liquid-metal magnetohydrodynamics. *Atomic Energy Rev*, 1975. **13**(3): p. 527–581.

[4] M. Frank, L. Barleon, U. Muller, Visual analysis of two-dimensional magnetohydrodynamics. *Physics of Fluids*, 2001. **13**(8): p. 2287-2295.

[5] Y. B. Kolesnikov, A. B. Tsinober, Experimental investigation of two-dimensional turbulence behind a grid. *Fluid Dynamics*, 1974. **9**(4): p. 621-624.

[6] W. K. Hussam, M.C. Thompson, and G. J. Sheard, A numerical study on the fluid flow and heat transfer around a circular cylinder in an aligned magnetic field. *International Journal of Heat and Mass Transfer,* 2011. **54**(5): p. 1091-1100.

[7] P.J. Schmid, Stability and transition in shear flows. 2001: *New York :Springer*.

[8] S.C. Reddy, P.J. Schmid , J. S. Baggett , On stability of streamwise streaks and transition thresholds in plane channel flows. *Journal of Fluid Mechanics*, 1998. **365**: p. 269-303.

[9] O.Y. Zikanov, On the instability of pipe Poiseuille flow. *Physics of Fluids*, 1996. **8**(11): p. 2923-2932.

[10] D. Biau, H. Soueid, and A. Bottaro, Transition to turbulence in duct flow. *Journal of Fluid Mechanics*, 2008. **596**: p. 133-142.

[11] H.M . Blackburn, D. Barkley, and S.J. Sherwin, Convective instability and transient growth in flow over a backward-facing step. *Journal of Fluid Mechanics*, 2008. **603**: p. 271-304.

[12] C.D. Cantwell, D. Barkley, and H.M. Blackburn, Transient growth analysis of flow through a sudden expansion in a circular pipe. *Physics of Fluids*. **22**(3): p. 1-15.

[13] J.M. Chomaz, Global instabilities in spatially developing flows: Non-normality and nonlinearity, *in Annual Review of Fluid Mechanics.* 2005. p. 357-392.

[14] F. Gianetti, and P. Luchini, Structural sensitivity of the first instability of the cylinder wake. *Journal of Fluid Mechanics*, 2007. **581**: p. 167-197.

[15] O. Marquet, D. Sipp, and L. Jacquin, Sensitivity analysis and passive control of cylinder flow. *Journal of Fluid Mechanics*, 2008. **615**: p. 221-252.

[16] N. Abdessemed, A. S. Sharma, S.J. Sherwin, and V. Theofilis, Transient growth analysis of the flow past a circular cylinder. *Physics of Fluids*, 2009. **21**(4): p. 044103-13.

[17] Airiau, C. and M. Castets, On the Amplification of Small Disturbances in a Channel Flow with a Normal Magnetic Field. *Physics of Fluids*, 2004. **16**(8): p. 2991-3005.

[18] D. Gerard-Varet, Amplification of small perturbations in a Hartmann layer. *Physics of Fluids*, 2002. **14**(4): p. 1458-1467.

[19] D.S. Krasnov, E. Zienicke, O. Zikanov, T. Boeck, and A. Thess, Numerical study of the instability of the Hartmann layer. *Journal of Fluid Mechanics*, 2004(504): p. 183-211.

[20] D. Krasnov, O. Zikanov, M. Rossi, and T. Boeck, Optimal linear growth in magnetohydrodynamic duct flow. *Journal of Fluid Mechanics,* 2010. **653**: p. 273-299.

[21] J. Sommeria, and R. Moreau, Why, how, and when, MHD turbulence becomes two-dimensional. *Journal of Fluid Mechanics*, 1982. **118**: p. 507-518.

[22] G.J. Sheard, T. Leweke, M.C. Thompson, and K. Hourigan, Flow around an impulsively arrested circular cylinder. *Physics of Fluids*, 2007. **19**(8): art. no. 083601

[23] G.J. Sheard, M.J. Fitzgerald, and K. Ryan, Cylinder with square cross-section: wake instabilities with incidence angle variation. *Journal of Fluid Mechanics*, 2009. **630**: p. 43-69.

[24] H. M. Blackburn, and , G. J. Sheard., On quasiperiodic and subharmonic floquet wake instabilities. *Physics of Fluids*, 2010. **22**: art. No. 031701.

[25] G. E. Karniadakis, M. Israeli, and S. A. Orszag, Higher-order splitting methods for the incompressible Navier-Stokes Eqs, *J. Compt. Phys.*, 1991. **97:** p. 414-443.

2011 International Conference on Mechanical, Industrial, and Manufacturing Engineering
Lecture Notes in Information Technology Vols. 1-2

Encapsulation of Inorganic Particles by Dispersion Polymerization through Ultrasonic Irradiation

Zhang Kai Fan Jinghui Wu Juying
Institute of System Engineering, China Academy of Engineering Physics, P.O.box 919-412, Mianyang 621900, China

Abstract: In this paper, the polystyrene/nano-silica composite particles were prepared and characterized according to the following steps. First, the nano-silica particles were pretreated with the surfactants under ultrasonic field. Second, the dispersion polymerization of styrene in a water-ethanol (1/6 wt/wt) medium, with poly(N-vinyl pyrrolidone) (PVP) as stabilizer and 2,2'-azobisizobutyronitrile (AIBN) as initiator in the presence of nano-silica particles was initiated with N2 purging through ultrasonic irradiation by taking its advantages of multieffect, i.e., dispersion, crushing, activation, and initiation. Finally, the polymerization kinetics characteristics were studied, and the encapsulation of composite particles were investigated with optical microscope, SEM, TEM, FTIR, X-ray photoelectron spectroscopy (XPS), thermogravimetric analysis (TGA), and differential scanning calorimetry (DSC).
Keywords: Composite Particle, Dispersion Polymerization, Ultrasonic Irradiation

1. Introduction

In recent literature, several processes have been described to synthesize particles that consist of an inorganic core surrounded by a polymer shell. The technique of polymer encapsulation is becoming more and more popular since polymer-encapsulated particles offer very interesting actual and potential applications. Encapsulated pigments are involved in the manufacture of cosmetics, inks, and paints to improve the compatibility between the filler and the binder. The process of encapsulation is of particular interest in agriculture and pharmaceutical industries to produce controlled-release products such as encapsulated pesticides and drugs. Encapsulation technologies have developed to reduce toxicity, to mask taste and odor, to facilitate storage or transport, and to improve the stability of the encapsulated product. Polymer-encapsulated inorganic particles may also have interesting properties in areas as adhesives, textiles, optics, and electronics[1,2].

Most methods of encapsulation included emulsion polymerization, surfactant-free emulsion polymerization, emulsion-like polymerization and suspension polymerization have been employed[1]. Dispersion polymerization is characterized by the fact that the monomer and the initiator are soluble, and the polymer insoluble, in the reaction medium. This is a kind of precipitation polymerization in which the insoluble polymer, that first forms small aggregates and next larger particles, is stabilized by a suitable steric stabilizer present in the reaction medium[3]. Dispersion polymerization has already been employed for the preparation of composite materials made of ultrafine silica particles. However, the goal in the works was not encapsulation of the silica particles by the polymer, but electrostatic stabilization of the large polymer particles by the negatively charged silica particles located at the surface of the polymer particles[4]. Bourgeat-Lami et al. have prepared polymer encapsulation of nano-silica particles, using dispersion polymerization of styrene in aqueous ethanol medium with ploy(N-vinyl pyrrolidone) (PVP) as stabilizer. In the works, nano-silica particles directly synthesized by stöber process in an aqueous ethanol medium are either unreacted or coated with 3-(trimethoxysilyl)propyl methacrylate (MPS), which is grafted at the silica particles surface. When the bare silica particles are used as the seed, there is a strong tendency of the silica beads to cover the surface of the polystyrene particles and obviously encapsulation does not occur. On the contrary, when the silica surface is made hydrophobic by coating, the inorganic particles are entirely contained in the polystyrene particles as evidenced by microscopy techniques (TEM, SEM, AFM) [5].

However, the big challenge encountered in preparing polymer/inorganic nano-particle encapsulation is that the nano-particle cannot be dispersed in polymer matrix at the

nano level by conventional techniques, because the surface energy of the tiny particles is very high, and these particles tend to agglomerate during mixing. Xia et al. have employed ultrasonic induced encapsulating emulsion polymerization of monomer in presence of nano-particles. The inorganic nano-particles in the aqueous solution can redisperse more effectively through ultrasonic irradiation than by conventional stirring. Ultrasonic induced encapsulating emulsion polymerization of BA monomer in the presence of nano-silica can produce poly(butyl acrylate) (PBA)/nano-silica composite[6]. To our knowledge, there is no description in the literature of encapsulation of inorganic nano-particles by a polymer using dispersion polymerization under ultrasonic field.

In this paper, we describe the dispersion polymerization of styrene in a water-ethanol (1/6 wt/wt) medium, with poly(N-vinyl pyrrolidone) (PVP) as stabilizer and 2,2'-azobisizobutyronitrile (AIBN) as initiator in the presence of nano-silica particles through ultrasonic irradiation inducement. The polymerization kinetics characteristics were studied, and the encapsulation of nano-silica particles were investigated with optical

2.2 Apparatus

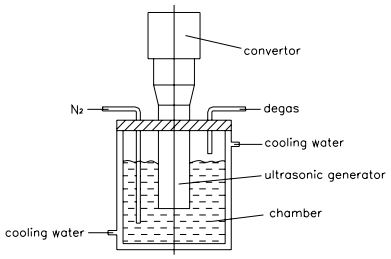

Figure 1 Schematic diagram of the ultrasonic reactor

The equipment employed in this research was 20KHz ultrasonic generator, DG-2000 (Dejia Electron Equipment Factory, Jiangshu, China). Ultrasonic irradiation was carried out with the probe of the ultrasonic horn immersed directly in the reaction dispersion system (Figure 1). During the polymerization, cooling water was circulated to decrease reaction system temperature, and constant N_2 purging rate was kept.

2.3 Preparation of polystyrene/nano-silica composite particles through ultrasonic irradiation

The polystyrene/nano-silica composite particles were prepared according to the following steps. First, 1.0g of nano-silica particles, 0.5g of SDS or CTAB, 10mL deionized and distilled water were introduced into a 50mL beaker. Then the nano-silica particles were pretreated under the ultrasonic irradiation of 600W for 2.0h. Second, 10mL of styrene, 0.1g of AIBN, 0.5g of PVP, 80mL of absolute alcohol were added to a 250mL three-necked flask and stirred into a transparent homogeneous phase solution. After bubbling nitrogen through the reaction medium for 2.0h, the pretreated nano-silica particles were added to the dispersion polymerization solution and mixed under stirring at 150 rpm for 24h. Third, the mixed reaction system was introduced into the reaction vessel, cooling water was circulated to decrease reaction system temperature, and constant N_2 purging rate was kept. Then the ultrasonic generator was switched on and the dispersion polymerization was subjected to ultrasonic irradiation of 300W for 3.0h. Fourth, the polymerized composite particles were cleaned with ethanol by a repeated sedimentation-redispersion process, and the composite particles were dried at 40℃ in a vacuum box for 24h.

2.4 Characterization

Samples were removed at various times throughout the

2. Experimental

2.1 Materials

Nano-silica particles: 60nm, Zhoushan Nanomaterial Limited Company, Zhejiang, China.

Styrene (St): AR, Beijing Fuxing Chemical Reagent Factory, was washed three times with 10% aqueous solution of sodium hydroxide, and distilled water to remove the inhibitors, dried with anhydrous sodium sulfate, then vacuum distilled. The sealed purified sample was stored at 4℃ until required.

2,2'-azobis(isobutyronitrile) (AIBN): AR, Beijing Chemical Reagent Factory, used as supplied.

Poly(N-vinylpyrrolidone) (PVP K-30): AR, Tianjin Jinyu Chemical Reagent Factory, used as supplied.

Cetyl trimethylammonium bromide(CTAB): AR, Beijing Chemical Reagent Factory, used as supplied.

Absolute alcohol (EtOH): AR, Chengdu Chemical Reagent Factory, used as supplied.

ultrasonic irradiation and the monomer conversion was determined gravimetrically.

Images of the silica beads alone and of the polystyrene particles polymerized in the absence and presence of silica beads were obtained from three different microscopy techniques: optical microscope (OM, MINGCA1800), scanning electron microscopy (SEM, Hitachi 4500), and transmission electron microscopy (TEM, JEM 100CX).

IR analysis of the samples was performed on a Nicolet 560 FTIR spectrometer.

TGA analysis of the samples was performed on Perkin-Elmer TGA7 instrument.

DSC analysis of the samples was performed on Seiko EXSTAR 6000 instrument.

The C, N, O, and Si content of the samples surface was determined by XPS performed on XSAM 800 instrument.

3. Results and discussion

3.1 Polymerization kinetics characteristic

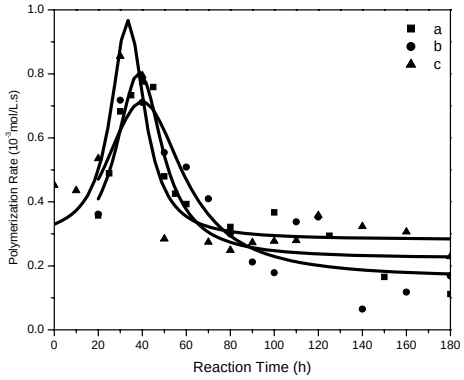

Figure 2 Monomer conversion and polymerization rate as functions of reaction time
(a)PS; (b)PS/SiO_2 (untreated); (c)PS/SiO_2 (treated)

Specific amounts of reactants were subjected to ultrasonic irradiation with a power output of 300W for 3.0 h, and the reaction system was changed from faint opalescence at the outset of the reaction to light milk white, then to milk white at the completion of the polymerization. The monomer conversion and polymerization rate as functions of reaction time is shown in Figure 2. As seen in Figure 2, the polymerization in the presence of unmodified nano-silica particles has similar polymerization kinetics characteristic to the polymerization in the absence of nano-silica particles. This phenomenon indicates that encapsulating polymerization did not occur during the polymerization in the presence of unmodified nano-silica particles, and the polymerization process of St did not occur at the surface of nano-silica particles, but for itself. On the contrary, the polymerization in the presence of modified nano-silica particles has higher monomer conversion and polymerization rate than those of the polymerization in the absence of nano-silica particles. In the polymerization in the presence of modified nano-silica particles, the conversion of monomer can reach about 70% in 3.0h, and the polymerization rate can reach the maximum in 35min. At the outset of the reaction, the system of polymerization of St was homogeneous solution, and it took some time to reach critical molecule chain length forming two-phase system. However, the polymerization in the presence of modified nano-silica particles was inhomogeneous system at the outset of the reaction, and modified nano-silica particles could become the nucleation centers. After modified nano-silica particles with the surfactants, their surface properties changed from hydrophilicity to hydrophobicity. Then the dispersion polymerization of St was easier to be initiated in the zones containing much monomer and initiator, which formed surrounding the nano-silica particles.

3.2 Particle size and morphology

From TEM and SEM micrographs the size and morphology of the nano-silica particles were determined. As seen in Figure 3, the nano-silica has size of about 60nm, and shape of sphericity-like. Because the surface energy of the nano-silica particles is very high, these particles tend to agglomerate after dispersion. During polymerization, nano-silica particles should be redispersed with ultrasonic irradiation.

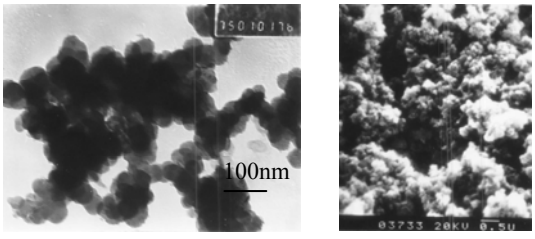

(a) (b)

Figure 3 Micrographs of nano-silica particles
(a) TEM, (b) SEM

The polystyrene particles obtained by dispersion polymerization are rather large (up to 1μm) and can be conveniently imaged using optical microscope and scanning electron microscope. Figure 4a shows SEM picture of polystyrene particles prepared in the absence of nano-silica particles. Particles exhibit a regular spherical shape and homogeneous distribution, which are characteristics of the conventional polystyrene latex particles usually obtained under the same experimental conditions. Compared with the polystyrene particles prepared by routine heat initiation, the polystyrene particles prepared by ultrasonic irradiation have broader size distribution. Ultrasonic cavitations create a very extreme environment, i.e. extremely high local temperature and pressure, as well as heating and cooling rates for chemical reaction. Local high temperature point can create a nonuniform initiation process.

Let us now examine what kind of composite particles is obtained in the presence of nano-silica particles. Figure 4b is composite particles mixed directly polystyrene particles and nano-silica particles. As seen in Figure 3b and 4b, polystyrene particles and nano-silica particles exist independently. Nano-silica particles tend to agglomerate obviously. As seen in Figure 4c, when bare nano-silica particles without pretreatment are introduced into the polymerization medium, investigation of the morphology of the resulting composite particles by SEM reveals that polystyrene particles are covered with some small silica beads and complete encapsulation does not occur. From this observation, the nano-silica particles stay free during polymerization and more or less anchor on the polymer particles during the polymerization, but remained at the surface because of their high hydrophilicity. On the contrary, the surface of the polystyrene particles obtained in the presence of pretreated nano-silica particles is smooth, and no silica bead is detected on the whole surface of the samples. An example is given in Figure 4d. These observations can lead to the conclusion that, once modified by the surfactant, CTAB, the nano-silica particles are encapsulated in the polystyrene particles in the course of the dispersion polymerization process. The transmission electron micrographs of polymer particles synthesized in the presence of modified nano-silica particles are shown in Figure 5. Because the composite particles have large size, the electron beam cannot penetrate the particles effectively. As seen in Figure 5, few nano-silica particles are found outside polystyrene particles, and the dispersion of most nano-silica particles inside composite particles cannot be seen distinctly.

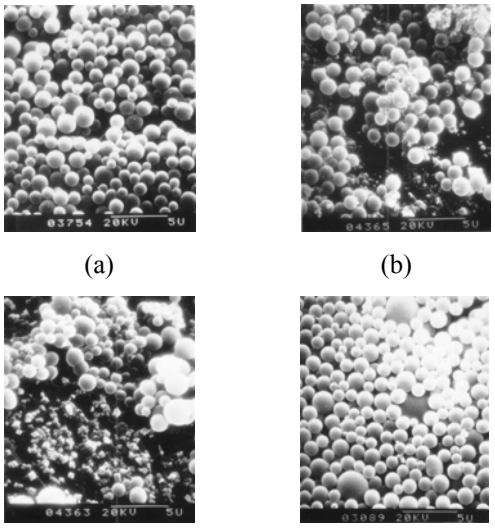

(a) (b)

(c) (d)

Figure 4 SEM photographs of some kinds of particles (a) PS particles; (b) mixture with PS and SiO_2; (c) PS/SiO_2 (untreated); (d) PS/SiO_2 (treated)

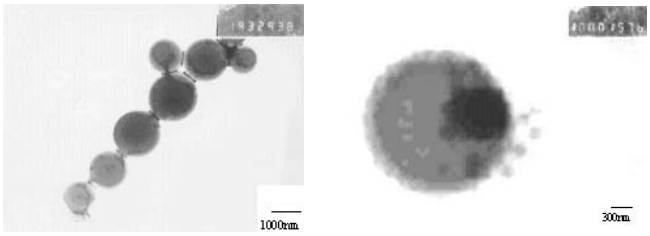

Figure 5 TEM photographs of SiO_2/PS composite particles

3.3 FTIR analysis

In order to confirm the structure of SiO_2/PS composite particles, the IR spectra of SiO_2/PS composite particles and particles mixed nano-SiO_2 and PS are compared in Figure 6. As shown in Figure 6, the two IR spectra are different. The major differences are marked with three circles in the IR spectra of SiO_2/PS composite particles. These differences show that SiO_2/PS composite particles prepared through ultrasonic induced encapsulation dispersion polymerization had formed different structure from particles mixed mechanically nano-SiO_2 and PS. In FTIR analysis, dose the peak at 2364 cm^{-1} probably belong to the gas CO_2 which did not be remove completely as characterizations

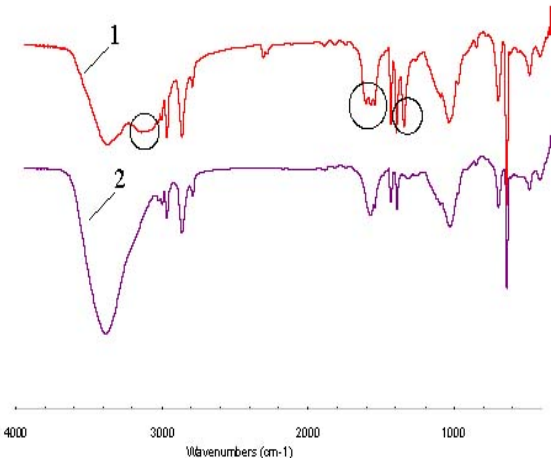

Figure 6 FTIR spectra of two sorts of composite particles (1) SiO_2/PS composite particles, (2) particles mixed nano-SiO_2 and PS

3.4 XPS analysis

Figure 7 shows survey X-ray photoelectron spectra of the sample of SiO_2/PS composite particles obtained through ultrasonic irradiation. The peak of binding energy of every element is slightly shifted due to the change of environment. The ratio of the atom number of C and Si (C/Si) in the surface of SiO_2/PS composite particles is determined from the ratio of peak areas corrected with the empirical sensitivity factors. The C/Si ratio in the surface of SiO_2/PS composite particles is 80/1, which is higher than that in the bulk (～54/1). The results provide supporting evidence for the polystyrene encapsulated nano-silica particles structure.

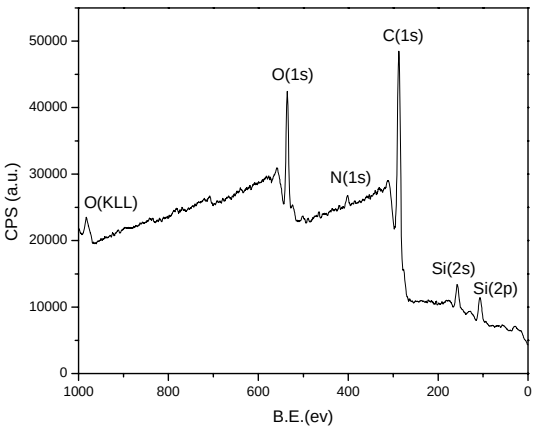

Figure 7 Survey X-ray photoelectron spectra of SiO_2/PS composite particles

3.5 TGA and DSC analysis

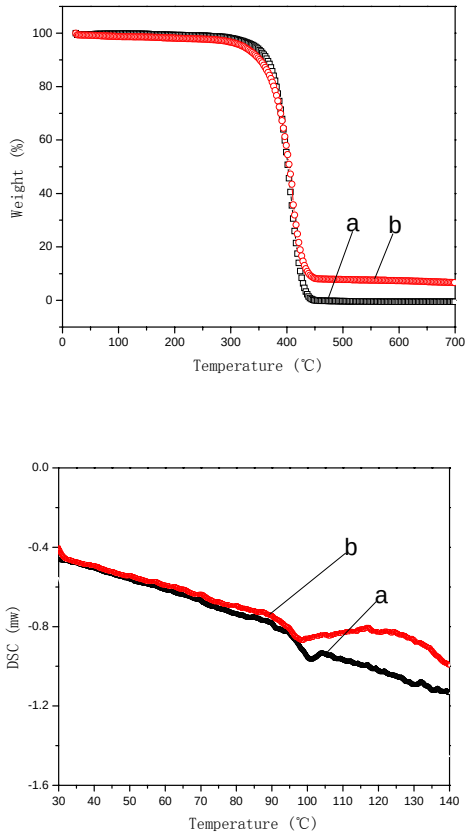

Figure 8 TGA and DSC curves of PS and SiO_2/PS particles (a) PS particles; (b) SiO_2/PS composite particles

Figure 8 are the TGA and DSC curves of the SiO_2/PS composite particles. As seen in TGA curve, the SiO_2/PS composite particles do not decompose before 300℃, and the mass loss is very low. When temperature reaches to 300℃, the SiO_2/PS composite particles start to decompose until 450℃. The residual mass of the SiO_2/PS composite particles is the mass of SiO_2 encapsulated. The SiO_2 content in the SiO_2/PS composite particles is 7.41% that can be calculated through the TGA curve. According to the ratio of mass of SiO_2 and styrene (1/10) in the raw recipe, the encapsulation ratio of SiO_2 is 66.7%. As seen in DSC curve, the Tg of the SiO_2/PS composite particles is about 100℃, and the value is lower than pure PS particles. The result shows that new structure formed in SiO_2/PS composite particles.

4. Conclusions

Encapsulation of nano-silica particles by polystyrene had been achieved by dispersion polymerization through ultrasonic irradiation, with the aid of a surfactant attached to

the nano-silica particles. The aggregation of nano-silica in the reaction media could be broken down under ultrasonic irradiation, and at the same time much monomer and initiator surrounding the surface of the nanoparticles through the attached surfactant were initiated. The primary composite particles continued to seize more monomer and initiator, and increased the molecular length until precipitating from the reaction media and forming sphere particles with micron size. Using three microscopy techniques, OM, SEM, and TEM, these composite particles were characterized. The surface of the polystyrene particles obtained in the presence of pretreated nano-silica particles was smooth, and no silica bead was detected on the whole surface of the samples. On the other hands, the FTIR and XPS spectroscopies of the composite particles provided another supporting evidence for the polystyrene encapsulated nano-silica particles structure. From TGA and DSC curves, some properties of composite particles could be drawn out, including the encapsulation ratio of SiO_2 was 66.7%, and the Tg of the composite particles was about 100℃.

REFERENCES

[1] Cao T., Liu Q., Hu J. Preparation, Property and Application of Polymer Emulsion. Chemical Industry Press: Beijing, China, 2002.

[2] Liang Z. Technology and Application of Microcapsule. Chinese Light Industry Press; Beijing, China, 2002.

[3] Barrett, K.E.J., Br.Polym.J., 5,259 (1973).

[4] Maeda,S., Gill,M., Armes,S.P., Langmuir 11,1899 (1995).

[5] Bourgeat-Lami, E., Lang, J., J.Colloid Interface Sci., 197,293 (1998).

[6] Hesheng Xia, Qi Wang. J.Appl.Polym.Sci., 80,1130 (2001).

2011 International Conference on Mechanical, Industrial, and Manufacturing Engineering
Lecture Notes in Information Technology Vols. 1-2

PUMA 560: Robot Prototype with Graphic Simulation Environment

Antonio Benitez[1], Ignacio Huitzil[1], Azgad Casiano[2], Jorge De La Calleja[1] and Medina M. A.[1]
Department of {Informatics[1], Mechatronics[2]} Engineering
Polytechnic University of Puebla
Tercer Carril del Ejido "Serrano" s/n, 72840.Juan C. Bonilla, Puebla., México
abenitez@uppuebla.edu.mx

***Abstract* – This paper presents the necessary elements to manipulate kinematic applications for a PUMA 560 models using a graphic simulation tool to present forward and inverse kinematics methods. Besides an implementations and applications to forward kinematic has been download through prototype robot based on Dynamixel AX-12 servo motors. Hence kinematics chains with six degrees of freedom are modeled and solved. As promising results a platform to simulate on three dimension space is presented as an important tool to verify the movements programmed on the robot.**

Index Terms - Forward and Inverse Kinematics Treatment, Robot prototype mechanism, and Programming and 3D Simulation.

I. INTRODUCTION

Robotics area has been important grown on last decades. Different kind of robotics mechanism has emerged to perform a wide variety of task. Inside this developed, articulated robots begins to play an important role on different applications, for example; manufacture process, especial applications and research and teaching process. The interest on develop of these robots is supported besides on electronics and computation grown. Particularly, computer graphics allow the user to build realistic environments for every problem that we wish. These changes could not be made at profitable costs and timely results without the use of computer simulation tools, since not only the robots, but also the environment must be setup several times to the desired initial conditions to repeat the experiment. Due to the process results, an original environment could be non-reconfigurable without human intervention (e.g. drilling a piece, moving parts to another place). One solution to the depicted issue is to account on graphical (morphological) and mathematical models to determine the interactions between robots and its external environment and then execute a desired task with intelligent (reactive or planned) obstacle avoiding in the trajectory.

Actuality teaching and research areas of robotics are based
on standard configurations such as the PUMA, STANDFORD and SCARA because these contain the robotics fundamental. Other inconveniences are the high construction costs to account on one model. Therefore, simulation is a good alternative solution to show the performance and testing of robots in real life through computer programs reducing construction and development costs.

In this work we present two types of implementations, initially, morphological models of the PUMA 560 robot is presented inside a graphic simulation environment, because of PUMA 560 is a manipulator under several industry applications and research topics are based. Hence, part of this work describes the necessary elements to get a 3D graphic interface that simulates the PUMA 560 using numeric and geometric methods to move the kinematic chain that represent the mathematic model and showing applications for inverse kinematic to paint figures and curves. On the other hand, a prototype for this robot has been developed using dynamixel servo motors to test kinematic solutions. An articulated with three degrees of freedom (DOF) was build to test forward kinematic applications.

This work will be presented as follows. In section II, the main structure for PUMA 560 is described. Next, in section III, joints characteristics and the problems of forward and inverse kinematic is presented. In section IV, we describe a graphic user interface for a tree dimensional environment to simulate the PUMA movements. Prototype for an articulated robot with four DOF is shown in section V. Finally in section VI conclusions and work in process is discussed.

II. THE PUMA 560 STRUCTURE

A robot is a servo controlled manipulator that made various programmed tasks. A robotic arm is the constituted by a kinematic chain which is a set of rigid bodies (links) attached to articulations (joints) that permit the relative motion between two elements [8] and [7]. In the kinematic chain the links have parameters such as weight, inertia, and size, among others. The joints have features of articulation type and DOF.

The PUMA 560 robot has six links and six DOF (rotary type joints in function of an angle θ). The first three DOF are located in the arm which allows determining the robot position. The following three DOF's are located in the end effectors to provide orientation, Figure 1. shows the physical constitution of this model and Table 1. the extent to which each articulation account.

A. Joints

The essential characteristic of a joint is that it permits some degree of relative motion between the two segments it connects. Modeling real joints can be very complex, since the motion limits depend on many factors, especially in the articulations of living organisms, and particularly, the human body [1]. Moreover, joints may be dependent on each other, especially in living organisms. This coupling (of motion and limits) can be integrated directly in the body definition, with the concept of joint group [1], or at the application level, with kinematic constraints resolved by an inverse kinematics engine (for example, the scapulo-thoracic constraint [5]).

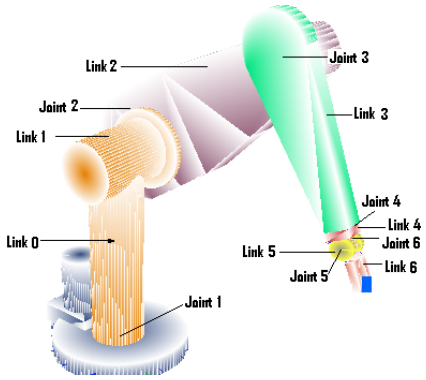

Fig. 1 Links and joints for PUMA 560 Structure.

TABLE I
MOTION LIMITS FOR SIX DOF FOR PUMA 560

Joint	Range (degrees)
1	-160° – 160°
2	-245° – 45°
3	-45° – 225°
4	-110° – 170°
5	-100° – 100°
6	-266° – 266°

B. *Ball-and-Socket Joint*

A ball-and-socket joint owns three rotational degrees of freedom. Hence, it is the most mobile of the purely rotational joints. It allows an axial motion (or twist) of the segment (one DOF), as well as a spherical motion (or swing) that determines its direction (two DOFs). Ball-and-socket joints are used to model articulations such as the human shoulder and hip.

II. KINEMATICS PROBLEMS

The kinematics is the science that studies the movement of bodies (is a matter of robotic structures mechanically multi-jointed) [4]. To set the locomotion on the robot kinematics it is necessary to solve two problems, the *"forward kinematic and inverse kinematic"*. The first problem consists on determining position and orientation of the final end-effector for the robot respect to a coordinate system reference, knowing the joint angles and geometric parameters. The second problem concerns the configuration to be taken by the robot for a position and orientation (configuration) determined from the end effector [3].

A. *Forward kinematic for PUMA 560*

The mathematic representation for a kinematic chain is A_1 A_2 A_3, . . . A_n, a set of n elements, and i that $1< i < n$, where the element A_i is connected to element A_{i+1}, so any motion of A_{i+1} is given by A_i [8].

Forward kinematic solution on a kinematic chain can be defined as a sequence matricial of multiplications from base frames to end effector frame, in order to obtain the position and orientation of this last element and is defined as follows:

$$T={}^{0}A_1\ {}^{1}A_2\ {}^{2}A_3 \ldots {}^{n-1}A_n.$$

Where n represent the number of joints used and end effector and A is the matrix representation for ball-and-socket joint:

$$A_{R_{xyz}}(\theta_x,\theta_y,\theta_z)=\begin{bmatrix} C_yC_z & C_yS_z & -S_y & 0 \\ S_xS_yC_z-C_xS_z & S_xS_yS_z+C_xC_z & S_xC_y & 0 \\ C_xS_yC_z+S_xS_z & C_xS_yS_z-S_xC_z & C_xC_y & 0 \\ T_X & T_Y & T_Z & 1 \end{bmatrix} \quad (1)$$

Where x, y and z are the rotation angles respect to X, Y and Z axes respectively [6]. T_X, T_Y and T_Z are the offset vector between current articulation and its predecessor one.

The morphology to every articulation for PUMA 560 is represented using a rotary joint, hence, for this work six ball-and-socket joints were used to represent the joints, taking account only one DOF for this kind of join. Because of the PUMA 560 only has six DOF, the matrix multiplication sequence will be:

$$\mathbf{T={}^{0}A_1\ {}^{1}A_2\ {}^{2}A_3 \ldots {}^{5}A_6.}$$

A. *Inverse kinematic*

To achieve a desired end-effector position (p_x, p_y, p_z) relative to the base frame by means of an articulated movement of the robot joints (q_1,q_2,q_3), we have to find an inverse mapping relating both sets of variables. Also, we have to consider the effect of robot configuration parameters such as links lengths and offsets (e.g., a_i and l_i in Fig. 2) for proper calculations.

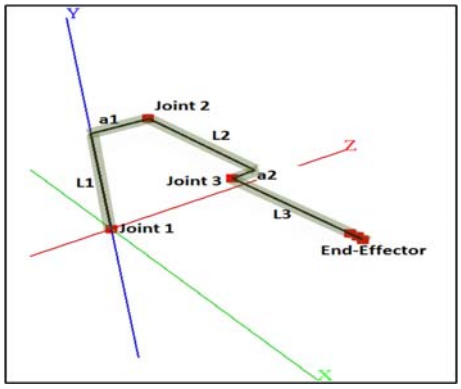

Fig. 2 Kinematic chain parameters for inverse kinematic problem.

As mentioned above, we obtained this mapping, commonly known as the Inverse Kinematics (IK) using a geometric approach. This method involves the planar projection of robot lengths and angles to obtain useful relating triangles in the 3D

space. In order to calculate the first joint angle, let us consider some auxiliary variables:

$$\begin{aligned} r &= \sqrt{p_z^2 + p_x^2 - a_1^2} \\ \alpha_1 &= \arctan\frac{a_1}{r} \\ \phi_1 &= \arctan\frac{p_x}{p_z} \end{aligned}$$

Thus, the first joint angle can be computed as:

$$q_1 = (\phi_1 - \alpha_1) - \left(\frac{\pi}{2}\right) \qquad (2)$$

To obtain the second joint angle, the following auxiliary variables are used:

$$\begin{aligned} R &= \sqrt{p_z^2 + p_x^2 + (p_y - l_1)^2 - a_1^2} \\ \alpha_2 &= \arctan(\frac{(p_y - l_1)}{r}) \\ \beta_2 &= \arctan(\frac{\sin\beta_2}{\cos\beta_2}) \end{aligned}$$

Where $\cos\beta_2 = [l_2^2 + R^2 - (l_3^2 + a_2^2)]/2l_2R$ and by trigonometry relation, $\beta_2 = \pm\sqrt{1 - \cos^2\beta_2}$ sin thus, the second joint angles can be calculated as:

$$q_2 = \alpha_2 + \beta_2 \qquad (3)$$

For the third joint the geometric relations used are:

$$\begin{aligned} \phi_3 &= \arctan\left(\frac{\sin\phi_3}{\cos\phi_3}\right) \\ \beta_3 &= \arctan\left(\frac{l_3}{|a_2|}\right) \end{aligned}$$

Where $\cos\phi_3 = [l_2^2 + (l_3^2 + a_2^2) - R^2/2l_2\sqrt{l_3^2 + a_2^2}]$ and by trigonometry relation $\sin\phi_3 = -\sqrt{1 - \cos^2\phi_3}$ Finally, the third joint angle can be computed as:

$$q_3 = \left(\frac{\pi}{2}\right) - (\phi_3 - \beta_3) \qquad (4)$$

Evidently, this geometric analysis is somewhat complex although there are only 3 DOF. Expanding to more degrees of freedom would turn calculations more complex and harder to compute, but for now we will not tackle that issue.

III. Simulation Environment for Kinematic Problems

The Graphic User Interface (GUI) for PUMA 560 was supported on GEMPA environment [2]. Hence, simulation environment for kinematic problems on PUMA was developed under C++ language with OpenGL Library.

A. *Functionalities*

Important elements behind this developed must be mentioned. As it was described in previous sections, forward kinematic needs six angles as input parameter. However, this values can be set by the user or can be generated from inverse kinematic process. So, there exists a natural relation between forward an inverse kinematic. On the other hand, inverse kinematic parameters can be set form the user or can be computed since PUMA kinematic application.

For this simulation environment, 3D visualization must be supported on matrices transformation that is applied on PUMA geometric model.

B. *Navigation Tools*

GUI is provided of navigation options through the mouse control to allow user operations such as translation, rotation and zoom effects on the 3D environment. Besides, the interface has been divided in three sections. The 3D visualization scenario; forward and inverse kinematic control interface; and PUMA kinematic applications interface.

The 3D visualization scenario. Here, PUMA 560 is painted using a 3D environment. Each link is painted using different color, reference frame *(X, Y, Z)* is included for every articulation so the user can see rotation reference between two consecutive joints. Besides, global reference frame is painted using green color for *X - axes*, blue color red for *Y - axes* and red one for *Z - axes*. On the other hand, values for inverse kinematic parameters are shown when inverse kinematic process is running. This features of visualization scenario can be seen in Figure 4.

Forward and inverse kinematic control interface. A window tool is presented to allows the user iterate with forward an inverse kinematics processes. To manipulate forward kinematic parameters, the tool offers movement's bars to allow the user determine the values for every articulation performing this operation and its visualization on real time. Movement range is restricted to Table 1. Figure 4 presents different position for PUMA model. Below forward kinematic control, a little section to set the inverse kinematic parameters is included, there the user can capture o modify the *(x,y,z)* position of the end effector. Application result will be presented in next section.

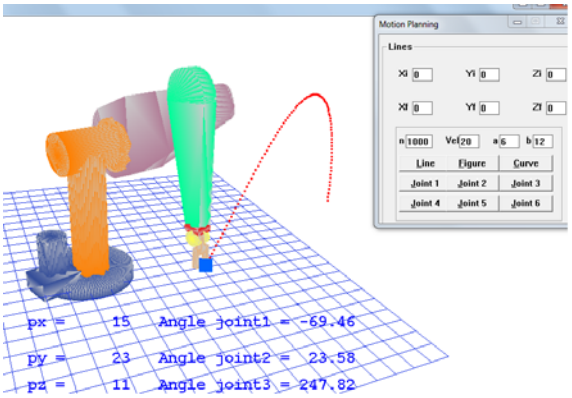

Fig. 4 GUI Model Diagram to Kinematics Operations.

PUMA Kinematic Applications. Initial kinematics applications were developed to test the forward and inverse kinematic process. A window tool is presented to allow the user to choice what kind of figure wants to paint. Figure 5. presents the GUI window interface proposed to select the figure to be painted and to set parameters to move the robot.

Besides, ranges for each join in PUMA 560 can be painted through this window, as it is shown in Figure 5.

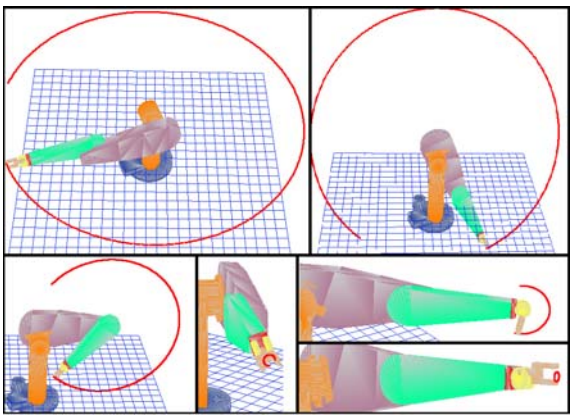

Fig. 5 Operations Ranges for PUMA 560.

IV. PUMA PROTOTYPE

Forward kinematic applications were tested and simulated on graphic environment, but as a important tests were implemented on a physical prototype for a kinematic chain with four DOF. Hence, the project includes the design and built for an articulated robot which is supported on *Dynamixel AX-12* servomotors.

Figure 6. presents the structure and morphology for articulated robot. Distances links and articulation positions can be identified. It is important to mention that each servomotor has been initialized and of course each one has a different operation range (restricted to Table 1). Subroutines capable to perform forward kinematics through programming servomotors were implemented.

Hence, a set of sequences can be send to servomotors to move the robot and simulate the end effector change its configurations from initial value to end value. In Figure 7. two illustrations where articulated robot is placed in different configurations (initial and goal configurations).

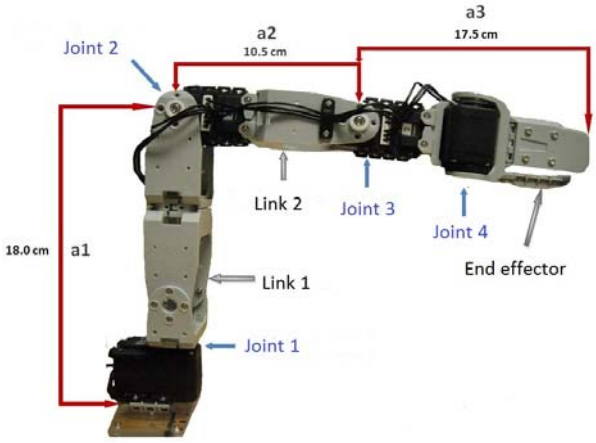

Fig. 6 Prototype representation for articulated robot with 4 DOF.

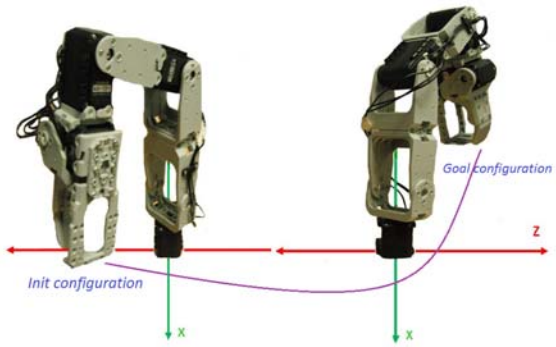

Fig. 7 Articulated robot moves from initial configuration (left side) to goal configuration (right side).

V. CONCLUSIONS AND WORK IN PROGRESS

This paper describes the use of graphic and geometric techniques to support the computation of forward and inverse kinematic problems. These techniques were implemented on PUMA 560 robot, a kinematic chain with six DOF. The implementation became successful and application results were presented in section III. Besides, implementation to forward kinematic was tested on a prototype robot based on Dynamixel AX-12 servomotors using four DOF. Even though, there exist many applications to kinematic chains and graphic simulation environments, this proposal tend to grown until supporting methods capable to solve the inverse kinematics problem to *n*-DOF. Hence, this work represents the essential platform to propose news challenges about inverse kinematic applications. Actually, the *Advanced Computer Perception and Automation Lab* is working on developing algorithms to solve for kinematic chains with more than six DOF.

ACKNOWLEDGMENT

This works was supported for The Program for Improvement the Teaching and Research (PROMEP-MEXICO).

REFERENCES

[1] M. King, B. Zhu, and S. Tang, "Optimal path planning," *Mobile Robots*, vol. 8, no. 2, pp. 520-531, March 2001.
[2] H. Simpson, *Dumb Robots*, 3rd ed., Springfield: UOS Press, 2004, pp.6-9.
[3] M. King and B. Zhu, "Gaming strategies," in Path Planning to the West, vol. II, S. Tang and M. King, Eds. Xian: Jiaoda Press, 1998, pp. 158-176.
[4] B. Simpson, et al, "Title of paper goes here if known," unpublished.
[5] J.-G. Lu, "Title of paper with only the first word capitalized," *J. Name Stand. Abbrev.*, in press.
[6] Y. Yorozu, M. Hirano, K. Oka, and Y. Tagawa, "Electron spectroscopy studies on magneto-optical media and plastic substrate interface," *IEEE Translated J. Magn. Japan*, vol. 2, pp. 740-741, August 1987 [*Digest 9th Annual Conf. Magnetics Japan*, p. 301, 1982].
[7] M. Young, *The Technical Writer's Handbook*, Mill Valley, CA: University Science, 1989.
[8] W. Ademir. Cinemática Directa Aplicada a un Actor Digital. PhD thesis, Universidad Iberoamericana Puebla, 2006.

2011 International Conference on Mechanical, Industrial, and Manufacturing Engineering
Lecture Notes in Information Technology Vols. 1-2

Resilient $H\infty$ control for 2D discrete time delay nonlinear systems in the second FM model

Lai Yongbo, Yan Hui
Department of Electrical Engineering
Jiangsu College of Information Technology
Wuxi ,China
Yongbo100@sina.com

Wei Yiqun
School of city
Jiangsu College of Information Technology
Wuxi ,China
Weiyiqun1234@163.com

***Abstract* - In this paper, it is investigated that the resilient robust $H\infty$ controller design for nonlinear time delay discrete two dimensional (2D) systems in the second FM model, the nonlinear function of systems satisfies Lipschitze condition, based on the robust stability theorem, firstly a sufficient condition of the resilient controller existence is established; then the designing controller which have additive and multiplicative forms are obtained by the linear matrix inequalities(LMI) theory. The designed state feedback controller guarantees the closed loop system is stable and impuls free for time delays and disturbance,which has optimal $H\infty$ performance norm, last a numerical example is provided to demonstrate the effectiveness of the proposed method.**

Index Terms - 2D discrete system;resilient control;H∞;LMI..

I. INTRODUCTION

In the past decades,discrete linear repetitive processes have been applicated in many areas,such as image processing and transmission,thermal processes,gas absorption,etc.Attempts to control these processes using stadard systems stability theory fail,precisely because these approaches ignor their inherent 2D systems structure.A long time the 2D linear discrete systems extensively studied by many researchers[2-15].From *Hinamoto*[1]first appllied the 1D Lyapunov stability theory to the 2D systems and filtering analysis, so far, many results have been reported in the literature , [3,4,5]*I.Trinh H and DU C*, etc.presented robust and real positive control problems for 2D difference systems. Recently,the robust control problem has drawn a great deal of researchers interests,much more significent results have been obtained for the continuous time 2Dcase and discrete 2Dcase[7,12].The guaranteed cost control problem for 2D discrete uncertain systems in the ROESSER model has been considered[6,9,10], furthmore,the 2D disrete systems stability discribed by the FMLSS (Fomasini-Marchesini second state space model) have been investigated extensively[1,7].

The $H\infty$ norm of the system transfer function from the input noise and disturbance to the output is one of popular performance measures in systems control theory.*Chen S. F.*,etc.[9,10,14]discussed $H\infty$ filtering control for uncertain 2-D systems, Up to date,the problem of resilient robust H∞ control for 2D discrete delays systems with nonlinearities and dynamics perturbation has not been fully investigated that the designed nominal controllers should be capable of tolerating some level of controller gain variations,Both $H\infty$ control and resilient control are more successful in solving 2D delayed nonlinear systems control ,this paper deals with the control problem of 2D discrete nonlinear delay systems, which discribed by FMLSS model. In this paper,a sufficient condition of resilient controller is presented,then designed the state feedback additive and multiplicative controller based on the LMIs.

II. PROBLEM FORMULATION

Consider a class of uncertain nonlinear 2D(FMLSS model) delay system,discribled by the following equations:

$$\begin{cases} x(i+1,j+1) = A_1x(i,j+1) + A_2x(i+1,j) + A_3f(\times) + \\ A_{1d}x(i-t_1,j+1) + A_{2d}x(i+1,j-t_2) + B_{11}\omega(i,j+1) \\ +B_{12}\omega(i+1,j) + B_{21}u(i,j+1) + B_{22}u(i+1,j), \\ z(i,j) = Cx(i,j) + D\omega(i,j). \end{cases} \quad (1)$$

where $x(i,j) \in \mathbb{R}^n$, $u(i,j) \in \mathbb{R}^m$ represent the state and control input respectively, $z(i,j) \in \mathbb{R}^p$ is control output, $\omega(i,j) \in \mathbb{R}^q$ is disturbance input,which belongs to $L_2\left\{[0,\infty),[0,\infty)\right\}$, t_1, t_2 are unknown positive interger time delays, $A_1, A_2, A_3, A_{1d}, A_{2d}, B_{11}, B_{12}, B_{21}, B_{22}, C, D$ are appropriate dimensions constant matrices.

In the system (1),the function $f(\times)$ is a class of generalized Lipschitze nonlinearities,satisfies:

Assumption 1:

$f(\times) = f(x(i+1,j), x(i,j+1), x(i+1,j-t_1), x(i-t_2,j+1))$

There exist constant matrices H_1, H_2, H_3, H_4 ,to all $x_1, x_2, x_3, x_4 \in R^n$, the function $f(\times)$ satisfies

$$\left\|f(x_1,x_2,x_3,x_4)\right\| \le \left\|H_1x\right\| + \left\|H_2x\right\| + \left\|H_3x\right\| + \left\|H_4x\right\| \quad (2)$$

It is assumed that the system(1)has a set of initial condition and exist two positive interger l_1, l_2 numbers, such that:

$$\begin{cases} x(i,j) = 0, \forall i \ge l_2, j = -t_2, -t_2+1, ..., 0 \\ x(i,j) = 0, \forall j \ge l_1, i = -t_1, -t_1+1, ..., 0 \end{cases} \quad (3)$$

Definition 1 For the 2D system (1),designed the state feedback resilient controller which to be of the form:

$$u(i,j) = [K + \Delta K]x(i,j) \quad (4)$$

K is the controller gain , ΔK is gain variations and two forms will be considered:

a) Additive controller gain variations:

$$\Delta K = J_1 F(k) E_1 \quad , \; F^T(k)F(k) \le I \tag{4a}$$

b) Multiplicative controller gain variations:

$$\Delta K = J_2 F(k) E_2 K \, , F^T(k)F(k) \le I \tag{4b}$$

where J_1, J_2, E_1, E_2 are know real constant matrices.

Definition 2[15] For the 2D system (1) and the designed resilient controller(4),which have the follow performances:

1.when $\omega(i,j) = 0$,the closed-loop system is asymptoticaly stable.

2.Given scalar $\gamma > 0$ and system (1) zero initial condition,

there exists $\left\| z(i,j) \right\|_2^2 \le \gamma^2 \left\| \omega(i,j) \right\|_2^2$, which

$$\left\| z(i,j) \right\|_2^2 = \sum_{i=0}^{\infty} \sum_{j=0}^{\infty} \left\| \begin{matrix} z(i,j+1) \\ z(i+1,j) \end{matrix} \right\|^2$$

$$\left\| \omega(i,j) \right\|_2^2 = \sum_{i=0}^{\infty} \sum_{j=0}^{\infty} \left\| \begin{matrix} \omega(i,j+1) \\ \omega(i+1,j) \end{matrix} \right\|^2 .$$

For this paper,in the following we introduce a Lemmal

Lemmal 1:[*Schur* complement] For a given matrix

$$S = \begin{bmatrix} S_{11} & S_{12} \\ S_{12}^T & S_{22} \end{bmatrix} \text{ with } S_{11} = S_{11}^T \, , \; S_{22} = S_{22}^T$$

then the following conditions are equivalent:

(1) $S < 0$, (2) $S_{22} < 0, S_{11} - S_{12} S_{22}^{-1} S_{12}^T < 0$.

III. ROBUST H_∞ PERFORMANCE ANALYSIS

From system equation (1) to (4),it follows that the closed-loop system

$$\begin{cases} x(i+1,j+1) = \bar{A}_1 x(i,j+1) + \bar{A}_2 x(i+1,j) + A_3 f(\times) + \\ A_{1d} x(i-t_1, j+1) + A_{2d} x(i+1, j-t_2) + B_{11} \omega(i,j+1) \\ + B_{12} \omega(i+1,j), \\ z(i,j) = Cx(i,j) + D\omega(i,j). \end{cases} \tag{5}$$

where $\bar{A}_1 = A_1 + B_{21}[K + \Delta K], \bar{A}_2 = A_2 + B_{22}[K + \Delta K]$

In this section, we present a sufficient condition of the resilient robust $H\infty$ performance control for the system (5).

Theorem 1: Consider the 2D discrete system (5),if there exist scalar $0 < \alpha < 1$, $\varepsilon > 0$, $\gamma > 0$ positive definite matrices P , $M_1, M_2 \in \mathbb{R}^{n \times n}$ and matrix $K \in \mathbb{R}^{m \times n}$ such that inequality

$$S = \begin{bmatrix} \Omega_1 & \bar{A}_1^T P \bar{A}_2 & \bar{A}_1^T P A_{1d} & \bar{A}_1^T P A_{2d} & \bar{A}_1^T P A_3 \\ * & \Omega_2 & \bar{A}_2^T P A_{1d} & \bar{A}_2^T P A_{2d} & \bar{A}_2^T P A_3 \\ * & * & \Omega_3 & A_{1d}^T P A_{2d} & A_{1d}^T P A_3 \\ * & * & * & \Omega_4 & A_{2d}^T P A_3 \\ * & * & * & * & \Omega_5 \\ * & * & * & * & * \\ * & * & * & * & * \end{bmatrix} \rightarrow$$

$$\leftarrow \begin{bmatrix} B_{11}^T P \bar{A}_1 + C^T D & B_{12}^T P \bar{A}_1 \\ B_{11}^T P \bar{A}_2 & B_{12}^T P \bar{A}_2 + C^T D \\ B_{11}^T P A_{1d} & B_{12}^T P A_{1d} \\ B_{11}^T P A_{2d} & B_{12}^T P A_{2d} \\ B_{11}^T P A_3 & B_{12}^T P A_3 \\ B_{11}^T P B_{11} + D^T D - \gamma^2 I & B_{12}^T P B_{11} \\ * & B_{12}^T P B_{12} + D^T D - \gamma^2 I \end{bmatrix} < 0 \tag{6}$$

here $\Omega_1 = \bar{A}_1^T P \bar{A}_1 - \alpha P - M_1 + \varepsilon H_1^T H_1 + C^T C$

$\Omega_2 = \bar{A}_2^T P \bar{A}_2 - \alpha P - M_2 + \varepsilon H_2^T H_2 + C^T C$,

$\Omega_3 = A_{1d}^T P A_{1d} - M_1 + \varepsilon H_3^T H_3$

$\Omega_4 = A_{2d}^T P A_{2d} - M_2 + \varepsilon H_4^T H_4$

$\Omega_5 = A_3^T P A_3 - \varepsilon I$

holds for all state delays,then the closed-loop system is asymptotical stable ,and the controller (4) is a state feedback resilient $H\infty$ controller for 2D system (1).

Proof: firstly,we define Lyapunov function as follow

$$V(x(i,j) = V_1(x(i,j) + V_2(x(i,j)$$

$$= [x^T(i,j) P x(i,j) + \sum_{l=-d_1}^{-1} x^T(i+l,j) M_1 x(i+l,j)]$$

$$+ [x^T(i,j) \alpha P x(i,j) + \sum_{l=-d_2}^{-1} x^T(i,j+l) M_2 x(i,j+l)] \tag{7}$$

It is obviously $V(x(i,j)) > 0$, when $\omega(i,j) = 0$,taking the Lyapunov function difference along any trajectory of the closed loop system (5) with inequality (2) is given by

$$\Delta V(i+1,j+1) = V_1(x(i+1,j+1) + V_2(x(i+1,j+1)$$

$$- V_1(x(i,j+1) - V_2(x(i+1,j)$$

$$\le \bar{\xi}(i,j) \left(\begin{bmatrix} \bar{A}_1^T \\ \bar{A}_2^T \\ A_{1d}^T \\ A_{2d}^T \\ A_3^T \end{bmatrix} P \begin{bmatrix} \bar{A}_1^T \\ \bar{A}_2^T \\ A_{1d}^T \\ A_{2d}^T \\ A_3^T \end{bmatrix}^T + \begin{bmatrix} \bar{\Omega}_1 & 0 & 0 & 0 & 0 \\ * & \bar{\Omega}_2 & 0 & 0 & 0 \\ * & * & \bar{\Omega}_3 & 0 & 0 \\ * & * & * & \bar{\Omega}_4 & 0 \\ * & * & * & * & \bar{\Omega}_5 \end{bmatrix} \right) \bar{\xi}^T(i,j) \tag{8}$$

Here

$$\bar{\xi}(i,j) = [x(i,j+1), x(i+1,j), x(i-t_1, j+1),$$

$$x(i+1, j-t_2), f(*)]$$

$\bar{\Omega}_1 = -\alpha P - M_1 + \varepsilon H_1^T H_1$

$\bar{\Omega}_2 = -\alpha P - M_2 + \varepsilon H_2^T H_2, \bar{\Omega}_3 = -M_1 + \varepsilon H_3^T H_3$

$\bar{\Omega}_4 = -M_2 + \varepsilon H_4^T H_4, \bar{\Omega}_5 = -\varepsilon I$.

From inequality (6),by ***schur*** complement,we can obtain

$$\begin{bmatrix} \bar{A}_1^T \\ \bar{A}_2^T \\ A_{1d}^T \\ A_{2d}^T \\ A_3^T \end{bmatrix}^T P \begin{bmatrix} \bar{A}_1^T \\ \bar{A}_2^T \\ A_{1d}^T \\ A_{2d}^T \\ A_3^T \end{bmatrix} + \begin{bmatrix} \bar{\Omega}_1 & 0 & 0 & 0 & 0 \\ * & \bar{\Omega}_2 & 0 & 0 & 0 \\ * & * & \bar{\Omega}_3 & 0 & 0 \\ * & * & * & \bar{\Omega}_4 & 0 \\ * & * & * & * & \bar{\Omega}_5 \end{bmatrix} < 0 \quad (9)$$

then it follows from the inequality (8) that

$$\Delta V(i+1, j+1) < 0 \quad (10)$$

So the system (5) is asymptoticaly stable.

Next we will give the *H*∞ performance γ analysis, considering the disturbenc input $\omega(i, j) \in \mathbb{R}^q$ and control input $u(i, j) = 0$,we have

$$J_\infty = \sum_0^\infty \sum_0^\infty \left\{ \Delta V(i+1, j+1) + \begin{bmatrix} z(i, j+1) \\ z(i+1, j) \end{bmatrix}^T \begin{bmatrix} z(i, j+1) \\ z(i+1, j) \end{bmatrix} \right.$$

$$\left. -\gamma^2 \begin{bmatrix} \omega(i, j+1) \\ \omega(i+1, j) \end{bmatrix}^T \begin{bmatrix} \omega(i, j+1) \\ \omega(i+1, j) \end{bmatrix} \right\} = \sum_0^\infty \sum_0^\infty \xi(i, j)^T S \xi(i, j) \quad (11)$$

here $\xi(i, j) = [x(i, j+1), x(i+1, j), x(i-t_1, j+1),$

$x(i+1, j-t_2), f(*), \omega(i, j+1), \omega(i+1, j)]$

By LMI (6),it can be obtained the equation (11) $J_\infty < 0$.

Using system initial condition (3),we can derive

$$\sum_{i=0}^\infty \sum_{j=0}^\infty \left\| \begin{matrix} z(i, j+1) \\ z(i+1, j) \end{matrix} \right\|^2 < \gamma^2 \sum_{i=0}^\infty \sum_{j=0}^\infty \left\| \begin{matrix} \omega(i, j+1) \\ \omega(i+1, j) \end{matrix} \right\|^2 \quad (12)$$

Which has $\left\| z(i, j) \right\|_2^2 \le \gamma^2 \left\| \omega(i, j) \right\|_2^2$.

This completes the proof of the Theorem1.

Now, we are in a position for the solvability of the robust resilient H_∞ performance control of the proposed problem.

Theorem 2 :For 2D discrete system (1),if there exist positive scalar $\alpha > 0, \varepsilon > 0$, $\gamma > 0$ matrix $X \in \mathbb{R}^{m \times n}$ and symmetric positive matrices $\bar{P}, \bar{M}_1, \bar{M}_2 \in \mathbb{R}^{n \times n}$ such that the following LMI (13) holds,

$$\begin{bmatrix} \Omega_{11} & \Omega_{12} & \Omega_{13} \\ * & \Omega_{22} & 0 \\ * & * & \Omega_{33} \end{bmatrix} < 0 \quad (13)$$

then the system (5) has a state feedback suboptimal H_∞ resilient controller (4) with respect to the additive gain variations:

$$u(i, j) = (X\bar{P}^{-1} + J_1 F E_1) x(i, j) \quad (14)$$

here $\Omega_{11} = -diag[\bar{P}, \alpha\bar{P}, \bar{M}_1, \bar{M}_2, \gamma^2 I, \gamma^2 I]$

$\Omega_{22} = -diag[\bar{P}, \varepsilon I, \varepsilon I, \varepsilon I, \varepsilon I]$

$\Omega_{33} = -diag[I, I, I, I, I, I]$

$$\Omega_{12} = \begin{bmatrix} A_1^T \bar{P} + B_{21}^T X & H_1 & 0 & 0 & 0 \\ A_2^T \bar{P} + B_{22}^T X & 0 & H_2 & 0 & 0 \\ A_{1d}^T \bar{P} & 0 & 0 & H_3 & 0 \\ A_{2d}^T \bar{P} & 0 & 0 & 0 & H_4 \\ A_3^T \bar{P} & 0 & 0 & 0 & 0 \\ 0 & 0 & 0 & 0 & 0 \end{bmatrix}$$

$$\Omega_{13} = \begin{bmatrix} \bar{P}C^T & 0 & \bar{P}B_{21}J_1 & 0 & \bar{P}E_1 & 0 \\ 0 & \bar{P}C^T & 0 & \bar{P}B_{22}J_1 & 0 & \bar{P}E_1 \\ 0 & 0 & 0 & 0 & 0 & 0 \\ 0 & 0 & 0 & 0 & 0 & 0 \\ D^T & 0 & 0 & 0 & 0 & 0 \\ 0 & D^T & 0 & 0 & 0 & 0 \\ 0 & 0 & 0 & 0 & 0 & 0 \end{bmatrix}$$

***Proof*:** according the *Theorem 1* and repetitive applying *Schur* complement,the inequality (6) can be rewritten as

$$\begin{bmatrix} \bar{\Omega}_{11} & \bar{\Omega}_{12} & \bar{\Omega}_{13} \\ * & \bar{\Omega}_{22} & 0 \\ * & * & \bar{\Omega}_{33} \end{bmatrix} < 0 \quad (15)$$

here $\bar{\Omega}_{11} = -diag[P, \alpha P, M_1, M_2, \gamma^2 I, \gamma^2 I]$

$\bar{\Omega}_{22} = -diag[P, \varepsilon I, \varepsilon I, \varepsilon I, \varepsilon I]$

$\bar{\Omega}_{33} = -diag[I, I, I, I, I, I]$

$$\bar{\Omega}_{12} = \begin{bmatrix} A_1^T + K^T B_{21}^T & H_1 & 0 & 0 & 0 \\ A_2^T + K^T B_{22}^T & 0 & H_2 & 0 & 0 \\ A_{1d}^T & 0 & 0 & H_3 & 0 \\ A_{2d}^T & 0 & 0 & 0 & H_4 \\ A_3^T & 0 & 0 & 0 & 0 \\ 0 & 0 & 0 & 0 & 0 \end{bmatrix}$$

$$\bar{\Omega}_{13} = \begin{bmatrix} PC^T & 0 & PB_{21}J_1 & 0 & PE_1 & 0 \\ 0 & PC^T & 0 & PB_{22}J_1 & 0 & PE_1 \\ 0 & 0 & 0 & 0 & 0 & 0 \\ 0 & 0 & 0 & 0 & 0 & 0 \\ D^T & 0 & 0 & 0 & 0 & 0 \\ 0 & D^T & 0 & 0 & 0 & 0 \\ 0 & 0 & 0 & 0 & 0 & 0 \end{bmatrix}$$

Now, pre-and post-mutiplying both side of inequality (15) by $diag[P^{-1}, ..., P^{-1}, I, ..., I]$, and denoting

$\bar{P} = P^{-1}, \bar{M}_1 = \bar{P}M_1\bar{P}, \bar{M}_2 = \bar{P}M_2\bar{P}, X = K\bar{P}$

we can obtain inequality (13).

This end the proof.

In addition, by solving the following optimization problem:

$$\begin{cases} \min\limits_{\alpha,\bar{P},\bar{M}_1,\bar{M}_2,X} \gamma^2 \\ s.t.(13) \end{cases} \tag{16}$$

We can obtain a state feedback resilient controller such that the H_∞ attenuation norm γ is minimized, and the controller (14) is said to be the optimal H_∞ controller for the 2D system (1).

Remark: 1. In the inequality (13) we substitute J_2, E_2 for J_1, E_1 ,which have the multiplicative controller form $u(i,j) = [I + J_2 F E_2] X \bar{P}^{-1} x(i,j)$.

2.The results proposed here are static independent of the delays,The approach of this paper can be applied to the discrete uncertain 2D systems with unknown time varying delays.

Numerical Example

Conside the 2D discrete nonlinear delays system (1) with parameters as follow:

$$A_1 = \begin{bmatrix} 0.3 & 0 \\ 0.2 & 0.1 \end{bmatrix}, A_2 = \begin{bmatrix} 0.2 & 0 \\ 0.1 & 0.2 \end{bmatrix}, A_3 = \begin{bmatrix} 0.1 & 0 \\ 0.2 & 0.2 \end{bmatrix}$$

$$A_{1d} = \begin{bmatrix} 0.01 & 0 \\ 0 & 0.01 \end{bmatrix}, A_{2d} = \begin{bmatrix} 0.02 & 0 \\ 0 & 0.01 \end{bmatrix},$$

$$B_{11} = \begin{bmatrix} 0.2 \\ 0.04 \end{bmatrix}, B_{12} = \begin{bmatrix} 0.1 \\ 0.04 \end{bmatrix}, B_{21} = \begin{bmatrix} 0.1 \\ 0 \end{bmatrix}, B_{22} = \begin{bmatrix} 0 \\ 0.1 \end{bmatrix}$$

$$C = \begin{bmatrix} 1 & 1 \end{bmatrix}, D = 0.5$$

$$J_1 = 0.12, J_2 = 0.15, E_1 = -0.1, E_2 = 1.0$$

The nonlinear function $f(*)$ satisfing assumption 1:

$$H_1 = H_2 = \begin{bmatrix} -1 & 1 \\ 0 & 0 \end{bmatrix}, H_3 = H_4 = \begin{bmatrix} 1 & -1 \\ 0 & 0 \end{bmatrix}$$

Applying the methods proposed in Theorem 2,and solving the optimization problem (16) by the LMI toolbox of Matlab,we can compute an optimal solution as:

$\alpha = 0.35$, $\varepsilon = 10.095$, $\gamma = 0.8650$, the additive controller gain $K = [-2.1895 \quad -6.1907]$, the multiplicative controller gain $K = [-2.2546 \quad -5.9975]$.

Assuming LMI (13) $J_1 = J_2 = E_1 = E_2 = 0$ the designed controller $K = [-2.8167 \quad -8.0570]$, and the H_∞ performance norm $\gamma = 0.9946$, the resilient control performance norm decreased 13%, which the design approach of this paper is effective.

IV. CONCLUSIONS

This paper considered the design problem of resilient robust $H\infty$ performance controller for a class of uncertain 2D discrete systems with time delays. By linear matrix inequalities(LMIs) approach and matrix Schur complement, A sufficient condition of the existence of the state feedback robust controller is established. Then a suboptimal resilient controller is obtained, using the proposed method and system transformation, an optimal controller could be solvable. Then given a numerical example to demonstrate the proposed design method is effective.

REFERENCES

[1] HINAMOTO T. 2D Lyapunov equation and filter design based on the Formasini-Marchesini second model [J]. IEEE Taans on circuits Systems,1993,40(1),pp:102-110.

[2] R N, Bracewell.Two dimensional Imaging,Prenstice-Hall,signal Processing Series,Prentice-Hall,Englewood,Cliffs,NJ,1995.

[3] I. Trinh H, Fernando T. Some new stability conditions for two dimensional difference systems [J]. Int J of system science,2000,31(2),pp:203-211.

[4] DU C,XIE L.Stability analysis and stabilization of 2D discrete systems [J] Int J Control,1999,72(2):,pp:97-106.

[5] Trinh H,Fernando T.Some new stability conditions for two dimensional difference systems [J].Int J of Systems Science,2000, 31(2),pp:203-211.

[6] GUAN X P, LONG C N, DUAN G R.Robust optimal guaranteed cost for 2D discrete systems J. IEE Pro Control Theory and applications,2001,148(5),pp:355-361.

[7] H.Kar, V.Singh,Stability analysis of 2D digital filters discribed by the Fornanisi-Marchesini second model using overflow nonlinearities, IEEE Trans Circuits Systems I 2001(48),pp:612-617.

[8] Chen S. F., Fong I.K.Delay dependent robust *H*∞filting for uncertain 2-D state-delayed systems[J].Signal processing,2007,87(11),pp:2659-2672.

[9] Xu S,Lam J,Lin Z Positive real control for uncertain two dimensional systems[J].IEEE Transactions on circuits and systems I Foundamental theory and Applications,2002,49(11),pp:1659-1666.

[10] Wojciech P, James L,Krzysztofg,Robust stability and stabilization of 2D discrete state-delayed systems[J].Systems & Control Letters,2004, 51(2),pp:277-191.

[11] Galkowski., Lam J,Rogers E,Xu S.,etc..LMI based stability analysis and robust controller design for discrete linear repetitive processer [J].International Journal of Robust Nonlinear control,2003,13(13), pp:1195-1211.

[12] A.Dhawan, H.Kar,Optimal guaranteed cost control of 2Ddiscrete uncertain systems:An LMI approach,Signal Processing,2007(87), pp:3075-3085

[13] Shi J.,Gao F., Wu T.J.From two-dimensional Linear quadratic optimal control to iterative learning control.Paper1[J] Industrial and engineering Chemistry Research,2006,45(13),pp:4603-4616.

[14] Wu L.,Wang Z.,Gao H. Filtering for uncertain 2D discrete sysyems with state delays.[J] ,Signal Processing,2007,87(11),pp:2213-2230.

[15] Xu Jian-Ming, Yu Li. *H*∞Control for 2-D Discrete State Delayed Systems in the Second FM Model[J],ACTA AUTOMATICA SINICA,2008,Vol34,No.7,PP:809-813.

2011 International Conference on Mechanical, Industrial, and Manufacturing Engineering
Lecture Notes in Information Technology Vols. 1-2

A Forecast Model of the Speed Change of Tornado Based on Function Singular Rough Sets

Wei,Ling-ling，
(Department of Computer of JiangXi BlueSky University, NanChang JiangXi 330029)
E-mail:rainweiling@163.com

Yang Wei
(Department of Computer of JiangXi BlueSky University, NanChang JiangXi 330029)
E-mail:yangwei@163.com

Abstract: The Tornado speed is estimated according to its path length and width, but sometimes the information detected by the Dopper radar has shown the fact that there are not directly relation between the speed rank of Tornado with its path length and width. Although the forecast of the speed rank is accurate, the Tornado speed may change owing to various influences from some unknown factors. The Rough Sets is a new and effective tool for dealing with uncertain knowledge, and singular rough sets is the extension of Rough Sets. In this paper, based on function singular rough sets a forecast model of the change of Tornado speed is presented in the complex condition.

Keywords: Function Singular Rough Sets; Tornado; Path Length; Path Width

Ⅰ.Introduction

It is application widely in many domains from the mathematician Z.Pawlak of the Poland put forward the rough sets in 1982. Because the sets X ($X \subset U$) is considered a static state in rough sets, but there are many dynamic data sets in the real word. So Shi Kai-Quan professor was put forward the conception of singular rough sets in 2002[1][4], the sets X ($X \subset U$) is regarded as dynamic that there are one direction dynamic $X=X^{\circ}$ or two direction dynamic $X=X^{*}$ in the singular rough sets. In the static-dynamic frame of sets, the rough sets of Z.Pawlak is special example of the singular rough sets, and singular rough sets is common form of it. In the system of fact application, it have some outside interferential factors that it can not forecast in advance, but can forecast the influence of the system will tend towards when its happen. In this paper, it is use a real example that forecast of tornado. There are known that the damage degree is related with the intension of the tornado, and the intension of tornado can be estimate by maximum wind power, path length and width. It may change the rank or intensity of the tornado because of the influence of other unknown factors. If it is forecast the rank and intensity by apply with the theory and method of rough sets in the static state, it is very difficult to obtain the satisfactory forecast result. Therefore it is put forward a new method for the tornado forecast, the method is research the rank and intensity of tornado by use function singular rough sets in this paper.

Ⅱ.Conception of Function Singular Rough Sets

Before it is introduced some symbols that will be use below :Function equivalence classes [u(x)] denoted as [u],Function u(x) and v(x)denoted as u and v；Function domain D(x)denoted as D, Function sets Q(x) ($Q(x)=\{u(x)1,u(x)2,\ldots,u(x)m\} \subset D$ (x)) denoted as Q ($Q=\{u1,u2,\ldots,um\} \subset D$). Function singular sets are classified function one direction singular rough sets and two direction singular rough sets.

A. the Function one direction singular rough sets

Definition 1: Let D is function domain, $Q=\{u_1,u_2,\ldots,u_m\} \subset D$ is function sets, if it has and $v \overline{\in} Q$，v turn to in action of it is called function move of D, and $F=\{f_1,f_2,\ldots,f_m\}$ is

called a function move family of D; or $\exists v\in D$, $v\overline{\in} Q\Rightarrow f(v)=u\in Q$.

Definition 2: Let $Q \subset D$, if $Q^{\circ}=Q\cup\{v|v\in D, v \overline{\in} Q, f(v)=u\in Q\}$ then Q° is called the one direction singular function sets of the Q, and Q^f is called f-expand of the Q，and that $Q^f=\{u|v\in D, v\overline{\in} Q, f(v)=u\in Q\}$.

B. the Function two direction singular rough sets

Definition 3 : Let D is function domain, $Q=\{u_1,u_2,\ldots,u_m\}\subset D$ is function sets, if it has $\overline{f}\in\overline{F}$ that made u_j turn to $\overline{f}(u_j)=v_j\overline{\in}Q$ and $v\overline{\in}Q$，v turn to in action o in action $\overline{f}$ is called function move in domain D, $F=\{f_1,f_2,\ldots,f_m\}$，$\overline{F}=\{\overline{f}_1,\overline{f}_2,\ldots,\overline{f}_n\}$ are called the function move family in domain D; or

$\exists v\in D, v\overline{\in} Q\Rightarrow f(v)=u\in Q$,

$\exists u_j\in Q\Rightarrow \overline{f}(u_j)=v_j\overline{\in}Q$

Definition 4: Let $Q\subset D$, if

$Q^*=Q'\cup\{v|v\in D, v\overline{\in} Q, f(v)=u\in Q\}$,

$Q'=Q-\{u\,|\,u\in Q, \overline{f}(u)=u\overline{\in}Q\}$ then Q^* is called the two direction singular function sets of Q; $Q^{\overline{f}}$ is called $\overline{f}$-shrink，moreover $Q^{\overline{f}}=\{u\,|\,u\in Q, \overline{f}(u)=v\overline{\in}Q\}$.

III Forecast of the Tornado

A. the estimate of the rank of wind speed

According to the character and trait of the history tornado, scientist estimated the damage degree is related to the intensity of tornado that decision by the most wind power(V_{max})、path length[L] and width[W][2]. Fujita was divided path length and width into six grade and denoted as 0~5, which is called Fujita grade (eg table1).

Table1 Fujita grade

Grade(F)	Most wind speed(V_{max})	Path length(Pl)	Path width(Pw)	damage grade
F0	18.0-32.2m/s	0.6-1.5km	5-15m	light destroy
F1	32.3-50.1m/s	1.6-5.0km	16-50m	middle destroy
F2	50.2-70.2m/s	5.1-16.0km	51-160m	Large destroy
F3	70.3-92.1m/s	16.1-50km	0.2-0.5km	severity mar
F4	92.2-116.2m/s	51-160km	0.6-1.5km	truculency mar
F5	>116.3m/s	161-507km	1.6-5.0km	uncertain destroy

And there are below relation form:

$L=1.61*10^{(Pl-1)/2}$ (km) (1)

$W=1.61*10^{(Pw-5)/2}$ (km) (2)

$V_{max}=6.30*(F+2)^{3/2}$ (m/s) (3)

Where F is determined by the surface wind speed V_{max}, Pl and Pw is determined by the path length and width of tornado. It can calculated the F，Pl and Pw by formula（1）、（2）、（3）.

Note: Sometimes the information returned from the Doppler radar are showed the path length and width, according to Fujita-grade calculated there are distributed in different grade. In this case, we consider all possible values taken to estimate the maximum grade of tornado.

B. The forecast of the rank change of wind speed

Let [u] is function equivalence classes of α-,and $[u]=\{u_1,u_2,\ldots,u_m\}$;α is attribute sets of [u][1], and $\alpha=\{\alpha_1,\alpha_2,\ldots,\alpha_k\}$, if $\alpha^*=\{\alpha_1,\alpha_2,\ldots\alpha_k,\alpha_{k+1},\ldots,\alpha_{k+\lambda}\}$then the [u]turn to $[u]^*$,and $[u]^*=\{u_1,u_2,\ldots,u_n\}\subset\{u_1,u_2,\ldots,u_m\}=[u]$；or if $card(\alpha)\leqq card(\alpha^*)$ then $card([u]^*)\leqq card([u])$, and attribute $\alpha_{k+1},\alpha_{k+2},\ldots,\alpha_{k+\lambda}$ are called confounding attributes, confounding factors are inevitable in the weather forecast.

Here are the one direction function singular rough sets in the change of wind speed rank..Let T is system for the wind speed rank forecast of

tornado. And it have attribute sets $\alpha=\{\alpha_1,\alpha_2,\ldots,\alpha_k\}$;the behavior state of T can be donate by $u_1,u_2,\ldots,u_m$; and that make up of the α-function equivalence classes of [u],

and [u]={u1,u2,…,um} (4)

Where $u_j \in [u]$ is the behavior state of the jth subsystem of T, $u_j$at the time $[t_1,t_n]$ is a data form on:

$$u_j=\{u_{j,1},u_{j,2},\ldots,u_{j,n}\} \quad (5)$$

$u_{j,\lambda}$ $_j$ that u_j is a eigenvalue of at t_λ $_1$,t_n].

From the above formula (4)and (5) is obtained data point row:

$(1,y_1),(2,y_2),\ldots,(n,y_n)$,where

$$y_p=\sum_{k=1}^{m} u_{k,j},\ j\in(1,2,\ldots,n),\ p=1,2,\ldots,n$$

By Lagrange interpolation function P(X) ，

$$P(x)=\sum_{j=1}^{n+1} y_j \prod_{i\neq j}\frac{x-x_i}{x_j-x_i}$$

Gained

$$P(x)=a_n x^n+a_{n-1}x^{n-1}+\ldots+a_1 x+a_0 \quad (6)$$

Formula (6) is a rough rule of prediction system of tornado with wind speeds , Because the wind speed rank may be effected by other environmental factors, made at any point t, attribute sets α turn to $\alpha^*=\{\alpha_1,\alpha_2,\ldots,\alpha_k,\alpha_{k+1},\ldots\alpha_{k+\lambda}\}$,and α-function equivalence classes [u] turn to[u]* of the system T,and that [u]*={u1,u2,…,uk+λ}

(7)

From above can be find card([u]*)<card([u])，system T rough rule change from P(x) to Q(y),

$$Q(y)=b_n y^n+b_{n-1}y^{n-1}+\ldots+b_1 y+b_0 .$$

Where Q(y) is the change rank and intensity of the tornado that at confounding of attribute sets $\{\alpha_{k+1},\alpha_{k+2},\ldots,\alpha_{k+\lambda}\}$.

Ⅳ Conclution

In this essay, it is forecast the tornado change at the influence of unknown factors by use function singular rough sets. It is taken the unknown factors as attribute joined with the known factor as attribute in forecast, and forecast the trends of the tornado once again, so it can better hold the extent of disasters caused by the tornado. From the characteristics of function S-rough sets, in addition to the weather forecast, it is very broad application prospects, for medical care, the use of products and so on.

References:

[1] Shi kai-quan,Cui yu-quan. Singular rough sets and rough decision[M].BeiJing:science press,2006.(in chinese)

[2] Wang feng-yun.,application analysis of single Doppler radar image[J].Journal of Tropical Meteorology,2003,(3):1-12.(in chinese).

[3] Liu qing,rogh sets and rough Reasoning[M].BeiJing: science press,2001.(in chinese)

[4] Shi kai-quan.function rough sets and system law mining [J]. computer science,2005,(8A):1-3.

2011 International Conference on Mechanical, Industrial, and Manufacturing Engineering
Lecture Notes in Information Technology Vols. 1-2

Dynamics of a system of two nonlinear difference equations

Qianhong Zhang

Guizhou Key Laboratory of Economics System Simulation
Guizhou College of Finance and Economics
Guiyang, Guizhou Province 550004,.China
zqianhong68@163.com

Daixi Liao

Basic Science Department
Hunan Institute of Technology
Hengyang, Hunan Province,421002, China
liaodaixizaici@sohu.com

***Abstract* - In this paper, we study the global behavior of positive solution for a system of two nonlinear difference equations**

$$x_{n+1}=\frac{x_n}{A+\sum_{i=0}^{k}a_i y_{n-i}},\quad y_{n+1}=\frac{y_n}{B+\sum_{i=0}^{k}b_i x_{n-i}},\quad n=0,1,2,\cdots,$$

where $k\in\{0,1,2,\cdots,\}, A,B,a_i,b_i\in(0,\infty)$,

$x_{-k},\cdots,x_{-1}\in[0,\infty)$, $y_{-k},\cdots,y_{-1}\in[0,\infty)$.

We prove the unique positive equilibrium is globally attractor but unstable.

Index Terms - Difference equation; Global attractor; Unstable

I. INTRODUCTION

In this paper, we investigate the global behavior of solutions of the following system

$$x_{n+1}=\frac{x_n}{A+\sum_{i=0}^{k}a_i y_{n-i}},\quad y_{n+1}=\frac{y_n}{B+\sum_{i=0}^{k}b_i x_{n-i}},\quad n=0,1,2,\cdots, \quad (1)$$

and

$$A,B,a_i,b_i\in(0,\infty),\ k\in\{0,1,2,\cdots,\} \quad (2)$$

The initial conditions

$$x_{-k},\cdots,x_{-1}\in[0,\infty),\ y_{-k},\cdots,y_{-1}\in[0,\infty);$$

$$\sum_{i=0}^{k}a_i\bar{x}(k-1)\le 1\ x_0,y_0\in(0,\infty).$$

In Sys.(1) if $A=B;a_i=b_i;x_n=y_n$, then Sys.(1) can be rewritten as the following difference equation

$$x_{n+1}=\frac{x_n}{A+\sum_{i=0}^{k}a_i x_{n-i}},\quad n=0,1,2,\cdots, \quad (3)$$

where

$$A,a_i\in(0,\infty),k\in\{0,1,2,\cdots\} \quad (4)$$

The equilibria of Eq.(3) is the solution of the following equation

$$\bar{x}=\frac{\bar{x}}{A+\sum_{i=0}^{k}a_i\bar{x}},$$

So $\bar{x}=0$ is always an equilibrium, and when

$$A<1 \quad (5)$$

Eq.(3) has a unique positive equilibrium

$$\bar{x}=\frac{1-A}{\sum_{i=0}^{k}a_i}$$

Kocic. et al.[6] have studied the stability of all positive solution of Eq.(3) under certain conditions. We summarize the results as follows

Theorem 1. [6] Assume that (4) holds. Then the following statements are true.

(i) Assume that $A<1$. Then every positive solution of Eq.(3) decreases zero.

(ii) Assume that (5) holds. Then Eq.(3) is permanent.

(iii) Assume that (5) holds, and one of the following three conditions is satisfied:

$$(a)\quad \sum_{i=0}^{k}a_i\bar{x}k\le 1;$$

$$(b)\quad \sum_{i=0}^{k}a_i\bar{x}k\le 1+a_0\bar{x};$$

$$(c)\quad \sum_{i=0}^{k}a_i\bar{x}(k-1)\le 1;$$

Then $\bar{x}$ is a global attractor of all positive solutions of Eq.(3)

If $n=-k,-k+1,\cdots,$, then Eq.(3) becomes to

$$x_{n+1}=\frac{x_n}{A+a_0x_n},n=0,1,\cdots, \quad (6)$$

which also has been investigated in [3], and whose global behavior of solutions is described as follows.

Theorem 2.[3] Assume that (4) and (5) hold, then the unique positive equilibrium $\bar{x}$ of Eq.(6) is globally asymptotically stable.

Furthermore, in 2007, L. X. Hu and W. T. Li [10] have investigated an open problem [6], i. e., Let $A,a_i\in(0,\infty)$, $i=0,1,\cdots,k$. the global asymptotical stability of the equilibrium points of Eq.(2) with positive initial conditions. Other related results can refer to [1,2,4,5,7-9].

Motivated by above discussion, we study the global behavior all positive solutions of Sys.(1) under certain conditions.

A pair of sequences of positive real numbers $\{(x_n,y_n)\}$ that satisfies Sys.(1) is a positive solution of Sys.(1). The equilibria $(\bar{x},\bar{y})$ of Sys.(1) is the solution of the following

equation

$$\overline{x}=\frac{\overline{x}}{A+\sum_{i=0}^{k}a_i\overline{y}},\quad \overline{y}=\frac{\overline{y}}{B+\sum_{i=0}^{k}b_i\overline{x}} \tag{7}$$

A positive solution $\{(x_n, y_n)\}$ of Sys.(1) is bounded and persists if there exist positive constants M, N such that

$$M \le x_n \le N,\ M \le y_n \le N,\quad n=-k,-k+1,\cdots,$$

II. MAIN RESULT

In this section we study the global behavior of positive solution of Sys.(1).

Theorem 3 Considering the system of difference equations (1). Then the following statements are true.

(i) Assume that (2) holds and

$$A<1, B<1 \tag{8}$$

Then Sys.(1) has a unique positive equilibrium $(\overline{x}, \overline{y})$ with

$$\overline{x}=\frac{1-B}{\sum_{i=0}^{k}b_i},\quad \overline{y}=\frac{1-A}{\sum_{i=0}^{k}a_i}$$

(ii) Every positive solution converges to the unique positive Equilibrium $(\overline{x}, \overline{y})$ as

$$\begin{cases} x_{n+1}=\frac{x_n}{A+a_0y_n}<\frac{x_n}{A}<x_n \\ y_{n+1}=\frac{y_n}{B+b_0x_n}<\frac{y_n}{B}<y_n \end{cases} n\to\infty.$$

Proof. (i) Let $(\overline{x}, \overline{y})$ satisfy (7). By simply calculating and noting (8) we have

$$\overline{x}=\frac{1-B}{\sum_{i=0}^{k}b_i},\quad \overline{y}=\frac{1-A}{\sum_{i=0}^{k}a_i}$$

from which it follows that $(\overline{x}, \overline{y})$ is a unique positive equilibrium of Sys.(1).This completes the proof of (i).

(ii) Let (x_n, y_n) be a positive solution of Sys.(1). Set

$$l_1=\liminf_{n\to\infty} x_n,\ l_2=\liminf_{n\to\infty} y_n,$$

$$L_1=\limsup_{n\to\infty} x_n,\ L_2=\limsup_{n\to\infty} y_n \tag{9}$$

from (1) and (9), we have

$$l_1\ge\frac{l_1}{A+\sum_{i=0}^{k}a_iL_2},\ l_2\ge\frac{l_2}{B+\sum_{i=0}^{k}b_iL_1},$$

$$L_1\le\frac{L_1}{A+\sum_{i=0}^{k}a_il_2},\ L_2\le\frac{L_2}{B+\sum_{i=0}^{k}b_il_1}.$$

from which it follows that

$$l_1=\frac{1-B}{\sum_{i=0}^{k}b_i}=L_1,\ \ l_2=\frac{1-A}{\sum_{i=0}^{k}a_i}=L_2 \tag{10}$$

It is obvious that

$$\lim_{n\to\infty}x_n=\overline{x},\ \lim_{n\to\infty}y_n=\overline{y}$$

This proves that the unique equilibrium $(\overline{x}, \overline{y})$ is a global attractor of all positive solutions of Sys.(1). This completes the proof of (ii).

Next we study the behavior of solution (x_n, y_n) of Sys.(1) about the equilibrium $(\overline{x}, \overline{y})$ .Firstly we consider the following system.

$$x_{n+1}=\frac{x_n}{A+a_0y_n},\quad y_{n+1}=\frac{y_n}{B+b_0x_n},\quad n=0,1,\cdots, \tag{11}$$

Theorem 4. Consider the difference equation system (11). Then the following statements are true

(i) Assume that (8) holds . Then system (11) has a unique positive equilibrium $\overline{x}=\frac{1-B}{b_0},\ \overline{y}=\frac{1-A}{a_0}$

(ii) Assume that (8) holds . Then the unique positive equilibrium $(\overline{x}, \overline{y})$ is locally unstable .

(iii) Assume that $A>1, B>1$. Then the equilibrium $(0,0)$ is globally asymptotically stable.

Proof. (i) It is obviously true because it is directly corollary of Theorem 3.

(ii) We can easily obtain that the linearized system of (11) about the positive equilibrium $(\frac{1-B}{b_0}, \frac{1-A}{a_0})$ is

$$\begin{cases} X_{n+1}=X_n+\frac{a_0}{b_0}(B-1)Y_n \\ Y_{n+1}=\frac{b_0}{a_0}(A-1)X_n+Y_n \end{cases} \tag{12}$$

from which we can easily obtain there is an eigenvalue $\lambda=1+\sqrt{(A-1)(B-1)}>1$ of Jacobian matrix of (12). i.e., it lies outside the unit disk. This implies that the positive equilibrium $(\frac{1-B}{b_0}, \frac{1-A}{a_0})$ is locally unstable.

(iii) The linearized system of (11) about the equilibrium $(0,0)$ is

$$\begin{cases} X_{n+1}=\frac{1}{A}X_n \\ Y_{n+1}=\frac{1}{B}Y_n \end{cases} \tag{13}$$

Its characteristic equation is

$$(\lambda-\tfrac{1}{A})(\lambda-\tfrac{1}{B})=0 \tag{14}$$

It is obvious that all the roots of (14) lie inside the unit disk. Hence the equilibrium $(0,0)$ is locally asymptotically stable .

On the other hand, from (11) we have

$$\begin{cases} x_{n+1}=\frac{x_n}{A+a_0y_n}<\frac{x_n}{A}<x_n \\ y_{n+1}=\frac{y_n}{B+b_0x_n}<\frac{y_n}{B}<y_n \end{cases} \tag{15}$$

which implies that $\lim_{n\to\infty}x_n=0,\ \lim_{n\to\infty}y_n=0$. So the equilibrium $(0,0)$ is globally asymptotically stable.

Corollary 1. Assume that (8) holds, then the unique positive equilibrium of (11) is a global attractor but unstable.

Theorem 5. Assume that (2) and (8) hold , then the positive solution of system (1) is locally unstable.

Proof. We can easily obtain that the linearized system of (1) about the positive equilibrium $(\overline{x}, \overline{y})$ is

$$\Psi_{n+1} = D\Psi_n$$

where $D = (d_{ij}), 1 \le i, j \le 2k+2$ is an $(2k+2)\times(2k+2)$ matrix such that

$$D = \begin{pmatrix} 1 & 0 & \cdots & 0 & 0 \\ 1 & 0 & \cdots & 0 & 0 \\ 0 & 1 & \cdots & 0 & 0 \\ \vdots & \vdots & \ddots & \vdots & \vdots \\ 0 & 0 & \cdots & 1 & 0 \\ \frac{b_0(A-1)}{\sum_{i=0}^{k} a_i} & \frac{b_1(A-1)}{\sum_{i=0}^{k} a_i} & \cdots & \frac{b_{k-1}(A-1)}{\sum_{i=0}^{k} a_i} & \frac{b_k(A-1)}{\sum_{i=0}^{k} a_i} \\ 0 & 0 & \cdots & 0 & 0 \\ 0 & 0 & \cdots & 0 & 0 \\ \vdots & \vdots & \ddots & \vdots & \vdots \\ 0 & 0 & \cdots & 0 & 0 \\ \frac{a_0(B-1)}{\sum_{i=0}^{k} b_i} & \frac{a_1(B-1)}{\sum_{i=0}^{k} b_i} & \cdots & \frac{a_{k-1}(B-1)}{\sum_{i=0}^{k} b_i} & \frac{a_k(B-1)}{\sum_{i=0}^{k} b_i} \\ 0 & 0 & \cdots & 0 & 0 \\ 0 & 0 & \cdots & 0 & 0 \\ \vdots & \vdots & \ddots & \vdots & \vdots \\ 0 & 0 & \cdots & 0 & 0 \\ 1 & 0 & \cdots & 0 & 0 \\ 1 & 0 & \cdots & 0 & 0 \\ 0 & 1 & \cdots & 0 & 0 \\ \vdots & \vdots & \ddots & \vdots & \vdots \\ 0 & 0 & \cdots & 1 & 0 \end{pmatrix}$$

from which it can easily follows that $\rho(D) > 1$. This implies that there exists at least eigenvalue of D lying outside the unit
disk. Hence the unique positive equilibrium $(\overline{x}, \overline{y})$ is unstable. This completes the proof of Theorem 5.

ACKNOWLEDGMENTS

This work is partially supported by the Doctoral Foundation of Guizhou College of Finance and Economics and supported by the Scientific Research Foundation of Hunan Provincial Education Department(10B023)

REFERENCES

[1] R. DeVault, G. Ladas, S. W. Schultz, "Necessary and sufficient conditions the boundedness of $x_{n+1} = A/x_n^p + B/x_{n-1}^q$", *J. Difference Equations Appl*.3, 1998, pp.259-266.

[2] R. M. Abu-Saris, R. DeVault, "Global stability of $y_{n+1} = A + \frac{y_n}{y_{n-k}}$", *Appl. Math. Lett.* 16, 2003, pp.173-178.

[3] S. N. Elaydi, "An introduction to Difference Equations", *Springer Verlag*, New York, 1996.

[4] R. P. Agarwal, W. T. Li, Y. H. Pang, "Asymptotic behavior of a class of nolinear delay difference equations", *J. Differ. Equat. Appl.* 8, 2002, pp.719-728.

[5] V. L. Kocic, G. Ladas, "Global Behavior of Nonlinear Difference Equations of Higher Order with Application", *Kluwer Academic Publishers*, Dordrecht,1993.

[6] V. L. Kocic, G. Ladas, "On rational recursive sequence", J. *Math. Anal. Appl*.173,1993, pp.127-157.

[7] M. R. S. Kulenonvic, G. Ladas, "Dynamics of Second Order Rational Difference Equations with Open Problems and Conjectures", *Chapaman & Hall/CRC*, Boca Raton, 2002.

[8] W. T. Li, H. R. Sun, "Dynamic of a rational difference equation", *Appl. Math. Compt.* 163, 2005, pp. 577-591.

[9] Y. H. Su, W. T. Li, "Global attractivity of a higher order nonlinear difference equation", *J. Differ. Equat. Appl*.11, 2005, pp.947-958.

[10] L. X. Hu, W. T. Li, "Global stability of a rational difference equation", *Appl. Math. Compt.* 190, 2007, pp.1322-1327.

2011 International Conference on Mechanical, Industrial, and Manufacturing Engineering
Lecture Notes in Information Technology Vols. 1-2

Study on the State Equation of the Position Loop and Speed Loop in the PMSM Cascade Sliding Mode Control

Xinkai Wu
School of Information and Electrical Engineering
Hu'nan University of Science and Technology
Xiangtan, Hu'nan Province, China
wxk-xtpu@163.com

Hongpei Xu, Shuangguang Peng and Minhai Zhang
School of Information and Electrical Engineering
Hu'nan University of Science and Technology
Xiangtan, Hu'nan Province, China
maozedong.888@163.com

***Abstract* - For the problems of the phase space mathematic model of the system in the design of the PMSM cascade sliding model variable structure control, based on an analysis of the dynamic mathematical model of PMSM and combined with the design methods of sliding mode variable structure, the state equations of the position loop and speed loop have been deduced respectively and the unified state space model has been got.**

Index Terms* - *cascade sliding model variable structure control; position and speed loop; state equation; PMSM

I. INTRODUCTION

In the modern AC servo system of PMSM, the sliding mode variable structure control technology for its excellent control performance has been applied more and more widely. But using single sliding mode controller to control position and speed variables will give the amplitude limitation of system and the decoupling control to bring major difficulties, limiting its application ranges. Therefore, from the engineering application angle, adopting cascade sliding model variable structure control not only can solve problems of the speed amplitude limit, but also further enhance the anti-interference ability of system and effectively eliminate the high amplitude chattering generated by the strong interference torque [1,2]. In the design of the cascade sliding model variable structure for the position and speed loop, we have to introduce the phase space mathematical model of the system. But there is currently no unified standard model, which affects the correctness of design for the cascade sliding mode controller. In order to solve the problem and conveniently for future research, the paper has studied the state equations of the position loop and speed loop in the PMSM cascade sliding mode variable structure control.

II. PMSM DYNAMIC MATHEMATICAL MODEL

Considering having no impact on the control performance, we have assumptions as follows [3]: 1) Ignore the saturation of the motor iron core; 2) Ignore the influences of cogging, commutation process and armature reaction; 3) Three-phase windings are completely symmetric and the magnetic field of permanent magnets steel is sinusoidal distribution along the air gap around; 4) The armature windings in the inner surface of the stator are uniformly continuous distribution. Furthermore, assume that the rotor of PMSM is cylindraceous (namely $L_d = L_q = L$), then get a series of equations of PMSM in the two-axis d-q synchronous rotating coordinate system as follows:

The stator flux equation:

$$\begin{aligned} \psi_d &= L i_d + \psi_f \\ \psi_q &= L i_q \end{aligned} \qquad (1)$$

The stator voltage equation:

$$\begin{aligned} u_d &= R_s i_d + \frac{d}{dt}\psi_d - \omega_e \psi_q \\ u_q &= R_s i_q + \frac{d}{dt}\psi_q + \omega_e \psi_d \end{aligned} \qquad (2)$$

The electromagnetic torque equation:

$$T_e = 1.5 p_n \psi_f \cdot i_q \qquad (3)$$

The mechanical motion equation:

$$J\frac{d\omega_m}{dt} = T_e - T_L - B\omega_m \qquad (4)$$

where, u_d and u_q are respectively the d and q axis stator voltages; i_d and i_q are respectively the d and q axis stator currents; ψ_d and ψ_q are respectively the d and q axis stator flux; L_d and L_q is respectively the d and q axis stator equivalent inductance; ψ_f is the equivalent flux of the rotor magnetic field; R_s is the stator resistance; T_e is the electromagnetic torque; T_L is the load torque; B is the viscous friction coefficient; p_n is the motor pole pairs; ω_m denotes the mechanical angular velocity of the rotor; ω_e denotes the electrical angular velocity of the rotor and $\omega_e = p_n \omega_m$; J is the moment of inertia of the motor Rotor.

From all the equations above, the state equation of PMSM in the d-q coordinate system can be obtained as follows:

$$\begin{bmatrix} \frac{di_d}{dt} \\ \frac{di_q}{dt} \\ \frac{d\omega_m}{dt} \end{bmatrix} = \begin{pmatrix} -R_s/L & p_n\omega_m & 0 \\ -p_n\omega_m & -R_s/L & -p_n\psi_f/L \\ -1.5p_n\psi_q/J & 1.5p_n\psi_d/J & -B/J \end{pmatrix} \begin{bmatrix} i_d \\ i_q \\ \omega_m \end{bmatrix} + \begin{bmatrix} u_d/L \\ u_q/L \\ -T_L/J \end{bmatrix} \quad (5)$$

From Eq.(5), PMSM is a nonlinear, multivariable and strong coupling time-varying system, so it is necessary to establish its decoupling state equation. Taking convex-mounted PMSM as an example, using the vector control mode of $i_d \equiv 0$, the decoupling state equation of PMSM in the d-q coordinate system is determined as:

$$\begin{bmatrix} \frac{di_q}{dt} \\ \frac{d\omega_m}{dt} \end{bmatrix} = \begin{bmatrix} -R_s/L & -p_n\psi_f/L \\ 1.5p_n\psi_f/J & -B/J \end{bmatrix} \begin{bmatrix} i_q \\ \omega_m \end{bmatrix} + \begin{bmatrix} u_q/L \\ -T_L/J \end{bmatrix} \quad (6)$$

III. State Equation of the Position Loop and Speed Loop in the Cascade Sliding Mode Control

On the basis of an analysis of the dynamic mathematical model of PMSM and obtaining its decoupling state equation in the d-q coordinate system, and combined with the design methods of the sliding mode variable structure controller, the state equations of the position loop and speed loop have been deduced respectively and the unified state space model obtained, which will be introduced as follows:

A. State Equation of the Speed Loop

Defines the state variable $x_1 = \omega_{ref} - \omega_m$ (where ω_{ref} is the given speed, and ω_m is the speed feedback), and the state variable $x_2 = \dot{x}_1$, so $x_2 = \dot{x}_1 = \dot{\omega}_{ref} - \dot{\omega}_m$, $\dot{x}_2 = \ddot{\omega}_{ref} - \ddot{\omega}_m$.

From Eq.(6),we get

$$\dot{\omega}_m = (1.5p_n\psi_f/J)\cdot i_q + (-B/J)\cdot\omega_m + (-T_L/J),$$

so the following equation can be obtained.

$$\ddot{\omega}_m = (1.5p_n\psi_f/J)\cdot\dot{i}_q + (-B/J)\cdot\dot{\omega}_m \quad (7)$$

From $x_2 = \dot{\omega}_{ref} - \dot{\omega}_m$, we get $\dot{\omega}_m = \dot{\omega}_{ref} - x_2$, then substituting it into Eq.(7) as follows:

$$\begin{aligned} \ddot{\omega}_m &= (1.5p_n\psi_f/J)\cdot\dot{i}_q + (-B/J)\cdot(\dot{\omega}_{ref} - x_2) \\ &= (B/J)\cdot x_2 + (1.5p_n\psi_f/J)\cdot\dot{i}_q - (B/J)\cdot\dot{\omega}_{ref} \end{aligned} \quad (8)$$

Substituting Eq.(8) into $\dot{x}_2 = \ddot{\omega}_{ref} - \ddot{\omega}_m$,we get

$$\begin{aligned} \dot{x}_2 &= \ddot{\omega}_{ref} - [(B/J)\cdot x_2 + (1.5p_n\psi_f/J)\cdot\dot{i}_q - (B/J)\cdot\dot{\omega}_{ref}] \\ &= (-B/J)\cdot x_2 - (1.5p_n\psi_f/J)\cdot\dot{i}_q + (B/J)\cdot\dot{\omega}_{ref} + \ddot{\omega}_{ref} \end{aligned} \quad (9)$$

On the assumption that the second derivative of the given speed is zero, namely $\ddot{\omega}_{ref} = 0$, we can obtain the phase space mathematical model of the system in the sliding mode design of the speed loop:

$$\begin{cases} \dot{x}_1 = x_2 \\ \dot{x}_2 = (-B/J)\cdot x_2 - (1.5p_n\psi_f/J)\cdot\dot{i}_q + (B/J)\cdot\dot{\omega}_{ref} \end{cases} \quad (10)$$

Eq.(10) can be rewritten in the form of a matrix as follows:

$$\begin{bmatrix} \dot{x}_1 \\ \dot{x}_2 \end{bmatrix} = \begin{pmatrix} 0 & 1 \\ 0 & -B/J \end{pmatrix} \begin{bmatrix} x_1 \\ x_2 \end{bmatrix} + \begin{bmatrix} 0 \\ -1.5p_n\psi_f/J \end{bmatrix} \cdot u_1 + \begin{bmatrix} 0 \\ (B/J)\cdot\dot{\omega}_{ref} \end{bmatrix} \quad (11)$$

where the control variable $u_1 = \dot{i}_q$.

Ignoring the impact of viscous friction coefficient, that is, letting $B = 0$,and also giving $K_t = 1.5p_n\psi_f$,so the phase space mathematical model of the system can be further simplified as:

$$\begin{bmatrix} \dot{x}_1 \\ \dot{x}_2 \end{bmatrix} = \begin{pmatrix} 0 & 1 \\ 0 & 0 \end{pmatrix} \begin{bmatrix} x_1 \\ x_2 \end{bmatrix} + \begin{bmatrix} 0 \\ -K_t/J \end{bmatrix} \cdot u_1 \quad (12)$$

where the control variable $u_1 = \dot{i}_q$.

At this point, we can begin to design the sliding mode variable structure controller for the speed loop of the system. In the design, in order to weaken the torque chattering of the sliding mode control, smoothen the torque, and further improve the steady-state accuracy, meanwhile enhancing the load-bearing ability of the system, the integral compensator should be introduced between the sliding mode controller and the controlled object [4,5]. Thus, the structure diagram of the sliding mode variable structure controller of the speed loop is shown in Fig.1.

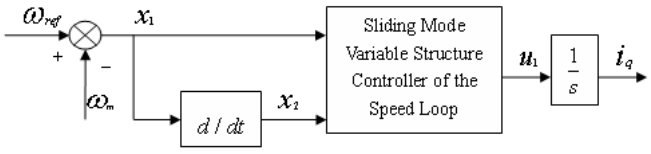

Fig.1 structure diagram of the sliding mode variable structure controller of the speed loop

B. State Equation of the Position Loop

Defines the state variable $y_1 = \theta_{ref} - \theta_m$ (where θ_{ref} is the given position, θ_m is the position feedback), and the state variable $y_2 = \dot{y}_1$,so $y_2 = \dot{y}_1 = \dot{\theta}_{ref} - \dot{\theta}_m$, $\dot{y}_2 = \ddot{\theta}_{ref} - \ddot{\theta}_m$。

Because $\omega_{ref} = \dot{\theta}_{ref}$, $\omega_m = \dot{\theta}_m$, thus $y_2 = \omega_{ref} - \omega_m$, then we get the following equation.

$$\dot{y}_2 = \ddot{\theta}_{ref} - \ddot{\theta}_m = \dot{\omega}_{ref} - \dot{\omega}_m \quad (13)$$

From Eq.(6), we get

$$\dot{\omega}_m = (1.5 p_n \psi_f / J) \cdot i_q + (-B/J) \cdot \omega_m + (-T_L / J)$$,

then substituting it into Eq.(13) as follows:

$$\begin{aligned} \dot{y}_2 &= \dot{\omega}_{ref} - \left[(1.5 p_n \psi_f / J) \cdot i_q + (-B/J) \cdot \omega_m + (-T_L / J) \right] \\ &= \dot{\omega}_{ref} - (1.5 p_n \psi_f / J) \cdot i_q + (B/J) \cdot \omega_m + T_L / J \end{aligned} \quad (14)$$

From $y_2 = \omega_{ref} - \omega_m$, we get $\omega_m = \omega_{ref} - y_2$, then substituting it into Eq.(14) as follows:

$$\begin{aligned} \dot{y}_2 &= \dot{\omega}_{ref} - (1.5 p_n \psi_f / J) \cdot i_q + (B/J) \cdot (\omega_{ref} - y_2) + T_L / J \\ &= (-B/J) \cdot y_2 + (B/J) \cdot \omega_{ref} - (1.5 p_n \psi_f / J) \cdot i_q + T_L / J + \dot{\omega}_{ref} \end{aligned} \quad (15)$$

Substituting Eq.(3) and $\ddot{\theta}_{ref} = \dot{\omega}_{ref}$ into Eq.(15), then it is obtained as follows:

$$\begin{aligned} \dot{y}_2 &= (-B/J) \cdot y_2 + (B/J) \cdot \omega_{ref} - T_e / J + T_L / J + \ddot{\theta}_{ref} \\ &= (-B/J) \cdot y_2 + (B/J) \cdot \omega_{ref} - (T_e - T_L) / J + \ddot{\theta}_{ref} \end{aligned} \quad (16)$$

Assume that the second derivative of the given position is zero, namely $\ddot{\theta}_{ref} = 0$, we can get the phase space mathematical model of the system in the sliding mode design of the position loop:

$$\begin{cases} \dot{y}_1 = y_2 \\ \dot{y}_2 = (-B/J) \cdot y_2 + (B/J) \cdot \omega_{ref} - (T_e - T_L)/J \end{cases} \quad (17)$$

Eq.(17) can be rewritten in the form of a matrix as follows:

$$\begin{bmatrix} \dot{y}_1 \\ \dot{y}_2 \end{bmatrix} = \begin{pmatrix} 0 & 1 \\ 0 & -B/J \end{pmatrix} \begin{bmatrix} y_1 \\ y_2 \end{bmatrix} + \begin{bmatrix} 0 \\ B/J \end{bmatrix} \cdot u_2 + \begin{bmatrix} 0 \\ -(T_e - T_L)/J \end{bmatrix} \quad (18)$$

where the control variable $u_2 = \omega_{ref}$.

Similarly, based on the phase space mathematical model, we can design the sliding model variable structure controller for the position loop of the system, and as is shown in Fig.2.

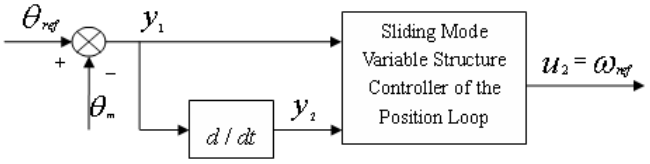

Fig.2 structure diagram of the sliding mode variable structure controller of the position loop

IV. CONCLUSIONS

Based on an analysis of the dynamic mathematical model of PMSM, combined with the design methods of sliding mode variable structure, the paper has respectively deduced the state equations of the position loop and speed loop in the PMSM cascade sliding model variable structure control, and has provided the unified phase space mathematical model of the system for the design of the sliding mode variable structure controller.

REFERENCES

[1] Jin Zhao, Shuyun Wan, and Xiaopeng Sun, “A Survey to Control Strategies of AC Servo Systems Based on Sliding Mode Control,” Electric Drive, Vol.1, pp.2-6, March 1996 (In Chinese).

[2] Utkin V I, Asif Sabanovic, “Sliding Modes Applications in Power Electronics and Motion Control Systems[C],”IEEE International Symposium on Industrial Electronics, Bled, pp.22-31, February 1999.

[3] Zhibing Shu, “AC Servo Motion Control System[M].Beijing,” Tsinghua University Press, pp.68-71, December 2006 (In Chinese).

[4] Jin Zhao, Shuyun Wan, and Lijiu Wang, “Cascade Sliding Mode Control for an AC Servo System,” Transactions of China Electrotechnical Society, Vol .3, pp.32-36, June 1996 (In Chinese).

[5] Yasser Abdel Rady Ibrahim Mohamed, “ Adaptive self-tuning speed control for permanent-magnet synchronous motor drive with dead time [J],” IEEE Transactions on Energy Conversion, vol.4, pp.855-862, May 2006.

2011 International Conference on Mechanical, Industrial, and Manufacturing Engineering
Lecture Notes in Information Technology Vols. 1-2

A New Inference Method on Fuzzy Control and Simulation

Benliang Xie
College of Science
Guizhou University
Guiyang,Guizhou 550025,China
ie.blxie@gzu.edu.cn

Qiao Liu
College of Science
Guizhou University
Guiyang,Guizhou 550025,China
liuqiao1955@163.com

***Abstract* - To one unsuitable property of Mamdani inference method, a new inference method is proposed in this article, which is called "translation method". In addition, how the new method affects the defuzzification method has been discussed. The simulation result on tank gunnery control system verifies the availability of the new method.**

Index Terms - Fuzzy control, inference method, Tank gunnery control system

I. INTRODUCTION

Fuzzy control is a practical alternative for a variety of challenging control applications since it provides a convenient method for constructing nonlinear controllers via the use of heuristic information [1]. In recent years, it plays an important role in many fields such as industry process control, inverted pendulum control [2] and so on.

As the statement in ref. [1], fuzzy control contains five steps:

1) Quantify the meaning of the linguistic values using membership function.
2) Input fuzzification. Actually, it is can be ignored mostly.
3) Premise quantification via fuzzy logic.
4) Inference. Determine conclusions for each rule.
5) Defuzzification. Convert Decisions into Actions.

In this article, we don't discuss the steps 1/2/3, but focus on the step 4. The step 5 is following, so we must discuss how the changes in the former affect the latter.

Many fuzzy inference methods have been developed in history, such as CRI method [3], III method [4], AARS method [5] and so on. This article follows the Mamdani method, and to avoid its improper property, a new inference method is present.

In section 2, we point out one unsuitable property of two conventional Mamdani inference methods: "minimum" and "product", and a new inference method is proposed to avoid the unsuitable property. In section 3, we discuss how the new inference method affects defuzzification step. In section 4, simulation result on tank gunnery control system verifies the availability and efficiency of the new inference method.

II. A NEW INFERENCE METHOD "TRANSLATION METHOD"

After the former three steps, we have got the certainty of premise in each rule, which is denoted by $\mu_{premise}$. The task of inference step is to decide the membership function for each conclusion of each rule under the certain of premise, which is denoted by $\mu(u)$. The "minimum" or "product" inference method is used usually.

The "minimum" method is given by

$$\mu(u) = \min\{\mu_{premise}, \mu_{conclusion}(u)\} \tag{1}$$

where $\mu_{conclution}(u)$ denotes the membership function of output linguistic variable in the rule with certain of premise $\mu_{premise}$. Taking triangle membership function as a sample, it is shown in Figure 1(a).

The "product" method is given by

$$\mu(u) = \mu_{premise} \times \mu_{conclution}(u) \tag{2}$$

and shown in Figure 1(b).

The justification for the two methods is that we can be no more certain about our conclusion than our premise. Let $d(u)$ denotes the reduction of membership function value of conclusion by the certain of premise, we can see that in minimum method

$$d(u) = \begin{cases} \mu_{conclusion}(u) - \mu_{premise} & \text{if } \mu_{conclusion}(u) > \mu_{premise} \\ 0 & \text{if } \mu_{conclusion}(u) \le \mu_{premise} \end{cases} \tag{3}$$

in product method

$$d(u) = \mu_{conclusion}(u) \times \left(1 - \mu_{premise}\right). \tag{4}$$

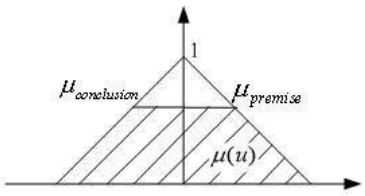

(a) Minimum inference method

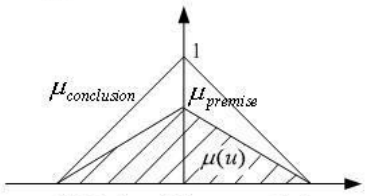

(b) Product inference method

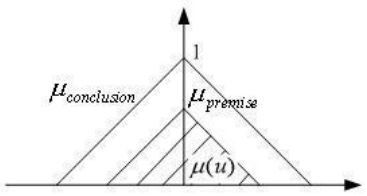

(c) Translation inference method

Fig. 1 The results of inference methods

It is clearly that for $\forall u_1, u_2$ if

$$\mu_{conclusion}(u_1) > \mu_{conclusion}(u_2)$$

then $d(u_1) > d(u_2)$, no mater what method we use.

It implies that the u with higher membership function value suffers from the certain of premise more, and the u with lower value suffers less or even not be suffered. It sounds not very suitable. In human's logic, the things with low certain to happen will be not happen if its premise with low certain too. But in the two methods above, the certain will reduce a litter or not reduce.

To avoid the unsuitable property mentioned above, a new inference method called 'translation method' is proposed, which is given by

$$\mu(u) = \max\{0, \mu_{conclusion}(u) - (1 - \mu_{premise})\} \quad (5)$$

and shown in Figure 1(c).

It is clearly that the translation inference method satisfies the basic law that certain about conclusion is less than premise. If premise happens sure, which means $\mu_{premise} = 1$, the certain about the conclusion will not be changed. And when premise absolutely not happens, which means $\mu_{premise} = 0$, the conclusion will not happen too because for every u $\mu(u) = 0$.

In this method,

$$d(u) = \begin{cases} 1 - \mu_{premise} & \text{if } \mu_{conclusion}(u) > 1 - \mu_{premise} \\ \mu_{conclusion}(u) & \text{if } \mu_{conclusion}(u) \le 1 - \mu_{premise} \end{cases} \quad (6)$$

It implies that each u suffers from the certain of premise equally, no matter its membership function value high or low, until $\mu(u) = 0$.

Sometimes, each rule has an additional rule certainty, which will be denoted by μ_{rule}. Then $\mu(u)$ should be changed as

$$\mu(u) = \max\{0, \mu_{conclusion}(u) - (1 - \mu_{premise} \times \mu_{rule})\} \quad (7)$$

But usually, the $\mu_{rule} = 1$.

III. Defuzzification Under "Translation Inference Method"

The input to a fuzzy controller will make more than one rule active at a time mostly. For each rule i, we will get $\mu_i(u)$ through inference step. The task of defuzzification step is that convert all active rules to an output by combining each $\mu_i(u)$.

Different inference method will give different membership function for the conclusion, but different membership function for the conclusion may not give the different single output, which is denoted by u^{crisp}, because the finally output also depends on defuzzification method.

There are many defuzzification methods. Take "center average" (CA) and "center of gravity" (COG) as samples.

CA method is given by

$$u^{crisp} = \frac{\sum_i b_i \mu_{premise(i)}}{\sum_i \mu_{premise(i)}} \quad (8)$$

where b_i denotes the center of the membership function of the conclusion of rule i (Usually it reaches its peak).

It is clearly that the result only depends on the certain of premise $\mu_{premise(i)}$ and the membership function of output linguistic variable $\mu_{conclusion(i)}(u)$. It has nothing to do with the membership function of the output $\mu_i(u)$. So the final output u^{crisp} will be the same no matter what inference method have been used.

COG method is given by

$$u^{crisp} = \frac{\sum_i b_i \int \mu_i(u)}{\sum_i \int \mu_i(u)} \quad (9)$$

and is shown in figure 2, where $\int \mu_i(u)$ denotes the area of the membership function of output linguistic variable in rule(i).

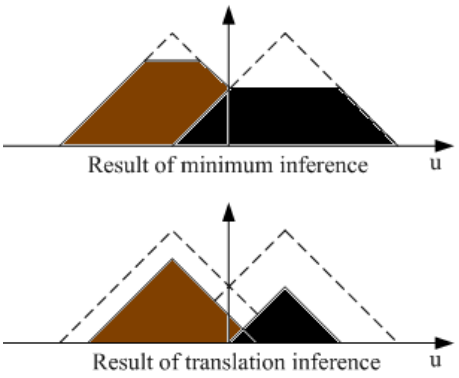

Fig. 2 Results in defuzzification step

It is clearly that different inference methods make different areas of membership function of output, so the final output u^{crisp} depends on what inference method we use.

It is strongly recommended that using the methods which depend on the result of inference step.

IV. Simulation On Tank Gunnery Control System

Tank gunnery control is an important topic on military project. Its main task is making sure the rotational speed of gun tube reach the given speed steadily fast and accurately.

The structure of tank gunnery control system is shown in figure 3(a).

Treat the inverter, AC motor and gun tube as a general plant. Through identification data such as step response, frequency response and triangle response, a nonlinear model has been established, which is shown in figure 3(b).

Because of the model's nonlinear property, linear controllers such as state space controller and lead lag network will be unsuitable. A fuzzy controller with translation inference method has been developed.

There are two input linguistic variables given by

$e(t) = r(t) - y(t)$ and $\frac{d}{dt}e(t)$, and one output linguistic variable the control voltage $u(t)$. Triangle membership function is used for the three variables. $e(t)$ and $u(t)$ are classified linguistically as "NB NM NS ZE PS PM PB", and $\frac{d}{dt}e(t)$ is classified as "N Z P".

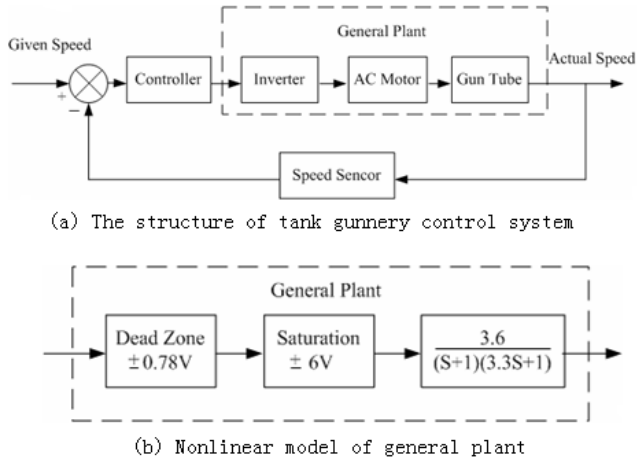

Fig. 3 The structure of tank gunnery control system

Simulation result is shown in figure 4. Remark that the speed of gun tube is expressed by voltage.

It is clearly that the steady time (95%) of open loop system is 14.04 second, and it is improved to 4.56 second by fuzzy controller. The rise time (60%) is improved from 4.25 second to 2.23 second. Control voltage is steady without higher-order oscillation. The small overshoot in fuzzy control is acceptable.

V. CONCLUSION

The translation method obeys human's logic, and satisfies the basic law that we have no more certain about conclusion than premise. The simulation result verifies its

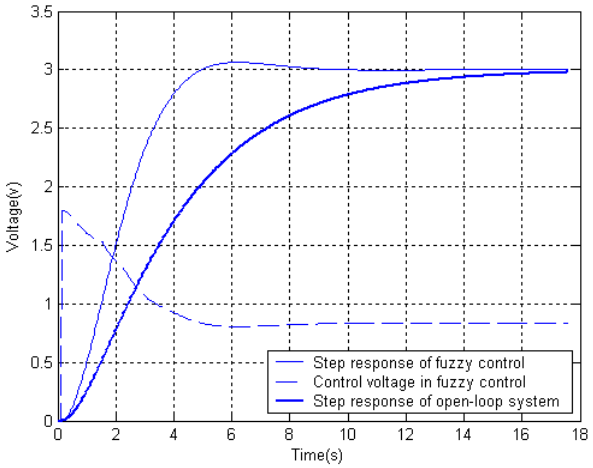

Fig. 4 Tank gunnery control system simulation result

availability, and operation of control is very soft and steady. The idea that making sure membership function values of all u reduce equally by the certain of premise until reach zero can try to apply in other inference methods.

REFERENCES

[1] Kevin M. Passino, Stephen Yurkovich. "Fuzzy control". Addison Wesley Longman, Inc. 1998

[2] Zhang N R, C Ebert, R Belschner, etc. "Fuzzy cascade control of an inverted pendulum". *Control and Decision*. 1996,11(1):85-88.

[3] Zadeh L A. "The concept of a linguistic variable and its applications to approximate reasoning (I;II;III)". *Information Science*. 1974,8:199-294; 1974,8:301-357; 1975,9:43-93.

[4] Wang G J. "On the logic foundation of fuzzy reasoning". *Information Science*. 1999,117:47-88.

[5] Turksen I B, Zhong Z. "Approximate analogical reasoning approach based on similarity measures". *IEEE Transactions on Systems, Man and Cybernetics*. 1998, 16(6):1049-1056.

2011 International Conference on Mechanical, Industrial, and Manufacturing Engineering
Lecture Notes in Information Technology Vols. 1-2

A Critical Analysis of Sense and Avoid Technologies for modern UAVs

MSc. Adrian MURARU
Faculty of Economics and Public Administration
University "Stefan cel Mare" of Suceava
Suceava, Str. Universitatii nr.13, 720229
muraruady@gmail.com

***Abstract* - Advances in computing, imaging and data transmission technologies are precursors to an important role for UAVs in warfare. The concept of unmanned aerial vehicles is a new step in modern warfare. UAVs are likely to revolutionize the reconnaissance and surveillance, to increase the capabilities of small units and also help in future network-centric formations. The purpose of this article is to show the importance of mission planning in a fully automatic flight and the critical role of implementing Sense & Avoid (S&A) procedures at different categories of UAVs.**

Index Terms -
UAV - Unmanned Aerial Vehicle
UAS - Unmanned Aircraft System
S&A – Sense and Avoid

I. INTRODUCTION

An unmanned aerial vehicle is an aircraft that flies without a human pilot on board. The responsibility for the control of this type of aircraft falls on either a human operator on the ground or its flight is autonomously based on pre-programmed flight plans using more complex dynamic automation systems. At first, UAVs were simply target drones for military aircrafts or artillery. Nowadays, the technology has advanced to the point where human pilots could be replaced by the sense and avoid system.

The problem of sense & avoid can be divided in two separate functions: the sense function and the avoid function, each with having several sub-functions (either allocated to a technical system or to a the human operator). The development of a Sense & Avoid System raises a couple of questions, each of which requires its own dedicated experimental design. According to a FAA (Federal Aviation Administration) definition in 2009 "Sense and Avoid (SAA) is the capability of an UAV to remain well clear and avoid collisions with other airborne traffic". The task of identifying possible conflicts and avoiding them is still in the responsibility of the human operator. Studies show, that even for an experienced pilot, it takes already a few seconds to identify possible conflicts after detecting an intruder.

Future unmanned systems within the armed forces will be highly heterogeneous in nature, with vehicles from multiple domains: aerial, underwater, and land, working in collaborative teams to complete a variety of missions. The complexity of supervising these teams will be enormous and will rely on human creativity, judgment, and experience. Therefore, the design and development of mission planning and monitoring technologies must be rooted in a deep understanding of the human operator's role as mission manager, and must effectively address the reasoning skills and limitations of both the human and autonomous intelligent system.

II. BASIC ASPECTS OF SENSE AND AVOID TECHNOLGY

A key requirement for routine access to the NAS is ROA compliance with 14 CFR 91.113, "Right-of-Way Rules: Except Water Operations." This is the section that contains the phrase "see-and-avoid," being is the primary restriction to the normal operations of UAVs. The intent of "see-and-avoid" is for pilots to use their sensors (eyes) and other tools to find and maintain situational awareness of other traffic and to yield the right-of- way, in accordance with the rules, when there is a traffic conflict. Since the purpose of this regulation is to avoid mid-air collisions, this should be the focus of technological efforts to address the issue as it relates to UAVs rather than trying to mimic and/or duplicate human vision. See figure 1.

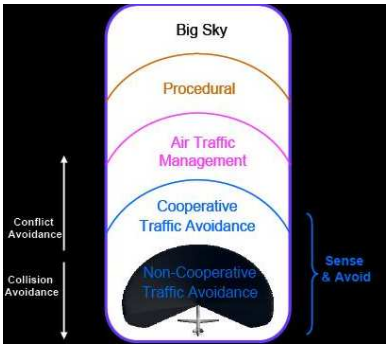

Figure 1: Types of air traffic encountered

The FAA does not provide a quantitative definition of see-and-avoid, largely due to the number of combinations of pilot vision, collision vectors, sky background, and aircraft paint schemes involved in seeing oncoming traffic. Having a sufficient field of regard (FOR) for a UAV S&A system, however, meeting the goal of assured air traffic separation is fundamental.

Although an elusive issue, one fact is apparent. The challenge with the S&A issue is based on a capability constraint, not a regulatory one. A possible definition for S&A systems emerges: sense-and-avoid is the onboard, self-contained ability to:s

- Detect traffic that may be a conflict
- Evaluate flight paths
- Determine traffic right-of-way
- Maneuver well clear according to the rules in Part 91.113, or
- Maneuver as required in accordance with Part 91.111.

A. Detection Requirements and Methods

According to the right-of-way rules (14 CFR 91.113), any aircraft must detect traffic that might be a conflict (becomes less than 500 feet separation) and then yield if required. Based on analysis, this means it must yield to aircraft from about 10 degrees left of the nose (approximately head on) to 90 degrees right of the nose depending on class. Prudence suggests that the search volume should include 90 degrees left of the nose as well. NASA studies[1] have shown for climbing or descending traffic, plus or minus 15 degrees search in elevation will adequately scan for converging aircraft which are using as much as 20 degree angles of climb.

While it does not specifically address *where* a pilot should be looking, it does exclude those areas where a pilot is *not* expected to be looking. Another FAA document (P-8740-51) provides guidance for pilots on "How to Avoid a Mid-air Collision." It suggests scanning methods, rates, and locations that will increase the probability of detecting a mid-air threat within the pilot's field of regard.

In the international community, ICAO has also set standards which offer yet more guidance on azimuth search areas. A summary of these detection requirements and others is provided in the table, and the technology available to search these defined regions is described in detail in the following sections.

This suggests the following requirement for an S&A systems standard: *Sense-and-avoid systems should provide a minimum traffic detection capability of plus or minus 110 degrees in azimuth measured from the longitudinal axis and plus or minus 15 degrees in elevation from the cruise speed level line.* The 15 degree elevation value is based on independent NASA and OSD analysis to detect climbing or descending threats.

TABLE I

Source	Azimuth	Elevation
FAA P-8740-51: How to Avoid a Mid-Air Collision	+/- 60 degrees	+/- 10 degrees
International Standards, Rules of the Air, Section 3.2 (ICAO)	+/- 110 degrees	No guidance
FAA Advisory Circular 25.773-1 (Transport Aircraft Design)	+/- 120 degrees	Variable: +37 and -25 degrees (varies with azimuth)

B. Range Requirement

In addition to the detection location relative to the ROA, the range of the potential collision threat must also be considered. The system will need to detect the aircraft in adequate time to process the information, determine the conflict, and execute the maneuver according to the right-of-way rules. Department of Defense (DoD) has conducted computer based simulations and analysis that confirm independent NASA findings[2] that the time needed to complete the avoidance maneuver depends primarily on the bank angle of the maneuver for speeds greater than about 80 knots. Because ROA will limit the angle of bank for preplanned maneuvers, the time required to perform the limited angle of bank maneuver is determined. Any additional time necessary for processing and/or operator response can be added to the maneuver time to determine the total time necessary to detect the traffic prior to collision.

Once this total time required is determined, the range is calculated dependent on the ROA's velocity and a representative traffic closing velocity vector. The range required of the detection system is then a function of the maneuverability and velocity of the ROA and its operational traffic. The Air Combat Command-sponsored joint working group mentioned above, using the terminology remotely operated aircraft, has proposed that:

The sense-and-avoid system must detect the traffic in time to process the sensor information, determine if a conflict exists, and execute a maneuver according to the right-of-way rules. If pilot interaction with the system is required, transmission and decision time must also be included in the total time between initial detection and the point of minimum separation.[3]

C. Sensor Requirement

The onboard systems of the UAVs can be co-operative or non-cooperative. The cooperative systems can be T-CAS (Traffic Collision Alerting System), ADS-B (Automatic dependent surveillance-broadcast), and ACAS (Airborne Collision Avoidance System). T-CAS monitors the airspace around an aircraft for other aircraft equipped with a corresponding active transponder, independent of air traffic control, and warns pilots of the presence of other transponder-equipped aircraft which may present a threat of mid-air collision (MAC). It is a type of airborne collision avoidance system mandated by the International Civil Aviation Organization. ADS-B is a radically new technology that redefines today the paradigm of communications - navigation - surveillance in air traffic management (ATM) today. ACAS is being used to describe short-range systems intended to prevent actual metal-on-metal collisions. The non-cooperative systems don't require other aircraft or obstacles in area to support the detection methodology. They can be used to detect ground-based obstacles. They split in active and passive systems.

[1] NASA Environmental Research and Sensor Technology (ERAST) program analysis conducted in support of See-and-Avoid Flight testing, March 2002 and 2003.

[2] OSD-FAA MARCAT and NASA ERAST program studies.

[3] *Sense-and-Avoid Requirement for Remotely Operated Aircraft (ROA),* 25 June 2004, HQ ACC/DR-UAV SMO.

Active systems transmit a signal to detect obstacles in flight path (radar, laser). Passive systems do not transmit a signal but rely upon detection of signals emanating from the obstacle (Motion detection sensors (MD), Electro-optical sensors (EO), Infrared sensors (IR).

C.1. Active, cooperative

The active, cooperative scenario involves an interrogator monitoring a sector ahead of the ROA to detect oncoming traffic by interrogating the transponder on the other aircraft. Its advantages are that it provides both range and bearing to the traffic and can function in both visual and instrument meteorological conditions (VMC and IMC). The disadvantages are its relative cost. Current systems available in this category include the various Traffic-alert and Collision Avoidance Systems (TCAS).

C.2. Active, non-cooperative

The active, non-cooperative scenario relies on a RADAR or laser-like sensor LIDAR scanning a sector ahead of the ROA to detect all traffic, whether transponder-equipped or not. The returned signal provides range, bearing, and closure rate, allowing prioritization of oncoming traffic for avoidance, in either VMC or IMC. Its potential drawbacks are its relative cost, the bandwidth requirement to route its imagery (for non-autonomous systems), and its weight. An example of an active, non-cooperative system that is currently available is a combined microwave radar and infrared sensor originally developed to enable helicopters to avoid power lines.

C.3. Passive, cooperative

The passive cooperative scenario, like the active cooperative one, relies on everyone having a transponder, but with everyone's transponder broadcasting position, altitude and velocity data. The advantages are its lower relative cost (no onboard interrogator required to activate transponders) and its ability to provide S&A information in both VMC and IMC. The disadvantage is its dependence on all traffic carrying and continuously operating transponders. In this scenario, ROA should have the capability to change transponder settings while in flight.

C.4. Passive, non-cooperative

The passive non-cooperative scenario is the most demanding one. It is also the most analogous to the human eye. An S&A system in this scenario relies on a sensor to detect and provide azimuth and elevation to the oncoming traffic. Its advantages are its moderate relative cost and ability to detect non-transponder equipped traffic. The disadvantages are its lack of direct range or closure rate information, potentially high bandwidth requirement (if not autonomous), and its probable inability to penetrate weather. The gimbaled EO/IR sensors currently carried by reconnaissance UAVs are examples of such systems, but if they are looking at the ground for reconnaissance then they are not available to perform S&A. An emerging approach that would negate the high bandwidth requirement of any active system is optical flow technology, which reports only when it detects an object showing a lack of movement against the sky, instead of sending a continuous video stream to the ground controller. Imagery from one or more inexpensive optical sensors on the UAV is continuously compared to the last image by an onboard processor to detect minute changes in pixels, indicating traffic of potential interest. Only when such objects are detected is their bearing relayed to the ground.

For comparison between the methods see the table below:

TABLE II

Oncoming Traffic is…

Onboard Systems are…	Cooperative	Non-Cooperative
Active	Pro: - Both range and bearing provided - Functions in VMC and IMC Con: - SWAP - Cost Example: TCAS systems	Pro: - Range, bearing, and closure rate proviled - Functions in VMC and IMC Con: - Data link required - SWAP - Cost Example: radars
Passive	Pro: - Cost Con: - VMC only Example: High Visibility Paint	Pro: - Cost - Detects non-transponder (all) aircraft Con: - Bearing only provided - Data link required - VMC only Example: EO/IR sensors

D. Avoidance Requirements and Methods

Once the "sense" portion of S&A is satisfied, the UAV must use this information to execute an avoidance maneuver. The latency between seeing and avoiding for the pilot of a manned aircraft ranges from 10 to 12.5 seconds according to FAA and DoD studies[4]. If relying on a ground operator to see and avoid, the UAV incurs the same human latency, but adds the latency of the data link bringing the image to the ground for a decision and the avoidance command back to the ROA. This added latency can range from less than a second for line-of-sight links to more for satellite links. See figure 2.

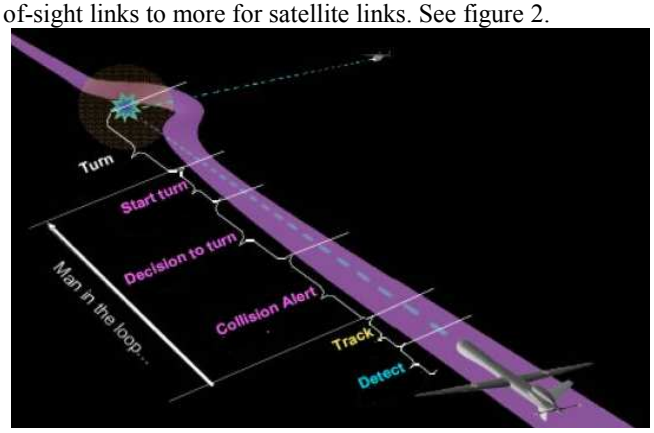

Figure 2: Collision avoidance time needed

[4] Tyndall Air Force Base Mid-Air Collision Avoidance Study; FAA P-8740-51; see also Krause, Avoiding Mid-Air Collisions, p. 13

D.1 Pilot-in-the-loop

Current UAVs are flown with varying degrees of human control and/or oversight. When flying in the NAS this oversight must adhere to the requirements of 14 CFR Part 91 (see ANNEX1) and its intent for pilots to see and avoid other aircraft. For reference, the regulations, including right-of-way rules for pilots, are provided below. These regulations apply to all aircraft (civil and military).

Section 91.111(a) makes it clear that the intent of this statutory language is to ensure that operators avoid creating "a collision hazard." Section 91.113 provides the right-of-way rules to clarify which aircraft should yield. In order of decreasing priority, right-of-way is granted to vehicles 1) in distress, 2) landing, 3) a balloon, 4) a glider, 5) an airship, 6) towing or air-air refueling, 7) on the right-hand, 8) in-front, and 9) below.

From "How to Avoid a Midair Collision" (FAA document P-8740-51), "Collision avoidance involves much more than proper eyeball techniques. You can be the most conscientious scanner in the world and still have an in-flight collision if you neglect other important factors in the overall see-and-avoid picture." The document describes a "see-and-avoid checklist" that includes proper procedures on the ground (e.g., flight planning, adding high-visibility features to the aircraft, etc.) to good en-route practices (e.g., avoiding crowded airspace, using radios effectively, etc.).

D.2 Autonomous

The pilot-in-the-loop scenario is one possible way to recognize an impending collision and initiate the required resolution maneuver. For beyond line-of-sight ROA operations, however, other methods to initiate action are required. S&A must be developed and must work throughout all phases of flight. In the case of ROA, where the operator and crew are off-board and connected via a data-link, the sense-and-avoid system must work even if the data-link malfunctions.

An alternative is to empower the ROA to determine autonomously whether and which way to react to avoid a collision once it detects oncoming traffic, thereby removing the latency imposed by data links. This approach has been considered for implementation on TCAS II-equipped manned aircraft, since TCAS II already recommends a vertical direction to the pilot; but simulations have found the automated maneuver worsens the situation in a fraction of the scenarios. For this reason, the FAA has not certified automated collision avoidance algorithms based on TCAS resolution advisories; doing so would set a significant precedent for ROA S&A capabilities.

III. CONCLUSION

Unmanned aerial vehicles (UAVs) present major challenges for the task of sense and avoid, especially in the case of miniature systems. It is necessary better implementing procedures that require new and innovative technologies, with better and safer capabilities in the automation and optimization of mission planning in unstructured environments within the entire flight envelope. It is also necessary to accommodate subsystem/component failure modes without major performance degradation (the maximal takeoff weight and the aerodynamics of small vehicles are very sensitive to all the additional equipments) or loss of vehicle and to perform extreme maneuvers without violating stability limits. An integrated/hierarchical approach to vehicle instrumentation, computing, modeling and control seems to provide possible solutions. The UAV community is accomplishing major milestones towards this goal. More recently, researchers have been concerned with multiple and heterogeneous UAVs flying in formation in order to take advantage of their complementary capabilities. The future work regarding the swarm problem opens new avenues of research where the intelligent control community can contribute significantly in terms of smart coordination / cooperation technologies.

The importance of mission planning in a fully automatic flight and the critical role of implementing Sense & Avoid (S&A) procedures at different categories of UAVs was presented. The focus was on the emerging capability to handle separation provision and collision avoidance in a way similar to the manned aircrafts. The main contributions are related to the critical analysis of the possibilities of integration S&A procedures for small UAVs in the context of simplicity and low-cost solution and the proposal to implement the organizing of a special course dedicated to the technical knowledge of the procedures for mission planning and utilization of UAVs; a critical. The article concludes with a technical perspective on the developments of S&A solutions for UAVs.

REFERENCES

[1] Advanced Technology Demonstration, Proceedings of the American Institute of Aeronautics and Astronautics InfoTech, 2005

[2] AERONAUTICAL COMMUNICATIONS PANEL (ACP) EIGHTEENTH MEETING OF WORKING GROUP F Montréal, Canada 12 – 22 May 2008

[3] Airspace Integration Plan for Unmanned Aviation November 2004

[4] Boşcoianu, M., *Optimal Path Control for Small UAVs equipped with VTO system,* International Conference UAV World, 3rd International Conference UAV World, Frankfurt, Germany, 2009

[5] Boscoianu M**,** Axente C., Pahonie R, Some aspects regarding the cooperative control problem for flying wing air vehicles, Computational Methods and Intelligent Systems, 10th WSEAS Int. Conf on Mathematical Methods and Computational Techniques in Electrical Engineering (MMACTEE'08), Sofia, Bulgaria, May 2-4, 2008, ISSN 1790-5117, ISBN 978-960-6766-60-2

[6] Boscoianu M, Pahonie R, Coman, A, Some aspects regarding the adaptive control of a flying wing micro air vehicle with flexible wing tips, Computational Methods and Intelligent Systems, 10th WSEAS Int. Conf on Mathematical Methods and Computational Techniques in Electrical Engineering (MMACTEE'08), Sofia, Bulgaria, May 2-4, 2008, ISSN 1790-5117, ISBN 978-9606766-60-2

[7] Developing Sense & Avoid For All Classes of UAV, Defense Research Associates

[8] INTEGRATING UAVs WITH CONVENTIONAL AIR OPERATIONS: SOME REGULATORY [1] ISSUES G.F. Marsters, AeroVations Associates and Mac Sinclair, AeroVations Associates

[9] McCalmont, J., Utt, J. and Deschenes, M., "Sense and Avoid Phase 1 (Man-in-the-Loop)

2011 International Conference on Mechanical, Industrial, and Manufacturing Engineering
Lecture Notes in Information Technology Vols. 1-2

Investigation on Multiple Sensor Fusion Applied in Service Humanoid Robot*

Haibo Chen[1], Wanmi Chen[1,2**],Yulin Xu[1,2],Xin Li[1,2]Yonghuan Yang[1], Dexing Zhang[1],Junfeng Qian[1],Lu Liu[1]

1.School of Mechatronics Engineering and Automation,Shanghai University ,Shanghai 200072,China
2.Shanghai Key Lab. of Power Station Automation technology ,Shanghai 200072,China
*** To who correspondence should be addressed at Box 3#,No.149,Yanchang Rd.,Shanghai,China.*
chb1985@gmail.com,wanmi@shu.edu.cn

Abstract - With the advances of computer science, robotics, and other related areas, service robots attract much attention to improve quality of human life from both academia and industry. Service robots present interesting technical challenges to working environments of robots from industries to homes and offices, and to extend markets for robots from industrial markets to commercial home appliance markets. Current practice of robot development, however, often fails to satisfy this requirement. Nowadays robots can recognize their environment in a limited way. Future robots designed for operations in a natural environment and for communicating with humans in a natural way require the fusion of data acquired from spoken words and sensory data from the surrounding area .In this paper, an intelligent service robot has been developed by means of intelligent sensors for speech recognition, proximity measurement, and image processing. This robot can understand the names of objects or users that a user has told the robot to take, recognize for it by color segmentation and calculate the depth of the target object by a stereo camera. After it has found and identified the object, the robot grasps it and brings it to the user through face recognition.

Index Terms - Service Robot; Sensor Fusion; Speech Recognition; Manipulator; Face Recognition

I. INTRODUCTION

The next generation robots such as service robots must be able to solve the complex goals which up to now only the people can handle. They utilize various technology-intensive components such as speech processors, vision recognizer, actuators to offer services and the robot applications can coordinate these components in harmony way with those people they are supposed to support[1-2]. The key technologies for service robots are intelligent systems which analyze and fuse comprehensive sensor data and derive execution strategies in order to accomplish a task.

In the Shanghai Key Laboratory of Power Station Automation Technology, there is a service robot whose name is 'Sklpat' with visual and speech sensors produced by Harbin Institute of Technology. Sklpat is equipped with binocular vision and network cameras, three front ultrasonic sensors, two lateral ultrasonic sensors, seven chassis obstacle avoidance sensors, two speakers, two manipulators and a 7 inch touch screen allow it to interact with humans through the man-machine interface. Besides, Sklpat is also equipped with TL-WN322G+ Wireless LAN Card of TP-Link, which possess the communication facilities of 54Mbps, contributing to the more convenient control of remote users. The appearance part of Sklpat is illustrated in Fig.1.It recognizes the spoken instruction and acts accordingly by grasping the target object.

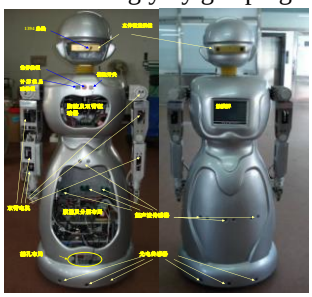

Fig.1. Appearance part description of Sklpat

Sensor fusion algorithms for robots have been developed by several research groups[3-4]. This paper focuses on the integration of intelligent sensors, sensor fusion, speech recognition, grasping and fetching objects with respect to humanoid robots.

II. SYSTEM ARCHITECTURE

A service robot needs to know the task to be accomplished, working environments, the ability to plan and perform actions depending on the working environments and find the right user. Those require the following functions (Fig. 2):

(1) Acquiring data: Sensing by means of multiple sensors in order to acquire all necessary data about the environment includes getting to know the goal to be met, e.g. by understanding a spoken instruction.

(2) Data preprocessing: In the data acquisition process, the information collecting is often accompanied by disturbances because of the impact of objective circumstances, so it is necessary to filter before it is processed in order to gather the purity information.

(3) Fusion of data: Fusion of the data acquired from multiple sensors in order to calculate the situation.

(4) Calculation and decision-making: Plan how to achieve the target object, execute of the necessary steps by controlling

* This paper is supported by State Key Laboratory of Robotics and System (HIT), support number: SKLS-2009-MS-10.This paper is also supported by Shanghai University, "11th Five-Year Plan" 211 Construction Project.

the robot motors, find the right user and give the target object to the user.

A distributed data base provides reference information e.g. for the pattern recognition algorithms in intelligent sensors, for strategies to fuse data or for setting an optimal execution plan. It is important that the data base can be adapted to new situations by methods such as learning algorithms. A robot embedding the features described above can be regarded as intelligent because it can perform tasks depending on a goal in a complex environment and can adapt to new situations by learning.

Depending on the area of activity the robot is equipped with some or all of the following sensors: speech recognition sensor, stereo camera.

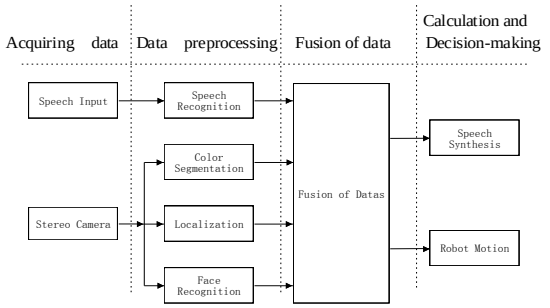

Fig.2 the function of sensor fusion technology

In order to cope with new situations, the speech sensor can learn new words and the vision sensor can learn the color of new object and the face of uses.

In order to measure the distance to an object, stereo camera is used for calculating the depth of the target object. The stereo camera currently also can differentiate between blue and red objects.

III. SPEECH RECOGNITION

Speech interaction module including speech synthesis and speech recognition (Fig.3) is mainly to complete real-time speech control, which is the bridge between man and robot. The robot's speech function module is developed in the Visual C++ 6.0 environment with Microsoft Speech SDK5.1. The Microsoft Speech SDK5.1 provides a high-level interface between an application and speech engines. Microsoft Speech SDK5.1 implements all the low-level details needed to control and manage the real-time operations of various speech engines. The two basic types of SAPI engines are text-to-speech (TTS) systems and speech recognizers. TTS systems synthesize text strings and files into spoken audio using synthetic voices. Speech recognizers convert human spoken audio into readable text strings and files. Microsoft Speech SDK5.1 is easy to use and has high recognition rate. Especially, no training is needed for the user and the feature of n non-specific people has been achieved since the engine is done. Management tools supplied by the API enable users to freely define their own vocabulary and grammar for different applications.

When the system is sub-playing voice, any interruption from the surrounding can't stop the task, which avoids hearing the speech which is played by itself. The system is in support of the adjustment of parameters, such as speed, style, volume, etc, allowing the speech of synthesis is continuous, understandable and nature, just like ordinary people's voice.

The speech signal is input, such as the user's input speech is "looking for green tea ".After processing and recognition by the system, converted into the corresponding action code to control the robot, it executes the corresponding action, while the robot can be by way of speaking to the feedback, such as when the robot will complete the action it can say" I have found ".

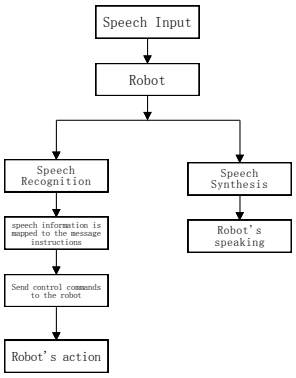

Fig.3. Speech interaction module

The intelligent speech recognition enables the robot to understand spoken instructions. These are either single words or a sequence of words which are spoken without breaks in between. After data acquisition, each word is assigned to an instruction, so that the robot now knows its task, e.g. which object to search for.

IV. OBJECT RECOGNITION AND LOCALIZATION

A binocular stereo camera is used in the system, which is from Point Grey Company. We extract one frame from the right camera of the binocular stereo camera. RGB (red, green, blue) color space data points from an image are projected into HSV (hue, saturation, value) color space to provide data points that are insensitive to the variations of illumination after the median filting.

A threshold segmentation algorithm is employed to extract the object. The 3D position is computed by the disparity picture, which is then passed to the manipulator module to grasp the object.

A. Traditional binocular stereo vision model

Stereo vision is based on the parallax theory as shown in Fig.4[5]. B is baseline length, f is the focal distance of the camera. Matching the corresponding pixel with a variety of algorithms[6], we can get the parallax d as following:

$$d = x_R - x_L \quad (1)$$

Then the depth information z can be obtained by the method based on the triangulation:

$$Z = f \times B / d \quad (2)$$

The model is adopted in the most existing system of stereo vision.

The Bumblebee[7] of Point Grey Company is shown is Fig.5, which is used in our robot. The camera specifications are shown in Table 1.

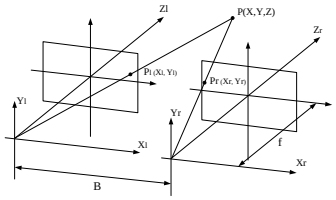

FIG.4 TRADITIONAL BINOCULAR STEREO MODULE FIG.

5 THE BUMBLEBEE USED IN THE ROBOT

B. RGB to HSV

A color can be represented by many color space modules. The RGB (red, green and blue) color space is the most common one. In digital images, the RGB values are between 0 and 255. Since the accuracy of the color detection affects the results of locating the object, choosing the suitable color space for color segmentation is very important. In this sense, RGB color space is not suitable because it is very sensitive to the variations of intensity. Since the segmentation results must be insensitive to the strength of illumination, color segmentation based on hue, saturation and value (HSV) has been chosen as suitable for this research.

TABLE 1. THE SPECIFICATIONS OF BUMBLEBEE

Specification	Low-Res(640×480)	High-Res(1024×768)
Imaging sensor	Two Sony progressive scan CCD	
	IC×424(648×488 max pixels)	IC×204(1024×768 max pixels)
	7.4μm square pixels	4.65μm square pixels
Baseline	12cm	
Lens Focal Length	3.8mm with HFOV	
Frame rates	48,30,15,7.5,3.75,1.875 FPS	18,30,15,7.5,3.75,1.875 FPS
Interfaces	6-pin IEEE-1394 for camera control and video data transmission 4 general-purpose digital input/output (GPIO)pins	

The HSV coordinate system, proposed originally in Smith[8], is cylindrical and is conveniently represented by the hex cone model shown in Figure 6[9-10]. The saturation is a measure of the lack of whiteness in the color, while the hue is defined as the angle from the red color axis, and value refers to the brightness. The motivation for using the HSV space is found in experiments performed on monkeys and anthropological studies, because it corresponds more closely to the human perception of color. This user-oriented color space is based on the intuitive appeal of the artist's tint, shade, and tone.

The set of equations listed in (3) are used to transform a point in the RGB coordinate system to the appropriate value in the HSV space.

C. Object Recognition and Localization

We first learn the HSV values of the object color off-line, with the thresholds of HSV being recorded. Figure 7 shows the color filter off-line mode program in VC++ 6.0. In on-line mode, the thresholds are read from the file, which is used to check each pixel in the picture. The points owned to the object are saved in a point list structure. Then the 3D position of the object is computed by the stereo vision. The flow of image processing is shown in Figure 8.

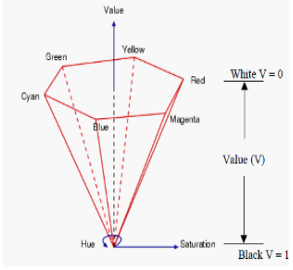

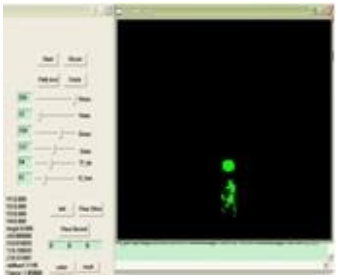

FIG.6 THE HSV COLOR SPACE FIG.7 THE COLOR FILTER MODULE

$$\begin{cases} h = cos^{-1}\dfrac{\frac{1}{2}[(R-G)+(R-B)]}{\sqrt{(R-G)^2+(R-B)(G-B)}} \\ s = 1-\dfrac{\min(R,G,B)}{v} \\ v = \dfrac{(R+G+B)}{3} \end{cases} \quad (3)$$

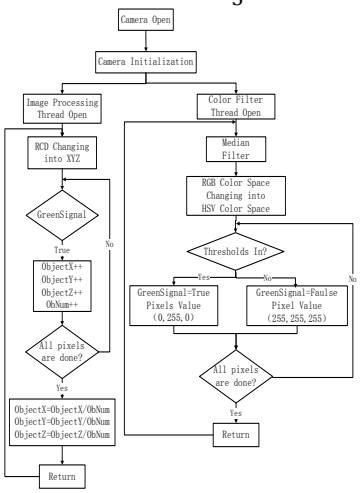

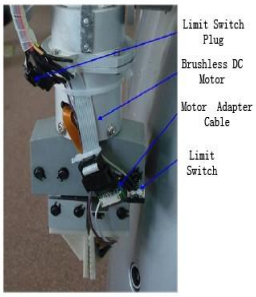

FIG. 8 THE FLOW OF IMAGE PROCESSING

FIG.9 THE GRIPPER OF THE MANIPULATOR

Target identification is by the color extraction, Robot eyes can look the color which is extracted from the target. Once Robot finds the color that the number of colur points must be more than 70,and then the Robot can go straight towards to target unless encountering obstacles. If robot finds obstacles, firstly, it stops for about 5S,If the obstacles still appear, entering into the obstacle avoidance program. There are not obstacles or avoiding obstacles, The Robot need adjust the direction according the colure. While the number of colure point is more than 300,the distance of target is almost accurate. Specific operation, as shown in diagram:

V. MANIPULATOR CONTROL

When the robot has moved to the target object in the appropriate position, we can learn the position of target object by color segmentation and stereo camera. The appropriate

position is that the object is in the workspace of the right arm of the robot. With the 3D position of the object, passed from the stereo vision module, the robot can grasp the object with the manipulator.

Each manipulator of the robot has six rotate degrees of freedoms (DOF). A gripper is set to the end of the manipulator, which has two limit switches as shown in Figure 9.

A. Manipulator kinematics

To evaluate the kinematics of the proposed robotic arm, the Denavit-Hartenberg (D-H) representations of the robotic arm is presented as shown in Fig. 10. The D-H representation is used to formulate the forward kinematics. The D-H representation of the robotic arm is characterized in terms of the D-H table, as shown in Table 2. Where d_3, d_6 and a_4 are shown in Fig. 10, and they are fixed distance, angles of θ_1 toθ_6 are joint angles of the robotic arm, and they are adjusted in terms of the harmonic drive gear motors, l1 to l6 in Table 2 are listed as Table 3.

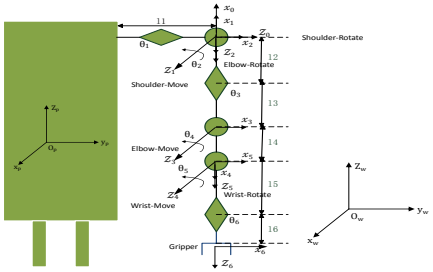

FIG. 10 THE D-H REPRESENTATIONS OF THE ROBOTIC ARM

TABLE 2 THE D-H TABLE OF THE ROBOTIC ARM

	θ_i	d_i	a_i	α_i
1	θ_1	0	0	-90°
2	θ_2 - 90°	0	0	90°
3	θ_3	l3+	0	-90°
4	θ4 - 90°	0	l4	0
5	θ5 +	0	0	90°
6	θ6	l5+	0	0

TABLE 3 THE LENGTH OF EACH LINKS

l1	l2	l3	l4	l5	l6
8	5	19	22	4	13

According to the D-H representation table, the matrix representations can be also desired as shown in (4). The gripper coordinates (Px, Py, Pz) can be calculated in term of (5). Therefore, the forward kinematics is finally evaluated when the joint angles of harmonic drive gear motors (θ_1 to θ_6) are given.

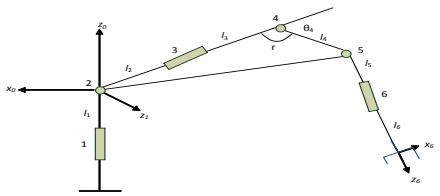

FIG.11 THE STRUCTURE DIAGRAM FOR THE INVERSE KINEMATICS

On the other hand, the inverse kinematics is applied for the trajectory planning requirements. Due to the structure of the robotic arm, it is impossible to find a unique solution for a given end effector position and orientation. Therefore, a geometry based approach is proposed in the paper. The structure diagram for the inverse kinematics is shown in Figure11.

$$A_1=\begin{vmatrix}\cos\theta_1 & 0 & -\sin\theta_1 & 0\\ \sin\theta_1 & 0 & \cos\theta_1 & 0\\ 0 & -1 & 0 & 0\\ 0 & 0 & 0 & 1\end{vmatrix} \quad A_2=\begin{vmatrix}\sin\theta_2 & 0 & -\cos\theta_2 & 0\\ -\cos\theta_2 & 0 & -\sin\theta_2 & 0\\ 0 & 1 & 0 & 0\\ 0 & 0 & 0 & 1\end{vmatrix}$$

$$A_3=\begin{vmatrix}\cos\theta_3 & 0 & -\sin\theta_3 & 0\\ \sin\theta_3 & 0 & \cos\theta_3 & 0\\ 0 & -1 & 0 & l_2+l_3\\ 0 & 0 & 0 & 1\end{vmatrix} \quad A_4=\begin{vmatrix}\sin\theta_4 & \cos\theta_4 & 0 & l_4\sin\theta_4\\ -\cos\theta_4 & \sin\theta_4 & 0 & -l_4\cos\theta_4\\ 0 & 0 & 1 & 0\\ 0 & 0 & 0 & 1\end{vmatrix} \quad (4)$$

$$A_5=\begin{vmatrix}-\sin\theta_5 & 0 & \cos\theta_5 & 0\\ \cos\theta_5 & 0 & \sin\theta_5 & 0\\ 0 & 1 & 0 & 0\\ 0 & 0 & 0 & 1\end{vmatrix} \quad A_6=\begin{vmatrix}\cos\theta_6 & -\sin\theta_6 & 0 & 0\\ \sin\theta_6 & \cos\theta_6 & 0 & 0\\ 0 & 0 & 1 & l_5+l_6\\ 0 & 0 & 0 & 1\end{vmatrix}$$

$$T = A_1A_2A_3A_4A_5A_6 = \begin{bmatrix} n_x & o_x & a_x & p_x \\ n_y & o_y & a_y & p_y \\ n_z & o_z & a_z & p_z \\ 0 & 0 & 0 & 1 \end{bmatrix} \quad (5)$$

B. Grasping Experiment

This experiment investigates the performance of the grasping task with a stereo camera and color segmentation. Only the color information about the object was used in this experiment. The robot itself was stationary. It grasped the object, lifted it ten centimeters and placed it back in the same position. This was repeated 40 times all with different locations of the object. The object had been placed by hand arbitrarily in the workspace of the arm. To get different position height the object was placed on different furniture and boxes. During one run the object was static. The experiment was done without artificial light only with natural sun light. The flow of the grasping can be seen in figure 12.

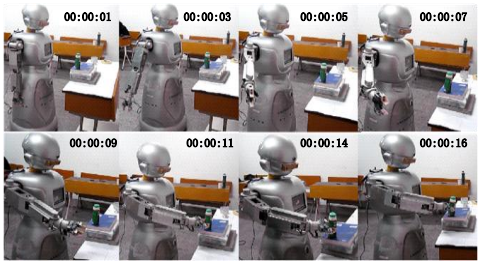

FIG. 12 THE FLOW OF THE GRASPING

The object was a colored cup. Because the vision system used could only compute the position without the orientation of the object, the arm always grasped the object in horizontal orientation. In other words the last arm segment was parallel to the floor. During the experiment no other object with the same color was in the visual field of the camera. The vision system ran at 15 frames per second and with a resolution of 640×480 pixel.

The robot tried 40 times to grasp the object. Nine times the arm pushed the object over. Ten times the arm moved the

object by approaching it.One time the stereo camera could not calculate the depth. This is a success rate of 50%.

This experiment showed that nine times the position calculation of the object was imprecise. This can be handled by using an infrared sensor of the hand to detect if the object is in the hand. This could prevent the arm for pushing the object over. Also the arm path is not yet complete. It was also shown that the color segmentation approach with a stereo camera is also working.

VI. Sensor Fusion, Planning and Motion Control

By fusing the speech, visual and color data, the robot knows all objects within its reach and their position as well as the goal it is advised to reach.

The fusion algorithm used is hierarchical and works as follows:

1. Speech and visual data are fused by matching the speech (derived from the speech sensor data) with one of the object identifiers (derived from the camera data). We overcome the binding problem by not dealing with sensor data themselves but by fusing classification results. The algorithm generates one of the following hypothesis:

-A negative match result (e.g. no object or the wrong object) leads to the hypothesis" object not found " . This requires no additional fusion of visual and color data and causes the robot to repeat the search.

- A match of one of the object results in the hypothesis "object found".

2. The robot moves towards the object until the object numbers gained by means of color segmentation are above the threshold value got by doing the experiment. In the next fusion step the hypothesis generated by the color segmentation is verified by the data acquired from the depth calculation of a stereo camera. If the distance equals the hypothesis it is regarded as true. Otherwise the hypothesis is rejected.

Currently we apply the fusion approach to differentiate 2 kinds of objects, a blue bottle and a red bottle.

Depending on the outcome of the sensor fusion the robot develops different execution plans and controls the robot motors accordingly:

• If the demanded object has been identified, the robot approaches it and grasps it in order to bring it to the user.

• If no or the wrong object has been spotted, the robot repeats the search by turning the robot and by moving in order to change the position.

The robot grasps the objects by gripper. It stops the gripper movements if a feedback signal indicates a resistance. Then robot gives the object to the user by means of face recognition as follows:

• If the user is the right one demanded, the robot approaches and brings the bottle to the user.

• If no or the wrong user has been found, the robot repeats the search by turning the robot and by moving in order to change the position until it finds the right user by the way of face recognition.

VII. Application Example

One typical example of the robot's performance is to search for objects and bring it to the user. This was repeated 20 times all with different locations of the object. The object was a stack of colored cups. The blue and red cups had been taught. The blue and red cups were placed on a desk. The experiment was done without artificial light only with natural sun light.

If the user says "Find blue cup and give it to xiaohong", the robot understands its task and searches for the cup. After detection, it grasps the cup and brings it to xiaohong(Fig.13).

Fig.13 the process of example

In a scenario of the example, the robot tried 20 times to grasp the object:

• One time the robot could not recognize the speech.
• One time the stereo camera could not calculate the depth.
• Two times the robot could not find the right user.
• Two times the robot could not grasp the object.

This is a success rate of 70%.

VIII. Summary

A robot has been developed which understands spoken instructions and can act accordingly. If the user advises the robot to bring a specific object, the robot uses its smart camera and other sensors to search for the object and brings it to the user. As future work additional applications such as home service robots, cleaning robots, entertainment robots are being developed.

References

[1] L. Brethes, P. Menezes, F. Lerasle and J. Hayet, Face tracking and hand gesture recognition for human–robot interaction, in: Proc. IEEE Int. Conf. on Robotics and Automation, New Orleans, LA, pp. 1901–1906 (2004).

[2] L. Aryananda, Recognizing and remembering individuals: online and unsupervised face recognition for humanoid robot, in: Proc. IEEE/RSJ Int. Conf. on Intelligent Robots and Systems,Lausanne, pp. 1202–1207 (2002).

[3] Matthias Zobel,Joachim Denzler. Integration of vision and dialogue in service robots, Machine Vision and Applications (2003) 14: 26–34.

[4] RIE KATSUKI, ROLAND SIEGWART. Reasoning of abstract motion of a target object through task order with natural language—pre-knowledge of object-hndling-task programming for a service robot, Advanced Robotics, Vol. 20, No. 4, pp. 391–412 (2006).

[5] Hyun-Jeong Lee, Min Cheol Lee. Technique for Localization and Visual Servoing of Mobile Manipulators. IEEE International Symposium on Industrial Electronics, 2009

[6] R Y Tsai. A versatile camera calibration technique for high-accuracy 3D machine vision metrology using off-the-shelf tv cameras and lenses[J]. IEEE Journal of Robotics and Automation,1987,3(5):323-344.

[7] Point Grey Research. Bumblebee 2 Getting Started Manual.2006.

[8] Smith, A.R.. Color gamut transform pairs. Computer Graphics (SIGGRAPH'78 Proceedings), 1978.

[9] Foley, J.D., vanDam, A., Feiner, S.K., Hughes, J.F. Fundamentals of Interactive Computer Graphics. Addison Wesley, Reading, M.A,1990.

[10] Kasson M.J., Ploaffe, W. An analysis of selected computer interchange color spaces. ACM Transaction of Graphics, 1992.

2011 International Conference on Mechanical, Industrial, and Manufacturing Engineering
Lecture Notes in Information Technology Vols. 1-2

Little-Shear-Modulus Model for Solving the Lamination Rotor Eigenfrequency Problems

Xu Yang
Institute of Nuclear and New Energy Technology
Tsinghua University, Beijing 100084, China
xuxu@tsinghua.edu.cn

Xu Chang
Nanning College for Vocational Technology
Nanning, Guangxi 530008, China
1196401@qq.com

Yu Suyuan
Institute of Nuclear and New Energy Technology,
Tsinghua University, Beijing 100084, China
suyuan@tsinghua.edu.cn

***Abstract* - In some mechantronic machines' design, the lamination stack structures are generally to be part of the rotor. It consists of pieces of stalloy, which is designed as very thin steel plate coating with special isolative paint. These sheets of assembly stacking stalloy will definitely influence the eigenfrequency and other dynamic effects of the rotor. But, considering the lamination's mechanical character, this influence is difficult to be well counted during design period. Some simplified ways are used to approximatively solve this kind of problem, such as modeling the lamination as a part of the rotor and neglecting its mechanical rigidity influence. In this paper, two of these useful simple traditional models are studied and compared. Finally, the Little Shear Modulus (LSM) Model, a new idea model will be demonstrated, which could exactly simulate the mechanical characters of the lamination stack and be easily understand as well. An assumed simple rotor example is used to evaluate this model, and the result proves that the LSM model can give more reasonable result. Finally, an real example is shown that how this LSM model is applied to solve the eigenfrequency of an actual grinder rotor.**

Index Terms* - *Lamination, Rotor Dynamics, Eigenfrequency, FEA

I. Introduction

The active magnetic bearing rotor laminations are constructed of low loss, electrical grade steel, which can well reduce the eddy current losses under high frequency electric-magnetic control signal.

The alternating magnetic flux creates electro motive forces inside the material it flows through. These electro motive forces fluctuate at the same speed as the flux and similarly create eddy currents normal to the flux path, i.e. the eddy currents circle around the flux. The eddy current power loss can be presented as the following equation:

$$P_{ec} = \frac{V_{lam}(\pi f \hat{B} \tau)^2}{6\rho_{lam}} \quad (1)$$

The structure of lamination stack solves the problem of eddy current losses, but it also brings difficulty in dynamic analysis. Now, the dynamic analysis, including modal analysis and eigenfrequency analysis are mostly dealed by Finite Element Analysis (FEA) through computer, and the most important work of FEA is to set up an appropriate model.

II. Two Traditional Lamination Models

Of cause, the lamination stack changes the rotor dynamic effect. Consider the structure of lamination stack, it supplies a notable mass but only small rigidity to the rotor. That is just why it is difficult to set up an FEA modal for it. In this paper, three solution models for this case will be introduced. Two of them are commonly used and the other is a new one.

A. Middle-Result (MR) Model

There are two excessive situations to simplify the lamination structure. One is to consider the lamination as a part of the rotor, which will provide both mass and rigidity to the rotor, and the FEA eigenfrequency calculated result will be higher than the true eigenfrequency. The other is to consider the lamination as additional mass of the rotor, without stiffness. And then, the eigenfrequency calculated result will be lower than the truth value. When the lamination stack is placed near by the stationary point of a bending axis, or when the lamination stack is just a very small part of a rotor, its influence to the bending eigenfrequency is not very strong, and the middle result of these two excessive situations can be well close to the true value. So it is called Middle-Result (MR) Model. But if the lamination stack is placed over the peak of a bending axis, these two excessive situations will bring to two distinct results, and the middle result of them will lose its meaning.

B. Small-Rigidity (SR) Model

Another reasonable model to simulate the lamination stack is Small-Rigidity Model. It is known that the lamination will be very rigid when it is pressed by outer force, but when

it is dragged, it will present to be very flexible, even very easy to be separated. Also consider the bending modal shape of the rotor, when the rotor is ideally purely bended, half of the cross section is under pressed and the other half is under dragged. So, assume that the lamination has only half rigidity of common steel, it comes out the half-rigidity model. In fact, each piece of the lamination stack is coating with the insulation layer. So mostly, when the lamination is under pressed, it can not even provide half rigidity of the steel material, just because the insulation layer is much softer than the steel. Base on the actual analysis object, some other models like one third or one fourth rigidity model under experiences are used. They are here looked like as the similar method, it is call Small-Rigidity model, which is often used in special situation when the object rotor has been well studied.

III. LITTLE-SHEAR-MODULUS (LSM) MODEL

Consider the actual lamination stack, to each piece itself, it has the same basic mechanical character as the ordinary steel material, but there is little relationship between each isolated piece of stalloy when the bending deformation is not very large. When the lamination stack is modeled as a big block of solid mass, it ought to be such a kind of material which is hard to be pressed and very easy to be sheared off between the layers. So, in finite element analysis, it can be assumed to be an ideal anisotropic material which has little shear modulus on the plane direction parallel to the steel plate, this is called Little-Shear-Modulus material model. In addition, the idea of half-rigidity model is borrowed here, in the direction parallel to the axis, only half elastic ratio will be used. The other modulus in the other directions of this model is kept as usual. This LSM anisotropic material model can nearly simulate the full mechanical character of the lamination stack on the rotor.

If this LSM model is used to solve the rotor dynamics problem, several important factors should be carefully considered, such as balance of Poisson's coefficients and the change of Young's modulus. These will be shown in the following example.

As a test of the LSM model, modal analysis of a simple rotor shown in figure 1 is performed by the above three solutions. The different bending eigenfrequency results are compared.

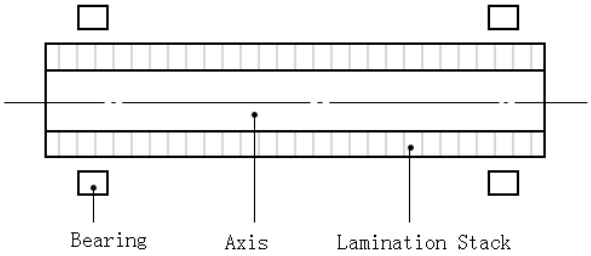

Fig. 1 A beam model for lamination analysis

To this rotor, its eigenfrequency is largely changed when the outside lamination stack is added up. Assume the length of this rotor is 180mm, the rotor diameter is 14.6mm, the lamination diameter is 40mm, and the bearing stiffness is 1x105N/m, the distance from the AMB to the axis top is 30mm.

A. Material Property

The material of the rotor is assumed to be ordinary steel, which has the following steel material properties: density ρ_S is 7800kg/m^3, Young's modulus E_S is 200GPa, and Poisson's coefficient μ_S is 0.3.

The lamination steel property is differed from ordinary steel: density ρ_L is 7550kg/m^3, Young's modulus E_L is 200GPa, and Poisson's coefficient μ_L is 0.3. But this property will be assumed to be different with different model.

MR model will use two different Young's modulus: E_{MR1} = 200GPa, E_{MR2} = 0, other material properties are the same.

SR model will use 1/8 of the ordinary Young's modulus: E_{SR} = 25GPa, other material properties are the same.

LSM model will use the following assumed anisotropic material properties:

Young's modulus:

$E_X = E_Z = 200e9, \quad E_Y = 100e9$

Shear Modulus:

$G_{XY} = G_{YZ} = 80e7, \quad G_{XZ} = 80e9$

Poisson's coefficient:

$\mu_{XY} = \mu_{XZ} = \mu_{ZY} = \mu_{ZX} = 0.3,$

$\mu_{YX} = \mu_{YZ} = 0.15$

Density:

$\rho = 7850$ kg/m^3

Here, the Y direction is parallel to the axis direction. And the six Poisson's coefficients are not fully isolated, they have to fit the function show as Eq.2.

$$\begin{cases} E_X \cdot \mu_{YX} = E_Y \cdot \mu_{XY} \\ E_Y \cdot \mu_{ZY} = E_Z \cdot \mu_{YZ} \\ E_Z \cdot \mu_{XZ} = E_X \cdot \mu_{ZX} \end{cases} \tag{2}$$

And the shear modulus can not be set to zero because of two reason. One is to avoid the instable of stiffness matrix, and the other is to represent the friction.

B. FEA model

Except for the material property, these three solutions will use the same boundary conditions, the same finite element mesh, and the same FEA software.

Firstly, the FEA calculation is based on 3D model, and a higher order 20-node 3D solid brick element is used in meshing. This kind of element has quadratic displacement behavior, and supports large deflection. The bearing suspension will be modeled as two directions springs connection from the middle node of the axis to the fix boundary, which have the same stiffness as the AMB. This FEA model is shown in figure 2.

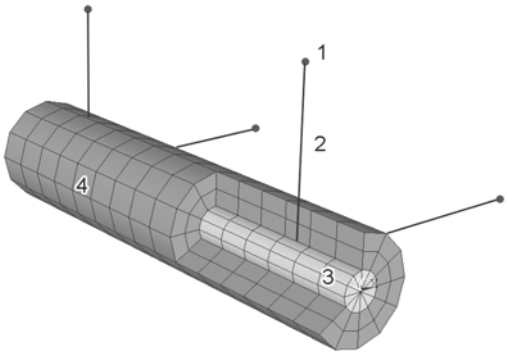

1). Fix Boundary 2). Spring Element
3). Axis 4). Lamination

Fig. 2 The FEA model of the beam example

This FEA 3D model includes totally 544 elements and 2832 nodes.

C. Modal Analysis Results

The eigenfrequency of modal analysis results from different models are listed below:

TABLE I
EIGENFREQUENCY SOLUTIONS

Eigenfrequency Solution	MR	SS (1/8 rigidity)	LSM
1st Rigid	53	54	53
2nd Rigid	61	62	61
1st Bending	2816	1918	2114
2nd Bending	6587	4663	3693

The two rigid eigenfrequency is all the same in different model calculation results, because it only depends on the rotor mass and the bearing stiffness. But the bending eigenfrequency results are quite different.

Judging by the frequency, it is hard to tell which model can give the best result. Thus, the simulated modal shapes of different models are also compared. It is obvious that the LSM model gives a quite different bending modal shape to the others. The following figure 3 shows the 1st bending modal shape of LSM model result and the ordinary bending modal shape.

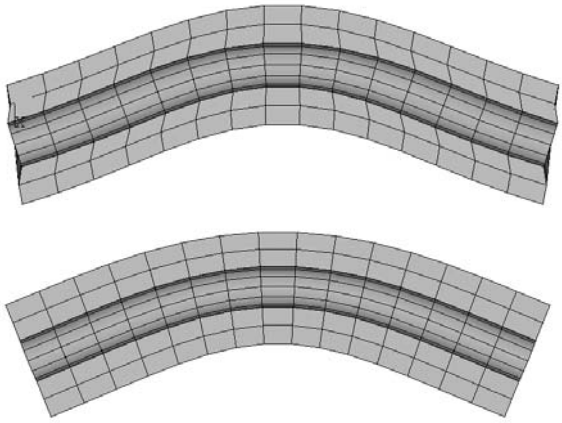

1) Bending of LSM Model 2) Ordinary Bending
(Displacement scale is largely amplified)

Fig. 3 The 1st bending modal shape

Because each steel plate of the lamination stack is isolated, when the rotor is bending, these lamination plates are much easier to be sheared off than to be pressed, which is correctly showed in the LSM model bending shape. In other words, the bending of lamination stack is not a theoretical pure bending, and through an ideal anisotropic material, it can be well simulated by FEA calculation.

IV. AN EXAMPLE OF AN ACTUAL GRINDER ROTOR

Finally, the LSM model is used to demonstrate the eigenfrequency of an actual grinder rotor, which is an active magnetic bearing (AMB) suspending rotor. This grinder rotor is shown in figure 4.

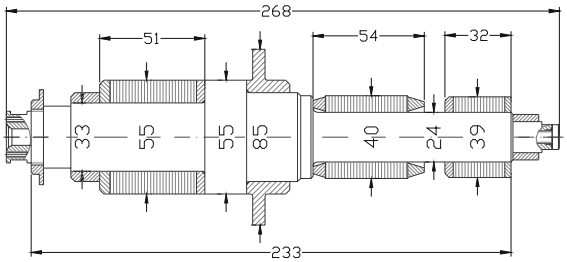

Fig. 4 The grinder rotor

There are three sections on this rotor using lamination structural: two for AMB and the middle one for electric motor. The FEA method with LSM model is used to solve the first bending eigenfrequency of this rotor. The detail of how to process the calculation will not be repeated again.

The FEA calculation result of the first bending eigenfrequency of this grinder rotor is about 1879Hz, and the experiment test result is about 1800Hz. The relative deviation of the first bending eigenfrequency which solve by using LSM model is about 4.4%. And the other eigenfrequencies are not tested in the experiment.

IV. CONCLUSIONS

The LSM model can well represent the property of lamination stack. Using the LSM model in FEA modal analysis can not only get the actual eigenfrequency, but also can show more actual bending shape of the rotor. This LSM model will be very useful in solving the dynamics problem of the rotor with lamination structure.

REFERENCES

[1] Schweitzer G, Bleuler H, Traxler A. Active Magnetic Bearings, Zurich, vdf Hochschulverlag AG., 1994

[2] Allaire PE, Kasarda MEF, Fujita LK: Rotor power losses in planar radial magnetic bearings – effects of number of stator poles, air gap thickness, and magnetic flux density. Proc. 6th Internat. Symp. on Magnetic Bearings, MIT Cambridge, 1998, August 5-7, 383-391.

[3] Rotating Machinery and Controls Laboratory. 2003 Romac Newsletter. http://www.virginia.edu/romac/

2011 International Conference on Mechanical, Industrial, and Manufacturing Engineering
Lecture Notes in Information Technology Vols. 1-2

Introducing the Cases Study of Application of Digital Factory for SMEs in KOREA

SangSu Choi, Hyunjei Jo and YongJu Cho
Manufacturing System R&D Department
Korea Institute of Industrial Technology, Cheonan-si, Chungcheongnam-do 331-825, KOREA
{ sschoi & hjjo & yjcho }@kitech.re.kr

***Abstract* - Manufacturing companies are putting their utmost efforts to improve their productivity. In order to achieve this, they introduce various solutions into IT area. Especially, digital manufacturing has the potential to transform the businesses environment and significantly improve the competitiveness. Digital manufacturing supports the whole manufacturing activities based on digital factory. Here mentioned digital factory means the computer model that realizes the integrated modeling of the product, process, production equipment and environment as for one actual manufacturing plant. In this paper, we introduce the case studies of improving productivity using digital factory in the SMEs in Korea and propose the process modeling system for manufacturing simulation.**

Index Terms - Digital Manufacturing, Digital Factory, Lean Manufacturing, Manufacturing Simulation, Improving productivity

I. INTRODUCTION

Manufacturing companies are putting their utmost efforts to improve their productivity. In order to achieve this, they introduce various solutions into IT(Information Technology) area. Especially, Digital Manufacturing has the potential to transform the businesses environment and significantly improve the competitiveness. Digital manufacturing supports the whole manufacturing activities based on digital factory. [1] Here mentioned digital factory means the computer model that realizes the integrated modeling of the product, process, production equipment and environment as for one actual manufacturing plant. [2]

As many automobile companies such as Toyota, GM, and DaimlerChrysler run digital factory based beforehand inspection to find out any possible problems caused during production, the effectiveness of such production simulation based on digital factory is already proved by many of these examples. [3][4] The Korean Government puts huge efforts on planning and implementing of improvement for small and medium sized companies and KITECH (Korea Institute of Industrial Technology) is to improve the competitiveness and technologies of small and medium sized companies in automobile, machine assembly, electric/electrical, shipbuilding and aerospace industries by supporting their IT which can improve their competitiveness and technical skills by applying IT to the existing MT (Manufacturing Technology). This paper introduces examples of collaboration of IT and MT based on above mentioned digital factory and the system that is being developed to support small and medium sized companies and proposes the process modeling system for manufacturing simulation.

II. CASES OF SUPPORTING COMPANIES

As it is well aware, significant funds and professional labor are required for fusion of IT and MT such as building digital factory. However, most of small and medium sized companies in Korea are facing difficulties due to lack of quality labor, technologies and funds for R&D and deterioration of the facilities. It is essential to find and develop a core manufacturing competitiveness to cut down the production cost to increase the productivity and improve technical skills in order to compete with other oversea companies who earn their competitiveness with low labor cost.

KITECH applied the methodology of IT and MT confusion to two selected small and medium sized companies and analyzed the caused problems and results of the application.

A. E Company, Inc.

E company produces robots and automatic line of distribution system. They want to extend 'DISK & DRUM' automatic supply line anew and simulate the line for prevention of encounter problems.

1) *The purpose of project*: The purpose of project is to build digital factory of E company with 3D simulation model creation of 'DISK & DRUM' automatic supply line (Fig. 1) and verify the production process by simulation analysis. (an output, the rates of operation of equipment etc.) And then draw efficient plan.
2) *The goal of project*: Building the 3D simulation model of DISK & DRUM automatic supply line.
   - Verification of the process
   ① Correction of quantitative result and Examination of achievement of target output per a day.
   ② Checking the rates of operation of equipment and bottleneck of process.
   ③ Suggestion of solution about occurred problems and weak point.
   - To-Be planning by analysis of AS-IS.
3) *Used software*: DELMIA / QUEST (Discrete Event S imulation)
4) *The result of project*: We build 3D digital factory as s

hown in Fig. 2 by simulation preparation and analysis of related basic data include 2D layout.

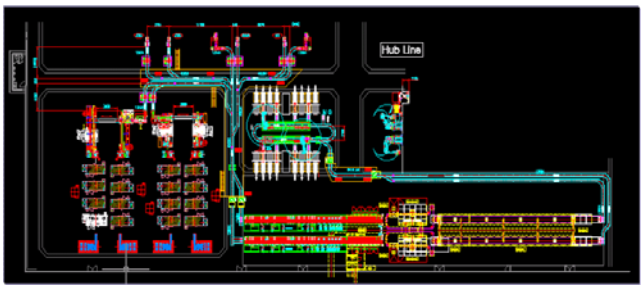

Fig. 1 2D layout of DISK & DRUM automatic supply line

Fig. 2 Digital factory of E company

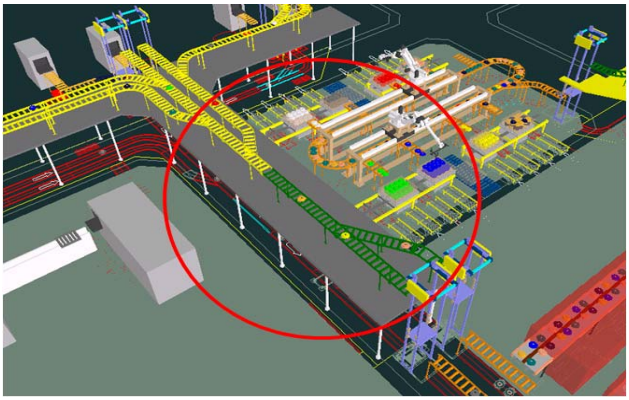

Fig. 3 Bottleneck states

As the result of analysis of new DISK & DRUM automatic supply line, two serious bottleneck states are found as shown in Fig. 3 and it can be big problem causes for operation of the line. These can be resolved by changing properties of facilities that are expected to put into the layout and optimizing the production process which we optimized to meet the initial target output.

1) Analysis of Simulation Results

- AS-IS Total Output of 20 hours Operation: Bottleneck State.
- TO-BE (1st ROUND) Total Output of 20 hours Operation: 14,904EA.
- TO-BE (2nd ROUND) Total Output of 20 hours Operation: 15,984EA.

B. M Company, Inc.

M company is manufactures car parts produce part such as door assembly and panel assembly hood etc. We conducted prior-simulation because it is necessary to build up the production line that various systems can be operated due to the troubles caused by diversification of product type, subdivision of process, increase of the process scale and etc.

1) The purpose of project: The purpose is to draw out an efficient solution and prove the production process of the whole line through the simulation analysis (output and rate of resource operation) by using 3D modeling and building digital factory of new front panel production line.

2) The goal of project: Building 3D simulation of new front panel manufacturing production line.

- Verification of the process

① Collect the information whether daily target output has been accomplished and the quantitative results.

② Check the rate of manufacturing resources operation and bottleneck sections.

③ Check working hours and work efficiency of the worker.

④ Check expected problems and weak points and draw out the solution.

- TO-BE plan in advance through AS-IS Analysis.

3) Used software: DELMIA / QUEST (Discrete Event S imulation)

4) The result of project: Fig. 4 shows new production lin e modeling by Quest.

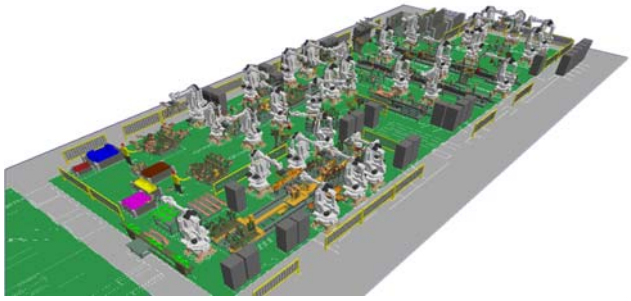

Fig. 4 New production line modeling by Quest

Below table 1 is a summary of the issues for results of the simulation. In table 1, we can see whether the bottleneck state that was occurred during As-Is Model simulation is happening, the number of times that the bottleneck state happened and the output differences accordingly while we also can check the fact that the bottleneck states are all resolved by correcting the problems through To-Be Model.

TABLE I
ANALYSIS BETWEEN AS-IS AND TO-BE

The simulation time		The amount of input	The amount of output	Occurrence of bottleneck or NOT (Count)
1 Hour	As-Is	54	50	Occurrence (12)
	To-Be	54	54	Nonoccurrence (0)
8 Hour	As-Is	430	397	Occurrence (40)
	To-Be	430	430	Nonoccurrence (0)
24 Hour	As-Is	1288	1191	Occurrence (105)
	To-Be	1288	1288	Nonoccurrence (0)

III. SUPPORT POLICY AND PROPOSED SYSTEM FOR SMES

First of all, the importance of beforehand inspection for design and manufacturing was carefully reviewed through the aforementioned example. Irregular and nonscheduled order and pressure to shorten the delivery are few of the difficulties that small and medium sized companies are facing. The above introduced solutions may help to find an appropriate solution for small and medium sized companies. However, the tools for such beforehand inspection are very expensive and hard to use. Despite of these disadvantages, large companies adopt the system since its effectiveness is already proven but small and medium companies are hardly able to not only purchase such system but also employ professional people. Also, in order to conduct the simulation of the above examples, modeling work is supposed to be done in advance and this modeling work is very time consuming and causes many other difficulties.

In regard to process planning, KITECH is currently developing low price modeling tool for small and medium sized companies and planning to use this tool for increase of the productivity and training human resources of small and medium sized companies while providing technical consulting to them.

Fig. 5 is a screenshot of the simulation modeling tool currently under development.

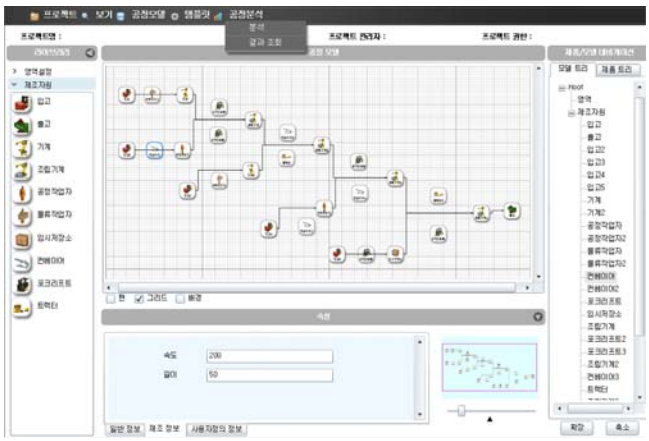

Fig. 5 Screenshot of process modeling tool

The modeling tool that KITECH is developing is online based system which allows ease of use if the user can use the PowerPoint of MS. GUI (Graphic User Interface) is developed on web 2.0 based by using Silverlight and the system is being developed to interwork between various heterogeneous commercial simulation engine.

Most of time, small and medium sized companies use excel or depend on their work experiences when they produce process plan. All expected effects when the system that we developed applied to an automobile parts manufacturing company are shown in table 2.

TABLE II
EXPECTED EFFORTS

	The change of process planning (The change each a day or a week)	The change of production line (The change each a month)	The setting up new lines (The change each a year)
Task	- The method of input material - The materials transport and workers - The allocation processes and working time - Warehouse and handling products, etc	- A type of manufacturing line - Removal or supplement working cells	- Setting up new lines and arrangement of working cells
As-Is	- Dependence of expert experience - Using MS-Excel - Occurrence of unforeseen circumstances	- Determination through the meeting with the person in charge - Impossibility of prior verification	- Consulting experts - Using commercial simulations S/W
To-Be	- Easy decision of process planning using the proposed system	- Possibility of prior verification using the proposed system	- Easy cooperation with consulting company using the system

For ease of modeling, it provides template for not only each tools but also each industries and each type of business. If the user uses the provided templates, he can reduce the modeling time.

IV. CONCLUSION

As it is well aware, significant funds and professional labor are required for collaboration of IT and MT such as building digital factory. However, most of small and medium sized companies in Korea are facing difficulties due to lack of quality labor, technologies and funds for R&D and deterioration of the facilities. KITECH developed the process modeling tool to provide easy process planning for small and medium sized companies and we will support small and medium sized companies by using this system. This system tool will be provided in online and provides templates for each industries and types and the library that allows an easy process modeling. The process modeling system suggested in this study is under beta-test and will be supplemented through examples of application of the system to real companies. In near future, we will introduce examples of application of the system and services provided to real companies.

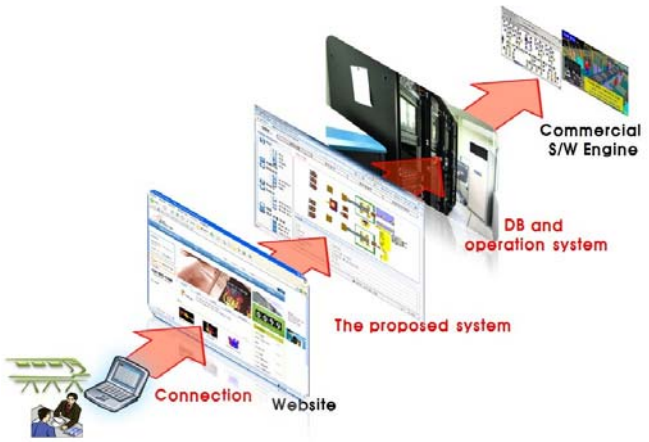

Fig. 6 Usage Process

ACKNOWLEDGMENT

This study is partially supported by “Development of Manufacturing Supporting Platform Technology Coupled with DMS” project which is R&D Program of MKE (The Ministry of Knowledge Economy) and planning project of KITECH.

REFERENCES

[1] K. Iwata, M. Onosato, K. Teramoto and S. Osaki, “A Modeling and Simulation Architecture for Virtual Manufacturing Systems”, *CIRP Annals - Manufacturing Technology*, vol. 44, no. 1, pp. 399-402. 1995.

[2] KUEHN, W, “Digital factory: integration of simulation enhancing the product and production process towards operative control and optimization”, *International Journal of Simulation*, vol. 7, no. 7, pp. 27-29. 2006.

[3] Toyota V-Comm., “The Toyota Production System.”, *http://www.toyotageorgetown.com/gpc.asp.* Access date: 23 July 2010 at 14.00. 2003.

[4] Delmia, “Case Studies - Daimler Chrysler.”, *http://www.3dskorea.co.kr/03_success01.asp*. Access date: 08 June 2010 at 09.30. 2002.

2011 International Conference on Mechanical, Industrial, and Manufacturing Engineering
Lecture Notes in Information Technology Vols. 1-2

Flow past a Square Cylinder at Small Incidence Angles: Characteristics of Leading Three-Dimensional Instabilities

Gregory J Sheard
Department of Mechanical and Aerospace Engineering, Monash Unviersity, VIC 3800, Australia
Greg.Sheard@monash.edu

***Abstract* – A detailed linear stability analysis is conducted on the flow past a square cylinder inclined at an angle to an oncoming flow. At shallow incidence angles two distinct three-dimensional instabilities present as the first-occurring modes in the wakes with increasing Reynolds number. At incidence angles below 10.5 degrees, the flow becomes three-dimensional via the classical Mode A instability seen behind circular cylinders. However, at higher incidence angles the wake experiences a period-doubling bifurcation as a subharmonic instability develops in place of the Mode A wake.**

Index Terms* – *Square cylinder, three-dimensional, wake instabilities.

I. Introduction

The flow past a square cylinder serves as a model for myriad applications in engineering, including offshore structures, buildings, bridges and pylons. These flows are characterized by the Reynolds number, which relates inertial to viscous effects in a flow. At low Reynolds numbers the flow is steady and laminar, and at higher Reynolds numbers the flow transitions first to time-dependent flow and then to three-dimensional flow, before eventually becoming turbulent. Three-dimensional transition in the flow past cylinders leads to abrupt changes in vortex shedding frequency and both lift and drag characteristics. It is therefore of interest as these transitions can have serious implications for the predictions of loading and fatigue of structures.

A useful method for analysis of three-dimensional transition in wake flows is linear stability analysis, which yields growth rates (σ) for linear three-dimensional instability modes with given spanwise wavelength λ growing on a two-dimensional base flow. A Floquet linear stability analysis was conducted by [1] on the wake of a circular cylinder. Their analysis accurately predicted the critical Reynolds number, spanwise wavelength, and spatio-temporal symmetry of the first-occurring three-dimensional instability, and their predictions matched very well to laboratory observations [2, 3]. Mode A emerges at a Reynolds number (based on freestream velocity and cylinder diameter) of $Re \approx 180$-190, and it is characterized by a spanwise wavelength approximately 4 times the cylinder diameter. The wake subsequently transitions to a second three-dimensional mode (Mode B), over $Re \approx 230$-260, which is characterized by a shorter spanwise wavelength of approximately 1 cylinder diameter. This second mode was also predicted by [1].

These modes have subsequently been found to be common to other extruded geometries, such as slender rings facing an oncoming flow [4, 5], staggered tandem circular cylinders [6], and cylinders with square cross-section [7, 8]. For these geometries, Mode A is usually observed at a lower Reynolds number than Mode B. In addition, a number of studies have also detected a third instability mode in these systems. For circular cylinders [9] and square cylinders at zero incidence [8], a quasi-periodic mode is predicted, whereas behind rings [10, 11] and inclined square cylinders [12, 13], a subharmonic mode is predicted. These modes are distinguished by their temporal properties arising from the respective eigenvalues of the evolution operator of the linearized Navier—Stokes equations used to determine the stability of the flow. A subharmonic eigenvalue lies on the negative real axis, whereas a quasi-periodic mode occurs as a complex-conjugate pair. A subharmonic mode invokes a period-doubling of the flow once the instability develops, whereas a quasi-periodic mode has the physical effect of introducing a new frequency into the flow. Analysis by [14] has shown that quasi-periodic modes are permitted in flows exhibiting a half-period reflective symmetry about the wake centreline (e.g. a square cylinder at zero incidence), whereas those systems do not allow a subharmonic mode. In contrast, subharmonic modes are permitted in systems which break this symmetry (e.g. an inclined square cylinder).

The system under investigation is shown in Fig. 1. It comprises a cylinder with a square cross-section inclined at an angle α to the oncoming flow, placed perpendicular to a uniform flow with speed U. The square cross-section has side length d, and the characteristic length is taken to be the projected height of the cylinder facing the oncoming flow, h. This gives a Reynolds number

$$Re = \frac{Uh}{\upsilon},$$

where υ is the kinematic viscosity of the fluid. The control parameters for the system are Re and α.

Laboratory investigations have previously investigated square cylinders at both a zero incidence [15] and at inclination [16]. These studies employed dye visualization and hot-wire measurements to elucidate transitions in the flow, and proposed the first map of two- and three-dimensional regimes in the Reynolds number-incidence angle parameter space for inclined square cylinders. A linear stability analysis [12], supported by direct numerical simulation, determined that the first-occurring three-dimensional transition behind inclined square cylinders was Mode A at incidence angles near 0° and 45°, and a subharmonic mode (Mode C) at intermediate angles. The subharmonic mode was most unstable at approximately $\alpha \approx 25°$, and the transition Reynolds number

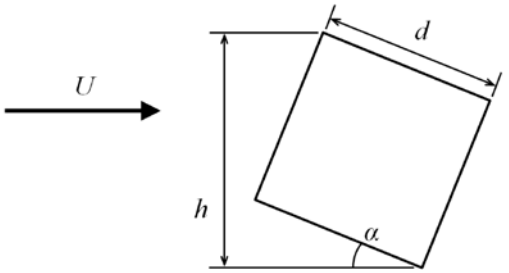

Fig. 1 A schematic representation of the inclined square-cylinder system, showing inclination angle α, characteristic length scale *h*, and free-stream velocity *U*.

increased substantially towards both 0° and 45°. At a zero incidence angle, [8, 12] identified a quasi-periodic mode, which was predicted to become unstable well above the critical Reynolds numbers for Modes A and B, but no evidence was found for the quasi-periodic mode at non-zero incidence angles. However, that analysis was only conducted at 7.5° increments in incidence angle, which raised a question as to whether the subharmonic mode immediately replaces the quasi-periodic mode the instant that the wake symmetry is broken at non-zero incidence angles, or whether the quasi-periodic mode persists at small non-zero angles.

Ref. [17] sought to address this question by investigating the effect of breaking reflective wake centreline symmetry at small increments. It was found that the quasi-periodic mode persisted while the symmetry-breaking was small but finite, and as it was further increased the complex-conjugate pair of eigenvalues smoothly migrated towards the negative real axis where it split into a pair of subharmonic eigenvalues. This study demonstrated that with increasing incidence angle, the quasi-periodic mode *changes into* the subharmonic mode, rather than being *replaced* by it through the emergence of a distinct eigenvalue.

A more recent numerical study [13] calculated the stability of an inclined square cylinder flow at a number of additional incidence angles, refining the Reynolds number-incidence angle regime map. Two notable features arose from their results: firstly, in keeping with the results of [17], the quasi-periodic mode branch was found to extend to non-zero incidence angles (they detected the quasi-periodic mode up to approximately 2°, but included no data on the quasi-periodic/subharmonic branch up to $\alpha = 10.2°$), and secondly, while interpolation suggested in [12] that the crossover from Mode A to the subharmonic mode occurred at approximately 12°, [13] detected the subharmonic mode and not Mode A at a lower angle of 10.2°. Thus [12] over-estimated the threshold incidence angle for the crossover from Mode A to the subharmonic mode, and considering the data in [13], the crossover could potentially occur anywhere down to 7.5°. Furthermore, why is Mode A not detected at all at α=10.2°? The present study addresses these questions through a more detailed stability analysis of the inclined square cylinder wake.

II. Numerical Treatment

A two-dimensional code [18, 19] employing a nodal spectral element method for spatial discretization and a third-order time integration scheme based on backwards differentiation is used to solve the time-dependent incompressible Navier—Stokes equations. Linear stability analysis is performed by evolving a three-dimensional perturbation on the two-dimensional base flow using the linearized Navier—Stokes equations [1]. Stability eigenvalues are determined using the ARPACK package [20], where the complex eigenvalues are Floquet multipliers (μ), and eigenvectors give the instability mode shape (for details see [12, 17]). Floquet multipliers represent amplification factors, and relate to the exponential growth rates (σ) of modes through $\sigma = \log|\mu| / T$, where T is the temporal period of the base flow. A Floquet multiplier with $|\mu| > 1$ corresponds to a positive growth rate ($\sigma > 0$) and an unstable mode.

The meshes employed here were adapted from those employed for the square-cylinder calculations in [17]. The domain size and element distribution were maintained for all incidence angles. The meshes have 644 elements with a polynomial degree 9. The distances from the cylinder to the upstream, transverse, and downstream boundaries were 20*h*, 20*h*, and 35*h*, respectively. On all boundaries except the downstream boundary a high-order Neumann pressure gradient boundary condition was imposed to preserve the third-order time accuracy of the computations [21], and on the downstream boundary a constant reference pressure was imposed. A uniform horizontal velocity was imposed at the upstream boundary, and stress-free conditions were imposed on the transverse boundaries. A no-slip condition was imposed on velocity at the surface of the cylinder, and a zero normal gradient of velocity was weakly imposed naturally on the downstream boundary by the Galerkin treatment of the diffusion sub-step of the time integration scheme.

The aim of this study is to develop a detailed map of transition regimes at small incidence angles. Hence incidence angles over $0° \le \alpha \le 12°$ are computed at approximately 1° increments. Analysis was targeted at narrow ranges of Reynolds numbers and spanwise wavelengths surrounding the dominant modes, minimising the intervals between data points and enhancing the precision of the predictions. Polynomial curve fitting was used to determine the wavenumber *m* (which relates to the spanwise wavelength through $\lambda/h = 2\pi/m$) corresponding to the peak growth rate for an instability mode at a given Reynolds number, and interpolation was performed to find the critical Reynolds number and wavenumber at which the mode first becomes neutrally stable (i.e., zero growth rate). Typically, 15 to 20 Floquet multipliers were computed to obtain each critical Reynolds number in the results to follow.

III. Results

A. The Mode A Branch

Fig. 2 shows the key Reynolds number curves for the Mode A instability branch at small angles. At $\alpha = 0°$, the present stability calculations for the onset of the Mode A instability are in agreement with [12], predicting $Re_{crit} = 164$ at a wavenumber $m = 1.24$. With an increase in α, the critical Reynolds number for the onset of the Mode A instability also

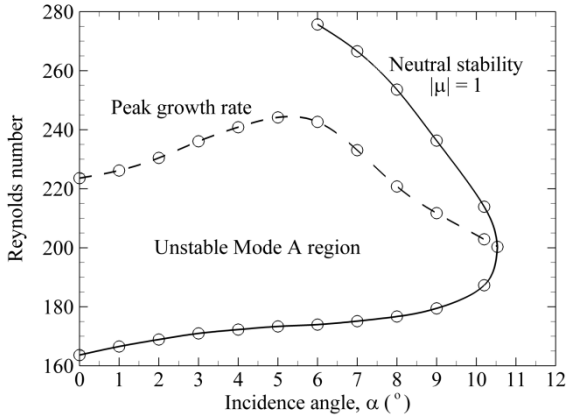

Fig. 2 Critical Reynolds numbers for the Mode A instability plotted against incidence angle. The unstable region of the parameter space is shaded, and a dashed line marks the point at which the maximum growth rate was found in the Mode A waveband for each incidence angle.

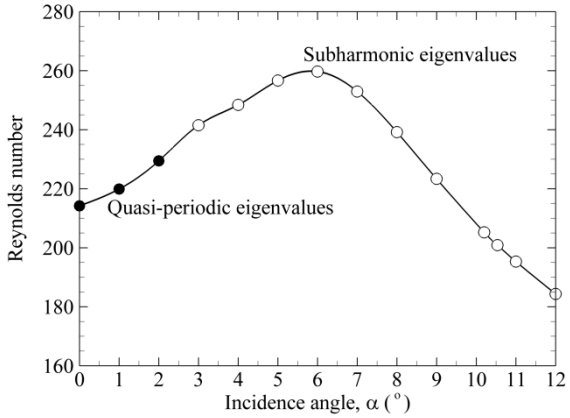

Fig. 3 Critical Reynolds numbers for the quasi-periodic and subharmonic modes plotted against incidence angle. Black and white symbols denote modes with quasi-periodic and subharmonic eigenvalues, respectively.

increases. Unusually, for a given α, the growth rate reached a maximum value, before subsequently decreasing again at higher Reynolds numbers. The Reynolds number for peak for Mode A growth rate is predicted to be $Re = 224$ at $\alpha = 0°$; it increases to $Re = 244$ at $\alpha \approx 5°$, and at higher incidence angles the peak occurs at lower Reynolds numbers. With increasing incidence angle, the Mode A instability was unstable over a decreasing range of Reynolds numbers. These computations predict that by $\alpha = 10.5°$, the Mode A waveband is not unstable for any Reynolds numbers considered in this study. At $\alpha = 10.5°$, the critical Reynolds number at which Mode A grazes the neutral stability threshold is $Re = 200$. This shows that the flow becomes less sensitive to the Mode A instability as the incidence angle is increased from 0°.

The achievement of positive growth rates for the Mode A instability in these computations at $\alpha = 10.2°$ (and indeed up to $\alpha = 10.5°$) is in contrast to the calculations in [13], where Mode A was not detected at $\alpha = 10.2°$. Given the close (but not exact) agreement between their critical Reynolds number curves and those of [12], the differences between the two sets of computations may be attributed to the different domain sizes and numerical techniques employed in the two studies. It is highly likely that the suppression of Mode A observed in the present calculations most likely occurred at an incidence angle just below $\alpha = 10.2°$ in their model, which explains their detection of only the subharmonic (Mode C) instability at that incidence angle.

B. Subharmonic and Quasi-Periodic Modes

The critical Reynolds number curve for the quasi-periodic/subharmonic mode branch is shown in Fig. 3. Ref [17] showed that the transition from quasi-periodic to subharmonic eigenvalues occurred at an incidence angle of $\alpha = 5.9°$ for a cylinder with a square cross-section. That study conducted the stability analysis at a constant Reynolds number (based on the cylinder side length) of $Re_d = 225$. At $\alpha = 5.9°$, this corresponds to a Reynolds number here of $Re = 247$. At that Reynolds number the Floquet multiplier resided inside the unit circle ($|\mu| < 1$), which corresponds to a decaying mode and a stable flow. In this study eigenvalues are determined at precisely the transition Reynolds number and peak wavenumber for all incidence angles. At the critical Reynolds number, the shift from quasi-periodic to subharmonic mode characteristics occurs somewhere between α=2° and 3°, in good agreement with [13], which detected a quasi-periodic mode at $\alpha \approx 2°$.

At $\alpha = 0°$, the mode has a critical Reynolds number of $Re_c = 214$, consistent with [12]. The critical Reynolds number increases with incidence angle to a maximum of $Re_c \approx 260$ at $\alpha \approx 6°$, before subsequently decreasing with further increases in α. The trend of the critical Reynolds number rising over $0° \le \alpha < 6°$ and falling beyond $\alpha \approx 6°$ closely mirrors the trend in the maximum growth rate of the Mode A instability.

Highlighting the consistency across the quasi-periodic and subharmonic states, Fig. 4 shows the perturbation fields at several incidence angles along the neutral stability curve. The topologies of the perturbation field mode structures are qualitatively consistent across these incidence angles, supporting the view that the quasi-periodic and subharmonic regimes are part of the one mode branch. No sudden change in structure is detected through the switch between these regimes.

IV. Summary and Conclusions

This study provides a clearer description of the stability of the wake behind an inclined square cylinder than is available from earlier attempts to map these regimes [12, 13]. The updated regime map is plotted in Fig. 5. This study demonstrates that with increasing incidence angle from $\alpha = 0°$, the flow is first unstable to the Mode A instability. This mode is progressively suppressed, so that by $\alpha = 10.5°$ the flow is no longer unstable to Mode A. Thereafter, the first-occurring instability is the subharmonic Mode C instability. As the incidence angle approaches 45°, which corresponds to a recovery of reflective symmetry about the wake centreline, [12] showed that Mode C is replaced again by Mode A as the first-occurring instability mode.

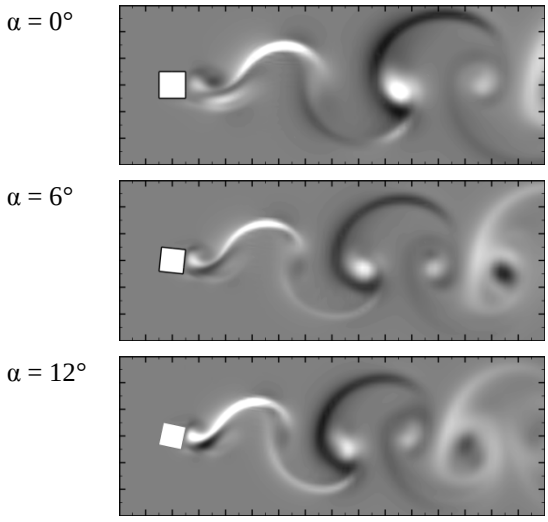

Fig. 4 Contour plots of the horizontal component of velocity in the perturbation field of the dominant mode in the quasi-periodic/subharmonic waveband at the neutral stability threshold (the curve in Fig. 3) at several incidence angles. Light and dark shading correspond to positive and negative velocities, respectively.

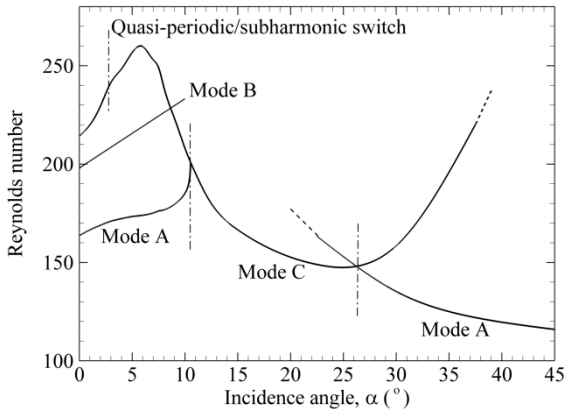

Fig. 5 The updated regime map for linear instability modes in the wakes behind inclined square cylinders, with critical Reynolds number curves plotted against incidence angle. The various modes are labelled, and dash-dotted lines are used to mark important incidence angles in the parameter space. The terms "QP" and "C" refer to the quasi-periodic and subharmonic (Mode C) parts of that transition curve.

This study also shows the critical Reynolds number curve for the quasi-periodic mode branch to be unbroken. While this mode is not the first-occurring instability for $\alpha < 10.5°$, and therefore may not be detectable at these incidence angles in a physical setting, this finding is important from the perspective of understanding the relationship between quasi-periodic and subharmonic instability modes in generic time-periodic flows exhibiting the same spatio-temporal symmetry properties as these flows.

This study has also shown that at the critical Reynolds number, the switch from quasi-periodic to subharmonic properties occurs between $\alpha \approx 2°$ and 3°. The combination between these results and those in [17] could potentially be used to seek a universal criterion for the critical amount of asymmetry required to invoke the subharmonic switchover.

ACKNOWLEDGMENT

This work was supported by a Monash University Faculty of Engineering Small Grant. Simulations were performed using the resources of the NCI National Facility, which is supported by the Australian Commonwealth Government.

REFERENCES

[1] D. Barkley, and R.D. Henderson, "Three-dimensional Floquet stability analysis of the wake of a circular cylinder," *Journal of Fluid Mechanics*, vol. 322, pp. 215–241, 1996.

[2] C.H.K. Williamson, "The existence of two stages in the transition to three-dimensionality of a cylinder wake," *Physics of Fluids*, vol. 31, pp. 3165–3168, 1988.

[3] C.H.K. Williamson, "Mode A secondary instability in wake transition," *Physics of Fluids*, vol. 8, pp. 1680–1682, 1996.

[4] G.J. Sheard, M.C. Thompson, and K. Hourigan, "From spheres to circular cylinders: The stability and flow structures of bluff ring wakes," *Journal of Fluid Mechanics*, vol. 492, pp. 147–180, 2003.

[5] G.J. Sheard, M.C. Thompson, and K. Hourigan, "From spheres to circular cylinders: Non-axisymmetric transitions in the flow past rings," *Journal of Fluid Mechanics*, vol. 506, pp. 45–78, 2004.

[6] B.S. Carmo, S.J. Sherwin, P.W. Bearman, and R.H.J. Willden, "Wake transition in the flow around two circular cylinders in staggered arrangements," *Journal of Fluid Mechanics*, vol. 597, pp. 1–29, 2008.

[7] J. Robichaux, S. Balachandar, and S.P. Vanka, "Three-dimensional Floquet instability of the wake of a square cylinder," *Physics of Fluids*, vol. 11, pp. 560–578, 1999.

[8] H.M. Blackburn, and J.M. Lopez, "On three-dimensional quasi-periodic Floquet instabilities of two-dimensional bluff body wakes," *Physics of Fluids* vol. 15, pp. L57–L60, 2003.

[9] H.M. Blackburn, F. Marques, and J.M. Lopez, "Symmetry breaking of two-dimensional time-periodic wakes," *Journal of Fluid Mechanics*, vol. 522, pp. 395–411, 2005.

[10] G.J. Sheard, M.C. Thompson, K. Hourigan, and T. Leweke, "The evolution of a subharmonic mode in a vortex street," *Journal of Fluid Mechanics*, vol. 534, pp. 23–38, 2005.

[11] G.J. Sheard, M.C. Thompson, and K. Hourigan, "The subharmonic mechanism of the Mode C instability," *Physics of Fluids*, vol. 17, article no. 111702, 2005.

[12] G.J. Sheard, M.J. Fitzgerald, and K. Ryan, "Cylinders with square cross section: Wake instabilities with incidence angle variation," *Journal of Fluid Mechanics*, vol. 630, pp. 43–69, 2009.

[13] D.H. Yoon, K.S. Yang, and C.B. Choi, "Flow past a square cylinder with an angle of incidence," *Physics of Fluids*, vol. 22, article no. 043603, 2010.

[14] F. Marques, J.M. Lopez, and H.M. Blackburn, "Bifurcations in systems with Z2 spatio-temporal and O(2) spatial symmetry," *Physica D*, vol. 189, pp. 247–276, 2004.

[15] S.C. Luo, X.H. Tong, and B.C. Khoo, "Transition phenomena in the wake of a square cylinder," *Journal of Fluids and Structures*, vol. 23, pp. 227–248, 2007.

[16] X.H. Tong, S.C. Luo, and B.C. Khoo, "Transition phenomena in the wake of an inclined square cylinder," *Journal of Fluids and Structures*, vol. 24, pp. 994–1005, 2008.

[17] H.M. Blackburn, and G.J. Sheard, "On quasi-periodic and subharmonic Floquet wake instabilities," *Physics of Fluids*, vol. 22, article no. 031701, 2010.

[18] G.J. Sheard, T. Leweke, M.C. Thompson, and K. Hourigan, "Flow around an impulsively arrested circular cylinder," *Physics of Fluids*, vol. 19, article no. 083601, 2007.

[19] A. Neild, T.W. Ng, G.J. Sheard, M. Powers, and S. Oberti, "Swirl mixing at microfluidic junctions due to low frequency side channel fluidic perturbations," *Sensors and Actuators B: Chemical*, vol. 150, no. 2, pp. 811-818, 2010.

[20] R.B. Lehoucq, D.C. Sorenson, and C. Yang, *ARPACK Users' Guide*. SIAM: Philadelphia, PA., 1998.

[21] G.E. Karniadakis, M. Israeli, and S.A. Orszag, "High-order splitting methods for the incompressible Navier-Stokes equations," *Journal of Computational Physics*, vol. 97, pp. 414–443, 1991.

2011 International Conference on Mechanical, Industrial, and Manufacturing Engineering
Lecture Notes in Information Technology Vols. 1-2

Cubic Convergence and Applications of a Variant of Newton -Method for Systems of Nonlinear Equations*

Liu Zhongli

College of Biochemical Engineering, Beijing Union University, Beijing 100023, China

Liuzhongli2@163.com

Zheng Quan

College of Sciences, North China University of Technology, Beijing 100144, China

zhengq@ncut.edu.cn

Abstract - Numerical solutions for nonlinear equations and systems of nonlinear equations have always appealed greatly to people. Newton method is a universally acknowledged classical algorithm. This paper probes into the third-order semilocal convergence of a variant of Newton method or Traub formula for the systems of nonlinear equations and presents the numerical examples for proving the correctness of the analysis of such convergence and confirming the efficiency and feasibility of the iterative formula. That is, we extend the iterative formula from one dimension to n dimensions and get its convergence ball.

Index Terms - systems of nonlinear equations; Traub formula; semilocal convergence; convergence ball

I. Introduction

In terms of the following systems of nonlinear equations:

$$F(x)=0, \tag{1}$$

where $F:\ R^n \to R^n$ is a given vector of nonlinear functions, we can adopt the classical Newton method and quasi-Newton method to find the solution [1]. Newton's method is one of the most elementary, popular and important one. One of the advantages of the method is its local quadratic convergence. Following is the iterative formula of a variant of Newton method we use to solve the above systems (1):

$$x_{n+1}=x_n-F'(x_n)^{-1}[F(x_n)+F(y_n)], \tag{2}$$

Thus we can get $y_n=x_n-F'(x_n)^{-1}F(x_n)$ by using Newton's method. Traub presented the one-dimension form as well as its efficiency and asymptotic convergence constant of (2) in his works [2]. Now we change (2) into the equivalent form in n variables as follows:

$$\begin{cases} y_n=x_n-F'(x_n)^{-1}F(x_n), \\ x_{n+1}=y_n-F'(x_n)^{-1}F(y_n). \end{cases} \tag{3}$$

The above iterative formula (3) is divided into two steps. In the second iteration step, we have known y_n and $F'(x_n)$. Now we only need to calculate a new value of function $F(y_n)$. In this paper, we extend Traub formula to n-dimension and analyze the semilocal cubic convergence of the iterative formula (2) and present the numerical examples in the following part.

II. Semilocal cubic convergence

The cubic convergence analysis of formula (2) is deduced as follows.

Construct a majorant function:

$$h(t)=Kt^2/2-t/\gamma+\eta/\gamma, \tag{4}$$

where $K,\gamma,\eta>0$, such that

$$\left\|F'(x_0)^{-1}\right\|\le\gamma,\ \left\|F(x_0)\right\|\le\eta/\gamma; \tag{5}$$

$$\left\|F'(x)-F'(y)\right\|\le K\left\|x-y\right\|, \text{ when } \left\|x-x_0\right\|\le 1/K\gamma. \tag{6}$$

Apply the iterative formula (3) to $h(t)$, we get the following result:

$$\begin{cases} s_n=t_n-h'(t_n)^{-1}h(t_n) \\ t_{n+1}=s_n-h'(t_n)^{-1}h(s_n) \end{cases},\ t_0=0.$$

Lemma 1 If $\alpha=K\gamma\eta<6\sqrt{2}-8<1/2$, then

(a) $h(t)$ has two positive real roots:

$$t^*=(1-\sqrt{1-2\alpha})\eta/\alpha,\ t^{**}=(1+\sqrt{1-2\alpha})\eta/\alpha;$$

(b) The sequences $\{t_n\}$ and $\{s_n\}$ satisfy the following:

$$0=t_0<s_0\cdots<t_n<s_n<t_{n+1}<s_{n+1}\cdots<t^*;$$

(c) $t^*-t_n\le(\sqrt{2}\lambda)^{3^n}/(\sqrt{2}-(\sqrt{2}\lambda)^{3^n})(t^{**}-t^*)$,

$$\lambda=(1-\sqrt{1-2\alpha})/(1+\sqrt{1-2\alpha}).$$

Proof Obviously (a) holds.

As for (b), because $s_n-t_n=-h'(t_n)^{-1}h(t_n)>0$ and $t_{n+1}-s_n=-h'(t_n)^{-1}h(s_n)>0$, then $t_n<s_n<t_{n+1}$. $n=0,1,2,\cdots$:

* This work is supported by Science-Research Foundation of Beijing Union University(No. zk200910x)

Let $u_n = t^* - t_n$, $v_n = t^{**} - t_n$; $a_n = t^* - s_n$, $b_n = t^{**} - s_n$, then
$h(s_n) = Ka_nb_n/2$, $h'(s_n) = K(a_n + b_n)/2$, $h(t_n) = Ku_nv_n/2$,
$h'(t_n) = -K(u_n + v_n)/2$,
and $a_n = u_n - u_nv_n/(u_n + v_n) = u_n^2/(u_n + v_n)$,
$b_n = v_n - u_nv_n/(u_n + v_n) = v_n^2/(u_n + v_n)$,
$u_{n+1} = (u_n^4 + 2u_n^3v_n)/(u_n + v_n)^3$, $v_{n+1} = (v_n^4 + 2v_n^3u_n)/(u_n + v_n)^3$,
that is,
$u_n/v_n \le 2(u_{n-1}/v_{n-1})^3 \le 2^{3^0}2^{3^1}\cdots 2^{3^{n-1}}(u_0/v_0)^{3^n} \le (\sqrt{2}\lambda)^{3^n}/\sqrt{2}$.
It is obvious that when $(\sqrt{2}\lambda)^{3^n} \to 0$, $u_n \to 0$, and then $t_n \to t^*$.
Therefore, (b) holds.
Substitute $v_n = t^{**} - t^* + u_n$ into the above inequation and we have (c).

Lemma 2 Suppose $F(x)$ satisfies (5) and (6), then the sequence $\{x_n\}$ resulting from the iterative formula (2) satisfies:

(a) $x_n \in S(x_0, t^*)$, $\|F'(x_n)^{-1}\| \le -h'(t_n)^{-1}$,

(b) $\|F(x_n)\| \le h(t_n)$, $\|y_n - x_n\| \le s_n - t_n$,

(c) $\|F(y_n)\| \le h(s_n)$, $\|x_{n+1} - y_n\| \le t_{n+1} - s_n$.

Proof As $\|F'(x_0)^{-1}\| \le \gamma$,
$\|F'(x_n) - F'(x_0)\| \le K\|x_n - x_0\| = h'(\|x_n - x_0\| + 1/\gamma < 1/\gamma$, then
$F'(x_n)^{-1}$ exists by Banach Lemma and
$$\|F'(x_n)^{-1}\| \le -h'(\|x_n - x_0\|)^{-1}.$$
From (2), we know that
$F(y_n) = \int_0^1 [F'(x_n + t(y_n - x_n)) - F'(x_n)]dt(y_n - x_n)$ and
$F(x_{n+1}) = F(y_n) + F'(y_n)(x_{n+1} - y_n) + \int_0^1 [F'(y_n + t(x_{n+1} - y_n)) - F'(y_n)]dt(x_{n+1} - y_n)$
.
Then we prove Lemma 2 by assumption of induction. When n=0, (a), (b) and (c) hold. In fact,
$$x_0 \in S(x_0, t^*),\ \|F'(x_0)^{-1}\| \le \gamma = -h'(t_0)^{-1};$$
$$\|y_0 - x_0\| = \|-F'(x_0)^{-1}F(x_0)\| \le -h'(t_0)h(t_0) = s_0 - t_0;$$
$$\|F(y_0)\| \le \int_0^1 Kt\|y_0 - x_0\|^2 dt \le K/2(s_0 - t_0)^2$$
$$= K/2(s_0 - t_0)^2 + h'(t_0)(s_0 - t_0) + h(t_0) = h(s_0),$$
$$\|x_1 - y_0\| \le \|-F'(x_0)F(y_0)\| \le -h'(t_0)^{-1}h(s_0) = t_1 - s_0.$$
Assume (a), (b) and (c) hold when $n \le m$, then
$\|x_{m+1} - x_m\| = \|x_{m+1} - y_m + y_m - x_m\| \le \|x_{m+1} - y_m\| + \|y_m - x_m\| = t_{m+1} - t_m$

Since $\|x_{m+1} - x_0\| \le \sum_{n=0}^{m}(t_{n+1} - t_n) = t_{m+1} - t_0 < t^*$, then
$$x_{m+1} \in S(x_0, t^*);$$
$$\|F'(x_{m+1})^{-1}\| \le -h'(\|x_{m+1} - x_0\|)^{-1} \le -h'(t_{m+1} - t_0)^{-1} = -h'(t_{m+1})^{-1};$$
$\|F(x_{m+1})\| =$
$\|F(y_m) - F'(y_m)F'(x_m)^{-1}F(y_m) + \int_0^1 [F'(y_m + t(x_{m+1} - y_m)) - F'(y_m)]dt(x_{m+1} - y_m)\|$
$\le \|I - F'(y_m)F'(x_m)^{-1}\|\|F(y_m)\| + K\|x_{m+1} - y_m\|^2/2$
$\le K\|x_m - y_m\|[-h'(t_m)^{-1}]h(s_m) + K(t_{m+1} - s_m)^2/2$
$= [h'(s_m) - h'(t_m)][-h'(t_m)^{-1}]h(s_m) + K(t_{m+1} - s_m)^2/2$
$= h(s_m) + (t_{m+1} - s_m)h'(s_m) + K(t_{m+1} - s_m)^2/2 = h(t_{m+1})$;
$\|y_{m+1} - x_{m+1}\| = \|-F'(x_{m+1})^{-1}F(x_{m+1})\| \le -h'(t_{m+1})^{-1}h(t_{m+1}) = s_{m+1} - t_{m+1}$;
$\|F(y_{m+1})\| \le K\|y_{m+1} - x_{m+1}\|^2/2 + h'(t_{m+1})(s_{m+1} - t_{m+1}) + h(t_{m+1}) = h(s_{m+1})$
$\|x_{m+2} - y_{m+1}\| = \|-F'(x_{m+1})^{-1}F(y_{m+1})\| \le -h'(t_{m+1})h(s_{m+1}) = t_{m+2} - s_{m+1}$;
So (a), (b) and (c) hold.
Thus Lemma 2 is proved.

Theorem 1 Let $F: D \subset R^n \to R^n$ be Frechet differentiable in a convex set $S(x^*, \delta) \subset D$, with $F(x)$ satisfying (5) and (6).
If $\alpha = K\gamma\eta < 6\sqrt{2} - 8 < 1/2$, then the sequence $\{x_n\}$ resulting from the iterative formula (2) is third-order convergent to the unique solution $x^* \in S(x_0, t^*)$ and
$$\|x_n - x^*\| \le t^{**} - t_n \le (\sqrt{2}\lambda)^{3^n}(t^{**} - t^*)/(\sqrt{2} - (\sqrt{2}\lambda)^{3^n}).$$

Proof As $K > 0$, $\gamma > 0$, $\eta > 0$ and $\alpha < 6\sqrt{2} - 8$, then
$0 < \sqrt{2}\lambda < 1$. From Lemma 1 and 2, we have $\{x_n\}$ remaining in the ball $S(x_0, t^*)$ and $\|x_{n+1} - x_n\| \le t_{n+1} - t_n$, then
$\|x_{n+m} - x_n\| \le t_{n+m} - t_n$. Since $\{t_n\} \to t^*$, $\{x_n\}$ is Cauchy sequence, which has a limit. We denote it as x^*. Then when $m \to \infty$, $\|x_n - x^*\| \le t^* - t_n \le (\sqrt{2}\lambda)^{3^n}/(\sqrt{2} - (\sqrt{2}\lambda)^{3^n})(t^{**} - t^*)$.
Besides, as $\|F(x_n)\| \le h(t_n)$ and
$\lim_{n\to\infty}\|F(x_n)\| \le \lim_{n\to\infty} h(t_n) = h(t^*) = 0$, then $F(x^*) = 0$.
Finally, to show uniqueness, we suppose $y^* \in S(x_0, t^{**})$ be another solution for $F(x) = 0$, then,
we have
$\|\int_0^1 F'(y^* + \theta(x^* - y^*))d\theta - F'(x_0)\| \le \int_0^1 \|F'(y^* + \theta(x^* - y^*)) - F'(x_0)\|d\theta$
$\le \int_0^1 (K\|y^* + \theta(x^* - y^*) - x_0\|)d\theta$
$\le \int_0^1 K[(1-\theta)\|y^* - x_0\| + \theta\|x^* - x_0\|]d\theta$
$\le K\int_0^1 [(1-\theta)t^{**} + \theta t^*]d\theta \le K(t^{**} + t^*)/2 < K\eta/\alpha = 1/\beta$,
where $0 \le \theta \le 1$.
By Banach Lemma and the median value theorem, we get that
$L = \int_0^1 F'(y^* + \theta(x^* - y^*))d\theta$ is non-singular;
and
$0 = F(x^*) - F(y^*) = \int_0^1 F'(y^* + \theta(x^* - y^*))d\theta(x^* - y^*) = L(x^* - y^*)$,

Therefore, we obtain $y^* = x^*$.This completes the proof of Theorem 1.

III. NUMERICAL EXAMPLES

Now apply the above formula to the following systems of nonlinear equations.

Example 1.
$$\begin{cases} 3x_1 - \cos(x_2 x_3) - 1/2 = 0 \\ x_1^2 - 81(x_2 + 0.1)^2 + \sin x_3 + 1.06 = 0 \\ e^{-x_1 x_2} + 20x_3 + (10\pi - 3)/3 = 0 \end{cases}$$

Give an initial guess $x_0 = (0.1, 0.1, -0.1)'$ and $D = \{x \mid -1 \le x_i \le 1, i = 1,2,3\}$.

Using the iterative formula (2), we get the following numerical result:

Table 1

k	$x_1^{(k)}$	$x_2^{(k)}$	$x_3^{(k)}$
1	0.499985832592680	.00878774734579	0.52316688002454
2	0.500000256581610	.00002819234869	0.52359803671133
3	0.500000000000010	.00000000000112	0.52359877559827
4	0.500000000000000	0.00000000000000	0.52359877559830

k	e_k	r_k	$\|F(x_k)\|$
1	0.008798	0.58939	0.1484
2	2.820e-05	0.59112	4.559e-04
3	1.120e-12	0.59113	1.817e-11
4	0.0	0.59113	1.790e-15

$x^* = (0.5, 0, -\pi/6)'$, $e_k = \|x_k - x^*\|$, $r_k = \|x_k - x_0\|$.

Starting with initial values $x_0 = (0.1, 0.1, -0.1)'$, we find the solution inside the ball whose center is x_0 and radius is 0.59113.

Example 2.
$$\begin{cases} x_1^2 + x_2^2 + x_3^2 = 1 \\ 2x_1^2 + x_2^2 - 4x_3 = 0 \\ 3x_1^2 - 4x_2^2 + x_3^2 = 0 \end{cases}$$

Give an initial guess $x_0 = (0.5, 0.5, 0.5)'$ and $D = \{x \mid -1 \le x_i \le 1, i = 1,2,3\}$.

Using the iterative formula (2), we get the following numerical result:

Table 2

k	$x_1^{(k)}$	$x_2^{(k)}$	$x_3^{(k)}$	$\|x_k - x_0\|$
1	0.67625000000000	0.62300000000000	0.34325000000000	0.2660
2	0.69827680505888	0.62852407959171	0.34256418976030	0.2839
3	0.69828860997151	0.62852429796021	0.34256418968957	0.2839
4	0.69828860997151	0.62852429796021	0.34256418968957	

Starting with initial values $x_0 = (0.5, 0.5, 0.5)'$, we find the solution $x^* \approx x_4$ inside the ball whose center is x_0 and radius is 0.28394.

Example 3.
$$\begin{cases} 4x_1 + 0.1e^{x_1} - x_2 - 1 = 0 \\ 0.5x_1^2 - x_1 + 4x_2 + 0.1 = 0 \end{cases}$$

Give an initial guess $x_0 = (0,0)'$ and $D = \{(x_1, x_2) \in R^2 \mid |x_1| < 0.5, |x_2| < 0.5\}$.

By simple computation, $\|F'(x) - F'(y)\|_\infty = \|x_1 - y_1\|_\infty \le \|x - y\|_\infty$, Let $K = 1$, we can get

$\beta = 0.328$, $\eta = 0.2985$, $\alpha = K\beta\eta = 0.098 < 6\sqrt{2} - 8$.

Furthermore, we also obtain the radius $r = t^* = 0.315$. Using the iterative formula (2), we get the sequences $\{x_k\}$ convergent to the unique solution $x^* \approx x_3$ inside the ball $S(x_0, 0.315) \subset D$. Numerical results are as follows:

Table 3

k	$x_1^{(k)}$	$x_2^{(k)}$	$\|F(x_k)\|$
1	0.22487102521119	0.02476114473255	5.464e-004
2	0.22492104815252	0.02490657730038	5.979e-015
3	0.22492104815252	0.02490657730038	5.979e-015

In this paper, we extended the Traub formula from one dimension to n dimensions and proved its semilocal convergence. From the above numerical results, we can see that the formula this paper probes into is third-order convergent when used to solve the systems of nonlinear equations. Therefore, the application of such formula to the systems of nonlinear equations is efficient and feasible. In addition, this formula can be used to find the solutions to discretized nonlinear partial differential equations.

REFERENCES

[1] J. M. Ortega, W.G. Rheinboldt, I*terative Solution of Nonlinear Equations in Several Variables*. Academic Press, New York, 1970.

[2] J. F. Traub, *Iterative Methods for the Solution of Equations*, Prentice-Hall, Englewood Cliffs, New Jersey, 1964.

[3] Danfu Han, Jingfen Zhu, "Convergence and error estimate of a deformed Newton method", *Applied Mathematics and Computation* 173: (2006) 1115-1123.

[4] Argyros I.K., "On a theorem of L. V. Kantorvich concerning Newton's method", *J. Comput. Appl. Math.*, 2003, 155: 223-230.

[5] S.Abbasbandy, "Extended Newton's method for a system of nonlinear equations by modified Adomian decomposition method", *Applied Mathematics and Computation*, 2005, 170: 648-656.

[6] Predrag M.R, "On q-Newton-Kantorovich method for solving systems of equations", *Applied Mathematics and Computation*, 2005, 168: 1432-1448.

[7] P. N. Brown and Y. Saad, "Hybrid Krylov methods for nonlinear systems of equations", *SIAMJ. Stat. Comput.*, 1990, 11(3), 450-481.

[8] Zhongli Liu, Quan zheng, Peng zhao, "A variant of Steffensen's method of fourth-order convergence and its applications", *Applied Mathematics and Computation*, 2010, 216, 1978-1983.

2011 International Conference on Mechanical, Industrial, and Manufacturing Engineering
Lecture Notes in Information Technology Vols. 1-2

New Research and Development of CE in Metalforming Equipment Manufacturing*

Baojian Yang, Qinxiang Xia
School of Mechanical and Automotive Engineering
South China University of Technology
Guangzhou,China
kurt.yang@163.com

Weiping Ruan, Zhenshi Li
Department of Technology
Guangdong metalforming machine works Co., LTD
Foshan, China
ruanweiping2007@sina.com

***Abstract* - The product development in equipment manufacturing industry has been constrainted by serial design for a long period of time. The implementation of concurrent engineering takes all elements of product lifecycle well into account while in the process of concept design. It aims at the corporation of all departments, so as to realize the TQCS goals. The content and research status of CE are discussed, moreover, its application and development trend for product development in equipment manufacturing industry are further expounded. It is able to reduce the development cycle and cost dramatically by implementing CE, thus keep the enterprise competitive in the market.**

Index Terms* - *Concurrent engineering; Metalforming equipment; Process integration; Product lifecycle

I. INTRODUCTION

The serial design has been applied in product development in equipment manufacturing industry for a long period of time, it follows the sequence of concept design--parts design--process design--manufacturing—practise test—redesign [1]. So developing new product with higher quality & higher capability with lower cost in the shortest time becomes new focus for the market competition. Concerning the problem of long cycle, high cost and low quality, Institute of Defense Analysis U.S.(IDA) proposed concurrent engineering(CE) concept for the first time in Oct.1988 by presenting a report named the role of concurrent engineering in weapons system acquisition[2]. The implementation of CE changes the organization structure, produce mode and the way people think for traditional manufacturing industry greatly, moreover, it aims at product lifecycle management, and has a significant meaning in improving enterprise`s core competiveness and ensuring it to response to user requirements rapidly.

II. CONNOTATION AND RESEARCH OF CE

A. Definition & characteristic of CE

The concurrent engineering represents a comprehensive philosophy of business, engineering, and management[3,11]. Its innate character is process integration, including synergy and concurrent [4,5]. Fig. 1 shows the temporal relation between serial engineering(SE) and concurrent engineering (CE). The serial engineering adopts “thrown over the wall” design method while CE completes product development concurrently and then modifies the design by analysis and evaluation in order to obtain the optimal scheme. CE has 4 characters, such as concurrence, constraints, coordination and fast feedback [2].

Many researchers define the CE from different point of view, however, the most representative and popular definition is the one given by Winner R.I. America:

Concurrent Engineering is a systematic approach to the integrated, concurrent design of products and their related processes, including manufacture and support. This approach is intended to cause the developers, from the outset, to consider all elements of the product life cycle from conception through disposal, including quality, cost, schedule, and user requirements [6].

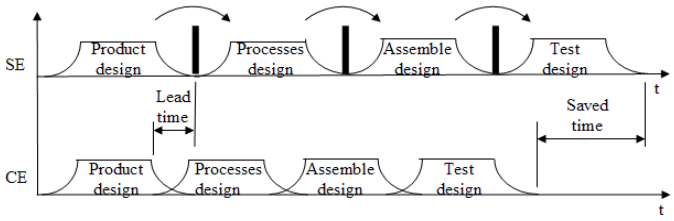

Fig. 1 Temporal relation between design activities of CE and SE

B. Research status of CE

The research achievement and application of concurrent engineering in foreign enterprises, such as Boeing, Ford, Motorola, GE, are quite notable. Moreover, there is a famous theory overseas about CE called shadow pricing, it means the product design process only takes 5% out of the total cost, but it determines 85% of the total cost as shown in Fig. 2 [7,8]. Also, there is a notable “28 principle”, it indicates the product design process only takes 20% out of the total lifecycle, but it determines 80% of the total cost, thus ERP (Enterprise Resource Plan) can only be operated within the left 20% [6]. Nevertheless, domestic research of CE is still at the preliminary stage, and the research of CE in metal forming equipment manufacturing is still a new issue though certain progress has been made since it was introduced in 1992.

C. International research status

The R&D of all aspects for CE general framework overseas involves in two levels: national level and enterprise level. For national level, U.S. Defense Ministry Advanced Defense Technology Research Agency spent $400M in

* This work is partially supported by CAS. Grant # 20090925 to W.P. Ruan

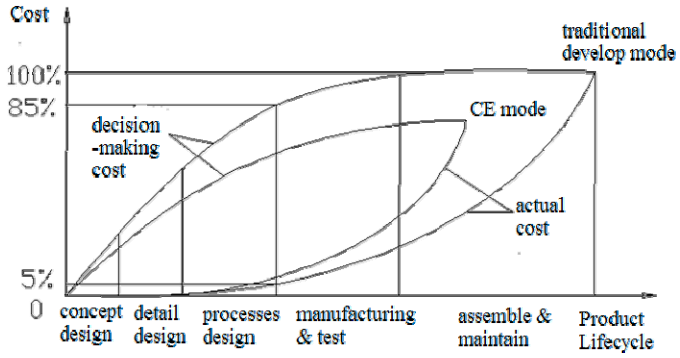

Fig. 2 Curve of decision-making cost and actual cost in different development mode

establishing CE research center in West Virginia University, and did research on all aspects for CE general framework. While for enterprise level, only in management or several technical measures of CE were implemented, such as DFM (Design For Manufacturing), DFA (Design For Assemble) & QFD (Quality Function Deployment). All in all, the international research & application of CE can be divided into 3 stages as follows [9]:

1) Research and preliminary practice (1985-1992), such as DARPA /DICE Plan supported by U.S. Department of Defense, European ESPRIT II&III Plan, Japanese IMS Plan, etc.

2) Application in enterprise(1991-1996) ,such as Boeing 777,737-X, McDonnell Douglas, Northrop B-2 bomber; Lockhead / Thaad missile development; Ford 2000 C3/P, Chrysler Viper, Renault; Simens, DEC, HP, IBM, GE , etc.

3) New development age(after 1995), the new technique appears constantly, such as reusable product development methods, network technique in collaborative design, virtual-reality technique in design, design methodology for product life cycle, product data reuse based on knowledge, product data management and share technique, etc. Reference [10] did research on CE manufacturability critic theory based on the blackboard architecture framework of several experts, and it was being implemented in large shell parts manufacturing successfully. Reference[11] did research on the integrated develop supported environment (IDSE) for CE, IDSE supported the integration of two fields, both data and function, and it was being implemented in the ARPA RAPIDCIM project and at the Air Force Logistics Center at Oklahoma City.

D. Domestic research status

Tsinghua University & CASIC(China Aerospace Science and Industry Corporation) spent tens of millions RMB in doing research on general framework of CE, but it was hardly used in enterprises because of develop ability, ROI(Return On Investment) and management tactic. In order to participate in the international competition of equipment manufacturing, the product development ability should be improved and CE is one of the best strategies for it. The research and application of CE in China includes several stages as follows [12]:

1) CE pre-research (before 1992), several CE projects were granted by 863/ CIMS (Computer Integrated Manufacturing System) plan and NSFC(National Natural Science Foundation of China), such as DFM, concurrent design method study, develop process modeling & simulation study, etc.

2) In 1993, 863/CIMS center organized Tsinghua University, Beijing University of Aeronautics & Astronautics, Shanghai Jiaotong University, Huazhong University of Science & Technology and Beijing Aerospace Corporation No.204 Institution to build CE feasibility demonstration team, and proposed to do key research on CE based on CIMS experiment.

3) On May, 1995, 863/CIMS center approved and initiated the important CE key technique project, and invested large amount of money to do research on CE methods, key technique and its application.

4) May,1995 to Dec.1997, research on tackling CE critical issue was carried out. From 1998 till now, great CE research achievement has been acquired and further research is being done. Reference [13] proposed a human oriented knowledge-based distributed collaborative design system, and CE was being implemented in QRRS(Qiqihar Railway Rolling Stocks) as the first step towards this system.

III. RESEARCH OF CE IN METALFORMING EQUIPMENT DEVELOPMENT

As Chinese backbone industry of civil economy, manufacturing industry involves in civil economy`s future and national security, thus determines the national comprehensive strength and international competitiveness. Metalforming equipment is one of machine tools for manufacturing industry, it is an important strategic unit of our national economy and the fundation of mechanical manufacturing industry[14].

A. The development mode of metalforming equipment based on CE

In traditional metalforming equipment product development mode, there is a rigid development program. It divides the develop process into several stages: feasibility analysis, requirement analysis, system analysis, schema design, detail design, processes formation and manufacturing, etc. Moreover, each stage is separated by clear boundaries between them as shown in Fig. 1, and each one also has complete document record. The periodic future of traditional development mode is very obvious with one-way style information flow, therefore, finding and resolving the problem of manufacturability & assembly in time is nearly impossible though for the experienced designers [2].

The development mode for metalforming equipment product based on concurrent engineering aims for short development cycle (Time), high quality(Quality), low cost (Cost), and good service ((Service) which is shorted for TQCS goal[15]. By organizing a multidisciplinary team that consider various elements for the whole product life cycle at the beginning of design, and forming the unitive development mode, it can realize the development integration and process integration of the product, thus make sure the product has good manufacturability, assembling, and maintainability even at the design stage. It reduces the redesign times, and keeps the product competitive in the market.

In the development mode based on CE, each designer can work in the CAD station like before. With the help of appropriate communication tools, product database and

network, the designers can communicate with each other and also can call important data such as criterion, material information from product database freely. Based on the requirement, everyone can modify their own design according to other`s requirements, and also can ask others to reply their requirements. Moreover, the design group can work concurrently and harmoniously with the coordination mechanism as shown in Fig. 3 [16]. So it is obvious that the development mode based on CE is concurrent in broad view, and serial in microscopic view.

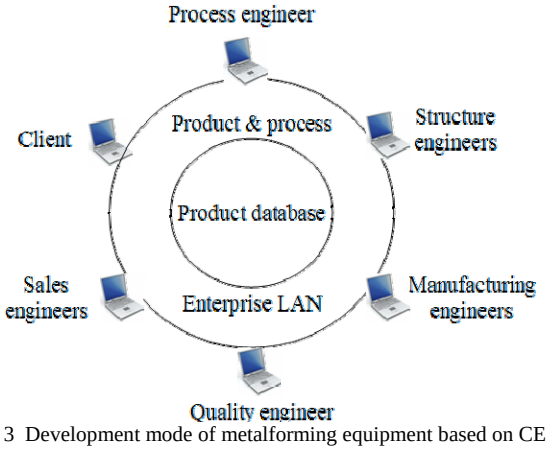

Fig. 3 Development mode of metalforming equipment based on CE

B. *The core content of implementing CE*

The framework of CE refers to decision layer, application layer and service layer, and its core content includes four aspects: development team reconstruction, support of the collaborative work environment, product definition digitalization and design process reconstruction[15].

1) Development team reconstruction. Building IPT (Integrated Product Team) with representatives from departments of sales, purchases, technique, quality control, manufacturing, etc. Given the relevant responsibility and right by the superior departments, IPT is responsible for the quality of the products they developed, moreover, it forms the develop schedule and commits the work of each department.

2) Design process reconstruction. Aiming at the overall optimization, it converts the traditional serial develop process to integrated & concurrent process and implements the design of body structure, hydraulic system, and control system by ways of team work & concurrent design on enterprise`s CAD platform foundation. The process parallelization mainly refers to the participation of downstream process in the early period of design rather than that of activities. Another aspect is process improvement, which aims at improving the efficiency of information flow & share for metalforming equipment products.

3) Product definition digitalization. Including product digital modeling, definition of digital tools and information integration, such as DFA, DFM, CAD /CAM/CAE[17]. For example, dividing the whole body model of metalforming equipment into several parts(such as slider, body, bedplate, base and upper beam, etc.) by building the whole skeleton line model of the body using layout in Pro/E and skeleton line function. Each part is modeled individually, and their design criterion & standard are identical. Finally, all the parts are integrated together for the complete body model.

4) Support of the collaborative work environment. Referring to the internet, PDM (Product Data Management) and computer platform that used for supporting the IPT. The environment is based on WAN (Wide Area Network), and provides the function of multi-media E-mail, document base, electronic notice, project management, electronic review and meeting management, etc.

C. *Strategy for implementing CE in metalforming equipment development*

The implementation of CE for metalforming equipment is a complex systematic engineering, it should be carried out through the proper processes.

1) Subdivide the project. The further subdivide of project is the key to implement CE at the develop stage. It subdivides each step of the traditional product development process further into more activities (include marketing, product design, processes design, sample machine manufacturing, small scale trial-manufacture, finalized production, etc.), and the next activity begins while the last activity is partly completed. So it breaks the boundaries between activities by concurrent cross process, thus reduces the development cycle dramatically [18].

2) Engineering analysis. In order to reduce the risk during manufacturing and assemble for the product, and make sure the product has good manufacturability, assembling and maintainability while in the process of design, the manufacturability and assembly are analyzed with DFM and DFA tools, and the ability of the manufacturing system is checked before trial-manufacture of metalforming equipment[19].

3) Formulate the flow. For guiding the concurrent development process, the concurrent development flow is built according to the relationship between activities and resource needed, such as staff, equipment and time, etc.

4) Control and adjust. The development flow is adjusted according to the change of interior & exterior environment and development process, so as to shorten the development time and ensure concurrent design be implemented successfully.

IV. DEVELOPMENT TREND OF CE TECHNOLOGY IN EQUIPMENT MANUFACTURING INDUSTRY

A. *The core of equipment manufacturing technique transfers from material processing to information processing Authors and Affiliations*

Completing the development of metalforming equipment in information field is not only the need of CE, but also a symbol for equipment manufacturing industry shifting to the information age from the industry age. It will bring about profound revolution in equipment manufacturing industry because the product then have two different kinds of forms (material form & information form) by realizing this target.

The activity with the highest profit is information processing rather than material processing because the most innovative and valuable parts of production lies in the development process and information format of the product. Hence, the product development based on information field will be put to the important position in production activities in equipment manufacturing industry. Once the core of activity is transfer to information processing from material

processing, it marks the turning for equipment manufacturing industry from the industry age to the information age[20].

B. Cross-nation collaborative virtual development by multifunction team

As CE being further applied in metalforming equipment manufacturing industry, the cross-nation manufacturing corporations will be able to realize the integrated development of metalforming equipment in the virtual environment [21].

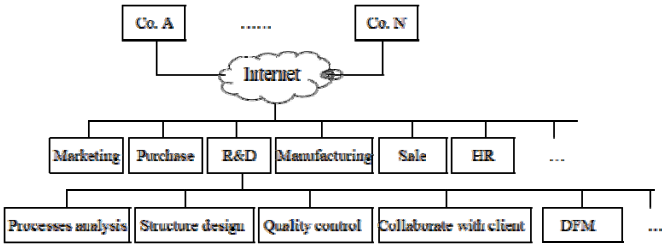

Fig. 4 Cross-nation virtual development based on CE

Reference [22] introduced FRID （Frequency Reader Integrated Design ）for the CE globalization of equipment manufacturing. Every FRID system contains reader, antenna and tag. Designers and process engineers would be able to control the process change using wireless signals to directly update the FRID tags, thus reduce paperwork and human interference and improve the efficiencies obtained through automation.

In this way, the equipment manufacturing using FRID technology has the possibility of integrating the relationship between customers, vendors, design & process planning, marketing and warehousing with real-time information as shown in Fig. 4. The business is thus enabled to provide customer satisfaction through tailor-made products supplied reliably and efficiently with competitive response time.

V. CONCLUSION

As the best way to put the CE theory into practice, the concurrent development of product is vital for the corporation to response to user requirement rapidly and improve its core competiveness. Implementing CE in metalforming equipment manufacturing process can make the product has good manufacturability , assembly and maintainability while in design process, so as to reduce the redesign times largely. The business is thus enabled to provide customer products efficiently with competitive response time.

ACKNOWLEDGMENT

This work is supported by Guangdong province & CAS (Chinese Academy of Sciences) comprehensive strategic cooperation projects. The authors would like to thank Mr. R. D. Mo.

REFERENCES

[1] Yunxian Zhu, “Reestablish the product development process in manufacturing industries on the basis of the concurrent engineering concept”. Mechanical Manufacturing,1998.6

[2] Cheng Wu, Introduction to contemporary integrated manufacturing system-- concept, method, technique and application. Tsinghua University Press, 2002.6

[3] Michael K. Painter, Richard J. Mayer, and Thomas E Cullinane, “The many faces of concurrent engineering”, AUTOFACT Conference Proceedings. November 10-14, 1991, pp.17-25

[4] Smith P R, “The historical roots of concurrent engineering fundamentals”, IEEE Transactions on Engineering Management. 1997,Vol.44(1), pp.67~78

[5] Dowlatshahi S., “A comparison of approaches of concurrent engineering”. Int. J Advance Manufacturing Technology, 1994, 9(2), pp.106-113

[6] Robert I. Winner, James E Pennell, Harold E. Bertrand, Marko M. G. Slusarczuk, “The role of concurrent engineering in weapons system acquisition”, IDA Report R-338.December, 1988

[7] Di Pan, Lieping Zhang, Huanchen Wang, “Concurrent engineering and its application in translating enterprise`s management mechanism”.JOURNAL OF SHANGHAI JIAOTONG UNIVERSITY, 1995.29

[8] Oh C H. Park C S, “An economic evaluation model for product design decisions under concurrent engineering”. The Engineering Economist,1993,38(4), pp.275-297

[9] Weisheng Xu, Qidi Wu, Yunshi Xiao, “Status and problems of concurrent engineering research”. Control and decision, 1996

[10] R Gadh, D Herbert, A Kott, C Kollar, “Feature-based design for manufacturability critique in concurrent engineering”, Information Security and Privacy, 9th Australian conference. Sydney, Australia, ACISP 2004, July 13-15.

[11] THOMAS M. BLINN, KEITH A. ACKLEY, RICHARD J. MAYER, “An integrated concurrent engineering environment for life cycle management”. Journal of Systems Integration, 2004(4), pp.51-65

[12] Guangleng Xiong, Heming Zhang, Bohu Li, “Research and application of concurrent engineering in China”.COMPUTER INTEGRATED MANUFACTURING SYSTEMS,2000.6(2)

[13] Heming Zhang, David Chen, “Developing a multidisciplinary approach of concurrent engineering”. CSCWD 2004, LNCS 3168, 2005, pp.230-241

[14] Caiyuan HUANG, Zhiqiang SONG, “The present and the future of the Chinese metalforming machine”. China Metalforming Equipment & Manufacturing Technology,2006.2, pp.12-17

[15] Meixia LIU, Tiancheng SHOU, Dong WANG, “Research on Product Design Based on Concurrent Engineering”. Modern Machinery, 2009.5

[16] Yan-hua SHI， Hua ZHOU, “Concurrent Engineering Application in Machine Tool Manufacturing”. Equipment Manufacturing Technology, No.4, 2009

[17] Ishii K, Modeling of concurrent engineering design in concurrent engineering. Automation Tools and Techniques, New York,John Wiley&Sons,1993. pp.19-39

[18] Pourbahei B, Pecht M, “Management of design activities in concurrent engineering environment”. Int. J Prod Res,1994. 32(4), pp. 821-892

[19] G. Kovacs ,I. Mezgar,E. Szelke, “Application of concurrent engineering in design for one-of-a-kind production”. International Conference on Robotics and Automation, Nice, France, May.1992

[20] Ping JIANG, Shaolin TANG, Yuxiang HU, “The discussion about the concurrent engineering”. Manufacturing Design Technology, 2000,2

[21] Yan-ming SUN, Jin-fan CHEN, De-yu QI, Ping HUANG, “Development of the concurrent design system based on internet”. Machine Design and Manufacturing Engineering, 2001.30(1)

[22] Zhekun Li, Fuyu Li, Lei Gao, Yujing Fan, “Concurrent intelligent manufacturing based on FRID”. Advanced Design and Manufacture to Gain a Competitive Edge, Springer London, Jul. 2008. pp.521~530

2011 International Conference on Mechanical, Industrial, and Manufacturing Engineering
Lecture Notes in Information Technology Vols. 1-2

Scheduling and Performance Evaluation of Robotic Flexible Assembly Cells under Different Dispatching Rules

Khalid Abd, Kazem Abhary, Romeo Marian
School of Advanced Manufacturing and Mechanical Engineering
University of South Australia
Mawson Lakes, SA 5095, Australia
Abdkk001@mymail.unisa.edu.au,{Kazem.Abhary & Romeo.Marian}@unisa.edu.au

***Abstract* - This paper addresses scheduling and evaluation of Robotic Flexible Assembly Cells (RFACs). Even though RFACs are capable of assembling a variety of products using the same resources, all previous studies have been devoted to scheduling RFACs for assembling a single product.**

The objective of the paper is to propose an algorithm deal with scheduling RFAC for assembly of multi-products. Four experiments are illustrated to schedule RFAC under different dispatching rules. Also, four performance measures are suggested to evaluate the cell performance. A case study is presented to illustrate applications of the proposed algorithm. The results of study demonstrate the effectiveness of the proposed algorithm to manage scheduling RFAC in a multi-product assembly environment.

Index Terms – Assembly cells, Scheduling rules, Robotics.

I. INTRODUCTION

Nowadays, with increasing global competition and responding to unpredictable demand, today's enterprises are forced to develop flexible systems adaptable to manufacture products with minimal reconfiguration. One class of such systems are Robotic Flexible Assembly Cells (RFACs) [1, 2].

RFAC consists of one or more robotic assembly stations linked by an automated material handling system, all controlled by a central computer [3, 4]. RFAC has several advantages, particularly in flexibility and dexterity to assemble a variety of products using the same equipment. In addition, RFAC is easy to modify and reconfigure [5]. On the other hand, the difficulties of RFAC are the need for more complicated scheduling system to prevent collisions between robots and other equipments in the cell [6].

Few studies have been devoted to scheduling RFACs. These studies can be categorised into three approaches. Some of these studies applied heuristic approaches to solve scheduling problem. For example, Lee and Lee [7], Nof and Drezner [8], Lin et al. [9], Pelagagge et al. [10], Sawik [11], Jiang et al. [12] and Rabinowitz et al. [13]. Other studies investigated simulation as an approach to scheduling RFACs. For instance, Glibert et al. [14], Hsu and Fu [15] and Basran et al. [16]. Only two studies, Brussel et al. [17] and Dell Valle and Camacho [18], implemented expert systems approaches to solve scheduling problems.

In addition, from the literature review, the studies have been used different types of performance measure to evaluate scheduling results. Table I summaries performance measures used in previous studies. Time-based measures have attracted significant attention.

TABLE I
PERFORMANCE MEASURES USED IN RFAC SCHEDULING STUDIES

Performance measures	Reference number of publications
Time-based measures	[7], [9], [10], [11], [12], [14], [15], [16], [17], [18]
Utilisation-based measures	[11], [13], [15]
Cost-based measures	[13]
Others	[8]

Based on the literature review, the following limitations can be identified:

- None of them have been described the scheduling RFACs for assembly of multi-products.
- Most of these studies have been used only one performance measure to evaluate the results of scheduling RFACs.

The aim of this paper is to propose a strategy for scheduling RFACs for concurrent assembly of multi-products. Then, the scheduling outcomes are evaluated using several performance measures.

This paper is structured as follows: RFAC are described in section II. In section, III the proposed algorithm is presented. Performance measures are formulated in section IV. In section V, a case study is provided. Experimental results and discussion are reported in section VI. Finally, conclusion and further research are presented in section VII.

II. DESCRIPTION OF RFAC

The multi robot assembly cell is composed of two robots (R1 and R2) that can use a number of tools that can be changed in a tool magazine (GC), assembly stations (AS1, AS2, AS3, AS4 & AS5) where components are assembled, transfer table (TT) to be transferred partial assemblies from one robot to another. There are also two conveyors. The first one (IC) supplies components to the cell and the second one (OC) is for conveying out a final product when assembly processes are completed, as shown in Figure 1.

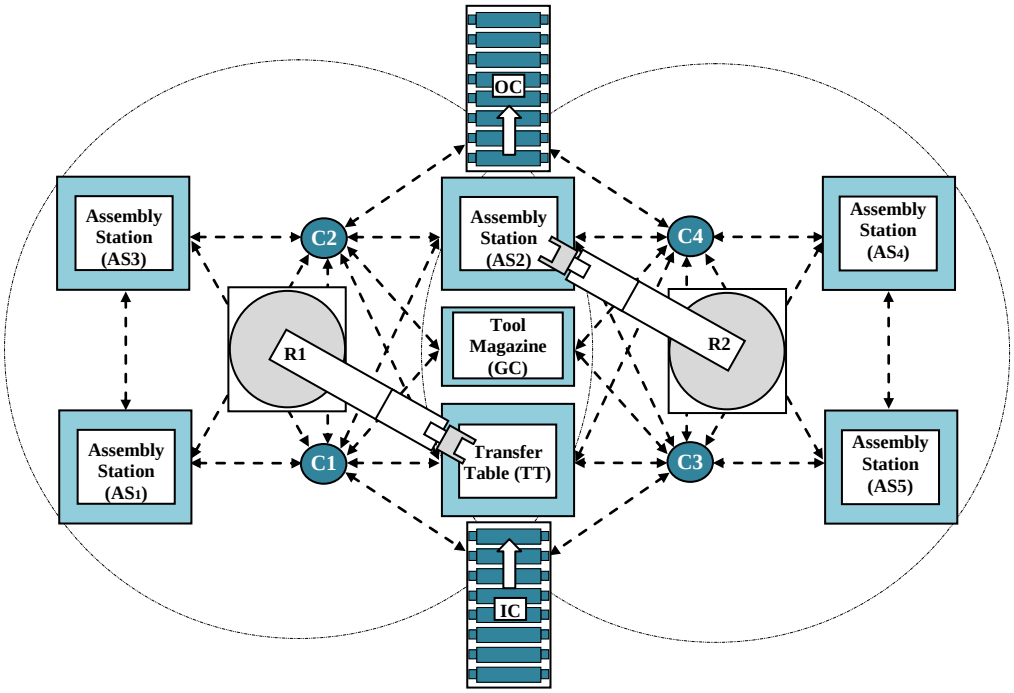

Fig. 1 A robotic flexible assembly cell

To provide a reliable solution to practical cases, the following requirements have been taken into account.

The first requirement is the robot move constraints. Robot cannot move from one place to another directly. This can be achieved by assigning four control points in the cell: C1 and C2 to robot 1, C3 and C4 to robot 2. For example, R1 cannot move from AS1 to AS2 directly. To move from AS1 to AS2, R1 should move via control point C1 or C2, as shown in Figure 2. Control points are set to simplify path planning and avoid collision.

The second one addresses the robot access restrictions. To prevent collisions between robots at shared area, such as component transfer table (TT), tool magazine (GC), assembly station (AS2) and conveyors: IN and OUT, R1 and R2 cannot access these areas concurrently.

The third requirement is the tooling resource constraints. To fetch and assemble, the hand of each robot should be equipped with a right tool; however, a specific tool may be not available for the two robots concurrently, due to the restricted number of available tools.

III. Proposed Algorithm

The scheduling of the RFAC requires finding a way which determines how to use cell resources in an optimal manner to assemble multi-products. Let us consider an assembly cell in which a set of tasks are performed using a set of resources to assemble multi-products concurrently.

In the algorithm, there are three major steps that are performed to generate schedules: (1) Determine a job's priority, (2) assign resources to carry out assembly operations; and (3) Evaluate the performance of RFAC, as shown in figure 2 which is also show the structure of the proposed algorithm.

In the proposed algorithm, the following assumptions are considered.

1. The optimum assembly sequence of each product is given in advance.
2. Each product uses some or all of the cell resources.
3. Each robot can perform only one task at a time.
4. No interruptions like resources breakdown in cell.
5. The processing time of each task is deterministic and is known in advance.
6. The set-up times are not considered.

The proposed algorithm is described by the following steps:

Step 1 T_{ij}, T_{hj} & $T_{lk\to s}$ are given as input data. Set manipulation of R_1& R_2 at position C_1& C_2 respectively.

Step 2 Set T_{now} = 0, where T_{now} represents the scheduling time.

Step 3 Determine a job's priority.

Step 4 Assign robot *l* to carry out assembly operation *i* at T_{now}.

Case 1 If operation *i* perform at AS_1or AS_3, assign robot *1*.

Case 2 If operation *i* perform at AS_4or AS_5, assign robot *2*.

Case 3 If operation *i* perform at sharing area AS_2, assign available robot *l*.

Step 5 Check if the operation *i* requires specific tool.

Step 6 If all operations of job *j* have been performed, go to step 7; otherwise, go to step 4.

Step 7 Compute the next T_{now}.

Step 8 Calculate performance measures; T_{max}, γ_l, U_R & W_R

Step 9 If all jobs *j* have been scheduled, Stop; otherwise, go to step 3.

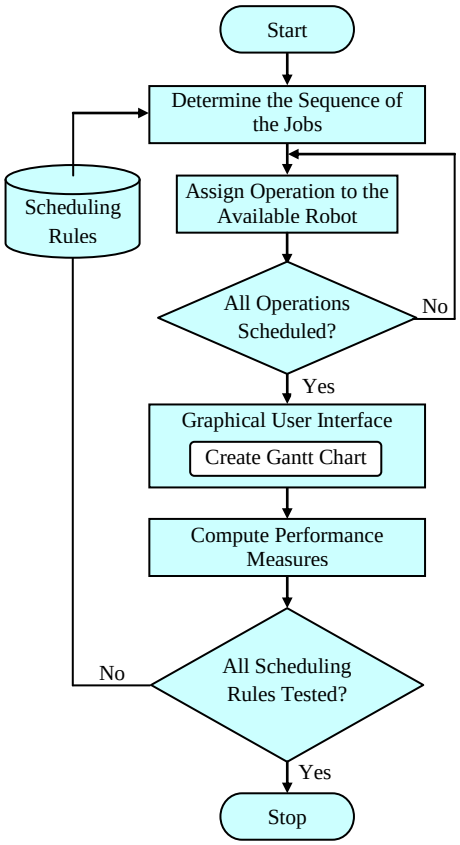

Fig. 2 Overview of the proposed algorithm

IV. Suggested Performance Measures

In this paper, time-based measures and utilisation-based measures will be considered to evaluate scheduling RFAC. To formulate the mathematical expressions of performance measures, the following notations are used:

h	Part index (h = 1, . . . ,n)
i	Assembly operations index (i = 1, . . .,p)
j	Product index (j = 1, . . . ,q)
k	Resource index (k = 1, . . . ,s)
l	Robot index
T_{ij}	Time of Assembly operation *i* of product *j*
T_{hj}	Time of tool change to transfer/assemble component *h* of product *j*
$T_{lk\to s}$	Time taken by robot *l* to travel between two resources
ε	Total time of Assembly operations of all products
α_l	Total Time of Assembly operations performed on robot *l*
β_l	Total Time of tool changes performed on robot *l*
γ_l	Total Time taken by robot *l* to travel between cell resources
Tl_{ct}	Total completion time performed on robot *l*

Four performance measures are formulated and given as follow:

A. *Scheduling Length*

One of the most common performance measures in scheduling is called scheduling length or cycle time (T_{max}). In field scheduling RFACs, T_{max} represents the maximum total completion time performed on robot *l*. T_{max} can be formulated as below.

$$T_{max} = max(Tl_{ct}) \qquad \forall\, l \in [1,2] \tag{1}$$

B. *Total Transportation Time*

The sum time required to travel the robot between cell resources to finish assembly of products. Total transportation time (γ_1) aims at measuring the amount of the movement of each robot in RFAC, during one cycle time. γ_l can be expressed as follows.

$$\gamma_l = \sum_k^s T_{lk\to s} \qquad \forall\, l \in [1,2] \tag{2}$$

C. *Utilisation rate*

Another important measure, that gives a clear perception as to whether the robots are used efficiently. Utilisation rate (U_R) can be formulated as below.

$$U_R\,\% = \frac{\delta_l}{T_{max}} \times 100 \tag{3}$$

$$\delta_l = [\alpha_l + \beta_l + \gamma_l] = \left[\sum_j^q \sum_i^p T_{ij} + \sum_j^q \sum_h^n T_{hj} + \sum_k^s T_{lk\to s}\right] \quad \forall\, l \in [1,2] \tag{4}$$

D. Workload rate

Workload rate (W_R) is a measure of RFAC balance. W_R can be expressed as follows.

$$W_R\,\% = 1 - \frac{|\alpha_1 - \alpha_2|}{\varepsilon} \times 100 \tag{5}$$

V. Case Study

Assume that three sizes of supply tanks are to be assembled in the RFAC presented as shown in Figure 3. The tanks are, essentially, chambers of constant level which supply, through gravity, liquid fuel for burners. They are composed of 13, 15 and 31 parts, respectively, as shown in Table II. During assembly, a silicone compound is applied to seal the gaps between the tank and the lid, and between the lid, the level control and the safety valve.

TABLE II
COMPONENTS OF THE SUPPLY TANKS

No	Part name	Quantity		
		Tank 11	Tank 21	Tank 51
1	Tank T	1,T1	1,T2	1,T3
2	Lid L	1,L1	1,L2	1,L3
3	Screws M6x16	4	6	10
4	Level control LC	1	1	2
5	Screws M3x12	4	4	12
6	Inlet I	1	1	2
7	Outlet O	1	1	2
8	Safety valve SV	0	0	1
Total parts number		13	15	31

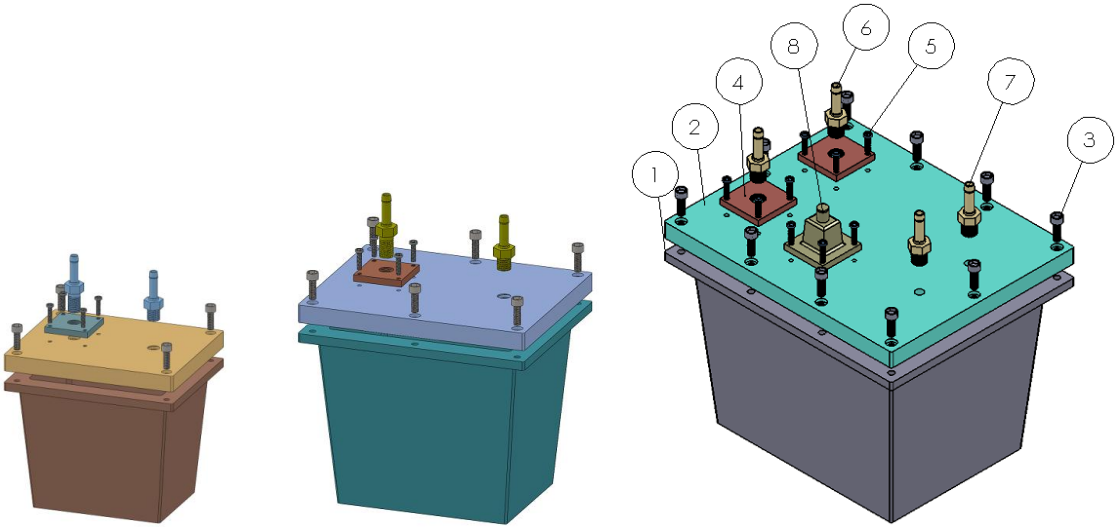

Fig. 3 Exploded view of supply tanks 11, 21 and 51

Further, assume that RFAC does not have to be stopped to load the AS with consumables like fasteners, parts and sealants (a realistic assumption for modern assembly machines with magazines of parts and components). The Assembly Stations in the RFAC are dedicated to the specific assembly operations, as shown in table III. Also this table gives details of description and time for each assembly operations.

TABLE III
ASSEMBLY OPERATIONS REQUIREMENTS

Description	Assembly Station	Time of Assembly operations		
		Tank 11	Tank 21	Tank 51
Sealant on Tank	AS1	5	10	18
Assemble Lid	AS2	5	5	5
Insert screws M6x16	AS2	8	12	20
Sealant on Lid	AS1	5	5	10
Fit the Level Control unit	AS3	5	5	10
Fit the Safety Valve	AS4	0	0	5
Insert screws M3x12	AS2	8	8	24
Assemble Inlet & Outlet	AS5	10	10	20
Total processing time (s)		46	55	112

For manipulation within the cell, the tanks are loaded on a pallet that requires a gripper G1 (to be used for T1, T2 and T5), whereas for the lids, a second pallet is utilised, requiring another gripper G2 (for L1, L2 and L5). The grippers are interchangeable. Each robot can work with either G1 or G2, as required. The time needed to perform tool change operations is listed in Table IV.

TABLE IV
TOOL CHANGE REQUIREMENTS

Tool name	Number of available tools	Part assignment	Tool change time (s)
Gripper 1	2	T1, T2, T3	3
Gripper 2	1	L1, L2, L3	3

Table V shows the time required to move the robot between two positions in the cell.

TABLE V
TRANSPORTATION TIME FOR ROBOTS BETWEEN CELL RESOURCES

Path description	Position	Trans. Time (s)
Robot move from resource to control point	AS1,2,3/GC/TT→C1,2 AS2,4,5/GC/TT→ C3,4	1
Robot move from control point to resource	C1,2→AS1,2,3/GC/TT C3,4→AS2,4,5/GC/TT	2
Robot move between control point and conveyor	C1, C3←→IC C2, C4←→OC	1.5
Robot move between two control points	C1←→C2 C3←→C4	1
Robot move directly from station to another	AS1←→AS3 AS4←→AS5	2

VI. EXPERIMENTAL RESULTS AND DISCUSSION

In order to examine the effectiveness of the proposed algorithm, four experiments are executed. Each experiment is performed with different dispatching rule. These rules set a job's priority. In this paper, each product is considered as independent job. Table VI shows the list of dispatching rules adopted in this study.

TABLE VI
LIST OF DISPATCHING RULES AND THE PRIORITY OF THE JOBS

No	Dispatching Rule	Sequence
1	Short Processing Time (SPT)	$Tank_{11}$ → $Tank_{21}$ → $Tank_{51}$
2	Long Processing Time (LPT)	$Tank_{51}$ → $Tank_{21}$ → $Tank_{11}$
3	Random (RAND1)	$Tank_{21}$ → $Tank_{11}$ → $Tank_{51}$
4	Random (RAND2)	$Tank_{11}$ → $Tank_{51}$ → $Tank_{21}$

Figure 4 illustrates Gantt chart of the experiments, and table VII shows the results of these experiments.

From the study, it has been found that the RAND2 rule performs the best result with respect to T_{max} (257 sec) and U_R (R1= 86% and R2 = 59%), while the same rule performs the worst result with respect to W_R (74%). Additionally, the LPT rule achieves very well with respect to W_R(85%), whilst, the same rule achieves the worst result with respect to $T_{tran.}$, the LPT rule shows large difference between the movement of robots (R1= 92 sec and R2=54 sec) compared with other rules.

Moreover, the SPT rule performs the best result with respect to $T_{trans.}$, this rule shows relatively small difference between the movement of robots (R1= 69 sec and R2=65 sec), however, the same rule performs unacceptable value of T_{max} (296 sec).

The results also showed an inverse relationship between U_R and T_{max}. This means U_R increase when T_{max} decreased, as shown in figure 5A & 5D. In addition, the results revealed that $T_{trans.}$is directly proportional to W_R, as shown in figure 5B & 5C.

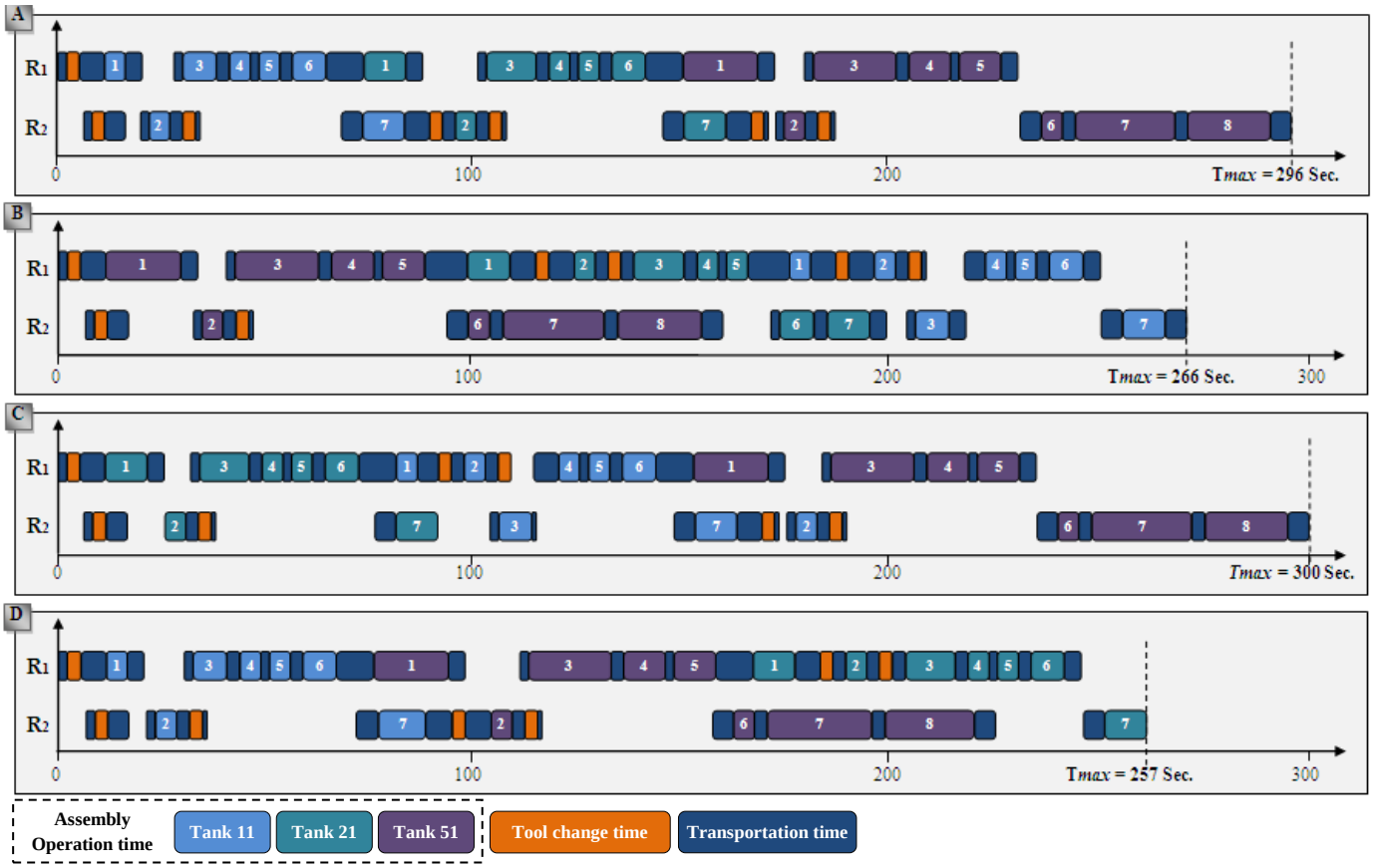

Fig. 4 Gantt chart of experimental studies

TABLE VII
THE RESULTS OF EXPERIMENTS

Dispatching Rules	T_{max}	Robot 1				Robot 2			
		α_1	β_1	γ_1	$T1_{ct}$	α_2	β_2	γ_2	$T2_{ct}$
SPT	296	129	3	69	231	84	18	65	296
LPT	266	123	15	92	246	90	6	54	266
RAND 1	300	126	9	78	264	87	12	60	300
RAND 2	257	134	9	77	237	79	12	60	257

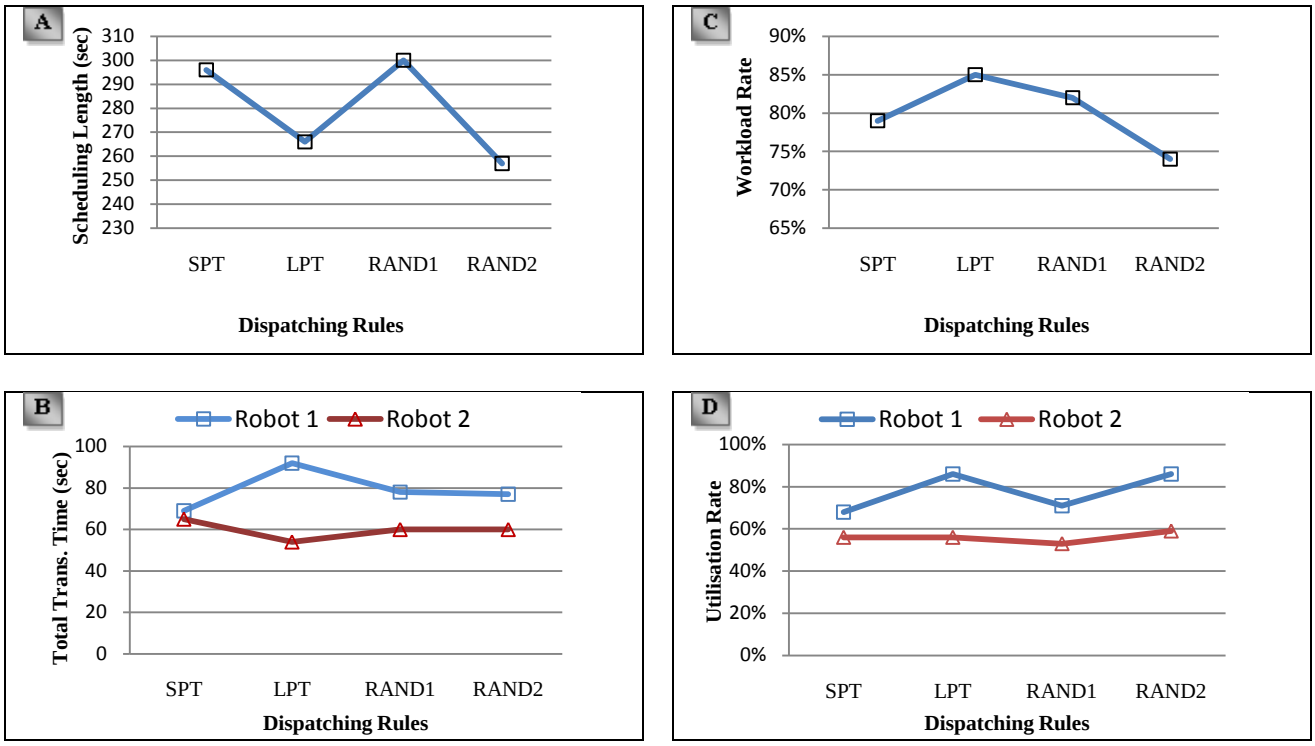

Fig. 5 Interaction plots with respect to performance measures

VII. Conclusion

This paper has dealt with the problem of scheduling RFAC with consideration of assemble multi-product, under different dispatching rules. Time-based measures and utilisation-based measures are applied to evaluate the RFAC performance. The existing algorithm and proposed performance measures have been tested by a case study.

Depending on the experimental results, make a decision of the best scheduling policy based on one performance measure is a simple way; but determination of the optimal scheduling through consideration of multi-performance measures is a considerably more complex task. The experimental results show that the algorithm and suggested performance measures are very effective for scheduling RFAC to assemble multi-products.

References

[1] R. M. Marian, A. Kargas, L. H. S. Luong, and K. Abhary, "A framework to planning robotic flexible assembly cells," in *32nd International Conference on Computers and Industrial Engineering*, Limerick, Ireland, 2003, pp. 607-615.

[2] K. Abd, K. Abhary, and R. Marian, "A scheduling framework for robotic flexible assembly cells," in *the 10th Global Congress on Manufacturing and Management*, Bangkok, Thailand 2010, pp. 111-116.

[3] T. Sawik, *Production planning and scheduling in flexible assembly systems*. poland: springer, 1999.

[4] S. Manivannan, "Robotic collision avoidance in a flexible assembly cell using a dynamic knowledge base," *IEEE transactions on systems, man, and cybernetics*, vol. 23, pp. 766-782, 1993.

[5] S. B. Mohamed, D. J. Petty, D. K. Harrison, and R. Rigby, "A cell management system to support robotic assembly" *The International Journal of Advanced Manufact. Technol.*, vol. 18, pp. 598-604, 2001.

[6] S. Y. Nof and J. Chen, "Assembly and disassembly: an overview and framework for cooperation requirement planning with conflict resolution," *Journal of Intelligent and Robotic Systems* vol. 37, 2003.

[7] J. K. Lee and T. E. Lee, "Automata-based supervisory control logic design for a multi-robot assembly cell" *International Journal Computer Integrated Manufacturing*, vol. 15, pp. 319-334, 2002.

[8] S. Y. Nof and Z. Drezner, "The multiple-robot assembly plan problem," *Journal of Intelligent and Robotic Systems* vol. 7, pp. 57-71, 1993.

[9] H. C. Lin, P. J. Egbelu, and C. T. Wu, "A two-robot printed circuit board assembly system," *International Journal of Computer Integrated Manufacturing*, vol. 8, 1995.

[10] P. M. Pelagagge, G. Cardarelli, and M. Palumbo, "Design criteria for cooperating robots assembly cells," *Journal of Manufacturing Systems*, vol. 14, pp. 219-229, 1995.

[11] T. Sawik, "Integer programming models for the design and balancing of flexible assembly systems," *Mathematical and Computer Modelling* vol. 21, pp. 1-12, 1995.

[12] K. Jiang, L. D. Seneviratne, and S. W. E. Earles, "Scheduling and compression for a multiple robot assembly workcell," *production Planning & Control*, vol. 9, pp. 143-154, 1998.

[13] G. Rabinowitz, A. Mehrez, and S. Samaddar, "A scheduling model for multi-robot assembly cells," *International Journal of Flexible Manufacturing Systems* vol. 3, pp. 149-180 1991.

[14] P. R. Glibert, D. Coupez, Y. M. Peng, and A. Delchambre, "Scheduling of a multi-robot assembly cell," *Computer Integrated Manufacturing Systems*, vol. 3, pp. 236-245, 1990.

[15] H. Hsu and L. C. Fu, "Fully automated robotic assembly cell: scheduling and simulation," in *IEEE International Conference on Robotics and Automation* National Taiwan University, 1995, pp. 208-214.

[16] D. Barral, J.-P. Perrin, and E. Dombre, "Flexible agent-based robotic assembly cell," New Mexico, 1997.

[17] H. Van Brussel, F. Cottrez, and P. Valckenaers, "SESFAC: A scheduling expert system for flexible assembly cell," *Annals of The CIRP*, vol. 39, pp. 19-23, 1990.

[18] C. Del Valle and E. F. Camacho, "Automatic assembly task assignment for a multirobot environment," *Control engineering practice*, vol. 4, pp. 915-921, 1996.

2011 International Conference on Mechanical, Industrial, and Manufacturing Engineering
Lecture Notes in Information Technology Vols. 1-2

Improvement of Cutting Performance for Friction Welding Material in Turning Process

Jong-Hwan Choi
Education Center for Vehicle Safety Component Technology
Pukyong National University
Busan, Korea
choijh2007@pknu.ac.kr

Dae-Min Kang
Department of Mechanical Engineering
Pukyong National University
Busan, Korea
dmkang@pknu.ac.kr

Jae-Seob Kwak
Department of Mechanical Engineering
Pukyong National University
Busan, Korea
jskwak5@pknu.ac.kr

***Abstract* - In order to obtain the good surface roughness in turning process, the cutting conditions are selected as the optimal value based on the prediction model of the surface roughness. However, it is difficult to satisfy the requirement condition for the high performance due to the changes of the cutting conditions during the machining. In this paper, the sliding mode control scheme based on surface roughness model has been suggested for the improvement of surface roughness in a turning process. The controller modulates the rotational speed of the workpiece to improve the roughness even if the cutting parameters change irregularly. First, the surface roughness model is constructed using the important four cutting parameters based on the experimental results in a turning process. Also, the dynamic characteristic of the electrical motor is included in the model. Second, applying the sliding mode control theory to the suggested model, the surface roughness is closed to the desired value. Finally, the effectiveness of this approach is verified through simulation.**

Index Terms – Surface Roughness, cutting parameter, turning Process, Sliding Mode Control.

I. INTRODUCTION

In the manufacturing industry, a high productivity has been required as the good quality products and the short processing time. In order to satisfy these requirements, the researchers have made an effort to find the optimal cutting conditions for the improvement of the quality of a product. Surface roughness of the product is one of evaluating the manufacturing performance. Because surface roughness affects the accurate dimension and fatigue strength of the product, the worker regard surface roughness of the product as the important factor during estimating the machining performance. Among surface roughness, the average roughness is the area between the roughness profile and its mean line, or the integral of the absolute value of the roughness profile height over the evaluation length. The turning process is a widely used machining process in which a single-point cutting tool removes material from surface of a rotating the workpiece. Surface roughness in a turning process is influenced by the cutting parameters, such as cutting speed, depth of cut, and insert radius[1-3]. Hong and Lian[2] have investigated the effect of the cutting parameters on surface roughness based on the experimental results and have proposed the prediction model of surface roughness by the orthogonal design in turning process. Also, they presented the optimal cutting parameters for the good roughness in turning process. However, it is difficult to maintain the optimal cutting parameters due to the high rotational speed of the workpiece and the variation of cutting depth between the workpiece and tool. In order to improve the roughness of the workpiece in presence of the irregular change of the cutting parameters, the control system which regulates the rotational speed in a spindle is needed.

In this study, the aim is to maintain the average roughness even though the insert radius and the depth of cut of the cutting condition are irregularly changing within the predictable range due to the cutting tool wear and the high rotational speed. First, the surface roughness model influenced by cutting conditions is constructed based on the experimental results in a turning process. Also owing to rotating the workpiece by the electronic motor, the transfer function defined as motor operation characteristic is added. Second, applying the sliding mode control theory to the turning process model which is composed of surface roughness model and the motor transfer function, the surface roughness is closed to the desired value. Finally, executing the computer simulation, the effectiveness of this approach is demonstrated.

II. MODEL OF SURFACE ROUGHNESS

In a turning process, the workpiece rotated by the spindle of a turning machine is manufactured as a cutting tool moving along surface of the workpiece. Surface roughness evaluating the machining performance relates to many cutting parameters. Among the parameters, there are the important four factors such as cutting speed, feed rate, depth of cut, and insert radius. Cutting speed is the rotational speed of the workpiece by the spindle, feed rate is the velocity of tool moving along surface of the workpiece, depth of cut is the depth between edge of tool and surface of the workpiece and insert radius is the radius of edge of tool. Therefore, the model of surface roughness is represented consequently as the function of the parameters.

The model of surface roughness in a turning process can be expressed as the following equation;

$$R_a = f(v_c, v_f, a_p, r_e) \tag{1}$$

where, R_a is average roughness, v_c is cutting speed, v_f is feed rate, a_p is depth of cut, r_e is insert radius.

Hong[2] has suggested the model of surface roughness using cutting parameters based on experimental results in a turning operation. The cutting experiments were carried out on the CNC lathe using SM45C steel bar(Diameter=48mm, Length=250mm), the condition is dry cutting. Applying the orthogonal design, surface roughness model can be expressed as the following equation;

$$R_a = 111.6\ v_c^{-0.372}\ v_f^{1.316}\ a_p^{0.09}\ r_e^{-0.528} \tag{2}$$

According to the model of surface roughness in Eq.(2), the surface roughness may be a low value if the values of cutting speed and insert radius increase, respectively. Also the roughness value increases if the values of cutting speed and insert radius decrease, respectively.

Meanwhile, cutting speed is dependent on the diameter of the workpiece and the rotational speed of the spindle in a machining. The spindle is rotated by the electrical motor. As the rapid response and the nonexistent overshoot, the model of the motor is regarded as the first order system. Therefore, the transfer function from the electrical signal to cutting speed can be expressed as the following Eq.(3). Also, the feed rate is regarded as the first order time delay as the following Eq.(4).

$$G_1(s) = \frac{V_c(s)}{I(s)} = \frac{C_1}{\tau_1 s + 1} \tag{3}$$

$$G_2(s) = \frac{V_f(s)}{V_{f0}(s)} = \frac{C_2}{\tau_2 s + 1} \tag{4}$$

where, $I(s)$ means the electrical signal acting the motor, $V_c(s)$ means cutting speed and $V_f(s)$ means feed rate in a turning process. τ_1 and τ_2 are the time constants, C_1 and C_1 are constants.

III. Design of Sliding Mode Controller

In this paper, sliding mode controller is suggested for surface roughness regulation in presence of the variations of cut depth and inset radius caused by the high spindle speed of turning process. The block diagram of the suggested control system is shown in Fig. 1.

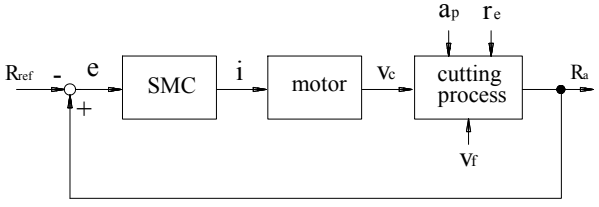

Fig. 1 Block diagram of control system for surface roughness model

The control system consists of the sliding mode controller, the electrical motor and the cutting process. Surface roughness of the cutting process is compared with a reference roughness. The difference between R_{ref} and R_a means error, which is used as an input to sliding mode controller. The transfer function of the model from the electrical signal on the motor to the roughness can be represented as following Eq.(5) and the state space equation of the model can be represented as the following Eq.(6).

$$G(s) = \frac{R_a(s)}{I(s)} = \frac{K}{(\tau_1 s + 1)(\tau_2 s + 1)} \tag{5}$$

$$\ddot{R}_a(t) = \alpha(t)(\dot{R}_a(t) + a\,R_a(t)) + b\ i(t) \tag{6}$$

where, $K=111.6C^{-0.372}a_p^{0.09}r_e^{-0.528}$ and $\alpha(t)$ means the nonlinear term including the disturbance and $i(t)$ means the control input as the electrical signal.

Let the roughness error and the sliding surface be defined as the followings[4];

$$e = R_a - R_{ref} \tag{7}$$

$$S = \left(\frac{d}{dt} + \lambda\right) e = \dot{e} + \lambda e \tag{8}$$

where, λ is a positive constant.

Differentiating the sliding surface with respect to time and substituting Eq. (6) and Eq. (7) gives

$$\dot{S} = \ddot{e} + \lambda \dot{e} = f + b i + \lambda \dot{e} \tag{9}$$

Then the control input can be chosen as the following equation;

$$i = \hat{i} - k\,\mathrm{sgn}(S) = b^{-1}(-\hat{f} - \lambda \dot{e} - k\,\mathrm{sgn}(S)) \tag{10}$$

where, the control discontinuity gain $k=F+\eta$ and the function $F \geq \left|\hat{f} - f\right|$ is satisfied. sgn(.) means the sign function.

In order to satisfy the sliding condition[5], the control discontinuity gain is chosen as the following equation;

$$\begin{aligned} \frac{1}{2}\frac{d}{dt}S^2 = S\dot{S} &= S(f - \hat{f} - k\,\mathrm{sgn}(S)) \\ &= (f - \hat{f})S - k\left|S\right| \leq -\eta\left|S\right| \end{aligned} \tag{11}$$

where, η is a positive constant.

The control input expressed as Eq.(10) includes the discontinuity across the sliding surface and generates the chattering that involves high control activity and may excite high frequency system. The chattering can be reduced by a thin boundary layer neighboring the sliding surface[5,6]. Continuous sliding mode control can be realized by replacing the sign function in Eq.(10) with the saturation function.

Therefore, the control input can be expressed as the following equation;

$$i = b^{-1}(-\hat{f} - \lambda \dot{e} - k\,\mathrm{sat}(S/\Phi)) \tag{12}$$

And the saturation function can be defined as the following equation;

$$\mathrm{sat}(x) = \begin{cases} x & \text{if } |x| < 0 \\ \mathrm{sgn}(x) & \text{otherwise} \end{cases} \tag{13}$$

IV. Simulation Results

In this paper, the sliding mode control scheme based on the model of surface roughness has been suggested for the improvement of surface roughness in a turning process even if the cutting parameters change irregularly. The performance of the suggested control system has been verified through simulation with controlling the rotational speed of the spindle in a turning. The reference value of surface roughness is preset at 2[μm] and the cutting parameters is used in the computer simulation as shown in Table 1. The spindle speed is 3333[rpm] based on cutting speed and diameter of the workpiece. In a turning process, the depth of cut changes irregularly due to a high rotational speed of the workpiece and insert radius increases because of the wear between the workpiece and the cutting tool tip. Considering these situations, the depth of cut is selected as the sine wave and it is assumed to the disturbance. The insert radius is assumed as increasing constant. Fig. 2 shows the simulation result during rotating the spindle as constant speed. The rotational speed is chosen as about 134.56[rad/s] according to the diameter of the workpiece and the cutting speed. If depth of cut and the insert radius are maintained as the initial conditions, surface roughness is constant. However, surface roughness decreases and the range of surface roughness is large as shown in Fig. 2(a) because the cutting conditions change irregularly. The average error is about 0.145[μm]. It indicates that surface roughness becomes worse due to the variation of cutting parameters. Fig. 3 show the simulation results of the suggested control system. As the result, it is shown that surface roughness is changing consistently. Surface roughness

TABLE I
CUTTING CONDITIONS USED IN SIMULATION

Conditions	Value
Dia. of the workpiece	48 [mm]
Cutting speed	193.77 [m/min]
Feed rate	0.2 [mm/rev]
Depth of cut	0.5 [mm]
Insert radius	0.8 [mm]

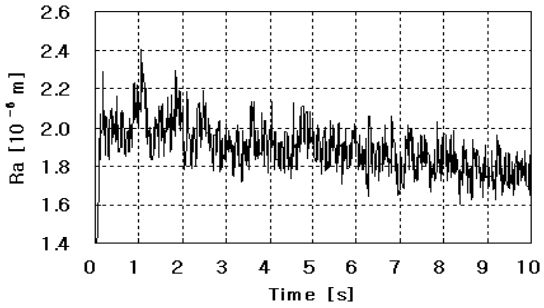

(a) Surface roughness

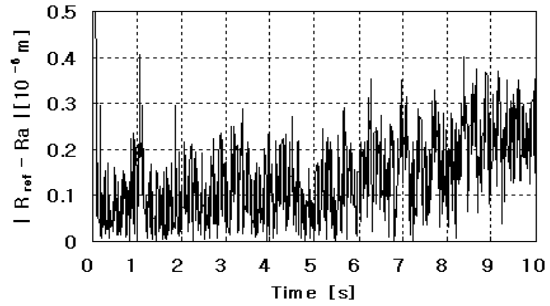

(b) Absolute error of Ra

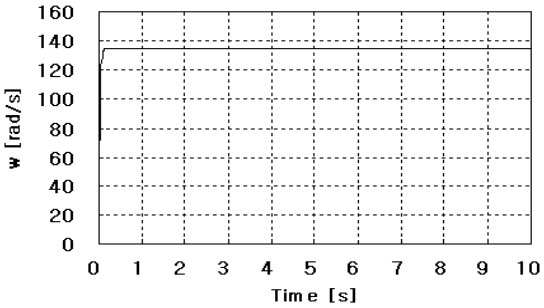

(c) Rotational speed of spindle

Fig. 3 The nominal model without SMC

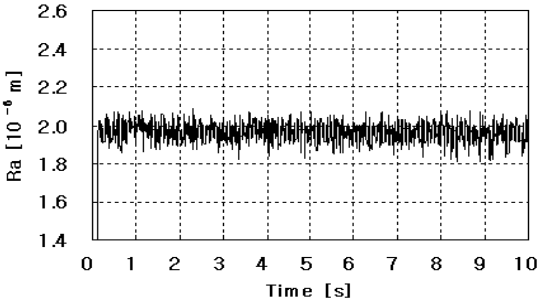

(a) Surface roughness

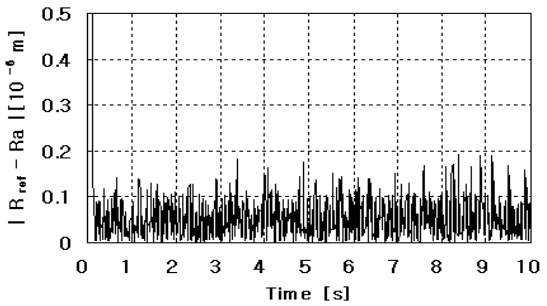

(b) Absolute error of Ra

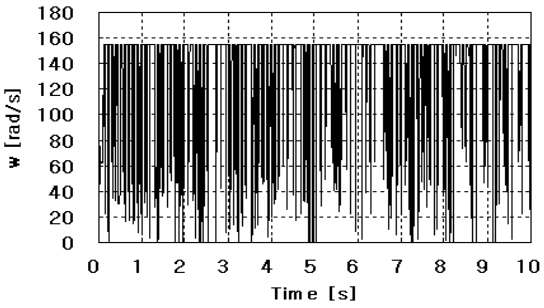

(c) Rotational speed of spindle

Fig. 4 The control model with SMC

is maintained as the little small value than the reference roughness. The roughness error between the model and the reference is about 0.067[μm] and the machining performance is improved as about 54[%] compared to the previous result. But, the control signal operating the electrical motor is doing the excessive action on account of the chattering and can not be applied to the real turning operation because of the occurrence of the high vibration in the system.

Fig. 4 shows the simulation result of the control system applying a boundary layer. If the amplitude of the saturation function decreases, the range of the rotational speed increases great. According to this condition, the amplitude is selected as 100. Surface roughness deteriorates slightly and the roughness error is about 0.078[μm]. The machining performance is improved as about 46[%] compared to the result of the constant rotational speed. However, the variation of the rotational speed is reduced remarkably due to the application of the boundary layer neighboring the sliding surface. Therefore, the suggested control system adopting the saturation function can be applied to the control of the electrical motor in a turning operation.

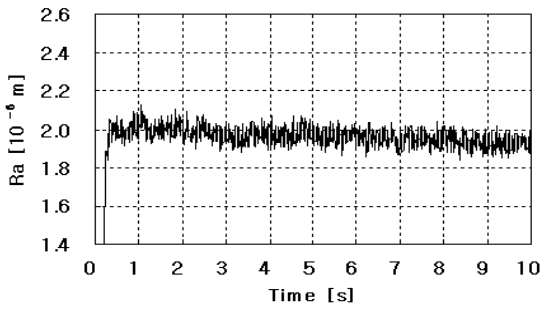

(a) Surface Roughness

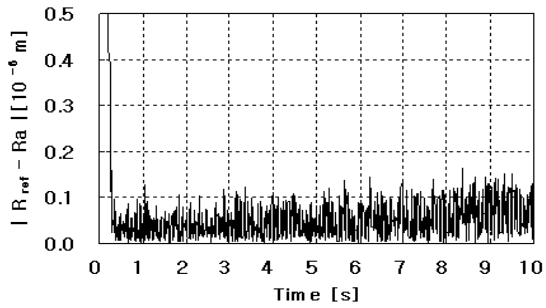

(b) Absolute error of Ra

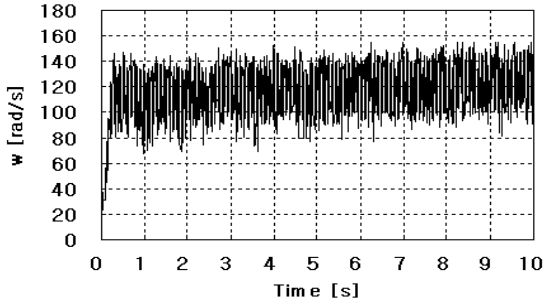

(c) Rotational speed of spindle

Fig. 5 The case of SMC with the boundary layer

V. Conclusions

This paper has presented the improvement of surface roughness of the workpiece by controlling the rotational speed of a spindle in a turning process even though the cutting parameters change. The following conclusions can be drawn based on the computer simulation results of this study;

1. The model of surface roughness can be expressed by the function of cutting parameters and the model is regarded as the second order system. For the maintenance of surface roughness, the rotational speed of the spindle is selected as the control object.
2. For the good surface roughness, the control of the rotational speed of the spindle based on the sliding mode control scheme is suggested and surface roughness can be improved in presence of the variations of the cutting parameters through simulation study. The sliding mode controller applied to the model of surface roughness leads to the chattering of the rotational speed in a spindle with the high frequency and further may causes a serious problem in a turning machine although surface roughness can be improved. The chattering problem is solved by using the thin boundary layer neighboring the sliding surface. Thus, the high frequency vibration of the rotational speed is decreased with satisfying the roughness.

Acknowledgment

Following are results of a study on the "Human Resource Development Center for Economic Region Leading Industry" Project, supported by the Ministry of Education, Science & Technology(MEST) and the National Research Foundation of Korea(NRF).

References

[1] K. A. Risbood, U. S. Dixit, and A. D. Sahasrabudhe, "Prediction of surface roughness and dimensional deviation by measuring cutting forces and vibrations in turning process," *Journal of Materials Processing Technology*, vol. 132, no. 1-3, pp. 203-214, January 2003.

[2] A.H. El-Sinawi and Reza Kashani, "Improving surface roughness in turning using optimal control of tool's radial position," *Journal of Materials Processing Technology*, vol. 167, no. 1, pp. 54-61, August 2005.

[3] M. Nalbant, H. Gokkaya, and G. Sur, "Application of Taguchi method in the optimization of cutting parameters for surface roughness in turning," *Materials and Design*, vol. 28, no. 4, pp. 1379-1385, 2007.

[4] Slotine, J. J. and Li, W. *Applied Nonlinear Control*, Prentice-Hall, Englewood Cliffs, NJ, 1991.

[5] Y. B. Park, T. Y. Kim, J. W. Woo, D. W. Shin, and J. W. Kim, "Sliding mode cutting force regulator for turning process," *International Journal of Machine Tool & Manufacture*, vol. 38, no. 8, pp. 911-930, August 1998.

[6] X. N. Luo, and Q. Zhang, "Sliding mode controller for force constrained cutting process," *Proceedings of American Control Conference*. pp. 1121-1126, 1990.

2011 International Conference on Mechanical, Industrial, and Manufacturing Engineering
Lecture Notes in Information Technology Vols. 1-2

Derivation of Cost-Tolerance Functions for Automated Manufacturing Systems

Chensong Dong
Department of Mechanical Engineering
Curtin University
Perth, WA 6845, Australia
c.dong@curtin.edu.au

***Abstract* - In this paper, the cost-tolerance functions of automated manufacturing are examined. The cost-tolerance functions where there are process mean shifts are derived from the data obtained from Monte Carlo simulation.**

Index Terms - Automated; Manufacturing; Cost; Tolerance

I. Introduction

As manufacturing industries strive to increase productivity and improve the quality, tolerance optimization has become an integral part of design.

It is obvious that implementing tight tolerances on an assembly provides higher quality but increases production costs. The problem is how to tradeoff these conflicting criteria to determine the most economical tolerance for the assembly.

Two cost factors need to be considered: operating costs and rejection costs. First, a manufacturing process with a higher precision usually results in higher operating costs because it requires better equipment and more highly trained personnel. Secondly, nonconforming products falling outside the tolerance limits need to be reworked or scrapped. With a given process precision, a tighter tolerance results in higher rejection costs.

Many cost-tolerance functions have been proposed, e.g. Sutherland function; reciprocal function; reciprocal square function; exponential function and Michael-Siddall function. In automated manufacturing, cost is directly related to process yield. In this paper, the cost-tolerance functions of automated manufacturing are examined.

II. Process Yield

In production, some products fail to meet the specification and have to be reworked or scraped. However, the cost for manufacturing these rejects has been incurred. If the process yield is Y, the associated cost can be simply given by

$$C = \frac{1}{Y} \quad (1)$$

The process variation can be represented by normal distributions, as shown in Fig. 1. When there is process mean shift, the yield will significantly decrease.

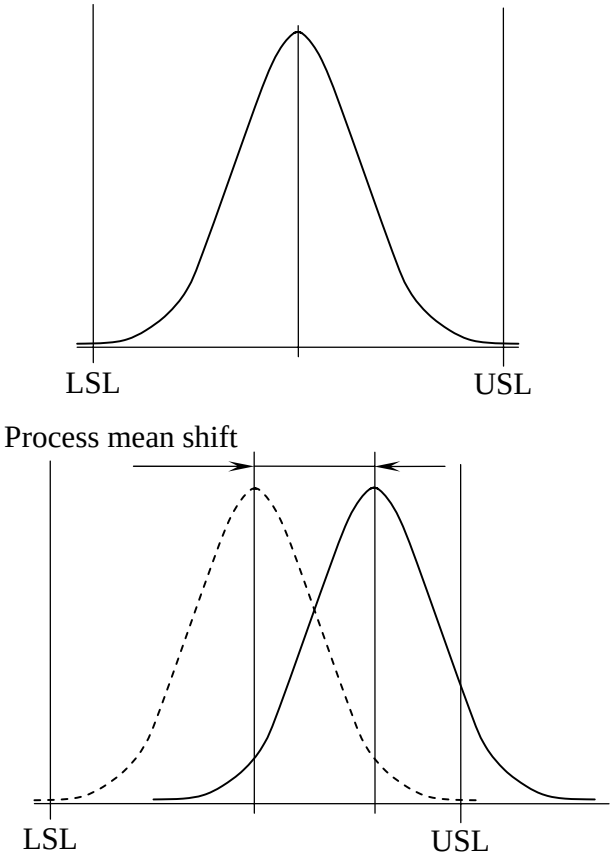

Fig. 1: Upper: process without mean shift; lower: process with mean shift

For the convenience of discussion, if the process standard deviation is 1 and USL-LSL = 6, the yield vs. process mean shift is shown in Fig. 2.

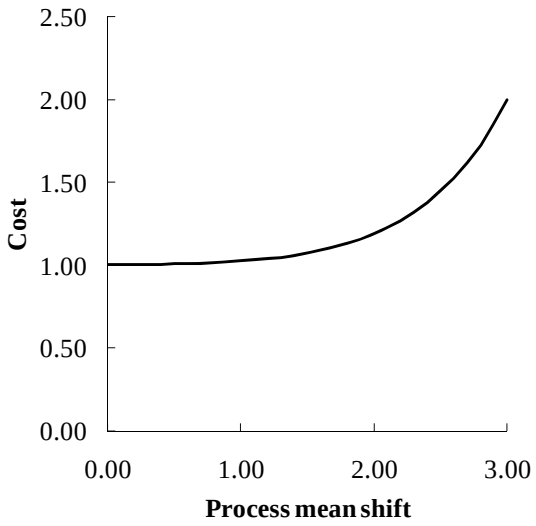

Fig. 2: Cost vs. process mean shift

III. Cost-Tolerance Functions

Five commonly used cost-tolerance functions are shown below [1].
Sutherland function: $C = bt^{-a}$;
Reciprocal function: $C = a/t$;
Reciprocal square function: $C = b/t^{a}$;
Exponential function: $C = a\exp(-bt)$;
Michael-Siddall function: $C = at^{-b}\exp(-dt)$.
When there is no process mean shift, these five cost-tolerance functions are fitted to the cost data, as shown in Fig. 3.

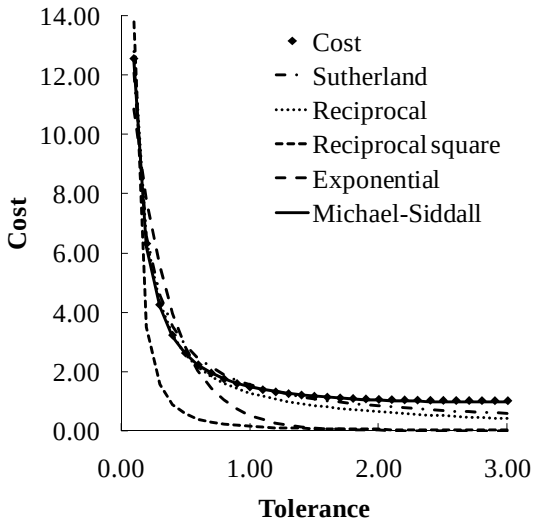

Fig. 3: Comparison of cost-tolerance functions

IV. Case Study

When the process mean shift follows *N*(0, 0.5), the cost for any given tolerance level was simulated by Monte Carlo simulation. For example, when the tolerance level is 2, the distribution of cost is shown in Fig. 4.

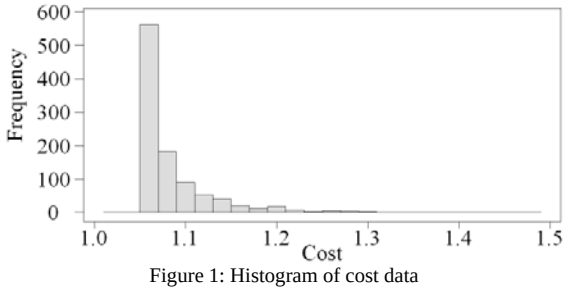

Figure 1: Histogram of cost data

The mean and upper bound of the data from Monte Carlo simulation are found and plotted vs. tolerance as shown in Fig. 5.

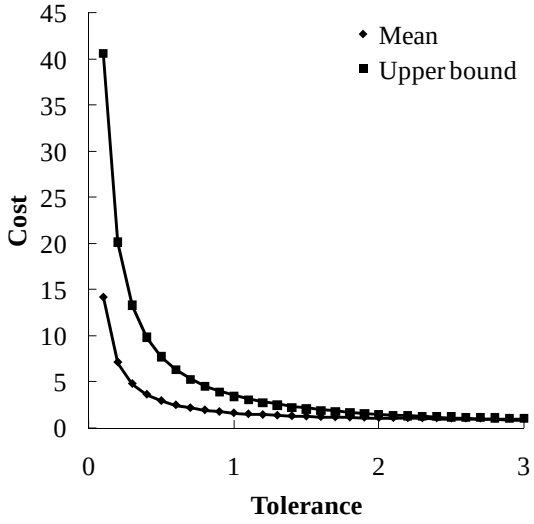

Fig. 5: Mean and upper bound of cost-tolerance data from Monte Carlo simulation

Two models can be fitted to the data, i.e.
For mean:

$$C = 1.189t^{-1.068}\exp(0.322t) \quad (2)$$

For upper bound:

$$C = 4.203t^{-0.898}\exp(-0.171t) \quad (3)$$

V. Conclusions

In this paper, the cost-tolerance functions of automated manufacturing are examined. The cost data are obtained using Monte Carlo simulation and represented by Michael-Siddall functions.

References

[1] Wu, Z., ElMaraghy, W. H. and ElMaraghy, H. A. (1998) Evaluation of cost-tolerance algorithms for design tolerance analysis and synthesis. *ASME Manufacturing Review*, **1**(3): p. 168-179.

2011 International Conference on Mechanical, Industrial, and Manufacturing Engineering
Lecture Notes in Information Technology Vols. 1-2

Quasi-Steady State Numerical Modeling of Pigging Operation in Gas Pipelines

Xu Jingyuan
School of Petroleum Engineering,
Southwest Petroleum University
No 8. Xindu Avenue, 610500, Chengdu, China
Katharine_Shmily_2005@yahoo.com.cn

Li Changjun
School of Petroleum Engineering
Southwest Petroleum University
No 8. Xindu Avenue, 610500, Chengdu, China
lichangjunemail@sina.com

***Abstract* - Pigging operation is an indispensable work in construction and operation of pipelines, which ensures the transportation efficiency for pipelines. In accordance with the flow behaviors of gas and liquid in horizontal isothermal gas pipelines during a pigging operation, a pigging physical model was established, in which the gas pipelines could be divided into three flowing sections. Then the pigging mathematical model was developed on the basis of the pigging physical model coupling with the quasi-steady state flow model by use of a mixed Eulerean-Lagrangean method in a mixed moving and fixed coordinate system. Finite difference method and Eular method were utilized to solve the mathematical model. For this purpose, a computer code was written and implemented to simulate pigging process by an iterative manner afterwards. The application example calculated finish time of a pigging operation and distributions of parameters, including gas flowrate, pressure and liquid holdup, through this numerical method. The results show that the numerical method can be used to monitor pigging operation and to judge pigging failures in gas pipelines.**

Index Terms* - *gas pipelines; liquid; pigging; numerical simulation

I. INTRODUCTION

Pigging operation is executed periodically to accumulate and remove the existing liquid in pipelines. This operation is able to keep the pipeline free of liquid, reduce the overall pressure drop and increase the pipeline flow efficiency.

McDonald and Baker [1] assumed that a steady-state method can be used, which means that the liquid holdup and pressure drop can be calculated with the steady-state two-phase empirical correlations at each time step. Barua [2] attempted to improve the McDonald and Baker pigging model and remove some limiting assumptions from the main model. Kohda et al. [3-4] proposed the first pigging simulation based on full two-phase transient formulations according to drift flux model. Minami and Shoham [5] developed a pigging model and coupled it with the Taitel [6] simplified transient simulator.

On the basis of previous studies, in accordance with the flow behavior of gas-liquid two-phase in horizontal isothermal gas pipelines during a pigging operation, a pigging physical model was established, in which the gas pipeline was divided into three flowing sections, as shown in Figure 1. The zone just ahead of the pig is the liquid slug section which is taken as slug flow because of the accumulation of liquid. In this paper, we consider the zone behind of the pig to the pipe inlet is the single-phase gas section by assuming 100% pigging efficiency. Downstream of the slug section, considering interaction between the two phases, is the two-phase flow section which is taken as stratified flow. Then the pigging mathematical model was built, which couples the pigging physical model with the quasi-steady-state flow model by use of a mixed Eulerean-Lagrangean method. Finite difference method and Eular method were utilized to solve the model. Based on the mathematical model, a computer code was written and implemented to simulate pigging process.

II. PIGGING MODEL

During a pigging operation, fluid flow abides by basic laws of fluid dynamics. According to the gas-liquid two-phase flow behavior during a pigging operation, the pipeline is divided into three flowing sections, as shown in Fig. 1. Far away from the pig to the outlet is the downstream undisturbed two-phase flow section where the effects of the pig are not yet felt. As the pig moves, the liquid slug section forms just ahead of the pig and expands by scooping the liquid from the downstream undisturbed two-phase flow section. The pig removes a lot of liquid, so the zone close to the left of the pig is a very low liquid-holdup section or a single-phase gas section. In this paper, we view the upstream section behind the pig as the single-phase gas section by ignoring the phase change during a pigging operation.

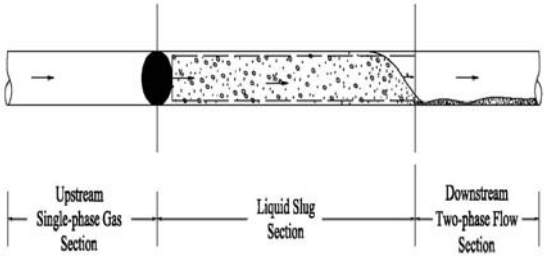

Figure 1. Pigging physical model

A. Liquid slug flow section

Just ahead of the pig is the liquid slug section in which great effects of pig are felt. For modeling the pigging operation, mass and momentum conservation equations are applied to the

liquid slug section. A mass-balance equation for a moving and expanding control volume is expressed as below [7]:

$$\frac{\mathrm{d}}{\mathrm{d}t}\int_{V(t)}\rho\,\mathrm{d}V+\int_{A(t)}\rho\left(\vec{v}-\vec{v}_{cs}\right)\mathrm{d}\vec{A}=0 \tag{1}$$

Where, t is the independent time variable, s; V is the volume of the control volume, m^3; A is the area of the control surface, m^2; v_{cs} is the velocity of the control surface, m/s.

By applying (1) with the finite difference method for the liquid phase inside the control volume described in Fig.1 and assuming that the liquid density and the liquid holdup of slug body are independent of time in a time step, (1) can be given by [5]:

$$y_{ls}\frac{\mathrm{d}L_S}{\mathrm{d}t}+\left(v_l-v_t\right)y_l+v_p\left(1-E\right)=0 \tag{2}$$

Where L_s is the length of the liquid slug section, m; y_{ls} is the liquid holdup of slug body; y_l is the liquid holdup of downstream two-phase flow section ahead of the slug front; v_t is the slug front translational velocity, m/s; y_l is the liquid-phase velocity ahead of the slug front, m/s; v_p is the pig velocity which equals to the gas velocity behind it, m/s; E is the pigging efficiency fraction or the gas void fraction left after the passage of the pig. In this paper, the upstream zone is taken as single-phase gas section by assuming 100% pigging efficiency.

The time rate of change of length of the liquid slug can be expressed in terms of difference between translational velocity and slug velocity, expressed by [5]:

$$\frac{\mathrm{d}L_S}{\mathrm{d}t}=v_t-v_p \tag{3}$$

Therefore, the translational velocity is obtained as:

$$v_t=\frac{y_{ls}v_p-y_lv_l-v_p\left(1-E\right)}{y_{ls}-y_l} \tag{4}$$

Besides, we assume that the liquid slipping past the pig has zero velocity relative to the pipe wall, that is:

$$v_s=v_p \tag{5}$$

Where, v_s is the slug velocity, m/s.

In this study, the Gregory et al. [8] correlation is used, that is:

$$y_{ls}=\frac{1}{1+\left(\frac{v_S}{8.66}\right)^{1.39}} \tag{6}$$

A momentum conservation equation applied to the control volume shown in Fig.1 is expressed by [5]:

$$\frac{\mathrm{d}}{\mathrm{d}t}\int_{V(t)}\rho\vec{v}\,\mathrm{d}V+\int_{A(t)}\rho\vec{v}\left(\vec{v}-\vec{v}_{cs}\right)\mathrm{d}\vec{A}=\vec{F} \tag{7}$$

Where, F is the net external force exerted by the surroundings on the control volume, N.

For horizontal pipelines, by use of finite difference method, (7) can be expressed as below by assuming that the liquid density, liquid-phase velocity and liquid holdup of slug body are unchangeable in a time step.

$$\begin{aligned}&\rho_l v_s\left(v_t-v_p\right)y_{ls}A+\rho_l v_l\left(v_l-v_t\right)y_lA\\&=\left(p_p-p_f\right)A-\tau_s\pi dL_s\end{aligned} \tag{8}$$

Where P_p is the pressure at the pig position, Pa; P_f is the pressure at the slug front, Pa; τ_s is the average shear stress between the liquid slug section and the pipe wall, Pa; d is the inside diameter of pipeline, m; ρ_l is the liquid density, kg/m^3; A is the cross-sectional area of pipeline, m^2; (P_p - P_f) is the total pressure drop across the liquid slug section, Pa.

The average wall shear stress in slug section, τ_s, is given by:

$$\tau_s=\frac{1}{2}f_s\rho_s{v_s}^2 \tag{9}$$

Where, f_s is the Fanning friction factor of the liquid slug section.

The relational expression between the overall pressure drop across the pig and the pig velocity has been found through experiments, that is [9]:

$$\Delta p_p=\exp\left(1.102-0.0047v_p\right)\left(15.876323\right)+10.49 \tag{10}$$

For horizontal pipelines, the gas velocity of slug body is determined in the manner as Hasan and Kabir [10] suggested:

$$v_{gs}=C_0\cdot v_s \tag{11}$$

Where, proposed by Nicholas Peta and Khalid Aziz [11], C_0 is a velocity distribution coefficient determined by liquid modified Reynolds number, whose empirical formula is $C0=1.64\mathrm{Re}_{\mathrm{mL}}^{-0.031}$ for horizontal pipelines; v_{gs} is the gas velocity of slug body, m/s.

Applying a continuity balance, as L.E. Gomez [12] proposed, on cross section in the liquid slug body, the liquid velocity of slug body can be determined by:

$$v_{ls} y_{ls} + v_{gs} \left(1 - y_{ls}\right) = v_s \tag{12}$$

Where, v_{ls} is the liquid velocity of liquid slug body, m/s.

B. Numerical solution

To model the quasi-steady state flow behavior during a pigging operation, we need to couple the pigging physical model with the quasi-steady state flow model. The pig is assumed to be a moving boundary through which no gas is allowed to pass. The front of the liquid slug is also a moving boundary. The key steps at each time step for coupling are to track the positions of the two moving boundaries, simultaneously, and to assume that all parameters are just the function of location in a time step and they are just the function of time at every location. Fig.2 gives the pigging mathematical model for the discretization.

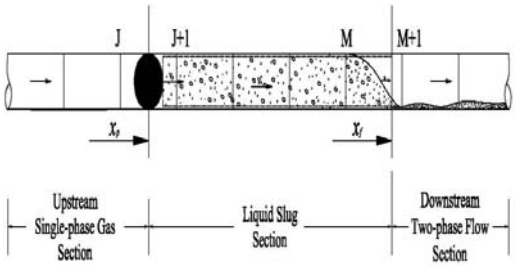

Figure 2. Pigging mathematical model

As shown in Fig.2, the pig is located between grid points J and $J + 1$, the slug front is located between M and $M + 1$. The x coordinate for the pig is x_p, the x coordinate for the slug front is x_f. Thus, while the pig and the slug front are in the pipeline, two additional grids are used.

At each time step the new positions of pig and slug front are calculated by using pig velocity and the translational velocity, respectively. That is [5]:

$$x_p^{k+1} = x_p^k + v_p^{k+1} \Delta t_k \tag{13}$$

$$x_f^{k+1} = x_f^k + v_t^{k+1} \Delta t_k \tag{14}$$

Where, x_p^{k+1} is the coordinate for the pig; v_p^{k+1} is the pig velocity, which equals to the gas velocity v_g^{k+1} behind it; x_f^{k+1} is the coordinate for the slug front; v_t^{k+1} is the translational velocity of the slug front.

After the positions of the pig and the slug front are found in a time step, the quasi-steady state flow model is performed to solve the upstream single-phase gas section and the downstream gas-liquid two-phase flow section by an iterative manner with the assumed inlet pressure.

C. Upstream single-phase gas section

The zone behind the pig is mainly composed of gas because of pigging operation. In this paper, this section is taken as single-phase gas section by ignoring the phase change during a pigging operation. The pressure just behind the pig and the given inlet gas volume flow rate under standard state are treated as the outlet boundary condition and the inlet boundary condition, respectively.

For quasi-steady state flow, every flow parameter is independent of time in a time step, so by use of the Weymouth's formula to calculate hydraulic friction loss, the pressure at each node in horizontal gas pipelines can be determined by [13]:

$$P_{g(i)} = \sqrt{P_Q^{\,2} - \frac{q^2 R_a T \cdot \Delta L}{0.3967^2 d^{16/3} R_g}} \tag{15}$$

Where, q is the natural gas volume flow rate under standard state, Nm^3/s; R_a is the gas constant of air, $m^2/(s^2 \cdot K)$. P_Q is the pressure at the inlet of pipeline, Pa; $P_{g(i)}$ is the pressure corresponding to node i, Pa; T is the transportation temperature, K; ΔL is the calculated length, m; R_g is the gas constant of natural gas, $m^2/(s^2 \cdot K)$.

D. Downstream two-phase flow section

Stratified flow is performed to solve the two-phase flow section located downstream of the slug section by considering interaction between the two phases. Basic assumptions are that the two phases remain thermodynamic equilibrium at each time step, and the velocity of each phase is constant, but not necessarily equal.

The separator pressure at the pipeline outlet is treated as the pressure boundary condition. The gas and liquid volume flow rates at the slug front just upstream of node $M + 1$ are used as the flowrate boundary conditions in the downstream two-phase flow section. Besides, the gas volume flow rate is determined by using a gas mass balance between a cross section in the liquid slug section and a cross section in the downstream two-phase flow section, expressed by [5]:

$$\left(1 - y_{ls}^{k+1}\right)\left(v_t^{k+1} - v_s^{k+1}\right) = \left(1 - y_l^k\right)\left(v_t^{k+1} - v_g^{k+1}\right) \tag{16}$$

So the gas volume flow rate $Q_{gx=xf}^{\,k+1}$ will be obtained by:

$$Q^{k+1}_{gx=x_f} = A\left[v_t^{k+1}\left(y_{Ls}^{k+1} - y_{L_{M+1}}{}^{k}\right) + v_s^{k+1}\left(1 - y_{Ls}{}^{k+1}\right)\right] \tag{17}$$

Similarly, the liquid flow rate is determined by using a liquid mass balance between a cross section in the liquid slug section and a cross section in the downstream two-phase flow section. That is,

$$Q_{lx=x_f}^{k+1} = v_{l_{M+1}}^{k+1} \cdot A_{l_{M+1}}^{k+1} = \frac{\left[v_t^{k+1} \left(y_{l_{M+1}}^{k} - y_{ls}^{k+1} \right) + v_s^{k+1} \cdot y_{ls}^{k+1} \right]}{y_{l_{M+1}}^{k}} \cdot \left(A - \frac{Q_{gx=x_f}^{k+1}}{v_g^{k+1}} \right) \tag{18}$$

Dukler II method [14] is performed to calculate the pressure drop in downstream two-phase flow section, formulas are as follows:

$$-\frac{\mathrm{d}P}{\mathrm{d}l} = \frac{\lambda}{d} \frac{u^2}{2} \rho_m \tag{19}$$

$$\rho_m = \rho_l \frac{R_l^2}{y_l} + \rho_g \frac{(1-R_l)^2}{(1-y_l)} \tag{20}$$

Where, *-dP/dl* is the gradient of pressure drop in pipeline, Pa/m; u is the mixed velocity of the two-phase, m/s; ρ_m is the mixed density of the two-phase, kg/m^3; R_L is the ratio of liquid volume containing in the two-phase; y_l is the liquid holdup of the two-phase; λ is the hydraulic friction factor. For horizontal two-phase pipelines with interphase slip, λ is determined by:

$$\lambda = C\left(0.0056 + \frac{0.5}{\mathrm{Re}^{0.32}} \right) \tag{21}$$

Where, R_e is Reynolds number of the gas-liquid two-phase; *C,* to be the function of the ratio of liquid volume, is the coefficient which can be understood as the multiples of the hydraulic friction factor increasing in two-phase pipelines compared with that in single-phase liquid pipelines.

The relation curve about C and R_L summed up with the measured data from database is expressed by:

$$C = 1 - \frac{\ln R_L}{S_0} \tag{22}$$

$$S_0 = 1.281 - 0.478(-\ln R_L) + 0.444(-\ln R_L)^2 - 0.094(-\ln R_L)^3 + 0.00843(-\ln R_L)^4 \tag{23}$$

Where, S_0 is the coefficient related to the ratio of liquid volume containing in the two-phase.

After the pressure at the last node of the pipeline is calculated by above methods, the difference between the separator pressure and the calculated pressure at the last node is obtained, by which the assumed inlet pressure is corrected until meeting the accuracy requirement.

So far, it is done that the calculation of all pipeline parameters in a time step. As time goes on, this calculation yields the pressure, liquid holdup, and gas volume flow rate distributions for all sections, completing the whole pipeline calculation for every time step.

III. APPLICATION EXAMPLE

A horizontal isothermal gas pipeline is 1.0km in length. The dynamic viscosity of gas is 1.2×10^{-5} Pa·s. The range of gas volume flow rate under standard state is 3096Nm^3/h ~4896Nm^3/h. The separator pressure at the pipeline outlet is 4.0MPa. The transportation temperature is 298.15K. The observation stations No.1 and No.2 are located at 300m and 700m from the pipeline inlet. The pigging time and the distributions of gas volume flow rate, pressure and liquid holdup at the two observation stations during a pigging operation are obtained through calculation.

The pigging time variations of different gas volume flow rate are shown in table 1.

TABLE I. COMPUTATIONAL DATA

No.	Gas volume flow rate(Nm^3/h)	pigging time(min)
1	3096	30
2	3384	38.5
3	4500	20.5
4	4680	20
5	4896	19.5

Fig.3 and Fig.4 show the pressure variations in the two observation stations. When observation stations are located in the undisturbed two-phase flow section, the pressure fluctuates slightly. In the case of No.1 observation station, when the slug front arrives, the pressure sharply increases to a local maximum until the pig passes through the station. Then the station is in single-phase gas section, the growth of liquid slug length causes more increase of the pressure. Discharging the slug into the separator causes the sharply decreasing of the pressure in the station. As the liquid slug is completely produced into the separator and the pig is removed from the pipeline, the pressure restored to its original state. Similar behavior is observed in the other observation station.

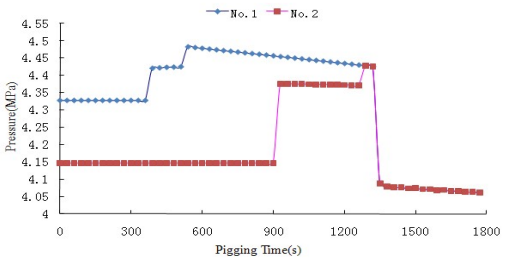

Figure 3. Pressure variations in No.1 and No.2 stations (gas flow rate 3096Nm^3/h)

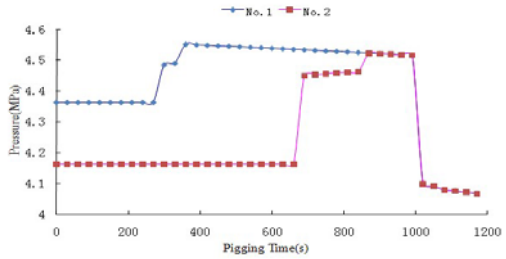

Figure 4. Pressure variations in No.1 and No.2 stations(gas flow rate 4680Nm^3/h)

Fig.5 and Fig.6 represent the liquid holdup variations in the No.1 station and the No.2 station, as well as the length of the liquid slug section changing over time. The predicted trend of liquid holdup variations seems to be reasonable. When observation station is in the undisturbed two-phase flow section, the liquid holdup remains unchanged taking no account of the phase transition. The liquid holdup approaches 1.0, when the slug reaches stations. After the slug flows through stations, the liquid holdup at stations is zero. Also, it can be seen that the length of the liquid slug section at No.2 station is longer than that at No.1 station for the liquid slug expanded by scooping the liquid from the downstream two-phase flow section.

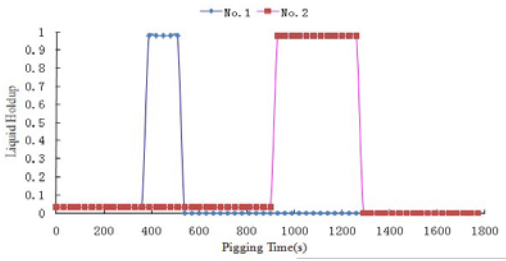

Figure 5. Liquid holdup variations in No.1 and No.2 stations(gas flow rate 3096Nm^3/h)

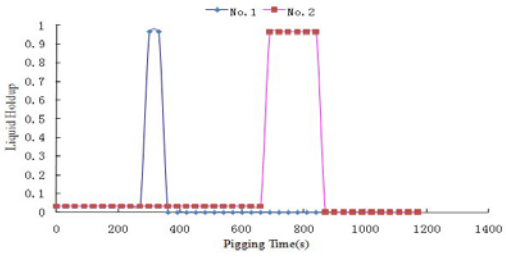

Figure 6. Liquid holdup variations in No.1 and No.2 stations(gas flow rate 4680Nm^3/h)

In Fig.7 and Fig.8, gas volume flow rates under actual state variations are shown in the two stations. When the station is in the undisturbed two-phase flow section, the gas volume flow rate fluctuates slightly. Immediately, after the slug reaches the station, the gas volume flow rate decreases dramatically. Later the station is in single-phase gas section where the flow rate increases rapidly to a local maximum. The flow rate increases to the maximum when the pressure drops drastically as the result of discharging the slug into the separator.

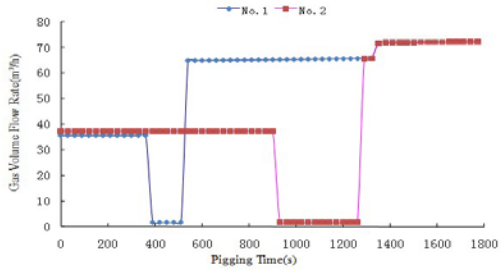

Figure 7. Gas volume flow rate variations in No.1 and No.2 stations(gas flow rate 3096Nm^3/h)

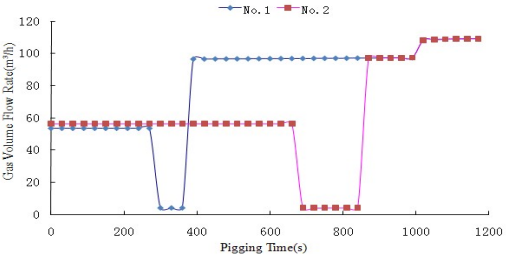

Figure 8. Gas volume flow rate variations in No.1 and No.2 stations(gas flow rate 4680Nm3/h)

The pressure variations at pipeline inlet and outlet are illustrated in Fig.9 and Fig.10, respectively. With the pressure variations at the pipeline inlet and outlet under normal pigging operation, field engineers could quickly judge whether pigging failures have occurred. Just to name a few, if the pressure at pipeline inlet increases dramatically and the outlet pressure decreases constantly, this phenomenon indicates that the pig is blocked inside pipeline. In addition, if the total pressure drop across the pipeline has no increase during a pigging operation, it shows that a gapping exists between the pig and the pipe wall.

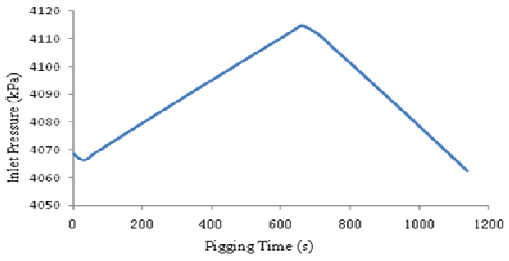

Figure 9. Pressure variation at pipeline inlet (gas flow rate 4500Nm^3/h)

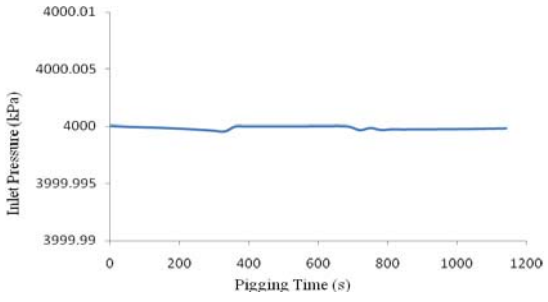

Figure 10. Pressure variation at pipeline outlet (gas flow rate 4500Nm^3/h)

IV. CONCLUSION

During a pigging operation, horizontal isothermal gas pipelines could be divided into three flowing sections which are single-phase gas section, liquid slug section and two-phase flow section from inlet to outlet. A pigging matematical model is built, coupling the pigging physical model with the quasi-steady-state flow model.

A computer code based on the pigging mathematical model was written and implemented to simulate pigging process. Then the pigging mathematical model was solved in a mixed moving and fixed coordinate system by Finite difference method and Eular method. It provides a measure to simulate pigging operation in gas pipelines.

The variable work conditions during a pigging operation in horizontal isothermal gas pipelines were simulated. Parameters in the liquid slug section and in two-phase flow section were calculated as slug flow and stratified flow, respectively. The study shows that the numerical method can be used to calculate the distributions of pigging process parameters, which provides guiding significance for monitoring pigging operation and judging pigging failures in gas pipelines.

ACKNOWLEDGMENT

This paper is supported by China National Petroleum Corporation (CNPC) tackling key subject: Research and Application of Ground Key Technicals for CO_2 flooding, JW10-W18-J2-11-20.

REFERENCES

[1] McDonald, A.E., Baker, O., "A Method of Calculating Multiphase Flow in Pipe Lines Using Rubber Spheres To Control Liquid Holdup," Drilling & Production Practice, API, 1964, pp. 56-64.

[2] Barua, S., *An Experimental Verification and Modification of the McDonald and Baker Pigging Model for Horizontal Flow*, MS Thesis, University of Tulsa, 1982.

[3] Kohda, K., Suzukawa, Y., Furukawa, H., "New Method for Analyzing Transient Flow After Pigging Scores Well," Oil & Gas Journal, Vol. 86, No. 19, pp. 40-47, May 1988.

[4] Kohda, K., Suzukawa, Y., Furukawa, H., "Pigging Analysis for Gas-Liquid Two-Phase Flow in Pipelines," ASME Annual Energy Resources Technology Conference & Exhibition, New Orleans, pp. 33-38,1988.

[5] Kazuioshi Minami, Ovadia Shoham, "Pigging Dynamics in Two-Phase Flow Pipelines: Experiment and Modeling," SPE Production & Facilities, Society of Petroleum Engineers, Vol. 10, No. 4, pp. 225-231, November 1995.

[6] Y. Taitel, O. Shoham, J. P. Brill, 1989, "Simplified transient solution and simulation of two-phase flow in pipelines," Chemical Engineering Science, Elsevier Science Ltd, Vol. 44, Issue 6, pp. 1353-1359,1989.

[7] Scott, S.L., *Modeling Slug Growth in Pipelines*, Ph.D.dissertation, University of Tulsa, January 1987.

[8] Gregory, G. A., Nicholson, M. K., Aziz, K., "Correlation of the Liquid Volume Fraction in the Slug for Horizontal Gas-Liquid Slug Flow," International Journal of Multiphase Flow, Elsevier Ltd, Vol.4, Issue 1, pp. 33-39, March 1978.

[9] Yuxing Li, Shuchu Feng, Xinlong Wang, "Prediction of Pigging Time and Velocity for Two Phase Flow in Pipelines," Nature Gas Industry,Vol.23, No.4, pp. 99-102, 2003 (in Chinese).

[10] A. Rashid Hasan and C. Shah Kabir, "A Study of Multiphase Flow Behavior in Vertical Wells," SPE Production Engineering, Society of Petroleum Engineers, Vol.3, No.2, pp. 263-272, May 1988.

[11] Nicholas Petalas, Khalid Aziz, "A Mechanistic Model For Multiphase Flow In Pipes," Journal of Canadian Petroleum Technology, Petroleum Society of Canada, Vol.39, No.6, pp. 48-61, June 2000.

[12] L.E. Gomez, Ovadia Shoham, Zelimir Schmidt, R.N. Chokshi, Tor Northug, "Unified Mechanistic Model for Steady-State Two-Phase Flow: Horizontal to Vertical Upward Flow," SPE Journal, Society of Petroleum Engineers, Vol.5, No.3, pp. 339-350, September 2000.

[13] Changjun Li, P*ipeline Transportation of Natural Gas*, Petroleum Industry Press, Chapter 2, August 2008 (in Chinese).

[14] Hong Jiang, Wu Liu, *Crude Oil Gathering and Transportation Engineering*, Petroleum Industry Press, Chapter 3, January 2006 (in Chinese).

2011 International Conference on Mechanical, Industrial, and Manufacturing Engineering
Lecture Notes in Information Technology Vols. 1-2

RMS Technical Performance Measurement method

Zhang WenJin
Department of Engineering System of Engineering
Beihang University
Beijing City, China
zwjok@buaa.edu.cn

Qiu YanLin and Wen Jia
Department of Engineering System of Engineering
Beihang University
Beijimg City, China

***Abstract* - In order to control the materiel's reliability, maintainability and supportability (RMS) through its life-cycle, a Technical Performance Measurement (TPM) method for RMS was presented in detail: first of all, a parameters tree for the TPM was constructed based on the Work Breakdown Structure (WBS); then, appropriate models for the RMS parameters during the materiel's life cycle were chosen and the RMS baselines were established; thereafter, the RMS parameters' value would be predicted, measured and demonstrated on the basis of the models in different phases ; eventually, reports on the corrective actions and the impact on performance, cost and schedule were provided.**

Index Terms* - T*echnical Performance Measurement; parameters tree; RMS baseline

I. INTRODUCTION

With the development of the design and manufacturing technology of the materiel and its increasing complexity, the importance of the special characteristics such as the reliability maintainability and supportability (RMS) has been recognized by more and more people, which urged the development of RMS theories and techniques including FMECA, RCMA and other techniques to improve the RMS of the materiel in the past few years. However, many problems still exist in the RMS management. For instance, the standardization of RMS management is not complete; the collection of necessary reliability tests data is not timely and the results of the analysis to the data are ignored by the designer. The problems above result in bad influences to the development of the materiel as follows: firstly, the improvement of RMS doesn't match the design, development and production process. Secondly, the RMS capability of product cannot satisfy the anticipated goal and modification of design is needed which result in the delay of consignment and waste of resources.

In order to monitor the change of RMS capability constantly during the design and developing phase, the RMS parameters must be monitored and evaluated efficiently in scheduled time. At present, Technical Performance Measurement (TPM) is used regularly in the engineering process to control and evaluate the RMS parameters. To implement the TPM for RMS, scheduled engineering analysis and test is needed to validate and forecast the value of the RMS parameters, which could provide the status of RMS capability and match the RMS management with the design, development and production of the materiel.

An efficient TPM method was provided in this paper for the measurement and evaluation of the materiel's RMS capability, which could not only monitor the values of the parameters but also give the predicted values of the parameters and evaluate them based on the different model of the parameters during different phases.

II. TECHNICAL PERFORMANCE MEASUREMENT

In the TPM process, existing data of Technical Performance is applied to forecast the distribution curve of the predicted value of RMS parameters, and the deviation is calculated to verify the distribution curve of the predicted value by comparing the predicted value with demonstrated data. Then, the evaluation will be implemented based on the results above and the corrective actions will be suggested.

During the concept phase, the key technology of the product could be determined by the work breakdown structure and the main RMS parameters, which need to be monitored and measured, should be chosen and put on a list. At the milestones and key points, RMS baseline should be established and predicted values of parameter should be achieved, and according to failures' distribution the distribution curve of predicted RMS data could be drawn to establish the integrated model to estimate and predict the value of RMS parameters.

During the design and development phase, the practical data of failures must be achieved by periodical evaluation and test to calculate the demonstrated value of the RMS parameters. Based on the deviation between the predicted value and demonstrated value of the RMS parameters, the distribution curve of the predicted value could be modified and a report on the problem analysis and corrective actions should be provided.

In the production phase, the affection of the design alteration should be evaluated using TPM and the status of the RMS parameters should be monitored.

Fig. 1 shows the workflow of the TPM.

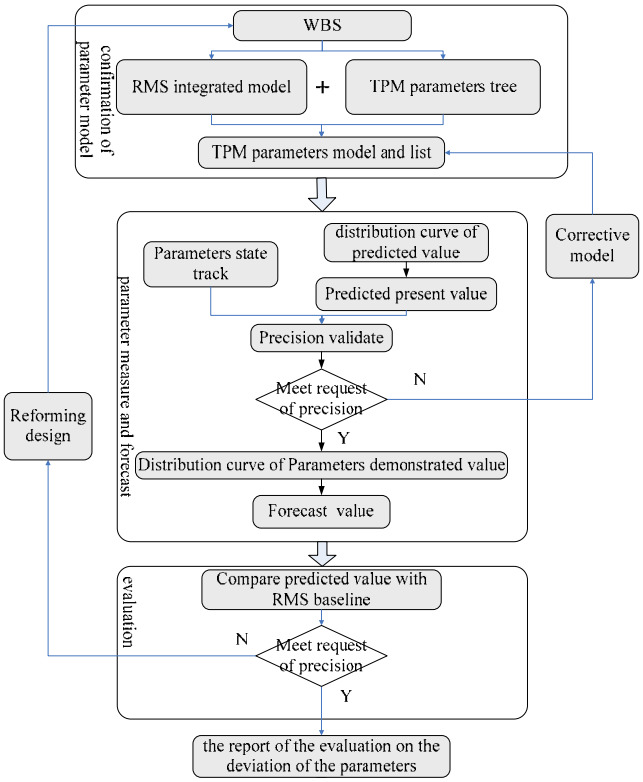

Fig. 1 Technical Performance Measurement process

The technique performance of RMS is analyzed and the analysis data is collected based on the main RMS parameters, the delivery of TPM report should be the time point of RMS evaluation.

III. RMS PARAMETERS MODEL IN LIFE CYCLE

A. *TPM parameters tree*

The parameters chosen should be the key parameters which could determine the success of the engineering system. Only a few key system parameters will be chosen because the number of the parameters should be restricted to implement TPM more economically and effectively.

Availability is chosen to be the basis for the parameter list and the guide line of the final integrated evaluation because it can reflect the readiness of the materiel and its formula can easily be broken in to several parameters for analysis and design.

TPM parameters tree could be determined by work units of WBS. The number of parameters related to each work unit will increase when the WBS become more detailed. Fig. 2 shows the TPM parameters tree of system based on WBS.

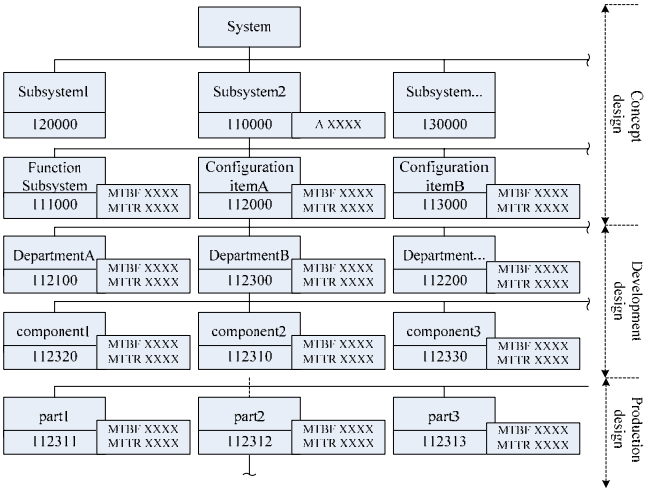

Fig. 2 TPM parameters tree of system

B. *Choosing the TPM parameters*

The models of the parameters chosen by TPM depend on the stage of design, development and production because a certain model can only be applied in certain way and the granularity of the data gathered vary in different phases.

The administrative logistics delay time and preventive maintenance time is not concerned in the concept and preliminary design phases. Therefore, Inherent availability (Ai) could be applied and MTBF MTTR of the units in the function subsystem of TPM parameters tree should be considered.

$$A_i = \frac{MTBF}{MTBF + MTTR}$$

In detailed design phase, achieved availability (Aa) could be applied for evaluation.

$$A_a = \frac{OT}{OT + CMT + PMT}$$

In utilization phase, operational availability (Ao) could be used from parts to system level because not only MTBF and MTTR but also OT, PMT, ST, CMT and ALDT should be considered by TPM during this period.

$$A_o = \frac{OT + ST}{OT + ST + PMT + CMT + ALDT}$$

IV. RMS PARAMETERS MODEL IN LIFE CYCLE

RMS baseline is the basis of TPM and also the start point to implement TPM in every phase, in return, TPM can optimize and alter RMS baseline.

The technique configure of the product is always altered during the total life cycle. Configuration baseline established at every developing phase can prevent the random alteration and control the alteration efficiently. RMS baseline is included in the configuration baseline but need to separateness convenient for measure\monitor\manage. The establishing of RMS baselines is as shown in Fig. 3.

During the conceptual design phase, based on the TPM parameters tree, the technical and economic feasibility of RMS requirement should be studied and the RMS work units of sub-system should be chosen. The parameters could choose availability in this phase. The details is contained in the <Operational requirement and specifications> and <Technical and economic feasibility study report>.

During the concept phase, further study of the feasibility of RMS requirements should be carried out, and the goal and thresholds of the RMS parameters should be determined, then, the reliability work plan should be made, and the functional FMEA should be implemented, at last, the RMS function baseline should be established and contained in <preliminary product specification>. The parameters data extracted in the RMS function baseline reflect the parameters data of function subsystem, technical condition items or subsystem in the TPM parameters tree.

In the preliminary design phase, RMS design criterion should be achieved and detailed work of RMS should be implement, then, RMS function baseline and distribution baseline should be established and contained in < product specification >and < preliminary system(subsystem) specification > which mainly include reliability parameters system report, environmental requirement, support resources allocation requirement and the reliability evaluation. The RMS parameters' data extracted form RMS distribution baseline should be considered as RMS parameters' data of component or subassembly in the TPM parameters tree.

In the detailed design phase, the RMS allocation baseline and the RMS product baseline could be determined by reliability analysis, design and supportability analysis, which includes the RMS parts of <system (sub-system) specification >, <preliminary system (sub-system) specification >, <Item specification >, and <technical document for trial-manufacture>. It contains the reliability modeling, predicting and allocating reports, FMECA reports, supportability analysis reports and the reliability evaluation. The RMS parameters data should be extracted from the RMS product baseline, and expressed as the RMS parameters data of parts in the TPM parameters breakdown structure.

In the production phase, the RMS product baseline should be determined by reliability test and evaluation, which contains the RMS parts of <preliminary craftsmanship specification>, <technical document for finalizing the design>, <craftsmanship specification >, <material specification > and <technical document for production and support>, and it is also the important parts of the production Bidding Documents and the technical manual.

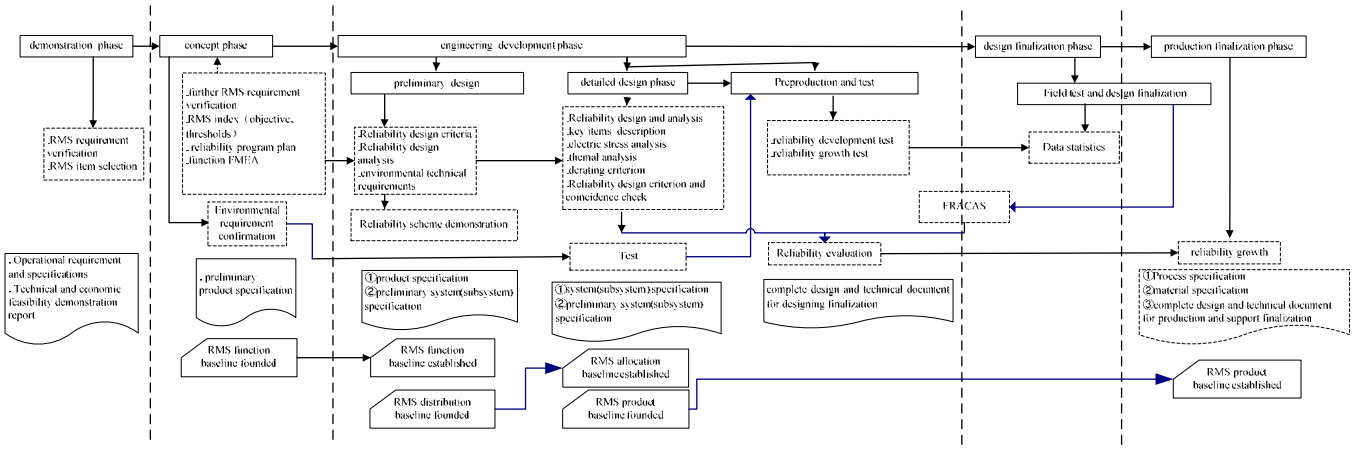

Fig. 3 The establishing of RMS baselines

V. TECHNICAL PERFORMANCE MEASUREMENT FOR RMS

Different models should be chosen to monitor and predict the parameters with the changing of the failure rate in the life cycle of the materiel. For instance, the Duane model could be used to monitor and predict the MTBF growth process during the design and usage phase.

The procedure of the technical performance measurement of the RMS is as follows:

1) The required value of the RMS parameters should be confirmed.

2) The predicted value of the parameters and their distribution curve should be determined.

In order to measure the change trend of RMS during the design and development phase, the distribution curve of the predicted value of the RMS parameters should be presented. Fig. 4 presents the expectation of MTBF trend using Duane Model.

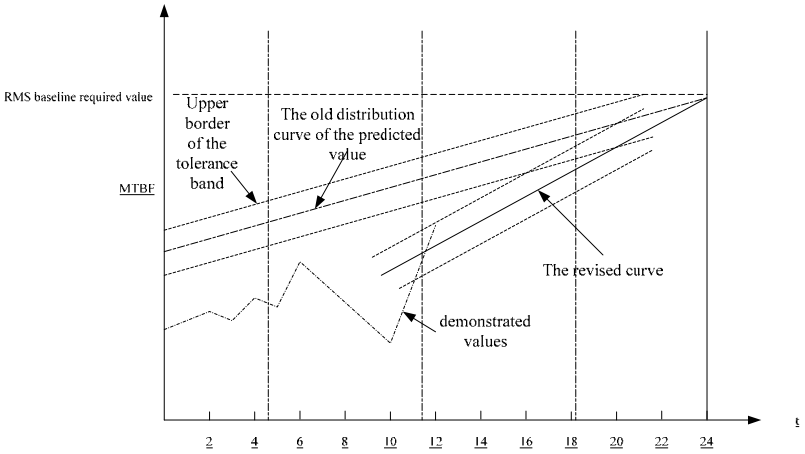

Fig. 4 distribution curve of MTBF predicted value on the Logarithmic coordinates bilateral Paper

The tolerance band of the curve should be given. And the border of the tolerance band determines the upper and lower threshold of the availability. As long as the value of the parameters is in the tolerance band, it could be achieved under the given time and cost. The tolerance band will become narrower with the design process.

In the concept phase, the expectation distribution curve of the parameters is determined by the statistics data, design experience and design draft, which is generally higher than the eternal value of the availability. Therefore, it cannot reflect the pattern of the parameters during the entire design process correctly. However, with the progress of the design, the curve will be revised by demonstrated values obtained by simulation and testing. The revised curve could reflect the changing process of the parameters' value and its effect on the model.

Fig. 5 presents the measurement and tracking curve of the parameters during different stages of the design phase.

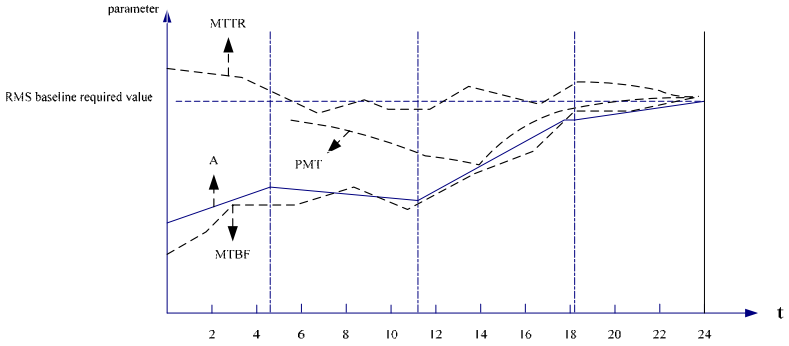

Fig. 5 the measurement and tracking curve of the parameters during different stages of the design phase

3) Obtaining the demonstrated values and drawing the distribution curve

The demonstrated values could be obtained by analysis, simulation and test. On the initial stage of the design phase, the analysis and Scaled Model Simulation methods could be used, but the analysis approach should the primarily used because most of the design is still on the paper on this stage. However, the simulation and Scaled Model testing could be approved with the progress of the design, which will provide more accurate demonstrated value. On the late stage, the mathematical model, sub-system testing and system testing could be used and more precise value will be achieved.

According to the demonstrated values obtained in different stages, the distribution curve of the demonstrated values could be drawn piece wisely which could be used by the designer to revise the former distribution curve of the expected value of the main parameters.

4) Calculating the deviation between the demonstrated value and predicted value

The deviation between the demonstrated value and predicted value should be calculated to check whether the deviation is allowed by the tolerance band.

5) Forecasting the currently estimated value of the parameters

The currently estimated value of the parameters could be forecasted based on the distribution curve of the predicted value and the demonstrated value. In the preliminary design phase, the comparison method and decision-making method could be used. And the comparison method, simulation model, experience, decision-making method could be adopted in the detailed and development phase. The experience and decision-making method could be used in the production phase.

6) Confirming and checking the predicted deviation

The predicted deviation's value of the parameters could be calculated based the required value and the currently

estimated value. The deviation should be checked to see whether it satisfies the requirement in the contract or not, and the parameters whose deviation exceeds the threshold must be marked and confirmed.

7) Analyzing and evaluating the parameters if the deviation exceeds the threshold

The impact of the deviation on other parameters and the whole system's performance should be analyzed as well as the impact on the distribution curve and the tolerance band of the predicted value. Then, the impact of the design change due to the elimination of the deviation on the change of the technical performance and production should be analyzed, as well as the impact on the cost and schedule of the project.

TABLE 1
THE REPORT OF THE EVALUATION ON THE DEVIATION OF THE PARAMETERS

Report of the evaluation on the deviation of the parameters WORK ITEM POWER SOURCE ON THE AIRPLANE WBS WORK ITEM REFERENCE 011200			
The deviation's value of availability			
Main parameter	Predicted value	demonstrated value	Deviation
MTBF			
Impact on the system performance			
Eigenvalue			
availability			
Impact on the cost to eliminate the deviation			
budget	Excepted cost	The growth of cost	usage
Impact on the schedule to eliminate the deviation			
project	schedule	Excepted schedule	Change of the schedule

8) Analyzing and evaluating the parameters if the deviation exceeds the threshold

If the currently estimated value is lower than the required value and the deviation exceeds the threshold, the following corrective actions could be applied:

Firstly, the value of Low-level parameters could be redistributed to assure that the value of the system parameters and the up-level parameters achieve the required value. However, it will be restricted by the schedule, resources and technology to follow the ways above. And if the method above cannot be taken, an alternative scheme should be applied, which includes changing the former design or using different hardware or software.

VI. FORMAT OF THE TPM REPORT

TPM report could take the format of the table or chart.

TABLE II
TPM REPORT TABLE

Project: POWER SOURCE ON THE AIRPLANE WBS 011200							
parameter	date			item			
	Predicted value	demonstrated value	deviation	currently estimated value	Required value		Expected deviation
					initial	current	

VII. CONCLUSION

1) It is vital to choose appropriate parameters models for the RMS parameters in different phases during the materiel's life cycle, which will be applied to predict the value of parameters at a certain time after they have been modified by the data of tests, simulation and experience.

2) The TPM method for RMS presented this paper can monitor the change of the parameters in different phases timely and analyze the impact of the parameters on the availability of the materiel to ensure the RMS management matching up to the design, development, production and utilization process of the materiel.

REFERENCES

[1] GB/T 19017-1997, Quality management—Guidelines for configuration management[S]. 1997.

[2] Qingtang Zhen, Dengke Yan. The used of WBS (work breakdown structure) in the engineering construct management [J]. Heilongjiang technology information, 22, 2008.

[3] Xiaoqiao Zhou. Work breakdown structure [J]. Project management technology, 2006(1): 65-66.

[4] Zongning Wu, Songjiang Wang. WBS in the engineering item management [J]. Project management technology, 6(6), 2008.

[5] R C Larrabee.Effective Work Breakdown Structures [J]. Software, IEEE, 2003, 20(5): 86-93.

[6] Mi-lung Choi, Hyoun-Mi Choi, and James W. Hong. XML-Based Configuration Management for IP Network Devices [J]. IEEE Communication Magazine. July 2004.

[7] Ruan lian, Wenjin Zhang. Aerocraft develop system engineering[S]. Beihang publishing house, 2008, 9.

2011 International Conference on Mechanical, Industrial, and Manufacturing Engineering
Lecture Notes in Information Technology Vols. 1-2

Vendor Selection, Using Fuzzy Approach

Nour Mohammad Yaghoubi
Department of Nuclear Power Engineering
University of Sistan & Baluchestan
Zahedan, Iran
yaghoobinor@yahoo.com

Hamid Hajihosseini*
Department of Industrial Engineering
Islamic Azad University, Zahedan Branch
Zahedan, Iran
intelsat605@gmail.com

***Abstract* - Vendor selection is an evaluation process that is based on many criteria that uses inaccurate or uncertain data. But while the criteria are often numerous and the relationships between higher-level criteria and lower-level sub-criteria are complex, most conventional decision models cannot help us clarify the interrelationships among the sub-criteria. Our proposed integrated fuzzy multiple criteria decision making (MCDM) method addresses this issue within the context of the vendor selection problem. First, we use triangular fuzzy numbers to express the subjective preferences of evaluators. Finally, using Fuzzy TOPSIS written in C++ language, the ranking of the vendors for a manufacturing company in supply chain and the consequences of the mentioned above were discussed and investigated.**

Index Terms - Chain management, Vendor evaluation and selection, Multiple criteria decision making (MCDM), Fuzzy logic, FUZZY TOPSIS.

I. INTRODUCTION

Various industries pay millions of dollars annually to improve their products and services. Products and services move in coming through the supply chain. Chains constantly change and face unexpected conditions. More investment in "product development" and "operations" are spending a lot of impact and affect the supply chain. A vendor selection problem usually involves more than one criterion, and criteria often conflict with each other. In multiple criteria decision making (MCDM), it is usually assumed that the criteria are independent. A considerable number of decision models have been developed based on the MCDM theory, such as preference ranking organization method (PROMETHEE) [3], analytical hierarchy process (AHP) [15,9], discrete choice analysis (DCA) [17], total cost ownership (TCO) [5], and data envelopment analysis (DEA) [18,14]. In response to increasing competition, reduction of product life cycle and rapidly change in customer tastes, most of companies consider developing long-term capabilities of vendors and this matter increases the importance of the vendor selection [8]. In today's intense competition, producing high quality products with minimum cost without satisfactory vendors is not possible.
However, in real life the available information in a MCDM process is usually uncertain, vague, or imprecise, and the criteria are not necessarily independent. To tackle the vagueness in information and the essential fuzziness of human judgment/preference, fuzzy set theory was proposed by Zadeh in 1965 [19], and a decision making method in a fuzzy environment was developed by Bellman and Zadeh [2]. A number of subsequent studies used fuzzy set theory to deal with uncertainty in the vendor selection problem. Holt [10] applied seven decision methods to contractor selection. The design process pointed out the advantages and disadvantages in the vendor selection model by Morlacchi in 1999 [13]. De Boer et al. [4] provided a comprehensive review of the literature concerning vendor selection. In these papers, fuzzy set theory was suggested as a way to improve upon the vendor selection problem. Mikhailov [12] proposed the fuzzy AHP method to determine the weight of each criterion and to score each alternative for each criterion. Kumar et al. [11] presented a fuzzy goal programming approach to solve the vendor selection problem with three objectives. In order to select a suitable partner for strategic alliance, fuzzy set theory can also be used to analyze a multiplicity of complex criteria in an MCDM environment [6]. Moreover, Shyur and Shih [16] developed a hybrid MCDM method for strategic vendor selection by using both the ANP and TOPSIS techniques. In order to solve the measurement of qualitative items, an approach was developed using both quantitative and qualitative data for vendor selection [7]. In sum, fuzzy set theory is useful when the purchase situation is full of uncertainty and imprecision due to the subjectivity of human judgment. Likewise, we will use fuzzy set theory in this paper. Furthermore, the weights represent general forms used to represent the preference structure of a decision maker. If the importance of a criterion can be properly captured through the weights, the quality of the decision making will be enhanced. Normally, the methods used to demonstrate the importance of criteria often assume additive weights and independence among criteria. But an additive model is not always suitable due to the varying degrees of interactions among the criteria.

II. PROPOSED MODEL

Optimization models after the industrial movement and especially after the Second World War are the center attention of mathematicians and industry mans. Main emphasis on classical optimization models is having a measure (or objective function); as following:

$$f: E1 \rightarrow En$$

F (x): optimized to

* Corresponding author

$$s.t: g_i(x) \begin{bmatrix} \leq \\ \geq \\ = \end{bmatrix} \quad 0?i = 1, 2, \ldots, m \quad ?E^n \rightarrow E^m$$

That the above model can be as total linear, nonlinear, or mixed. But the researchers in recent decades focused on Multiple Criteria Decision-Making (MCDM) for complicated decisions. The decisions instead of using a measure of optimality of several criteria may be used. This decision making model is divided into two main types as represented: Multiple Objective Decision-Making (MODM) and Multiple Attribute Decision-Making (MADM). Note that MODM used to design and MADM applied to select best option [1].
TOPSIS method is a common method used in MCDM problems that plays the main role to select vendors in developed models. The best option in TOPSIS method is the option that has the minimum distance from the positive ideal solution (PIS) and maximum distance from the negative ideal solution (NIS). In many conditions, Crisp and classic data for modeling real conditions seems inadequate.

III. Evaluating and Selection of Vendors in a Manufacturing Company with Fuzzy TOPSIS Approach

In this research required information for problem solving has been gathered through questionnaires and data obtained from FUZZY TOPSIS program and analyzed. Linguistic terms and their importance used in this research shown in table 1.

TABLE 1
THE IMPORTANCE DEGREE OF CRITERIA

	Low	Medium	High
1. very bad	( )	( )	( )
2. bad	( )	( )	( )
3. fair	( )	( )	( )
4. good	( )	( )	( )
5. very good	( )	( )	( )

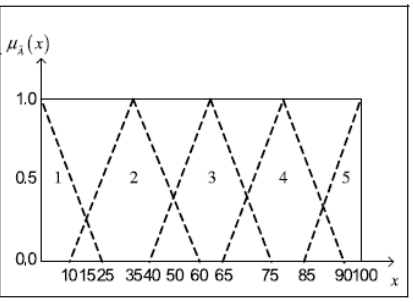

Decision matrix "D" and the criteria weight matrix "W" in the figure 1 are shown.

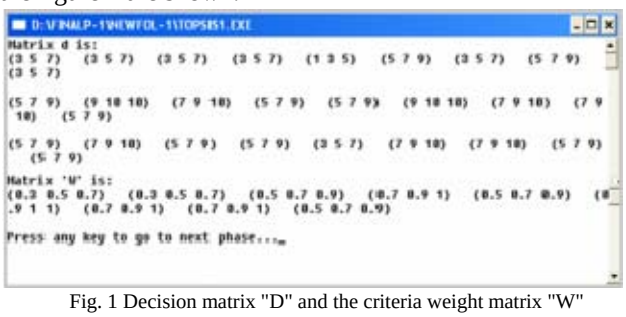

Fig. 1 Decision matrix "D" and the criteria weight matrix "W"

The output of each stage of the FUZZY TOPSIS program as results is given in figures 2 to 7.

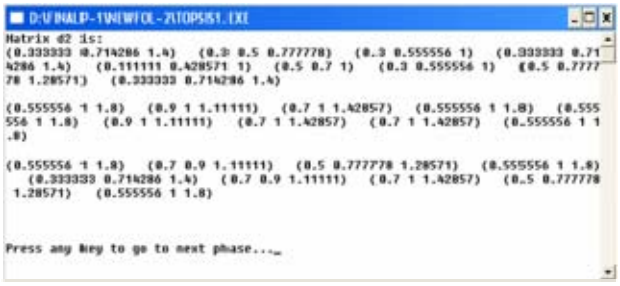

Fig. 2 Normalized decision matrix in FUZZY TOPSIS

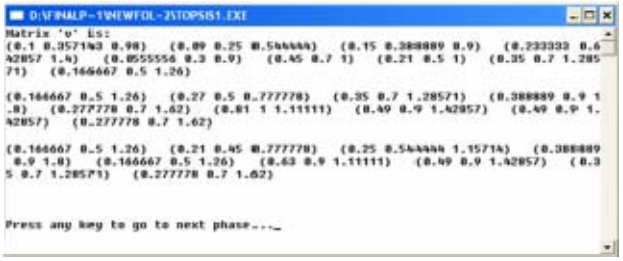

Fig. 3 weighted normalized decision matrix in FUZZY TOPSIS

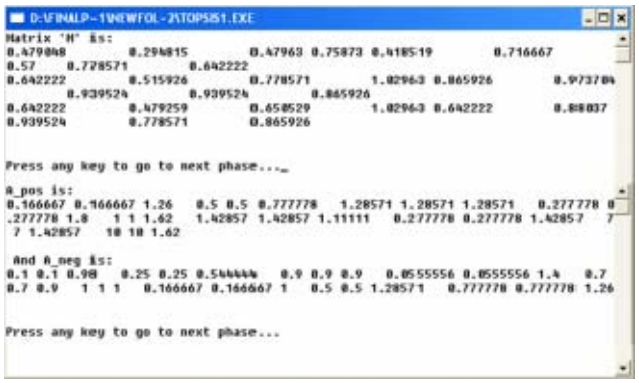

Fig. 4 Matrix "M" and the positive ideal solutions (PIS) and negative ideal solution (PIS)

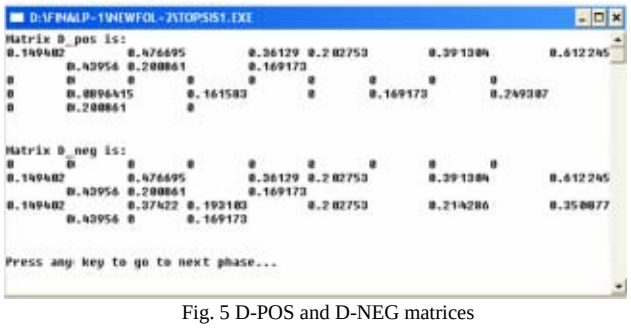

Fig. 5 D-POS and D-NEG matrices

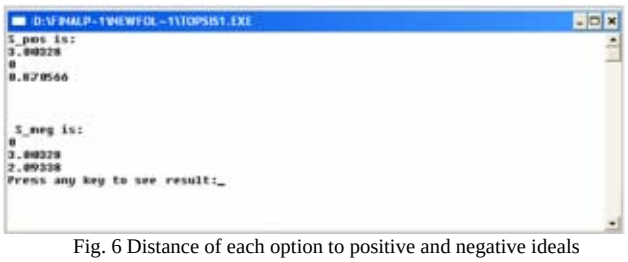

Fig. 6 Distance of each option to positive and negative ideals

Fig. 7 Final score and ranking suppliers by FUZZY TOPSIS method

IV. Conclusion

In the purchasing process, as a purchaser, one has many responsibilities and tasks, but the most important aspect of purchasing is selecting the correct vendor. There are a few basic guidelines, whether you're buying tools, raw materials or machinery, the purchasing principles remain the same. Now, more the ever, the right thing, at the right time at the right price determines the success of the purchasing department. As companies are forced to improve their own products and services, vendors are pressured to upgrade their performance on quality, service and price. The selection process does not always follow the same path and is not always applied in the same way, because circumstances differ and product and services required differ. The information available for use in multiple criteria decision making is usually uncertain, vague, or imprecise, and the criteria are not necessarily independent. In addition, if a criterion were to contain additional sub-criteria, there would be a stronger possibility of correlation among sub-criteria. However, traditional MCDM methods are based on the assumption of independence among sub-criteria, and the analytical framework for vendor selection processes has failed to consider the violation of this assumption. In this paper, we demonstrate an integrated fuzzy MCDM technique, which is more appropriate for selecting the best vendor. Here we introduce fuzzy numbers to express linguistic variables that express the subjective judgment of evaluators. Our proposed method may avoid overestimation when the criteria have substitutive effects or underestimation when the criteria have multiplicative effects. Our results show that the fuzzy integral method is better and more reasonable than the traditional method. Therefore, we demonstrate that the non-additive multiple criteria evaluation techniques are more appropriate than the traditional method and provide practitioners with a valuable tool for use in a fuzzy MCDM environment to solve vendor selection problems.

References

[1] M.J. Asgharpour, "Multiple criteria decision-making", Tehran university press: 2006, pp. 1-10.

[2] R.E. Bellman, L.A. Zadeh, Decision making in a fuzzy environment, Management Science, vol. 17, no. 4, pp. 141–164, 1970.

[3] J.P. Brans, P. Vincke, A preference ranking organization method, Management Science, vol. 31, no. 6, pp. 647–656, 1985.

[4] L. De Boer, E. Labro, P. Morlacchi, A review of methods supporting supplier selection, European Journal of Purchasing and Supply Management, vol. 7, no. 2, pp. 75–89, 2001.

[5] Z. Degraeve, E. Labro, F. Roodhooft, An evaluation of supplier selection methods from a total cost ownership perspective, European Journal of Operational Research, vol. 125, no. 1, pp. 34–59, 2000.

[6] J.F. Ding, G.S. Liang, Using fuzzy MCDM to select partners of strategic alliances for liner shipping, Information Sciences, vol. 173, no. 1-3, pp. 197–225, 2005.

[7] R. Florez-Lopez, Strategic supplier selection in the added-value perspective: a CI approach, Information Sciences, vol. 177, no. 5, pp. 1169–1179, 2007.

[8] V. B. Gargeya & J. su,, "Strategic sourcing and Supplier selection: A Review of survey- based empirical research", Second world conference on POM and 15th Annual POM conference, Cancun, Mexico, 2004.

[9] S.H. Ghoudsypour, C.O. O'Brien, A decision support system for supplier selection using an integrated analytic hierarchy process and linear programming, International Journal of Production Economics vol. 56–57, no. 1–3, pp. 199–212, 1998.

[10] G.D. Holt, Which contractor selection methodology?, International Journal of Project Management, vol. 16, no. 3, pp. 153–164, 1998.

[11] M. Kumar, P. Vrat, R. Shankar, A fuzzy goal programming approach for vendor selection problem in a supply chain, Computers and Industrial Engineering, vol. 46, no. 1, pp. 69–85, 2004.

[12] L. Mikhailov, Fuzzy analytical approach of partnership selection in formation of virtual enterprises, Omega, vol. 30, no. 2, pp. 393–401, 2002.

[13] P. Morlacchi, Vendor evaluation and selection: the design process and a fuzzy –hierarchical model, in: Proceedings of the 8th IPSERA Conference, Dublin, 1999.

[14] R. Narasimhan, S. Talluri, D. Mendez, Supplier evaluation and rationalization via data envelopment analysis: an empirical example, Journal Supply Chain Management, vol. 37, no. 3, pp. 28–37, 2001.

[15] R.L. Nydick, R.P. Hill, Using the analytic hierarchy process to the supplier selection problem, International Journal of Purchasing and Materials Management, vol. 28, no. 2, pp.31-36, 1992.

[16] H.J. Shyur, H.S. Shih, A hybrid MCDM model for strategic vendor selection, Mathematical and Computer Modelling, vol. 44, no. 8, pp. 749–761, 2006.

[17] R. Verma, M.E. Pullman, An analysis of the supplier selection process, Omega, vol. 26, no. 6, pp. 739–750, 1998.

[18] C.A. Weber, J.R. Current, A. Desai, An optimization approach to determining the number of vendors to employ, Supply Chain Management: An International Journal, vol. 5, no. 2, pp. 90–98, 2000.

[19] L.A. Zadeh, Fuzzy sets, Information and control vol. 8, no. 3, pp. 338–353, 1965.

2011 International Conference on Mechanical, Industrial, and Manufacturing Engineering
Lecture Notes in Information Technology Vols. 1-2

Performance Prediction of Wind Turbine Using Actuator-Disk Model

Qiuhua Chen, Xu Lai, Ling Chen and Xiong Hu
State Key Laboratory of Water Resources and Hydropower Engineering Science
Wuhan University
Wuhan, Hubei Province, China
adachenqh@gmail.com

***Abstract* - This paper focuses on the applications of actuator-disk model which is a simplified substitution of wind turbine. The approaches of modeling in Fluent and compiling programmes in UDF are both adopted in order to exert forces upon the incoming flow on the grids in actuator-disk model. Then the performances of wind turbines are predicted and influences of axial spacing between wind turbines on performance are analysed as well. The results show that actuator-disk model predicts the performances of wind turbine accurately to some extent during the low wind speeds.**

Index Terms – Performance of Wind Turbine, Fluent, Actuator-Disk Model

I. Introduction

Using the software of three-dimensional flow field calculation to analyse aerodynamic characteristics of wind turbine has attracted much attention, but the characteristics of aerofoil's structure and the irregular shape in the spanwise direction cause difficulty in modeling work of numerical simulation. Not only the meshing of wind turbine is sophisticated but the boundary layer's fine mesh grids lead to great total number of grids, obviously taking up a lot of computer resources and computation time.

Alternative models of wind turbine have been studied by some scholars with the purpose to solve this problem, such as actuator-disk model[1] with equal swept area and actuator-line model which replaces the geometry of each blade by a cylindrical volume positioned along the blade axis. The cylinder has the same length as the blade and the cross-section area, comparable with that of the real blade. There are relatively few research applications fucusing on the use of alternative models of wind turbine by domestic scholars. And different from the research methods as in [1], which calculates the body forces, the surface forces are adopted in this paper to achieve the replacement.

This paper takes actuator-disk model as the object, compiles programmes independently with user-defined function UDF in Fluent to calculate forces according to the blade element theory and finally exerts reaction forces to the incoming fluid to achieve the replacement. The actuator-disk model simplifies complex modeling and meshing due to the irregular shape of wind turbine blades, saving computer resources and computing time significantly, so calculating the characteristics of several wind turbines in a wind farm at the same time can be realized on a general computer.

II. Bacial Theory and Governing Equations

Blade element theory[2] is the basic theory to analyse and calculate the forces on wind turbine blades. It is assumed that the forces on a blade element can be calculated by means of two-dimensional aerofoil characteristics using an angle of attack determined from the incident resultant velocity in the cross-sectional plane of the element; the velocity component in the span-wise direction is ignored. Three-dimensional effects are also ignored.

In addition, the fluid governing equations are listed here because they reflect the rules of fluid motion and the basis of flow calculation in Fluent.

A. Blade Element Theory

Blade element theory considers each blade being divided up into finite elements along the spanwise. Each of the blade elements will experience a slightly different flow as they have a different rotational speed (Ωr), different chord length (c) and twist angle (β). Then characteristics of whole wind turbine can be obtained by integration along radial direction.

Consider a turbine with B blades and of tip radius R, rotating at angular velocity Ω. The vortex induced by wind turbine's rotation affects the coming flow, reducing the axial velocity V_n by $-aV_n$, where a is called the axial flow induction factor. The flow exiting the disk does have rotation and that rotation remains constant as the fluid progresses down the wake. The transfer of rotational motion to the air takes place entirely across the thickness of the disk. And the change in tangential velocity is expressed in terms of a tangential flow induction factor a'. The induced tangential velocity is $\Omega r a'$ at a radial distance r from the axis of rotation. Then axial and tangential velocities are expressed as $V_n(1-a)$ and $\Omega r(1+a')$. So the relative velocity is $V_{\text{rel}} = \sqrt{(V_n(1-a))^2 + (\Omega r(1+a'))^2}$.

Velocities and forces of a blade element are shown in Figure 1, here α represents attact angle which is the included angle between chord and relative velocity, and Φ represents the angle of incoming flow which is the included angel between rotation plane and relative velocity.

The angle of attack α is then given by

$$\alpha = \Phi - \beta \tag{1}$$

In Fig. 1, the lift forces acting upon the element, perpendicular to the direction V_{rel}, is therefore

$$F_L = \frac{1}{2}\rho C_L c V_{rel}^2 \tag{2}$$

and the drag force parallel to V_{rel} is

$$F_D = \frac{1}{2}\rho C_D c V_{rel}^2 \tag{3}$$

where C_L and C_D are lift and drag coefficients, seperately.

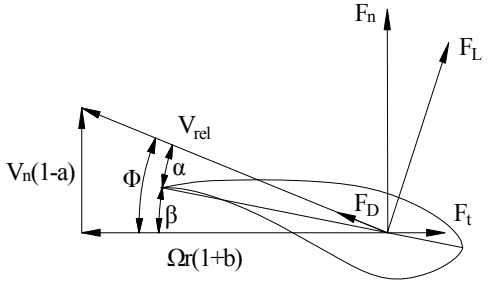

Fig. 1 Velocities and forces of blade element

The projections of F_L and F_D on axial direction **n** and tangential direction **t** are

$$F_n = \frac{1}{2}\rho V_{rel}^2 c(C_L \sin\theta + C_D \cos\theta) \tag{4}$$

$$F_t = \frac{1}{2}\rho V_{rel}^2 c(C_L \sin\theta - C_D \cos\theta) \tag{5}$$

B. Governing Equations[3]

All calculations of CFD are based on the fundamental governing equations of fluid dynamics — the continuity, momentum and energy equations which are the mathematical statements of three fundamental physical principles: 1) mass is conserved; 2) Newton's second law; 3) energy is conserved. In wind farms, it is allowable that just continuity and momentum equations are taking into consideration.

1) The Continuity Equation:

Consider a control volume of arbitrary shape and finite sizes. The surface that bounds this control volume is called the control surface *S*. The fluid moves through the fixed control volume, flowing across the control surface. The net mass flowing out this volume through surface *S* equals to the time rate of decrease of mass inside control volume. Therefore, the continuity equation is given by

$$\frac{\partial \rho}{\partial t} + div(\rho \mathbf{V}) = 0 \tag{6}$$

where the parameter **V** is velocity vector and ρ is the density of fluid. Suppose that the fluid is homogeneous, incompressible and with constant density, then the continuity equation can be simplified as

$$div\mathbf{V} = 0$$

or

$$\frac{\partial u}{\partial x} + \frac{\partial v}{\partial y} + \frac{\partial w}{\partial z} = 0 \tag{7}$$

where *u*, *v* and *w* represent the projections of **V** in the *x*, *y* and *z* directions, seperately.

2) The Momentum Equation:

The momentum equation is another fundamental physical principle to a model of the flow, based on Newton's second law $F = ma$, where F is the force and a is acceleration. Consider a control volume τ, the time rate of moment change is given by

$$\int_\tau \rho \mathbf{V} \delta\tau$$

the sum of body forces **F** is

$$\int_\tau \rho \mathbf{F} \delta\tau$$

and the sum of surface forces $\mathbf{P}_n$ is

$$\int_S \mathbf{P}_n \delta S$$

The time rate of momentum change equals to the sum of body forces and surface forces, which is

$$\frac{d}{dt}\int_\tau \rho \mathbf{V} \delta\tau = \int_\tau \rho \mathbf{F} \delta\tau + \int_S \mathbf{P}_n \delta S \tag{8}$$

Also the differential form is

$$\rho \frac{d\mathbf{V}}{dt} = \rho \mathbf{F} + divP \tag{9}$$

where *P* is the stress tensor.

Those equations are the basic rules that numerical calculation software CFD obeys to compute characteristics of fluid.

III. The Calcualtion Model

A. Actuator Disk Model

The actuator disk model concept consists in modeling the wind turbine rotor as a permeable surface, taking up the same swept area of wind turbine, on which the forces wind turbine acting upon incoming flow are exerted. These exerted forces are reaction forces of incoming flow to simulate the effect of the rotor, aiming to achieve replacement of real wind turbine. For Horizontal-Axis Wind Turbines (HAWTS), the actuator disk geometry is defined by the blades' swept area. Figure 2 illustrates a typical actuator disk for HAWT, where *x* means the axial direction and γ is the coning angle of the blades. On this drawing, the blade coning angle has been exaggerated for clarity. The surfacial force exerted on an element of the actuator disk *dA* may be decomposed onto normal direction **n** and tangential direction **t** (see Fig. 2).

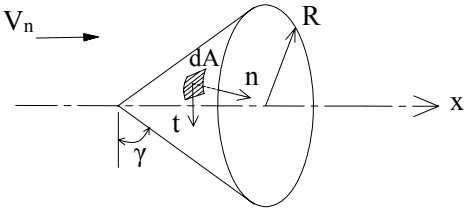

Fig. 2 Description of the actuator disk

B. Mathematical Model

The critical step is to develop a mathematical model to figure out surfacial force applied by the rotor onto the fluid. Consider the blade element *dr*, located at a distance *r* from the

rotational axis, is delimited by $\theta(r)_{\min} \le \theta \le \theta(r)_{\max}$ on dA (see Fig. 3). Hence, the mean force applied onto the fluid by the blade element over this path is expressed as follows:

$$dF = \frac{-1}{\theta(r)_{\max} - \theta(r)_{\min}} \int_{\theta(r)_{\min}}^{\theta(r)_{\max}} (F_n \mathbf{n} + F_t \mathbf{t}) dr d\theta \qquad (10)$$

The time-averaged force applied by B blades onto the fluid comprised in the control area can be expressed as:

$$dF = -\int_{r_{\min}}^{r_{\max}} \frac{B}{2\pi} \int_{\theta(r)_{\min}}^{\theta(r)_{\max}} (F_n \mathbf{n} + F_t \mathbf{t}) dr d\theta \qquad (11)$$

Hence

$$dF = -\int_A \frac{B}{2\pi} (F_n \mathbf{n} + F_t \mathbf{t}) dA \qquad (12)$$

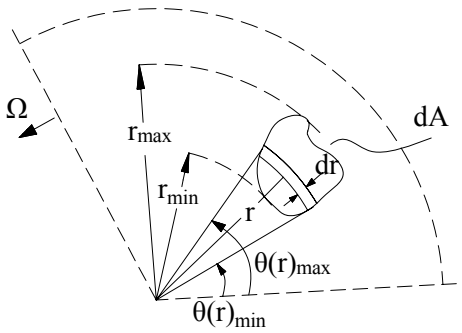

Fig. 3 Surface force integration over dA

IV. Numerical Method

A. Calculation Domain

A rectangular block is modeled as the calculation domain, and suppose the incoming flow along x axis, normal to the rotor plane. Set a thin disk to replace wind turbine at the origin of coordinates (see Fig. 4a) to represent the actuator disk model. The sizes of rectangular block are decided by wind turbine's geometries. The length along y axis is four times of diameter as well as the length along z axis. The inlet boundaries are surfaces located upstream of the wind turbine and the distance from inlet to rotor plane is twice of diameter. The outlet boundaries are surfaces located downstream of the wind turbine and the length between outlet and rotor plane is trible of diameter.

As illustrated in Fig. 4b, owing to the regular geometries of structures in the calculation domain, the grids are all divided into hexahedron elements. And the elements are not very fine in order to reduce the total number of grids and save calculation time, except the domain near the virtual wind rotor. The more fine grids must be used in the immediate vicinity of the rotor to capture the wide variations of flow properties and obtain better simulation. The grid size is then increased as distance from the turbine increases.

B. Numerical solution

Numerical method is applied to predict the performance of wind turbine. Programs are compiling through the user define function (UDF) in Fluent to calculate the forces based on blade element theory and exert computed forces upon the points of the grid (see Fig. 4b). At the beginning of the interation, according to initial velocity of incoming flow and dynamic coefficients, the normal force F_n and tangential force F_t are computed, then those forces are taken as the boundary conditions transfered to the solver to calculate a new velocity. UDF uses this new velocity to produce forces again, then the interation is conducted until results reach convergence. Therefore, certain dynamic characteristics are attained to realize the performance prediction.

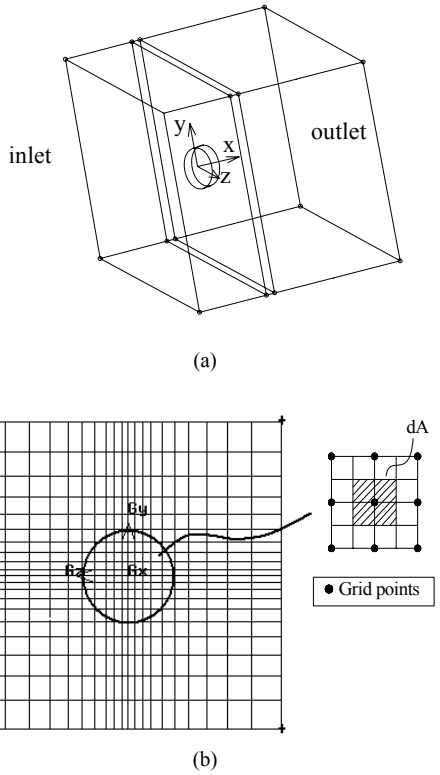

Fig. 4 Computational domain and grid topology

V. Results

The results presented in this section illustrate practicability and accuracy of performance prediction with the actuator-disk model. Then the model is applied on the setting of wind turbines in wind farm. This essay only makes some analysis of a two-row turbine park.

A. Performance Prediction of an Single Wind Turbine

The power performances of three experimental rotors tested by NERL during phases II, IV and VI are presented here, comparing with the results of actuator disk model.

1) NREL Phase II Turbine:

NREL phase II turbine has three blades, with a rotor diameter of 10.1 meters, 71.63 rpm synchronous speed, constant chord and no twist (see [4]).

The influence of incoming flow velocities has been studied and is presented in addition to predictions on performances (see Fig. 5). The performance increases as the velocity increases for both measurements and numerical

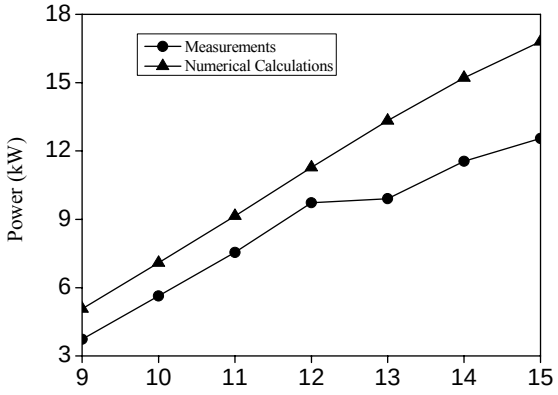

Fig. 5 Performance predictions for the NREL phase II rotor

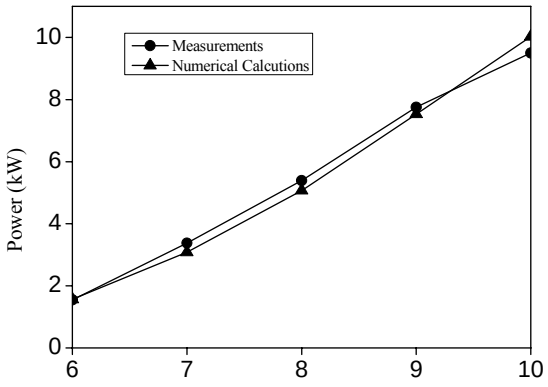

Fig. 6 Performance predictions for the NREL phase IV rotor

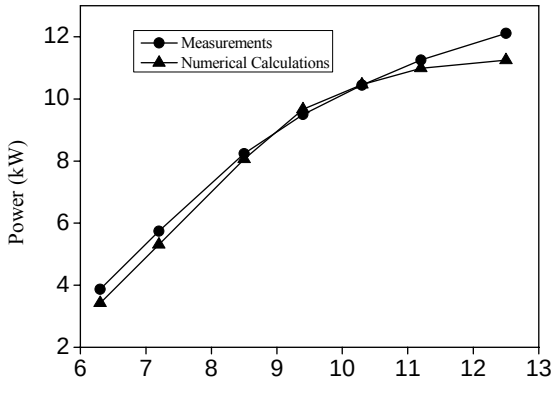

Fig. 7 Performance predictions for the NREL phase VI rotor

calculation. Phase II experimental results are less than numerical calculations generally, to be more exactly, the discrepancy is approximately 26% for low wind velocities, then added up to about 34% when wind velocity reaches 15m/s. This phenomenon is a common feature of blade-element actuator-disk-based methods, which cannot account for stall delay effects without appropriate modeling, so the gap between two methods becomes more abviously with high velocities. In addition, the dynamic geometries of phase II rotor, no twist and constant chords, may lead to some unsatisfied characteristics results.

2) NREL Phase IV Turbine:

NREL phase IV turbine has three blades, with a rotor diameter of 10.046 meters, 71.63 rpm synchronous speed and constant chord, but twists vary along the spanwise (see [4]).

The velocities of incoming fluid increase gradually from 6m/s to 10m/s. Results are expressed in Fig. 6. On the whole, values of numerical calculation are close to experiment data. Only at 10m/s, numerical result is a bit higher than that of experiment. In general, actuator disk model predicts the performance accurately to some degree at low wind velocities. From the tendency, it can be predicted that numerical results may still be higher at the condition of high speeds.

3) NREL Phase VI Turbine:

The basic parameters for NREL phase VI turbine are: two blades, a rotor diameter of 10.06 meters and 71.63 rpm synchronous speed, but both of chords and twists vary along the spanwise (see [5]).

The performances with the two methods are compared and analysed when the velocities change from 6.3m/s to 12.5m/s in Fig. 7. The results show that there are not obvious disparities based on experiments and actuator disk model. The results according to actuator disk model are less slightly than that of experiment at 6.3m/s and 7.2m/s, then almost equivalent from 7.2m/s to 11.2m/s. But actuator disk model predicts a little less than experiment's result when velocities get higher, about 7% at 12.5m/s.

B. Performance Prediction of Two-Row Turbines

The practicability and accuracy of performance prediction with the actuator disk model have been proved in section *A* above. Furthermore, the simplicity of modeling which produces less grids and saves much resource on computer contributes a lot convenience to the simulation of wind turbines' setting in wind farm. Because of the limitation of time, only the influences of axial spacing between two-row turbines on performace are discussed here, but more work will be conducted in the near future.

Two rotors based on actuator-disk-method are modeled in Fluent with axial spacing L and NREL Phase VI are taken advantage of here to predict the effect of axial spacing on performance (see Table I). Consider wind velocity is 8.5m/s, and the predicted power of an single wind turbine is 8.08 kilowatt according to Fig. 7, then we would use this number to make comparisons which are shown in Table I. The power of the anterior turbine is expressed as P_1, and P_2 for the back turbine. The axial spacing L between these two rotors inceases from six times of rotor diameter D to sixteen times of it. At

TABLE I
THE INFLUENCE OF AXIAL SPACING ON WIND TURBINE PERFORMANCE IN WAKE REGION

Axial Spacing	P_1 / kW	P_2 / kW	P_2 / P_1•100%
L = 6D	8.08	2.74	30.9%
L = 8D	8.08	3.48	43.1%
L = 16D	8.08	7.66	95%

the condition of constant incoming wind velocity, the performance P_1 keeps constant as the distance increases but the output power P_2 leaps greatly from 2.74 kilowatt to 7.66 kilowatt, almost 95% of 8.08 kilowatt (see [6]). A conclusion can be drawn that when axial spacing reaches a length of sixteen times of diameter, the wake effect can be ignored. Therefore, the effect of wake flow can be reduced through increasing the axial spacing in order to enhance performance of the turbine in the wake region.

VI. Conclusions

A program based on actuator-disk-theory has been compiled through the user-define-function UDF in Fluent to predict the power of wind turbine. This method calculates surfacial forces according to blade element theory, then exerts them upon the nodes of grids to realize the repalcement of a real wind turbine.

The practicability and accuracy of performance prediction of Horizontal-Axis Wind Turbines (HAWTS) by the adoption of actuator-disk model has been tested in this paper. This method simplifies the model work of the unregular geometries and saves calculation time. At the condition of low wind velocities, actuator disk model predicts performances accurately to some degree for the single wind turbine from the comparison with experiments. By numerical simulations, it can also be drawn that increasing the axial spacing between two rotors can reduce the influence of wake flow. Therefore, actuator-disk model can be considered as a useful tool for analysis the arrangements of wind turbines in wind farm.

Acknowledgment

This work was supported by "the Fundamental Research Funds for the Central Universities" of China. We also wish to thank the assistance of State Key Laboratory of Water Resources and Hydropower Engineering Science in Wuhan University.

References

[1] I. Ammara, C. Leclerc, and C. Masson, "A viscous three dimensional differential/actuator-disk method for the aerodynamic analysis of wind farms," Journal of solar energy engineering, vol. 124, Novermber 2002, pp. 345-356.

[2] T. Burton, D. Sharpe, N. Jenkins, E. Bossanyi. Wind Energy Handbook. New York: John Wiley & Sons, 2001.

[3] John D. Anderson, JR. "Computational Fluid Dynamics," Mcgraw-Hill Companies, 2005, pp. 37-93.

[4] D.A. Simms, M.M. Hand, L.J. Fingersh, and D.W. Jager. "Unsteady aerodynamics experiment phases II-IV: test configurations and available data campaign," National Renewable Energy Laboratory, 1999, pp. 45-54.

[5] D.A. Simms, M.M. Hand, L.J. Fingersh, and D.W. Jager. "Unsteady aerodynamics experiment phase VI: wind tunnel test configurations and available data campaigns," National Renewable Energy Laboratory, 2001, pp. 72-73.

[6] K. Chen, D.X. He. "The study for the wake model of wind turbine and the wake effects on the performance of wind turbine," aerodynamics research and development center of China, vol. 17, March 2003, pp. 84-87.

[7] D. Le Gouriérès, "WIND POWER PLANTS-Theory and Design," PERGAMON PRESS, 1982.

[8] Fujun. Wang. "The analyse of computational fluid dynamics-the theory and application of CFD," Beijing: Qinghua University Press, 2004.

[9] R. Mikkelsen. "Actuator Disc Methods Applied to Wind Turbines," Ph.D thesis, Techical University of Denmark, 2003.

[10] L.J. Pohlen, T.J. Mueller. "Boundary Layer Characteristics of the Miley Aerofoil at Low Reynolds Numbers," *J. Aircr.*, vol. 21, September 1984, pp: 658-664.

2011 International Conference on Mechanical, Industrial, and Manufacturing Engineering
Lecture Notes in Information Technology Vols. 1-2

Factors Affecting Launching and Implementing Activity Based Costing System Employing FAHP in Iran

Ali Khozein
Islamic Azad University, Aliabad Katoul Branch, IRAN
Khozain@yahoo.com

Morteza Dankoob
Islamic Azad University, Aliabad Katoul Branch, IRAN

Ghasem Barani
Islamic Azad University, Aliabad Katoul Branch, IRAN
Barani_Ghasem@yahoo.com

***Abstract*- The present study tried to point out factors affecting launching and implementing Activity Based Costing System among Iranian companies; Fuzzy AHP was employed as one of the important items regarding multi-criteria decision making. Finally, those factors were ranked according to their importance. To this end, first of all, major factors were classified and ranked into four main groups such as; organizational, environmental, individual, and technical factors; then minor factors were examined and then ranked. Regarding results of Fuzzy AHP technique, organizational factors are the most important ones and then are environmental, individual, and technical ones. Enough attention to factors affecting launching and implementing Activity Based Costing System is of crucial help for useful application and more efficiency of such systems.**

Index Terms: Activity Based Costing System, Fuzzy AHP, Factors, Launching, Implementing.

I. INTRODUCTION

Practically, Activity Based Accounting (ABC) System recognizes the relationship between necessary activities and costs in order to render services which make economic value for the organization [1]. Activity Based Accounting System is derived from this belief that products use activities and activities use resources and it leads to decimation of value adding activities and non-value adding activities [2]. In fact, by the use of this method, cost of each product or service equals total cost of activities relevant to the production at that product or service. In traditional costing, costs are generally allocated on the basis of the volume while according to the costing thinking and activity based management, products and the produced services are not directly users of the resources but are users of the activities [3].

Therefore, Activity Based Accounting System is one of the most modern costing systems; such as system can alone or with current costing systems be applied to provide essential information to make decisions [1]. As the zone of market changes, companies as well as organizations try world competitions in which more and more information and technology of information is of need to win. ABM and ABC are of pioneer systems in this field [4] and have made organizations and companies use them. If we are aware of factors affecting implementing and running, it will help the system to reach its goals successfully and prevents waste of financial as well as intellectual capital and then leads to more organizational participation and trust [5]. Now, it is time to refer to the research question:

- what are Ranking major and minor factors implementing and launching Activity Based Costing System among Iranian Companies?

II. REVIEW OF THE LITERATURE

ABC system can be taken into account as a development and extension of two-stage assignment for costing and is underlying for modern cost system, measuring products and program cost, more efficient operational budgeting and appropriate product pricing. ABC system will put an emphasis on activity as a cost object since activity is the main reason for costing. In such a system first, costing will be assigned to the activities and then through the activities, it will be given to other objects such as programs, plans, products, services. Having, determined the cost, the managers will give much more credence to the new cost object i.e. activities. Measuring the products and program cost appropriately, product price, product processing improvement, eliminating the additional activities, identifying the cost drivers, value added activities identification, eliminating non value added activities, operation programming, determining trade strategy of entity and finally measuring its operation appropriately need some information provided by ABC system much better compared to the management accounting conventional systems.

Horngren, et al [1] believes that Activity Based Accounting System is one the most modern costing systems which can separately or with current systems provide proper information for decision making. Prior to this, Cooper and Kaplan [6] claimed that companies can decrease costs, run modern pricing politics, recognize improvement opportunities and specify product combinations if they apply reliable financial statements approved by ABC system.

Cokins [5] classified problems (failures) ahead of running costing projects and activity based management into four

categories which are as follows: the biggies or showstoppers, the users' rejection, the organization obstacles and the nuisances. Some of the items include: unemploying all financial and nonfinancial sections of the organization, lack of enough and on time training, courage of implementation team, full time work, grossly underestimating of the magnitude of resistance to change, underestimating the degree of disbelief of the newly calculated numbers by project team, overengineering the design of the new system, autocratically mandating the new system by higher-level organization unit, and …[5]. Cokins in his following findings asserted that 90 percent of success in implementation and running Activity Based Costing System is due to organizational factors and the rest due to mathematical factors. Accountants as well as other organization sections are responsible for implementing such system. To this aim, factors such as education and plan to implement and communicate, true selection of activity are of importance [7]. Since too much attention to essential technical considerations to implement is necessary, little attention is paid to withstanding versus implementation [8]. To sum up, Activity Based Accounting System is better and more accurate in comparison with traditional Accounting system, though there are a lot of obstacles ahead of them. One of the biggest problems that this system faces is that companies know how to implement a new system but they do not know enough why they should do such activities and ignore them [4].

Thus regarding former researches, factors affecting implementing and running Activity Based Costing Systems in Iranian Companies are classified into four groups such as: organizational, individual, environmental and technical factors; minor factors are shown in table 1. Organizational factors consider formal and informal relationships between employees and managers. These factors can be controlled and managed by managers. On the other hand, environmental factors are related to conditions which are outside the enterprise and managers can not control them. Individual factors include characteristics and attribute of the planning and implementing (project) team. Finally, technical factors contain items which are derived from the nature of Activity Based Costing and Management System. The present study tries to prioritize and rank such factors.

III. METHODOLOGY

In this research, first of all, factors (criteria) affecting implementing and launching ABC System were recognized then using Fuzzy Analytical Hierarchy Process (FAHP) they were ranked. Analytic Hierarchy Process (AHP) is one of the well-known Multi-criteria decision making techniques that was first proposed by Saaty [9]. Although the classical AHP includes the opinions of experts and makes a multiple criteria evaluation, it is not capable of reflecting human's vague thoughts. The classical AHP takes into consideration the definite judgments of decision makers [10]. Different methods for the fuzzification of AHP have been proposed in the literature. Experts may prefer intermediate judgments rather than certain judgments. Thus the fuzzy set theory makes the comparison process more flexible and capable to explain experts' preferences [11].

In this study, Chang's [12] extent analysis method is used to compare the performances of banks because of the computational easiness and efficiency of this method. Let $X=\{X_1,X_2,\ldots, X_N\}$ be an object set, and $U=\{u_1,u_2,\ldots, u_N\}$ be a goal set. According to the method of Chang's extent analysis, each object is taken and extent analysis for each goal is performed, respectively. Therefore, m extent analysis values for each object can be obtained, with the following signs:

(1)

$$M_{gi}^{1}, M_{gi}^{2},....,M_{gi}^{m} \qquad where \qquad i=1,2,....,n$$

where all the $M_{gi}^{j}(j=1,2,....,m)$ are TFNs.

The steps of Chang's (1996) extent analysis can be given as in the following:

Step 1: The value of fuzzy synthetic extent with respect to the *i*th object is defined as

(2)

$$S_i=\sum_{j=1}^{m} M_{gi}^{j} \otimes [\sum_{j=1}^{n}\sum_{j=1}^{m} M_{gi}^{j}]^{-1}$$

To obtain $\sum_{j=1}^{m} M_{gi}^{j}$ perform the fuzzy addition operation of m extent analysis values for a particular matrix such that

(3)

$$\sum_{j=1}^{m} M_{gi}^{j}=(\sum_{j=1}^{m} l_j, \sum_{j=1}^{m} m_j, \sum_{j=1}^{m} u_j)$$

and to obtain $[\sum_{i=1}^{n}\sum_{j=1}^{m} M_{gi}^{j}]^{-1}$, the fuzzy and to addition operation of $M_{gi}^{j}(j=1,2,....,m)$ values is performed such as

(4)

$$\sum_{i=1}^{n}\sum_{j=1}^{m} M_{gi}^{j}=(\sum_{i=1}^{n} l_i, \sum_{i=1}^{n} m_i, \sum_{i=1}^{n} u_i)$$

and then the inverse of the above vector is computed in this equation such as

$$[\sum_{i=1}^{n}\sum_{j=1}^{m} M_{gi}^{j}]^{-1}=(\frac{1}{\sum_{i=1}^{n} u_i}, \frac{1}{\sum_{i=1}^{n} m_i}, \frac{1}{\sum_{i=1}^{n} l_i})$$

Step 2: As M_2 and M_1 are two triangular fuzzy numbers, the degree of possibility of

$$M_2=(l_2,m_2,u_2) \geq M_1=(l_1,m_1,u_1)$$

Is defined as

$$V(M_2 \geq M_1)=\sup[\min(\mu_{M1}(x),\mu_{M2}(y))]$$

and can be equivalently expressed as follows:

$$V(M_2 \geq M_2)=hgt(M_1 \cap M_2)=\mu(d)=\begin{cases} 1, & if\ m_2 \geq m_1, \\ 0 & if\ l_1 \geq u_2, \\ \dfrac{l_1-u_2}{(m_2-u_2)-(m_1-l_1)}, & otherwise \end{cases}$$

where d is the ordinate of the highest intersection point D between μ_{M1} and μ_{M2} (Fig. 1).

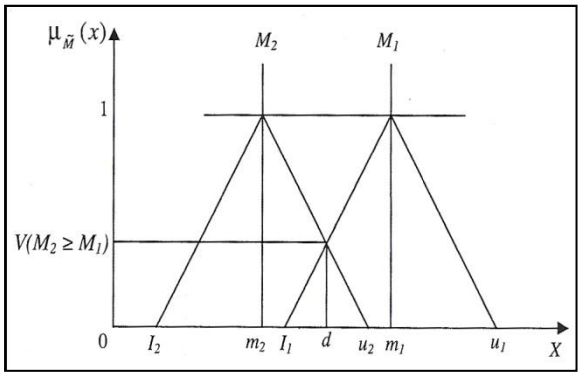

Fig. 1 The intersection between μ_{M1} and μ_{M2}

Step 3: The degree of possibility for a convex fuzzy number to be greater than k convex fuzzy numbers $M_i(i=1,2,....,k)$ can be defined by

$$V(M_1 \geq M_2,...,M_k) = V(M_1 \geq M_2),...,V(M_1 \geq M_k)$$

$$d(A_i) = Min\{V(S_i \geq S_k)\},$$

For k=1,2,…. , n; $k \neq i$. Then the weight vector is given by

$W'=(d'(A1), d'(A2),..., d'(An))^T$,

Where A_i *(i= 1,2, ..., n)* are *n* elements.

Step 4: Via normalization, the normalized weight vectors are $W=(d(A1), d(A2),..., d(An))^T$,

where *W* is a non-fuzzy number.

The respondent of this research were managers, financial managers, researchers, university professors and experts of ABC system. For gathering data needed for FAHP tables, the researchers used interviews, questionnaire and making expert work groups. After recording the answers, combining pair wise comparison matrix for each participant would be started.

IV. Findings

In this study, the effect of 25 minor factors (criteria) in 4 major groups on implementing and launching Activity Based Costing System among some accepted companies in Tehran Stock Exchange were examined. As table 1 illustrates, regarding findings of the research, the importance of organizational factors (0.484) is more than other factors; then are other factors such as: environmental factors (0.231), individual factors (0.153), and technical factors (0.132). Among organizational factors, the importance of participation of nonfinancial sections in planning and running system and considering information needs of different sections in organization, and enough and on time education is more than other factors. Among environmental factors, the importance of standardization and directions relevant to the new system and teaching the system in universities and educational centers is more than other factors. Among individual factors, the importance of eligibility of the designing team, logical timing of the designing and running and full time work of project team is more than other factors. Among Technical factors, the importance of eligibility of the finding the clear cost objects, small number of cost reinforces and centers and strong correlation of reinforces and costs is more than other factors.

Among all minor factors, participation of nonfinancial section is planning and launching the system, standardization and directions relevant to the new system, teaching the system in universities and education centers, considering information needs of different sections of the organization, enough and on time training, monitoring and supervising the operation, identification of all advantages of the system by society and directions to run the system are of vital importance; and little contradiction between the results taken from the new system, applying simulating techniques, no strict attention to details while planning and enough trust from the employees' part regarding information derived from system are the least important factors.

V. Conclusion

The head of the designing team of Activity Based Costing System should be brave enough; he/she should be the most interested person among all qualified individuals; he/she should be interested in consulting the matters with experienced counselors. Universities should also train students regarding Activity Based Costing System.

All taken together, implementing and launching Activity Based Costing System leads to less failures in companies; otherwise, while implementing and launching the system, different weak points of the system would be known; items which already have been predictable and controllable but not enough attention has been paid to them.

When we are aware of the reasons of the failures, we can easily solve the problems and predict the probable problems and find solution for them. As results, we will experience more success and can enjoy benefits of ABC system more than ever and finally value of the organization would be added.

TABLE 1
RANKING MAJOR AND MINOR CRITERIA IMPLEMENTING AND LAUNCHING ACTIVITY BASED COSTING SYSTEM BY FUZZY AHP

Criterion	Weight of Criterion	Minor Criteria	Weight of Minor Criterion	Total Weight	Rank
Organizational criterion (I1)	0.484	participation of nonfinancial segments in planning and running system	0.228	0.110	1
		No withstand from employees' part versus new information system	0.068	0.033	12
		readiness of the employees' of different sections	0.076	0.037	11
		enough and on time training	0.149	0.072	5
		directions to run the system	0.103	0.050	8
		monitoring and supervising the operation	0.133	0.064	6
		considering informational needs of different sections of the organization	0.165	0.080	4
		unification of the new system with other systems	0.078	0.038	10
Environmental criterion (I2)	0.231	Identification of all advantages of the system by society	0.198	0.046	7
		Standardization and directions relevant to the new system	0.404	0.093	2
		Teaching the system in universities and educational centers	0.398	0.092	3
Individual criterion (I3)	0.153	No strict attention to details while planning	0.098	0.015	19
		Applying simulating techniques	0.082	0.013	20
		Logical timing of the designing and running	0.186	0.028	13
		Full time work of project team	0.143	0.022	14
		Enough courage from project team	0.106	0.016	18
		Eligibility of the designing team	0.259	0.040	9
		Proper interaction	0.127	0.019	15
Technical criterion (I4)	0.132	Enough trust from the employees' part regarding information derived from system	0.113	0.015	19
		Small number of cost reinforces and centers	0.145	0.019	15
		Finding the clear cost objects	0.166	0.022	14
		Considering all costs of chain value	0.131	0.017	17
		Strong correlation of reinforces and costs	0.14	0.018	16
		Organizational design to run and implement the system	0.12	0.016	18
		Accurate definition of activities	0.118	0.016	18
		Little contradiction between the results taken from the new system	0.067	0.009	21

REFERENCES

[1] Horngren, C.T., Foster, G, Datar, S, Rajan,M, Ittner, C., *Cost Accounting – A Managerial Emphasis*, 12th edition, Pearson Education, Upper Saddle River, New Jersey. 2005.

[2]. Wickramsinghe D. and Alawattage C., *Management Accounting Change: approaches and Perspectives*, Rowtledge, 2007.

[3]. H. Thomas Johnson and Robert S. Kaplan, *Relevance Lost: The rise and Fall of Management Accounting*, Boston, MA: Harvard Business School Press, 1987.

[4] Kuchta, D., and Troska, M., "Activity-based Costing and Customer Profitability*", Cost Management*, 2007.

[5] Cokins, Gary, *Activity Based Cost Management*, Mc Graw-Hill Companies, Inc., USA, 1996.

[6]. Cooper, R. and Kaplan, R. S., "Profit Priorities From Activity-Based *Costing," Harvard Business Review, Vol. 69, No. 3, pp. 130-135, 1991.*

[7] Cokins, Gary, *Activity Based Cost Management: an Executive's Guide*, John Wiley & Sons, Inc., USA, 2001.

[8] Rotch, W., "Activity Based Costing in service industries, in Reev,j. (ed)" *Readings and Issues in Cost Management*, Warren, Gorham & Lamont, 1995.

[9] Saaty, T.L., *The Analytical Hirarchy Process, Planning, Priority, Resource Allocation*, RWS Publication, USA, 1980.

[10]. Wang, T. C., & Chen, Y. H., "Applying consistent fuzzy preference relations to partnership selection", *International Journal of Management Science*, 35, 384–388, 2007.

[11]. Kahraman, C., Cebeci, U., & Ulukan, Z., *Multi-criteria supplier selection using fuzzy AHP. Logistics Information Management*,16(6), 382–394, 2003.

[12]. Chang, D-Y., *Extent analysis and synthetic decision. Optimization Techniques and Applications*, 1, 352,1992.

2011 International Conference on Mechanical, Industrial, and Manufacturing Engineering
Lecture Notes in Information Technology Vols. 1-2

Criticality of Product Recovery Management in Sustainable Supply Chain

Swee S. Kuik, Sev V. Nagalingam and Yousef Amer

School of Advanced Manufacturing & Mechanical Engineering
University of South Australia
Mawson Lakes, Adelaide, Australia

{Swee.Kuik, Sev.Nagalingam and Yousef. Amer}@unisa.edu.au

***Abstract* - The challenge of sustainability in manufacturing is to have efficient and effective supply chain management with particular focus on product recovery operations. However, currently numerous manufacturers neglected product return policy and strategy due to the lack of measureable criteria to justify product recovery operations and management. In order to address this current gap, this paper suggests a new business model that caters for product recovery management in achieving sustainable supply chain. To minimise unexpected returned product quality and quantity, 6R *(reduce, reuse, recycle, recover, remanufacture, and redesign)* approach is introduced in this paper for integration within product recovery business processes to create a hybrid system to achieve sustainability in manufacturing. Future research should concentrate on the integration of this 6R approach within the supply chain process of returns management for establishing this hybrid system to resolve the production planning and management issue of uncertain returns quality and quantity in order to gain sustainable advantage.**

Index Terms – Product recovery, sustainable supply chains, sustainability in manufacturing, 6R methodology

I. INTRODUCTION

In recent years, there is a growing interest in promoting environmental conscious manufacturing that helps achieve efficiency and effectiveness in supply chain management. Existing conventional supply chain management frameworks such as Supply Chain Operations Reference model (SCOR) and Global Supply Chain Forum model (GSCF) do not incorporate 6R methodology in order to attain a closed loop system [1, 2]. An innovative 6R *(reduce, reuse, recycle, recover/reclaim, remanufacture and redesign)* methodology that is derived based on a previous 3R *(reduce, reuse and recycle)* approach has been recently proposed to assess organisational activities and to handle multiple product lifecycles. The introduction of 6R methodology aim is to balance environmental, economic and social dimensions in promoting sustainability in manufacturing. However, most organisations have not realised the importance of incorporation of this 6R methodology within supply chain management processes in terms of cost savings, customer satisfaction and reduction of environmental impacts.

In view of significance of product recovery management, Ref. [3] reported that a large amount of commercial product recovery within organisations may increase operational costs which is estimated around $100 billion annually. Since there are no measureable criteria to justify product recovery operations yet, numerous manufacturers are having difficulty to manage returns management processes and to monitor reverse global supply chains systematically. Moreover, Ref. [4] stated that the returns management process is one of the critical supply chain management processes that may assist organisations in achieving a sustainable competitive edge and help increase the profitability of an organisation.

Therefore, this paper is organised as follows: Firstly, a discussion on 6R methodology strategy that is aimed at waste minimisation including the opportunity for improvement and practical limitation is presented. This is followed with the analysis on business costs associated with 6R methodology incorporation. Secondly, a business model for waste minimisation within supply chain management is proposed and analysed to show that the supply chain process of returns management is one of the critical requirements for achieving sustainability in manufacturing. Thirdly, the criticality of the returns management process is reviewed. Furthermore, a summary of the potential gaps in conventional return management process is discussed. Finally, a conclusion is made and future research is suggested.

A. Enhancing sustainability management

To achieve sustainability in manufacturing, justification and definitions on sustainability incorporation within product, process and system levels needs to be defined clearly. More specifically, streamlined sustainability incorporation is concerned with the development of environmental friendly products that are physically more durable, efficient in terms of energy consumption and processing, avoidance of the use of hazardous materials and ease for manufacturing processes [5, 6]. The proposal of sustainability in manufacturing might have appeared to be overly futuristic, but with today's advanced technological development in terms of efficient communication and shared information, it is possible to reach this aspiration of sustainability in manufacturing without much sophistication.

In view of waste minimisation within any stage of multiple product lifecycles, the utmost important step for manufacturers is to take into consideration of innovative 6R methodology [5, 6]. Opportunity for improvement in the aspects of 6R consideration is discussed to help assess practical limitations within operational processes. Table I summarises the sustainability in manufacturing with respect to

opportunities to minimise waste and improve efficiency and effectiveness within the operational processes through 6R incorporation perspectives. Sustainability in manufacturing should take an entire product lifecycle perspective to analyse [6, 7]. However, one stage may need to compromise the trade-offs in another [2, 8, 9] within the holistic analysis. This trade-offs consideration is really important to achieve what is called sustainability management within the triple bottom-line, that is, to meet the balance of economic, environmental and social dimensions [1, 10, 11].

TABLE I
6R METHODOLOGY IN WASTE MINIMISATION

Opportunity for improvement	***Rectified by***	***Practical limitation***
*1R:**Reduce** potential*	• *Incorporate strategy for facilitation of disassembly and components* • *Use less complex materials during operational processes* • *Use of less components*	• *Significant initial cost involved for a design with disassembly feature and have less components with same functionality* • *Continuous improvement programme needed to execute and monitor improvement progress*
*2R: **Reuse** potential*	• *Extend product life* • *Utilise reuse option after use and post-use stages* • *Develop secondary markets*	• *Increase complexity* • *Increase risk of failure* • *Product warranty*
*3R: **Recycle** potential*	• *Reduce number of components* • *Utilise recyclable material* • *Discuss opportunity to increase number of recyclable components with customers*	• *Some recycled material may have significant environmental impact* • *Quality issue during processing* • *Need to get customer's support to increase recycled material usage*
*4R: **Reclaim/ recover** potential*	• *Incorporate recovered components as the alternative in new system* • *Extend product /component life*	• *Increase risk of failure with extended product life* • *Need to compromise quality issue*
*5R:**Remanufacture** potential*	• *Use of simple process for remanufacturing* • *Extend product / component life* • *Conserve product identity*	• *Increase operational cost* • *Increase risk of failure during extended product life*
*6R: **Redesign** potential*	• *Extend product / component life* • *Require significant time and effort for this investment* • *Apply other 5R into design options*	• *Increase risk of failure* • *Increase complexity* • *Not totally a new product with extended product life components*

B. Business cost on 6R methodology incorporation

Previous research [12-14] indicates that there is significant deficit on the interconnection between manufacturers' responsibility and environmental conscious manufacturing. In certain cases, the cost associated with the environmental conscious manufacturing is transferable to customers via increase in selling price of the product [13, 15]. However, this market strategy may not be a primary push to manufacturers. It depends largely on three significant trends such as market dominance, branding and product differentiation [13]. To a certain extent, only those monopolistic manufacturers can hold substantial price inelasticity as their business advantage for a short period [13]. 6R methodology incorporation may incur additional costs that are associated with operational activities for a short term or an internal period of learning-by-doing [16]. Over a period of learning-by-doing, most manufacturers incrementally acquire some advanced technology techniques to improve their operational activities, for instance, improvement in recycling or remanufacturing within operational processes [6, 13]. This scenario can directly bring cost benefits to all manufacturers. Table II illustrates some potential costs associated with manufacturing processes in response to sustainable development that incorporates 6R methodology. By optimising supply chain management processes, these potential costs within global supply chain networks can be minimised significantly thus gaining profitability for the organisation.

TABLE II
BUSINESS COST FOR SUSTAINABILITY IN MANUFACTURING

Potential Costs	***Description***
Transaction costs	*Customer and negotiation agreement, information sharing and system upgrades*
Collection costs	*Testing, sorting, refurbishing and disposition involving labour, transportation, equipments, planning schedule and storage*
Remanufacture costs	*Require more complicated operational process to conserve returned product's identity*
Recycle processing costs	*Required to further processing and activities*
Redesign for environment costs	*Significant effort required by considering all options for 5R within design constraints*
Miscellaneous costs	*Waste management strategy, environmental restriction from government regulatory system*

Although the interconnection between manufacturer's responsibility and environmental conscious manufacturing is relatively new and less focused in current literature [14, 17, 18], economic principles provide justification for the implementation of an appropriate strategy within the organisations and thus influence one of the triple bottom-line dimension of sustainability development [8]. Trade-off consideration may take into account significant economic principles as a major guideline towards any implementation [2, 9]. Sometimes, it is evident that environmental regulatory systems such as prohibition of material usage may affect the overall managerial decision of the organisation. However, the potential costs listed in Table II provide some initial guidelines for manufacturers to undertake cost benefit analysis on the product disposition decision within operational

processes. Also, the authors believe that this analysis gives manufacturing industry a basic understanding for the categorisation of the business costs involved in considering 6R methodology incorporation. Adding environmental aspects at earlier stages of the design process, process and system levels is a favourable approach [6]. In general, it is strongly recommended not to add the environmental aspects of the product at the later stages of the product lifecycle.

II. Supply Chain Integration

A. *Waste minimisation within supply chain management*

Due to limited evidence of the interconnection between supply chain management processes and 6R methodology incorporation, this research intends to provide a guideline proposal for manufacturers to construct an analysis on waste minimisation within supply chain management processes. This proposal consists of inputs or sustainability drivers, process interface and waste rectification for sustainability in manufacturing and provides generic relationships among these issues. Fig. 1 illustrates a new business model of sustainable supply chain practices that are associated with 6R methodology incorporation at four phases of product lifecycle stages. These phases are: (i) Pre-manufacturing, (ii) manufacturing, (iii) use and (iv) post-use. For maximum benefits, sustainability in manufacturing needs to be achieved from pre-manufacturing to post-use stages of the product lifecycles and an opportunity for improvement between these stages needs to be created for controlling and monitoring performance across supply chains.

The four layers that have different representations on sustainability in manufacturing are explained as follows: the first layer (outer layer) depicts five sustainability drivers to promote the implementation of sustainable supply chain practices. Wide community awareness and government legislation and regulatory systems become a major pivot of sustainable movement. In addition, the organisational characteristics may impact on the progress of sustainability development due to the complexity of decision synchronisation among collaborating members. Often, overall performance for measuring the achievement of sustainable level needs to be associated with economic (i.e. available resources, profitability, etc.) and social (safety, customer acceptance, etc.) mechanisms to meet the triple bottom line. The second layer depicts the product lifecycle and an opportunity for improvement between use and post-use stages may impact overall performance level of sustainability in manufacturing. The third layer depicts the eight supply chain management processes (proposed by GSCF Team [19, 20]) that need to be integrated towards current market trends and sustainability in manufacturing. These processes include demand management, order fulfilment, manufacturing flow management, product and commercialisation, supplier relationship management, customer service management, customer relationship management and returns management. The fourth layer introduces additional 6R incorporation within supply chain management processes as currently there is lack of research focus on improving supply chain management process through 6R methodology. By fully integrating this 6R methodology incorporation, the final outcome of sustainability in manufacturing with sustainable supply chain practices (depicted as inner circle in Fig 1) can be achieved by global supply chain networks.

Top management commitment and leadership on sustainable development will help boost the internal sustainability drivers for all employees. Even though, significant investment effort is required to support organisational learning curve and those investment costs are initially very high, as a result of these investments, a long term opportunity will be an increase in overall productivity and improved design capability.

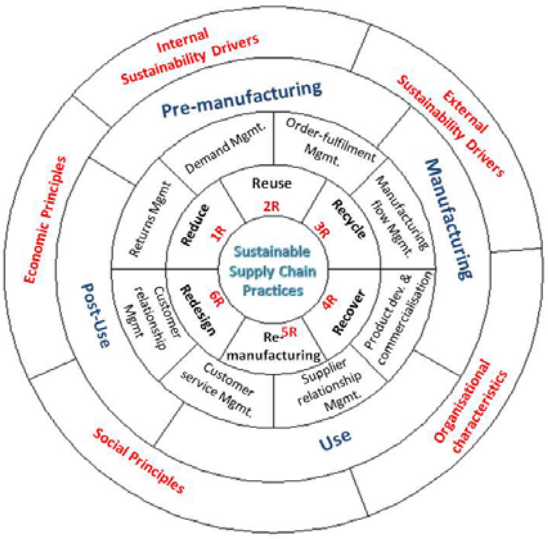

Fig. 1. A new business model for supply chain management processes and 6R methodology incorporation

B. *6R Criteria for returns management process*

In many circumstances, the product returns policy and operational strategy have been neglected by numerous industry practitioners due to lack of measureable criteria to justify product recovery in returns management process. If an organisation is able to manage returns management efficiently, the benefits will include identifying critical productivity improvement, promoting continuous breakthrough improvement projects and reducing communication conflicts [4, 21]. 6R incorporation within returns management is summarised in Table III.

Conventional supply chain processes of returns management handles five key elements. There are: (i) consumer returns, (ii) marketing returns, (iii) asset returns, (iv) product recalls and (v) product recalls and (vi) environmental returns. Each of these key returns elements is analysed against 6R incorporation as proposed in Table III. Section III presents a discussion of the importance of product recovery in returns management for competitive sustainable advantage within current literature and recommends a research direction.

TABLE III
PERFORMANCE INDICATORS FOR WASTE MINIMISATION BY 6R

6R incorporation	*Description*
1R: Reduce material usage and pollution risk	*Use of less material in designing product and process levels and less material waste during operations by considering product returns quality*
2R: Increase recyclable material	*Always discuss opportunity for increasing use of recyclable materials in designing products and processes. These design may not affect the functional capability by the utilisation of returned product*
3R: Target for secondary market for reuse product	*If the newest product to be designed, it may incur high cost associated with this kind of design and seek any secondary market opportunity for product having reused component. (e.g. to consider reuse in developing countries)*
4R: Recover or reclaim component for further processing	*Always seek for any opportunity to recover components for further processing*
5R: Remanufacture for returns products to be usable product	*Always consider major cost involved for remanufacturing operations after use or post-use stages*
6R: Redesign product with incorporating sustainability for product lifecycle	*In considering 5R criteria as a foundation for redesign product to extend product lifecycle during use and post-use stages*

III. SUMMARY OF CRITICALITY IN RETURN MANAGEMENT

Sustainability in manufacturing focuses on minimising environmental impacts and maximising economic returns. Many researchers are having difficulties to assess the trade-off considerations among environmental and economic dimensions, as these trade-offs play a significant role in making the decisions for implementing sustainable development [8, 9, 22]. Furthermore, given the unexpected quality and quantity of the returned products, conventional returns management processes may face some problems such as inability to integrate returned products to maximise the post-use performance and handling the product disposal processes. Numerous manufacturers are striving to integrate this returns management into their current system to increase the potential for post-use returned products. A review summary and observation of sustainable returns management in current literature identifying that there is a need to integrate current returns management with the 6R approach into hybrid system for the reduction of waste given below:

(a) Decision synchronisation and configuration to extend product lifecycle:

Decision making is a critical in regards to product returns [21]. A systematic approach must take into consideration the policy planning, product development, communications and logistics and information systems. However, there is still lack of 6R methodology incorporation to handle use and post-use stages in order to extend product lifecycle due to unexpected product returns' quality and quantity.

(b) Isolated and inappropriate operations management on product returns system:

By considering a return-handling system, manufacturers can generate cost savings through treating returned goods as goods for sales, designing efficient routes for returned products and proving independent and separated management system for return handling [23, 24]. Returned product has potential in secondary markets. However, the return handling system linkage relationship between 6R incorporation and current returns management is isolated. For an optimised return handling system with fast and efficient return management, detailed examination is required due to uncertainty in returned product quality and quantity. There is also need to improve production planning tasks by designing both manufacturing and 6R approach into one hybrid system to meet customer demand and thus achieve profitability via these operations.

(c) Limitation of measureable criteria on assessing product returns operation and management:

Past research studies have discussed some types of product returns within supply chain networks such as consumer returns, marketing returns, asset returns, product recalls and environmental returns [4, 25]. However, a guideline of returns avoidance, gate keeping and disposition method for handling product recovery may not able to resolve the product disposal to landfills. 6R incorporation within returns management is to further extend the product lifecycles after use and post-use stages. The conventional returns management process does not guarantee a reduction of the product disposal to landfill; this is due to the limitation of measureable criteria to assess the performance of product recovery.

IV. CONCLUSION

This paper has highlighted some essential problems within current conventional product recovery operations and recommended that there is a need to be integrated 6R approach into one hybrid system to meet market trends and thus gain profitability from post-use of the returned product.

In addition, the authors also found out that numerous manufacturers have been neglected product recovery operations due to the limitation of measureable criteria that is not established to provide essential guideline for practicing sustainable returns management process. Therefore, future research recommends that performance measurement metrics for product recovery operations need to be established meaning that it is to be integrated with 6R approach into one hybrid system to achieve sustainability in manufacturing.

REFERENCES

[1] S. S. Kuik, S. V. Nagalingam, and Y. Amer, "Challenges in implementing sustainable supply chain within a collaborative manufacturing network," in *8th International Conference on Supply Chain Management and Information Systems* Hong Kong, 2010.

[2] S. Byggeth and E. Hochschorner, "Handling trade-offs in Ecodesign tools for sustainable product development and procurement," *Journal of Cleaner Production*, vol. 14, pp. 1420-1430, 2006.
[3] J. D. Blackburn, V. D. R. G. Jr, G. C. Souza, and L. N. V. Wassenhove, "Reverse supply chains for commercial returns," *California Management Review*, vol. 42, pp. 6-22, 2004.
[4] S. D. Rogers, M. L. Douglas, L. C. Keely, and J. G.-D. Sebastian, "The returns management process," *International Journal of Logistics Management, The*, vol. 13, pp. 1-18, 2002.
[5] I. H. Jaafar, *et al.*, "Product design for sustainability: A new assessment methodology and case studies," in *Environmentally conscious mechanical design*, ed New Jersey: John Wiley & Sons, 2007, pp. 25-65.
[6] A. D. Jayal, F. Badurdeen, O. W. D. Jr, and I. S. Jawahir, "Sustainable manufacturing: Modeling and optimisation challenges at the product, process and systems levels," *CIRP Journal of Manufacturing Science and Technology*, vol. 2, pp. 144-152, 2010.
[7] F. Badurdeen, D. Lyengar, T. J. Goldsby, H. Metta, and S. Gupta, "Extending total life-cycle thinking to sustainable supply chain design," *International Journal of Product Lifecycle Management*, vol. 4, pp. 49-67, 2009.
[8] M. A. Toman, "Economics and sustainability: Balacing trade-offs and imperatives," *Land Economics*, vol. 70, pp. 339-413, 1994.
[9] R. J. Welford, "Editorial: Corporate environmental management, technology and sustainable development: postmodern perspectives and the need for a critical research agenda," *Business Strategy and the Environment*, vol. 7, pp. 1-12, 1998.
[10] R. Nidumolu, C. K. Prahalad, and M. R. Rangaswami, "Why sustainability is now the key driver of innovation " *Harvard Business Review*, vol. 87, pp. 56-64, 2009.
[11] A. Sharma, L. Gopalkrishnan R, A. Mehrota, and R. Krishnan, "Sustainability and business-to-business marketing: A framework and implications," *Industrial Marketing Management*, vol. 39, pp. 330-341, 2010.
[12] L. Argument, F. Lettice, and T. Bhamra, "Environmentally conscious design: matching industry requirements with academic research," *Design Studies*, vol. 19, pp. 63-80, 1998.
[13] A. Gottberg, J. Morris, S. Pollard, C. Mark-Herbert, and M. Cook, "Producer responsibility, waste minimisation and the WEEE Directive: Case studies in eco-design from the European lighting sector," *Science of The Total Environment*, vol. 359, pp. 38-56, 2006.
[14] S. M. Gupta and A. J. D. F. Lambert, *Environment conscious manufacturing*. Boca Raton: CRC Press, 2008.
[15] T. Cooper, "WEEE, WEEE, WEEE, WEEE, all the way home? An evaluation of proposed electrical and electronic waste legislation," *European Environment*, vol. 10, pp. 121-130, 2000.
[16] E. Kutsoati and J. Zábojník, "The effects of learning-by-doing on product innovation by a durable good monopolist," *International Journal of Industrial Organization*, vol. 23, pp. 83-108, 2005.
[17] A. Gungor and S. M. Gupta, "Issues in environmentally conscious manufacturing and product recovery: a survey," *Computers & Industrial Engineering*, vol. 36, pp. 811-853, 1999.
[18] M. A. Ilgin and S. M. Gupta, "Environmentally conscious manufacturing and product recovery (ECMPRO): A review of the state of the art," *Journal of Environmental Management*, vol. 91, pp. 563-591, 2010.
[19] D. M. Lambert, "The eight essential supply chain management processes," *Supply Chain Management Review*, vol. 8, pp. 18-26, 2004.
[20] D. M. Lambert, *Supply chain management: processes, partnerships, performance*, Third ed. Sarasota, Florida: Supply Chain Management Institute, 2008.
[21] N. C. Smith, R. J. Thomas, and J. A. Quelch, "A strategic approach to managing product recalls," *Harvard Business Review*, vol. 74, pp. 102-112, 1997.
[22] P. R. Kleindorfer, K. Singhal, and L. N. Van Wassenhove, "Sustainable Operations Management," *Production and Operations Management*, vol. 14, pp. 482-492, 2005.
[23] V. Jayaraman, V. D. R. G. Jr, and R. Srivastava, "A Closed-Loop Logistics Model for Remanufacturing," *The Journal of the Operational Research Society*, vol. 50, pp. 497-508, 1999.
[24] J. Stock, T. Speh, and H. Shear, "Many happy (product) returns," *Harvard Business Review*, vol. 80/7, pp. 16-17, 2002.
[25] C. R. Carter and D. S. Rogers, "A framework of sustainable supply chain management: moving towards new theory," *International Journal of Physical Distribution and Logistics Management*, vol. 38, pp. 360-387, 2008.

2011 International Conference on Mechanical, Industrial, and Manufacturing Engineering
Lecture Notes in Information Technology Vols. 1-2

A Framework of Product Recovery to Improve Sustainability in Manufacturing

Swee S. Kuik, Sev V. Nagalingam and Yousef Amer

School of Advanced Manufacturing & Mechanical Engineering
University of South Australia
Mawson Lakes, Adelaide, Australia

{Swee.Kuik, Sev.Nagalingam and Yousef Amer}@unisa.edu.au

***Abstract* – Product recovery operation is widely recognised and practiced as an ecological alternative for end-of-life products processing that promotes the utilisation of returned products, components and materials. 6R *(reduce, reuse, recycle, recover, remanufacture, redesign)* incorporation is a proactive practice that primarily focuses on the improvement of product, process and system levels along supply chains and makes the returned product economically and environmentally viable. However, conventional product returns policy and strategy that has its limitation on measureable criteria for product recovery operations. In this paper, a framework of supply chain process of returns management is proposed to describe the dynamics of product recovery operations within multiple product lifecycle stages from pre-manufacturing, manufacturing, use and post-use. Future research should concentrate on sustainable manufacturing activities to improve sustainability of supply chain networks.**

Index Terms – 6R approach, sustainability in manufacturing, product recovery, supply chain

I. INTRODUCTION

In the past decade, globalisation of manufacturing industries and high competitive economy has become predominant. Many global manufacturing investors have their established facilities around the world to meet the high demand of the customers' requirement. This distributed facilities is essential in today's market to have competitive advantage among the supply chain networks [1, 2]. Further, recent issues such as climate change, resource scarcity, security and new government regulations bring significant challenges to industry [3-5]. There are various drivers that are requesting the attention towards sustainability in manufacturing. However, the implementation of sustainability in manufacturing may not be simple to exercise and incorporate within organisation's inter- or intra-organisational activities that are related to the supply chain management processes. In fact, the returns management including customer returns, marketing returns, asset returns, product recalls and environmental returns has been highlighted as one of the major issues of supply chain due to the uncertainty of the product returns in terms of its quality and quantity.

The intend of this paper is to propose a framework of product recovery to attain the goal of sustainability in manufacturing by minimising environmental impact on returns management process within multiple lifecycle stages of the product. More specifically, the final outcome of the research may assist manufacturing industry to (i) shorten time to market (from product returns to re-market launch), (ii) develop product returns by optimising the key factors, e.g. quality, time to market, and cost (iv) improve product returns quality and minimise waste (changes, errors and reworks) and (v) responsive to the customer's demands and global market changes.

Firstly, open loop and closed loop supply chains are discussed and it is asserted that sustainability in supply chain is a globalised trend. Secondly, the effectiveness of product recovery operation is discussed based on a set of quantifiable parameter-metrics typically falling into the following four broad categories: - quality, time, financial and waste. Thirdly, a framework of product recovery is proposed based on Design for Six Sigma (DFSS) methodology according to the Identify, Design, Optimise and Validate (IDOV) phases. However, this paper only discusses the "identify (I)" phase through the application of first level of quality function deployment (QFD) with 6R consideration *(reduce, reuse, recycle, recover/reclaim, remanufacturing, redesign)* to the key supply chain process of returns management by providing key performance indicators. This analysis presents an understanding of how to improve performance monitoring of the supply chain. Finally, a conclusion is made and future research is suggested.

A. Supply chain management

Conventional supply chain practices focus on material flows from a supplier to end user or customer. This supply chain is considered as an open loop or forward supply chain management [1, 6]. However, green supply chain management which has an emphasis on reverse or closed loop supply chain management is currently an active topic among researchers [7-9]. A closed loop supply chain consists of returns management process meaning the integration of the forward supply chain activities as well as the supplementary activities which are associated with the reverse supply chain [10-13]. To a certain extent, those activities of the closed loop supply chain differ significantly from the activities of the forward supply chain. Table I provides a comparison between an open loop supply chain and a closed loop supply chain by areas of responsibility. Due to current pressures on environmental conscious manufacturing public awareness on environmental impacts, the lifecycle of a product should go beyond the

current idea of green supply chain management to explore the new paradigm of managing a sustainable supply chain.

TABLE I
COMPARISON ON RESPONSIBILITY

Factor	*Open loop*	*Closed loop*
1: Product innovation	*Product acquisition*	*Product recovery and waste management*
2: Operational process	*Testing, sorting, refurbishing, and disposition*	*Incorporating 5R methodology (reduce, reuse, recycle, remanufacture and recover)*
3: Information and technology	*Partially automated and manual information systems*	*Fully automated information record system to retrieve any product*
4: Order cycle time	*Short and medium*	*Long and medium*
5: Product value appreciation	*Moderate and low*	*High*
6: Improved redesign potential	*One way approach*	*Two way approach*
7: Finance and cost	*More hidden excluding product recovery and returns costs*	*More visible including product recovery and returns cost*
8: Logistic channel	*Less complicated and single or multi-echelon*	*More complicated or diverse or multi echelon*
9: Marketing	*Simple and visible market*	*Need to create markets for direct use, recover, remanufacture, recycle and disposal*

However, many organisations need to take an initiative to fine-tune their supply chains in order to implement sustainable supply chains. Nevertheless, sustainable supply chain practices are not easy to achieve within organisations due to the complication of multiple lifecycles of the products involved. There are some distinctions between sustainable supply chains and green supply chains [14]. These distinctions are still not well interpreted in many contexts and the scenario is complicated when involving many types of product returns and recovery. More specifically, in the green approach emphasis is only on the environmentally friendly product lifecycle within its use whereas a sustainable supply chain approach examines multiple product lifecycle within its use and post-use stages to balance environmental, economic, and social dimensions. Table II shows the relationship between green and sustainable approaches within supply chain practices in details.

TABLE II
COMPARISON OF SUPPLY CHAIN PRACTICES

Green practice	*Sustainable practice*
Simple and straightforward lifecycle approach	*Comprehensive and multi-lifecycle approach*
An environmental friendly designed product in its "use" stage only	*An environmental friendly designed product from "use" to "post-use" stages*
Emphasise on 3R methodology and some cases on 5R methodology except redesign	*Emphasise on 6R methodology incorporation*
Environmental concern only	*Environmental, social, and economic concerns*
Without interaction equity between economic and environmental dimensions	*With interaction equity among economic, environmental and social dimensions*
One way approach	*A closed loop approach*
More hidden excluding product recovery and returns costs	*More visible including product recovery and returns costs*

B. Product recovery for returns management

In view of the importance of operational product recovery, there are a few reasons that affect the progress assessment of sustainability in manufacturing. Firstly, the organisational structure is slightly different compared to the traditional structure of an enterprise where utilisation of shared resources and competency are not considered. Sharing information and allocating shared resources in achieving sustainability in manufacturing among collaborating members for their activities in reaching an optimal decision is very complicated especially dealing with the returns management process. As currently there is no system wide approach to assess the unexpected product returns in terms of their quality and quantity. This requires significant efforts to compromise on collaborating members' limitations in order to smoothen returns management systems. Secondly, although collaborating members from geographically dispersed locations can share their core competencies, resources, systems and knowledge via a collaborative manufacturing approach for satisfying mass customisation demands and achieving profits, a successful sustainable manufacturing strategy is not merely based on this configuration. More importantly, this strategy is to be aligned to promote sustainable manufacturing and processes such as synchronisation in material movement, reduction of process cycle time, use of recyclable products, reuse of components, remanufacturing etc. However, to date most research focuses on organisational issues and decision synchronisation on production-distribution planning but not on environmental conscious manufacturing, recycling, reusing, remanufacturing or product recovery.

II. A FRAMEWORK FOR PRODUCT RECOVERY

A. Process-based product recovery

The examination of a returned product potential and the review of returned product design focusing on improving the returns management system can have variety of characteristics at different levels of product representation. However, today supply chain design in many industries exhibit deficiencies including modest level of quality, ignorance of customer needs, and too much performance metrics used that created complexity [15]. Such limitations generate a large amount of non-valued added activities within supply chain management. In order to achieve sustainability in supply chain, a system design methodology must be in place to assist manufacturers. To a certain extent, several sources of variation in the service processes need to be addressed while conceptualising a solution in managing supply chain [15]. The implementation of Six Sigma has delivered quality products to customer satisfaction and thus may increase the potential of delivering the same outcome for supply chain design [15, 16]. In the following sections, pertinent characteristics in terms of quality, time, financial and waster are discussed. This is followed by analysis of the first phase (Identify) of DFSS and

identification of performance indicators for product recovery through 6R consideration as illustrated in Fig. 1.

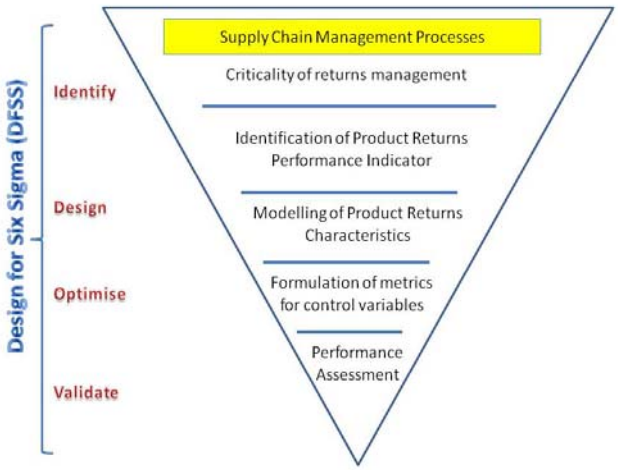

Fig. 1. A new framework for the product recovery to achieve sustainability in manufacturing

B. Performance measure criteria

The development of performance criteria for utilisation of product returns is important for assessing sustainability in manufacturing. This product recovery framework aiming for waste minimisation based on DFSS is represented by its pertinent characteristics of (i) quality, (i) time, (iii) financial and (iv) waste in order to achieve sustainability in manufacturing. Table III illustrates the performance measure for the identification of control variables for returns management process.

TABLE III
PERFORMANCE MEASURE OF THE CONTROL VARIABLES IN PRODUCT RETURNS

Performance measure	***Description***
Quality	*Unexpected quality of product returns may impact the other manufacturing processes. In addition, the extended life of product returns may have significant quality issue. Customer expectation and requirement are considered important to extend product return lifecycle*
Time	*There are many ways to define time to develop product return. Worldwide manufacturers are constantly striving to improve their performance and thus reduce product returns cycle time.*
Financial	*Product returns costs are generally categorised into product returns development costs and product returns manufacturing costs. Sometimes, the return on investment (ROI) on traditional terms hinder the implementation of product recovery operations*
Waste	*Product returns may generate unexpected outcome such as inappropriate planning, poor implementation and poor remanufacturing/recycling/recover/reuse processes may increase product disposal to landfills*

III. ANALYSIS OF IDENTIFICATION OF PERFORMANCE INDICATORS FOR PRODUCT RECOVERY

Quality function deployment (QFD) is a matrix based configuration that consider customer "what" as an input and translate them into design specifications "How" [17, 18]. This prioritised way is generated a list of "what" is strongly correlated with the proposed listed of "How". Within this relationship analysis, the scale indicator for strong relationship is *"9"* while the weak relationship is *"3"*. However, if there is no significant relationship, it is categorised into *"0"*. The outcome of first level QFD is to prioritise the list of critical requirements. In the first level of QFD matrix, scale indicator, R_{ij} represents the intensity of relationship factors of "what" with the possible "how" to handle with. The cumulative weight, CW_j is estimated based on the relationship function in Eq. (1) [17].

$$CW_j = \sum_{i=1}^{n} W_i R_{ij} \quad (1)$$

where j = 1,2...m

W_i = the importance assigned to each "what" on the scale of 5-1

HOWs / Outputs / WHATs / Inputs	Kano Classification	Importance (1-5)	Reduce materials usage and pollution risk	Increase recycleable material upon customer agreement	Target secondary market to reuse product	Recover components for further processing	Remanufacture for return products to be usable product	Redesign product with incorporting sustainability for proudct lifecycle			
Direction of Improvement											
Consumer returns		1	3	3	9	3	9	9			
Marketing returns		2	3	3	9	3	9	9			
Asset returns		3	3	3	9	3	3	9			
Product recalls		4	3	9	3	3	9	9			
Environmental returns		5	3	0	3	3	3	9			
Importance of the HOWs			45	54	81	45	87	135	0	0	0
% Weight			10	12	18	10	19	30			
Importance in next level			2	2	3	2	3	5			

Fig. 2. First level QFD analysis for products returns through 6R consideration

Based on the first level of QFD, the major controlled variables that need to be controlled are (i) secondary markets development to reuse the product after use and post-use stages, (ii) redesigned product by incorporating sustainability within product lifecycles and (iii) remanufacture of usable product with product returns. Table IV provides these variables.

TABLE IV
MAJOR VARIABLES FOR ACHIEVING SUSTAINABILITY IN MANUFACTURING WITHIN RETURNS MANAGEMENT PROCESS

Major variables	***Description***
Secondary market for reuse	*Opportunity for secondary market may bring profitability for the organisation. This is considered as better option to extend product lifecycle of returned products*
Redesign product	*By considering sustainability elements, e.g. reuse materials and recyclable or remanufacturable components for sustainable product. Product redesign enables to reduce the product disposal to landfill. Usual method to simplify by understanding of design for environment and disassembly*
Remanufacture for product returns	*Remanufacturing approach is more complicated process than recycling. Valued-added recovery and high cost involved within this operational process in order to conserve the originality of product identity that becomes marketable product.*

There are several important implications from this 6R incorporation strategy. Firstly, the response of sustainability

drivers is continuously changing over a certain period especially handling environmental legislation and regulatory systems [19]. These sustainability drivers may affect and involve any change in return policy and standard returns guidelines. By pro-active dealing with incremental change, sustainable competitive advantage and consumer protection can be achieved [20, 21]. In addition, these changes may influence overall operational processes including information sharing flow and financial flow along supply chains and thus the scope of such influence for the integration process is considered huge and borderless. Secondly, this system requires a high level of functional integration within business processes of collaborating members and top management commitment and leadership to dissolve any conflict within this returns management process. Finally, in many cases, the integration processes involving the forward and reserve supply chains may have a certain level of complexity [22, 23]. An efficient integration process may reap benefits in terms of product, process and system design to minimise returns quantity and increase reliability of processes bring down the cost involved within use and post-use stages of product lifecycles [24, 25].

IV. Conclusion

This paper has demonstrated how the DFSS methodology can be implemented to supply chain design to identify major control variables for the supply chain process of returns management. A framework of product recovery is proposed to meet this new business paradigm for sustainability in manufacturing that help improves product recovery operation and management. Future research may determine the inter-relationship between performance measures and the major controlled return management variables in order to formulate metrics to control these variables. The methodology described in this paper that may be applied to diverse supply chain management processes to promote a systematic way to achieving sustainability in manufacturing.

References

[1] S. S. Kuik, S. V. Nagalingam, and Y. Amer, "Challenges in implementing sustainable supply chain within a collaborative manufacturing network," in *8th International Conference on Supply Chain Management and Information Systems* Hong Kong, 2010.

[2] S. S. Kuik, S. V. Nagalingam, Y. Amer, and Y. P. Saw, "Implementation of six sigma methodology to improve supply chain network in the context of Malaysian manufacturing industries," in *8th International Conference on Supply Chain Management and Information Systems* Hong Kong, 2010.

[3] H. Walker, L. D. Sisto, and D. McBain, "Drivers and barriers to environmental supply chain management practices: Lessons from the public and private sectors," *Journal of Purchasing and Supply Management*, vol. 14, pp. 69-85, 2008.

[4] Q. Zhu, Y. Geng, and K.-h. Lai, "Circular economy practices among Chinese manufacturers varying in enironmental-oriented supply chain cooperation and the performance implications," *Journal of Environmental Management*, 2010.

[5] Q. Zhu and J. Sarkis, "An inter-sectoral comparison of green supply chain management in China: Drivers and practices," *Journal of Cleaner Production*, vol. 14, pp. 472-486, 2006.

[6] D. M. Lambert, "The eight essential supply chain management processes," *Supply Chain Management Review*, vol. 8, pp. 18-26, 2004.

[7] A. A. Hervani, M. M. Helms, and J. Sarkis, "Performance measurement for green supply chain management," *Benchmarking: An International Journal*, vol. 12, pp. 330-353, 2005.

[8] J. Sarkis, "Manufacturing strategy and environmental consciousness," *Technovation*, vol. 15, pp. 79-97, 1995.

[9] J. Sarkis, Ed., *Greening the supply chain*. Berlin: Springer-Verlag London Limited, 2006, p.^pp. Pages.

[10] J. D. Blackburn, V. D. R. G. Jr, G. C. Souza, and L. N. V. Wassenhove, "Reverse supply chains for commercial returns," *California Management Review*, vol. 42, pp. 6-22, 2004.

[11] V. D. R. Guide, V. Jayaraman, R. Srivastava, and W. C. Benton, "Supply chain management for recoverable manufacturing systems," *Interfaces*, vol. 30, pp. 125-142, 2000.

[12] V. D. R. Guide and L. N. V. Wassenhove, "The reverse supply chain," *Harvard Business Review*, vol. 80, pp. 25-26, 2002.

[13] P. Rao, O. la O' Castillo, J. P. S. Intal, and A. Sajid, "Environmental indicators for small and medium enterprises in the Philippines: An empirical research," *Journal of Cleaner Production*, vol. 14, pp. 505-515, 2006.

[14] S. Byggeth and E. Hochschorner, "Handling trade-offs in Ecodesign tools for sustainable product development and procurement," *Journal of Cleaner Production*, vol. 14, pp. 1420-1430, 2006.

[15] Y. Amer, L. Luong, S.-H. Lee, and M. A. Ashraf, "Optimisating order fulfilment using design for Six Sigma and fuzzy logic," *International Journal of Management Science*, vol. 3, pp. 83-89, 2008.

[16] B. El-Haik and D. M. Roy, *Service design for Six Sigma: A roadmap for excellence*. Hoboken: New Jersey: Willey Interscience Publication, 2005.

[17] Y. Amer, L. Luong, and S.-H. Lee, "Case study: Optimising order fulfillment in a global retail supply chain," *International Journal of Production Economics* 2009.

[18] D. Johnson and R. Srivastava, "Design for sustainability: Product development tools and life cycle economics," in *Proceedings of the 39th Annual Meeting of the Decision Sciences Institue*, Maryland, USA, 2008, pp. 1711-1716.

[19] T. Cooper, "WEEE, WEEE, WEEE, WEEE, all the way home? An evaluation of proposed electrical and electronic waste legislation," *European Environment*, vol. 10, pp. 121-130, 2000.

[20] A. Gottberg, J. Morris, S. Pollard, C. Mark-Herbert, and M. Cook, "Producer responsibility, waste minimisation and the WEEE Directive: Case studies in eco-design from the European lighting sector," *Science of The Total Environment*, vol. 359, pp. 38-56, 2006.

[21] R. W. Kates and T. M. P. a. A. A. Leiserowitz, "What is sustainable development? goals, indicators, values and practice," *Environment: Science and Policy for sustainable development*, vol. 47, pp. 8-21, 2005.

[22] J. Ammenberg and E. Sundin, "Products in environmental management systems: drivers, barriers and experiences," *Journal of Cleaner Production*, vol. 13, pp. 405-415, 2005.

[23] S. Seuring and M. Muller, "From a literature review to a conceptual framework for sustainable supply chain management," *Journal of Cleaner Production*, vol. 16, pp. 1699-1710, 2008.

[24] S. D. Rogers, M. L. Douglas, L. C. Keely, and J. G.-D. Sebastian, "The returns management process," *International Journal of Logistics Management, The*, vol. 13, pp. 1-18, 2002.

[25] N. C. Smith, R. J. Thomas, and J. A. Quelch, "A strategic approach to managing product recalls," *Harvard Business Review*, vol. 74, pp. 102-112, 1997.

2011 International Conference on Mechanical, Industrial, and Manufacturing Engineering
Lecture Notes in Information Technology Vols. 1-2

Reliability Sensitivity Analysis of Structural System with Multiple Failure Modes

Hao Lu and Yimin Zhang
School of Mechanical Engineering and Automation
Northeastern University
Shenyang, 110004, People's Republic of China
hao.lu.neu@gmail.com

***Abstract* - A reliability sensitivity analysis method for structural system with multiple failure modes is proposed. For arbitrarily distributed random variables, the perturbation technique and the Edgeworth expansion are employed to approximate the cumulative distribution function of each failure mode. The reliability of the system is then calculated based on reliability theory. Reliability sensitivity of random variables are derived with the gradient method.**

Index Terms - Multiple failure modes; Reliability; Reliability sensitivity; Arbitrarily distributed random variables.

I. INTRODUCTION

Standard of reliability has become one of important indicators to evaluate the product quality. During the design process of mechanical structures, it is essential to take uncertainties of design variables into account, which may have different influence on the reliability to varying degrees. A quantitative analysis of reliability dependency of the variables, i.e., reliability sensitivity analysis, is thus needed to perform and rank the reliability sensitivity with respect to design variables. In recent decades, a great many of research results on the theories and methods of reliability and reliability sensitivity are put forward [1-3].

Generally, there are many potential failure modes in the structural system. Thus, only take all potential failure modes into account can accurately reflect the situation of the structure. Cornell put forward the bounds theory on the reliability estimation of structural systems, which could be used to get rough estimate results [4]. Feng gave a high accuracy method with two- and three-order joint probabilities based on the narrow reliability bounds [5]. Zhao presented moment methods for reliability analysis applicable to both series structural systems and non-series structural systems [6].

In the present paper, the random perturbation method is adopted firstly to obtain the statistical characteristic of the limit state function $g_i(\boldsymbol{X})$ of each failure mode. In the case that the basic random variables is non-normal, the Edgeworth series is utilized to approximately express the cumulative distribution function of $g_i(\boldsymbol{X})$ with known first few moments of the random variables. Based on the gradient method, the numerical models of reliability sensitivity with respect to the mean and variance of design variables are derived.

II. RELIABILITY ESTIMATION OF STRUCTURAL SYSTEM

A. Reliability Estimation of Failure Modes

The reliability of structural system with multiple failure modes can be expressed as

$$R = P(G > 0) = \int_0^{\infty} f_G(G)dG \tag{1}$$

$$G(\boldsymbol{X}) = \left(g_1(\boldsymbol{X}), g_2(\boldsymbol{X}), \cdots, g_n(\boldsymbol{X})\right)^{\mathrm{T}} \tag{2}$$

where $\boldsymbol{X} = \left[X_1, X_2, \ldots, X_n\right]^{\mathrm{T}}$ denotes the random variable vector with known first few moments and $G(\boldsymbol{X})$ defines the limit state function of multiple failure modes. According to the perturbation method, the mean, variance, the third moment and the forth moment of the limit state function $g_i(\boldsymbol{X})$ of each failure mode can be expressed as

$$\mu_{g_i} = \mathrm{E}\left[g_i(\boldsymbol{X})\right] = \bar{g}_i(\boldsymbol{X}) = g_{i\mathrm{d}}(\boldsymbol{X}) \tag{3}$$

$$\sigma_{g_i}^2 = \mathrm{Var}\left[g_i(\boldsymbol{X})\right] = \left(\frac{\partial g_{i\mathrm{d}}(\boldsymbol{X})}{\partial \boldsymbol{X}^{\mathrm{T}}}\right)^{[2]} \mathrm{Var}(\boldsymbol{X}) \tag{4}$$

$$\theta_{g_i} = \mathrm{C}_3\left[g_i(\boldsymbol{X})\right] = \left(\frac{\partial g_{id}(\boldsymbol{X})}{\partial \boldsymbol{X}^{\mathrm{T}}}\right)^{[3]} C_3(\boldsymbol{X}) \tag{5}$$

$$\eta_{\mathrm{g}_i} = \mathrm{C}_4\left[g_i(\boldsymbol{X})\right] = \left(\frac{\partial g_{id}(\boldsymbol{X})}{\partial \boldsymbol{X}^{\mathrm{T}}}\right)^{[4]} C_4(\boldsymbol{X}) \tag{6}$$

where the subscript *i*d defines the determine part of $g_i(\boldsymbol{X})$, $(\bullet)^{[k]}$ represents the Kronecker product, and$(\bullet)^{[k]}=(\bullet)\otimes(\bullet)\otimes\cdots\otimes(\bullet)$, $\mathrm{Var}(\boldsymbol{X})$ is the variance matrix, $C_3(\mathrm{X})$ and $C_4(\mathrm{X})$ are the third and the fourth central moment matrix. $\sigma_{g_i}^2$, θ_{g_i} and η_{g_i} are the variance, the third and the fourth central moment of the limit state function $g_i(\boldsymbol{X})$ of each failure mode, respectively.

In the case that the random variables are normally distributed, for a given limit state function $z_i=g_i(\boldsymbol{X})$, the reliability index and reliability could be defined as

$$\beta_{SMi} = \frac{\mathrm{E}\left[g_i(\boldsymbol{X})\right]}{\sqrt{\mathrm{Var}\left[g_i(\boldsymbol{X})\right]}} = \frac{\mu_{\mathrm{g}_i}}{\sigma_{\mathrm{g}_i}} \tag{7}$$

$$R_i = \Phi(\beta_{SMi}) \tag{8}$$

where $\Phi(\bullet)$ is the standard normal distribution function.

However, the distribution of random variables are unknown in most cases, the assumption of normal distribution may not exactly reflect the actual conditions. As a matter of fact, the statistical data acquired in engineering practice are generally sufficient to evaluate the first few moments of random variables. In that case, by using the Edgeworth series expansion, the unknown probability cumulative distribution function of each failure mode $g_i(\mathrm{X})$ can be approximated as a

standard normal cumulative distribution function. On the basis of this, the reliability and reliability sensitivity of structural system with arbitrarily distributed variables can be further obtained. According to the Edgeworth series expansion [7], the probability cumulative distribution function of a standardized variable with arbitrary distribution could be approximately expressed as standard normal distribution function as follows

$$F(y)=P_1(y)+P_2(y)+P_3(y) \tag{9}$$

$$P_1(y)=\Phi(y), \tag{10}$$

$$P_2(y)=-\lambda_{1i}H_2(y)\phi(y)/6, \tag{11}$$

$$P_3(y)=-\left(3(\lambda_{2i}-3)H_3(y)+(\lambda_{1i})^2H_5(y)\right)\phi(y)/72 \tag{12}$$

where $y=(z_i-\mu_{gi})/\sigma_{gi}$, $\lambda_{1i}=\theta_{gi}/\sigma_{gi}^3$, $\lambda_{2i}=\eta_{gi}/\sigma_{gi}^4$, $\Phi(\bullet)$ is the cumulative distribution function of a standard normal random variable, $\varphi(\bullet)$ is the standard normal probability density function and $H_j()$ is the Hermite polynomial, the iterative formula of which is expressed as follows,

$$\begin{cases} H_{j+1}(x)=xH_j(x)-jH_{j-1}(x) \\ H_0(x)=1,\ \ H_1(x)=x \end{cases} \tag{13}$$

Thus, the failure probability of each failure mode $P_{\mathrm{FM}i}$ is represented as

$$P_{\mathrm{FM}i}=\Phi(-\beta_{\mathrm{SM}i})-\varphi(-\beta_{\mathrm{SM}i})\left[\frac{1}{6}\lambda_{1i}H_2(-\beta_{\mathrm{SM}i})+\frac{1}{24}(\lambda_{2i}-3)H_3(-\beta_{\mathrm{SM}i})+\frac{1}{72}(\lambda_{1i})^2H_5(-\beta_{\mathrm{SM}i})\right] \tag{14}$$

$$\beta_{\mathrm{FM}i}=-\Phi^{-1}(P_{\mathrm{FM}i}) \tag{15}$$

$$R(\beta_{\mathrm{FM}i})=P(g_i(\boldsymbol{X})\ge 0)=1-P(-\beta_{\mathrm{SM}i}) \tag{16}$$

In case reliability $R(\beta_{\mathrm{SM}i})>1$ appears, a modifier formula is employed

$$R'(\beta_{\mathrm{FM}i})=R(\beta_{\mathrm{SM}i})-\frac{R(\beta_{\mathrm{SM}i})-\Phi(\beta_{\mathrm{SM}i})}{\left\{1+\beta_{\mathrm{SM}i}\left[R(\beta_{\mathrm{SM}i})-\Phi(\beta_{\mathrm{SM}i})\right]\right\}^{\beta_{\mathrm{SM}i}}} \tag{17}$$

B. Reliability Estimation of Structural System

For a structural system, failure modes can be defined by performance functions $g_i(\boldsymbol{X})$. Under the assumption that the failure modes are mutually independent, the performance function of a series system can be expressed as the minimum of the performance functions,

$$G(\boldsymbol{X})=\min\left[g_1,g_2,\ldots,g_n\right] \tag{18}$$

where $g_i=g_i(\boldsymbol{X})$ is the performance function of the ith failure mode.

Depending on the assumption that all failure modes are mutual independence, the reliability of structural system can be represented as follows

$$R_{\mathrm{S}}=\min(1-P_i)=\min R_i \tag{19}$$

where R_i denotes the reliability of the ith failure mode.

III. Reliability Sensitivity Analysis

Reliability sensitivity refers to the partial derivative of the reliability with respect to basic random variables. It ranks the design variables and guides the reliability design. The reliability sensitivity with respect to the mean and variance of random variables is approximately derived as follows:

$$\frac{\mathrm{D}R_{\mathrm{S}}}{\mathrm{D}\bar{\boldsymbol{X}}^{\mathrm{T}}}=\sum_{i=1}^{m}\frac{\partial R_i(\beta_{FMi})}{\partial\beta_{SMi}}\frac{\partial\beta_{SMi}}{\partial\mu_{gi}}\frac{\partial\mu_{gi}}{\partial\bar{\boldsymbol{X}}^{\mathrm{T}}}*\left(\prod_{j=1}^{m}R_j(\beta_{FMj})\Big/R_i(\beta_{FMi})\right) \tag{20}$$

$$\frac{\mathrm{D}R_{\mathrm{S}}}{\mathrm{DVar}(\boldsymbol{X})}=\sum_{i=1}^{m}\left(\frac{\partial R_{ri}(\beta_{FMi})}{\partial\beta_{SMi}}\frac{\partial\beta_{SMi}}{\partial\sigma_{gi}}+\frac{\partial R_{ri}(\beta_{FMi})}{\partial\sigma_{gi}}\right)*\frac{\partial\sigma_{gi}}{\partial\mathrm{Var}(\boldsymbol{X})}\left(\prod_{j=1}^{m}R_{rj}(\beta_{FMj})\Big/R_{ri}(\beta_{FMi})\right) \tag{21}$$

where,

$$\frac{\partial R_{ri}(\beta_{FMi})}{\partial\beta_{SMi}}=\phi(-\beta_{SMi})\left\{1-\beta_{SMi}\left[\frac{1}{6}\lambda_{1i}H_2(-\beta_{SMi})+\frac{1}{24}(\lambda_{2i}-3)H_3(-\beta_{SMi})+\frac{1}{72}(\lambda_{1i})^2H_5(-\beta_{SMi})\right]-\left[\frac{1}{3}\lambda_{1i}H_1(-\beta_{SMi})+\frac{1}{8}(\lambda_{2i}-3)H_2(-\beta_{SMi})+\frac{5}{72}(\lambda_{1i})^2H_4(-\beta_{SMi})\right]\right\} \tag{22}$$

$$\frac{\partial\beta_{SMi}}{\partial\mu_{gi}}=\frac{1}{\sigma_{gi}} \tag{23}$$

$$\frac{\partial\beta_{SMi}}{\partial\sigma_{gi}}=-\frac{\mu_{gi}}{\sigma_{gi}^2} \tag{24}$$

$$\frac{\partial R_i(\beta_{FMi})}{\partial\sigma_{gi}}=\phi(-\beta_{SMi})\left[\frac{1}{2}\lambda_{3i}H_2(-\beta_{SMi})+\frac{1}{6}\lambda_{4i}H_3(-\beta_{SMi})+\frac{1}{12}\lambda_{5i}H_5(-\beta_{SMi})\right] \tag{25}$$

$$\frac{\partial\sigma_{gi}}{\partial\mathrm{Var}(\boldsymbol{X})}=\frac{1}{2\sigma_{gi}}\left[\frac{\partial\bar{g}_i}{\partial\boldsymbol{X}}\otimes\frac{\partial\bar{g}_i}{\partial\boldsymbol{X}}\right] \tag{26}$$

$$\frac{\partial\mu_{\mathrm{g}i}}{\partial\boldsymbol{X}^{\mathrm{T}}}=\left[\frac{\partial g_i(\bar{\boldsymbol{X}})}{\partial X_1}\ \ \frac{\partial g_i(\bar{\boldsymbol{X}})}{\partial X_2}\ \cdots\frac{\partial g_i(\bar{\boldsymbol{X}})}{\partial X_n}\right] \tag{27}$$

$$\lambda_{3i}=\frac{\theta_{gi}}{\sigma_{gi}^4} \tag{28}$$

$$\lambda_{4i}=\frac{\eta_{gi}}{\sigma_{gi}^5} \tag{29}$$

$$\lambda_{5i}=\frac{\theta_{gi}^2}{\sigma_{gi}^7} \tag{30}$$

As reliability $R_i>1$ appears, sensitivity with respect to reliability index $\beta_{\mathrm{FM}i}$ is described as follows,

$$\frac{\partial R_i^{'}}{\partial \beta_{FMi}}=\frac{\partial R_i\left(\beta_{FMi}\right)}{\partial \beta_{SMi}}+\left[\frac{\partial R_i\left(\beta_{FMi}\right)}{\partial \beta_{SMi}}-\phi\left(\beta_{SMi}\right)\right]\frac{\beta_{SMi}\left(\beta_{SMi}-1\right)\left[R_i\left(\beta_{FMi}\right)-\Phi\left(\beta_{SMi}\right)\right]-1}{\left\{1+\left[R_i\left(\beta_{FMi}\right)-\Phi\left(\beta_{SMi}\right)\right]\beta_{SMi}\right\}^{\beta_{SMi}+1}}$$
$$+\frac{\left[R_i\left(\beta_{SMi}\right)-\Phi\left(\beta_{SMi}\right)\right]\left(\left\{1+\left[R_i\left(\beta_{SMi}\right)-\Phi\left(\beta_{SMi}\right)\right]\beta_{SMi}\right\}\ln\left\{1+\left[R_i\left(\beta_{SMi}\right)-\Phi\left(\beta_{SMi}\right)\right]\beta_{SMi}\right\}+\left[R_i\left(\beta_{SMi}\right)-\Phi\left(\beta_{SMi}\right)\right]\beta_{SMi}\right)}{\left\{1+\left[R_i\left(\beta_{SMi}\right)-\Phi\left(\beta_{SMi}\right)\right]\beta_{SMi}\right\}^{\beta_{SMi}+1}} \quad (31)$$

Substituting equations (22-31) into equations (20) and (21), the reliability sensitivity of random variables $\mathrm{D}R_\mathrm{S}/\mathrm{D}\bar{\boldsymbol{X}}^\mathrm{T}$ and $\mathrm{D}R_\mathrm{S}/\mathrm{DVar}(\boldsymbol{X})$ can be obtained.

IV. Numerical Examples

As showed in Fig. 1 is a simple beam-cable structural system. The length of the beam is 2*l*, the length of cables is *L*=3m. The cross section of the beam is a rectangle with width *b* and height *h*. The cross sectional area of the cable are A_i(*i*=1,2). The plastic limit bending moment of the beam is *M*. The yield limit stress of the cable and the beam are σ1 and σ2, respectively. The uniformly distributed load is *q*. The random variables are independent with each other, and their probabilistic properties with known first four moments are listed in Table I.

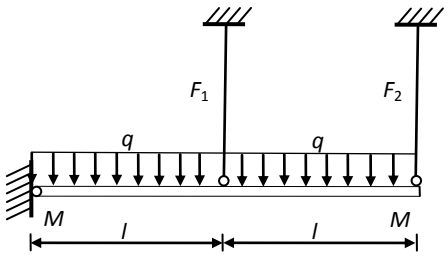

Fig. 1 Beam-cable structural system

TABLE I
Probabilistic Properties of Random Variables

Random variables	mean	standard deviation	The third moment	The fourth moment
b(mm)	152	0.76	1.4223e-1	1.1723
h(mm)	200	1	3.2400e-1	3.5140
A_1(cm^2)	6.45	0.032	1.0617e-5	3.6847e-6
A_2(cm^2)	3.32	0.017	1.5918e-6	2.9349e-7
σ_1(MPa)	300	6	69.984	4.5541e3
σ_2(MPa)	300	6	69.984	4.5541e3
q(kN/m)	37	0.74	0.13129	1.05373

There are four failure modes of the beam-cable structural system, the performance functions of failure modes are listed below:

$$g_1=6M-ql^2/2$$
$$g_2=A_1\sigma_1 l+2A_2\sigma_2 l-2ql^2$$
$$g_3=M+A_2\sigma_2 l-ql^2/2$$
$$g_4=2M+A_1\sigma_1 l-ql^2$$

where $M=Wf_y$, $W=bh^2/6$.

Then the reliability R_i can be calculated according to equation (16).

$$R_1=1.0$$
$$R_2=0.997357$$
$$R_3=1.0$$
$$R_4=1.0$$

On the basis of the above results, the reliability index β_S, the reliability R_S and the relative error of the system are obtained, β_S=2.78907, R_S=0.997357, R_MCS=0.981658, $\varepsilon_R=\left|R_\mathrm{S}-R_\mathrm{MCS}\right|/R_\mathrm{MCS}=1.6\%$. R_MCS is the reliability computed by Monte Carlo simulation with 10^6 samples.

According to equations (20) and (21), the reliability sensitivity with respect to the mean and variance of system variables is derived as follows

$$\frac{\mathrm{D}R_\mathrm{S}}{\mathrm{D}\bar{\boldsymbol{X}}^\mathrm{T}}=\frac{\partial R_4}{\partial \bar{\boldsymbol{X}}^\mathrm{T}}R_3R_2R_1+\frac{\partial R_3}{\partial \bar{\boldsymbol{X}}^\mathrm{T}}R_4R_2R_1+\frac{\partial R_2}{\partial \bar{\boldsymbol{X}}^\mathrm{T}}R_4R_3R_1+\frac{\partial R_1}{\partial \bar{\boldsymbol{X}}^\mathrm{T}}R_4R_3R_2$$

$$\frac{\mathrm{D}R_\mathrm{S}}{\mathrm{DVar}(\boldsymbol{X})}=\frac{\partial R_4}{\partial \mathrm{Var}(\boldsymbol{X})}R_3R_2R_1+\frac{\partial R_3}{\partial \mathrm{Var}(\boldsymbol{X})}R_4R_2R_1+\frac{\partial R_2}{\partial \mathrm{Var}(\boldsymbol{X})}R_4R_3R_1+\frac{\partial R_1}{\partial \mathrm{Var}(\boldsymbol{X})}R_4R_3R_2$$

$$\mathrm{D}R_\mathrm{S}/\mathrm{D}\bar{\boldsymbol{X}}^\mathrm{T}=\begin{bmatrix}\partial R_s/\partial q\\ \partial R_s/\partial \sigma_1\\ \partial R_s/\partial \sigma_2\\ \partial R_s/\partial A_1\\ \partial R_s/\partial A_2\\ \partial R_s/\partial b\\ \partial R_s/\partial h\end{bmatrix}=\begin{bmatrix}\text{-2.63168e-5}\\ \text{1.22000e-53}\\ \text{2.62105e-9}\\ \text{7.89505e2}\\ \text{1.57901e3}\\ \text{2.39881e-44}\\ \text{3.64619e-44}\end{bmatrix}$$

$$\mathrm{D}R_\mathrm{S}/\mathrm{DVar}(\boldsymbol{X})=\begin{bmatrix}\partial R/\partial \mathrm{Var}(q)\\ \partial R/\partial \mathrm{Var}(\sigma_1)\\ \partial R/\partial \mathrm{Var}(\sigma_2)\\ \partial R/\partial \mathrm{Var}(A_1)\\ \partial R/\partial \mathrm{Var}(A_2)\\ \partial R/\partial \mathrm{Var}(b)\\ \partial R/\partial \mathrm{Var}(h)\end{bmatrix}=\begin{bmatrix}\text{-7.47950e-3}\\ \text{-1.48791e-9}\\ \text{-4.42317e-11}\\ \text{-2.68383e12}\\ \text{-6.88748e12}\\ \text{-5.79607e9}\\ \text{-1.33912e10}\end{bmatrix}$$

The example displays that the reliability of the beam-cable structural system increases as the dimension parameter *b*, *h*, A_i and yield stress σ_i, increases, but descends as the load *q* rises. In other words, the results show that the reliability has a high dependency on A_i, moderate dependency on *q*, and slight dependency on *b*, *h* and σ_i.

V. CONCLUSIONS

The numerical method of reliability sensitivity analysis of structural system with multiple failure modes is proposed in this paper. With known statistical properties of random variables, the first four moments of each failure modes are calculated by the perturbation method. Based on the reliability theory and reliability sensitivity technology, the reliability of the structural system is obtained and the reliability sensitivity with respect to design variables are ranked. The approach could be a guild to the reliability estimation and optimal design of structural system.

ACKNOWLEDGMENT

The research reported here is supported by "the Fundamental Research Funds for the Central Universities" (N100603008). We would also like to express our appreciation to Key National Science & Technology Special Project on "High-Grade CNC Machine Tools and Basic Manufacturing Equipments" (2010ZX04014-014), Chinese National Natural Science Foundation (50875039) and Key Projects in the National Science & Technology Pillar Program in the Eleventh Five-year Plan Period (2009BAG12A02-A07-2).

REFERENCES

[1] Y. M. Zhang, "Reliability sensitivity design for mechanical elements with arbitrary distribution parameters," *Chin. J. Mech. Eng.*, vol. 40, no. 8, pp. 100-105, 2004.

[2] Y. T. Tsai, and H. C. Chang, "Reliability-based optimum design for mechanical problems using genetic algorithms," *Proc. Instn Mech. Engrs, Part C: J. Mechanical Engineering Science*, vol, 222, pp: 1791-1799, 2008.

[3] J. Li, J. b. Chen, and W. l. Fan, "The equivalent extreme-value event and evaluation of the structural system reliability," *Struct. Saf.*, vol, 29, no. 2, pp, 112-131, 2007.

[4] C. A. Cornell, "Bounds on the Reliability of Structural Systems," *J. STRUCT. DIV.-ASCE*., vol, 93, no.S1, pp, 171-200, 1967.

[5] Y. S. Feng, "A method for computing structural system reliability with high accuracy," *Comput. Struct*., vol, 33, no. 1, pp, 1-5, 1989.

[6] Y. G. Zhao, and A. H. S. Ang, "System reliability assessment by method of moments," *J. Struct. Eng., ASCE*. Vol, 129, no. 10, pp, 1341-1349, 2003.

[7] H. Cramer, *Mathematical Methods of Statistics*. Princeton University Press, Princeton, NJ, 1964.

2011 International Conference on Mechanical, Industrial, and Manufacturing Engineering
Lecture Notes in Information Technology Vols. 1-2

Fabrication and Characterization of Nanocrystalline Diamond Films Using Hot Filament CVD*

FENG Jie, MEI Jun, LI Jianguo and HU Dongping
Institute of system engineering
China academy of engineering physics
Mianyang 621900, China
fjie168@sina.com

YU Zhiming and FENG Jie
School of Materials Science and Engineering
Center South University
Changsha 4100083,China
zhiming@mail.csu.edu.cn

Abstract: **Nanocrystalline diamond films were deposited on Si substrates using bias-enhanced hot filament chemical vapour deposition (HFCVD) technique. Effect of hot filament structure and substrate bias on morphology and Raman spectroscopy of diamond films were investigated during deposition. Friction characteristics and nano-mechanical performance of diamond films deposited by this system were researched. The results show that the double layer filament structure can enhance the voltage of positive substrate bias and increase the energy of particles and H content in the gas mixture. Thus the double layer hot filament structure can increase the ratio of precursors re-nucleation and restrict the grain coarsening. The grain size was observed to be approximately 3 nm. The high quality nanocrystalline diamond films were deposited on a 75 mm diameter Si substrate, the thickness of film was about 50 micron and roughness was less than 8 nm by Ar/CH4/H2 gas mixture. Furthermore, the friction coefficient of the films was 0.10 at the room temperature in the air. The film has excellence wear and friction properties. The modulus is lager than 850GPa, and hardness large than 86GPa. This film may be implemented into existing Si-based micro-system technologies and may have extensive foreground at MEMS technology field.**

Keywords: Surface characterizations; Nanocrystalline diamond film; Hot filament chemical vapor deposition

I. Introduction

As the microstructure material of micro electron mechanical system (MEMS) the film of CVD diamonds has more unexampled characteristic because the diamond film is an ultra hard material with high mechanical strength, exceptional chemical inertness and outstanding thermal stability. But the normal microcrystalline diamond (MCD) film has large surface roughness, and consistency of thickness can't obtain, polishing of MCD film is difficult. So it could not application in filed of micro-electron and MEMS comprehensive. Nanocrystalline diamond film has not also the characteristic of MCD film but also less roughness and less coefficients of friction (COF) and more wearable[1~4]. The NCD film is more than MCD film for using in the field of MEMS. It could increase the capability and the reliability of MEMS components.

In the present study, using reformative HFCVD system the fabrication methods of deposited NCD films was researched. The technics of deposited NCD films was studyed with the gases mixture, chamber pressure, the structure of filaments and bias of substrate and so on. The films was obtained at the gases mixture of H_2, Ar, CH_4. It have large dimension (dia. is 75mm), large thickness (about 50 micrometer), and roughness less than 8 nm. The modulus is lager than 850GPa, and hardness large than 86GPa. And the friction coefficient of the films was 0.10 at the room temperature in the air. The film has excellence wear and friction properties. This film may be implemented into existing Si-based microsystem technologies and may have extensive foreground at MEMS technology field.

II. Experiments and methods

A. Deposition equipment

The HFCVD equipment of self-designed was used for deposited NCD films. The main amelioration was the hot

* This work was partially supported by the Foundation of China Academy of Engineering Physics (Project No. 2010A0302013).

filaments structure. The hot filaments were double layer instead single layer. The excellence of the hot structure is that the double layer filaments structure can enhance the positive substrate bias and increase the energy of particles and H content in gases mixture. Thus the double layer hot filament structure can increase the ratio of precursors re-nucleation and grain coarsening does not occur. The same time, the bias of substrate is modifiable by different methods in double layer filament structure HFCVD system. The schematic illustration of hot power supply system and substrate bias was shown in Fig.1.

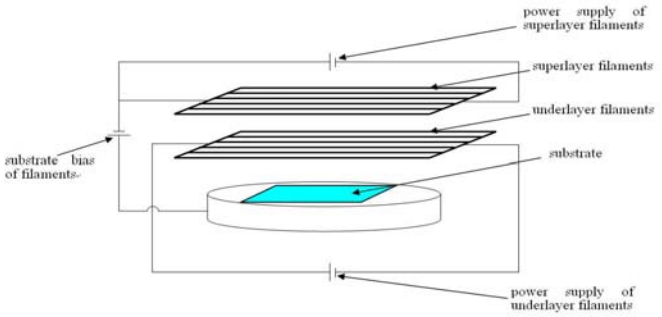

Fig. 1 Schematic illustration of the power supply system

B. Condition of deposition

The gases mixture system of CH_4, Ar, H_2 is universal in the MWCVD system for NCD films. But in HFCVD system the heat decompose of gases is dissimilitude with MWCVD system, the processing parameters of MWCVD is not direction for the HFCVD deposition. In this study the processing parameters were designed consulting the CH_4, H_2 of HFCVD. Mono-crystalline <100> oriented Silicon(Si) wafers of 75 mm diameter, pre-treated in ultrasonic bath with a suspension of 40-μm grain sized diamond powder in ethanol[5], were used for the deposition of nanocrystalline diamond (NCD) by HFCVD technique. The typical deposition parameters of NCD films was shown in tab.1.

C. Characterization

The morphology and quality of the NCD films were determined by scanning electron micro-scopy (SEM) and Raman spectroscopy. Surface roughness measurements are performed on the films surface with an atomic force microscope (AFM). The average roughness of the films surface is measured with a profilometer.

Subsequently, using pin-on-disk tribometer the coefficients of friction (COF) of the films was measured. The nano-mechanical properties were measured with MTS Nano indenter DCM test system.

Tab. 1 Typical deposition parameters of nanocrystalline diamond film

Parameters	Value
Acetone concentration（CH_4/H_2+Ar），%	1~2
Ar concentration, %	0~100
Chamber pressure，KPa	1.5~2.0
Filament structure	Single layer、double layer
Filament temperature，℃	2200±200
Filament to substrate distance，mm	6～8
Substrate temperature，℃	880～950
Deposition time，h	30

III. Results and discussion

A. Effect of Ar concentration for morphology and Raman spectra

Fig.2 shown the Raman spectra of diamond films deposited on different Ar concentration in single layer HFCVD system. From the Raman spectra, when the concentration of Ar was 0%, it was the gases mixture of the MCD films on HFCVD. The spectrum was typical 1332 cm^{-1} peak of diamond band. When the concentration of Ar was 50%, the spectrum was different from the spectrum of the conventional diamond film. As the Ar concentration in the reactant gas was increased, carbon peaks around 1350 cm^{-1} and 1580 cm^{-1} assigned to D and G bands were significantly broadened and there existed an extra broad band near the 1140 cm^{-1} which could evidence the presence of nanocrystalline diamond. Broadening of the diamond band was the result of the nano dimension of the grain size, Raman scattering in the region 1400 cm^{-1}~1600cm^{-1} was attributed to sp^2-bonded carbon existing between the nanocrystalline diamond grains. Noted that the spectra had an extra Raman shift at approximately 1140 cm^{-1} compared with conventional diamond spectrum. Raman scattering was approximately 50 times more sensitive to amophous carbon and graphite phase than to diamond, hence the diamond component dominated in the films. When the Ar concentration is up to 90%, the deposited matter is always graphite.

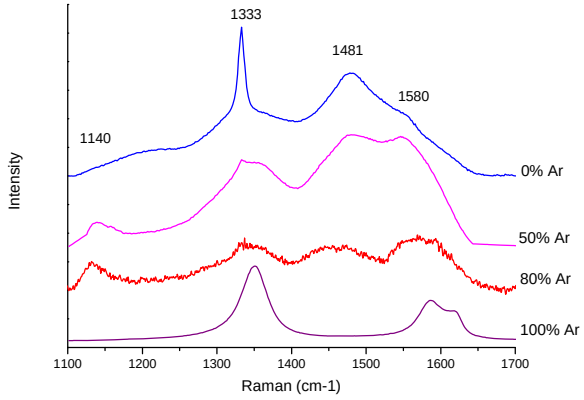

Fig.2 Raman spectra of the diamond films on different Ar concentration by single layer HFCVD

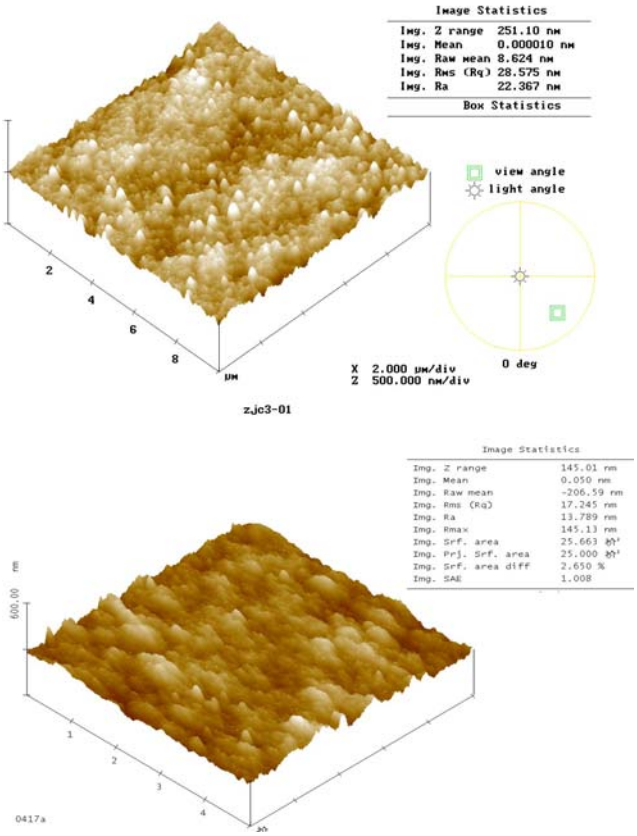

Fig.3 AFM images of NCD films with different Ar concentration by single layer HFCVD，A）50% Ar，B） 80%Ar

The surface AFM images of the diamond films were presented in fig. 3. When the Ar concentration was 0%, and the pressure was 2KPa the diamond grains were very sharp, with increasing concentration of Ar, the diamond grains became small. It could be clearly seen that when the Ar concentration was increased to 80%, the surface of diamond films was smoothest, the grains size was the finest. The Ra surface roughness of 0%Ar in a 5μm × 5μm area was about 150nm. While when the Ar concentration was 50% and 80%, the pressure of gases was 2KPa, the Ra surface roughness was 28nm and 25.5nm, respectively.

B. Effect of hot filament structure for morphology and Raman spectra

Fig.4 shown the measurement of different Ar concentration in chamber pressure of 2KPa, CH_4 concentration was 4% by double layer HFCVD. It was shown that Raman spectrum of 0%Ar, 50%Ar, 80%Ar concentration was accordant in the main. There were typical 1332cm^{-1} peak of diamond band, 1355cm^{-1} and 1580 cm^{-1} assigned to D and G bands, and an extra Raman shift at approximately 1140 cm^{-1} compared with conventional nanocrystalline diamond spectrum. The nanocrystalline diamond films were deposited by 0% Ar, 50%Ar, and 80%Ar concentration, respectively. The grains of diamond films were very small.

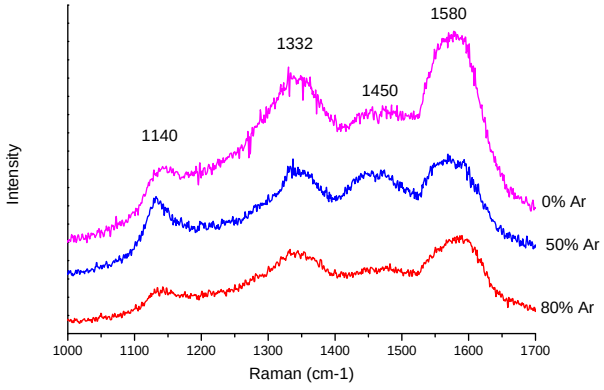

Fig.4 Raman spectra of the diamond films on different Ar concentration by double layer HFCVD

The surface AFM images of diamond films deposited by double layer HFCVD were presented in fig. 4. When the Ar concentration was zero, and chamber pressure was 2KPa the diamond grains were big and very sharp, with increasing concentration of Ar, the diamond grains became ball-like and very fine. It could be clearly seen that when the Ar concentration was increased to 80%, the surface of diamond films was smoothest; the grains size was the finest. The Ra surface roughness in a 5μm × 5 μ m area was approximately 20.4nm of 0%Ar. While when the Ar concentration was 50% and 80%, the Ra surface roughness was 13nm and 9nm,

respectively.

Surface roughness values measured by AFM could only demonstrate morphology state in the area of 5 μ m × 5 μ m, and could not reflect the whole surface area. Therefore, a surface scanning profilometer was employed to measure the surface roughness of diamond films with 10mm scanning length in the work. The Average Surface Roughness (Ra) for the diamond films deposited with Ar concentration of 0%, 50%, 80% and pressure of 2KPa were 45nm, 23nm and 12nm, espectively. The Root Mean Square (RMS) Roughness were 68 vs. 32 and 18nm,respectively. The surface roughness of diamond films was directly related to the Ar concentrations, and pressure of gases.

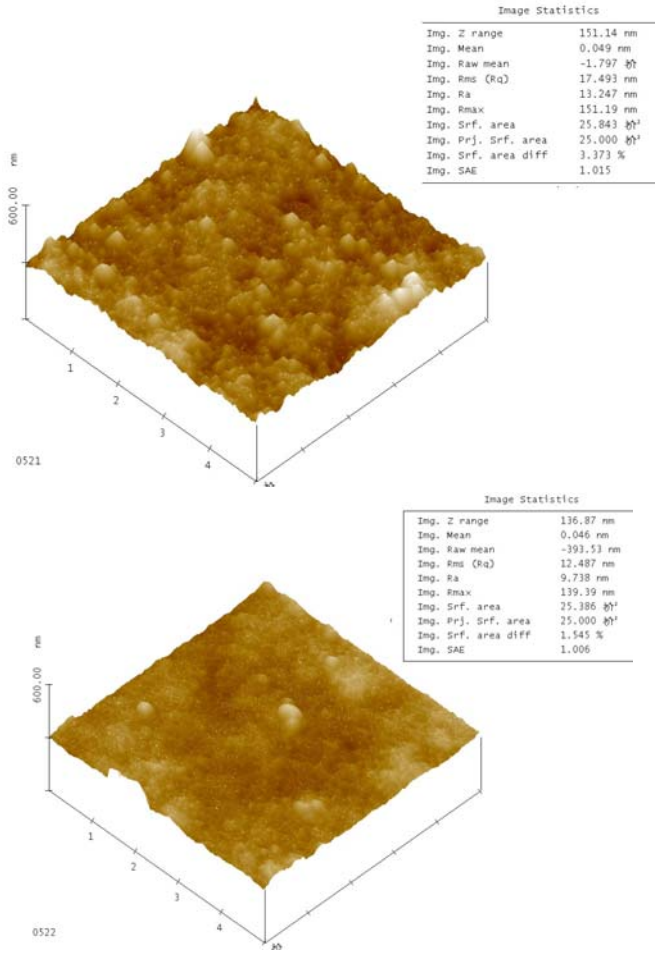

Fig.5 AFM images of NCD films with different Ar concentration by double layer HFCVD, a) 50%Ar, b) 80%Ar

Fig.6 is the cross-sectional SEM of specimens and the thickness with 80%Ar concentration, 2KPa pressure by double layer HFCVD. The surface was very smooth. The thick of film could be up to 50 μ m.

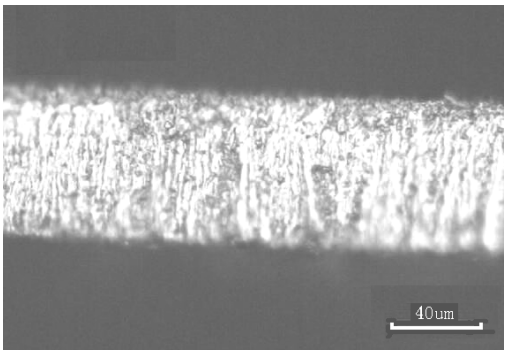

Fig. 6 Cross-sectional SEM of film

C. Effect of gas component for surface friction performance

The friction and wear performance was against of films deposited at 0%Ar and 50% Ar concentration using double layer HFCVD system. The surface roughness of the films was measure with micro-profilometer before test, respectively. The result of Average Surface Roughness is, 0%Ar, Ra0.032μm, 50%Ar, Ra 0.012μm. It was agreement with the result of AFM method. It was proved that nano-crystalline diamond films can be deposited using double layer filaments HFCVD method no matter whether Ar. But the roughness of films was more small if gases mixture existed Ar concentration. The COF-times curves of the films on different Ar concentration was shown in fig.7. The COF and grinding crack depth as shown in Tab.2.

Tab. 2 Friction and wear characteristics of NCD films on different filament structure

Deposited parameters	Filament structure	Grinding crack depth	COF
0%Ar，4%CH4，1.5KPa	Double layer	0.04μm	0.131
50%Ar，4%CH4，1.5KPa	Double layer	0.02μm	0.098

Thus it could be seen that the COF of NCD films was less than 0.15 at the different gases mixture using double layer HFCVD method. The COF of film at 50%Ar concentration was less than at 0%Ar. The reason is that the surface of the films is more slippery. At this test condition the both films have not obvious wear and tear. And the films was intact. The result shown that the films was wearable and less COF all right. It was the material for making turn components of MEMS.

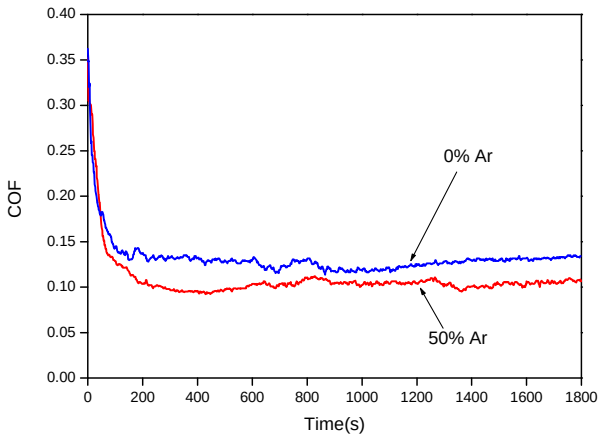

Fig. 7 COF-times curves of NCD films on different Ar concentration

D. Effect of different gases mixture for nano-mechanical performance

Effect of Ar concentration for the nano-mechanical properties at 4% CH_4 and 2KPa pressure using the nano impress instrument test system by double layer HFCVD method. The results of films hardness and modulus show in Tab.3. It is observed that the hardness and modulus reduce with the Ar concen-tration increase. When Ar concentration is up to 90%, the hardness and modulus already drop down to Si basal body. The reason is Ar has the action of refined grain, but at the same time the SP^2 bond and graphite phase are introduced more. The content of the SP^2 bond and graphite phase is determinable the micro-mechanics characteristic. In the main, test result reflect the trend of mechanical properties of films in different mixtrue gases.

Tab. 3 Effect of Ar concentration for modulus and hardness of NCD films

Ar concentration	0%	50%	80%	100%
Modulus [GPa]	1005.0	850.8	654.78	210.8
Hardness [GPa]	100.2	86.4	61.4	24.2

IV. Conclusion

The nano-crystalline diamond films are posited on Si substrates by adjusting the Ar concentration and selecting the reactive pressure in CH_4-H_2-Ar mixture gases using HFCVD equipment.

The double layer filament structure can enhance the voltage of positive substrate bias and increase the energy of particles and H content in the gas mixture. Thus the double layer hot filament structure can increase the ratio of precursors re-nucleation and restrict the grain coarsening. The NCD films whose grain size was observed to be approximately 3 nm and surface roughness was less than 8 nm was deposited by the filament structure. The modulus of the film can be up to par 850GPa, and the hardness can be up to 86 GPa.

Furthermore, the friction coefficient of the films was exceptionally low. The cof can be up to 0.10 at the room temperature in the air. The film has excellence wear and friction properties. It may be implemented into existing Si-based micro-system technologies and may have extensive foreground at MEMS technology field.

References

[1] Gruen Dieter M. Nanocrystalline diamond films[J] . Annu Rev Mater Sci ,1999 ,29 :211 - 259.

[2] T. Wang, H.W. Xin, Z.M. Zhang, Y.B. Dai, H.S. Shen，The fabrication of nanocrystalline diamond films using hot filament CVD[J]，Diamond and Related Materials 13 (2004) 6–13

[3] P.W. May a, J.A. Smith a, Yu. A. Mankelevich，Deposition of NCD films using hot filament CVD andAr/CH4/H2 gas mixtures[J]，Diamond & Related Materials 15 (2006) 345 – 352

[4] Shr-Ming Huang, Franklin, Chau-Nan Hong. Low temperature growths of nanocrystalline diamond filmsby plasma- assisted hot filament chemical vapor deposition[J]，Surface & Coatings Technology, 200 (2006) 3160 – 3165

[5] Feng Jie, Li Jianguo, Mei Jun, Hu Dongping. Development of single-and double-layered hot filament for growth of diamond nano-crystalline film, Chinese journal of vacuum science and technology, 30 (2010), 474-478

2011 International Conference on Mechanical, Industrial, and Manufacturing Engineering
Lecture Notes in Information Technology Vols. 1-2

Study on the Mineral Structure of Mould Powder*

Ying Xu
College of Materials Science and Engineering
Hebei United University
Tangshan,Hebei Province 063009, China
yuyingdd@yahoo.com.cn

Liguang Zhu
College of Metallurgy Science and Engineering
Hebei United University
Tangshan,Hebei Province 063009, China
zhulg@heut.edu.cn

***Abstract* - Mineral analysis of the mould powder is tested by X-diffraction, which is used to study the infullence on mineral properties caused by the chemical composition. The results show that the mineral structure composition of the mould powder is mainly calcium melilite, and a small amount of cuspidite, lithium aluminate, magnesium feldspar, sodalite, etc. Compared with other minerals, calcium melilite has a low heat conduction coefficient, which can reduce the thermal capability of flux and heat flow in continuous casting process, and then the longitudinal cracks are reduced, mould friction is aslo significantly reduced. While the crystallization properties and glass performance of mould powder are not only determined by CaO/SiO_2, but also by NaO/Al_2O_3 and other factors.**

Index Terms - mould powder, mineral structure, continuous casting process.

I. INTRODUCTION

Crystallized character of mould powder has become an important part of its development. Precipitation types and micro-crystal structure, that is the mineral structure of mould powder, will have important impact on the abilities of lubrication and heat transfer. To this end, it is necessary to do a deep research on mineral structure and influence laws of mould powder after solidified, which can be beneficial to optimize metallurgical behavior and performance, also be good to rational design of mould powder.

II. RESEARCH PROGRAMS

A. Research on mineral composition of mould powder

1) Combined with industrial practice, standard orthogonal experimental methods are used to design slag composition. It is shown in Table I .

TABLE I
THE EXPERIMENT SCHEME OF MOULD FLUX FOR STUDY OF T_C

Number	R	CaO	SiO_2	Al_2O_3	MgO	CaF_2	Na_2O	Li_2O	B_2O_3	BaO
1	0.8	34.7	43.3	5.0	2	6	6	1	1	1
2	0.8	29.8	37.2	5.0	4	8	8	2	3	3
3	0.8	24.0	30.0	5.0	6	10	10	4	5	6
4	0.8	19.6	24.4	5.0	8	11	11	5	7	9
5	0.8	15.6	19.4	5.0	10	12	12	6	9	11
6	0.9	28.0	31.0	5.0	10	6	6	2	5	9
7	0.9	26.1	28.9	5.0	2	8	8	4	7	11
8	0.9	26.5	29.5	5.0	4	10	10	5	9	1
9	0.9	27.0	30.0	5.0	6	11	11	6	1	3
10	0.9	25.1	27.9	5.0	8	12	12	1	3	6
11	1.0	29.5	29.5	5.0	8	6	6	4	9	3
12	1.0	28.5	28.5	5.0	10	8	8	5	1	6
13	1.0	27.5	27.5	5.0	2	10	10	6	3	9
14	1.0	26	26	5.0	4	11	11	1	5	11
15	1.0	27.5	27.5	5.0	6	12	12	2	7	1
16	1.1	30.4	27.6	5.0	6	6	6	5	3	11
17	1.1	30.9	28.1	5.0	8	8	8	6	5	1
18	1.1	28.3	25.7	5.0	10	10	10	1	7	3
19	1.1	28.3	25.7	5.0	2	11	11	2	9	6
20	1.1	27.8	25.2	5.0	4	12	12	4	1	9
21	1.2	32.7	27.3	5.0	4	6	6	6	7	6
22	1.2	29.5	24.5	5.0	6	8	8	1	9	9
23	1.2	28.9	24.1	5.0	8	10	10	2	1	11
24	1.2	30	25	5.0	10	11	11	4	3	1
25	1.2	33.3	27.7	5.0	2	12	12	5	5	3

2) To close to actual state, slag samples are pre-melt first, and then crushed, ground into powder of 200 mesh.

3) X-diffraction instrument is used for qualitative analysis of mould powder minerals.

III. TEST RESULTS AND DISCUSSIONS

A. Analysis of crystallization properties and vitrification abilities of mould powder

5 representative samples of X-diffraction are selected, which is shown in Fig.1 to Fig.5. From the figures, we can analyze the results which are shown in Table II.

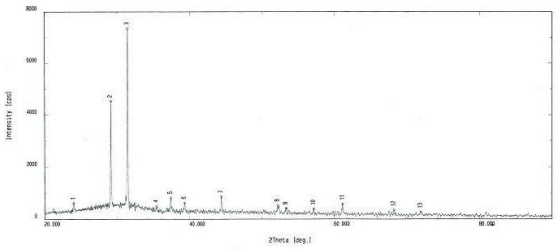

Fig. 1 XRD pattern of No.7 mould powder

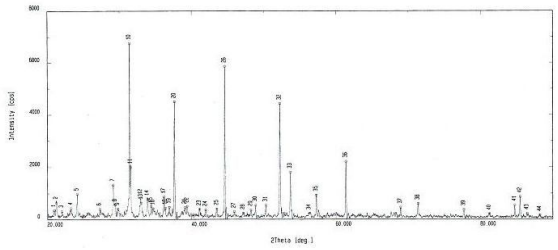

Fig. 2 XRD pattern of No.2 mould powder

* This work is partially supported by National NSF Grant #51074063 and HEBEI NSF Grant # E2010000930 to Liguang Zhu

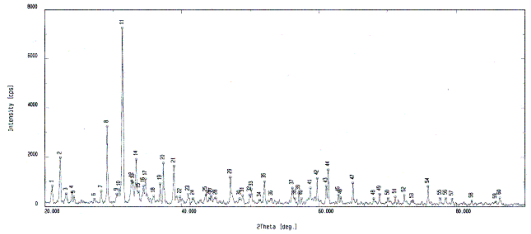

Fig. 3 XRD pattern of No.9 mould powder

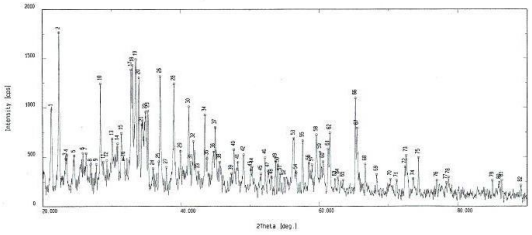

Fig. 4 XRD pattern of No.5 mould powder

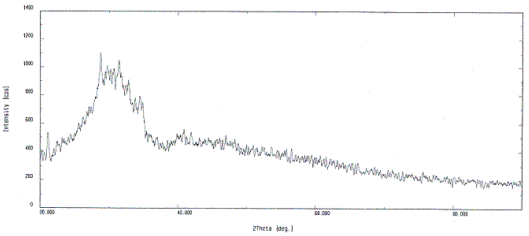

Fig. 5 XRD pattern of No.15 mould powder

Mould powder of $7^{\#}$, $2^{\#}$, $9^{\#}$, $5^{\#}$, $15^{\#}$ are representative samples, from Fig.1 ~ Fig.5, we can see that from sample $7^{\#}$ to $15^{\#}$, the intensity of diffraction peak is becoming weaker and the width is increasing, crystallization condition is decreased; precipitation of crystals were from simple single phase to complex crystal phase, and the precipitation amount of the crystals also decreased. As is shown in Fig.5, $15^{\#}$ sample are almost totally non-crystals.

TABLE II

THE XRD RESULTS OF SAMPLES

samples	chemical composition	samples	chemical composition
1	natrium melilite, cuspidite	14	calcium melilite
2	calcium melilite, magnesium feldspar	15	non-crystals(small amount of calcium melilite, lithium aluminate, cuspidite)
4	lithium aluminate, Kilalaite	16	calcium melilite
5	lithium aluminate, calcium aluminum, lithium alumina silicate	17	calcium melilite, lithium aluminate
6	Bredigite, silicon calcium borate	18	calcium melilite
7	calcium melilite	19	non-crystals(small amount of calcium melilite)
8	calcium melilite, magnesium feldspar	20	calcium melilite
9	calcium melilite	21	calcium melilite
10	calcium melilite	22	non-crystals(small amount of calcium melilite, sodalite)
11	calcium melilite	23	calcium melilite
12	calcium melilite, lithium aluminate	24	calcium melilite
13	calcium melilite, lithium aluminate	25	calcium melilite, magnesium melilite

The crystallization properties of mould powder are mainly related to the chemical composition. Reducing the ratio of NaO/Al_2O_3 is an effective way to inhibite precipitation of nepheline crystals. Riboud[1], who believed that tendency of the precipitation of crystals in the cooling process is related with two factors, that are the alkalinity and viscosity which are determined by CaO/SiO_2. The alkalinity is higher or the viscosity is lower, the tendency of precipitation of crystals is greater. It can be qualitatively interpreted by the chain-ion model of oxidized residue. Low viscosity or high alkalinity of slag means that silicon-oxide chain of the melt is short, ion migration is fast, and short-range of chain is orderly, these are all the nucleation conditions. On the contrary, high viscosity or low alkalinity of the slag show that ionic bond is elongated. It is difficult to show order in short-range, and thus the super-cooling phenomenon of non-crystals is prone to appear. That the content of Na_2O is too high promotes the precipitation of nepheline, and is aslo not conducive to vitrification of slag[2,3]. Comparison of $7^{\#}$ and $2^{\#}$, crystallization properties are improved with the increasing alkalinity under the same ratio of NaO/Al_2O_3. The same trend of change is reflected in $9^{\#}$ and $5^{\#}$ with their X-ray diffraction patterns. The alkalinity and ratio of NaO/Al_2O_3 of $15^{\#}$ is larger, and it is manifested for the full glass. Therefore, the study is showed that the crystallization properties and vitrification performance of slag are not only determined by CaO/SiO_2, but also by NaO/Al_2O_3 and other factors.

B. Influence on the continuous casting caused by mineral composition of the mould powder

As it can be seen from Table II, slag of $15^{\#}$, $19^{\#}$, $22^{\#}$ have a good performance of vitrification. For mould powder with good crystallization ability and poor performance of vitrification, its crystallization temperature is higher than its solidification temperature; crystalline is precipitated directly from the slag. In the cooling process, viscosity of slag is increased, so the fluidity and lubrication performance of slag are reduced. In the casting process, this can result in lower quality of casting blank, and bonding breakout problems. For the better vitrification performance of mold powder, its solidification temperature is higher than the crystallization temperature. Crystalline is precipitated from solid phase of mould powder, lubrication is good.

Table II showed that calcium melilite is the mainly mineral composition of the sample $1^{\#}$-$25^{\#}$, there are a small number of cuspidite, lithium aluminate, magnesium feldspar, sodalite, etc. Among various minerals, the network of CaO-Al_2O_3-SiO_2 system glass whose main component is calcium melilite (C_2AS) has skeleton of $[SiO_4]$[4]. In the void spaces, it is filled with outnetwork of ions, and some of the Si^{4+} is replaced by Al^{3+}. A network of silica tetrahedron is constituted by the way of vertices connection. In the glass network, when the $Ca^{2+}/2Al^{3+} > 1$ and the $Al^{3+}/Si^{2+} < 1$, all of Al^{3+} exist by the form of $[AlO_4]$, that is all the Al^{3+} are network forming ions, but there is some non-bridging oxygen in the glass network, structure of network is relatively loose.

Therefore, the calcium melilite-based slag has good vitrification performance, which is a good glass structure, allows slag film with good lubricating function, so that friction will be as low as possible during the downward movement of slab in the mould.

Thermal conductivity of different minerals in the mould powder is different, which affects the solidification of the slab. The mineral composition of self-flux is calcium melilite-based. Compared with other minerals, calcium melilite has a lower thermal conductivity, which can reduce the thermal capacity of the flux, so the heat flow is reduced and the longitudinal cracks can be reduced too.

There is significantly dependent relationship between bond breakout rate and the mineral composition. As the difference of mineral properties, friction of mould is different. The friction will be increased rapidly because of the use of slag which produces a large number of nepheline, while the friction caused by the use of calcium melilite is decreased. Therefore, self-flux will significantly reduce the mould friction. After the applications of above composition of mould powder in Tangshan Iron and Steel and Chengde Sheng Feng steel, the effect is very good.

IV CONCLUSION

(1) As is known by studying the microstructure of mould powder, the crystallization properties and glass performance of mould powder are not only determined by CaO/SiO_2, but also by NaO/Al_2O_3 and other factors.

(2) The mineral composition of self-flux is mainly melilite. compared with other minerals, calcium melilite has a lower thermal conductivity, which can reduce the thermal capacity of the flux, so the heat flow is reduced and the longitudinal cracks can be reduced too.

REFERENCES

[1] Reveson. Ironmaking and Steelmaking, vol.5. no.4, pp: 181-186, 1988.

[2] W-C Jung, E Toshihiko, S.Hiroyuki and S. Mikio. Heat Transfer across Mold Flux Film in Mold during Initial Solidification in Continuous Casting of Steel . ISIJ International, vol.38. no.8.,pp:834-842, 1998

[3] W-C Jung, S, Hiroyuki. Effect of solidification of mold fluxes on the heat transfer in casting mold .Journal of Non-Crystalline Solids, vol. 282, pp. 110-117, 2001

[4] L. Kaiming. Study on precipitation dynamics of glass during constant temperature process. Academic journal of QingHua, vol. 6, pp. 96-100, 1998

2011 International Conference on Mechanical, Industrial, and Manufacturing Engineering
Lecture Notes in Information Technology Vols. 1-2

Information Guidance System applying IR Line in Line Tracer

Hye-Mi Lee, Nam-Hoon Ryu, Seung-Hyeok Yoo, Mi-Jeong Park and Eung-Kon Kim

Department of Computer Engineering
Sunchon National University
Maegok-dong, Suncheon-si, Jeollanam-do, Korea
{lhrooh & nhryu & sh-yu & mj_park & kek}@sunchon.ac.kr

Jong-Wook Jeong

SRC Corporation

Haeryong-myeon, Suncheon-si, Jeollanam-do, Korea
jeong@robotsrc.com

***Abstract* - Line Tracer is a robot that follows the black line using infrared rays sensor board. This paper proposes and implements Expo Guidance System grafting line tracer using IR ink. Because the black line which is used in existing line tracer is glaringly obvious visually, we have a difficulty with applying the diverse industrial fields. This system can control the action of line tracer without expressing the route where line tracer moves using Invisible IR ink. We also graft multimedia for enhancing the ability of information delivery of Expo Guidance System, and reinforce interaction with users. If we implement the proposed method, the working process becomes simple so that the time of making becomes short. We create the economic value about using line tracer increasing the accessibility to various industrial fields.**

Index Terms – Line Tracer, Invisible IR Ink, Expo Guidance System

I. INTRODUCTION

Line Tracer is a robot that moves following the black line. It uses reflection and absorption of light through light emitting diode suite and photodiode suite of sensor board. It is a method that uses infrared rays sensor. LED lamp sends infrared rays to the ground. Line Tracer is a structure that rolls the wheel controlling the motor of both sides to follow the black line as the infrared rays sensor detects the intensity of radiation of infrared rays that is reflected by the white and black. When it processes, it stops at the certain position, and it plays the voice or can play the appointed display image at some section. However, the route itself can be seen certainly, Line Tracer has a difficulty with using the various industries.

The existing Line Tracer uses black and thick line for maximization of cognition rate about line, and is glaringly obvious visually. This line has no difficulty with using robot basic education such as a robot competitive exhibition, but should solve the problem of arousing interest and improving immersion for using industrial fields[1-3].

Infrared rays is an electromagnetic wave that has wavelength range of 0.75㎛~1mm and is outer than the edge of red line when we disperse the emitted light of sun with prism. Because it has the heat, it is called heat line, and its heat effect is the characteristic of infrared rays. It also has no harmlessness to body, and uses and applies the various fields because of the characteristic of invisibility.

This paper escapes the existing line tracer method using the black line that is glaringly obvious visually for getting the economic effect beyond the education field, and offers and implements the invisible line tracer method that can be tracked by the infrared rays ink. To prove the result of this, we make the exhibition set that introduces 2012 Yeosu Expo, and the line tracer where we add the guide broadcasting using multimedia of sound and video for maximization of immersion and interest about introduction of the exhibition set. If we use the proposed method, the immersion is increased and the problem of delivery ability decline of guide system of expo can be solved due to not using the visible line.

II. EXPO GUIDANCE SYSTEM

This paper makes Multi Guidance System that can introduce the exhibition center of 2012 Yeosu Expo. Users can get the information of the exhibition center they want to know with line tracer, and they can have a strong interaction due to controlling it for themselves. The information users want to know are delivered by voice guidance and playing the appointed display video. We use infrared rays that can be invisible to human eyes on the route that are used in line tracer and the guidance time mark. This is for enhancing the quality of the exhibition center and maximizing the ability of information delivery about Expo exhibition center reinforcing concentration of guidance. This system consists of Sensor Module, Behavior Module, Remote Control Module, Control Module, and Interface Module. The figure 1 shows the composition of Multi Guidance System.

A. Sensor Module

Sensor module consists of Light Emitting Diode Suite, Photodiode Suite, and Analysis Suite. We use reflection and absorption of light through Light Emitting Diode Suite and Photodiode Suite of sensor board. In the existing line tracer, the black that means a line absorbs all the light and the white that means background reflects all the light so that we control the action. If we, however, use infrared rays luminescence ink, the route line that we made with infrared rays reflects stronger light and the section that means background reflects weaker light relatively when we light from Light Emitting Diode Suite. Analysis Suite judges all this processes, and controls the action with direction algorithm.

The figure 2 is Key map of line tracer. (a) is the method that uses the black line that is used in the existing line tracer.

Because Viewpoint that can control the exhibition model we want to introduce and Behavior in line tracer coexist as simple form, it is difficult to increase the economic value. (b), however, doesn't mark the moving route of line tracer and is a form that has a general introduction set of the exhibition center. Because the black line can't be seen visually, we can have the opportunity of aesthetic design and make a lot of forms according to characteristic and situation of the exhibition set. Line tracer recognizes the line that is made up of infrared rays ink like (c) as the route and viewpoint that are necessary. Infrared rays ink is invisible to human eyes because of invisibility, but we can trace with infrared sensor node. Since we don't have to process and can mark all of viewpoint that is necessary to behavior and control and interface, implementation becomes simpler as advantage. The implementation result that we use finally is a combination form of (b) and (c) together.

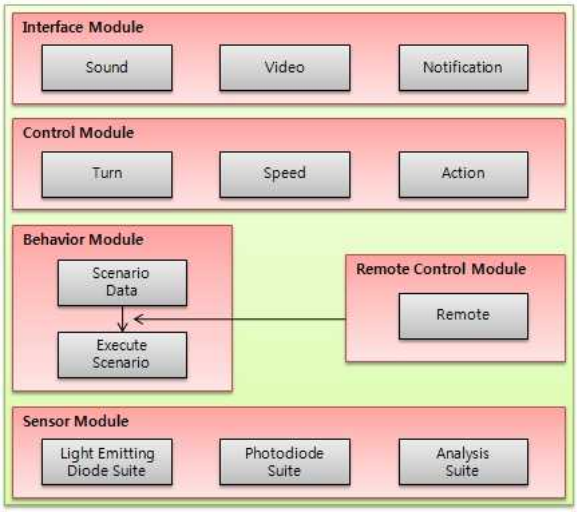

Fig. 1 Block diagram of multi guidance system

B. *Behavior Module / Remote Control Module*

Behavior Module has scenario data that can introduce and move following the fixed route through scenario. When interaction with users does not exist, it will move according scenario that is built in. If users control line tracer remotely with remote control, arousing interest and immersion can be increased by moving the position that users want immediately and being changed to action scenario.

C. *Control Module*

Control Module controls actions of turn, speed control, going straight and stop in viewpoint.

D. *Interface Module*

Interface Module is a module grafting multimedia for delivering information in detail and easily. When we are moving, it will play theme song. When we arrive to viewpoint, it will start relevant voice introduction. We can acquire more dynamic information increasing delivery efficiency of information with playing display video that are built in the certain position of guidance system when necessary. The figure 3 is a test screen in line tracer that is developing and will be used in Expo 2012 Yeosu Korea Guidance System.

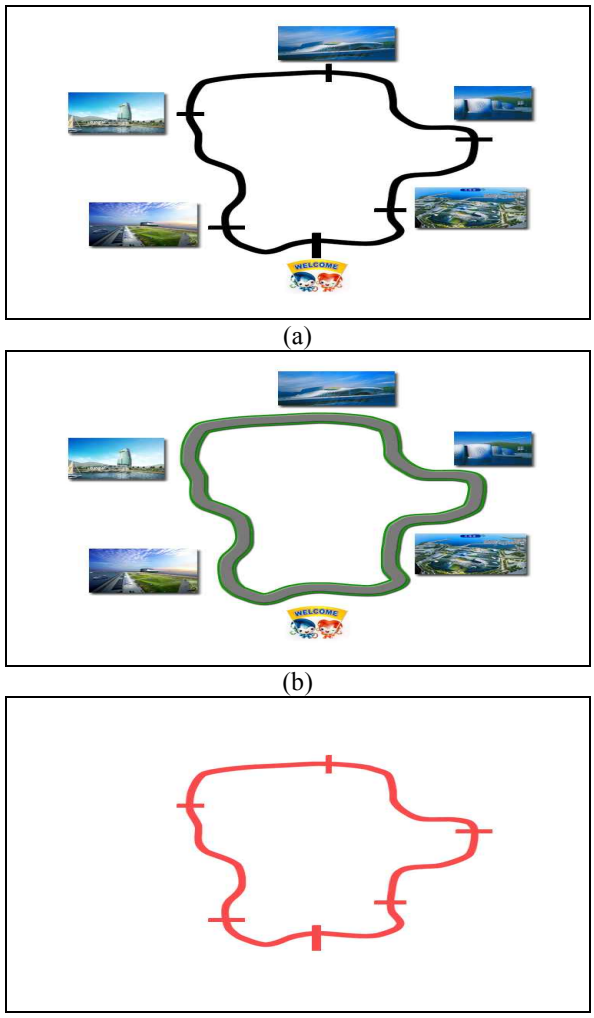

Fig. 2 Key map of line tracer

Fig. 3 Expo 2012 Yeosu Korea guidance system test image

III. CONCLUSION

Line tracer is a robot that moves following the black line with infrared rays sensor board. Because the existing line

tracer should recognize the route through the black line and applying to the diverse fields is limited, it is difficult to create the economic effect. This paper make line tracer apply to the various industrial fields beyond the fixed applying range with Expo Yeosu Korea Guidance System. We enhance the quality substituting the black line that is used for recognizing the route of line tracer by the invisible IR ink. To remove visual inconvenience, we cut down time of production due to making the route for maximizing the rate of recognition only without processing line and viewpoint. Because we can apply design according characteristic and situation of the exhibition set so that the range of applying becomes broad, we can expect the economic effect. We can also acquire information more dynamically applying multimedia with line tracer and arousing interest and immersion are increased as we expected emphasizing interaction with users. We can apply guidance system of museum and exhibition centre from now on.

ACKNOWLEDGMENT

This research was financially supported by the Ministry of Education, Science Technology (MEST) and National Research Foundation of Korea(NRF) through the Human Resource Training Project for Regional Innovation

REFERENCES

[1] Shimada, Yasuyuki, Ohtsuka, Hirofumi, Yamamoto, Yoshiichi, Matsumoto, Tsutomu, and Kawaji, Shigeyasu, "Design of System and Control Engineering Education Curriculum Based on the Growth of Line Tracer," Journal of Japanese Society for Engineering Education, vol. 55, no. 3, pp. 99-104, 2007.

[2] Seung-Ki Min, Suk-Hyun Seo, Jin-Ho Kim, Key Ho Kwon, Sung-Ho Hwang, and Jae Wook Jeon, IEEE International Symposium on Industrial Electronics(ISIE 2009), pp. 960-965, 2009.

[3] Hong-Hyu Kim, and Jeung-Jin Moon, Route Tracking of Moving Magnetic Sensor Objects and Data Processing Module in a Wireless Sensor Network, International Conference on Smart Manufacturing Application(ICSMA 2008), pp. 343-348, 2008.

2011 International Conference on Mechanical, Industrial, and Manufacturing Engineering
Lecture Notes in Information Technology Vols. 1-2

Stability of a Rotating Tank Source-Sink Setup to Model a Polar Vortex

Tony Vo and Gregory J. Sheard
Department of Mechanical and Aerospace Engineering
Monash University
Clayton, Victoria 3800, Australia
{Tony.Vo & Greg.Sheard}@monash.edu

Luca Montabone
Atmospheric, Oceanic and Planetary Physics
University of Oxford
Parks Road, Oxford OX1 3PU, United Kingdom
Montabone@atm.ox.ac.uk

The fundamental instabilities forming on a numerical rotating source-sink model is reported. The rotation of fluid combined with fluid injection from a source ring placed an appreciable distance away from the axis and the fluid withdrawal from a central sink generates a vortical structure similar to that seen in atmospheres.

Axisymmetric flow is computed on the meridional semi-plane using a spectral-element discretisation, and stability to non-axisymmetric perturbations is determined using a linear stability analysis. Direct numerical simulation (DNS) via a spectral element-Fourier method verifies the stability predictions. The solutions produce similar vortex structures to the experimental physics.

A global linear stability analysis predicts a structure with azimuthal wavenumber 13 arising from the flow which is higher than what was observed experimentally (wavenumbers of 1 to 6). Contour levels of the perturbation field indicate that perturbation structures are located at the source, rather than the sink, where laboratory dye visualization has been focused. Three-dimensional simulations suggest that these outer disturbances agitate lower-wavenumber instabilities near the axis (pole).

Index Terms – Polar vortex, Source-Sink, Numerical, Barotropic instabilities.

I. Introduction

Atmospheric vortices are abundant in nature and arise due to the ordinary rotation of the Earth. They are known for their coherent structures and the ability to harness great amounts of energy as seen in tornadoes. Distinct vortices, known as polar vortices have been observed to form at the polar regions on Earth. They are large in size and circular in shape. Polar vortices have been observed on planets with atmospheres, including Venus, Mars, Jupiter and Saturn, and their size, configuration and strength differs.

The combination of planetary rotation together with conservation of angular momentum causes circumpolar jets to develop at polar latitudes, which encircle the polar vortex. This structure can take on various geometric configurations, such as a dipole observed on Venus through to a hexagonal configuration, observed on Saturn by the Cassini spacecraft [3]. These configurations are not always stable and have demonstrated swift vacillation between states in over timescales in the order of days. A recent example was observed on Venus via the European Space Agency Venus Express probe where the southern structure transitioned between a dipole to a monopole, and back again over the span of a few Earth days, where one Venusian day equates to 243 Earth days [8].

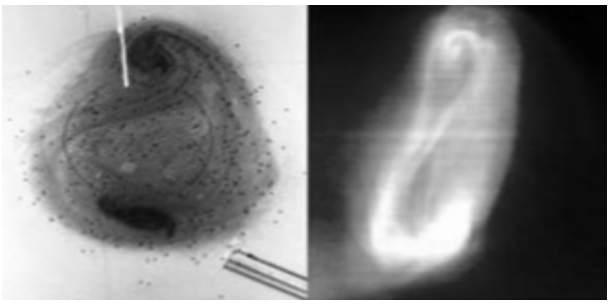

Fig. 1 An analogue between a mode-2 structure created in a laboratory (left) and its atmospheric counterpart (right). This figure is reproduced from [6]. The images represent a Venus dipole polar vortex.

Strong coherent vortices have the ability to trap particles in their cores and isolate them from the surrounding flow for extended periods [9]. This property poses issues for Earth's climate as polar vortices are prominent during winter, exacerbating chlorine build up. The onset of spring weakens and breaks up the polar vortex. This releases the chlorine which reacts with the ozone, depleting the ozone layer. Consequently, climate variability has been observed in the high-latitude Southern Hemisphere [13]. The effects propagate equatorward impacting countries such as Australia through prolonged drought conditions [7].

In pursuit of an understanding of the stability of polar vortices, models have recently been studied in the laboratory [6]. Vortex structures were generated which closely resembled the various configurations observed in the atmospheres. Fig. 1 depicts a comparison between a laboratory-produced vortex and a Venusian atmospheric polar vortex. A 5-metre diameter Coriolis tank in Trondheim, Norway, was used to produce model polar vortices with configurations featuring 1 to 6 repetitions around their circumference, which were observed via dye visualisation. The vortices were produced by rotating the cylindrical tank, and injecting fluid poleward from a source ring offset by extraction of fluid from a sink at the tank axis (the pole). Conservation of angular momentum increases the rotation rate of the poleward-moving fluid, thus generating the vortex near the axis. The injection and extraction of fluid also induces upwelling and downwelling effects, which are seen naturally in the Earth's atmosphere arising from temperature differences across latitudes. Thus the present source-sink method faithfully models several features of the polar atmospheric physics.

978-0-9831693-1-4/10/$25.00 ©2011 IERI

Given the complexity and current limited understanding of the dynamics involved in producing, stabilising and the vacillation of polar vortices, the immediate study is focused on the fundamental instabilities that form. As a result, the forcing parameters dictating the simulations in this preliminary study are lower than to those explored in [6].

II. Methodology

In this study the source-sink system in [6] will be numerically produced. A schematic representation of the apparatus is shown in Fig. 2. The polar vortex is generated by the rotation of the tank at angular velocity Ω, and the poleward flux flow from the source to sink.

The two determining factors for the stability of a polar vortex have been found to be most dependent on the Rossby number and the volume flux [6]. The Rossby number relates inertial forces to Coriolis forces, though in this configuration it is not a control parameter. Hence we instead define a Reynolds number given by

$$Re = \frac{{R_i}^2 \Omega}{\nu} \tag{1}$$

where R_i is the sink radius, and ν the kinematic viscosity of the working fluid. An experiment in [6] utilised water with one tank revolution per minute which equates to $Re \sim 21{,}200$.

The axisymmetric mesh is shown in Fig. 3, which represents the *z-r* plane of the apparatus over which the flow is computed. The meridional semi-plane is discretised into a mesh of quadrilateral elements. The vertical dotted line denotes the axis of rotation and spatial symmetry.

To simulate and invoke the appropriate dynamics acquired in the laboratory, certain boundary conditions have been applied. The bottom and side walls rotate at a rate of Ω, while the top boundary acts as a stress-free surface. The inlet and outlet vertical velocity for the source and sink are parabolic in profile, peaking at their radial centreline and relatively stationary at their edges. The curvature of the sink accounts for the β-effect at the planet's pole [5].

The working fluid is assumed to be incompressible and Newtonian. The flow is described by the Navier-Stokes equations

$$\frac{\partial \mathbf{u}}{\partial t} + (\mathbf{u} \cdot \nabla)\mathbf{u} = -\nabla P + \nu \nabla^2 \mathbf{u} \tag{2a}$$

$$\nabla \cdot \mathbf{u} = 0 \tag{2b}$$

where $\mathbf{u}$ is the velocity vector field and P is the kinematic pressure field. These equations are solved in cylindrical coordinates using an in-house code employing a spectral-element discretisation in space and a third-order time-integration scheme based on backward differentiation. The axisymmetric solver has been validated in studies [10, 11]. Within each macro element, Lagrangian tensor-product polynomial shape functions describe the flow: the polynomial degree can be varied to control spatial resolution. The polynomials are interpolated at the Gauss-Legendre-Lobatto quadrature points. This scheme is based on high-order splitting methods presented in [4].

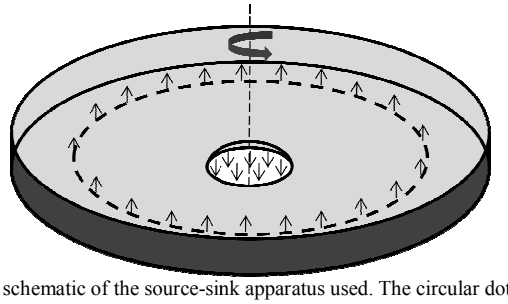

Fig. 2 A schematic of the source-sink apparatus used. The circular dotted line represents the source ring where fluid is injected and the vertical dotted line representing the axis of rotation. The arrows display flow direction.

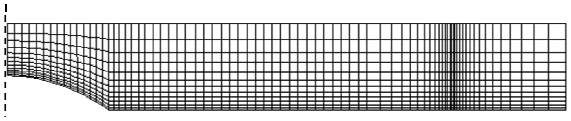

Fig. 3 Two-dimensional axisymmetric mesh of the *z-r* semi plane.

Our interest is in non-axisymmetric structures in the vortex flow and its stability, and thus a linear stability analysis is used to predict the fastest growing three-dimensional modes that develop on the underlying axisymmetric flow. An algorithm is executed which operates by computing the base flow and each of the perturbation fields separately. The saturated base flow is frozen and decoupled from the evolving three-dimensional perturbation fields. The eigenvalues of the system are obtained through a Floquet analysis [1]. Over sufficient periods of the flow solution, the leading eigenvalue is determined which corresponds to the Floquet multipliers μ of the system. The relationship between the Floquet multiplier and the growth rate σ is given by

$$\mu = e^{\sigma T} \tag{3}$$

where T denotes the time period. Thus, $|\mu| < 1$ represents a stable flow and $|\mu| > 1$ an unstable flow - the respective growth rates being positive and negative. The present implementation in cylindrical coordinates follows [12], and was recently validated in [2].

Focusing on the fundamental stability of the system, simulations have been performed for controlling parameters at lower values than those employed in [6]. Table I summarises the parameters used here and in an experiment from [6] as a comparison, as functions of *Re* and a poleward flux parameter

$$\bar{Q} = \frac{Q}{2\pi\Omega {R_o}^2 H}, \tag{4}$$

where Q denotes the injected/extracted fluid flow rate, R_o the radial distance from the axis to the source centreline and H representing the tank height.

TABLE I

Tabulated case studies and an experiment from Montabone *et al.* (2009) as defined by *Re* and $\bar{Q}$.

Case	*Re*	$\bar{Q}$ (10^{-4})
1	1325	3.04
2	4639	3.32
3	7952	3.61
4	11266	3.89
Laboratory	21206	4.75

III. Results

A. Axisymmetric Flow

Steady state solutions were obtained on the meridional semi-plane for the four flow cases. Fig. 4 represents the typical velocity fields exhibited by the flow in its steady state condition, via contours of vertical (axial) and radial velocity. It is apparent that the dominant dynamics occur in the boundary layer on the bottom boundary, known as the Ekman layer, and in the vicinity of the source and sink.

From [5], the measured relative azimuthal velocity profile (the local azimuthal velocity relative to the rotation of the tank) was observed to scale directly with r for regions between the axis and the sink's outer radius, and scales with $1/r$ thereafter. Azimuthal velocity data along the surface of the flow is presented in Fig. 5. A general trend of increasing peak velocities with increased Re and $\bar{Q}$ is demonstrated. The profile is qualitatively consistent with laboratory results. These profiles were found to be independent of height outside of the Ekman layer above the sink, verifying that the flow is strongly barotropic and that the setup reproduces the experimental physics. The peak location of the azimuthal velocity differed between the numerical and experimental results, with the latter peak closer to the sink edge. Further investigation has determined that to obtain the relative azimuthal velocity profile seen in the laboratory, the bulk of the sink outflow must have occurred near to the radial edge of the sink.

B. Linear Stability Analysis

Stability analysis was computed on each saturated axisymmetric base flow, and perturbations with azimuthal wavenumbers ranging from 1 to 20 were investigated. The global instability growth rates are shown in Fig. 6. The wavenumber is defined as $k = 2\pi/\lambda$ where λ is the azimuthal wavelength in radian. In each case the growth rate reaches a peak at a particular wavenumber before decreasing again at higher wavenumbers. The Re = 1325 case is found to be completely stable, with $k = 7$ the dominant wavenumber. This peak growth rate wavenumber correspondence increases with increasing Re and $\bar{Q}$.

Fig. 4 Contours of vertical (top) and radial (bottom) velocity depicting dynamic locality and boundary layers respectively for Re = 11266. Greyscale contours are used where light and dark shadings denote positive and negative values respectively.

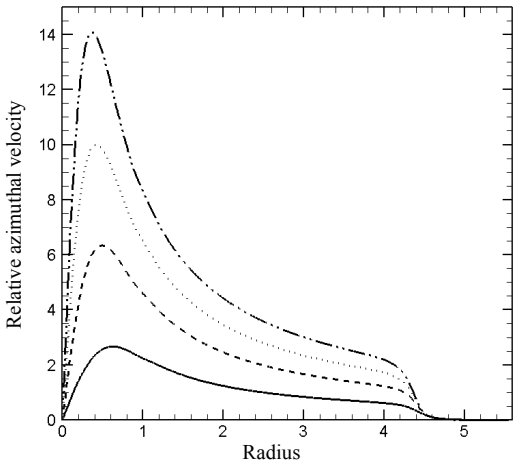

Fig. 5 Plots of the relative azimuthal velocity against normalized radius extracted from the surface of the flow for Re = 1325 (solid), Re = 4639 (dashed), Re = 7952 (dotted) and Re = 11266 (dash-dot-dot).

The case simulated with parameters most closely matching the laboratory conditions predicts a dominant instability mode with azimuthal wavenumber k = 13. This is higher than the wavenumbers observed in polar vortices and their laboratory models. A point of note is that the analysis is global and peak wavenumbers reflect modes across the entire flow. These do not necessarily correlate with the stability of the polar vortex region in isolation.

In the laboratory, visualization has been confined to the sink region near the axis, whereas stability analysis has predicted perturbation structures to be strongest in the vicinity of the source ring, as illustrated in Fig. 7.

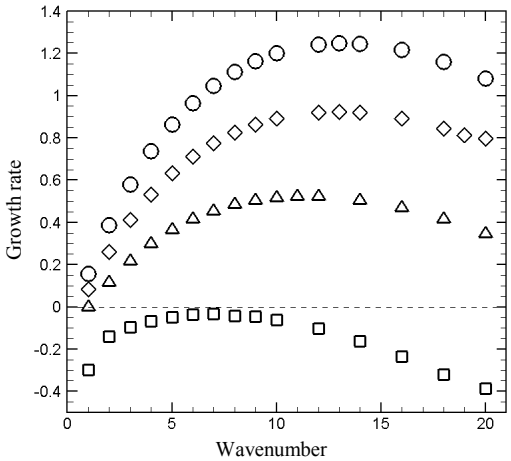

Fig. 6 Plots of growth rate against wavenumber obtained via linear stability analysis for Re = 1325 (square), Re = 4639 (triangle), Re = 7952 (diamond) and Re = 11266 (circle). The growth rates are non-dimensional and their values are deduced from the global domain.

Fig. 7 Perturbation contours of vertical vorticity displaying strong growth around the source radius for $Re = 4639$, $k = 13$. Greyscale contours are used where light and dark shadings denote positive and negative values respectively.

C. *Three-dimensional DNS*

Three-dimensional DNS computed over 16 Fourier mode expansions yield evolution of the predicted instability modes and are comparative to polar vortex configurations. The location of the prevailing instabilities agrees well with the linear stability results. Low-wavenumber disturbances have been observed near the sink.

Perturbation vorticity contours at the fluid surface are shown in Fig. 8, depicting an inner coherent structure with wavenumber 2. This structure has been seen to vacillate between a mode-1 and mode-2 configuration respectively representative of a circular and dipole structure in the atmosphere. The outer high-wavenumber disturbances developing around the source ring are unstructured and appear to act as a forcing perturbation that incites low-wavenumber instability structures to emerge near the sink. Regular patterns have been observed around the source under different forcing conditions. In such cases, the polar vortex remains to exhibit a low-wavenumber configuration. Global stability analysis did not detect structures forming near the axis, thus suggesting that stability analysis should be confined to the sink region.

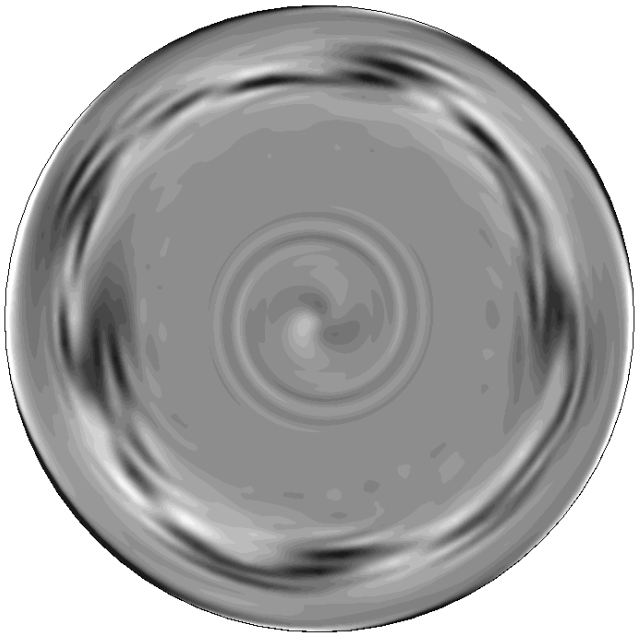

Fig. 8 A plan view of the surface where contours of vertical vorticity are shown. Greyscale contours are used where light and dark shadings denote positive and negative values respectively.

III. Conclusion

The fundamental instabilities occurring in polar vortices produced via a source-sink configuration have been numerically investigated. A computational mesh set up to emulate the dynamics of an experimental study [6], is the basis of this study. Base flow solutions indicate major dynamics taking place in the Ekman layer, source and sink locality.

Montabone *et al.* (2009) observed through dye visualisation, the polar vortex forming around the sink. Stability analysis dictates major growth appearing around the source ring which is visible in 3D DNS, although a polar vortex in the centre was also observed. This implies stability analysis should be performed on a truncated domain enclosing only the sink, in order to obtain growth rates that are reflective of the polar vortex.

Acknowledgments

T.V. received support through an Engineering Research Living Allowance and acknowledges the Monash University E-research centre for the access to its high performance computing facility, Sun Grid. Computations were also carried out with the support of a grant under the NCI Merit Allocation Scheme. NCI is supported by the Australian Commonwealth Government. G.J.S. is supported by a Faculty of Engineering Small Grant.

References

[1] D. Barkley, R. D. Henderson, "Three-dimensional Floquet stability analysis of the wake of a circular cylinder," Journal of Fluid Mechanics., 1996, vol. 322, pp. 215-241.

[2] S. J. Cogan, K. Ryan, G. J. Sheard, "Symmetry breaking and instability mechanisms in medium depth torsionally driven open cylinder flows," Journal of Fluid Mechanics, 2011, In Press.

[3] L. N. Fletcher, *et al*., "Temperature and composition of Saturn's polar hot spots and hexagon," Science, 2008, vol. 319, pp. 79-81.

[4] G. E. Karniadakis, M. Israeli and S. A. Orszag, "High-order splitting methods for the incompressible Navier-Stokes equations," J. Comput. Phys., 1991, vol. 97, no. 2, pp. 414-443.

[5] L. Montabone, *et al.*, "Barotropic instability of planetary polar vortices: CIV analysis of specific multi-lobed structures," Proceedings of the HYDRALAB III Joint User Meeting, Hannover, February 2010.

[6] L. Montabone, *et al.*, "Coherent Structures in Planetary Polar Vortices: A Laboratory View," International Conference on Comparative Planetology: Venus – Earth – Mars, ESTEC, Noordwijk, Netherlands, 11-15 May, 2009.

[7] B. F. Murphy and B. Timbal, "A review of recent climate variability and climate change in southeastern Australia," International Journal of Climatology, 2008, vol. 28, pp. 859-879.

[8] G. Piccioni, *et al.*, "South-polar features on Venus similar to those near the north pole," Nature, 2007, vol. 450, pp. 637-640.

[9] A. Provenzale, "Transport by coherent barotropic vortices," Annu. Rev. Fluid Mech., 1999, vol. 31, pp. 55-93.

[10] G. J. Sheard, "Flow dynamics and wall shear stress variation in a fusiform aneurysm," Journal of Engineering Mathematics, 2009, vol. 64, no. 4, pp. 379-390.

[11] G. J. Sheard and K. Ryan, "Pressure-driven flow past spheres moving in a circular tube," Journal of Fluid Mechanics, 2007, vol. 592, pp. 233-262.

[12] G. J. Sheard, M. C. Thompson and K. Hourigan, "The subharmonic mechanism of the Mode C instability," Physics of Fluids, 2005, vol. 17, no. 11, article no. 111702.

[13] D. W. J. Thompson and S. Solomon, "Interpretation of recent Southern Hemisphere climate change," Science, 2002, vol. 296, pp. 895-899.

2011 International Conference on Mechanical, Industrial, and Manufacturing Engineering
Lecture Notes in Information Technology Vols. 1-2

Research of Vertical Shaft Impact Crusher Rotor Channels' Number Based on EDEM*

Song Wang, Fang Zhao* and Derong Duan
Department of Mechanical Engineering
University of Jinan
Jinan, Shandong Province, China
wangs1985@163.com

Abstract - The vertical shaft impact crusher virtual prototype model was established based on the EDEM to simulate the motion stage and mechanical properties of rock materials flow in rotors with different number of channels. The results show that the structure of the vertical shaft impact crusher rotor with 6 channels is most reasonable and the accelerating effect is best. At the same time, the rotor with excessive channels will make most of particles leave the rotor without full acceleration. However, the fewer the number of rotor channels are, the fewer particles thrown off the rotor are in unit time, the longer accelerating time is, which can reduce the crushing efficiency.

Index Terms – EDEM; Vertical Shaft Impact Crusher; Rotor; Virtual Prototype Technology; Channel

I. INTRODUCTION

The vertical shaft impact crusher (hereinafter referred to as VSI) has been widely used in the production of gravel with its simple structure, light weight, low cost, stable operation, high efficiency and production of better cube aggregate [1].

Being an important part in VSI, the rotor although plays an accelerating role in rock materials broken; the stone could be collided and broken only after accelerated in the rotor. It has been founded that the sand production rate, fineness modulus and the life of rotor wearing parts were all influenced by the number of rotor channels in the manufacturing and maintenance for many years of VSI manufacturers. The accelerating effect of rotor to particles was determined by the number of channels, thereby affecting the sand production rate and the fineness modulus of VSI. There is a great difference of stone lithology in China, and the adaptation of different stone to different number of channels is various. Therefore, it has been urgently required by VSI manufacturers that the relationship between the rotor accelerating effect and the number of channels, then the appropriate number of channels will be selected to the specific stone broken.

II. STRUCTURE AND WORKING PRINCIPLE OF VSI

The VSI was mainly made of hopper, rotor, crushing chamber, transmission and frame structure, as it can be seen in Fig.1. Stone fell into the rotor through the hopper under the gravity, and were equally divided into every channels by separating cone. Accelerated by the role of friction and the runner plate, stone gradually gained the kinetic energy and were ejected off the rotor by centrifugal force at the ejected speed which almost reached the liner speed of rotor edge. At this ejected speed, the collision between stone accelerated with the crushing chamber and the waterfall stone from the sub-feeder had happened, and the process of collision continued about 5s~20s.Finally, the stone without kinetic energy left the crushing chamber under the gravity[2].

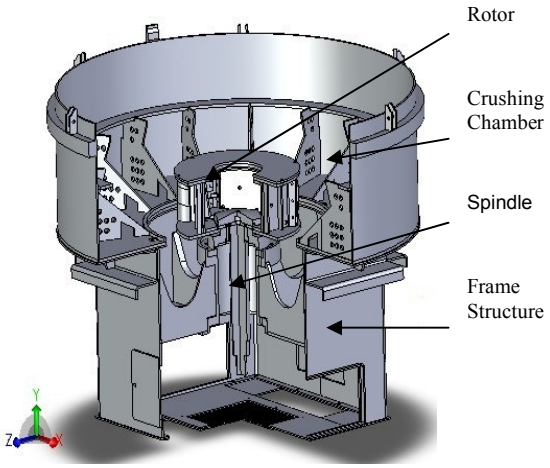

Fig.1 Rotor Structure

III. VIRTUAL PROTOTYPE TECHNOLOGY AND EDEM SOFTWARE

Virtual prototyping technology is a new product design and process development method appeared in early 1990s. It had established a highly visible prototype of the digital simulation of physical prototypes through combining virtual reality, computer simulation technology and CAD technology [3].

EDEM™ is the first multi-purpose Discrete Element Modeling software tool in the world, which is designed for the simulation and analysis of industrial particle handling and manufacturing operations.

IV. ROTOR MODELING

In this paper, the rotor was modeled by SolidWoks with the Sandvik RP109 as prototype. Without affecting the simulation results, the rotor three-dimensional model was

* This work was financially supported by Shandong Natural Science Foundation of China Grant No. Y2007F40.

Simplified by removing and merging certain parts, and keeping the same parameters of rotor radius, separating cone radius, runner plate installation angle, the size and installation angle of butt ends, total channel export spacing. Respectively, the rotor was modeled with 3~8 channels and imported into EDEM through the IGES format, the configuration distribution was showed in Fig.2.

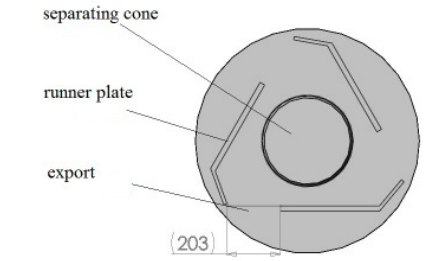

(a) Rotor with 3 channels

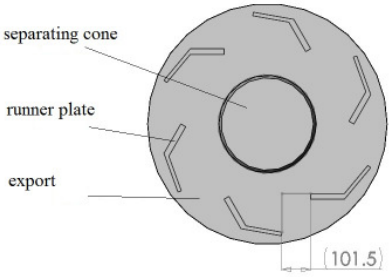

(b) Rotor with 8 channels

Fig.2 Configuration distribution of different rotors

V. CONSTRAINT SETTINGS

A. *Global Settings*

The rotor model was imported into EDEM, in which the red frame was the computational domain. The physical properties was set as the interaction between the particles and the particles to geometry, the acceleration of gravity g along the z axis was -9.81m/s^2.according to the documentation and the survey data, the material of rotor was steel, the material properties were: Poisson's ratio ν 0.28, the shear modulus G 7.1e+7Pa,density ρ 7800Kg/m^3.The interaction coefficient of material was defined as follows, the restitution coefficient of particles s_1 0.1,the static friction coefficient f_1 0.545,the rolling friction coefficient g_1 0.01;the restitution coefficient of particles to rotor s_2 0.2,the static friction coefficient f_2 0.5,the rolling friction coefficient g_2 0.01[4],it was can be seen in Fig.3.

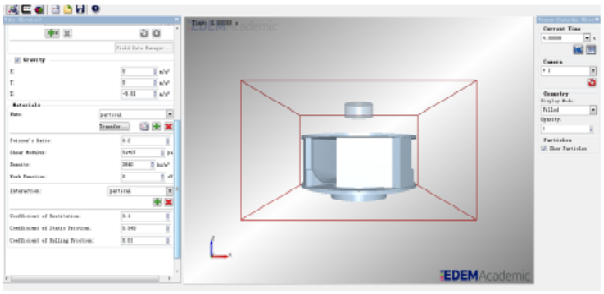

Fig.3 EDEM global settings graph

B. *Defining Particles*

According to need to set particle size, particle radius of where to set 20mm, material selection limestone, as shown in Figure 4.

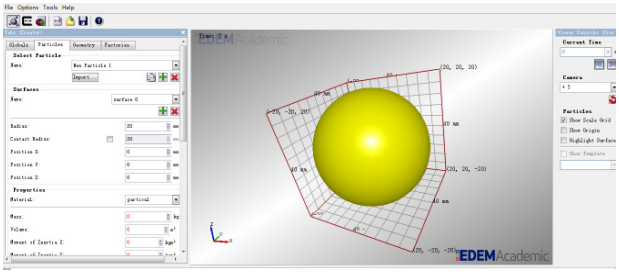

Fig.4 EDEM defining particles graph

C. *Defining the Geometry*

Set in the rotor speed for 1400r/min, in order to simulate the practical feeding flow, set particles factory shape for cylinder of the radius:160mm, high:100mm, and The same axis with the rotor, produced a total of 200kg grain, generating speed for 140kg/s, particle generation time for initial 1e-12s, generating position inside the particles factory random distribution.

D. *Simulator Settings*

To ensure the simulation accuracy and the rotor can throw all the particles, set total simulation time step of 1e-4s, simulation time is 2.5s; cell size of 40mm, a total of 9196 cells, set after completion of operations.

VI. ANALYSIS OF SIMULATION RESULTS

In order to properly compare the rotors with different channels, respectively, the average speed-time graph was made with the average speed of particles thrown off the rotor as the vertical axis and the time as the horizontal axis, as shown in Fig.5.

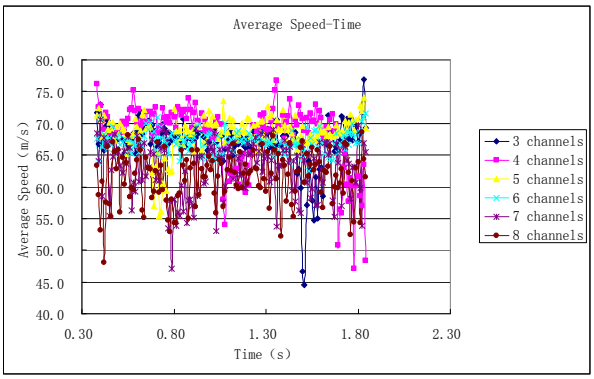

Fig.5 average speed-time graph

Seen from Figure 5, speed of particles thrown off the rotor with 7,8channels is lowest with significant fluctuations in the average as time progresses. Speed of particles thrown off rotor with 6 channels live in the middle, not the highest, however, the fluctuation is very small. Although the speed of particles thrown off the rotor with 3~5 channels is slightly larger than that of rotor with 6 channels, their fluctuations are also great, as shown in Table 1.

TABLE I

ARITHMETIC MEAN AND STANDARD DEVIATION OF PARTICLES EJECTED SPEED

Number of channels	3	4	5	6	7	8
arithmetic mean (m/s)	67.1	68.1	68.5	67.8	62.8	61.5
standard deviation	3.89	4.14	2.90	1.64	4.38	3.90

Seen from Table 1, from 3channels to 6channels the arithmetic mean of particles speed has not changed much, but the standard deviation decreased, indicating that fluctuation in the arithmetic mean is smaller and the overall speed of the particles thrown off rotor has risen. From 6 channels to 8 channels, the arithmetic mean decreased significantly, and the standard deviation also increased, indicating that the overall speed of particles thrown down. Therefore, the speed of particles increases as the number of channels increases, in the 6 channels reaches a peak and then begins to decline. Thus, rotor with 6 channels is the most reasonable design and accelerates particles best.

Suppose the reasons for this phenomenon are: with the increase in the number of channels, the time of particles thrown off the rotor was becoming faster and faster in order from 3 channels to 8 channels. With too many channels, particles thrown off the rotor were numerous, resulting in many particles in rotor without full acceleration and fall off the rotor, leading to the arithmetic mean of particles ejected speed was low in rotors with 7 and 8 channels, standard deviation was high; however, the fewer numbers of channels would result in the fewer particles thrown off the rotor in unit time, the longer accelerating time, and the reduction of production efficiency. In order to prove this hypothesis, it was made that the number of particles of each rotor-time graph, as shown in Fig.6.

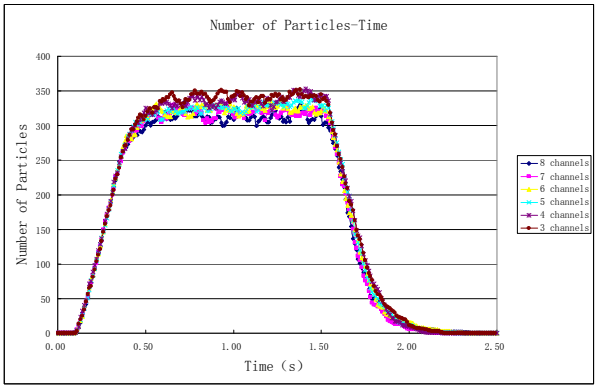

Fig.6 number of particles of each rotor-time graph

Seen from Fig.6, after 0.4s, the number of particles in rotor reduced in order from 3 channels to 8 channels at each time point. In the case of equal feeding quantity, it was indicated that the fewer particles remaining in the rotor, the faster the particles were thrown off the rotor with the shorter accelerating time. In the time from 0.4s to 0.6s, the number of particles in rotor grew slowly, because of that the rotor began to throw particles out; meanwhile, the curve slope declined in order from 3 channels to 8 channels, which means the growth rate of particles' number decreased, indicating that particles were thrown off the rotor faster and faster. After 1.5s, none of particles generated, and the remaining particles were thrown off the rotor, resulting in the reduction of the particles' number; the curve slope increased in order from 3 channels to 8 channels, which means the reducing rate of particles arose, showing that the particles were thrown off the rotor faster and faster also. This is consistent with the content hypothesis, proving the correctness of inference.

VII. CONCLUSIONS

(1) The more the number channels are, the more easily the particles are thrown off the rotor, the shorter the accelerating time is.

(2) The rotor with excessive channels will make most of particles leave the rotor without full acceleration. However, the fewer the number of rotor channels are, the fewer particles thrown off the rotor are in unit time, the longer accelerating time is, which can reduce the crushing efficiency.

(3) The structure of the vertical shaft impact crusher rotor with 6 channels is most reasonable and the accelerating effect is best.

ACKNOWLEDGMENT

This work was financially supported by Shandong Natural Science Foundation of China (grant No. Y2007F40).

REFERENCES

[1] Minggao Zheng, "Brief Discussion on the development of the system sand equipment," *Mining & Processing Equipment*, vol. 8, no. 2, pp. 18-20, January 2004.(In Chinese)

[2] Yaoqing Xin, "Brief Discussion of vertical shaft impact crusher," *Mining & Processing Equipment*, vol.33, no. 7, pp. 27-28, September 2004. (In Chinese)

[3] Ruyi Shen, “Jaw Crusher simulation of key organizations,” *Mechanical Engineering and Automation*, vol. 18, no.5, pp. 66-67, January 2009. (In Chinese)
[4] Guoqiang Wang, Wanjun Hao, and Jixin Wang, “Discrete element method and its practice on EDEM,” Xian: Northwestern polytechnical university Press, 2010, pp. 45-70. (In Chinese)

2011 International Conference on Mechanical, Industrial, and Manufacturing Engineering
Lecture Notes in Information Technology Vols. 1-2

Supply Chain Strategic Decision Analysis Using ANP and SD Simulation Method

Nasim Nezamoddini
Department of Industrial Engineering
Sharif University of Technology, Tehran, Iran
n_nezameddini@ie.sharif.ir

Farhad Kianfar
Department of Industrial Engineering
Sharif University of Technology, Tehran, Iran
fkianfar@sharif.edu

***Abstract* – This paper presents a novel approach that integrates the analytical network process technique and system dynamics to model the decision variables in manufacturing company's strategy selection regarding elements of its supply chain. Alternative strategies are evaluated based on obtained simulation results of system dynamic model using Super matrix tools of ANP. This integration increases the level of confidence in decision process with eliminating biased judges of experts and taking into account board of decision and variables' long term effects in system.**

Index Terms – Decision making, System dynamics, Analytical Network process, Supply chain, Strategic management

I. INTRODUCTION

In today's global marketplace, individual firms no longer compete as independent entity in market, but rather as integral part of supply chain. Therefore, final success of company completely depends on its managerial ability to coordinate the network of business relationships among supply chain parts. A supply chain is integrated system synchronizing interrelated business processes in order to transform raw materials into finished products and distribute them to costumers in integrated flow of information, money and material. Business strategy forces the supply chain operation to activate that as a customer facing entity serving the competitive goals of the enterprise—not merely an operational department [1], [2].

In strategy research, the importance of supply chain strategic management concepts has long been discussed and recognized to hold the potential to lead to business success.

To identify an supply chain base organization's strategy this paper suggests taking all important parts of supply chain and its markets variables into account and detects all relations among them. Accordingly, we propose an Analytic Network Process(ANP) and System Dynamics(SD) modelling to handle relations. Both of them are effective tools in decision making due to their feedback support natures. Integration of SD and ANP not only help managers to eliminate their disadvantages such as quality of dependency to expert judgments in analytical network process and unorganized nature of system dynamic approach but also provide comprehensive methodology to detect best alternative for strategy selection with considering decision board and long term effects of variables in decision making process.

II. EVALUATION METHODS

B. System Dynamics

Jay Forrester principally introduces system dynamics as a modelling method in Industrial Dynamics books [3]. Since then considerable advances have been made and it has become a valuable tool to represent, analyse and understand the dynamic behaviour of complex systems for strategic and policy related decision-making [4], [5], [6].

There is evidence that people don't make optimal decisions in dynamic environment and more so where there is a huge uncertainty attached to key variables [7], [8]. This fact can undermine all of the methods that use people's judgment in these circumstances such as ANP. System dynamic is useful methodology especially in complex systems such as supply chain with large amount of factors that influence each other in feedback loops where lack of information or large amount of data prohibits us from modelling the system precisely. Three main advantages of SD models, Deterministic evaluation, Sensitivity and Probabilistic Analysis, can help decision maker to predict any future status of system and effect of any policy in uncertain environment [9].

SD analysis includes four main steps:

1) causal-loops or influence diagrams:

The structure of a system in SD modelling is described using causal-loops diagrams (CLD). A CLD consists of variables connected by arrows denoting the causal influences among the involved variables as positive or negative loop in system boundaries identified according to the system objectives [3]. In our case it consist all of the factors that can affect our decision such as market, supply chain sections and other allied important variables. Fig. 1

2) simulation model :

The next step of the SD methodology involves the mapping of the causal loop diagram into a dynamic simulation model using specialized software. We used the Ithink software for this purpose. Mathematical equations are provided by statistical analysis on past ten years statistics gathering in Mapna equipment manufacturing Company.

3) Model validation:

In this stage we can use different method in order to find equations with high accuracy. The model is validated by confirmation of every element of it by the management of

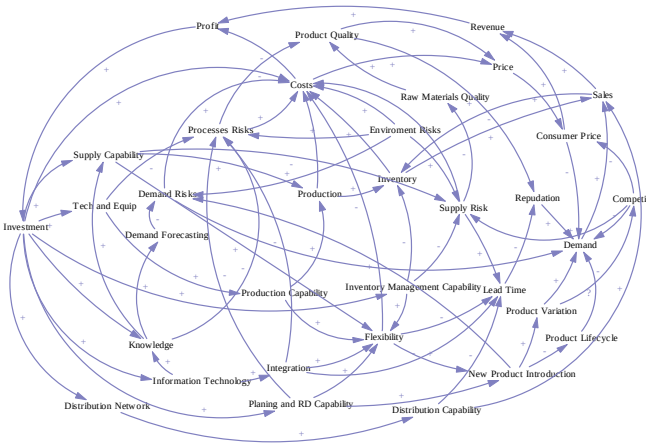

Fig.1 Supply chain causal loop diagram

subject Company. This is one of confident validation methods for system dynamics [3].

4) Scenario description:

After running model and sensitivity analysis the experts reach to scenarios guarantying success of company. Product's Price and Cost reduction, Lead time reduction and Increase in variation of products by introducing new ones are defined scenarios In this case.

Supply chain major driving forces behind supply chain linkage consist of Customer, monetary value, and Information, Knowledge and Risk elements [10]. In this case we consider them and other factors such as market variables and supply chain sections, other key components in Supply chain strategic decision process.

Although system dynamics is one of the powerful tools in decision making it is not void of problems especially in large systems. SD models often don't evaluate system's behaviour over time explicitly and only the pattern of behaviour preferred by modeller is presented and rationale of decision is omitted behind decision and as a result consequents don't evaluate formally. Therefore it is necessary to combine this method with another organized one like ANP to obtain more effective decision support system.

A. *Analytical Network Process*

The Analytical Network Process (ANP) extends the Analytical Hierarchy Process (AHP) to cases of dependence and feedbacks introduced by Thomas L. Saaty in 1980. it deals systematically with all kinds of interrelationships between the decision levels and attributes by obtaining the composite weights through the development of a ''super matrix.'' [11].

The ANP approach has been defined as a non-linear, capable to model more complex and dynamic environments and Due to rationale and abstract structure of analytical network process that facilitate decision, it was used to determine best choice in supply chain as complex systems[12], [13], [14].

The ANP is composed of four major steps [11]:

1) Model construction and problem structuring:

The problem are stated in a rational system, like a network obtained by decision-makers through brainstorming or other appropriate methods.

2) Pair wise comparison matrices and priority vectors:

Pairs of decision elements at each cluster are compared with respect to their importance towards their control criteria and Decision-makers are asked to respond to a series of pair wise comparisons of two elements.

3) Super matrix formation:

The super matrix concept is similar to the Markov chain process, where each matrix segment represents a relationship between two clusters in a system. Local priority vectors make the columns of super matrix and to obtain global priority of each element in each column elements of any cluster are multiplied in priority of that cluster obtained in pair wise evaluating of importance of clusters and final matrix is named weighted matrix. Raising a matrix to exponential powers gives the long-term relative influences of the elements on each other. To achieve convergence on the importance weights, the weighted super matrix is raised to the power of 2k þ 1, where k is an arbitrarily large number; the new matrix is called the limiting super matrix.

4) Selection of the best alternatives:

The alternative with the largest overall priority should be selected, as it is the best alternative determined by the calculations made using matrix operations.ANP model derived from causal loop diagrams and system dynamic model is shown in Fig.2.

Although, this method can handle the problems appropriately, it strongly depends on the experts' opinions completing pair wise comparison matrix. Sometimes due to the complexity of system and its long term behaviours they cannot correctly judge. Other factors such as bias Judgments and models misconception also affect the results of comparison. Considering all of these possibilities, we need another reliable method like system dynamics to solve mentioned problems.

III. METHODOLOGY

A. *Proposed Structure*

In this paper, we choose combination of system dynamics and analytical network process to offers integrated decision structure. Both fields are concerned with providing practical approaches to support decision makers across a wide spectrum of application areas especially at higher managerial levels by employing quantitative and qualitative models. The basis of ANP and SD is causal loop diagram that shows the relations

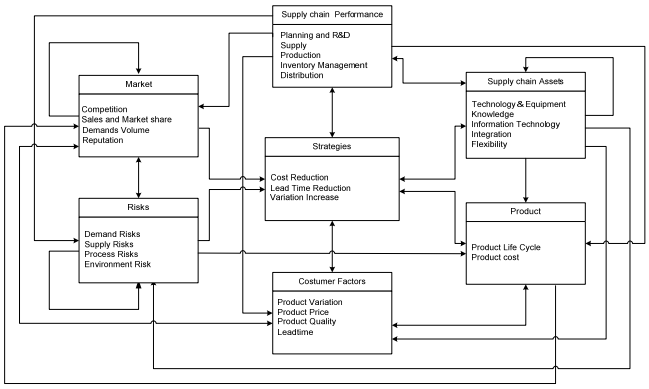

Fig. 2 Analytical Network Process model for supply chain strategy selection

and feedbacks among the model parameter. In fact SD model provides long term forecast for decision elements to determine their priorities and ANP model organizes our data and uses them to choice best alternative[15], [16]. Fig. 3 shows an overview of proposed structure in this paper.
strategic decision systems should be guarantee competitive advantage and explain clearly link between Costumers' criteria and performance Criteria. Moreover, It should be based on a systems thinking approach to manage system relations among business processes and allow scenario analysis[2].

Integration of System dynamics with analytical network process provide systematic framework to meet these 4 needs in our study.

B. Application of proposed model

It is necessary to describe how the supply chain should operate in order to compete. In manufacturing companies, consist an extensive supply chain, its business strategy determine rules in supply chain to gain success in competition with other companies.

In this case, Mapna Equipment Company, results of SD modelling leads to three proposed strategy. Managers can set all details aspects of these scenarios such as investment rate of the company in any field by observing long term effects. ANP model derived from CLD diagram and SD results also was illustrated before. To better understand, in Fig.2 we didn't merge clusters and considered them separately. However, due to flexibility of suggested method that let us to compare all of relations between elements, there are no need to consider several clusters and we can minimize them to 2 group including criteria and alternatives.

Super matrix is one of the powerful tools in analytical network process that allows a resolution of the effects of inter-dependence that exists between the elements of the system. In this paper, we suggest new method for completing super matrix to eliminate all of mentioned problems related to experts' judge. Simulation results are normalized in order to be compared with each other in same standard.

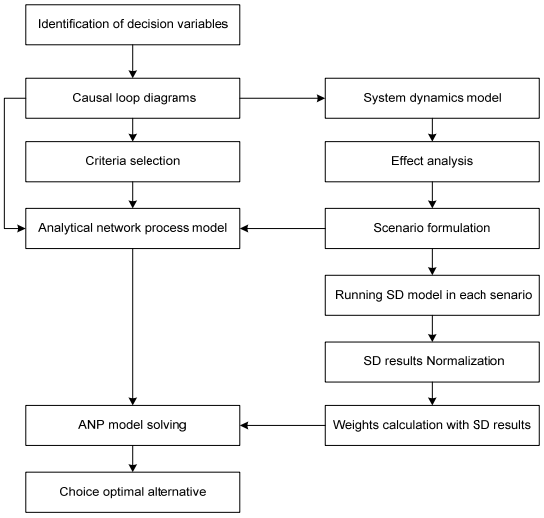

Fig. 3 Proposed decision support model

We encounter three types of comparison in this case:

1) First group consists of comparing relations between sub criteria and determining priorities. The results of simulation can help us to generate these priorities more accurate than before. Another advantage of this method is eliminating the clusters comparison that due to its general define and misconception can be misleading in some cases. Comparison between clusters is necessary because calculated weight in ANP model for every element in any cluster is not equal to overall priority of that element. In suggested model we can find overall priority of elements using results of simulation and calculating steeps. Steeps are best estimators of the influence for all elements of model. Fig. 4 shows 3 variables' trends (B, C, D) during time under influence of other decision variable (A). Priorities can be determined in each column based on calculations in Table.1

All of the similar priorities for criteria in ANP model are calculated by this method. Relative Results are imported in Super decision, a sophisticated and user friendly software that implements ANP [11].

2) Second type of relations includes the effects of criteria on alternatives. We want to know which of the strategies satisfies a criterion more and has more desirable influence for supply chain and business and rank three alternatives . This method helps us to consider important factors impact like time. Accepting our limitation in predicting long term behaviour of system, Time can change direction of decision and lead to failure. Therefore, simulation can assist us to predict them and take into account any possible change in future. We set board of decision and consider variables value in that time. To reach accurate estimation of priority of factors we use 3 & -3 as high & below border of normal distribution and calculate distance from these borders for special factors in any scenario based on its desirable or undesirable effect on system. Final score of a policy is calculated by dividing its distance to cumulative distances of all three scenarios' results. To better understand,

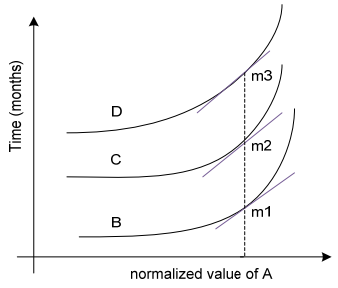

Fig.5 Flowchart of A's effect on other variables

TABLE 1
PRIORITIES OF RELATION BETWEEN VARIABLES

	A	B	C	D
A	1			
B	$\frac{m_2}{\sum_{i=2}^{3} m_i}$			
C	$\frac{m_3}{\sum_{i=2}^{3} m_i}$			
D	$\frac{m_2}{\sum_{i=2}^{3} m_i}$			

Table.2 clearly describes Suggested calculations for relative priorities in any column.

3) Third type of relations explains the effects of alternatives on criteria. Each strategy due to its investment policy changes the attributes differently. To assess these priorities we use first value of criteria and final value of them resulted from SD model running, for finding effect of each policy on related factors. The priorities of effects are calculated by dividing any change to overall value in each particular policy (a_i) as shown in Table.3.

$$x_{A/a_i} = |Final\ value\ of\ A\ in\ a_i - Initial\ value\ of\ A|. \quad (1)$$

Priorities derived from second and third part also are imported in super decision to further calculations. In the illustrative example the results of the logistics strategic analysis by Super Decision tools point to selection of Alternative lead-time reduction for System, which has the largest normalize desirability index of "0.42".

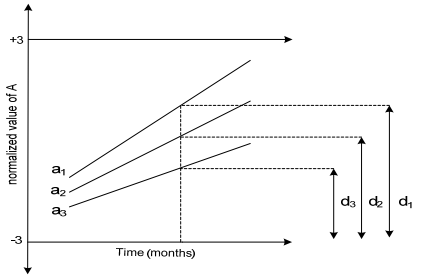

Fig. 5 Changes of A in 3 proposed strategies

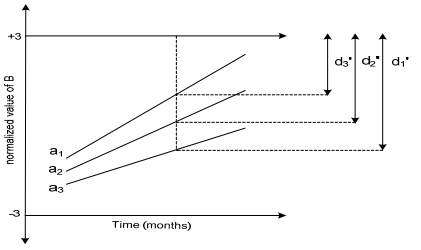

Fig. 6 Changes of B in 3 proposed strategies

Table 2
PRIORITIES OF STRATEGIES FOR CRITERIA

	A	B	C
a_1	$\frac{a_1^1}{\sum_{i=1}^{3} a_i^1}$	$\frac{a_1^2}{\sum_{i=1}^{3} a_i^2}$	
a_2	$\frac{a_2^1}{\sum_{i=1}^{3} a_i^1}$	$\frac{a_2^2}{\sum_{i=1}^{3} a_i^2}$	
a_3	$\frac{a_3^1}{\sum_{i=1}^{3} a_i^1}$	$\frac{a_3^2}{\sum_{i=1}^{3} a_i^2}$	

Table 3
PRIORITIES OF VARIABLES THAT STRATEGIES AFFECT THEM

	a_1	a_2	a_3
A	$\frac{x_{A/a_1}}{x_{A/a_1} + x_{B/a_1} + x_{C/a_1}}$	$\frac{x_{A/a_2}}{x_{A/a_2} + x_{B/a_2} + x_{C/a_2}}$	
B	$\frac{x_{B/a_1}}{x_{A/a_1} + x_{B/a_1} + x_{C/a_1}}$	$\frac{x_{B/a_2}}{x_{A/a_2} + x_{B/a_2} + x_{C/a_2}}$	
C	$\frac{x_{C/a_1}}{x_{A/a_1} + x_{B/a_1} + x_{C/a_1}}$	$\frac{x_{C/a_2}}{x_{A/a_2} + x_{B/a_2} + x_{C/a_2}}$	

IV. CONCLUSION

This paper presents potentials of integrating two powerful decision methods, System Dynamics and Analytical Network Process, in strategic supply chain management. Both are based on causal loop diagrams and consider interdependencies among decision parameters. The supply chain is source of the value generated by firm would benefit from having its strategy formulated in parallel with the firm's business level strategy in order to reduce inefficiency of strategy by participation of higher management instead of middle level managers.

System dynamics basis is system thinking and it helps us to model system without requirement to detail and exact data and traces long term behaviour of system's elements. It is important especially in strategic decision making to know consequents of decisions which are usually subjects of this analysis. Combination of these two methods allows us to increase confidence level of decision with eliminating pair wise comparison in ANP and organizing the results of SD model. We illustrate method in extended case conducted by Strategic planning department of Mapna Equipment Company.

This decision support system has the potential to be used in integration with other strategies of supply chain by adding other variables to causal loops diagrams or breaking down to detail levels in supply chain sections.

REFERENCES

[1] D.M., Lambert, M.C., Cooper, Issues in supply chain management, Industrial marketing management, 29, 65-83..

[2] G.N., Stock, N. P., Greis, J. D., Kasarda, 1998, "Logistics, Strategy, and Structure: A Conceptual Framework," International Journal of Physical Distribution & Logistic Management, Volume 29 Number 4.

[3] J.W., Forrester, 1961,Industrial Dynamics. The M.I.T. Press.

[4] S. A., Cavaleri, J. D., Sterman, (1997). Towards Evaluation of Systems Thinking Interventions: A Case Study. System Dynamics Review, 13(2), 171-186.

[5] P., Otto, A system dynamics model as a decision aid in evaluating and communicating complex market entry strategies, Journal of Business Research 61 (2008) 1173–1181.

[6] E., Zahn, R., Dillerup, U., Schmid, 1998, Strategic evaluation of flexible assembly systems on the basis of hard and soft Decision criteria. System Dynamics Review, 14(4), 26.

[7] B., Brehmer, Dynamic Decision Making: Human Control of Complex Systems. Act Psychologica, 81, (1992), 206-223.

[8] J. D., Sterman, (2000). Business Dynamics: Systems Thinking and Modeling for a Complex World. Boston: Irwin/McGraw-Hill.

[9] R., Dhawan, 2006, "System dynamics and its impact on managerial decision making" University of Sydney (Hrsg.), Sydney.

[10] H., Min, G., Zhou, Supply chain modelling: past, present & future, Computers and Industrial engineering, 43(2002) 231-249.

[11] T.L., Saaty, 2001, Decision Making with Dependence and Feedback: The Analytic Network Process, second ed. RWS Publications, USA.

[12] A., Agarwal, R., Shanker, M.K., Tiwari, Modelling the metrics of lean, agile and leagile supply chain: An ANP-based approach, European Journal of Operational Research 173 (2006) 211–225.

[13] A. K., Choudhury, M. K., Tiwari, S. K., Mukhopadhyay, Application of ANP to strategic planning problems of a supply chain cell, Production Planning & Control, Vol. 15, No. 1, January 2004, 13–26.

[14] L., Mead, J., Sarkis , 1998, Strategic Analysis of logistics and supply chain management systems using the Analytical Network .

[15] J., Ashayeri, R., Kajy, Global business process re-engineering: a system dynamics approach, International journal of Operations, Vol. 18,No 9/10, 1998.

[16] D., Tesfamariam, B., Lindberg , Aggregate analysis of manufacturing systems using system dynamics and ANP, Computers & Industrial Engineering 49 (2005) 98–117.

2011 International Conference on Mechanical, Industrial, and Manufacturing Engineering
Lecture Notes in Information Technology Vols. 1-2

Development of Graphical User Interface for Reconfiguration of Manufacturing Automation System

Muhamad Arfauz A Rahman
Manufacturing and Materials Engineering
RMIT University
Bundoora, Victoria 3083, Australia
s3223098@student.rmit.edu.au

John P.T. Mo
Manufacturing and Materials Engineering
RMIT University
Bundoora, Victoria 3083, Australia
john.mo@rmit.edu.au

***Abstract* – The main objective of this work is to create a new method in developing a highly flexible manufacturing framework which will be easily reconfigurable for upcoming production needs. In this paper, the initial development of Graphical User Interface (GUI) for compensating the current development of the reconfiguration framework of manufacturing automation system is described. A user friendly interface to the system engineer for ease of system reconfiguration has been developed. The GUI is divided into three main sections. The first contain the requirement, specifications and constraint component. The next section consists of the steps and options component while the final section shows the optimization stage of the works. The components are mainly extracted from the steps and work descriptions provided by the user requirements and specifications as well as some constraints. In order to simplify the configuration and reconfiguration works, these information are essentials. Later, the layout of this GUI will be integrated with the specific rules and algorithm which is concurrently being developed.**

Index Terms – Reconfiguration, Manufacturing Automation System, Framework for flexible configuration, Graphical User Interface.

I. Introduction

Due to the fluctuating and changing market demand in product needs, the available current system is sometimes not capable to produce the product accordingly. Changes in system requirements and low flexibility of the system are amongst the challenges that limit the system's ability [1]. The system need to be configured and reconfigured accordingly from time to time in order to adapt with the new situation. Currently, the way system design engineers reconfigure their flexible system is through a time consuming evaluation and costly redevelopment [2-4]. Introducing the more suitable method which allows the manufacturer to easily reconfigure with less time and investment is an immense step towards competitive manufacturing.

A. Manufacturing Automation System Reconfiguration

Rahimifard and Weston define reconfiguration as a change capability to be invoked when requirement arises to realize a new set of reachable states [5]. Currently, the most common method in system reconfiguration which is done by the system/design engineer is through traditional system reconfiguration [6]. The current system will be reconfigured accordingly to suit with the manufacturing process of the product and requires heaps of discussions, paper works and human involvement. In this case the entire process of reconfiguration of the system requires a lot of effort, time and sometimes cost. Those factors indeed give a huge burden to company to set up their new system in many ways. A simple yet cost effective method needs to be introduced for simplifying the reconfiguration process.

At this stage, the research requires diverse concept not limited to initially configure a new system but also to reconfigure the existing system. In a flexible reconfigurable framework, the goal is therefore not about adapting one system to another, but rather to develop a system design from a task description independent of the platform, and subsequently carry out a matching process that assigns components to achieve the specified function [7]. To achieve this goal, the system development process is divided into two stages as shown in Fig. 1.

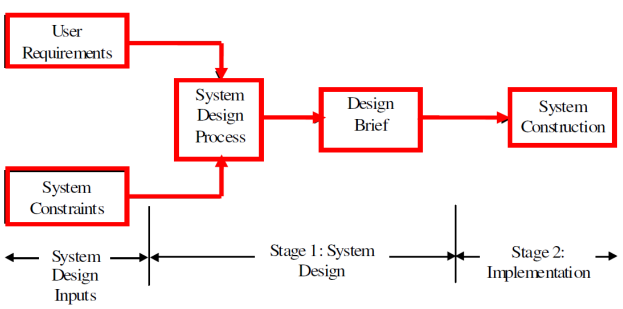

Fig. 1: Platform/framework stage

The level of configuration and reconfiguration process shown in Fig. 1 can be divided as follow:

1) Initial Design inputs level - input: This includes capturing the user requirements/specifications and constraint, analyzing the user requirements/specifications and constraint, and determining the required steps.

2) System Design level - stage 1: This stage will relate the steps and combine with an appropriate condition as well as choosing available, suitable and additional new parts.

3) Implementation level - stage 2: This stage involves representing and optimization the system.

All levels perform different activities in order to achieve the configuration and reconfiguration target. This research work concentrates mostly on all level. The initial development of Graphical User Interface (GUI) is described.

The goal is to provide a user friendly interface to the system engineer for ease of system reconfiguration. It is crucial to come out with the good interface for the user to capture the requirements and specifications as well as to manipulate the inputs.

Due to various changing needs, such as for new product development, addition or removal of physical components in the system will be severely occur as well as for financial reasons. On top of that, Mo et al. state that in building an automation system, components required may be associated through physical or non physical specifications at different types [8].

II. FLEXIBLE RECONFIGURATION FRAMEWORK

The main activity is the system design process. Firstly, capturing user requirements and specifications is essential steps to simplify the configuration and reconfiguration works. In this work, system process conditions are required in order to commence the automation system reconfiguration. The general view of the automation system can be obtained once all the necessary conditions are in place. All the conditions may describe the current state or situation of the propose automation system. These conditions give only a general view of the system in which any suitable components are possible to be used as long as it can successfully complete the given task based on the specifications. Base on the levels of the system development process, the general instruction of the propose automation system in stage 1 is called process instructional guide as shown in Fig. 2. This process instructional guide provides design brief for the specific task which can be obtained from the user specification.

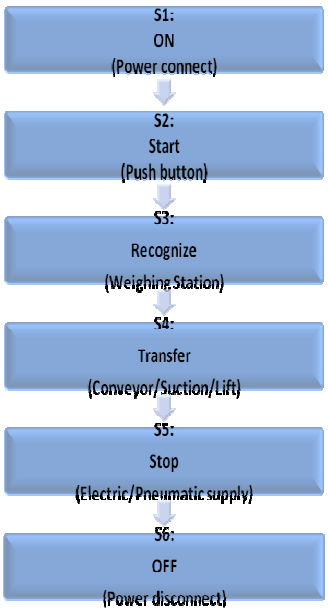

Fig. 2: Process Instructional Guide with Component Specification

At the later stage, the initial process instructional guide needs to be complemented with more sufficient information. At this stage various possible and suitable components are being matched with the process instructional guide. The process requires some sort of intelligence aspect in order to carefully match with the instruction. All the possible components may best suit with the current state or situation of the propose automation system accordingly. These components are possible to be used as long as it can successfully complete the given task based on the specifications. Additional possible components may be added or changed accordingly from time to time to suit with the updated the conditions of the automation process.

The framework will then search for the components that can be used to fulfil the specified user requirements and specifications. Accessory repository has a number of components including cylinders of different length, several types of sensors, a wide variety of connector tubes, clamps, etc. Mo et al. elaborated that system parameters such as length of cylinders and sensors are selected from the component repository as shown in Fig. 3.

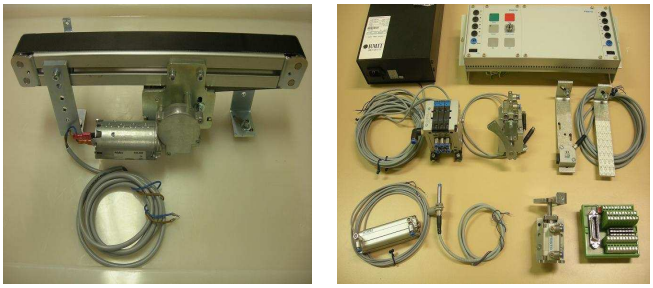

Fig. 3: The conveyor and components

Generally, the proposed system may be more than one system. More complete work description which incorporates the steps, instructions and possible component specification is now implemented. At this stage, engineers will have more clear view of the propose automation system. Nevertheless, the components listed can be changed accordingly to suit with the physical or non physical constraints.

III. DEVELOPMENT OF GRAPHICAL USER INTERFACE (GUI)

A. Interface for System Requirements and Specifications

The first step is to capture the user requirements either in a form of verbal or written requirements. The users requirements will describe the environment, the way it should be, after the system or machine is integrated. It consists of functional and non-functional requirements. Functional requirements state how the system should act. On the other hand, non-functional requirements concern quality characteristics such as efficiency or user-friendliness. The next step is to identify and capture the user specifications. Specifications are the descriptions that are sufficient for building the system or machine. Fig. 4 shows the proposed the

basic model of manufacturing reconfiguration for capturing user requirements and user specifications.

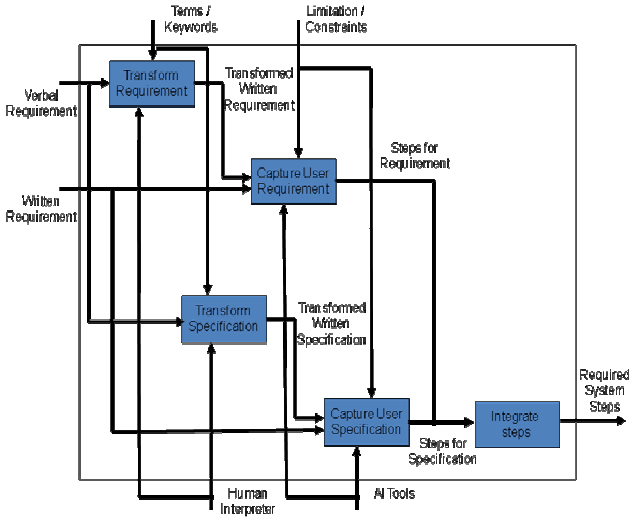

Fig. 4: User Requirements and Specifications Model

The next step is to generate a methodology for putting the entire user requirement and the possible design of the manufacturing system into one context which later provide the best design outcome for the design of manufacturing system. The form of interface for obtaining all necessary information such as user requirements, user specifications and other constraints is shown in Fig. 5.

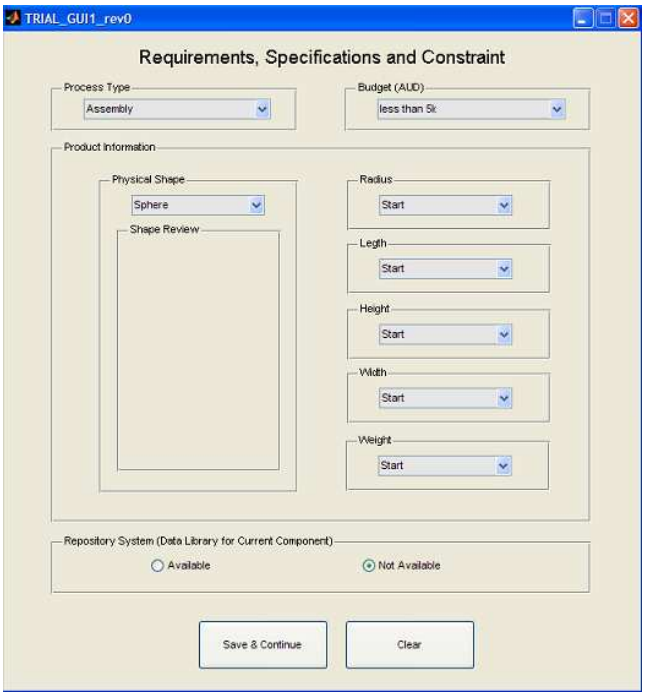

Fig. 5: Interface for Inputs Gathering

The work scenario descriptions which are generally present user requirements and user specifications for the intended manufacturing automation system will be used to enter all information required. These requirements and specifications are the key information for the design of the proposed system and need to be extracted. In order to simplify the extraction efforts, this research introduces method of capturing these requirements and specifications.

B. Identification of Steps and Options

Once the requirements, specifications and constraints are extracted, these crucial components are further manipulated to provide an optimum steps for the complete process of the system. Further configuration and reconfiguration process will be conducted base on these steps. The next interface will let the system/design engineer to decide on the manufacturing process route suitable for their application. The following Fig. 6 shows the interface for identification of necessary steps and available options for user.

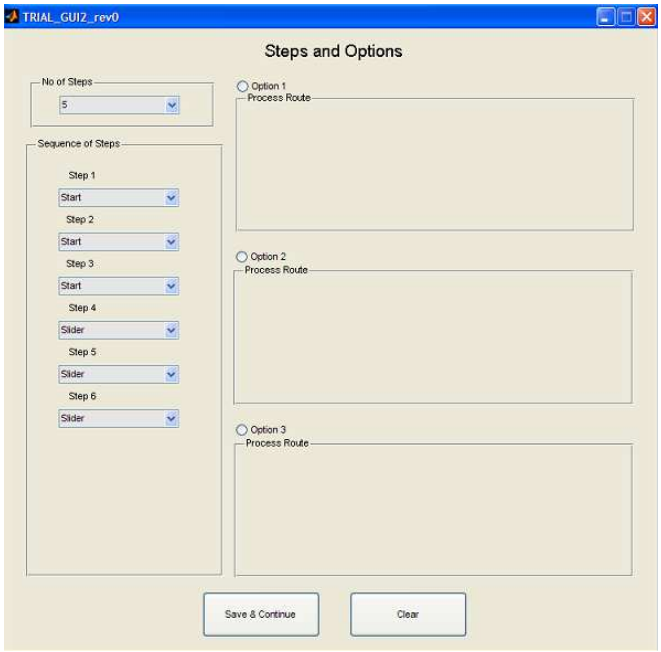

Fig. 6: Steps and Options Identification

At this stage, the configuration and reconfiguration has been simplified and can be used to develop the proposed flexible reconfigurable framework. The framework also requires a set of list of components which can be obtained from the current system or initially stored in the framework data library. This data library which is developed from the previous configuration study is known as library of component.

C. Optimizations Interface

In this section, the process involves determining the best possible components for the system to be configured and reconfigured for various conditions based on work scenario

descriptions. The following Fig. 7 shows the optimization interface which has been develop.

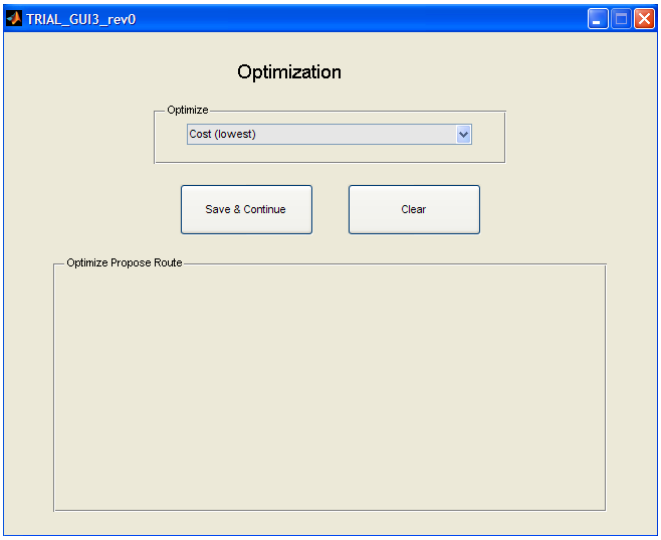

Fig. 7: Optimization Interface

Some of the key components include in this section of the interface are the cost, number of components and process time. The interface will give the user the freedom to choose the final optimization factor.

IIV. FURTHER WORKS

Concurrent with the development of this GUI layout, the main rules and algorithm are also being developed. The construction of all rules and algorithm are based on the study conducted prior to this development stage. The rules and algorithm will be constructed using the MATLAB programming language.

Later in this research work, the rules, algorithm, GUI layout will be combined to form the initial platform for manufacturing system reconfiguration. This platform will be tested using the current laboratory setup in the school of Aerospace, Mechanical and Manufacturing Engineering at RMIT University. The development process will then hope to continue with implementing a series of intelligent algorithms for planning a highly complex robotic production line using a PC based virtual reality analysis tool to provide visualization capability to the research.

V. CONCLUSIONS

At this stage, the basic layout of GUI using GUIDE platform in MATLAB to capture and manipulate the user requirements and specifications and later provide an optimum solution for the design of flexible and reconfigurable manufacturing automation system is developed. The basic idea is to develop an interface for flexible reconfigurable framework in order to assist the system/design engineer to easily reconfigure a new set up based on new user requirements through capturing user requirements and specifications. Introducing the user friendly interface for flexible reconfigurable framework allows the manufacturer to easily reconfigure their automation system faster and with no or low investment is an immense step towards competitive manufacturing. This research work is hoped to benefit the industry through reducing human involvement while trying to optimize the current system and at the same time minimizing the risk of future investment.

ACKNOWLEDGMENT

The present work involves physical experiments through exploring a unique platform of flexible manufacturing cell called Targeted Technology Introduction Module (TTIM) system supplied by SAGE Automation, several types and models of robots, various associated automation equipments and other manufacturing facilities in the School of Aerospace, Mechanical and Manufacturing Engineering at RMIT University, Australia.

REFERENCES

[1] Ferscha, A., et al., *Building FlexibleManufacturing Systems Based on Peer-Its.* EURASIP Journal on Embedded Systems, 2008. **vol. 2008**.

[2] Abdi, M.R., *Layout Configuration Selection for Reconfigurable Manufacturing Systems Using the Fuzzy AHP.* International Journal of Manufacturing Technology and Management, 2009. **vol. 17**(1/2): p. pp.149-165.

[3] Álvarez, R., et al., *Redesigning An Assembly Line Through Lean Manufacturing Tools.* The International Journal of Advanced Manufacturing Technology, 2009. **vol. 43**(9): p. pp. 949-958.

[4] ElMaraghy, H.A., O. Kuzgunkaya, and R.J. Urbanic, *Manufacturing Systems Configuration Complexity.* CIRP Annals - Manufacturing Technology, 2005. **vol. 54**(1): p. pp. 445-450.

[5] Ramimifard, A. and R.H. Weston, *A Resource-Based Modelling Approach to Support Responsive Manufacturing Systems.* The International Journal of Advanced Manufacturing Technology, 2009. **vol. 45**(11): p. pp. 1197-1214.

[6] Galan, R., et al., *A Methodology for Facilitating Reconfiguration in Manufacturing: The Move Towards Reconfigurable Manufacturing Systems.* The International Journal of Advanced Manufacturing Technology, 2007. **vol. 33**(3-4): p. pp. 345-353.

[7] Rahman, M.A.A. and J.P.T. Mo. *Design Methodology for Manufacturing Automation System Reconfiguration*. in *ASME 2010 International Mechanical Engineering Congress & Exposition*. 2010. Vancouver, British Columbia, Canada: ASME.

[8] Mo, J.P.T., P. Dawson, and M.A.A. Rahman. *Active Learning Approach in Developing Engineering Design Skill through Open Ended System Specification*. in *20th Australasian Association for Engineering Education Conference*. 2009. University of Adelaide, Adelaide, Australia.

2011 International Conference on Mechanical, Industrial, and Manufacturing Engineering
Lecture Notes in Information Technology Vols. 1-2

Issues in Model Building for Multiple Response Surface Problems

Amineh Zadbood
Department of Industrial Engineering
Iran University of Science & Technology
Tehran, Iran
zadbood85@ind.iust.ac.ir

Kazem Noghondarian
Department of Industrial Engineering
Iran University of Science & Technology
Tehran, Iran
noghondarian@iust.ac.ir

***Abstract* –Selection of optimum conditions on control variables often involve considering multiple response characteristics simultaneously. This is called a Multiple Response Surface Problem and encounters in many manufacturing applications. Optimization phase has been the main focus of attention in most research so far. However, data collection and statistical model building are challenging issues. The main aim of this paper is to take a detailed look at the most prominent works that has discussed building the model in Multiple Response Surface Problems. In addition, classifies optimization techniques that have been used after each type of model building. In the conclusion it is suggested that the model Robust Regression Technique, a semiparametric method can be substituted in the modeling phase of well-known works in the literature to obtain better results. In addition, applying artificial neural networks instead of polynomial regression methods may lead to a better estimate of the relationship between responses and variables.**

Index Terms – multiple response surface problem, Model Robust Regression, Model Building , Response Surface Methodology, Artificial Neural Networks.

I. INTRODUCTION

Response surface methodology (RSM) is a group of statistical and mathematical techniques used in product/process optimization [1]. Most common problems in RSM studies have paid more attention to the relationship between one response of interest and several input variables. However, many manufacturing applications deal with Selection of optimum conditions of control variables considering multiple response characteristics simultaneously. This is called a Multiple Response Surface (MRS) Problem.

The multiple response surface problems have three seminal stages: data collection, model building and optimization. Optimization phase has been the main focus of attention in most research so far. However, data collection and statistical model building are challenging issues. In this paper we will focus on the model building phase.

For building the regression model three major techniques have been applied in the MRS studies: Parametric, non parametric and semiparametric.

In order to construct the regression model, suppose there is a response variable y, and m controllable input variables, $x_1,...,x_m$. The form of the relationship is written in equation (1):

$$y = f(x_1,...,x_m) + \varepsilon \quad (1)$$

The form of the true response function f is not known, and the random error (ε) in the system or process is included in the equation.

Ref. [2] states that a parametric model can describe most of the data. However, if data derivate from the specified model a parametric model would not be much sufficient [2].

A nonparametric would not consider the significant information of the researcher when it fits the model [2].

A model robust regression technique, a semiparametric method has exhibited more robustness to model misspecification than the two other methods [3].

In this paper, we review and discuss existing methods for model building phase of an MRS problem. Section 2 reviews the parametric,nonparametric and semiparametric methods. Section 3 discusses a data mining approach that is recently presented for Multiresponse optimization. It is presented by Lee and Kim (2008) and presents a way to solve the optimization problem without building a statistical model. Section 4 is about the use of artificial neural networks to estimate the relationship between some responses and input variables. Section 5 discussed the optimization techniques that have been used for each type of model building. Section 6 presents the conclusions and future areas for research.

II. MODEL BUILDING TECHNIQUES REVIEW

A. *Parametric Method*

In this method we assume known linear form for f, and write the model in the following form:

$$y = X\beta + \varepsilon \quad (2)$$

For n response variables, X is a n*s matrix and β is a s*1 vector of parameters. β is unknown and the parameters should be estimated.

Ordinary least squares (OLS) is a common method that is usually used to estimate the fits.

$$\hat{y} = X\hat{\beta} = X(X'X)^{-1}X'y \quad (3)$$

B. *Nonparametric Method*

In the situations when the parametric function in equation 2 is not correct, a nonparametric method would be a good option [3].In this method there is no assumption about the parametric relationship between the response and variables [3].Among the different smoothness fitting techniques in nonparametric approach, here we just review the Local Polynomial Regression (LPR) as is described by Ref [3].

Ref. [3] focuses on the 1st order polynomial and find the fit at $x_1 = (x_{11}, ..., x_{m1})$ as follows:

$$\hat{y}_1 = \tilde{x}_1 (\tilde{X}' W_1 \tilde{X})^{-1} \tilde{X}' W_1 y \qquad (4)$$

W is the local weight matrix [3].

C. *Semiparametric Method*

Semiparametric method has the advantages of both parametric and nonparametric method [3]. Model Robust Regression (MRR) is introduced first by 3 .It is very suitable for the situations when the researcher has incomplete knowledge about the model and can be used in designed experiments problem [3].

the parametric fit with the nonparametric one are combined with a mixing parameter Landa[3].

The fit at x_1 is as follows :

$$\hat{y}_1 = \hat{x}(X'X)^{-1} X'y +_1 \lambda \tilde{x}_1 (\tilde{X}' W_1 \tilde{X})^{-1} \tilde{X}' W_1 y \qquad (5)$$

For a detailed study of the mixing parameter and smoothing parameter see [3].

III. Direct Optimization without Building a Model

In Ref. [4] the authors state that a good empirical model is sometimes difficult to obtain from the process data. Therefore an approach is required that directly solves the multiple response problem without a model building [4].

The approach is called patient rule induction method (PRIM) .The objective in this approach is to find small box-shaped regions of control variables that in that region the average value of the response variable is significantly larger than its average value over the whole region [4].

IV. Artificial Neural Networks

Noorossana et al.(2009) proposed the use of artificial neural networks in order to estimate quantitative and qualitative responses [5].They explain that in some situations polynomial regression methods have difficulties in estimating the relationship between responses and input variables because of the complexity of the problem[5] .Therefore, artificial neural networks would be a suitable alternative[5].

Another recent work in this area is the paper by Aminnaseri et al. (2010) [6].They estimate the relationship by artificial neural networks, and in the optimization phase apply Genetic Algorithm [6].

V. Optimization

Numerous Methods have been introduced for multiple response optimizations in the literature. Here we just focus on the most prominent ones: constrained optimization, the desirability function approach and the loss function approach.

A. *Desirability function approach*

This approach is about transforming an estimated response like $\hat{y}_i(x)$ to a scaled free value called desirability. Desirability changes from 0 to 1. The overall desirability (D) in the [0, 1] interval is acquired by combining all the desirabilities (d_i) [7]. Derringer and Suich (1980) extended the idea and proposed a method to construct an overall desirability [8].

Here a Desirability function for the larger-the-better case is shown:

$$d_i = \begin{cases} 0 & \hat{y}_i(x) \le y_i^{min} \\ \left[\dfrac{\hat{y}_i(x) - y_i^{min}}{y_i^{max} - y_i^{min}}\right]^t & y_i^{min} \le \hat{y}_i(x) \le y_i^{max} \\ 1 & \hat{y}_i(x) \ge y_i^{max} \end{cases} \qquad (6)$$

In the above equation, the min and max indexes on the y shows the lower and upper limits accepted for $\hat{y}_i(x)$ respectively.

B. *Loss function approach*

Pignatiello (1993) proposed a squared error loss function as follows [9]:

$$L(y(x)) = (y(x) - \Phi)' C (y(x) - \Phi) \qquad (7)$$

Where:

y(x) = response vector,

Φ = target vector,

C = cost matrix.

The cost matrix states the relative importance of the response variables.

More detailed studies about this approach can be found in Vinning (1998) [10], Tsui (1999) [11], Riberio et al. (2000) [12].

C. *Constrained Optimization*

A distinguished approach is to consider the problem as a constrained optimization [1]. Kim gave the name priority

based approach to it [13]. The priority based approach selects the response with the highest importance as the objective function and the rest of the functions are considered as constraints, though it is not always much straightforward.

The idea was first proposed by Myers and Carter (1973) [14]. Two responses are referred as a "primary response" and a "constraint response". The objective here is to find optimum conditions on a set of design variables which maximize the primary response function subject to the constraint response function. Biles (1975) considered multiple process responses and extended the Myers and Carters idea [15]. The priority based approach was also studied in the later years by Delcastillo and Montgomery (1993) [16].

The table below classifies works in the literature considering the model building method and the optimization technique. It can be noticed that when semiparametric approach or artificial neural networks have been used for model building, most authors prefer to use desirability function for the optimization phase.

TABLE I
CLASSIFICATION

Types of Model	Most popular MRS approaches

Building	Constrained Optimization	Desirability Function	Loss Function
Parametric	✓	✓	✓
Nonparametric		✓	
Semiparametric		✓	
No modeling, direct optimization		✓	
Artificial Neural Networks		✓	

CONCLUSIONS

In this article existing approaches in model building for a multiple response surface problem are reviewed and discussed. Semiparametric approach has the advantages of both parametric and nonparametriv methods. Although semiparametric method has shown significant properties, most works in the literature have used the parametric approach. It would be a good idea to substitute the semiparametric method, for instance model robust regression in the modelling phase of prominent works in the MRS to lead to better results.Another good alternative is using artifiaical neural networks to estimate relationships.

Future studies can focus on the use of artificial neural networks approach in problems that have used loss function or process capability approach in the optimization phase.

REFERENCES

[1] Myers, R.H., and Montgomery, D.C., Response Surface Methodology: Process and Product Optimization using Designed Experiments,second edition,USA , Wiley ,2002

[2] Mays JE, Birch JB, Starnes BA, "Model Robust Regression: combining parametric, nonparametric, and semiparametric methods",*Nonparametric statistics*, vol. 13, pp. 245-277, 2001.

[3] Wan W, Birch JB, , "a Semiparametric technique for the multi response optimization problem" Tech report,Virginia tech university , 2009.

[4] Lee M.S,Kim K.J "MR-PRIM:patient rule induction method for Multiresponse optimization," *quality engineering*,vol 20,pp. 232-242,2008.

[5] Noorossana. R., Davanloo Tajbakhsh S.,Saghaei A, "An artificial neural network approach to multiple response optimization", *International journal of advanced manufacturing technology*,40:1227-1238,2009.

[6] Aminnaseri M.R., Baradaran Kazemzadeh R.,Salmasnia A,Salehi M,"optimization of multi response process using artificial neural networks and genetic algorithm",7th international conference on Industrial Engineering,Iran,Isfahan,2010.

[7] Harrington. E.Jr, "the desirability function",*industrial quality control*, 21,494-498,1965.

[8] Derringer, G., and Suich, R.,. "Simultanous Optimization of Several Response Variables", *Journal of Quality Technology*, Vol. 12, No. 4.pp. 214-219,1980.

[9] Pignatiello, J. J., Jr., "Strategies for Robust Multi-response Quality Engineering", *IIE Trans*., 25, 5-15 ,1993.

[10] Vinning ,G G. ,"a compromise approach to Multiresponse optimization", *Journal of Quality Technology,* 30, pp. 309-313,1998.

[11] Tsui, K. ,"robust design optimization for multiple characteristics problems", *international journal of production research,* 37,.pp. 433-445,1999.

[12] Riberio,J and Elsayed,E. ,"a case study on process optimization using the gradient loss function" , *international journal of production research,* 33,.pp. 3233-3248,1999.

[13] Kim, K. J., Byun, J. H., Min, D., Jeong, I. J., "Multiresponse Surface Optimization: Concept, Methods, and Future Direction", (Tutorial), *Korea Society for Quality Management*, 2001.

[14] Myers R.H., and Carter W.H., "Response surface techniques for dual response systems",*Technometrics*,15,1973,301-317

[15] Biles, W., "A response surface method for experimental optimization of multi response processes,industrial and engineering chemistry", process design and deployment,14, ,152-158,1975.

[16] Del Castillo, E., Montgomery, D. C.," A Nonlinear Programming Solution to the Dual Response Problem", *Journal of Quality Technology* 25, pp. 199-20,1993.

161-171

2011 International Conference on Mechanical, Industrial, and Manufacturing Engineering
Lecture Notes in Information Technology Vols. 1-2

Inertial Navigation System for Omni-directional AGV with Mecanum Wheel

Jungmin Kim, Jungje Park and Sungshin Kim
School of Electrical Engineering
Pusan National University
Geumjeong, Busan 609-735, Korea
{kjm16, parkjj & sskim} @pusan.ac.kr

Abstract **- This paper presents INS (inertial navigation system) as the localization for an omni-directional AGV (automatic guided vehicle) with Mecanum wheels. The Mecanum wheel is one design for the wheel which can move in any direction, is a conventional wheel with a series of rollers attached to its circumference. The localization techniques for the general mobile robot use basically encoder. Otherwise, they use gyro and electronic compass with encoder. However, it is difficult to use the encoder because the Mecanum wheel occurs frequently the slip by the rollers attached to conventional wheel's circumference. Hence, we propose the localization of the omni-directional AGV with the Mecanum wheel. The proposed localization uses encoder, gyro, and accelerometer. In this paper, we ourselves designed and made the AGV with the Mecanum wheels for experiment. And we analyzed the accuracy of the localization when the AGV moves sideways to 20m distance at about 20cm/s and 38cm/s, respectively. In experimental result, we verified that the accuracies of the proposed localization have 27.4944mm and 29.2521mm, respectively.**

Index Terms - AGV, INS, Mecanum wheel, omni-directional

I. Introduction

Recently, the interest in the AGV has been increased as the amount of logistics has been increasing. However, the existing AGVs don't work effective in the narrow workspace because its direction can only change during moving forward or backward. Hence, the interest in the omni-directional AGV was growing, and there are many studies [1-7]. The Mecanum wheels are a conventional wheel with a series of rollers attached to its circumference. These rollers have an axis of rotation at 45° to the plane of the wheel in a plane parallel to the axis of rotation of the wheel. As well as moving forward and backward like conventional wheels, they allow sideways movement by spinning wheels on the front and rear axles in opposite directions. However, it is difficult to use the encoder because the Mecanum wheel occurs frequently the slip by the rollers attached to conventional wheel's circumference. Hence, we propose the localization of the omni-directional AGV with the Mecanum wheel. The proposed localization uses encoder, gyro and accelerometer.

II. Measurement System

In this paper, we designed and made the AGV with the Mecanum wheels for experiment of localization.

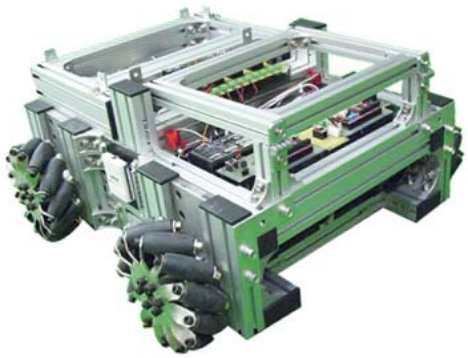

Fig. 1 Omni-directional AGV

The AGV has four Mecanum wheels, four 300W BLDC motors (TM-90D0321), motor drivers which control each of the motors. In addition, we use a laptop for rapid development, and a DAQ (data acquisition) to control the motor driver efficiently. Fig. 1 shows the designed omni-directional AGV with Mecanum wheels.

A. Kinematics

Fig. 2 shows the kinematics of AGV with Mecanum wheel.

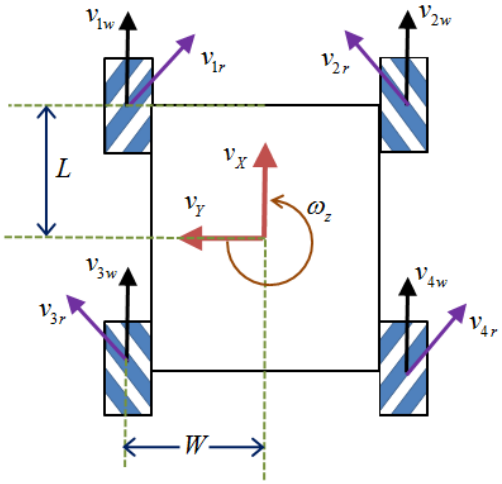

Fig. 2 Kinematics of robot with Mecanum wheel

In Fig. 2, L is the distance between the instantaneous center of rotation (ICR) and the center of front wheels or rear wheels. And W is the distance between front wheels or rear wheels. v_{iw} is the linear velocity by rotation of the wheels, and v_{ir} is actual force acting on the ground by rollers on Mecanum wheel. Because the rollers have an axis of rotation at 45° to the plane of the wheel, v_{iX} and v_{iY} are calculated by v_{iw} and v_{ir} as follows.

$$\begin{aligned} v_{1X} &= v_{1w} + \frac{v_{1r}}{\sqrt{2}}, v_{1Y} = \frac{v_{1r}}{\sqrt{2}} \\ v_{2X} &= v_{2w} + \frac{v_{2r}}{\sqrt{2}}, v_{2Y} = \frac{v_{2r}}{\sqrt{2}} \\ v_{3X} &= v_{3w} + \frac{v_{3r}}{\sqrt{2}}, v_{3Y} = \frac{v_{3r}}{\sqrt{2}} \\ v_{4X} &= v_{4w} + \frac{v_{4r}}{\sqrt{2}}, v_{4Y} = \frac{v_{4r}}{\sqrt{2}} \end{aligned} \quad (1)$$

To summarize the above equation into v_{1w}, v_{2w}, v_{3w}, v_{4w} is represent by

$$\begin{aligned} v_{1w} &= v_X - v_Y - (L+W)w_z \\ v_{2w} &= v_X + v_Y + (L+W)w_z \\ v_{3w} &= v_X + v_Y - (L+W)w_z \\ v_{4w} &= v_X - v_Y + (L+W)w_z \end{aligned} \quad (2)$$

Here, the above equation represented by a matrix is as follows.

$$\begin{bmatrix} v_{1w} \\ v_{2w} \\ v_{3w} \\ v_{4w} \end{bmatrix} = \begin{bmatrix} 1 & -1 & -(L+W) \\ 1 & 1 & (L+W) \\ 1 & 1 & -(L+W) \\ 1 & -1 & (L+W) \end{bmatrix} \begin{bmatrix} v_X \\ v_Y \\ v_Z \end{bmatrix} \quad (3)$$

That v_X, v_Y and w_Z are calculated through the inverse equation is as follows.

$$T = \frac{1}{(L+W)}$$

$$\begin{bmatrix} v_X \\ v_Y \\ w_Z \end{bmatrix} = \frac{1}{4} \begin{bmatrix} 1 & 1 & 1 & 1 \\ -1 & 1 & 1 & -1 \\ -T & T & -T & T \end{bmatrix} \begin{bmatrix} R_w \cdot \dot{\theta}_1 \\ R_w \cdot \dot{\theta}_2 \\ R_w \cdot \dot{\theta}_3 \\ R_w \cdot \dot{\theta}_4 \end{bmatrix} \quad (4)$$

Where R_W and Θ_i are the radius of the wheel and are the rotational speed of each of the wheels, respectively. And the speed of each of the wheels can be expressed as $R_W \times \Theta_i$. Finally, the (x, y, Θ) position of the AGV can be calculated by accumulated eq. (4).

TABLE I
MAJOR SPECIFICATIONS OF SENSORS

Item (model)	Specification	
Accelerometer (myAccel3LV02)	Voltage	3.3V
	Interface	I2C
	Typ. Range	2.0/ 6.0g
Encoder (TMC-D03)	Voltage	5V
	Resolution	1000 pulse
Gyro (myGyro300SPI)	Voltage	5V
	Interface	SPI
	Sensitivity	±300°/s

B. Sensors for localization

We use an accelerometer (myAccel3LV02), four encoders (TMC-D03), and a gyro (myGryo300SPI) for the localization of the AGV, and measure them through CAN (controller area network) communication on AT90CAN128 MCU (micro controller unit). Table I shows the major specifications of each of the used sensors.

III. PROPOSED LOCALIZATION

Fig. 3 shows the flowchart of a proposed localization.

First, the proposed localization uses information of encoder to resolve the accumulated errors of accelerometer and gyro. Next, each velocity of encoder and gyro are calculated by data from encoder and gyro. And then errors of encoder are calculated through difference between two angular velocities. Next steps are similar to the steps above, but encoder and accelerometer are used.

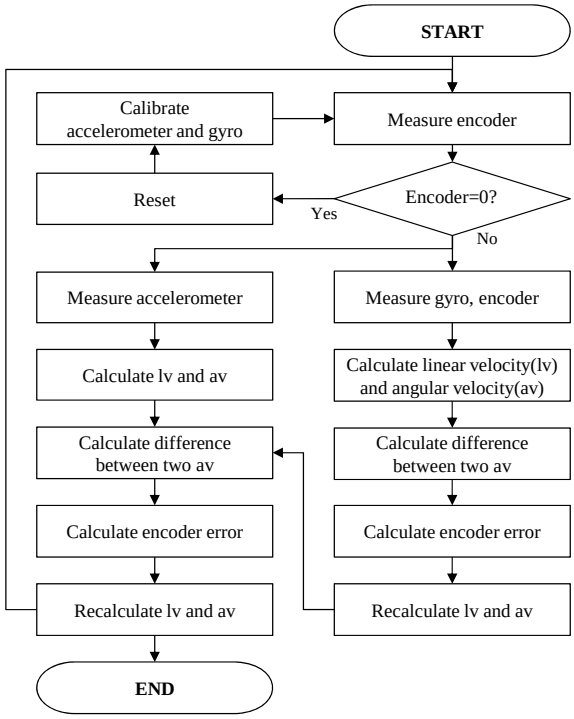

Fig. 3 Flowchart of proposed localization

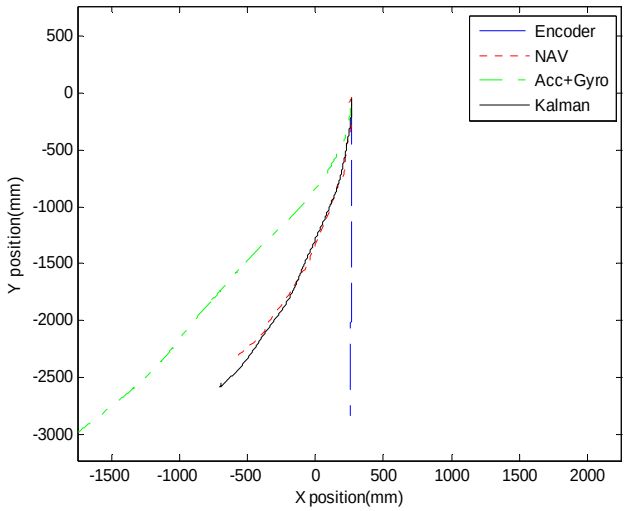

Fig. 4 Result of sideways driving (20cm/s)

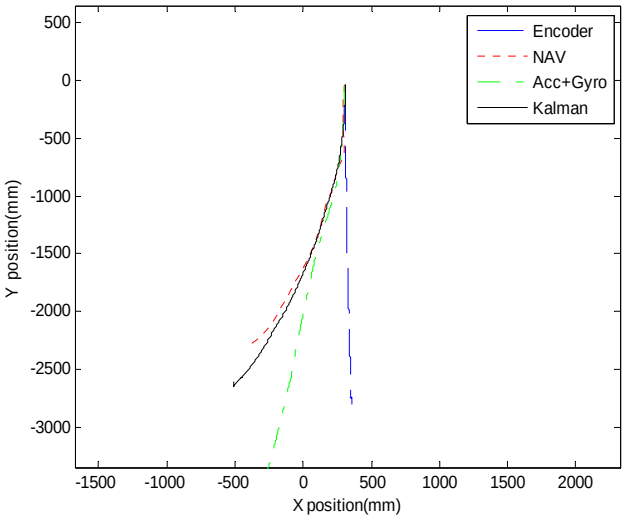

Fig. 5 Result of sideways driving (38cm/s)

IV. Experiment

In the experiment, the performance of the proposed localization is compared with NAV200 when the AGV moves sideways to 20m distance at about 20cm/s and 38cm/s, respectively. NAV200 which has ±3mm accuracy is able to measure very accurate positioning, but is very expensive. Table II shows the major specifications of NAV200.

Fig. 4 and Fig. 5 show representative experimental results, respectively

In the result (--) which uses only the encoder, the driving result of the AGV seems like moving straight. But if you see the result (:) using NAV200, we can verify that the AGV don't moved straight by the slip. In case of using accelerometer and gyro, the result (-.) has high errors by the double integral of accelerometer. However, the result (-) of the proposed method

TABLE II
Major Specifications of NAV200

Item	Specification
Power supply	24V
Operating range	1.2~28.5m
Scanning frequency	8Hz
Field of view	360°
Angular resolution	0.1°

is similar to the result of NAV200. Table II shows each of the experiments.

When the AGV moves sideways at about 20cm/s and 38cm/s, the proposed localization has 27.4944mm and 29.2521mm, respectively. And we verify that the proposed localization is effective though sideways driving causes severe slip.

V. Conclusion

This paper presents the localization for an omni-directional AGV with Mecanum wheels. The localization techniques for the general AGV use basically encoder. Otherwise, they use gyro and electronic compass with encoder. However, it is difficult to use the encoder because the Mecanum wheel occurs frequently the slip by the rollers attached to conventional wheel's circumference. Hence, we propose the localization for the AGV with Mecanum wheels, and it used encoder, gyro, and accelerometer. For experiment, we designed the AGV with the Mecanum wheels, and compared the proposed localization with NAV200 when the AGV moves sideways to 20m distance at about 20cm/s and 38cm/s, respectively. In experimental results, we verify that the proposed localization is effective though sideways driving causes severe slip.

Acknowledgment

"This work was supported by the Grant of the Korean Ministry of Education, Science and Technology" (The Regional Core Research Program/Institute of Logistics Information Technology)

TABLE III
Experimental Results

#	Specification	
	20cm/s	**38cm/s**
1	22.7019	29.3039
2	34.7432	29.4895
3	29.6854	43.0997
4	36.6345	21.4171
5	34.5811	33.8901
Avg.	**27.4944**	**29.2521**

REFERENCES

[1] I. A. Vis, "Survey of Research in the Design and Control of Automated Guided Vehicle Systems," *European Journal of Operational Research* vol. 170, no. 3, pp. 677-709, 2006.

[2] C. W. Tan, S. S. Park, "Design of accelerometer-based inertial navigation systems," *IEEE Transactions on Instrumentation and Measurement*, vol.54, no. 6, pp. 2520-2030, 2005.

[3] K. L. Han, O. K. Choi, J. W. Kim, H. S. Kim, J. S. Lee, "Design and Control of Mobile Robot with Mecanum Wheel," *ICCAS-SICE*, pp. 2932-2937, 2009.

[4] A. Dogandzic, J. Riba, G. Seco, and A. Lee Swindle-hurst, "Positioning and Navigation with Applications to Communications," *IEEE Signal Proc. Magazine*, vol. 22, no. 4, pp. 10-11, 2005.

[5] C. W. Tan, S. S. Park, "Design of accelerometer-based inertial navigation systems," *IEEE Transactions on Instrumentation and Measurement*, vol.54, pp. 2520-2030, 2005.

[6] J. K. Hwang, M. Uchanski, C. K. Song, "Vehicle Speed Estimation based on Kalman Filtering of Accelerometer and Wheel Speed Measurements," *International journal of automotive technology*, vol. 6, no. 5, pp. 475-481, 2005.

[7] Q. Pingping, F. Li, Z. Xin, "Design of Inertial Navigation System Based on Micromechanical Gyroscope and Accelerometer," *Control and Decision Conference*, pp. 1351-1354, 2009.

2011 International Conference on Mechanical, Industrial, and Manufacturing Engineering
Lecture Notes in Information Technology Vols. 1-2

Detection of Chatter during High Speed Milling, using Chaos Theory

Afshin Koohestani
Manufacturing and Materials Engineering
RMIT University
Melbourne, Victoria, Australia
Afshin.koohestani@student.rmit.edu.au

John P.T. Mo
Manufacturing and Materials Engineering
RMIT University
Melbourne, Victoria, Australia
john.mo@rmit.edu.au

***Abstract* - The purpose of this work is to investigate chaos theory as a new method for detection of chatter in milling of metals especially Titanium. This paper introduces application of Chaos in detection of chatter during high speed milling (HSM) process. The preliminary stage has been done on Aluminum and the results show that theory of Chaos has potential power of chatter detection during machining.**

Index Terms* - *High Speed Milling, Chatter, Chaos Theory, Condition Monitoring

I. INTRODUCTION

High Speed Milling (HSM) is one of the most common manufacturing processes and is used for milling of metals such as aluminum, steel, titanium, etc to reduce the time and cost of fabrication [1]. HSM performs a vast range of complex operations as well as high speed production. Material removal rate and surface generation rate are two most important parameters that should be considered for an efficient machining process.

First trial of this method goes back to the early years of twenty century when proposed by Carl Salomon [2]. According to his theory, by increasing the speed of machining five to 10 times more than normal speed, the chip tool interface temperature would decrease. Based on other experiments, it has been identified that cutting speed is different for different materials.

Many advantages are identified for this method of production such as reduction of process time, mechanical stress, and heating of work piece, the surface finish improvement, ability to use smaller tools, as well as improvement of dynamical stability.

High speed milling process reduces some of barriers occur during milling such as less reduction of heating in work piece and then reduce thermal stress at the cutting edges [2]. Although, amount of heat produced during milling is still one of the main barriers in milling of some materials, especially for Titanium.

Titanium and its alloys are non-ferrous metals with excellent corrosion resistance, fatigue properties, and high strength-to-weight ratios, as well as they are ductile. Titanium and its alloys are categorized as difficult to cut materials because of some properties such as low thermal conductivity, high chemical reactivity, and the high cutting forces [3]. Different researches have been done to improve machining properties of Titanium. The issue which has been focused in this work is chatter during machining. High cutting force during machining is the reason of chatter and it produces tool failure and work piece low quality surface.

A. Chatter

Chatter is a self-excited vibration that occurs during material removal, and it is the result of flexibility between cutting tool and work piece [4,5]. The forces acting on each tooth can be considered function of thickness of the chips being removed by the tooth during machining process. These forces will cause a movement between tool and work piece that the movement imparts a wavy surface finish on the work piece. As tool rotates, the next tooth cuts this wavy surface. Now, chip thickness is function of current relative displacement and previous displacement. The result is a natural feedback process or self-excited vibration [6].

Chatter is classified as primary and secondary. Primary chatter occurs at low spindle rotational speed and it is mainly due to physical mechanisms such as friction between tool and work piece. Secondary chatter is caused by the regenerative effect, which is behavior of the uncut chip thickness due to a combination of the instantaneous tool–work piece relative vibrations with the waviness produced by the previous tooth passage [7,8]. Most machining operations are mainly affected by the regenerative effect [9].

Chatter is the main issue against machining and the causes of instability during the machining process [10]. The chatter produces poor surface and noisy workplace. Hence, the chatter causes unusual tool wear, damage of tooling structure, spindle bearings, and poor dimensional accuracy of the work piece [9]. All these issues will bring poor productivity during machining process. Therefore, it is necessary to predict chatter occurrence before happening, which after that, the cost, time, and quality of production are not in acceptable condition.

Different methods of chatter detection have been investigated and identified in the industry, which most of them have been investigated under the time and frequency domain.

In the frequency domain method, a variety of signals such as sound pressure, displacement, force, or acceleration is used for the analysis. The first effective solution in the frequency domain was derived by Altintas and Budak in1995 [11]. They considered the Fourier series expansions of the periodic matrices truncated at the zeroth-order constant terms. The applicability of this technique is limited to the slot-milling configuration. It is not capable to represent highly intermittent

milling processes with small radial immersions, whose cutting force trends require more harmonics to be approximated [9].

Time domain method analyses mathematical functions or physical signals with respect to time. This approach is very time consuming, and its applicability in industrial conditions is limited [9].

B. Chaos Theory

Simplicity and regularity are associated with predictability, which always complexity and irregularity are synonymous with unpredictability [12]. Thus, disordered systems consider as complex system and usually unpredictable. Although by finding an order underlying in the random data can help to predict the systems. The theory which describes disordered systems named Chaos theory. This theory tries to find the underlying order in the disordered systems or random data.

Chaos can be considered a new theory, first was introduced in the 1880s, and now is applied in wide range of knowledge such as Mathematics, biology, engineering, robotics, computer science, physics, etc to predict the behavior of dynamical systems. Chaos is mathematically defined as "randomness" generated by simple deterministic systems. This randomness is a result of the sensitivity of chaotic systems to the initial conditions. However, chaos implies order to some extent as the systems are deterministic. This mixture of randomness and order allows taking a different approach in studying processes that were thought to be completely random. Hence, a system can transfer from a regular periodic system to a chaotic system by altering one of the controlling parameters [12].

Chaos theory can be used in a dynamical system. Dynamical systems are systems with fixed rule for description of time dependence of each point in the space. Each dynamical system has one specific state in any time, which is identified by a set of real numbers or vectors, and that point in space state can represent the system. Any change in the state of the system will correspond to change in the numbers or vectors. Hence, the rule of system is a fixed rule, which explains the future state of the system from current one, as well as each state in the future can follow just one state in the current state for a specific time period.

A dynamical system should have 3 properties to be classified as chaotic. These three properties are sensitivity to initial condition, topologically mixing, and dense in periodic orbits and they play main role to predict the behavior of dynamical systems by chaos theory.

Explanation of chaotic behavior may be sought through analysis of a chaotic mathematical model, or through analytical techniques such as recurrence plots and phase space plots.

In many cases chaotic behavior is found only in a subset of phase space. In the other word, by plotting the phase space diagram and investigate state of system, it can be identified if the system has chaotic behavior, or detects any changes in state of system [12].

The evolution of a dynamical system is best described in its phase space, which is a coordinate system whose coordinates are all the variables that enter the mathematical formulation of the system. The variables are necessary to describe the state of the system at any moment. To each possible state of the system, there corresponds a point in the phase space. In the other word, a phase space is a space that all states of a system are represented and possible state of system point out in to one specific point in the phase space. E.g. the space consists of values of position and momentum variables are a phase space for mechanical systems [12].

In a phase space, all freedom or parameters of system are represented by an axis of multidimensional space. Every state of the system will be plotted as a point in this multidimensional space. In the end, the phase space diagram represents all state of system, and its shape can explains qualities of the system that might not be obvious in the other respects.

A system can transform from regular periodic system to a chaotic system simply by altering one of the controlling parameters. This transformation can be identified by plotting phase space for two nearby states, or in general plotting phase space of X_n and X_{n+T}, which T is specified delay step which can be specified based on the process and requirements of analyze. If the evolutions do not diverge, the dynamics will not be chaotic. T is specified delay step which can be specified based on the process and requirements of analyze. T will be calculated by calculation of autocorrelation factor for each X_n [13,14]. This factor can be calculated by using (1) and if k=1 then the factor will be calculated for each point of series.

When the correlation is calculated between a series X_n and its delay series, then it is called autocorrelation. A high correlation is likely to indicate a periodicity in the signal of the similar time duration. Below equation is being using to calculate auto correlation coefficient of a series and the series of its delay.

$$autocorr(k) = \frac{\sum_{i=0}^{N-1}(x_i - mx)(x_{i+k} - mx)}{\sum_{i=0}^{N-1}(x_i - mx)^2} \qquad (1)$$

$$-1 < autocorr\ (k) \leq 1$$

Where mx is the average of series, k is delaying of the series x_0, x_1, x_2… x_{N-1}. When the term i+k extends past the length of series N, then two options are available. The series can be considered 0, or in the usual Fourier approach the series can be assumed to wrap. The autocorrelation factor always has its maximum amount in the x_0 which is 1.

II. Design of Experiment

Based on description of dynamical systems, the process of milling can be considered as a dynamic system. Therefore, by analyzing signals and plotting phase space diagram based on data, it is possible to investigate behavior of system during the machining, as well as detection of any chatter happening.

The experiment includes cutting of six slots. Depth and radius of cut were similar in all slots, but rotation speed and feed rate were varied. The cutting parameters are shown in

Table 1. Aluminum is considered for machining and as the material. The work piece was a block of aluminum alloy 6061, temper T651.

The experimental test was performed with a 4-axis Milling Machine. Hence a flat end mill-cutting tool with 2 flutes, 6 mm diameter, and 35 mm length was used in order to cut the work piece. A miniature, wide frequency response, and voltage mode triaxial accelerometer Kistler 8694M (± 500 g of range) was used for chatter identification. The signals were sampled at 1 kHz by National Instruments Data Acquisition device.

Accelerometer and National Instruments data acquisition (NI DAQ) card recorded amplitude of vibration along three axes X, Y, and Z. The slot was cut along Y-axis, and depth of cut was along Z-axis.

One adaptor was used in order to mounting accelerometer on the spindle tool and record vibration of the spindle tool (see Fig. 1). In previous experiment, sensor was mounted on the surface of lubricant fluid block which the data recorded was not enough pure. Hence from experimental measurements, it is appeared that signals along Z-axis are more unstable than data from other two axes by using adaptor. Although, signal along Y-axis was more unstable in previous experiments which accelerometer was mounted on the block of lubricant fluid.

III. Analysis of Experiment

As mentioned in phase space section, transformation from regular to a chaotic system could be identified by plotting phase space of X_n and X_{n+T}, which X is amplitude of signal recorded by accelerometer. T is delay which was identified based on autocorrelation factor in each period of time. To plot the phase space diagram, autocorrelation factor was used to identify the delay. Autocorrelation diagram was plotted based on calculated factors for each period of time. The point that autocorrelation factor was zero considered as delay (Fig. 2). Comparing with previous experiments,

The experiment was done as described in previous section. The slots were cut and the accelerometer recorded signals. By identifying delay point for each period of time during each test using autocorrelation diagram, the phase space diagram was plotted. All periods of time were divided to equal sections for each test, which the length of sections were depended on behavior of the process and if the sections are able to identify behavior changes. Each part of time covers a part of process in the previous part.

TABLE 1
Cutting Parameters

Test No.	Radial Speed (RPM)	Feed Rate (mm/min)	Feed per Tooth (mm)	Depth of Cut (mm)	Radius of Cut (mm)
1	3500	360	0.06	5	3
2	4000	360	0.06	5	3
3	4000	420	0.06	5	3
4	3000	420	0.06	5	3
5	3000	480	0.06	5	3
6	3500	480	0.06	5	3

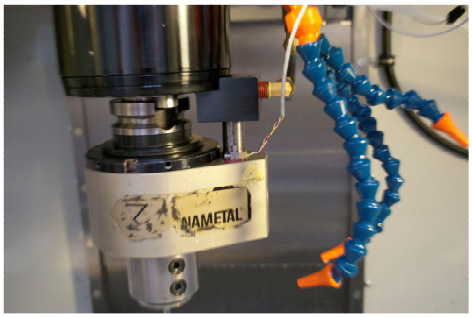

Fig. 1 Accelerometer mounted on the adaptor.

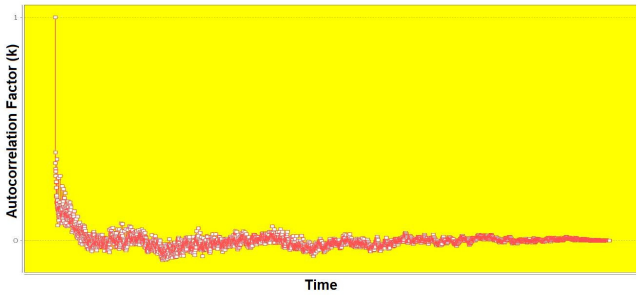

Fig. 2 Autocorrelation diagram to define delay of T.
Time: 6-11 (sec), Radial Speed: 4000 (rpm), Feed Rate: 360 (mm/min)

By plotting phase space diagrams for signals from Z-axes, it was identified that the points (each point is state of system) are dense when system is in regular state (see Fig. 3). Even though, the phase space diagram is going to be expanded when the system starts going to irregular states or chatter is going to be happened (see Fig. 4).

Density of points might be a better visual judgment about behavior of the system. Thus, a-3D-diagram was plotted in order to specify density of points. The slope of peaks can be a parameter of chatter detection, which is smooth when the system is in regular state. The system is unstable, if the slope of peaks is sharp (see Fig. 5 and 6). Time period is effected on the shape of this diagram. The peaks might be grown up by considering smaller time periods.

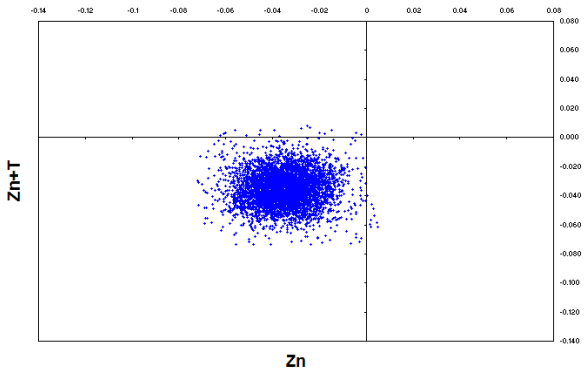

Fig. 3 Phase Space diagram – Stable state.
Time: 6-11 sec, Radial Speed: 4000 rpm, Feed Rate: 360 mm/min

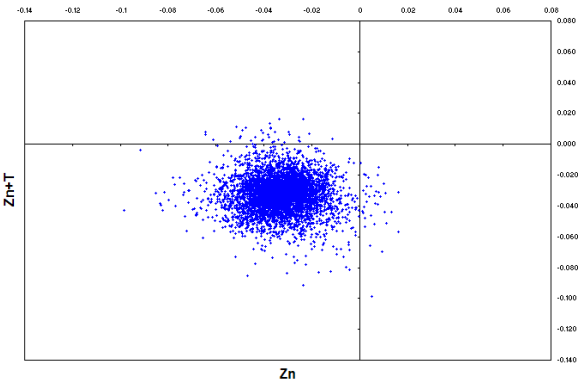

Fig. 4 Phase Space diagram – unstable state.
Time: 10-15 sec, Radial Speed: 4000 rpm, Feed Rate: 360 mm/min

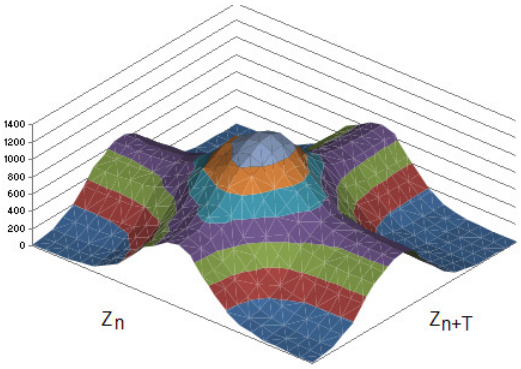

Fig. 5 Density of points – Stable state.
Time: 6-11 sec, Radial Speed: 4000 rpm, Feed Rate: 360 mm/min

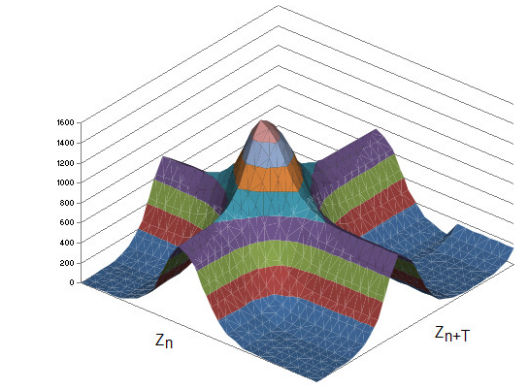

Fig. 6 Density of points – unstable state.
Time: 10-15 sec, Radial Speed: 4000 rpm, Feed Rate: 360 mm/min

IV. Conclusion

In recent years, chaos theory has been evolving in prediction of system states. The growing of chaos theory and using regularly to predict state of system shows that it can be used in prediction of chatter during HSM process by industries.

This investigation is in the early stage of introducing chaos theory and phase space for detection of chatter before happening. The results of this experiment show that Chaos theory has enough potential to detect chatter during milling process. Although this investigation is in preliminary stage, the results show that the chaotic method and phase space diagrams can be used in order to detect chatter.

At this stage, chatter can be detected in periods of time and it is required to propose a new method of image processing in order to monitor chatter on-line and during the process. Hence, more investigation is required in order to using adaptor and if the direction of critical acquired data will be changed.

Acknowledgement

This project is supported by an industry grant provided by Production Parts Pty Ltd, Australia. The authors would like to thank the generous support and on-going technical inputs by the industry partner to this project.

References

[1] H. Schulz and T. Moriwaki, "High – speed machining", *Ann. of the CIRP* t. 41, nr 2, s. (1992) 637–642

[2] R. Pasko, L. Przybylski, and B. Slodki, "High speed machining – The effective way of modern cutting" *International Workshop CA Systems and Technologies* 72-79

[3] P. E. Leigh, J. K. Schueller, S. Smith, J. Tlusty, "Advanced Machining Techniques on Titanium Rotor Parts" *American Helicopter Society*, 56th Annual Forum (2000)

[4] F.F. Ehrich, "Chapter 5: Self excited vibrations" *Harris' shock and vibration handbook* (2010)

[5] C.S. Anderson, S.E. Semercigil, O.F. Turan, "A passive adaptor to enhance chatter stability for end mills" *International Journal of Machine Tools & Manufacture* (47) (2007) 1777–1785

[6] N.D. Sims, B. Mann, and S. Huyanan, "Analytical prediction of chatter stability for variable pitch and variable helix milling tools" *Journal of Sound and Vibration* (317) (2008) 664–686

[7] G. Stepan, "Delay-differential equation models for machine tool chatter" *Nonlinear Dynamics of Material Processing and Manufacturing*, New York (1998), 165–219

[8] S.A. Tobias, "Machine Tool Vibration" *Blackie & Sons Ltd.*, (1965)

[9] G. Totis, "RCPM - A new method for robust chatter prediction in milling" *International Journal of Machine Tools & Manufacture* (49) (2009), 273–284

[10] E. Budak, "Improving productivity and part quality in milling of titanium based impellers by chatter suppression and force control" *Annals of CIRP* 49 (2000), 31–36

[11] Y. Altintas and E. Budak, "Analytical prediction of stability lobes in milling" *Annals of the CIRP* 44 (1995), 357–362

[12] A.A. Tsonis, "Chaos from theory to application", *Plenum Press, NY* (1992)

[13] MT. Rosenstein, JJ. Collins, CJ. Deluca, "A practical method for the calculating largest Lyapunov exponents from small datasets" *Physica D,* 65 (1993), 117–34.

[14] P. Shange, X. Na, S. Kamae, "Chaotic analysis of time series in the sediment transport phenomenon" *Chaos, Solitons & Fractals* 41 (2009) , pp. 368-379.

2011 International Conference on Mechanical, Industrial, and Manufacturing Engineering
Lecture Notes in Information Technology Vols. 1-2

Task Automation for Modelling Deflection Prediction On Machining Thin-Wall Part with Catia V5

R. Izamshah R.A
Faculty of Manufacturing Engineering
Universiti Teknikal Malaysia Melaka
Hang Tuah Jaya, Melaka 76100, Malaysia
izamshah@utem.edu.my

John P.T Mo and Songlin Ding
School of Aerospace, Mechanical and Manufacturing Eng.
RMIT University
Bundoora East, Australia
{john.mo & songlin.ding}@rmit.edu.au

***Abstract* - Accuracy of machined components is one of the most critical considerations for many manufacturers especially in aerospace industry where most of the part used a thin-walled monolithic structure. However, because of the poor stiffness of thin-wall part, deformation is more likely to occur in the machining process which resulting a dimensional form errors and has been largely ignored by CAD/CAM software. This paper proposed task automation for predicting the surface errors when machining a thin-wall low rigidity component. The proposed model would be an efficient means for analysing the root cause of errors induced during machining of thin-wall parts and provide an input for downstream decision making on error compensation. A set of machining tests have been done in order to validate the accuracy of the model and the results between simulation and experiment were in good agreement.**

Index Terms – Task Automation, CAD/CAE, Thin-wall Machining, Deflection Modelling

I. INTRODUCTION

Thin-wall machining of monolithic parts allows for higher quality and precise parts in less time, impact business issues including inventory and Just-In-Time (JIT) manufacturing. Because of the poor stiffness of thin-wall part, deformation is more likely to occur in the machining of thin-wall part which resulting a dimensional form errors. In current industry practice, the resulting errors are usually compensated through one or more of the following techniques: (i) using a repetitive feeding and final 'float' cut to bring the machined surface within tolerance; (ii) manual calibration to determine 'tolerable' machining conditions; and (iii) a lengthy and expensive trial and error numerical control validation process. Noticeably all of these existing techniques have a tendency to lower productivity. On the other hand, most of the CAD/CAM software can only provide tool path simulation without considering the dynamical effects of the machining process on part errors. Hence, the development of a system which simulating the entire machining process is necessitate.

There were few reported work been done in predicting the deformation of thin-wall part. Budak and Altintas [1] used the beam theory to analyse the form errors when milling using slender helical endmill for peripheral milling of a cantilever plate structure. The slender helical endmill is divided into a set of equal element to calculate the form errors acting by the cutting forces on both tool and the workpiece. Kline et al. [2] used a thin-wall rectangular plate element model clamped on three edges. He used an equivalent concentrated force to calculate the deflection of the tool and the workpiece. The form errors are obtained by summing the tool and the workpiece deflection. The effects of workpiece and cutter dynamic deflections on the chip load are proposed by Elbastawi and Sagherian [3]. Included in their model is the tracking of the changing of dynamics stiffness of workpiece geometry. In addition, the effects of cutter deflection for estimating the instantaneous uncut chip thickness were proposed by Sutherland and DeVor [4]. Later, Tsai and Liao [5] developed an iteration schemes to predict the cutting forces and form error on thin-wall rectangle plate. The cutting force distribution and the cutting system deflections are solved iteratively by modified Newton-Raphson method. Ratchev et al. [6] investigated the modelling and simulation environment for machining low-rigidity components. Later in his work, he modelled the material removal process using voxel-based representations by cutting through the voxels at the tool/part contact surface and replacing them with equivalent set of mesh. He used Aluminium Alloys 6082 for the experimental analysis and verification. Rai and Xirouchakis [7] consider the effects of fixturing, operation sequence and tool path in transient thermo-mechanical coupled milling simulation of thin-walled components. Recently, Izamshah et al. [8] adopted the Lagrangian method in his machining simulation, in which each individual node of the mesh follows the corresponding material particle during motion. The workpiece is modelled as a plastic object so that the material can be deform and cut by the endmill teeth.

Despite of several significant works on modelling thin-wall machining that has been developed, there still a requirement for more efficient approach on modelling the thin-wall machining especially for minimizing the analysis time from initial part creation to analysis result. The advantages of the proposed model over previous work are the integration between CAD and CAE, fast design-analysis loop and the flexibility to create complex finite element models while maintaining associativity with the master design, thereby avoiding time-consuming and error-prone transfer of geometry. This paper discuss on task automation for predicting the part deflection when machining thin-walled workpiece. The proposed methodology is implemented with CATIA V5 platform using the Mechanical Design workbench, Generative Structural Analysis workbench and Advanced Meshing workbench.

978-0-9831693-1-4/10/$25.00 ©2011 IERI

II. METHODOLOGY

The proposed modelling and simulation system for machining thin-wall components is shown in Fig. 1. The system consist of several model, namely, feature based geometry model, material removal model and deflection analysis model. The methodology is performed within the CAD environment and the analysis model is fully associative with the CAD geometry and its specification. The simulation is perform by automate the task for modelling solids object, material removal process and structural analysis using Catia V5 through the use of macros, with Windows as the operating system and Visual Basic as the programming language. The methodology consists of several procedures with different functions as follows:

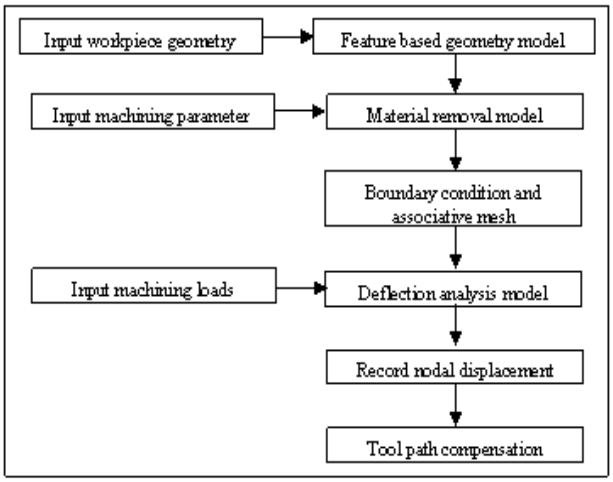

Fig. 1. System methodology for deflection prediction.

A. *Catia programming languages*

Catia V5 allows the creation and execution of macros through the use of distinct object-based programming languages. A macro is a series of functions, written in a scripting language, that group in a single command in order to perform the requested task automatically. It can also be a good means to store intricate interactions or describe a document in a clear text file easy to edit and requiring less memory than a document. Catia automation provides a way to store operations in the form of a *.CATScript* file which is written in a language similar to the Visual Basic language.

The automated objects in the application are organized in a parent-child hierarchical structure. The main object from which all the others descend is an 'Application' that directly represents the Catia programme as shown in Fig. 2. The feature based geometry model and material removal model are implemented using Catia V5 Mechanical Design workbench while Advanced Meshing Tool workbench and Generative Structural Analysis workbench are used for the part deflection analysis.

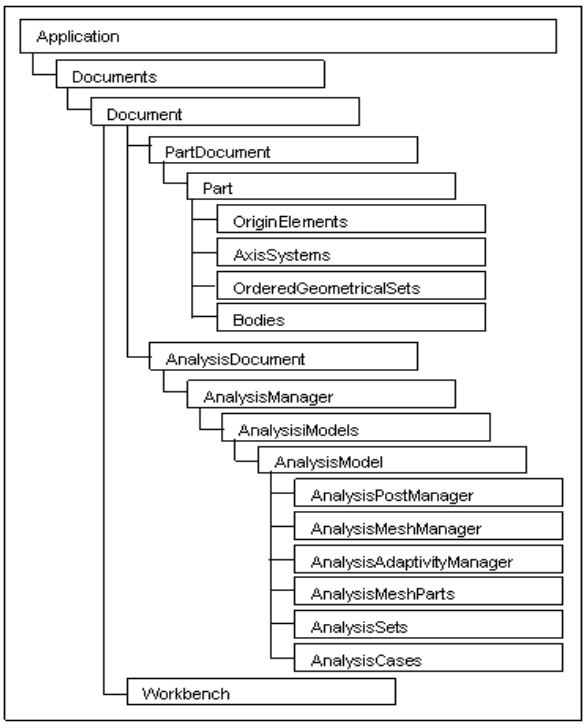

Fig. 2. System architecture for object automation.

B. *Feature based geometry model*

The component feature attributes such as the initial workpiece dimensions and material properties are created by automating the task for modelling solids object with Catia V5 through the use of macros, using Visual Basic as the programming language. By using a simple form, the dimensions are enter which define the geometry of the part (length, thickness and height). This application automatically and immediately creates the part compare with the manual process that would require construction of lines and generation of solid model. The created component is saved in *.CATPart* file format and work as a master part. Any changes and update of material removal process need to be done in this master part. At this stage, the part material properties needs to be define by calling the built in Catia material library.

C. *Material removal model*

To model the material removal process during machining, the cutter shape and the cutter path that is coincidence with the workpiece material will be remove using 'Extrude' (cut) and 'PowerCopy' function in the Catia Mechanical Design workbench. Again, by using a simple form, the machining parameter are enter which define the tool diameter, axial depth of cut, radial depth of cut and the machining length. For the first step, the cutter is set at the entry of the workpiece and the material which is coincidence with the cutter shape are remove

and saved as a new *mrr(i).CATPart* file, where *i* denotes the machining length. Then, the *mrr(i).CATPart* file will be input to Catia Advanced Meshing Tool workbench for generation of associative mesh for the solid component. At this stage, global parameters such as the shape and the size of the elements needs to be specify before performing the finite element analysis.

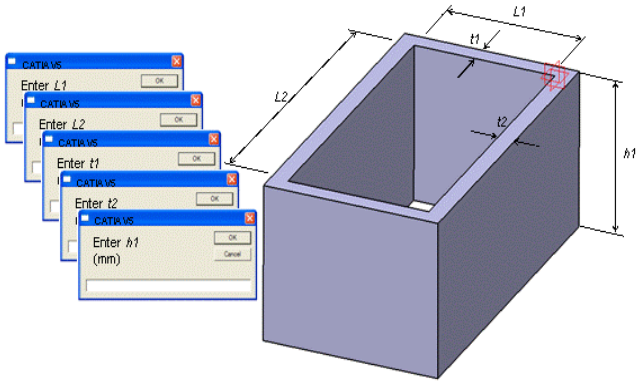

Fig. 3. Interactive windows for part generation.

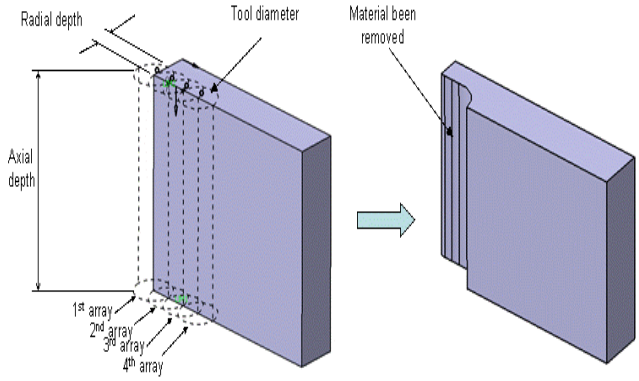

Fig. 4. CAD based material removal model for machining process.

D. Deflection analysis model

Catia Generative Structural Analysis workbench are used to perform a static analysis for part deflection prediction. At this phase analysis information such as nodes, elements, material properties, boundary conditions and the machining load will be input to calculate the deflection. The FEA results which contain the elements and nodes values is stored and saved in a native *ASCII* file format and *.CATAnalysis* file and stored in a knowledge-based template. The cutter feed position is then move to the next position and the material on the new feed step will be removed and saved as a new *mrr(i+1).CATPart* file to perform the subsequent analysis. Finally, after repeating this procedure at different location along the feed direction, the complete surface form errors of the component are obtained and used for tool path compensation and NC verification.

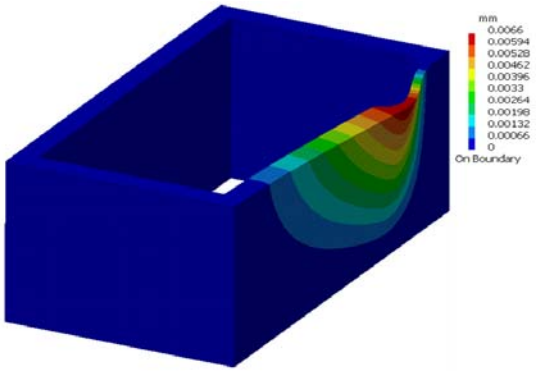

Fig. 5. Simulation result for deflection analysis.

II. MODEL VALIDATION

The proposed model was experimentally tested by comparing the simulation results with the results of experiment for an identical set of test components. The geometry of the component used in the simulation and experiment is 150x150x17 mm with 1.8 mm of wall thickness. The experimental set-up is shown in Fig. 6. All experimental tests were performed on a HAAS VF1 vertical machining center. Three component Kistler dynamometer (type 9257B) and Kistler charge amplifier (type 5070A) are used to measure the cutting loads, while National Instrument DAQ card is used to acquire the signal. The wall deflection is measured using three Lion Precision ECL 130 inductive displacement sensors. The sensors are mounted at three different equal locations (37.5, 75 and 112.5 mm) at the back of the workpiece. Both the signals from the dynamometer and displacement sensors are then been analyse using LabVIEW 8.5.1.

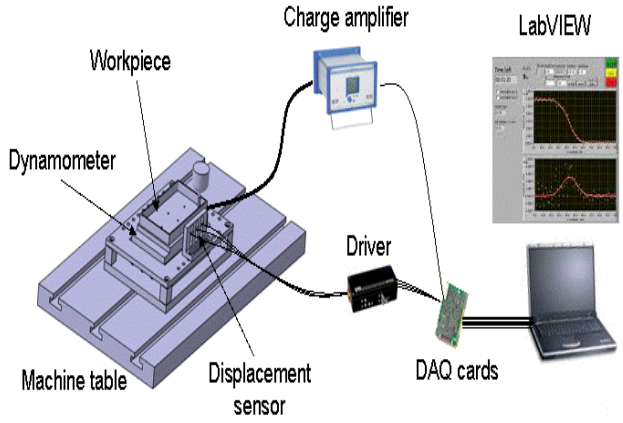

Fig. 6. Experimental set-up.

The workpiece material used in the simulation and experimental is annealed alpha-beta titanium alloy (Ti6Al4V). The cutting parameters used in the simulation and experiment are listed in Table 1.

Table 1. Machining parameters used for simulation and experiment.

Tool	4 flutes carbide flat endmill

Tool diameter	6 mm
Helix angle	38°
Ramp down angle	5°
Cutting speed	4244 rpm
Feed rate	340mm/min
Axial cutting depth	15 mm
Radial cutting depth	0.3 mm

Fig. 7 shows the displacement values for three sensors between simulation and experiment. The cutter feed step is set at 30 equally space location at one side of the wall along the feed direction. It can be seen that both the displacement obtained from simulation and experiment are closely match with the agreement value between 80.3% and 99.9% for predicted and measured value.

Fig. 8 shows the simulation result of the displacement magnitudes at the middle location of cutter feed step. From the cut plane analysis of the wall, it shows that the form errors are smallest at the bottom of the part. The form errors magnitudes increase towards the middle of the part and decrease towards the end of the part, where the wall flexibility decreases. Due to the decreasing stiffness of the wall as a result of material removal, there is an increasing value of form errors between two regions (start and end) in the feed direction. To a large extent, the more flexible the wall, the higher surface errors result during cutting. Once the deflection of the workpiece is established, the tool path is optimised by recalculating the coordinates of the cutter. To compensate the resulting profile error, the cutter location needs to be modified from the initial position to the compensated position by a distance of the resulting displacement value at certain cutter feed position.

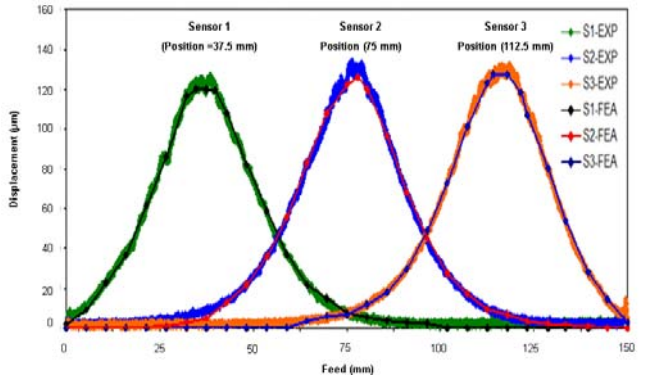

Fig. 7. Comparison between simulation and experiment of displacement along the workpiece length.

III. CONCLUSIONS

A good agreement between simulation and experimental results prove the validity of the proposed model in handling real-field problems. Prediction of the surface errors due to the flexibility of the workpiece can be easily predicted with the proposed model. On the other hands, the proposed model can minimize the analysis time, fast design-analysis loop, multidiscipline collaboration and the flexibility to create complex finite element models while maintaining associativity with the master design, thereby avoiding time-consuming and error-prone transfer of geometry. The proposed model would be an efficient means for analysing the root cause of errors induced during machining of thin-wall parts and provide an input for downstream decision making on error compensation. To a large extent, the manufacturers can further enhance their productivity by eliminating the need of expensive preliminary cutting trials often require for validating the designed machining process plan.

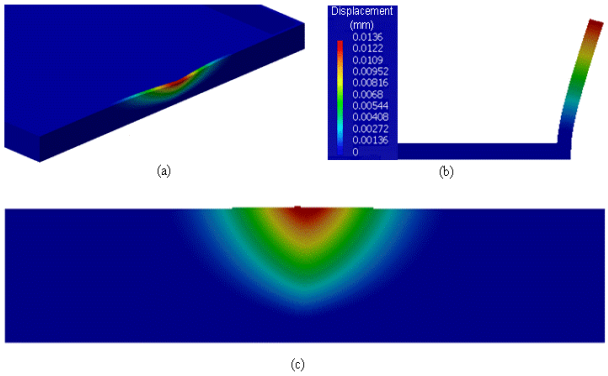

Fig. 8. (a) Machining simulation for deflection analysis at the middle location of cutter feed. (b) Cut plane analysis of the part. (c) Back view of the part.

ACKNOWLEDGMENT

The authors would like to thanks Production Parts Pty Ltd Australia, for providing the experiment material and technical supports.

REFERENCES

[1] E. Budak, Y. Altintas, Peripheral milling conditions for improved dimensional accuracy, Int. J. Mach. Tools Manuf. 34 (1994) 907-918.
[2] W.A Kline, R.E. DeVor, I.A. Shareef, The prediction of surface accuracy in end milling, ASME J. Eng. Ind. 104 (1982) 272-278.
[3] M.A Elbestawi, R, Sagherian, Dynamics modelling for the prediction of surface errors in the milling of thin-walled sections, J. of Materials Processing Tech 25 (1991) 215-228.
[4] J.W Sutherland, R.E DeVor, An improved method for cutting force and surface error prediction in flexile end milling system, ASME J. Eng. Ind. 108 (1986) 269-279.
[5] J.S Tsai, C.L. Liao, Finite element modelling of static surface errors in the peripheral milling of thin-walled workpiece, J. of Materials Processing Tech 94 (1999) 235-246.
[6] S.Ratchev, W.Huang, S.Liu, A.A Becker, Modelling and simulation environment for machining of low-rigidity components, J. of Materials Processing Tech 153-154 (2004) 67-73.
[7] J.K Rai, P.Xirouchakis, Finite element method based machining simulation environment for analyzing part errors induced during milling of thin-walled components, Int. J. of Mach. Tools Manuf. 48 (2008) 629-643.
[8] R. Izamshah R.A, John P.T Mo, Songlin D, Finite element analysis of machining thin-wall parts, J. of Key Eng Materials Vol. 458 (2011) 283-288, in press.

2011 International Conference on Mechanical, Industrial, and Manufacturing Engineering
Lecture Notes in Information Technology Vols. 1-2

Effect and Analysis of Vertical Roller Mill Grinding method on Grinding Layer

Jingliang Nie, Xiangbo Ze, Chaoyang Zhang and You Fu
School of Mechanical Engineering
University of Jinan
Jinan, Shandong Province, China
niejl521@163.com

***Abstract* - The state of grinding layer is the key factor which affects the grinding effect of vertical roller mill. The state of grinding layer depends on the grinding method of vertical roller mill. Combining the mathematical model of vertical roller mill to study the grinding layer which using the cylindrical roller. The analysis showed that the grinding method of vertical roller mill mainly affect the pressure distribution of grinding layer. Through the simulation of vertical roller mill grinding process by the discrete element analysis software EDEM, the distribution form of material granule and the pressure distribution curve of grinding layer in different grinding method are obtained. We can draw the following conclusion from the curve: the uneven fineness products are easily product by mill which using the flat shape roller model; the uniform fineness products are easily product by mill which using the circular-arc roller model.**

Index Terms - vertical roll mill; grinding layer; material bed

I. INTRODUCTION

As the high efficiency energy saving grinding equipment, the vertical roller mill has been used more widely in cement industry. Especially for grinding the cement raw materials. In China, the application of vertical roller mill starts relatively late. And the research of its comminution mechanism is not very much. It restricts the development of vertical roller mill and the ability to deal with some related issues in China. The grinding device which composed by grinding roller and grinding disc is the key component， which affect the state of grinding layer. So this paper used the grinding layer of vertical roller mill as the research object to analysis the grinding layer's state of vertical roller mill which using different structure of grinding roller and grinding disc.

II. THE OPERATION FORM OF VERTICAL ROLLER MILL

Let's investigate the operation form of vertical roller mill before discuss the state of its grinding layer. The grinding process is completed by a comminution device which is composed mainly of grinding roller and grinding disc. The materials are ground into powder between the grinding roller and the grinding disc [1]. Take the HRM vertical roller mill which is designed by Hefei cement research institute for an example. The main structure of the HRM is shown in Fig. 1. The materials enter the center of the grinding disc from the feed inlet which located in the top of the mill. Under the action of centrifugal force which generated by the grinding disc rotation, the material is left to the grinding region which between grinding roller and disc. The large particles are crushed first and formed the material bed. Then under the action of the roller's extrusion, grinding and the extrusion between particles, the particles are comminuted to powder. In addition to the gravity of roller, the grinding pressure is mainly provided by a hydraulic device. After grinding the material overflow from the edge of the grinding disc and are brought into the separator. After the selection of separator, the qualified fine powder is taken out the mill through the mill's exit. The meals fall to the grinding disc and repeat the above grinding process.

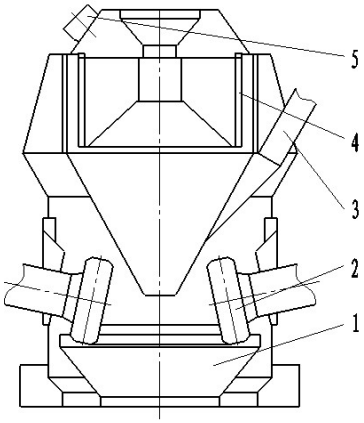

1-grinding disc; 2-grinding roller; 3-feed inlet; 4-separator; 5-mill exit
Fig. 1 Structure of the HRM

III. THE COMMINUTION MECHANISM OF VERTICAL ROLLER MILL

The comminution mechanism of vertical mill is material bed grinding. That is to say, the material forms the material bed under the high pressure. The transfer of stress depends mainly on the particles. Under the interaction of particles, the crack, fracture, splitting and crushing arise on and on [2]. The layer crushing refers to a phenomenon which a large of particles aggregate into particle swarm and were crushed because of the action of stress, namely there is interaction between particles [3]. In fact, the grinding process of vertical roller mill is that the material is extruded and rolled by the grinding device and the extrusion between the particles [4]. Because the velocity difference exists between the grinding roller and the grinding disc, the particle is milled at the same time [5]. The working diagram of vertical roller mill is shown

in Fig. 2. The material bed features of the vertical roller mill are that the part of material bed is limited and the side of material bed is free.

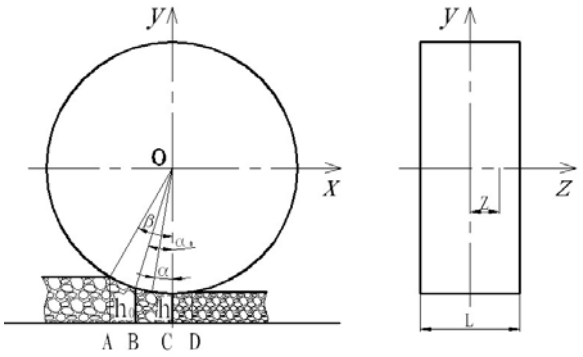

Fig. 2 Working diagram of the vertical roller mill

In the grinding region of vertical roller mill, the material is ground through the following three stages: compacting stage, the material layer compressed and crushed stage, expansion stage.

IV. The Effect of Vertical Roller Mill Grinding Method on Grinding Layer

Vertical roller mill grinding method means that using the different structure of grinding roller and the grinding disc to grind the material. In the grinding region, the distribution form of pressure plays a vital role in the process of materials crushed. It also determines the efficiency of vertical roller mill. While the vertical roller mill grinding method plays a decisive role on the distribution form of pressure.

A. The Pressure Distribution of Grinding Layer along the Roller Surface under Columniform Roller

The working diagram of columniform roller is shown in Fig. 2. In order to analyze the pressure distribution of material layer along the roller surface, make the following assumptions:

1) In the compacting stage, the relative density of material is unchanging, the value is constant as δ_0;

2) In the material layer compressed and crushed stage, there is no relative sliding between the materials and the roller surface, that is, the material moving speed is equal to the speed of the roller surface, the materials are only deformed in the vertical direction;

3) The end of the material layer compressed and crushed stage locates in the vertical plane C, where the material relative density reaches the maximum, the value is δ_C;

4) In center of the roller (along the axial direction), the compression properties of the material are the same with the uniaxial compression properties, the material uniaxial compression curve formula is as in (1).

$$p_p = p_c\left[\ln\left(\frac{1-\delta_0}{1-\delta}\right)\right]^{\frac{1}{n}} \tag{1}$$

Where:

p_p -The pressure acts on the material in the compressed and crushed stage;

p_c -The specific pressure of the material;

δ_0 -The initial relative density of the material, $\delta_0 = \rho_0 / \rho$;

ρ -The density of the material block;

n -The curve compression factor.

According to the assumption 2), any mass of the vertical layers is equal, which can be derived that in the material compressed and crushed stage, the pressure of the materials located at any point (α, λ) of the roller surface can be described as equation (2):

$$p(\alpha,\lambda) = p_c \cdot \left[\ln\left(\frac{1-\delta_0}{1-\delta_\alpha}\right)\right]^{\frac{1}{n}} \cdot (1-2|\lambda|)^m \quad 0 \le \alpha \le \alpha_0 \tag{2}$$

Where:

δ_α -The relative density of the materials located at any point (α, λ) of the roller surface;

λ=Z/L (Where: Z—the axial distance which from a point on the roller to the center of the roller, L— the roller width);

m-Axial pressure distribution coefficient, m> 1.

According to the equation (2), it can conclusion that the factors which influence the pressure distribution of grinding layer as follows: the diameter of grinding roller, the width of grinding roller and the relative density of the material located at any point of the roller surface. In the case of the same gap between the grinding roller and the grinding disc, the larger the roller diameter is, the larger the region of the grinding layer crushed is. The roller width mainly affects the pressure distribution of grinding layer which along the roller's axial direction. The material relative density mainly affects the pressure distribution of grinding layer which along the roller's radial direction. The material relative density related to the roller structure and the fit form of the grinding roller and the grinding disc.

B. The Effect of the Different Roller Structure on the Grinding Layer

There are mainly two types of the grinding structure used, one is flat-shaped, the other is circular-arc. Transformed into the grinding roller and the grinding disc structure are columniform roller (or conical roller) combined with flat grinding disc or the tire roller combined with the groove-type grinding disc.

The EDEM model is established in this paper, which simulates the material layer crushed under the different roller structure. EDEM is the world's first multi-purpose discrete element modeling software tool designed for the simulation and analysis of industrial particle handling and manufacturing operations. With EDEM you can quickly and easily create a parameterized model of your granular solids system. CAD models of real particles can be imported to obtain an accurate representation of their shape. Add the mechanical, material

and other physical properties to form your model particles. These can be stored in a library allowing you to build a collection specific to your processes [6].

B.1. Model Building and Simulation

In order to analyze the effect of the grinding mill structure on the state of grinding layer, a simplified model of the vertical roller mill is built, which only retain the comminution device (the grinding roller and the grinding disc), and omitting the other structures. Using SolidWorks software, Simplified model is built, the simplified model of the vertical roller mill is shown in Fig. 3.

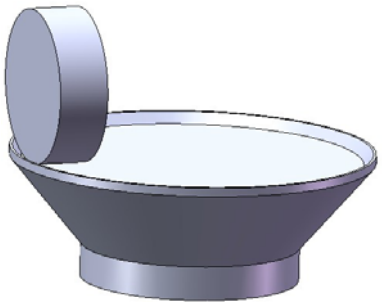

a. the simplified model of columniform vertical roller mill

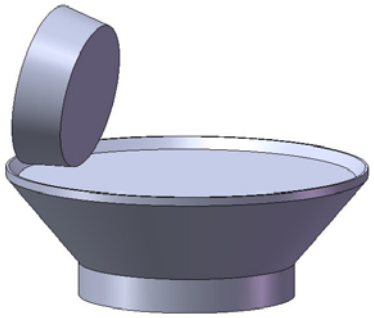

b. the simplified model of conical vertical roller mill

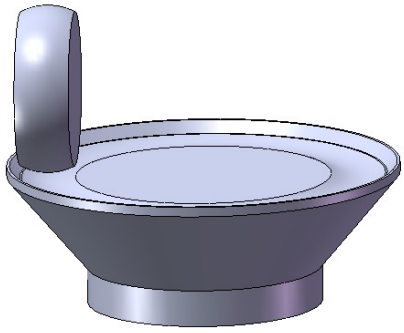

c. the simplified model of tire vertical roller mill

Fig. 3 The simplified model of vertical roller mill

Import the simplified model into discrete element simulation software EDEM for simulation, the simulation steps are as follows:

Step 1: Set the model parameters. The parameters including the gravity, materials, the interaction between particles, the interaction between particles， the geometry and so on. The limestone and the steel 45 are used here. The material properties are shown in table I. The interaction between particles: the coefficient of restitution is 0.1, the static friction coefficient is 0.545, and the rolling friction coefficient is 0.1. The interaction between particles and geometry: the coefficient of restitution is 0.2, the static friction coefficient is 0.5, and the rolling friction coefficient is 0.1.

TABLE I

MATERIAL PROPERTIES

Item / Material	Poisson's ratio	Shear modulus(pa)	Density(kg/m^3)
Limestone	0.2	5e+7	2640
45	0.3	7e+10	7800

Step 2: Define the particles.

Step 3: Define the material and the motion characteristics of geometry. The material of grinding roller and grinding disc is defined as 45. And the grinding disc's speed is set to 25r/min.

Step 4: Create the particle factories. Setting the number, the initial state， and other parameters of particle according to the actual feed volume.

Step 5: Set the time parameter and run the simulation of the vertical roller mill grinding process.

B.2. Analysis of Simulation Results

The EDEM software post-processing module is used, and pressure distribution of three types grinding mill structure under all materials along the roller grinding layer is mapped out, as showed in fig. 4.

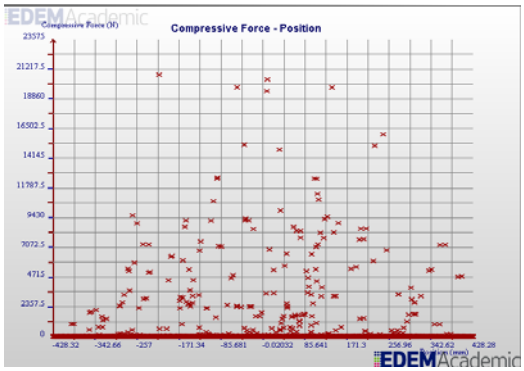

a. columniform roller

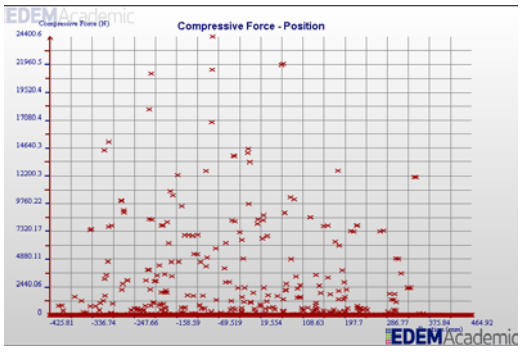

b. conical roller

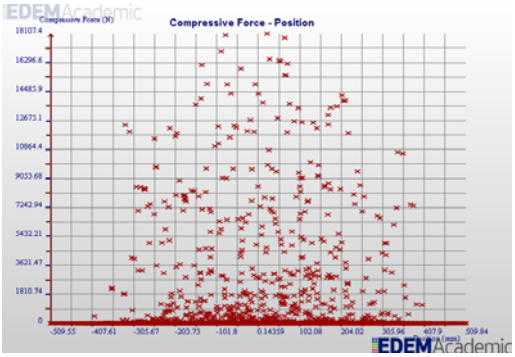

c. tire roller

Fig. 4 pressure distribution of material along grinding roller

The pressure distribution shown in figure 4 indicate that using the cone-shaped vertical roller mill, the pressure has a horizontal component, and most of the material in the grinding layer and the maximum pressure of grinding layer are in the big tip-to-face side, and it has a low stress zone in the small tip-to-face side which plays a pre-grinding effect on material. Using the tire-shaped vertical roller mill, because of the hindering effect on material from the circular roller conveyor, from the center to roll axial sides extensions, the grinding particles in grinding zone are uniformly distributed, compare to the particles distribution state is center little and side more which using the columniform vertical roller mill.

The pressure distribution curve along the roller grinding materials of three different roller structures is mapped by figure 4, and the grinding pressure distribution under different grinding structures is shown in fig. 5.

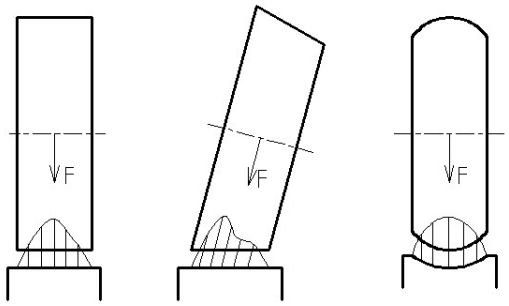

Fig. 5 the grinding pressure distribution under different grinding structures

By the pressure distribution curve shown in fig. 5, there are two kinds of grinding layer pressure distribution curve under different grinding methods, one kind is sharp, the other is evenly. The fine particles are generated in the sharp high pressure, and the thicker particles are generated in the side low pressure, the particle size curve and the pressure curve are consistent. Therefore, the grinding way can be chosen reasonably according to the demand when design and choose the models of vertical roller mill.

V. CONCLUSION

The conclusions obtained by analysis as follows:

1) The grinding method of vertical roller mill causes grinding layer pressure distribution exists gradient along the axial and radial direction of grinding roller in the grinding region. The pressure distribution gradient is related to the roll grinding size and structure form.

2) The fit form of grinding roller and grinding disc determines the grinding method. There are usually two kinds fit forms of grinding roller and grinding disc, one is flat shape, the other is circular-arc shape. The fit form influences the pressure distribution of grinding layer along the mill roller, then influences the particle size of the product. The pressure distribution curve of the flat shape mill is sharp, and the particle size is uneven thickness. The pressure distribution curve of the circular-arc shape is evenly, and the particle size is evenly.

ACKNOWLEDGMENT

Supported by National Key Project of Scientific and Technical Supporting Programs Funded by Ministry of Science & Technology of China During the 11th Five-year Plan (NO.2006BAF02A24) and the Key Subject Research Foundation of Shandong Province (XTD0713).

REFERENCES

[1] Nairen Zhao, “Running mechanism of roller mill and its selection principle,” *Cement Engineering*, no. 1, pp. 4-10, January 2004.

[2] Yunlong Yue, Ya Qu, “Advantage of roller mill applied to pre-grinding of cement,” *China Powder Science and Technology*, vol. 6, no. 5, pp. 37-39, October 2000.

[3] Zhichao Liu, Liangchen Wu, Tonglong Xue ed., “Theory and application of material crushing equipment,” Xuzhou: China University of Mining and Technology Press, 2006, pp. 82-84.

[4] Zhengyu Liu, Zhen Liu, Wenwu Liu, “Application of rolling mill to powder engineering,” *China Powder Science and Technology*, vol. 6, no. S1, pp. 96-105, October 2000.

[5] Zhongqi Han, “Application and development of vertical mill technology,” *China Cement*, no. 12, pp. 53-56, 2009.

[6] Guoqiang Wang, Wanjun Hao, Jixin Wang, “Discrete element method and practice in EDEM,” Xian: Northwestern Polytechnical University Press, 2010, pp. 9-13.

2011 International Conference on Mechanical, Industrial, and Manufacturing Engineering
Lecture Notes in Information Technology Vols. 1-2

Node-based FlexRay Scheduling Method for Reducing the Scheduling Complexity

Young Hun Song, Man Ho Kim and Suk Lee
School of Mechanical Engineering
Pusan National University
Busan,Korea
{embedded, kmh & slee}@pnu.edu

Kyung Chang Lee
Department of Control and Instrumentation Engineering
Pukyong National University
Busan,Korea
gclee@pknu.ac.kr

***Abstract* - FlexRay was developed to replace CAN protocol in chassis networking systems, to remedy the shortage of transmission capacity and unsatisfactory real-time transmission delay of conventional CAN. However, FlexRay network systems require a complex scheduling method for the static and dynamic segment, which is a barrier to their implementation as chassis networking systems. In particular, if we want to migrate from a CAN network to a static segment of a FlexRay network using the well-defined CAN message database, which has been specifically constructed for chassis networking systems by automotive vendors, a new type of scheduling method is necessary to reduce complexity during the software development process. This paper presents a node-based FlexRay scheduling method for reducing the scheduling complexity in FlexRay network systems.**

Index Terms – in-vehicle networking(IVN) systems, FlexRay, node-based scheduling method, scheduling complexity, software complexity index.

I. INTRODUCTION

Recently, as increasing needs of driver about safety and reliability of vehicle, high speed transmission rate and predictable transmission quality of service (QoS) have become necessary [1]-[5]. Academically, controller area network (CAN) is unsuitable for the chassis networking systems to require real-time characteristics of braking or steering system because it has low transmission rate and non-deterministic property [6]-[8].

To solve these problems, time-triggered chassis control network system has been developed such as FlexRay, automotive vendors have tried expanding the application area of FlexRay protocol. Because of the complexity of the protocol itself, however, FlexRay is more difficult than CAN to implement applications. According to many years of developing and applying process, various developing methodologies are presented in the CAN protocol. In addition, in order to guarantee smooth transmission of various sensor or actuator signals generated from each ECUs, CAN message standard has been well established from automotive vendors. Specifically, CAN protocol is applied various chassis network system with stable operation presently [9].

In order to change the CAN network system to FlexRay network system in the chassis networking system, complex scheduling method about system design level to network configuration and operation level is necessary. In particular, FlexRay needs more complex network configuration and parameter setting procedure, because it support various functions to compare with traditional features of CAN functions. As well as, in spite of the importance of scheduling compared to CAN network, absence of network scheduling methods and know-how are the biggest problems to apply FlexRay protocol to chassis networking system [10].

Numerous studies related to FlexRay have been conducted. Schmidt researched about the message scheduling method of static segment and dynamic segment in the FlexRay network systems. Armengaud sought ways of message slot of dynamic segment using the CAN ID priority method [11]. Seo suggested hybrid scheduling method using the FlexRay and CAN network [12]. In addition, Sethna mentioned that FlexRay implementation from the starting of the conversion with existing CAN system is useful [13]. As well as research about the FlexRay network scheduling, Commings conducted that FlexRay network design method rather than using the two CAN network with gateway was more effective as increasing the network traffics [14].

This paper presents a node-based FlexRay scheduling method for reducing software complexity in the FlexRay network systems when CAN network message database is migrated to static segment of FlexRay network systems. Node-based scheduling method proposed in this paper encloses all CAN messages of that node as one FlexRay node frame in the network and transmits one FlexRay node frame in the static segment. In other words, transmitting node broadcast with one FlexRay node frame enclosed all CAN message of that node, and the other nodes are disassembled and delivered necessary CAN message to application layer when received the FlexRay node frame. The remainder of this paper is organized as follows. Section II describes the overview of FlexRay protocol. Section III describes node-based FlexRay scheduling method. Finally, a summary and conclusion is given in Section IV.

II. Overview of the FlexRay protocol

FlexRay developed by the FlexRay consortium including BMW and Daimler Chrysler, Motorola, Philips is distributed real-time vehicle networking protocol [15]. FlexRay provides high speed transmission rate between 1Mbps and 10Mbps and guarantee network fault tolerance using the redundant dual channel. Also, FlexRay has deterministic and predictable transmission delay characteristic.

FlexRay communication cycle consists of four elements as shown in the Fig 1(a): a static segment, a dynamic segment, a symbol window, and a network idle time. First, a static segment can be transmitting synchronous frame with static time division multiple access method. Second, a dynamic segment can be transmitting asynchronous frame with dynamic mini-slotting based on the arbitration. Third, a symbol window send single symbol that is defined FlexRay protocol version. Finally, network idle time serves as a phase during which the node calculates and applies clock correction terms.

Fig 1(b) shows the media access control method of static segment in the FlexRay network systems. In the static segment, FlexRay transmits the frame using the time division multiple access (TDMA) method. In the figure, static segment divides static slot with the same length that is consist of an identical number of macroticks. Scheduling design of each node is performed for each channel. When the network is started, each node inserts frame into the slot, which has the same frame ID and slot counter values with each node, and transmits. At this time, each node can be transmitting the same frame ID to each channel for fail safety of transmitting frame.

Fig 1(c) shows the media access control method of dynamic segment in the FlexRay network systems. In the dynamic segment, FlexRay transmits the frame using the dynamic mini-slotting method. In the figure, dynamic segment divides very small length of mini slot. Here, slot counter is set

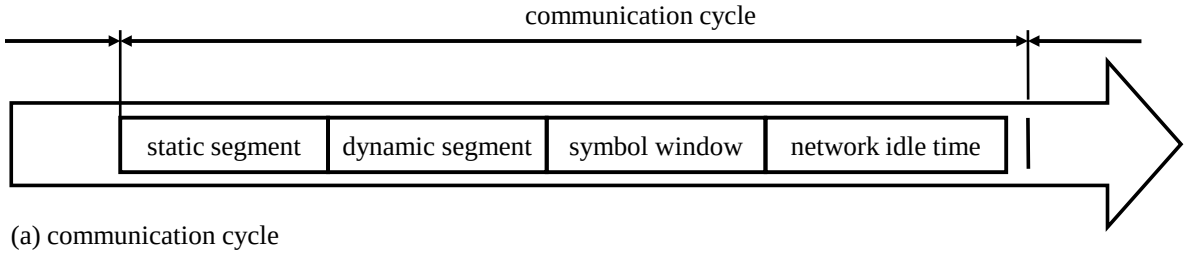

(a) communication cycle

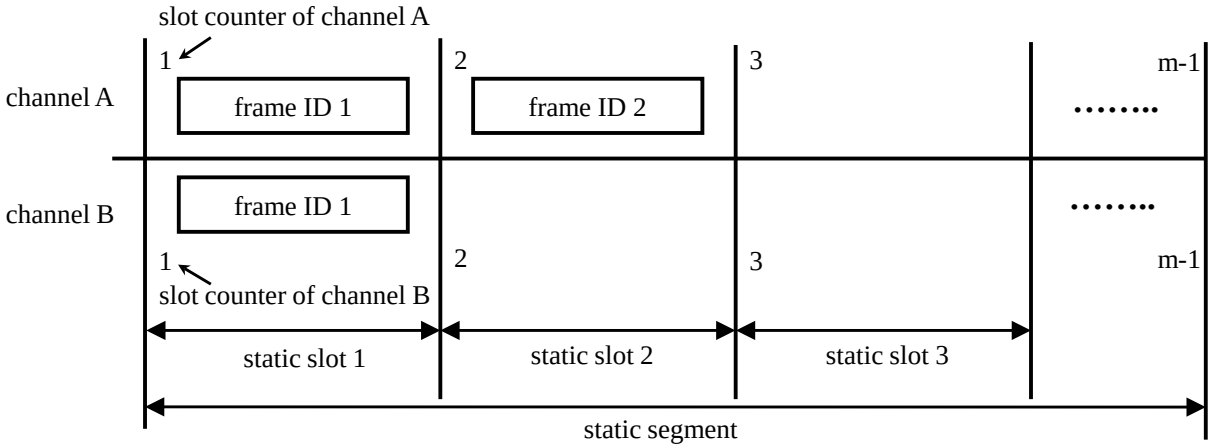

(b) medium access control in the static segment

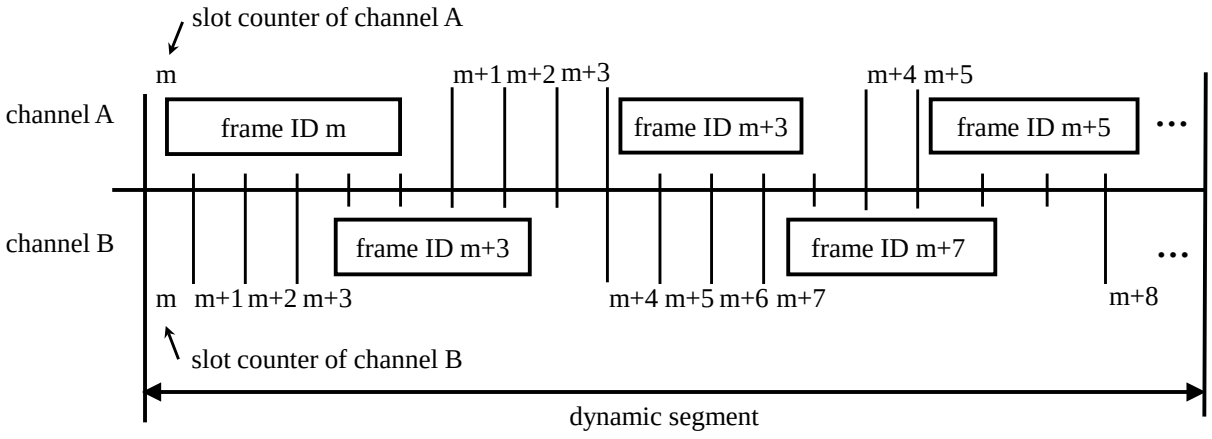

(c) medium access control in the dynamic segment

Fig 1. FlexRay communication cycle and medium access control method

a greater value than end of static slot number. In the dynamic segment, frame transmission method is similar to the static segment frame transmission. Namely, the frame generated from each node has a unique frame ID, and each node inserts frame into the mini-slot, which has the same frame ID and slot counter values with each node, and transmits. However, the number of mini-slot is allocated dynamically with the size of the frame length. In the figure, frame ID m is allocated as 6 mini-slots due to have a 5 or 6 mini-slot length. At this point, slot counter of next 7th mini slot is set to m+1, and frame with m+1 frame ID can be transmit in corresponding mini-slot.

III. FlexRay network system design using a node-based scheduling method

Generally, the scheduling of the FlexRay network systems consists of the following two steps. The first is cluster configuration to determine the structure of the network systems, and the second step is node configuration to determine the detailed function of each node. In the cluster configuration step, various network parameters, such as communication speed, communication cycle length, frame size, and static segment size, are set according to the frame information such as data length or generation period. In the node configuration step, various message parameters of the nodes, such as communication channel and frame ID, are set according to the frame information. These scheduling processes are carried out in the off-line state.

Unfortunately, the assigned static slot numbers and the software coding load increase rapidly during the node configuration step, as the number of messages in the FlexRay network systems increases. In particular, the scheduling process for migrating from well-defined CAN messages to static slots of the FlexRay is both extensive and complex, because commercial CAN message database has hundreds of messages with various data length and generation period. Furthermore, when the FlexRay network systems are configured in the off-line state, it is very difficult to add nodes or messages. In general, if we want to add a node or a message to the FlexRay network systems, all of the systems must be stopped, and scheduling information must be reloaded for all nodes.

To migrate efficiently from the commercial CAN messages to static slots of FlexRay network systems, this paper presents the node-based FlexRay scheduling method. In the node-based scheduling method, only one static slot of the FlexRay network is assigned to one node in a one-to-one correspondence. That is, the number of static slots in the static segment is the same as the number of nodes in the FlexRay network systems. And then, the transmitting node makes a single frame by assembling its all CAN messages and broadcasts the frame using the pre-assigned static slot in the static segment. While, the other nodes receives all FlexRay frames, disassembles CAN messages enclosed with FlexRay frame, and delivers necessary CAN messages to its application layer. In this way, an application layer engineer, which designs the majority of ECU functions, will be able to develop an ECU application software on the basis of the only well-defined CAN message database without regard to the configuration of FlexRay network system. While, a network layer engineer will be able to construct and maintain the FlexRay network system without regard to message features such as generation period or length. Consequently, this node-based scheduling method can reduce the scheduling complexity required to design the FlexRay network system.

Fig 2 shows the layer architecture of a FlexRay node for the node-based scheduling method to assemble a FlexRay frame from various CAN messages and disassemble a CAN message from a FlexRay frame. In general, a conventional FlexRay node consists of a physical layer, a data link layer, a transport layer, and an application layer. However, a slot management sub-layer is added to the application layer in the node-based scheduling method. The slot management sub-layer holds the slot assembly, slot disassembly, and message filtering functions. The slot assembly function furnishes the procedure for assembling the ID and data of a CAN message from the application layer, and creating an appropriate FlexRay frame format. The slot disassembly function provides the procedure for disassembling the ID and data of a CAN

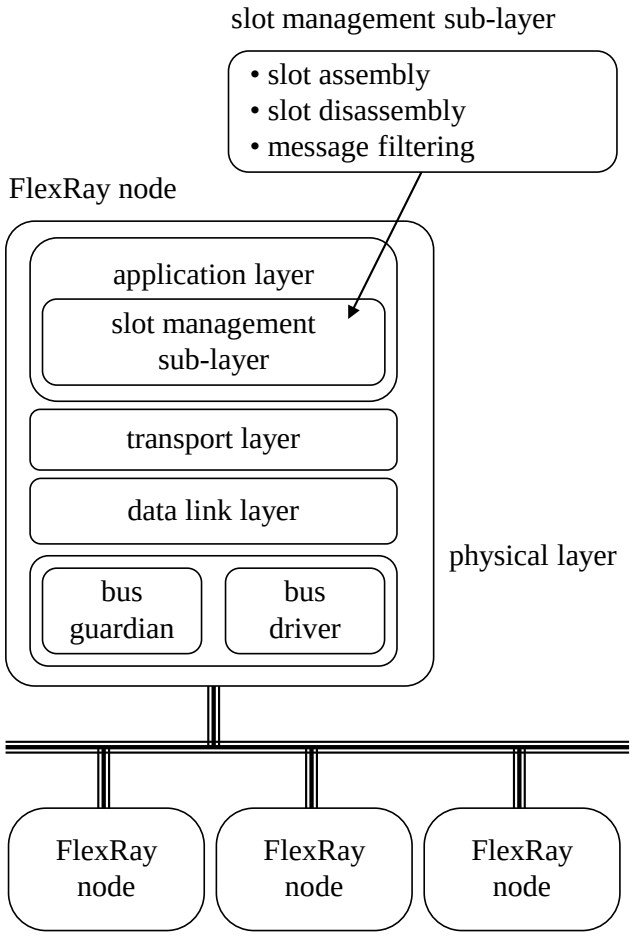

Fig 2. Layer architecture of a FlexRay node for the node-based scheduling method.

message from the lower layer, and creating the CAN message format. Finally, the message filtering function furnishes the procedure for receiving a designated message from the CAN message created with the disassembly function, and ignoring undesignated messages.

IV. Summary and Conclusions

This paper presents a node-based scheduling method for the static segment, to reduce software complexity in FlexRay networks in which the systems are designed using the CAN message database. To develop a node-based scheduling method, the communication structure for FlexRay network systems and the layer architecture for FlexRay nodes are suggested. The conclusions derived from this research are as follows.

First, the FlexRay network systems design consists of cluster and node configurations. Accordingly, when FlexRay network systems are designed using the automotive industry's CAN message database, effective system design is essential.
Second, when a network layer design engineer defines system design variables via a cluster or node configuration in the off-line state, the application layer design engineer that designs the majority of the main ECU functions will be able to develop an ECU application program that refers only to the CAN message database. Consequently, our node-based message scheduling method can reduce the effort required to design FlexRay network systems.

This research has been limited to testing the feasibility of the node-based scheduling method for simple experimental test code and specific network systems. Hence, the software complexity performance of the proposed method should be evaluated using a more realistic application, such as a chassis control system with a CAN message database. Besides, the development of various scheduling techniques will be needed to increase effective scheduling for the node-based scheduling method.

ACKNOWLEDGMENT

"This work was supported by the Grant of the Korean Ministry of Education, Science and Technology" (The Regional Core Research Progran/Institute of Logistics Information Technology)

REFERENCES

[1] S. Lee, D. H. Lee, M. H. Kim, and K. C. Lee, "Traffic-balancing algorithm for CAN system with dual communication channels to enhance the network capacity," International Journal of Automotive Technology, vol. 11, no. 4, pp. 525-531, August. 2010.
[2] E. Armengaud, A. Steininger, and M. Horauer, "Towards a systematic test for embedded automotive communication systems," IEEE Transactions on Industrial Infomatics, vol. 4, no. 3, pp. 146-155, August. 2008.
[3] M. H. Kim, S. Lee, and K. C. Lee, "Kalman predictive redundancy system for fault tolerance of safety-critical systems," IEEE Transactions on Industrial Infomatics, vol. 6, no. 1, pp. 46-53, Febuary. 2010.
[4] T. H. Hwang, K. Park, S. J. Heo, S. H. Lee, and J. C. Lee, "Design of integrated chassis control logics for AFS and ESP," International Journal of Automotive Technology, vol. 9, no. 1, pp. 17-27, February. 2008.
[5] E. G. Schmidt and K. Schmidt, "Message scheduling for the FlexRay protocol: the dynamic segment," IEEE Transactions on Vehicular Technology, vol. 58, no. 5, pp. 2160-2169, June. 2009.
[6] M. Rahmani, K. Tappayuthpijarn, B. Krebs, E. Steinbach, and R. Bogenberger, "Traffic shaping for resource-efficient in-vehicle communication," IEEE Transactions on Industrial Informatics, vol. 5, no. 4, pp. 414-428, November. 2009.
[7] N. Navet, Y. Song, F. Simonot-Lion, and C. Wilwert, "Trends in automotive communication systems," Proceedings of the IEEE, vol. 93, no. 6, pp. 1204-1223, June. 2005.
[8] J. Ryu, M. Yoon, and M. Sunwoo, "Development of a network-based traction control system, validation of its traction control algorithm and evaluation of its performance using net-HILS," International Journal of Automotive Technology, vol. 7, no. 6, pp. 687-695, December. 2006.
[9] H. Kopetz, and G. Grunsteidl, "TTP - a protocol fault-tolerant real-time systems," IEEE Computer, vol. 27, no. 1, pp. 14-23, January. 1994.
[10] M. H. Kim, K. N. Ha, S. Lee, and K. C. Lee, "Implementation of FlexRay network system using node-based scheduling method," Transaction of KSAE, vol. 18, no. 2, pp. 39-47, March. 2010.
[11] E. Armengaud, A. Steininger, and M. Horauer, "Towards a systematic test for embedded automotive communication systems," IEEE Transactions on Industrial Infomatics, vol. 4, no. 3, pp. 146-155, August. 2008.
[12] S. H. Seo, T. Y. Moon, J. H. Kim, S. H. Hwang, and J. W. Jeon, "A gateway system for an automotive system: LIN, CAN and FlexRay," 6th IEEE International Conference on Industrial Informatics, pp. 967-972, 2008.
[13] F. Sethna, E. Stipidis, and F. H. Ali, "What lessons can controller area networks learn from FlexRay," IEEE Vehicle Power and Propulsion Conference, pp. 1-4, 2006.
[14] R. Cummings, "Easing the transition of system designs from CAN to FlexRay," SAE Paper No.2008-01-0804, 2008.
[15] FlexRay consortium, FlexRay protocol specification 2.1 revision A, 2005.

2011 International Conference on Mechanical, Industrial, and Manufacturing Engineering
Lecture Notes in Information Technology Vols. 1-2

Localization for Fork-lift AGV using Extended Kalman Filter

Eunkook Jung and Kyunghoon Jung
Department of Interdisciplinary cooperative Course :Robot
Pusan National University
Geumjeong, Busan 609-735, Korea
{silverkook & hooraring}@pusan.ac.kr

Jungmin Kim and Sungshin Kim
School of Electrical and computer Engineering
Pusan National University
Geumjeong, Busan 609-735, Korea
{kim16 & sskim}@ pusan.ac.kr

Abstract - This paper presents improving the accuracy of the localization using the extended Kalman filter for AGV (automatic guided vehicle). In general, the existing localizations for AGV use the global sensor and the local sensors for localization. However, the local sensors were not suitable for AGV which is required to high accuracy because the local sensors have an accumulative error. Therefore, this paper proposes the improved method to measure a position of AGV using the extended Kalman filter. For experiment, we tested the accuracy of the localization while AGV moves 10 times, and verified that the localization accuracy was improved.

Index Terms - Extended Kalman Filter, Localization, AGV, Local Sensor, Sensor Fusion

I. INTRODUCTION

The unmanned transportation systems have been developed in 1955. The AGV has been used at the manufacturing industry, warehouse, and container terminal. There are two existing guidance systems for the AGV. They are wire guidance and magnet-gyro guidance. The sensor of the wire guidance system is placed on the bottom of the AGV, and wire is placed approximately 1 inch below the ground. The sensor detects the radio frequency being transmitted from the wire. It has an advantage that can turn off the wire's power in urgent situation and stop immediately the system of AGV. The magnet-gyro guidance system is similar to wire guidance system, but it uses the transponders of gyro which are embedded in the floor of the work place [1-5]. In Recent years, the laser guidance system is studied actively without a guided wire. However, the method is difficult to measure an accurate position because the laser navigation has slow response time. Therefore, we studied the method using a local sensor to supplement the method using laser navigation system because local sensor has high speed response time. However, this method using local localization sensor is not suitable for AGV which is required high accuracy. However, local sensor has many error values. Therefore, this paper proposes the improved method to measure a position of AGV using the extended Kalman filter, EKF is used to minimize the error of local localization sensor. The measured local position data is fused with the global position data to use for localization of AGV.

Fig. 1 Used fork-lift AGV

II. AGV SYSTEM

For experiment, we designed the fork-type AGV. The actuator of the AGV is axletree driving system. Fig. 1 shows the fork-type AGV used in this study.

A. Measurement System

We used the NAV200 of SICK Co., Ltd to receive the global position data. Also, we used the encoder and gyro as local Position data. Table 1 shows the specification about used sensors for localization of the fork-lift AGV.

TABLE I
Spec. of used sensors

Item (model)	Sensor specification	
Laser navigation	Voltage	24
	Resolution	approx. 15(mm)
	Typ. range	1.2 ~ 28.5(m)
Encoder	Voltage	12(V)
	Resolution	1000(pulse)
Gyro	Voltage	5(V)
	Sensitivity	±300˚/s

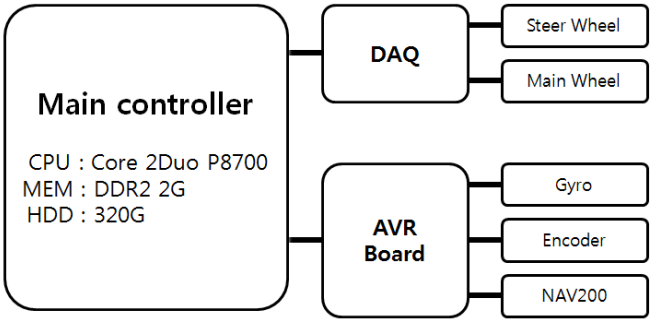

Fig. 2 System configuration of AGV.

The position data is received by NAV200 within 400ms and by encoder and gyro within 100ms. The received position data is transmitted from DAQ to control actuator. The entire system of the AGV is briefly shown in Fig. 2.

B. Kinematics

The wheels of the used fork-type AGV are consisted of the driving wheel and road wheel. Fig. 3 shows the kinematics model on the curve driving of the fork-type AGV. Then it shows the global coordinates (*O*-*X*-*Y*) and local coordinates (*o*-*x*-*y*). The driving of fork-type AGV is performed by an angle and velocity of driving wheel with velocity of load wheel. In Fig. 3, h_1 is the length between the center axletree of fork-type AGV (O_{ICR}) and the center of the driving wheels is calculated by Eq. (1).

$$h_1 = \frac{l}{\sin\delta} \tag{1}$$

At the time of rotation of the wheel on the floor, if there is no slip, the linear velocity of the wheel is the actual velocity of the fork-type AGV. The v_d is the linear velocity of the fork-type AGV, the linear velocity is calculated as following.

$$v_d = r_d\, w_d \tag{2}$$

In Eq. (2), r_d is the radius of driving wheel and w_d is the angular velocity of driving wheel. r_d and w_d are expressed by the coordinates and the direction angle as following.

$$\begin{aligned} \dot{X} &= v\cos\theta = r_d w_d \cos\theta \\ \dot{Y} &= v\cos\theta = r_d w_d \cos\theta \\ \dot{\theta} &= \frac{r_d w_d \sin\delta}{l} \end{aligned} \tag{3}$$

III. Localization System

The localization of AGV using encoder and gyro should consider slip of wheel and increased cumulative errors. Therefore, we present the localization method using the extended Kalman filter for minimizing the error of local sensors for localization.

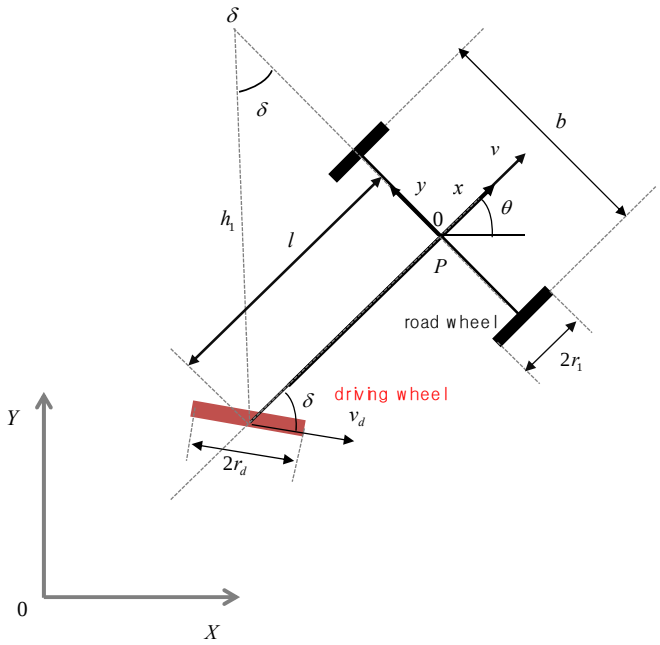

Fig. 3 Kinematics model of fork-type AGV

A. The Extended Kalman Filter

The Kalman filter produces minimum error variance by probabilities from the motion model and the observation model [6]. Especially, the Kalman filter can assist computers to track objects with low latency. Although the tracking of objects is a dynamic problem, the Kalman filter has simple algorithm, low steady state time. Then it is useful to real-time computing. However, to reduce the noise using the Kalman filter, the system must be linear. Therefore we use the extended Kalman filter. It is the nonlinear version of the Kalman filter which linearize about the current mean and covariance

B. Motion Model

AGVs motion model is defined as current position of AGV through kinematics. The input of current AGV (u_k) is calculated by the linear velocity and angular velocity that used data of encoder and gyro. The nonlinear equation of motion model can be expressed linear equation as Eq. (5).

$$z^{-} = A_k x_{k-1}^{T} + W_k u_k^{T} \tag{4}$$

Then, a Jacobian matrix (A_k, W_k) is calculated by the following Eq. (6) and (7).

$$W_k = \frac{\partial f(x_{k-1}, u_k, 0)}{\partial u_{k+1}} = \begin{bmatrix} 1 & 0 & \cos(\theta_k - \delta_k) \\ 0 & 1 & \sin(\theta_k - \delta_k) \\ 0 & 0 & 1 \end{bmatrix} \tag{5}$$

$$W_k = \frac{\partial f(x_{k-1}, u_k, 0)}{\partial u_k} = \begin{bmatrix} \cos(\theta_k - \delta_k) & 0 \\ \sin(\theta_k - \delta_k) & 0 \\ 0 & 1 \end{bmatrix} \tag{6}$$

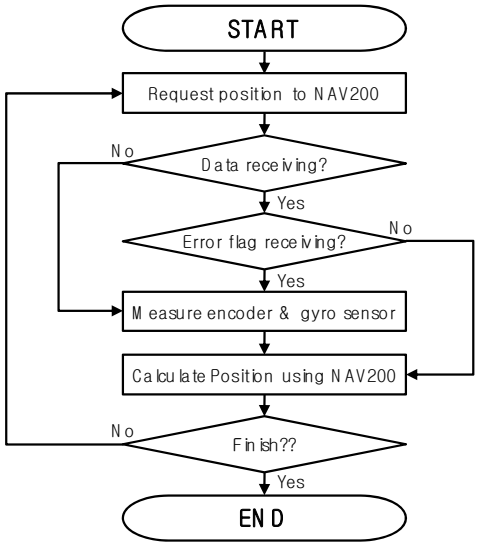

Fig. 4 Algorithm of sensor fusion.

C. *Measurement Model*

An observed variable (z) is used predicted value through the extended Kalman filter. The predicted value represents a current position (x, y) and angle (θ) of AGV as equation (9); therefore, it is applied to a measurement.

$$z^{-} = H \begin{bmatrix} x_k^{nav} \\ y_k^{nav} \\ \theta_k^{nav} \end{bmatrix} \tag{9}$$

D. *Sensor Fusion*

The laser navigation is able to measure the global position of AGV, however it has low response time and lack of data when the AGV move care or it has high speed because of problem is not correctly recognized the reflects. we achieved high accuracy of localization by fusing the predicted position data through the extended Kalman filter and the global position data. The flowchart of the sensor fusion is shown in Fig. 4

IV. Experiments and Results

A. *Experimental Environment*

To verify the performance of the proposed sensor fusion, we experiment on actual AGV. The 13 reflectors are installed for the laser navigation sensor.

B. *Localization Result*

we tested accuracy of localization of AGV as circle road driving because the AGV has high error when moving curve. In the test, the driving speed and steer angle were fixed to drive stable. The result of the experiments with former method is shown in Fig. 2. As shown in Fig. 2, it is accurate position data as close as the circle.

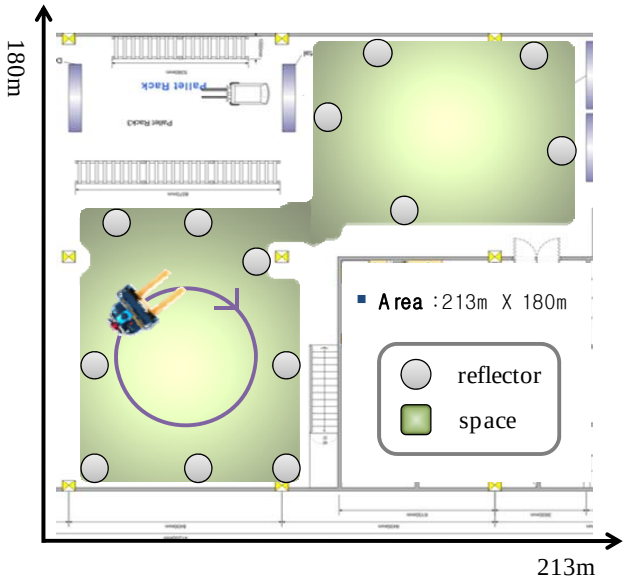

Fig. 5 Experimental environment

In the results, we are able to verify that the former method has many errors because of it doesn't consider the errors measured by local position data, and we was able to verify that the proposed method has higher accuracy.

V. Conclusions

This paper presents the localization method using the extended Kalman filter to minimize the error of local sensors. For experiment, we designed a fork-lift type AGV. The localization sensors are used a laser navigation, a gyro and two encoders. To reduce the accumulative error of local sensors, we applied the extended Kalman filter, and minimized the error of local sensors that is caused by the slip of the wheels and the error by numerical integration. For experiment, we tested the accuracy of the localization while AGV moves 10 times, and verified that the proposed method is efficiently.

Acknowledgment

This work was supported by the Grant of the Korean Ministry of Education, Science and Technology" (The Regional Core Research Program/Institute of Logistics Information Technology)

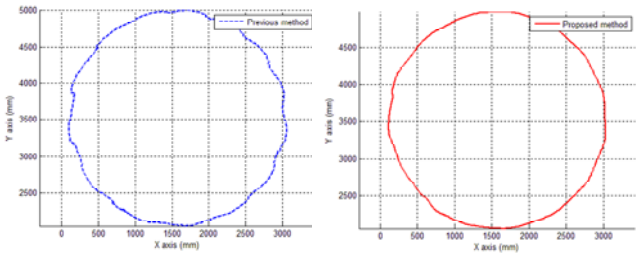

(a) general method (b) proposed method

Fig. 6 Localization result

REFERENCES

[1] J. Borenstein, "The OmniMate: A Guidewire and Beacon-free AGV for highly Reconfigurable Applications," *International Journal of Production Research*, vol. 38, no. 9, pp. 1993-2010, 2000.

[2] C. Y. Chan, *A System Review of Magnetic Sensing System for Ground Vehicle Control and Guidance*. California PATH Research Report, UCB-ITS-PRR-2002-20, 2002.

[3] M. J. Caruso, T. Bratland, C. H. Smith and Rober Schneider, "A New Perspective on Magnetic Field Sensing," *Sensor Magazine*, Vol. 15, No. 12, pp. 34-46, 1998.

[4] C. Y. Chan, and H. T. Tan, *Evaluation of Magnetic as a Position Reference System For Ground Vehicle Guidance and Control*, California PATH Research Report, UCB-ITS-PRR-2003-8, March, 2003.

[5] Y. J. Ryoo, E. S. Kim, and Y. C. Lim "Intelligent Positioning System for Magnetic Sensor Based Autonomous Vehicle," *SCIS & ISIS*, 2004. Y. J.

[6] Deok-Jein Lee and Kyle T. Alfriend "Precise Real-Time Orbit Estimation Using The Unscented Kalman Filter," Advances in the Astronautical Sciences, Vol. 114, 3, pp. 1853-1872, 2003.

[7] L. Jetto, S. Longhi, and G. Venturini "Development and Experimental Validation of an Adaptive Extended Kalman Filter for the Localization of Mobile Robots," *IEEE Transactions on Robotics and Automation*, vol 15, no 5, pp. 219-229. April, 1999.

2011 International Conference on Mechanical, Industrial, and Manufacturing Engineering
Lecture Notes in Information Technology Vols. 1-2

Rework Center Attached to a Queueing-Inventory System with Budgetary Constraint

Rasoul Haji, Ehsan Khodabandeh and Alireza Haji
Industrial Engineering Department
Sharif University of Technology
Tehran, Iran
haji@sharif.edu, e_khodabandeh@ie.sharif.edu, ahaji@sharif.edu

***Abstract* - In this paper we consider a single retailer with an attached rework center. Retailer faces a Poisson demand with a known rate and adopts a base stock policy, that is, as soon as a demand arrives he orders a unit to a supplier with an ample stock. All demands must be satisfied. If retailer is out of stock, the demand will be backlogged. The lead time of the retailer is a random variable with a general distribution function. Each arriving unit to the retailer is defective with a known probability. When a customer finds that his purchased unit is defective he sends this defective unit to the rework center of the supplier, which is attached to the retailer, and waits for the rework of his unit. We assume that the rework processing time for a defective unit is a random variable with a general distribution function and there is an investment constraint on the average inventory and queue size at the rework center. In this paper first we derive the long run unit total cost of the system consisting of holding and backordering cost of retailer, queueing and processing cost of the rework center. Then we obtain the optimal inventory position of the retailer with the above investment constraint.**

Keywords - Base Stock, Defective Item, Backorder, Investment Constraint

I. Introduction

Recently, many researchers have worked on queueing systems with inventory control where customers arrive one by one and require service. Customers need exactly one item form the inventory and the on-hand inventory is dropped by one at the moment of satisfying customer's demand. Served customer departs immediately from the system and replenishment of the inventory is placed with an external supplier. These systems are called queueing-inventory systems [1].

Several models in this field, especially those related to our work, have been developed up to now. Reference [2] considered a two-echelon repairable inventory system consisting of a central depot and multiple stocking centers where centers inventory replenishment policy is one-for-one. In their model, centers received defective items and passed them to the depot for repair. They assumed that depot replenishment lead times are different across stocking centers. They investigated the impact of such assumptions on system performance and derived probability distributions of the random delays at the depot experienced by center replenishment orders.

Reference [1] considered M/M/1 queueing system with inventory under continuous review, different inventory management policies, and with lost sales. They assumed that service times and lead times are exponentially distributed. They derived stationary distributions of queue length and inventory processes in explicit product form.

Reference [3] considered a similar model with backorders for unsatisfied demands. They computed performance measures, presented an approximation scheme for it, and derived optimality conditions under different order policies.

Reference [4] considered a queueing-inventory system with two classes of customers when service times and supplier's lead time follow exponential distributions. They showed a priority service rule to minimize the long-run expected waiting cost by dynamic programming method and also, they found the necessary and sufficient condition for stability of the priority queueing- inventory system.

Reference [5] dealt with a multistage queueing-inventory model by decomposing it into multiple single-stage inventory queues. This decomposition approach let them provide an accurate performance estimates and also, enabled them to solve an optimization problem that minimizes the total inventory cost subject to a required service level.

To our knowledge, we have not found any literature studying a queueing-inventory system with two successive and related queues, one-for-one replenishment rule, backordering policy, and also an investment constraint. The rest of the paper is organized as follows. The model, notations and problem formulation are all described in section II. In section III we discuss our numerical studies and we conclude in section IV.

II. Model description

Consider a network for a single item that consists of a retailer and a rework center. Customers arrive at retailer according to a Poisson process with rate λ and each customer needs exactly one item from the inventory. The retailer replenishment ordering policy is based on base stock or (R-1, R) inventory system, with R being the maximum inventory level. So each time a customer arrives, an order is placed immediately with an external supplier with infinitive capacity. Thus every customer is served by an item if available, backlogged otherwise. Note that the replenishment lead time, which is the time between ordering of goods and receiving them, is a random variable with a general distribution function.

But, a certain fraction, say α of the goods is defective. Each time a customer receives a defective item, he goes to the rework center to be served. The distribution of rework processing time is unknown with finite mean and variance, μ and σ^2 respectively. Thus customers leave the system with rate $\lambda(1-\alpha)$ and join the rework center queue with rate $\lambda\alpha$ (see Fig. 1).

978-0-9831693-1-4/10/$25.00 ©2011 IERI

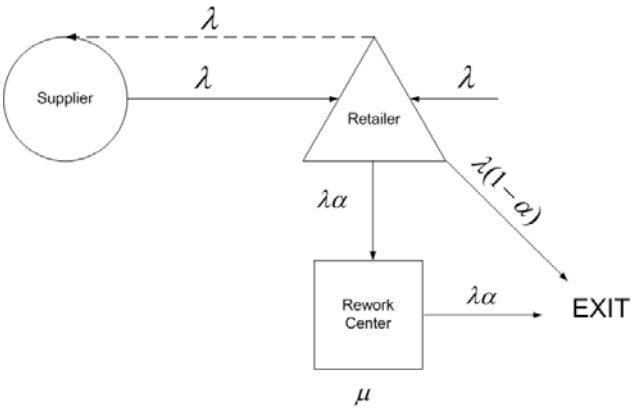

Fig. 1 Queueing-inventory system with one retailer and an attached rework center

Based on these assumptions, one can see that we have a queueing-inventory system with two consecutive queues. The supplier queue and the rework center queue.

In this paper we consider the following costs: holding cost for on-hand inventory at retailer, shortage or delay cost, queueing and processing cost of the rework center. Note that based on our (R-1, R) policy, we assume that ordering cost in comparison with holding and shortage costs is negligible.

A. Notations and Problem Formulation

The objective is to find the optimal base stock level which minimizes the system total cost. Let us introduce the following notations:

λ : Demand rate (mean customer arrival rate)

μ : Mean service time at rework center

σ^2 : Variance of service time at rework center

α : Percentage of defective items

L : Length of retailer's lead time

$\bar{L}$: Expected value of L

$D(L)$: Mean demand during lead time of the retailer

N : Average number of customers at rework center

h : Unit holding cost per unit time at the retailer

$\hat{\pi}$: Unit backorder cost per unit time at the retailer

R : Inventory position of the retailer

R^* : The optimal value of R

$\bar{I}(R)$: Retailer expected number of on-hand inventory

$\bar{b}(R)$: Retailer expected number of backorders

C_1 : Unit penalty cost for customer's waiting time at rework center

C_2 : Unit processing cost of defective items at the rework center

C : Unit cost of investment (in retailer's inventory and rework center's queue size)

B : Maximum available budget

$TC(R)$: Expected total cost per unit time

According to the above notations, we consider the following cost function for the system in which N is the average number of customers at rework center:

$$TC(R) = h\bar{I}(R) + \hat{\pi}\bar{b}(R) + C_1 N + C_2\lambda\alpha \quad (1)$$

One can easily show [6] that the average inventory in retailer is:

$$\bar{I}(R) = R - D(L) + \bar{b}(R) \quad (2)$$

Form (1) and (2) we have:

$$\begin{aligned} TC(R) &= h(R - D(L) + \bar{b}(R)) + \hat{\pi}\bar{b}(R) + C_1 N + C_2\lambda\alpha \\ &= h(R - D(L)) + (h + \hat{\pi})\bar{b}(R) + C_1 N + C_2\lambda\alpha \end{aligned} \quad (3)$$

For computing this cost function, we need to know the values of $D(L)$, N, and $\bar{b}(R)$ which the latter can be determined by formula (4).

$$\bar{b}(R) = \sum_{j=R}^{\infty}(j - R)P_j \quad (4)$$

Where $P_j = P(D(L) = j)$ is the probability that the lead time demand is equal to j, which in base stock system is the same as the number of outstanding orders at retailer.

For further computations first, we should take a look at our queueing-inventory system. As we know, at the time $t + L$ all replenishments that were ordered before t, have been received. So the outstanding orders are those occurred between t and $t + L$. Since the demand is Poisson with rate λ, the number of outstanding orders follows a Poisson distribution with mean $\lambda\bar{L}$.

Moreover, by a result due to [7], the number of outstanding orders in a one-for-one inventory system with Poisson demands, complete backlog of unsatisfied demands, and arbitrary but independent lead times, is the same as the number of customers in an M/G/∞ queueing system. In other words, the steady state occupancy level in an M/G/∞ system is Poisson with mean $\lambda\bar{L}$ where λ is the arrival rate and $\bar{L}$ is the average retailer's replenishment lead time.

On the other hand, according to the arrival rate and service time at rework center, we have an M/G/1 queueing system in this center.

Now considering these two consecutive queues, we can determine the cost function's components as follows:

$$P_j = \frac{(\lambda\bar{L})^j e^{-\lambda\bar{L}}}{j!} \quad (5)$$

By substituting (5) in (4) and with some algebra the following expression can be concluded for $\bar{b}(R)$:

$$\bar{b}(R) = \lambda\bar{L}\left(1 - F(R-2, \lambda\bar{L})\right) - R\left(1 - F(R-1, \lambda\bar{L})\right) \quad (6)$$

Where $F(a,b) = \sum_{i=0}^{a}\frac{e^{-b}b^i}{i!}$ is the Poisson cumulative distribution function with parameter b in which the number of random events occurring will be between zero and a.

Now, mean amount of demand during lead time and the average number of customers at rework center are of interest.

By using Little's formula [8], we see that the value of $D(L)$ is equal to $\lambda\bar{L}$. Therefore, using (6) and (2) we can write:

$$\begin{aligned}\bar{I}(R) &= R - D(L) + \bar{b}(R)\\ &= R - \lambda\bar{L} + \lambda\bar{L}\left(1 - F(R-2,\lambda\bar{L})\right) - R\left(1 - F(R-1,\lambda\bar{L})\right)\\ &= R\left(F(R-1,\lambda\bar{L})\right) - \lambda\bar{L}\left(F(R-2,\lambda\bar{L})\right)\end{aligned} \quad (7)$$

Moreover, as one knows the value of N for an M/G/1 system is obtained by Pollaczek-Khintchine formula [8] that is:

$$N = \rho + \frac{\rho^2 + (\lambda\alpha)^2\sigma^2}{2(1-\rho)} \quad ; \ \rho = \lambda\alpha\mu \quad (8)$$

From (6), (8), and (3) we can easily show that:

$$\begin{aligned}TC(R) &= \hat{\pi}\left(\lambda\bar{L} - R\right)\\ &+ (h+\hat{\pi})\left[R\left(F(R-1,\lambda\bar{L})\right) - \lambda\bar{L}\left(F(R-2,\lambda\bar{L})\right)\right]\\ &+ C_1\left(\rho + \frac{\rho^2 + (\lambda\alpha)^2\sigma^2}{2(1-\rho)}\right) + C_2\lambda\alpha\end{aligned} \quad (9)$$

But as we mentioned before, we have an investment constraint on the average inventory and queue size in the rework center. From (7) the average investment in retailer's inventory is:

$$C * \bar{I}(R) = C * \left(R\left(F(R-1,\lambda\bar{L})\right) - \lambda\bar{L}\left(F(R-2,\lambda\bar{L})\right)\right) \quad (10)$$

Also, form (8) the average investment in queue size of the rework center is:

$$C * N = C * \left(\rho + \frac{\rho^2 + (\lambda\alpha)^2\sigma^2}{2(1-\rho)}\right) \quad (11)$$

Therefore from (10) and (11) the investment constraint for the average inventory and queue size can be writhen as:

$$C\left[\begin{aligned}&R\left(F(R-1,\lambda\bar{L})\right) - \lambda\bar{L}\left(F(R-2,\lambda\bar{L})\right)\\ &+ \rho + \frac{\rho^2 + (\lambda\alpha)^2\sigma^2}{2(1-\rho)}\end{aligned}\right] \le B \quad (12)$$

To find R^*, the optimal value of R, which minimizes (9) subject to (12), first we obtain R_0 which minimizes the cost function (9) regardless of the budgetary constraint (12). Clearly, R_0 is the smallest integer for which

$$\Delta TC(R) = TC(R+1) - TC(R) \ge 0, \quad (13)$$

Or equivalently,

$$\Delta TC(R) = -\hat{\pi} + (\hat{\pi} + h)\left[F(R,\lambda\bar{L})\right] \ge 0 \quad (14)$$

That is R_0 is the smallest integer for which the following relation holds:

$$F(R,\lambda\bar{L}) \ge \frac{\hat{\pi}}{\hat{\pi} + h} \quad (15)$$

If R_0 satisfies the budgetary constraint (12), then $R^* = R_0$. Otherwise, the optimal base stock, R^*, is obtained from budgetary constraint (12). That is, R^* is the largest integer which satisfies the following relation:

$$C\left[\begin{aligned}&R^*\left(F(R^*-1,\lambda\bar{L})\right) - \lambda\bar{L}\left(F(R^*-2,\lambda\bar{L})\right)\\ &+ \rho + \frac{\rho^2 + (\lambda\alpha)^2\sigma^2}{2(1-\rho)}\end{aligned}\right] \le B \quad (16)$$

In order to illustrate the obtained results, we present a numerical study in the next part.

III. Numerical example

Let's assume that there is a retailer which faces demands according to a Poisson Process with rate of 2 per day, and each customer needs exactly one unit of item. The retailer immediately places an order to the supplier to replenish the inventory. Customer's demand will be satisfied if enough inventory is available, backordered otherwise. We assume that retailer's lead time is constant and it is equal to 1 for each item and also 10% of the items are defective. Customers who have received imperfect items send their goods to the rework center whose service time follows an Erlang-2 distribution with mean 2 days. Moreover, we use holding cost per unit per unit time of 1, and backorder cost per unit per unit time of 5. Furthermore, $C_1 = 2$, $C_2 = 1$, $C = 2$, and investment cannot be more than 4.

Considering these parameters and based on the previous section results, we obtain the optimal base stock level to minimize the system total cost. The following table shows these calculations with respect to different values of base stock.

According to the cost function, one can see that the optimal value of base stock which minimizes the total cost function is 5. But since we have a budgetary constraint on the average inventory and queue size, the costs cannot exceed 4. Thus, the optimal base stock level is equal to 3, which satisfies the investment constraint. Fig.2 illustrates these results.

IV. Conclusion

We studied a queueing-inventory system consisting of a single retailer with an attached rework center. Retailer faces a Poisson demand with a known rate and adopts a base stock policy. Unsatisfied demands at retailer are backordered. We assumed that a certain fraction of the arriving unit to the retailer is defective and when a customer finds a defective unit he will sent it to the rework center of the supplier to be reworked. It is assumed that the rework processing time for a defective unit is a random variable with a general distribution function and also the lead time of the retailer is a random variable with a general distribution function. Under these assumptions and subject to an investment constraint on the average inventory and queue size in the rework center, we derived the long run unit total cost of the system and obtained the optimal inventory position of the retailer which minimizes the total cost.

TABLE I
TOTAL COST (TC) AND INVESTMENT CONSTRAINT WITH RESPECT TO DIFFERENT BASE STOCK VALUES (R)

Base Stock (R)	Total Cost (TC)	Investment Constraint
2	9.343612051	3.047870684
3	6.882752538	3.894250846
4	5.76614387	5.188714623
5	5.657723338	6.819241113
6	6.154215685	8.651405228
7	6.953164474	10.58438816
8	7.88173745	12.56057915
9	8.858919498	14.55297317

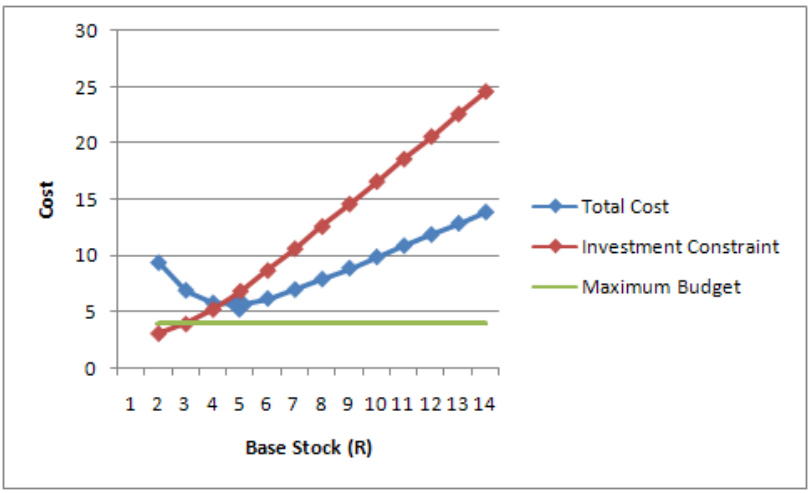

Fig. 2 Optimal base stock with respect to investment constraint and maximum budget

Reference

[1] Schwarz M, Sauer C, Daduna H, Kulik R, Szekli R, "M/M/1 Queueing systems with inventory", *Queueing Syst*, vol. 54, pp. 55–78, 2006.
[2] Y. Wang, M.A Cohen, and Y-S Zheng, "A two echelon repairable inventory system with stocking-center-dependent depot replenishment lead times", *Management Science*, vol. 46, no.11, pp. 1441-1453, 2000.
[3] Schwarz M, Daduna H, "Queueing systems with inventory management with random lead times and with backordering", *Math. Meth. Oper. Res*, vol. 64, pp. 383–414, 2006.
[4] Zhao N, Lian Z, "A queueing-inventory system with two classes of customers", *Int. J. Production Economics*, vol. 129, pp. 225–231, 2011.
[5] L. Liu, X. Liu, D.D. Yao, "Analysis and Optimization of a Multistage Inventory-Queue System", *Management Science*, vol. 50, no. 3, pp. 365-380, 2004.
[6] G. Hadley, T.M. Whitin, *Analysis of Inventory Systems*, Prentice Hall Inc, 1963.
[7] C. Palm, "Analysis of the Erlang traffic formulae for busy- signal arrangements", *Ericsson Tech*. vol. 4, pp. 39-58, 1938.
[8] D. Gross, C.M. Harris, *Fundamentals of Queueing Theory*, John Wiley and Sons Inc, 3rd Ed, 1998.

2011 International Conference on Mechanical, Industrial, and Manufacturing Engineering
Lecture Notes in Information Technology Vols. 1-2

Estimation and Distribution in the Mass Budget Process for Satellite

Jose Alvarez, Student.
Department of Spacecraft Technology, School of Astronautics.
Beijing University of Aeronautics and Astronautics- BUAA.
Beijing. People's Republic of China. 100191.
Josegalvarez07@gmail.com.

***Abstract*— The estimation and distribution of the mass budget for satellite is an delicate process in the approach for the design in a spacecraft. The accuracy in it can prevent overload of work and mistakes in the development process that could increase the cost of production. All this estimation and distribution process of the mass is done for groups of work that have to be linked with every sub systems or design teams, this conforms the preliminary tasks for the design of the communications satellite. For the investigation was used information in the Vx-Sat project which is a system engineering exercise, realized in the China Academy of Space Technology (CAST). The objective of the paper is to demonstrate an analysis of the procedures in the estimation and distribution in the mass budget process for satellite using suitable software's and shows the importance of the whole process to get the more reliable results. Likewise includes the most important information of the Vx-Sat system, preliminary requirements in the structure and finally all the methodology used to the analysis of the general estimation of the mass properties with its results.**

Keywords- CoG: Center of Gravity, Mass Budget, Moment of Inertia, Mass Balance.

I. INTRODUCTION

The structure subsystem withstand loads to meet environmental requirements for ground, ascent and in-orbit operations without failure or harmful deformation and maintain the necessary dimensional stability to satisfy all mission requirements throughout the service life. [1]. The satellite structure provides the mechanical supports for the units and others subsystems in the configuration that meets the systems requirements of thermal control, mass properties, alignment, launch vehicle interface and assembly integration and test. [2].

The principal factor driving structural design is that of minimizing mass. It must be extremely efficiently used and utterly reliable. The prime requirement is for the minimum structure which can achieve the goals during the dynamic loading with which it is presented during the testing and launch phases and finally in the zero-gravity operational environment. What makes spacecraft structural engineering perhaps unique is that its goals are strongly dependent on other subsystems such as thermal design, attitude control, communications and power. Structural design does not only encompass materials selection and configuration but must also include analysis and verification testing as part of the process, with an increasing reliance being placed upon analytical methods as experience grows.[3].

II. OVERVIEW OF THE SYSTEM

The structure of the satellite unit is used to provide the physical support for all the units in a configuration that meets the system requirements and the launch vehicle constraints. The main structure of the Vx-Sat is a typical satellite bus, with the limited modifications to accommodate features to it. Consist of Communications Module (C.M), Service Module (S.M.) and Propulsion Module (P. M.). The reference coordinate system of the structure shall be defined as follow:

- The origin O, is the center of the circle Φ 1194 in the satellite / launch vehicle separation plane.
- The Z axis is perpendicular to the separation plane from the origin O toward the top of the satellite.
- The X axis is included in the separation plane and toward east side.
- The Y axis completes the direct orthogonal system (X, Y, Z).

The +Z direction is the earth direction, the +Y direction is the south direction and the +X direction is the east direction, when the satellite is on geostationary orbit in the on-station attitude.

The Vx-Sat consists of 16 active Ku-band repeaters to receive, amplify and transmit the communications signals over the defined coverage areas; Vx-Sat has two coverage areas which are showed in Figure 1. Ground stations will be considered as fixed in the coverage zone. The Vx-Sat, is a geosynchronous communications satellite developed for CAST by Venezuelan trainees. The launch mass is less than 2600 Kg. the system design is based in DFH-3 bus with limited codifications to accommodate to the communications payload.

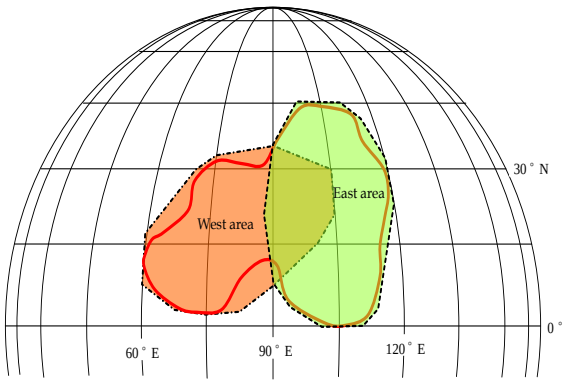

Fig. 1. Coordinates of coverage areas of the Vx-Sat.

III. REQUIREMENTS

A. *Structural Requirements.*

The structure shall be designed to withstand loads without permanent deformations (beyond specified limits or fracture loads) to comply with environmental requirements for ground, ascent and in-orbit operations. The relevant load and environmental requirements (with the maximum expected duration if pertinent) like thermal effects on the structure, including temperature, thermal stresses and deformations, mechanical and physical property changes of the materials have to be also considered. The structure subsystem will hold on and maintain the necessary dimensional stability to satisfy all mission and systems requirements [4].

B. *MassProperties.*

The mass of the structure should not exceed 200 kg. This mass includes all the constituting parts of the structure subsystems. There is no specific value to meet about the position of the gravity center and inertias: these constraints are already integrated at system level in the application interface and layout drawings. The center of gravity (COG) position should be calculated with ±10% accuracy in a coordinate system parallel to the reference coordinate system in which the origin is the structure center of gravity.

C. *The General Mass Budget.*

Dry mass budget of satellite is 10009.664 kg, the mass with balance weight was used for the propellant calculation, a margin of 22.64 kg is reserved giving a dry launch mass 0f 1041 kg and a total launch mass of 2428.643 kg approximately 2429 kg. The spacecraft mass budget is shown in the table I, harness and connectors calculation is included in each subsystem mass, additional 14 kg is included as others assembly, cables and pipelines.

TABLE I. MASS BUDGET

Subsystem / System	Specified Mass(kg)
Payload	183.84
TC&R	38.95
OBDH	43.9
EPS	275.212
AOCS	87.456
UPS	336.454
Thermal	51.584
Structure	178.268
Others (Pipe lines, Cables, Assembly)	14
Dry Mass Sub-Total	1009.664
Balance Weight	31.36
Total for UPS Propellant Calculation	1041.024
Margin	22.64
Total Mass Dry Budget	1063.664
Helium	3.759
MON-1	862.37
MMH	521.49
Total Propellant Mass	1387.619
Total Launch Mass	248.643

D. *Layout.*

The primary structure of Vx-Sat has a parallel hexahedral box organized around a central cylinder which interfaces with the launch vehicle. The box main body of the satellite is: 2208mm (L) x 1720mm (W) x 2238mm (H). The inner of the main body houses most of the satellite units. The outer of main body are attached with all the appendages. Solar arrays are attached to each side of the north and south, Ku bands antennas are attached to each side of the west and east, other bands antennas are mounted in the top. The preliminary layout configuration of the Vx-Sat is composed as is show in the table II.

TABLE II. STRUCTURE COMPONENTS

Quantity	Component	Module
1	North Lower Panel	Service Module
1	South Lower Panel	Service Module
1	North Panel	Communication Module
1	South Panel	Communication Module
1	West Panel	Communication Module
1	East Panel	Communication Module
1	Earth Panel	Communication Module
1	Anti Earth Panel	Propulsion Module
2	Anti Earth Lateral Web 1	Propulsion Module
4	Anti Earth Lateral Web 2	Propulsion Module
2	Earth Panel Web	Communication Module
1	Central Cylinder	Propulsion Module
1	Internal Panel	Propulsion Module
1	East Low Panel	Propulsion Module
1	West Low Panel	Propulsion Module

In the Figure 2 is possible check the layout of the Vx-Sat according to the components in each module as follow:

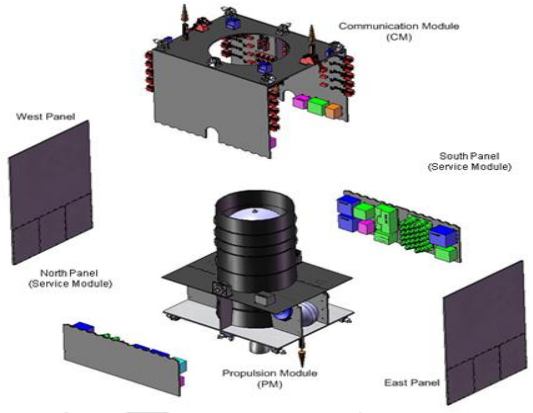

Fig. 2. Vx-Sat Layout.

IV. THE PROCESS OF ESTIMATION AND ANALYSIS FOR THE MASS BUDGET

The process of estimation and analysis for the mass budget begins with the development of all the tasks related with the calculation of the mass properties; first at all, is necessary introduce some basic concepts used in the next steps with the use of the software for the results.

A. Center of Gravity.

The Center of gravity is the average location of the weight of an object. Determining the center of gravity is very important for any flying object. In a general form of the center of gravity equations 1 and 2 could be define as follow:

$$x_{cg} = \frac{\sum m_i x_i}{\sum m_i} \tag{1}$$

$$y_{cg} = \frac{\sum m_i y_i}{\sum m_i} \tag{2}$$

B. Moment of Inertia.

The moment of inertia is a term used to describe the capacity of a cross section to resist bending. The moment of inertia is defined with respect to a specific rotation axis. The general form of the moment of inertia involves an integral like the equation 3.

$$I = \int dI = \int_0^M r^2 dm \tag{3}$$

C. Calculation.

The process of estimation implies since know very well the requirements of the satellite user, to with the other subsystems, carry out the entire tasks to finish the design of the satellite. The main tasks are named as follow:

- Obtain all the information related with the requirements from the user of the satellite through meeting held with System team.
- With the primary information, begins the first task, including the preparation of the tools to be used in the calculation of the mass budget; while the others subsystems are doing their calculations according with their budgets. These budgets must be more close for the one's indicated for the System team.
- When the structure subsystem gets all the budgets from the other subsystems, begin the principal task for the calculation of the mass properties. It begins with the estimation of the mass and volume of each component from each subsystem. This phase is very important, because structure subsystem according with the limitations could make decisions that could rearrange the budget of any subsystem.
- When all the arrangements are made and each subsystem has assigned their mass budget, the structure subsystem, begin with the layout of all the devices to be set in the satellite. The modeling of all the pieces was made with Solidworks software. With all the pieces modeled, begin the task of assign the place according of the subsystem. This phase is very important and has to be very careful with it, because all the components have to be checked one by one, to be very sure of the mass added for each subsystem.
- The next step is the calculation with the MSC Patran Nastran software, which let the assignment of the masses, estimation of total mass of each equipment, center of gravity, moments of inertia and mass balance.
- The process of calculation consisted, in the use of the software MSC Patran Nastran; this process should consider the calculations from the inferior levels to the next superior level. In this process, the software begun accumulating the total values of masses to each level corresponding of the design of the VX-SAT, which allowed verify the masses assigned to each one of the components and modules, with this gave as a result the total mass assigned to the general design.

D. Results.

The results given for the MSC Patran Nastran software are showed in the table III to VI; these results were verified in parallel with the STA software to get more accuracy in the calculations.

TABLE III. RESULTS WITH MSC PATRAN NASTRAN SOFTWARE

Satellite Status	Mass (kg)
Communications Module	269.790
Service Module	212.958
Propulsion Module	259.214
Dry Satellite	1009.664
Dry Satellite with Balance Weight	1041.024
Launch Configuration	2428.64
Transfer Orbit Attitude Control	2423.17
1st Maneuver	1855.55

Satellite Status	Mass (kg)
2nd Maneuver	1342.37
3rd Maneuver	1323.54
BOL	1317.94
Station Acquisition	1314.74
N/S	1124.82
E/W	1107.16
Synchronous Orbit Attitude Control	1095.91
EOL	1092.05
De-Orbiting	1089.64
Propellant Residuals	1075.99
Margin (2%-5%)	1066.58

TABLE IV. RESULTS WITH MSC PATRAN NASTRAN SOFTWARE

CoG Location (mm)		
X_{SAT}	Y_{SAT}	Z_{SAT}
2.26E-02	2.32E-02	1.537
7.45E-03	1.17E-02	3.57E-01
-2.21E-02	-2.55E-02	6.76E-01
-1.08E-03	1.62E-03	9.71E-01
-1.04E-03	1.57E-03	9.75E-01
-4.49E-04	6.72E-04	8.63E-01
-4.50E-04	6.74E-04	8.61E-01
-5.88E-04	8.80E-04	9.52E-01
-8.13E-04	1.22E-03	1.07E+03
-8.24E-04	1.23E-03	9.37E-01
-8.28E-04	1.24E-03	9.40E-01
-8.29E-04	1.24E-03	9.42E-01
-9.69E-04	1.45E-03	9.74E-01
-9.85E-04	1.48E-03	9.80E-01
-9.95E-04	1.49E-03	1.03E+03
-13.98	1.50E-03	9.54E+02
-1.00E-03	1.50E-03	9.52E+02
-1.01E-03	1.52E-03	9.78E-01
-1.02E-03	1.53E-03	9.78E-01

TABLE V. RESULTS WITH MSC PATRAN NASTRAN SOFTWARE

Moment of Inertia ($kg.m^2$)		
I_{XX}	I_{YY}	I_{ZZ}
2.38E+02	2.00E+02	3.00E+02
1.17E+02	7.24E+01	1.83E+02
1.53E+02	1.94E+02	1.30E+02
9.04E+02	9.79E+02	9.33E+02
9.25E+02	1.03E+03	9.77E+02
1.61E+03	1.75E+03	1.28E+03
1.61E+03	1.75E+03	1.28E+03
1.34E+03	1.47E+03	1.17E+03
1.08E+03	1.22E+03	1.07E+03
1.07E+03	1.21E+03	1.07E+03
1.07E+03	1.20E+03	1.07E+03
1.07E+03	1.20E+03	1.06E+03
9.78E+02	1.14E+03	1.07E+03
9.69E+02	1.13E+03	1.06E+03
9.59E+02	1.09E+03	1.03E+03
9.57E+02	1.09E+03	1.03E+03
9.56E+02	1.09E+03	1.03E+03

TABLE VI. RESULTS WITH MSC PATRAN NASTRAN SOFTWARE

Moment of Inertia ($kg.m^2$)		
I_{XY}	I_{YZ}	I_{XZ}
5.465	2.398	3.463
-2.59E+01	-1.58	2.62E-01
-1.23	-3.13E-01	8.44E-01
-2.21E+01	-3.9	3.385
-2.21E+01	-3.89	3.381
-2.21E+01	-4.07	3.503
-2.21E+01	-4.07	3.505
-2.21E+01	-3.93	3.406
-2.21E+01	-3.96	3.43
-2.21E+01	-3.95	3.422
-2.21E+01	-3.95	3.418
-2.21E+01	-3.94	3.416
-2.21E+01	-3.89	3.381
-2.21E+01	-3.88	3.375
-2.21E+01	-3.9	3.39
-2.21E+01	-3.9	3.387
-2.21E+01	-3.9	3.385

V. CONCLUSIONS

The structure subsystem of Vx-Sat is a complex system because has to consider and provides the mechanical support to the other subsystem in their configuration, so in this paper was described the Vx-Sat system, main features and preliminary design of its structure subsystem, so the core of this investigation was related the mass budget and all its process to obtain the best results.

The design of the structure is a complex process that depends of the constant communication and many trade-off with the other subsystems of the satellite to get the more suitable layout to fulfilling the user demands.

The determination of the mass budget in the design of a satellite is very important because with this information is possible to assure the stability of the design in the conditions of operation during the whole life of the satellite.

Is possible to find complications in the whole process of the estimation of the mass budget related with the models designed in software not suitable with the choosen software, in this case the MSC Patran Nastran; so is very important take care about because this detail could decrease the accuracy in all the calculations.

An important recommendation is to use in parallel other software in the estimation of the mass budget, so the designer can verify and compare if the results are really close to the acceptable values in this kind of investigation.

REFERENCES

[1] China Academy of Space Technology, Structure *of Communications Satellite*, Space Technology International Training Series, 2006.

[2] China Academy of Space Technology, *Mechanical Subsystem of Spacecraft*, Space Technology International Training Series, 2005.

[3] P. Fortescue, and J. Stark, Spacecraft Systems Engineering, 2nd ed., pp.237, 1995.

[4] China Academy of Space Technology, Introduction to the *Spacecraf Engineeringt*, Space Technology International Training Series, 2005.

2011 International Conference on Mechanical, Industrial, and Manufacturing Engineering
Lecture Notes in Information Technology Vols. 1-2

Research on Financing Selection of Chinese Energy Performance Contracting

Shanghua Hu
School of Management
Tianjin University
Tianjin, China
shanghuahu@126.com

Haiyang Qi
School of Management
Tianjin University
Tianjin, China
well-qihaiyang@163.com

Abstract - In the process of carrying out Chinese Energy Performance Contracting (EPC), the biggest barrier that Chinese EPC encounters is financing difficulties. This article discusses the current financing situation of Chinese EPC, introduces several financing patterns and its characters that Chinese EPC has been applied, and then analyses several key factors that influence Chinese EPC financing, namely, EPC's self-specialty, business life-cycle, financing structure & financing cost, information asymmetry, financing environment & financing policy. Based on these proposed some suggestions on Chinese EPC financing.

Index Terms - Energy Performance Contracting (EPC), financing pattern, influence factor, suggestion, China

I. INTRODUCTION

Energy Performance Contracting (EPC) is a new market-oriented energy-saving mechanism, and its essence is to get the full cost of energy conservation projects by means of reducing energy expenses. Energy Service Company (ESCO) is a professional profitable company which based on Energy Performance Contracting.

EPC model in China began in 1998, which was supported by the World Bank (WB) and the Global Environment Facility (GEF).Currently, there are three basic types of EPC contracts in China, namely, Share Savings Contract, Guaranteed savings Contract and Outsourcing of Energy System Management. At present, the most frequently EPC type used in China is Share Savings Contract, that the ESCO provides full project funding.

II. THE CURRENT FINANCING SITUATION OF ENERGY PERFORMANCE CONTRACTING IN CHINA

When the ESCO provides EPC services for the customers, they need to pay for all the investments in advance, including the purchase of energy-saving equipments; therefore, the implementation of EPC project must be based on the premise of adequate funding. However, the majority of Chinese ESCO is still in the early stages of development, with little registered capital, poor financial system and low credit rank and so on, it is difficult for them to obtain credit from financial institutions. Even if they can get the loan, the amount is relatively low, and need to provide collateral security and other items of fixed assets. Currently, the possible way for ESCO to obtain secured loans is to get guarantee from China National Investment &Guarantee Co., LTD (CNIG), which was entrusted by the WB / GEF funds.

However, until the end of 2008, there were only 41 ESCOs received loan guarantees, while there were more than 300 ESCOs during the same period in the country and most of the ESCOs are still in weak financial predicament. According to statistics, China has more than 90% of the ESCOs facing financing difficulties, if the financing difficulties can be resolved, at least 50% of the ESCOs would double the speed of development [1]. Contrasted to the financing difficult situation for the ESCO, China's demand for energy services is strong. A report from China Energy Conservation Service Industry Association Committee (EMCA) showed that China's energy service industry output value reached 41.73 billion Yuan in 2008, more than 4,000 energy conservation projects had been implemented, while there were only 41 ESCOs, 127energy-saving projects won the guarantee from the CNIG, the total investment is 790 million Yuan [2], less than 4% of the total investment in the year. ESCOs are facing a huge funding gap.

III. MAIN FINANCING PATTERNS OF CHINESE EPC

A. Internal Financing

Internal financing is the most common form of EPC financing in China, the fund is mainly from the enterprise self-capital and corporate earnings converted into increased capital. According to an investigation of 351 ESCOs of non-EMCA, 72.1% of the total funds were from the enterprise interior. The advantage of this financing pattern is that it can save transaction costs for firms, reduce financing costs, and enhance control, while the disadvantage is lacking of financial capacity, poor growth, as it would be influenced by the profitability of the business, net assets and future earnings expectations and other factors.

B. Domestic commercial bank loans

Domestic commercial bank lending is the most important financing pattern for ESCO in China. As the historical development of Chinese EPC is not very long, most commercial banks don’t have a good understanding of EPC, as well as the ESCOs are mostly small and medium enterprises (SMEs), commercial banks set series of harsh, complicated loan procedures. In these cases, funds from them could not be much, and are far from the needs of EPC.

C. SMEs credit guarantee funds

At present, 31 provinces, municipalities and autonomous regions in China have been established more than 100 SMEs credit guarantee agencies. The origin of SMEs credit guarantee funds is local government funds, members of voluntary funds, social funds, etc. Most of these institutions are public service, industry self-regulation of non-profit organization, and are based on membership management. When the EMCA members seek funding, they can be guaranteed by SMEs.

D. Government subsidies and energy funds

In 2010, the Ministry of Finance arranged 2 billion Yuan energy funds, which was designed to support ESCO take EPC model. In addition, some local governments also have established "post-grant" policy to support EPC projects. For example, the Beijing Municipal Government formulated a policy that give the ESCO no more than 20~30% of the project investment subsidy, according to the energy-saving rate from 15% to25% above, and subsidies for individual projects can get a subsidy of 5 million Yuan at most.

E. International institutions loans, grants and EPC credit secured loans

In the first implementation process of the "WB / GEF China Energy Conservation Project", the WB provided a loan of $63 million, the GEF and the European Commission $ 5million, $ 22million in grants, respectively. Project Phase II established the "EPC Loan Guarantee Scheme"; the GEF provided $ 22 million as security grant funds.

IV. THE MAIN FACTORS AFFECTING CHINESE EPC FINANCING

A. EPC's self-specialty

Statistics show that, in China, 70% of more than 500 ESCOs are SMEs. They are too weak at economic strength; therefore, they are unable to deal with the whole process of energy saving services, either the overall system energy conservation or technological transformation. Meanwhile, ESCO recover funds by sharing the efficiency of energy conservation, which has a long payback period, generally 3-5years, and some even up to 10 years. As previously stated, most ESCOs are technical-service companies with little fixed assets, they have no ability to provide guarantees or sufficient mortgage to banks in the financial security of their loans. This factor makes the EPC face a very big financial pressure.

B. Business life-cycle

According to the business life-cycle theory, ESCO life-cycle can be divided into four stages, namely, start-up stage, growing stage, maturity stage and decline stage. In different stages, the financing pattern is different.

In the start-up stage, EPC model has not been widely spread, as well as the acceptance of customers is poor and the probability of energy services provided to meet customer's requirements is also uncertain. Above all, great risk of corporate management means most ESCOs should adopt internal financing, and equity financing is the most appropriate [3].

In the growing stage, products and services from ESCO have been improved, and the public and customers' knowledge about EPC model as well as its benefits has been enhanced, so the potential demand is also growing. ESCO need more funds to support its rapid development. It is also necessary to control the financial risk of funding sources. Continuing to adopt equity financing is a good choice and the best financing strategy is to issue shares [3].

In the maturity stage, although the energy market is still huge, it is saturated basically. The risk of corporate management is reduced to the middle class. With the disappearing of high-risk factors of start-up stage and growing stage, the sales volume, market share and profitability get stable and cash flow becomes easy to predict. In this stage, shareholders hope that companies stay in the maturity stage, not only generating large amount of cash flow in a long term, but also would like to enter other industries to get more earnings. Therefore, the best strategy is to absorb large numbers of debt financing [3].

C. Financing structure and financing costs

Financing structure means the each size of equity capital and long-term debt capital. At present, the most important financing means of Chinese EPC is debt financial from financial intermediaries. According to the financing structure theory, corporate should take a synthetically consideration of the cost of capital, risk and agency when it decides its capital structure. The high proportion of the debt financing would increase the risk of corporation. When the cost of risk is greater than the profit of tax deduction from debt, the profit of agency of debt will be insufficient to offset the agency costs of debt, then, this would cause more harm than good[4]. Therefore, the blind pursuit of the debt financing is not the best choice, and ESCO should increase equity financing appropriately.

Financing costs is also an important factor affecting the selection of financing mode of EPC. Financing costs means the cost to obtain funds or capital, including fee generated in the financing process (called financing fee) and the minimum necessary return on investment when using the funds(called financed with fees). The pecking order financing theory suggests that, the lowest cost financing mode is enterprise self-capital and retained profits, followed by the venture capital/private equity funds, policy funds, debt or issue bonds or the issuance of convertible bonds, issue new shares, namely, the internal financing first, the external financing second; Then in the external financing, debt financing came after the equity financing, the share financing finally [5].

D. Information asymmetry

Information asymmetry refers to both sides of the business transaction have a different mastery of the relevant

information, and it may bring adverse effects to the weak party. For the information asymmetry in the credit market, there are adverse selection models, moral hazard models and signal display theory [6]. According to the different time of occurrence, theory of asymmetric information can be divided into pre and post information asymmetry. Prior information asymmetry would lead to adverse selection, while post information asymmetry would lead to moral hazard. When an enterprise approach to internal financing, information asymmetry would not occur, only when external financing was adopted, information asymmetry would be happened.

Since the existence of asymmetric information, some commercial banks may not provide loans or guarantees to the ESCOs which would not pay or the repayment ability is not high. However, those ESCOs which were trustworthy and high ability of repayment would also be excluded, that means adverse selection was occurred. In the same way, commercial banks would have the doubt that the ESCO may engaged in non-EPC project or other outside activities (these activities are high risk) after they received the funds, that means moral hazard was occurred, and also the lender would reduce the willingness to lend. To sum up, the existence of information asymmetry makes the EPC financing more difficult.

E. Financial conditions and financing policy

As the cost and efficiency are different from different sizes of financial institutions providing financial services, large financial institutions are usually more willing to provide financing services to large enterprises, less willing to provide financing services to SMEs [7].Besides, because of China's current financial system was built on the basis of state-owned banks, State-owned Banks naturally reluctant to provide financing service to the SMEs, especially to the ESCO.

Furthermore, the imperfect financing support policy to the ESCO also causes financing difficulties. The Chinese government hasn't made any formal laws or regulations to govern the ESCO and the authority energy detection and identification section were also lacked, as well as the existing fiscal management system is not conducive to the implementation of EPC projects. All these factors make the EPC financing hard to go forward.

V. SUGGESTIONS ON THE CHINESE EPC FINANCING

A. Financing by green financial products of small and medium financial institutions

Small and medium financial institutions own less capital. As they are unable to provide financing services for large enterprises, they have a stronger motivation to provide financing services for the ESCO. More importantly, small and medium sized financial institutions have information superiority. Through long-term cooperation, small and medium financial institutions' understanding of operating conditions of ESCO is getting deeper, which is helpful to solve the problem of asymmetric information between ESCO and themselves and it would ease the difficulty of EPC financing.

B. Absorbing venture capital (VC) / private equity (PE)

Since most of the ESCOs are still in the start-up stage or the growing stage, the introduction of VC / PE would not only increase their equity capital and reduce financial risk, but also could bring advanced concepts, standardized management and wide range of resources to enhance the overall capacity rapidly. The success of an ESCO often requires multiple rounds of financing and years of hard working, therefore, in the long run, matching development planning with the financing strategies as well as the VC / PE impetus would be conducive to the rapid development of the ESCO.

C. Choosing a good time to issue shares on the Growth Enterprises Market (GEM)

China has been launched the GEM since October of 2009 in the Shenzhen Stock Exchange. The requirements for size and profitability are lower in GEM, relative to the main board market. Most companies do not have to provide high profitability, and all of their shares can be traded. Therefore, GEM is an ideal place of financing for EMCO, which has small size but high technology, and represents the new direction of economic development with broad prospects.

D. Using the third-party financing platform

In June of 2010, China established an investment and financing platform for EPC in Beijing, with the help of third party investment, trade the EPC as a public trading exchange-traded varieties, ESCO can use this platform to attract social investment in energy saving.

E. Developing new financing models

Some of the SMEs in other fields have started supply chain financing, which is a new financing model. EPC in China can draw lessons from this kind of financing ways, by using higher credibility company such as client company or equipment manufacturers to achieve the purpose of financing.

REFERENCES

[1] G. Wang, F. Liu, and W. Wang, "Promoting the development of Chinese Energy Performance Contracting," *Chinese Investment of Science and Technology*, pp. 41-43, Oct. 2009.

[2] Ministry of Energy-saving and Comprehensive Utilization of Industry and Information, *Report of Development of Chinese Energy Conservation Service*, Beijing: EMCA, 2009.

[3] Chinese Institute of Certified Public Accountants, *Management of Financial and Cost*, Beijing: Press of Financial and Economic, 2010, pp.297-302.

[4] M. Jensen and W.Meelding, "Theory of the Firm: Managerial Behavior, Agency Costs and Ownership Structure," *Journal of Financial Economies*, pp. 305-360, Mar. 1976.

[5] Chinese Institute of Certified Public Accountants, *Company Strategy and Risk Management*, Beijing: Press of Economic and Science, 2010, pp.183-187.

[6] C.Myers and S.Majlu, "Corporate Financing and Investment Decision When Firms Have Information that Investors Do Not Have," *Journal of Financial Economics* vol.21, no.13, pp. 187-221, Jul. 1984.

[7] Y. Ling, and Y. Liu, "Promoting the Growth of Medium and Small-size Enterprises through the Development of Medium and Small-sized Financial Institutions," *Economic Research*, pp. 10-18, Jan. 2001.

2011 International Conference on Mechanical, Industrial, and Manufacturing Engineering
Lecture Notes in Information Technology Vols. 1-2

Significance of Haptization in Multilateral Information

[1]Eiji AOKI*, [2]Junji HIROOKA, [3]Nobuhiro NAGATOMO, [3]Toshihiko OSADA,
[1,4]Hiroaki NISHINO, [1,4]Kouichi UTSUMIYA
[1]Institute for Hypernetwork Society, Oita, Japan.
[2]Kyushu Telecom Promotion Center, Fukuoka, Japan.
[3]AVOC Co., Ltd., Miyazaki, Japan.
[4]Oita University, Oita, Japan.
**corresponding author: blue@hyper.or.jp*

Abstract— **We are paying attention to tactile information, the sensation of touch, as a way for enabling multisensory communication. We have been conducting a research project for designing and developing a "haptization" based communication framework and its application systems. Since its inception is to classify human sensations, the phrase of "five senses" consisting of vision, hearing, touch, taste, and smell, has been used from olden days. This classification is triggered by the ancient Greeks. However, there are at least nine types or over twenty types of human sensory channels if the classification is considered from a practical standpoint. The touch sensation contains not only simple skin sensations such as pains, and temperatures, but also other types induced by some physical stimuli like pressures and vibrations. As you can easily experience when you browse web pages on the Internet, the current web technology fully depends on information visualization. It does not, however, provide any means to convey other sensory information. We conducted a survey on the effect of haptization for disabled people and the weak in information technology like pregnant and elderly. Such people ordinarily have difficulties for obtaining digital information with various reasons. We also developed a prototype system using tablet personal computers (PCs) presenting touch-enabled interactions based on a vibration display function. We carried out a public demonstration experiment for conducting the survey. In this paper, we report our past activities and the results of the survey.**

Keywords- haptization; digital divide; the weak in information technology; information accesibility

I. INTRODUCTION

Information terminals in the current society have been designed for use by healthy people. Homogeneous and uniform industrial products, however, do not match individual expectations from end users' viewpoints. As this is true even for the healthy people, it goes without saying that the issue is suicidal for disabled persons who occupy about 5 percent population in Japan. Additionally, an unprecedented super-aged society that about 23 percent of the elderly constitutes a major portion is predicted in Japan in no distant future. Designing and implementing information access methods allowing the weak for easily acquiring a wide variety of information are expected to become a next big challenge. The weak including not only the disabled persons but also the users in various layers are struggling with PCs and mobile phones for exploring important information.

We have been conducting various activities for promoting informatization usable by the weak. These activities include launching communities and organizations for improving the information literacy of the weak, and introducing welfare information services based on assistive computer technologies. We are also working on the training of teachers who lead novices to common Internet users and designing the manner of utilization for assistive software such as screen reader. In 2003, we started a social action program funded by Microsoft Corporation called UP (Unlimited Potential) program [1] in our local region. The purpose of the project is to educate the weak in information technology. This five-year program triggered the spontaneous formation of some groups operated by the elderly, disabled persons, and mothers of small children. Three NPOs (nonprofit organizations) are formed including the NPO Disabilities UP Oita Project, the NPO Oita Senior Net, and the NPO Power Wave Hiji. They have been working on the promotion of information technology in each field. These activities thereby contribute to enrich life, retirement, and work at home for the weak in the local region.

II. QUESTIONNAIRE SURVEY ABOUT HAPTIZATION FOR THE WEAK IN INFORMATION TECHNOLOGY

The above mentioned activities have been fostered the people who received the benefits of informatization and enhanced their information literacy. Their accomplishments are really remarkable ones. These social changes enable the weak to widen their views and give them a chance for working in new fields. Therefore, we conducted a survey on the usefulness of information haptization based on the hypothesis that new communication means pursuing greater convenience and user friendliness are continuously required. The survey has been conducted at the end of 2009.

This work was supported in part by Ministry of Internal Affairs and Communications (MIC) in Japan, Strategic Information and Communications R&D Promotion Programme (SCOPE) No.092310005.

A. *Essential Matter of Survey*

Modern society depending on the Internet cannot stop a deluge of information. If you can reach a target web site among a tremendous number of candidate pages by using a search engine like Google, and even if the found site include important information, you may not possible to access such significant information because of the poorly organized contents. The web accessibility heavily depends on an authoring skill of the site creator. You may face other problems such as useless functions caused by immature or awkward devices and unfriendly operational environment without any instructions or explanations. The web accessibility will be increasingly important issues.

Through this questionnaire survey, we tried to learn about how respondents (the weak persons who are belonging to a crop of "digital divide") feel the current situation of the Internet and its accessibility, and what they think about the role and potential power of information haptization. We, however, include only basic questions in this trial because the word "haptization" seems to be an uncommon word for the public.

B. *Survey Contents and Results*

Subjects of this survey are the members of the three NPOs as described in Section 1. There are the NPO Disabilities UP Oita Project run by the disabled persons, the NPO Oita Senior Net run by the elderly, and the NPO Power Wave Hiji run by mothers of small children. Most of them are rather active users of the Internet. We sent the questionnaire to these organizations and received 139 responses.

The contents of the questionnaire and their results are as follows:

a. *Age*: The age distribution of the subjects that 20s is 3 percent, 30s is 24 percent, 40s is 18 percent, 50s is 11 percent, 60s is 26 percent, 70s is 18 percent.

b. *Gender*: Male is 22 percent and female is 78 percent.

c. *Residence area*: The distribution of the subjects' residence area that 71 percent of them are living in Oita city, the capital city in Oita prefecture. Remains are dispersed in seven cities in the prefecture.

d. *IT equipment in-use* (multiple answers allowed): The types of IT equipment used by the subjects on a daily basis. The top three devices are PCs, mobile phones, and digital cameras.

e. *Type of Internet access line in-use* (multiple answers allowed): The types of Internet access lines used by the subjects. The top three types are optical fiber lines, CATV lines, and ADSL lines.

f. *Type of indoor connection line in-use* (multiple answers allowed): The types of indoor connection lines used by the subjects. Most subjects use Ethernet lines or wireless lines.

g. *Internet applications in-use* (multiple answers allowed): The number of Internet applications used by the subjects. Mail is the clear winner. Online shopping and blog are the next class applications.

h. *Type of inconvenience in using IT equipment* (multiple answers allowed): The types of objects and entities the subjects feel inconvenient when they use IT equipment. Flawed manual and complexity caused in multi-functional usage are the top two reasons.

i. *Type of inconvenience in using application software* (multiple answers allowed): The types of operations or entities the subjects feel inconvenient when they use application software. Flawed manual again is the most visible source. Other factors are laboriousness in following operational rules and vexatiousness in performing software version up.

j. *New modality other than audio-visual interface used in the Internet*: This item inquires the subjects about "Can you imagine a new modality other than traditional audio-visual interface used in the Internet?" Only 20 percent of the subjects answered yes.

k. *Prospective modality other than visual interface used in the Internet* (multiple answers allowed): This item inquires the subjects about "Please select prospective sensory channels to be usable on the Internet as much as you think." Hearing is the top and haptic (touch sensation) is the next-best choice.

l. *Usability in multimodal interface*: This item inquires the subjects about "Can you feel user-friendliness if you can use more sensory channels such as touch sensation in addition to the visual feedback?" 31 percent of the subjects answered yes and 38 percent answered no preference.

m. *Application software leveraged by haptic modality* (multiple answers allowed): This item inquires the subjects about "What are prospective applications leveraged by haptic interface?" The online shopping and electronic voting systems are selected as most probable applications. Traffic information system is the next choice.

n. *Benefits of the Internet*: This item inquires the subjects about "Do you enjoy the benefits of using the Internet in your daily life?" 80 percent of the subjects answered yes.

o. *Improvements of the current Internet services*: This item inquires the subjects about "What are your requirements to improve the current Internet services?" The following opinions are collected:

- A voice service for telling me my today's schedule in the morning is preferred.
- A service for notifying more detail information of the local government is desired.
- A service for automatically showing the live information about local region on the desktop screen is expected.
- I want a cheaper and easier-to-use audio input function.
- Please attach an easy-to-understand document.
- Please avoid any disabled connection states when using the Internet.
- A service to politely guide how to use the Internet is desired.

- An easy-to-use and safe online shopping service is preferred, because I am scared to use the current services.
- A thorough filtering service is preferred.
- A service for prohibiting connections to dark websites is desired.
- I need to improve my skill for using the Internet.
- More easy-to-understand system messages are desired, because many notes, warnings, and news are written with technical terms and very difficult to understand.
- A service to use PCs and the Internet like public telephones in the town is useful.
- A service for preserving from crime and trouble is desired to get a convenient and safe usage environment.
- A TV Internet service easily manageable by a simple zapper is preferred.
- I am conscious of increasing risks associated with the increasing serviceability and functionality of the Internet.
- A Braille display for stereoscopically showing the whole screen is desired.
- Functions for automatically switching the Internet access method (connection optimization), appropriate filtering, and connecting to appliances are desired.

C. Discussions

We expected that the subjects (the weak persons) claim inconvenience in using hardware devices and software applications and such problems are depend on functionality of the devices and poor interface of the applications. We, however, found that the device functionality and application interface are considerably well designed and accepted by the subjects. We learned from the results of the questionnaire that the subjects' frustrations over the Internet operations are caused by poor documentations and insufficient explanations of the devices and applications they are using. System response also is an important factor for satisfying the users' requirements.

As mentioned in Question ***j***, imaging a new communication modality other than traditional audio-visual interface is very difficult for many subjects. The result met our expectation. As regards the potential ability of the haptic modality (touch-based communication), we found a positive result. As described in Question ***l***, about 31 percent subjects answered that they feel the touch sensation will improve the user-friendliness in the Internet usage. If we add the subjects who answered "no preference (may become supporters in the future)", the number becomes about 69 percent. This suggests that well designed haptic interface may become a principal modality for supporting wide variety of users including the weak persons.

As described in Question ***m***, many subjects expect the haptic interface to be used in practical applications such as online shopping, electronic voting, and street guidance rather than recreational use like electronic museum guidance. As shown in Question ***n***, most subjects feel that using the Internet is beneficial to their good life; on the other hand, many of them feel that their technical skills are not enough to fully enjoy the potential ability of the Internet. The results of Question ***o*** suggest that many subjects want practical problem-solving solutions for currently available services rather than futuristic solutions or new technologies.

III. A PROTOTYPE SYSTEM WITH TABLET PCS AND PUBLIC DEMONSTRATION EXPERIMENT

Based on our previous discussions and findings in Section 2, we designed and developed a prototype system using tablet personal computers (PCs). We used the TouchScreen™ haptic display developed and marketed by Immersion Corporation [2]. When you touch the part of the screen, you feel some tactile sensations with vibrations. The types of vibration, intensity, and patterns are variable parameters. We developed the system capable of presenting various touch sensations by using such features. The different GUIs placed on the screen produce different touch sensations.

As shown in Figure 1, there are four kinds of "Trial" buttons (A, B, C, and D) placed on the top of the screen. Each button generates a different vibration pattern. Subjects are required to push each button and remember its vibration pattern. Next, they should try the "Question" button, a bigger center button on the screen, generating an identical pattern with one of four patterns. Then, they should select a same vibration pattern of the question among four vibration patterns (A, B, C, or D). They choose one answer by pushing a button among the four "Answer" buttons placed at the bottom.

We conducted a public demonstration experiment using the prototype system as shown in Figure 2 at the end of 2010. The purpose of the experiment is to find a set of vibration patterns to be stably used for tactile communications. There were more than 100 subjects attended. They examined the system and tried various vibration patterns. We conducted a questionnaire survey in the experiment.

A. Survey Contents and Results

Subjects of this experiment include engineers and administration staff working in IT companies, students in a career college, and the weak in information technology. The contents of the questionnaire and their results are as follows:

a. *Difficulty of the question (for selecting an identical vibration pattern)*: Most subjects answered difficult.

b. *Feeling of tremble PCs*: The top three feeling are fresh, interesting, and peculiar feeling.

c. *Feeling of touch*: Most subjects answered fingertip feeling and focus of consciousness.

d. *Usefulness of vibration technology*: Half of the subjects answered yes.

e. *Thinking about the different vibration patterns*: Most subjects answered technological progress is required.

f. *Improved usability with tactile information*: Most subjects answered yes.

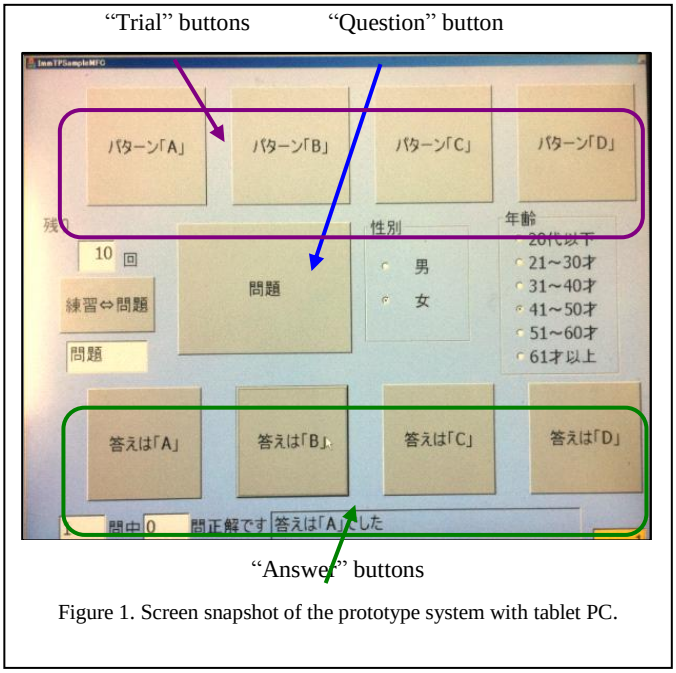

Figure 1. Screen snapshot of the prototype system with tablet PC.

(a) scene 1

(b) scene 2

Figure 2. Snapshots taken in the experiment.

B. *Discussions*

As mentioned in Question ***a***, it seems difficult to remember the difference between four vibration patterns and accurately select one. We do not usually care about subtle vibrations in our daily life. But as mentioned in Question ***b***, many of them enjoyed the touch-based operations with tactile feedback, even feel difficulty. Most subjects are interested in sense of touch. As regards the potential ability of the tactile information, we found the positive result.

Question ***c*** inquires the subjects about "Did you feel that you touched something?" At first most subjects felt that they were sensitive or insensitive, then concentrated to the fingertip, and focus on the consciousness. As mentioned in Question ***d***, about half of them were positive and the rest answered no preference.

Question ***e*** inquires the subjects about "What do you think about presenting different vibration patterns in the part of the screen?" At first most subjects surprised, then they tried many times of touching the screen. We learned from the result of the questionnaire that subjects firstly felt strange, then think technological progress. As mentioned in Question ***f***, the result met our expectation. This suggests that well designed haptic interface may become a principal modality for supporting wide variety of users including the weak persons.

IV. Conclusions

In this paper, we reported a questionnaire survey conducted in 2009 for exploring problems "digital divide" people and a hearing survey conducted for revealing the problems the Internet users are facing. We especially eye on the haptic technology (touch-based communication modality) and conducted another survey in 2010. In the survey, we asked subjects some questions on the technology such as what is a potential impact of the haptic modality on their usage, and which services can receive the benefits of the touch-based interactions. Most subjects answered that there are many influential fields such as traffic control system like car driving and traffic light control systems, ticket vending machines, bank systems like cash dispensers, medical care systems, social welfare systems, voting systems, entertainment machines like TV screens, remote control devices, game machines, and tablet PCs like iPad™, e-book, smart-phone.

Although the survey still is a preliminary trial, the results seem promising. Because we are also working on developing some practical application systems with haptic interface, we would like to conduct more elaborative survey focusing more on the haptic technology in the near future.

References

[1] Oita UP program, http://www.microsoft.com/japan/citizenship/ca/up/up_oita.mspx.

[2] Hiroaki Nishino, Ryotaro Goto, Tsuneo Kagawa, Kouichi Utsumiya, Junji Hirooka, Eiji Aoki, Toshihiko Osada, Nobuhiro Nagatomo, "An Electronic Voting System for Haptic Touchscreen Interface," *Proc. of the 4th Int'l Conf. on Complex, Intelligent and Software Intensive Systems (CISIS-2010)*, pp.1164-1169, Feb.15-18 2010.

[3] Eiji Aoki, Junji Hirooka, Toshihiko Osada, Nobuhiro Nagatomo, Hiroaki Nishino, Kouichi Utsumiya, "Effects of Haptization on Disabled People," *Proc. of the 4th Int'l Conf. on Complex, Intelligent and Software Intensive Systems (CISIS-2010)*, pp.1153-1157, Feb.15-18 2010.

2011 International Conference on Mechanical, Industrial, and Manufacturing Engineering
Lecture Notes in Information Technology Vols. 1-2

Modeling Volatility of Financial Markets using an AR/GARCH Model in Tehran Stock Exchange

Fatemeh Hosseini Tash, Mohammad Modarres
Department of Industrial Engineering
Sharif University of Technology
Tehran, Iran
hoseini85@gmail.com , modarres@sharif.edu

***Abstract* – In this paper, we apply an AR/GARCH model to three main indices of Tehran Stock Exchange: the Price (TEPIX), Finance and Industry indices. The main purpose of this modeling is firstly to have a validated quantitative model as the foundation for forecasting the market's status, and secondly to remove the linear and heteroskedasticity effects from the data to make the residuals ready to be investigated in the light of deterministic, nonlinear characteristics. We find strong evidence of ARCH/GARCH specifications in all indices. In addition, we forecast the model with four different k-step(day)-ahead horizon. The Mean Absolute Errors (MAE) of these predictions are compared with each other. Obviously, the one step ahead forecast indicates the least MAE measure. The 90-step-ahead prediction plot, on the other hand, demonstrates notable imprecision due to the sudden upward change in volatility, which is reflected in the prediction with observable delay. In addition, we conclude that the most significant proportion of the bias of the forecast is due to covariance, indicating non-structural bias.**

Keywords: Volatility, Autoregressive (AR), GARCH, Financial Time Series, Forecasting

I. INTRODUCTION:

Building models that can explain the behavior of the financial data is an important challenge for finance researchers and professionals. One of the most addressed questions in this regard, has been how to model volatility of financial assets. During the last two decades, emphasis has been given to forecasting the volatility of financial time series. This issue is crucial for policy makers, option traders and investors. Volatility forecasts are important for many financial decisions, such as implementation and evaluation of asset pricing theories and risk management. Thus, several developments in financial econometrics have been allocated to using quantitative models which not only consider the risk and return of the assets, but also are able to explain investors' attitude toward volatility. These models must be capable of dealing with volatility in The ARCH class of models, pioneered by Engle (1982) and generalized by Bollerslev (1986), is by far the most popular class of econometric models for describing a series with time-varying conditional variance. Fat tails and volatility clustering are two important characteristics within financial time series, which can be captured by the GARCH family models.

The performance of GARCH models on explaining the volatility of stock markets has been the subject of several studies. But few have tested GARCH models using daily data from Middle East stock markets. Mecagni and Sourial (1999) examined the behavior of stock returns as well as the market efficiency and volatility effects in the Egyptian stock exchange using GARCH models. Furthermore, Tooma (2003) investigate the impact of price limits on volatility dynamics in the Egyptian Stock Exchange using several GARCH models under four different error distributions. Alberg et al. (2006) estimate stock market volatility of Tel Aviv Stock Exchange indices using asymmetric GARCH models. Meric et al. (2007) study the co-movements of the US, UK and Middle East stock markets (Egyptian, Israeli and Turkish).

In this paper, we apply an AR/GARCH model to three main indices of Tehran Stock Exchange: the Price (TEPIX), Finance and Industry indices. The main purpose of this modeling is firstly to have a validated quantitative model as the foundation for forecasting the market's status, and secondly to remove the linear and heteroskedasticity effects from the data to make the residuals ready to be investigated in the light of deterministic, nonlinear characteristics of the Chaos Theory. Autoregressive (AR) with Generalized Auto-regressive Conditional Heteros-kedasticity (GARCH) model is a non-linear time series model which combined the linear AR with conditional variance GARCH. ARIMA/GARCH has been applied to model many financial time series. French at al. (1986) examined the daily values of S&P composite portfolio with an ARIMA/GARCH-in-mean model to analyze the interrelation between stock return and market volatility. Ferenstein and Gasowski (2004) estimated and AR(1)/GARCH model for stock returns of two enterprises in Warsaw Stock Exchange. Floros (2008) evaluated the performance of ARMA/GARCH family models on the Egyptian CMA index and the Israeli TASE-100 index.

II. AR/GARCH MODEL

AR/GARCH is a combination of linear AR(m) with GARCH(p,q) variance, which consists of a conditional mean and conditional variance model. The AR part of the model, represents the mean of log returns of the index as an autoregressive model with the lag of m, and the GARCH equation, model the conditional variance of the time series as an autoregressive nonlinear model with lags p and q. We introduced GARCH model to explain the changing volatility characteristic. The most important contribution of GARCH model is its dynamic variance, where the variance varies over time.

A. Stationarity

To develop an AR/GARCH model for the time series of the return on TEPIX, we need to examine the data to make sure of their stationarity, which is the foundation of time series analysis. Many economic and financial time series exhibit trending behavior or non-stationarity in the mean. An important econometric task is determining the most appropriate form of the trend in the data, and transforming the data to stationary form prior to analysis. Augmented Dicky-Fuller test, Said and Dickey (1984) can be used to determine if trending data should be first differenced or regressed on deterministic functions of time to render the data stationary. It tests the null hypothesis of that time series is non-stationary.

B. AR(m) model

Frequently, we find that the values of a series of financial data at particular points in time are highly correlated with the value which precede and succeed them. An autoregressive (AR) model is a type of random process which is often used to model and predict various types of natural and social phenomena. Dependent variable is a function of itself at the previous period or moment of time. The notation AR(m) refers to the autoregressive model of order m. The AR(m) model is defined as

$$Y_t = c + \sum_{i-1}^{m} \varphi_i Y_{t-i} + \varepsilon_t$$

Where $\varphi_1, \varphi_2, \ldots, \varphi_p$ are the parameters of the model, c is a constant and ε_t is the white noise

In traditional AR estimation, the basic assumptions on the error terms include zero mean and constant variance, or specifically (i) $(\varepsilon_t) = 0$, (ii) $E(\varepsilon_t^2) = \sigma^2$, and (iii) $E(\varepsilon_t \varepsilon_s)$, for $s \neq t$. In particular, the homoscedastic assumption (ii) of constant variance does not necessarily need to hold.

C. Autocorrelation and Partial Autocorrelation

Consider a weakly stationary return series r_t . When the linear dependence between r_t and its past values r_{t-i} is of interest, the concept of correlation is generalized to autocorrelation. The correlation coefficient between r_t and r_{t-l} is called the lag-l autocorrelation of r_t and is commonly denoted by ρ_l.

The partial autocorrelation function (PACF) plays an important role in data analyses aimed at identifying the extent of the lag in an autoregressive model. The use of this function was introduced as part of the Box-Jenkins approach to time series modeling, where by plotting the partial autocorrelative functions, one could determine the appropriate lags p in an AR(p). Given a time series z_t, the partial autocorrelation of lag k is the autocorrelation between z_t and z_{t+k} with the linear dependence of z_{t+1} through to z_{t+k-1} removed. See Box, Jenkins, and Reinsel (1970) or Brockwell (1996) for the mathematical details.

Partial autocorrelation plots (Box and Jenkins, pp. 64–65, 1970) are a commonly used tool for model identification in Box-Jenkins models. The partial autocorrelation of an AR(p) process is zero at lag p+1 and greater. If the sample autocorrelation plot indicates that an AR model may be appropriate, then the sample partial autocorrelation plot is examined to help identify the order.

In addition to ACF and PACF, Box and Pierce (1970) propose the Portmanteau statistic as a test statistic for the null hypothesis $H_0 : \rho_1 = \cdots = \rho_m = 0$ against the alternative hypothesis $H_1 : \rho_i = 0$ for some $i \in \{1, \ldots, m\}$. Ljung and Box (1978) modify the $Q^*(m)$ statistic to increase the power of the test in finite samples. Accepting the null hypothesis above means that the data have no significant serial correlation.

By looking at the autocorrelation function (ACF) and partial autocorrelation (PACF) plots of differenced series, we can identify the AR model and the number of terms needed. The general features of ACF and PACF for AR(p) model is that the ACF has form of exponential decay or damped sinusoid or a mixture of both, and PACF cuts off after lag p.

D. Heteroskedasticity

A sequence of random variables is heteroskedastic if the random variables have different variances. In contrast, a sequence of random variables is called homoscedastic if it has constant variance. When using some statistical techniques, such as ordinary least squares (OLS), the assumption that the error term has a constant variance is made. This might not be true even if the error term is assumed to be drawn from identical distributions. White (1982) proposed a consistent estimator for the variance-covariance matrix of the asymptotic distribution of the OLS estimator. This validates the use of hypothesis testing using OLS estimators and White's variance-covariance estimator under heteroskedasticity. The most widely used method to test for the presence of heteros-kedasticity is the White, which establishes whether the residual variance of a variable in a regression model is constant (homoscedasticity).

E. ARCH/GARCH

ARCH and GARCH models treat heteroskedasticity as a variance to be modeled. As a result, not only are the deficiencies of least squares corrected, but a prediction is computed for the variance of each error term. The ARCH process explicitly recognizes the difference between the unconditional and the conditional variance allowing the latter to change over time as a function of past errors. A useful generalization of the ARCH model is the GARCH parameterization introduced by Bollerslev (1986). The most widely used GARCH specification asserts that the best predictor of the variance in the next period is a weighted average of the long-run average variance, the variance predicted for this period, and the new information in this period that is captured by the most recent squared residual.

Let the dependent variable be labeled r_t, which could be the return on an asset or portfolio. The mean value m and the variance h will be defined relative to a past information set. The GARCH(p,q) model is defined by

$$\begin{cases} y_k = \sigma_k \varepsilon_k \\ \sigma_k^2 = \omega + \sum_{i=1}^{p} \alpha_i y_{k-1}^2 + \sum_{j=1}^{q} \beta_j \sigma_{k-j}^2 \end{cases} \quad (1)$$

Where $\omega > 0, \alpha_j \geq 0, \beta_j \geq 0$, and the innovation sequence $\{\varepsilon_t\}_{t=-\infty}^{\infty}$ is independent and identically distributed with $E(\varepsilon_0) = 0$ and $E(\varepsilon_0^2) = 1$.

The autocorrelation and partial autocorrelation functions for the squared process are useful in identifying and checking time series behavior in the conditional variance equation of the GARCH form. The partial autocorrelation function for ε for a GARCH(*p, q*) process is in general non-zero but dies out. Thus, the appropriate orders for *p* and *q* could be identified by standard Box-Jenkins methodology applied to the squared residuals, $(y_t - \hat{\mu})^2$. According to Bollerslev (1986), PACF cuts off after lag q for an ARCH(*q*) process. The PACF for ε^2 for a GARCH(*p, q*) process is in general non-zero but dies out.

III. Case Study: Tehran Exchange

In this paper, we try to apply the AR/GARCH model to three main indices of Tehran Stock Exchange in Iran. The overall price index is called TEPIX. There are two main categories of different companies in Tehran Exchange, which are Industry and Finance. In addition to the market index, we apply our model to Industry and Finance price indices. The model is estimated on daily data from 28th March 1998 to 21th April 2010, i.e., a total of 2919 observations, using ordinary least squares. All the data were collected from the Library of Tehran Exchange Organization. TABLE I gives the descriptive statistics for daily stock market prices and returns. Daily log returns of the Price Index are calculated from $r_t = \ln X_t - \ln X_{t-1}$, Where X_t is the TEPIX value of day t. Fig. 1 presents the plots of TEPIX and its returns over time (We only show TEPIX results to preserve space). We have also calculated three statistics using observations in the full sample; Skewness, Kurtosis, Jarque-Bera. The TEPIX and Industry index show negative skewness implying that the distribution has a long left tail. However, positive skewness of the Finance index is an indication of long right tail. The values for kurtosis are high in all cases. So, the distributions are peaked relative to normal.

TABLE I
DESCRIPTIVE STATISTICS FOR INDEX VALUES AND RETURNS

A.Index	TEPIX	Finance	Industry
Mean	7298.315	16923.3	5905.149
Std. Dev.	4067.208	10972.68	3130.638
Skewness	-0.1488	0.579347	-0.22694
Kurtosis	1.472279	2.475239	1.482497
Jarque-Bera	294.6359	196.7824	305.1347
Probability	0	0	0
Observations	2919	2919	2919
B.Return	TEPIX	Finance	Industry
Mean	0.078321	0.078321	0.072001
Std. Dev.	0.785264	0.785264	0.518251
Skewness	-0.8933	-0.8933	1.295784
Kurtosis	50.11353	50.11353	32.96009
Jarque-Bera	270357.3	270357.3	109988.3
Probability	0	0	0
Observations	2919	2919	2919

To examine stationarity, we first examine the test to the daily values of the TEPIX. The t-statistic of the test accepts the null hypothesis of the unit root and proposes that we use the differences of the index values. The result for the first differences shows that the first difference of TEPIX has a stationary structure. Therefore, we work with daily log returns of the Price Index. This removes the trends from the series. The results of the two ADF tests for TEPIX are shown in the TABLE II. As it is noted, the null hypothesis of unit root test is rejected, meaning that the series are stationary.

TABLE II
RESULTS OF THE ADF TEST ON DAILY TEPIX VALUES AND RETURNS.

Augmented Dickey-Fuller test statistic	t-Statistic	Prob.*
TEPIX	4.050430	1.0000
Return	-8.071407	0.0000
*MacKinnon (1996) one-sided p-values.		

IV. Empirical Results

A. Estimation

First, it is more convenient to work with a time series which demonstrates the deviation from the mean of the return time series, also called the residual time series. This is obtained from $u_t = r_t = r_t - \mu$, where μ is the mean of the return time series. Then, we filter conditional mean structure in the data by estimating AR(*m*) model, with the dependent variable of returns. AR(*m*) order is determined by reference to the ACF, PACF, and Q-statistics of the residuals. The *Akaike information criterion* (AIC), Akaike (1974), can be useful in choosing the best lag (*m*) for our AR model. The ACF for the residuals of TEPIX has almost sinusoid decay, and the PACF dies out after 10 lags. Thus, an AR(10) seems to be a well-fitting model for the data. The same result can be achieved for the Industry and Finance indices.

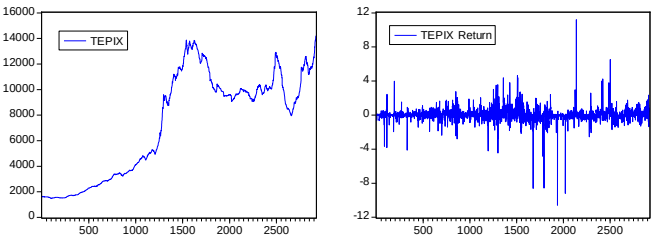

Fig. 1
Plot of TEPIX and its returns over time

After estimating the AR(10) for three indices, we test the homoscedasticity of the residuals of the AR model using the White test statistic. The results of the test for TEPIX can be found in TABLE III. TEPIX and Industry index statistics reject the homoscedasticity hypothesis and imply that the heteroskedasticity is the problem of the model. The AR(10) model for Finance index accepts the homoscedasticity hypothesis and eliminates any further development of GARCH model. However, the ARCH LM test, rejects the null hypothesis that there is no ARCH up to order 1 in the residuals. So, for Finance index, we only implement ARCH for the variance. To examine whether the GARCH model can be used in modeling the variance of the returns, we plot the ACF and

PACF for the second power of the residuals, i.e. ε_t^2. These Plots show significant values for PACF, indicating that GARCH can be an appropriate methodology to remove heteroskedasticity. To simplify the model estimation, we consider the GARCH(1,1), which has been shown to be accurate enough for financial data in Bollerslev (1992).

TABLE III
WHITE TEST RESULTS FOR THREE INDICES' RESIDUALS

TEPIX			
nR^2	502.3965	Prob. $\chi^2(65)$	0.00

Therefore, the final estimated model, after considering the GARCH equations, will be as follows.

1. TEPIX:

$$r_t = 0.075 + u_t$$
$$u_t = 0.488u_{t-1} + 0.085u_{t-4} + 0.068u_{t-5} + 0.05u_{t-8} + 0.049u_{t-9} + 0.035u_{t-10} + \varepsilon_t$$
$$\varepsilon_t = z_t\sigma_t$$
$$\sigma_t^2 = 0.023 + 0.596\sigma_{t-1}^2 + 0.318\varepsilon_{t-1}^2 \quad (1)$$

2. Industry Index:

$$r_t = 0.071 + u_t$$
$$u_t = 0.43u_{t-1} + 0.079u_{t-2} + 0.09u_{t-4} + 0.072u_{t-5} + 0.069u_{t-9} + 0.044u_{t-10} + \varepsilon_t$$
$$\varepsilon_t = z_t\sigma_t$$
$$\sigma_t^2 = 0.008 + 0.829\sigma_{t-1}^2 + 0.154\varepsilon_{t-1}^2 \quad (1)$$

3. Finance Index:

$$r_t = 0.078 + u_t$$
$$u_t = 0.45u_{t-1} + 0.044u_{t-9} + \varepsilon_t$$
$$\varepsilon_t = z_t\sigma_t$$
$$\sigma_t^2 = 0.427 + 0.326\varepsilon_{t-1}^2 \quad (1)$$

For both TEPIX and Industry index, the sum of ARCH and GARCH coefficients is very close to one, indicating that volatility shocks are persistent. We conclude that strong GARCH effects are apparent in the financial market. Also, the coefficient of lagged conditional variance is significantly positive and less than one, indicating that the impact of 'old' news on volatility is significant.

B. Model Validation

In this step, rigorous statistical hypothesis testing is applied to validate the model assumptions of the GARCH specification. These tests include the Ljung-Box and ACF, PACF plot for the residuals and the squared residuals of the GARCH model, as well as ARCH LM test.

Correlogram and Q-statistics of the residuals displays the autocorrelations and partial autocorrelations of the standardized residuals. It can be used to test for remaining serial correlation in the mean equation and to check the specification of the mean equation. If the mean equation is correctly specified, all Q-statistics should not be significant. Correlogram of Squared Residuals displays the autocorrelations and partial autocorrelations of the squared standardized residuals. It can be used to test for remaining ARCH in the variance equation and to check the specification of the variance equation. If the variance equation is correctly specified, all Q-statistics should not be significant. ARCH LM Test: carries out Lagrange multiplier tests to test whether the standardized residuals exhibit additional ARCH. If the variance equation is correctly specified, there should be no ARCH left in the standardized residuals. We can examine different lags with this test and make sure that all significant lags have been added.

These tests were implemented on the residuals of all three AR/GARCH models; neither signs of remained autoregressive component nor ARCH or GARCH lags were observed in them. Thus our models of these three indices are ready to be forecasted in different steps ahead.

C. Forecasting indices and returns

The three main purposes of forecasting volatility are for risk management, for asset allocation, and for taking bets on future volatility. In this paper, we not only forecast the market volatility, but also present the prediction of returns and indices' values. To do so, after estimating the parameters, we can build the AR/GARCH prediction model. The problem of one-step-ahead prediction of the log return of TEPIX, and extending it to the 10, 30, and 90-step-ahead (a steps is considered as a day) forecasts are considered here. To compare different k-step-ahead forecasts, we use some forecast accuracy metrics. The forecasted TEPIX and its volatility are illustrated in Fig. 2 and Fig. 3 as an example. To plot the volatility, we first forecast the varianve from the GARCH model, and then we multiply it by 250 (days of a year) and take the square root.

The reported forecast error statistics in this study are the Root Mean Squared Error (RMSE), the Mean Absolute Error (MAE) and the Theil Inequality Coefficient (TIC).

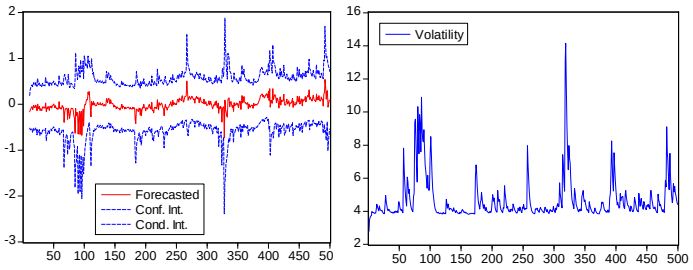

(a) (b)

Fig. 2
One-step-ahead forecast of (a) residuals
and (b) volatility of TEPIX's AR/GARCH model.

The mean squared forecast error can be decomposed to define three proportions of error: Bias Proportion, Variance Proportion and Covariance Proportion. The bias proportion tells us how far the mean of the forecast is from the mean of the actual series. The variance proportion tells us how far the variation of the forecast is from the variation of the actual series. The covariance proportion measures the remaining unsystematic forecasting errors. Note that the bias, variance, and covariance proportions add up to one. If the forecast is "good", the bias and variance proportions should be small so that most of the bias should be concentrated on the covariance

proportions. The Results of these measures are shown in TABLE IV for TEPIX. As it can be observed, the most significant proportion of errors belongs to non-structural errors such as exogenous variables.

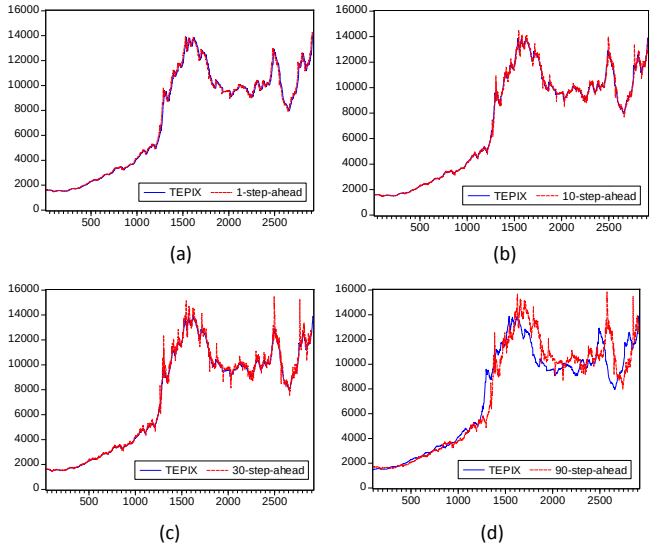

Fig. 3
One-step-ahead, (b) 10-step ahead, (c) 30-step ahead, and (d) 90-step-ahead forecasted values of TEPIX

TABLE IV
FORECAST ACCURACY EVALUATION FOR TEPIX

Root Mean Squared Error	0.44
Mean Absolute Error	0.26
Theil Inequality Coefficient	0.58
Bias Proportion	0.00
Variance Proportion	0.23
Covariance Proportion	0.77

Besides, we calculate the MAE measure for different k-step-ahead forecasts of TEPIX. The results are shown in TABLE V. It is clear that the least MAE belongs to the least lag of prediction, which is one-step-ahead.

TABLE V
MEAN ABSOLUTE ERROS (MAE) FOR DIFFERENT K-STEP-AHEAD FORECASTS OF TEPIX

K	1	10	30	90
MAE	0.26	0.29	0.33	0.37

V. Conclusion

Many lines of research have been examining financial returns to address the question of whether GARCH family models have the capability of capturing volatility clustering. The results of this paper probe the issue by providing estimates from AR/GARCH models for daily returns of three main indices of Tehran Stock Exchange: TEPIX, Industry Index, and Finance Index. In summary of our results, we found strong evidence of ARCH/GARCH specifications in all indices. The some of the estimated coefficients in almost all cases are close to 1, indicating the persistence of conditional variance. In addition, we forecasted the model with four different k-step (day)-ahead methods. The MAEs of these predictions were compared with each other. Obviously, the one step ahead forecast indicates the least MAE measure. The 90-step-ahead prediction plot, on the other hand, demonstrates notable imprecision due to the sudden upward change in volatility, which is reflected in the prediction with observable delay. The most significant proportion of the bias of the forecast is due to covariance, indicating non-structural bias. This bias should be taken seriously, since it causes a considerable error in forecasting the returns of the indices. Different exogenous variables with different linear and nonlinear models should be implemented and compared to the results of the AR/GARCH model. Some further research can be conducted on other types of GARCH family models, such as EGARCH, TGARCH, CGARCG, PGARCG, and GARCH-M. In addition, research can be concentrated on examining elaborate nonlinear effects such as Chaos Theory, which is the subject of our future studies on the residuals of the presented AR/GARCH.

VI. References

[1] Bollerslev, T. (1986) "Generalised autoregressive conditional heteroscedasticity", *Journal of Econometrics*, Vol 31, pp. 307-27

[2] Bollerslev, T. and Wooldridge, J. M. (1992) "Quasi maximum likelihood estimation and inference in dynamic models with time varying covariances", *Econometric Reviews*, Vol 11, pp. 143-179.

[3] Box, George E.P., and Jenkins, Gwilym M. (1970), *Time Series Analysis Forecasting and Control,* San Francisco: Holden-Day.

[4] Engle, R. F. (1982) "Autoregressive conditional heteroscedasticity with estimates of the variance of UK inflation", *Econometrica*, Vol 50, pp. 987-1008.

[5] Floros, C (2008), "Modelling Volatility using GARCH Models: Evidence from Egypt and Israel", *Middle Eastern Finance and Economics*, Vol. 2, pp. 31-41.

[6] French, K. R., Schwert, G. W. and Staumbaugh, R. F. (1987) "Expected stock returns and volatility", *Journal of Financial Economics*, Vol 19, pp. 3-29.

[7] Jenkins, G. Box, G., Reinsel, G., (1970), *Time Series Analysis, Forecasting and Control*, 1th ed., Wiley, pp. 64-65

[8] P.Brockwell and R.Davis, "*Introduction to Time Series and Forecasting*", Springer, 1996.

[9] Ljung, Greta M., and George E. P. Box, "On a Measure of Lack of Fit in Time Series Models," *Biometrika 65* (1978), 297-303.

[10] Mandelbrot, B., 1963, The variation of certain speculative prices, *Journal of Business* 36, 394-419.

[11] Mecagni, M. and Sourial, M. S. (1999) "The Egyptian stock market: Efficiency tests and volatility effects", IMF Working paper No. 99/48.

[12] Meric, G., Ratner, M., and Meric, I. (2007) "Co-movements of the U.S., U.K., and Middle East Stock markets", Middle Eastern Finance and Economics, Issue 1, pp. 60-73.

[13] Nakatsuma, T. and Tsurumi H., "ARMA-GARCH models: Bayes Estimation Versus MLE, and Bayes Non-stationary Test", department working papers with number 199619, department of Economics, Retgurs University, 1996.

[14] Tooma, E. A. (2003) "Modeling and forecasting Egyptian stock market volatility before and after price limits", Working Paper 0310, Economic Research Forum, Cairo, Egypt.

[15] White, Halbert, 1982, Maximum likelihood estimation of misspecified models, Econometrica 50, 1-25.

2011 International Conference on Mechanical, Industrial, and Manufacturing Engineering
Lecture Notes in Information Technology Vols. 1-2

The Existence of Periodic Orbits In the Satellite Motion Systems Under the Periodic Perturbation

Li Jia
Pearl River College Tianjin University of Finance and Economics, Tianjin, 3001811, China
Jiali0@yahoo.cn

Lizhen Zhang*
Department of Mathematics, Tianjin Polytechnic University Tianjin,300160, China
*Corresponding author:Lzhzhang0@yahoo.com.cn

***Abstract* - In this paper, we obtain the existence of periodic orbits in the satellite motion systems under the periodic perturbation on R^2. Using the Melnikov methods on R^2, we get the situations of keeping periodic orbits in this system. This means that the system is stability in these situations.**

Index Terms* - *Melnikov methods , Subharmonic Periodic Orbits, Resonance, Periodic Perturbation.

I. INTRODUCTION

With the deeper understanding of the world，people are aware of many systems have very complex dynamics growing. The chaotic and stability nature properties are prevalent in these complex systems and its a very important dynamic properties. I recent years, people's understanding of some complex systems are gradually in-depth. Chaos theory and the stability of the complex system have made great progress and these theorys are increasingly becoming a powerful tool for these systems. In this paper, we research the periodic perturbation system on R^2, and get the situations of keeping periodic orbits in this systems.

From the reference[1], we know that the equation of motion describing the librational motion of an arbitrarily shaped satellite in a planar , the elliptical orbit is

$$(1+\varepsilon\mu\cos\theta)\,\psi''-2\varepsilon\mu\sin\theta\,(\psi'+1)+3\beta sin\theta cos\theta=0 \quad (1)$$

Here $\psi''=\frac{\partial\psi}{\partial\psi}, \psi\in(-\pi,\pi], \theta\in(0,2\pi), \beta$ is a physical parameter, freedom of movement of any plane shape of the satellite orbit equation as follows, $\varepsilon\mu$ is the eccentricity of the elliptical orbit, and $0<\varepsilon\ll 1$. The elliptical orbit sketch map of the librational motion of an arbitrarily shaped satellite in a planar is follow figure 1,

For the very small ε, we use the Taylor expansion $\frac{1}{1+\mu\cos\theta}=1-\varepsilon\mu\cos+\mathcal{O}(\varepsilon^2)$, We can change the system (1) into,

$$\psi''+3\beta\sin\psi\cos\psi=\varepsilon[2\mu\sin(\psi'+1)+3\mu\beta\sin\psi\cos\psi\cos\theta]+\mathcal{O}(\varepsilon^2) \quad (2)$$

Let $\psi=x, \psi'=y$, we can get the equivalent system of (2),that is a two-dimensional periodic perturbations system,

$$\begin{cases} x'=y \\ y'=-\frac{3}{2}\beta\sin 2x+\varepsilon[2\mu(y+1)\sin\theta+\frac{3}{2}\mu\beta\sin 2x]+\mathcal{O}(\varepsilon^2) \end{cases} \quad (3)$$

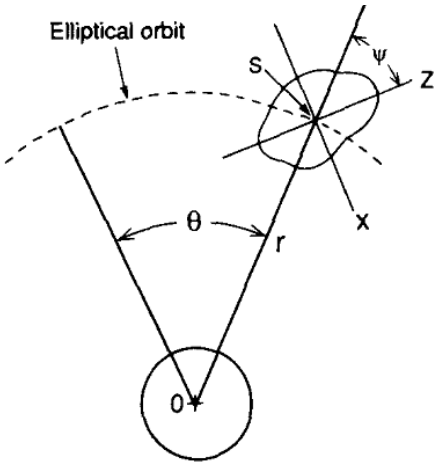

Figure 1 The elliptical orbit sketch map of the librational motion of an arbitrarily shaped satellite in a planar

This is the system to research in this paper.

II. The phase diagram of the unperturbed system

In this section, we consider that the existence of periodic orbits of the system (3) and the conditions of the periodic orbits in the periodic perturbation system still exist. When $\varepsilon=0$, we can get the unperturbed system of (3),

$$\begin{cases} x'=y \\ y'=-\frac{3}{2}\beta\sin 2x \end{cases} \quad (4)$$

This system (4) is a Hamilton system, the Hamilton function of this system is

$$H(x,y)=\frac{1}{2}-\frac{3}{4}\beta\cos(2x)=h. \quad (5)$$

from

$$\begin{cases} x'=0 \\ y'=0 \end{cases} \quad (6)$$

That is

$$\begin{cases} y=0 \\ -\frac{3}{2}\beta\sin 2x=0 \end{cases} \quad (7)$$

From the properties of plane hamilton system, we know that there are a center point$A(0,0)$, and two saddle points $B(+\frac{\pi}{2},0)$,$C(-\frac{\pi}{2},0)$ when$\beta<0$. When $\beta>0$, there are a saddle point $A(0,0)$ and two center points $B(+\frac{\pi}{2},0)$,$C(-\frac{\pi}{2},0)$ in system (4). For $\beta<0$, the phase diagram of (4) is following,

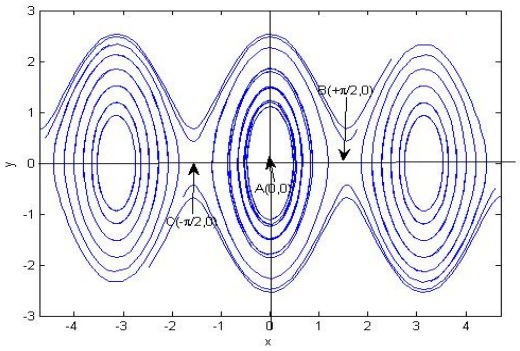

Figure 2 .When $\beta<0$, the phase diagram of (4)

when$\beta>0$, we can get the phase diagram of (4) similarly. In this paper, we only consider the situation of $\beta<0$.

III Existence of Subharmonic periodic orbits.

In this section, we consider the situation of $\beta<0$, then from the theory of the system stability, we know that when $0<h<-\frac{3}{4}\beta$, there corresponds to a cluster of periodic orbits around the center $B(+\frac{\pi}{2},0)(orC(-\frac{\pi}{2},0))$, we can calculated the parameter expression of the periodic orbits,

$$\begin{cases} x(\theta)=\pm\arctan\frac{k}{k'}cn(\sqrt{-3\beta}\theta,k) \\ y(\theta)=\mp\frac{-\frac{k}{k'}\sqrt{-3\beta}sn(\sqrt{-3\beta}\theta,k)dn(\sqrt{-3\beta}\theta,k)}{1+\frac{k^2}{k'^2}cn^2(\sqrt{-3\beta}\theta,k)} \end{cases} \quad (8)$$

where cn,sn,dn are elliptic functions[4], $k=\sqrt{\frac{3\beta-4h}{6\beta}},k'=\sqrt{1-k^2},b=\sqrt{\frac{4h+3\beta}{3\beta-4h}}=\frac{k'}{k}$, and their periodic are

$$T(k)=\frac{4K(k)}{\sqrt{-3\beta}},$$

where $K(k)$ is the first complete elliptic integral. In order to analyze this cluster periodic orbits with the small periodic perturbation, that is the system (3), we suppose that the periodic orbits are satisfied with the resonance situations,

$$T(k)=\frac{2\pi m}{n},$$

That is

$$\frac{4K(k)}{\sqrt{-3\beta}}=\frac{2\pi m}{n}$$

where m,n are relatively prime positive integers. Now we calculate the $Melnikov$ function of the these periodic orbits. The $Melnikov$ function is following,

$$\begin{aligned} M_1^{\frac{m}{n}}(\theta_0,\beta,\mu) &= \int_0^{nT}F(q(\theta-\theta_0))\wedge f(q(\theta-\theta_0),\theta)d\theta \\ &= \int_0^{nT}y(\theta-\theta_0)\{2\mu\sin y(y(\theta-\theta_0)+1) \\ &\quad +\tfrac{3}{2}\mu\beta\sin 2x(\theta-\theta_0)\cos\theta\}d\theta. \end{aligned} \quad (9)$$

Put the periodic orbit parameter equation (8) into the above equation, and in accordance with $x(\theta),y(\theta)$ the parity into the above equation can be changed into the following form,

$$M_1^{m/n}(\theta_0,\beta,\mu)=2\mu\cos\theta_0 J_1+2\mu J_2\sin\theta_0-\frac{3}{2}\beta J_3\sin\theta_0. \quad (10)$$

where

$$\begin{cases} J_1 = \int_0^{nT}y(\theta)\sin\theta d\theta \\ J_2 = \int_0^{nT}y^2(\theta)\cos\theta d\theta \\ J_3 = \int_0^{nT}y(\theta)\sin\theta\sin 2x(\theta)d\theta. \end{cases} \quad (11)$$

Following, we calculate separately J_1,J_2,J_3, and Put $x(\theta)$ of the system (8) into (11), and can get

$$\begin{aligned} J_1 &= \int_0^{nt}y(\theta)\sin\theta d\theta \\ &= -\frac{k}{k'}\int_{-2nK}^{2nK}\frac{sntdnt\sin(\frac{m\pi}{2nK}t)}{1+\frac{k^2}{k'^2}cn^2t}dt \end{aligned} \quad (12)$$

We calculate $\oint_L f_1(z)dz$ using the residue theorem, here

$$f_1(z)=\frac{snzdnzexp(\frac{m\pi}{2nK}z)}{1+\frac{k^2}{k'^2}cn^2z}$$

where the road L is taken by a parallelogram *ABCD*, its graph is following the figure 3,

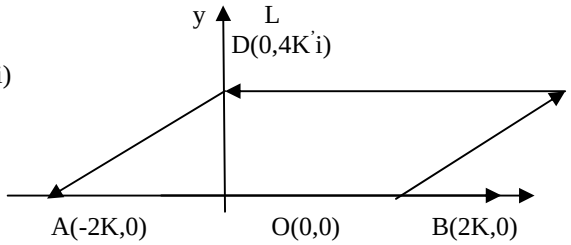

Figure 3 the road L passed by the path

we can get there are four level one poles, they are

$$\begin{aligned} z_1&=K+K'i, \\ z_2&=-K+K'i, \\ z_3&=K+3K'i, \\ z_4&=3K+3K'i. \end{aligned}$$

So we can calculate the residues of function $f_1(z)$ at these poles,

$$\begin{cases} Res_{z=z_1} = \frac{k'}{2ki}e^{-\frac{m\pi K'}{2nK}}(\cos\frac{m\pi}{2n}+i\sin\frac{m\pi}{2n}) \\ Res_{z=z_2} = -\frac{k'}{2ki}e^{-\frac{m\pi K'}{2nK}}(\cos\frac{m\pi}{2n}-i\sin\frac{m\pi}{2n}) \\ Res_{z=z_3} = -\frac{k'}{2ki}e^{-\frac{3m\pi K'}{2nK}}(\cos\frac{m\pi}{2n}+i\sin\frac{m\pi}{2n}) \\ Res_{z=z_4} = \frac{k'}{2ki}e^{-\frac{m\pi K'}{2nK}}(\cos\frac{3m\pi}{2n}+i\sin\frac{3m\pi}{2n}) \end{cases} \quad (13)$$

from the residue theorem, we can get

$$\begin{aligned}\oint_L f_1(z)dz &= \int_{L_1} f_1(z)dz + \int_{L_2} f_1(z)dz \\ &\quad + \int_{L_3} f_1(z)dz + \int_{L_4} f_1(z)dz \\ &= \int_{AB} f_1(z)dz + \int_{BC} f_1(z)dz \\ &\quad + \int_{CD} f_1(z)dz + \int_{DA} f_1(z)dz\end{aligned}$$

(14)

where

$$\int_{AB} f_1(z)dz = \int_{-2K}^{2K} \frac{snzdnzexp(i\frac{m\pi z}{2nK})}{1+\frac{k^2}{k'^2}cn^{2z}}dz \quad (15)$$

$$\int_{CD} f_1(z)dz = (-1)^m e^{-\frac{2m\pi K'}{nK}} \int_{AB} f_1(z)dz \quad (16)$$

from the odevity of the functions snz, dnz, cn^2z and the symmetry of the integration path L, we can get

$$\int_{BC} f_1(z)dz + \int_{DA} f_1(z)dz = 0. \quad (17)$$

then take the formula (15),(16),(17) into (14), we get

$$\begin{aligned}\int_{L_1} f_1(z)dz + \int_{L_3} f_1(z)dz &= (1+(-1)^m e^{-\frac{2m\pi K'}{nK}})* \\ &\quad \int_{-2K}^{2K} \frac{sntdnte^{(\frac{m\pi}{2nK}t)}}{1+\frac{k^2}{k'^2}cn^2t}dt\end{aligned}$$

(18)

Further more, we take (13) into the above formula, combined the residue theorem and we obtain

$$J_1 = \begin{cases} 0 & when \ \ n>1 \ or \ m \ is \ even \ number \\ (-1)^{[\frac{m}{2}]}\pi sech\frac{m\pi K'}{2K}, & when \ \ n=1 \ andm \ is \ odd \ number \end{cases}$$

(19)

Similarly ,we obtain

$$J_2 = \begin{cases} 0 & \\ & when \quad n>1 \ or \ m \ is \ even \ number, \\ (-1)^{[\frac{m}{2}]} & \frac{K}{m}(\frac{m\pi}{2K} - \frac{1-7k'}{12k^2})cn\frac{m\pi K'}{2K}sech\frac{m\pi K'}{2K}, \\ & when \quad n=1 \ andm \ is \ odd \ number. \end{cases}$$

(20)

$$J_3 = \begin{cases} 0 & \\ & when \quad n>1 \ or \ m \ is \ even \ number \\ (-1)^{[\frac{m}{2}]} & \frac{\pi k^2}{2k}(\frac{m\pi}{4k} - \frac{3k'^2}{k^2K})cn\frac{m\pi K'}{2K}sech\frac{m\pi K'}{2K}, \\ & when \quad n=1 \ andm \ is \ odd \ number \end{cases}$$

(21)

where $[\frac{m}{2}]$ is the integer part of $\frac{m}{2}$. We take the J_1, J_2, J_3 into (10),and can get the formula of function $M_1^{\frac{m}{n}}(\theta_0, \beta, \mu)$, and easily know ：when n>1 or m is even number,

$$M_1^{\frac{m}{n}}(\theta_0, \beta, \mu) = 0.$$

If we want consider the properties of these periodic orbits, it must be use the higher order Melnikov theory[2,3]. When n=1 and m is an odd number, we have

$$M_1^{m/1}(\theta_0, \beta, \mu) = 2\mu\cos\theta_0 J_1 + (2\mu J_2 - \frac{3}{2}\mu\beta J_3)\sin\theta_0$$

(22)

From the formula (19), we know $J_1 \neq 0$, so when $\mu \neq 0$, the function $M_1^{\frac{m}{n}}(\theta_0, \beta, \mu)$ has always the simple zero.

Consequently we have the following theorem according to the related results of the literature [2,3],

Theorem For the sufficiently small ε, there always exists periodic orbits satisfied with the resonance condition $T(k) = 2m\pi$ and m is odd number in the system (3) ,the periodic orbits form is the same as formulas (8).

REFERENCES

[1] [1] V.S. Modi, R.C. Brereton , Periodic solutions associated with the gravity-gradient-oriented system: Part I. Analytical and numerical determination. AIAA J.7,pp.1217-1225,1969.

[2] [2]S. Wiggins. Introduction to applied nonlinear Dynamical Systems and Chaos, Springer-Verlag: New York,1990.

[3] [3]J. Guckenheimer, P. Holmes. Nonlinear Oscillators, Dynamical Systems, and Bifurcations of Vector Fields. Springer-Verlag: New York, 1983.

[4] [4]P.F. Byrd, M.D. Friedman. Handbook of Elliptic Integrals for Engineers and Scientist. Springer-Verlag: New York,1971.

2011 International Conference on Mechanical, Industrial, and Manufacturing Engineering
Lecture Notes in Information Technology Vols. 1-2

Application of Desirability Based Multiresponse Optimization for Reciprocating Pump Design*

Yangdong Wu
Lab of Contemporary Manufacturing Technology
Guizhou University
Guiyang, Guizhou Province, China
Qxyd2000@yahoo.com.cn

Lifang Wang
Reciprocating Pump Technology Institute
Benxi Water Pumps co., ltd
Benxi, Liaoning Province, China
gydujing71@163.com

***Abstract* - Response surface methodology based robust design is a fine technique to improve product quality. This paper presents rationale of response surface methodology, using response surface methodology to solve multiple variables problems, for multiple design targets, applying desirability function to calculate them, so the multiple responses can be changed into one single function. Simulated annealing is used to solve overall desirability function. Finally, master structure parameter of reciprocating pump is designed using our method.**

Index Terms - Response surface methodology*; *Multiresponse optimization*; *Desirability function*; *Simulated annealing*; *Reciprocating pump.

I. INTRODUCTION

Reciprocating pump belongs to positive displacement pump, it make the liquid medium volume change periodically by plunger reciprocation. Reciprocating pump suit to transport high pressure, low flow and high viscosity liquid, but it can not transport corrosive liquids usually. Sometimes, it would be driven by steam engine for transporting flammable liquid and explosive liquid. Reciprocating pump could start without injecting liquid, so reciprocating pumps possesses self-priming capability, but the suction capability would change along with the atmospheric pressure, the liquid nature and temperature, so the installation altitude of reciprocating pump is restricted. Reciprocating pump discharge can not be adjusted by valves, but it should be changed through bypass pipe or changing the operation frequency of the piston, changing the piston stroke. Before reciprocating pump starting, discharge pipe valve must be open. Reciprocating piston connects with motor by pump crankshaft and connecting rods. The pump can be driven by electromotor or steam engine.

Among various modern design methods, robust design is a fine technique to improve reciprocating pump product quality, since G.Taguchi put forward the method, many study commit themselves to improve on the robust design technique through statistics analysis method [1], many methods introduce response surface methodology (RSM) to instead of signal noise ratio method which was brought forward by G.Taguchi [2]. Figure 1 shows the RSM robust design principle.

Along with product become more and more complicated and diversifications of customer requirement, product quality characteristics possess Multi target frequently [3]. So multiresponse optimization shows its important academic value and applied value progressively. Multiresponse optimization need optimize multi-responses at the same time [4]. This paper presents rationale of response surface methodology, multi-response transforming method based on desirability function and overall desirability function optimization using intelligent algorithm.

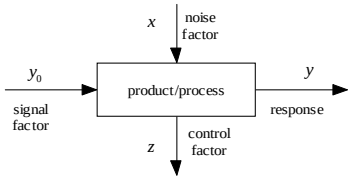

Fig. 1 RSM robust design principle

II. RESPONSE SURFACE METHODOLOGY AND EXPERIMENTAL DESIGN

Response surface methodology is a collection of mathematical and statistical techniques that are useful for modeling and analysis of problems in which a response of interest is influenced by several variables and where the objective is to optimize this response. We use the RSM to model the response of multiple quality characteristic caused by various control and noise factors [5]. There control factor is design factor that designer could control them and noise factor is un-control factor that influence quality characteristic.

The RSM is an important branch of experimental design. It is a critical technology for optimizing product performance and improving the design formulation of new products. Response surface methods can lead to a rapid and accurate exploration of the parameter space and to the estimation of optimum conditions with a small expenditure on experimental data. The experimental design, multivariate regression analysis, and optimization techniques form the foundation of response surface methodology.

Experimental design is used to select parameter combinations for efficient experimentation. Using the resulting data, a second-order estimation model is constructed using regression analysis techniques relating the output response surface to input parameters. Response surface methodology could fit the model that include control and noise factors, when we carry out experimental design, two kinds of factors

* This work is partially supported by the Science and technology Foundation of Guizhou Province, China (Grant No. [2009]2233) and the introduced talents scientific research Foundation of Guizhou university, China (Grant No. (2008)014).

may arrange on one array. If two kinds of factors were defined as

$$x^T = (x_1, x_2, \cdots, x_n),\ z^T = (z_1, z_2, \cdots, z_k)$$

the empirically fitted second-order model may be written as

$$\hat{y}(x,z) = b_0 + x^T b + x^T \hat{B} x + z^T \hat{R} z + z^T \hat{\gamma} + z^T \hat{D} x \quad (1)$$

where b, $\hat{B}$, $\hat{R}$, $\hat{\gamma}$ and $\hat{D}$ are appropriate vectors or matrices of unknown regression parameters. The model regression coefficient could be calculated by least square method. The second-order model was applied widely at present.

When using the response surface model, in order to sure that the regression is significant, analysis of variance can be used to indicate that the regression of experimental data is significant for the regression analysis.

The basic of response surface methodology is design of experiments (DOE). Design of experiments or experimental design is the design of any information-gathering exercises where variation is present, whether under the full control of the experimenter or not. However, in statistics, these terms are usually used for controlled experiments.

Design of experiments is thus a discipline that has very broad application across all the natural and social sciences. The DOE methodology ensures that all factors and their interactions are systematically investigated. Therefore, information obtained from a DOE analysis is much more reliable and complete than results from one-factor-at-a-time experiments that ignore interactions and may lead to incorrect conclusions. The figure 2 shows the face-centered central composite design for three factors.

When the experimenter wants to investigate more factors (for instances, more than 4 factors) in an experiment one cannot expect to obtain a good result without the use of modern experimental designs. We need some efficient fractional factorial designs, as central composite design, orthogonal design etc.

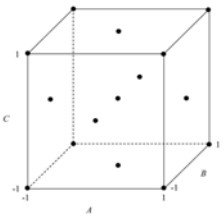

Fig. 2 Face-centered central composite design for three factors

The Uniform design is another such efficient fractional factorial design. It has been successfully used in various fields such as chemistry and chemical engineering, pharmaceutics, quality engineering, system engineering, survey design, computer sciences and natural sciences. The uniform design has been recognized as an important space-filling design by the international community.

III. MULTIPLE RESPONSE OPTIMIZATION ALGORITHM

The goal of multi-response problem is to find the setting of the design variables that achieve an optimal balance of the response variables. Desirability function method can be used to combine multiple responses into one single function and attempt to find the optimal balance. Each response function is transformed into a desirability function. Here we adopt the three kinds of desirability functions which were discussed in paper of hezheng [6], they may adapt to various design requirements.

All the individual desirability functions are combined to form an overall desirability function, the overall desirability function can be defined as weighted geometric mean of the individual desirability. The levels of various factors and response value corresponding to the maximum value of overall desirability function represent the optimum solution and its response.

Multiple response optimization is complicated, the overall desirability function is a nonlinear function usually, design variable and its restriction include both continuous variable and disperse variable, so it is difficult to solve the problem using ordinary optimization algorithm. An intelligent optimization method, such as simulated annealing (SA) can be used to optimize the overall desirability function. The flow in simulated annealing is illustrated in figure 3.

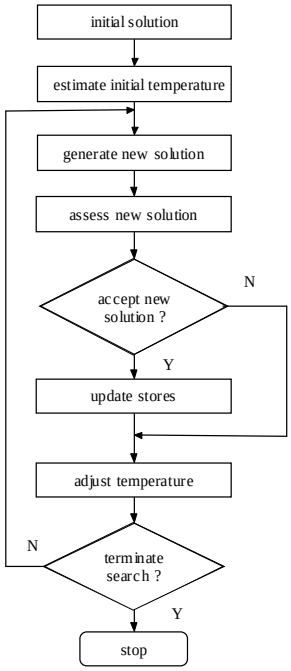

Fig. 3 Flowchart of optimization algorithm

Simulated annealing is a generalization of a Monte Carlo method for examining the equations of state and frozen states of n-body systems [7]. The concept is based on the manner in which liquids freeze or metals recrystallize in the process of annealing.

The original Metropolis scheme was that an initial state of a thermodynamic system was chosen at energy E and temperature T, holding T constant the initial configuration is

perturbed and the change in energy dE is computed [8]. If the change in energy is negative the new configuration is accepted. If the change in energy is positive it is accepted with a probability given by the Boltzmann factor exp -(dE/T). This processes is then repeated sufficient times to give good sampling statistics for the current temperature, and then the temperature is decremented and the entire process repeated until a frozen state is achieved at T=0.

By analogy the generalization of this Monte Carlo approach to combinatorial problems is straight forward. The current state of the thermodynamic system is analogous to the current solution to the combinatorial problem, the energy equation for the thermodynamic system is analogous to at the objective function, and ground state is analogous to the global minimum. Furthermore, avoidance of entrainment in local minima (quenching) is dependent on the "annealing schedule", the choice of initial temperature, how many iterations are performed at each temperature, and how much the temperature is decremented at each step as cooling proceeds.

IV. RECIPROCATING PUMP MASTER STRUCTURE PARAMETER DESIGN USING MULTIPLE RESPONSE OPTIMIZATION

Reciprocating pump consists of transmission parts, hydraulic parts, pipelines subassembly and accessory and so on, each portion contains relevant components. It has abundant variety and less production batch, and its performance parameter is often a series. The figure blow shows a typical three plungers reciprocating pump.

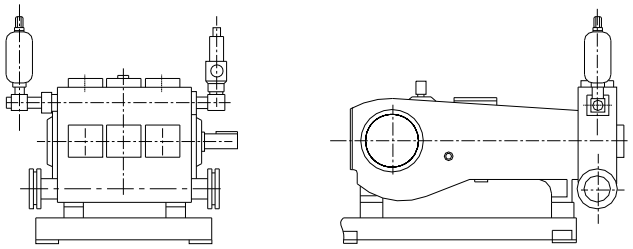

Fig. 4 Three plungers reciprocating pump

Reciprocating pump original design parameters includes discharge rate (Q), discharge pressure (P_q), number of plunger (Z), number of action (K), volume efficiency (η_v), power of motor(P), structure mode, operation temperature etc. On the basis of original design parameter, we can identify motor power and master structure parameter, i.e. plunger diameter (D), plunger stroke (S) and pump rate (n), accordingly transmission end, hydraulic end, pipeline subassembly and accessory may be designed and structure dimension of these parts may be gained.

Figure5 illustrates reciprocating pump principle. When it works, the piston moves from left to right, form a negative pressure pump cylinder, then the suction tank fluid through the valve into the pump cylinder. When the piston moves from right to left, the liquid of cylinder is squeezing, and the pressure increasing, liquid discharged from the discharge valve. A reciprocating piston, if suction and discharge fluid known as a work cycle, the pump called the single-action pump. When the piston rounds one circle, the suction and discharge of pump are twice, the pump known as double-acting pump. Piston from one end to another end, called a stroke.

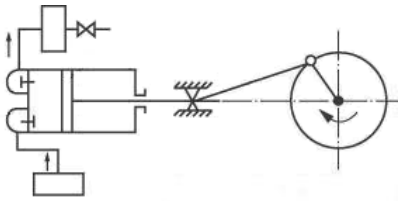

Fig.5 Reciprocating pump schematic diagram

The key of reciprocating pump design is master structure parameter design. The design of master structure parameter decide whether whole dimension is harmonious and technology parameter is matching, it decide whole design project of product and become the important foundation of particular design of other parts. Thus design of master structure parameter is the most important portion of reciprocating pump design. Figure blow shows relation among reciprocating pump parts. Figure blow shows relation among reciprocating pump parts.

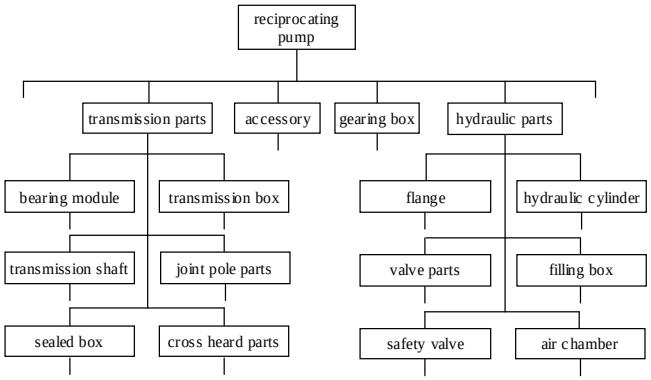

Fig. 6 Reciprocating pump parts

Master structure parameter ought to satisfy the requirement of product performance parameter, and make product have enough life and reliability and maintenance convenience. In reciprocating pump design, consumer requirement may express by two basal performance parameters, namely displacement and pressure. Pressure is never related to displacement, it lies on characteristic of equipment, and that displacement lies on master structure parameter, the same displacement may make up of different master structure parameter. For obtaining right master structure parameter, we should choose appropriate average speed of plunger firstly, then revolution of crank and stroke length are gained, finally, according to the ratio of stroke length and plunger diameter, regulating these parameter and gaining plunger diameter, so a group of right master structure parameter are found. The parts structure design could operate based on master structure parameter.

We would design a reciprocating pump, its discharge rate is 10.2m^3/h and discharge pressure is 11Mpa. According as reciprocating pump design theory, power(P), torque(T) and plunger fore(F) are quality characteristics, the factors that would be calculated in design are plunger diameter(D), plunger stroke(S), pump rate(n) and volume efficiency(η_V), discharge rate(Q) is considered as a restriction. In design process, according to initialization condition and design criterion, a restriction is given as

$$A \cdot S \cdot n \cdot D \cdot \eta_V = 712 \qquad (2)$$

A is section area of plunger.

The formulations of Q, P, T and F are given in *reciprocating pump* [9]. Due to formulation of F is simpler than other, we only calculate response surface of Q, P and T, desirability function of F could be defined directly.

According to design criterion of reciprocating pump, control factors include D, n, S and η_V, system restriction are plunger average speed(u_m) and ratio of plunger stroke to plunger diameter(ψ), their range of value from references to *reciprocating pump*.

Response Surface Regression: q versus d, s, n, v

The analysis was done using coded units.

Estimated Regression Coefficients for q

Term	Coef	SE Coef	T	P
Constant	1.34958	0.090767	14.869	0.000
d	0.36395	0.035696	10.196	0.000
s	0.05495	0.015207	3.613	0.006
n	0.03792	0.013845	2.739	0.023
v	0.03275	0.016219	2.020	0.074
d*d	0.11350	0.004060	27.958	0.000
d*s	0.09491	0.004067	23.335	0.000
d*n	0.01189	0.003544	3.355	0.008
d*v	0.03067	0.004323	7.095	0.000

S = 0.04241 R-Sq = 100.0% R-Sq(adj) = 100.0%

Analysis of Variance for q

Source	DF	Seq SS	Adj SS	Adj MS	F	P
Regression	8	151.922	151.92197	18.99025	10556.66	0.000
Linear	4	148.989	0.19221	0.04805	26.71	0.000
Square	1	1.274	1.40607	1.40607	781.63	0.000
Interaction	3	1.659	1.65904	0.55301	307.42	0.000
Residual Error	9	0.016	0.01619	0.00180		
Total	17	151.938				

Unusual Observations for q

Obs	StdOrder	q	Fit	SE Fit	Residual	St Resid
10	10	9.790	9.848	0.034	-0.058	-2.23 R

R denotes an observation with a large standardized residual.

Fig. 7 Regression analysis result of Q

In experimental design of response surface, uniform design is applied [10], the fitted second-order model could be obtained, the figure 7 shows the regression result of Q, there we use v instead of η_V. Figure 8 illustrated the relation among q, d and s.

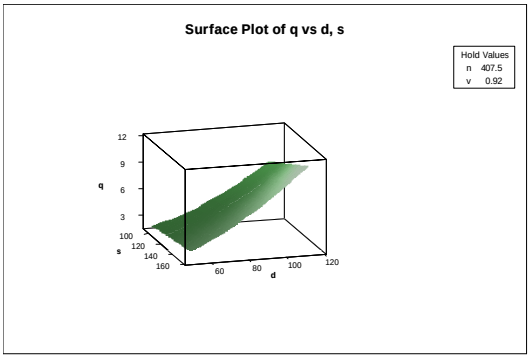

Fig. 8 Q in relation to d and s

Then in term of design criterion, each desirability function can be defined according as aforementioned method. The weight value of response is established by designer [11]. Using simulated annealing, the design results are as D is 46mm, S is 92mm, n is 403min^{-1} and η_V is 0.92. The performance of reciprocating pump was improved using these parameters.

ACKNOWLEDGMENT

This paper obtains the support form colleagues of Benxi water pumps co., ltd and Lab of Contemporary Manufacturing Technology of Guizhou University, I wish to express my gratitude to everyone who contributed to this work.

REFERENCES

[1] Chen, Shikui, "Multiresponse and multistage metamodeling approach for design optimization", *AIAA Journal*, vol.31, no.1, pp.206-218, January 2009.

[2] Myers R H, Montgomery D C. Response Surface Methology.New York: John Wi1ey&Sons, Inc, 1995.

[3] V.I. Vitanov, N. Javaid, "Application of response surface methodology for the optimisation of micro friction surfacing process", *Surface and Coatings Technology*, vol.204 (15), pp.3501-3508, 2010.

[4] G. Steenackers, F. Presezniak, "Development of an adaptive response surface method for optimization of computation-intensive models", *Computers & Industrial Engineering*, vol.57(3), pp.847-855, 2009.

[5] Shah H K. "Impact of Correlated Responses on the Desirability function", Department of Industrial Engineering, Arizona State University, 2001.

[6] Hezhen, Zhongzhiyu, "Application of Improved Desirability Function Method to the Multi-Response Optimization," *Journal of Tianjin University*, vol.39, pp. 1136-1140, Sep. 2006.

[7] Davidson, Ron and David Harel, "Drawing Graphs Nicely Using Simulated Annealing". *ACM Transactions on Graphics*, vol. 15, no. 4, pp. 301-331, 1996.

[8] Wangdingwei, Wangjunwei, *Intelligent optimization methods*, high education press, Beijing, 2007

[9] reciprocating pump design compile group, *reciprocating pump design*, mechanical industury press, Beijing, 1987.

[10]Fangkaitai, Machangxing, *orthogonal and uniform experiment design*, science press, Beijing, 2001.

[11]Kovach, J., "Development of a multidisciplinary-multiresponse robust design optimization model", Engineering Optimization, Vol. 40, No. 9, p 805-819, September, 2008.

2011 International Conference on Mechanical, Industrial, and Manufacturing Engineering
Lecture Notes in Information Technology Vols. 1-2

Kinematic Motion System and Structural Analysis of Aileron Actuator Using FEM

Byeong Sam Kim[1)] . Kyoungwoo Park[4)] . JungHyun Park[3)]
Department of Automotive Engineering
Hoseo University
Asan City, Cheongnam, 336-795, Korea
kbs@hoseo.edu

KiWon Jang[2)]. SangBeom Kim[2)]. DaeHyun Kim[2)]
Hanwha Corporation Aeropace R&D Center[2)], Hanwha Corporation Aeropace R&D Center[3)], Asan-City, Korea

***Abstract* - The wings are mounted inside the actuator system in order to needs of aileron design and kinematic motion system and structural analysis, to ensure the structural safety analysis results are presented. Using kinematic analysis program Sim Design(motion platform), applied in aileron force acting on the joints. It is feasible to change torque the layout of aileron requirements. A finite element representation of the mechanism as a structure is developed. Using the predicted aerodynamic loads, a structural analysis is performed. These results are beneficial for the next phase of model development of the mechanism.**

I. INTRODUCTION

The share of air flight control device wing aileron, elevator, rudder control of the main control device (Primary control system) and secondary day personal flap, spoiler, leading edge flap control of a secondary control device (Secondary control system), they are divided into domestic demand, despite the abundance of technology received recognition in the civil aircraft market, has not been adopted. Medium-class business jet existing parts of the aircraft wing flaps protruding actuators have been called for air resistance and fuel economy. In this study, the protruding parts of an aircraft wing flaps actuators (aileron actuator) mounted inside the wing to remove the protruding part, and the resulting increase in air resistance and fuel economy were targeted.

In this study, the wings are mounted inside the actuator system in order to meet the requirements for the design and kinematic analysis of aileron (kinematic motion system) and structural analysis to ensure the structural safety through the analysis results are presented.

Kinematic motion analysis program by Sim Designer acting on each joint of aileron force and torque aileron requirements for information corresponding to the conditions that were identified, based to identify the characteristics of each part and the structural basis of this analysis using ABAQUS 6.5 model was developed separately by each working on structural analysis, structural characteristics and performance and forecasts were performed. In addition, components of the safety margin for hydraulic components were confirmed by checking the structural safety.

II. AILERON MECHANISM

A. *3-axis motion of the aircraft*

The center of gravity (CG) of the aircraft's three axis was penetrating the lines of 3 points in the virtual. The rotation axes of two wings, an imaginary spirit by nature can be thought. Each other on three dimensions of each axis by 90 degrees through the center of gravity should remain happened. From nose to tail axis connecting the breeder (longitudinal axis) is known, the right wing between the ends the left wing tip and the horizontal axis (lateral axis) is called, the gas passing through the vertical axis, vertical axis is called. Longitudinal axis for the movement of aircraft roll, horizontal (lateral axis) aircraft for the movement of the pitch, vertical axis around the movements of aircraft (yaw) is called.

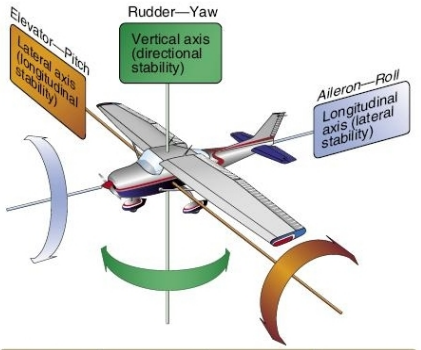

Primary Control Surface	Airplane Movement	Axes of Rotation	Type of Stability
Aileron	Roll	Longitudinal	Lateral
Elevator/ Stabilator	Pitch	Lateral	Longitudinal
Rudder	Yaw	Vertical	Directional

Fig. 1 Aircraft control system movement

B. *Configuration of Aileron*

In the generic fighter of aileron example discussed in this paper, linear models will be used. This is not a requisite, but

for the analysis based on non-linear models, more detailed information and motion algorithm. The linear actuators of mechanism can be either hydraulic rams or electric spindle devices. The aileron actuator motion-bases generally utilise a mechanism known's as the Stwart Platform or "hexapod", which was originally proposed for a base-frame, six actuator legs (the jacks). This method can be applied to both the gravitational forces and the aerodynamic load and gravitational forces categories. The positioning of the links and joints are not changed within the analysis, because of the nature of the design synthesis performed on the mechanism. By changing the lengths of members or moving the links or joints, the desired motion for morphing the wing may no longer be achievable.

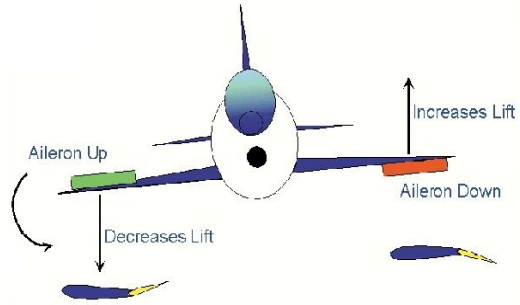

Fig. 2 Aircraft right turn for aileron motion

C. *Mechanism Analysis model*

Aileron's system as shown in the 3D model is composed of the larger piston, bell crank, clevis, stroke and flap. By using kinematic motion system analysis, all of the above free design variable and constraints can be combined to yield the most architecture aileron actuator of the four major parts. This is part of joint connecting the four joint. For simplified system analysis, in this point unnecessary pin were also removed.

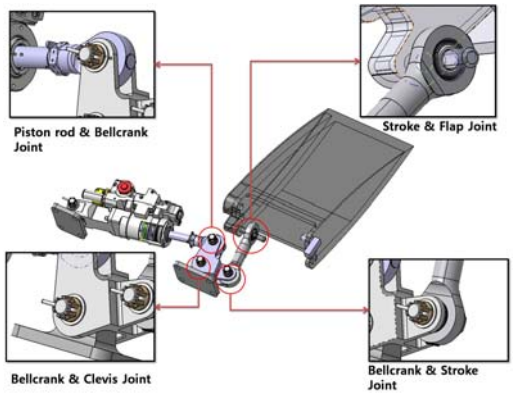

Fig. 3 Aileron composition and joint mechanism

This method can be applied to both the gravitational forces and the aerodynamic load and gravitational forces categories for aileron mechanism. Aileron mechanism have moved up the wing when the maximum angle of 19 ° (TEU 19 °), went down to below 11 ° (TED 11 °) at Case1 and when the wings moved up 24 ° (TEU 24 °) , went down to below 16 ° (TED 16 °) Case2 a time were compared. The rated pressure of the pressure piston (rated pressure) 2775psi, the maximum pressure 3000psi applied when compared in each case. The motion analysis represented a Sim Design@ and, Adams@' program. See Table 1.

D. *Results of Mechanism Analysis*

In Case 1, bellcrank and clevis joint of the connection to the force and torque is the most that can be seen that occur. Also, when you went down to below the angle of the wing (TED 11 °) moved up more when (TEU 19 °) force and torque generation can see that the two larger. Table 2 kinematic motion analysis of a Case 1 is shown the results. Case 2 as well as the connection of bellcrank and clevis joint force and torque on the highest was found to occur. Also, when you went down to below the angle of the wing (TED 16 °) moved up more when (TEU 24 °) force and torque generation can see that the two larger. Table 3 kinematic motion analysis of a Case 2 shows the results. Case 1 and Case 2 when compared to the kinematic motion system analysis of piston and connecting bellcrank joint in part except in Case 1 Case2 more than the forces and torques can be seen that occur. This change in the angle of the wing, larger loads acting on each joint is known to be greater.

TABLE I
Kinematic Analysis in each case

Case	Aileron Angle	Pressure (psi)
Case1	TEU 19°	2775
		3000
	TED 11°	2775
		3000
Case2	TEU 24°	2775
		3000
	TED 16°	2775
		3000

III. STRUCTURAL ANALYSIS

A. *Model design and Boundary conditions*

Aileron's structural analysis model can be divided into three. The piston rod, bellcrank, stroke is these three different parts. The results of kinematic motion analysis were used for the structural analysis based on data that the load applied to each part. The statics pressure range because it contains the maximum pressure in the range of a maximum pressure of 3000psi was the result of applying the data. Case 1 and Case 2 also occurs in the value of the force and torque limit value because they are included within the scope of Case 2 is a TEU 24 ° TED 16 ° and in the context of structural analysis was carried out.

TABLE II
The result of kinematic motion analysis for Case 1

Joint	Pressure (psi)	TED 11°		TEU 19°	
		Force (N)	Torque (in-lb)	Force (N)	Torque (in-lb)
Piston & Bell crank	2775	37936	2929.2	37936	2929.2
	3000	41012	3166.8	41012	3166.8
Bell crank & Clevis	2775	54983	8222.8	67412	11340.4
	3000	59441	8889.8	72878	12260.6
Bell crank & Stroke	2775	37926	3141.5	49128	4068.0
	3000	41001	3396.3	53112	4397.9
Stroke & Flap	2775	37926	2900.3	49128	3791.8
	3000	41001	3135.4	53112	4099.2

The pressure of piston can be used the maximum pressure 3000psi. Each model defines a material density as well as linear, elastic isotropic values of modulus of elasticity, and Poisson's ratio. As with the real constants sets, the first tentative designs are modelled after the second generation model. The materials property include stainless steel (AMS5862 15-5PH) was applied, element type the Tetra mesh (C3D4) were used for ABAQUS 5.7@.

TABLE III
The result of kinematic motion analysis for Case 2

Joint	Pressure (psi)	TED 16°		TEU 24°	
		Force (N)	Torque (in-lb)	Force (N)	Torque (in-lb)
Piston & Bell crank	2775	37936	2929.2	37936	2929.2
	3000	41012	3166.8	41012	3166.8
Bell crank & Clevis	2775	56979	8497.3	79347	14713.8
	3000	61600	9186.8	85781	15907.1
Bell crank & Stroke	2775	39473	3269.7	61413	5081.8
	3000	42674	3534.9	66392	5493.8
Stroke & Flap	2775	39473	3031.2	61413	4717.5
	3000	42674	3094.4	66392	5100.0

B. Margin of Safety

Structural analysis in margin of safety should be considered. The margin of safety is calculated by dividing the critical stress by the limit stress and subtracting one. This ultimate stress with Von Mises is divided by a safety factor of 1.5 in order to have the limit stress. The critical stress is found by dividing the critical force by the cross sectional each area of all the connection link (bell crank, stroke, piston). The yield shear stress of the material chosen is the safety factor is defined as follows.

$$F \cdot S = \frac{S_o}{S_\alpha}$$

TABLE IV
Result of FE Structural Analysis in each parts

	Pressure (psi)	Angle	Von-Mises Stress (Mpa)	Margin of Safety	Max. Displacement (mm)
Bell crank	3000	16°	659.8	0.434	0.253
		24°	662.1	0.429	0.256
Stroke	3000	16°	443.6	1.133	0.796
		24°	620.1	0.527	0.923
Piston	3000	.	274.6	2.446	0.105

C. Result of FE Analysis

Table 4 shows the result of FE analysis in each part. The results of margin of safety for bellcrank (TED 16°) and (TED 24°) with this final design are 0.434 and 0.429 when the load is estimated to be insufficient to withstand. Bell crank joint connection with the piston rod in the most stress and displacement results showed values of the angle did not differ significantly. The stroke is associated with the bellcrank joint was the most stress and displacement. However, the resulting values were different angle, TEU 24 ° at a TED 16 ° greater than the stress and displacement angles seen representing the larger part that the recipient can know the load is greater. The stroke, but also belong within the range of margin of safety is sufficient to withstand the loads are evaluated. When applied to the piston displacement amount 3000psi maximum pressure 0.105mm, Von-Mises Stresses 274.6Mpa 2.446 calculated by the margin of safety is sufficient to withstand the loads are evaluated.

TED16°

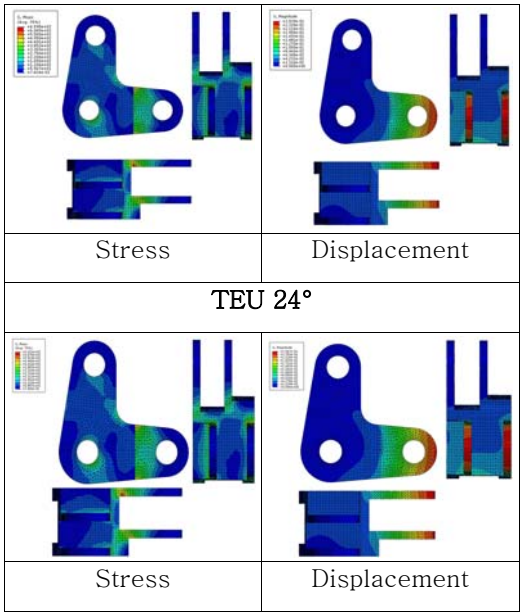

Fig. 4 Bellcrank Structural Analysis result

IV. CONCLUSION

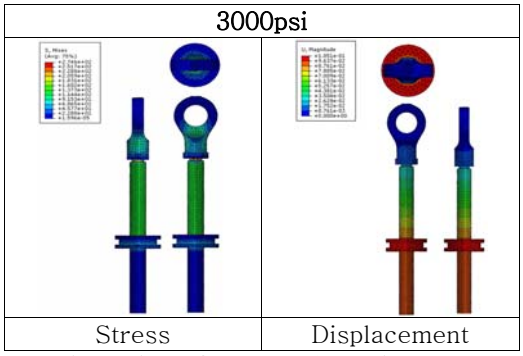

Fig. 5 Piston Structural Analysis result

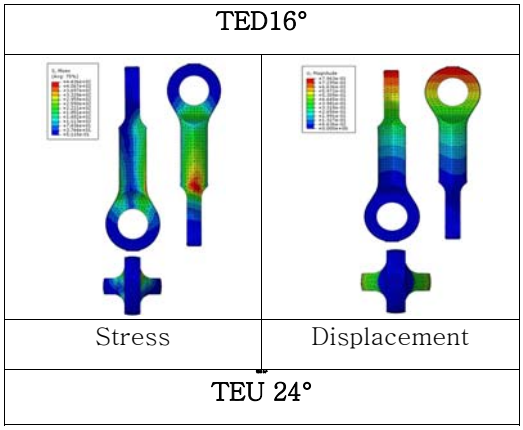

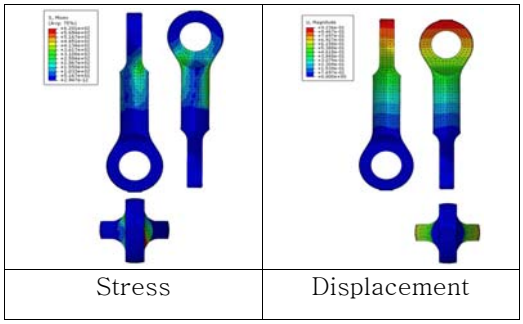

Fig. 6 Stroke Structural Analysis result

In this paper, kinematic motion system analysis and FE structural analysis of the flight control actuators for capacity are presented. Aileron actuator 3 main parts of the piston, bell crank, divided by the stroke of 3D analysis model was developed. Verification calculations prove the model developed in Sim Design and ABAQUS 5.7 as being accurate. Kinematic motion analysis and FE structural analysis performed on the basis of stress distribution and the amount of displacement could be predicted. Analysis of aileron actuator model experiments and simulations to create the actual equipment that would reduce costs and time are considered. In addition, through the optimization of the analytical model analysis time and results can be predicted more accurately than is believed to be.

ACKNOWLEDGMENT

This work was supported by grant No. 2009-0666 from the Korea Aerospace Technology Research Association of the Ministry of Knowledge Economy (MKE).

REFERENCES

[1] D. Stewart, “A platform with sis-degrees-of-freedom”, In Processing International of mechanism engineers, Vol. 180, part 1, pp.371-386, 1966.

[2] S.K. Advani, D. Giovannetti, and M. Blum, “Design of a hexapod motion cueing system for the NASA ames vertical motion simulator “, AIAA Modeling & Simulation Technologies Conference, 08, 2002.

[3] K. Sung, J. Lim, “A strength analysis of rack and pinion of steering gear assay using a commercial finite element program", KSAE08-*S0214*, pp. 1296-1301, 2008.

[4] D. W. Leonard , “Structural Design and Analysis of a Kinematic Mechanism for a Morphing Hyper-Elliptic Cambered Span Wing”, Thesis, Virginia Polytechnic Institute and State University, 2003.

[5] Y. S. Kim, Y. H. Jeon, and all., “Multi-Objective and Multidisciplinary Desing Optimization of Supersonic Fighter wing", Journal of Aircraft, Vol. 43, No. 3, 2006.

[6] C. W. Jun, K.Y. Park and Q. S. Kang , "On the Static Test of Aileron Control System for a Basic Trainer" KSAS journal, Vol. 28, No. 3, pp. 150-155, 2000.

2011 International Conference on Mechanical, Industrial, and Manufacturing Engineering
Lecture Notes in Information Technology Vols. 1-2

Target Range of Chinese House Price Regulation

Lin cheng
Basic Department of Xi'an Politics Institute
Shaanxi Province, China
linch@sina.com

***Abstract* - The development of real estate industry is significant to the national economy and the people's livelihood, and the regulation of real estate is an important content of macroeconomic regulation and is controversial invariably. The key of real estate regulation is the regulation of house price, i.e. to control the rising extent of house price within a normal range. The article calculates the target range of house price regulation in 3σ Method. According to the conclusions, should control the house price rising rate in first-tier cities within [-10.84%, 10.56%], and that in second-tier cities within [-5.13%, 15.99%].The conclusions can provide a theoretical support for the stipulation of real estate regulation policies and the evaluation of the effects of real estate regulation policies.**

Index Terms* - *real estate, house price, regulation, normal range.

I. INTRODUCTION

From 2003, the nation has made a series of real estate regulation policies for alleviating the economic and social contradictions resulted from the too fast rising of house price. From the second half year of 2009, the Chinese real estate market walked out the adjustment situation during the international financial crisis, with both volume and price rising, and the government is facing the difficulty of real estate regulation again. The regulation of house price is the key of real estate regulation. But the target range of house price regulation, i.e. whether the rising rate of house price is normal and requires the regulation of the government, and whether the regulation measures have achieved the predicted target, hasn't a clear definition until now. This is the purpose of the article.

II RESEARCH IDEAS

The target range of house price regulation is the reasonable range of house price fluctuation, and means the rising or declining extent of house price is coordinative with the situations of economic growth and does not need the government to intervene. When the rising extent of house price year on year is within this range, it is considered as normal and does not need to be regulated and controlled. When the rising extent of house price exceeds the upper limit of normal fluctuation range, it may be considered as "overheated" of the real estate market, and needs contractionary regulation; vice versa, when the declining extent of house price exceeds the upper limit of normal fluctuation range, it may be considered as "overcolded" of the real estate market, and needs expansionary regulation. According to this, the running states of real estate market can be divided into three types: normal, basically-normal, abnormal (overcolded or overheated). Currently, the main target of Chinese house price regulation is to prevent too large house price rising extent and overheated real estate market.

For convenient to study the target range of house price regulation, the article chooses two important indexes, house price rising rate and house price rising rate/urban GDP growth rate, and calculates the normal range of these two indexes in Composite Simulation Method. The Composite Simulation Method was established on the basis of Japanese experience, determined the critical values of the indexes according to the statistical law, and so to judge the running state of real estate market.

The traditional method to determine critical values is Empirical Data Method. Due to its poor accuracy, two new methods to determine critical values, Neural Network Method and 3σ Method based on normal distribution assumption, have grown up recently. Currently, the application of Neural Network Method is still at the start, not mature and perfect enough. Therefore, the article determines critical values in the modified 3σ Method.

III. THEORY OF 3 Σ

Normal distribution is the most common type of probability distribution type. 3σ Method assumes that the index variables are distributed normally, and accordingly studies the change law of indexes[ ]. The probability function of normal distribution is:

$$F(X) = \frac{1}{\sqrt{2\pi}s}\int_{-\infty}^{p} e^{-\frac{(x-m)^2}{2s^2}}\,dx \qquad (1)$$

Of which, is the mean value of overall samples, and is the standard deviation of overall samples.

According to the normal distribution law and formula can calculate the following probability:

$$\Phi(x) = p(\mu-\sigma<x<\mu+\sigma) = p[-\sigma<(x-\sigma)<\sigma] = p\{-1<\frac{x-\mu}{\sigma}<1\} \qquad (2)$$

So,

$$F(x) = F(1) - F(-1) = 0.8413 - 0.1587 = 0.6826 \qquad (3)$$

Similarly, can obtain:

$$p(\mu-2\sigma<x<\mu+2\sigma) = \Phi(2)-\Phi(-2) = 0.9546 \qquad (4)$$

$$p(\mu-3\sigma<x<\mu+3\sigma) = \Phi(3)-\Phi(-3) = 0.9973 \qquad (5)$$

$$p(\mu-4\sigma<x<\mu+4\sigma) = \Phi(4)-\Phi(-4) = 0.999937 \qquad (6)$$

13 978-0-9831693-1-4/10/$25.00 ©2011 IERI

Accordingly, can obtain the following conclusion:

Firstly, assuming that all the characteristic values of indexes are subject to normal distribution, then in the total data of characteristic values near 70% are within $\pm\sigma$, 95.46% within $\pm2\sigma$, and only less than 5% exceed $\pm2\sigma$. It shows that most of the characteristic values are distributed within ±2σ; at the same time, the indexes within ±2σcan represent the random distribution law of indexes in real estate industry.

Secondly, the principle of 3 σ is not affected by the value of σ. No matter what size the value of σ is, 68.3% characteristic values are contained within $\pm\sigma$. 95.46% and 99.73% characteristic values are contained respectively within $\pm2\sigma$ and within $\pm3\sigma$.

For more accurately defining the normal range of house price fluctuation, it is necessary to calculate those of first-tier cities and those of second-tier cities respectively. Currently, the house price in first-tier cities is on the high side, with large investment risk, weakening attraction to investment capital, and has exceeded the house purchasing ability of residents. Comparing to the second-tier cities, the normal range of house price rising in first-tier cities shall be smaller and that of declining shall be larger. Therefore, the range of one time of standard deviation can be chosen as the upper limit of the normal range of rising extent fluctuation of house price, and the range of three times of standard deviation can be chosen as the lower limit of the normal range of declining extent fluctuation of house price. For the second-tier cities with lower house price, one time of standard deviation is too conservative, thus, two times of standard deviation is chosen as the upper limit of the normal range of house price rising extent, and the range of one to two times of standard deviation is considered as the normal range of house price fluctuation.

Taking the mean value of each index as the central value of its fluctuation, firstly calculate its central value, then determine the normal growth range. According to the above analysis, for the first-tier cities, can regard the range of one time of standard deviation from the central value as the upper limit of normal range, and the range of three times of standard deviation as the lower limit of the normal range, i.e. $[\mu-3\sigma, \mu+\sigma]$. for the second-tier cities, can regard the range of one time of standard deviation from the central value as the normal range, i.e. $[\mu-\sigma, \mu+\sigma]$. regard the range of one to two times of standard deviation from the central value as the basic normal range, i.e. $[\mu-\sigma, \mu-2\sigma]$ and $[\mu+\sigma, \mu+2\sigma]$. regard the range of over two times of standard deviation from the central value as the abnormal (overcolded or overheated) range, i.e. $[-\infty, \mu-2\sigma]$ and $[\mu+2\sigma, +\infty]$. In this way, the normal range of indexes in the second-tier cities is $[\mu-2\sigma, \mu+2\sigma]$, and its boundary is the critical value for judging whether regulation is needed.

Obviously, the analysis on the regulation standards of real estate market is taking a specific economic development situation as premise. The above calculation is obtained from the statistical data of 2003～2008, therefore, its analysis conclusion is suitable for the similar macroeconomic situations. In this period, the yearly average growth rate of GDP in Chinese cities reached 10.68%, the financial institutions' loan rate of five years above was 6.12～7.20%, yearly average inflation rate was 3.2%, and the cities were in the fast urbanization development stage with yearly average growth rate of urban population of about one percent.

According to the above principles, can calculate the normal range of house price rising rate and house price rising rate/urban GDP growth rate.

IV. Normal Range of House Price Rising Rate

The indexes of house price are the most important indicators for reflecting the trend of house price variation and the situation of real estate market. According to *the China Statistical Yearbook*, can calculated the house price rising rate in these 35 cities in 2003～2008 (table I).

TABLE I
HOUSE PRICE RISING RATE IN 35 LARGE AND MIDDLE CITIES（%）

	2000	2003	2004	2005	2006	2007	2008
Total	1.1	4.8	9.7	7.60	5.51	7.60	6.46
Beijing	-0.5	0.3	3.7	6.68	8.75	11.40	9.45
Tianjin	0.0	4.1	13.5	5.97	6.70	6.90	5.84
Shijiazh	1.8	0.3	3.6	5.55	4.34	7.60	5.75
Taiyuan	1.1	2.8	6.4	5.60	3.90	4.40	5.70
Huhehaote	2.0	0.7	5.2	11.78	9.46	4.40	1.23
Shenyang	3.0	7.6	15.9	7.50	6.58	6.10	4.57
Dalian	0.2	0.7	4.6	9.15	10.87	7.20	4.82
Changchun	6.6	0.2	0.2	1.93	1.60	6.40	6.97
Ha'erbin	1.8	0.2	4.7	4.60	3.27	6.80	6.36
Shanghai	-1.4	20.1	15.9	9.72	-1.33	3.40	5.91
Nanjing	1.6	9.8	15.3	8.05	4.33	6.60	2.75
Hangzhou	4.9	6.1	11.7	9.72	2.63	7.30	8.58
Ningbo	5.5	16.6	13.9	6.35	2.16	8.60	9.16
Hefei	0.0	4.1	5.6	6.15	1.25	1.80	8.35
Fuzhou	0.3	1.1	3.6	4.40	6.67	6.80	3.85
Xiamen	0.1	2.8	7.3	8.00	6.95	7.00	2.71
Nanchang	3.2	4.8	7.3	8.30	6.23	6.80	4.15
Jinan	2.8	3.1	10.3	7.55	4.27	5.20	7.22
Qingdao	2.3	14.6	15.3	10.93	6.92	6.50	5.09
Zhengzhou	-0.5	2.0	4.0	6.97	5.69	6.30	3.32
Wuhan	1.5	3.8	8.4	6.83	3.03	5.20	4.91
Changsha	-0.4	0.5	3.3	2.83	5.30	8.40	6.66
Guangzhou	-2.7	-0.7	2.7	4.65	6.22	6.60	-0.16
Shenzhen	-0.8	2.2	4.6	7.22	12.29	16.30	-1.86
Nanjing	-0.7	2.1	5.7	4.93	4.12	7.60	8.16
Haikou	-0.6	2.7	5.9	2.53	2.80	6.60	10.43
Chengdu	1.3	2.9	7.9	7.20	3.00	6.90	6.29
Guiyang	3.9	1.3	2.6	9.78	7.12	7.60	3.39
Kunming	0.2	-0.9	2.3	2.60	4.41	6.90	6.60
Chongqing	1.8	6.1	13.9	2.90	1.33	3.50	3.22
Xi'an	1.3	1.4	5.0	4.28	3.59	6.40	8.06
Lanzhou	0.5	1.8	8.7	5.55	4.72	6.00	9.77
Xining	1.1	1.9	4.0	3.35	2.79	3.80	7.51
Yinchuan	2.2	2.1	4.4	2.65	2.33	3.90	11.76
Wulumuqi	2.4	-0.1	0.7	0.92	1.19	9.00	15.50

Then calculate the mean value and mean square deviation in these 35 cities, and determine the critical value of house price rising rate when the real estate market is under normal state in the method of 3σ (table Ⅱ).

According to this can obtain the critical value of these 35 large and middle cities under abnormal state (overcolded or

overheated). When the house price rising rate exceeds the critical value in a city, it can be considered that the real estate market is overcolded or overheated in the city.

TABLE Ⅱ
CRITICAL VALUE OF HOUSE PRICE RISING RATE IN 35 LARGE AND MIDDLE CITIES（%）

	μ	σ	$\mu+\sigma$	$\mu-\sigma$	$\mu-2\sigma$	$\mu+2\sigma$	$\mu+3\sigma$	$\mu-3\sigma$
Total	6.1	2.53	8.6	3.59	3.59	11.16	13.69	-1.46
Beijing	5.7	4.28	10.0	1.40	1.40	14.25	18.53	-7.17
Tianjin	6.1	3.72	9.9	2.42	2.42	13.59	17.31	-5.03
Shijiazh	4.1	2.30	6.4	1.83	1.83	8.74	11.04	-2.77
Taiyuan	4.3	1.72	6.0	2.55	2.55	7.71	9.43	-0.89
Huhehaote	5.0	3.93	8.9	1.04	1.04	12.82	16.74	-6.81
Shenyang	7.3	3.82	11.1	3.51	3.51	14.96	18.77	-4.13
Dalian	5.4	3.73	9.1	1.63	1.63	12.82	16.55	-5.82
Changchun	3.4	2.88	6.3	0.54	0.54	9.16	12.04	-5.21
Ha'erbin	4.0	2.21	6.2	1.75	1.75	8.37	10.58	-2.66
Shanghai	7.5	7.66	15.1	-0.19	-0.19	22.79	30.45	-15.51
Nanjing	6.9	4.35	11.3	2.57	2.57	15.61	19.96	-6.12
Hangzhou	7.3	2.83	10.1	4.45	4.45	12.93	15.75	-1.20
Ningbo	8.9	4.60	13.5	4.30	4.30	18.09	22.69	-4.90
Hefei	3.9	2.79	6.7	1.10	1.10	9.47	12.26	-4.47
Fuzhou	3.8	2.30	6.1	1.51	1.51	8.42	10.73	-3.09
Xiamen	5.0	2.83	7.8	2.15	2.15	10.65	13.48	-3.52
Nanchang	5.8	1.70	7.5	4.13	4.13	9.22	10.92	0.73
Jinan	5.8	2.52	8.3	3.26	3.26	10.81	13.33	-1.77
Qingdao	8.8	4.56	13.4	4.25	4.25	17.92	22.47	-4.86
Zhengzhou	4.0	2.44	6.4	1.53	1.53	8.85	11.29	-3.35
Wuhan	4.8	2.15	7.0	2.66	2.66	9.10	11.25	-1.63
Changsha	3.8	2.96	6.8	0.84	0.84	9.72	12.68	-5.08
Guangzhou	2.4	3.37	5.7	-1.00	-1.00	9.11	12.49	-7.74
Shenzhen	5.7	6.22	11.9	-0.51	-0.51	18.15	24.37	-12.96
Nanjing	4.6	2.87	7.4	1.69	1.69	10.29	13.16	-4.05
Haikou	4.3	3.33	7.7	1.01	1.01	10.99	14.31	-5.64
Chengdu	5.1	2.41	7.5	2.66	2.66	9.88	12.29	-2.15
Guiyang	5.1	2.86	8.0	2.24	2.24	10.82	13.67	-3.48
Kunming	3.2	2.77	5.9	0.39	0.39	8.70	11.47	-5.15
Chongqing	4.7	4.02	8.7	0.65	0.65	12.72	16.75	-7.39
Xi'an	4.3	2.30	6.6	1.99	1.99	8.88	11.18	-2.60
Lanzhou	5.3	3.11	8.4	2.18	2.18	11.51	14.62	-4.04
Xining	3.5	1.90	5.4	1.59	1.59	7.29	9.19	-2.21
Yinchuan	4.2	3.20	7.4	0.99	0.99	10.59	13.79	-5.40
Wulumuqi	4.2	5.40	9.6	-1.17	-1.17	15.04	20.44	-11.98

Finally, can divide the 35 cities into first- and second-tier cities by experience. Generally, first-tier cities mean Beijing, Shanghai, Hangzhou, Shenzhen, and Guangzhou, and all the others are second-tier cities. Here taking eight typical cities, Nanjing, Tianjin, Shenyang, Wuhan, Chengdu, Chongqing, Xian, and Urumchi, to calculate their critical values of house price rising rate (table Ⅲ-Ⅵ).

TABLE Ⅲ
UPPER LIMIT OF HOUSE PRICE RISING RATE IN FIRST-TIER CITIES(%)

City	Beijing	Shanghai	Hangzhou	Shenzhen	Guangzho	Average
Critical Value for Overheated	10.0	15.1	10.1	11.9	5.7	10.56

TABLE Ⅳ
UPPER LIMIT OF HOUSE PRICE RISING RATE IN SECOND-TIER CITIES(%)

City	Shenyang	Chengdu	Xi'An	Nanjing	Wuhan	Chongqing	Average
Critical Value for Overheated	14.96	14.99	8.88	15.61	9.10	12.72	14.47

TABLE Ⅴ
LOWER LIMIT OF HOUSE PRICE RISING RATE IN FIRST-TIER CITIES(%)

City	Beijing	Shanghai	Wuhan	Gunagzhou	Average
Critical Value for Overcold	-7.17	-15.51	-12.96	-7.74	-10.84

TABLE Ⅵ
LOWER LIMIT OF HOUSE PRICE RISING RATE IN SECOND-TIER CITIES(%)

City	Shenyang	Chengdu	Xi'an	Nanjing	Wuhan	Chongqing	Average
Critical Value for Overcolded	-4.13	-2.15	-2.60	-5.03	-1.63	-7.39	-5.13

It can be seen from the calculated results that, the upper limit of normal rising rate is 10.56%, lower limit is -10.84%, and the target range of regulation is [-10.84%, 10.56%] in first-tier cities; the upper limit of normal rising rate is 12.47 %, lower limit is -5.13%, and the target range of regulation is [-5.13%, 12.47%] in second-tier cities.

Ⅴ. NORMAL RANGE OF HOUSE PRICE RISING RATE GDP GROWTH RATE

Firstly, calculate the house price rising rate/GDP growth rate in first-tier cities. According to the China Statistical Yearbook and the statistical yearbook in all cities over the years, can sort out the house price rising rate/GDP growth rate in first-tier cities in 2004～2008.

According to the above table calculate the mean value of house price rising rate/GDP growth rate in first-tier cities. Considered the practical situations of high-speed development of urban real estate industry in recent years, taking ±2σ as normal range is too conservative, therefore, taking [$\mu-3\sigma$, $\mu+3\sigma$] as the normal range of the index.

Then calculate the house price rising rate/GDP growth rate in second-tier cities. Considered the integrality of statistical data, selecting Xian, Nanjing, Shenyang, Wuhan, and Chongqing as the typical representatives of second-tier cities to calculate the normal range of house price rising rate/GDP growth rate.

Via calculation, can obtain the mean value of house price rising rate/GDP growth rate in second-tier cities.

It can be seen from the calculated results that, the mean value 0.86 of house price rising rate/GDP growth rate in first-tier cities is the upper limit when the real estate market is under normal state, the mean value -0.31 is the lower limit, and the target range of regulation is [-0.31, 0.86]; the mean value 1.17 of house price rising rate/GDP growth rate in second-tier cities is the upper limit when the real estate market is under normal state, the mean value -0.42 is the lower limit, and the target range of regulation is [-0.42, 1.17].

Ⅵ. CONCLUSION

The real estate market is a typical regional market. Due to the unbalanced economic development in Chinese regions and the large difference of running states of real estate market in cities, therefore, should select the regulation target and corresponding policies and tools via classification.

House price regulation is the most important content of real estate regulation. For the comparison of house price fluctuation range, should inspect whether the growth rate of house price in the same period is within the normal range by monthly data. That is to say, comparing the mean values of commercial residential building of all months to those in the same period of last year, if the growth rate in the same period exceeds the normal range determined in this article, the central and local governments should consider publishing regulation measures for the city or region. According to the practical situations in China, currently the main target of house price regulation is to prevent fast rising of house price, i.e. prevent overheating of real estate market.

According to the calculations in the article, should control the house price rising rate in first-tier cities within [-10.84%, 10.56%], and that in second-tier cities within [-5.13%, 15.99%]; control the ratio of house price growth rate and economic growth rate in first-tier cities within [-0.31, 0.86], and that in second-tier cities within [-0.42, 1.17]. Looking from the practical situations of real estate market in recent years, the normal range of house price fluctuation determined in the article is reliable. In some years real estate market was overheated, looking from the monthly comparative indexes, the house price rising extent exceeded the upper limit of normal range and needed the government to regulate and control in Beijing, Shenzhen, shanghai, Hangzhou, and Haikou, etc.

REFERENCES

[1] Huang Zhengxin, Several Theoretical Problems on Bubble Economy and Its Measurement, Financial Research, 2002,06

[2] Duan Y.,Tian P.,Zhang X., "Relative efficiency control fuzzy system", Proceeding of the 46'th ISSS Annual Conference, Shanghai,China, 2002.

[3] He Yan and Zhang Bin.(2006)."Research on influence of macro-regulation on real estate industry in China"(In Chinese). Price Theory and Practice.(12):45-46

[4] Yin Huibin and Tan Shiya.(2006)."Policy orientation of macroeconomic regulation on Chinese Real estate market"(In Chinese).Statistics and Decision.(10):100-102

2011 International Conference on Mechanical, Industrial, and Manufacturing Engineering
Lecture Notes in Information Technology Vols. 1-2

Study on Yacht Product Innovation Connotation and Design Technology

Gangqiang Zheng
School of Art and Design
Wuhan University of Technology
Wuhan, Hubei Province, China
zhenggq@whut.edu.cn

Sijia Wan
School of Art and Design
Wuhan University of Technology
Wuhan, Hubei Province, China
dirkjomo@gmail.com

***Abstract* - Aiming at the design and innovation of yacht product, the innovation connotation of yacht product designing is summarized on the basis of the analysis of the constitution of yacht product system. The innovation of yacht product shall lay emphasis on the research of yacht shape and space blending law of the cabin. With the research of basic theory and method application of yacht designing, the theoretical research of yacht designing shall be consistent with the technical application. Initial design technical analysis is conducted to the key question of the yacht product innovation and yacht design and research scheme is elaborated in three aspects, namely, research method, technical way and experimental means. The initial mode of yacht research is constructed and the exploration of direction, pattern and method is conducted for further research of yacht product innovation.**

Index Terms-Yacht; Product design; Product innovation; Style and cabin space;

I. INTRODUCTION

Yachts are unique high-end consumer products. Yet the yacht industry of China is going through the quick start-up progress, promoted by the amazing development of economy, the Chinese yacht design hasn't taken off and is not prepared to meet the needs of the yacht industry. Most domestic yacht companies had to seek the cooperation with foreign designers [1]. Therefore, in order to cope with the urgent needs of innovation in yacht product and avoid plagiarism, it is high time to analyze yachts systematically, cognize the intension and key technologies of the innovation of yachts and discover the advanced and effective research models.

II. THE INTENSION OF INNOVATION IN YACHT PRODUCT

A. the Innovation Research about Yacht Product

The innovation in yacht product refers to the design innovation of yachts' shape and inner declaration. More specifically, it includes yachts' exterior and interior design (interior space and declaration design and transitional indistinct space design), yacht's ancillary facilities design and so on. The basic theories and application methods can be constructed on the basic of the knowledge systems of vehicle, interior, architecture and product design.

To achieve the innovation in yacht design, it is necessary to use scientific methods and combine the subjects with practical cases in order to systematically analyze the design of yacht shape and cabin space with a multi-interdisciplinary sight. Exploring the integration issue between yacht engineering technologies and industrial design involves several subjects, such as modeling design, aesthetics, space construction, configuration and structure, engineering technology, material and craft [2]. By following the progress of analyzing practical questions, exploring basic theories, creating new methods and design practices, it is possible to enhance the quality of yacht design.

The research about the innovation of yacht product should focus on the following three key points:

1) Elementary research about the regulation of yacht style and interior space: Analyzing the system of yacht product and studying the phenomenon and cause of the amalgamation of exterior style and interior space, as well as the correspondence between them are necessary for discovering the characteristics and regular pattern of their coupling. After the factors related to yacht design are found out by analyzing them systematically, the influence and correlation properties among them have to be dug out. Thus the integration patterns and

design methods can be revealed, providing the scientific foundation theoretical guide for the design progress. At the same time, in order to furnish necessary evidence of norm and standard for yacht design, a fundamental data set of yacht style and interior space have to be completed.

2) Innovative research about the elementary theories of yacht design: Proposing and establishing the relative principles on the design of yacht style and interior space, such as the heterogeneous isomerism theory in yacht design --"same in general, vary in details". The "same" includes the homogeneity of culture, technology, material, space, form, color, and market and so on. The word "vary" appears in the ever changing design presentation.

3) Innovative research about the methods and application of yacht design: Establish the hybrid design system by associating the relationship between form and function, analyzing yachts' systematical correlation design methods and technology roadmap, creating modern design techniques. In other words, by integrating analysis of industrial design mode, engineering knowledge of ships and digital modeling design, the goal to discover the advanced and effective design innovation modeling system and apply the system in the practice of yacht design and model making can be achieved, also deepening the theory and accomplishing the interaction and promotion of the circulation.

B. The primary objectives of yacht product innovation research

The research of yacht product innovation aims at exploring basic theories of yacht design and improving the innovation level. The goal of the research can be divided into two aspects.

1) The purpose about basic theory: By analyzing the integration phenomena of yacht style and cabin space, guided by the combination of ship engineering technology and industrial design, it is available to discover the features and regulations of their integration, and propose the localizing aesthetic concept of yacht design, then access the heterogeneous isomerism theory of yacht design and systematical correlation design methods primarily. The relative contents are discussed at length in the articles about the analysis of yacht design system and principles.

The purpose about practical applications: Using systematical correlation design methods to improve the innovation of modern yacht design techniques and applying the principles and relative methods of integration in yacht design, observing the design results and reviewing the mechanism of action.

C. The features of yacht product innovation research

1) Interdisciplinary. The research can either choose to study the integration of academic knowledge and practical technology by industries, universities and research institutes or use the information of comprehensive designing, ship engineering and material technology to study the multi-interdisciplinary project.

2) The Combination of quantitative and qualitative analysis. With using quantitative demonstration to analyze and abstract data, measuring and testing yacht style and cabin space for rational analysis, yacht design should be investigated "essentially". In order to amalgamate rational analysis and perceptual sublimation, the inherent laws need to be discovered by taking advantage of the relative methods of data management [3].

D. The Conclusion of Yacht Product Innovation Connotation

Over all, the connotation sketch map can be concluded according to the analysis of the research content, primary objectives and features of yacht product innovation as Table I.

TABLE I

THE CONNOTATION SKETCH MAP OF YACHT PRODUCT INNOVATION

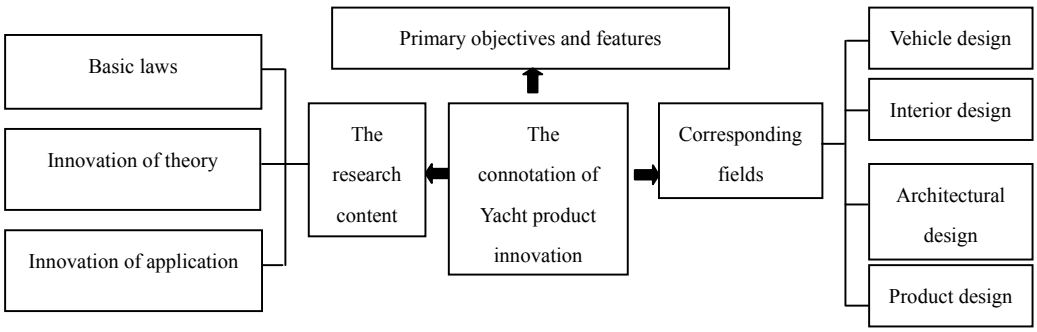

III. THE ANALYSIS AND RESEARCH ON YACHT PRODUCT DESIGN TECHNOLOGY

A. The Key Issues about the Creativity of Yacht Product

The key issues to solve about the creativity of yacht product are exploring the core basic theory of yacht designing as well as satisfying independent innovation of yacht designing. Specific issues are described below:

Main body characteristics analysis: To analysis yacht product system in form and functions. Establish knowledge base and specialized dataset in the field of yacht designing; analysis the appearance of yacht and the "assimilation" characteristics as well as the regular patterns of blending of compartment space system, exploring appearance of yacht and compartment space blending mechanism as well as their coupling congruent relationships. The key technique is the rationalized plane layout of yacht compartment space and design technique of space integration.

Induction of related principles: clarifying concepts of localized yacht assimilation design and the "isometric" principle and related theories, differentiating and analyzing character of their same innate natures in cultures, technologies, spaces and materials, researching its "different structures" application methods in practical design.

Abstract of designing methods: Researching the key factors of yacht appearance and system associated designing methods of compartment space and their technology roadmap. Establishing yacht appearance and mixed type design system of compartment space: Pattern analysis of industrial design + Professional knowledge of shipping engineering + Digitizing modeling etc. and doing practical application of yacht designing and model building. The key techniques are 3D simulate modeling and rendering technique of yacht appearance and compartment space.

B. Yacht Product Innovation Research Program

The basic idea of yacht product innovation research program is an answer to the demand of the development of yacht industry from a methodological point of view of theoretical innovation. The innovation research program is combined with academic development, focusing on empirical investigations, making breakthrough by seizing the yacht design core and essence. This program is relegated to the forward-looking and innovative application-oriented basic research. Yacht design theory research should be unity with the technology appliance and set up a design theory and method with local characteristics. The research program includes the research method, the technological lines, and experimental means etc. following is the brief introduction.

1) *Research Methods*

Innovation research of yacht product must be considered with development direction of domestic yacht industry, adopting scientific ways to research and to induce, by means of modern technology, To integrate rational logic data quantitative analysis (quantitative study) and emotional speculation analysis (qualitative research), theoretical discriminating discussion and empirical study, macroscopic holding and analysis of individual cases, to materialize scientific, standardization and conscientiousness of research methods. The specific methods following can be applied:

a. Literature and investigation comprehensive analysis method：According to the purpose of study, collecting yacht design literature to induce and to analysis on the one hand, investigating the circumstance of yacht industry to know the relative need by means of scientific methods such as individual case study, test, questionnaire and interview on the other hand. After that, analyzing and refining the materials from the two dimensions of vertical deducing and horizontal comparison then come up with some conclusions. By doing this, conditions from all aspect about yacht appearance and spatial design are grasped. In the comprehensive study, innovative opinions and design theory aiming at yacht appearance and the "blending" features of compartment space can be come up with to gain the criterions of yacht appearance and the "blending" features of compartment space and to construct "blending" pattern from the aspects of sculpt and space.

b. Quantitative empirical study method: To study shipping related technology and the norm of yacht design, to analysis and refine selected typical cases placed in related background. Doing rationalized and digitized decomposing and analysis to the sculpt of yacht and compartment space by measuring and testing. In that way, the systematic basic knowledge base information of yacht design and a dataset are established as well as the yacht practical design model and the mixed design system are constructed.

*c. Qualitative theoretical study metho*d: to do the

"naturalizing" analysis about yacht appearance and compartment space. Studying foreign design theory while pay great attention to localizing spirit and aesthetic character study. To experience the object of study by investigate on the spot to get subjective feeling under such circumstance. Creating theoretical assumption from literature material and case study by means of "look-ahead and feedback method". By adopting methods such as induce and deduce analysis and synthesis, abstract and summarization, modeling and diagram to do thought process about acquired materials. By comparing, gradually enriching and systematizing, the inner regular pattern is revealed.

d. Multi-directional crossed study method. "Multi-directional crossed" reflected as "manufacture, study and research" co operational research, namely higher educational institutes cooperate with enterprises as the form of knowledge alliance aiming at the design objective of yacht to integrate theoretical knowledge and practical technologies. On the other hand, it is reflected as research crossed disciplines. Synthesizing design theories, shipping aesthetic theories, shipping design, material technology and economics etc., taking literature analysis, survey study and market demand as a whole to study.

2) *The technological lines*

Yacht product innovation research is an intercross comprehensive research. The technological lines can be analyzed from the aspect of the basic theory and the technological method. The technological lines can be separated as dark and light clues throughout the two technologies system. The outside clue is yacht space modeling and design (technological method level), while the inside clue is the assimilation of shape and space (principle level). One of the two technological systems is the basic theoretic system of yacht modeling and space design, the other one is the system of basic knowledge base and data set.

The research structure: information summary (raise problem) → rule identification (analysis problem) → feature induction (refine ideas) → theory analysis (theory exploration) → extraction method (design innovation) → method validation (practical application) →loop upgrade.

3) Experimental methods

Yacht product Innovation research can adopt the methods related to industrial design to carry out the yachts modeling and space design experiments. Including:

a. Project Design: With the same background conditions and parameters, the plane and elevation "blending" design of yacht styling and cabin space can be carried out. It also can explore the combination of rules and characteristics and the interactions of external shape of boat and the cabin space.

b. Simulation analysis: Apply the common principle of "isomeric" in the modeling yachts and cabin space design practice and on the basis of the flat and facade design, the three-dimensional simulation modeling and rendering program performance can be done. And then make the comparison different programs and verify the applicability of design theory and innovation [4].

c. Model analysis: Select the best solution, on the basis of the three-dimensional simulation model do the model making on the proportion of clay or composite materials, then the model will be comparative analysis, check the influence of the research and analysis of design principles, and enrich and adjust the design methodology.

d. The summary of experimental result: On the basis of the first three types of experimental study, through the experimental results and analysis do the research analyses of yacht design mechanism. Use the relevant theories of various factors and their inter-relationship to make the summary so as to obtain a variety of factors influencing the relationship between the pattern and logic.

TABLE II

YACHT PRODUCT INNOVATION RESEARCH LINES

Raise →	Solve →	Setup →	Evaluate →	Conclude
Raise problem (Basic rule)	Problem analysis (Assimilation)	Construction model (Isomerism)	Method validation (System design)	Conformed expectance (Loop upgrade)

IV. CONCLUSION

This paper discussed the product design and innovation of yachts, analyzed the constitution of the yacht product system, and concluded the connotation of yacht product design innovation, pointed out the necessity of studying the amalgamation rule of yacht style and cabin space, as well as the research about the application of yacht design theories and methods. Moreover, the yacht design theory study should be connected with its technology application. The paper also elementarily investigates the key question of yacht product innovation and expatiates on the research project according to study methods, technical paths and experimental measures, builds up the rudimentary mode of yacht investment, explores the direction, manner and measures of the further research of yacht product innovation.

References

[1] Meunier, M，Fogg, R．Challenges Associated with Design and Build of Composite Sailing Super Yachts[J]，International Conference – Design，Construction and Operation of Super and Mega Yachts – Papers，2009，p 105-113

[2]Feng Bowei, Liu Zuyuan, Chang Haichao. The Appliance of Multi-interdisciplinary Optimal Design in Boat Elementary Design, China Shipbuilding [J], 2009, 50(4):109-116 (In Chinese)

[3]Hu Jie, Jiang Zhiyong. Intelligent Design of Ship Parts Based on Catia, Ship & Ocean Engineering, December 2009, 38(6):49-51 (In Chinese)

[4]Tao Wei, Chen Hanming, Zhu Yingfu, Ying Wen Ye. Research on Ship Virtual Design. Ship Engineering [J], 2009, 31(2); 56-59 (In Chinese)

2011 International Conference on Mechanical, Industrial, and Manufacturing Engineering
Lecture Notes in Information Technology Vols. 1-2

Balancing Flexible Production Lines

Ana Filipa Espírito Santo Martins Pereira
Department of Mechanical and Industrial
Faculdade de Ciências e Tecnologia, FCT-UNL
Campus Universitário, 2829-516 Caparica, Portugal
anaespereira@gmail.com

Alexandra Maria Baptista Ramos Tenera
Department of Mechanical and Industrial- UNIDEMI
Faculdade de Ciências e Tecnologia, FCT-UNL
Campus Universitário, 2829-516 Caparica, Portugal
abt@fct.unl.pt

***Abstract* – The current market is characterized by being extremely competitive in which customer satisfaction expectations has long become a law of survival. In this sense, industries have been forced to develop more and new production methods. This new methods aim not only to satisfy customers' requirements, but also to improve the production process in order to increase companies competitiveness in their highly competitive and dynamic markets. One example of these is the automotive industry. One tactic used in this market to accomplish this is through the modification of existing assembly lines in order to make them more flexible as they need to produce more and new types of products, so automotive assembly lines needs to increase their levels of flexibility in order to satisfied the needs of today's market moving assembly lines from the classics approaches to the mix-model assembly line. These changes may involve not only line rebalancing but also, layout changes. Therefore, in this article using IDEF concepts we will present and discuss an implementation model for setting up and balancing of mix-models assembly lines that was tested in an automotive industry company.**

Index Terms - Flexibility, Balancing Assembly Lines, Mix-Models, Automotive Industry

I. Introduction

The current world market is characterized by being a place where industries have evolved and become increasingly more dynamic and competitive [1], so they have to develop these features over time along to cope with the customer requirements increasing demand [2].

The increasing requirements from the customer are expressed by product acquisition's that must satisfy both physical necessities and psychological needs requiring tailored products. This fact makes industries to manufacture higher product variety which must, also, present a high product quality and low costs [3].

In order to manufacturing industry meet the needs of the actual generation of customers, they are obliged to modify their production systems aiming to introduce production flexibility which can be seen as the ability of the production process has to adapt to different input variables in order to be possible to manufacture several models simultaneously [4].

According with Zhang, Vonderembse and Lim [5], the concept of production flexibility must be separated into two different aspects, volume flexibility and product flexibility. Volume flexibility can be seen as the capacity to adjust the volume of production to different product quantities. Product flexibility can be seen as the variation of product models to manufactures the product mix. So, product flexibility allows industries to satisfy the customer necessities, whereas, the volume flexibility supports the industries productivity increasing [4], as synthesized in Fig. 1, next presented.

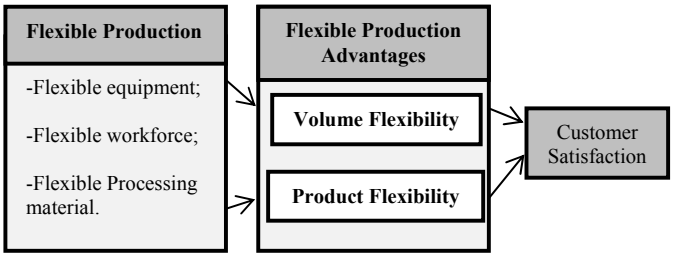

Fig. 1 Flexible production: capacity of industrial and consumer satisfaction (Adapted from Zang et al. 2003, p176)

For most industries the implementation of flexible production systems implies deep changes in the production systems becoming essential production lines deep transformations in order to keep pace with market developments. The productions lines that seem to best fit the characteristics of current markets are called assembly lines-mix models. These lines have the particularity of being able to produce a number of models of the same product without any stop between the productions of each model. Examples of the application of such lines can be found in the automotive industry since in this type of market customer purchasing selection is based on an extensive range of options [6].

II. Assembly Lines characterization

An assembly line is mostly characterized by a line consisting of a sequenced set of workstations in which assembly tasks of a product are performed. The product allocated to a specific workstation moves to the next workstation generally using a transportation system [7]. Transportation systems most used in product handling on assembly lines can be classified into three main categories [4]:

1) Continuous transportation, in which conveyor device moves with constant speed;

2) Synchronized transportation, in which the device carrier moves at constant time intervals;

3) Unsynchronized transportation, in which the device carrier moves according to the operators speed.

On an assembly line each workstations is responsible for making a particular product and piecemeal assembly which arriving to the end of the line, the product will be completely finished [8]. In a typical workstation it can be considered two forms of work: one consisting mostly of manual work; the other, consisting of two work forces: manual and automatic.

In the first form (manual) may be required simple tools; in the second, the semi-automatic, equipment utilization may also be required [9].

Notice that workstations may still also be qualified in two ways [4]: open and closed workstations. On closed workstations, the operator can not violate the limits of your workstation to complete the tasks assigned to it. On open workstations, the operator may use the next workstation to fully perform his tasks. In both cases task allocation is defined through the task process time and precedence diagramming. The process time is based on the time required to perform each individual task and the precedence diagramming is based on the inter-relationship between tasks.

A. Assembly Lines Classifications

In order to meet the need to manufacture a high variety and number of products, industries have developed their assembly lines in order to meet this target [10]. Thus, over the years, it was possible to observe the typology development of different forms of assembly lines. They appeared to respond to the manufacture of various products and the desired quantity of each product.

Currently, there is large range of assembly lines that can be divided into different categories according to the flow of material, product diversity and automation level as shown in Fig. 2.

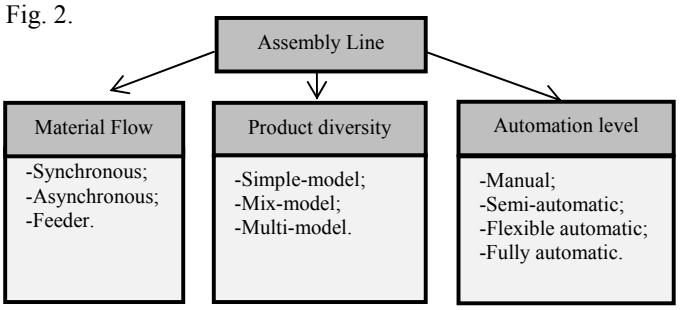

Fig. 2 Assembly lines classifications

In the category of material flow can be identified three different types of assembly lines: Synchronous, Asynchronous and feeder lines. In synchronous or paced assembly line the cycle time limits the content of work in the workstation. In the Asynchronous or unpaced assembly line, no cycle time is associated to workstations. Thus, just when the operator finished their work sends the pre-assembly for the following workstation. The feeder lines can be seen as supplemental lines in which pre-assemblies of the product are become fulfilled to manufacture [11].

The automation level category lines are categorized by the automation level that can be performed in the assembly line. In the manual assembly line all the work is performed by hand. In the semi-automatic assembly line two types of work can be performed, manual and automatic. In fact, this type of automation is frequently used in problematic workstations, like the ones that have a high process time or ergonomics contains. The last two categories, flexible automatic assembly line and fully assembly line are very similar. The main difference between them is based in the production level. The first one is used for high volume production and second for mass production [12].

The product diversity category has three main sub-categories: Straight; Mix-model and Multi-model according with the product mix produced, because this is the most important classification in this work it will be detailed in following section.

B. Product Diversity Assembly Lines

Simple assembly lines are characterized by large scale single product manufacturing [13]. Therefore the production costs associated with a single product are reduced. However, it presents a major constraint, inflexibility. This line is designed only for the fabrication of a product model with no variants, which currently is not a good option because currently, market needs tends to personalize products; so industries are pressed to produce different part numbers without, however, unduly increasing their costs [1].

To minimize this problem, manufacturers have developed assembly lines in which the construction of more than one model becomes possible. This kind of lines comes in two forms: the mix-model assembly lines and the multi-model assembly lines.

In the mix-model assembly the production of different models is made in a certain order. In the multi-model assembly line different product references are also manufactured but between each reference there is a stop line to adapt the line to the product to be manufactured, these stops are called setup time [10], which turn this assembly lines less flexible compared with mix-model assembly lines.

The industrial used of these two last types of assembly indicates that their productivity levels are high, as well as its flexibility, due to the existence of a short production cycle, low production volumes and a high diversity of manufacturing [1].

C. Assembly Lines Main Configurations

Due to the strict guidance of the existing process for the assembly lines, the configuration of assembly lines is due mostly to the flow of material along the line [10]. Nevertheless, several classical categories can be identified as:

1) In straight assembly lines, the workstation is physically in straight line and only has works on the one side of the line

2) In U-shaped assembly line, the line has the form of an U and the operators can work in more than one workstation;

3) In C-shaped assembly line, the line has the form of a C and has the same property of the u-shaped in which the operators can also work in more than one workstation;

4) In circular shaped assembly line, workstations are arranged in a circular layout and the product covers each one of the stations until arriving at the final workstation,

5) In Double-sided assembly line workstation can be found in both of sides, right and left side. In this configuration, the operators can perform work on both sides of the line or just work on one side [11], but in both cases operators are disposed, face to face, as seen in Fig. 3, next presented.

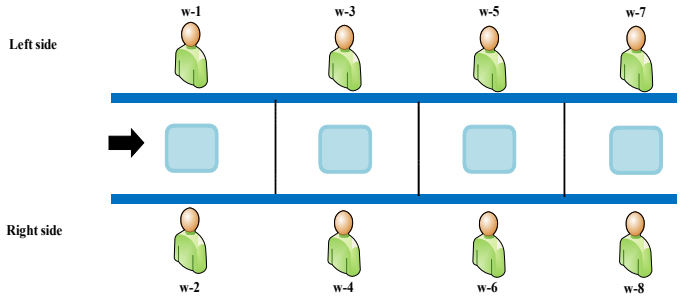

Fig. 3 Schematic example of double-sided assembly line

D. *Double -Sided Assembly Lines*

As we can see in Fig. 3 in double-sided assembly lines both sides can be seen as assembly lines in which there are two sides, the right and left side. The most common form of this application is the existence of stations on both sides of the line where operators are facing each other while they do not perform the same operations.

These assembly lines are mostly used in large size production, such as, automotive industry [14]. The assembling process of this type of product is differentiated from smaller ones, because of the product dimensions and other characteristics like heavy weight, that occurs when a specific task exists but not in the same of side of the line, the movement of the product becomes complicated [1].

The use of such lines provides a decrease in the size of the line, the number of equipment to use and handling of materials [15]. In contrast to all these advantages there is an important constraint, in the precedence definition, because it becomes necessary to take account to face to face interference. This interference is defined by the waiting time that side station operators have to "use" before start its work. This waiting time is referred to as work idle time [1].

Fig.4 shows an example of this work interference. The precedence diagram presented has several letters associated to each task: R and L for right and left side tasks and the letter E for either side tasks which are the ones that can be performed in both line sides. As shown in Fig.4, task 1 and 2 are examples of either side tasks and in this case both tasks have no precedence between them. However, the same is not true for tasks 3 and 4. Task 3 may not begin before task 1 is complete and tasks 3 and 2 must be finalized in order to start task 4.

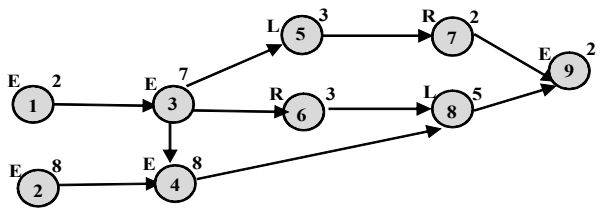

Fig. 4 Interference example in a double-sided assembly line

Observing Fig.4, from the left side and considering a workstation for task 1 and task 3 with a cycle time of 9 units of time and a workstation in right side with task 2 assigned, which lasts for 8 units of time. On the right side of the station, there will be a gap of 1 unit of time. So, considering that no other task can now be started, a unit of time in the left side will be the idle time originated by the interference of task 3 to task 4.

E. *Balancing Assembly Lines*

Balancing an assembly line consists of tasks allocation to workstations so that the precedence relations between the stations are satisfied and the total duration of activities in all work stations is approximately the same [16] enabling the optimization of the production capacity [8]. An assembly line balanced implies better use of productive resources and thus lower production costs due to the reduced investment in equipment, material flow, number of operators and other factors used [4].

A classic problem of balancing assembly lines are characterized by allocating each task to a workstation not exceed the cycle time determined to minimize downtime and verifying the sequencing of all tasks [17], which can be a very complex problem. Balancing assembly lines problems can be classified, in the following categories [11]:

1) Single assembly line balancing problems (SALBP);
2) U-shaped assembly line balancing problems (UALBP);
3) Mix-model assembly line balancing problems (MALBP);
4) Robotic assembly line balancing problems (RALBP);
5) Multi-objective assembly line balancing problems (MOALBP).

The MALBP gives as solutions to the assembly of more than one product reference or Mix-model assembly line balancing which can also be further classified in the following way according to their objective function [11]:

1) MALBP-1: for minimizing the number of workstations given a certain cycle time;
2) MALBP-2: for minimization of the cycle time given a certain number of workstations;
3) MALBP-E: for maximizing line efficiency.

III. Implementation of a Mix-Model Assembly Line

Designing mixed-product assembly line MALBP-E is characterized by three basic stages [18]:

1) Theoretical layout development of the assembly line;
2) Sequence definition of the mix of models and;
3) Preparation of the physical layout of the assembly line.

Using these stages and adapting it to flexible assembly lines configuration three slightly distinct stages can be characterized:

1) Balancing and configuration of a theoretical layout of an assembly line;
2) Balancing and configuration of the assembly line final layout;
3) Balancing and configuration improvements on the assembly line.

To outline these three main steps the Integration Definition for Function Modeling (IDEF) approach will be used. This approach consists of a family of several process modeling methods [19]. In this work a mixture between two families, the IDEF0 and the IDEF3 methods was selected because with this integration both the description, layout and analysis of system processes can be achieved. The family IDEF0 allows the schematic construction where we can identify the inputs and outputs in study and using the family IDEF3 boxes we can represent the activities of the process to be described in which the arrows will represent the flow of material and information between activities (see Fig. 4).

From the analysis of the first part of diagram in Fig. 4 we can identify the main subject under study, balancing and setting up mix-model assembly lines which represented here as a square. Other important data can also be visualize, for example, which data are necessary to achieve the desired objective, in this case, the entries correspond to the assembly tasks required to make the product for which the final balance is achieved and setup a mix-model assembly line to suit the products and quantities produced. At the bottom of the main activity there is also the entry of three different mechanisms that are necessary for the proper preparation of assembly tasks to be carried out [20]. The data concerning the demand for it, is to go over the main activity which indicates that this data requires some kind of control at the extent to which different volumes of production configuration and balancing the assembly line are different.

This IDEF approach will also allow the representation of children diagrams. This fact is possible to be observed in Fig.4, through decomposition of the main step in three main activities by which they must pass to design a mix-model assembly line.

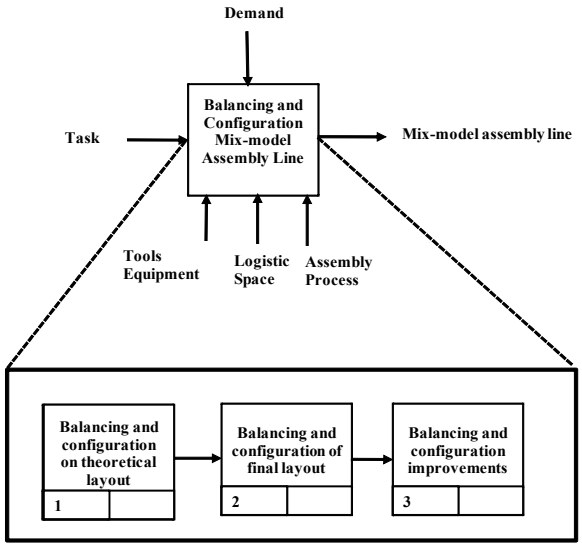

Fig. 4 Implementation of mix-model assembly line diagram

The first main phase is the balancing and configuration of a theoretical layout of the assembly line. This process can be decomposed into smaller process or activities, like: tasks determination, tasks aggregation, tasks allocation and balance validation according with installation restrictions and if necessary new re-allocation to new workstations processes as it can be seen in Fig. 5.

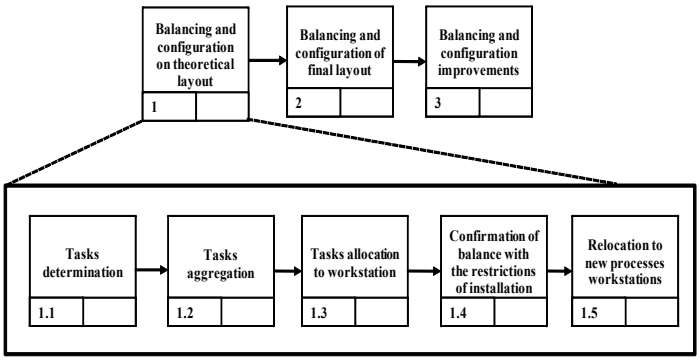

Fig. 5 Diagram of the main activity: balancing and configuration on theoretical layout

The second main phase is balancing and configuration the assembly line of the final layout. This phase is needed due to the fact that in the planning and installation of an assembly line there are several factors to be taken into account, the product demand, the available physical space, equipment and tools to be bought or reuse. Thus, as rule, these planning starts with some time in advance to avoid any problems that may occur. However, within the planning time span may arise several changes being one of most common the variation of products demand. This phase can also be break down into smaller process or activities, such as, identification of changes, rebalancing the assembly line, balance verification with the installation restrictions, re-allocation the processes to new workstations and change implementation (see Fig. 6).

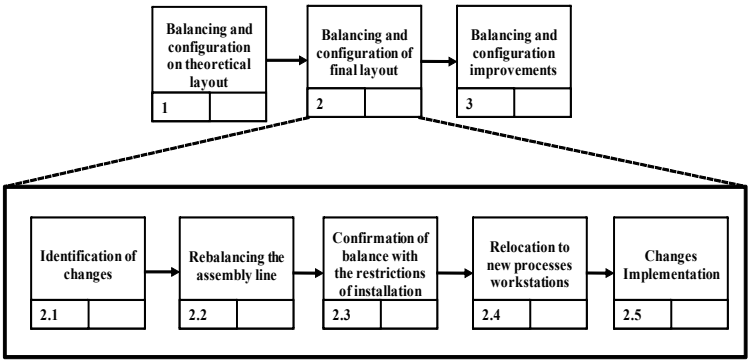

Fig. 6 Balancing and configuration of final layout diagram

The third and last phase the balancing and configuration improvements on the assembly line come after a change in the assembly line as defined.

The changes identified here are generally due to the introduction of new models or optimization of the existing assembly line. This last phase also includes several process or activities as shown in Fig. 7.

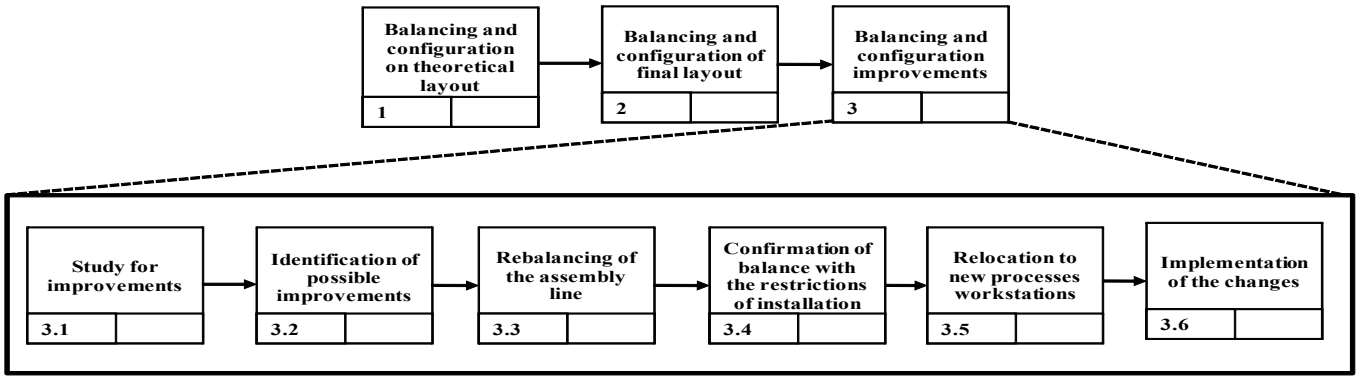

Fig. 7 Balancing and configuration improvements diagram

This phase includes study for line balancing and configurations improvements, identification of possible improvements, rebalancing of the assembly line, confirmation of balance with the installation restrictions, relocation to the new processes workstation and implementation of changes.

For demonstration of the applicability of the proposed approach the following section will present and discussed the implentation test done in a real mix-model assembly line from an automative industry. However, only the last phase will be detailed.

IV. Case Study Implementation

In previous section it was briefly exposed the general proposed approach for designing mix-model assembly lines. Although the proposed approach for balancing mix-model assembly lines implementations includes all the three characterized main phases in this section will be focus only on the third phase (see Fig.7), corresponding to balancing and configuration improvements on mix-model assembly lines because in the case study used to test the model there were already a mix-model assembly line installed in the automotive company where the proposed procedure was tested.

The implementation process described is described in the following two main sections; the first will include the improvement study, identification and selection of possible points of improvement, resulted from steps 3.1 to 3.2 of the proposed approach. In the second section the main results obtained from the 3.3 to 3.6 step will be present and discussed, including the assembly line rebalancing and improvements results achieved from the implantation changes, in line represented in Fig.8.

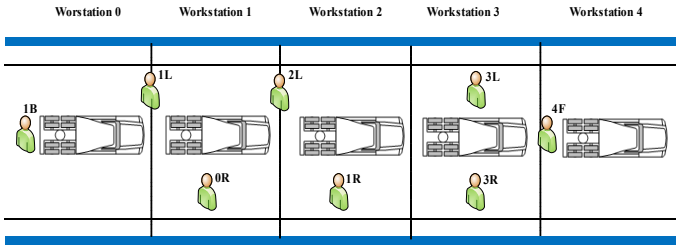

Fig. 8 Location of operators in initial status

A. Assembly Line Initial Status

The assembly lines under study have about a hundred workstations but to demonstrate the proposed procedure let's just considered the first 5 workstations on the assembly line (see Fig.8).

In these workstations the equipment that helps some assembly tasks in the product and the product, moves from one station to another on a conveyor system. As for the existing operators in these stations it was considered that they have versatility so they can perform any tasks of this assembly line area. The study will be focus only on the first five seasons of the worked assembly line as presented in Fig. 8 which includes the location of the operators in the assembly line under study.

As shown in the Fig. 8, the line shows a total of eight operators including three operators performing tasks on the right side of the product, and other three performing tasks on the left side of the product and finally two more located at the front and back of the products. Each of these operators has an alphanumeric code to make it easier to identify his working area. The operator assigned to the station 1B (Back) is located physically at the workstation 0 which would be expected since the numbering 1B means that his work area should be at the workstation 1. Further, this situation is repeated with the other five operators in workstation 1L, 2L, 0R, 1R and 4F (Front).

Operators of workstation 0R, 1R and 4F are physically within a single workstation. However, the numbering of these workstations does not match their numbering. Operators in 1L and 2L show a worst case since their work areas are not located on a single workstation, but rather between two workstations. The occurrence of this situation may lead to interferences between the operators as they can sometimes have a physical proximity rather large when carrying out its tasks, which can lead to waiting times by some of them.

An important factor for the characterization of any assembly line relates to the location of components that each operator must have at his disposal to make the assemblies in the product. In this sense, Fig.9 presents the occupation of the existing logistics space on the workstations in question.

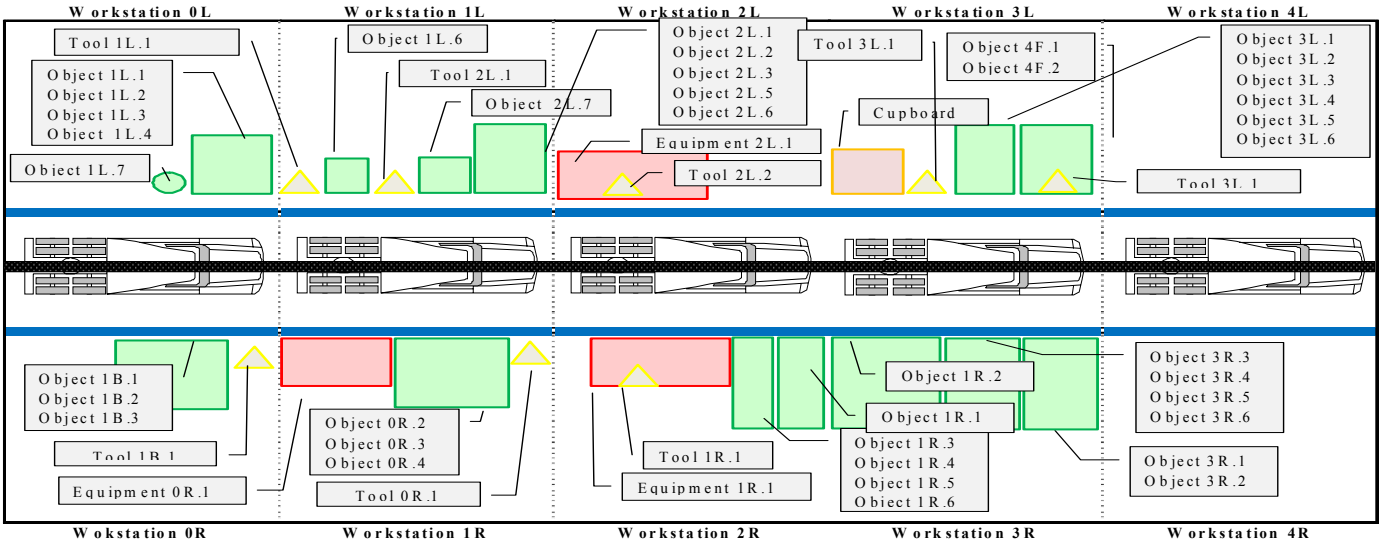

Fig. 9 Logistic space occupation, initial status

The coding process of the objects in Fig. 9 is the same for all workstations presented, which includes the work area and the number of objects that the operator of this workstation needs to assemble. So, for example, objects belonging to the station 1L is represented by 1L.x with x = 1,2,3,4,5,6,7. From careful analysis of Fig.9 we can see that objects belonging to the work operator 1B are on the side of the workstation 0R which are incorrect positioned for the operator assigned to the Workstation 1L. As the space station logistics are not properly positioned it can be predicted that the logistics space corresponding to the other workstations also evidence that fact, the only exceptions are the 3L and 3R workstations where the objects are correct.

Looking further to Fig. 9 it is also possible to noted, that workstations 1L and 2L have an operator working between the two workstations. This problem is due to the fact that the material to build the stations mentioned is shared by the two stations. So, the operator performs his work among the stations.

Analyzing the use of the space logistics was possible to identify the origin of wicked positioning of operators. The bad distribution of components by the stations had also another consequence, the increase in displacement that operators make to accomplish their tasks. That can be seen in the spaghetti diagram shown in Fig. 10.

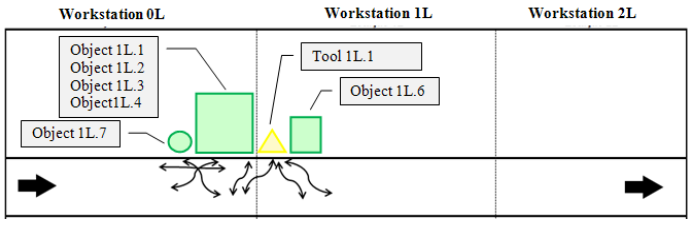

Fig. 10 Spaghetti diagram of workstation 1L, initial status

The spaghetti diagram tool was chosen because allows a simple graphical representation of the records journeys made by identities under observation during the conduct of its operations [21].

In Fig. 10 we can see that the operator performs a large number of offset by not having to move between more than one workstation, but also by constant need to move to the side to fill with objects to assemble the product.

Another important factor is to study the existing work to processes in each workstation, The work is to be performed by a single work shift which produces 75 units of model α and 150 units of model β which makes a total of 225 units per shift and a cycle time of 116 seconds. Table I presents the description of the work process for the workstation 1L, in which the coding process used in the logistic study was also considered to describe it.

In Table I we can see what tasks are performed and which models requires the execution of each tasks. Another detail, also visible in this table, is the time that each operator needs to perform each task. For all other workstation the same process was made. With the values shown in Table I it is possible to construct the load diagram that it is show in Fig. 11, in which it appears for each model and for each of the stations, the workload divided into two distinct parts: bottom part of the bar (green color) and top part (red color): the first one represents all the operations that add value to the product and the other represente operations that add no value to the product. The criterion for this classification, consisted of tasks that are clearly designated as movements or tasks that correspond to object removals, since they to not perform any task of added value. All other tasks were classified as value add tasks.

Looking again to the Fig. 11 it can be observed that the workstations 1L, 2L, 0R and 1R have higher wasted time. This can be a problem since they correspond to time that doesn't add value to the product, and yet, the company has costs associated with this. Another fact visible in Fig.11 is the

unbalance workload of the models within the same workstation, the example of that can be seen in the workstations 2L, 3L, 1R, 3R and 4F. These workstations present large differences in workload on the operator allocated in the workstations.

TABLE I
DESCRIPTION OF THE INITIAL PROCESS FOR THE WORKSTATION 1L

Nº Task	Description of the process	Model	Time (sec.)
1	Take subject 1L.1	$\alpha;\beta$	2
2	Prepare object 1L.1	$\alpha;\beta$	7
3	Assembling the subject 1L.1	$\alpha;\beta$	8
4	Take subject 1L.2	$\alpha;\beta$	2
5	Prepare object 1L.2	$\alpha;\beta$	11
6	Remove object 1L.3	α	3
7	Remove object 1L.4	β	3
8	Take object 1L.5	$\alpha;\beta$	2
9	Take object 1L.1	$\alpha;\beta$	2
10	Take object 1L.6	$\alpha;\beta$	2
11	Moves to the product	$\alpha;\beta$	5
12	Assembly object in the product 1L.1	$\alpha;\beta$	4
13	Assembly object in the product 1L.6	$\alpha;\beta$	2
14	Remove object 1L.7 product	$\alpha;\beta$	6
15	Moves to the side and put the object 1L.7	$\alpha;\beta$	4
16	Take the object 1L.2 and object 1L.8	$\alpha;\beta$	4
17	Moves to the product	$\alpha;\beta$	4
18	Assembly object 1L.2 and object 1L.8 in the product	$\alpha;\beta$	16
19	Moves to the tool support 1L.1	$\alpha;\beta$	4
20	Take the tool 1L.1	$\alpha;\beta$	2
21	Moves to the product	$\alpha;\beta$	4
22	Assembly 1L.2 subject and object 1L.8	$\alpha;\beta$	18
23	Moves the tool support 1L.1	$\alpha;\beta$	4
24	Put tool 1L.1	$\alpha;\beta$	2

The description of the process also allowed the construction of the precedence diagram in Fig. 12. This diagram was built with the information on the total study made just parcialy presented here in the Table I, already discussed.

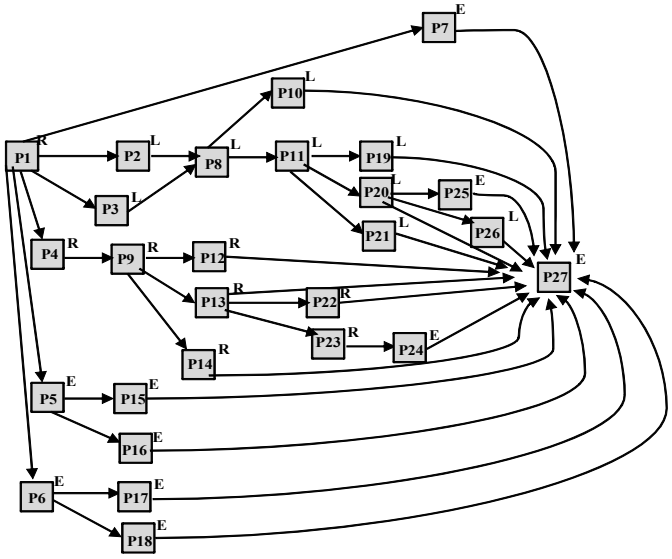

Fig. 12 Line study precedence diagram

For the precedence diagram a letter was used in each process. This letter indicates which side of the workstation should be used to performe the process work. If the letter is an L means that this process work should be performed on the left side of the workstation. For the letter R, the process work must be carried out on the right. When a letter is represented is an E indicates that this process can be carried out both in the left or right side. The processes represented by this letter are generally those that are in the back of the product or on the front of it so that it is indifferent the allocation of these processes to the left or right side of the assembly line.

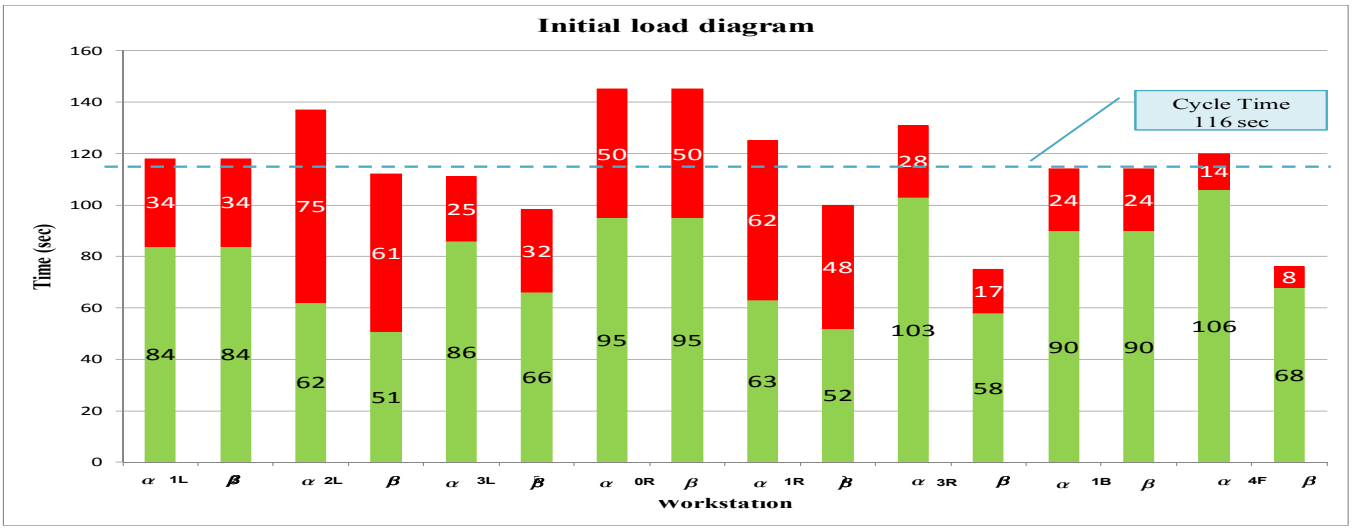

Fig. 11 Initial load diagram

For a better understanding and visualization of the sides operations that are allocated to each workstation processes in question, a product area diagram of the assigned operations was built as presented in Fig. 13.

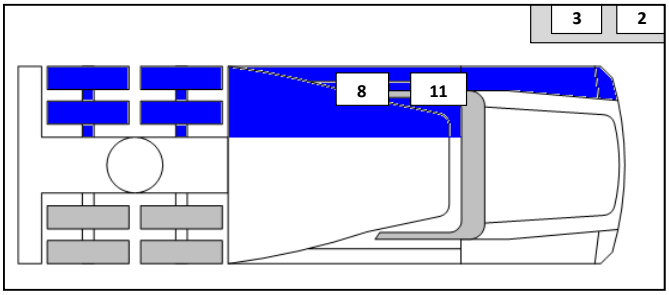

Fig. 13 Diagram allocation process of the workstation 1L

Fig. 13 shows just an example of the operations side allocated to the workstation 1L, in which arises the numbers of existing processes presented in Table II. For other workstations the same procedure was performed.

TABLE II
MAIN PROCESS OF WORKSTATION 1L

Process Nº	Main Process	Process Time	
		α	β
P2	Process of prepare the object 1L.1	17	17
P3	Process of prepare the object 1L.2	13	13
P8	Process of take place the objects 1L.3, 1L.4, 1L.5, 1L.6 and 1L.7	30	30
P11	Process of assembly the object 1L.2	58	58

By the analyze of Table II and Fig. 13, it can be seen that workstation 1L processes are made on the left side of the product in which take place the process 8 and 11 and the process 2 and 3 are carried out on a bench located on the side of the assembly line.

The diagram allocation processes in Fig. 14 aims to identify where the work of each workstation in done in the product. From Fig.14 we can identify that we have workstation operating in more than one work area, and workstations 3L and 3R are those who have a greater number of work areas, three areas. All other workstations have two zones with the exception of the workstation 1L which operate in one zone only.

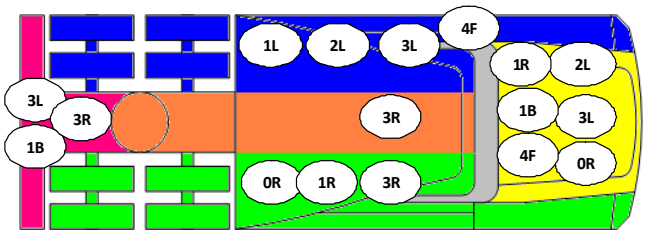

Fig. 14 Diagram allocation process for all workstations, initial status

Ending process 3.1 of the proposed approach it is now possible to go to 3.2 identifing several areas for improvement, which were:

1) Correct positioning of operators on the workstations;

2) Improve logistics management, particularly in suitable placement of the material on the workstations;

3) Improve the existing balance in order to balance the loads on the workstations and reduce the number of product areas to work;

4) Improve the initial working conditions so that we can help decrease the displacements made by the operators.

B. Final status of assembly line

This section aims to characterize the final assembly line in study so that it is possible to introduce the improvements identified, as well the test results of the proposed procedure. Thus, this section begins with the process 3.3 of the proposed aproach (Fig. 8).

Process 3.3 is characterized by a rebalancing of the assembly line stations in question. To rebalance the assembly line the precedence diagram shown (see Fig. 12) was used and data exemplified in Table I. To improve the implementation results the used of supporting cars was considered. The inclusion of this support cars on the assembly line allowed the reduction of movements made by operators in carrying out their duties to the extent that the objects to assemble the product are at their fingertips so operators wil no loger need to move to the side of the assembly line to catch it.

Assuming the rebalancing of the assembly line, it is possible to decrease a job, including the workstation 4F, and the insertion of five support cars on the assembly line stations 1L, 3L, 0R, 3R and 1B. The stations 2L and 2R do not have the necessary conditions for the implementation of the support cars to the extent that these stations have to install a device for that.

The allocation of cases to the product area was a factor that was taken into account in the rebalance. This can also lead to reduction of waste. Thus, adjusting the allocation the processes under the new balancing assembly line, originates the results presented in Fig. 15 in which we can see that workstations, 1L, 3L and 1R, will perform operations in one single area of the product . All other stations will operate in more than one area of the product. However, this is not considered a major obstacle because the introduced support cars can help the task development in different areas of the product, thus enabling the reduction of dislocations, without reducing the number of zones.

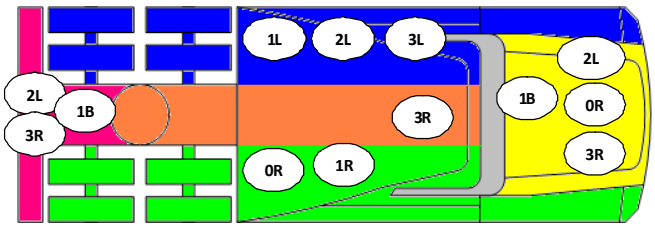

Fig. 15 Diagram allocation process for all workstations, final status

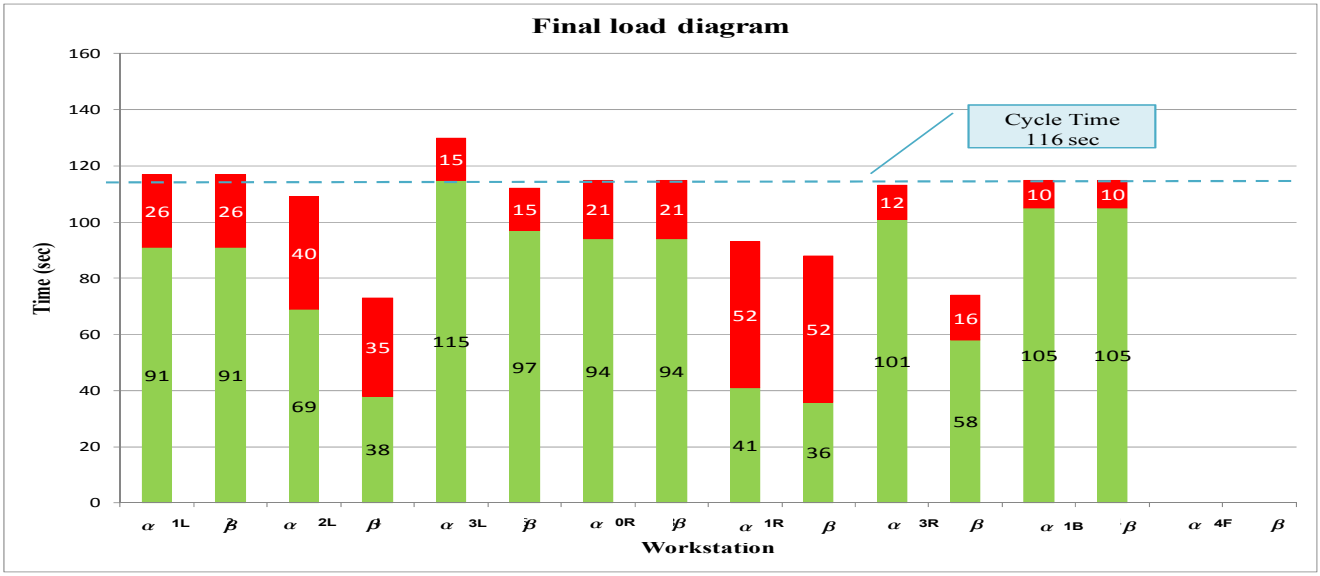

Fig. 16 Final load diagram

Rebuilding the load diagram for the new situation it's possible to observe the decrease of waste in all workstations, as presented in Fig.16, for each model in each used workstation.

In Fig. 16 although there is not yet a balance between loads of the two models for the same workstation. However, there was an improvement since the initial situation had five workstations, the station 2L, 3L, 1R, 3R and 4F, and the final status contains only three, the station 2L, 3L and 3R.

Ending process 3.3 of the proposed approach, the process 3.4, verification of installation conditions, will then start (see Fig.8). In this process installation restrictions checking is done. This restriction can be for example:

1) Workstations Identity;
2) Level of work area;
3) load Balance on the workstation;
4) Multiple operators;
5) Operations multi-operator;
6) Ergonomic restrictions;
7) Physical space limitation.

In this case all restrictions mentioned were taken into account in this study. However this article will focus only the most relevant, physical space limitation. This restriction imposses verification whether or not exits, poor logistic space management. In the initial status, it was found that the logistic occupation did not have a good solution, see Figs. 10 and 11.

The new rebalancing the logistic space are represented in Fig. 17 from which we can see that now every tool and objects are in the right position.

After checking all the installation restrictions, starts the the reallocation of processes to new workstations step (see Fig. 8). Like in the previous step was not observed non-compliances with installation restriction, then, the last step, 3.6, implementation of changes, can be taken in place. This step aims to implement the rebalancing of the assembly line made in step 3.3, as well as the changes in step 3.4 and 3.5.

V. Main Conclusions

Assembly lines have changed to be able to make more than one product model and, thus having increased productive line flexibility. The evolution of the assembly lines turned out to be significant since can be identified several different types of assembly lines. From all the existing assembly lines studied mixed-model lines appears to be more prepared to meet the requirements of the new markets and For better implementation of these assembly lines, this article proposes a implementation procedure for balancing this type of assembly lines.

To test the proposed procedure an actual mixed-model assembly line from an automotive company was used from which it was possible to achieve significant improvements, particularly in correcting the problems identified with the initial state of the assembly line.

These improvements were mainly in shortening the level load of the workstations, due to the reduction of waste in operators time so that they are now able to receive new work processes that will replace the existing waste time.

The reduction of this waste led to the relocation of some objects on the assembly line so that they are now physically on the corresponding workstations reducing the number of areas where an operator works and to the inclusion of support cars to assist replacement of assembling objects.

The implementation of the proposed changes also improved the general working conditions in which the operators performed their operations.

However, the results this approach still presents some fragilities. The proposed procedure doesn't specify an algorithm to balance the mixed model assembly line. One improvement point would be the development of an algorithm capable to satisfy all the requirements in this approach in order to be able to cope to any assembly line.

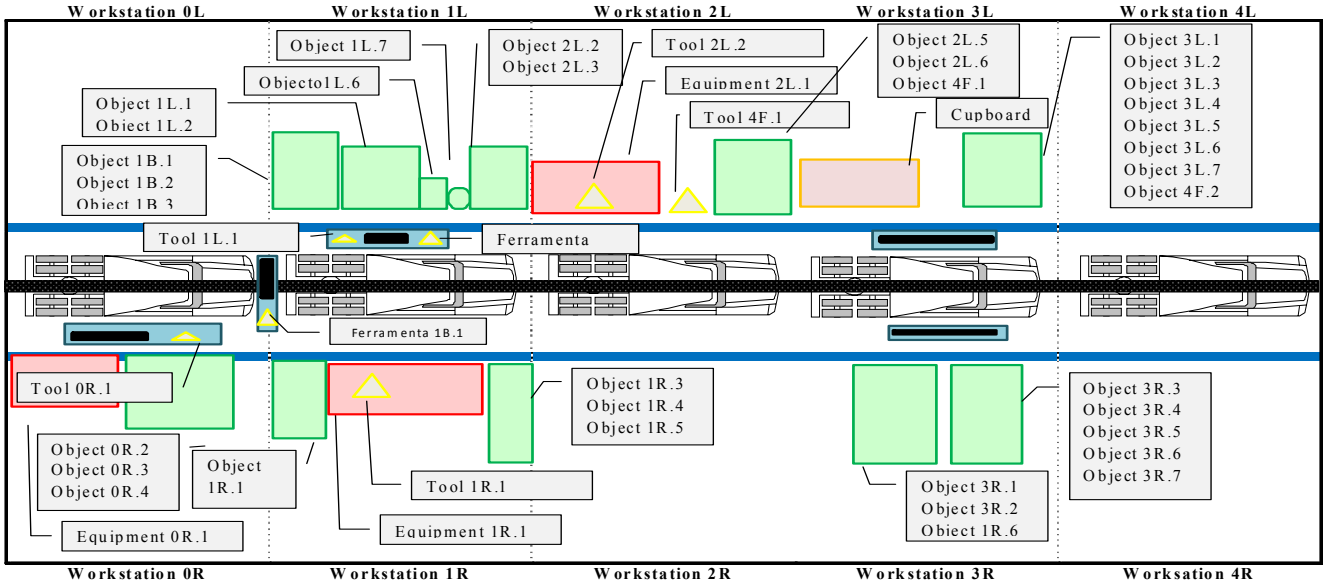

Fig. 17 Logistic space occupation, final status

ACKNOWLEDGMENT

The authors woulk like to thanks all employees of the case study company for the support, availability and information for this study used in this study.

REFERENCES

[1] Simaria, A. S., *Assembly Line Balancing: New perspectives and procedure*. PhD Dissertation in Industrial Engineering and Management, Aveiro University, Department of Economics, Management and Industrial Engineering, Aveiro, 2006.

[2] Su, J., Ferguson, M., & Chang, Y.-L., "Evaluation of postponement structures to accommodate mass customization," Journal of Operations, vol. 23, no. 3-4, pp. 305-318, 2004.

[3] Boone, C., Craighead, C., & Hanna, J., "Postponement: an evolving supply chain concept," International Journal of Physical Distribution & Logistics Management, vol. 37, no. 8, pp. 594-611, 2007

[4] Gerhardt, M. P., *Systematic implementation of procedures for Balancing Assembly Lines and Multi-Model*, Post-Graduation in Production Engineering, Federal University of Rio Grande do Sul, Porto Alegre, 2005.

[5] Zhang, Q.,Vonderembse, M., & Lim, J.-S., "Manufacturing flexibility: defining and analyzing relationships among competence, capability, and customer satisfaction", Journal of Operations Management, vol. 2, no 2, pp.173-191, 2003.

[6] Coronado, Lyons, Kehoe, & Coleman, "Enabling mass customization: extending build-to-order concepts to supply chains," Production Planning & Control, vol. 15, no. 4, pp.398-411, 2004.

[7] Gonçalves, J. F., & Almeida, J. R, "A hybrid genetic algorithm for assembly line balancing," Journal of Heuristics, vol. 8, no. 1, pp. 629-642, 2002.

[8] Gokçen, H., & Baykoç, F., "A new line remedial policy fot the paced lines with stochastic task times," International Journal of Production Economics, vol. 58, pp. 191-197, 1999.

[9] He, D., & Babayar, A., "Scheduling manufacturing systems for delayed product differentiation," International Journal of Production Research, vol. 40, no. 11, pp. 2461-2481, 2002.

[10] Becker, C., & Scholl, A., *A survey on problems and methods in general assembly line balancing*, Jenaer Schriften Zur Wisfschaftwissenchaft, FSU – Jena, 2003.

[11] Betancourt, L. C., *ASALBP: the Alternative Subgraphs Assembly Line*, Doctorial Program: Advanced Automation and Robotic, Catalonic Technical University, Institute of Industrial and Control Engineering, Catalonic, 2007.

[12] Heilala, J., & Voho, P., "Modular reconfigurable flexible final assembly systems," Journal Assemble Automation, vol. 21, no. 1, pp.20-30, 2001.

[13] Groover, M. P., *Automation, Production System, and Computer-aided Manufacturing*, Prentice Hall, 1980.

[14] Lee, K., Jeong, H., Park, C., & Park, J., "Construction and performance analysis of a Petri net model based on a function model in a CIM system," International Journal Advance Manufacturing Technologic, vol. 23, no. 1-2, pp.139-147, 2003.

[15] Kim, Y. K., Kim, Y., & Kim, Y. J, "Two-sided assembly line balancing: a genetic algorithm approach," Production Planning & Control, vol. 11, no.1, pp.44-53, 2000.

[16] Aguiar, G., Peinado, J., & Graeml, A., *Simulations of physical arrangements for product and production line balancing: case study of a real education for engineering students*. XXXV Brazilian Congress of Engineering Education. Conbenge, 2007.

[17] Rekiek, B., Dolgui, A., & Delchambre, A., "State of art of optimization methods for assembly line design," Annual Reviews in Control, vol. 26, no. 2, pp.163-174, 2002.

[18] Rekiek, B., Lit, P., & Dechambre, A., "Designing mixed-product assembly lines," Transactions on Robotics and Automation, vol. 16, no. 3, pp. 268-280, 2000.

[19] Lee, T. O., Kim, Y., & Kim, Y. K., "Two-sided assembly line balancing to maximize work relatedness and slackness", Computers & Industrial Engineering, vol.40, pp.237-292, 2001.

[20] Noh, S., Park, Y., Kong, S., Han, Y., Kim, G., & Lee, K., "Concurrent and collaborative process planning for automotive general assembly," International Journal of Advance Manufacturing Technology, vol. 26, nº 4, pp.572-584, 2005

[21] Liker, J. (2005). O Modelo Toyota, 14 *Princípios de Gestão do Maior Fabricante do Mundo*. Bookman.

2011 International Conference on Mechanical, Industrial, and Manufacturing Engineering
Lecture Notes in Information Technology Vols. 1-2

Exploring a Promising Research Theme based on Academic Knowledge Map using the GTM Method*

Byungun Yoon
Dept. of Industrial & Systems Engineering
Dongguk University-Seoul
Seoul, South Korea
e-mail: postman3@dongguk.edu

Ahyeon Kim, Wonbae Jeon
Dept. of Industrial & Systems Engineering
Dongguk University-Seoul
Seoul, South Korea
e-mail: ahyeonkim@dongguk.edu, esunhong@nate.com

***Abstract* – Since many researchers are looking for promising, novel research ideas, they normally want to explore research vacuum that has not been studied and is able to even suggest a breakthrough in existing research environment. However, traditional approaches just deal with qualitative method or are dependent of the individual capability to create promising research ideas. Therefore, this research aims at proposing a systemic process to explore influential research theme, using bibliometric data and methods. For this, first, a research area that is proper to this approach is selected and related academic papers are collected from academic database. Second, text mining is conducted to extract keywords from the papers. Third, academic knowledge map is visualized and research vacuums are derived by GTM. Fourth, the characteristics of the research vacuums are grasped by applying the algorithm of GTM. Finally, with keywords that can represent the features of the vacuums, existing research are investigated to evaluate the level of related research activities in the areas of interest.**

Index Terms – Academic Knowledge Map, Generative Topology Mapping, Text Mining, Research Theme.

I. INTRODUCTION

The selection of promising research subjects is often a critical issue in R&D budgeting because the amount of R&D investment is insufficient and a lot of research proposals are submitted to governments as well as companies. Thus, the evaluation of public research and development (R&D) programs has been highlighted since the 1980s when the concept of strategic research management was introduced [1]. In particular, important research proposals should be prioritized in order of economical and technical impact in the level of firms. In a bibliometric-related research area, the past data on academic paper and reports are utilized to investigate the trend of research and core research subjects. Bibliometric assessments are economical, non-invasive, and simple to implement, permitting updates and rapid inter-temporal comparison with more quantitative data [2]. A wider use of bibliometrics to evaluate the quality and efficiency of research activities is realized in areas of scientific investigation that are well represented by articles in international journals [3].

However, existing research focuses on the examination of research trends and current core research areas and little attentions are paid to the investigation of promising future research themes. In addition, most of researchers are interested in visualizing relationship among present R&D activities without quantitative analyses. If any, such studies are based on statistical analysis, providing basic implications such as a network of researchers and a trend map of research. However, the more important issue is how to identify the vacuum of research subjects and evaluate the value of vacuum. Thus, this paper deals with a process to explore the research vacuum and evaluate the possibility of new research by drawing an academic knowledge map on the basis of the generative topology mapping(GTM). Since the GTM method is a novel machine learning tool for data modelling and visualization, many researchers apply it to visualize original data into a 2 or 3-dimensional space and derive the characteristics of unoccupied cells of the map. In this paper, an approach to positioning existing academic papers and exploring the research vacuums that are not occupied by the previous research is proposed. For this, text mining is applied to extract important keywords that are able to present the features of academic papers because the textual format of papers is composed of natural language. In particular, the GTM is a core method to visualize the relationship among papers and explore research vacuums. Since such vacuums can be promising or useless, the process of evaluation should be considered. The results of this research can help researchers to catch meaningful research themes from the previous research history and enhance the R&D budgeting process for policy-makers.

II. BACKGROUND

A. GTM(Generative Topographic Mapping)

The GTM model which is provided by Bishop is a probabilistic version of the Self Organizing Maps (SOM).

Both SOM and GTM are useful for visualizing data by low-dimensional views from original high-dimensional data. The potential application of techniques above could be classification, clustering, visualizing data, pattern recognition and patent mapping [5] [6] [8].

SOM is artificial intelligence model based on learning process which was proposed by Kohonen. Even it simply provides a model in forms of discrete nodes, it does not

* This research was supported by the Basic Science Research Program through the National Research Foundation (NRF) and funded by the Ministry of Education, Science, and Technology (Grant No. 2009-0073285).

include general proofs of convergence, ambiguous dimensions and subjective identification of patent vacuums [6].

GTM overcomes these limitations of the SOM by probabilistic method based on Bayesian theory and offers a number of advantages compared with the standard SOM. This technique provides concept of deriving a probability density model of low dimension space data by offer relatively small level of latent variable or hidden variable from origin data [4]. GTM is a non-linear latent variable model whose parameters could be optimized using the EM (expectation-maximization) algorithm. [4]

One of the advantages of GTM is can provide probabilistic framework by automatic identification of latent variables by inversing mapping [7]. The document vacuums are extracted automatically and help to understand object by keywords vectors. GTM based data visualization approach can estimates feature document simultaneously with the training of the visualization model. It provides better extrapolation by modeling different features with a separate noise model and gives feature document values.

B. Bibliometrics

Bibliometrics is applied very frequently in the field of Knowledge management and Technology Management. For example, Patent data and Research fund data are applied a lot. co-citation analysis, trend analysis would be used by calculating the journal impact, the importance of technology, to identify trends. The term of Bibliometrics was named in 1969 by Pritchard [9]. For 50 years before 1969, it has been called as "statistical analysis" [10].

Recently, some researchers have demonstrated that bibliometric techniques provide useful information that can counterbalance shortcomings and mistakes in peer judgment, such as distortions arising from subjectivity in assessments [11]. In various studies, bibliometric data have been applied to assess research performance and anticipate promising research areas, particularly for the natural and life sciences, because scientific progress is generally achieved by researchers who study research topics by building upon the work of other scientists [12] [13]. In general, conventional bibliometric methods evaluate the research trend by investigating the publication outputs of different countries, research institutes, journals, and research fields or by doing the citation analysis [14]. However, focusing on the changes in the quantities of citations or publications alone may not be adequate to provide a clear indication of the developing trends or future orientation of a research field. Information based on the content of studies, such as source titles, author keywords, keyword plus and abstracts should be introduced in research-trend studies. Arrue and Lopez first attempted to evaluate the growth pattern of conservation tillage research based primarily on abstracts published on Soils and Fertilizers [15]. Qin used keywords plus to investigate the development of antibiotic resistance research [16].

III. FRAMEWORK

A. Overall Process

In order to explore promising research themes, academic papers are positioned on a research map which is drawn by applying the GTM method. For this, the first step is to choose the research area which is of interest and academic papers in the category are collected from database such as SCI. Second, text mining is applied to extract keywords of each paper and keyword vectors of papers are constructed on the basis of the occurrence frequency with the extracted keywords. Third, academic knowledge map is developed by adopting GTM, visualizing the relationship among the papers. Fourth, research vacuums are identified to explore meaningful research themes. In the academic knowledge map, unoccupied cells that existing academic papers did not deal with are derived, providing the characteristics of the cells. GTM can present the keywords of the unoccupied cells in the map. Finally, the keywords are utilized to evaluate the value of potential research themes which are grasped from the map. By retrieving papers with the keywords of the vacuums, the research opportunities can be evaluated. Fig. 1 shows the overall process of this approach.

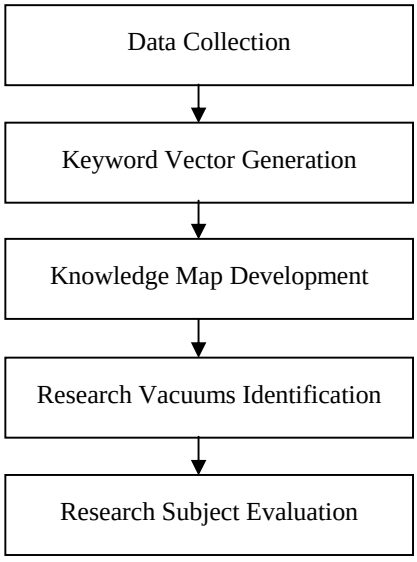

Fig. 1 Overall Process of This Paper.

B. Development of Academic Knowledge Map

The development of academic knowledge map is conducted by applying the GTM. First of all, keyword vectors should be prepared to visualize the information of papers. Keywords are extracted by TF/IDF(term frequency–inverse document frequency) which is a weight often used in information retrieval and text mining. This weight is a statistical measure used to evaluate how important a word is to a document in a collection or corpus. However, the approach might bear a problem to be unable to consider the domain knowledge of the selected research subject. Thus, keywords that are extracted by using TF/IDF are screened by applying the knowledge of domain experts. Then, keyword vectors of

collected papers are built on the basis of occurrence frequency of the keywords. The data fields of the vectors are filled with the frequency. Fig. 2 exemplifies the keyword vectors of the papers.

Paper 1 = (3, 2, 1, 23, 31, …., 3, 6, 8)
Paper 2 = (13, 7, 0, 0, 11, …., 2, 7, 2)
…
…
Paper n = (7, 8, 2, 27, 24, …., 11, 3, 2)

Fig. 2 Example of Keyword Vector.

Second, vectors of academic papers are used as inputs of the GTM. Matlab which allows matrix manipulations, plotting of functions and data, implementation of algorithms is adopted to apply GTM to mapping the collected papers. Although two and three-dimensional maps can be generated, the two-dimensional map is chosen to enhance the understanding of research distribution.

C. Exploration and Evaluation of Research Vacuums

After academic papers are positioned on the grids of academic knowledge map, unoccupied cells in the grids are identified. The knowledge map is composed of m*n grids and if k points are occupied by existing papers, the number of new research opportunity becomes to be (mn-k). Each cell has the proper keyword vectors, enabling the mapping of papers. GTM can identify the keywords of unoccupied cells (i.e. research vacuums). Fig. 3 shows a mechanism to derive the keywords of research vacuums from the map. In the figure, keyword vector of vacuums are extracted, and the first and third keywords can characterize the features of the vacuum (V1).

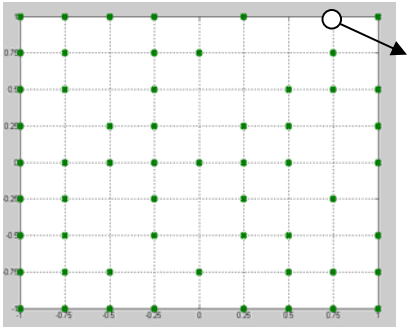

Fig. 3 Keyword Vector of Vacuums.

Although there are many research vacuums, important research vacuums should be evaluated to screen meaningful opportunities from useless research themes. For this, the extracted keywords of the identified research vacuum are used to retrieve the relevant academic papers from paper searching databases. In this paper, the number of searched papers is calculated to analyze the value of vacuums. If a lot of related papers which deal with the similar subject in the other research area are searched, the vacuum in the selected research category has influential opportunities for study but it remains unoccupied. Thus, the important papers which are cited from subsequent papers are listed to explore future research themes.

IV. Results

A. Data

Academic papers are downloaded from *Sciencedirect* which provides a database of papers in thousands of journals. In this paper, electric/telecommunication research category is chosen because the papers in the category are sufficient to conduct this approach. 129 papers in the category are collected for the analysis. In the category, several sub-categories such as semiconductor, antenna and telecommunication systems are included.

B. Academic Knowledge Map

Keywords are extracted from 129 papers by applying text mining. Stemming, TF-IDF and stopwords exclusion are conducted to derive meaningful keywords. Consequently, 50 keywords are selected to be utilized for mapping. Table 1 presents the list of 50 keywords from 129 papers.

TABLE I
Extracted Keywords

Keywords
Packet, electric, computing, efficiency, nodes, power, electron, GHz, Broader, Influenced, Network, Nm, One-dimensional, Hydroxide, Heat, Signal, Inhomogeneities, Miniaturized, Broadband, EO, two-dimensional, watermarking, band, codewords, substrate, space, video, wireless, transformer, Simulation, Optical, Circle, 3D, Ge, Clustering, Channel, Conventional, Digital, Watermark, Nanometer, Multipath, Overhead, dB, FCFS, Synchrotron, Media, Paging, Electrical, Block, Viterbi

An academic knowledge map is generated by keyword vectors that are composed of the occurrence frequency of 50 keywords in each paper. GTM is used to visualize the relations among papers, applying 9*9 grids in mapping the vectors.

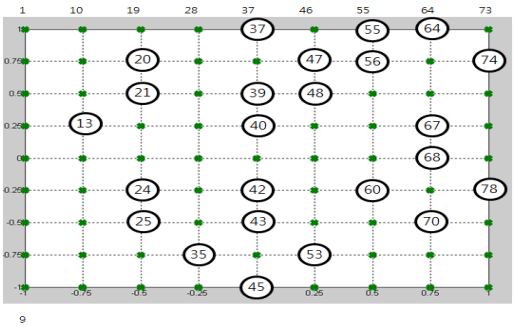

Fig. 4 Research Vacuums in Knowledge Map.

Potential research themes in the knowledge map are shown in Fig. 4. 24 research vacuums are identified from 81 total sets of research areas. In order to understand the characteristics of the 24 research vacuums, keywords of the

vacuums are derived by applying GTM. Table 2 depicts the keywords that can characterize each research vacuums.

TABLE II
KEYWORDS OF EACH VACUUM

No.	Keywords	No. of Papers
63	Broadband, heat	2255
52	Power, signal, GHz, dB	1527
34	channel, multipath	751
24	multipath, block	486
38	electric, nm, dB, efficiency, broader	399

The first research vacuum has two keywords (broadband and heat) and the number of papers which are searched by the keywords is 2255. Thus, although a lot of related papers in the other research areas are written, little attention is paid to the theme in the electric/ telecommunication area. Table 3 shows the top 5 ranked papers which are frequently cited in the research vacuum. Thus, the papers should be investigated in order to explore new research ideas.

TABLE III
TOP 5 RANKED PAPERS RELATED TO NO. 63 VACUUM

Rank	Paper Title	Cited Counts
1	Doubling of sensitivity and bandwidth in phonon cooled hot electron bolometer mixers	70
2	Temperature-independent strain sensor using a chirped Bragg grating in a tapered optical fibre	79
3	Ultra-broadband semiconductor laser	95
4	Increase of the SBS threshold in a short highly nonlinear fiber by applying a temperature distribution	74
5	High-bandwidth graded-index polymer optical fiber	246

V. CONCLUSIONS

Since governments and companies want to identify new opportunities for economical and technological sustainability, potential technology development and research should be explored. This paper deals with mapping past research activity and deriving promising research vacuums. For this, text mining and GTM are applied to visualize research papers and investigate the characteristics of vacuums. The proposed approach can provide useful information on promising research themes and R&D budgeting.

However, this approach has several limitations. First, although a proper criteria to judge meaningful research vacuums needs to be suggested, this paper insufficiently tackles the issue by presenting the number of related papers and the cited counts of the papers. Thus, a good indicator such as *a relevance ratio* to analyze the exact value of vacuums should be proposed. Second, the process to select keywords is incomplete because it is mostly dependent on text mining software. Thus, a research dictionary that consists of keywords in each research category will be useful to extract meaningful keywords. Finally, although a cell in the academic knowledge map is identified as a research vacuum, the cell sometimes includes small number of keywords and a large scale of related papers. Therefore, an additional process needs to be intervened in order to separate such vacuums from genuine research vacuums. This paper will help researchers to anticipate future research subjects and policy-makers to select influential research proposals.

REFERENCES

[1] T. Hayashi, “Bibliometric analysis on additionality of Japanese R&D programmes”, *Scientometrics*, vol. 56, no. 3, pp. 301–316, 2003.

[2] G. Abramoa, C.A. D’angeloa, A. Capraseccaa, “Allocative efficiency in public research funding: Can bibliometrics help?” *Research Policy*, vol. 38, pp. 206–215, 2009.

[3] A.F.J. Van Raan, “Fatal attraction: conceptual and methodological problems in the ranking of universities by bibliometric methods”, *Scientometrics*, vol. 62, no. 1, pp. 133–143, 2005.

[4] C. Bishop, M. Svensen, "The Generative Topographic Mapping", *Neural Computation*, vol. 10, no. 1, pp. 215-234, 1998.

[5] J.H, Choi, "pattern Classification by Using Bayesian GTM", proceedings of KFIS 2001 fall conference, 2001.

[6] Changho Son, Yongyoon Suh, Jeonghwan Jeon, Yongtae Park, "Development of a GTM-based Patent Map for Identifying Patent Vacuums", Expert System with Applications, in press.

[7] C. Bishop, M. Svensen, "developments of the Generative Topographic Mapping", *Neurocomputing*, vol. 21, pp.203-223, 1998.

[8] I. Olier, A. Vellido, "Advanceds in clustering and visualization of time series using GTM through time", *Neural Networks*, vol. 21, pp. 904-913, 2008.

[9] Y. Okubo, “Bibliometrics “Bibliometric Indicators and Analysis of Research Systems, Methods and Examples”, OECD, STI Working Paper 1997/1).

[10] E.W. Hulme, *Statistical bibliography in relation to the growth of modern civilization*, 1923.

[11] D.W. Aksnes, R.E. Taxt, “Peers reviews and bibliometric indicators: a comparative study at Norvegian University”, *Research Evaluation*, vol. 13, no. 1, pp. 33–41, 2004.

[12] F. Narin, *Evaluative Bibliometrics: The Use of Publication and Citation Analysis in the Evaluation of Scientific Activity*, National Science Foundation, Washington, DC, 1996.

[13] A.F.J. Van Raan, “Advanced bibliometric methods as quantitative core of peer review based evaluation and foresight exercises”, *Scientometrics*, vol. 36, pp. 397–420, 1996.

[14] W.T. Chiu, Y.S. Ho, “Bibliometric analysis of homeopathy research during the period of 1991 to 2003”. *Scientometrics*, vol. 63, pp. 3–23, 2005.

[15] J.L. Arrue, M.V. Lopez, “Conservation tillage research trends and priorities”, *Suelo Y Planta*, vol. 1, no. 4, pp. 555–564, 1991.

[16] J. Qin, “Semantic similarities between a keyword database and a controlled vocabulary database: An investigation in the antibiotic resistance literature”, *Journal of the American Society for Information Science*, vol. 51, no. 2, pp. 166–180, 2000.

2011 International Conference on Mechanical, Industrial, and Manufacturing Engineering
Lecture Notes in Information Technology Vols. 1-2

Analysis of Flow Characteristics in WIG -vehicle with Direct Under Pressurization Device

Kyoungwoo Park, Jong-Kwan Ahn and Sung-Tae Shim

Department of Mechanical Engineering

Hoseo University, Asan 336-795, Rep. of Korea

kpark@hoseo.edu

Chol-Ho Hong, Byeong-Sam Kim and Juhee Lee

Department of System Control, Automotive, and Mechatronics

Hoseo University, Asan 336-795, Rep. of Korea

{chhong, kbs, juheelee}@hoseo.edu

***Abstract* – In the present work, numerical investigations for the three-dimensional WIG effect vehicle with direct underside pressurization (DUP) have been performed to analyze aerodynamic characteristics and static height stability. The computational model consists of all compartments of a WIG effect vehicle such as propeller, fuselage, air chamber, main wing, and tail. As the results of this study, the DUP is not favorable for both stability and aerodynamic performance of the WIG effect vehicle because the accelerated air produces an excessive drag, negative pitching moment and 3-dimensional effects (that is, yawing and rolling moments). The result shows that the effect of yawing and rolling moments is not serious.**

Index Terms - Aerodynamic characteristics, CFD , DUP (direct underside pressurization); Ground effect; WIG (Wing-in-ground) effect vehicle, Yawing and Rolling moments.

I. INTRODUCTION

Wing-in-ground (WIG) effect vehicles are the advanced vehicle that cruises close to water or ground surface (i.e., at a height of 30% of its chord length or lower) by utilizing an air cushion among the wing, the fuselage and the ground. Due to the air cushion at low heights, there is a considerable increase in lift and a decrease in drag and therefore enhancement of the lift–drag ratio. The enhancement of the lift-drag ratio makes the WIG effect vehicle to consider one of the potential means of transportation. Therefore, much attention has been paid on the prediction of performance in WIG vehicle both by numerical and experimental methods from as early as the 1900s. In 1922, Wieselsberger [1] performed a theoretical investigation to determine the conditions for taking off and landing of an airplane using Prandtl's wing theory. Jung et al. [2] conducted a smoke trace test to visualize the flow pattern around the NACA6409 in ground effect and measured the pressure distributions on the surface of the airfoil. Staufenbiel and Schlichting [3] insisted that the static height stability is a part of the dynamic stability as well as a necessary condition for the stability. It means that the dynamic stability cannot be satisfied without the static height stability.

For designing a WIG effect vehicle with high cruise performance, it is difficult to satisfy the design requirements such as efficiency and stability, simultaneously, because of the trade-off phenomena between them. Park and Lee [4] performed a multi-objective optimization for the 2-dimensional WIG effect vehicle by integrating CFD and MOGA (multi-objective genetic algorithm). Because the vehicle in ground effect skims over the surface, its cruise performance is generally improved. However, the vehicle is required about 2 times larger engine power to obtain sufficient thrust during both takeoff and landing since part of a fuselage is sunk in water. In order to obtain additional thrust, these engines bring on an increase in the drag so that give rise to a structural problem to support the heavy engines in cruise [5].

In the present study, the 3-dimensional flow characteristics and the height static stability of WIG effect vehicle with DUP that consists of all compartments such as fuselage, wings, DUP and T-tail are investigated numerically. Numerical analyses are performed by solving the Reynolds averaged Navier-Stokes (RANS) of turbulent flow. The aerodynamic characteristics are obtained and compared for various conditions such as pitch angles and non-dimensional heights.

II. COMPUTATIONAL MODEL AND VALIDATION

2.1. Computational Models

Air is taken as the working fluid and is assumed to be steady, incompressible, and turbulent flow. The fluid properties are taken to be constant and the effect of viscous dissipation is assumed to be negligibly small. Using the aforementioned assumptions, the Reynolds-Averaged Navier-Stokes (RANS) equations for mass and momentum, which are written in a tensor notation, have to be solved.

$$\frac{\partial(\rho u_j)}{\partial x_j} = 0 \tag{1}$$

$$\frac{\partial(\rho u_i u_j)}{\partial x_j} = -\frac{\partial P}{\partial x_i} + \frac{\partial}{\partial x_j}\left[\mu\left(\frac{\partial u_i}{\partial x_j} + \frac{\partial u_j}{\partial u_i}\right) - \overline{\rho u_i' u_j'}\right] \tag{2}$$

The new term, $\overline{\rho u_i' u_j'}$, the Reynolds stress, must be modeled by using a turbulence model in order to solve the RANS equations. In this study, the flow domain was divided into two regions such as near wall and fully turbulent regions, and then adopted a standard turbulent model [6] and wall function next to the wall. According to this model, turbulent kinetic energy (k) and its dissipation rate (ε) are expressed in a tensor form as follows:

$$\frac{\partial}{\partial x_j}(\rho u_i k) = \frac{\partial}{\partial x_j}\left[\frac{\mu_t}{\sigma_k}\frac{\partial k}{\partial x_j}\right] + P_k - \rho\varepsilon \tag{3}$$

$$\varepsilon = \frac{k^{3/2}}{l_\varepsilon}\left(1+\frac{C_\varepsilon}{\mathrm{Re}_y}\right) \quad (4)$$

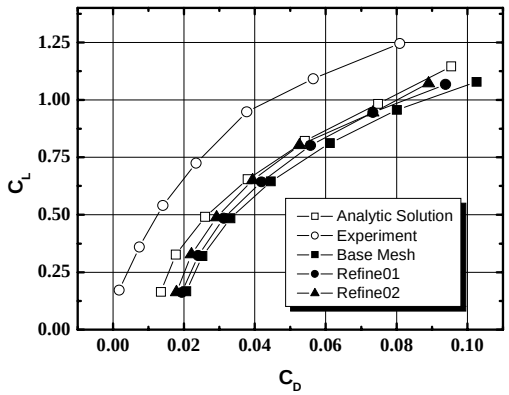

Fig. 1 Comparision of drag polars; analytic solution [Anderson, 1999], experiment[McAlister and Takahashi, 1991] and this study

where i = 1,2 and 3 denote x, y, and z -directions, respectively. The term P_k in Eq. (3) stands for the production term. The model constants and various functions used in the turbulent model are detailed in reference [6].

The numerical simulations presented in this work were done by means of STAR-CCM+ [7] which is a general purpose commercial software. The pressure-velocity coupling phenomenon is resolved through the SIMPLE algorithm [8]. For representing the exact flight conditions, the moving wall boundary condition with a flight velocity is applied at the ground. The solutions are treated as converged ones when the sum of normalized residual is less than 1×10^{-5}. The propeller was modelled with the moment source with a fan curve.

2.2. Validation of CFD Model

To valid the present CFD model, the experiment [9] and analytical results [10] for lift and drag coefficients are plotted in Fig. 1. For this, a rectangular wing of the untwisted NACA 0015 profile (i.e., aspect ratio of 6.6) with Reynolds number of 1.5×10^6 is used. The 3-dimensional shaped wing is placed far away from the ground (that is, ground effect is negligible). Figure 1 shows that the computational results of three consecutive numbers of grids (basic: 170k cells, refine#1: 250k cells, and refine#2: 450k cells) have a little discrepancy compared with those of experiments. This is due to the fact that the measurement data were listed without proper corrections of the blockage factor and lift interference, as the authors mentioned in their paper. On the contrary, the results of this study have a good agreement with the analytic solutions as shown in Fig. 1.

III. RESULTS AND DISCUSSION

The computational domain considered in this study is extended 6 times of a vehicle length for each direction in order to avoid the influence of the far boundaries, but it is extended 10 times for the downstream direction. To take the no-slip boundary condition on the surface into account correctly, 6 layers of the prism grid with high aspect ratio along the surface are used next to the surface. To evaluate the forces on the vehicle surface, locally refined grids next to the vehicle are employed. The computational domain are shown in Fig. 2. The non-dimensional height between the wing and the ground is measured at the trailing edge, and the nose-up pitching moment is positive as shown in Fig. 2. The numerical calculations are performed from $h/c = 0.24$ to 0.45 and $\alpha = -2^o$ to 10^o degrees except at $h/c = 0.24$ and $\alpha = -2^o$ due to the fuselage contacting with the ground.

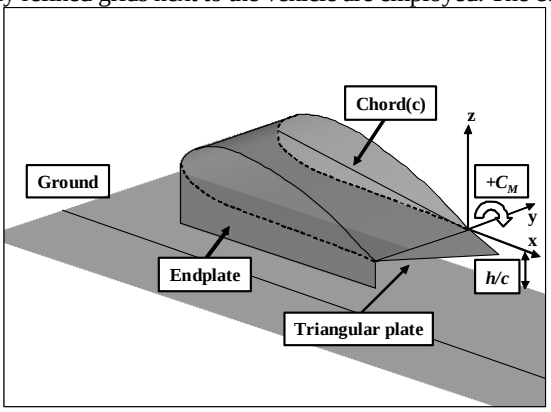

Fig.2 Geometric configuration of WIG vehicle

Table 1 Specification of model vehicle

Maximum Speed	About 25 m/s (72 km/h)
Cruise Speed	15 m/s (54km/h)
Engine Power	1 ps at 10000 rpm
Propeller Diameter	24 cm (9.5 inch)
Main Wing Area	0.10976 m2
Tail Wing Area	0.07558 m2
Control Surface	Rudder
Total Weight	About 2.7 kg
Total Length	1 m
Span	0.7 m
Chord Length	33.4 cm

The boundary conditions are configured to identify the free-flight condition. The upstream boundary is modeled using an inlet velocity with a uniform distribution. A pressure outlet boundary condition is adopted at the downstream. A slip wall boundary condition is imposed on the undisturbed far boundary, thus imposing a zero cross flow condition. The wing and ground plane are modeled as solid walls with a no-slip boundary condition. In addition, the ground surface is provided with a velocity equal to free stream for identifying free flight through calm air. The Reynolds numbers based on both free stream velocities (v_{in} = 10 and 15 m/s) and chord length of the vehicle are 2.14×10^5 and 3.21×10^5, respectively. The detail specifications of the model vehicle are listed in Table 1.

3.1. Aerodynamic Characteristics and Static Height Stability

Fig. 3 presents the flow streams along the center line of the vehicle for $\alpha = 9^o$ and $h/c = 0.24$ (i.e., the vehicle is close to

the ground) in order to explain the overall flow pattern around the WIG vehicle. The accelerated air coming to the DUP flows

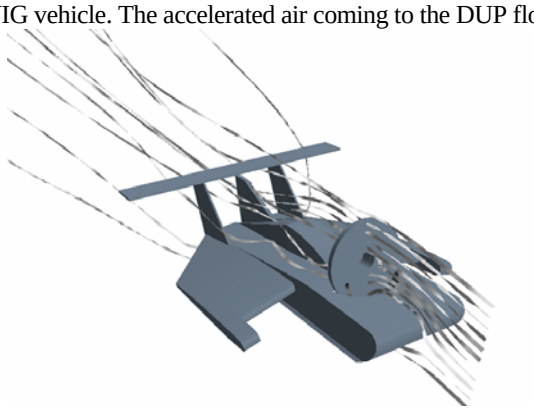

Fig. 3 Streamlines around a model vehicle

along the surface of the fuselage with high dynamic pressure. It is also shown that a part of the accelerated air comes into the lower surface of the fuselage and run through the small gap between ground and wing with the reduced, as shown in Fig. 3. There is another flow passage leading the air into air chamber; the fore gap between fuselage and ground. From the figure, higher pressure on the aft body of the vehicle is expected because of air stagnation in the air chamber. Note that this higher dynamic pressure can augment both the lift and drag forces and the pitching moment as the vehicle is approaching to the ground.

In general, the ground effect improves the aerodynamic forces because of an increase in pressure on the lower surface and a decrease in the influence of the wing tip vortex. Figure 4 shows the lift coefficients (C_L) as the function of dimensionless height (*h/c*) for with and without DUPs. As shown in Fig. 5, except for the case of negative pitch angle ($\alpha = -2^o$), the lift coefficients of all cases (that is, $v_{in} = 10$ without DUP, $v_{in} = 10$ and $v_{in} = 15$ with DUP) are increased as *h/c* decreases due to the ground effect. A larger pitch angle results in a higher increase in lift coefficient. This result, higher lift at lower height, is agreed well with those of other researches [18, 25-27]. It is also shown in Fig. 4 that for the same inlet velocity ($v_{in} = 10$ *m/s*). Figure 4 also shows that the lift force for the case of with DUP is higher than that for without DUP. It implies that DUP has a great influence on lift augmentation. When the pitch angle is greater than *3* degree, the lift coefficient for $v_{in} = 15$ *m/s* becomes smaller than that for $v_{in} = 10$ *m/s* since the pressure fraction by the DUP to the dynamic pressure is relatively small. It is interesting that all lift coefficients at $\alpha = -2^o$ decrease when the vehicle gets close to the ground and the cases with DUP have a larger decrease in lift coefficient at this pitch angle (to be discussed later). This result is mainly due to the shape of the fore part of the fuselage; venturi effect or diverge-converge effect between fuselage and ground. It is also shown in Fig. 4 that C_L is linearly proportion to α at $h/c = 0.45$, but not at $h/c = 0.24$ where the effect of ground is stronger. The similar non-linear increase in lift can be seen in many researches. The non-linear increase is due to the fact that when the vehicle is in ground effect above the critical pitch angle (between -2^o to 0^o), the oncoming air through the DUP and leading edge is stagnated because of the small gap between fuselage and ground so that

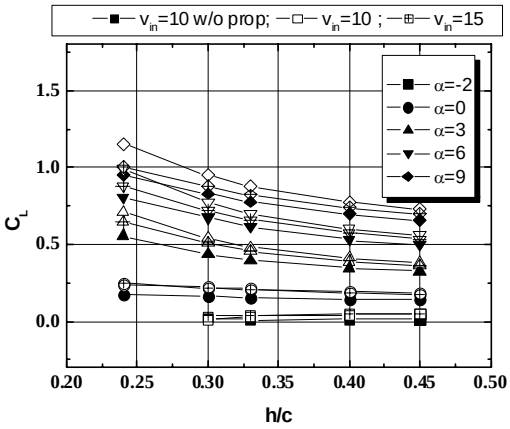

Fig. 4 Lift coefficient vs. height at various pitch angles for with and without DUP

the pressure is suddenly increased. However, for the out of critical pitch angle and height, the increasing rate of pressure is slow and thus it increases linearly as the general airplane does.

The aerodynamic characteristics of lift and drag can be wrapped into a single diagram; the drag polar. Virtually improving the aerodynamic performance of wings in ground effect can be achieved by increasing in the lift and reducing in the drag at the same time. Thus, a high performance airfoil or vehicles may be placed at the left in a drag polar diagram. The drag polar according to the heights for three cases are plotted in Fig. 5 and the total drag consists of zero-lift drag and drag due to lift in the present work. In general, the drag due to lift is reduced as the vehicle approaches to the ground so that the aerodynamic efficiency, range, and endurance can be improved. As shown in Fig. 5, the total drag for $v_{in} = 10$ *m/s* with DUP becomes the largest followed by $v_{in} = 15$ *m/s* (with DUP) and $v_{in} = 10$ *m/s* (without DUP). For the subsonic flow, the total drag of the WIG effect vehicle or generic airplane is comprised of three components such as form, friction, and induced drags. Fig. 5 shows that the zero-lift drag for $v_{in} = 10$ *m/s* with DUP has the largest value among three cases. This implies the negative effect of DUP on the dynamic pressure; increasing in the friction and

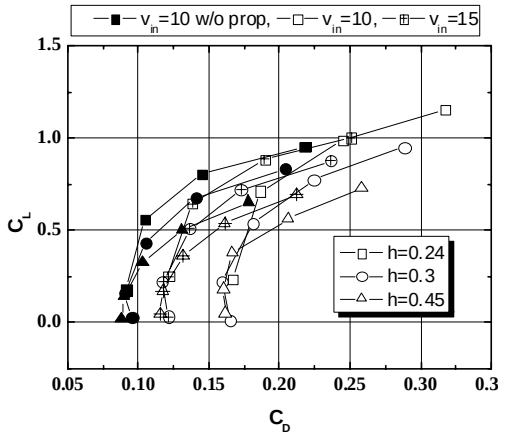

Fig. 5 Drag polars for various heights

form drags. However, the drag for $v_{in} = 15$ *m/s* with DUP becomes lower because the rate of pressure rise by a propeller to dynamic pressure is low so that its value is placed on the left compared to that of 10 *m/s*. The DUP by the augmented dynamic pressure increases lift and drag, simultaneously. As a result, the two cases with DUP are placed on the right side in Fig. 5, and thus low operating performance is predicted. For the case of $h/c = 0.45$, the minimum drag is occurred at $C_L = 0$ whereas it appears at around $C_L = 0.25$ for $h/c = 0.25$. It implies that the vehicle obtains the minimum drag when it has a small pitch angle. The cruising vehicle in ground effect with a small pitch angle obtains better operational efficiency.

The aerodynamic forces of the vehicle in ground effect, which are varied with α and h/c, lead to a different stable condition from out of ground effect such as a general airplane. The static height stability ($H.S.$), a condition considered both α and h/c for the vehicle in ground effect, was proposed by Irodov [10]. Irodov derived with a coordinate system that has an origin at a trailing edge. In this study, the same coordinate system was used for convenience. The *H.S.* includes the differentiations of lift coefficient and pitching moment coefficient against heights and pitching angle and is defined as;

$$\boldsymbol{H.S.} = \frac{\boldsymbol{C_{M,\alpha}}}{\boldsymbol{C_{L,\alpha}}} - \frac{\boldsymbol{C_{M,h}}}{\boldsymbol{C_{L,h}}} = \boldsymbol{X_\alpha} - \boldsymbol{X_h} \le 0 \qquad (5)$$

where the subscripts h and α in the moment and the lift coefficients represent the derivative of height and pitching angle, respectively. Eq. (5) implies that the aerodynamic center of height (X_h) should be placed upstream of the center of the pitch angle (X_a) in order to maintain the stability of the vehicle in ground effect. Fig. 6 shows the static height stability of three cases with various angles of attack. $H.S.$ in Fig. 6 apparently shows that the case with DUP is less stable than that without DUP when the vehicle is in ground effect. The pressure on the aft-portion of the air chamber for the case with DUP is increased as the height approaches the ground so that the high pressure contributes to moving X_h downward. Thus the DUP is not favorable for H.S. However, in the case of $v_{in} = 10$ *m/s* and $\alpha = 9$ deg., the pressure on the air chamber and the lift on the T-tail increases with the patch angles and therefore $C_{M,a}$ in Eq. (5) decreases so that X_a moves further downstream and thus improves the stability as shown in Fig. 9. It is obvious in Fig. 6 that the vehicle has not increased its cruising height suddenly, which might be a cause of the overturn.

IV. CONCLUSIONS

A 3-dimensional numerical investigation of the WIG effect vehicle with DUP has performed and analyzed aerodynamic characteristics and static height stability. The WIG effect vehicle with all compartments such as propeller, fuselage, air chamber, main wing, and tail was considered. The DUP with increased pressure in the air chamber can considerably reduce take-off speed and thus minimize the effect of the hump drag while the vehicle accelerates to take off on water. However, it also increases the drag by high dynamic pressure on the entire surface of the vehicle and stunts high performance.

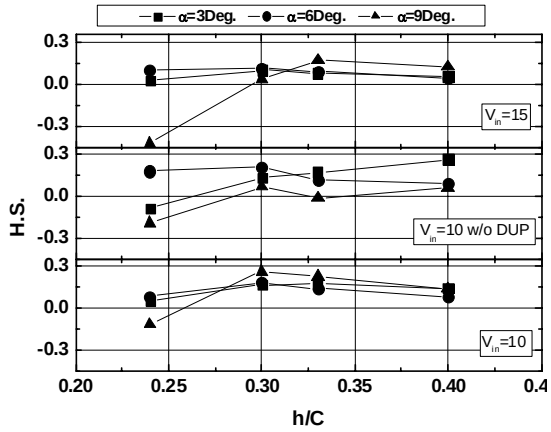

Fig. 6 Static height stability vs. heights for various pitch angles

The computational results clearly show that the DUP can dramatically improve lift but is not favorable for aerodynamic performance and stability. The air with high energy through the DUP slows down and turns its energy to lift in the air chamber under the fuselage. When the vehicle is in ground effect such as $h/c < 0.35$ and $\alpha > 3^o$, stagnation of the air results in high pressure at the aft part of the air chamber, generating sufficient lift. However, the high pressure naturally leads to negative pitching moment and moves X_h downstream. The closer the height of the vehicle is to ground, the higher the pressure is. As a result, this is one of the major factors for aggravating the $H.S.$ It is also necessary that designers for WIG effect vehicle be careful with designing the DUP to enhance takeoff.

ACKNOWLEDGMENT

This research was supported by Basic Science Research Program through the National Research Foundation of Korea NRF) funded by the Ministry of Education, Science and Technology (No. 2010-0015597)

REFERENCES

[1] C. Wieselsberger, *Wing Resistance near the Ground*, NACA TM77 (1922).

[2] K.H. Jung, H.H. Chun and H.J. Kim, Experimental investigation of wing-inground effect with a NACA6409 section, *Journal of Marine*, 13 (3) (2008) 317–327.
[3] R.W. Staufenbiel, and U.-J. Schlichting, Stability of Airplanes in Ground Effect, *Journal of Aircraft*, 25(4) (1988) 289–294.
[4] K.W. Park and J.H. Lee, Optimal design of two-dimensional wings in ground effect using multi-objective genetic algorithm, *Ocean Engineering*, 37 (2010) 902-912.998, pp. 158-176.
[5] H.H. Chun, J.H. Chang, K.J. Paik and M.S. Shin, Wind Tunnel Test on the Aerodynamic Characteristics of a PARWIG Craft, *Journal of the Society of Naval Architects of Korea*, 37 (3) (2000) 57~68.
[6] W. Rodi, Turbulence Models and Their applications in Hydraulics-a State Art of Review, *Book Publication of International Association for Hydraulic Research*, Delft, Netherlands (1984).
[7] STAR-CCM+ v4.02, Methodology, *Computational Dynamics, Co.*, London. U. K (2008).
[8] S.V. Patankar, Numerical Heat Transfer and Fluid Flow, *McGraw-Hill Book Company*, New York, (1980).
[9] K.W. McAlister and R.K., Takahashi, *NACA 0015 Wing Pressure and Trailing Vortex Measurements*, NACA Technical Paper 3151 (1991).
[10]R.D. Irodov, Criteria of Longitudinal Stability of Ekranoplan, *Ucheniye Zapiski TSAGI*, 1 (4) (1970) 63-74.

2011 International Conference on Mechanical, Industrial, and Manufacturing Engineering
Lecture Notes in Information Technology Vols. 1-2

Discussion of Mechanism of Martensite Phase Transformation

Zongchang Liu, Yunping Ji, Haiyan Wang,
Huiping Ren
School of Material and Metallurgy
Inner Mongolia University of Science and Technology
Baotou, Inner Mongolia, China
lzchang75@163.com

***Abstract* - The mechanism of martensite phase transformation was discussed based on the surface relief phenomenon, shear model, shear energy, resistance and driving force for the transformation. The author points out the defect of the shear mechanism and considers that the surface relief is a common phenomenon of supercooled austenite transformation. The surface relief of martensite has no evident difference with that of pearlite or bainite, thus the shear mechanism of martensite transformation lacks of experiment basis. The existing shear models on the basis of the orientation relationship are not in accord with the practice. The resistance of marensite transformation includes the shear strain energy, the stored energy of the crystal defects due to the phase transformation and the volume expansion energy. The driving force is too small to overcome the resistance to fulfill the shear process. The shear mechanism can not achieve crystal lattice parameter and substructure of martensite crystal. So the study on the new mechanism of martensite phase transformation is put forward in this paper.**

Index Terms - Martensite. Supercooled austenite. Shear. Surface relief

I. INTRODUCTION

Since the 30s of the last century, the shear mechanism of martensite phase transformation has been put forward, which has been accepted by the academia, it seems to be a mature theory. However, the author's research indicates that the reasonableness of the shear mechanism is well worth deliberating.

In this paper, experimental and theoretical testing of the shear mechanism was carried out from the aspects of morphology, crystallography, and thermodynamics and so on. The defect of the shear mechanism was analyzed form the surface relief phenomenon, shear models, shear energy, and the resistance and driving force for phase transformation. The author points out that the shear mechanism of martensite phase transformation lacks of the experimental evidence: any kind of shear model does not conform to the reality; the energy consumption for the shear is excessive; the resistance of phase transformation is large, while the driving force isn't enough to shear. So it is thought that the shear mechanism of martensite phase transformation is imperfect, and then it is significant theoretically to study the new mechanism of martensite phase transformation further.

II. SHORTAGE OF EXPERIMENTAL EVIDENCE OF THE SHEAR MECHANISM

It has been believed that the surface relief of martensite is caused by shear since the 20th century. The surface relief was described as *N* type and was regarded as the experimental evidence of shear mechanism.

Up to now, it has been found that the surface relief exists in pearlite, bainite, martensite, and widmanstatten microstructure. The general shape of the relief is the tent type (∧) while it is taken as *N* type in another angle of view. The surface relief has become a universal phenomenon of supercooled austenite transformation in the surface of the sample.

Although the surface relief morphology of transformation products of various steels is different, the relief shape is basically similar. The relief of a single plate phase is all in tent (/\) type and the adjacent two pieces of reliefs combined are regarded as in *N* type. Experimental results indicate that, compared with the surface relief of pearlite, widmanstatten, and bainite, the martensite relief has no special nature. All the lath martensite surface relief shows the tent type (∧), meanwhile the surface relief of the plate martensite of the Fe-Ni-C alloy also shows the tent type[1].

Fig.1 is the observed results of the surface relief of lath martensite. The shape of the surface relief shows tent type (∧). From another perspective, if the surface relief of martensite is *N* type, the surface relief of pearlite, bainite is *N* type as well. In recent years, the observed results form different researchers are consistent. The accurate determination of the size and the morphology of the relief by means of STM and AFM show that the surface relief of martensite is nothing special, which can not reflect the characteristics of "shear".

The phase transformation condition of the supercooled austenite on the surface and inside of the specimen is different. Many experiments show that: the surface martensite nucleates along the austenite grain boundary, and grows up toward the surface of sample; the formation of bainite ferrite on the surface of the sample also nucleates along the austenite grain boundary. However, for the specimen interior, martensite and lower bainite nucleate can at the defects in the

austenite crystal grain interior. Martensite generated along the austenite grain boundary can not keep the coherent relations.

When the surface supercooled austenite of sample transforms into pearlite, the surface relief forms as a result of the uneven expansion of phase transformation, which is caused by the specific volume difference of different phase [2-3]. When the austenite of the sample surface transforms into bainite or martensite, the heterogeneous volume expansion also occurs and the complex surface aberration stress generates, thus giving rise to the surface distortion. The new phase formed firstly is bound to stand out at the surface of the specimen, resulting in the relief phase adapt to the morphology and microstructure, that is, surface relief.

Fig.2 is the morphology of the surface relief of plate martensite in high-carbon steel polished, etched and then observed by optical microscope [4]. The author of this paper marked martensite lath with M on it, showed the location of surface relief with arrow and drew a horizontal line along the surface of sample. It is obvious that the parts produced martensite lath protrude without sinking, which indicates it is the result of the volume expansion. The morphology of the relief is tent type (∧), not *N* type, and there is no shear characteristics. Therefore in the Fig.2 (b), the point that the original author described it as the *N* type is not correct.

Thus, according to the latest observations, such as STM, AFM, SEM and LPM devices combining with theoretical analysis, the surface relief is caused by volume expansion during phase transformations. It is clearly inappropriate to take it granted as the evidence of the shear mechanism of martensite transformation.

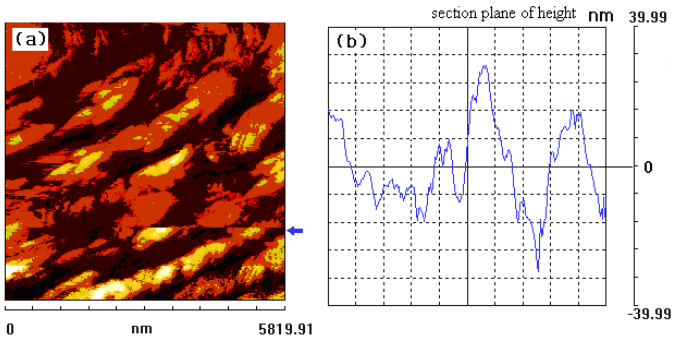

Fig.1 STM, Surface relief of lath martensite of 2Cr13 steel
(a) Relief pattern (b) Height section line of position marked with arrow in Fig. 1 (a)

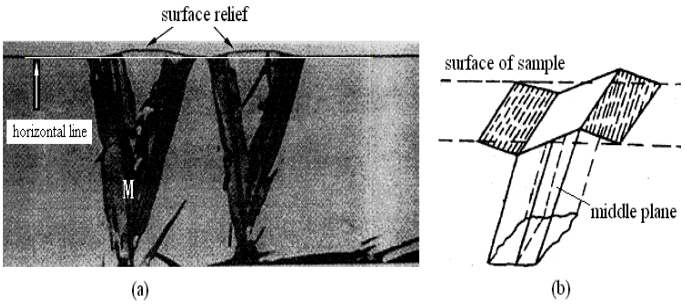

Fig.2 Surface relief and sketch map of high-carbon martensite

III. MARTENSITE SHEAR MODELS DO NOT MATCH WITH THE ACTUAL

A. *Defect of shear models*

In the 1930's, Γ.B. koor Azimov and G. Sachs, first measured that there existed a certain crystallology relationship between the martensite and austenite in the 1.4% C steel, which was later known as the K-S relations. Then the K-S shear model was designed.

In the 1934's, the Western Hills measured there existed a certain orientation relationship during martensite transformation, later known as the Nishiyama relationship, and the shear model of the Western Hills was designed.

However, the two models do not match with the actual habit plane. In addition to this, it can not produce high-density dislocations and fine twin crystal. Therefore, the K-S model and the Western Hills model are both inconsistent with the actual [4-5].

In the 1949's, A. B. Greninger and A. R. Troiano determined the orientation relationship of martensite in Fe-22% Ni-0.8C% alloy and found the G-T relations, then the G-T shear model was designed. However, the model is still not fully in line with the actual. Although indicating the existence of dislocations in martensite, but it can not explain the causes of dislocation tangles and stacking faults in martensite.

Between 1953 and 1954, two presentational hypotheses of martensite transformation were put forward independently, one known as the "W-L-R theory", the other called "B-M theory". However, the physical model of the calculation is wrong, and therefore its results do not conform to the actual phase transition in steel.

Later, scientific researchers proposed or improved some shear models, like Boggers-Burgers dual-shear model and Fan collaboration model. Except Bain strain model, the remaining models are shear model or improved model based on shear.

Since the 20th century, eight kinds of shear models were put forward, but it is regrettable that any kind of the shear models can not be fully in line with the actual, especially for the martensite transformation in steel. Therefore, the shear mechanism of martensite transformation is only a hypothesis at best.

B. *Inappropriate design of shear mechanism according to the orientation relationships*

As mentioned above, since the beginning of the 30s last century, scholars have designed a series of shear models according to the orientation relations between martensite and austenite. Although these models meet their own relationship, it is difficult to explain more experiment phenomena. In fact, the orientation relationships only reflect the corresponding lattice relationship between the parent phase and the new phase. However, this crystal relationship is usually macroscopical, it can not reflect the real structure and its evolution of the interface between the parent phase and the new phase, and it can not reflect the way of atomic migration, either. It has been found that there all exist K-S relationship in the martensite, bainite, pearlite, and Widmanstatten

microstructure, but they have a completely different phase transformation mechanism, moreover, the way of atomic displacement in them is not the same either. Therefore, the only way of the orientation relationship can not fully reflect the micro-mechanisms of the phase transformations and the actual movement of atoms, which lacks of experiment and theoretical basis. Moreover, there has no new progress and breakthrough in the shear models in recent 30 years and the study comes to a standstill, the vital reason of which is that they cannot withstand the test of practice.

IV. DRIVING FORCE OF MARTENSITE TRANSFORMATION IS NOT ENOUGH TO SHEAR

A. *Energy consumption of shear process*

The needed stress to make the crystal shear is expressed as $\tau = G\cdot\gamma$, in which G is elasticity modulus of shear (for Fe, G=81.6 × 10^3 MN/m^2, γ is shear strain (the unit of γ is radian).

According to the K-S model, when γ-Fe transforms to α martensite (0% C), the first shear angle is 19°28' which is equivalent to 0.34 radian, so the calculation of the shear stress is 27.8×10^3 MN/m^2. When the molar volume of martensite lath (V) is equal to 7.5 cm^3/mol[6], the energy consumption of shear calculated is 208×10^3 J/mol, that is the required energy for the first shear according to the K-S model. The second shear angle of K-S model is 10°32', which needs the shear energy of 112×10^3J/mol else. The total energy consumption of the twice shear is 320×10^3 J/mol.

According to the Western Hills shear mod, only the first shear occurs which is identical with that of the K-S model. The required shear energy is 208×10^3 J/mol.

For the G-T model proposed in 1949, an average shearing displacement measured according to the surface relief effect is 10.75°, so the energy consumption of the shear is 115×10^3 J/mol. The second shear of the G-T model is twin of 12 ~ 13 ° on the $(112)_M$ plane of martensite, then the second shear is 133×10^3 J/mol. The total shear energy is 248×10^3 J/mol.

It is clear that a great deal of energy is consumed after the completion of the shear for the above shear models. However, after the shear, the actual martensite lattice is not yet obtained. So the lattice parameter needs to be adjusted, which also needs the movement of atoms and needs energy consumption further. It is visible that these shear models just take account of the change from face-centered cubic structure to body-centered structure (but not body-centered cubic), without attention of the source of energy and the amount of phase transformation resistance.

B. *Strain energy caused by shear process*

Aaronson calculated the strain energy (Wε) caused by the shear process using the following equation [5]:

$$W_\varepsilon = \frac{E(\varepsilon_{13}^T)^2}{1+\nu}\cdot\frac{\pi(2-\nu)V}{4(1-\nu)}\cdot\frac{c}{b} \quad (1)$$

In the equation, E is elastic modulus, ε_{13}^T is shear straintensor free of stress, ν is Poisson's ratio, V is the molar volume of bainite ferrite lath, and c/b is the ratio of thickness and length. The shear strain energy calculated is about Wε=1400 J/mol (350℃) when using c/b＝0.02 and ε_{13}^T ＝0.18.

Elastic modulus E is related to the temperature. The value of elastic modulus increases with the decrease of phase transformation temperature, and then the shear strain energy (Wε) will increase. When the elastic modulus of 45Cr steel (Ms = 360℃) at 350 ℃ (E)is taken as 21020 KG/mm^2, the molar volume of martensite laths (V) is taken as 7.5 cm^3/mol, the ratio of thickness and length (c/b) of lath martensite is still taken as 0.02 and Poisson's ratio (ν) is taken as 0.3, and then they are substituted into formula (1), the shear strain energy calculated is 1468 J/mol. For the convex-lens-shaped high-carbon martensite, when c/b is 0.1, Wε calculated is 7340 J/mol. It is obvious that the strain energy caused by shear is too high.

C. *Stored energy of crystal defects and strain energy of volume expansion*

A large number of crystal defects come into being during the process of martensitic transformation, such as high density dislocation and fine twin, and these sub-structures have high stored energy. In addition, when austenite transforms to martensite, the specific volume increases, the volume expansion energy can be caused.

Assuming the energy required for the formation of dislocations and twins in the internal martensite is Γ_d and Γ_t respectively, the energy required for the formation of dislocations in the austenite around martensite is Γ_d and the interfacial energy (and the surface energy) is Γ_s, then $\sum\Gamma=\Gamma_s+\Gamma_d+\Gamma_t$. Based on the literature [5], the storage energy of crystal defects of martensite is total as 202 cal / g atom, or 845J / g atom.

To sum up, if martensite transformation is a shear process, the phase transformation will encounter the resistance including the shear strain energy, the stored energy of the crystal defects due to the phase transformation, such as high density dislocations, stacking faults, fine twin, and the volume expansion energy.

D. *Driving force of martensitic transformation*

The driving force of martensite transformation in Fe-C alloy was calculated in Reference [4], and the critical driving force of martensite phase transformation in pure iron is about 1.18×10^3 J/mol, while the driving force of martensite phase transformation in Fe-C alloy of (0.4~1.2)%C is 1.337~1.714 × 10^3 J/mol.

Compared with the resistance of martensite transformation in accordance with the K-S model, the Western Hills model and G-T model, it is clear that the driving force is too small to overcome the resistance to shear.

V. NEEDS OF RESEARCH ON NEW MECHANISM OF MARTENSITE TRANSFORMATION

Martensite transformation needs a great deal of energy according to the mechanism of shear. The driving force of the phase transformation calculated by the current methods is too small to complete the shear process.

Until now, the shear process of martensite lath is not directly observed by any detection equipment. The only so-called evidence is the surface relief. While the experimental study shows that the surface relief is the result of the volume expansion in phase transformation, which is not caused by shear. All shear models are inconsistent with the habit plane of martensite and the substructure, such as high-density dislocations, twins and stacking faults. These shear models have not been significantly improved during several decades.

At the higher temperature range, the phase transformation of the supercooled austenite is eutectoid decomposition, in which the formation of pearlite is the interface diffusion of atoms [7]. In the middle temperature region of bainite transformation, carbon atoms can diffuse by long term, but the iron and the replacement atoms is hard to diffuse. In order to complete the transformation from the over-cooling austenite to bainite with lower free enthalpy, the iron and substitutional atoms at the interface transit from the parent phase into the new phase by heat thermal activation transition of non-cooperative to realize the restructuring of the lattice and transform into Bainite. However, by the control of carbon atoms long-term diffusion, the transformation is very slowly. So bainite transformation neither diffuses nor shears [8-9]. At the lower temperature region of martensite transformation, the displacement of carbon atoms and iron atoms is in the way of no diffusion. However, this displacement is not a simple shear process. The only shear can not achieve crystal lattice parameter and substructure of martensite crystal. So it is necessary to study the new mechanism of martensite phase transformation.

VI. CONCLUSIONS

(1) Compared with the surface relief of pearlite, widmanstatten and Bainite, the surface relief of martensite has no special nature and the shape of the relief is the tent type (∧). Therefore, the shear mechanism of martensite transformation lacks of experimental evidence.

(2) No shear model can fully conform to reality. It is short of experimental and theoretical basis to design the shear models only by orientation relationship. So the shear mechanism is not mature.

(3) The required energy of the shear process according to the K-S model, the Western Hills model or G-T model is very great which is far more than the driving force of martensite transformation.

(4) Martensite transformation in steel is a process of the coordinated displacement of carbon and iron atoms without diffusion, which is not a mechanical shear process. It is necessary to study the new mechanism of martensite phase transformation.

REFERENCES

[1] Xiaoping Lin, Yong Zhang, Nanju Gu, et al, "AFM observation and quantitative analysis of γ（fcc）→α（bcc）martensitic surface relief," Transaction of Materials and Heat Treatment, vol. 22, no. 4, pp. 4-9, February 2001.

[2] Zongchang Liu, Baoyu Duan, Haiyan Wang and Huiping Ren, "Morphology and formation of the surface relief of pearlite," Metal heat treatment, vol. 34, no. 1, pp. 24-28, January 2009.

[3] Baoyu Duan, Zongchang Liu, Huiping Ren, et al, "Surface relief in T8 steel," Journal of Inner Mongolia University of Science and Technology, vol. 27, no. 2, pp. 108-114, June 2008.

[4] Zuyao Xu, Martensitic transformation and martensite (2nd edition). , Beijing: Science Press, 1999.

[5] Zongchang Liu, Quenching crack and prevention of steel (2nd edition). , Beijing: Metallurgy Industry Press, 2008.

[6] Zuyao Xu, Martensitic transformation and martensite (1nd edition). , Beijing: Science Press, 1982.

[7] Liu Zongchang, "Recent evolution of pearlite transformation theory," Metal heat treatment, vol. 33, no. 4, pp. 1-8, April 2008.

[8] Zongchang Liu, Haiyan Wang and Ren Huiping, "Investigation of bainite ferrite nucleation mechanism," Transaction of Materials and Heat Treatment, vol. 28, no. 1, pp. 53-58, February 2007.

[9] Zongchang Liu, Haiyan Wang, Yufeng Wang, et al, "Morphology and formation mechanism of bainitic carbide," Journal of Material Heat Treatment, Transaction of Materials and Heat Treatment, vol. 29, no. 1, pp. 32-37, February 2008.

2011 International Conference on Mechanical, Industrial, and Manufacturing Engineering
Lecture Notes in Information Technology Vols. 1-2

Towards a decentralized coordination in an agent-based approach for flow-shop manufacturing system

Noria Taghezout
ORAN University, Algeria
IRIT- Toulouse University, France
taghezoutnour@yahoo.fr
Noria.Taghezout@irit.fr

Seddik Reguieg
ORAN University, Algeria
rseddiko@hotmail.com

***Abstract*— Multi-agent system (MAS) design has emerged as a powerful approach to perform tasks or solve problems in a decentralized environment. In this paper, we address the problem of achieving coordination in a flow-shop manufacturing system. Without such coordination, potential conflicts among the agents can become obstacles in the implementation of the system and lead to total disorder. Agents communicate through the JADE platform, which includes many predefined performatives to aid the participating agents in carrying out their different tasks. The proposed model consists mainly of five components: Resource Agent, Interface Agent, Supervisor Agent, Data Manager Agent and Coordinator Agent, and a coordination protocol which ensures the exchange of messages among them. Agents interact to solve problems of resource allocation, conflict management, and better reaction during a resource's failure. The coordinator agent has learning features that facilitate decision-making in the system. A simple scenario is given to illustrate the feasibility of our approach.**

Index Terms - Multi-Agent Systems (MAS). Coordination. coordination protocols. JADE platform. flow-shop manufacturing system.

I. INTRODUCTION

In the classical flow-shop problem, a set of jobs (tasks) flow through multiple stages in the same machine order, where each stage consists of only one machine.

An ordinary flow-shop model is a multi-stage production process, where the jobs have to visit all stages in the same order, whereas a flexible flow-shop model, a generalization of the classical flow-shop model, is more realistic, and it assumes that at least one stage must have multiple machines. Moreover, a machine can process at most one job at a time and a job can be processed by at most one machine at a time. Preemption of processing is not allowed. The problem consists of assigning the jobs to machines at each stage and sequencing the jobs assigned to the same machine so that some optimality criteria are minimized [22].

In a real world situation, it is common to find newer or more modern machines running side by side with older and less efficient machines. Even though the older machines are less efficient, they may be kept in the production lines because of their high replacement costs. The older machines may perform the same operations as the newer ones, but would generally require a longer operating time for the same operation. In this paper, the flexible flow-shop problem with unrelated parallel machines is considered.

A detailed survey for the flexible flow-shop problem has been given by Linn and Zhang (1999) and Wang [21]. Most researchers develop existing heuristics for the classical flexible flow-shop problem with identical machines by using a particular sequencing rule for the first stage.

Regarding the issue of agent integration in flow-shop systems, we cite for example the work described in [25]. The authors considered here, the feasibility model of multi-agent scheduling on a single machine where each agent objective function is to minimize the total weighted number of tardy jobs. Lee et al. (2009) discussed a multi-agent scheduling problem on a single machine in which each agent is responsible for its jobs and wishes to minimize the total weighted completion time of its own set of jobs [23].

Leitao (2009) surveyed the literature in manufacturing control system using distributed AI techniques. He also discussed the reasons for the weak adoption of these approaches by industry and pointed out the challenges and research opportunities for the future [24].

Production systems have complex interactions among tasks that require material flow and other coordination. In addition, the unexpected event such as demand variation and processing delay due to machine down time cause the system to become unstable. Solutions among entities become infeasible and need more coordination.

As a result, it can be difficult for a centralized control/scheduling approach to achieve its objective in highly dynamic and chaotic systems. To meet the need of communication and coordination between entities in the environment, a distributed scheduling algorithm has been developed in which the coordination mechanisms are adopted to resolve the conflicts or simple interactions, in this paper.

The remainder of this paper is organized as follows: In Section 2, we introduce our study, starting by a short background on the coordination approaches, then we'll present a general description of our prototype, the structure of our coordination protocol, and algorithms that solve some resource allocation problems. A scenario is given in Section 3 to illustrate the feasibility of the proposed approach. Some concluding remarks are given in Section 4.

II. PROPOSED APPROACH

In multi-agent systems, coordination can be expressed by different techniques, which are summarized in: coordination languages, coordination algorithms and coordination protocols. Several works have appeared in the field of coordination [14] [15] [16] which propose solutions that can provide consistency in production systems. Among those works, we can cite [13]; this approach is a centralized one. It is composed of a single agent which is responsible of the system coordination. This is on the one hand but on the other, several architectures [17] based on the distributed

aspect were developed in order to provide a large number of interactions. We have developed a hybrid architecture where we shared the coordination tasks among agents and agent resources coordinator. The goal is to make the system more flexible, reactive and produce a quick execution.

In this section we present a general architecture of our multi-agent system, the internal structures of our agents, our coordination protocol and some algorithms that solve some problems of dynamic production management such as resource allocation, conflict management, information retrieval and response to resources failures.

A. *General architecture of our prototype*

The proposed system mainly includes five components: Resource Agent (RA), Coordinator Agent (CA), Supervisor Agent (SA), Interface Agent (IA), Data Manager Agent (DMA). With each agent processing capabilities and reasoning, communication and coordination is managed by the coordinator Agent (CA). As shown in Fig. 1, the general architecture is:

1) Resource Agent (RA): It interacts directly on the resource, each agent is responsible for a resource (Fig. 2). The RA has the following components:

- A Database (DB) contains dynamic data; the most important for our study can be summarized in status data, resource status (normal, breakdown, repairing etc.), data of current executing scheduling.
- A Knowledge Base: contains the knowledge and rules and provides the needed scheduling and production information.
- Interface Module: is a graphical interface that is used to control the resource management messages and interacting with different parts of the system.
- Control Module: controls the tasks of each agent.
- Coordination Module: It performs the coordination process, and processes the received messages.

2) Coordinator Agent (CA) : It performs tasks such as resource allocation, task allocation, scheduling and priorities management. It also provides useful information for various agents as required. CA has the same structure as RA, with 03 additional modules. Fig. 3 gives a description :

- Decision Module: is applied when each agent evaluates the alternative solutions. It considers all related attributes of the given task and gives a utility assessment to represent the satisfaction level of a proposal.
- Learning Module: it contains the learning algorithm (Case-Base Reasoning), which is used to enrich the database with new cases of deadlock and failures encountered during the execution of the coordination process.
- Prevention Module: It contains procedures for preventing failures and deadlock using the cases already recorded by the Learning Module.

3) Interface Agent (IA) : It is responsible for managing all the interface modules of other agents. It has an interface for viewing results and messages exchanged between agents, it gives glimpses of other interfaces and controls access to the system.

4) Supervisor Agent (SA): It checks if there is no breakdown or blockage via Monitoring Module.

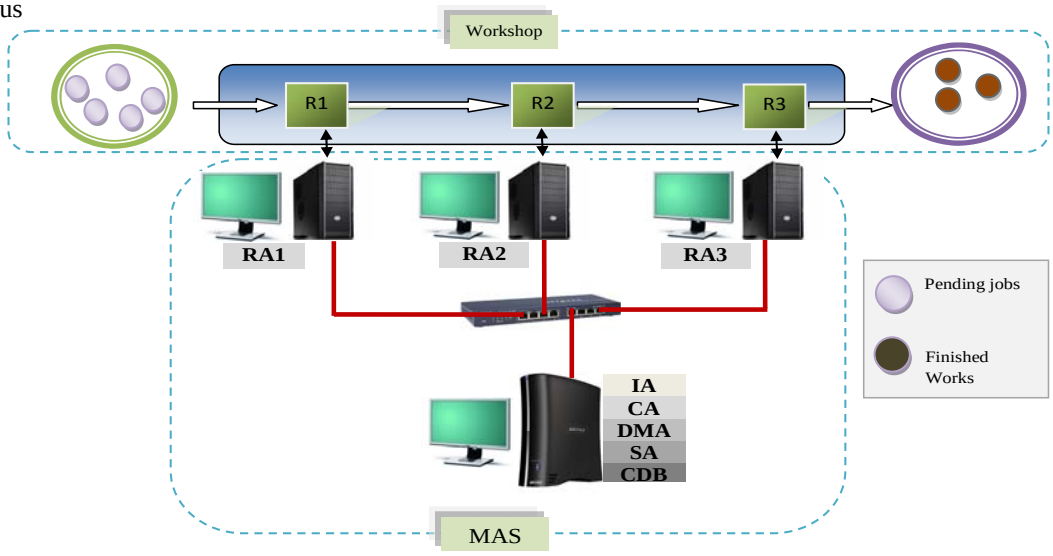

Fig. 1 General architecture of our prototype.

The AS's internal database (DB) contains a table where it records the history of supervision made by the agents, and another that contains the performance of each agent calculated with Performance's Evaluation Module. Interface Module is a graphical interface that displays the different supervisions, alerts and warnings in case of blockages or breakdowns during production process (See Fig. 4). Performances of each agent are calculated as in (1):

$$Per(A_i)=NE/NR*100 \quad (1)$$

Per (A_i): A_i Performance Agent.

NE: number of messages sent from SA to the agent A_i.

NR: Number of message received by SA from agent A_i.

5) Data Manager Agent (DMA): **c**omprises, manages and updates databases.

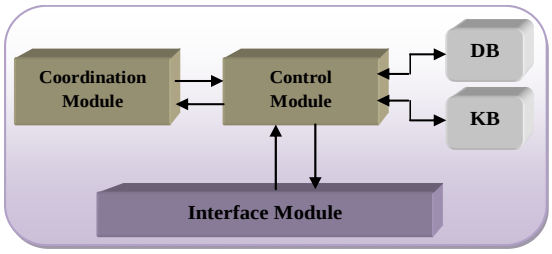

Fig. 2 Internal architecture of the Resource Agent.

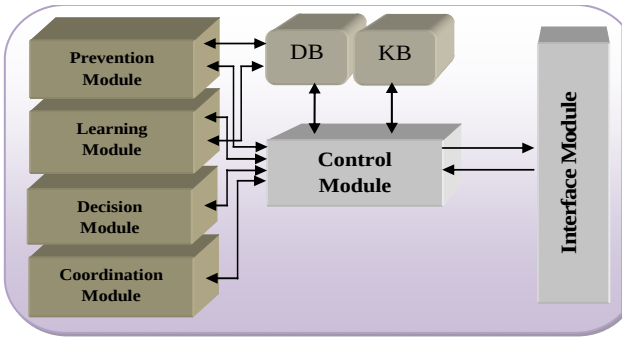

Fig. 3 Internal architecture of the Coordinator Agent.

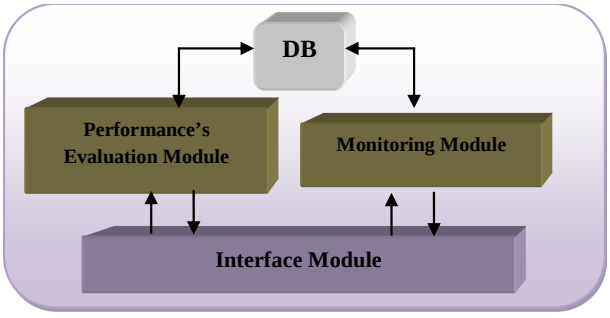

Fig. 4 Internal architecture of the Supervisor Agent.

B. Our protocol

An agent sends a message in two cases: (i) When receiving a message that needs an answer; and (ii) When executing an action . Each message sent of our protocol is designed using the language Communication FIPA-ACL [18].

C. Towards a decentralized coordination : new algorithms

The advantage of the proposed approach is that it can prevent the blockage of the whole system, and increase the operating efficiency. Moreover, the multi-agent platform allows the message transfer and coordination among agents through the communication language, or through the coordination mechanism. The Coordinator Agent is the heart of our architecture; it provides reasoning capabilities according to Case-Based Reasoning (CBR) paradigm. As mentioned in [26], CBR is able to utilize the specific knowledge of previously experienced, concrete problem situations (cases). Here, a case consists at least of a problem description (e.g. symptoms, faults) and a solution (e.g. a therapy or an action of cure). The Prevention Module is in permanent execution to prevent failures and deadlocks already encountered. The phases in the resource allocation algorithm are summarized in Fig. 5. Whereas the system response to failure is described in Fig. 6.

III. ILLUSTRATION

The software developed includes two parts: the JADE platform for the multi-agent system (MAS) environment, and the model developed under Borland Jbuilder. The Data Base management is implemented by using MySQL server. The agents communicate through the JADE platform, which includes many predefined performatives to aid the participating agents in carrying out their different tasks.

In this work, Sniffer Agent provided by JADE was employed to monitor the communication among agents on the agent platform. Fig. 7 shows the communication during the analysis and coordination phases. The CA receives two requests for an allocation of a resource R from the RA1 and RA2, it asked the Supervisor Agent (SA) to provide the performance of the two agents, and then it evaluates two performances. Agent RA1 has the highest performance; in this case the CA accepts the allocation request for agent RA1 via the performative "AGREE" and refuse the request of RA2 via the performative "REFUSED".

```
1 - Repeat
2 - Reception of allocation requests of resource Ri from Resource Agents
3 - TasckList[] = list of tasks performed by agents which request the
allocation
4 – Identifying the status of the resource Ri
5 – Identifying of Case"C" / / collect all parameters of the case
6 - Search for C in the DB of cases already encountered
7 - Queue[] = List of resources identical to Ri
8 - If (Ri.State == Failure)
      All requests are rejected with suggestion Queue[]
   Else
      If (Ri.State == busy)
        Identification of the release time of the resource
        D = duration of the release of the resource
        Send Callback of request resource after D
      Else
         If (C exists in base case)
           Allocation done for the agent cited in case C
        Else
            / / According to the tasks' priorities
          TaskList[] = MaxPriority(TaskList[])
          If (TaskList[] contains one record)
            Allocation done for the agent which hold TaskList[]
          Else
              Identification of agent's performances
            / / Acording to the agents' performances
            TaskList[] = MaxPerformance(TaskList[])
            If (TaskList[] contains one record)
              Allocation done for the agent which hold TaskList[]
            Else
               ListePos [] = Position of tasks TaskList[] in the schedule
              If (NbreMax [ListePos[]]== 1)
                Allocation to the later task
              Else
                TaskList[] = MaxStockOutstanding(TaskList[])
                / / ressources' stock outstanding (input stream))
                If (TaskList[] contains one record)
                  Allocation done for the agent which hold TaskList[]
                Else
                   Random between TaskList[]
10 - Save the new case C'
11 - Until agent-terminate-work
```

Fig. 5 Resource allocation algorithm.

IV. CONCLUSION

We propose in this paper, a coordination protocol for a multi-agent system applied to dynamic production management. This decentralized approach involves each agent in the environment having the necessary information

to make autonomous decisions, while a common goal is reached through cooperation among the community. We intend to apply our system to INOTIS campany which is located in ORAN city (Inotis wants to be an international front-runner in the development, marketing and production of spunlace nonwovens for critical environments where contamination control is of vital importance). A future research direction is to integrate other performance measures of each agent and perform other experiments on hybrid flow-shop production system.

```
1- Resource « R » of resource agent RAi broke down
2- Update internal database of RAi
3- Request the DMA to update the Central DataBase (CDB)
4- Identification of the failure P
   If (repair procedure known and repair time is short)
     LocaleRepair() ;
   Else
     Search resources identical to R
     Queue[] = queue resources identical to R
     If (Queue[] != Empty)
       Request to agents which hold Queue[] the duration and the repair
procedure of failure P
       Duree[]= repair time
       Queue[]=QueueMaxTime(Queue[],Duree[])
       D=Duree;
       If (D is short)
         LocaleRepair() ;
       Else
         Request to Coordinator Agent CA to choose between agents
which hold Queue[]
         If (Choice is received)
           Agent_orient=Choice_received;
           If (OrientationProduction(RAi, Agent_orient,D) == true)
             Successful Orientation
           Else
             Orientation refused
         Else
           Wait() ;
   Else
     There is no agent holding a identical resource
     Apply a new maintenance procedure to a new failure
     Update the internal DB of RA with the new failure
```

Fig. 6. Response to a resource failure algorithm.

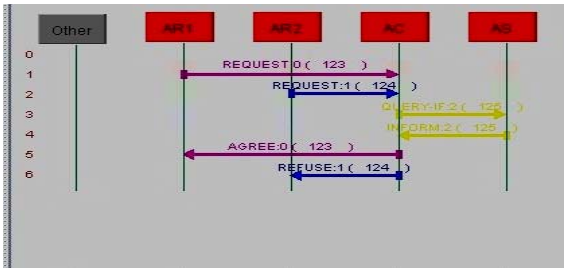

Fig.7 JADE's sniffer results.

REFERENCES

[1] Brînzei N., Drăghici G., Ferney M., Zerhouni N. - «L'état de l'art sur la conduite des systèmes flexibles de production», A VIII-a Conferinþă internaþionalã de inginerie managerialã oi tehnologicã Tehno'98 1998, vol 2, p.261-268.H.

[2] Adamou M., « Contribution à la modélisation en vue de la conduite des systèmes flexibles d'assemblage à l'aide des réseaux de Petri orientés objet », Thèse de doctorat, Université de Franche-Comté, 1997.

[3] Kouiss K., Pierreval H. « Systèmes multi-agents : directions actuelles pour La productivité dans un monde sans frontières», Congrès International de Génie Industriel de Montréal 2029-2038.

[4] Ferber J., «Les systèmes multiagents : vers une intelligence collective», InterEdition, 1995.

[5] Greaves M., Holmback H., Bradshaw J., « What is Conversation Policy ?», in F. Dignum, M. Greaves (eds), Issues in Agent Communication, Springer-Verlag : Heidelberg, Germany, p. 118-131, 2000.

[6] Koning J.-L., « Operational Semantics Rules as a Computational Coordination Mechanism in Multi-Agent Systems », International Journal on Intelligent Control and Systems, vol. 2, n± 12, p. 167-178, 2007.

[7] Charif Y., « Chorégraphie dynamique de services basée sur la coordination d'agents introspectifs », Thèse de doctorat, Université Pierre et Marie Curie Paris VI.

[8] Malone T., Crowston K., « The interdisciplinary study of coordination », ACM Comput. Surv., vol. 26, n± 1, p. 87-119, 1994.

[9] Shehory O., Kraus S., « Feasible Formation of Coalitions among Autonomous Agents in Nonsuperadditve Environments », Computational Intelligence, vol. 15, p. 218-251, 1999.

[10] Caillou P., Aknine S., Pinson S., « A Multi-Agent Method for Forming and Dynamic Restructuring of Pareto Optimal Coalitions », Proc. of the 1st International Joint Conference on Autonomous Agents and Multiagent Systems (AAMAS), ACM Press, New York, NY, USA, p. 1074-1081, 2002.

[11] Durfee E., «Coordination of Distributed Problem Solvers», Kluwer Academic Publishers, Norwell, MA, USA, 1988.

[12] Gelernter D. et Carriero N., Coordination Languages and Their Significance.Communications of the ACM, n°35(2), pp. 96-107, 1992. (Ch. 1)

[13] Francisco, P.M. and Douglas, H.N. (1996) 'Multi-agent mediator architecture for distributed manufacturing', *J. of Intelligent Manufacturing*, Vol. 7, pp.257–270.

[14] Sikora, R. and Shaw, M.J. (1998) 'A multi-agent framework for the coordination and integration of information systems', *Management Science*, Vol. 44, pp.65–78.

[15] Blecker, T. and Graf, G. (2003) 'Multi agent systems in internet based production environments-an enabling infrastructure for mass customization', Paper presented at the *Second Interdisciplinary World Congress on Mass Customization and Personalization* (pp.1–27). Munich, Germany. In proceedings.

[16] Liu, S. and Young, R.I.M. (2004) 'Utilizing information and knowledge models to support global manufacturing co-ordination decisions', *Int. J. of Computer Integrated Manufacturing*, Vol. 17, pp.479–492.

[17] Wang, D., Nagalingam, S.V. and Lin, G.C.I. (2005) 'Development of an agent-based Virtual CIM architecture for small to medium manufacturers', *Robotics and Computer-Integrated Manufacturing*, forthcoming, doi:10.1016/j.rcim.2005.09.001.

[18] The FIPA ACL Message Structure Specifications. http://www.fipa.org/specs/fipa00061/, 2002.

[19] Jérôme Euzenat. A protocol for building consensual and consistent repositories. Rapport de recherche 3260, INRIA Rhône-Alpes, Grenoble (FR), septembre 1997, 46p.

[20] J.L. KONING and S. PESTY: Modèles de communication, in "Principes et architectures des systèmes multi-agents", édité par Jean-Pierre Briot et Yves Demazeau, Collection IC2, Hermes Science Publications, Paris, 2001.

[21] Wang H., "Flexible flow-shop scheduling: optimum, heuristics, and artificial intelligence solutions". *Expert Systems* **22** (2), 2005, p. 78–85.

[22] Jungwattanakit Jitti., Reodecha Manop., Chaovalitwongse Paveena., Frank Werner. "A comparison of scheduling algorithms for flexible flow shop problems with unrelated parallel machines, setup times, and dual criteria". *Computers & Operations Research, Volume 36, Issue 2, February 2009, p. 358-378.*

[23] Lee K.B., Choi B.C., Leung J.Y.T., and Pinedo M.L., " Approximation algorithms for multi-agent scheduling to minimize total weighted completion time". *Information Processing Letters* **109** , 2009, p. 913–917.

[24] Leitao P., "Agent-based distributed manufacturing control: A state-of-the-art survey". *Engineering Applications of Artificial Intelligence 22*, 2008, p. 979-991.

[25] Cheng T.C.E., Ng C.T., and Yuan J.J., " Multi-agent scheduling on a single machine to minimize total weighted number of tardy jobs". *Theoretical Computer Science* **362**, 2006, p. 273–281.

2011 International Conference on Mechanical, Industrial, and Manufacturing Engineering
Lecture Notes in Information Technology Vols. 1-2

Exploratory Studies on Grain Refinement in Medium Chromium Ferritic Stainless Steel Welds

Muhammed Olawale Hakeem Amuda and Shahjahan Mridha

Department of Manufacturing and Materials Engineering
International Islamic University Malaysia
Gombak, Kuala Lumpur 53100, Malaysia

mwalehakeem@gmail.com & Shahjahan@iium.edu.my

Abstract **- The fusion welding of ferritic stainless steel is associated with several challenges principal among which is the grain coarsening in and around the weld section. This leads to loss in ductility and toughness. It may be possible to improve ductility in the ferritic weld if refined grain structure can be produced. Available literatures indicate that formation of refined grains in weld is promoted by ensuring low net heat input and faster transfer dynamics. This may be achieved by controlling the proportion of arc heat input that is actually delivered to the workpiece or enhancing the solidification process by artificially agitating the weld pool. Addition of elemental powder ex-situ as well as the use of cryogenic cooling offer means for controlling net heat input and ensuring faster cooling from the grain coarsening temperature. In the present work, exploratory studies are conducted on grain refinement in medium chromium ferritic stainless steel weld via ex-situ elemental powder addition and cryogenic cooling. It emerged from the study that grain refinement averaged 40% with cryogenic cooling, 35% with aluminum and titanium, 55%. The refinement from cryogenic cooling is due to the steep thermal gradient provided by the cooling liquid while ex-situ elemental powders provide sites for heterogeneous nucleation of equiaxed grains leading to higher microhardness value which is indicative of greater resistance to flow stress and a measure of strength.**

Index Terms **- Grain refinement, cryogenic cooling, elemental powder, heat input.**

I. Introduction

The growing interest in the use of ferritic stainless steels for structural application in engineering systems is facing some challenges due to the difficulties in producing a defect free weld with acceptable ductility and toughness [1-3]. While it might not be difficult to produce crack free joint in ferritic stainless steel, it is a challenge to fabricate structure with improved ductility. Ductility loss in the ferritics could add up to 35% [4]. This may probably change the fracture mode from dimple-ductile to cleavage-brittle resulting in the loss of effective mechanical properties. The loss in ductility accompanying the fusion welding of the ferritics is due to the high grain coarsening in the grade caused by the weld heat input. Grain size control in weld is often practice to combat the problem.

It may be possible to improve ductility in the ferritic weld if refined grain structure can be produced. Available literatures indicate that formation of refined grains in weld is promoted by ensuring low net heat input and faster transfer dynamics. This may be achieved by controlling the proportion of welding arc heat input that is actually delivered to the workpiece or enhancing the solidification process by artificially agitating the weld pool. Several techniques for ensuring this have been reported in the literature [5-7]. Such techniques include inoculation with heterogeneous nucleants, current pulsing, electromagnetic stirring and vibratory welding, and the addition of elemental powder [5]. More specifically, attempts had been made to refine ferritic stainless steel welds through the introduction of elements with similar atomic diameter as iron such as Al, Cu and V including titanium [6, 7].

The implementation of current pulsing technique in ferritic stainless steel weld provides marginal improvement of about six percent in ductility [4]. In another work, appreciable improvement in weld tensile strength was reported by Reddy and Meshram [8] when magnetic arc oscillation technique was adopted. Villafuerte et al. [9] also reported the formation of equiaxed grain in TIG welded ferritic stainless steel containing different amounts of aluminum and titanium under different conditions of heat input and welding speeds. However, the material used was experimental steel and as such the titanium and aluminum were constitutive rather than elemental. The use of enhanced convective flow in the weld pool via liquid metal chilling has equally been reported to lead to grain refinement in ferritic stainless steel weld [10]. It flows from these reported works that while the addition of elemental powder had provided grain refinement in ferritic stainless steel welds, the technique is only applicable to the second and third generation ferritics and not to the common medium chromium variety approximating the first generation grade. Thus, these elements are deliberately added during the AOD steel making process invariably resulting in a costlier grade. Furthermore, while magnetic arc stirring and liquid metal chilling provides enhanced convective fluid flow in the weld pool to refine the grains, these techniques virtually have no effect on the effective heat input into the workpiece.

Low net weld energy input can be achieved by implementing a heat intervening system that acts as heat sinks and reduce the effective heat that goes into the fusion of the base alloy. A major promise in the envisaged technique is that the peak temperature and the time spend above the grain

coarsening temperature are both reduced thus the grain structure in the weld is controlled.

Virgin elemental powder addition via preplacement technique can assist in ensuring low net heat input during the fusion welding of medium chromium ferritic stainless steel. They not only act as heat sinks but also provide sites for heterogeneous nucleation during post-weld solidification. This enables the formation of fine equiaxed grains with better weld properties. Also, additional cooling through the use of cryogenic liquid improves the cooling rate and can be beneficial for the control of grain size in the weld. These techniques are well practiced procedure in laser melting for surface engineering and welding to control microstructure and properties of laser treated materials [11]. Such techniques have not been reported in the gas tungsten arc welding process. It may be worthwhile to extend these procedures to gas tungsten arc melting process.

In the present work, exploratory studies are conducted into two initiatives for the control of grain structure in GTA welded medium chromium ferritic stainless steel. The first initiative involves the preplacement of elemental titanium and aluminum powders on medium chromium ferritic stainless steel followed by arc melting under gas tungsten torch. The other procedure encompasses the use of liquid nitrogen for cryogenic cooling of the weld pool.

II. MATERIAL AND METHODS

A. *Materials*

Cold rolled 1.5mm medium chromium ferritic stainless steel whose composition is given in Table 1 was used for the study. Virgin 3µm titanium and 15µm aluminum powders of 99.9% purity each were supplied by Rheina Phenols & Chemicals GmbH. Polyvinyl alcohol solution was used as adhesive to clad the powder to the substrate surface. Liquid nitrogen was supplied by Mox-Linde Gases Sdn. Bhd, Malaysia.

TABLE I
CHEMICAL COMPOSITION OF AISI 430 FERRITC STAINLESS STEEL

Material Spec.	Composition											VHN	GS (µm)
	C	Cr	Ni	Si	Mn	Mo	Cu	P	S	N	Ti		
AISI 430	0.12	16.19	-	0.75	1.0	-	-	0.04	0.30	-	-	166.5	5.05

B. *Experimental Procedure*

The stainless steel plate was prepared into test coupons of dimensions 65mm x 25mm x 1.5mm. The substrates were sanded with 300 grit size emery paper, cleaned and oxide de-scaled in acetone. A paste containing different amount of the titanium and aluminum powders were separately prepared in an organic binder solution of polyvinyl alcohol (PVA) and then applied to the substrate. The binder was to ensure effective adherence of the powder to the substrate. The coupons with the moisten paste were oven dried at 60^0C for 30 minutes. Table 2 indicates the ordinary limiting composition of titanium and aluminum in ferritic stainless steel. The extremes of these compositions and the centre points were used to create a three-level powder composition for the exploratory study.

TABLE 2
TYPICAL COMPOSITIONS OF TITANIUM AND ALUMINUM IN FERRITIC STAINLESS STEEL [9]

	Composition (%)	
Element	Min.	Max
Ti	0.25	1.06
Al	0.010	0.11

Direct current autogenous single pass arc melting was used to deposit full bead-on-plate weld track on the prepared coupons in pure argon gas environment. The set-up for the powder preplacement technique is shown in Fig. 1. The elemental powder investigation was conducted using 3-level factorial design with welding speed and amount of powder as the primary experimental variables and type of powder as the categorical variable at a fixed welding current of 90A. The design matrix is shown in Table 3.

Cryogenic weld cooling was investigated by making full bead-on-plate autogenous weld track on acetone pre-cleaned coupons and exposing them to high pressure liquid nitrogen from a Dewar under argon shielding. The welding condition for the cryogenic cooling is presented in Table 4.

Transverse section of the coupons normal to weld direction were cut for metallographic examination and prepared for microstructural observation through conventional metallographic technique. Detailed observations of the microstructure were made using Nikon Epiphot 200 light optical microscopy incorporated with image analysis software.

Vickers microhardness machine was used for measuring the hardness of the weld section at a test load of 500g for a dwell time of 10s.

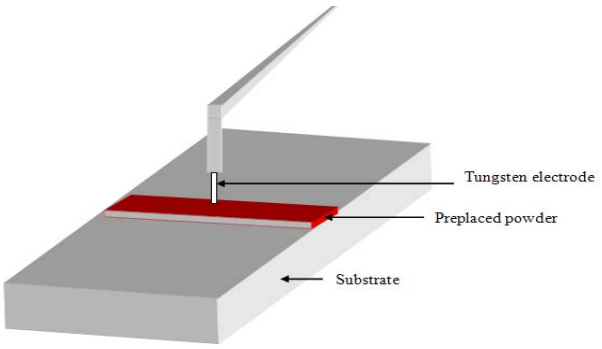

Fig.1 Schematic illustration of TIG torch elemental powder preplacement technique

TABLE 3
DESIGN MATRIX FOR ELEMENTAL POWDER ADDITION

Weld Run	Voltage (V)	Arc Length (mm)	Argon Flow rate (dm^3/s)	Current (A)	Speed (mm/s)	Heat Input (J/mm)	Powder Amount (mg)	Type of Powder
1	30	1.5	0.12	90	1.00	1296	30	Al
2	30	1.5	0.12	90	2.50	518.4	20	Al
3	30	1.5	0.12	90	3.00	432	40	Al
4	30	1.5	0.12	90	1.00	1296	40	Ti
5	30	1.5	0.12	90	2.50	518.4	180	Ti
6	30	1.5	0.12	90	1.00	1296	40	Al
7	30	1.5	0.12	90	3.00	432	30	Al
8	30	1.5	0.12	90	1.00	1296	110	Ti
9	30	1.5	0.12	90	2.50	518.4	110	Ti
10	30	1.5	0.12	90	3.00	432	40	Ti
11	30	1.5	0.12	90	2.50	518.4	40	Ti
12	30	1.5	0.12	90	3.00	432	20	Al
13	30	1.5	0.12	90	3.00	432	110	Ti
14	30	1.5	0.12	90	2.50	518.4	30	Al
15	30	1.5	0.12	90	1.00	1296	20	Al
16	30	1.5	0.12	90	1.00	1296	180	Ti
17	30	1.5	0.12	90	2.50	518.4	40	Al
18	30	1.5	0.12	90	3.00	432	180	Ti

TABLE 4
MELTING CONDITIONS FOR EXPLORATORY CRYOGENIC WELD COOLING

Process	DCEN straight polarity full bead on plate penetration GTA weld
Position	Flat
Melting Conditions	
Current	90A
Voltage	30V
Speed	1, 2.5, 3 mm/s
Arc length	1.5mm
Torch orientation	Vertical
Electrode configuration	2.44mm W-2 pct. Th., 60^0 cone included angle
Electrode stickout	3mm
Cryogenic coolant	Liquid nitrogen
Shielding environment	99.9 pct argon at a flow rate of $0.12 dm^3/s$

III. RESULTS AND DISCUSSION

The microstructure of the base metal is shown in Fig. 2. The microstructure revealed a mixture of fine-grained recrystallized ferrite and chromium carbide precipitate aligned in the rolling direction. The average grain size of the base metal has been determined via Abrams three-circle procedure. The average value is 5.05μm as listed in Table 1.

The heat input in welding is directly related to the heat flux, welding speed and process efficiency. It can be calculated from the relationship given in equation 1[12]

$$HI = \frac{\eta IV}{v} \qquad (1)$$

where η= efficiency, I= current in A, V= voltage and υ= welding speed in mm/s. For the same materials and welding process, the efficiency is constant and for GTA process it is taken as 0.48 [12]. The equation indicates that the heat input can be adjusted with the change of the arc current or welding speed. In the present investigation, a fixed arc current of 90A and different welding speeds have been considered. The heat input conditions with the corresponding primary process parameters are listed in Table 3. These heat input conditions were used to produce control weld tracks for the grain refinement study.

During welding the surfaces of the metals are raised to fusion temperature and the resolidified fused metal is deposited as weld bead. The weld bead dimensions changes proportionally to the energy input. Low magnification stereo microscope of Carl Zeiss make was used to observe the modifications in the weld bead with changes in heat input. The macrographs at the different heat input conditions are shown in Figs. 3a-c. The figure revealed that the weld dimension respond to changes in heat input. There is greater distortion at 1296J/mm than at 518.4J/mm. The figure equally revealed slight broadening at the top side of the weld with increase in heat input. One significant observation in the figure is that the penetration is not affected by the level of heat input. This is probably influenced by the thickness of the specimen, though the heat affected zone (HAZ) as well as the fusion zone (FZ) are greatly affected by the level of the heat input.

The changes in weld dimensions with heat input are presented in Table 5. The table indicates that the largest size of the weld in terms of the FZ and the HAZ occurs at heat input of 1296J/mm. However, there is no significant difference in the weld dimension at the heat input of 518.4 and 432 J/mm. This is probably due to the fact that cooling rate decreases with increasing heat input. Thus, when the heat input is higher, more volume of the metal is melted and the welding heat has more time to play on top the metal particularly at low welding speed. Also, Fig.3a exhibit elongated grains at the top and equiaxed grains at the underside. The grain morphology in Fig.3c is, however, generally equiaxed.

Figs. 4 and 5 are the macrographs of ferritic stainless steel weld produced with different amount of aluminum and titanium powder respectively.

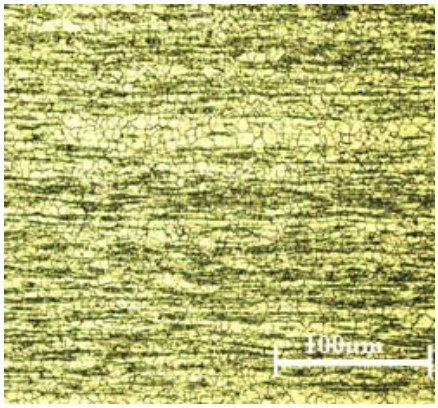

Fig.2 Optical micrograph of the base metal

Fig.3 Cross section macrograph of weld under different heat input (a) 1296J/mm, (b) 518.4J/mm and (c) 432J/mm

Figure 4 revealed that the weld geometry changes with increase in aluminum composition. Furthermore, the penetration of the weld also reduces with increase in the amount of aluminum. For instance, while there is full penetration and slight difference in the weld width between the top and bottom at aluminum content of 20mg (Fig.4a), the penetration is incomplete and the difference between the top and bottom of the weld is wide when the amount of aluminum is 40mg. This is because as the amount of aluminum powder increases greater proportion of the heat input is converted to melt the powder and in the process, the net heat input delivered to the workpiece is less leading to shallow penetration. However, this is effective in producing equiaxed grains in the weld since the reduced heat input implies faster cooling rate. Thus, the time spend above the grain coarsening temperature is reduced. Fig.5 presents the effect of titanium composition on weld geometry. The figure shows that the trend is similar to aluminum but the weld geometry is relatively wider and deeper. This is due to the poor thermal property of titanium unlike aluminum.

The geometry of weld produced under different heat inputs but cooled in liquid nitrogen is shown in Fig.6. The figure revealed the presence of equiaxed grains in all the heat input conditions. The difference in the weld profile relative to Fig. 3 is quite obvious.

Fig.7 shows the comparative evaluation of the effect of cryogenic cooling and elemental powder addition. The figure revealed that both cryogenic cooling and elemental powder addition constricts the weld profile leading to reduced weld dimension particularly the creation of a very narrow band of heat affected zone. However, elemental powder addition appears more effective in this regard. Cryogenic cooling produces an average constriction of 35 percent while titanium and aluminum powders provide an average of 58 and 65

TABLE 5
SIZE OF THE WELD BEAD AT DIFFERENT HEAT INPUTS

Weld Run	Current (A)	Speed (mm/s)	Heat Input (J/mm)	Weld dimension (mm)	
				Fz	HAZ
1	90	1.00	1296	10.82	4.50
2	90	2.50	518.4	6.45	2.44
3	90	3.00	432	5.77	2.27

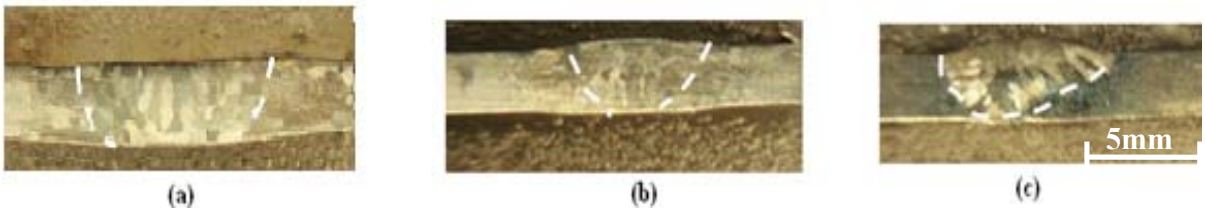

Fig. 4 Cross section macrograph of weld at heat input of 518.4J/mm and different amount of aluminum powder (a) 20mg, (b) 30mg and (c) 40mg

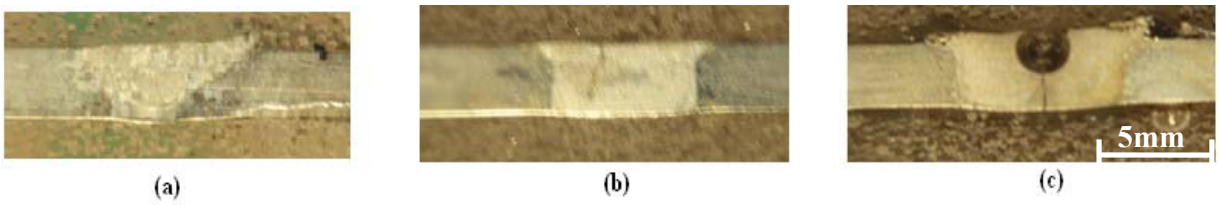

Fig. 5 Cross section macrograph of weld at heat input of 518.4J/mm and different amount of titanium powder: (a) 20mg, (b) 110mg and (c) 180mg

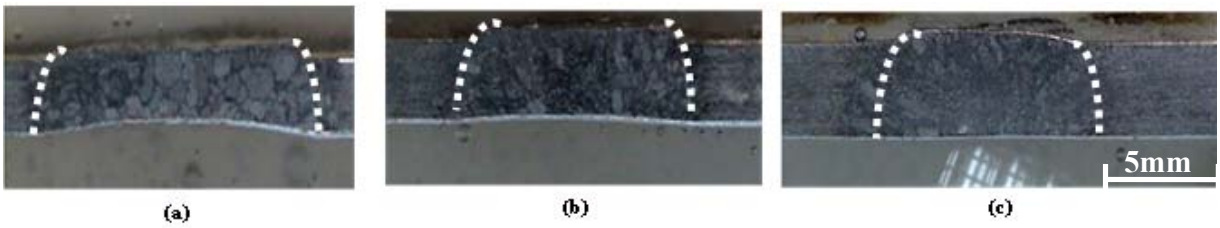

Fig. 6 Macrostructure of welds produced at different heat inputs but cooled in liquid nitrogen (a) 1296 J/mm, (b) 518.4 J/mm and (c) 432 J/mm

percent respectively. The performance of aluminum powder is enhanced due to the better heat transport property of the powder relative to titanium.

The fusion zone microstructure of the weld produced without any external treatment is shown in Fig.8. The microstructure revealed the transition from columnar to equiaxed grains as the heat input reduces. However, the grain structure is generally coarse and elongated in direction normal to the fusion boundary. The apparent equiaxed grains in Fig. 8c are due to the higher welding speed which reduces the time spend above the grain coarsening temperature. Even at that the grains size is still about seven folds larger than the base metal.

However, the use of cryogenic cooling as shown in Fig.9 induce grain refinement with the formation of more equiaxed grains and clearly defined grain boundaries, particularly in Figs 9a and b relative to Figs. 8a and b. The grain refinement observed in the weld is enhanced by the very sharp steep thermal gradient induced by the cryogenic liquid.

Figs. 10 and 11 are the fusion zone microstructure of welds produced with ex-situ addition of aluminum and titanium powders respectively. The microstructure generally revealed formation of refined equiaxed grains in the weld with well defined grain boundary delineation; though Fig. 10a show the presence of columnar grains but the width is narrow unlike in Fig. 8a. Formation of refined grains is promoted in these welds because greater part of the energy input is converted to melt the preplaced powder thus reducing the effective energy available to melt the substrate. Furthermore, these powders acts as nucleation sites for the resolidified weld pool and subsequent grain growth is effectively pinned at the grain boundary. However, the microstructures revealed that grain refinement from titanium powder is better than from aluminum. This is probably due to the higher heat capacity of titanium powder which implies greater latent heat of fusion for titanium (419KJ/Kg) than aluminum (398KJ/Kg)[13] and this effectively generate a lower peak temperature in welds pretreated with titanium producing fusion zone of finer grain structure as shown in Fig. 11. The differential average particle size of the elemental powders could equally have contributed to the grain refinement dynamics. The average particle size of titanium powder is 3 micron while aluminum is 15 micron.

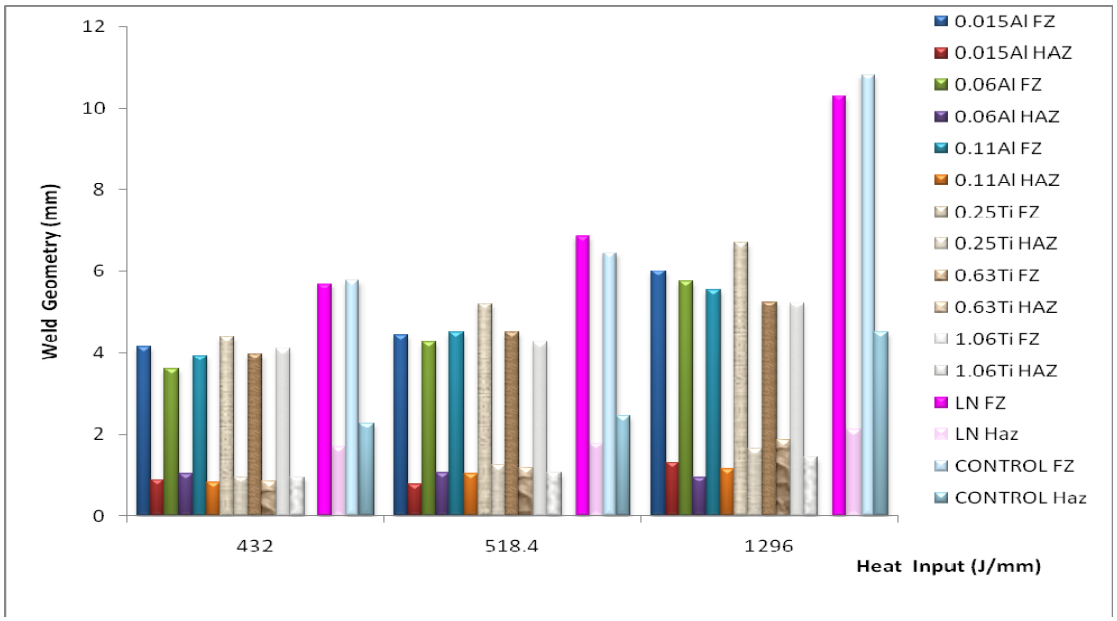

Fig. 7 Effect of liquid nitrogen and elemental powder on weld profile

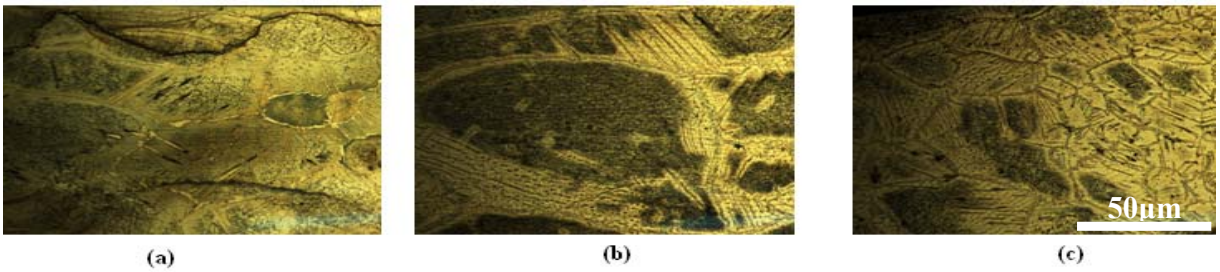

Fig.8 Fusion zone grain structure of weld produced at different heat input condition, (a) 1296J/mm, (b) 518.4J/mm (c) 432J/mm

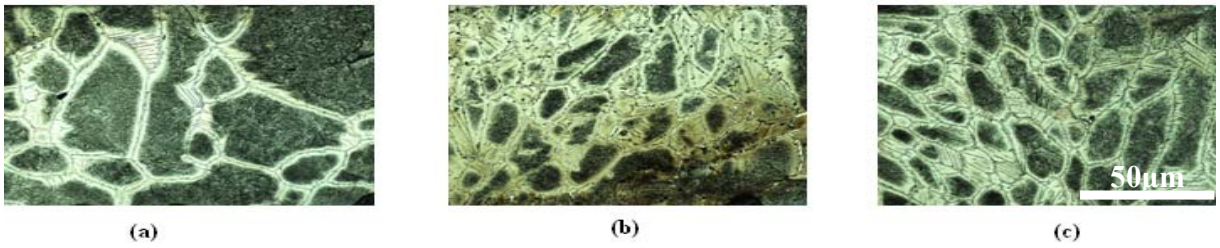

Fig.9 Grain structure of welds produced under different heat conditions but cooled in cryogenic nitrogen, (a) 1296J/mm, (b) 518.4J/mm (c) 432J/mm

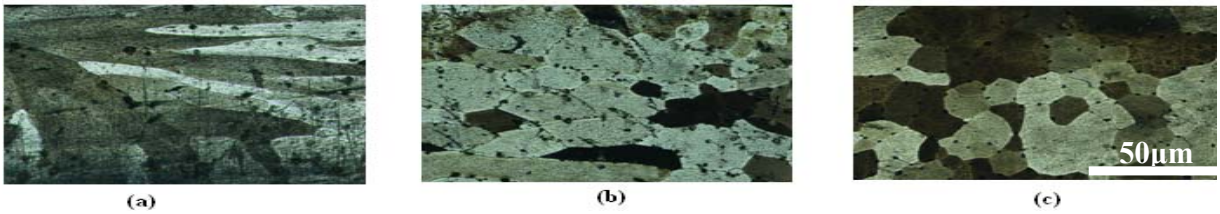

Fig. 10 Effect of aluminum addition on grain structure in welds produced under different heat conditions (a) 1296J/mm, (b) 518.4J/mm (c) 432J/mm

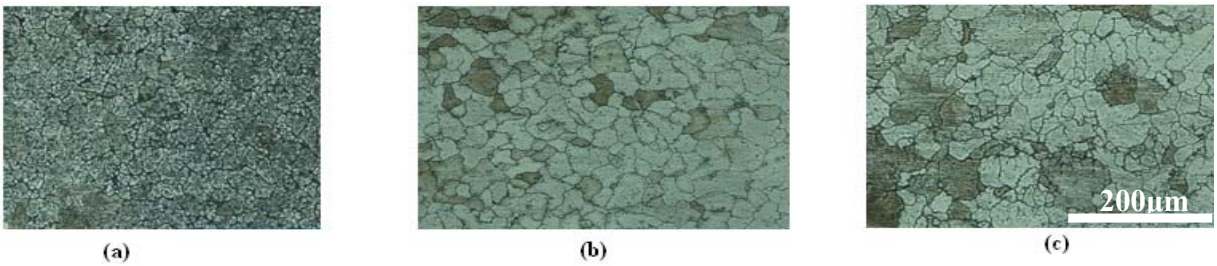

Fig. 11 Effect of titanium addition on grain structure in welds produced under different heat conditions (a) 1296J/mm, (b) 518.4J/mm (c) 432J/mm

The average grain size of the welds produced under various process conditions have been evaluated using Abrams three-circle procedure and the result is presented in Fig. 12. Titanium powder pretreated-welds have the most significant grain refinement attributes with an average of 55 percent improvement relative to the control welds across all energy input conditions. Cryogenic cooling provides 40 percent while aluminum on the other hand presents the least grain refinement of 35 percent on the average. Though, titanium provides the best grain refinement attribute, it, however, also forms cracks in certain spot of the weld microstructure particularly in welds pretreated with 1.06 percent titanium powder. This is shown in Fig. 13 with the indicated arrow. The crack is through the thickness of the weld. The weld microstructure from the other two treatment conditions are however free from cracks.

Microhardness can be used as a measure of resistance to flow stress and an indication of strength. Longitudinal microhardness evaluation of the welds is presented in Figs. 14a-c.

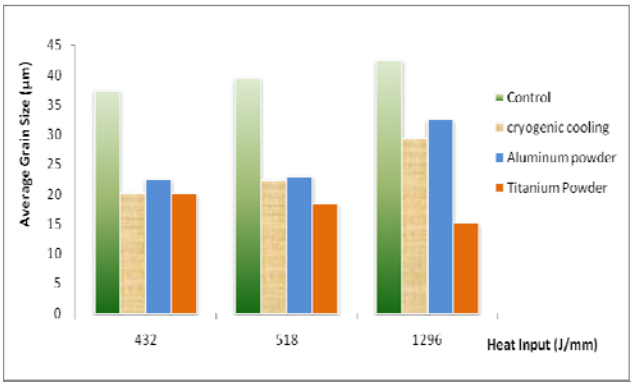

Fig. 12 Effect of elemental powder addition and cryogenic cooling on average grain size of weld

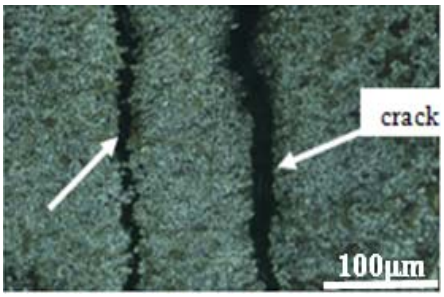

Fig. 13 Cracks in the fusion zone microstructure of welds pre-treated with 1.06wt% titanium powder

The figure indicates that across all energy input conditions, the elemental powder treated weld substrate exhibit higher microhardness value. Specifically, titanium powder produces the highest value. This correlate to the average grain size of the weld in Fig. 12 which shows that titanium powder treated welds produced highest grain refinement. This is indicative of the relative strength of the grain refinement techniques. The figure equally revealed that the base metal is not really affected by the treatment conditions of the weld irrespective of the energy input. However, Fig. 14c indicates discontinuity at three different spots in welds pretreated with titanium powder. This is suggestive of the presence of cracks. Indeed, the existence of cracks in welds made at these conditions is validated in Fig. 13.

Cryogenic cooling ensures grain refinement by enhancing the cooling cycle from the peak temperature thereby effectively shortening the time spends above the grain coarsening temperature. Elemental powder on the other hand control the net energy input into the substrate as well as providing substantial heterogeneous sites for nucleation and growth of equiaxed grains. This apparently explains the mechanisms of grain refinement observed in the two strategies that have been investigated in the present work.

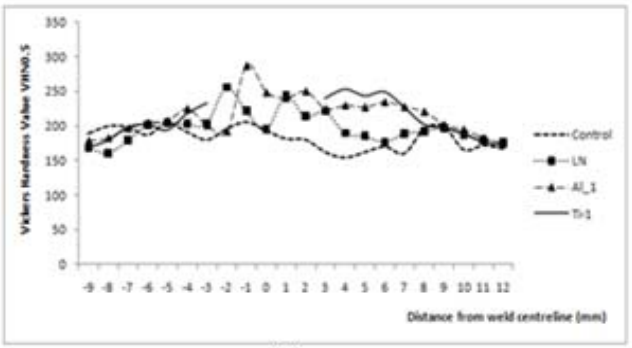

(a)

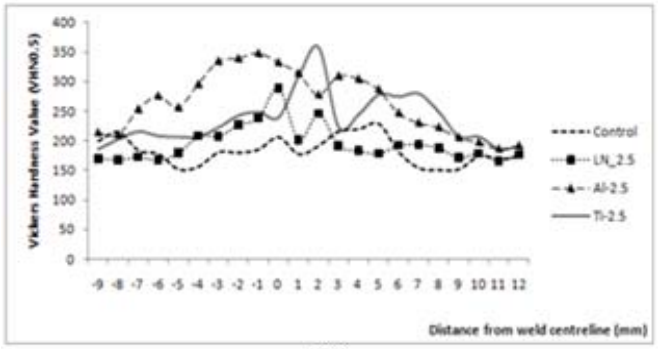

(b)

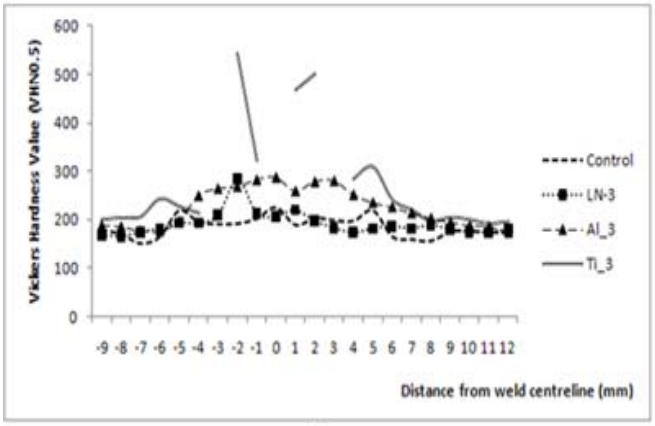

(c)

Fig.14 Microhardness profile across the weld longitudinal dimension at different heat input (a) 1296J/mm, (b) 518J/mm and (c) 432J/mm

IV. CONCLUSIONS

The present investigation has attempted grain refinement in medium chromium ferritic stainless steel weld via cryogenic cooling and preplacement of titanium as well as aluminum elemental powder. The study provides the following findings:

i. The weld penetration is not affected by the level of the energy input probably due to the thickness of the material.

ii. The use of cryogenic cooling and elemental powder preplacement reduces the weld dimension. However for elemental powder addition, the reduction is proportional to the amount of powder preplaced. Titanium powder provides 65 percent constriction in the weld geometry; aluminum is 58 percent while cryogenic cooling provides 35 percent.

iii. Titanium powder pretreated-welds have the most significant grain refinement attributes with an average of 55 percent improvement in grain size relative to the control welds across all energy input conditions. Cryogenic cooling offers 40 percent while 35 percent on the average is recorded with aluminum. While titanium provides the best grain refinement attribute, it, however, also forms cracks in certain spot of the weld microstructure particularly in welds pretreated with 1.06 percent titanium powder.

iv. Microhardness value can be used to approximate the resistance to flow stress and can be indicative of the strength. In the present study, the microhardness value validates that titanium powder treated welds exhibit superior resistance to flow stress.

v. The refinement from cryogenic cooling is due to the steep thermal gradient provided by the cooling liquid while ex-situ elemental powders provide sites for heterogeneous nucleation and growth of equiaxed grains.

ACKNOWLEDGMENT

The authors acknowledge Prof. Hassan Ali Khan, Department of Manufacturing and Materials Engineering, International Islamic University Malaysia, for providing some metal powder used for the exploratory study. Technical assistance from Dyuti Sarker is also acknowledged.

REFERENCES

[1] G. M. Reddy, T. Mohandas, "Explorative studies on grain refinement of ferritic stainless steel welds", *Journal of Materials Science Letters* 20, 721-723, 2001.

[2] K. Shanmugan, A.K. Lakshminarayanan, and V. Balasubramanian, "Effect of weld metal properties on fatigue crack growth on behaviour of gas tungsten arc welded AISI 409M grade ferritic stainless steel', *International Journal of Pressure Vessels and Piping* 86, 517-524, 2009.

[3] T. Mohandas and G.M. Reddy, "A comparison of continuous and pulse current gas tungsten arc welds of an ultra high strength steel", *Journal of Materials Processing Technology* 69, 222-226, 1997.

[4] V. Anbazhagan and R. Nagalakshmi, "Metallurgical studies in ferritic stainless steel weld", WRI Journal 23, 25-37, 2002.

[5] M.O.H Amuda and S. Mridha, "Grain refinement in ferritic stainless steel welds: The journey so far" *Advanced Materials Research*, 83-86, 1165-1172, 2010.

[6] P. Sathiya, S. Aravinda, S. and A. Noorul Haq, "Effect of friction welding parameters on mechanical and metallurgical properties of ferritic stainless steel", *International Journal of Advanced Manufacturing Technology* 31, 1076-1082, 2007.

[7] J. L. Cavazos, "Characterization of precipitates formed in ferritic stainless steel stabilized with Zr and Ti additions", *Material Characterization* 56, 96-101, 2006.
[8] G. M. Reddy and S. D. Meshram, "Grain refinement in ferritic stainless steel welds through magnetic arc oscillation and its effect on tensile property", *Indian Welding Journal* 39, 35-41, 2006.
[9] J. C. Villafuerte, E. Pardo and H. W. Kerr, "The effect of alloy composition and welding conditions on columnar-equiaxed transitions in ferritic stainless steel gas tungsten arc welds', *Metallurgical Transactions* 21A, 2009-2019, 1990.
[10] J. C. Villafuerte, H. W. Kerr and S. A. David, "Mechanism of equiaxed grain formation in ferritic stainless steel gas tungsten arc welds", *Materials Science and Engineering* 194, 187-191, 1995.
[11] R. Braun, "Nd: YAG laser butt welding of AA6013 using silicon and magnesium containing powders", *Materials Science and Engineering* 426, 250-262, 2006.
[12] K. E. Easterling, Introduction to the physical metallurgy of welding (2nd ed). Oxford: Butterworth-Heinemann, 2004.
[13] http://www.engineeringtoolbox.com/fusion-heat-metals-d_1266.html, "Metals and latent heat of fusion", accessed Wednesday 15, December 2010.

2011 International Conference on Mechanical, Industrial, and Manufacturing Engineering
Lecture Notes in Information Technology Vols. 1-2

Design and Analysis of Active Hood Lift System Used for Pedestrian Head Protecting

YE Hui and LU Shanbin
State Key Laboratory of Automobile Dynamic Simulation
Jilin University
Changchun, Jilin Province 130022, China
{yehui & lusb}@jlu.edu.cn

HU Ping*
School of Automotive Engineering
Dalian University of Technology
Dalian, Liaoning Province, 116024, China
pinghu@dlut.edu.cn

***Abstract* - In the car accident casualties, Pedestrian occupied a large proportion of the injuries. Pedestrian protection became a key problem of vehicle safety. The engine hood was the most possible position impacted by head of pedestrian. The pedestrian protection of engine hood was an important performance of vehicle. The active engine hood was used to improve the pedestrian protection performance of vehicle and to meet the regulations. According to the active hood technology that had been developed, a new lift mechanism of hood was developed based on an original vehicle in this research. This lift mechanism could pop up backward and upward at the same time with both front and rear portions of engine hood. The crank rod mechanism was used and it was linked with the hinges of hood in rear portion and lock of hood in front. Spring was used in the front of lift mechanism to protect the pedestrian who crash into the front of hood. The pedestrian protection performance of active engine hood which was installed with designed lift mechanism was analyzed by finite element simulation of headform-to-hood crash. The results were compared with those of original hood. It was shown that the pedestrian protection performance of hood with the designed lift mechanism was improved.**

Index Terms –vehicle, pedestrian protection, active engine hood, lift mechanism, design.

I. INTRODUCTION

In the car accident casualties, pedestrian occupied a large proportion of the injuries[1]. Pedestrian protection became a key problem of vehicle safety. The engine hood was the most possible position impacted by head of pedestrian. Some studies showed that more than 50% of pedestrian fatalities were caused by head injuries and most of them were impacted by engine hood or windshield. The pedestrian protection of engine hood was an important performance of vehicle[2].

In order to avoid the human life loss caused by pedestrian-to-vehicle collisions, many passive and active safety devices to decrease the possibility of head injury has been proposed in industry recently. The active engine hood was one of these devices to be used to improve the pedestrian protection performance of vehicle and to meet the regulations[3].

The active hood system lifted up the rear portion of the hood for a distance at the time when pedestrian-to-vehicle impact happened. This provided a free space between the hood and the hard components underneath the hood. When the head of pedestrian crashed into the pop-up hood, free space underneath the hood would allow the hood to deform and absorb more impacting energy through structural deformation. As a result, the possibilities of head injury could be reduced. The active hood system was mainly composed of lift mechanism and detecting sensor system. The performance of lift mechanism directly affected the pedestrian protection of active hood system.

The lift mechanism of active hood system was used to transmit the motion of actuator to engine hood. This mechanism determined the raising position and height of engine hood. Many types of lift mechanism of active hood system have been developed. Martin Krenn et al. studied the mechanics and kinematics of an active hood and investigated the integration and effects of the active hood in a feasible safety concept of modern cars. A simple mechanism with leaf spring was used to raise the rear portion of engine hood[4], as shown in fig. 1. Kaoru Nagatomi et al. developed a pop-up hood system to reduce the severity of head injuries to pedestrian in pedestrian-to-vehicle accidents. This system employed sensors located on the bumper to detect impact of a pedestrian and raised the rear portion of the engine hood approximately 100mm[5], as shown in fig. 2. Keun Bae Lee et al. developed an active hood lift system and raised up the rear portion of the hood approximately 120mm[6], as shown in fig. 3. These lift mechanism of active hood raised either the rear portion or the front portion of engine hood only.

In this research, a new lift mechanism which could pop up backward and upward with both front and rear portions of engine hood was developed based on an original vehicle. The raising of rear and front portions of engine hood could reduce the possibilities of head injuries more than just raising one portion. Beyond this, the engine hood's raising both backward and upward could cover the windscreen base, windscreen scuttle and wiper spindle where the injury was very severe.

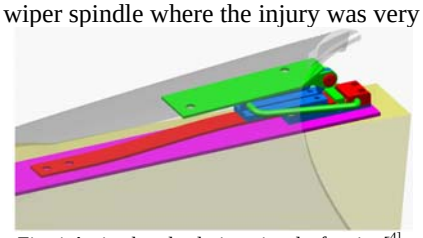

Fig. 1 Active hood solution via a leaf spring[4].

* Corresponding author

Fig. 2 Setup for hood lift operation testing[5].

Fig. 3 Child headform impacting pop-up engine hood[6].

II. THE REQUIREMENT ANALYSIS OF DESIGN

The principle of active engine hood was: firstly, the space underneath the engine hood could be enlarged through the raising of hood. This enlarged the deformation of the hood and avoided hood contact with the hard parts underneath the hood; Secondly, the energy of collision could be absorbed effectively by enlarging the deformation of hood. Thus, the head injury of pedestrian could be reduced to least. According to the principle of active engine hood and the analysis of lift mechanism, the following points should be considered in design of lift mechanism:

(1) The position and direction of raising;
(2) The length of action time of the mechanism;
(3) The height of raising;
(4) Whether the mechanism could be recovered;
(5) The magnitude of modification to the original vehicle.

In order to improve the performance of pedestrian protection system, the pop-up position of hood was located at the rear and front portions at the same time. The pop-up direction of engine hood was backward and upward.

According to time-sequence of pedestrian contact with vehicle, the time from the first contact to the head contact with the hood for the child was 60ms and for the adult was 140ms. In order to reserve adequate time for the trigger of sensor and signal transmission, the motion time of mechanism was set as 40ms.

Experiment of pedestrian-to-vehicle collision showed that the distance between hood and underneath hard parts should be at least 70mm for adult headform and 50mm for child headform to guarantee that the value of HIC was less than 1000. According to this conclusion, the raising height of the front hood portion was set as 50mm and the rear portion 70mm.

The recovery of lift mechanism of hood could save the cost of use and maintenance of active hood system. So the newly designed lift mechanism should be recovered. Because the lift mechanism of engine hood must be assembled to the vehicle, the modification to the original vehicle should be simplified when designed lift mechanism.

III. THE LIFT MECHANISM DESIGN OF ACTIVE ENGINE HOOD

The slider-crank and link mechanism were used as the base of lift mechanism, as shown in fig. 4. The principle of this lift mechanism was that the driving force of actuator drove the slider moving towards the right direction and the hinge of engine hood could do circular motion guided by slider; this raised the rear portion of hood. The lock of hood moved with the link and this raised the front portion of hood. Thus, the engine hood could be raised both backward and upward at the same time and recover alike.

This mechanism was divided into two portions. The front portion was assembled with the lock of hood and the other end was connected with car body. The rear portion was assembled with the hinge of hood and the other end was connected with car body. The modification of lock and hinge of hood were avoided by this design, as shown in fig. 5.

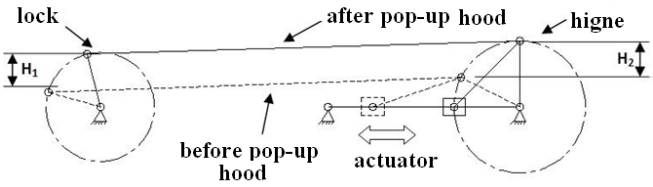

Fig. 4 The slider-crank and link mechanism of lift mechanism.

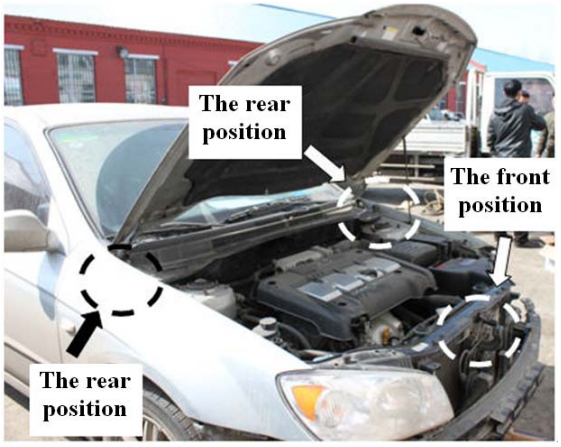

Fig. 5 The position of lift mechanism assembled.

According to the dimension of the original vehicle and the requirement of 50mm front raising and 70mm rear raising space, the length of the crank and the link was calculated, and the angles of the crank with horizontal was also calculated. The fig. 6 showed the calculated dimension of the rear portion of lift mechanism. As can be seen from the fig. 6, the lift

mechanism could raise rear portion 74.12mm and the moving length of end of link need to be more than 96.59mm. In order to improve the pedestrian protection performance of the front of hood where children's heads were impacted, a spring was used in the front portion of lift mechanism.

The CAD models were constructed according to the calculated dimension using CATIA software. The fig. 7 showed the components of the front portion of lift mechanism. The fig. 8 showed the assembly of the front portion. The fig. 9 and fig. 10 were the components and assembly of the rear portion.

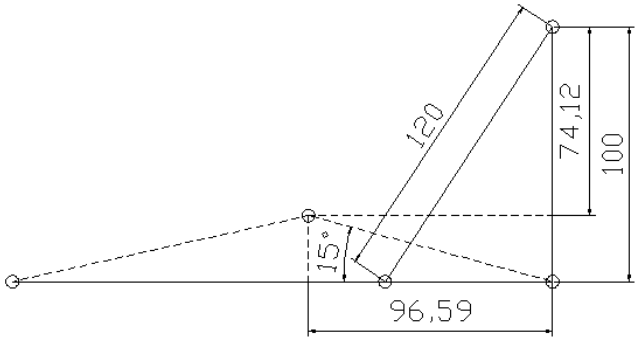

Fig. 6 The dimension of the rear portion of lift mechanism.

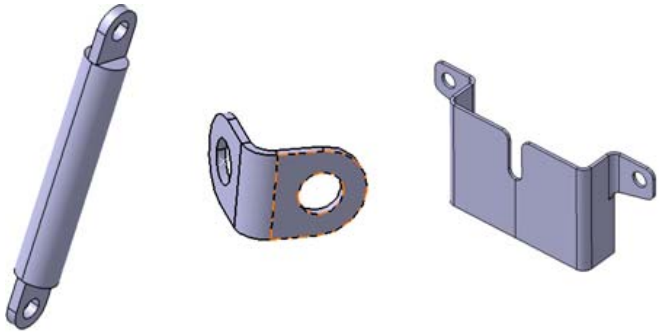

(a) cylinder link (b) connector (c) lock of hood

Fig. 7 The components of front portion of lift mechanism.

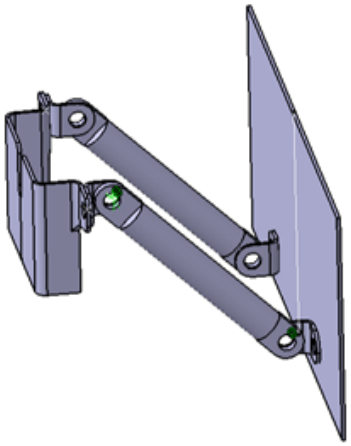

Fig. 8 The assembly of the front portion.

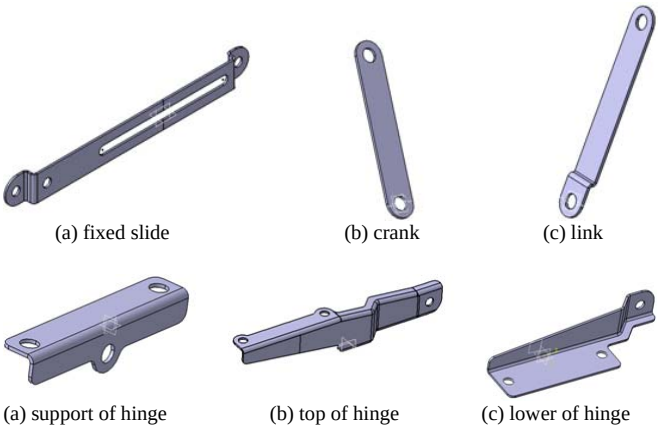

(a) fixed slide (b) crank (c) link

(a) support of hinge (b) top of hinge (c) lower of hinge

Fig. 9 The components of the rear portion.

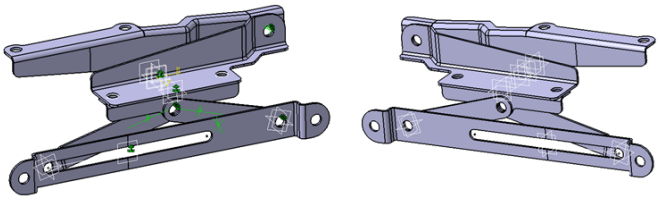

(a) left part (b) right part.

Fig. 10 The assembly of the rear portion.

IV. THE PEDESTRIAN PROTECTION ANALYSIS OF ACTIVE HOOD

In order to analysis the pedestrian protection of the designed active engine hood system, finite element model of lift mechanism was fixed with a Ford Explorer finite element model. The CAD model was saved as iges type file, then was imported into the HyperMesh software to be meshed. HyperMesh was a most constantly used preprocessing software of CAE. The mesh was mainly composed of quad elements and the size of element was set as 5 mm. The fig. 11 showed the finite model element of the front portion of lift mechanism. The fig. 12 showed the finite model of the rear portion of lift mechanism.

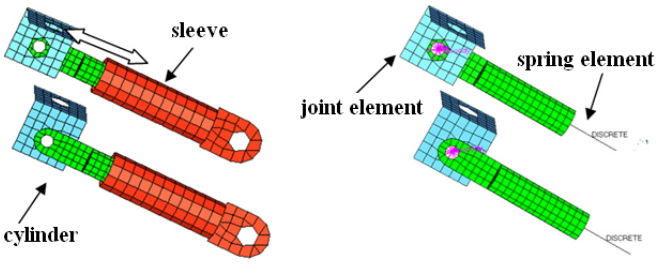

Fig. 11 The finite element of the front portion of lift mechanism

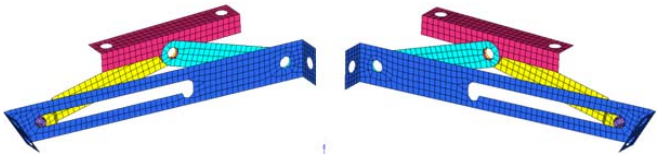

Fig. 12 The finite element of the rear portion of lift mechanism

The finite element model of lift mechanism was fixed on the car body. The fig. 13 showed the assembly of the front portion of lift mechanism of active engine hood system. The fig. 14 showed the assembly of the rear porttion of lift mechanism. While these assemblies were done, some modifications of the original vehicle were necessary. The lift mechanism was connected to the car using revolute joint elements and rigid link elements.

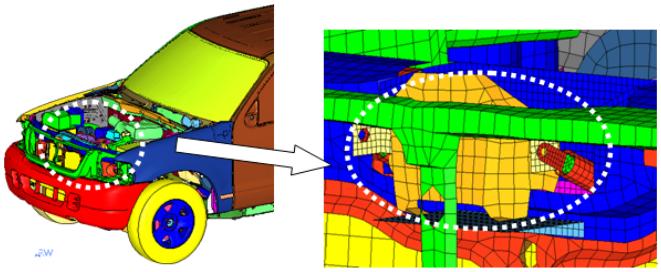

Fig. 13 The assembly of the front porttion of lift mechanism on the car

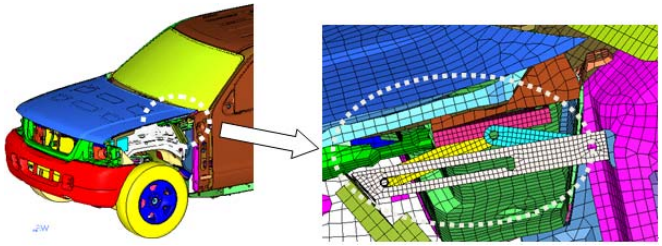

Fig. 14 The assembly of the rear portion of lift mechanism on the car

The simulation of headform to the engine hood impact was carried out to analyze the pedestrian protection performance of active engine hood system with LS-DYNA software. This test was accorded to the Euro-NCAP regulation. The child and adult headforms were developed and certificated according to the regulation. The fig. 15 showed the finite element model of adult headform. The engine hood was marked up with program developed based on HyperMesh software. The fig. 16 was the marked up engine hood. The fig. 17 showed the positioned headform on the deployed engine hood. The simulation HIC values of headform were obtained and compared with those of the original hood. Table 1 was the comparison between the active hood and the original hood in HIC values and peak accelerations. As can be seen from the table, child and adult HIC values were decreased a lot by active engine hood system. So were child and adult peak accelerations.

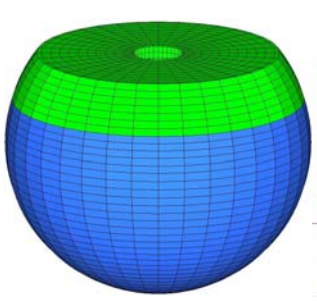

Fig. 15 The adult headform

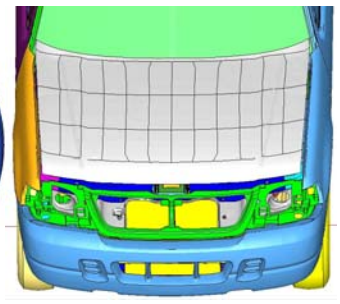

Fig. 16 The marked up engine hood

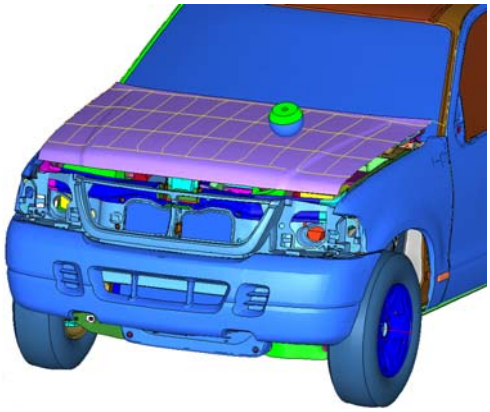

Fig. 17 The positioned headform on the deployed hood

Table 1 The comparison of HIC value and peak acceleration between active and original hood

	Impact position	Origin hood	Active hood	Decreased
Mean HIC_{15}	child	1173.6	576.083	50.91%
	adult	893.341	449.75	49.65%
Peak Acc/g	child	198.604	129.154	34.96%
	adult	140.127	136.603	2.51%

V. Conclusion

A new lift mechanism of active engine hood system was developed. This lift mechanism allowed both front and rear portions of engine hood pop up backward and upward. The crank rod mechanism was used and it was linked with the hinges of hood in the rear portion and the lock of hood in front. Spring was used in the front of lift mechanism. The CAD model and finite element model were constructed. The simulation test of headform impact engine hood according to Euro-NCAP was carried out. The results showed that adult and child HIC values were decreased a lot by active engine hood system. So were the child and adult peak accelerations.

References

[1] C.E. Neal-Sturgess, E. Carter, R. Hardy, R. Cuerden, L. Guerra, J. Yang, “APROSYS European in-depth pedestrian database,” *Innovations for Safety: Opportunities and Challenges*, 2007.

[2] I. Kalliske, F. Friesen, “Improvements to pedestrian protection as exemplified on a standard-sized car,” *17th International Technical Conference on the Enhanced Safety of Vehicles (ESV)*, Paper No. 283, 2001.

[3] J. Hoffmann, A. Kretzschmar and M.V. Blundell, “Investigation into the use of adaptable car structures concepts for pedestrian impact protection,” *International Conference on Vehicle Safety*, 2002.

[4] Martin Krenn, Bernd Mlekusch, Christoph Wilfling, et al., "Development and evaluation of a kinematic hood for pedestrian protection," *Society of Automotive Engineers (SAE)*, Paper No. 2003-01-0897, 2003.

[5] K. Nagatomi, K. Hanayama, T. Ishizaka, et al., "Development and full-scale dummy tests of a pop-up hood system for pedestrian protection," *19th International Technical Conference on the Enhanced Safety of Vehicles (ESV)*, Paper No. 05-0113, 2005.

[6] K.B. Lee, H.J. Jung and H.I. Bae, "The study on developing active hood lift system for decreasing pedestrian head injury," *20th International Technical Conference on the Enhanced Safety of Vehicles (ESV)*, Paper No. 07-0198, 2007.

2011 International Conference on Mechanical, Industrial, and Manufacturing Engineering
Lecture Notes in Information Technology Vols. 1-2

ALD Research of the Liver Analogs Constructed with Multi Cell Assembling Technology*

Haixia Liu
School of Instrument Science and Optoelectronic Engineering
Beihang University
Beijing, China
Liuhx02@mails.tsinghua.edu.cn

Shengjie Li, Yongnian Yan and Xiaohong Wang
Department of Mechanical Engineering
Tsinghua University
Beijing, China
Lishengjie99@mails.tsinghua.edu.cn

***Abstract* - Preliminary experiment results indicated that the multi cell assembling technology can realize two hybrid cell-matrix spatial distributions according to predesigned digital models, thereby can fabricate the liver-like construct which can mimic the natural liver structure and main components. After a period of time culturing in vitro, it has the ability to form liver analog. Using the rat liver analog constructs cultured in vitro for some days in the research of alcoholic liver disease (ALD), through add alcohol to stimulate, and make a control with adding vitamin E and vitamin C, a notability test data can be gained. ALD is considered an important factor in liver cancer, the pathogenesis is complex, the mechanism is still not entirely clear. Formerly, the basic researches of pathogenesis and drug prevention are based on animal models such as baboons or rats. However, this application is limited because of the peculiar animal requirements and high costs, and commonly challenged by ethic. There is a need to have more experiment researches, perfect the multi cell assembling technology, establish the technological process and test means, directly construct the human liver analogs containing various human liver cells for deep studying. A potential for this technology to be used in the research of ALD pathogenesis will be very promising. Therefore, a series of problems leaded by adopting animal model will be solved; ALD pathogenesis and related drug research also will be speed up at the same time.**

Index Terms* - *multi cell assembling, liver analog construct, alcoholic liver disease.

I. INTRODUCTION

The liver is a huge chemical plant and plays an important role in metabolic processes; over 95% of Human alcohol intake is via hepatic metabolism. Alcoholic liver disease (ALD) refers to the damage that is caused to the liver due to prolonged alcohol abuse. ALD is a major cause of morbidity and mortality both in the United States and worldwide. It is projected that the mortality for cirrhosis with superimposed alcoholic hepatitis is much worse than that of many common types of cancer [1-2]. There are increasing trends recently; it became an important health problem facing the developed and developing world.

ALD mechanism is complex, the pathogenesis is still not entirely clear. At present, the basic researches of pathogenesis and drug prevention are based on animal models such as baboons or rats [3]. However, this application is limited because of the peculiar animal requirements and high costs, and commonly challenged by ethic [4-5]. Liver analog based on 3D cell assembling technology have some similar natural liver function in the physiological environment [6-7]. This paper has a progressed research based on multi cell assembling technology [8], through select the appropriate extracellular matrix material, liver cells and adipose derived stem cells (ADSCs) to build the liver analogs with vascular access, after culturing in vitro and biological evaluation, applied to the ALD model.

Reference [9] studies have shown that the metabolism of alcohol in the liver makes the malondialdehyde (MDA) product of lipid peroxidation increased. MDA level indirectly reflects the degree of liver injured. MDA will also damage the normal function of endothelial cells distributed in the liver vascular network, the content of vascular endothelial diastolic factor NO reflects the normal degree of endothelial cell function [10].

Vitamin E and vitamin C are powerful antioxidants, combined application will improve the proliferation of liver cells, protect the liver's detoxification ability and normal metabolism [11].

Through adding alcohol to stimulate liver analog constructs fabricated by multi cell assembling technology during in vitro culturing, test changes of MDA and NO levels, and make a control with added vitamin E and vitamin C [12].

As well known, the liver is composed of two branched vascular networks and numerous hepatic lobules. The blood supply system is very abundant and important for liver functions. Through constructing three-dimensional structure containing pipeline system, simulate the liver structure, after in vitro culturing, come into being liver analog. Liver cells and matrix materials gelatin (Tianjin Green-Island Company, China, medical level)/ chitosan (Sigma, USA)/ sodium alginate (Sigma, USA) (G / C / A system) constitute a liver lobular; ADSCs and gelatin / fibrin (Sigma, USA)/ sodium alginate (G / F / A system) constitute vascular channels.

II. MATERIALS AND METHODS

Use special software to establish the heterogeneous CAD model to mimic the liver organization structure (Fig.1), calibrate the materials component in accordance with the model structure, using the preprocessing software Aurora (Yinhua, China), the digital model was transferred to a

* This work is supported by CNSF Grant #50905009 to H.X. Liu.

common layer interface (CLI) file for digital-controlled assembling.

Liver cells were isolated from 6-week-old Sprague–Dawley (SD) rats (Laboratory Animal Center, Health Science Center, Peking University, China) by following a two-step collage-nase (Invitrogen, USA) perfusion method [13]. About 96% of the cells were typical hepatocytes while the others were nonparenchyma cells. ADSCs were isolated from the inguinal fat of SD rats, as described previously, and then differentiated into endothelial cells after 4 days induced. Respectively prepare 15G0.5C1.25A and 15G2.5F1.25A sol materials, for distinguish visibly, relevant to the solvents are phosphate-buffered saline (PBS) solution and DMEM/F12 medium (GIBCO, USA). Both sols were mildly stirred to even and avoid air bubbles mixed, with the liver cell density of 5×10^6 cells/mL and endothelial cell induced by ADSCs density of 1×10^6cells/mL. They were loaded into standard medical disposable sterile syringe (Shanghai Kangshou, 1mL) with 26G needle (OD: 0.45, ID:0.25, L:10mm) respectively, and fitted in the Multi-nozzle Cell Assembler. Fig. 2 is a formed 3D liver analog construct. The red tube-like part was made of ADSC/GAF hydrogel, the red color is due to the solvent of GAF was DMEM/F12, while the white meshwork part was made of hepatocytes/GAC hydrogel. This complex structure with vascular-like network was almost as accurate as the designed digital model (Fig. 1).

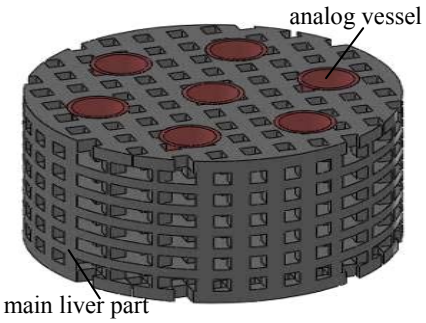

Fig.1. liver analog CAD model

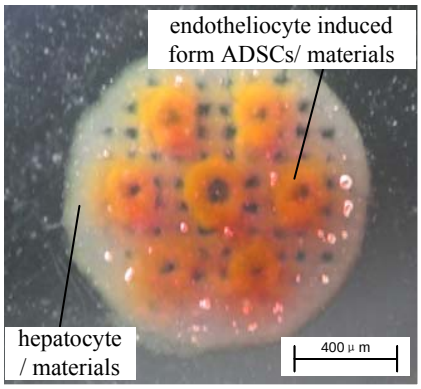

Fig.2. liver analog construct

Removed the liver analog from Multi-nozzle Cell Assembler working chamber and had a posttreatment [14]. Statically cultured at 37℃, 5% CO_2 in MCO-15AC incubator (Sanyo, Japan) with DMEM medium supplemented with 15% fetal bovine serum (FBS), 100 IU/mL penicillin/streptomycin, and 1 IU/mL aprotinin (Sigma, USA). Culture medium was changed every other day. During the culture time, the morphology and proliferation of cells in the construct were observed daily with an inverted microscope CK40 (Olympus, Japan).

III. Results

Cultured for 10 days, observe all cells distribution and growth status by immunohistochemical staining. The construct was rinsed with PBS, fixed with 4% (w/v) paraformaldehyde (Tianjing Keou, China) at 48℃ for 2 h, followed by several washes in distilled water, embedded in optimal cutting temperature (Tissue-Tek® O.C.T) medium, and then sectioned into 10μm slices using a HM525 freezing microtome (MICROM, Germany). Some of the slices were stained with 50 mg/mL propidium iodide (PI) (Sigma, USA), followed by immunofluorescence with primary antibody CD31 (goat antirat, polyclonal, Santa Cruz, USA, 1:200, PBS) and secondary antibody FITC-conjugated antigoat IgG (Sigma, 1:100, PBS). These slices were observed under a fluorescence microscope X-Cite series150 (EXFO, Canada).

The rest of the samples were stained with 50 mg/mL PI at 48℃ for 30min, then extensively washed with PBS, and incubated overnight at 48℃ with primary antibody albumin (ALB) (rabbit antirat, monoclonal, Santa Cruz, USA, 1:200, PBS). After being washed with PBS, the samples were incubated with a secondary antibody, FITC-conjugated antirabbit IgG (Sigma, 1:100, PBS) at 37℃ for 30min.

In Fig. 3, PI-ALB immunofluorescence staining was positive for the nuclei, which is a distinct biomark for mature hepatocytes. This confirmed that the hepatocytes were alive with secretion ability.

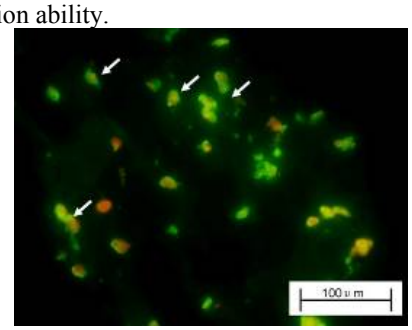

Fig.3 Immunofluorescence staining pictures of hepatocytes with PI- ALB, the scale bar is 100 mm.

In Fig. 4, the cells were stained positive with PI-CD31, which is a distinct biomark for mature endothelial cells. This indicated that the endothelial cells induced by ADSC were alive with secretion ability and distributed in the vascular structure.

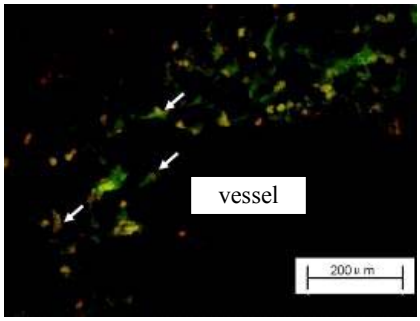

Fig.4 Immunofluorescence staining pictures of endothelial cells with PI-CD31, the scale bar is 200 mm.

After 10 days culturing and testing, it shows that the assembled construct with a vascular-like network could provide a suitable environment for both hepatocytes and endothelial cells induced by ADSC to exist, proliferate, and maintain normal metabolism functions, holds the potential to be functional liver, namely liver analogs. Hereafter, the residual liver analogs were randomly divided into two sets, namely alcohol set and drug set.

1) In alcohol set, the liver analog was cultured with DMEM/12 medium supplemented with 15% FBS, 50mM alcohol (Beijing Yili, China). After 12h culture, the medium was changed with normal DMEM/F12 with 15% FBS, 100 IU/mL penicillin/streptomycin. All the removed supernatant medium was preserved at -20℃ for further tests.

2) In drug set, the liver analog was cultured with DMEM medium supplemented with 15% FBS, 50mM alcohol, 2.3μM Vitamin E and 2.3μM vitamin C (Sigma, USA). After 12h culture, the medium was changed with normal DMEM/F12 with 15% FBS, 100 IU/mL penicillin/streptomycin. All the removed supernatant medium was preserved at -20℃ for further tests.

3) Have alcohol and drug effect on the all test groups every 2 days and sampling. The regular reserved culture media were analyzed using an automatic biochemical analyzer (Hitachi 7600, Japan) to test. The each group of test consisted of five samples, and the data were presented as mean ±SD values. MDA content were tested with the modified thiobarbituric acid (TBA) method, the absorption peak at 532 ~ 535nm [15]. NO content were tested using the nitric oxide test box (Nanjing Jiancheng).

The MDA test results after 8d culture are shown in Fig. 5. The MDA concentration increased at the early stages and then decreased in the alcohol set, an explanation for the changes in the MDA concentration may be that the hepatocytes were damaged irreversibly by alcohol, thus the MDA concentration decreased gradually. Comparatively, in the drug set with vitamin E and vitamin C, MDA concentration has change little during the test period.

The NO test results after 6d culture are shown in Fig. 6. It is showed that adding vitamin E and vitamin C, the set compared to the role of pure alcohol set, there are a slight increase of the NO content, it indicated that both the vitamin E and vitamin C existence play a certain active protection on the endothelial cells.

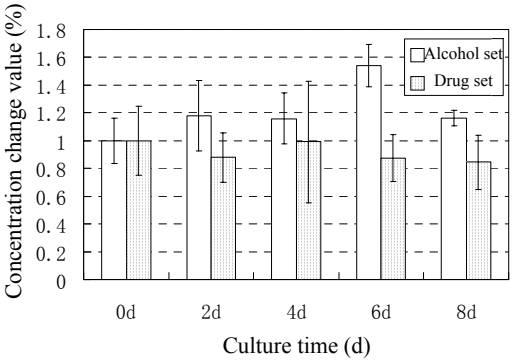

Fig.5 The changes of MDA concentration during 8d culture.

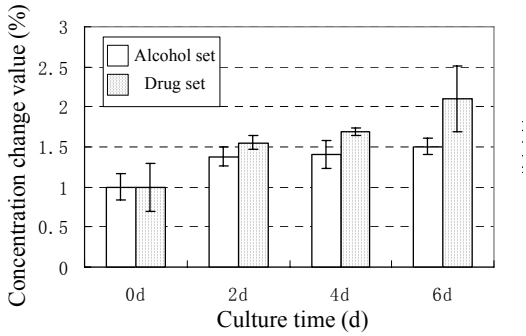

Fig.6. The changes of NO concentration during 6d culture.

IV. CONCLUSIONS

Preliminary experiment results indicated that the multi-cells assembling technology can realize two hybrid cells-matrix spatial distributions according to predesigned digital models, thereby can fabricate the liver-like constructs which mimic the natural liver structure and main components. After a period of time culturing, it can form liver analogs. A notability test data can be gained when use this liver analog constructs in alcoholic liver disease researching. There is a need to have more experiment research, perfect the test means and establish the technological process, a potential for this technology to be used in the research of ALD pathogenesis is very promising. Therefor, a series of problems leaded by adopting animal model will be solved; ALD pathogenesis and related drug research also will be speed up contemporarily.

REFERENCES

[1] A. Barve, R. Khan, L. Marsano, K. V Ravindra, and C. McClain, "Treatment of alcoholic liver disease," *An of Hepatol*, vol. 7, no. 1, pp. 5-15, January-March 2008.

[2] C. J. McClain, Z. Song, S. S. Barve, D.B. Hill, and I. Deaciuc, "Recent advances in ALD. IV. Dysregulated cytokine metabolism in ALD," *Am J Physiol Gastrointest Liver Physiol*, vol. 287, no. 3, pp. 497-502, September 2004.

[3] S. Stewart, D. Jones, and C. P. Day, "Alcoholic liver disease: new insights into mechanisms and preventative strategies," *Trends Mol Med*, vol. 7, no. 9, pp. 408-413, September 2001.

[4] Z. Song, C. J. McClain, and T. Chen, "S-Adenosylmethionine protects against acetaminophen-induced hepatotoxicity in mice," *Pharmacol*, vol. 71, no. 4, pp. 199-208, December 2004.

[5] C. Ji, and N. Kaplowitz, "Betaine decreases hyperhomocysteinemia, endoplasmic reticulum stress, and liver injury in alcohol-fed mice," *Gastroenterology*, vol. 124, no. 5, pp. 1488-1499, May 2003.

[6] H. X. Liu, Y. N. Yan, X. H. Wang, J. Cheng, F. Lin, Z. Xiong, et al, "Construct hepatic analog by cell-matrix controlled assembly technology," *Chin Sci Bull*, vol. 51, no. 15, pp. 1830-1835, August 2006.
[7] X. H. Wang, Y. N. Yan, Y. Q. Pan, H. X. Liu, J. Cheng, F. Lin, et al, "Generation of three-dimensional hepatocyte/gelatin structures with rapid prototyping system," *Tissue Eng*, vol. 12, no. 1, pp. 83-90, January 2006.
[8] S. J. Li, Z. Xiong, X. H. Wang, Y. N. Yan, H. X. Liu, R. J. Zhang, "Direct fabrication of a hybrid cell/hydrogel construct by a double-nozzle assembling technology," *J Bioact and Compat Pol*, vol. 24, no. 3, pp. 235-248, May 2009.
[9] E. Mezey, J. J. Potter, L. Rennie-Tankersley, J. Caballeria, and A. Pares, "A randomized placebo controlled trial of vitamin E for alcoholic hepatitis," *J Hepatol*, vol. 40, no. 1, pp. 40-46, January 2004.
[10] B. Ganaraja, D. DS. Crystal, BM. Vijayalakshmi, AK. Nayanatara, BM. Ramesh, and C. Ramaswamy, "Use of vitamin C on effect of ethanol induced lipid peroxidation in various tissues, sperm count & morphology in the wistar rats," *J of chin clin med*, vol. 3, no. 11, pp. 627-631, November 2008.
[11] C. A. Oyinbo, W. N. Dare, G. R. A. Okogun, L.C. Anyanwu, N.M. Ibeabuchi, C.C. Noronha, et al, "The hepatoprotective effect of vitamin C and E on hepatotoxicity induced by ethanol in sprague dawley rats," *Pakistan J of Nutr*, vol. 5, no. 6, pp. 507-511, June 2006.
[12] L. P. Tantcheva, E. S. Stoeva, A. S. Galabov, A. A. Braykova, V. M. Savov, and M. M. Mileva, "Effect of vitaminamin E and vitaminamin C combination on experimental influenza virus infection," *Methods Find Exp Clin Pharmacol*, vol. 25, no. 4, pp. 259-264, May 2003.
[13] P. Papeleu, T. Vanhaecke, T. Henkens, G. Elaut, M. Vinken, S. Snykers, and V. Rogiers, *Isolation of Rat Hepatocytes*, 3rd ed., Totowa: Humana Press, 2006, pp.26-39.
[14] H. X. Liu, Y. N. Yan, and X. H. Wang, "Structure stability research of cells assembly in vitro culturing," *J of tsinghua univ(in chinese)*, vol. 50, no. 8, pp. 1009-1011, August 2010.
[15] B. Tokur, K. Korkmaz, and D. Ayas, "Comparison of two thiobarbituric acid (TBA) method for monitoring lipid oxidation in fish," *J of Fish & Aquat Sci*, vol. 23, no. 3-4, pp. 331-334, March 2006.

2011 International Conference on Mechanical, Industrial, and Manufacturing Engineering
Lecture Notes in Information Technology Vols. 1-2

Using Genetic Algorithm for Optimizing of High Speed Flip-Flop

Alireza rezaee
Islamic azad university Hashtgerd branch
arrezaee@yahoo.com

Amir Nasser Khaleqhi
Islamic azad university Hashtgerd branch
nasser.khaleqhi@gmail.com

Abstract **- In this paper, we report an algorithm known as genetic algorithm for the optimization of power-delay-product (PDP) via transistor sizing. In this optimization, genetic algorithm is used to minimize the PDP of Modified Hybrid Latch Flip-Flop (MHLFF).**
Genetic algorithm is implemented in MATLAB; the fitness function, a function of power and delay, is accurately computed using Hspice for a 65nm CMOS technology.
The results show 31% reduction in PDP comparison with the previous one.

Index Terms - Genetic algorithm, Flip-Flop, Optimization.

I. INTRODUCTION

Increasing the power dissipation in VLSI circuits not only discourage their use in portable applications because of the limitations of battery life, but also degrades the performance and reliability of these circuits. Moreover, scaling of feature size has allowed chip density to increase, make the total power greater. So, power reduction and performance boosting is important for system development and success. Flip-Flop, an important block of any blocking system in synchronous VLSI designs, is critical to the performance of digital systems [1].
Reduction in charge and discharge time of capacitors in Flip-Flop circuit is used to increase its speed. Reducing the charge and discharge time of these capacitors has a great impact on its speed. In order to reduce this time, current flowing through these capacitors should be increased. Therefore, power consumption becomes greater. All these reasons show the trade off between power and delay. So, PDP is proposed as a fitness function. The aspect ratio of transistors should be optimized to minimize the PDP of circuit. In this work, genetic algorithm is employed to optimize the sizing of MHLFF which results significantly improvement in PDP.
In section II, an overview of MHLFF circuits is described. Section III gives a brief introduction on genetic algorithm. Section IV explains how the optimization is. Section V gives a simulation results. Conclusion is explained in section VI.

II. MHLFF

The structured of MHLFF Flip-Flop and timing diagram are shown in figure1 [2].
When the clock makes a transition from low to high, during a time equal to the delay of three inverters, CLKBD remains high. This period creates a short pulse at node C1.
During this pulse, MN3 becomes on; if D is low and Q is high which means that D was high in the previous clock, MN1 becomes off but MP2 becomes on forcing the output to low. If D and Q are high or both of them are low, node X (internal node) will not change, so redundant transitions are avoided. If D is high and Q is low, node X discharges turning on MP3 forcing the output to high. Redundant transitions are minimized in this Flip-Flop. So, MHLFF is faster and less power consuming than the previous ones [3, 4].

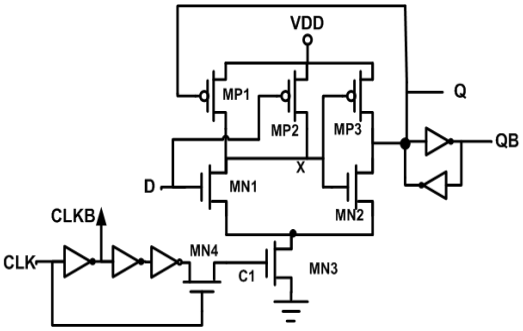

(a)

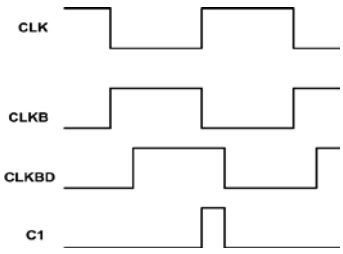

(b)

Fig1. (a) Schematic of MHLFF, (b) timing diagram

III. GENETIC ALGORITHM

Genetic algorithm is a powerful tool that has been used to solve a range of complex VLSI problems such as size and power minimization. As mentioned in previous sections, genetic algorithm is used to optimize PDP of MHLFF in this paper.

A general flow of a typical genetic algorithm is shown in fig 2.

The algorithm steps must be iterated until relatively good specification is obtained. The parameters are grouped in the chromosome like structure. These chromosomes are a population of each generation.

After evaluating the fitness function of each generation, new population is created by operators such as selection, crossover, and mutation [6, 5, 7].

IV. PDP OPTIMIZATION

To reach our aim, PDP optimization, we select four transistor's width as genes of one chromosome. Each population consists of 25 chromosomes. The genetic algorithm process ends when the end condition is satisfied.

We select two parent chromosomes from a population, in selection step. Our selection type is Roulette wheel in which the probability to choose a certain individual is proportional to its fitness.

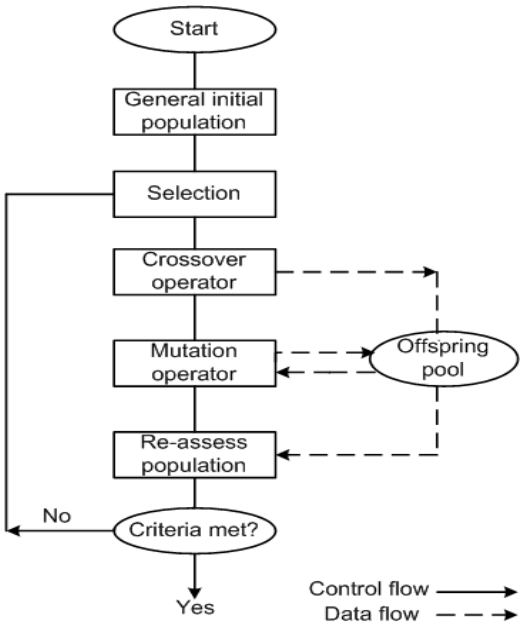

Fig2. Process of genetic algorithm

In crossover step, two individual or parents combine to form a crossover child for the next generation. Crossover function that is applied in this work is Heuristic which creates a child that lies on the line containing the two parents, a small distance away from the parent with the better fitness value in the direction way from the worse one. The parameter Ratio enables the algorithm to determine how far the child from the better parent. This equation shows the relation between child and two parents.

$$Child = parent2 + R \times (parent1 - parent2)$$

Parent1 has the better fitness value and parents2 has the worse fitness value. In this paper, crossover Ratio is 0.8.

Genetic algorithm is started to generate chromosome from the number which is set by initial range.

As the population size is finite, the crossover operator alone can not bring enough variation to the population. Mutation is very important factor to make small random changes in the individual or chromosome and create a child. Therefore, mutation can generate chromosomes whose genes do not exist in initial population.

The mutation function used in our optimization is Gaussian which adds a random number taken from a Gaussian distribution with mean 0 to each gene. The variance of this distribution is determined by the parameters Scale and Shrink.

Scale specifies the variance at the first generation. For (i) th gene, variance is given by:

$$Scale \times (V(i, 2) - V(i, 1))$$

V (i, 2) is a second coordinate of initial range for (i) th gene.

Shrink controls how the variance shrinks. In next equation, relation between the (k) th generation and (k-1) th is shown:

$$Var_k = Var_{k-1} \times (1 - Shrink.K/generation)$$

So, variance of next generation decreases. As a result, jumping into local minimum is prevented.

The type of mutation function, crossover, and other operators are summarized in table.1

Table1. Genetic algorithm's options

Options	Type/value
Population	25
Initial range	[0.50;0.55]
Selection	Roulette
Crossover, Rate	Heuristic,0.8
Mutation	Gaussian
Mutation parameter, Scale	2
Mutation parameter, Shrink	0.5

V. RESULTS

In order to reduce the PDP and increase the speed of MHLFF, genetic algorithm is applied by using Hspice as a simulator and MATLAB as a function evaluator. This circuit is modeled by 65nm CMOS technology [8]. Four main transistor's lengths are assumed 65nm and width are chosen as a variable of fitness function. These variables and the initial ones in nm are shown in table2. In table.3, new value of PDP and delay are compared with initial ones.

VI. CONCLUSION

Genetic algorithm is a beneficial tool to optimize the PDP in FLIP-FLOP circuits. In this paper, we presented how this tool is applied in MHLFF circuit by using transistor sizing. The results of simulation showed that optimized circuit has 31% better PDP than the previous one.

Table II.
Value of transistors' widths before and after the optimization

W(nm)	W_{MN1}	W_{MN2}	W_{MP2}	W_{MP3}
Old value	200	700	300	850
New value	804.3	1141.8	858	1098.2

Table III.
camparison PDP and speed before and after the optimization

	PDP(μw. ps)	Delay(ps)
Before optimization	77	61
after optimization	52.8	41
improvement	31%	33%

REFERENCES

[1] Hamada, M., Terazawa, T., Higashi, T., Kitabayashi, S., Mita, S., Watanabe, Y., Ashino, M., Hara, H., and Kuroda, T.: 'Flip-flop selection technique for power-delay trade-off'. Dig. Tech. Pap. IEEE Int. Solid-State Circuits Conf., February 1999, pp. 270–271

[2] Rasouli, S.H., Khademzadeh, A., Afzali-Kusha, A., and Nourani, M., " Low power single and double edge-triggered flip-flop for high speed applications," IEE Proc.-Circuits Devices Syst., Vol. 152, No. 2, April 2005.

[3] Nedovic, N., and Oklobdzija, V.G.: 'Hybrid latch flip-flop with improved power efficiency'. IEEE Symp. On Integrated Circuits and Systems Design, September 2000, pp. 211–215.

[4] Kim, C., and Kang (Sen), S.-M.: 'A low-swing clock double-edgetriggered flip-flop', IEEE J. Solid-State Circuits, 2002, 37, (5).

[5] Klass, F.: 'Semi-dynamic and dynamic flip-flops with embedded logic'. Symp. VLSI Circuits Dig. Tech. Papers, June 1998, pp. 108–109.

[6] Marek Obitko, "GENETICS ALGORITHMS", available online: http://cs.felk.cvut.cz/~xobitkolga.

[7] Frederic Dreier," Genetic Algorithm Tutorial (GA)", July 2002, available online: http://www.google.com/search?hl=en&lr=&q=%22genetic+algorithm+tutorial%22%22ga%22%22frederic%22pdf.

[8] http://www-device.eecs.berkeley.edu/~ptm

2011 International Conference on Mechanical, Industrial, and Manufacturing Engineering
Lecture Notes in Information Technology Vols. 1-2

Convection Heat Transfer on a Stretching Surface with an Imposed Variable Wall Temperature

Lin Lin
School of Mechanical Engineering
University of Science and Technology Beijing
Beijing, CHINA
linlin@ustb.edu.cn

***Abstract* - A theoretical analysis the flow and heat transfer over a continuously moving/stretching surface with variable wall temperature is made and the similarity solutions are presented The results indicated that the heat transfer characteristics are strongly affected by the values of wall parameters of velocity and temperature and the Prandtl numbers. For small value of rPr/(m+1), the surface temperature gradient could be expected to be proportional to the Prandtl number. However, for large value of rPr/(m+1), the temperature gradient at the surface could be approximated by the square of root of the value.**

Index Terms - Heat transfer. Boundary layer. Similarity solutions. Shooting technique.

I. INTRODUCTION

Flow and heat transfer on a continuous moving/stretching solid surface with imposed temperature gradient occurs in a number of engineering processes. Examples of such technological processes are hot rolling, wire drawing, glass fibre and paper production, drawing of plastic films, metal and polymer extrusion, metal spinning, etc. Both the kinematics of stretching and the simultaneous heating or cooling during such processes has a decisive influence on the quality of the final products.

Following the pioneering work of Sakiadis[1-2], the problems of boundary layer over a continuous moving surface moving in an otherwise quiescent fluid medium have attracted considerable attention during the last few decades. The great majority of theoretical investigations in this field described the heat transfer and fluid flow in the vicinity of the continuous moving surface with the aid of similarity solutions of boundary layer equations. Later an experimental and theoretical treatment was made by Tsou et al.[3] , who also determined heat transfer rates for certain values of Prandtl number. For a list of the key references of a vast literature concerning this subject we refer to the recent papers [4-8].

The boundary layer on a continuous moving solid surface represents a different class of boundary layer problem which has a solution substantially different from that of the classical boundary layer flow over a semi-infinite flat plate. In this paper, we study the flow and heat transfer over power law moving/stretching continuous solid surface with a variable surface velocity and a variable wall temperature which both are power-law function of the location, see Fig.1.

II. BOUNDARY LAYER GOVERNING EQUATIONS

Suppose that the flow is two-dimensional and incompressible. The physical properties of the fluid are constant except the surface tension. For laminar boundary flow over a flat plate, the Navier-Stokes equations can be reduced to the continuity equation and the boundary layer momentum equation:

$$\frac{\partial u}{\partial x}+\frac{\partial v}{\partial y}=0 \ . \tag{1}$$

$$u\frac{\partial u}{\partial x}+v\frac{\partial u}{\partial y}=\nu\frac{\partial^2 u}{\partial y^2} \ . \tag{2}$$

The boundary layer energy equation is:

$$u\frac{\partial T}{\partial x}+v\frac{\partial T}{\partial y}=a\frac{\partial^2 T}{\partial y^2} \ . \tag{3}$$

The corresponding boundary conditions at the surface are:

$$u=u_w(x)=cx^m, \ \ v=0, \ T(x,0)-T_\infty=Ax^{\ r} \ . \tag{4}$$

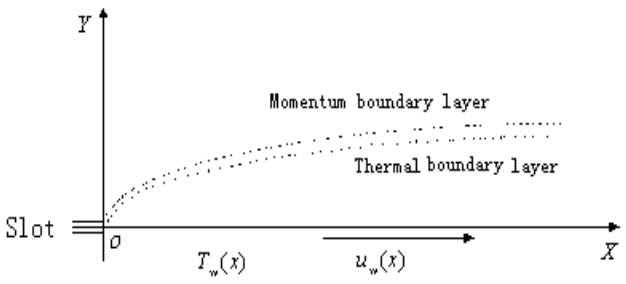

Fig.1 Schematic representation of the boundary layer on a moving/stretching wall with $u_w(x)=cx^m$, $T_w(x)=T_\infty+Ax^{\ r}$

Far from the surface, the boundary conditions are:

$$u(x,\infty)=u_\infty=0,\quad T(x,\infty)=T_\infty\ . \tag{5}$$

where m and r are respectively the velocity parameter and the temperature parameter. When $m=0$, the surface is moving in a constant velocity; and when r =0, the thermal boundary condition becomes isothermal. Proceeding with the analysis, we define the stream function ψ, the similarity variable η and the dimensionless temperature $\theta(\eta)$ as follows[16-19]:

$$\psi(x,y)=A(x)F(\eta),\quad \eta=B(x)y\ ,$$
$$\theta(\eta)=(T-T_\infty)/(T_w-T_\infty)\ . \tag{6}$$

where $A(x)$ and $B(x)$ are functions to be determined, $F(\eta)$ denotes the dimensionless stream function. The velocity components are respectively $u=\dfrac{\partial\psi}{\partial y}$ and $v=-\dfrac{\partial\psi}{\partial x}$. Substituting (6) into (1)-(5), in terms of the similarity solutions, by choosing

$$A(x)=\sqrt{u_w(x)\nu\ x/(m+1)}\ =\sqrt{c\nu/(m+1)}\ x^{(m+1)/2},$$

and

$$B(x)=\sqrt{(m+1)u_w(x)/\nu\ x}=\sqrt{(m+1)c/\nu}\ x^{(m-1)/2}\ .$$

We obtain the following nonlinear ordinary differential equations:

$$F'''(\eta)+\frac{1}{2}F(\eta)F''(\eta)-\frac{m}{m+1}(F'(\eta))^2=0\ . \tag{7}$$

$$\theta''(\eta)+\frac{1}{2}\Pr F(\eta)\theta'(\eta)-\frac{r\Pr}{m+1}F'(\eta)\theta(\eta)=0\ . \tag{8}$$

and the transformed boundary conditions are:

$$F(0)=0,\ F'(0)=1,\ F'(+\infty)=0\ . \tag{9}$$

$$\theta(0)=1,\quad \theta(+\infty)=0\ . \tag{10}$$

The local wall heat flux is defined as:

$$-k\frac{\partial T}{\partial y}\Big|_{y=0}=-2kA\sqrt{\frac{u_w(x)}{3\nu}}\ x^{r-\frac{1}{2}}\theta'(0)\ . \tag{11}$$

The local Nusselt number based on the distance from the leading edge is defined as

$$Nu_x=\frac{x}{T_\infty-T_W}\left(\frac{\partial T}{\partial y}\right)\Big|_{y=0}=-2\sqrt{\frac{u_w(x)}{3\nu}}\ x^{\frac{1}{2}}\theta'(0)\ . \tag{12}$$

where the Relynolds number is defined as $\mathrm{Re}_x=u_w(x)x/\nu$ based on x.

III. Solutions and discussions

The governing equations (7)-(8) are solved subject to boundary conditions (9)-(10) numerically using the fourth-order Runge-Kutta method and shooting technique. It is seen that the numerical integration cannot be started at $\eta=0$ because $F''(0)$ is not there for momentum equation (7) and $\theta'(0)$ is not there for energy equation (8). The shooting technique is used to determine the unknown boundary conditions at $\eta=0$.

The momentum equation and the energy equation are decoupled since the fluid is incompressible. So, the solution to the momentum equation may be discussed first. At the beginning of the numerical computation, a value F_0'' is arbitrarily guessed and a positive increment $\Delta F_0''$ is picked. The shooting technique takes care of the infinity condition on F' at $\eta_{\max}$ (let the range of numerical integration be restricted to the finite dimensions, here $\eta_{\max}=20$ is considered). If not, the initial guess for F'' at $\eta=0$ will be replaced by $F_0''+\Delta F_0''$ and this process be repeated until the infinity condition is satisfied. Therefore, the outer boundary condition given in (9) must be changed into a more general form

$$F'=0,\ F''=0\quad \text{for } \eta\ge\eta_k\ . \tag{13}$$

The solutions for momentum boundary layer equations are shown in Figs.2-4. A comparison is given for m=1/3 with the result of Arafune and Hirata[16] for $F''(0)=-0.5869$ and the present result of $F''(0)=-0.5869939$.

The results indicated that velocity $F'(\eta)$ approaches to zero for any exponent m for larger η. The dimensionless shear stress profile $F''(\eta)$ is always negative for all range of η which decreases with m and increases with increasing η.

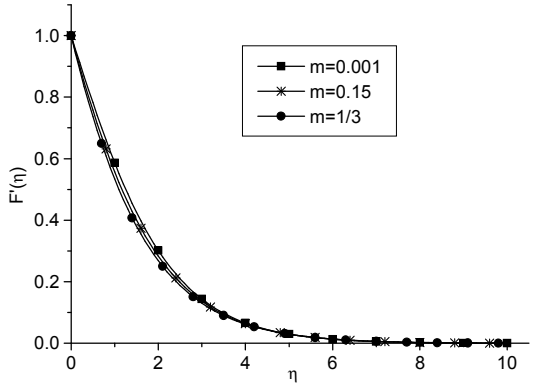

Fig.2 Velocity profiles for m=0.001 to 1/3

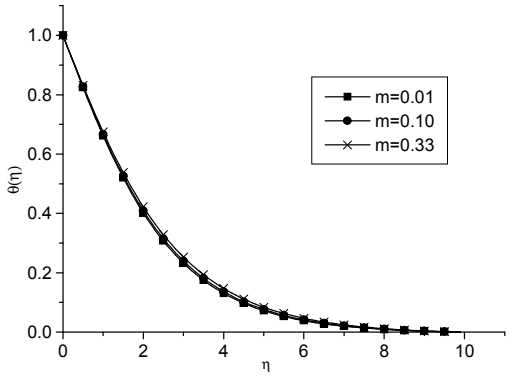

Fig.3 Temperature profiles for Pr=0.72,r=0.0,m=0.01 to 0.33

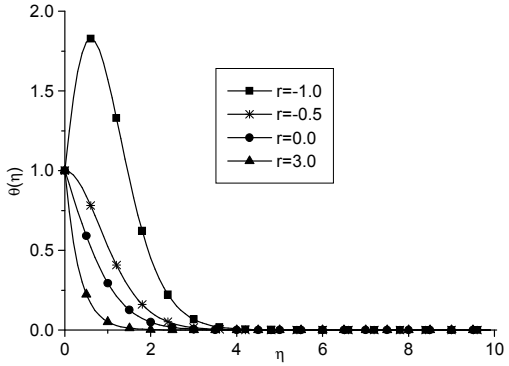

Fig. 4 Temperature profiles for m=0.001,Pr=3.0, r = -1.0 to 3.0

The temperature distribution function $\theta(\eta)$ and the surface temperature gradient $\theta'(0)$ are both function of the parameters of the velocity exponent m, the Prandtl number Pr and the wall temperature exponent r. Utilizing the solutions of momentum boundary layer equations, we may obtain the solutions of energy equation, the numerical results are presented in Figures 3-5.

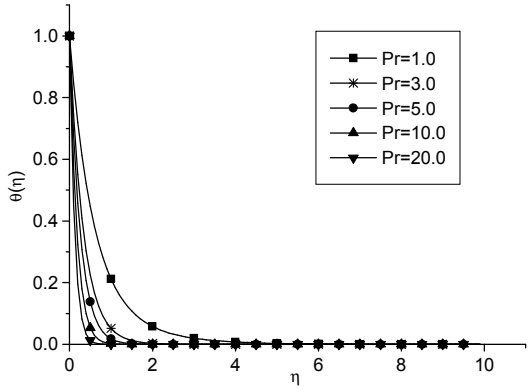

Fig.5 Temperature profiles for m=0.01,r=3,Pr=1to20

The typical temperature distribution profiles for energy boundary layer are shown in Figs.3 –5 for several values of velocity power law index parameter m, the Prandtl number Pr and the wall temperature exponent r. The results indicated the heat transfer characteristics affected by velocity exponent are weak but it strongly depended on the wall temperature exponent r and the Prandtl number. The magnitude of the slop of the temperature profiles at the surface sharply decreases with decreasing Prandtl number as the thermal boundary layer gets very thick for low Prandtl numbers and the thermal boundary layer is much thinner for high Prandtl numbers.

The surface temperature profiles for a small value of temperature gradient exponent r is steeper near the leading edge which provides more flow. For larger values of temperature gradient exponent r, the slope of the temperature profile is steeper near the trailing edge where the boundary layer is thicker and the additional acceleration of the flow has less effect.

We may make further analysis for the heat transfer characteristics. It may be seen from the table 1-3, the figures 5-12 and the (8) that for small value of $r\,\mathrm{Pr}/(m+1)$ (≥ 0), the thermal boundary layers are much thicker than that of the momentum boundary layers. Therefore, over most of the domain, the functions $F'(\eta)$ may be replaced by zero and $F(\eta)$ may be replaced by $F(+\infty)$. So, the energy equation may be approximated by

$$\theta''(\eta)+\frac{1}{2}\mathrm{Pr}\,F(+\infty)\theta'(\eta)=0\ . \tag{14}$$

The solution of (14) subject to the boundary conditions (10) is

$$\theta(\eta)=e^{-\frac{1}{2}\mathrm{Pr}\,F(+\infty)\eta}\ . \tag{15}$$

The temperature gradient at the surface for small value of $r\,\mathrm{Pr}/(m+1)$ may be approximated by

$$\theta'(0)=-\frac{1}{2}\mathrm{Pr}\,F(+\infty)\ . \tag{16}$$

Therefore, the surface temperature gradient could be expected to be proportional to the Prandtl number for small value of $r\,\mathrm{Pr}/(m+1)$.

The local wall heat flux and the local Nusselt number given by (11) and (12) can be respectively written as:

$$-k\frac{\partial T}{\partial y}\Big|_{y=0}=kA\,\mathrm{Pr}\,F(+\infty)\sqrt{\frac{c}{3\nu}}\,x^{\frac{m-1}{2}+r}\ . \tag{17}$$

and

$$Nu_x=\frac{x}{T_\infty-T_W}\left(\frac{\partial T}{\partial y}\right)\Big|_{y=0}=\mathrm{Pr}\,F(+\infty)\sqrt{\frac{c}{3\nu}}\,x^{\frac{m+1}{2}}\ . \tag{18}$$

For large value of rPr/(m+1), the thermal boundary layer thickness is thinner than that of the momentum boundary layer thickness. So, the energy equation can be approximated by assuming that $F(\eta)$ is essentially zero and that $F'(\eta)$ is essentially $F'(0)=1$ for small η. Therefore, for large value of $r\,\mathrm{Pr}/(m+1)$, the energy equation may be approximated by

$$\theta''(\eta)-\frac{r\,\mathrm{Pr}}{m+1}\theta(\eta)=0 \quad . \tag{19}$$

Equation (19) subject to the boundary conditions (10) has the solution:

$$\theta(\eta)=e^{-\sqrt{\frac{r\,\mathrm{Pr}}{m+1}}\eta} \quad . \tag{20}$$

The temperature gradient at the surface for small value of $\frac{r\,\mathrm{Pr}}{m+1}$ could be approximated by

$$\theta'(0)=-\sqrt{\frac{r\,\mathrm{Pr}}{m+1}} \quad . \tag{21}$$

The local wall heat flux and the local Nusselt number given by (11) and (12) can be respectively written as:

$$-k\frac{\partial T}{\partial y}\Big|_{y=0}=2kA\sqrt{\frac{cr\,\mathrm{Pr}}{3\nu(m+1)}}\,x^{\frac{m-1}{2}+r} \quad . \tag{22}$$

and

$$Nu_x=\frac{x}{T_\infty-T_W}\left(\frac{\partial T}{\partial y}\right)\Big|_{y=0}=2\sqrt{\frac{cr\,\mathrm{Pr}}{3\nu(m+1)}}\,x^{\frac{m+1}{2}} \quad . \tag{23}$$

IV. Conclusions

This paper presents a similarity analysis for the flow and heat transfer for laminar boundary layer over a continuous moving/stretching surface with variable wall velocity and variable wall temperature. The similarity solutions are numerically presented and the associate transfer characteristics are discussed. The heat transfer characteristics are strongly affected by the value of rPr/(m+1). For small value of rPr/(m+1), the surface temperature gradient could be expected to be proportional to the Prandtl number. However, for large value of small value of rPr/(m+1), the temperature gradient at the surface could be approximated by the square of root of the value.

Nomenclature

u_w surface velocity
u velocity component along x
v velocity component along y
ψ stream function, F dimensionless stream function
m power law exponent relating to surface velocity,
r power law exponent relating to surface temperature
k thermal conductivity
a thermal diffusivity
Re_x the Relynolds number is defined as based on x.
Nu_x the local Nusselt numbe is defined as based on x
Pr Prandtl number

Acknowledgment

The work is supported by the National Natural Science Foundations of China (No.50936003, 51076012).

References

[1] Sakiadis, B. C. "Boundary-Layer Behavior on Continuous Solid Surfaces: I. Boundary-Layer Equations for Two-Dimensional and Axisymmetric Flow", *A.I.Ch.E. Journal*, vol. 7 pp. 26-28, 1961.

[2] Sakiadis, B. C. "Boundary-Layer Behavior on Continuous Solid Surfaces: II. The Boundary-Layer on a Continuous Flat Surface", *A.I.Ch.E. Journal*, vol. 7, pp. 221-225, 1961.

[3] Tsou, F.K., "Sparrow,E.M. and Goldstein,R.J., Flow and heat transfer in the boundary-layer on a continuous moving surface", *Int. J. Heat and Mass Transfer*, vol. 10, pp. 219-235, 1967.

[4] Erickson, L.E., Fan, L.T. and Fox,V.G., "Heat and mass transfer on a moving continuous flat plate with suction or injection", *Industrial Engineering Chemistry Fundaments*, vol. 5, pp. 19-25, 1966.

[5] Griffin, J.F. and Throne, J.L., "On thermal boundary layer growth on continuous moving belts", *A.I.Ch.E. Journal*, vol. 13, pp. 1210-1211, 1967.

[6] Moutsoglou, A. and Bhattacharya,A.K., "Laminar and turbulent boundary layers on moving, nonisothermal continuous flat surfaces", J*ournal of Heat Transfer*, vol.104, pp. 707-714, 1982.

[7] Abdelhafez, T.A., "Skin friction and heat transfer on a continuous flat surface moving in a parallel free stream", *Int. J. Heat and Mass Transfer*, vol. 28, pp. 1234-1237, 1985.

[8] Vleggar, J., "Laminar boundary-layer behavior on continuous, accelerating surface", *Chemical Engineering Science*, vol. 32, pp. 1517-1525, 1977.

[9] Jeng,D.R., Chang,T.A.,and DeWitt,K.J., "Momentum and heat transfer on a continuous moving surface", *Journal of Heat Transfer*, vlo. 108, pp. 532-539, 1986.

[10]Chappidi, P. R. and Gunnerson F.S., "Analysis of heat and momentum transport along a moving surface", *Int. J. Heat Mass Transfer*, vol. 32, pp. 1383-1989, 1989.

[11]Ali, M.E., "On thermal boundary layer on a power-law stretched surface with suction or injection". *Int. Heat Fluid Flow*, vol. 16, pp 280-290, 1995.

[12]Ali, M.E. and Al-Yousef, F., "Laminar mixed convection from a continuously moving vertical surface with suction or injection. *Heat Mass Transfer*, vol. 33, pp. 301-306, 1998.

[13]Elbashbeshy, E.M.A., Bazid M.A.A., "Heat transfer over a continuously moving plat embedded in non-Darcian porous medium", I*nt. J. Heat Mass Transfer*, vol. 43, pp. 3087-3092, 2000.

[14]Magyari, E., Keller, B., "Exact solutions for self-similar boundary-layer flows induced by permeable stretching walls", *Eur. J. B-Fluids*, vol. 19, pp. 109-122, 2000.

[15]Magyari, E, Ali, M.E. and Keller, B. "Boundary-layer flows induced by continuous surfaces stretched with rapidly decreasing velocities", *Heat and Mass Transfer*, vol. 38, pp. 65-74, 2001.

[16]Arafune K. and Hirata A., "Thermal and solutal Marangoni convection in In-Ga-Sb system", *J. Crystal Growth*, vol. 197, pp. 811-817, 1999.

2011 International Conference on Mechanical, Industrial, and Manufacturing Engineering
Lecture Notes in Information Technology Vols. 1-2

The Study on Relationship Between Organizational Inertia and Product Innovation

Min Liu[1, 2]

1. Glorious Sun School of Business and Management
Dong Hua University
Shanghai, China, 200051
E-mail: 7718cathy@sohu.com

Shuzhen Zhu[1]

2. School of International Business
Tianjin Foreign Studies University
Tianjin, China, 300204
E-mail: z_shuzhen@sohu.com

***Abstract*—This is the leading study of structural dynamics model and method to demonstrate the relationship between organizational inertia and product innovation in perspective of structural equation modeling. This study aims to establish the fundamental constructs of organizational inertia and the corresponding models. It reveals that the motivation of enlarging the dimensions of organizational inertia from the structural inertia is that empirical practice demands the relevant modeling foundations. Organizational inertia is regarded as the main study object in virtue of more uncertainties and complicatedly ever-changing environment. The organizational inertia is divided into three constructs and set up the dynamic evolutionary modeling with product innovation which one is exploitation and the other is exploration. The results illustrate that inertia is a two-edged sword that it is positive to foster the product innovation if change consistency and vice versa.**

Keywords- Organizational Inertia, Product Innovation, Structural Equation Modeling, Feedbak Constructs

I. INTRODUCTION

The knowledge has been focused which determines the way by which an individual, an enterprise or even a nation can gain wealth and prosperity. As a knowledge-based economy is emerging, winning through inertia, matching with ever-changing environment and favoring dynamic evolution have become popular buzzwords in organizational innovation. Thus, successful innovation of KIBS can be the chief determinant for the survival of an enterprise in a knowledge-based economy.

Enterprises are encouraged to adopt novel ideas while reforming old operational procedures and creating new ones (Nonaka, 1994). Faced with an ever-changing environment and increasing uncertainties, most of enterprises are supported by innovation with flexibility for changes, which is the key to its survival and successful development. Therefore, to weaken the negative effect of uncertainties and to meet current challenges, KIBS should seek ways to strengthen the positive effect of inertia, which has recently become an important subject in academic circles as well as in the business world.

There exists the discussion of organizational inertia if mentioned hurdles of innovation. This study frames inertia in organizations with respect to the laws of motion. It provides fresh insights into using the principles of inertia in physics to the study of KIBS innovation management. In physics, inertia refers to the principle that, unless acted upon by an external force, a body at rest remains at rest, and a body in motion remains in a state of uniform motion (Newton, 1995/1687). The inertia perspective has been imported into organizational theory from physics study (Hannan and Freeman, 1984) and this lens has played an essential role in understanding of organizational innovation conceptually and empirically.

II. THEORETICAL FRAMEWORK

A. Conceptual Understanding of KIBS

Generally speaking, KIBS are concerned with providing knowledge-intensive inputs to business process of other enterprises to the full extent, including private and public sector clients. Miles et al. (2005) explained the principal characteristics of KIBS: they rely heavily on professional knowledge; they either are themselves primary sources of information and knowledge or they use knowledge to produce intermediate services for their clients' production processes; they are of competitive importance and supplied primarily to business. More precisely, Miles identified KIBS as "services that involved economic activities which are intended to result in the creation, accumulation or dissemination of knowledge".

Tovoinen (2006), who provided another accepted assumption of KIBS, defined KIBS as "expert companies that provide services to other companies and organizations". Den Hertog (2000) suggested that "KIBS are private companies or organizations focusing on professional knowledge, i.e., knowledge or expertise related to a specific (technical) discipline or (technical) functional-domain to supply intermediate products and services that are knowledge based". Bettencourt et al. (2002) stated KIBS as "enterprises whose primary value-added activities consist of the accumulation, creation, or dissemination of knowledge for the purpose of developing a customized service or product solution to satisfy the clients' needs".

One essential point derived from the analysis of definitions is that KIBS refer to service firms that are characterized by high knowledge intensity and services to other firms and organizations, services which are predominantly non-routine (Muller, 2009).

To sum up, there is no standard approach and universally accepted explanation of KIBS. However, a certain consensus exists about the branches and organizations that comprise the KIBS sector. NACE (a European Classification of Economic Activities) provides the nomenclature with prevalent power to identify KIBS in Europe. KIBS sector includes computer and related activities, research and development, and other business services.

As described above, KIBS have come with the tide of knowledge economics and possess especially characteristic features and survival environment as well as being faced with much more uncertainty than the traditional industrials.

B. Organizational Inertia

This research analyzes inertia as a metaphor to explain organizational change and innovation. This stream of study places primary emphasis on clarifying singular changes in organizational structure. However, little research examines the

consistency of innovation, which describes the dynamic evolution of organizational inertia.

The law of motion provides the fundamental framework for inertia research. Every body perseveres in its state of rest, or of uniform motion in a straight line, unless it is compelled to change that state by forces impressed thereon (Newton, 1995/1687). Two elements are highlighted to be derived from the first law of motion. The first element emphasizes that a body at rest will remain at rest unless acted upon by a net external force. The second element states that a body in motion will remain in uniform motion in a straight line unless acted upon by a net external force. In organizational theory studies, it aligns, in particular, "a body in motion remains in uniform motion" with consistency of change in organizations.

A large body of diverse literature and research is devoted into understanding organizational inertia. The concept of organizational inertia is very broad; consequently, researchers and scholars have looked at it from a variety of perspectives. Hannan and Freeman (1984), in a population ecology perspective, proposed an evolutionary model of inertia as a starting point for this discussion. They (1984) indicated inertia in "relative and dynamic terms" which involved in the adjustment speed of organizational structure given change in the environment and claimed that "high levels of structural inertia in organizational populations could be explained as an outcome of an ecological-evolutionary process". Structures of organizations have high level of inertia pressure if the speed of reorganization is much lower than the rate at which environmental conditions change.

Considered sunk costs, KIBS are changed slowly although their structures are not of a deadweight quality unlike manufacturing industries. There are still large lags in response to environmental changes and to attempts by decision makers to implement change (Hannan & Freeman, 1984). Since lags can be longer than typical environmental fluctuations and longer than the attention spans of decision makers and outside authorities, inertia often blocks organizational innovation.

C. Inertia in System Dynamics (SD) Method

System dynamics (SD) theory was proposed by Jay W. Forrester in 1956. It is considered as "the complexity, nonlinearity, and feedback loop structures that are inherent in social and physical systems" (Forrester, 1994). Assumptions about how organizational inertia and organizational innovations illustrate the evolutionary dynamics of corporations and other institutions are frequently taken as primitive terms in empirical studies. Limited researches are available that examine these assumptions directly by representing inertia and its factors as fundamentally interdependent dynamic processes.

According to Hannan and Freeman (1984), structural inertia is not constant over the organizational life-course, but varies systematically with age and size. Dawn Kelly (1991) proposed a diagram to display a basic view of structural inertia theory.

It is the first time that the inertia theory has been demonstrated in light of the dynamic model including positive and negative feedbacks. However, there are so many limitations in this model. Some researchers regard organizational type as a moderator variable. Organizational type is a determinant factor in modern knowledge economic tide to reveal the inimitable features of organizational change.

Erik Larsen et al. (2002) redesigned Kelly's model to demonstrate the ecological model of organizational inertia and change. The model was contributed to the relationship of inertia, capabilities and changes. It made much progress to build an incommensurable empirical models but it did not pinpoint the specific dimensions of inertia in light of organizational innovation. Hence, this study aims to provide a tentative study of inertia and the relative dynamic model to fulfill the investigation of the inertia theories.

III. RESEARCH METHOD

Beginning with the notion of organization as change-resistant complex systems for which innovation is to some extent as risky as inaction, Hannan and Freeman pointed out a well-structured framework for modeling processes of organizational change. However, they could not consider the dynamic of inertia with the previous change on the scent of variability consistency.

KIBS regard the specialism-generalism knowledge and knowledge workers as the core competitive advantages in response to more uncertainty and more complicated ever-changing environment. As described above, although the core concerns addressed by these mutually contentious perspectives on organizational innovation are a little bit different, there also exist domains of substantial overlap that could be practically investigated.

Against the background of this general discussion, this research aims at making out the specific component of organizational inertia of KIBS because KIBS have the prominently different characteristics from the traditional industries. Accumulation processes of organizational inertia are developed in the context of a feedback representation of a model of change inspired by ecological theories. The study uses system dynamics (SD) methods to simulate the model, test its internal consistency, and explore the full dynamic implications of a theory with time delay. It relates to dynamic evolution of organizational inertia to explode its positive effects to organizational innovation and meanwhile to restrain and divert the negative effects.

A. Feedback Loops on Organizational Inertia and Change

As noted above, the limitations in regard to the theoretical framework should be solved imperiously. The first step is to identify and represent dynamic elements that are telegraphed through the described above and the second objective is to explore conceptual connections between core features of inertia theories of organizational innovation that are typically believed to set up incommensurable empirical models. In this regard, innovation is considered to change for enterprises.

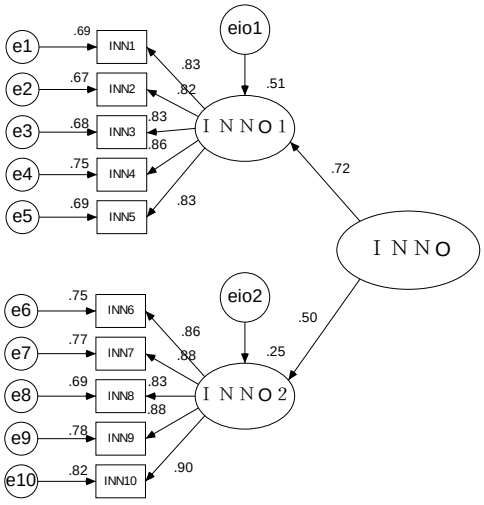

Figure 1. Product Innovation Model

According to Fig. 1, there are four feedback loops to illustrate the dilemma in deciding how organizations are faced with change pressure caused by uncertainty and ever-changing environment. Innovation endeavor enables operating routine to disrupt in the performance of the routine. It is important to believe innovation with variance on the degree of core component change and an unchanged work flow pattern. The combination of the incremental innovation and modular innovation is implicit in the part of component change. Thus the temporal consistency plays an essential catalyst in reinforcing change from the time since previous change.

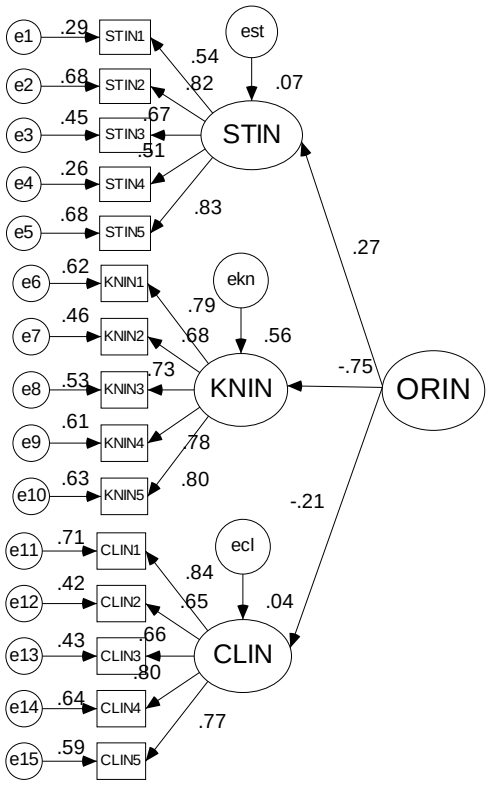

Figure 2. Organizational Inertia Model

In view of KIBS' special elements, such as knowledge worker, flexible organization, special business cultures, and more determinant factors, it should be designed in dynamic model with time delay. At the end of the arrow there are symbols "+"and "-" to represent the positive (reinforcing loop) and negative (balancing loop) feedback respectively.

As regards Fig. 2, there is a great deal of information to identify the inertia dimensions. Environment change is highlighted in the first loop that it involves with political, technological, integration of industrial structures and new international economic order as well. The loop reveals the function of routine that mentioned above which is the direct resistance to change. Any management activity in KIBS can not leave participation of individuals and thus, individual cognitive capabilities in light of environmental change take effect in the loop to influence the operating routines of KIBS.

In the second loop, one way of apprehending routines is the set of collective actions that it can do from memory (Hannan & Freeman, 1984). Nelson and Winter (1982) presented organizational memory was an organization's repertoire of routines. Among others, organizational memory is influenced by unlearning, failure and successful pattern which are the main factors of all to generate enterprises' inertia separately or jointly based on certain probability.

In the third loop, organizational learning is crucial in KIBS because of the high frequency of increasing knowledge and knowledge workers in KIBS need to reinvest in learning to keep skills and capabilities at their former levels. Individuals and organizations that have the chance to exert a broad repertoire of routines do so with too many investments in learning.

The forth loop directly illustrates knowledge inertia which Liao et al. initially proposed in 2002. This loop can be evolved more complicatedly with time delay and be endued with self-determination of an individual knowledge worker.

B. Dynamic Model of Organizational Inertia

A SD feedback loop demonstrates every element of inertia. It is very intuitive but more scientific to explore the essence in the organizational inertia during enterprises' innovation. Fig. 3 is a causal loop of inertia of KIBS which more feedback loops (reinforcing loops and balancing loops, time delay) are added to describe the dimensions of inertia in detail. The diagram identifies the nonlinear and complicated dynamic system of organizational inertia and its subsystems by virtue of every feedback loop which represents a dimension of organizational inertia and elaborates an aspect or a perspective of inertia mentioned above.

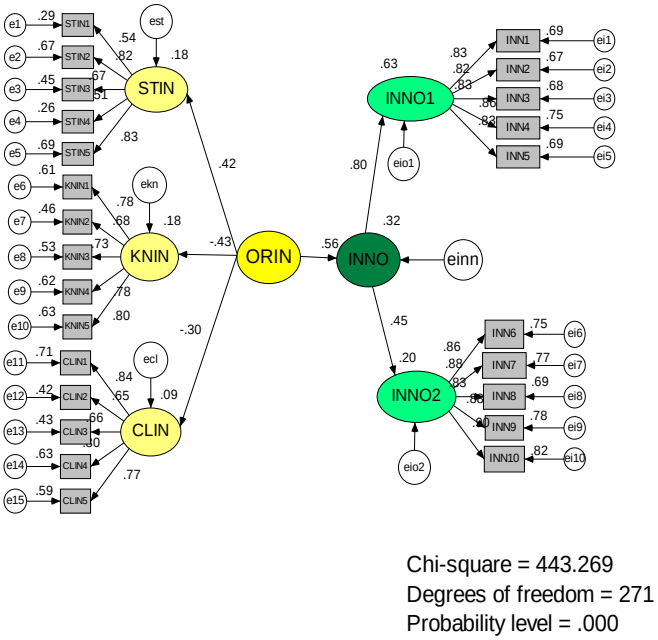

Figure 3. Model of Organizational Inertia and Product Innovation 1

It is included the cognitive and action inertia loop, structural inertia loop and knowledge inertia loop as well. In evolutionary perspective there is stronger inertia at some period of the life-cycle and sometimes weaker inertia. Thus, what we are eager to do is that no matter what kind of inertia will be expected not to hinder the process of organizational innovation.

The following will be given the relative functional equations to explain the main causal loops noted above in view of dynamic evolution. Organizational inertia (It) is represented as a stock (or accumulator) variable that integrates the corresponding net flow, defined as the balance between increase in inertia (I (+)) and decrease in inertia (I (-)).

$$I_{t_i} = \int_{t_0}^{t_i} [I^{(+)}(t_i) - I^{(-)}(t_0)]dt + I(t_0) \quad (1)$$

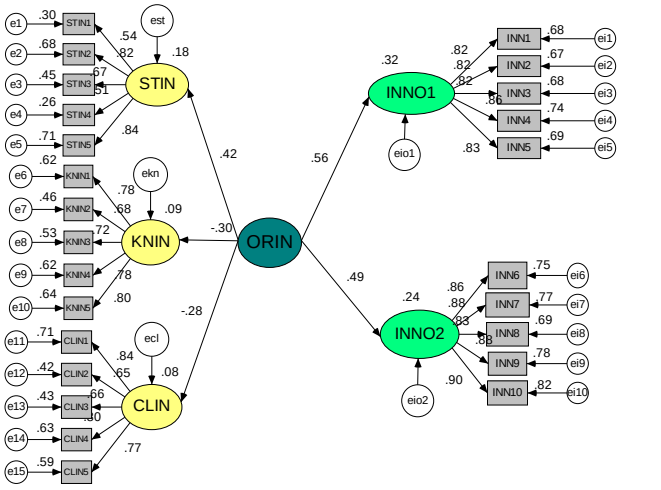

Figure 4. Model of Organizational Inertia and Product Innovation 2

According to the original formulation of the theory (Hannan & Freeman, 1984), structural inertia is affected by organizational age, size (S) and organizational memory (M). However, KIBS are not so remarkable in these variables due to the general impression of KIBS: younger, smaller size, novel design, flexible structures and independent innovation and humanized management as a core. The functional relations, which might be linear or nonlinear, are regarded as an auxiliary variable.

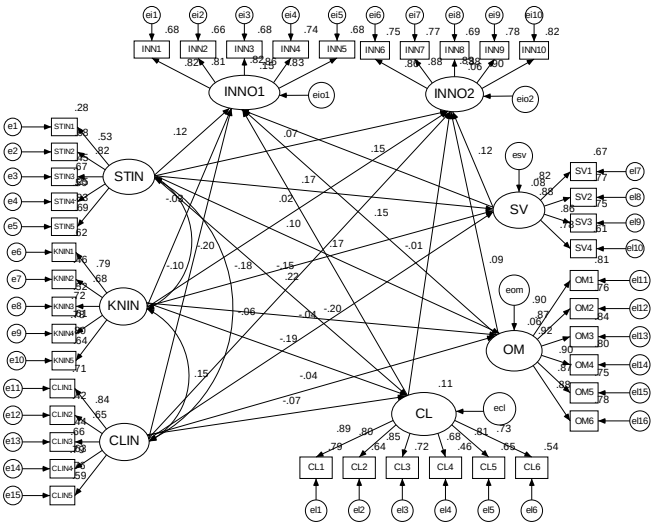

Figure 5. Model of Organizational Inertia, Organizational Learning and Product Innovation 3

IV. CONCLUSIONS

It is the first time to make KIBS as the main researching object which is always regarded as the modulator of inertia in the previous study; this paper has established a system dynamic model of KIBS' organizational inertia, namely the dynamic accumulation processes with delay; it enlarges the domains of inertia from its original theoretical foundation (structural inertia) to organizational inertia by considering features of KIBS with uncertainty and ever-changing knowledge. Inertia exists not only in structures, but also in human cognition and behavior in the process of learning knowledge and innovation activities.

From Hannan and Freeman's structural inertia, it has been peeling off the mystic veil of inertia derived from the physical field. The dynamic evolutionary study of organizations directly deals with organizational inertia and change. It is combined the features of KIBS and organizational learning and moreover, it reformulates some of the central assumptions and propositions in terms of System Dynamics. One motivation for transforming the ecological theory of structural inertia into a SD model with dynamic evolution is that empirical studies that have aimed to test the theory have been yielded to focusing on the complex feedback relations linking with individual propositions. By this causal feedback loops it is available to explore more specific dynamic feedback processes implicit in the original formulation to test its internal change consistency and the link among inertia factors.

The current modeling efforts have two limitations: the first one is that absence of necessary data which makes the dynamic simulation model unavailable; the second is that some feedback loops and their functional relations should be explored more elaborately, which is the next step in the further study.

REFERENCES

[1] Nonaka. A dynamic theory of organizational knowledge creation. Organization Science, 1994; 15 (1): 14-37.

[2] Newton. The Principia. Translated by A. Motte. Prometheus Books: Amherst, NY, 1995. Original work published in 1687.

[3] Hannan M.T., Freeman J. Structural Inertia and Organizational Change. American Sociological Review, 1984; 49(2): 149-164.

[4] Huff J O, Huff A S, Thomas H.Strategic Renewal and theInteraction of Cumulative Stress and Inertia. Strategic Management Journal, 1992; 13.

[5] Miles I, Kastrinos N, Flanagan K, Bilderbeek R, Den Hertog P. Knowledge-intensive Business Services: Users, Carriers and Sources of Innovation. European Innovation Monitoring Systems. EIMS Publication No 15. Innovation Programme, DGXIII, Luxembourg, 1995.

[6] Toivonen M. Future Prospects of Knowledge-intensive Business Services (KIBS) and Implications to Regional Economies. ICFAI Journal of Knowledge Management, 2006: 4, 3.

[7] Den Hertog. PD. Knowledge-intensive Business Services as Co-producers of Innovation. International Journal of Innovation Management, 2000; 4(4):491–528.

[8] Bettencourt LA, Ostrom AL, Brown SW, Roundtree RI. Client Co-production in Knowledge-intensive Business Services. California Management Review, 2002; 44:100–28.

[9] Emmanuel Muller, David Doloreux. What we should Know about Knowledge-intensive Business Services. Technology in Society, 2009; 31: 64-72.

[10] Shu-hsien Liao, Wu-Chen Fei, CT Liu. Relationships between knowledge inertia, organizational learning and organization innovation. Technovation, 2008(28): 183-195.

[11] Jay W Forrester. System Dynamics, Systems Thainking, and Soft OR. System Dyanmics Review. 1994; 10 (2).

[12] E. Larsen, A Lomi. Representing Change: a System model of Organizational Inertia and Capabilities as Dynamic Accumulation Processes. Simulation Modelling Proactice and Theory, 2002; 10: 271-296.

[13] Jing K. Bai. Organizational Evolution Study in Perspective of Inert. Reform and Strategic, 2008 (3): 157-158. In Chinese.

[14] Nelson R, Sidney Winter. An Evolutionary Theory of Economic Change. Cambridge: Belknap, 1982.

[15] Kelly D, Amburgey T. Organizational inertia and momentum: a dynamic model of strategic change. Academy of Management Journal, 1991 (34): 591–612.

2011 International Conference on Mechanical, Industrial, and Manufacturing Engineering
Lecture Notes in Information Technology Vols. 1-2

Looping With Colebrook Friction Factor During Liquid Flow In Pipes

Peter Ohirhian.

Dept. of Petroleum Engineering, University of Benin, Benin City, Nigeria.

(e-mail: okuupet@yahoo.com, okuopet@gmail.com)

***Abstract* - A new equation for calculating the increase in the liquid volumetric flow rate due to the looping of two pipes has been developed. Unlike current equations that consider only pipe diameter and length, the new equation uses the Colebrook friction factor and pipe length. The Colebrook dimensionless friction factor is a function of both absolute roughness of the pipes and the viscosity of the fluid transported by the pipes.**

The increase in the liquid volumetric flow rate due to the looping of two pipes remains constant for all types of transported liquids , when only pipe diameter and length are considered. The new formula reveals that the gain in the flow rate that results from the looping of two pipes is not constant. It changes slightly from one liquid type to another.

For the purpose of comparison, the new equation was used to solve a problem whose solution is available in the literature. The new equation predicted an increase in the liquid volumetric rate as 17.882 %, while the current method that considers only pipe diameter and length calculated it as 17.913 %.

Further, the new equation was arranged in the form of an algorithm that can be used to calculate the pipe diameter needed to achieve a desired increase in volumetric flow rate during the looping of two pipes.

KEY WORDS: Pipe Looping, Colebrook Friction Factor, Liquid Flow, Optimum Diameter

1.0 INTRODUCTION

Equations for calculating the pressure drop or volumetric rate during fluid flow in pipes, generally involve the use of a dimensionless friction factor (f). The dimensionless friction factor(f) can be experimentally measured when the fluid properties (specific gravity and viscosity) and pipe properties (length, diameter and absolute roughness) are known. Colebrook [1] combined the equations developed from experimental measurement of the dimensionless friction factor (for complete turbulent fluid flow through rough pipes) with the equation of fluid flow through smooth pipes, to arrive at a general equation for the dimensionless friction factor. The dimensionless friction factor depends on the Reynolds number, which in turn, depends on the volumetric flow rate. Thus, developing an equation for the change of flow rate due to the joining of pipes with different absolute roughness and diameter is a formidable task when the dimensionless friction factor is involved.

Early attempts to calculate the change in the liquid volumetric flow rate due to the looping of two pipes, replaced the Colebrook friction factor with constants that can be read from tables. One early attempt was that of Hazen Williams.(Giles et al., [2]). Katz et al. [3] proposed an equation for calculating the increase in the gas volumetric flow rate that related to the Colebrook dimensionless friction factor. However, they could not propose a formula for calculating the dimensionless friction factor that appeared in their equation. It had to be experimentally measured. Ikoku [4] made use of Weymouth assumption (that the dimensionless friction factor can be approximately related to only pipe diameter) and came up with an equation for calculating the increase in the gas volumetric flow rate due to the looping of two pipes. An equation of this type that includes only pipe properties predicts a constant increase in the flow rate for all types of fluids that flow through equal lengths and diameters of pipes. Recently, Ohirhian and Ofoh [5] came up with an equation for calculating the increase in the liquid volumetric rate due to the joining of two pipes in parallel. The Ohrhian and Ofoh equation made use of the Colebrook dimensionless friction factor.

In this work, an equation for calculating the increase in the liquid volumetric flow rate that depends on the Colebrook dimensionless friction factor during the looping of two pipes is developed. The equation is also arranged in the form of an algorithm for calculating the exact diameter of a new pipe that is needed to loop an existing pipe in order to attain a desired increase in the liquid volumetric flow rate.

2. 0 DEVELOPMENT OF EQUATIONS

2.1 Equations for flow rate

Application of the Bernoulli equation to two points in a uniform diameter pipe that transports a liquid, leads to

$$\frac{P_1}{\omega}+\frac{V_1^{\,2}}{2g}+Z_1-H_L=\frac{P_2}{\omega}+\frac{V_2^{\,2}}{2g}+Z_2 \quad (1a)$$

Where

P_1 = Pressure at point (1)

P_2 = Pressure at point (2)

w = Specific weight of the liquid

V = Average velocity of the liquid

g = Acceleration due to gravity

d = Diameter of the pipe

L = Length of the pipe

Z_1 = Elevation of the pipe at point (1)

Z_2 = Elevation of the pipe at point (2)

The generally accepted expression for the loss of head during laminar and turbulent flow in pipes is that of Darcy-Weisbach. The expression for the loss head (H_L) is:

$$H_L=\frac{fLv^{\,2}}{2gd} \quad (1b)$$

Where, f =Dimensionless friction factor

Combination of equations(1a) and (1b) leads to :

$$\frac{P_1}{\omega}+\frac{V_1^{\,2}}{2g}+Z_1-\frac{fLv^2}{2gd}=\frac{P_2}{\omega}+\frac{V_2^{\,2}}{2g}+Z_2 \quad (1c)$$

During liquid (incompressible) flow in pipes,

$$Q=AV \quad (2)$$

Where

Q = Liquid volumetric rate

A= Cross-sectional area of the pipe

Also, $A=\frac{\pi}{4}d^2$. Combination of equations (1 c) and (2) produces

$$Q=\frac{\pi}{4}\frac{d^{\,2.5}\,y}{\sqrt{f\,L}} \quad (3)$$

where

$$y=\sqrt{2g}\left[\frac{[p_1-p_2]}{w}+(Z_1-Z_2)\right]^{0.5} \quad (4)$$

The variables in equations (3) and (4) remain as defined in previous equations.

The Reynolds number which is a ratio of viscous to inertia forces during fluid flow pipes is,

$$R_N=\frac{\rho Vd}{\mu}=\frac{wVd}{\mu\, g} \quad (5)$$

Where μ = absolute viscosity of the fluid and other variables remain as defined in previous equations. Then,

$$Q=\frac{\pi R_N\,\mu\, d\, g}{4\,w} \quad (6)$$

The kinematics viscosity of a fluid (ν) is defined by Giles et al (2009) as

$$\nu=\frac{\mu}{\rho}=\frac{\mu g}{w} \quad (7)$$

Then, the volumetric rate (Q) can be expressed as:

$$Q=\frac{\pi R_N\,\nu\, d}{4} \quad (8)$$

Simultaneous solution of equations (1 c) and (8) leads to

$$R_N\sqrt{f}=\frac{d^{\,1.5}\,y}{\nu\sqrt{L}} \quad (9)$$

The Colebrook (1938) equation is widely used for the calculation of the dimensionless friction factor (f). The equation is:

$$\frac{1}{\sqrt{f}}=-2\log\left(\frac{\epsilon}{3.7d}+\frac{2.51}{R_N\sqrt{f}}\right) \quad (10)$$

Where

$\in$ = Absolute roughness of the pipe and other variables remain as defined in previous equations.

Substitution of $R_N\sqrt{f}$ from equation (9) into equation (10) gives:

$$\frac{1}{\sqrt{f}} = -2\log\left(\frac{\in}{3.7d} + \frac{2.51\,\nu\sqrt{L}}{y\,d^{1.5}}\right) \qquad (11)$$

Simultaneous solution of equations (3) and (10) gives:

$$Q = -1.570796\frac{yd^{2.5}}{\sqrt{L}}\log\left(\frac{\in}{3.7d} + \frac{2.51\nu\sqrt{L}}{yd^{1.5}}\right) \qquad (12)$$

All the variables in equation (12) remains as defined in previous equations.

2.2 Calculation of the equivalent diameter of pipes in parallel

The pressure drop across pipes in parallel is same. Thus for two pipes in parallel,

$$\Delta p_t = \Delta p_A = \Delta p_B \qquad (13)$$

Where

ΔP_t = Total pressure drop.

ΔP_A = pressure drop across pipe A

ΔP_B = pressure drop across pipe B

The total volumetric rate for pipes in parallel is the sum the volumetric rates through the individual pipes. Thus for two pipes, A an B , in parallel,

$$Q_t = Q_A + Q_B \qquad (14)$$

Where

Q_A=Volumetric rate through pipe A

Q_B=Volumetric rate through pipe B

Q_t=Total volumetric rate through pipes A and B.

If the inlet pressure p_1, the exit pressure p_2 and change in elevation ($Z_1 - Z_2$) are same for two pipes in parallel, then from equation (3),

$$\frac{d_e^{2.5}}{\sqrt{f_e L_e}} = \frac{d_A^{2.5}}{\sqrt{f_A L_A}} + \frac{d_B^{2.5}}{\sqrt{f_B L_B}} \qquad (15)$$

The subscript e, refers to equivalent properties of a pipe that has the same flow rate as the two pipes joined in parallel. Choose pipe A as the reference for calculating the equivalent properties, then,

$$\frac{d_A e^{2.5}}{\sqrt{f_A L_A}} = \frac{d_A^{2.5}}{\sqrt{f_A L_A}} + \frac{d_B^{2.5}}{\sqrt{f_B L_B}} \qquad (16)$$

$$\text{Or} \quad d_{Ae}^{5} = d_A^{5}\left(1 + \left(\frac{d_B}{d_A}\right)^{2.5}\left(\frac{f_A}{f_B}\right)^{0.5}\right)^{2} \qquad (17)$$

Where d_{Ae} is the diameter of pipe A that gives the same flow rate as both pipes A and B joined in parallel.

2.3 Equations for equivalent length of pipes in series

The total pressures drop across pipes in series the sum of the pressure drop though the individual pipes. Thus for two pipes in series

$$\Delta P_t = \Delta P_A = \Delta P_B \qquad (19)$$

Then,

$$\frac{f_A L_A}{d_e^{5}} = \frac{f_A L_A}{d_A^{5}} + \frac{f_B L_B}{d_B^{5}} \qquad (20)$$

Subscript e refers to properties of a pipe whose pressure drop is same as the total pressure drop across pipes A and B joined in series. Chose pipe A as reference for calculating the equivalent properties (d_e, f_e, and L_e), then,

$$L_{Ae} = L_A + L_B\left(\frac{d_A}{d_B}\right)^{2.5}\left(\frac{f_B}{f_A}\right)^{0.5} \qquad (21)$$

Where L_{Ae} is the equivalent length of pipe A whose pressure drop is same as the combined pressure drops through pipes A and B.

Equation (21) can be written in dimensionless form as

$$L_{Ae} = 1 - x + x\left(\frac{d_A}{d_B}\right)^{2.5}\left(\frac{f_B}{f_A}\right)^{0.5} \qquad (22)$$

Where x , is the fraction of total length that is occupied by pipe B.

2.4 Calculation of increase in flow rate through pipes in series

Equation (3) can be written as:

$$Q = \frac{K^1}{\sqrt{f}} \frac{d}{\sqrt{L}}^{2.5} \quad (23)$$

Where

$$K^1 = \frac{\pi}{4}\sqrt{2g}\left[\frac{[p_1 - p_2]}{w} + (Z_1 - Z_2)\right]^{0.5}$$

The quantity K^1 is constant after joining two pipes in series, provided there is no change in the inlet, outlet pressures and elevation as a result of joining the pipes. Let Q_A be the flow rate through pipe A and Q_N be the new flow rate after joining pipe B in series to pipe A, then

$$Q_N = \frac{k'^1 de^{2.5}}{\sqrt{fe\ Le}} \quad (24a)$$

$$Q_A = \frac{K^1 d_A^{2.5}}{\sqrt{f_A L_A}} \quad (24b)$$

Where the equivalent properties d_e, f_e, and L_e are calculated with pipe A as the reference, then,

$$\frac{Q_N}{Q_A} = \frac{\sqrt{L_A}}{\sqrt{L_{Ae}}} \quad (25)$$

The ratio $\frac{Q_N}{Q_A}$ can be written as $\frac{Q_N}{Q_A} = 1 + \frac{Q_B}{Q_A}$ Then, from equation (22) $Q_N =$

$$1 + \frac{Q_N}{Q_A} = \frac{1}{\left[x\left(\frac{d_A}{d_B}\right)^5\left(\frac{f_B}{f_A}\right) + 1 - x\right]^{0.5}} \quad (26)$$

Let us denote the fractional increases in the volumetric flow rate by FI, then,

$$FI = \frac{Q_B}{Q_A} = \left[x\left(\frac{d_A}{d_B}\right)^5\left(\frac{f_B}{f_A}\right) + 1 - x\right]^{-0.5} - 1 . \quad (27)$$

2.5 Equation For Increase in Flow Rate Of Looped Pipes

Figure 1 shows a pipe A, with diameter d_A, and absolute roughness $\in_A$ to which pipe B, with diameter d_B and absolute roughness $\in_B$ is looped.

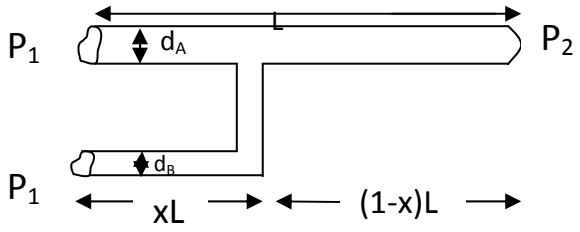

Fig 1. A schematic of a looped pipe line

Let L be the length of pipe A and x the fraction of L that is looped. Then application of equation (17) to the parallel section of the loop produces a pipe with a larger diameter than that of pipe A, that is joined in series to pipe A. The larger pipe has absolute roughness of pipe A and its diameter is:

$$d_{Ae}^{\ 5} = d_A^{\ 5}\left(1 + \left(\frac{d_B}{d_A}\right)^{2.5}\left(\frac{f_A}{f_B}\right)^{0.5}\right)^2$$

Equations (22) and (25) can be applied to the two pipes in series to get the fractional increase in the volumetric flow rate as:

$$FI = \left\{x\left(1 + \left(\frac{d_B}{d_A}\right)^{2.5}\left(\frac{f_A}{f_B}\right)^{0.5}\right)^{-2} + 1 - x\right\}^{-0.5} - 1 \quad (28)$$

Where $\left(\frac{f_A}{f_B}\right)^{0.5}$ is obtained from equation (11) as:

$$\left(\frac{f_A}{f_B}\right)^{0.5} = \frac{\log\left(\frac{\in_B}{3.7 d_B} + \frac{2.51 v\sqrt{L}}{y d_B^{1.5}}\right)}{\log\left(\frac{\in_A}{3.7 d_A} + \frac{2.51 v\sqrt{L}}{y d_A^{1.5}}\right)} \quad (29)$$

Example 1

Table 1 shows the diameters and lengths of a looped pipeline

The system transports natural gasoline with specific gravity 0.719 and kinematic viscosity 0.660 x 10^{-5} ft^2/sec.. What is the fractional increase in the volumetric flow rate? Use a pressure drop of 300 psig and absolute roughness of 0.0003 ft for both pipes A and B.

Table 1. Pipe properties of a looped pipeline.

Section	Internal diameter (inch)	Length L (miles)
A	4	3
B	6	3
C	4	7

Solution

Length of pipe A (L) = 10miles = 10 x 5280 ft = 52800 ft

Pressure drop (P_1 - P_2) = 300psig = 300 × 144 psf = 43200 psf

d_A = 4 in = 0.33333 ft. ,

d_B = 6 in = 0.50000 ft.

w = 62.4 × 0.719 lb / ft^3

= 44.8656 lb / ft^3

v = 0.66 × 10^{-5} ft^2 / sec

Fraction of looped length of pipe (x) = $3/10 = 0.3$

$$\frac{\in_A}{3.7d_A} = \frac{.0003}{3.7\times 0.3333} = 2.43246E\text{-}4$$

$$\frac{\in_B}{3.7d_A} = \frac{0.0003}{3.7\times .0.5} = 1.62162E-4$$

$$y = \sqrt{2g}\left[\frac{(p_1 - p_2)}{w} + (Z_1 - Z_2)\right]^{0.5}$$

$$= \sqrt{2\times 32.2}\left[\frac{43200}{44.8656} + 0\right]^{0.5} = 249.01647$$

$$\frac{2.51\,v\sqrt{L}}{yd_A^{1.5}} = \frac{1.52864E-5}{249.01647\times 0.33333^{1.5}} = 7.94317E-5$$

$$\frac{2.51v\sqrt{L}}{yd_B^{1.5}} = \frac{1.52864\,E-5}{249.01647\times 0.5^{1.5}} = 4.32366\,E-5\ \text{T}$$

hen, $\left(\frac{f_A}{f_B}\right)^{0.5} = \frac{\log(1.62162E-4+4.32366E-5)}{\log(2.43246E-4+7.94317E-5)}$

= 1.05619

$$\left[1+\left(\frac{d_B}{d_A}\right)^{2.5}\left(\frac{f_A}{f_B}\right)^{0.5}\right] = \left[1+\left(\frac{6}{4}\right)^{2.5}\times 1.05619\right]$$

= 3.91052

Then,

$$\text{FI} = \left\{x\left[1+\left(\frac{d_B}{d_A}\right)^{2.5}\left(\frac{f_A}{f_B}\right)^{0.5}\right]^{-2} + 1 - x\right\}^{-0.5} - 1$$

$$= \left(0.3\times 3.91052^{-2} + 0.9\right)^{-0.5} - 1.0$$

= 0.17882 = 17.882%

The solution of Ikoku [4] that does not consider the effects of fluid specific gravity and viscosity, and pressure drop across the inlet and exit ends of a looped pipeline follows:

$$L_{AB}{}^{1} = \left[\frac{1}{\left(\frac{1}{3}\right)^{0.5}\left\{1+\left(\frac{6}{4}\right)^{8/3}\right\}}\right]^2 = 0.19244\ mi$$

$$L_{AB} = L_c + L_{AB}{}^{1} = 7.19244\ \text{mi}$$

$$\frac{Q_N}{Q_A} = \left(\frac{10}{7.19244}\right)^{0.5} = 1.17913$$

Hence, $FI = \frac{Q_B}{Q_A} = \frac{Q_N}{Q_A} - 1 = 0.1793 = 17.913\%$

When this type of solution is used, the fractional increase in the flow rate remains CONSTANT for all types of liquids transported by a looped pipeline. Further, the absolute roughness of a new pipe that is used to loop an old pipe may not be the same. The change in absolute roughness can also influence the increase in the flow rate due to looping.

2.6 Effect of Fluid properties, pressure drop and absolute roughness on increase in flow rate

To illustrate the effect of fluid properties, pressure drop and difference in the absolute roughness of looped pipes in the increase in volumetric rate, we shall alter the fluid specific gravity and viscosity, pressure drop and absolute roughness of the new pipe, in the previous example

Example 2

Use the data shown in table I to calculate the increase in the volumetric flow rate; if the transported liquid is medium fuel oil at 80^0F. Medium fuel oil at 80 ° F, has specific gravity = 0.851 and kinematic viscosity =3.65 x10 $^{-5}$ ft^2/sec. Also use ΔP =400psig and the absolute roughness of the new pipe as 0.00008ft.

Solution

$$\frac{\in_A}{3.7d_A}=\frac{0.0003}{3.7\times.0.33333}=2.43246E-4$$

$$\frac{\in_B}{3.7d_B}=\frac{0.00008}{3.7\times0.5}=4.32432E-4$$

,

$$y=\sqrt{2\times32.2}\left(\frac{400x144}{0..851\times62.4}\right)^{0.5}$$

$$=264.29996$$

$$\frac{2.51\nu\sqrt{L}}{y\,d_A}=\frac{2.51\times3.65E-5\times\sqrt{52800}}{264.29996\times0.33333}=1.30881E-5$$

$$\frac{2.51\nu\sqrt{L}}{yd_B}=\frac{2.51\times3.65E-5\times\sqrt{52800}}{.264.29996\times0.5}=7.12413E-5$$

Then,

$$\left(\frac{f_A}{f_B}\right)^{0.5}=\frac{\log(4.32432E-4+7.12413E-5)}{\log(2.43246E-4+1.30881E-5)}$$

= 0.91832.

$$FI=\left\{0.3\left[1+\left(\frac{6}{4}\right)^{2.5}\times0.91832\right]^{-2}+0.7\right\}^{-0.5}-1$$

$$=(0.0240+0.7)^{0.5}-1$$

$$=0.17520\ \ =17.520\ \%$$

The increase in flow rate has changed form 17.882% to 17.520 %. Indeed, the change in flow rate IS NOT CONSTANT.

2.7 Selection of optimum diameter of pipe needed for looping

Equation (28) can be arranged as

$$\left(\frac{d_B}{d_A}\right)^{2.5}\left(\frac{f_A}{f_B}\right)^{0.5}=\left(\frac{x}{T^{-2}+x-1}\right)^{0.5}-1.0 \qquad .(30)$$

Where

T = 1 + FI
FI = Desired fractional increase in flow rate
x = Fraction of pipe that is looped, starting at the upstream end of the original pipe.

Then combination of equations (29) and (30) produces:

$$d_B=d_A G^{0.4}\left[\frac{H}{\log\left(\frac{\in_B}{3.7d_B}+\frac{2.51\nu\sqrt{L}}{yd_B}\right)}\right]^{0.4} \qquad (31)$$

Where:

$$G=\left[\left(\frac{x}{T^{-2}+x-1}\right)-1.0\right]$$

$$H=\log\left(\frac{\in_A}{3.7d_A}+\frac{2.5\nu\sqrt{L}}{yd_A^{1.5}}\right)$$

$$y=\sqrt{2g}\left[\left(\frac{p_1-p_2}{w}\right)+(Z_1-Z_2)\right]^{0.5}$$

Where x = 1, equation (31) reduces to the Ohirhian and Ofoh [5] equation for the increase in flow rate due to the placement of two pipes in parallel. The Ohirhian and Ofoh equation for the increase in flow rate by the addition of a new pipe in parallel to an existing pipe is:

$$d_B = d_A FI^{0.4}\left[\frac{H}{\log\left(\frac{\in_B}{3.7 d_B}+\frac{2.51\nu\sqrt{L}}{y d_B}\right)}\right]^{0.4} \quad (32)$$

A negative sign of the quantity G in equation (31) shows that a second pipe selected to loop an existing pipe CANNOT bring about the desired increase in the flow rate, by use of the fraction of the length old pipe that is to be looped.

Example 3

A 6 inch pipe is to be used to loop a 4 inch pipeline. Is it possible to achieve a 50% increase in flow rate, if 0.3 of the length of the existing pipeline is to be looped?

Solution

Here, fraction of old line to be looped (x) = 0.3

Desired increase in flow rate (FI) = 50% = 0.5

Then, T = 1 + F I = 1 + 0.5 = 1.5

$$G = \left(\frac{x}{T^2 + x - 1}\right)^{0.5} - 1$$

$$= \left(\frac{0.3}{1.5^{-2} + 0.3 - 1.0}\right) - 1 = -2.17391$$

The negative sign of G shows that it is not possible.

Example 4

A 6 inch pipe is to be used to loop a 4 inch pipe line. Is it possible to achieve a 25% increase in flow rate, if half of the length of the existing pipeline is to be looped?

Solution

$$G = \left(\frac{0.5}{1.25^{-2} + 0.5 - 1}\right) - 1 = 2.571428$$

Yes, it is possible!

Equation (31) is non linear. Numerical analysis groups this equation of type : x = f(x)

The solution to x = f(x) according to shield [6] is:

$$x_{I+1} = f(x_i) \quad (33)$$

Where x_i is an initial guess (approximate solution). The initial guess in equation (31) is $d_A G^{0.4}$. That is: $d_{B1} = d_A G^{0.4}$ .Then

$$d_{B\,i+1} = d_A G^{0.4}\left[\frac{H}{\text{Log}\left(\frac{U_1}{d_{B\,i}}+\frac{U_2}{d_{B\,i}^{1.5}}\right)}\right]^{0.4}$$

Where U_1 ,U_2, y and H are constants defined as:

$$U_1 = \frac{\in_B}{3.7 d_A}, \quad U_2 = \frac{2.51\nu\sqrt{L}}{y}$$

$$y = \sqrt{2g}\left[\left(\frac{p_1 - p_2}{w}\right) + (Z_1 - Z_2)\right]^{0.5}$$

$$H = \log\left(\frac{\in_A}{3.9 d_A} + \frac{2.51\nu\sqrt{L}}{y\, d_A^{1.5}}\right)$$

In order to start the computation, d_{B1} is taken as = $d_A G^{0.4}$

Convergence is $\left|d_{B\,i+1} - d_{B\,i}\right| < TOL$

Where, TOL is a small number that depends on needed accuracy.

Example 5

Find the diameter of a pipe needed to loop a 4 inch horizontal pipeline to half of its total length of 10 miles, if it is desired to achieve 25% increase in the volumetric flow rate. Take absolute roughness of the old 4 inch line as 0.0003 ft and that of the new pipe as 0.00008. Also. take pressure drop as 400 psig, specific gravity of transported liquid as 0.851 and its kinematic viscosity as 3.65 x10 $^{-5}$ ft^2/sec.

Solution

Here, $y = \sqrt{2g}\left(\frac{\Delta p \times 144}{w}\right)^{0.5} = \sqrt{2x32.2}\left(\frac{400x \times 144}{0.851 \times 62.4}\right)^{0.5}$

= 264.29996

$$U_2 = \frac{2.51\nu\sqrt{L}}{y}$$

$$= \frac{2.51 \times 3.65E-5 \times \sqrt{52800}}{264.29996}$$

= 7.965012E-5

G = 2.57143 (from example (4)

Initial guess = $d_{B1} = d_A G^{0.4}$ = 0.33333x2.57143$^{0.4}$ = 0.485262

$$U_1 = \frac{\in_B}{3.7} = \frac{0.00008}{3.7} = 2.162162E-5$$

$$H = \log\left(\frac{0..0003}{3.7 \times 0.33333} + \frac{2.51 \times 3.65E\text{-}3 \times \sqrt{52800}}{264.29996 \times 0.33333^{1.5}}\right)$$

$$= -3.18235$$

Then,

$$d_{B2} = 0.485262\left[\frac{-3.182351308}{\log\left(.\frac{2.162162E-5}{0.485262} + \frac{7.965012E-5}{0..485262^{1.5}}\right)}\right]^{0.4}$$

$$= 0.485262\left[\frac{-3.182351308}{-3.552559865}\right]^{0.4}$$

= 0.464364456

d_{B3}=0.485262 × PU . Where:

$$PU = \left[\frac{-3.182351308}{\log\left(.\frac{2.162162E-5}{0.464364456} + \frac{7.965012E-5}{.464364456^{1.5}}\right)}\right]^{0.4}$$

$$= 0.485262\left[\frac{-3.182351308}{-3.525389983}\right]^{0.4}$$

= 0.465792687

d_{B4}=$0.485262\left[\frac{-3.182351308}{-3.527286362}\right]^{0.4}$

= 0.465692501

Continuing in this manner,

d_{B5} = 0.465699516

$$\left|d_{B5} - d_{B4}\right| = 0.000007015$$

By use of a TOL =0.00001, the iteration has converged.

Expected accuracy iS 5 decimal places. Thus, the required diameter =0.46570 ft = 0.46570 x12 inches = 5.5884 inches

3 CONLUSIONS

1. A new equation for the calculation of the increase in the liquid volumetric flow rate that results from the looping of two pipes has been developed. The increase in flow rate from the new equation, depends on pipe properties, such as , diameter, length, and absolute roughness, and liquid properties-specific gravity and viscosity.

2. The increase in the liquid volumetric flow rate predicted by current equations use only the pipe properties – length and diameter. The restriction of current models to only pipe properties makes the increase in flow rate computed by them to be constant. The increase in the volumetric rate from the new model is not constant

3. An algorithm for selecting the exact diameter of a new pipe needed to loop an existing pipe in order to achieve a desired increase in the liquid volumetric rate has been developed.

SI Metric Conversion Factors

$(°F - 32)/18$	$= °C$
$ft \times 3.048000 * E-01$	$= m$
$m \times 2.540 * E+00$	$= cm$
$lbf \times 4.448222 E+00$	$= N$
$lbm \times 4.535924 E-01$	$= kg$
$psi \times 6.894757 E+03$	$= Pa$
$lb\,sec/ft^2 \times 4.788026 E+01$	$= Pa.s$

* Conversion factor is exact.

REFERENCES

[1] Colebrook, C.F.J, Inst.Civil Engineers, 11, p 133, 1938.

[2] R.V. Giles, L. Cheng, and J. Evert, Schaum's Outline Series of Fluid Mechanics and Hydraulics, McGraw Hill Book Company, New York, 2009

[3] D.L. Katz, C. Cornell, K. Kobashi,F.H. Poettman, J.A. Vary, J.H.Eliribaas,., and C.F. Weinaug,Hand Book of Natural Gas Engineering, New York, McGraw Hill Book Company, 1959

[4] C.U. Ikoku, Natural Gas Production Engineering, New York, John Wiley & Sons. New York, 1984

[5] P.U. Ohirhian, and E.P. Ofoh, "Direct calculation of the flow rate and pipe paralleling during liquid flow in pipes" Journal of Mathematics and Technology, **B**aku, Azerbaijan.No3, August, 2010

[6] F. Sheid, Theory and Problems of Numerical Analysis,Schaum's Outline Series of Fluid Mechanics and Hydraulics, McGraw Hill Book Company, New York, 1968

2011 International Conference on Mechanical, Industrial, and Manufacturing Engineering
Lecture Notes in Information Technology Vols. 1-2

A Study on Principle and Method of Design for Environment and Some Major Approaches to Implementation

Wang-Qi
Academy of Art and Design
Shandong Institute of Light Industry
Jinan, Shandong Province, China
wangqi8231356@126.com

***Abstract* - Along with the economic development and strengthening of people's awareness of the environmental protection, Design for Environment emerging as a whole new way of designing in view of products is more and more valued by people. The soul of designing thus has transferred from emphasizing the performance of products to the equal stress on performance and beauty, which will by any means prove to be a blessing for the shaping and establishment of a more healthy and sustainable society.**

Index Terms - design, product, sustainable development, ecology, pollution

INTRODUCTION

Since the proposal of "sustainable development" by the United Nations in 1987, "sustainable development" has begun attracting world wide attention, developing a hot issue in a global scale. To establish a sustainable society, that is, meet the various needs of our offspring and all alive species, we must base products designing on ecology to prevent pollution at source, building a new production and consumption system. Back to the earlier stage of designing, the central concept of designing has transferred from emphasizing the performance of products to the equal stress on performance and beauty. Nowadays, designers are required to further consider the environmental influence imposed by the designing and manufacturing of products in application. Therefore, ecology-based design seems to be a trend in years ahead.

1. Concept of "Design for Environment" and its development

Design for Environment, known also as Ecological Design, Green Design or Environment Conscious Design is originally proposed by American design theorist Victor Papanek in his work"Design for the Real World"in which the effective utilization of limited natural resources and designers' moral and social responsibility are equally emphasized for the sake of protecting earth, besides, design in essence is not merely intended for commercial value and winning the competition of design and package style, it is indeed a way of meeting the growing social needs in various respects. Papanek' theory has a persistent and universal impact on modern world and the "green" idea as a core notion of DFE is being more and more valued by an overwhelming number of consumers who advocate such concepts as rationally using, economizing and conserving resources as energy shortage appears as one of the major social crises confronting human beings, ideas like green-expenditure, green products, sustainable consumption are accordingly accepted as well.

It is agreed today product design is closely interrelated with sustainable development, for the former has a sustainable influence on human life and the whole society. Thus,designers are supposed at the earliest stage of designing to take en environmental elements and pollution precaution into account,taking environmental factor as goal and starting-point of designing, minimizing the negative impact of products on environment to the lowest scale.the central notion of DFE is conceived as "three R", ie, "Reduce，Recycle and Reuse" which does not only reduce the consumption of materials and resources and the disposal of toxic substance , but also recycle and reuse them with convenience. DFE is based on the reflection of environmental and ecological pollution caused

by modern technological culture, exemplifying a returning to nature and moral value for designers. DFE,therefore,is considered a concept of evolution going beyond a technical level which requires designers to abandon the seeking for novelty and originality of the appearance of products; designers instead are responsible for the creativity of products to prolong its life span as much as possible in a long run.

2. Design principles of DFE and its evaluation methods

2.1 Design principles:

To achieve the unity of systematization and integration, DFE must give the whole precess of production from raw materials option, designing, manufacturing, marketing and after-sale service into full consideration. In recent years, the principle for DFE is being widely and heated discussed across the whole design world.

Japanese scholar Ryoichi Yamamoto suggests that three elements are involved in a product's life circle: cost (short for C including the total cost of raw material, manufacturing, recycling, and disposal); impact (short for I including loss and wastage of resource, health hazard and environmental pollution etc,.); and performance (short for F including safety, convenience, beauty and construction situation). The comprehensive value indicators can be presented as P/IC, therefore, the best principle is to lengthen P and shorten I and C as much as possible. As a contrast, designers only consider P/C, maximizing the finest performance and lowering production cost, which makes all the difference between traditional design and DFE.

Prof. Vander Run S. of University of California puts forward "the five principle of DFE":

- integrate design with regional and cultural factors, as a consequence, the design methods will arise out of cultural and physical features based on different areas.
- design products "according to ecological accounting", namely, to design products on basis of LCA (ie, Life Cycle Assessment), or collect information of ecological accounting neglected by the previous economic theory and perfect it.
- to "design conforming to natural structure", ie, to design products making effective use of model and evolution embodied by nature itself.
- "everyone is likely to be the designer"
- "visualize nature". Given the fact that people living in era of modern industrialization are less likely to see the ecological process of crafts, their awareness, concern and imagination is dwindling at the same time, visualize nature will improve human awareness of protecting environment.

In addition to the above mentioned theoretical principles, many countries are considering and adopting the principle of "Three R": reduce, recycle and reuse.

2.1.1 Reduce

"reduce" includes (1) reducing volume in designing, that is, cutting the unnecessary components from the complex structure and function to achieve the essence of it, making the products smaller simpler in size; (2) reduce energy consumption, such as, reduce the weight of removable products to reduce the energy consumption it must pay for; (3) reduce pollution in the course of consuming.

2.1.2 Reuse

"reuse" includes (1) structural integrity of components; (2) integrity of subject products in term of its alternative structure, namely to say, subject products must be replaceable with each component embedded in. Draw an example of the interrelationship between camera and buttery. As an integrated structure, the function of replaceable butteries will not be fulfilled if the camera itself doesn't have an empty room of loading and unloading buttery; (3) systematization with regard to the function of products, ie, product is viewed as a work system and a unity jointed by components.

2.1.3 Recycle

"recycle" which requires designers to use recycling resources and recycled products to encourage its regeneration is rapidly gaining wide attention and often adopted as an effective strategy for its small investment and fast effect.

2.2 Evaluation method

As a theoretical foundation, Life Cycle Assessment also called LCA for short is taken to be the most significant usual method of analyzing environmental performance. The so-called Life Cycle is to mean the total process of product's returning to nature from its original natural form, specifically speaking, the procedures cover from gaining natural energy, exploitation, manufacturing, packaging, transportation, selling, application, recycling to disposal of wastage etc,. In the year of 1997, the International Organization for Standardization released the relevant

principles and framework concerning life cycle assessment in which LCA involves the confirmation of purpose and scope, list analysis, influential evaluation and result interpretation.

Prof. Han Brezet of Delft University of Technology divides DFE into four types according to the degree of innovation, see Fig 1. Type 1 stands for the innovation of products, to adjust and improve the existing products such as set up system of recycling tires or add equipment of preventing contamination in perspective of protecting environment and preventing pollution. Type 2 stands for redesigning of products: the concept of product remains unchanged, but the components of such products will be further developed and replaced by other materials, like adding non-toxic materials, using recycling and detachable components to encourage reuse. Type 3 stands for the innovative concept of products: to solve problems by re-examining or re-evaluating the function of products. Examples in point are like the change of communication from letter to electronic technique, or from owning private cars to rent cars. Type 4 stands for system innovation: in order to achieve sustainability-based society, it is necessary to innovate infrastructure facilities and arouse new types of service and products, such as, production or manufacturing base can be shifted from agricultural land to factory; or to organize, work, transport on basis of information technology.

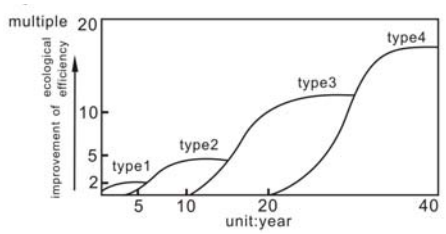

Fig 1, four types of innovation and its potential of bringing environmental improvement

3. Major procedures of DFE

Design for environment must take environmental factor into account, while traditional designing takes priorities over factors like performance and cost of production or manufacturing. Design for environment covers various aspects of modern life, it is exemplified in areas from designing, economic analysis, manufacturing to management etc,.in which the stage of designing will be given careful consideration in this paper. According to the Governing Council of the United Nations Environment Programme (UNEP), a typical design for environment can be specified into six procedures: organization of program, product option, confirmation of ecological strategy, birth of conception, detailed illustration of designing concept and release of the final new products into market.

3.1 Material option

"green materials" refer to those which are well compatible with environment in addition to meeting the basic functional requirements. Green materials are characteristic in reducing pollution and recycling or rousing materials, therefore, the choice of green material should follow the following principles in carring it out.

- give first priority on renewable resources or recycled materials in order to raise the utilization rate of resources and reduce the loss of waste, achieving the sustainable development. Select low energy-consuming and less pollutive materials.
- choose materials readily recycled,reused or degradable; do not choose toxic, harmful and radiating materials, nor combine the above two types of materials together.

3.2 Design approach

3.2.1 Recycling design

Recycling design aims at fully considering the problem of recycling and reusing into account at the very early stage of designing products, optimizing resources and minimizing pollution as much as possible. To be concrete, designers are will first think over problems like how to choose materials conveniently easy to detach and assembly, thus those sorts of materials will be in turn given first priority. Design based on recycling involves two methods: recycling of raw materials and reusing of components in which the latter is more reasonable on the ground of the difficulty and high cost. Major procedures and strategy of recycling design are listed as material mark, arts and crafts, economic evaluation and constructional design. In Japan, most manufacturers adopt an approach named Check-List to produce products with low environmental load.

3.2.2 Removable and detachable design

In order to reduce the cost of distribution and detachment, designers should design on basis of the following principles: choose products easily detachable, approachable and convenient in maintenance; adopt simple appearance and

structure; decreasing the types of components and using easy joint method to reduce the number of fasteners; predict structure of products in order to avoid the combination of interactive influence and pollution for different materials.

3.3 Industrial application and relative case studies

Difficulties EFE confronting with cover a variety of aspects: including notion, technology, design and talented designers. People have become aware of the importance of protecting environment, it still remains however a tough problem, that quite a many countries only focus attention on strategy of end-of-pipe pollution control, while designing has not been attached considerate concern to relieve energy and resource consumption from the stage of designing. For most of the enterprises, they fail to realize the solution to environmental pollution as an opportunity they could take advantage of to survive the fierce competition in business. The key to an enterprise's success, without a doubt, lies in how to utilize the resources effectively to produce goods of high performance-and-price ratio, which DFE caters to such requirements as reducing costs, decreasing risk, and fostering a good firm image.

Take an example of household electrical industry, a large number of electrical appliances are taking advantage of new energy and technology. In present China, "green electrical appliances" say no to freon and stand out the existing electrical appliances in view of reducing noise pollution and saving energy. Chinese manufacturing industry has put forward the "strategy of replacing freon". A case in point is the appearance of "green television" which reduces the TV radiation by embedding X-ray to limit electrical circuits and adding materials to absorb X- ray in picture tube. The following are applicable cases worthy of careful consideration:

- "magnesium alloy television" made by Matsushita Electric Industrial. It adopts magnesium alloy as the main substances of its shell for its abundant conservation, easily recycled and light weight. This new type of television will be more functional with the prevailing of large-sized television in the future years.
- watch of arm-swinging and automatically generating electricity. As the arm swings, The semi-circle hammer in quartz watch will rotate, increasing the speed up to 100 times faster, and driving the rotor to rotate in an amazing speed and generate electricity at the same time.
- make effective use of wind power to generate electricity. Wind power has been long adopted in Holland and Denmark due to its pollution-free feature.

SUMMARY

As a result of mutual understanding and global consensus, the appearance of DFE is a whole new and cross-cultural subject, requiring jointed cooperation of designers, ecologists and economists, besides, it also needs active participation of government, enterprises and consumers to grow into conglomeration in a large scale. The theoretical concept that DFE bases on is the concept of sustainable development which draws international attention, which declares it as the common interests and the same goal the global population is striving for. It can be expected DFE will develop into a complete social system and benefit both enterprises and consumers once a system is to be built up. Study of DFE has just begun, however, it reveals us a bright and prosperous future, bringing about a new "industrial revolution" and promoting human civilization to a new era.

REFERENCES

[1] Brezet Han, Hemel and Carolien V. Ecodesign —A Promising Approach to Sustainable Production and Consumption [EB/ OL].

[2] Ryoichi Yamamoto, Ecological Design, Trans: Wang Tian-min, Beijing: Beijing Publishing House of Chemical Industry, March 2003.

[4] Xie Da-kang, Effect of Ecological Design on Social Economic Development, May 2003.

[5] Environmental Management of Life Cycle Assessment Principles and Framework, ISO14040121997.

[6] Xu Ping and Pan Lin, Green Design, Jiangsu Fine Arts Publishing House, 2001.

[7] Han Brezet, Trend of Ecological Design, Industry and Environment, 1998, pp. 21-24.

[8] Liang Yi-ren and Lin Shi-ping, Theory and Practice of Ecological Design, Beijing: Journal of Beijing Forestry University, June 2004, pp.9-12.

2011 International Conference on Mechanical, Industrial, and Manufacturing Engineering
Lecture Notes in Information Technology Vols. 1-2

The analysis of influence that no-tillage seeding affectted on the soil water content based on BP neural networks*

Jia Honglei[1] Zhang Jinbo[1,2] Wang Baogang[1] Ye Wei[1] Ma Yunhai[1]
1. The Key Laboratory of Bionic Engineering (Jilin University), Ministry of Education, Changchun 130022, china.
2. College of Mechanical Engineering, Jiamusi University, Jiamusi 154007, China.
Corresponding author: ma yunhai
E-mail: myh@jlu.edu.cn

Abstract - **The prediction model of soil moisture content was set up using BP neural networks , and the influence that three kinds of farming, including non-farming, traditional farming and no-tillage seeding effected on the soil water content was analyzed. The water content is highest under the no-farming mode, secondly under the no-tillage, and least under the traditional farming within the 60 test days; Along with the change of time, the mean value of soil moisture content descended gradually in the condition of no plowing, there is only a little change during the traditional plowing, but the mean value of soil moisture content has up-trend in the no-tillage seeding process. The results showed that no-tillage seeding possess excellent effect of moisture conservation for small soil area in the short term, and this farming way is suitable for application and dissemination.**

Index Terms - BP neural network, no-tillage seeding, moisture conservation

I. INTRODUCTION

No-tillage seeding is a kind of important farming way of soil moisture conservation. As a sowing method, it realizes such combine operation as ditching, sowing, fertilization, suppression in the earth surface covered with straw residue. Because, this method can furthest lower the water evaporation and soil erosion because of not moving soil layer, in addition, the breathable conditions of soil was lowered, so the decomposition rate of organic matter was reduced, and the accumulation of organic matter was increased, the factors mentioned above are beneficial to the water-saving and crops growth[1].Because the sowing method have shown a lot of advantages, it has attracted great attention of related scholars who Committed to lucubrating and application[2-4].

Soil moisture content (moisture statu) is one of important indicator to measure soil property and sowing quality. It is important for analyzing soil property and selecting good seeding mode to establish prediction model for soil moisture variation law .It also has reference value for the analysis of plant distribution and even within the small scope of the climate change [5].Because soil moisture content is affected easily by many environmental factors, so the establishment of prediction model has a certain complexity. At present，the common building methods of prediction model include empirical formula, water balance method, holard kinetic method, time series models method and so on. But those models have some shortcomings, including the limited application scope of parameters and a large quantity of data, so it is restricted greatly in the practical applications. Therefore, the establishment of soil moisture prediction model, which can correctly reflect the soil moisture content change rule and easily to use, would has important practical significance [6-8].

Artificial neural network (NES) has had a wide application in the analysis of soil moisture [9,10]. At present, it has been used to the analyzing lowest value of two growth seasons and the dynamic changing of soil moisture [11-14]. The latest research results showed that the BP neural network modeling method based on PCA is more exact than that of the traditional ways of stepwise regression [11], but the related reports of research that use BP neural network to analyze the soil moisture are little. Therefore, the algorithm, which is known as precision clock of net measurement and control system that is IEEE1588 PTP time synchronization, was adopted in this paper. The excellent property of this algorithm is easy to transplant, and different users can use it according to frequency of their own equipment. The influence of no-farming, traditional farming and no-tillage to soil water content was analyzed.

II. TEST

A. Test apparatus and equipment

The 2BDM-4 multifunction no-tillage planter and Deere 804 tractor were used to planting operation tests. The soil moisture and related parameters were measured by soil moisture meter、thermometer、meter ruler、steel ruler、chronograph.

B. Test method

The test was processed at xinli town of Changchun suburban, the same piece of field is divided into three test areas, then three kinds of operation including no-farming seeding, traditional seeding, and no-tillage was carried out respectively. The soil moisture, temperature, air humidity, rainfall and other related parameter variation condition were observed and measured in 60 days before and after sowing.

* This work is partially supported by National Key Technology R&D Program (Grant No. 2011BAD20B09) to Jia Honglei and National Natural Science Foundation of Chain (Grant No.51075177) to Ma Yunhai.

Multipliers can be very confusing. Write “Magnetization (kA/m)” or “Magnetization (103 A/m).” Figure labels should be legible, at 8-point type.

III. BUILDING AND ANALYSIS OF PREDICTION MODEL BASED ON BP NEURAL NETWORKS

Steepest descent method was used to train sample data by BP network, the weights value and threshold value of network were adjusted through reverse spread in order to make the error of network square sum least. Thus the mapping relationship from input to output was obtained, and the mathematical equations of mapping relationship was got, that is mathematical model

A. Determination of model input-output and setting of network parameters

The soil moisture, temperature, air humidity and rainfall, which selected at the layer of 10cm, 15cm and 20cm below the earth surface, were determined as the input information of network. The input data and output data of network were normalized in order to make the network converge, increase the convergence rate speed of network, and decrease the computation. The research adopted three degree BP neural network to carry out forecasting, the principle photograph is followed as Fig.1.

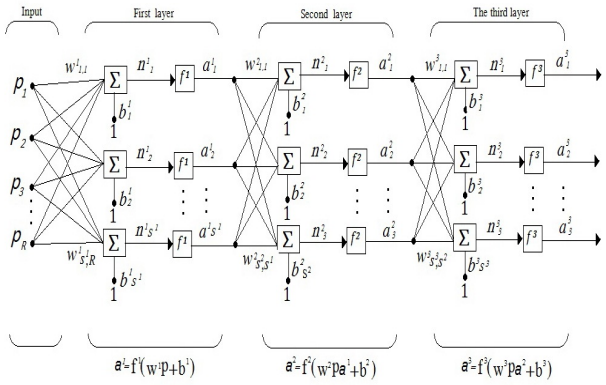

$a^1=f^3(W^3f^2(w^2f^1(w^1p+b^1)+b^2)+b^3)$

Fig 1 Three degree BP neural network

P -input vector
W-weight matrix
b -offset value vector
n -net input vector
a- output vector
f -transfer function

BP neural network model have six input nodes, three layers of soil moisture, three meteorological factors; the output node is soil moisture of 20cm layer. According to determination of the implicit layer nodes of reference formulas and practical correction, finally chosen hidden nodes is 10, the implicit layer transfer function is *tansig*, and output layer is *logsig*. With BP network’s *trangdx* algorithm was adopted, the maximum training times are 5000, training target is $1e^{-4}$, other parameters are given by default.

The model realizing process based on BP algorithm as follows:

Calculating according to the following formula [15,16]

$$I_j = \sum_{i=1}^{p} w_{1ij} y_i + b_{ij}, j = 1,2,\cdots, p. \quad (1)$$

$$O_j = f_1\left(I_j\right), j = 1,2,\cdots, q \quad (2)$$

$$S = \sum_{i=1}^{q} w_{2i} O_i + b_2, q \quad (3)$$

$$y = f_2\left(S\right), \quad (4)$$

$$E = \frac{1}{2}\sum_{i=1}^{n}\left(t_i - y_i\right)^2, \quad (5)$$

In the formula:

I, O are respectively input value and output value of implicit layers; *S* is input value of output layer; *y* is output value of network training; *t* is the input value corresponding to the measured values ; *p*、q are the nodes of input layer and implicit layer; *n* is sample size; w_1 is neuronic connection weight of hidden layer and input layer; w_2 is neuronic connection weight of layer output and hidden layer; b_1 、b_2 are neurons threshold value of hidden layer and output layer respectively; *E* is allowable error of network; f_1、f_2 are transfer function of hidden layer and output layer.

B. Forecast of soil moisture content by BP network model

The temperature, air humidity and rainfall were selected as inputs to give *P* according to the model mentioned above, the predicted value of soil moisture was made as output *T* on the 20cm level; According to learning algorithm and training parameters talked above, the measured soil moisture was selected as signal of teacher to train network, this could make different output get corresponding input. The training would be stopped when the error between the Calculating output value and signal of teachers is less than the setting allowable value. The obtained convergent curve of network through practical training is shown as figure 2.

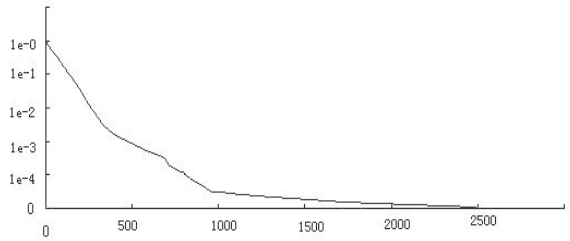

Fig 2 Convergence curve of BP neural network which obtained through the practical training

IV. ANALYSIS OF TEST RESULTS

Soil moisture content was analyzed according to the above mode under three different seeding methods, including no-farming, traditional faring and no-tillage, the results are

shown in Fig. 3 (a) ~ (f). From figures, the water content is highest under the no-farming mode, secondly under the no-tillage, and least under the traditional farming within the 60 test days; Along with the change of time, the mean value of soil moisture content descended gradually in the condition of no plowing, there is only a little change during the traditional plowing, but the mean value of soil moisture content has up-trend in the no-tillage seeding process.

In the traditional way of sowing, the stubble ploughing operation can make the soil moisture loss largely, and this mode also lead to a lower soil moisture. Nevertheless, the compacting has excellent effect of rising and preserving soil moisture during the process of seeding operation, and it can remain the soil moisture unchanged.

Using No-tillage seeding technique can cut the straw stubble fertilize,clean seeding strip,seeding, cover soil, compact and so on. It takes less time and reduces the times of turning over the soil and decreases the mixture of dry and wet soil, besides the compacting for soil moisture content's increase,So this can reduce soil moisture losing possibly, keep the soil moisture content. At the same time, soil has characteristics of incompact, excellent permeability and the balanced distribution of mineral, so the no-tillage seeding is best for crop growth in three seeding operation modes. The no-ploughing, which although has a high level of soil moisture content, generally make the content of oxygen and Nitrogen lower, lead to unbalanced distribution of mineral in soil, so the no-ploughing mode is disadvantageous for crops growth.

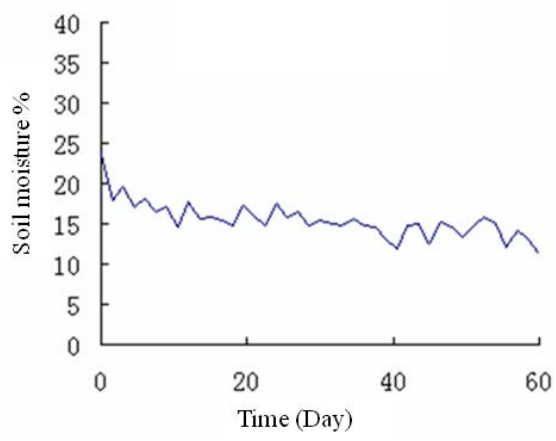

(a) soil moisture forecast map for the no-ploughing (ridge)

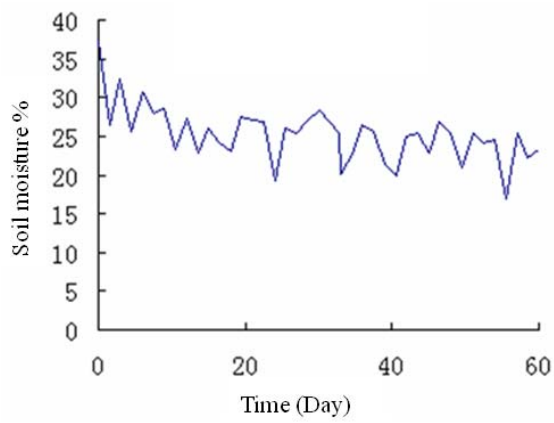

(b) soil moisture forecast map for the no-ploughing (furrow）

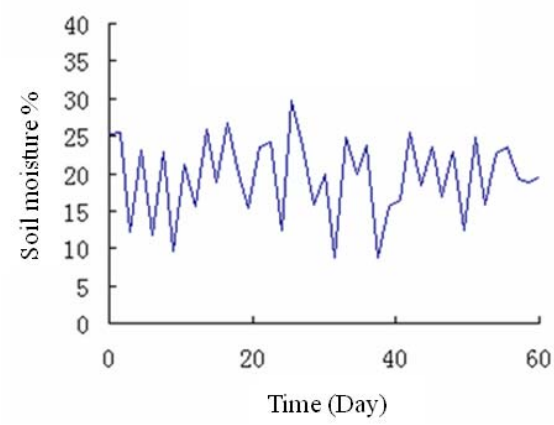

(c) soil moisture forecast map traditional farming (furrow)

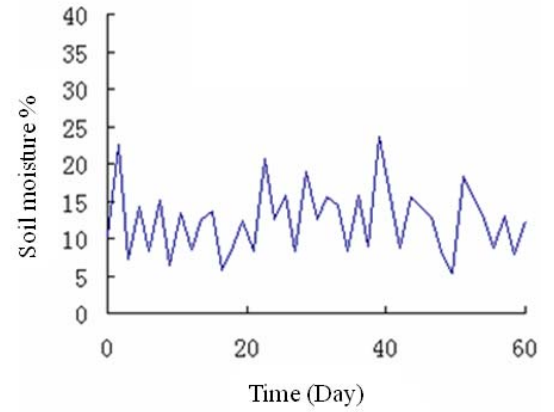

(d) soil moisture forecast map for the for the traditional farming (ridge)

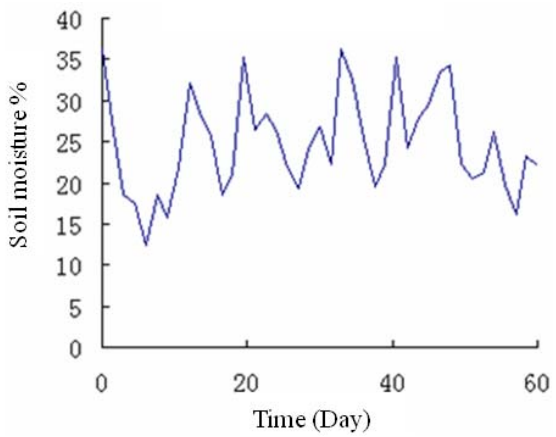

(e) soil moisture forecast map for the no-tillage seeding (ridge)

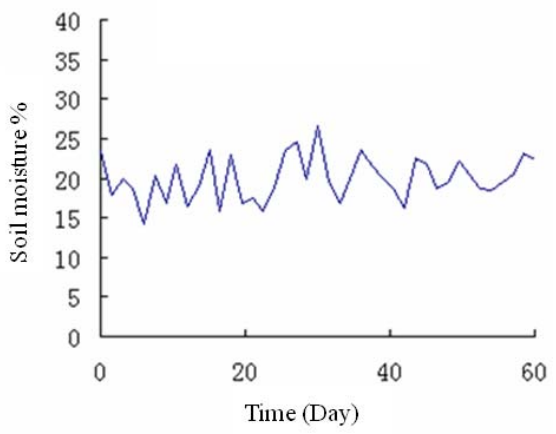

(f) soil moisture forecast map for the no-tillage seeding (furrow)

Fig. 3 Soil moisture forecast results of three kinds of sowing mode

V. CONCLUSION

Soil moisture is highest under the condition of no-ploughing, but as the time goes on, it will decline obviously; During the no-tillage process, the soil moisture content is placed in the middle, as the time goes on, it will remain unchanged or appear ascendant trend. For the traditional seeding mode, soil moisture is lowest, however, it remain unchanged mainly because of compacting.

The no-tillage seeding mode is the best in three kinds of sowing methods.

ACKNOWLEDGEMENTS

This project was supported by Jilin Provincial Science and Technology Department of China (Grant No. 20070518, 20091013), by "985 Project" of Jilin University, by National Key Technology R&D Program (Grant No. 2011BAD20B09), by Innovation Project of Scientific Frontier and Interdisciplinary of Jilin University (Grant No. 200903264) and by Supported by National Natural Science Foundation of China (Grant No. 51075177, 50635030).

REFERENCES

[1] Gosai, Kuldip; Arunachalam, Ayyanadar; Dutta, Biman Kumar, "Influence of conservation tillage on soil physicochemical properties in a tropical rainfed agricultural system of northeast India,"*Soil and Tillage Research*, vol. 105, no. 1, pp. 63-71, September 2009

[2] Imaz, M.J.; Virto, I.; Bescansa, P.; Enrique, A.; Fernandez-Ugalde, O.; Karlen, D.L."Soil quality indicator response to tillage and residue management on semi-arid Mediterranean cropland," *Soil and Tillage Research*, vol 107, no. 1, pp. 17-25, March 2010

[3] Fernández-Ugalde, O.; Virto, I.; Bescansa, P.; Imaz, M.J.; Enrique, A.; Karlen, D.L. "No-tillage improvement of soil physical quality in calcareous, degradation-prone, semiarid soils" *Soil and Tillage Research*, vol. 106, no. 1, pp. 29-35, January 2009

[4] Liu, Weidong; Tollenaar, Matthijs; Stewart, Greg; Deen, William "Impact of planter type, planting speed, and tillage on stand uniformity and yield of corn" *Agronomy Journal*, vol 96, no. 6, pp. 1668-1672, November/December 2004

[5] Khaledian, Mohammadreza; Mailhol, Jean-Claude; Ruelle, Pierre; Delage, Laurent; Rosique, Patrick "Direct seeding effects: Field tests and crop model simulation" *Computers in Agriculture and Natural Resources - Proceedings of the 4th World Congress*, pp. 636-641, 2006,

[6] Sinha, Sunil K.; Wang, Mian C. "Artificial neural network prediction models for soil compaction and permeability" *Geotechnical and Geological Engineering*, vol. 26, no. 1, pp. 47-64, February 2008

[7] Coelho, Leandro dos Santos; Freire, Roberto Zanetti; dos Santos, Gerson Henrique; Mendes, Nathan "Identification of temperature and moisture content fields using a combined neural network and clustering method approach" *International Communications in Heat and Mass Transfer*, vol. 36, no. 4, pp. 304-313, April 2009.

[8] Ma, DongHao; Shao, MingAn; Zhang, JiaBao; Wang, QuanJiu "Validation of an analytical method for determining soil hydraulic properties of stony soils using experimental data" *Geoderma*, vol. 159, no. 3-4, pp. 262-269, November 2010

[9] Guo, En-Ying; Zheng, De-Xiang; Chen, Ping-Liu; Wu, Bao-Guo; Chen, Ping-Teng "Study of the stand diameter distribution model of Eucalyptus plantation based on artificial neural network" *ICCASM 2010 - 2010 International Conference on Computer Application and System Modeling, Proceedings*, vol. 10, pp. v10498-v10502, 2010,

[10] Moreno, Raquel Salazar; Aguilar, Abraham Rojano; Cruz, Irineo López; Reyes, Manuel Galicia "Artificial neural network as a prediction tool in agricultural variables" *2006 ASABE Annual International Meeting, 2006, 2006 ASABE Annual International Meeting*

[11] Gretchen R. Miller ,Dennis D. Baldocchi ,Beverly E. Law ,Tilden Meyers. "An analysis of soil moisture dynamics using multi-year data from a network of micrometeorological observation sites". *Advances in Water Resources* . 2007, 30(5): 1065-1081.

[12] QinJu ,ZhongboYu ,ZhenchunHao ,GengxinOuc,JianZhao ,DedongLiu . "Division-based rainfall-run off simulations with BP neural networksand Xinanjiang model". *Neurocomputing* . 2009 ,72 (13-15):2873-2883.

[13] Amin Elshorbagy ,K. Parasuraman. "On the relevance of using artificial neural networks for estimating soil moisture content". *Journal of Hydrology* . 2008, 362,(1-2) :1-18.

[14] Fen He,Chengwei Ma. "Modeling greenhouse air humidity by means of artificial neural network and principal component analysis" .*Computers and Electronics in Agriculture* .2010, 71 : S19-S23.

[15] Sahimi M. "Fractal-wavelet neural-network approach to characterization and upscaling of fractured reservoirs". *Cumputers Geo-sciences*.2000,26(8):877-905.

[16] JING Yan-lin WU Yan-qing YANG Li-na "Assessment of loess collapsibility based on data mining"*Journal of Northwest Sci-Tech University of Agriculture and Forestry(Natural Science Edition)*, vol. 4, pp.130 -1342006.

2011 International Conference on Mechanical, Industrial, and Manufacturing Engineering
Lecture Notes in Information Technology Vols. 1-2

Study on Performance Evaluation of Listed Electric Power Companies with EVA

Jiang Yuanbin
School of business and management, North China Electric Power University,Beijing,China
jybthebest@ncepu.edu.cn

Abstract -This paper analyzes the necessity and availability in performance evaluation of listed company through the research of the basic introduction of EVA and the application of EVA in the evaluation on operating performance of listed electric power companies. Based on the accounting statement, it calculates the EVA of listed companies and ranks them in order to analyze company performance. Furthermore, it makes a further analysis on business condition by comparing with the net profit. This paper makes a conclusion that EVA operating performance evaluation system can make a real reflection on the operating performance of china Electric power listed companies by the way of combing theory with practice, which makes a analytical comparison between EVA index and traditional operating performance evaluation index.

Index Terms -Operating performance; listed electric power companies; EVA

I. INTRODUCTION

As the global financial crisis swept the world which breaks out in the United States, the world's stock market dropped sharply overall, and the general global economic growth slows down. Under the current complex economy circumstance, as an enterprise, it must improve operating performance for the sake of surviving. As the pillar industry of the national economy, the electric power company is the vital development part for world nations. It is significant for the development of electric utility industry that making a proper evaluation on Operating performance of china listed electric power companies.

Since Stern & Stewart put forward the concept “economic value added” and was dedicated to popularize it in 1980s, a storm come in the theory and practice field, which regarded the shareholder value as the core and pursued the concept of company value added. EVA is increasingly used in management practice and is regarded as “the current hottest evaluation index” by the U.S. magazine "Fortune".

After Introducing into China in the late 90s, EVA evaluation methods have been adopted by many enterprises, the SASAC (state-owned assets supervision and administration commission of the state council) in the second term encouraged the central enterprises to adopt EVA assessment system. There were 87, 93,100 central enterprises participating in the economic value-added assessment pilot project in 2007, 2008, 2009 respectively. In the working conference held in 2009 which is on operating performance assessment of central enterprises executives, The SASAC Deputy Director HUANG SHU HE signified that SASAC would fully implemented economic value-added assessment in central enterprises from the beginning of the third term of central enterprises executives in 2010. One of the aims is to guide enterprises to scientific decision-making, prudent investment and improve the ability to create value. In the end of 2009, SASAC issued the "the central enterprises implement economic value-added assessment program (draft)" which required State-owned enterprises to fully implement EVA assessment methods in 2010. Local SASAC also begun to proceed and popularized the pilot project intensely.

II. THE CALCULATION OF EVA

A. The Definition of EVA

Economic value added model is simply referred to as EVA, which is based on the thinking of residual income and develops to become a new model of value. From the point of view of arithmetic, EVA is residual income that is remaining part after netting of all costs, which is equal with the concept that NOPAT subtracts equity and debt capital cost. In other words, it means the value above or below the latter comparing NOPAT with the lowest returns which is the same capital investment by investors in other securities with similar risk. For the sake of making assessments of the net income status of enterprises all paid-in capital, it should deduct the cost of capital in capital gains to evaluate Current business benefits which have been achieved.

B. The Formula of EVA

Although the definition of EVA is simple, it is equal to the difference between NOPAT and all capital costs and is residual income that is remaining part after netting of all costs including opportunity cost. However, there is not Unification formula for the calculation of EVA. Commonly used method of calculating is:

EVA= Net Operating Profit after Taxes (NOPAT) - Cost of Capital

= Accounting Profit-Cost of Capital Rate ×Stockholder's Equity

The formula for calculating EVA in this paper is as follows:

EVA= Net Operating Profit after Taxes (NOPAT) – Total Cost of Capital

= Net Operating Profit After Taxes (NOPAT) -

Total Capital×Cost of Capital Rate

Thereinto：

Total Capital=Debt Capital + Equity Capital +

Equivalents Equity Capital - Construction in Progress Net

Thereinto：

Equivalents Equity Capital= Reserve for Uncollectible Accounts + Inventory Falling Price Reserves + Short and Long Term Investment + Fixed Assets/ Intangible Assets Depreciation Reserves

Cost of Capital Rate= Cost of Debt Rate ×Debt

Capital/(Debt Capital +Equity Capital)+ Cost of Equity

Capital Rate ×Equity Capital/(Debt Capital +Equity Capital)

Debt Capital= Short Term Loan+ Long Term Loan Due

Within One Year+ Long Term Loan + Long Term Payable

Cost of Equity Capital Rate= Riskless Rate of Return +β×

Market Risk Premium

Among them, debt cost ratio adopts the benchmark interest rate 5.58% of 3~5 years' long-term bank loans. Beta coefficient can be gained by regression computing stock return ratio to the return ratio of stock market index over the same period; Risk rate of return is gained from the Shanghai Stock Exchange in the year of the most long-term government bonds yields (20 years, 3.25%); Market risk premium is calculated at 4%; other major data is from SINA.COM.

C. Listed Electric Power Companies EVA

According to the balance sheets and income statements of 52 domestic listed companies in 2009 which are from SINA Finance website, making models by using office excel to Calculate domestic listed companies' EVA values and rank them in the following table (in the fourth column sort)

TABLE I

THE EVA OF THE COMPANIES

Ranking	Company Name	EVA	Capitalization/EVA
1	Shenzhen Auto Electric Power Plant	6492147.93	89.50
2	Guangzhou Development Industry	200320080.40	63.53
3	Jilin Power Share	38646515.27	61.92
4	Guangdong Electric Power Development	477225163.60	47.66
5	Sichuan Chuantou Energy	121590863.90	46.10
6	Shenergy Group	806372324.70	44.38
7	Sichuan Mingxing Electric Power	36311385.39	42.99
8	Sichuan Xichang Electric Power	29877543.32	37.89
9	Beijing Jingneng Thermal Power	88515342.19	33.15
10	Harbin Hatou Investment	128498078.10	27.98
11	Huadian Power International Corporation	227575908.00	27.45
12	Chongqing Jiulong Electric Power	125522807.70	25.71
13	Shenzhen Energy	1182254352.00	18.02
14	Guizhou Qianyuan Power	692606575.50	17.47
15	Shanxi Zhangze Electric power	493095853.70	16.16
16	Guangxi Guiguan Electric Power	876812637.40	14.80
17	Top Energy Company	160770323.50	14.69
18	Huadian Energy	1613914240.00	8.24
19	Guangdong Baolihua New Energy Stock	821872480.50	7.32
20	*ST Xinneng Taishan Power Generation	-951488177.70	-5.32
21	Tianjin Binhai Energy & Development	-113516713.40	-5.71
22	Shenzhen Nanshan Power Station	-590242643.40	-7.99
23	Sichuan Minjiang Hydropower	-168206561.90	-8.81
24	Guangdong Meiyan Hydropower	-348891273.40	-10.51
25	Dalian Thermal Power	-124637103.70	-11.83
26	Datang Huayin Electric Power	-826462385.10	-13.71
27	Xinjiang Tianfu Thermoelectric	-248335431.80	-15.80
28	Guangdong Shaoneng Group	-459234941.30	-15.26
29	Chongqing Fuling Electric Power Industrial	-54193503.72	-16.03
30	Guangdong Wedge	-546700323.30	-16.34
31	Guodian Changyuan Electric Power	-595723104.30	-16.74
32	Jointo Energy Investment	-558756837.10	-17.09
33	AnHui Wenergy Company	-521327450.10	-17.13
34	Guangxi Guiding Electric Power	-119312510	-19.23
35	Shenyang Jinshan Energy	-302885428.40	-19.36
36	China Datang Corporation	-4920906357.00	-22.80
37	Jiangxi Ganneng	-289685334.10	-23.17
38	SDICHuajing Power Holdings	-1859416162.00	-24.16
39	Shandong Jiangquan Industry	-63399645.30	-25.91
40	Three Gorges Water Conservancy and Electric Power	-36200442.46	-39.48
41	Leshan Electric Power	-30049182.70	-42.78
42	Kaidi Electric Power	-127773419.90	-48.073
43	Hunan Chen Dian International	-53379848.91	-49.93
44	GD Power Development	-1204356206.00	-59.22
45	InnerMongoliaMengDianHuaNeng	-333057930.20	-62.30
46	Shanghai Power	-351214767.50	-63.58
47	Guangzhou Hengyun	-79997646.54	-77.70
48	Yunnan Wenshan Electric Power	-18758036.21	-85.01
49	Nindong Electric Power	-28132456.82	-90.74
50	Huaneng Power International	-1411145022.00	-95.71
51	Changjiang Electric Power	-731130179.00	-165.91
52	Ningbo Thermal Power	-3207068.99	-177.35

III. LISTED ELECTRIC POWER COMPANY PERFORMANCE EVALUATION BASED ON EVA

A. Raising Problems

Based on the above calculation results of EVA and the net profit data of finance annual reports of electric power listed companies which are taken from SINA Finance website,

the distribution of positive and negative situation of the EVA and the net profits of electric power listed companies shows as follows: We can see that there is some difference between traditional company performance evaluation of net profits and EVA to reflect the operating performance of electric power listed companies. From the net profit index, there are 44 electric power listed companies gaining the net profit which accounts for 85% of electric power listed companies. Only eight electric power listed companies are in a loss. However, only 36 companies' EVA values are positive among 52 companies. What's more, some companies' EVA values are negative but their net profits are positive. Instead, some companies' net profits are negative, but their EVA values are higher than those of some companies whose net profits are positive. So what is the problem that the two indicators (Net profit and EVA) reflect different performance evaluation results? How should we treat the difference?

To this issue, the paper plan to adopt statistic methods to build linear regression models for the sake of analysis.

B. Sample Option and Data Sources

This paper was originally listed 55 electric power listed companies as the research objects. But in order to eliminate negative factors as far as possible, the paper selects samples of empirical studies adhere to the following principles:

1) Excluding companies which have non-standard audit opinion on financial reporting and incomplete data samples: Shenzhen Nanshan Power Station ，Guangdong Meiyan Hydropower.

2) Taking into account the extreme values having a negative effect on Statistical results, the paper eliminates extreme values companies within the range of 3 times standard deviation of the financial index: SDICHuajing Power Holdings, Changjiang Electric Power, GD Power Development and Huadian Energy.

3) Sample companies excluding companies which issue H stock and B stock at the same time: Huaneng Power International, Huadian Power International Corporation and China Datang Corporation. As the recognition of revenue and expenses in the accounting policies in these companies are significantly different.

Finally, there are 44 electric power listed companies meeting the above selection criteria.

C. Variable Set

Study of variables in the process of study involves in company market EVA, EVA and NP. Each sample of EVA is obtained by the calculation on the former part of the paper. Other data are from SINA.COM. Variables involved in the established model are explained respectively below:

1) Dependent variable. In the Empirical research of this paper, Dependent variable is the company market EVA. Bad or good operating performance can be reflected through the company performance in the market. That is to say, company market EVA can be used as a measurement of the operating performance of listed companies. Company's market value added (EVA) is equal to the company's market value (V) minus the number of the company's total capital investment. That is the book value of Paid-in capital. The market value (V) is for the corresponding point in time the stock price multiplied by the number of shares.

2) Operating performance variables. 1, net profits are Samples from the income statement in the 2009 Annual Report. 2, EVA is from this part of the calculation before.

D. A Simple Linear Analysis Model and Conclusions

Research methods and empirical results. The paper regards market value of the company as a standard to measure operating performance of electric power listed companies, which is the dependent variable in the model. Through the regression analysis of the market value of listed electric power companies and EVA, traditional accounting profit index, comparing the explanation level of explanatory variables on the dependent variable. According to the research aim of the paper and the definition of each variable, building the models as follows:

$$EVA1=\alpha 1+\beta 2EVA+\gamma 1+\mu 1 \quad (1)$$

$$EVA2=\alpha 2+\beta 2NOCF+\gamma 2+\mu 2 \quad (2)$$

Analysis data by regression analysis tool provided by office excel tool as follows:

Explained variable	Model Summary		Variance analysis		Coefficient		
	R2	adjusted R2	F	Sig.	Standardized partial regression coefficient	T	Sig.
EVA	0.187983	0.168648	9.723037	0.003281	1.507064	3.118178	0.003281
NP	0.410138	0.396094	29.203149	2.84306 3	1.346484	5.403993	2.84306 3

See the relevance of NP and EVA as a visual map from the above table:

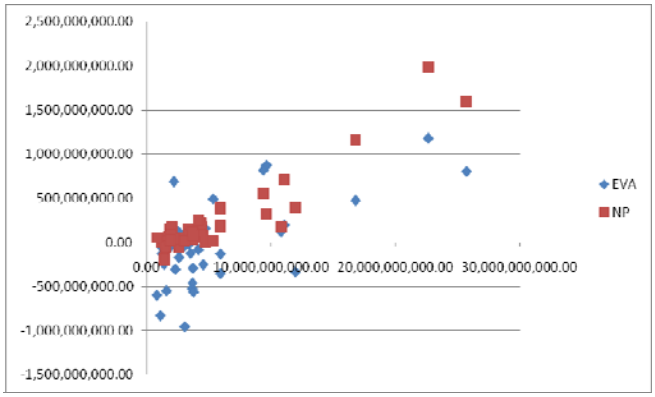

The results of regression analysis shows: in the case of significant level 0.05, model (1) explains that the effect of the overall linear regression of equation was significant by the analysis of Variance and T test, especially Sig F value and Sig T value approach to zero. All of these shows that EVA can make a proper reflection of operating performance of listed electric power companies and can explain company value well, so it can be used to illustrate the market value size of domestic electric power listed companies as well as the basic sorting and the basic evaluation of operating performance of electric power listed companies.

However, comparing with NP index, EVA has not special advantage. And its 18.80% explanation level to MVA is lower than 41.01% of NP. There are two reasons.

1) In china, capital cost is difficult to fix: Weighted average cost of capital consists of debt cost and equity cost, which is used to calculate EVA. Cost of debt is very easy to determine, but the cost of equity is more difficult to determine. Equity cost involves in Government bonds and corporate bonds which can be converted to the cost of preferred stock, common stock cost and risk fund cost. In a medium-long term perspective, assessment data of equity cost is from capital market. China's current capital market is not perfect, investors scatter, low portfolio. Therefore, risk-free interest rate, risk factors and market risk premium are difficult to determine. These factors result in inaccurate calculation of the cost of equity. Because calculating the weighted cost of capital is not accurate, it results in inaccurate calculation of EVA.

2) EVA appraisal method is affected by the fluctuation of capital cost: company can adopt capital cost by changing capital structure and business option. However, this can only be decided by the senior managers. At different times, the cost of capital is usually the most unstable and volatile variable in the EVA equation, which will cause the fluctuation of EVA.

IV. CONCLUSION

Research conclusions of the paper are as follows:

A. EVA is a new evaluation method of operating performance. Because of adding the factor of capital cost, the operating performance evaluation based on EVA can reflect the real condition of company operating performance.

B. As the pillar industry of the national economy, it is very important for electric utility industry to evaluate the operating performance of listed electric power companies. With the development of EVA appraisal method, it is a trend that EVA appraisal method replaces the traditional appraisal ways. Listed electric power companies can make a further understanding of its own operating performance and incentive itself to develop through EVA.

Although EVA appraisal method has an advantage over traditional appraisal ways, it also is not perfect. EVA index just shows the final result of company operating performance, which is bad for analysing the problems in the production and management process. Furthermore, EVA index is an absolute index, which goes against the horizontal comparison among different scale companies.

This thesis just makes a research on EVA operating performance appraisal method on the theory level, which hasn’t gone deep into practice. Only through the test of practice, in practice, continuing to be explored, forward, the performance evaluation based on EVA can be made to become better and more suitable for operating performance evaluation of electric power listed companies.

REFERENCES

[1] James L. Grant. Foundations of Economic Value Added. 2nd ed. John Wiley & Sons，Inc.2005

[2] Joel M. Stern. The EVA Challenge: Implementing Value Added Change in an Organization. John Wiley & Sons，Inc.

[3] Jame A. Abate. EVA: The Real Key to Creating Wealth .John Wiley & Sons，Inc. 2003

[4] M. Caputo. Foundations of Dynamic Economic Analysis. Cambridge University

[5] Paul A. Samuelson. Foundations of Economic Analysis. 1997

2011 International Conference on Mechanical, Industrial, and Manufacturing Engineering
Lecture Notes in Information Technology Vols. 1-2

Study and Application of Formation Protection Drilling-In Completion Fluid in Developing Low and Extra Low Permeability Reservoirs*

Guancheng Jiang and Yingying Li and Weixing Xu

MOE Key Laboratory of Petroleum Engineering
China University of Petroleum(Beijing)
18 Fuxue Road, Changping, Beijing, China

jgc5786@126.com echoes1984@hotmail.com xu.wei.xing@163.com

Ying Kong and Chunyan Feng

College of Chemistry&Chemical Engineering
China University of Petroleum(EastChina)
66 Changjiang Road, Qingdao, Shandong Province, China

Yingkong1967@yahoo.com.cn fcynqr2010@gmail.com

***Abstract* – Developing low and extra low permeability reservoirs becomes more and more important to the sustainable energy development in China. However, formation damage caused by water lock and other factors tends to occur in the reservoir with low and extra low permeability. Hence, conduct the research to formation damage control has important significance. Aiming at the disadvantages of current drilling-in completion fluids technology, the particularity of formation damage in low and extra low permeability reservoirs and the unpredictability of reservoir pore etc, a special surfactant FCS-08 and the film-forming amphiphilic polymer reservoir protecting agent LCM-8 have been used to develop a novel drilling-in completion fluid which controled the formation damage by improving the properties of rock surface. With large amount of tests in lab and field, both core plugging&recovery rate were more signifacant than 90%, this drilling-in completion fluid realizes the broad-spectrum temporary plugging effect and "zero damage" near the borehole. Compared with other drilling-in fluids commonly used, this one has better effect on reservoir protection and has gained greater daily oil production.**

Index Terms – Low and extra low permeability; Reservoir protection; Synergy; Film-forming material; Field application.

I. INTRODUCTION

Reservoirs with low and extra low permeability are characterized by the high argillaceous cement content,high capillary pressure,tiny pore throat, complicated structures, serious heterogeneity,large oil-gas flow resistance and so on, as a result,formation damage such as water sensitivity and water lock caused by the invasion of extraneous fluids occur easily in drilling process and the damage rate usually gets up to 70-90%. Hence, the protection quality of low and extra low permeability reservoir will be one of the key factors of its exploitation and development.

Although many drilling-in completion fluid technologies for formation damage control have been developed domestic and overseas over a long period,such as the temporary shielding technique[1,2], fractal geometry temporary shielding technique[3],broad-spectrum temporaryshielding technique[4], alkali soluble micron-sized cellulose temporary shielding technique[5], D50 temporary shielding technique[4], D90 ideal packing technique[6], film forming technique[7,8] , oil film technology[9-14] and so on. The effects of these novel techniques and technologies on low and extra low permeability reservoir protection are not so good. The essential reason is that all of these technologies didn't take the formation damage caused by instantaneous filtration into consideration. Besides, the plugging capacity of these techniques can be further enhanced under certain conditions.

In addition, Zhanghongxia proposed adding surfactants in drilling-in fluid to reduce water lock in low and extra low permeability reservoirs and has applied in the reservoir of Qiudong, which provides ideas for formation damage control [15]. However, it needs further improvement both in the choice of surfactant and establishment of protection technique.

In this paper,the novel surfactant FCS-08 and the new film-forming amphiphilic polymer protectant LCM-8 are firstly developed, and the new concept of "rock surface properties improvement" which combined with the novel film-forming and water lock prevention techniques are put forward. A novel drilling-in completion fluid has been established.

Through adding the FCS-08 and LCM-8 into the upper drilling-in fluid and transform it into the fluid of "rock surface properties improvement". Under the condition of downhole temperature and pressure, this drilling-in fluid improve the properties of reservoir rock surface with FCS-08 by avoiding the damage caused by hydration swelling and water lock. Besides, a layer of temporary plugging barrier with strong toughness and extra-low permeability is formed by the softening, deformation and adsorption of LCM-8, which stop the later fluid entering the reservoirs. The temporary shielding barrier can flow back through the flow of crude oil into the wellbore or be relieved by perforation. There is no need to predict exactly the distribution curve of throat diameter in the reservoir when designing , this drilling-in completion fluid has high applicability, low cost and convenient operation, etc.

1 Properties evaluation of the special surfactant FCS-08

1.1 Wettability of core surface

* This work is partially supported by the National Natural Science Foundation of China(Project NO.51074173)
This work is also supported by the National Science Fund for Distinguished Young Scholars(Project NO.50925414)

Immerse artificial cores with similar property into the FCS-08 solutions with concentration of 10% for 4 hours, and dry them naturally. The contact angle of distilled water, oilfield sewage, n-hexadecane and crude oil in core surface has been measured and the results are shown in Table 1.

In the surface of cores treated by the FCS-08, the contact angle of water reaches to 139.79° which is 137.27 ° higer than the untreated one and the rolling angle is 4.7°. The contact angles of oilfield sewage, n-hexadecane and crude oil are also significantly higher than the untreated. The wettability of core surface processed by FCS-08 has already changed from amphipathic to amphiphobic, which avoid the hydration swelling and water lock damages in drilling process by hindering the invasion of filtrate and the direct contact between rock and water.

1.2 Surface tension

The degree of water lock damage is not only related to lithologic features of reservoirs, the type and content of cement, pore structure and extraneous fluid properties also had a close relationship with gas log permeability, porosity and initial water saturation, and the water-oil interfacial tension after the invasion of foreign fluid. According to the information presented in Table 2, the surface tension of FCS-08 is far lower than the other surfactants.

2 Properties evaluation of LCM-8

2.1 Film-forming ability

The surface and flank of filter paper, the surface of the sandstone treated before and after film-forming are detected through the scanning electron microscopy (sem). The results are showed in Fig.1-3, the film-forming amphiphilic-polymer reservoir protectant LCM-8 has a good film-forming ability both in the surface of filter paper and in the surface of the sandstone.

2.2 Evaluation of reservoir protection

2.2.1 Visual sand-bed experiment

Using visual sand-bed filtration experimentation, the invasion depth of drilling-in completion fluid with LSM-8 and several other film-formers are measured, the results are showed in Fig.4, the invasion depth of drilling-in fluid with LCM-8 is lower than that of contrast samples, which shows that LCM-8 formed a film of higher quality in sand bed.

2.2.2 Plugging and recovery rate of permeability

2.2.2.1 Design of drilling-in completion fluid

To evaluate the reservoir protection effect of the reservoir protectant LCM-8, the upper inhibitive polymer drilling-in fluids of 33-531-4 well are chose to be the base mud. Reservoir protection materials of different types and different dosages are added to design 14 drilling-in completion fluid formulas, which are tabulated in Table 3.

Table 1 CA of Each Medium in the Surface of Different Cores

Medium / Core	Distilled water	Oilfield sewage	n-hexadecane	Crude oil
Untreated	2.52°	10.62°	2.20°	35.35°
Immersed by FCS-08	139.79°	122.31°	65.46°	85.68°

Note：The crude oil gets from Shengli Oilfield.

2.2.2.2 Evaluation of plugging rate

Using artificial rock and the LSY-1 core flow testing apparatus, the fluids prepared in 2.2.2.1 are evaluated in laboratory after 24h aging at 80℃, 3.5MPa according to the precesure stated in[16,17]. The results are showed in Fig.5.

Fig.5 shows that compared with the base mud, the mud dealt with temporary shielding techniques has an higher permeability plugging rate, it can cause more serious blocking at the pollution part; meanwhile, the fluids with LCM-8 in it has an better blocking effect than that of GPJ and other film-formers. In addition, when the LCM-8 content is more than 2.0% , the permeability plugging rate can reach to 90% and the increasing trend is not obvious along with the dosage more than 2.0%.

Table 2 Surface Tension of Common Surfactants

No.	Type of surfactant solution	Surface tension mN/m
1	0.3%FCS-08	8.26
2	0.3%ABS	26.06
3	0.3%OP-10	26.59
4	0.3% Tween-40	30.25
5	0.3% OS-15	36.73
6	0.3% Span60	29.56
7	0.3%Tween-80	41.36
8	0.3%ABSN	25.50

Table 3 Drilling-in Completion Fluid Formula

No.	Drilling-in completion fluid formula
1	the upper strata mud
2	1+ 1.0% another film-former B
3	1+ 1.0% broad spectrum “oil-film” temporary shielding agent GPJ
4	1+ 1.0% film-forming amphiphilic-polymer LCM-8
5	1+ 2.0 % another film-former B
6	1+ 2.0% broad spectrum “oil-film” temporary shielding agent GPJ
7	1+ 2.0% film-forming amphiphilic-polymer LCM-8
8	1+ 2.5% another film-former B
9	1+ 2.5% broad spectrum “oil-film” temporary shielding agent GPJ
10	1+ 2.5% film-forming amphiphilic-polymer LCM-8
11	1+ 3.0% another film-former B
12	1+ 3.0% broad spectrum “oil-film” temporary shielding agent GPJ
13	1+ 3.0% film-forming amphiphilic-polymer LCM-8
14	1+ 4.0% film-forming amphiphilic-polymer LCM-8

Note:The broad spectrum “oil-film” temporary shielding agent GPJ is a film-former that developed in our laboratory and has been well applicated in oilfield.

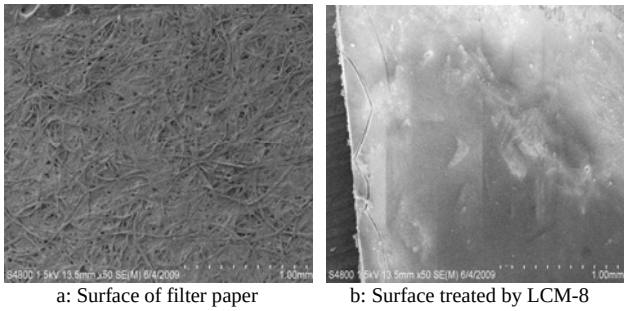

a: Surface of filter paper b: Surface treated by LCM-8

Fig.1 SEM photos of the filter paper surface before and after treated by LCM-8

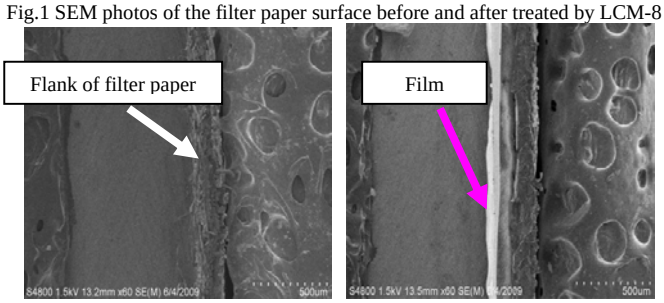

a:Flank of filter paper b: Flank treated by LCM-08

Fig. 2 SEM photos of the filter paper sflank before and after treated by LCM-8

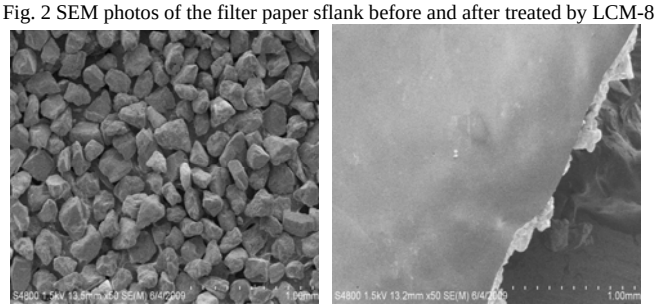

a:Surface of sandstone b:Surface treated by LCM-8

Fig. 3 SEM photos of the sandstone surface before and after treated by LCM-8

2.2.2.3 Evaluation of recovery rate

For further research of the protection effect of LCM-8, the pollution part of cores damaged in 2.2.2.2 are cut[17,18] and the permeability recovery rate of oil are mesured, the results showed in Fig.5**.**

According to the results, the permeability recovery rate of core was obviously improved after the pollution part was cut off, which shows that temporary shielding techniques could indeed form a shielding ring with extremely low permeability near the pollution surface, which stop the solid particles and filtrate of drilling-in completion fluids invading reservoirs; meanwhile, the fluids with GPJ or other film-formers in it has lower permeability recovery rate than that of LCM-8 in it. Moreover, we can see from Fig.5 that when the content of LCM-8 is 2.0% , the permeability recovery rate can reach more than 90% and the increasing trend is not obvious along with the dosage more than 2.0%. In consideration of the results of plugging rate evaluation, the optimal formula of temporary shielding is the upper strata mud with 2.0% LCM-8 in it.

2.2.2.4 Evaluation of flowback and plug removal

Selected the cores with plugging&recovery rate both more than 90% which damaged by drilling-in completion fluid with LCM-8 to measure its reverse oil permeability under different

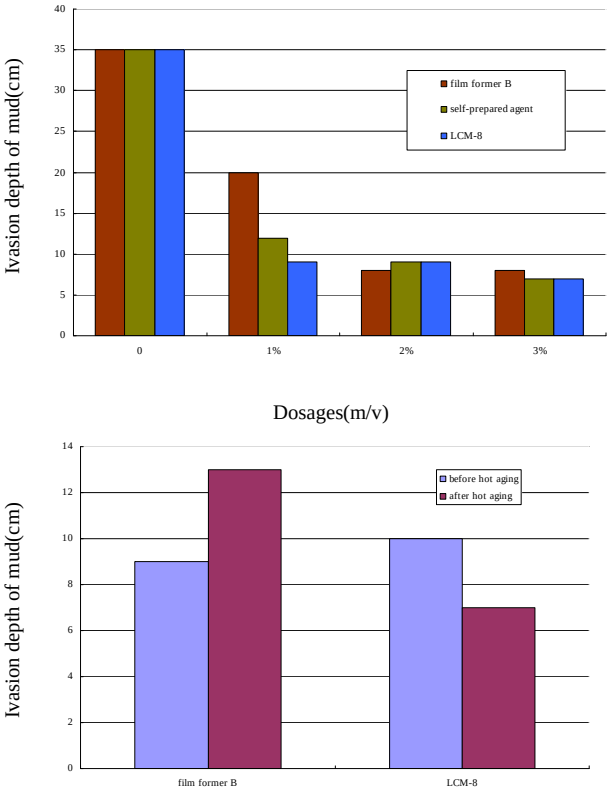

Fig.4 Contrast of depth of invasion of several film-formers (2% dosage)

flow pressures, the permeability recovery value under different conditions are calculated, as shown in Fig.6.

The results in Fig.6 shows that the permeability recovery increased along with the increasing of flowback pressure, the effects of plug removal are better; the permeability recovery of fluid with LCM-8 in it is higher than that of upper strata mud under the same flowback pressure. In the actual production process, the flowback pressure is higher than the pressure tested in this paper, as a result, the removal of plug could realize easily.

3 Field application of “rock surface properties improvement” drilling-in completion fluid

Take the fault block Chang-68 in Weibei Oilfield as an instance to illustrate the design of this “rock surface properties improvement” drilling-in completion fluid.

Fault block Chang-68 in Weibei Oilfield is characterized by the large differences in clay mineral content and the illite mixed layer content, high formation water salinity (about 30000mg/L), small pore size (maximum pore throat size is 0.494μm ~ 1.4835μm) and critical salinity 29106mg/L, and it belongs to low porosity ultra-low permeable reservoir, with medium partial strong water sensitivity and acid sensitivity and medium salt sensitivity. The potential damage factors of the reservoir include clay hydration expansion and dispersed, water lock and inorganic scale. Therefore, in the design of

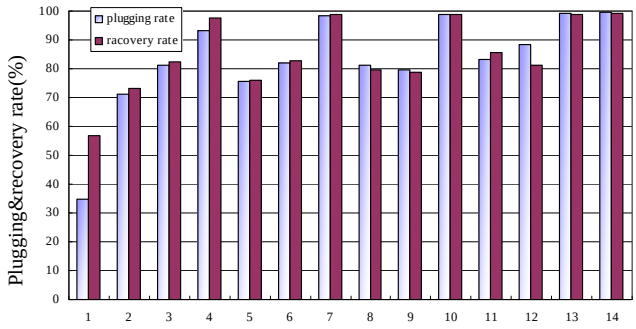

Fig-5 The flugging&recovery rate of damaged cores

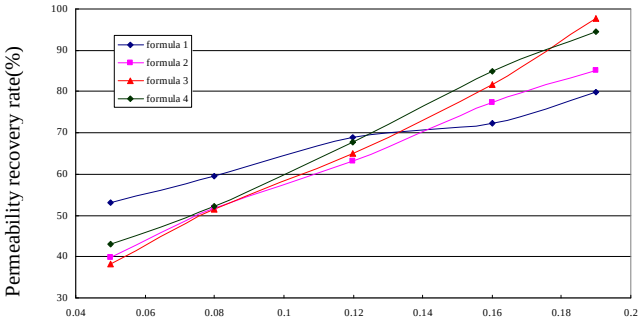

Fig.6 The permeability recovery and flowback pressure

drilling-in completion fluid, a compact mud cake is requred to be formed on the sidewall to stop drilling fluid filtrate entering reservoirs effectively; besides, the invasion fluid should have a lower surface tension in order to avoid water blocking damage and increase reverse discharging to reduce formation damage. Hence, through improving the upper drilling fluid, the drilling-in completion fluid of “rock surface properties improvement” to protect low and extra low permeability reservoirs are established.

In site operation process, when the well is almost drilled into production zone, add 2.0% LCM-8 and 0.3% surfactant FCS-08 into the upper drilling-in fluid and modify it into drilling-in completion fluid of "rock surface properties improvement " to protect low and extra low permeability reservoir. The general properies are tabulated in Table 4.

Table 4 shows that the rheology behavior of drilling fluid has little change pre and post modification, the surfactantFCS-08 and amphiphilic polymers reservoir protectant LCM-8 have better compatibility with other treatment agents; the filtration and shale inflation of the modified drilling-in completion fluid of " rock surface properties improvement" gets lower and the lithic recovery and permeability recovery rate are greatly increased, the daily output per well is 1.6 times as that of well next to it.

In addition, this drilling-in completion fluid has been applicated in Shengli oilfield, no complicated situation of drilling fluid appears in all wells. Compared to conventional reservoir protection technologies, this one significantly reduces reservoir damage accidents and greatly increases the average daily oil production pur-meter under unit pressure (shown in Table 5), get a better reservoir protection effect.

Table 4 General Performance Test

State	ρ g/cm^3	AV mPa•s	PV mPa•s	YP Pa	YP/PV	G_{10s} / G_{10min} Pa	API FL mL	K_f	pH	Lithic recovery, %	Shale inflation, %	Permeability recovery, %
Before modification	1.10	28	20	8	0.4	1.5/3.0	4.5	0.1	8.5	68.7	5.86	62.33
After modification	1.10	30	20	10	0.5	2.0/3.0	4.0	0.1	8.5	86.2	2.69	93.4

Table 5 Effects of Reservoir Protection in Shengli Oilfield

Well No.	Technique	Daily output(t/d)	Daily oil production pur-meter under unit pressure (t/m.d.MPa)	Stimulation ratio
Chun64-4	This method	3.2	0.064	1.408
Chun64-3	Conventional method	0.9	0.045	
Fan143-x10	This method	5.2	0.168	1.48
Fan143-13	Conventional method	4.7	0.113	
Liang38-p4	This method	24.8	0.016	1.186
Liang 38-p2	Conventional method	7.3	0.013	
Liang 23-x36	This method	5.9	0.12	21.83
Liang 23-12	Conventional method	0.5	0.005	
Liang 38-p7	This method	10.4	0.012	1.104
Liang 38-p3	Conventional method	2.2	0.011	
Fan 147-9	This method	5	0.303	1.697
Fan 147-1	Conventional method	2	0.179	

4 Conclusion

(1) Through adding the special drilling surfactant FCS-08 can avoid the water lock damage and hydration expansion damage problem caused by instantaneous filtration or other factors. The new film-former LCM-8 could form a layer of "film" with strong toughness and extremely low permeability on well rocks and has better plugging effect and reservoir protecting effect than other film-forming materials.

(2)Through adding 2.0% amphiphilic polymers reservoir protectant LCM-8 and 0.3% surfactant FCS-08 gradually into the upper drilling fluid and modifying it into drilling-in completion fluid of "rocks surface properties improvement", the problems of low and extra low permeability reservoir protection in drilling process are solved.

(3) The field application shows that, compared with the conventional reservoir protection techniques, this “rock surface properties improvement” drilling-in completion fluid has a better effect. The daily oil production per meter under unit pressure increased rapidly, getting a better reservoir protection effect and economic benefit.

ACKNOWLEDGMENT

Brief Introduction: Guancheng Jiang, male, born in 1966, doctor of science, professor, doctoral supervisor,.received his bachelor's degree from the Southwest Petroleum University (SWPU) in 1987, received his master’s and doctoral degree respectively from China University of Petroleum (huadong) in 1993 and form Ocean University of China in 2005. Now he is a professor in the Department of Petroleum Engineering at the China University of Petroleum(Beijing), where he is mainly engaged in the research and teaching of oilfield chemistry and formation damage**.**

REFERENCES

[1] Kexiang Li, *Dring-in completion fluid technology in formation damage control*, Beijing:Petroleum Industry Press, 1993,349-438.

[2] Shizhong Fan, Jienian Yan, Dacheng Zhou,*Dring and completion fluid and formation damage control technology*, Dongying:University of Petroleum Press,1996,615-653.

[3] Yingchun Cui and Yao Zhang, “Application of fractal theometry theory to optimal selection of themporary, ”Journal of The University of Petroleum, vol.24, no. 2, pp. 17-20,1997.

[4] Tongtai Xu, “The general- purpose temporary shield plugging technology in protecting hydrocarbon reservoir, ” Drilling Fluid and Completion Fluid, vol.20,no.2,pp.39-42,2003.

[5] Jienian Yan etc, “Advances in overseas technology of formation damage control-Investigations on the mechanisms andmethods of temporary plugging,” Dring Fluid and Completion Fluld. vol.20,no.1,pp.44-48,2003.

[6] Jienian Yan, Jianghua Wang, Jinbo Zhang, “New method for optimizing particle size of bridging agents in drilling fluids,” Journal of Oil and Gas Technology. vol.29,no.4,pp.129-135,2007.

[7] Guan-cheng Jiang etc,“Design and application of drilling and completion fluid system for formation protection in the key blocks of Dagang Oilfield,” Oil Drilling & Production Technology. vol.30,no.6,pp.58-61,2008.

[8] Hu Lu etc,“Application of extensive temporary plugging technology in Lungu Block,” Drilling & Production Technology. vol.26,no.5,pp.91-94,2003.

[9] Guancheng Jiang, Chaofeng Ji, Xianping Ma, Yihua Yao, Mutai Bao, “Study and Application of Reservoir Protection Fluid System For Drilling & Completion Using Oil-film Method”. *2009 SPE European Formation Damage Conference*, SPE 119811.

[10] Guancheng Jiang etc,“Study and Application on the Oil-film Method Used for Reservoir Protection Drilling & Completion Fluid Systems,” Journal of Dispersion Science and Technology. vol.31,no.4,2010.

[11] Guancheng Jiang, Chengliang Hu,Ying Xiong, Daoxuan Li,“Study on system of broad-spectrum oil-film temporary plugging drilling fluid,”Journal of China University of Petroleum(Edition of Natural Science) . vol.30,no.4,pp.53-57,2006.

[12] Guancheng Jiang, Dongliang Hu, Xunzhong Guan, Yong Jin,“Study on system of broad-spectrum oil-film temporary plugging drilling and completion fluid,” Journal of Basic Science and Engineering . vol.15,no.1,pp.74-83,2007.

[13] Guancheng Jiang, Xianping Ma, Chaofeng Ji, Shuxin Gao, “Application of a broad-spectrum oil-film temporary plugging agent to reservoir protection,” Chinese Journal of Applied Chemistry. vol.24,no.6,pp.665-669,2007.

[14] Ying Xiong, Chengliang Hu, Gucheng Jiang, Yuwen Song, Jialiang Zhang,“Study and preparation of broadly adaptable mud lost circulation plugging agents GPJ,” Drilling Fluid and Completion Fluid. vol.23,no.1,pp.1-4,2006.

[15] Hongxia Zhang etc,“Research and application of drilling fluids to mitigate porosity impairment of deep and low porosity reservoirs,”Drilling Fluid and Completion Fluid. vol.26,no.4,pp.4-7,2009.

[16] Guancheng Jiang, Chun Huang, Guorong Zhang, *The new technology of protection in Loose Sand Reservoirs reservoir* ,Dongying:University of Petroleum Press, 2006,137-205.

[17] Jienian Yan, Linji Huang,Drilling fluid optimization design and practical technology,Dongying:University of Petroleum Press, 1993,462-479.

2011 International Conference on Mechanical, Industrial, and Manufacturing Engineering
Lecture Notes in Information Technology Vols. 1-2

Does it fit Together? – State-of-the-art of Academic Research Regarding to Manufacturing Execution Systems and Business Intelligence

Tom Hänel
Chair of Information Systems
Technische Universität Bergakademie Freiberg
Freiberg, Germany
Tom.Haenel@bwl.tu-freiberg.de

Carsten Felden
Chair of Information Systems
Technische Universität Bergakademie Freiberg
Freiberg, Germany
Carsten.Felden@bwl.tu-freiberg.de

***Abstract* – Manufacturing Execution Systems (MES) have relevance for practice and academic research, since the number of publications within the topic is increasing. MES facilitate vertical integration as concept between an Enterprise Resource Planning (ERP) layer and an automation layer. MES are insufficiently embedded within the overall organizational decision-making process. Therefore, the paper investigates the role of Business Intelligence (BI) as decision support concept in context of MES to define a state-of-the-art by the method of literature review. 340 articles of selected scientific databases have been analyzed and evaluated to achieve this goal. Only 1.8 percent of these publications consider BI related to MES. This result leads to the conclusion that further research regarding to the integration of BI and MES is needed.**

Index Terms – Manufacturing Execution System (MES), Literature Review, Business Intelligence.

I. INTRODUCTION

Manufacturing Execution Systems (MES) close the gap between an Enterprise Resource Planning (ERP) layer and an automation layer [1]. This is relevant for organizations of manufacturing and process technology forced to restructure their production due to increased competitive pressure. Reasons are networking, dynamic sampling and an ongoing product individualization of, which requires permanent adaption capabilities in production, information management, and process control [2]. A challenge is the integration of MES within the overall organizational decision-making [3], because the data of the shop-floor level are needed for decisions in all enterprise levels, for instance to operate plants and machines, to control quality, for accounting or to appraise new technologies. Business Intelligence (BI) describes concepts to support management decisions by the usage of a data warehouse and online analytical processing (OLAP). A data warehouse is a persistent database decoupled from operational systems to support reporting and analysis activities within the whole organization [4]. The integration of BI and MES led to the generation of performance indices for production influencing operational, middle management and strategic decisions [5]. Motivated by the introduced issue, the paper intends to give a state-of-the-art of MES and BI in academic literature, which is defined as an overview about scientific questions and stimulates the further research [6]. This provides the basis to investigate the role of BI in context of MES and production environments. This is useful for collaboration of organizational entities between the different enterprise levels, which is especially relevant for organizations realizing the value creation in production.

As depicted in Fig. 1 the amount of published research in field of MES has been increased over the last period of 18 years. This includes several articles giving an overview about scientific issues and expediting the further research [3],[7],[8]. None of these publications, which are comparable to the definition of state-of-the-art, consider the term or concepts of BI. Furthermore they are not reviewing the underlying literature according to a dedicated method. Therefore, this paper contributes a state-of-the-art by analyzing the literature in field of MES under consideration of BI based on an appropriate approach [6], [9], [10]. This is important for researchers and practitioners, so that duplication can be avoided and relevant findings can be considered.

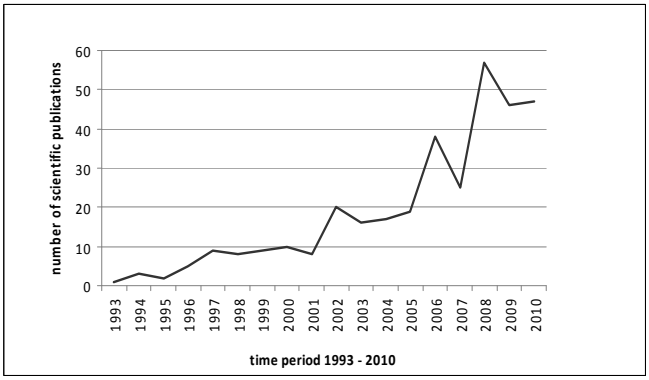

Fig. 1 Publications in field of MES from 1993-2010

The paper is organized as follows: Section II defines the term of MES as concept between ERP layer and automation layer and as submodule of BI. Furthermore the functions and architecture of MES are described. The method of literature review is explicated in Section III by presentation of a staged process. Section IV highlights the results of the literature review by evaluation and analysis of the located publications in context of MES and BI. Finally, the paper is summarized in Section V giving conclusions and further research perspectives.

II. BACKGROUND

This section defines the term Manufacturing Execution System (MES). After the definition basic functions of MES are described. Finally, this section points out architecture requirements of MES.

A. *Definition of MES*

The MES is placed between the layer of ERP and automation as shown in Fig. 2. It realizes a vertical integration by enabling of task-oriented compaction, communication and access of data [2]. The ERP system is responsible for order and resource planning. It communicates desired quantities to the MES, which reports the results back to the ERP. Therefore, the MES has to execute target-performance comparison permanently. This is to be done over the full production cycle by using real-time data. Operational performance shall be improved by reporting of crucial information regarding to the production process. MES delivers decision relevant information on shop floor level. Therefore, MES can be considered as submodule of BI, which provides decision relevant information to the whole organization [11].

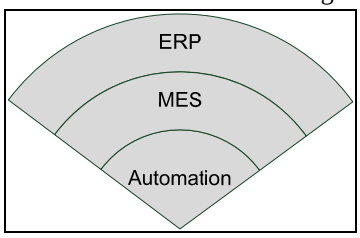

Fig. 2 MES as concept between ERP and automation layer

B. *Functions of MES*

Manufacturing environments are manifold depending on the complexity of the product and the underlying production process. To meet the different production conditions a MES has to cover eleven functions (see Fig. 3) [12].

Dispatching production units reacts on occurrences of the ongoing production. Orders and work plans are changed and adjusted if necessary. Data collection gathers and monitors all relevant data regarding to materials, operators, machines and processes. Quality management analyzes the measured data to avoid non-conformity. Maintenance management ensures functionality of machines and plants by recording the consumption of resources and hours of operation. Performance analysis compares the achieved efficiency of the production environment with desired quantities of the business or ERP level. Scheduling is planning sequences of process steps under consideration of available resources and capacities. Document control manages that all relevant information regarding to products, processes and design are accessible to the employees. Labor management records and organizes working time. Process management monitors the production process and provides information to operators about the production activities. Product tracking and genealogy creates the product history for progressing of production units. Resource allocation manages and monitors production relevant resources.

Data collection, quality management, performance analysis, document control, process management as well as product tracking and genealogy coincide with BI, because these functions of MES allegorize data aggregation and analysis to support the collection and distribution of decision relevant information. This is equal to the intention of BI [12]. Considering the aforementioned aspects there are intersections between the concepts, but MES is more versatile than BI, because of the focus on the shop floor level.

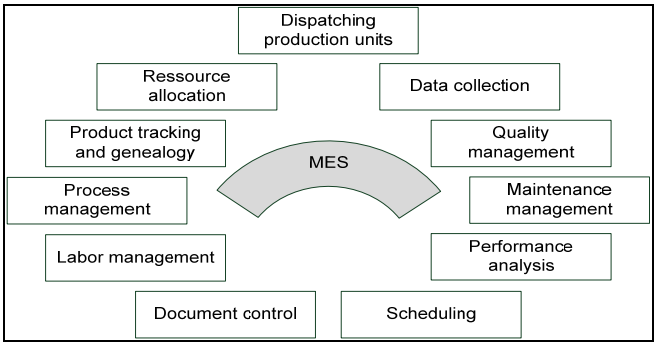

Fig. 3 Functions of MES

C. *Architecture of MES*

The architecture of MES consists of three layers [8]: application layer, functional layer, and data interface layer (see Fig. 5). The data interface layer enables the access to one or more databases, where persistent data are stored. The heart of a MES is the functional layer. It implements the aforementioned eleven functions of the MES especially scheduling or document control. This layer consists of single functional components and can be extended according to production requirements. The application layer presents the MES functions on several clients. Users are able to interact with the system by sending requests and getting desired results. In addition to the described layers the architecture of MES has to consider interfaces to the ERP and control systems.

BI is based on the extraction, loading and transformation of data from several operational databases as for instance ERP, supply chain management, customer relationship management and other external data sources within a data warehouse [13]. Since the architecture of MES proposes a data interface layer, an interface to the data warehouse and therewith integration within BI can be achieved.

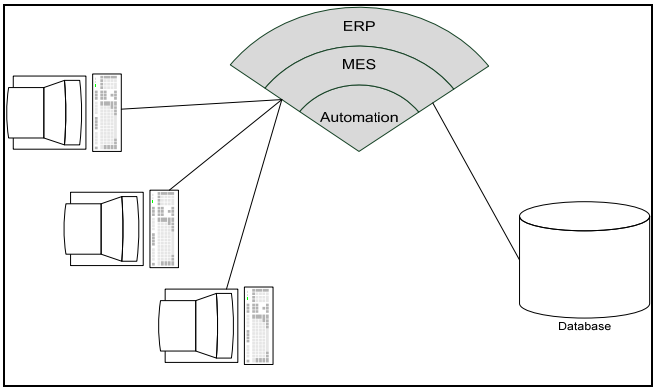

Fig. 4 Architecture of MES

III. METHOD OF LITERATURE REVIEW

A review is defined by the following characteristics: Based on primary investigations to one or more similar research questions, the review intents to describe, summarize, evaluate or integrate the findings of previous research [6]. From this it follows that a review identifies gaps within a research topic and raises new issues in a scientific field [9].

The review follows process consisting of five stages as depicted in Fig. 5 [6]. During the stage of problem formulation, the question that has to be answered by the review gets formulated, delimited and further specified. The next stage of literature search makes suitable literature for the given problem available. The third stage evaluates the located literature. The focus is to examine the identified literature concerning its relevancy. Subsequently, the literature has to be processed and proper systemized. After this, analysis and interpretation of the literature take place. Within this stage, the findings of literature evaluation will be explored and rated. This has to be done against the formulated problem. Finally, the research results are to be edited and presented to the general public.

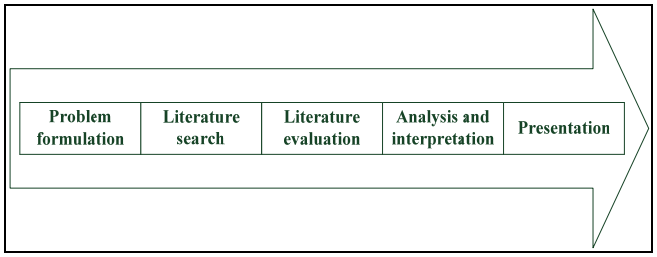

Fig. 5 Review process according to Ref. [6]

IV. Results

Since the problem formulation is been explicated in the introduction this section presents the results of the further steps regarding to the review process of literature.

A. Literature search

The scientific databases of IEEE Xplore, ACM Digital Library, Science Direct, EBSCOHOST, Emerald and AIS electronic Library (AISeL) are the basis of the literature search. This is been done, because the databases are covering a wide range on scientific publications. The search considered double-blind reviewed articles of the databases and references of them focusing on MES. The search terms were *Manufacturing Execution System*, *MES* or *Manufacturing Execution System MES*. Fig. 6 shows the result of the literature search. Altogether 340 articles are found, where the most (183) are listed in the IEEE Xplore database.

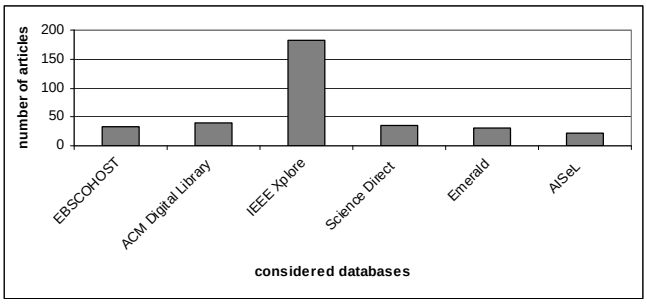

Fig. 6 Matches in selected databases

B. Literature evaluation

All of the 340 articles are evaluated for their relevance in context of BI. Therefore, the articles were searched in for the keywords of *Business Intelligence*, *BI*, *Data Warehouse* and *Operational Business Intelligence*. After this limitation the selected articles have been compared to the narrow understanding of BI, which equalizes the term with data warehousing and online analytical processing (OLAP) [11]. This is been done, because in the broader sense, BI considers applications used for direct and indirect decision support including evaluation and presentation functionality as well as data storage and processing [13]. Due to this understanding, a MES itself is a BI application. Table 1 shows the results of the evaluation. Only 2 percent of the articles consider BI in the narrow understanding (see Fig. 7).

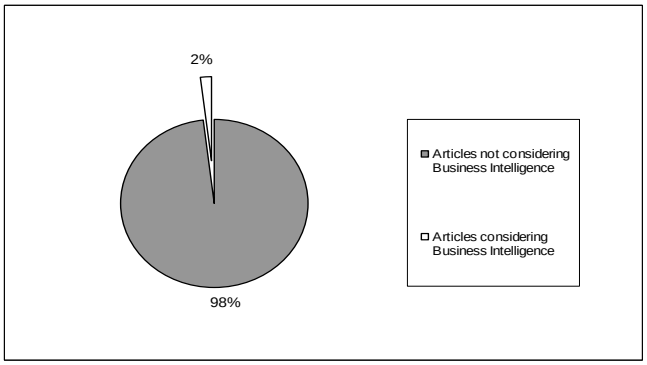

Fig. 7 Articles considering MES and BI

TABLE I
EVALUATION OF MES PUBLICATIONS FOR THEIR RELEVANCE IN CONTEXT OF BI

Database / Keywords	EBSCOHOST	ACM DL	IEEE Xplore	Science Direct	Emerald	AISeL	**TOTAL**
"Manufacturing Execution System"	32	39	183	35	30	21	**340**
"Manufacturing Execution System" + "Business Intelligence"	0	0	0	0	0	2	**2**
"Manufacturing Execution System" + "Data Warehouse"	1	0	2	0	0	0	**3**
"Manufacturing Execution System" + "Operational Business Intelligence"	0	0	0	0	0	1	**1**

C. Analysis and interpretation

The number of publications regarding to MES is increasing. This indicates the relevance of MES for practitioners and researchers. Considering the integration of MES within BI, the relationship between the concepts is hardly investigated, because the percentage of publications has a marginal value of 1.8 percent.

Table II summarizes the content and findings of articles considering BI. Addressed are implementation and integration aspects. The term Business Intelligence is only used in the last three publications. The previous articles consider data warehousing and OLAP, which is consistent to the narrow understanding of BI [11].

TABLE II
SUMMARY OF THE ARTICLES CONSIDERING BI

Ref.	Year	Summary
[14]	2005	The article presents a multi-dimensional data model and snowflake schema for MES data warehouse. Furthermore online analytical processing (OLAP) cubes are designed for an implementation case to analyze production indices.
[15]	2006	The article discusses an enterprise yield management (EYM) systems, which loads data from the MES and from ERP into a centralized data warehouse to identify problem areas in production.
[16]	2006	The article discusses integration of manufacturing execution system, data warehouse, online analytical processing (OLAP) and data mining.
[17]	2010	The article investigates the relationship between operational BI and MES and proposes an integration framework.
[18]	2010	The article presents architecture to integrate MES data in the BI-Tool of the ERP system. The investigation is based on a case study, where a prototype is modelled for extraction of MES data in real-time.
[5]	2010	The article presents a concept for operational management to organize the production process according to restrictions of original equipment manufacturers. Integration of BI and MES is part of the research framework and the base for operational decision support.

V. CONCLUSION

The role of BI to integrate MES in the overall decision making of organizations is hardly investigated, although it is advantageous for the following reasons:

- consideration of production performance indices within all organizational levels,
- real-time analysis of the shop floor to improve operational performance and
- integration of isolated applications to ensure a comprehensive operational decision making.

To close the indentified gap scientific approaches for integration of BI and MES have to be investigated and validated. This is needed to confirm the conclusions of this paper and to get further insights to the presented topic.

REFERENCES

[1] ISA ANSI/ISA-95.00.01-2000, “Enterprise Control System Integration, Part 1: Models and Terminology,” 2000.

[2] J. Kletti, *Manufacturing Execution System – MES*, Berlin: Springer, 2007.

[3] B. Saenz de Ugarte, A. Artiba, and R. Pellerin, “Manufacturing execution system – a literature review,” *Production Planning and Control*, vol. 20, no. 6, pp. 525-539, September 2009.

[4] P. Gluchowski, ”Data Warehouse,“ in Enzyklopädie der Wirtschaftsinformatik – Online-Lexikon, 4th ed., K. Kurbel, J. Becker, N. Gronau, E. Sinz, and L. Suhl, Eds. Munich: Oldenbourg, 2010, http://www.enzyklopaedie-der-wirtschaftsinformatik.de, last access: 2010-12-28.

[5] P. Louis and S. Olbrich, “Architecture for analyzing manufacturing execution data – using Business Intelligence logic,” *Proceedings of the Sixteenth Americas Conference on Information Systems*, Lima, Peru, August 12-15, 2010.

[6] P. Fettke, „State-of-the-Art des State-of-the-art – Eine Untersuchung der Forschungsmethode ‘Review’ innerhalb der Wirtschafts-informatik,“ *Wirtschaftsinformatik*, No.4, 2006, pp. 257-266.

[7] M. Younus, C. Peiyong, L. Hu, and F. Yuqing, “MES Development and Significant Applications in Manufacturing – A Review,” *2nd International Conference on Education Technology and Computer (ICETC)*, 2010.

[8] L. Fei, “Manufacturing Execution System Design and Implementation,” *2nd International Conference on Education Technology and Computer (ICETC)*, 2010.

[9] J. Webster and R. Watson, “Analyzing the past to prepare for the future: Writing a literature review,” *MIS Quarterly*, vol. 26, no. 2, pp. 13-23, 2002.

[10] J. vom Brocke, et al. “Reconstructing the Giant: on the importance of rigour in documenting the literature search process,” in S. Newell, E. Whitley, N. Pouloudi, J. Wareham, and L. Mathiassen, Eds. *17th European Conference on Information Systems*, Verona, 2009.

[11] C. Felden and G. Chamoni, “Project Blueprints as Basis for Business Intelligence Projects – Towards an Applicable Business Intelligence Maturity Model,” unpublished.

[12] MESA, “MES Functionalities and MRP to MES Data Flow Possibilities,” *MESA International – White Paper Number 2*, Pittsburgh, 1997.

[13] H.-G. Kemper, W. Mehanna, and C. Unger, *Business Intelligence Grundlagen und praktische Anwendungen*, 2nd ed., Wiesbaden: Vieweg, 2006.

[14] K.-Y. Chen and T.-C. Wu, “Data warehouse design for manufacturing execution systems,” *Proceedings of the 2005 IEEE international Conference on Mechatronics*, Taipei, Taiwan, July 10-12, 2005.

[15] S. Griffith, “It takes an enterprise to manage yield,” *Electronic Engineering Times*, May 2006.

[16] R.-S. Chen, Y.-S. Tsai and C.-C. Chang, “Design and Implementation of an Intelligent Manufacturing Execution System for Semiconductor Manufacturing Industry,” *IEEE International Symposium on Industrial Electronics*, 2006.

[17] M. Koch, H. Baars, H. Lasi, and H.-G. Kemper, “Manufacturing Execution Systems and Business Intelligence for Production Environments,” *Proceedings of the Sixteenth Americas Conference on Information Systems*, Lima, Peru, August 12-15, 2010.

[18] P. Hollstein and H. Lasi, “A CHANGEBILITY APPROACH FOR PROCESS MANAGEMENT AND DECISION SUPPORT ON THE SHOP FLOOR,” *Mediterranean Conference on Information Systems (MCIS)*, Paper 41, 2010.

2011 International Conference on Mechanical, Industrial, and Manufacturing Engineering
Lecture Notes in Information Technology Vols. 1-2

Studies and research on the use of Virtual Reference Station (VRS) and Precise Point Positioning (PPP) GPS in Romania.

Gabriel Bădescu, Rodica Bădescu, Ovidiu Ştefan,

Department Geodesy of Mines
The North University of Baia Mare
Baia Mare,Victor Babeş Nr. 62/A, ROMÂNIA

badescu_rodica@yahoo.com; gabrielbadescu@yahoo.com; o.stefan@ymail.com

Caius Didulescu

Department Geodesy
Tehnical University of Civil Engineering
Bucureşti,District 2, Bld Lacul Tei No.122-124 , ROMÂNIA

caiusdidulescu@yahoo.com;

Ioel Samuel Vereş

Department of Mines
The Petroşani University
Str. Universitatii nr. 20, Petrosani, Hunedoara, ROMÂNIA

veresioel@yahoo.com;

Cornel Păunescu

Department Geology and Geophysics
Bucharest University
Str. Traian Vuia 6, Sector 2, Bucureşti , ROMÂNIA

cornelpaun@gmail.com

Abstract

The Geodesy Group of the Department of Geodesy and Mines, Department of Mineral Resources and Environment of the North University of Baia Mare, made research on the optimal configurations to achieve long-range action of GPS as a basis for accurate positioning for aircraft used in various projects of air-photography and subsequent mapping. There have been several parallel strategies used to solve this problem: a virtual reference station (VRS), precise point positioning (PPP), and several reference sections (MRS). This paper summarizes the concepts behind positioning technology PPP and VRS techniques and presents the latest experimental results of our research in this area. Current comparisons of PPP and VRS techniques, with a trajectory of well-controlled and independent aircraft earth stations in Romania show that they can achieve an accuracy of about 4-5 cm. The issue for the future will be to make the implementation of these combined methods the main goal in solving the various issues in the field of Geodesy.

Keywords: GPS, VRS, PPP, kinematics positioning, RTK.

1. INTRODUCTION

In time, long-range action kinematics positioning was the target of mapping projects made from the air, which use as a primary positioning technique the relative GPS technique with phase differences. Nevertheless, this was difficult to execute in a production environment because of the effect, especially of the atmosphere, with GPS errors which increase with the base receiver distance, rover receiver. This is not exactly problematic in Romania, because in the case in which the air mapping projects are usually made in not so distant places, in which the geodesic control, occurs more often than in other countries, the project cost increase is not significantly great. Presently, there are three viable approaches to handling this issue:

- Multi-base station or multiple reference stations (MRS) approach (Wanninger, 1999, 2002; Vollath et al, 2000;. Fotopoulos and Cannon, 2001);
- The concept of virtual reference station (VRS) (e.g. Vollath et al, 2000;. Higgins, 2002; Wanninger, 2002; Hu et al, 2003) and
- The Precise point positioning (PPP) technique (e.g, 2001; Gao şi Shen, 2001; Witchayangkoon, 2000).

This article describes the initial results of our trials regarding the application of the VRS and PPP approaches. Here we will briefly describe the concepts of VRS and PPP, followed by the results of some of our initial trials, using our own internally developed software. This shows that both techniques can offer a precision of approximately 3-4 cm, but it is expected that the errors would decrease and the MRS approach module improved.

2. The VRS concept used widely in Romania, using also ROMPOS

The VRS concept is a derivate of the Multiple Reference Stations (MRS) approach, but differs in the fact that the GPS reference receivers are instead used to "synthetically" determine the double frequency code and to send GPS data from a virtual base station which is located near the user's receiver. The user data and the GPS virtual data station are then processed in the unique base mode in order to determine the coordinates of the user's receiver. This can be achieved almost in real-time (similar to real time kinematics RTK) or post-processing modes, but the almost real-time mode requires a large broadband between reference stations (in case the data are calculated virtually through GPS) and, later, for the user.

The concept of VRS allows the user to access data from a virtual GPS reference station from any collated location which is found close to the real GPS reference network. Also, with VRS the approach is more flexible in what concerns allowing the users to use their current receivers and software without involving any other special software or

communications equipment in order to simultaneously administrate the data in all reference stations.

With VRS, the users in the MRS network can operate from greater distances than with the conventional RTK or faster / quick static GPS modes (usually 10 and 20 km), without low precision. In ideal conditions, the VRS approach can provide a single precision coordinate point of a few centimeters for a network of MRS reference stations separated by 45-120 km, which is the case of the GNSS National Romanian Network and ROMPOS (reference stations A class, around 70). Regarding our issue concerning the specific application for aircraft positioning, it must be stated that the notion of VRS was initially created for fast / rapid-static users or RTK who work with relatively short distances (less than 9-12 km) from the interest area. Under these circumstances, an approximate utility position is enough for the data generating process of the Virtual Reference Stations (VRS). However, for long-range action for kinematic GPS positioning, the Rover can be used on long distances. Thus, it is necessary to frequently update the position of the Virtual Reference Stations (VRS), so that the separation between the VRS and Rover does not become too large, ideally within 12 km.

As a result, the VRS method suggested by Wanninger (2002) shall be modified for long-range action for post-processing kinematic GPS applications. During this method the VRS will be modified, VRS which is mentioned in a fix position according to the rover and the approximate initial position, and the corrections are applied to the Rover trajectory. When the current approximate position of the rover becomes greater than 12 km from the initial VRS position, a new Virtual Reference Station (VRS) is created. This process continues each time when the distance of 12 km is reached, in reality making the Virtual Reference Station the "trail" of the aircraft's (airplane's) trajectory.

3. Our own post-processing VRS software named Geoland Survey GNSS-VRS

Our own post-processing VRS software named Geoland Survey GNSS-VRS, for medium and long range (25-150 km) kinematic positioning, was developed inside the Geodesy Department of the North University in Baia Mare, in collaboration with the company S.C. Geoland Survey SRL in Baia Mare, and it generates modified VRS data for kinematic users in pure RINEX format, so that the Virtual Reference Stations (VRS) located away from the user are always no further than 10-15 km. Because of the altitude difference between the ground receivers and the ones on aircraft with GPS the delay of the signal due to the troposphere must be handled with special care.

The operation mode with the post-processing procedure allows the careful processing of GPS data and avoids frequent broadband problems, found in GNSS type RTK applications. Considering this aspect, we have used the International GPS Service (IGS) and the final orbit catalogues (precise orbits) instead of diffused ephemerides GPS.

4. Experiments using Virtual Reference Stations (VRS) with the subsequent test results

The double-frequency GPS data set from the air and from the permanent ground stations in Romania (the National GNSS Network Class A) 08:25-09:25 (GPS time), on June 7th 2005, was chosen from a trial flight in Romania, having a data collecting rate of 1 Hz. This test used five permanent reference stations in Romania (the National GNSS Network Class A) (BAIA, DEJI and BIST; Illustration no.1), in order to build a Multiple Reference Stations (MRS) network, also having a data sampling rate of 1 Hz. The reference stations were equipped with double-frequency MS750 Trimble receivers and TRM41249.0 antennas. The distance between the reference stations varies between 45 and 120 km.

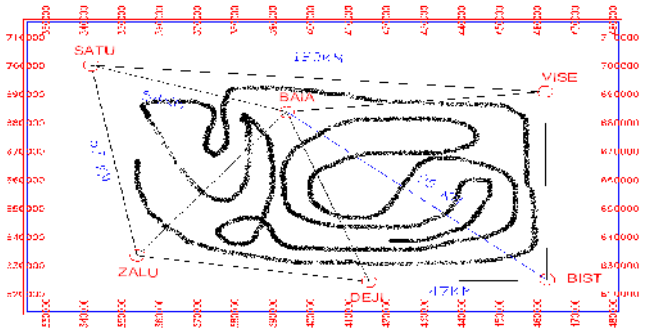

Fig. 1 shows the reference network and the flight trajectory during the trial period.

The VRS data were generated using my modified VRS method and the subsequent software (Geoland Survey GNSS-VRS), and then the aircraft's trajectory was uniquely determined in relation to the base, for each next VRS type station. The reference trajectory for the aircraft is known with a precision of a few centimeters from software comparisons and different independent positions determined by aerial triangulation. The modified positions using VRS estimate have been compared with the aircraft's reference trajectory. Two hours of flight for the aircraft's trajectory (red) and the reference network in the 6 stations in the National GNSS Network used for the VRS modified tests (stereo-graphical projection 1970).

Table no. 1 - The descriptive statistics for the differences (meters) between the VRS modified results and the reference trajectory for two hours of aerial kinematic testing using GPS in Romania.

	STD	Mean	Max	Min
North	0.023	-0.015	0.069	-0.063
East	0.032	0.013	0.078	-0.723
Height	0.057	-0.032	0.112	-0.191

Table no. 1 - The descriptive statistics for the differences (meters) between the VRS modified results and the reference trajectory for two hours of aerial kinematic testing using GPS in Romania.

Table no. 1 synthesizes the results of the comparisons made during the two-hour trial period. As Table no. 1 clearly shows, the standard deviations for North, East and height are

23 mm, 32 mm and 57 mm, when the modified VRS method is used, together with the corresponding software (Geoland Survey GNSS-VRS). It is important to mention that, it is proportional to the expected precision of the aircraft's reference trajectory. Considering that the GPS positioning precision is systematically weaker for the height element, it is necessary to pay special attention to the antecedent delay due to the troposphere's effect. The precision incongruity for the horizontal coordinates are likely and mainly caused by the multipath effect, due in turn to the aircraft's fuselage which is made out of metal and has a great power in reflecting the waves. The main incongruities for the vertical are most likely caused by the combination of multipath errors and by residual errors caused in turn by the crossing of the GPS signal through the troposphere.

5. The precise point positioning concept (PPP)

In the classic GPS positioning of a point, the precision is around 20 m, and is known as independent positioning, and implies a single tracking code for GPS receivers.

It is also possible to determine the positions of a single point from code measurements and phase measurements. Using precise GPS orbits and clock corrections (e.g. time corrections for clocks found in satellites), they are available from the IGS service, and it has been proven that the positioning using phase measurements for a single point can be improved up to the level of decimeter precision (e.g. Gao and Shen, 2001; Kouba and Heroux, 2001). This can be achieved by using free-ionosphere, pseudo-codes and phase measurements, together with precise IGS orbits and clock corrections.

This measurement approach is known as Precise Point Positioning (PPP). The Precise Point Positioning (PPP) approach is similar to the positioning of a single point using pseudo-codes (pseudo-range) made with a hand GPS receiver, with the exception that this (Precise Point Positioning) also uses data from GPS phase measurements, as well as improved orbits (precise orbits) and clock corrections through satellite. Under ideal circumstances, the PPP concept can insure precisions for a single point of 4-10 cm, regardless of the length of the GPS bases.

The concept of Precise Point Positioning (PPP) is relatively new (in Romania, and was presented for the first time as part of a doctorate thesis at the Gheorghe-Asachi Technical University in Iasi in 2010), is very current and generally implies lower costs. Very important is the fact that this (PPP) method requires a single GPS (GNSS) receiver with a double frequency which uses phase measurements and thus the necessary cost and logistics is avoided for the implementation of a network of GPS (GNSS) receivers around the interest area, as is necessary in the case of Multiple Reference Stations (MRS) techniques and Virtual Reference Stations (VRS). Considering these aspects mentioned, the Multiple Reference Stations (MRS) are still used globally through the data provided by the IGS.

5.1. Geoland Survey GNSS-VRS

This software is still under development for the application of the Precise Point Positioning (PPP) technique, in post-processing mode, according to two important mathematical models.

- The Kouba and Heroux model (2001), which uses free-ionosphere combinations with linear L1 and L2 phase measurement combinations, but cannot provide whole-fixed-ambiguity solutions (this model only offers float type solutions).
- The Gao and Shen model (2001), which uses a free-ionosphere combination with linear L1 and L2 phase measurement combinations which reduces the noise of code measurements and tries to solve whole ambiguities.

Presently, the Kouba and Heroux model (2001) is used in our software, as well as the Gao and Shen model (2001).

Because the PPP technique does not cancel the errors found in a position through a relative / differential GPS technique, different types of corrections have been included intxo the software that I have developed, namely Geoland Survey GNSS-VRS. In addition to the final IGS products presented above, these are: relativity corrections for satellite eccentricities "orbital and Earth rotation" (Sagnac correction), compensations of the satellite antenna at their gravity center (especially the so-called Y-bias), delays due to the troposphere effect, phase windup and solid Earth tides. A sequential procedure and a leveling filter, also, were put into application in our PPP software, Geoland Survey GNSS-VRS, in case the ambiguities are basically carried forward from one measuring date to another.

A common practice in processing GNSS measurements is that of creating linear combinations between measured sizes in order to solve ambiguities. These linear combinations give the advantage that they eliminate the influence of certain errors, helping in understanding and solving GNSS problems. Thus, we can identify the following types of linear combinations, when a single receiver is used: the linear combination between the code measurement and the phase measurement, recorded on the same frequency (GRAPHIC); narrow-lane and wide-lane linear combinations; the combination for reducing the ionosphere effect (Iono-free); the combination for eliminating geometrical effect (Geometry-free); the Melbourne – Wübbena.

5.2. Results and experiments using the PPP measuring mode

In our PPP experiments and results, while we wanted to perform an aerial kinematics positioning, we tested the software using static GPS data based on ground markers

(permanent ground stations), but processed as kinematics. The 'error' values are represented by the differences between one date of measurement and another, between the estimated PPP position and the control station with ground coordinates.

A large number of static GPS data sets have been used, the results being listed below, the trial data in Romania being typical for the ones made with other sets of data in other measurements. Using the date-to-date solution and the PPP method partially simulates a ground example for kinematics measurements.

Six GPS stations (Fig. 2) from a MRS station in Romania have been used. Although the distances between these six stations vary between 47 km and 120 km, this fact does not matter because the PPP method is of reference for independent GPS bases lengths. All six stations have been equipped with Trimble MS750 dual-frequency receivers and TRM41249.0 antennas. The data set used for testing the Geoland Survey GNSS-VRS software for the PPP type positioning was measured in the interval 09:15 – 13:35 (GPS time), on June 7th 2005, with a sample rate of 1 Hz.

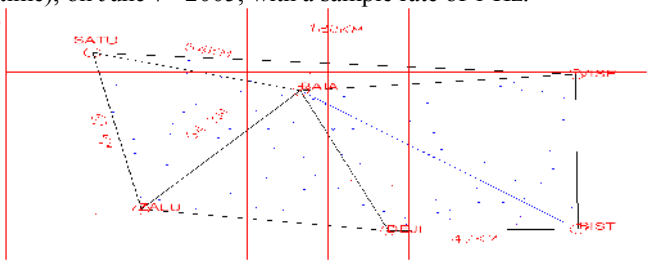

Fig. 2. Six GPS stations from a MRS station in Romania have been used.

The 3D coordinates for these six reference stations are known with a precision of approximately 1 cm horizontally and 2 cm vertically in the national coordinates system (the Official Coordinates System in Romania ETRF89, GRS-80 ellipsoid). They were determined through static measurements during the determination of the National GNSS Network class A, over a number of measuring days.

The values of the North, East and height errors, date by date, have been calculated by lowering the estimated PPP position in relation to the reference coordinates.

Table no. 2 – the descriptive statistics of the differences (meters) between the PPP results and the known results of the BAIA static station for the three hours (simulated) of GPS kinematics test in the National GNSS Network in Romania.

Station	STD			Mean		
	North	East	Height	North	East	Height
BAIA	0.026	0.034	0.088	0.036	-0.036	0.113
SATU	0.026	0.038	0.067	0.042	-0.128	0.045
ZALU	0.023	0.030	0.045	0.038	-0.132	-0.025
DEJI	0.028	0.033	0.038	0.032	0.006	0.057
VISE	0.018	0.015	0.022	-0.021	-0.025	0.081
BIST	0.005	0.023	0.031	-0.008	-0.034	0.098

Table no.2 shows the error values using the PPP method for all six stations.

Once can observe in table no. 2 that the solution of using the PPP method in strategy no. 1 reaches about 28 mm for the precision of the North, East and height elements as standard deviations, but this depends mainly on the quality of the data from the GPS stations.

The PPP method in strategy no. 2 reaches about 20 mm for the precision of the North, East and height elements as standard deviations, but this depends mainly on the quality of the data from the GPS stations and we have noticed an improvement of method 1, because they are taken into account inside the software.

6. Conclusions and suggestions regarding the use of the Precise Point Positioning technique.

We have hereby presented a part of our results for a wide-range action of the kinematics GPS positioning, with the help of the post-processing software kit developed by the Geodesy Department. For the software which is modified for the VRS method, the test results which use one hour of recording data at a frequency of 1 Hz and the aerial kinematics GPS method, show a precision of 2-4 cm in Romania for the horizontal elements and a precision of 7-9 cm for the height element.

For the PPP software, the test results using 4 hours of data at 1 Hz in Romania show a precision of about 2 cm, for all three elements (X, Y, Z) of the GPS determined coordinates. While these results are extremely interesting, they are correlated with the studies carried out by other authors (**N. Castleden, s.a. -Australia, C.O. Andrei-Romania)**, and now the emphasis falls on the post-processing approach of the Multiple Reference Stations (MRS), which will allow the use of restraints in the National GNSS Network class A in Romania, and the improvement of model errors produced by the atmosphere.

REFERENCES

[1] Chen X.M., Han S.W., Rizos C., Goh P.C. (2000) *Improving real-time positioning efficiency using the Singapore Integrated Multiple Reference Station Network (SIMRSN)*, Proc 13th Int. Tech. Meeting of the Satellite Division of the U.S. Inst. of Navigation, ION GPS-2000, Salt Lake City, September 19-22, 9-16.

[2] Fotopoulos G., Cannon M.E. (2001) *An overview of multi-reference station methods for cm-level positioning*, GPS Solutions 4(3): 1-10.

[3] Han S.W. (1997) *Carrier phase-based long-range GPS kinematic positioning*, Ph.D. dissertation, rep. UNISURV S-49, School of Geomatic Engineering, The University of New South Wales, Sydney, Australia.

[4] Hu G.R., Khoo H.S., Goh P.C., Law C.L. (2002) *Testing of Singapore Integrated Multiple Reference Station Network (SIMRSN) for precise fast static positioning*, Proceedings of the European Navigation Conference-GNSS2002, 27-30 May, Copenhagen, Denmark, CD-ROM.

[5] Muellerschoen, R., W. Bertiger, M. Lough (2000) *Results of an Internet-Based dual-frequency Global Differential GPS System*, Proceedings of IAIN World Congress in Association with the U.S. ION 56th Annual Meeting, San Diego, California, June 26-28, 2000.

[6] Teunissen P.J.G., Kleusberg A. (eds) (1998) *GPS for Geodesy*. 2nd enlarged edn. Springer, Berlin Heidelberg New York.

[7] Vollath U., Buecherl A., Landau H., Pagels C., Wager B. (2000) *Multi-base RTK positioning using virtual reference stations*, Proc 13th Int. Tech. Meeting of the Satellite Division of the U.S. Inst. of Navigation, ION GPS-2000, Salt Lake City, September 19-22, 123-131.

2011 International Conference on Mechanical, Industrial, and Manufacturing Engineering
Lecture Notes in Information Technology Vols. 1-2

Influence of Preparation Method on Microstructure and Tribological Properties of C/C-SiC Composites*

Qilong Shi, Peng Xiao, Zhuan Li
State Key Laboratory of Powder Metallurgy
Central South University
Changsha, Hunan Province, China
shiqilong@gmail.com

***Abstract* - In present study, two kinds of C/C-SiC composite had been elaborated by Isothermal Chemical Vapour Infiltration (ICVI) and Reactive Melting Infiltration (RMI) process, respectively. The 2.5 dimension needle carbon felt has been used to form porous C/C composites preforms by using Isothermal Chemical Vapour Infiltration, ether. Then, the C/C preforms with the same density were converted into the C/C-SiC composite by using the ICVI and RMI method respectively. The influence of preparation method on microstructure and tribological properties of C/C-SiC composites was studied. The result of microstructure observation showed that a denser microstructure had obtained by RMI method, and the smaller size of SiC grain was observed in the ICVI sample. Moreover, the results of braking test showed that the samples prepared by using RMI method had the better tribology properties than that of the samples prepared by using ICVI method, due to the softer superficial hardness. However, the latter one had the lower weight wear rate, due to the higher superficial hardness.**

Index Terms – Isothermal Chemical Vapor Infiltration (ICVI); Reactive Melt Infiltration (RMI); C/C-SiC composite; Microstructure; Tribological properties.

I. INTRODUCTION

C/C composites have distinct advantages as the friction material such as excellent thermal and mechanical properties with lower density (lower than 2.0 g·cm^{-3}) [1]. Presently, the C/C composites have been widely used in the advanced friction system, such as, Aircraft brakes and Formula 1 brakes [2]. However, the disadvantages such as insufficient stability of friction coefficient caused by humidity, high cost, and low oxidation resistance make C/C composites less attractive. Retaining the advantages of C/C composites, C/C-SiC composites promise to overcome most of the disadvantages of C/C composites, and show some others excellent properties such as high and stable friction coefficient, long lifetime, low wear rate, lower sensibility to humidity, and high oxidation resistance at high temperature (over 1000℃)[3,4].

In 1960s, the first kind C/C-SiC composite was fabricated by polymer impregnation pyrolysis (PIP) method [5]. However, the application of C/C-SiC composites was limited by the high cost and long production period of PIP process, then, the new processes have been introduced in C/C-SiC composites fabrication, which were reactive melt infiltration (RMI) and chemical vapor infiltration (CVI) process[6,7]. The RMI process was based on the infiltration of molten silicon into porous C/C composites and formation of silicon carbide matrix by chemical reaction at high temperature above melting point of silicon, which rapidly took as the high cost-effective fabricating route and has been widely used [8,9]. In contrary, the CVI process, which based on the infiltration of vaporous precursor into porous C/C composites by gas flow and deposition of silicon carbide in composite matrix by pyrolysis reaction under pyrolysis temperature, has been ignored for a longtime because of the similar drawbacks as PIP process [10]. Therefore, although CVI process is believed to be promising because it would not cause damage to carbon fibers and can produce finer silicon carbide particles, which could lead to improved strength of the materials, the tribological properties of C/C-SiC composites prepared using CVI are not fully understood, much less to compare the tribological properties with C/C-SiC composites prepared by RMI.

Then, in this paper, the work will mainly focused on the differences of tribological properties between the two kinds of C/C-SiC composites—the samples fabricated by CVI and RMI respectively, but the same kind of porous C/C composites have been used.—under the same testing condition.

II. EXPERIMENTAL PROCEDURES

A. Preparation of Sample

PAN-based carbon fibers (T300, 12K, Toray, Japan) were employed in this study, which accounts for a 30% volume fraction in the composites. Prior to CVI deposition, 2.5-dimensional fiber preforms were prepared using the needling method. Then, CVI was employed to deposit the pyrolytic carbon into the preform by decomposing propylene (C_3H_6)) to produce porous C/C composites with a same density about 1.3 g•cm^{-3}, which were graphitized at 2400℃ for 2 hours. The porous C/C composites were then converted into C/C-SiC composites by isothermal chemical vapor infiltration and reactive melting infiltration process, respectively. For CVI process, the porous C/C composites were placed in an chemical vapor infiltration facility where deposition of SiC particles occurred to produce C/C-SiC composites. Methyltrichlorosilane (CH_3SiCl_3, MTS) was used as a precursor together with bubbling hydrogen gas (H_2, the gas

* This work is partially supported by National Natural Science Foundation of China Grant # 51072231 and Major project in Hunan Science and Technology Grant # 2009FJ1011-3 to P. Xiao.

low is 80 ml•min^{-1}) in the reaction chamber to produce SiC particles with a typical deposition condition at 950℃ and 200~300 Pa for 100 ～ 400 hour. The reaction rate for producing SiC particles was controlled by introducing Argon (Ar, the gas low is 200 ml•min^{-1}) as the dilute gas. For RMI process, the porous C/C composites were placed in a graphite crucible and covered by the silicon powder, then, the graphite crucible was put into a vacuum sintered facility, where infiltration of liquid silicon and chemical reaction occurred to produce C/C-SiC composites with a typical reaction condition at 1700 ℃ for 1 hour. The schematic diagram of preparation process is shown in Fig. 1.

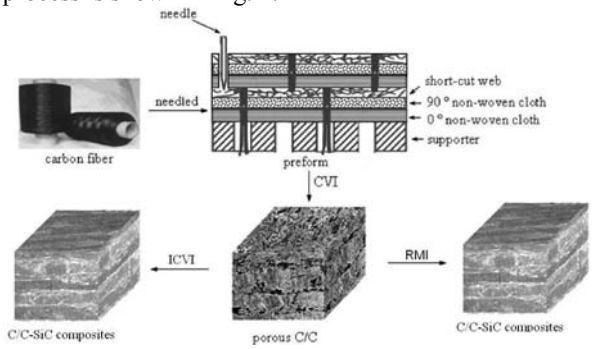

Fig. 1. Preparation process of 2.5D needle-punched C/C-SiC composites

B. Open porosity, density, thermal property and composition

The porosity and density of the samples were measured using the Archimedes displacement method. Thermal diffusivity of the samples was measured using flash method (JR-3 laser thermo-conduction meters, China) under a continuous flow of argon gas at a flow rate of 100 ml/min with a samples size of 10 mm in diameter and 3 mm in height.

The compositions of different samples were got through the different methods. For the samples prepared by using CVI process, the weight percentage of SiC and C in sample was calculated as:

$$W_{SiC} = \frac{\rho_{final} - \rho_g}{\rho_{final}} \quad (1)$$

$$W_C = 1 - W_{SiC} \quad (2)$$

Where W_{SiC} and W_C are the weight percentage of SiC and C respectively, ρ_{final} is the final density of C/C-SiC composites, ρ_g is the density of porous C/C composites after graphitization. For the samples prepared by using RMI process, the gravimetric analysis was employed to determine the fraction of C, Si, and SiC in the composites. Si was removed by dissolving the composite in a mixture of hydrofluoric and nitric acid (HNO_3:HF = 4:1) at 40 ℃ for 48 h, therefore, the fraction of Si could be calculated through the weight different of the sample before and after the dissolving, whereas the content of C was measured by burning it off at 700 ℃ for 20 h in air, then, the content of residual SiC can be calculated. Consequently, the fraction of C in composites could be got.

C. Friction and wear properties

The friction and wear properties of C/C-SiC composites were tested on a disk-on-disk type laboratory scale dynamometer (Fig. 2), simulating a normal landing condition of the aircraft. The kinetic energy absorbed by braking was supplied by the inertia wheels, which were driven by a DC motor. The test pieces are ring specimens with a thickness of 14mm and an inner diameter of 53 mm and an outer diameter of 76 mm. The tested ring specimens acted as both rotor and stator. When the inertial wheel, which rotated with the rotor specimen simultaneously, was accelerated to a certain rotational velocity, braking was achieved through the friction between the rotor and stator under a certain braking pressure. The moment of inertia, rotating velocity and brake pressure during braking were 0.1 kg • m^2, 25 m • s^{-1} and 1 MPa, respectively. The braking tests for each pair of brakes were repeated for 10 times under the same testing condition. The average friction coefficient μ_{cp} during each braking test was automatically recorded by the machine. Stability factor of coefficient of friction S during each braking test can be described as:

$$S = \mu_{cp} / \mu_{\max} \quad (3)$$

where μ_{max} represents the maximum friction coefficient during each braking test. The wear property was evaluated using weight wear rate, which was reckoned as the average weight difference of the test rings before and after braking tests in one particular braking test cycle.

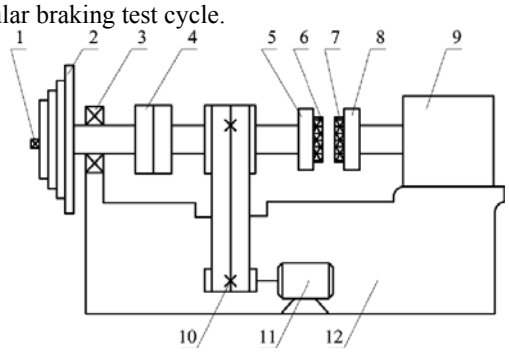

Fig.1 Schematic diagram of the dynamometer. (1) Clamp nut, (2) inertial wheel, (3) bearing, (4) clutch, (5) rotor holder, (6) rotor, (7) stator, (8) stator holder, (9) pressing cylinder, (10) strap, (11) motor, and (12) lathe bed.

D. Observation and analysis

The microstructure of sample was investigated by SEM (SM-6360LV, America) analysis. After braking test, the friction surface was observed and recorded by an optic microscope (POLYVAR-MET, Japan), the morphology of wear debris were analyzed by SEM (JSM-6360LV). The phases were analyzed by using X-ray diffraction (XRD, D/max-γ A, Japan) with nickel filtered Cu Kα radiation produced at 45 kV and 100 mA.

III. RESULTS AND DISCUSSION

A. Phases and microstructure in matrix of C/C–SiC composites analysis

The XRD phase analysis result of the C/C–SiC composites is shown in Fig. 2. It reveals that the silicon carbide and carbon have been found in both kinds of the C/C–SiC composites, and, the mainly phase of the silicon carbide is a face-centered cubic (fcc; β) type SiC. However, there is

some unreacted silicon in the samples prepared by using RMI method, which was never found in the samples prepared by using ICVI method. The composition of two kinds of C/C-SiC composites has been listed in TABLE Ⅰ.

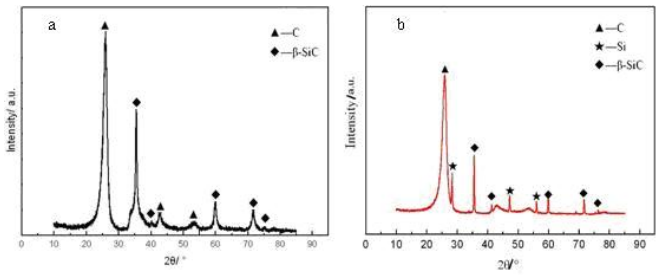

Fig.2 XRD patterns of the C/C–SiC composites
(a) preparing by using ICVI method; (b) preparing by using RMI method.

TABLE. I
The composition of two kinds of C/C-SiC composites

No.	Preparation method	Composition/ wt%		
		SiC	C (C_f and PyC)	Si
1	CVI	32	68	-
2	RMI	33	65	2

Fig 3 shows microstructure of them. Although the fabrication method for tow kinds of samples was completely different, they showed an similar microstructure. It can be seen that in the region with few carbon fibers, the carbon fibers were wrapped with a pyrolytic C layer first, and then surrounded by a thick SiC layer which is believed to be formed due to infiltration during deposition or siliconizing reaction during melting silicon infiltration, see Figure 3. And, in the regions rich of carbon fibers, the fairly dense C/C composites were formed. However, in the sample 2, there were lots of residual silicon have been found in the open macrospores of matrix (the white region in Fig. 3(b)), which was the most obviously distinguish between the two kinds of samples. The residual silicon can be commonly observed in samples prepared using RMI method, which is believed to decrease the open porosity extremely. Moreover, the morphology of SiC particle in the two kinds of C/C-SiC composites is completely different, as shown in Fig. 4. It could see that many semi-spherical silicon carbide particles, which expressed the cauliflower-like surface, have been observed on the SiC layer surface of sample 1, and the most of them is less than 5 μm (seen in Fig. 4 (a)). But, for sample 2, the SiC particles, which were bigger than 10 μm, shown the facetted surface, seen Fig. 4 (b).

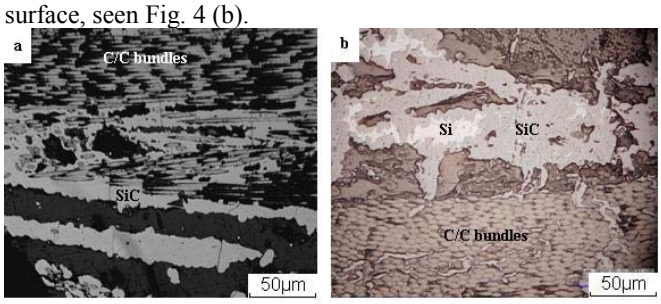

Fig.3 Optical micrographs of C/C-SiC composites materials
(a) the sample 1; (b)the sample 2

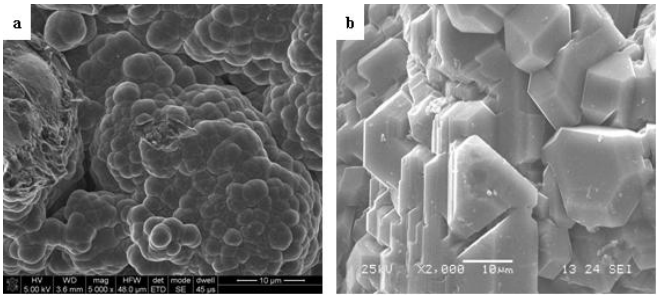

Fig.4. SEM micrographs of C/C-SiC composite.
(a) ICVI sample and (b) RMI sample.

The different shape of silicon carbide particles in two kinds of composites is mainly due to the different formation mechanism of silicon carbide layer during the preparing process, which has been shown in Fig. 5. During the CVI process, the gas precursor was infiltrated into the matrix and pyrolyzed to generate the SiC layer rapidly. After the original SiC layer was formed, the later SiC particles would deposit on the original SiC layer, which resulting into the growth of SiC layer. Therefore, the SiC layer formed during the ICVI process would be compact and continuous. Moreover, because of limitation of superficial energy, the SiC particles show the semi-spherical shape. In contrary, during the RMI process, because of excellent soakage ability between the liquid silicon and the pyrolytic carbon, the liquid silicon could be infiltrated into the inner position of C/C preform by the surface tension. Then, the melting silicon reacted with pyrolytic carbon to form the silicon carbide layers rapidly. After the original SiC layer has been formed, the growth of SiC layer would be controlled by the diffusion of Si atom [11]. Consequently, the SiC layer became relatively coarse and discrete. Besides, the interfacial tension between the SiC layer and melting Si is relatively low, thus, the silicon carbide particles show the facetted structure shape, which is determined by the diamond-like crystal structure of itself.

S. Fouquet etc. researched the mechanical properties of SIC layer in C/C-SiC composites fabricated by using different method [12]. They found that the superficial hardness of SiC layer in samples fabricated by using CVI method is much better than that in samples fabricated by using RMI method. It is mainly due to that the SiC layer in the former one is more compact and continuous than that in latter one. Therefore, the sample 1 must has the higher superficial hardness than sample 2 because of the similar composition in matrix.

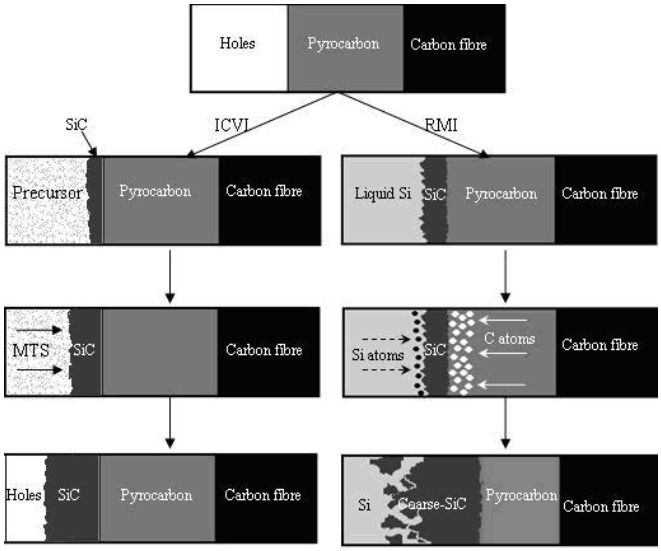

Fig. 5 Schematic representation of a model of SiC layer formation process during different fabrication process

B. *Open porosity, density, and thermal property*

The open porosity, density, and thermal property of two kinds of C/C-SiC composites are shown in TABLE Ⅱ. It could be seen that the sample 2 has the higher density and lower open porosity than the sample 1, which is mainly due to the residual silicon exit in the matrix of sample 2 as mentioned above. Besides, the considerable interlocking elongated cracks, which were done due to the relaxation of thermo-mechanical during the graphitization process, facilitated the infiltration of liquid silicon into the deeper position of porous C/C preform.

TABLE Ⅱ
The open porosity, density, and thermal property of C/C-SiC composite

No.	Density/ $g \cdot cm^{-3}$	Open porosity/ %	Transverse thermal diffusivity /$mm^2 \cdot s^{-1}$	
			//	⊥
1	1.91	13.02	23.5	8.1
2	1.99	8.3	23.7	16

The thermal properties of materials play an important role during braking, it is very necessary to measure the thermal diffusivity, especially transverse thermal diffusivity (heat diffuseness along the direction normal to friction surface) [6]. The measured results are shown in Table 2 as well. It could be seen that transverse thermal diffusivity of sample 2 in both testing directions is higher than that sample 1, especially, along the perpendicular direction. It is mainly due to the lower open porosity and the better uniformity of 2 helps to improve the thermal diffusivity in both direction.

C. *Friction property*

TABLE Ⅲ summarizes the friction testing results of two kinds of C/C-SiC composite. It can be seen that sample 2 has the better friction coefficient (0.30) than the sample 1(0.24), consequently, the shorter braking time (4.90 s) has been achieved. There were two reasons for this phenomenon. One is that the sample 2 has the higher transverse thermal diffusivity than sample 1 as mentioned above, and that will lead to remove the heat on the friction surface more easily and quickly, which generated from rotating kinetic energy by frictional force during the braking process, and resulting into the increase of friction coefficient. Moreover, because the compact SiC layer in sample 1 increased the superficial hardness as mentioned above, the hard SiC asperities were difficult to pierce into the friction surface deeply (as known as "ploughing effect") during the braking process. Consequently, the low friction coefficient has been achieved.

TABLE III
The results of friction testing

No.	μ	S	Braking time/s	Weight wear ratio/$mg \cdot time^{-1}$	
				Stator ring	Rotor ring
1	0.24	0.59	6.15	5.74	4.12
2	0.30	0.61	4.90	10.8	16.8

However, every coin has two sides. Although the friction properties of sample 1 was inferior than that of sample 2, the weight wear ratio of it was less than that of sample 2, which is lower than 5.74 $mg \cdot time^{-1}$. It is mainly due to that the relatively high compact SiC layer in sample 2 has decreased the friction coefficient, but this structure has increased the hardness of SiC layer, which lead to the layer difficultly broke by shearing and compressive force, and then the wear rate has been decreased. That may imply that if the SiC content in matrix is increased, the C/C-SiC composites prepared by using ICVI method should have a potential using in sealing material.

Although the friction coefficient and wear rate of two kinds of C/C-SiC composites were completely different, the coefficient stability of them was similar, which were 0.59 and 0.61 respectively. This is mainly due to the continuous friction film has been formed on both kinds of samples' friction surface.

D. *Friction coefficient curve*

The friction coefficient curve could express the friction properties and friction behaviors of material directly. Then, the typical friction coefficient curves of two kinds of C/C-SiC composites as a function of braking time are shown in Figure 6. In all curves, the friction coefficient increased sharply within less than half second to a peak value of about 0.38 to 0.6 (which was considered as the prior stage of braking process), followed by steady decrease to nearly a plateau which was less than half of the peak value, and then in the final stage increased progressively to a peak value again, which was about 0.35 to 0.42. This makes the curves look like a saddle. However, the maximum peak value (0.42) in curve of sample 2 was not presented at the prior stage of braking process (as sample 1 did), but at the final stage. And, espeicially, the difference between the maximum peak value and minimum value (0.31) of the curve is only 0.11 (in contrary, this difference in curve of sample 1 is more than 0.3.), which resulting in a relatively smooth shape of the curve. It is known that the friction coefficient would be decreased with the increase of surface hardness under the same

surface roughness [13]. As mentioned above, the superficial hardness of sample is higher than that of sample 2. Therefore, the ploughing effect of silicon carbide asperities, which was the main resource of friction resistance in the middle stage, has been limited, resulting in the obviously low friction coefficient.

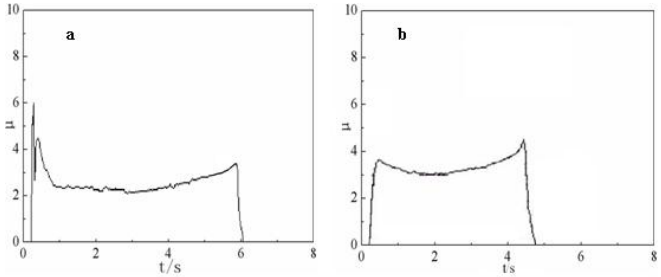

Fig.6. The typical friction coefficient curve of two kinds of C/C-SiC composites.
(a)Sample 1; (b) Sample 2.

Besides, the tail peak in the curve of sample 2 is the sharpest one in both curves, which imply that the adhesion and abrasion of the contact conjunctions and asperities have been enhanced greatly by the quickly decrease of sliding velocity and sharply increase of surface temperature at the final stage. And, this could be certificated by the following discussion of friction surface.

E. Friction surface and wear debris

Figure 7 show the morphology of friction surfaces of the two rings after braking test. It can be seen that the continuous friction film has been formed on both friction surfaces. Furthermore, there are some small pits have been found on the friction surfaces of Sample 2, which is the typical phenomenon of adhesive wear, but the similar morphology are hardly found on the sample 1, which has the relatively smooth surface. It implies that the adhesive effect is more effective in sample 2, which could improve the friction coefficient, and that matched with the different of tail peak in friction coefficient curve of two kind's composites.

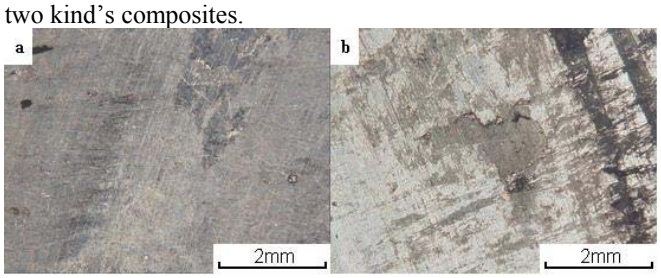

Fig.7. Macroscopic of friction surface of C/C-SiC testing ring
(a) Sample 1; (b) Sample 2

Figure 8 shows the further details of the friction surface after braking test. It can be seen that some grooves were left behind on the friction film of the tested rings (seen Fig 8 (a) and (b)). The grooves on the friction surface are typical character of ploughing effect, suggesting that the grain-abrasion friction have occurred during the braking process for both testing rings. However, in some grooves on friction surface of sample 1, some carbon fibers could be observed directly, and the similar phenomenon was hardly found in the sample 2. That implied that the thickness of friction film on the friction surface of sample 1 is thinner than that of sample 2. During the braking process, the friction film was formed by the wear debris under the braking pressure. Meanwhile, the new wear debris was continuously formed as the retained debris in the friction film was sloughed off [14]. Therefore, the easier wear debris form, the thicker friction film achieves. It was reported that high hardness of friction surface resulted in the difficult formation of wear debris [5]. Then, the high superficial hardness of friction surface for sample 1 may be responsible for the thinner friction film.

The change of thickness of friction film has an influence on the wear debris, too. Figure 9 shows the morphology and size of wear debris from different composites after braking test. Although, both particulate debris and plate-like debris have been observed in all samples, the size of them from sample 1 is smaller than that from sample 2. It can be seen that the size of the most particulate-type debris is smaller than 2 μm, and the most of plate-like debris is smaller than 5 μm, as shown in Figure 9 (a). In contrary, there are a lot of relatively big particulate-type debris have been observed in sample 2, which are bigger than 5 μm, meanwhile, the size of plate-like debris has been increased to about 10 μm, or even bigger. Moreover, it is noted that more particulate debris could be observed in sample 1. It is generally believed that the formation of particulate debris is usually due to the crushing and deformation of abrasive particles like hard SiC, whereas the formation of plate-like debris is mainly due to the pealing-off of carbon fiber and pyrolytic carbon which have a hexagonal crystal structure [16]. Therefore, the bigger size of particulate debris just matches the relatively bigger size of SiC particles in matrix of sample 2, which has mentioned above. Moreover, the increase of size and percentage of plate-like debris is mainly due to that the pyrolytic carbon in sample 2 is much easier attend the friction process than that in sample 1, because of the relatively incompact SiC layer in matrix.

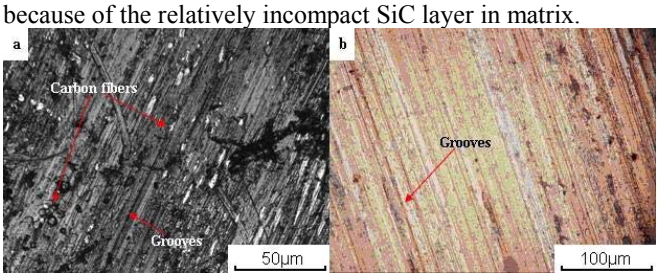

Figure 8 Optical micrographs showing the detail of friction surface after braking test.
(a) Sample 1; (b) Sample 2

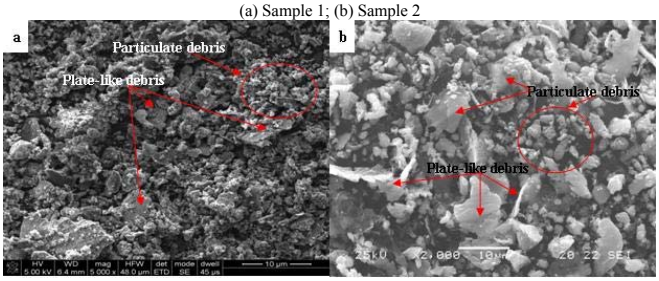

Figure 9 The SEM micrographs showing the wear debris of C/C-SiC composite after braking test
(a) Sample 1; (b) Sample 2

IV. CONCLUSIONS

(1)The two kinds of C/C-SiC composites have been fabricated by using ICVI (sample 1) and RMI (sample 2) process, respectively, and the same kind of porous C/C composites has been employed.

(2)Because of the different densification mechanism during the different fabrication process, sample 2 has some residual silicon in the matrix, which led to higher density than that of sample 1, and resulted in the lower open porosity and higher transverse thermal diffusivity.

(3)The SiC layer in the matrix of sample 1 was more compact and continuous than that in sample 2 due to the different formation mechanism of SiC layer, which resulting in the harder friction surface in sample 1. Moreover, the size of SiC particles in sample 1(which was smaller than 2 is finer than that in sample 2.

(4)The sample 2 had the better friction properties than sample 1, due to the softer friction surface of sample 2. The weight wear rate of sample 2, however, was higher than that of sample 1. That may imply that if the content of SiC in matrix is increased, the C/C-SiC composites fabricated by using ICVI method should have a potential using as the sealing material.

(5)The different superficial hardness led to the different wear behavior between the tow kinds of composite. The abrasive wear has been observed on both friction surface, but the adhesive wear is more obvious in sample 2. Meanwhile, the continuous friction film, particulate type and plate-like type wear debris have been found from both kinds of composites. However, the thickness of friction film and size of both type wear debris in sample 2 is higher than that in sample 1.

ACKNOWLEDGMENT

The authors wish to thank all colleagues from the advanced ceramic institute for their help and informative discussions.

REFERENCES

[1] Krenkel, W., “Cost effective processing of composites by melt infiltration (LSI-Process)”. Ceram. Eng. Sci. Proc., vol. **22**, no. 4, pp.442–444. March 2001,

[2] Mei, H., Cheng, L. F., Zhang, L. T. and Xu, Y. D., “Modeling the effects of thermal and mechanical load cycling on a C/SiC composite in oxygen/argon mixtures”. Carbon, vol. 45, no. 11, pp. 2195–2204, Dec. 2007,

[3] Odeshi, A. G., Mucha, H. andWielage, B., “Manufacture and characterization of a low cost carbon fibre reinforced C/SiC dual matrix composite”. Carbon, vol. 44, no. 6, pp. 1994–2001, Apr. 2006,

[4] Paris, J.-Y.,Vincent, L. and Denape, J., “High-speed tribological behaviour of a carbon/silicon carbide composite.” Comp. Sci. Technol., vol. 61, no. 5, pp. 417–423. May. 2001,

[5] Xu YD, Cheng LF, Zhang LT. “Carbon/silicon carbide composites prepared by chemical vapor infiltration combined with silicon melt infiltration”. Carbon, vol. 37, no. 7, pp. 1179–871, Jun. 1999

[6] Rak ZS. “A process for C_f/SiC composites using liquid polymer infiltration”. J Am Ceram Soc, vol. 84, no. 5, pp. 2235–2239. May 2001

[7] Xu YD, Zhang YN, Cheng LF, Zhang LT, Lou JJ, Zhang JZ. “Preparation and friction behavior of carbon fiber reinforced silicon carbide matrix composites”. Ceram Int, vol. 33, no. 6, pp. 439–454, Jun 2007;

[8] Guangpeng Jiang, Jianfeng Yang, Yongdong Xu, “Effect of graphitization on microstructure and tribological properties of C/SiC composites prepared by reactive melt infiltration”. Composites Science and Technology, vol. 68, no. 6, pp. 2468–2473, Jun 2008.

[9] Shangwu Fan, Litong Zhang, Yongdong Xu, “Microstructure and properties of 3D needle-punched carbon/silicon carbide brake materials”, Composites Science and Technology, vol. 67, no. 11, pp. 2390–2398, Nov. 2007

[10]Yanzhi Cai, Yongdong Xu, Bin Li, “Low-cost preparation and frictional behaviour of a three-dimensional needled carbon/silicon carbide composite”, Journal of the European Ceramic Society, vol. 29, no. 9, pp. 497–503, Sept. 2009

[11]Yonghui Zhang, Zhichao Xiao, Jiping Wang, “Effect of pyrocarbon content in C/C preforms on microstructure and mechanical properties of the C/C – SiC composites”, Materials Science and Engineering A, vol. 502, no. 1, pp. 64 – 69, Jan. 2009

[12]S. Fouquet, M. Rollin, R. Pailler, Tribological behaviour of composites made of carbon fibres and ceramic matrix in the Si–C system, Wear, vol. 264, no. 11, pp. 850–856, Sept. 2008

[13]S.W. Fan, Y.D. Xua,L.T. Zhang, “Three-dimensional needled carbon/silicon carbide composites with high friction performance”, Materials Science and Engineering A, vol. 467, no. 4, pp. 53–58, Mar. 2007

[14]S. Wen, Tribology Theory, Tsinghua University Book Concern, Beijing, 1991, pp. 398–470.

[15]Yongdong Xu, Yani Zhang, Laifei Cheng, “Preparation and friction behavior of carbon fiber reinforced silicon carbide matrix composites. Ceramics International”, , vol. 33, no. 1, pp. 439–445, Jan. 2007.

[16]Vaidyaraman S, Purdy M, Walker T, Horst S. “C/SiC material evaluation for aircraft brake applications”. In: Fourth international conference on high temperature ceramic matrix composites (HT-CMC4) proceedings. Munich, May, 2001.

2011 International Conference on Mechanical, Industrial, and Manufacturing Engineering
Lecture Notes in Information Technology Vols. 1-2

Efficient Method in Operational Transmission Power Grid

Daniel Morar
Sibiu Transmission Subsidiary
CN Transelectrica-SA
Bucharest, Olteni 030786, Romania
Daniel.Morar@transelectrica.ro

Basarab Guzun
Department of Energy Power and Utility
University "Politehnica" of Bucharest
Bucharest, Splaiul Independenței 060042, Romania
guzunbasarabdan@yahoo.com

***Abstract* - The paper present the methods propose by the authors to be applied in operating of the substations. The substations take in consideration was rehabilitates by replace the existing equipments to new equipments made in the last generation. The substations take in consideration, also are change their architecture itself. The mathematic methods and new analyses methods for resolve the operational substations tasks are issue. The analysis methods take in consideration the operational reliability, the technical parameters of equipments and those variations in operation, the importance of the equipments parameters, the statistics and the reliability and the specific parameters. The elasticity of several type of the system architecture is analyzed.**

Index Terms – Operational, Elasticity, Power Grid, Substation

I. Introduction

The high voltage power networks, operating activities undergoing a transition from equipment and systems whose life is exhausted in new equipment and systems.

Mining activity is booming and follows a Quality Plan, which is a modern policy of quality, environmental protection and operational safety and health.

The analysis is base on statistical data. This way we intend to reduce the number of failures of high voltage equipments. Another purpose of our analysis is to choose the best architecture for new substation. An important feature of the new architecture choice is the elasticity of substations.

In this context the authors propose a method of operation.

II. Errors and Failures

In the analysis of faults occurring in equipment most importance is finding the causes that led to their failure. The analysis performed shows that these cases are due to operating equipment parameters, quality of equipment or human error.

Another classification of causes of failure indicates "who causes" the appearance of the defect. Such cases are due to failure of the designer, manufacturer, network operator, users of the equipments, weather conditions, pollution, animals and birds' action.

The authors propose a different classification based on the time when an error has occurred, which subsequently led to equipment failure.

These periods are:

1) The request: is initially, the intention of making an investment
2) The market: is the "market place"
3) The design: the design phase
4) The production: production stage of the equipments
5) The assembly: the stage of equipment's installation
6) The operation: is using a network
7) The maintenance: maintenance of the equipment

In comparison with the steps to be taken to achieve an investment, we found that these steps are the same periods of occurrence of errors above. Therefore we have defined these stages as stages of error. While analyzing each period can be discovered errors in previous stages. Some of these errors can be corrected by the application of effective methods of managing projects, to each stage.

The stage error is:

$$\varepsilon_{stage} = \frac{|POp - PS|}{POm}. \quad (1)$$

In (1) ε is error, *POp* is efficiency parameter (minimum value), *PS* is number of errors in one stage and *POm* is maximum number of activities with or without errors [2].

II. Operational Method

The equipments used to calculus the operational reliability take apart from a system with different architecture type.

We study the how can use the equipments in several type of architecture of the system.

The study present which architectures types of systems are the most profitably.

The data from the operational reliability calculus of the equipments, which was present above, was use to calculus the reliability of the system. In calculus for operational reliability of the systems we use only the best result of the equipments reliability.

We archive an analysis about the solution offer by each system, with different architecture, from Power Grid.

We take in consideration the behavior of the system to each kind of failure.

For calculate the reliability and elasticity of the architecture for system, we take in consideration the following factors:

1) The safety of the scheme
2) The architecture type of scheme
3) The equipment's maneuvers action
4) The equipment's type and function
5) The equipment's reliability
6) The operational scheme
7) The spare capacity of the scheme
8) The operational mode of the equipment and the scheme (use, supervisor, maneuver, monitoring)

The results of the behavior of different systems over 5 years of operation are present in the Table I.

TABLE I
RELIABILITY OF THE SYSTEMS

	System type	*R*
1	double bus bare - OHTL - double bus bare	0.41
2	double bus bare - transformer - double bus bare	0.42
3	double bus bare with by-pass bus bare - OHTL - double bus bare with by-pass bus bare	0.52
4	double bus bare - OHTL - double bus bare with by-pass bus bare	0.45
5	double bus bare - transformer - double bus bare with by-pass bus bare	0.52
6	1.5 circuit breaker - OHTL - 1.5 circuit breaker	0.41
7	1.5 circuit breaker - OHTL - double bus bare	0.40
8	1.5 circuit breaker - transformer - 1.5 circuit breaker	0.44
9	1.5 circuit breaker - transformer - double bus bare with by-pass bus bare	0.45
10	hexagonal - OHTL - hexagonal	0.39
11	hexagonal - OHTL - 1.5 circuit breaker	0.40
12	hexagonal - transformer - hexagonal	0.40
13	hexagonal - transformer - double bus bare	0.38
14	"H" system - "H" system	0.10
15	"H" system - OHTL - 1.5 circuit breaker	0.21
16	1.5 circuit breaker - "H" system - OHTL - double bus bare	0.24
17	"H" system - cross function	0.38
18	"H" system - 2 OHTL with 1 transformer	0.18
19	OHTL in double bus bare with by-pass bus bare system in function on proper bay	0.84
20	OHTL in double bus bare with by-pass bus bare system in function on by-pass bus bare	0.80
21	transformer in double bus bare with by-pass bus bare system in function on by-pass bus bare	0.80

III. ELASTICITY

The elasticity of a substation's electric scheme is the ability of a system to keep as many circuit components after the occurrence of failures, leading to the unavailability of system elements (nodes, bays, etc.).

Elasticity of a system depends on:

1) Number of nodes in a system (N), which forming a graph

2) System connectivity (the connection graph)

3) Node degree

4) Number of cells (sides)

5) System response in case of failures (state system)

The correct choice of a station architecture results in a reduction of errors due to incompatible network station structure. To prevent these errors the authors propose a preliminary calculation of the elasticity system.

The equation for systems elasticity we propose to be:

$$E = N \cdot gr(N) \cdot \frac{C}{I} \prod K \cdot \qquad (2)$$

In (2) *E* is elasticity, *N* is number of nodes and bus-bars, *gr(N)* is rank of nodes and bus-bars, *C* is number of bays with circuit breakers, *I* is number of incoming equipments like overhead line or transformers units, *K* is a coefficient with depend of system status after the occurrence of failures [2].

The equation for probability of elasticity we propose to be:

$$Pe = \prod \left(\frac{Cd - Nd + 1}{Cn - Nn + 1} \cdot \frac{S}{Sm} \right)^2 \cdot \qquad (3)$$

In (3) *Pe* is probability of system's elasticity, *Cd* is number of bays with circuit breakers in function after the occurrence of failures, *Nd* is number of nodes in function after the occurrence of failures, *Cn* is number of bays with circuit breakers in function before the occurrence of failures, *Nd* is number of nodes in function before the occurrence of failures, *S* is the system status after the occurrence of failures, *Sm* is the system status before the occurrence of failures, each case of failures values are multiply [2].

The factors *S*, *Sm* and *K* are obtain by optimum roads methods transposed in optimum flow. For example may apply the Dijkstra's Shortest Path Method [1].

IV. RESULTS

The renewable for a 400/220kV substation was analyzed. The results are described in table II and are base on equation (2) and (3). In table II E_1 is elasticity for 8 circuits, E_2 is elasticity for 4 circuits.

TABLE II
ELASTICITY

Nr.	Elasticity			
	System type	E_1	E_2	*Pe*
1	Double Bus-bar	189	45	0.338
2	Polygonal	1260	52	0.355
3	1.5 circuit breaker	1950	151	0.411
4	"H"	-	60	0.318
5	Single Bus-bar	11.2	2.4	0.335

V. CONCLUSION

For the rehabilitation of the 400/220kV substation the "H" type system in 220kV substation and 1.5 circuit breakers type system in 400kV was chosen.

The conclusions of the analysis of the system's types are:

1) Can't function for long time with the equipment on the by-pass bus bare

2) The grate reliability of a system has in the following order 1.5 circuit breaker type, double bus bare type and hexagonal type

3) The most convenient system for function are "double bus bare with by-pass bus bare - installation - double bus bare with by-pass bus bare" and "1.5 circuit breaker - installation - double bus bare with by-pass bus bare"

4) The most reliability system is 1.5 circuit breaker type

REFERENCES

[1] S.C. Savulescu, *Grafos, Diagrafos e Redes Electricas*, IBEC, Sao Paulo, 1980, pp.1-278.

[2] D. Morar, "Metode performante privind exploatarea statiilor si retelelor de inalta tensiune" unpublished.

2011 International Conference on Mechanical, Industrial, and Manufacturing Engineering
Lecture Notes in Information Technology Vols. 1-2

Design and Implementation of Mobile Assistance System for Auto-Valet Parking Service*

Kyoung-Wook Min and Jeong-Dan Choi
Department of IT Converence Technology Research Laboratory
Electronics and Telecommunications Research Institute
Yusong-gu, Daejeon, Korea
{kwmin92 & jdchoi}@etri.re.kr

Sung-Il Jin
Department of Computer Science
Chungnam National University
Yusong-gu, Daejeon, Korea
sijin@cs.cnu.ac.kr

***Abstract* – The AVP (Auto-Valet Parking) service enables a vehicle to drive and park without any human interaction. The driverless vehicle has to follow the scheduled route on the road and be parked in a parking lot automatically. For this service, the technologies of infra-based detection server and controlling the vehicle automatically are needed. And if driver can request service remotely and monitor the moving state of the vehicle in real-time, the service is able to be more convenient to the driver. The mobile AVP system assists the request service and monitoring the state of the autonomous driving and parking in a mobile device. So, in this paper we design and implement the mobile AVP assistance system which is able to manage the parking area map data efficiently in the mobile device and provides AVP service remotely and user-centric parking slot selection.**

Index Terms – Auto-Valet Parking, Park GML, Mobile Spatial DBMS, Autonomous Driving Assistance System

I. INTRODUCTION

Parking task is recognized as the most difficult among the driving tasks since it includes finding free parking space and moving backward in large probabilities of collision [1]. To alleviate the aforementioned driver's burden, two different types of systems are studied and commercialized. The first is smart parking system [2] and the second is automatic parking assistance system [3].

Although these two types of systems give some degree of comfort and safety to the driver, they assume drivers presence in the car, and still need driver's much attention and constrained environment. In this dissertation, the mobile AVP technology is emphatically studied among the system framework to provide the full autonomous valet parking system framework.

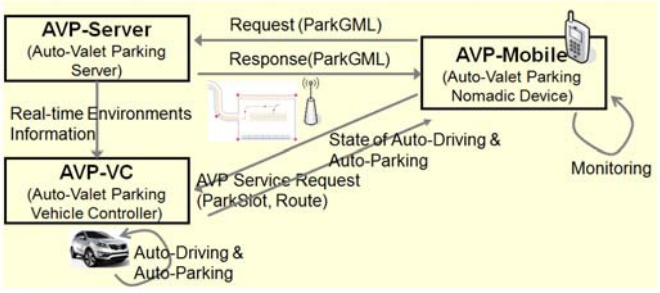

Fig. 1 The system framework for full auto-valet parking service.

The Fig.1 shows the system framework for auto-valet parking service.

- ***AVP-Server***: is responsible for high level multi-vehicle path planning and decision making according to the driving-situation. And also it is providing the information of detecting the positions of static/dynamic obstacles and the controlled vehicle. Also, it should detect occupancies of parking slots, and the attitudes of parked vehicles to determine the geometries of the free space. And it provides parking area map service for AVP-Mobile.
- ***AVP-VC:*** controls the movement of the vehicle. This receives parking area map, control commands, perception information from AVP-Server. It integrates and fuses the perception information with in-vehicle sensor information, producing reliable position of the vehicle and obstacles. Using the computed perception information, a local path, which guarantees collision-free, is generated and it is followed according to the path as controlling actuators through vehicle control interfaces.
- ***AVP-Mobile:*** provides the VAP assistance service in mobile device. It requests the service remotely and monitors the state of the vehicle moving. It manages the parking area map and provides the driver to choose the parking slots. Finally, the driver can know the location and state of parking in easy.

The following is the composition of this dissertation. The development factors for mobile AVP assistance service are explained in detail in section II. In section III, the prototype of the mobile AVP assistance system will be described. Finally section IV is the conclusion of this dissertation.

II. MOBILE AVP ASSISTANCE SYSTEM

The AVP-Mobile system can provide the convenience to driver to request AVP service and monitor the vehicle moving state remotely. For this assistance service, the parking area map data model is to be defined and managed efficiently in mobile device. And also user-centric slot selection policy is to be suggested.

* This work was supported by the Industrial Strategic Technology Development Program (10035250, Development of Spatial Awareness and Autonomous Driving Technology for Automatic Valet Parking) funded by the Ministry of Knowledge Economy(MKE, Korea).

A. Parking Area Map Data Model (ParkGML)

The GML (Geography Markup Language) was established as a standard in ISO TC211 and OGC (Open Geospatial Consortium) [4~6]. The GML serves as a modeling language for geographic systems as well as open interchange format for geographic transactions on the internet. The ParkGML that we have designed as the spatial data model for the AVP service is implemented as an application schema for the GML 3.1.

There are three kinds of data group as their specific properties. The static features are data which will be not changed for long time. The parking road and slot, etc. data are in case of the static one. The static data are generated by surveying and mapping. The semi-dynamic features are data which will be not changed during executing the AVP service after being generated at the time of the service start. The route and static obstacle data are in case of this semi-dynamic one. The dynamic features are data which will be changed continuously during executing the AVP service in rea time. The vehicle location and moving obstacle, etc. data are in case of the dynamic one. The features of the ParkGML have geometrical data type which defined in GML and semantic attributes. Fig. 2 shows the XML schema of the ParkGML.

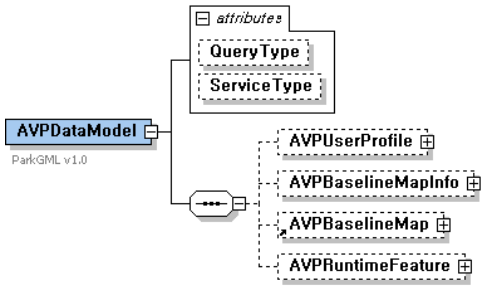

Fig. 2 The ParkGML XML Schema.

The ParkGML have the attributes of QueryType and ServiceType to implement the application protocol for AVP service. The AVPBaselineMap element contains the static features and the AVPRuntimeFeature element contains the semi-dynamic and dynamic features. There three profiles, that is, driver, nomadic device and vehicle profile in AVPUserProfile element. These profiles are helpful to choose the user-centric optimal parking slot. AVPBaselineMapInfo element describes the meta-information of AVPBaselineMap. This has information about the map dimension, SRS, version and so on. The detailed sub-elements of ParkGML will be described in sub section *C*.

B. Mobile Spatial DBMS for managing ParkGML data

In mobile device, there are several commercial DBMS for managing of data. But these cannot manage spatial data like the features of ParkGML efficiently because the spatial data type and queries are not supported in these DBMS. That is to say, the spatial query processor and storage system have to be needed to manage the large map data to guarantee the efficiency and high performance. So we have developed the mobile spatial DBMS to support spatial queries and navigation queries [7]. The summarized features of mobile spatial DBMS are presented in Table I.

TABLE I
THE FEATURES OF THE MOBILE SPATIAL DBMS

Function		*Mobile DBMS*
SQL/API		C/C++ API
DDL		Create / Drop Table-space, Table, Index
DML		Insert, Update, Delete
Search		Attribute Search (Match, initial Sound) Spatial Search (Windows, K-NN, Relational Search) Network Search (Physical Rid Search)
Transaction/Recovery		Begin, Commit, Redo, Undo
Object		Table (General Table, Network Table) Access Path (B+-tree, multilevel-GRID, R*-tree)
Data Type	General	char, varchar, int, uint, short, double, float, binary, date, time, blob
	Geometry	point, lineString, polygon
	Topology	node, link
Flash-aware		Block-level Spatial Clustering
Storage Media		Disk, Flash Memory
Supported Platform		Windows Mobile, Android

It is the DBMS in which the flash memory is used as the storage medium and being operated in mobile device. It provides the standard spatial data types and search operations [8]. And optimal route search query is provided as network search [9]. Some flash-aware functions are provided and this system is running in the windows and android mobile platform.

C. Protocols for Mobile AVP Service

The ParkGML represents the park area map data model and encoding/exchange format among the AVP systems. It provides 4 main services and defines the elements for these services. Table II shows the kind of AVP services and its elements. The QueryType and ServiceType attribute are defined in the root element of the ParkGML. The ServiceType attribute expresses the type of service shown in Table II. The QueryType attributes means the keyword of the query in the system side. For example, in case of the MapProvision service, the value of QueryType attribute will be "*REQUEST*" in AVP-Mobile system side. And in AVP-Server system side, the value of the QueryType attribute will be "*RESPONSE*" to transmit the ParkGML to the AVP-Mobile system. The "*REPORTING*" of the QueryType means the periodical reporting some information to the AVP system. And the "*NOTIFICATION*" of the QueryType means the notification some state to the AVP system.

TABLE II
THE AVP SERVICE AND ITS PROTOCOL ELEMENTS

Service	*Protocol Elements*			
	REQUEST	*RESPONSE*	*REPORTI*	*NOTIFICATION*
MapProvision (Mobile ↔ Server)	AVPUserProfile	AVPBaselineMapInfo AVPBaselineMap	-	-
AVPStart (Mobile ↔ VC)	ParkingSlot	AVPRoute	-	-
AVPMonitoring (VC → Mobile)	-	-	VehicleLoc	-
AVPFinished (VC → Mobile)	-	-	-	ParkedVehicle

- ***MapProvision:*** is requesting ParkGML to AVP-Server with AVPUserProfile element. The server transmits the static parking map data of ParkGML to AVP-Mobile. The AVPBaselineMap element will be used to store to the mobile spatial DBMS and visualize the map data and select parking lot in AVP-Mobile. Fig. 3 shows the XML example of the MapProvision service. In response, there are road, detailed road, service area, parking slots etc, as map data.

<REQUEST, AVP-Mobile → AVP-Server>

```
<?xml version="1.0" encoding="UTF-8"?>
<AVPSpatialModel xmlns:xsi="http://www.w3.org/2001/XMLSchema"
 xmlns:gml="http://www.opengis.net/gml" xsi:noNamespaceSchemaLocation="ParkGML.xsd"
 QueryType="REQUEST" SeerviceType="MapProvision">
   <AVPUserProfile>
      <UserProfile Handicap="false" Sex="Male" Age="30" Name="kwm in" Phone="010xxxxxxxx"/>
      <NomadicDeviceProfile Platform="Android" CPU="1GHz" Resolution="800x400"/>
   </AVPUserProfile>
</AVPSpatialModel>
```

<RESPONSE, AVP-Server → AVP-Mobile>

```
<?xml version="1.0" encoding="UTF-8"?>
<AVPSpatialModel xmlns:xsi="http://www.w3.org/2001/XMLSchema"
 xmlns:gml="http://www.opengis.net/gml" xsi:noNamespaceSchemaLocation="ParkGML.xsd"
 QueryType="RESPONSE" SeerviceType="MapProvision">
   <AVPBaselineMapInfo Name="ETRIPark" Release="2010.09.01" Dimension=2 SRS="WGS84"
        Provider="ETRI"/>
   <AVPBaselineMap>
      <!--Map Data ····-->
   </AVPBaselineMap>
</AVPSpatialModel>
```

Fig. 3 XML example of the MapProvision service.

- ***AVPStart:*** is requesting start AVP service to AVP-VC. In this time, it is optional to select the parking slot among avail slots by driver in AVP-Mobile. The AVP-VC transmits the route element to the destination slot to AVP-Mobile in Fig. 4.

Fig. 4 AVPSlot and AVPRoute Element.

- ***AVPMonitoring:*** AVP-VC is reporting the position of vehicle to AVP-Mobile periodically and it is monitored in mobile device in real-time.

- ***AVPFinishing:*** AVP-VC notifies the final parked state to AVP-Mobile. The parked state is presented by image or geometry in Fig. 5. In case of image, it can be created by stitching all around image of vision camera attached vehicle or infra-based vision camera. And In case of geometry, it can be extracted by image.

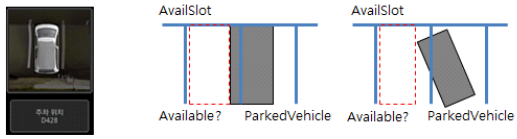

(a) by Image (b) by Geometry

Fig. 5 ParkedVehicle Element.

C. User-Centric Parking Slot Selection Model

The final parking slot has to be selected by considering the driver, vehicle, parking area information. In case of the driver information, the sex, age, handicapped person etc, have to be considered as choosing the optimal parking slot. In case of the vehicle information, the kind of vehicle, size, and electric vehicle etc, have to be considered. In case of the parking area information, inhabitant preference and exclusive use of woman parking area etc, have to be considered. For example, if the driver is a handicapped person, the vehicle must be parked at exclusive use of handicapped person slot and if the vehicle is an electric one, it has to be parked at the electric pluggable slot. The other factors to be considered to select the parking slot are ecological routing to minimize fuel consumption and time of transportation confusion and so on.

There are user-centric parking slot choice models in our dissertation: active slot selection model and passive one. The active slot selection model, the driver selects adaptive slot in AVP-Mobile. The passive slot selection model, the AVP-Server chooses the slot by analyzing the user and vehicle profile. In this case, the driver just does request the AVP service. In the active slot selection model, there are 3 kinds of policies and these are following.

- ***User-Centric:*** all avail slots which are transmitted from AVP-Server are displayed in AVP-Mobile and the user selects adaptive slot.
- ***System Recommend (AVP-Mobile):*** the driver selects slot among optimal candidate slots which are recommended by AVP-Mobile as analyzing the profile information.
- ***System Recommend (AVP-Server):*** the driver selects slot among optimal candidate slots which are recommended by AVP-Server as analyzing the profile information. In this case not all avail slots but recommended slots are transmitted from AVP-Server to AVP-Mobile.

In these models, the driver selects final parking slot in mobile device and this has to be verified whether slot is valid or not in AVP-Server because other vehicle was occupied the slot during the driver was selecting that. The Fig. 6 shows the message flows of three active slot selection models.

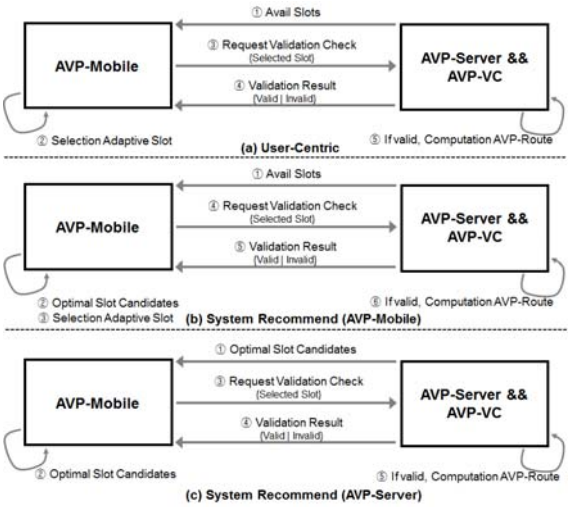

Fig. 6 Message flows of Active Slot Selection Models.

III. IMPLEMENTATION

We have implemented the AVP-Mobile system on the Android mobile platform (version 2.2). The architecture of AVP-Mobile system is shown in Fig. 7.

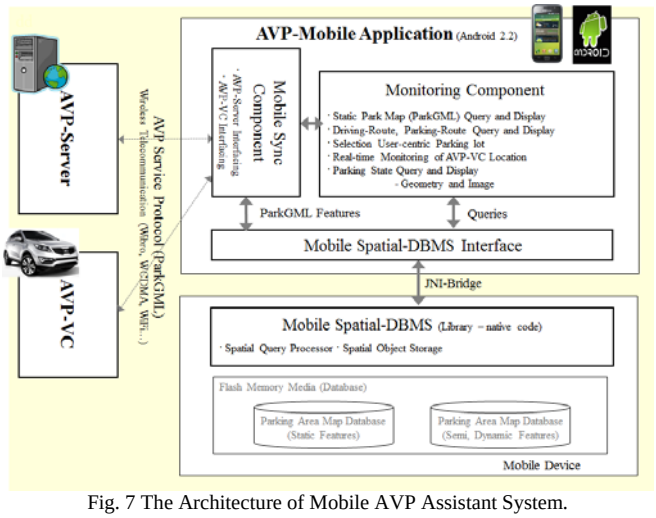

Fig. 7 The Architecture of Mobile AVP Assistant System.

There are two major parts: mobile spatial DBMS and AVP-Mobile application. The mobile spatial DBMS has been implemented by native code. It uses the NAND flash memory as storage media and creates two databases when receiving ParkGML element: static feature and (semi-)dynamic feature database. The real-time vehicle location is stored when reported from AVP-VC and the trajectories of vehicle can be searched. The spatial queries are executed when searching spatial objects to visualize the static features and selecting parking slot and so on.

The AVP-Mobile application has been implemented by Java and this can be interfacing with native code using JNI (Java Native Interface) bridge framework. The mobile sync components is encoding/decoding the XML message in compliance with ParkGML protocol and send/received to/from AVP-Server or AVP-VC via WCDMA or WiFi wireless telecommunication. The monitoring component is visualizing the park map and AVP route data as querying to the database. And it is monitoring the location of vehicle in real-time and after parked, the stat of the parking are displayed by image or geometry data. To provide the user-centric slot selection model, optimal slot candidates are created as analyzing the profile information in monitoring component and it provides the user interface to select the adaptive slot by driver.

Fig. 8 shows the screen captures of executing AVP-Mobile. In (a), the initial screen is shown and main menus which are “request ParkGML”, “request AVP service”, “Minitoring” and “Viewing Parked State” can be clicked. In (b), the static parking area map data and AVP route is displayed and location of vehicle is monitoring in real-time. In (c), the message of finishing parking is notified and in (d), parked state is displayed as image format.

(a) Initial Screen (b) Route, Monitoring (c) Parking Finished (d) Parked Vehicle

Fig. 8 The screen captures of AVP-mobile execution.

IV. CONCLUSION

In this dissertation, we have designed and implemented the AVP-Mobile system to supply more convenient AVP service to driver. We have defined the ParkGML data model to represent the parking area as GML extension. And we have developed the mobile spatial DBMS to manage large spatial map data efficiently. It provides the useful spatial and navigation queries in mobile device. The AVP service protocol among the AVP systems is also defined. The user-centric parking slot selection model is provided as analyzing the user, vehicle and parking area profile. We have implemented this system on the Android mobile platform and shown the system operation. This AVP-Mobile assistance system is expected to provide a high quality autonomous driving and autonomous parking service.

REFERENCES

[1] M. Wada, K. S. Yoon, and H. Hashimoto, “Development of Advanced Parking Assistance System,” IEEE Transactions on Industrial Electronics, vol. 50, No. 1, pp.4-17, Feb. 2003.

[2] M. Y.I. Idris, et al., “Car Park System: A Review of Smart Parking System and its Technology,” Information Technology Journal 8 (2), pp.101-113, 2009.

[3] Automatic Parking. http://en.wikipedia.org/wiki/Automatic_parking

[4] OGC Implementation Specification for Geographic Information-Simple feature access – Part1 Common Architecture v1.2.0, http://www.opengeospatial.org

[5] OGC Geographic Markup Language(GML) Implementation Specification v3.1.1, http://www.opengeospatial.org

[6] International Organization for Standardization, Text for FDIS 19115 Geographic Information, ISO/TC-211, http://www.iso.org

[7] K.W.Min, K.H.An, J.W.Kim and S.I.Jin, “The Mobile Spatial DBMS for the Partial Map Air Update in the Navigation”, Proceedings of The 11th International IEEE Conference on Intelligent Transportation Systems, Beijing, China, pp.476-481, Oct. 2008.

[8] Egenhofer, M.J., Herring, J.R., 1990, “A mathematical framework for the definition of topological relationships”, Proceedings of Fourth International Symposium on Spatial Data Handling, Zurich, Switzerland, pp.803-813.

[9] Fu. L., Sun, D., and Rilett, L. R. Heuristic shorest path algorithm for transportation applications: state of the art. In Comput. Oper. Res. 33, 11, 3324-3343, 2006.

2011 International Conference on Mechanical, Industrial, and Manufacturing Engineering
Lecture Notes in Information Technology Vols. 1-2

A Study on a Platform of Neighborhood EV Control System with Road-Infra Servers*

JeongDan Choi, KyoungWook Min
Department of Car/infra fusion Research Team
Electronic Telecommunication Research Institute
161,Kajeong-dong, Yuseong gu,Korea
{jdchoi & kwmin92}@etri.re.kr

KyungWhan Ahn and KyungBok Sung
Department of Car/infra fusion Research Team
Electronic Telecommunication Research Institute
161,Kajeong-dong, Yuseong gu,Korea
{mobileguru & kbsung}@etri.re.kr

Abstract – We propose a neighborhood EV control system that automatically maneuvering from a traffic lane to designated battery-switching or recharging stations supported by road-infra servers and nomadic device. The road-infra servers coordinate with the entire many neighborhood EVs processing the automatically path following missions such as the position-tracking and objects-recognition within the whole limited area. The user nomadic device is to reflect the best custom courses that will fit the driver's preferences or monitoring the neighborhood EV's status. To perform that, we suggest a platform of neighborhood EV control system based on distributed road-infra servers. And we developed the guidance protocol from road-infra servers to the neighborhood EV and the user nomadic devices. We aim to design this infra-based neighborhood EV control system to be robust of taking maneuvers in various circumstances as well as overcome and make up limitations of in-vehicle sensors.

Index Terms – Road-infra server, Neighborhood Electric Vehicle (NEV), Regeneration System, Nomadic device, Guidance protocol.

I. INTRODUCTION

The Kyoto Protocol aimed at fighting the global warming was initially adopted on 11 December 1997 in Kyoto. Under the Protocol, 37 countries commit themselves to a reduction of gases produced by them, and all member countries agreed to reduce their collective greenhouse gas emissions by 5.2% from the 1991 level. During the last few decades, increased concern over the environmental impact of the petroleum-based transportation infrastructure, has led to the interest in an electric transportation infrastructure.

An electric vehicle (EV) referred to as an electric drive vehicle, uses one or more electric motors for propulsion. Especially, a neighborhood electric vehicle (NEV) is for battery electric vehicles that are legally limited to roads with posted speed limits of 25 miles per hour (40 km/h) or less [1]. According that, green marketing and various studies are attracted new customers to the EV. One is Car-sharing services that support the consumer needs for better fuel savings, fewer traffic jam, and parking nightmares in busy city center.

There's an important problem to be solved in EV. The points are the few charging stations and the batteries should be frequently recharged. So, we introduce the NEV control system that automatically maneuvering from point to designated battery-switching or recharging stations. That are supported by road-infra servers which are connected with several kinds of sensors. The stations may be the parking lots, so that the core technologies are similar to the self parking ones of the unmanned ground vehicle.

Car-safety system has been actively researched and developed in most of automobile company for driver's safety and convenience. Recently developed vehicles are equipped with a self-parking system that autonomously maneuvers the vehicles into a parking space using in-vehicle sensors. But their commercialization is proceeding with difficult for many reasons such as cost or sensor's reliability. We'd like to suggest some technologies to overcome the limitations of in-vehicle sensors, and propose the architecture that are cooperative system with in-vehicle sensors and road-infra servers. We adapt our pilot system to the autonomous valet regeneration system of NEV.

II. PROBLEM STATEMENT

In the DARPA Urban Challenge [2], a vehicle performs on-road navigation and zone-navigation including a parking operation without human intervention. Until now, it's impossible to apply those systems to real world application since high cost devices such as laser scanners, radars, DGPS/INS, computers, networking devices should be mounted on those vehicles.

Several products of PAS (Parking Assistance System) support automatic steering control when performing parallel and perpendicular parking [3]. The driver should find free parking space by himself, and pass carefully by the region for the system to detect the free space by using in-vehicle sensors such as ultrasonic sensors and vision sensors. After the detection, the system propels the steering wheel, the driver controls the accelerator/brake pedals. This system has limitations since it does not help the driver to save the time to search the available slot and often fails to recognize the geometry of it.

And various studies on driving context-awareness using V2I (Vehicle to Infrastructure) communication have been tried. Recently, a system in which a sensor network is installed in an intersection to discriminate the speed of a

* This work is partially supported by the Industrial Strategic Technology Development Program (10035250, Development of Spatial Awareness and Autonomous Driving Technology for Automatic Valet Parking) funded by the Ministry of Knowledge Economy (MKE, Korea)

vehicle or catch a vehicle that violates a traffic signal is used. But a service that delivers information regarding a situation around the vehicle to a driver before an accident happens has not yet been used.

In general, application level protocols for intelligent transportation systems (ITS) define some important applications, their messages and message transmission sequences. These predefined applications are generally called use cases. The messages and message sequences of an ITS application protocol are fixed and applications should implement rigid-formatted message set and message sequences for each use case. Global Telematics Protocol (GTP) [4] and Mobile Location Protocol (MLP) [5] are typical examples of the use case based protocol. However, there are two important issues on existing protocols for ITS applications. The first is that message formats and message sequences in an application protocol are fixed. This can cause a problem because use cases in an application protocol can be frequently inserted, modified and deleted. The second is, more importantly, that a user device should implement all the use cases. ITS terminal devices are being shifted from vehicle attached on-board devices to nomadic devices (e.g. PDAs, smart phones, etc.). A nomadic device, by nature, requires light-weighted applications due to the limitation of resources. Although we present a protocol for a specific purpose, our scheme for making a protocol independent of use cases can be widely used in ITS and vehicle controlling domains.

In this paper, we integrated infrastructure based on distributed servers and in-vehicle sensors to lower the cost and incorporated nomadic device and to provide driving information and control vehicles to the battery-switching or recharging stations (Fig.1). And our main contribution of this paper is to develop a novel technique for designing the distributed vehicle control platform.

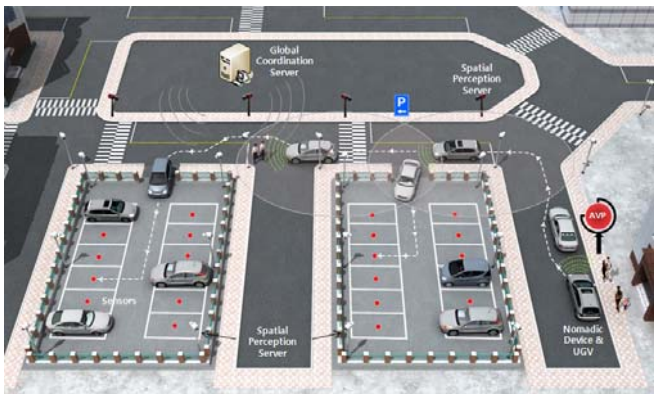

Fig. 1 The proposed system components and service overview

III. Cooperative Control Systems

A. *A platform overview*

The proposed system consists of four major subsystems: a nomadic device, a perception server, a coordination server, and a vehicle controller. The so-called nomadic device is a portable device designed to facilitate the development of the intelligent transportation service provision and multimedia use such as passenger information, automotive information, driver advisory and warning systems. The AVR program is installed on it, so as to user can require the AVR service and monitoring the vehicle's status. The vehicle controller is a device which is mounted on the car. The perception server and the coordination server is a road-infra server which equipped in road-infrastructure for perception and coordinate the vehicles. The detailed modules and relationships are presented in Fig.2.

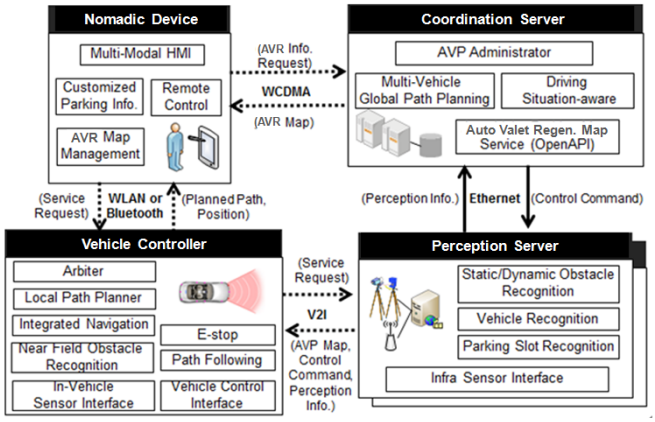

Fig. 2 System Architecture of the proposed system

In Fig.3, we show the software architecture of our road-infra servers and vehicle server. Basically the database is storing and maintaining the local dynamic map and vehicle's general information and also can be reconstructed by the vehicle on-demand service which request the automatic valet regeneration service within the restricted area.

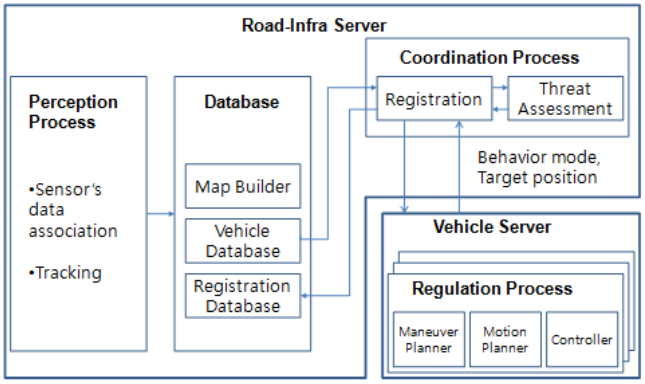

Fig. 3 Software components of the proposed system

B. *Road-Infra servers*

The perception server is located on the road side, and it's responsible for the recognizing the road environments from the connected sensors. We regard sensors detect some information related in road, such as traffic data, roadway shape information, the positions of static/dynamic obstacles and the controlled vehicle's position. Also, it should detect occupancies of power regenerating slots, and the spatial-geometry information of the free space. One or more perception servers are covered the restricted whole area since

there is limitation of the connectivity of the communication and sensing coverage of the sensors such as image, or laser scanner. And these all components are connected with V2I communications to satisfy the data transferring among the several perception servers.

The coordination server is in charge of handling the multiple vehicles within the whole service area. It is the highest up in the control hierarchy level, and prepares the path planning, makes a decision according to the driving-situation for each vehicle. The desired path is sent to the vehicle server through the perception server, and then the perception server schedules the go and stop command including emergency stop for vehicles in his territory. And also it provides the map for user device using the guidance protocol. The proposed protocol is used for driving guide and safety among our entire automatic valet regenerating system components. Operators can monitor overall systems and power regeneration zones by received perception information from perception servers and can sends emergency stop commands for abnormal situation or system fault case. The coordination sever is linked with the perception servers through the wired metwork (Ethernet) and coordinates the control handover when the vehicle pass through the overlapped coverage from the current servicing area to the next serviced one.

C. Vehicle Server

We consider that our target service is public transportation NEV and target area is limited. Most unmanned ground vehicles use many kinds of sensors for obstacle detection, recognition of driving environment, and tracking of its position. In our architecture, control system has remodeled steer, brake and accelerator to control the speed and heading position. But the road-infra servers conduct the other functions to go and stop, such as detection, position tracking, making decision and so on. It can be done the light-weighted control system. In Fig.4 shows the hardware components and software components of our test platform. We modified a pick-up sedan to control the vehicle electrically. It has 3 motors for handle, brake, and accelerator and controller. The controllers are processing the sensor's data fusion, path planning, and controlling motors. Data fusion computer is connected with add-on sensors, road-infra server and upper-lever in-vehicle controller. We use the wireless communication system between vehicle server and road-infra server. The add-on sensors are used for emergency stop function and assuring the position tracking. Examples of add-on sensors are digital compass, accelerometer, and GPS. In-vehicle sensors are wheel speed sensors in ABS and yaw rate sensors in vehicle dynamics control.

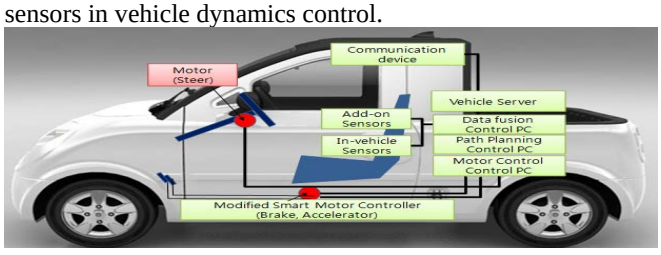

Fig. 4 The modified NEV system components

The so-called regulation process is embedded with vehicle server, which includes the maneuver planner, motion planner and low-layer controller (Fig.5). The maneuver planner make plan and control the only 1 vehicle's behavior, such as Ready, Lane following, Trajectory following, and Parking. The motion planner is composed of Velocity profile generator, Trajectory generator, and Road information, and creates the velocity profile and trajectory profile. The controller block controls the longitudinal controller and lateral controller to follow the desired path. And the Performance monitoring block give feedback about the current maneuver completion.

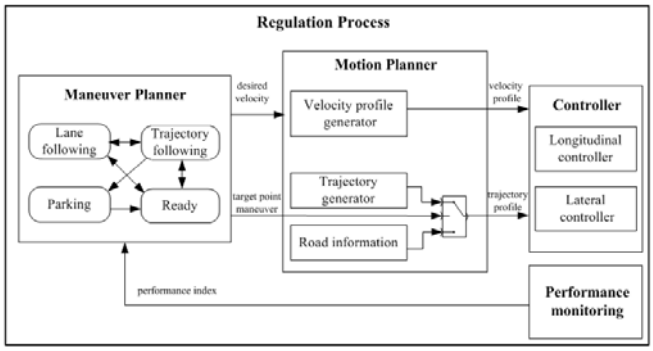

Fig. 5 The components of the Regulation Process

D. Nomadic Device

As mentioned before, we regard nomadic device as a smart device embedding our AVR program and guidance protocol. A user can request AVR service to the coordination server using nomadic device through the wireless communication (WCDMA) and then receive customized available slot information. If the driver wants to control the car automatically, the driver connects and registers his device to the registration database. And then the driver may leave from his vehicle as getting some information about the position and status of his unmanned vehicle. It is possible so that the vehicle server propels one or more electric motors according to the transmitted AVR mission from the road-infra servers. After the completion of AVR service, user can get the all- around image about the parked vehicle and status of the charged batteries.

E. Vehicle to Road-infra protocol

In this section, we propose an application protocol for safety warning and parking guidance considering aforementioned issues. The environments of road and parking lots are subject to change with time and place while driving, the use cases are frequently added, modified, and deleted on nomadic device. To provide those services for a nomadic device without installing necessary use cases in the device, we make a user nomadic device receive a necessary use case from a road-infra servers on-the-fly. For provide terminal devices with a use case, a road-infra servers can transmit a software module that implements the use case.

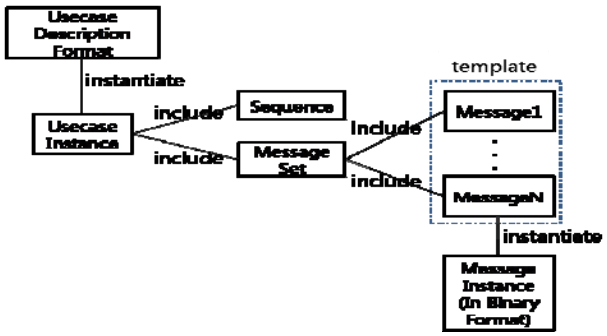

Fig. 6 Protocol design scheme

In our protocol, a road-infra servers transmits a use case description data instead of a software module. We use the term of use case instance to refer to such a use case description data. A use case instance specifies a set of message templates and a sequence of message exchanges. The client program in a terminal device exchange messages with a road-infra servers according to the sequence specified in the use case instance. A message transmitted to the terminal device is in a binary format. It is instantiated using the corresponding message template.

A use case instance is made by the XML document and should satisfy the description format. To express the use case in a machine readable format for both the server and nomadic device, the means are needed that include rules for the description of the use case. In our protocol, these rules are defined using a document type definition (DTD) [5] and the use case description format (UDF). The overall scheme is depicted in Fig. 6.

IV. Simulation Results

In this section, two main ideas will be presented through simulations: one is that the distributed road-infra architecture is robust enough to compensate for the in-vehicle sensors to service a specific autonomous driving. So, we use the CarSim model with 27 degree of freedom and control logic consisting of MATLAB/Simulink is used. Fig. 7 is shown the multiple vehicles' performed trajectory results under the proposed distributed architecture. The other is to show the longitudinal controller via the desired trajectory and velocity profile (Fig. 8).

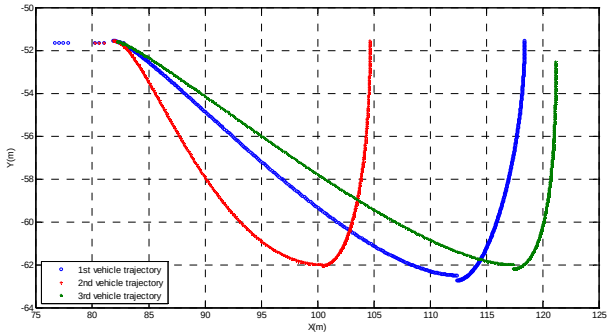

Fig. 7 Multiple vehicle's trajectory profile for mission completion

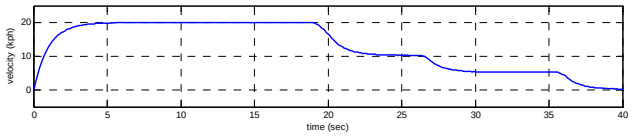

Fig. 8 velocity profile for desired trajectory following

V. Conclusions

In this paper, we suggested architecture for the NEV control system that automatically maneuver from a traffic lane to designated battery-switching or recharging stations supported by road-infra servers and nomadic device. We've simulated the spatial perception server and coordination server with sensors and nomadic device to support that the modified EV can drive into a slot autonomously. The proposed system incorporates both in-vehicle sensors and road-side servers connected with sensors on road, reducing device cost of individual vehicle and providing reliable performance of object detecting. And also we proposed a flexible application protocol for safety warning and parking guidance services. Unlike many other application protocols in ITS and Telematics domains, our protocol makes the client part independent of use cases for supporting light-weighted nomadic devices.

By using this system, it's possible to cut down the air pollution and energy consumption source from the transportation system by shortening waste time search for the available slot. In the future, we plan to apply our system and the protocol to the real road and battery recharging and replacement station of the electric vehicle.

References

[1] Eberle, Ulrich; von Helmolt, Rittmar, "Sustainable Transportation based on electric vehicle concepts: a brief overview," Royal Society of Chemistry.

[2] Andrew Bacha, et al., "Odin: Team VictorTango's Entry in the DARPA Urban Challenge," Journal of Field Robotics 25(8), pp.467-492, 2008.

[3] M.Wada, K. S. Yoon, and H. Hashimoto, "Development of Advanced Pakring Assistance System," IEEE Transactions on Industrial Electronics, vol. 50, No. 1, pp.4-17, Feb. 2003.

[4] M. Y.I. Idris, et al., "Car Park System: A Review of Smart Parking System and its Technology," Information Technology Journal 8 (2), pp.101-113, 2009.

[5] Joingik Kim, Oh-Cheon Kwon, and Hyunsuk Kim, "Development of an Event Stream Porcessing System for the Vehicle Telematics Environment," ETRI Journal, vol.31, no.4, Aug. 2009.

[6] Open Mobile Alliance, "Mobile Location Protocol (MLP)", Enabler Release Definition for Mobile Location Protocol (MLP) Candidate Version 3.1, March 2004.

2011 International Conference on Mechanical, Industrial, and Manufacturing Engineering
Lecture Notes in Information Technology Vols. 1-2

Applying on BLDCM Speed PID Controller of Optimizing BP Neural Network Based on GA

Zhengge Miao, Chao Song, Chunwan Hu and Lingshun Liu

Department Control of engineer
Naval Aeronautical and Astronautical University
YanTai 264001, China

morgenco@163.com

***Abstract* - A sort of optimized BP neural network PID control algorithm based on GA is proposed in this text, and applied to brushless DC motor (BLDCM) speed control system. A kind of optimized speed PID controller has been designed. The algorithm utilizes GA to optimize BP neural network initial weight at first, and uses BP neural network on-line regulate PID parameter. It solves the detrimental effect of network initial weight. The feasibility of algorithm has been proved according to emulation.**

Index Terms – GA. BP neural network. PID control. BLDCM. Optimize.

I. INTRODUCTION

With the development of intelligent control system neural network, PID control has been used widely. However, the initial weight of controller has a great randomicity, it causes direct effect to control results of the controller. If initial weight is chosen improperly, the output value will fluctuate considerably at beginning stage[1]. GA is used to optimize the initial weight of neural network, and BP neural network is used on-line to regulate PID parameter in this paper.

II. CONTROL SYSTEM STRUCTURE

System structure figure of BP neural network PID controller optimized by GA is shown in Fig 1. The control structure consists of three parts: the initial weight of neural network is optimized by GA, BP neural network on-line regulate PID parameter by modifying its coefficients, classical PID controller make a closed loop control of brushless DC motor.

The control system adopt incremental digital PID speed controller[2]. The format of incremental digital PID control algorithm is

$$u(k) = u(k-1) + \Delta u(k) \tag{1}$$

$$\Delta u(k) = k_p(e(k) - e(k-1)) + k_i e(k) + k_d(e(k) - 2e(k-1) + e(k-2)) \tag{2}$$

Where, k_p is proportion coefficient, k_i is integration coefficient , k_d is differentiation coefficient, $e(k)$ is the difference between desired output and actual output of current sampling time, $u(k)$ is the control variable of the current sampling time.

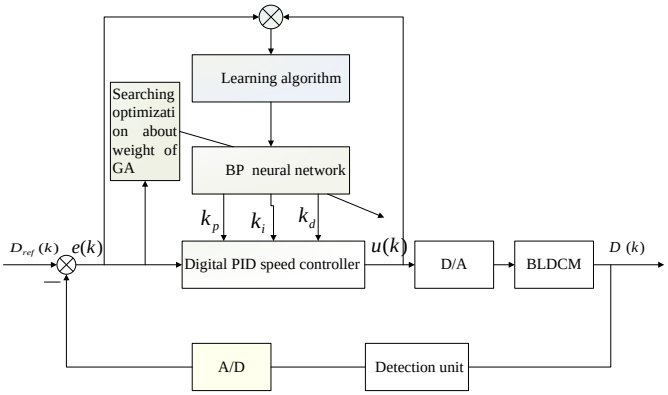

Fig 1 BP neural network PID control optimized by GA.

III. IMPLEMENTATION OF THE CONTROL ALGORITHM

A. Learning and searching of GA for optimized results in BP network about its initial weight and threshold.

BP neural network algorithm based on GA is defined as follow: in the learning of BP neural network, the weight and threshold is described as chromosome and selecting suitable fitness function, then GA iteration until convergent in a certain meaning [3].

Considering a neural network with an input node i, an implied node j, output node k, the training result of BP neural network will generate four matrices.

1) The weight matrix from input layer to implicit layer is follow:

$$W = \begin{bmatrix} W_{11} & W_{12} & \cdots & W_{1j} \\ W_{21} & W_{22} & \cdots & W_{2j} \\ \cdots & \cdots & \cdots & \cdots \\ W_{i1} & W_{i2} & \cdots & W_{ij} \end{bmatrix}$$

2) The threshold matrix of implicit layer is follow:

$$\gamma = \begin{bmatrix} \gamma_1 \\ \gamma_2 \\ \cdots \\ \gamma_j \end{bmatrix}$$

3) The weight matrix from implicit layer to output layer is follow:

$$V=\begin{bmatrix} V_{11} & V_{12} & \cdots & V_{1k} \\ V_{21} & V_{22} & \cdots & V_{2k} \\ \cdots & \cdots & \cdots & \cdots \\ V_{j1} & V_{j2} & \cdots & V_{jk} \end{bmatrix}$$

4) The threshold matrix of output layer is follow:

$$h=\begin{bmatrix} h_1 \\ h_2 \\ \cdots \\ h_k \end{bmatrix}$$

GA is utilized to optimize the weight of BP neural network, that is optimizing the above matrices W , γ , V and h . In order to achieve this optimization, these four matrices need to transform into chromosome string that is convenient to the operation of GA. Generally speaking，binary string is utilized to code by chromosome. Each X chromosome represent a coefficient. The range of X is determined by the scope and accuracy of weight coefficient. The mapping relation about chromosome bit string and the encoding of the weight set occurrence is shown in Figure 2[4].

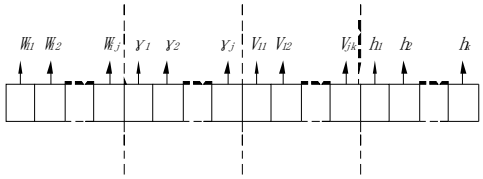

Fig 2 The mapping about chromosome and the encoding of the weight set occurrence

In order to use GA to optimize weight coefficient, a fitness function is needed to evaluate chromosome. Error square sum is available.

$$f(i)=1/E(i),\quad E(i)=\sum_{p}\sum_{k}(V_k-T_k)^2 \tag{3}$$

where the number of chromosome i=1,2…N , the node number of output layer k=1,2,3, the number of learning sample p=1,2,3,4, T_k is teacher's signal.

B. Digital PID controller based on BP network

Three layers BP network is adopted, its structure diagram is shown in fig 3.

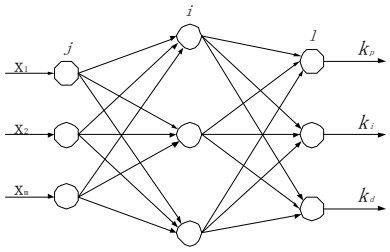

Fig 3 Structure diagram of BP neural network

The input value of input layer,

$$o_j^{(1)}=x(j) \quad (\text{j=1,2,…M}) \tag{4}$$

where M is the variables number of input and determined by complex degree of control system.

The input and output value of implicit layer is

$$net_i^{(2)}=\sum_{j=0}^{M}w_{ij}^{(2)}O_j^{(1)},\quad O_i^{(2)}(k)=f(net_i^{(2)}(k)) \quad (\text{i=1,2,…Q}) \tag{5}$$

Where $w_{ij}^{(2)}$ is the weighted coefficient of implicit layer and superscript（1）,(2), （3）represent input layer, implicit layer and output layer respectively.

Selecting positive-negative symmetric Sigmoid function of neurons in implicit layer as its activation function.

$$f(x)=\tanh(x)=\frac{e^x-e^{-x}}{e^x+e^{-x}} \tag{6}$$

Input and output of output layer of the network is:

$$net_l^{(3)}(k)=\sum_{i=0}^{Q}w_{li}^{(3)}O_i^{(2)}(k) \qquad O_l^{(3)}(k)=g(net_l^{(3)}(k))$$

（l=1,2,3）

$$O_1^{(3)}(k)=k_p\ O_2^{(3)}(k)=k_i\ ,O_2^{(3)}(k)=k_i \tag{7}$$

where $w_{ij}^{(3)}$ is the weighted coefficient of output layer.

The output node of output layer is respectively corresponding to three tunable parameters k_p, k_i, k_d Because k_p, k_i, k_d cannot be negative value, so we select nonnegative sigmoid function as the activation function of output layer neurons.

$$g(x)=\frac{1}{2}(1+\tanh(x))=\frac{e^x}{e^x+e^{-x}} \tag{8}$$

Selecting performance index function

$$E(k)=\frac{1}{2}(n_{ref}(k)-n(k))^2 \tag{9}$$

According to grads decline method which can correct the weight coefficient. That is searching and adjusting the weighted coefficient in negative grads direction according as $E(k)$ .And attach an inertia item result in a fast convergence to global minimum.

$$\Delta w_{li}^{(3)}(k)=-\eta\frac{\partial E(k)}{\partial w_{li}^{(3)}}+\alpha\Delta w_{li}^{(3)}(k-1) \tag{10}$$

Where η is learning rate, α is inertia coefficient. And,

$$\frac{\partial E(k)}{\partial w_{li}^{(3)}}=\frac{\partial E(k)}{\partial y(k)}\bullet\frac{\partial y(k)}{\partial \Delta u(k)}\bullet\frac{\partial \Delta u(k)}{\partial O_l^{(3)}(k)}\bullet\frac{\partial O_l^{(3)}(k)}{\partial net_l^{(3)}(k)}\bullet\frac{\partial net_l^{(3)}(k)}{\partial w_{li}^{(3)}(k)} \tag{11}$$

But $\frac{\partial y(k)}{\partial \Delta u(k)}$ is unknown, so a approximately sign function $\operatorname{sgn}\frac{\partial y(k)}{\partial \Delta u(k)}$ is used to take the place. The result of the impact of inaccurate can be compensated by adjusting learning rate η.

From formula(1) and formula(6),we conclude that

$$\frac{\partial \Delta u(k)}{\partial O_l^{(3)}(k)}=e(k)-e(k-1) \tag{12}$$

$$\frac{\partial \Delta u(k)}{\partial O_2^{(3)}(k)}=e(k) \tag{13}$$

$$\frac{\partial \Delta u(k)}{\partial O_3^{(3)}(k)}=e(k)-2e(k-1)+e(k-2) \tag{14}$$

According to above analysis , we conclude that the calculation formula of weight coefficient about BP neural network output layer is follow:

$$\Delta w_{li}^{(3)}(k)=\alpha\Delta w_{li}^{(3)}(k-1)+\eta\delta_l^{(3)}O_i^{(2)}(k) \tag{15}$$

$$\delta_i^{(3)}=e(k)\operatorname{sgn}(\frac{\partial y(k)}{\partial \Delta u(k)})\frac{\partial \Delta u(k)}{\partial O_l^{(3)}(k)}g'(net_l^{(3)}(k)) \tag{16}$$

For the same reason, we conclude the calculation formula of weight coefficient about implicit layer:

$$\Delta w_{ij}^{(2)}(k)=\alpha\Delta w_{ij}^{(2)}(k-1)+\eta\delta_i^{(2)}O_j^{(1)}(k) \tag{17}$$

$$\delta_i^{(2)}=f'(net_i^{(2)}(k))\sum_{l=1}^{3}\delta_l^{(3)}w_{li}^{(3)}(k) \tag{18}$$

Where $g'(\bullet)=g(x)(1-g(x))$, $f'(\bullet)=(1-f^2(x))/2$

B. Flow chart of GA optimizing the initial value of BP neural network weight.

A Flow chart of GA optimizing the initial value of BP neural network weight is shown in fig 4[5].

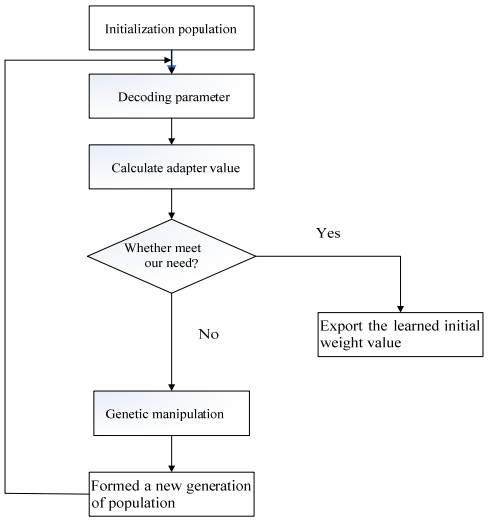

Fig 4 Flow chart that GA optimize the initial value of BP neural network weight

After we find the initial value of network optimized by GA, following algorithm is used to regulate PID controller on-line.

1) Deciding structure of BP network, that is, making sure of the input layer node number M and connotative layer node number Q, and then give out initial value of weight coefficient of each layer. That is ,we get weight initial value based on GA, and chosen learning rate η and inertia coefficient α ,here $k=1$.

2) From sampling, we obtain $n_{ref}(k)$ and n_k at $t=KT$,and calculate the error value at present time $e(k)=n_{ref}(k)-n(k)$.

3) Calculating input value and output value of neurons of every layer in neural network. Its output values are three adjustable parameters (k_p , k_i and k_d)of PID speed controller.

4) From formula(1), we calculate the output $u(k)$ of digital PID speed controller.

5) Start to learn BP neural network. According to formulae (14),(15),(16),(17), weight coefficients $w_{ij}^{(2)}(k)$ and $w_{ij}^{(3)}(k)$ of every layer are regulated on-line to regulate speed control parameters of PID on-line.

6) Let $k=k+1$ and return step(1), until the error meet our requirements.

IV. Simulation Study

Let the transfer function of speed loop equivalent controlled object is: $\frac{2.6}{S(0.0019S+1)}$

Chosen the structure of neural network is 4-5-3,learning rate is η=0.28,inertial coefficient is α =0.04,input vector is $x=[u(k),y(k),e(k),1]$,the number of species population in GA is

30,crossover probability P_c =0.6,mutation probability $P_m = 0.01$ .square error curve and match value curve draw by simulation are shown in Fig 5.From fig 5 we know that average fitness of chromosome is tended to be stable via about 300 Generations inheritance.

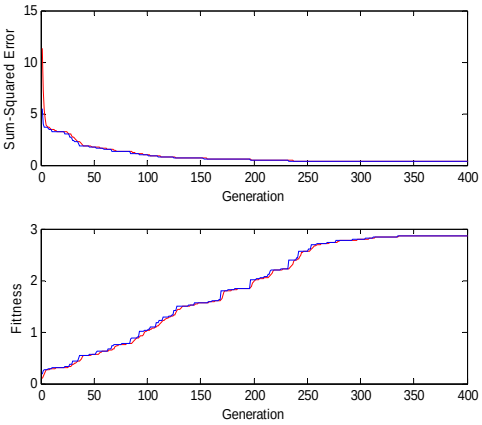

Fig 5 Curves of square error and match value

When the control signal is a step signal, the response curves of BP neural network which one is optimized and anther is not optimized are shown in fig 6.

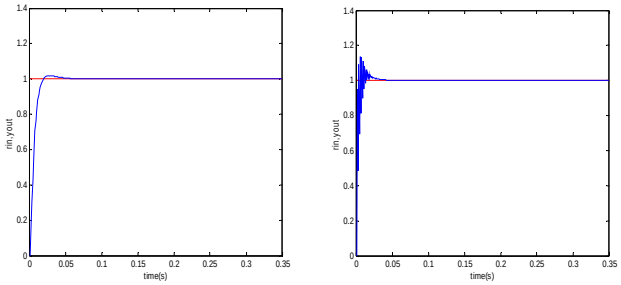

Fig 6 Response curves of BP neural network that are not optimized by GA

Error curves optimized and not optimized are shown in fig 7.

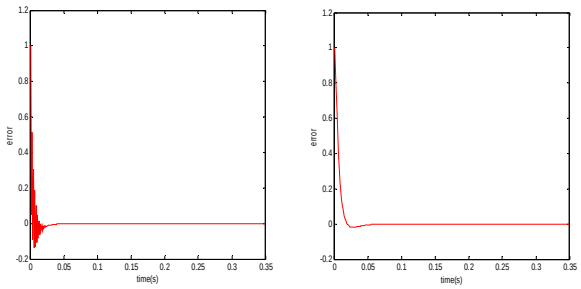

Fig 7 Error curves not optimized and optimized by GA

Tuning curves of PID controller parameter are shown in fig 8.

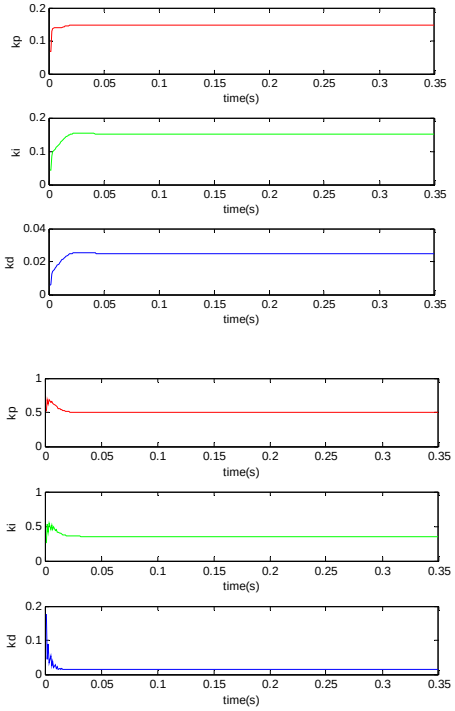

Fig 8 BP network regulate PID controller parameters curves that not optimized and optimized by GA

CONCLUSION

From the step response curve and error curve, we can see that the step response of BP neural network optimized by GA, is not fluctuate obviously in the initial stage, which proved that the improved method is feasible. In PID control parameters tuning curve, the parameters tuning process of optimized is quicker. We can clearly seen the superiority of the improved method for PID parameters optimization. The method solves the problem in some extent that traditional PID speed controller hard to tune parameters real-time and lack of effective control of some complex process and parameter time-varying systems.

REFERENCES

[1] Junshan Gao. A kind of PID control based on GA and neural network. Electric Machines and Control,Vol 8,pp.108-112,February 2004.

[2]Ju Long. Optimal design of Brushless DC motor speed control system.Chengdu:Xi'an Jiao Tong University Press,December 2006.

[3]Chongjun Wang. A kind of BP neural network algorithm based on GA and its application . Journal of Nanjing University, Vol 39,pp. 459-466,May 2003.

[4]Liqun Han. Intelligent Control Theory and Applications . Beijing: Machinery Industry Press, January 2008.

[5]Guojun Yang. Application and Accomplish of GA in Neural Network.Journal of System Simulation,Vol 13,pp.567-570,May 2001.

2011 International Conference on Mechanical, Industrial, and Manufacturing Engineering
Lecture Notes in Information Technology Vols. 1-2

Research on the End to End Congestion Control and Quality of Service on Overlay Network

Dengshi Li

School of Mathematics and Computer Science,
Jianghan University.
Wuhan China 430056
Email：reallds@126.com

Xi Guo

School of Computer , Wuhan University

Wuhan China 430072
Email：guoxi82222003@yahoo.com.cn

***Abstract* –Congestion control and quality of service are two interrelated research subjects. Due to the end to end essence of TCP, the source algorithm of congestion control can not acquire enough information of intermediate network to control traffic ideally. In order to solve this problem, a method based on the change rate of average queue length to enhance RED is proposed. However, the resulting average queue length is quite sensitive to the level of congestion and to the parameter settings of RED. To alleviate the problem of parameter dependence of RED, a new adaptive method based on the change rate of the average queue length to tune max is established. Extensive simulations show that the proposed mechanism can improve the robust property of RED considerably and outperforms the existing methods.**

Index Terms –Congestion control; Quality of Service; Active queue management; Adaptive method

I. INTRODUCTION

Multimedia application is a more rapid pace in recent years. From the VOIP to sound as real-time multi-cooperation has brought a new end-user experience. Such as multimedia conferencing, telemedicine, e-commerce. And the general data is different, with real-time characteristics of multimedia data, that is between the data must meet certain time requirements [1]. Currently the Internet has been based on best-effort multimedia applications and can not satisfy all users of network transmission quality. Therefore, in order to improve utilization of network resources, to provide users with a higher quality of service QoS for the target area of research is currently very dynamic [2]. There are two general ways to provide QoS including application-level QoS mechanisms and network-level QoS mechanisms. Congestion control is a good basis to improve service quality [3]. Congestion control mechanism is not strong, safeguard the quality of service to speak of. The main purpose of this article is from these two aspects of how to improve the utilization of network resources to protect the user's service quality.

90% of Internet traffic using a TCP / IP protocol, using the most current Internet congestion control mechanism is based on the source TCP window congestion control mechanism. This control is mechanism by detecting packet loss or ECN marking, etc. Congestion notification information to perceive the current state of the network, and then adjust the tentative size of the send window, and then control the amount of data into the network, in order to avoid network congestion or reduce network [4] The degree of congestion. However, this congestion control mechanism does not provide any Quality of Service. It will often result in excessive transmission delay and packet loss rate, so its role is limited. And as such as image, voice and other multimedia streams in large numbers, based on the source side of the TCP congestion control has appeared to be inadequate, then the network itself is also necessary to participate in the congestion control. Incidentally, the IP network layer-based congestion control algorithm, which is the most important active queue management algorithm, which through the router packet buffer queue management, as a reasonable state of network congestion information back to the sender, the sender as soon as possible in order to adjust its data transmission rate to ease congestion. Although this type of network congestion control algorithm to be a great success, but there are still many shortcomings and needs to be improved further study.

II. RELATED WORK

According to their location congestion control methods can be divided into two categories: source algorithm and the link algorithm. Source algorithm, that is, TCP congestion control, network edge devices in the host and perform. Its role is to adjust the sending rate based on feedback information. Link algorithm that is, IP congestion control, network equipments (such as routers and switches) are in the implementation. Its role is to detect the occurrence of network congestion, resulting in congestion feedback information [5]. Link algorithm is currently concentrated in the active queue management.

A. The Source Algorithm of Congestion Control

Its starting point is to make the source of the congestion level of the network to adjust its data transmission rate to control the network load [6]. TCP uses a window-based, end to end closed-loop control. Later, TCP Reno increased the fast retransmit and rapid recovery (fast recovery) algorithm to avoid network congestion is not enough for a serious caused by the slow start algorithm reduces the window size over the earth. TCP uses a plus-type increase of multiplication decreases (A workers MD), based on the window, end to end congestion control mechanisms. Practice shows that the congestion control mechanism for best-effort type of service has a good adaptability. However, studies have found that TCP congestion control is still many problems [7].

B. The Link Algorithm of Congestion Control

Such algorithms are also known as the IP congestion control. End of the TCP window-based control strategy for robust Internet plays a key role. However, the rapid growth of traffic makes the backbone of the growing congestion [8]. The emergence of new business, higher network quality of service requirements from the spoon. To meet these needs, end to end congestion control alone is not enough. Intermediate nodes need to take some strategies to prevent and control network congestion, thus ensuring the smooth flow and to provide a network of service quality assurance. View of the congestion control algorithm using the source of some shortcomings, in recent years, congestion control algorithm using the link of the growing importance for the people [9]. End to end nature of TCP due to its characteristics, it can not use the network data flow information of intermediate nodes to improve the efficiency of the equity security.

C. The QoS Of Overlay Network

QoS refers to the network data transmission range of services required to meet the requirements for the specific quantifiable, transmission delay, delay jitter, packet loss rate, bandwidth requirements, throughput and a series of indicators [10]. The service here specifically refers to packets (flow) through a number of network nodes accepted by the transport service, emphasizing the end or the network integrity of the border to the border. In order to meet the different users, the application QoS requirements, the sender in the control plane for QoS using RSVP, in consultation with each node on the transmission channel reserved for the necessary resources. If the network QoS remaining resources can not meet their requirements, the connection request is rejected [11].

III. The Intrusion Detection Model Based On Data Mining Technology

A. The Idea of Model Design

In this model, data mining technology is primarily used in cluster analysis. The non-supervised clustering is data mining anomaly detection system, a commonly used method. Anomaly detection model is the behavioral characteristics of the user's habits are stored in the feature database, and then the user behavior and characteristics of the current features of the database comparison, if the deviation between the two is large enough, then the invasion happened. Unsupervised anomaly detection rather than the method proposed is based on two premises [12]: One is the normal data in the network data is far greater than the invasion of the number of data, and the other provided that the invasion of normal data and there is a big difference between the data. This method can be labeled from a set of data is not found in any invasion, and not worry about the data source is pure.

B. The System Structure And Work Flow

Based on the above design, this data mining technique used in network intrusion detection system, based on the proposed building in the Snort data mining based network intrusion detection system. The system includes the following specific functional modules:

(1). Packet sniffer

The collection of data to the network, it is only a simple interface to capture information. Packet sniffer determines the location of intrusion detection level of local processing.

(2). Decoder

When a packet is captured, the need for data link layer to decode the original packet. In the decoding process, the captured data to Packet data structure to the pre-processor for subsequent analysis and detection engine in preparation.

(3). Data preprocessing

It is responsible for connecting the original data or data mining methods need to convert the data format. Include: further filtering, noise cancellation, third-party testing tools to detect known attacks.

(4). Exception analyzer

It is responsible for using the network model of normal behavior after pretreatment test packets, discarding those that meet the model of normal data packet, the packet will be exceptions to the rules and regulations to match the list, if the match is successful, indicating an intrusion, this time alarm information. If abnormal data packet does not match with all the rules, then that may be unknown type of packet data generated by intrusion packet, it may be normal behavior unknown network packets, these packets will be sent to the cluster analysis module

(5). Clustering Analyzer

Packet of these abnormal cluster analysis are in the clustering process will produce the new network model of normal behavior to abnormal parser, and for the failure to form a network model of normal behavior abnormal data packets, will be a record to the rules builder.

IV. The Improved Apriori And Ripper Algorithm

In statistical analysis test of this hypothesis, there are usually two types of errors: false alarm rate and false negative rate. The corresponding error probability is expressed as α and β. Usually these two types of errors are difficult to be estimated. The threshold method was given as:

$$\alpha \log \frac{\alpha}{1-\beta} + (1-\alpha) \log \frac{1-\alpha}{\beta} \le D(P_1 \| P_0) \qquad (1)$$

This type of errors include two types of threshold hypothesis testing related to the probability distribution of entropy: greater related entropy means the stronger detection capability. In order to make statistical analysis system security, statistical analysis needs to reduce the related entropy, or even make it to be zero to obtain a perfect secure statistical analysis system. On the contrary, in order to design

good statistical analysis algorithm, we need to look for characteristics of the probability distribution of carrier signal and the statistical analysis. While on the signals (images, audio, etc.) modeling, recent studies have made great progress, but on a unified model of the signal has not been established. However, given the situation that contains two kinds of signals (the original carrier signal and the statistical analysis signal); this problem can be solved through supervised learning approach. Therefore, statistical analysis faces enormous challenges in order to avoid changing the statistical features of cover signal when secret message has been embedded; conversely, statistical analysis is to seek the statistical difference between the feature vectors caused by information hiding.

As a dollar evolution of Gaussian probability density function, Gaussian mixture model (GMM) can be approximation of any probability density distribution of arbitrary shape, which is widely used in speech recognition. This paper also uses it to model the wavelet coefficients. In general, the Gaussian mixture distribution model can be the following using limited form of distribution and said:

$$f_k(x) = \sum_{j=1}^{k} \pi_j \phi(x, \theta_j) \qquad (2)$$

Here, $\phi(x, \theta_j)$ is the j^{th} component of GMM model, θ_j is the vector of the mixture parameters which consists of weight π_j, mean μ_j, variance σ_j^2. The weight π_j must satisfy:

$$\pi_1 + \ldots + \pi_k = 1, \pi_j \geq 0 \qquad (3)$$

As to a random variable X, its probability density function is denoted by $p(x)$. If it is Gaussian random variable with mean μ and variance σ^2, then its probability density is denoted by $N(\mu, \sigma^2)$. The characteristic function defined as follows:

$$\Phi(t) = \int_{-\infty}^{\infty} p(x) e^{jtx} dx \qquad (3)$$

Here, $j = \sqrt{-1}$. Corresponding probability density can also use the following type:

$$p(x) = \frac{1}{2\pi} \int_{-\infty}^{\infty} \Phi(t) e^{-jtx} dt \qquad (4)$$

The above discussion of the model concerns the generic situation, but it did not tell me if it is sensitive to the statistical and analysis operation. Even if we do not know the exact statistical model and which embedded algorithm is used, but as described above, statistical analysis personnel can capture the signals prior to knowledge of statistical models and general statistical characteristics of statistical analysis algorithms.

V. Simulation Experiment

In this section, we compare the performance of the proposed algorithm I with four known algorithms based on statistical moment. Each experiment randomly select 500 of the 1000 audios from wav database as cover audio. For each audio signal, we use same embedding frame length ($N = 4096$) and six embedding strength ($\alpha 1 = 1 \times 10^{-2}$, $\alpha 2 = 5 \times 10^{-2}$, $\alpha 3 = 5 \times 10^{-3}$, $\alpha 4 = 8 \times 10^{-3}$, $\alpha 5 = 5 \times 10^{-4}$, $\alpha 6 = 8 \times 10^{-4}$) to create the audio signal. As a result, 500 cover audios and their versions are used for training the classifier. Then from the remaining 500 audios, we can obtain 500 pairs. Each pair consists of the original audio and the corresponding version. These 500 pairs of audio are used for testing.

Among the four known reference algorithms considered for comparison, Farid proposed an approach which uses a wavelet-like decomposition to build higher-order statistical models. Harmsen used the histogram characteristic function to detect additive noise modelable information hiding. Shi's method is based on statistical moments of the characteristic function of wavelet sub-bands. Oktay Altun proposed method based on marginal distortion. In order to make a fair comparison of the performance, we implemented the referred algorithms which utilized the best parameters mentioned in algorithms. The first 5 moments for 4 wavelet decomposition levels were considered to extracting features. In algorithm, the order of distortion function is set to 1000 and the second embedding strength is $\alpha = 5 \times 10^{-4}$.

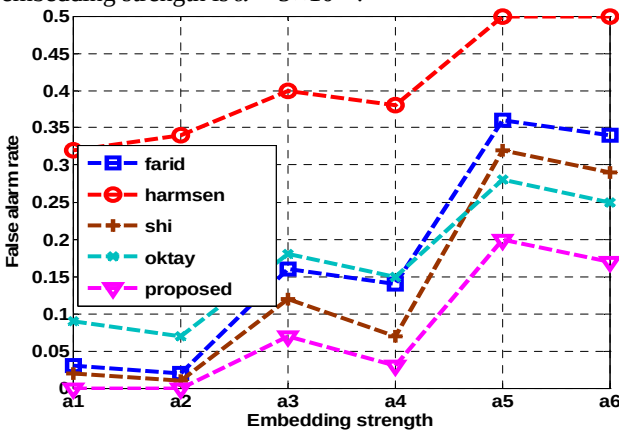

Figure1: Performance Comparison with similar algorithms

Figure1 shows the test results of false alarm rate (FAR) and false negative rate (FNR). It is clearly observed that both FAR and FNR achieved by our proposed algorithm I is lower than 10% with embedding strength α takes the level of 10^{-2} and 10^{-3} (a1, a2, a3, a4). Even when embedding strength α takes the level of 10^{-4} (a5, a6), both FAR and FNR can still achieve lower than 20%. On the other hand, although the algorithm Farid, Shi utilizing moments of wavelet coefficients is fairly good, our method can still get more than 5% reduction in both FAR and FNR when the α takes 10^{-3} or lower. Since these algorithms work very well in image cover due to their ability to capture the statistical difference in images which are not distinct in audio. The algorithm Oktay detects the hidden information in audio signal, but the detecting results are not so good. Due to the order of distortion function plays very important role in performance, if we set it as fixed value, the

detecting results is influenced seriously. The algorithm Harmsen has poor detecting performance even the bigger embedding strength (a1, a2) was taken which means the features did not capture the statistical difference causing by information embedding.

VI. CONCLUSION

This research work focused on the end to end network quality of service and link congestion control algorithms. In particular, active queue management mechanism was studied. But the research is still relatively narrow, focused on the research of its robustness. However, active queue mechanism should also meet the other requirements, such as TCP friendly flow three} BU environment exists to protect TCP flows. In this paper, on TCP flow bandwidth fairness J of research is limited to RTT factor, but inhibition the non-TCP flow is also very important. Also on the wireless network environment, the quality of the service is only in recent years' has just begun, there are many problems awaiting study.

This article about the fairness of TCP flows of the bandwidth is limited to one of the factors that RTT. On this issue, although the force of a law that the existing congestion in the network will fail when more serious and also suggested some solutions, but also limited to the layer from the previous simulation were discussed. Deeper theoretical requirement is a more realistic network model to explain theoretically, and then propose appropriate solutions to them with a broader scope. In addition, several other TCP flow bandwidth fairness of the issue also needs further study.

ACKNOWLEDGEMENT

This work supported by grant from the plan project of central colleges of special funds basic research and operating expenses)—Young Teacher Grant. The project number is: 3101014

REFERENCES

[1] Ying Wang, Pierre Moulin (2008) Perfectly secure steganography: capacity, error exponents, and code constructions. IEEE Transactions on Information Theory, 54(6):2706-2722

[2] Yossi Rubner, Carlo Tomasi, Lenoidas J. Guibas (2000) The earth mover's distance as a metric for image retrieval. International Journal of Computer Vision, vol. 40(2), pp.99-121

[3] Franks R G. Performance Analysis of Distributed Server Systems. [Ph D dissertation].Ottawa-Carleton Institute for Electrical and Computer Engineering, Carleton University, Ottawa, Ontario, Canada, December, 2009

[4] Jain, V.; Jain, M.; Queuing network model for link and path availability of ad hoc Networks. The International Conference on Wireless and Optical Communications Networks, pp: 5-9. 2006

[5] Farid, D.M.; Rahman, M.Z. Learning intrusion detection based on adaptive bayesian algorithm. 11th International Conference on Computer and Information Technology. pp: 652-656. 2009

[6] Meijuan Gao; Jingwen Tian; Mingping Xia. Intrusion Detection Method Based on Classify Support Vector Machine. Second International Conference on Intelligent Computation Technology and Automation. pp:391-394. 2009

[7] Tian-rui Li; Wu-ming Pan. Intrusion detection system based on new association rule mining model. IEEE International Conference on Granular Computing. pp: 512-515. 2005

[8] WenJie Tian; JiCheng Liu. A new network intrusion detection identification model research. 2nd International Asia Conference on Informatics in Control, Automation and Robotics. pp:9-12. 2010

[9] Yongquan Mo; Yizhong Ma; Liang Xu. Design and implementation of intrusion detection based on mobile agents. IEEE International Symposium on IT in Medicine and Education. pp: 278-281. 2008

[10] Yu-Xin Ding; Min Xiao; Ai-Wu Liu. Research and implementation on snort-based hybrid intrusion detection system. IEEE International Conference on Machine Learning and Cybernetics. pp: 1414-1418. 2009

[11] Yang Jianxi; Zhou Jianting; Wang Fan. A Study on the Application of GA-BP Neural Network in the Bridge Reliability Assessment. IEEE International Conference on Computational Intelligence and Security. pp: 540-545. 2008

[12] Shang, G.Q.; Sun, C.H. Application of BP Neural Network for Predicting Anode Accuracy in ECM. International Symposium on Information Science and Engineering. pp: 428-432. 2008

2011 International Conference on Mechanical, Industrial, and Manufacturing Engineering
Lecture Notes in Information Technology Vols. 1-2

Preparation and Properties of Flame Retardant Epoxy Resin*

Jing Dang, Junwei Gu(✉), Yusheng Tang and Guangcheng Zhang

Key Laboratory of Space Applied Physics and Chemistry, Ministry of Education, School of Science
Northwestern Polytechnical University
Xi'an, Shaanxi Province, China, 710072

Correspondence to Junwei Gu, E-mail Address: gjw@nwpu.edu.cn, nwpugjw@163.com

***Abstract* - A novel structural phosphorus-containing epoxy resin (ED) was prepared by bisphenol A epoxy resin(E-51) and DOPO, and a nitrogen-containing phenolic aldehyde curing agent (MFP) was synthesized by melamine, methanal and phenol. The products were analyzed and characterized by Fourier transform infrared (FTIR), nuclear magnetic resonance (^{1}H NMR), Thermo-gravimetric analyses (TGA) and Scanning Electric Microscope (SEM), and the flame retardant and thermal resistance properties of cured epoxy resin were investigated. Results showed that the flame retardant and thermal resistance properties were improved with the increasing mass fraction of phosphorus. The onset decomposition temperature of cured epoxy resin containing 3wt% phosphorus was over 330^{o}C, the charring rate reached 30% at 650^{o}C, could reach UL 94-V0 rating.**

Index Terms* - *Phosphorus-containing epoxy resin(ED), Nitrogen-containing curing agent(MFP), Flame retardant, Thermal resistance properties.

1 INTRODUCTION

Epoxy resins are one type of thermoset resins combining many excellent properties, such as high mechanical properties, excellent thermal and environmental stabilities, low cost & shrinkage rate and ease of forming, and are widely used in various industrial fields such as adhesive, surface coating, painting materials, laminates, semiconductor encapsulation, and insulating material for electric device **[1-4]**.

However, conventional epoxy resins are flammable, and they still represents a limitation in structural applications as an incidental fire event involves not only health risks, but also loss of mechanical properties **[5-7]**. To the best knowledge of us, the flame retardant of epoxy resin can be improved by adding flame retardants or by incorporating reactive flame retardants **[8-11]**.

In our present work, a novel structural phosphorus-containing epoxy resin (ED) was prepared by bisphenol A epoxy resin (E-51) and DOPO (9, 10-dihydro-oxa-20-phosph henanthrene-10-oxide), and a nitrogen-containing phenolic aldehyde curing agent 2, 4, 6-tri (phenol-methylene-amide)-trizone (MFP) was also synthesized by melamine, methanal and phenol. And the products were analyzed and characterized by FTIR, TGA, ^{1}H NMR and SEM, and the flame retardant and thermal resistance properties of cured epoxy resin were investigated.

2 EXPERIMENTAL

Materials. Epoxy resin (E-51), was received from Blue Star New Chemical Materials Co., Ltd (Jiangsu, China). Melamine and phenol were purchased from Bodi Chemical Co., Ltd (Tianjin, China). Tetrahydrofuran and methanal were supplied by Tianjin Ganglong Chemical Co., Ltd (Tianjin, China). DOPO was received from Huizhou Sunstar Technology Co., Ltd (Guangdong, China). 1-(β-cyanoethyl)-2-methylimidazole and triethylamine were purchased from Xi'an Chemical Reagent Co., Ltd (Shaanxi, China). Sodium hydroxide and p-toluenesulfoni were supplied by Weifang Shunfuyuan Chemical Co., Ltd (Shandong, China)

Synthesis of phosphorus-containing epoxy resin(ED). In a 500ml three-neck and round-bottom glass flask with a temperature controller, magnetic stirrer and a reflux condenser, DOPO, triethylamine and E-51 were mixed at 70^{o}C for 40min. After distilling the solvent, the mixture was gradually heated to 155-160^{o}C and reacted for 6h. The transparent yellow ED was prepared by cooling to room temperature. The synthetic route was shown in **Scheme 1**.

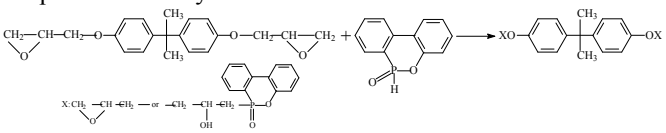

Scheme 1 Synthesis route of ED

Synthesis of MFP. Methanal and melamine were fed into a 500ml three-necked round-bottomed flask. The reaction mixture was heated to 80^{o}C and reacted for 40min (pH=9). And then, phenol and p-toluenesulfoni were added into the mixture above and maintained at 95^{o}C for an additional 24h. The product was neutralized by 10% NaOH. And then the precipitant was filtered and washed thoroughly by methanol. The white powder was dried under vacuum at 80^{o}C for 8h. The synthetic route was shown in **Scheme 2[12]**.

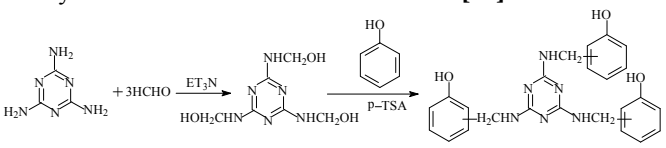

Scheme 2 Synthetic route of MFP

Preparation of ED/MFP. The ED, MFP and 1-(β-cyanoethyl)-2-methylimidazole were mixed, kept in a vacuum vessel to remove voids, and then to be quickly poured into the preheated die(110^{o}C). And the mixture was cured in a vacuum

* This work is supported by Fund for basic research from NWPU (Grant No. JC20100219) to Junwei Gu and Fund for basic research from National Scientifical and Industrial Technology Committee (Grant No. G9AL0001) to Yusheng Tang.

oven for 1h at 125°C, 2h at 145°C, 3h at 160°C, and 2h at 180°C, before undergoing properties testing.

Analysis and Characterization. FTIR spectra were obtained on Nicolet-550 equipment (Thermo Nicolet Corp., USA) with thin films on KBr; ^{1}H NMR spectrum was performed on a INOVA-400 NMR spectrometer(Varian Corp., USA) using CD_3COCD_3 as solvent; TG analyses were carried out at 10°C/min over the whole range of temperature (50-650°C) under N_2 on TGA Q50. The SEM morphologies of the cured epoxy resin were observed by JEM-6700F; The flame retardant properties of the cured epoxy resin were tested by UL-94 test(according to ASTM 1356-90).

3 RESULTS AND DISCUSSION

Structure analyses of MFP and ED. Figure 1 shows the FTIR spectra of DOPO(a), E-51 and ED(b).

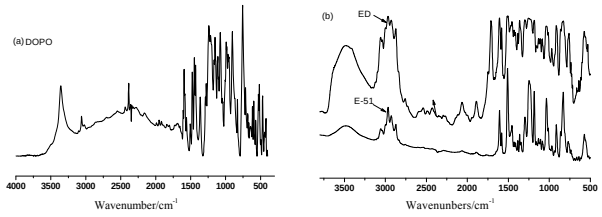

Figure 1 FTIR spectra of DOPO(a), E-51 and ED(b)

It can be seen that, the band at 2386cm^{-1} can be assigned to the characteristic stretching vibration peak of P-H, and the corresponding P-H peak disappears in the FTIR spectrum of ED. The characteristic stretching vibration peak at 3500cm^{-1}(-OH) can be attributed to the residual hydroxyl in E-51. And the characteristic peak at 3479cm^{-1}(-OH) in ED strengthens and broadens, which can be ascribe to the formed aliphatic series hydroxyl between DOPO and ring opening of E-51. Additionally, the other absorption peaks of P-O-Ph(755cm^{-1} and 1117cm^{-1}), P-Ph(1595cm^{-1} and 1493cm^{-1}), and P=O(1179cm^{-1} and 1244cm^{-1}) of DOPO appear in the FTIR spectra of ED. FTIR analysis reveals that ED has prospective chemical structure.

Figure 2 shows the ^{1}H NMR spectrum of MFP.

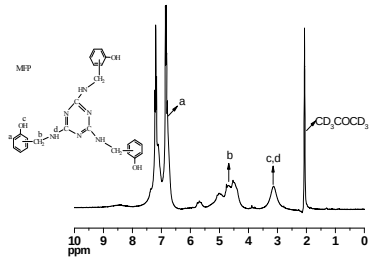

Figure 2 ^{1}H NMR spectrum of MFP

As seen from **Figure 2**, the signal at 4.3-4.5 ppm is induced from the chemical shift of methylene hydrogen (bH). And the signal at 6.7-7.2ppm stands for the chemical shift of benzene ring hydrogen (aH). The hydroxyl hydrogen of benzene ring (cH) and hydrogen of amino-group (dH) are corresponding to the active hydrogen. And the solvent, temperature and rapid proton exchange can influence the chemical shift of active hydrogen, leading to unfixing peaks. Therefore, the signal at 3.1ppm stands for the chemical shift of active hydrogen. ^{1}H NMR analysis reveals that MFP has prospective chemical structure.

Flame retardant properties of cured epoxy resin. The flame retardant properties of cured epoxy resin are presented in **TABLE 1**.

TABLE I The flame retardant properties of cured epoxy resin(ED)

Mass fraction of phosphorus /%	Average time of the first flame combustion(T_1)/s	Average time of the second flame combustion(T_2)/s	Flame droplets	standard
1(DDS)	23	24	none	V-1
1(MFP)	6.0	6.5	none	V-0
3(MFP)	self-extinguishing from a flame	self-extinguishing from a flame	none	V-0

At the same mass fraction of phosphorus, ED/MFP has more predominant flame retardant compared with ED/DDS. It is mainly due to good N-P flame retardant synergism between MFP and ED, further to increase the flame retardant effect.

It can be also seen that, the flame retardant of ED/MFP improves with the increasing mass fraction of phosphorus. It can be attributed to the increase of N-P flame retardant synergism and improving charring rate. The formed charred layers can prevent the volatilization of the combustion, and to effectively exclude oxygen and combustion heat. Moreover, MFP can release the ammonia gas, water vapour and nitrogen suffering from heat. The incombustible gas above and pyrophosphoric acid protective film can form C-C foam thermal barrier by foaming function, further to decrease the heat conduction. Additionally, the formed P-N-P and P-O-P can also break off the combustion chain reaction, finally to restrain the combustion.

Thermal properties of cured epoxy resin. The TGA curves of E-51 and ED containing 3wt% phosphorus are presented in **Figure 3**.

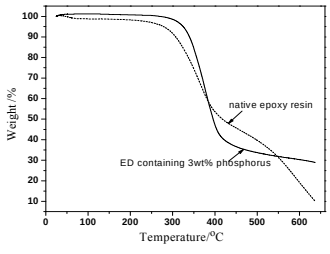

Figure 3 TGA curves of E-51 and ED

It can be seen that, both the onset decomposition temperature and maximal decomposition rate temperature increase by introducing of phosphorus, and the charring rate are also improved. When the mass fraction of phosphorus is 3%, the onset decomposition temperature is over 330°C, and the charring rate is 30% at 650°C. It reveals that the addition of DOPO helps to the charring. Meantime, the good N-P flame retardant synergism between MFP and ED can further increase the flame retardant effect.

The SEM observations of flexural fractures of E-51 and ED containing 3wt% phosphorus are presented in **Figure 4**.

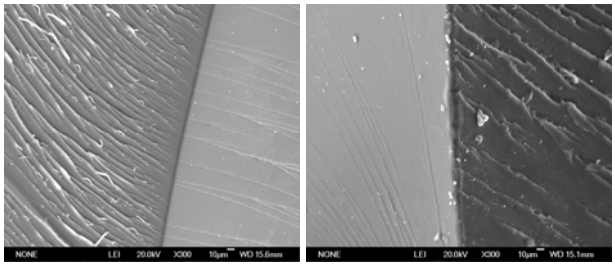

(a)native epoxy resin (b) ED(3wt% phosphorus)

Figure 4 SEM observations (×300) of flexural fractures of E-51 and ED containing 3wt% phosphorus

It can be seen that flexural fracture of ED containing 3wt% phosphorus presents more obvious brittle fracture feature, compared to native E-51. The reason can be ascribed that the masses of rigid DOPO aromatic ring lateral groups make the rigidity of molecular chain increase. When outside force takes action, stress concentration points are easy to form, residual stress can't be relieved easily, and crack extends quickly, finally to intensify the trend of brittle fracture.

4 CONCLUSIONS

A novel structural phosphorus-containing epoxy resin (ED) and a nitrogen-containing phenolic aldehyde curing agent (MFP) were synthesized successfully, the ^{1}H NMR and FTIR analyses revealed that MFP and ED had prospective chemical structures. The flame retardant and thermal resistance properties were improved with the increasing mass fraction phosphorus. When the mass fraction of phosphorus was 3%, the corresponding onset decomposition temperature of cured epoxy resin was over 330^{o}C, the charring rate reached 30% at 650^{o}C, could reach UL 94-V0 rating. SEM analyses revealed that the trend of brittle fracture intensified by introducing phosphorus.

ACKNOWLEDGMENT

The authors are grateful for the support and funding from Fund for basic research from NWPU(Grant No. JC20100219) to Junwei Gu and Fund for basic research from National Scientifical and Industrial Technology Committee (Grant No. G9AL0001) to Yusheng Tang.

REFERENCES

[1] Baljinder K. Kandola, Bhaskar Biswas, Dennis Price, *et al.,* "Studies on the effect of different levels of toughener and flame retardants on thermal stability of epoxy resin," *Polymer Degradation and Stability,* vol. 95, no. 2, pp. 144-152, February 2010.

[2] Ping Chen, Shengping Liu. "Epoxy Resin," *Beijing: Chemical Industry Press,* 1999, pp.18-40.

[3] S. Alessi, D. Conduruta, G. Pitarresi, *et al.,* "Hydrothermal ageing of radiation cured epoxy resin-polyether sulfone blends as matrices for structural composites," *Polymer Degradation and Stability,* vol. 95, no. 4, pp. 677-683, April 2010.

[4] Jie Kong, Yusheng Tang, Xingjun Zhang, *et al.,* "Synergic Effect of Acrylate Liquid Rubber and Bisphenol A on Toughness of Epoxy Resins," Polymer Bulletin, *Polymer Bulletin,* vol. 60, no. 2-3, pp. 229-236, March 2008.

[5] Dezhong Wang. "Production and application of epoxy resin," *Beijing: Chemical Industry Press*, 2001. pp.24-36.

[6] B.K. Kandola, A.R. Horrocks, P. Myler, *et al.,* "Mechanical performance of heat/fire damaged novel flame retardant glass-reinforced epoxy composites," *Composites Part A: Applied Science and Manufacturing,* vol. 34, no. 9, pp. 863-873, September 2003.

[7] A.P. Mouritz, S. Feih, E. Kandare, *et al.,* "Review of fire structural modelling of polymer composites," *Composites Part A: Applied Science and Manufacturing,* vol. 40, no. 12, pp. 1800-1814, December 2009.

[8] Xin Wang, Yuan Hu, Lei Song, *et al.,* "Flame retardancy and thermal degradation mechanism of epoxy resin composites based on a DOPO substituted organophosphorus oligomer," *Polymer,* vol. 51, no. 11, pp. 2435-2445, May 2010.

[9] Schäfer, Alexande, Seibold Sebastian, Lohstroh Wiebke, *et al.,* "Synthesis and properties of flame-retardant epoxy resins based on DOPO and one of its analog DPPO," *Journal of Applied Polymer Science,* vol. 105, no. 2, pp. 685-696, July 15, 2007.

[10]Xiaodong Wang and Qiang Zhang. "Synthesis, characterization, and cure properties of phosphorus-containing epoxy resins for flame retardance," *European Polymer Journal,* vol. 40, no. 2, pp. 385-395, February 2004.

[11]LiPing Gao, DeYi Wang, YuZhong Wang, *et al.*, "A flame-retardant epoxy resin based on a reactive phosphorus-containing monomer of DODPP and its thermal and flame-retardant properties," Polymer Degradation and Stability, vol. 93, no. 7, pp. 1308-1315, July 2008.

[12]Yuqin Min, Lin Fang, Xinghong Zhang, *et al.*, Study on the synthesis and properties of novel halogen-free flame retardant epoxy resins[J]. Journal of Zhejiang University(Science Edition), *vol*. 33, no .4, pp. 429-433, April 2008.

[13]M. Young, *The Technical Writer's Handbook*, Mill Valley, CA: University Science, 1989.

2011 International Conference on Mechanical, Industrial, and Manufacturing Engineering
Lecture Notes in Information Technology Vols. 1-2

Structure Strength Analysis for LPG Ship

Chunlin Zhang
School of Power and Mechanical Engineering of Wuhan University
Wuhan University, Hubei Province, China
linlitiankong@163.com

Jie Yang
Shanghai Marine Diesel Engine Research Institute
No.3111, Huaning Road, Minhang District, Shanghai, China
yangjun2268@126.com

Abstract
Liquefied petroleum gas (LPG) is safe,clean,and cheap, offering a viable alternative to conventional fuels, and is more and more important while the lack of energies all over the world. Nowadays, it is widely used in motor vehicles and people's daily life.LPG ship is a type of high-tech and high value ship widely used and high efficiency in transporting LPG. According to the special features of its structure, it is needed to have a direct calculation to ensure all the parts have sufficient strength.
In the present paper, a 6900m^3 LPG ship with two independent cargo tanks of type C was analyzed using the Finite Element Analysis (FEA) method. The analysis serves to check the structure strength and give suggests to optimizing the areas too strong or too weak. And in this paper some convenient formulas are derived for designers.

Keywords: LPG Ship, Strength Analysis, FEA Method, Reliability

I. INTRODUCTION

LPG has been widely used as a clean, safe and cheap fuel, which brings up the development of LPG ships. To have a high efficiency, the LPG ships are builded larger and larger. According to the special features of its structure, to ensure the reliability of the ships, it is needed to calculate the strength of the important areas. With the development of computer and math, the Finite Element Analysis method now has been developed commendable. The FEA method is used in many areas, and is a helpful method for ship design. During the process of design, with the finite element analysis, designers can know the strength distribution directly, and have an improvement for better design. This paper analyzed a 6900m^3 LPG ship with two independent toroidal cargo tanks depend on the rules of China Classification Society by the commercial programs of MSC.Software Company. In the analysis process, the most important and intricate load is the force on the saddles. In "*rules for construction and equipment of ships carrying liquefied gases in bulk*", it is recommended that the distribution using sine/cosine function to simulates the cargo tank loading applied to the saddle. To be efficient for the analysis in the future, some convenient formulas are derived in the paper for designers.

II. THE LOADS IN ANALYSIS

The loads for analysis the structure strength for LPG ships include cargo load, structural self-weight, seawater pressure, additional load for equilibrium, the forward collision force, half value of the gravitational component from each effective mass along the heeling plane for ship at a static heeling angle of 30°,load applied in the pressure testing [1].

A. Acceleration Components

The acceleration for analysis contains the gravity and the acceleration due to ship's motion corresponding to a probability level of 10^{-8} in the North Atlantic. The acceleration components include the direction of vertical, transverse and longitudinal [2].

1) Vertical acceleration: motion accelerations of heave, pitchan, possibly, roll (normal to the ship base):

$$a_z = \pm a_0 \sqrt{1 + (5.3 - \frac{45}{L_0})^2 (\frac{X}{L_0} + 0.05)^2 (\frac{0.6}{C_b})^{1.5}} \quad (1)$$

With

$$a_0 = 0.2 \frac{V}{\sqrt{L_0}} + \frac{34 - 600 / L_0}{L_0}$$

2) Transverse acceleration: motion accelerations of sway, yaw and roll; and gravity component of roll:

$$a_y = \pm a_0 \sqrt{0.6 + 2.5(\frac{X}{L_0} + 0.05)^2 + K(1 + 0.6K\frac{Z}{B})^2} \quad (2)$$

3) Longitudinal acceleration: motion accelerations of surge and pitch; and gravity component of pitch:

$$a_x = \pm a_0 \sqrt{0.06 + A^2 - 0.25A} \quad (3)$$

With

$$A = (0.2 - \frac{L_0}{1200} + \frac{5Z}{L_0}) \cdot \frac{0.6}{C_b}$$

Where:

L_0——length of the ship(m);
C_b——block coefficient(m);
B——greatest moulded breadth of the ship(m);
X——longitudinal distance(m) from amidships to the center of gravity of the tank with contents;
Z——vertical distance(m) from the ship's actual waterline to the center of gravity of the tank with contents;

B. Details of Loads

1) Cargo load: weight of cargo tanks and liquid cargos, with inertial forces induced by ship motions being considered;

2) Structural self-weight: hull structural weight in the model, may calculated automatically by computer program;

3) Seawater pressure: may be only hydrostatic pressure;

4) Additional load for equilibrium: used to add the difference between structural sole weight and buoyancy to the cargo load, applied on the bottom plating and superimposed on the buoyancy;

5) The forward collision force: equal to a half of the weight of cargo tank and cargo and one fourth for the backward

6) Half value of the gravitational component from each effective mass along the heeling plane for ship at a static heeling angle of 30°

7) Loads in the pressure testing

C. Loads on saddle

The location of cargo tank, saddle and ship structure is like Fig.1 below. There is sleeper between cargo tank and saddle to reduce stress concentrations. The angle of saddle is 150°. It is recommended that the distribution using sine/cosine function to simulate the cargo tank loading applied to the saddle [2].The load is simulated by cosine function in the following work.

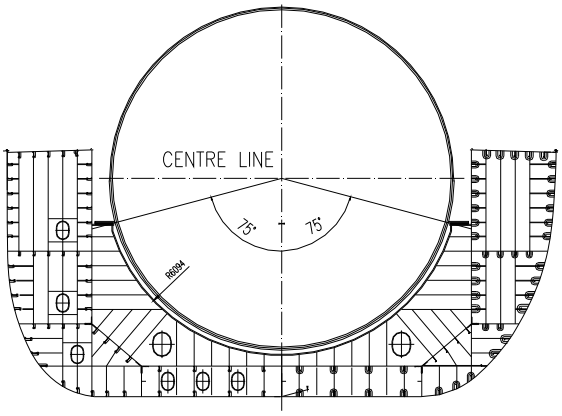

Fig.1 The location of cargo tank and ship structure

There are three conditions need to be calculate for the loads on saddle: vertical pressure, horizontal pressure, and the pressure when ship at a static heeling angle of 30°.

1) Vertical pressure added on the saddle:

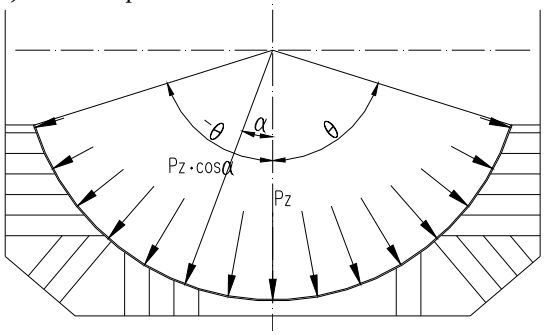

Fig.2 Vertical pressure distribution

$$\int_{-\theta}^{\theta} \cos^2\theta \cdot \mathrm{D} \cdot \mathrm{R} \cdot d\alpha = G$$

So

$$P_z = \frac{G}{D \cdot R \cdot (\theta + \frac{1}{2}\sin 2\theta)} = \frac{M \cdot a_z}{D \cdot R \cdot (\theta + \frac{1}{2}\sin 2\theta)} \quad (4)$$

2) Horizontal pressure added on the saddle:

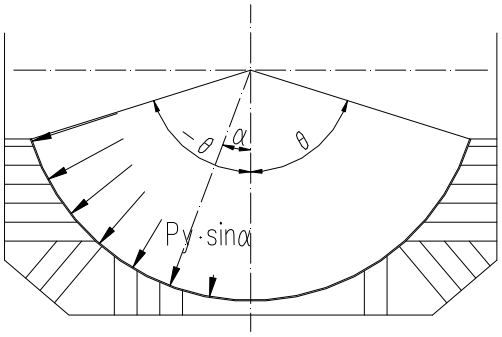

Fig.3 Horizontal pressure distribution

$$\int_{-\theta}^{\theta} P_y \cdot \sin^2\alpha \cdot D \cdot R \cdot d\alpha = F_y$$

So

$$P_y = \frac{F_y}{D \cdot R \cdot (\frac{1}{2}\theta - \frac{1}{4}\sin 2\theta)} = \frac{M \cdot a_y}{D \cdot R \cdot (\frac{1}{2}\theta - \frac{1}{4}\sin 2\theta)} \quad (5)$$

3)The pressure when ship at a static heeling angle of 30°:

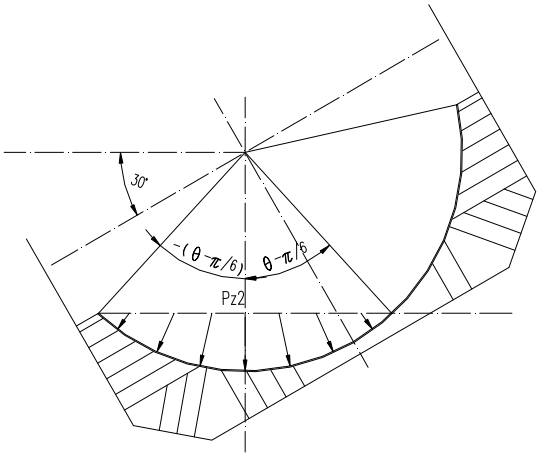

Fig.4 The pressure when ship at a static heeling angle of 30°

$$\int_{-(\theta-\pi/6)}^{\theta-\pi/6} P_{z2} \cdot \cos^2\theta \cdot D \cdot R \cdot d\alpha = G'$$

So

$$P_{z2} = \frac{M \cdot g}{D \cdot R \cdot (\theta - \pi/6 + \frac{1}{2}\sin(2\theta - \frac{\pi}{3}))} \quad (6)$$

Pz—— vertical pressure on saddle(Pa);

Py—— horizontal pressure on saddle(Pa);

P_{z2}——vertical pressure on saddle when ship at a static heeling angle of 30°(Pa);

G——weight of cargo tanks and liquid cargos, with inertial forces induced by ship motions being considered(N);

M——total mass of cargo and cargo tank(kg);

D—— the width of saddle faceplate(m);

R——: the ratio of saddle(m);

α——: the angle of saddle(rad);

III. THE FINITE ELEMENT MODEL

To conduct a finite element analysis, a fine model should be builded first.In this paper,the model was builded in MSC.patran contains two half- cargo-areas in longitudinal direction for each tank like the Fig.5 to Fig.7.This model contains most parts of this area, and is enough for the analysis.[3]

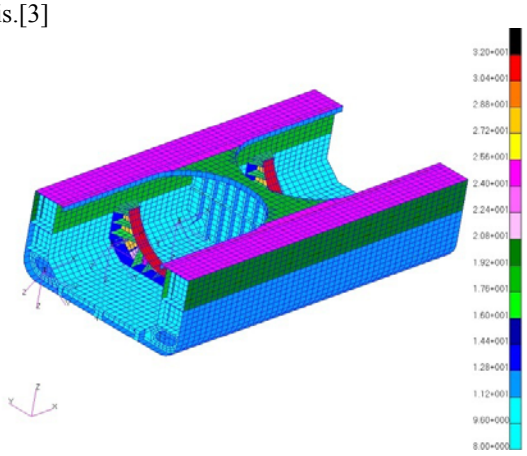

Fig.5 Finite element model

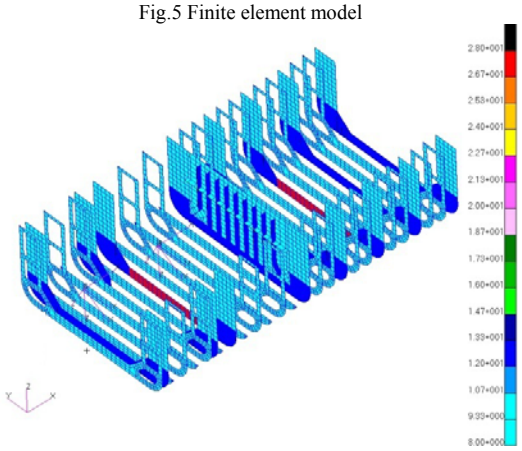

Fig.6 Finite element model of inner parts

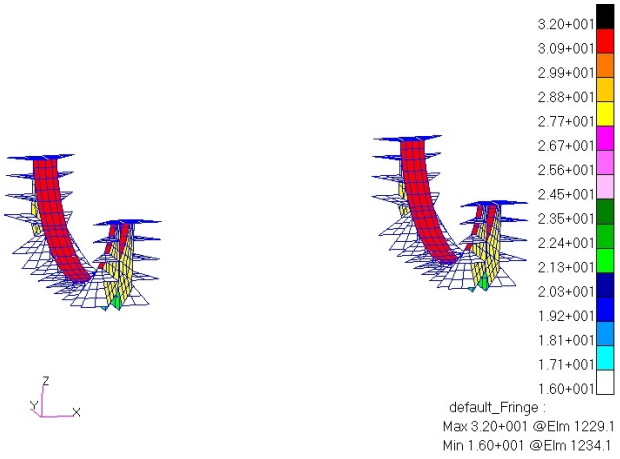

Fig.7 Finite element model of saddle

IV: THE BOUNDRAY CONGDITION AND LOAD COMBINATIONS

By the command of CCS, the boundary condition of the local model is set according to table. I. And the load combinations are generally taken from the table. II. [1]

TABLE I
BOUNDARY CONDITIONS OF THE LOCAL MODEL

Degree of Freedom / Supporting Point location	X	Y	Z	θ_x	θ_y	θ_z
Longitudinal centerline	free	fixed	free	fixed	free	fixed
For end plane	fixed	fixed	fixed	free	fixed	fixed
Aft end plane	free	fixed	fixed	free	free	free

TABLE II
LOAD CONDITIONS

Load item / Load condition	Cargo load			Structural self weight	Seawater Pressure	Additional load for equilibrium	1/2(tank+ cargo)forward collision force	1/4(tank+ cargo)backward collision force	Static heeling angle of 30°	Load in Pressure testing
	ax	ay	az							
Pitch+heave	1.0		1.0	1.0	1.0	1.0				
Roll +heave		1.0	1.0	1.0	1.0	1.0				
Pitch+roll+heave	0.8	0.8	0.9	1.0	1.0	1.0				
Independent(1)							1.0			
Independent(2)								1.0		
Independent(3)									1.0	
Independent(4)										1.0

Notes: The values in the table are the coefficients of the load combinations and where a blank exists, it means that the item is not taken into account under the combination considered.

V: RESULTS OF THE ANALYSIS

After the loads and boundary conditions were added on the model, the calculation can be taken by the MSC. Nastran. When the program finished, the results can be showed like the Figs below. Designers can easily read the level of stress.

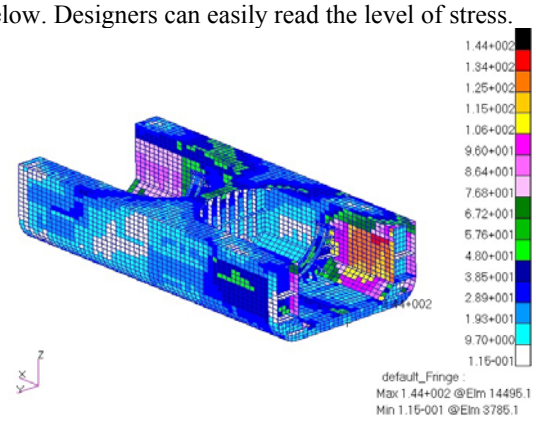

Fig.8 von Mises stress of the whole model

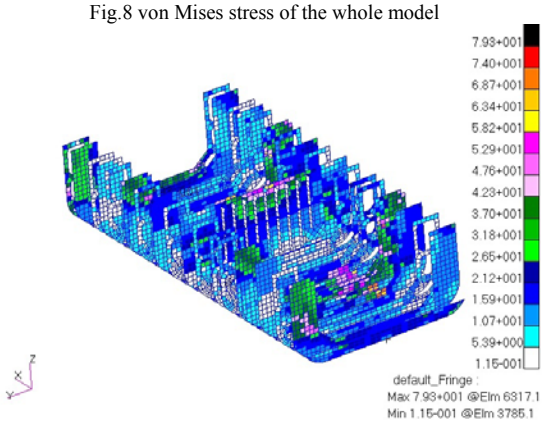

Fig.9 von Mises stress of the inner rings

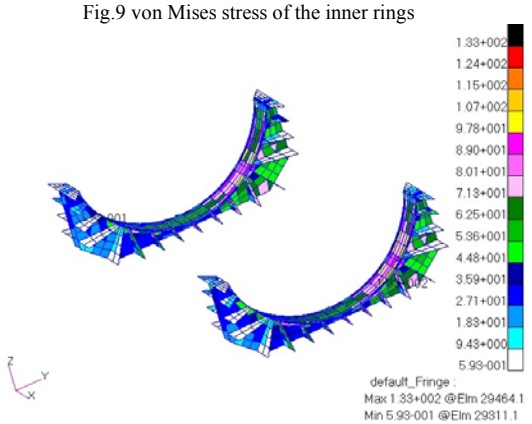

Fig.10 von Mises stress of the saddle

In the original design, analysis result shows that the areas below the saddles had serious stress concentrations. So it is advised to the designer to add one more ventral shield for each saddle, while the thickness of inner shell can be reduced from 20mm to 16mm.The followed calculation result shows like Fig.8 to Fig.10.The final result shows that the saddle areas have a good stress distribution, and the Max von Mises stress is only 144Mpa, much less than the admissible stress of material.

VI.CONCLUSION

The 6900m^3 LPG Ship analyzed in the paper is the largest full pressure LPG ship in China now. The finite element analysis for the 6900m^3 LPG Ship was conducted in the designing process. By the finite element analysis, some useful improvements were given to the designers. The areas not suitable were improved depend on the results of the stress distribution. Practice proves that the FEA method is useful and necessary in the ship design process especially in a new style of ship design, from which, the structure strength can be easily read, and designers have direction to improve the structural performance. By the strength analysis a new bigger ship can be builded more rational and reliable. The formulas given in the paper can be used in strength analysis for LPG ship conveniently.

REFERENCES

[1] Rules for Construction and Equipment of Ships Carrying Liquefied Gases in Bulk,CCS,2006
[2] Guidelines for Direct Calculations of Strength,CCS,2009
[3] MSC.Patran User's Manual

2011 International Conference on Mechanical, Industrial, and Manufacturing Engineering
Lecture Notes in Information Technology Vols. 1-2

Numerical Modeling of Heat and Moisture Transfer during Microwave Drying of Wood

Part Ⅱ:the Simulation above Fiber Saturation Point

Jian-fang Yu (College of Material Science and Art Design, Inner Mongolia Agricultural University, Huhhot 010018, yjf_112@163.com)
Xi-ming Wang (College of Material Science and Art Design, Inner Mongolia Agricultural University, Huhhot 010018, w_ximing@263.net)
Cai-qin Yang (College of Science, Inner Mongolia Agricultural University, Huhhot 010018, nmgycq@sina.com)
Jing-ya Nan (Institute of Chemical Industry of Forest Products, Chinese Academy of Forestry, Nanjing 210042, nanjingya123@yahoo.cn)
Bing-hu Sun (College of Material Science and Art Design, Inner Mongolia Agricultural University, Huhhot 010018, sbhmk2050810157@163.com)

Abstract：The heat and moisture transfer model above fiber saturation point (FSP) has been developed based on volume averaging theory in the last paper. It's numerical solutions under adequate initial and boundary conditions are obtained by adopting fully implicit finite difference method and MATLAB software in this paper. This paper verifies experimentally the model and describes theoretically the changeable and distributional patterns of moisture content and temperature in the process of microwave drying of wood. The numerical solutions show that the microwave drying process may be divided into two stages which are the stage of increasing drying rate and the stage of constant drying rate. And there are no significant moisture and temperature gradients that are indicated along thickness of wood in the process of wood drying.
Key words: Microwave drying; Heat and moisture transfer; Numerical solutions; Volume averaging theory; *Larix gmelin*

1. Introduction[1]

Conventional drying of wood is a slow process relying on heat conduction from the outer layers towards the interior. To advance the drying rate, drying time and quality of dry products, internal moisture transfer must be enhanced by controlling to match the heat and mass transfer in a boundary film layer on the materials. Many studies[1-2] indicate microwave heating offers an opportunity to enhance the rate of evaporation because the energy is absorbed throughout the volume. It has been widely applied in various industries[3-7]. However, the industrial application of wood drying hasn't achieved substantial progress[8]. Enriching and improving the theory of heat and moisture transfer during the microwave drying of wood has important theoretical meaning and practical value for controlling reasonably the microwave drying of wood and improving the quality of dried products. In the theoretical analysis, the last paper[9] developed a numerical model of heat and moisture transfer based on volume averaging theory above the fiber saturation point (FSP). This paper verifies experimentally the model and microwave drying is examined theoretically to specify preliminarily the effect of internal heating on the changeable and distributional patterns of moisture content and temperature during microwave drying of wet wood based on the numerical analysis by the model.

2. Verification of the Model

In order to verify the distribution and variation laws of wood temperature and moisture content in the process of microwave drying, the temperature and moisture content of each feature point in the thickness direction of the internal wood through the experiment will be measured.

2.1 Experiment Equipment

The weight monitoring system is KunLun Coast KL8000 Series Data Acquisition. Weight sensor range: ≤5kg; Accuracy: 1%g; using temperature: ≤200℃.

Fluorescent fiber 4-channel temperature monitoring system: the fluorescent optical fiber temperature sensor and 4-channel fluorescent optical fiber modem apply the LABVIEW software in PC to multi-point temperature monitoring for wood.

2.2 Experimental Materials and Methods

In the test green wood of *Larix Gemini* with the thickness of 40 mm, length 490mm were processed. In this paper, the optical fiber temperature measurement system is used to measure temperatures in 1/2 and 1/4 form the surface (i.e. the heart layer and the sub-surface layer), weight sensor is used to measure the average moisture content of wood, and the model mixer is applied to achieve the average heating of the microwave.

2.3 Determination of model parameters

In the process of establishing the model of heat and moisture transfer, as wood can be regarded as a system of multiphase mixtures which are composed with the real wood, free water, bound water and vapor, wood properties and other parameters used in the simulation are following [7-11]:
ρ_s=420kg/m^3, ρ_f=967 kg/m^3, ρ_b=967 kg/m^3, G=0.41, M_v=0.018kg/mol, R=8.314J/(mol·K), φ=0.6, k_f=1.26×10^{-7}m^2, k_v=4.93×10^{-7} m^2, c_f= c_b=4210J/(kg·℃), c_v=2000 J/(kg·℃), h_T=12W/(m^2·℃), h_M=9.37×10^{-9}kg/(m^2·Pa·℃).

The corresponding variables of model parameters, the effective thermal conductivity of the moist wood, dynamic viscosity of bound water, dynamic viscosity of water vapor

[1] * Project supported by the National Natural Science Foundation of China (Grant No. 30760192).
†Corresponding author: Xi-ming Wang

and latent heat of vaporization of water, are calculated using the following equations[8].

$$\lambda_{eff} = \frac{G}{1+MG}(0.1941 + 0.4064M) + 0.01864$$

$$\mu_f = \frac{0.001779}{(1 + 0.03368T + 0.000221T^2)}$$

Where T is the temperature of water, ℃.

$$\mu_v = \mu_0(\frac{T+273}{273})^n = 8.022\times10^{-6}\times(\frac{T+273}{273})^{1.27}$$

Where μ_0 expresses the dynamic viscosity at the temperature of 0℃, and its value is 8.022*10^{-6}Pa·s; T expresses the temperature of vapor, ℃; n expresses the coefficient, taking 1.27.

$$h_{vap} = (-2.5315\times T + 2506.9)\times10^3$$

2.4 The Comparative Analysis between Verified Results of the Model Experiment and Calculated Results of Model

Experimental curves and model simulated curves of temperatures and the average moisture contents in heart layer and sub-surface layer of the sample are shown in Fig. 2.

Seen from Fig. 2, the drying process is divided into two stages, namely the stage of increasing drying rate and the stage of constant drying rate, and the corresponding temperature curves express the stage of decreasing rate and the stage of constant rate. However, Fig. 2 show that, in the process of drying, experimental values of the sample's temperature are slightly lower than simulated values. The reason may be that during the model simulation, the microwave energy is regarded as a kind of internal heart source, but during the practical drying, the microwave penetration into wood decays exponentially. Therefore, in the process of practical drying, the microwave energy bound by wood is less than the simulated values. Generally speaking, the established model can be used to simulate the drying process and predict changes of moisture content and temperature in the drying process.

3.The numerical solutions of the model and simulated results

3.1 Numerical method

In the process of solving the problem on heat and moisture transfer of wood, it is rather difficult if directly solving the boundary value problems on differential equations of heat and moisture transfer. Therefore, no matter what kind of numerical method is adopted, the continuous problems must be discredited, and any numerical solution represents only approximate value of true value on each of the discrete points. Accordingly, partial differential equations should firstly be discreted in the computational domain, and then convert into the corresponding algebraic relationships or algebraic equations. Then algebraic relationships or equations can be solved to obtain the numerical solutions.

In the paper, according to the shape of the sample and the characteristics of the model, controlling equations of the model and corresponding boundary conditions are discreted in the computational domain by adopting fully implicit finite difference method, and boundary value problems on heat and moisture transfer are solved by using prediction-correction system, and then computational interface of numerical simulation can be achieved by applying MATLAB program. In the simulation program, parameters and conditions can make the appropriate increasing and decreasing changes, or the input data can be saved and reset correspondingly. And simulated results can be showed in the form of 2D or 3D map. Meanwhile, real-time data values can be captured to show variable values and parameter values in the time of n and the position of j within the wood.

3.2 Numerical simulated results and analysis

In the following, according to the model of heat and moisture transfer, the variation law and distribution law of moisture content and temperature with the drying time in the process of microwave drying will be conducted with numerical prediction and related analysis.

3.2.1 The variation law of moisture content and temperature with the drying time in the process of microwave drying

The variation law of moisture content and temperature with the drying time in the process of microwave drying is shown in fig. 3 and fig. 4. Simulated conditions are initial moisture content of the sample 60% and the thickness 60 mm (i.e. h in the model is equal to 30 mm).

In the process of conventional convective drying, heat is mainly transferred through the forms of convection heat transfer and heat conduction, so the rate of transfer is very slow. However, in the process of microwave drying, microwave energy in the form of electromagnetic waves penetrates directly into the internal wood, and interacts with polar molecules in the wood through the electromagnetic field to convert the electromagnetic energy into the heat energy instantly.

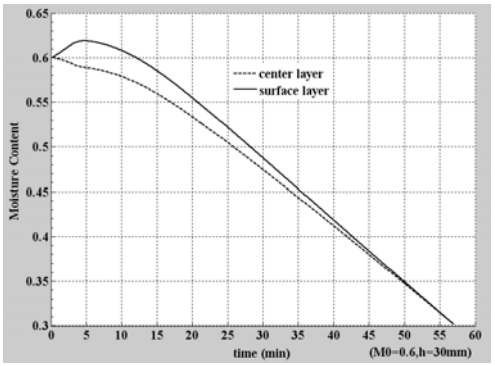

Fig. 3 Variations of moisture content with drying time

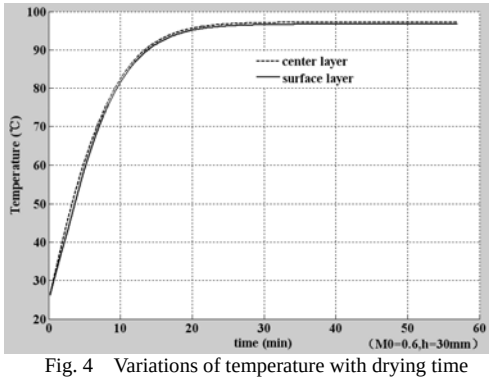

Fig. 4 Variations of temperature with drying time

Therefore, the transient behavior of temperatures in microwave drying is quite different from conventional drying by external heating. In particular, the increase of the wood temperature and the evaporation of water are going simultaneously along the wood thickness and the rate of increases in temperature is very fast at the beginning of drying.

The reason can be explained by the fact that the net heating rate falls gradually due to reduction of the temperature difference between hot air and the surface with elevation of the surface temperature in the convective heating while the microwave heating is adopted with a constant through the drying period in this model. Fig. 3 and Fig. 4 show that, while the initial moisture content of the sample is above FSP, the surface and heart layers of wood has not significant moisture content gradient and temperature gradient through the microwave drying period, particularly in the later period of drying, but represent the moisture content gradient that the inside is high yet the outside is low. This indicates that in the process of microwave drying, when the moisture content is above FSP, moisture content gradient is not the main driving force of water migration within the wood. The reason that causes the low surface temperature may be the evaporation of water in the wood surface, and the convection heat transfer of the drying medium make the temperature of wood surface decrease.

Fig. 3 also shows that, within 5 minutes which are at the beginning of drying, moisture content of the wood surface increase slightly compared with the initial moisture content. Because of the instantaneous nature of microwave energy, water within the wood absorb the heat, vaporize rapidly, and then migrate to the wood surface. Since the moving rate of water is faster is than the evaporation rate of water in the wood surface, the moisture content of wood surface is higher than the initial moisture content within a few minutes which are at the beginning of drying, and the moisture content difference between the surface layer and the heart layer increases. This is the same as the studying results of Ref. [12]. When researching the characteristics of extraordinary heat and moisture transfer within the porous medium, Ref. [12] also points out that the phenomenon of “local humidity increase” within the porous medium is caused by the couple action of extraordinary heat and moisture transfer. Ref. [7] also makes a theoretical analysis for the phenomenon of “local humidity increase” which appears in the process of microwave vacuum drying. With the acceleration of evaporation rate on the surface and the extension of moving path of internal water, this situation is gradually easing, the moisture content difference between the surface layer and the heart layer begins to decrease, and the water distribution within wood tends to be average.

Fig. 3 and Fig. 4 show that the whole drying process can be divided into two stages: the stage of increasing drying rate (the stage of increasing temperature) and the stage of constant drying rate (the stage of constant temperature). In 20 minutes, namely in the stage of increasing drying rate, the reduced range of wood moisture content is gradually increasing, the average rate is 0.27%/min, and the moisture content difference between the surface layer and the center layer firstly increases and then decrease. However, the increased range of temperature is fairly large, and the average rate is 3.5℃/min. This indicates that, during this period, the microwave energy that is bound by the wood is mainly used to increase the temperature of wet wood, yet the energy that is consumed by the water evaporation is very little. After drying for 20 minutes, namely entering into the stage of constant drying rate, the moisture content of wood decreases rapidly at a constant rate of 0.65%/min, and the rising rate of temperature decreases, then maintaining gradually a constant value nearly. This indicates that, in this stage, the microwave energy that is bound by the wood is mainly used to evaporate the moisture within wood. The proportion of the stage of constant drying rate accounting for the whole process of microwave drying is about 56.14%. In the whole process of microwave drying, the highest temperature is 97.14℃.

3.2.2 The Distribution Law of Moisture Content, Temperature and Pressure with the Drying Time in the process of Drying

For the distribution law of moisture content in the process of drying, many scholars do researches basing on different drying methods and different species. During the conventional drying, the distribution of moisture content is obtained generally by the method of stratified moisture content. However, as the time of microwave drying is very short, it is fairly reasonable using the model to predict the distribution of moisture content. During modeling in this paper, the initial moisture content of the sample is 60% and the thickness is 60mm (i.e. the h in the model is 30mm).

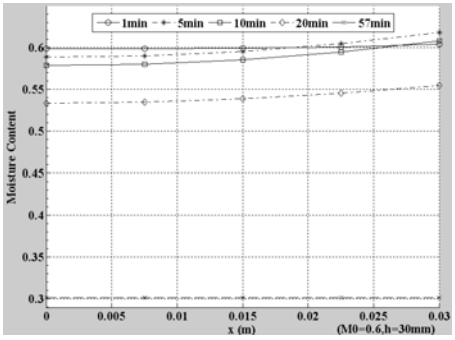

Fig. 5 distribution curve of moisture content

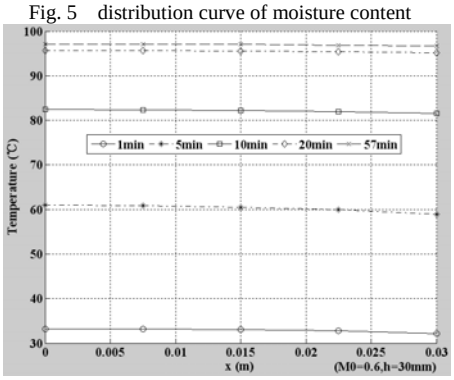

Fig. 6 distribution curve of temperature

In general, Fig. 5 and Fig. 6 show that, when the initial moisture content of the sample is above FSP, distributions of moisture content and temperature along the wood thickness are rather average, and the distribution pattern that the inside is high is shown obviously. The difference of temperature is less than 2.1℃.

The maximum value of temperature gradient in the thickness direction is 0.7℃/cm. However, the moisture content of the outer layer is higher than the inner, and the maximum value of the moisture gradient is 1%/cm.

4. Main conclusions

Microwave drying of wood is a complex coupling process of heat and moisture transfer. Laws of heat and moisture transfer have a direct effect on the distributions of temperature and moisture content within the wood. The main results are following.

The drying process can be divided into two stages: the stage of increasing drying rate and the stage of constant drying rate, namely the stage of rising temperature and the stage of constant temperature. The proportion of the stage of constant drying rate is about 56.14%. In the whole process of drying, obvious moisture content gradient and temperature gradient between the surface and heart layer are not shown, but the moisture content gradient that the inside is low and the outside is high, temperature gradient that the inside is high and the outside is low are shown.

5. Outlook

This study has a practical significance for the microwave heating technology, but the heat and moisture transfer during the microwave drying of wood is a very complex process containing the phase change, involving more mechanisms on the heat and moisture transfer. In the paper, when establishing the model, it is assumed that the wood doesn't deform. Although the deformation and the stress in the microwave drying of wood are smaller compared with the conventional convective drying, the development and distribution of stress and deformation in the process of wood microwave drying should be analyzed from a mechanical point of view. At the same time, the mechanism of stress release in the process of wood microwave drying combined specifically with changes in wood microstructure is investigated considering the interaction between the stress and the heat and moisture transfer.

The distribution laws of moisture content field and temperature field plays an important role in understanding the mechanism of heat and moisture transfer during the microwave drying. Therefore, the establishment of two-dimensional model of heat and moisture transfer should be combined with the wood anisotropy. And the advanced measurement methods such as the nuclear magnetic imaging and the CT scanning should be applied.

References:

[1] Dedic.A.,Zlatanovic.M,. "Some aspects and comparisons of microwave drying of beech and fir wood,".*Holz als Roh-und Werkstoff*, vol. 59, pp. 246-249, 2001.

[2] Bengtsson N., "Development of industrial microwave heating of foods in Europe over the past 30years," *Journal of microwave power and electromagnetic energy*, vol. 36, no. 4, pp. 227-240, 2001.

[3] Ratanadecho P.,Aoki,K.and Akahori M., "Experimental and numerical study of microwave drying in unsaturated porous material," *Int.Comm.Heat and mass transfer*, vol. 28, no. 5, pp. 605-617, 2001.

[4] A.L.Adamovich, N.N.Grinchik, S.P.Kundas, V.I.Terekhov, "Modeling of nonisothermal heat and moisture transfer in capillary-porous media in microwave heating," *Teplofiz.Aéromekh.*, vol.11, no. 2, pp. 257-272, 2004.

[5] Araszkiewicz, M.,Koziol,A., Oskwarek,A., Lupinski,M. "Microwave drying of porous materials," *Dry.Technol*, vol.22, no. 10, pp. 2331-2341, 2004.

[6] Michal Araszkiewicz, Antoni Koziol, Anita Lupinska, Michal Lupinski, "Microwave drying of various shape particles suspended in an air stream," *Transp Porous Med*, vol.66, no. 10, pp. 173-186, 2007.

[7] Li Xianjun, "Research on Characteristics of Wood Microwave-Vacuum Drying," *Ph. D. Dissertation of Beijing Forestry University*, 2005.

[8] Stanish M A, "The roles of bound water chemical potential and gas phase diffusion in moisture transport through wood," *Wood Science and Technology*, vol. 20, no. 1, pp. 53-70, 1986.

[9] Yu-jianfang, Wang-ximing, "Numerical Modeling of Heat and Moisture Transfer During Microwave Drying of Wood Above FSP(Part Ⅰ:the Model)", *The 6th International Conference on Physical and Numerical Simulation of Materials Processing (ICPNS 2010)（indexed by ISTP）*, pp. 318, 2010

[10] S.Pang,I.G.Simpson,A.N.Haslett, "Cooling and steam conditioning after high-temperature drying of Pinus radiata board experimental investigation and mathematical modeling," *Wood Science and Technology*, vol. 35, pp. 487-502, 2001.

[11] N.N.Grinchik, "Modeling off nonisorhermal heat and moisture transfer in capillary-porous media in periodic microwave heating," *Journal of Engineering Physics and Thermophysics*, vol. 80, no. 1, pp. 1-10, 2007

[12] Wang xin, Shi mingheng, Yu weiping, "Research on high intense and rapid heat and mass transfer in convective boundary condition", *Journal of engineering thermophysics*, vol. 23, no. 2, pp. 212-214, 2002

2011 International Conference on Mechanical, Industrial, and Manufacturing Engineering
Lecture Notes in Information Technology Vols. 1-2

The borehole method of rock massive stress state estimation

Valery Pavlov
Laboratory of computational methods in geophysics
Institute of Petroleum Geology and Geophysics
Novosibirsk,630090, Russia
vapavlov@bk.ru

Sergey Serdyukov and Peter Martynuk
Laboratory for oil production wave-engineering
Institute of Mining
Novosibirsk,630091, Russia
svserd@academ.org

***Abstract* - In permeable rock the hydraulic fracturing stress measurement is carried out using such impenetrable shell as a packer and a sleeve that prevents from fluid injection into the fracture and rock. The stress states are determined from several fracture reopening pressures on condition that cracks have different orientation in reference to a maximum stress. Numerical modeling of this problem shows the gradual character of the crack opening in the borehole and the influence of an indefinable initial crack length on the reopening pressure value Pr of other fractures. As a solution the using of a singular radial fracture and the measuring of fracture opening value on the outline dependence of the pressure in the impenetrable shell are proposed. The fractures are induced by hydraulic fracturing in advance. The test of the solution is carried out using singular integral equations of linear fracture mechanics. The fracture opening pressure and fracture opening value on the outline dependence of the fracture opening portion length and external stress field is determined. The principal stress ratio estimation algorithm is developed. The ratio of principal stresses is an additional parameter and it is used to find out the stress with the fracture reopening pressure on the borehole wall.**

Index Terms – hydraulic fracturing stress measuring, sleeve fracturing, numerical modeling.

I. Introduction

Hydraulic fracturing has been widely used for rock stress measurement [1]. The method is based on the relation of hydraulic fracturing pressure to rock mass stress. The state of the remote stresses in a plane perpendicular to a borehole axis is evaluated from the reopening pressure, the shut-in pressure and orientation of a pair of longitudinal cracks. Cracks are induced by hydraulic fracturing, which are parallel to the borehole axis. In this method, the shut-in pressure is used to estimate the remote compressive stress normal to the crack plane. This method assumes that no pressure penetration of the fracture occurs prior to the onset of fracture opening. However, as shown in laboratory works to examine permeability of fractures under compressive loads [2], pressure to penetrates the fractures before it begins to open. The sleeve fracturing method of stress measurement was first proposed by Stephansson [3]. A complete history of sleeve fracturing is given by Amadei and Stephansson [4]. The sleeve fracturing method can't be used in the condition of an irregular stress field in the massif $\sigma_{min}/\sigma_{max}<1$ [5]. This is referred to a single fracture method and a double fracture method. In the double fracture method it is connected with mistakes of the reopening pressure determination of the secondary fracturing system. In the single fracture technology the inaccuracy in external field parameters determinations connected with the impossibility to create linear extensive fractures by borehole flat jack, such as Goodman jack[5]. The method [6], based on the integrated use of measuring hydraulic fracture and deformational measurement is proposed for determination of σ_{max}, σ_{min} in the permeable rock. Performance of the following methods involves two stages. On the 1st stage (preliminary) the fracturing system is formed by hydraulic fracturing, but with high intensity of loading. On the 2nd stage the impenetrable shell is placed into the same borehole interval. As only two fractures are supposed to be produced, than the additional parameter for external stress field determination is necessary. As additional parameter it is suggested to use the fracture opening on the borehole outline during loading dependence on $\alpha= \sigma_{min}/\sigma_{max}$.

II. Numerical model

Mathematical model

A 2D problem, illustrated in Fig. 1, is considered. There is a vertical borehole with the radius R and with a pair of radial, lengthy fractures located in an infinite rock formation. The rock massive are subjected to the horizontal principal stresses σ_{max}, σ_{min}. The fractures are aligned in the direction of σ_{max}. Let us consider (x, y) to be a coordinate system (Figure 1). The datum point of coordinate system is coincident with the center of the borehole. Compressing stress field σ_{max}, σ_{min} takes place at infinites, the coefficient $\alpha= \sigma_{min}/\sigma_{max}$ characterizes irregularity of the compression field. The maximum compression stress σ_{max} acts in the direction of axis Ox (Figure 1).

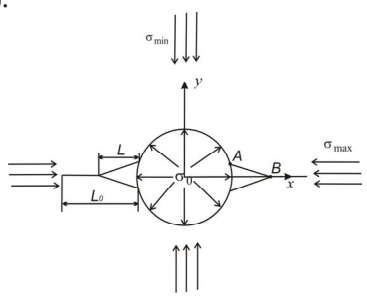

Fig. 1. Illustration of the fracture and borehole geometry.

A packer system is installed within the borehole and its packer element is inflated against the borehole wall. Due to the inflation, a pressure σ_0 is applied on the borehole wall but not on the fracture surfaces at anytime during pressurizations. Where σ_0 is lower than the borehole pressure at fracture reopening Pr the fracture surfaces contact each other. When σ_0 reaches σ_* (where $\sigma_*= \sigma_{max}(3\alpha\text{-}1)$ - i.e. P_r), the fractures begin to open from their mouths at the borehole. Afterwards the length of the opening portion of the fracture, L, increases with σ_0 (but always $L<<L_0$). Where L_0 is a length fractures are induced in advance.

Numerical calculations

For the borehole sectional area incremental size estimation the problem with the following boundary conditions on the round outline is solving:

$$\sigma_n = -\sigma_0; \tau_s = 0,$$

and on the crack edges(as a liquid does not penetrate cracks):

$$\sigma_n = 0; \tau_s = 0,$$

where σ_n and τ_s are normal and tangent stresses on boundaries. Using the complex potential integral expressions for the elastic plane with a round hole and a linear cut and considering the central symmetry, the problem comes down to the finding of the integrated singular integral equation solution (Savruk 1981):

$$\frac{1}{2\pi}\int_L [R(T,X)\cdot g'(t) + S(T,X)\cdot \overline{g'(t)}]dt = P(X), \qquad (1)$$

where T and X is the outline of the fracture L in the basic coordinate system xOy:

$$T = \xi \cdot l + (1+l) = t + z_0;\ l = L/2R;\ |\xi| \le 1;$$

$$X = \eta \cdot l + (1+l);\ |\eta| \le 1;$$

here z_0 is zero of local coordinate system, connected with the crack of a length L, i=√-1.

The cores R(T,X) and S(T,X) of the equation (1) are included into [7], and the 1st part is:

$$P(X) = p_+ - 2p_- \mathrm{Re}\left(\frac{1}{X^2}\right) + \left[(\sigma_0 + p_+)\cdot\frac{1}{\overline{X}^2} + p_+\cdot\left(2\cdot\frac{X}{\overline{X}^3} - 1 - 3\cdot\frac{1}{\overline{X}^4}\right)\right].$$

Where

$$p_+ = \frac{\sigma_{max} + \sigma_{min}}{2};\ p_- = \frac{\sigma_{max} - \sigma_{min}}{2}.$$

The unknown function g'(t) is proportional to the derivative from displacement discontinuity:

$$\frac{d}{dt}\left[(u+iv)^+ - (u+iv)^-\right] = i\cdot\frac{4(1-\upsilon^2)}{E}\cdot g'(t), \qquad (2)$$

where E – is the coefficient of elasticity, υ is the Poisson ratio, u and v are horizontal and vertical crack edges displacement in the local coordinate system, connected with them. Signs "+" and "-" near the brackets mean upper and lower crack edges respectively.

The algorithm of equations (1) numerical calculation is described in detail in [7]. As additional condition the finitude of crack edges displacement discontinuity on the hole outline is taken. Using the linearity of problems we get the expression for the intensity coefficient of stress K_1 as:

$$K_1 = \sigma_{max}\cdot\sqrt{L}\cdot A\left(\alpha, L/R\right) + \sigma_0\cdot\sqrt{L}\cdot B\left(L/R\right);$$

Where numerical factors A(α,L/R), B(L/R) are the result of additional problems solution (I, II). The value σ_0, which is necessary to open the closed fractures for the length L are found from the condition $K_1 \ge 0$ and are determined by the equation:

$$\frac{\sigma_0}{\sigma_{max}}\left(\alpha, L/R\right) = \frac{\sigma_0}{\sigma_*}\cdot\frac{\sigma_*}{\sigma_{max}} = \overline{\sigma_0}\cdot\frac{1}{(3\alpha-1)} = -\frac{A\left(\alpha, L/R\right)}{B\left(L/R\right)}.$$

This value σ_0 is presented in (3) and we get the numerical solution of the original problem, with the help of which the open fracture profile can be calculated including $[v]_A$, that is the coefficient of normal fracture opening on the hole outline. As displacement discontinuities in the tip of the crack $[u]_B=[v]_B=0$ (fig. 1), then if we integrate (2) from A to B and use Gaussian quadratures [8], we get:

$$[u]_A + i[v]_A = -i\frac{4(1-\upsilon^2)}{E}\cdot\int_{-l}^{l} g'(t)dt = -i\frac{4(1-\upsilon^2)\cdot\sigma_{max}}{E}\cdot l\cdot\int_{-1}^{1}\frac{\varphi(\xi)d\xi}{\sqrt{1-\xi^2}} = -i\frac{4(1-\upsilon^2)}{E}\cdot\sigma_{max}\cdot l\cdot\frac{\pi}{n}\cdot\sum_{k=1}^{n}\varphi(\xi_k).$$

Where $\varphi(\xi_k)$, are values of numerical solution in nodal points:

$$\xi_k = \cos\frac{\pi(2k-1)}{2n};\ (k = \overline{1,n});$$

(n - determines the odder of the solution approximation). Dividing the real and supposed parts of the formula we come to the equation:

$$[v]_A = -\frac{4\cdot(1-\upsilon^2)}{E}\cdot\sigma_{max}\cdot l\cdot\frac{\pi}{n}\cdot\sum_{k=1}^{n}\mathrm{Re}[\varphi(\xi_k)].$$

Thus we have the dependence of normal fracture opening on the hole outline $[v]_A$ on the mechanical constants E, υ, values σ_{max}, σ_0 and fracture length L. Also the dependences

$\overline{\sigma_0}\left(\alpha, L/R\right)$, $[v]_A(\alpha,L/R)$ и $[v]_A(\alpha, \overline{\sigma_0})$ for different $\alpha=\sigma_{max}/\sigma_{min}=0.5?1$ were found.

Let's introduce non-dimensional fracture opening on the hole outline:

$$\overline{[v]} = \overline{[v]}\left(\alpha, \overline{\sigma_0}\right) = \frac{[v]_A \cdot E}{4(1-\upsilon^2)\cdot \sigma_{\max} \cdot R}$$

For which the approximate formulas are produced:

$$\overline{[v]} = \beta_0(\alpha) + \beta_1(\alpha)\cdot\overline{\sigma_0} + \beta_2(\alpha)\cdot\overline{\sigma_0}^2 + \\ + \beta_3(\alpha)\cdot\overline{\sigma_0}^3 = \sum_{k=0}^{3}\beta_k(\alpha)\cdot\overline{\sigma_0}^k$$

for different α and having $\overline{\sigma_0}$ =1?4, which are depicted in the fig. 2.

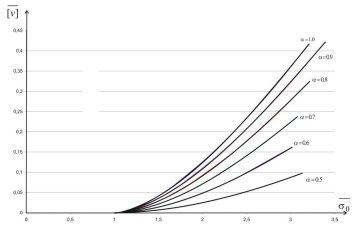

Fig. 2. Dependence of $\overline{[v]}$ on $\overline{\sigma_0}$ received from numerical modeling

Numerical calculation are carried out, showing the influence of stress acting along cracks σ_{max} on fracture opening on the borehole outline. The parameter of "cross-section area change dependence of probe pressure"-ζ, allows to determine stress state. By the way there is no P_s in the calculation model. The fracture opening on the borehole outline has a considerable influence on ζ. This allows to determine $\alpha= \sigma_{min}/\sigma_{max}$. Stress distribution calculation are carried out in the area close to borehole outline and to fracture (Fig. 2a). These calculations are made for two cases: σ_{max}=0,7 σ_{min} and σ_{max}=0. The change of stress distribution σ_{xx} is examined with the increase of the fracture length. The parameter σ_{max} has a significant influence on stress distribution in the area next to the fracture mouth – directly on the borehole wall. The existence of this dependence gives the opportunity to the parameter ζ in calculations stress measurement.

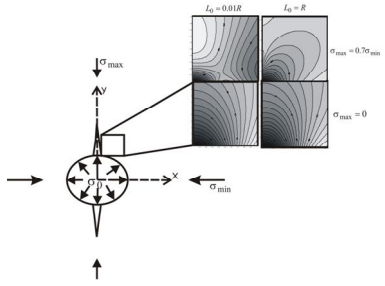

Fig. 2a. Stress distribution close to borehole outline and to fracture

III. THE ALGORITHM OF EXTERNAL FIELD PARAMETERS DETERMINATION

Using the received dependence the algorithm of external field parameters determination is proposed. The data receives from field experiments are given by the diagrams "pressure-volume". The total area of the deformed hole with $\overline{\sigma_0}>1$ will be written as:

$$S = S_{el} + {}_{\Delta}S_m$$

When the pressure in the hole is $\overline{\sigma_0}\in(1-4)$ ($\overline{\sigma_0}>1$), as a result of fracture opening cross sectional area of borehole gets the change:

$${}_{\Delta}S \approx 2\cdot[v]_A \cdot R = \pi R^2 \cdot \frac{8(1-\upsilon^2)}{\pi}\cdot\frac{\sigma_{\max}}{E}\cdot\overline{[v]}$$

Under the action of external field and the pressure in hole it turns into the elliptical one with semi axis:

$$a = R\left[1+\frac{\sigma_{\max}}{E}((1+\upsilon)\cdot\overline{\sigma_0}\cdot(3\alpha-1)+(1-\upsilon^2)\cdot(1-3\alpha)\right];$$
$$b = R\left[1+\frac{\sigma_{\max}}{E}((1+\upsilon)\cdot\overline{\sigma_0}\cdot(3\alpha-1)-(1-\upsilon^2)\cdot(3-\alpha)\right].$$

And its area will be:

$$S_{el} = \pi ab \approx \pi R^2 \cdot \\ \cdot\left[1+\frac{2\sigma_{\max}}{E}((1+\upsilon)\overline{\sigma_0}\cdot(3\alpha-1)-(1-\upsilon^2)\cdot(1+\alpha))\right]$$

Thus the total area can be marked as:

$$S = S_{el} + {}_{\Delta}S_f = \pi R^2\{1+\frac{2\sigma_{\max}}{E}((1+\upsilon)\cdot\overline{\sigma_0}\cdot(3\alpha-1)- \\ -(1-\upsilon^2)(1+\alpha)+\frac{4(1-\upsilon^2)}{\pi}\cdot\overline{[v]})\}$$

Let us show how to find σ_{max}, σ_{min} by using the results of calculations. The general diagram form of the equipment volume change V from $\overline{\sigma_0}$ is shown in the fig.3. In the section *OA* the equipment filling by fluid occurs. Therefore the volume V_0 with $\overline{\sigma_0}$ is:

$$V_0 = \pi R^2 h\left[1-\frac{2\sigma_{\max}}{E}\cdot(1-\upsilon^2)\cdot(1+\alpha)\right].$$

Let's examine the volumetric gain $\Delta V=\Delta V_1+\Delta V_m$, which results from the pressure action $\overline{\sigma_0}$ (ΔV_1 - линия AD) and fracture opening (ΔV_m with $\overline{\sigma_0}>1$):

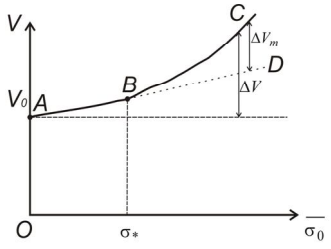

Fig. 3. Form of the received experimental curve

$$\Delta V = \Delta V_1 + \Delta V_m =$$
$$= \pi R^2 h \frac{2\sigma_{\max}}{E} \cdot (1+\upsilon)\left[\overline{\sigma_0} \cdot (3\alpha - 1) + \frac{4 \cdot (1-\upsilon)}{\pi} \cdot \overline{[v]}\right] =$$
$$= A_0 \cdot \sigma_* \left[\overline{\sigma_0} \cdot (3\alpha - 1) + \frac{4 \cdot (1-\upsilon)}{\pi(3\alpha - 1)} \cdot \overline{[v]}\right]$$

Where

$$A_0 = \pi R^2 h \frac{2}{E} \cdot (1+\upsilon)$$

is the slope ratio of *AD*. The inclination of this right line is easily determined. So if h=20cm, measuring the volume in cm^3, and E in mPa (mega Pascal), we get β is an angle of dip of the line *AD* to the horizontal axe, which is equal to ≈15?. We should remark that pitch angles of curves $\overline{[v]} = \overline{[v]}(\alpha, \sigma_0)$ are differentiated according to α (fig. 2). The same we can say about ΔV_m. This allows to find α and σ_* by the following algorithm. Let's examine the dependence $\Delta V_0(\overline{\sigma_0})$ received as a result of the experiment (fig. 4). as the angle β≈15? then one can distinguish ΔV_{0m} with $\sigma_i > \sigma_*$.

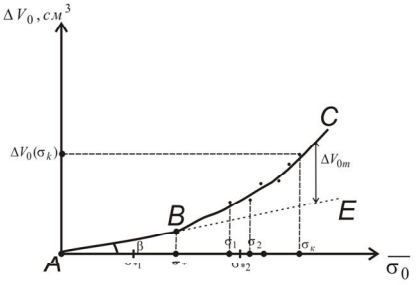

Fig. 4. Algorithm of σ* and α. determination

The true meaning σ_* is not distinguished, it is in the interval (σ_{*1}, σ_{*2}) Let's choose $\sigma_i > \sigma_*$ (i=1?k) and the volumes $\Delta V_0(\sigma_i)$ and $\Delta V_{0m}(\sigma_i)$ respectively. As true σ_* we take that whereby the function:

$$F_1(\alpha, \sigma_*) = \sum_{i=1}^{k-1}\left[\frac{\Delta V_m(S_k)}{\Delta V_m(S_i)} - \frac{\Delta V_{0m}(\sigma_k)}{\Delta V_{0m}(\sigma_i)}\right]^2,$$

achieves the minimum with α=0.5?1 and $\sigma_* = \sigma_{*1}$?σ_{*2}. Using the found σ* the squared deviation is calculated:

$$F_2(\alpha, \sigma_*) = \sum_{i=1}^{k}\left[\Delta V(S_i) - \Delta V_0(\sigma_i)\right]^2.$$

with different α. As α the value whereby this function have a minimum is chosen.

IV. The scheme of the performance of the experiment

The suggested method includes two stages. Preliminary stage is the producing of two symmetrical linear cracks by classical straddle packer probe. Using of high speed rate of fluid injection into isolated borehole interval. High speed injection is carried out using an electric pump or hydropneumatic accumulator. They are placed into a borehole next to an examined borehole interval for the hardening the working system. At the second (basic) stage an instrument with an isolated cover, which prevents the leak-off into the rock, is placed into the interval with already created stretched crack. The fracture reopening pressure P_r is fixed as in the method of double fracture. As an additional parameter one suggests to use the crack opening at the borehole outline during loading dependence on $\alpha = \sigma_{min}/\sigma_{max}$. The determination of maximum compressive stress is also carried out by the impression packer [9]. This method allows the monitoring of the rock mass state, as the crack is formed at a preliminary stage of measurements. During the loading of the borehole interval there will be elastic deformation, induced by injection into the change of cross-sectional area. These deformations are taken into accounts in the course of the solution with fracture opening on borehole outline. The magnitudes of cross-sectional area change of the borehole induced by fracture opening and elastic deformations are equals.

Conclusions

The method of the rock stress measurement based on the integrated use of hydraulic fracturing and of elastic deformations was suggested. The numerical modeling showed that the fracture opening on the borehole outline depends on relations of maximum and minimum stress in the rock mass. The advantage of the method is that the crack of hydraulic fracture as a system measuring element is created once. As a result the method could be used for a continuous monitoring of state change in the chosen point of rock mass in the process of field exploitation.

References

[1] Hayashi, K., T. Ito, H. Abe. In situ stress determination by hydraulic fracturing – A method employing an artificial notch. Int. J. Rock Mech. Min. Sci. & Geomech. Abstr. Vol. 26, pp. 197-202, 1989

[2] Zoback, M.D. & Rummel, F. & Jung, R. & Raleigh C.B. Laboratory hydraulic fracturing experiments in intact and pre-fractured rock. Int. J. Rock Mech. Min. Sci. and Geomech. Abstr.; 14:49-58, 1977.

[3] Stephansson O. Rock stress measurement by sleeve fracturing. In: Proceedings of the Fifth Cong. International Society of Rock Mechanics, Melbourne, vol. F. Rotterdam: A.A. Balkema, p. F.129-37, 1983.

[4] Amadei, B. & Stephansson, O. Rock stress and its measurement, 1st ed. London: Chapman & Hall, 1997.

[5] Charsley, A.D. & Martin, C.D. Sleeve-fracturing limitations for measuring in situ stress in anisotropic stress environment, Int. J. Rock Mech. Min. Sci. & Geomech. Abstr. Vol.40, pp. 127 – 136, 2003.

[6] Pavlov, V.A. & Yankayte, A.V. & Serdyukov, S.V. The development of hydraulic fracturing for the estimation of stress state of permeable rock [in Russian]. Mining informational and analitival bulletin (scientific and technical journal) № 12, 2009.

[7] Savruk, M.P. 2D Elastic Problems for Bodies with Fractures [in Russian], Naukova Dumka, Kiev, 1981.

[8] Panasyk, V.V. & Savruk, M.P. & Dacyshin, A.P. Stress distribution around crack in the plate and envelope [in Russian], Naukova Dumka, Kiev, 1976.

[9] Anderson, T.O. & Stahl, E.J. A study of induced fracturing using an instrumental approach, JPT (Feb. 1967) pp. 261-67; Trans., AIME, 240, 1967.

2011 International Conference on Mechanical, Industrial, and Manufacturing Engineering
Lecture Notes in Information Technology Vols. 1-2

Preparation and thermoelectric properties of Bi_2Te_3/Polythiophene nanocomposite materials*

Yong Du[1,2], Kefeng Cai[1] and Zhen Qin[1]
[1]*Functional Materials Research Laboratory*
Tongji University
1239 Siping Road, Shanghai 200092,China
kfcai@ tongji.edu.cn duyong212@163.com

Shirley Zhiqi Shen[2] and Philip S. Casey[2]
[2]*Materials Science and Engineering Division*
CSIRO
Private Bag 33, Clayton South, 3169, Victoria, Australia
Shirley.Shen@csiro.au

***Abstract* - Bi$_2$Te$_3$/Polythiophene (PTH) thermoelectric bulk nanocomposite materials were prepared by a two-step method. First, Bi$_2$Te$_3$ and PTH nanopowders were prepared by hydrothermal synthesis and chemical oxidative polymerization, respectively. Second, the mixture of the Bi$_2$Te$_3$ and PTH nanopowders was pressed under 80 MPa in vacuum at various temperatures.**

In this paper, Bi$_2$Te$_3$/PTH (50:50 wt) bulk nanocomposites hot pressed at 623 K were investigated. The electrical conductivity of the material is ~ 800 Sm^{-1}, which is several orders of magnitude larger than that of pure PTH. The Seebeck coefficient is ~ -46 μV/K, indicating n-type conduction, which agrees with the Hall effect measurement result. And the power factor is ~ 2.54 μWcm^{-1}K^{-2} at 473 K.

Keywords* - *bismuth telluride; polythiophene; thermoelectric properties; nanocomposite

I. INTRODUCTION

Thermoelectric (TE) device can convert waste heat to electric power using the Seebeck effect and act as cooler by means of the Peltier effect [1]. The conversion efficiency of a TE device is determined by the materials used. Whereas the effectiveness of a TE material is evaluated by a nondimensional figure of merit, ZT ($=\alpha^2\sigma T/\kappa$, where α is the Seebeck coefficient, σ is the electrical conductivity, κ is the thermal conductivity, and T is the absolute temperature) [2]. So, it is necessary to optimize these parameters simultaneously [3]. However, the α, σ, and κ are interdependent—changing one alters the others, making optimization extremely difficult [4]. Up to now, most researches in thermoelectrics are focused on inorganic semiconducting materials. However, the relatively high cost and poor processbility of the state-of-the-art inorganic semiconducting TE materials impede their widely applications.

Compared with inorganic TE materials, organic conducting polymers, mainly including polyacetylene [5], polyaniline [6, 7], polypyrrole [8], PTH [9] and their derivatives [10], possess unique features for potential applications as TE materials because of their low density, low cost, easy synthesis, and facile processing into versatile forms. Furthermore, polymers inherently possess low thermal conductivity. Therefore, to synthesize inorganic-polymer composites may be an effective strategy to achieve improved TE performance by combining the advantages of each component. To the best of our knowledge, no research on TE properties of Bi_2Te_3/PTH nanocomposite materials has been reported yet. The bulk Bi_2Te_3/PTH nanocomposite materials have been prepared through a hot pressing method at various temperatures. In this paper, the TE properties of Bi_2Te_3/PTH nanocomposite materials pressed at room temperature (RT) and hot pressed at 623 K were investigated.

II. EXPERIMENTAL

All chemical reagents used were of analytical grade.

A. Synthesis of Bi_2Te_3 nanopowders

About 60 ml deionized water was added into a Teflon-lined 100 ml autoclave, and appropriate amounts of $Bi(NO_3)_3\cdot 5H_2O$, $C_4H_4Na_2O_6\cdot 2H_2O$, TeO_2, KOH and KBH_4 were put into the autoclave sequentially, and then some deionized water was added until 80% of the volume of the autoclave was filled. The autoclave was sealed and maintained at 180 ^oC for 24 h and then naturally cooled to RT. The product was washed with deionized water and pure ethanol in sequence for several times then filtered. Finally the dark product was dried in vacuum.

B. Synthesis of PTH

A solution of 0.648 g (4 mmole) of anhydrous iron (III) chloride in 50 ml $CHCl_3$ was added dropwisely into a solution that was prepared by dissolving 0.084 g (1 mmole) of thiophene in 50 ml of $CHCl_3$. The reaction was stirred and kept at RT for 12 hours. The polymer was isolated by precipitation with 300 ml methanol, after that 1 M HCl was added (stirred 12 hours). The product was washed with 1 M HCl for several times until the filtrate become colorless, and then dried in vacuum.

C. Preparation of Bi_2Te_3/PTH bulk TE materials

The as-synthesized Bi_2Te_3, PTH powders were mixed according to 50:50 wt in an agate mortar for 1 h. The mixed powders were pressed in a graphite die (10 cm in diameter) at 80 MPa for 60 min at various temperatures under vacuum.

The phase structure of the hydrothermally synthesized powder, cold pressed and hot-pressed samples was examined by X-ray diffraction (XRD, Bruker D8 Advance), with Cu Kα radiation (λ = 1.5406 Å). The morphology of the powders

* This work are supported by National Natural Science Foundation of China #50872095, 973 Program #2007CB607500 to K.F.Cai and China Scholarship Council to Yong Du's study at CSIRO.

was observed by transmission electron microscopy (TEM, Philips TECNAI-20). The fracture surface and the composition of the hot pressed samples were examined by field emission scanning electron microscopy (FE-SEM, Quanta 200 FEG) equipped with energy dispersive X-ray spectrometry.

The Hall effect of the bulk Bi_2Te_3/PTH nanocomposite samples was measured using HMS-3000 (Ecopia) at RT with a magnetic field of 0.55 T, and then the samples were cut into rectangular pieces (~ 8 mm × 1 mm × 2 mm) for electrical transport property measurement from 298 to 473 K along the direction perpendicular to the hot pressing direction. The Seebeck coefficient was determined by the slope of the linear relationship between the thermoelectromotive force and temperature difference (~ 10 K) between the two ends of the sample. Electrical conductivity measurement was performed using a steady-state four-probe technique with a square wave current (~ 10 mA in amplitude).

III. Results and Discussion

It is clearly seen from the TEM image (Fig.1) of the as-prepared Bi_2Te_3 nanopowders via hydrothermal process that there are two morphologies of the powders (nanorods and hexagonal nanosheets). The sizes of the nanorods is ~ 40 nm in diameter and ~ 100 to 200 nm in length, and the size of the hexagonal nanosheets is (~100- 200 nm big with thickness <30 nm). The as-prepared PTH nanopowders are spherical with average diameter of ~ 200 nm.

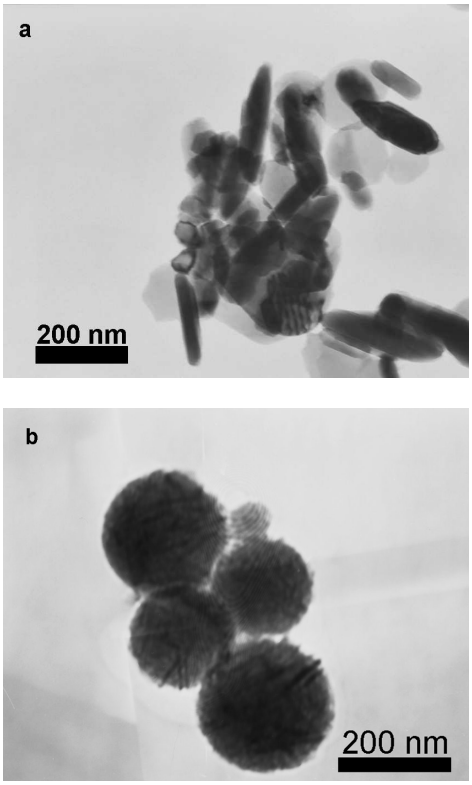

Fig. 1 TEM images of the Bi_2Te_3 nanopowders prepared by the hydrothermal synthesis method (a) and PTH prepared by the chemical oxidative polymerization (b)

Figs. 2b and d show the XRD patterns of the hydrothermal synthesized Bi_2Te_3 nanopowders and the Bi_2Te_3/PTH nanocomposite material pressed at 623 K, respectively. The pattern of PTH is not shown in the figure since the PTH is amorphous. All the peaks in Fig. 2 b can be indexed to rhombohedral Bi_2Te_3 (JCPDS card file, No 15-0863) with space group: R-3m (166). No impurity peaks are observed, indicating the hydrothermally synthesized Bi_2Te_3 powders with high purity. Based on Scherrer's formula $L = K\lambda/(\beta \cos\theta)$ (L is the grain size, K a constant, λ the X-ray wavelength, β the half width of the diffraction peak), the average grain size of the Bi_2Te_3 nanopowders is estimated to be about 48 nm. This agrees with the TEM observation results.

The rhombohedral Bi_2Te_2S (JCPDS card file, No 09-0447) with pace group: R-3m (166) was formed when the sintered temperature reached ~ 623 K. The reason might be that the PTH underwent a decomposition when the temperature was higher than 523 K [11], which produced :S free radical and • SH free radical. Therefore, the sulphur reacted with Bi_2Te_3 to form the single phase materials Bi_2Te_2S [12].

Fig. 3 shows the FTIR spectra of the Bi_2Te_3/PTH composite and PTH. It is seen from the Fig. 3 that the two spectra are similar only the peak positions with slight shift. For instance, the peaks at 3434, 2918 and 2368 cm^{-1} attributed to C–H stretching vibrations in PTH are shifted to 3435, 2918 and 2369 cm^{-1} in Bi_2Te_3/PTH composite; the absorption peaks at 784 cm^{-1} and 694 cm^{-1} due to C–H out of plane stretching vibration and C–S bending mode in PTH appear at 782 cm^{-1} and 691 cm^{-1}, respectively in Bi_2Te_3/PTH composite [11]; the absorption peak at 1033 cm^{-1} attributed to the in-plane C–H aromatic bending vibrations in PTH has been observed at 1031 cm^{-1} in Bi_2Te_3/PTH composite; the absorption peaks at 1654, 1437 cm^{-1} due to C=C stretching vibration in pure PTH and C=C stretching vibration of the PTH ring have shifted the most to 1637 cm^{-1} and 1459 cm^{-1} in the composite. The reason might be that the PTH underwent a partially decomposition and the insertion of Bi_2Te_3 in the polymer matrix.

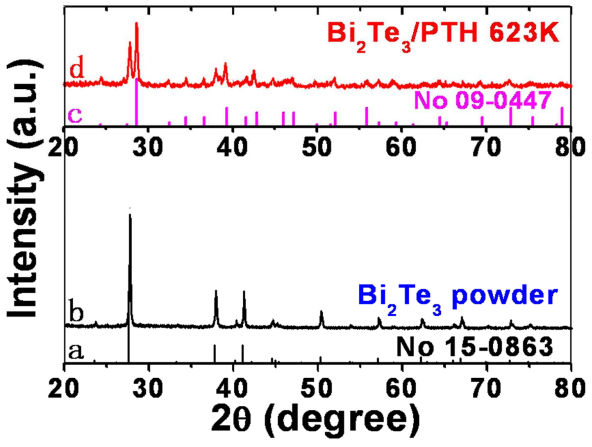

Fig. 2 XRD patterns of (a) Bi_2Te_3, JCPDS card file, No 15-0863, (b) hydrothermal synthesized Bi_2Te_3 nanopowders, (c) Bi_2Te_2S(JCPDS card file, No 09-0447) and (d) Bi_2Te_3/PTH nanocomposite materials pressed at 623 K

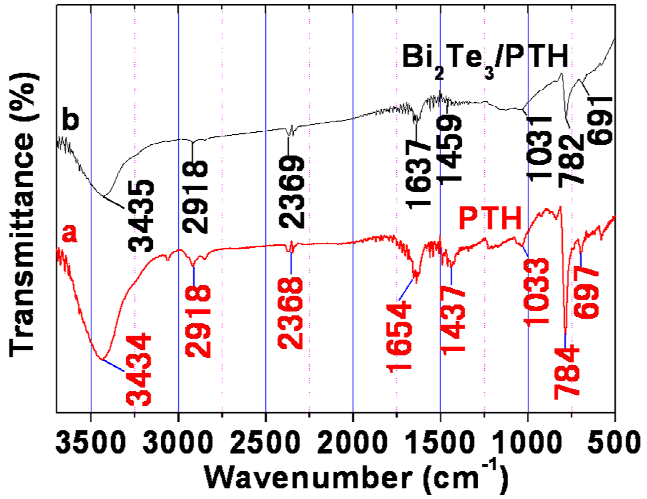

Fig. 3 FTIR spectra of (a) PTH prepared, (b) Bi_2Te_3/PTH nanocomposite hot pressed at 623 K

FESEM images of the fracture surface of the hot pressed sample are shown in Fig. 4 (a). The microstructure of the sample is aligned approximately perpendicular to the pressing direction and inhomogeneous. EDS analysis reveals that the darker contrast district in the FESEM image of the sample contains C, S and Cl with an atomic ratio of C: S = 7.72: 1, which deviates somewhat from the composition of PTH due to the PTH was partially decomposed. While the lighter contrast area contains C, S, Cl, Bi and Te, and the total mass fraction of C, S, Cl is much less than 50%, which deviates somewhat from the nominal composition (50:50 wt). This also implies that the PTH was partially decomposed. The atomic ratio of Bi: Te = 2.25:3, C: S = 5.3: 1, respectively. This indicates that this region is rich in Bi and that the content of S element is much higher than the darker contrast district. This should be because some S was doped into Bi_2Te_3 [13]. Note that there is Cl at both regions due to the sample was doped by HCl.

Table 1 lists the σ, carrier concentration, mobility and Hall coefficient of the samples measured by at Hall effect measurement RT.

Fig. 5 (a) and (b) show the temperature dependence of σ, α and power factor of the sample. The σ of the composite at RT is several orders of magnitude larger than that of PTH reported in Ref. [11]. The $|\alpha|$ at RT is much lower than that of PTH reported in Ref. [14] (~ 130 μV/K). The α of the sample is negative in all the temperature range measured, indicating n-type conduction, which agrees with the Hall effect measurement. As the temperature increases, the σ first slowly decreases and then increases gradually, while the temperature dependence of $|\alpha|$ is roughly opposite to that of the σ. When T < 325 K, the power factor slowly decreases, then increases with the temperature increasing. A maximum power factor reaches ~ 2.54 μWcm^{-1}K^{-2} at ~ 473 K. As low thermal conductivity of the sample can be expected, a high ZT value of the sample can be expected.

Table 1 RT electrical conductivity(σ), carrier concentration (n), mobility (μ_H) and Hall coefficient (R_H) of the sample hot pressed at 623 K

σ(S /cm)	n/cm^{-3}	μ_H/(cm^{2}V^{-1}s^{-1})	R_H/(cm^3/C)
5.843	6.46×10^{17}	56.46	-9.633

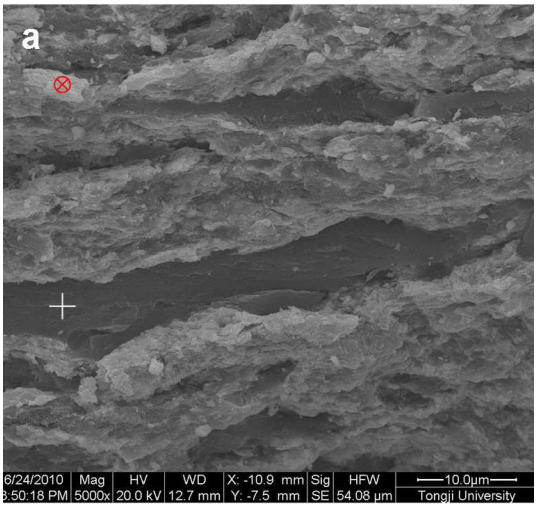

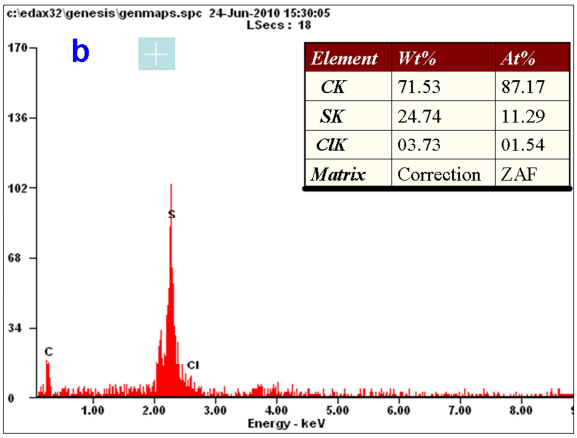

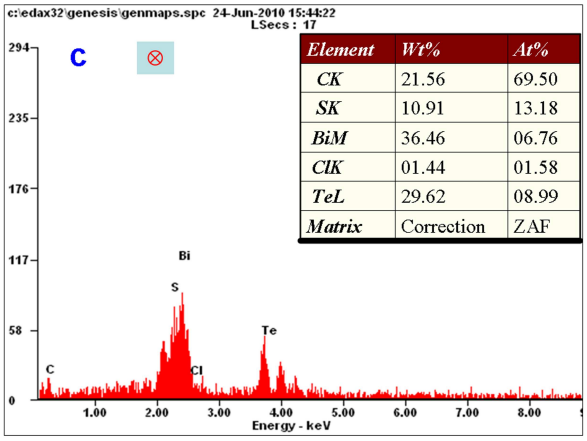

Fig. 4 FESEM images (a) of the fracture surface along the direction parallel to the hot pressing direction of the sample, and (b), (c) EDS spectra recorded on the darker and lighter contrast districts

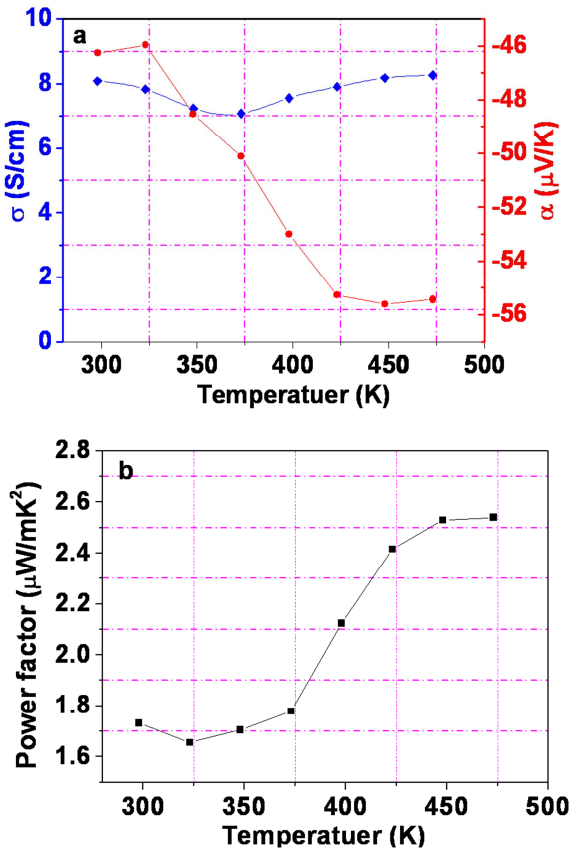

Fig. 5 Temperature dependence of (a) electrical conductivity and Seebeck coefficient, and (b) power factor of the sample pressed at 623 K

IV. Conclusion

Pure Bi_2Te_3 and PTH nanopowders were successfully synthesized by hydrothermal synthesis method and chemical oxidative polymerization, respectively, and bulk nanostructured Bi_2Te_3/PTH composites have been prepared by hot pressing the mixed nanopowders. The sample pressed at 623K under 80 MPa has a high σ and α, with a maximum power factor of ~ 2.54 $\mu Wcm^{-1}K^{-2}$ at ~ 473 K. This preparation route to produce inorganic-polymer TE materials is low-cost, high efficiency, and promising.

References

[1] H. Ohta, S. Kim, Y. Mune, T. Mizoguchi, K. Nomura, S. Ohta, T. Nomura, Y. Nakanishi, Y. Ikuhara, M. Hirano, H. Hosono, and K. Koumoto, "Giant thermoelectric Seebeck coefficient of a two-dimensional electron gas in SrTiO3," *Nat Mater*, vol. 6, pp. 129-34, 2007 Feb (Epub 2007 Jan 2007.

[2] K. F. Hsu, S. Loo, F. Guo, W. Chen, J. S. Dyck, C. Uher, T. Hogan, E. K. Polychroniadis, and M. G. Kanatzidis, "Cubic AgPb(m)SbTe(2+m): bulk thermoelectric materials with high figure of merit," *Science*, vol. 303, pp. 818-21, 2004 Feb 2004.

[3] L. E. Bell, "Cooling, heating, generating power, and recovering waste heat with thermoelectric systems," *Science*, vol. 321, pp. 1457-61, 2008 Sep 2008.

[4] A. Majumdar, "Materials science. Thermoelectricity in semiconductor nanostructures," *Science*, vol. 303, pp. 777-8, 2004 Feb 2004.

[5] M. Reghu, C. O. Yoon, C. Y. Yang, D. Moses, A. J. Heeger, and Y. Cao, "Superlocalization of the Electronic Wave-Functions in Conductive Polymer Blends at Concentrations near the Percolation-Threshold," *Macromolecules*, vol. 26, pp. 7245-7249, Dec 1993.

[6] N. Mateeva, H. Niculescu, J. Schlenoff, and L. R. Testardi, "Correlation of Seebeck coefficient and electric conductivity in polyaniline and polypyrrole," *Journal of Applied Physics*, vol. 83, pp. 3111-3117, Mar 1998.

[7] X. B. Zhao, S. H. Hu, M. J. Zhao, and T. J. Zhu, "Thermoelectric properties of Bi0.5Sb1.5Te3/polyaniline hybrids prepared by mechanical blending," *Materials Letters*, vol. 52, pp. 147-149, Jan 2002.

[8] E. Hu, A. Kaynak, and Y. C. Li, "Development of a cooling fabric from conducting polymer coated fibres: Proof of concept," *Synthetic Metals*, vol. 150, pp. 139-143, Apr 2005.

[9] X. Gao, K. Uehara, D. D. Klug, S. Patchkovskii, J. S. Tse, and T. M. Tritt, "Theoretical studies on the thermopower of semiconductors and low-band-gap crystalline polymers," *Physical Review B*, vol. 72, p. 7, Sep 2005.

[10] D. Kim, Y. Kim, K. Choi, J. C. Grunlan, and C. H. Yu, "Improved Thermoelectric Behavior of Nanotube-Filled Polymer Composites with Poly(3,4-ethylenedioxythiophene) Poly(styrenesulfonate)," *Acs Nano*, vol. 4, pp. 513-523, Jan.

[11] K. Majid, R. Tabassum, A. F. Shah, S. Ahmad, and M. L. Singla, "Comparative study of synthesis, characterization and electric properties of polypyrrole and polythiophene composites with tellurium oxide," *Journal of Materials Science-Materials in Electronics*, vol. 20, pp. 958-966, Oct 2009.

[12] O. Y. Plotinskaya, F. Damian, V. Y. Prokofiev, V. A. Kovalenker, and G. Damian, "TELLURIDES OCCURRENCES IN THE BAIA MARE REGION, ROMANIA," *Carpathian Journal of Earth and Environmental Sciences*, vol. 4, pp. 89-100, Oct 2009.

[13] D. C. Grauer, Y. S. Hor, A. J. Williams, and R. J. Cava, "Thermoelectric properties of the tetradymite-type Bi_2Te_2S-Sb_2Te_2S solid solution," *Materials Research Bulletin*, vol. 44, pp. 1926-1929, Sep 2009.

[14] Y. Bao, C. C. Liu, S. Lu, J. K. Xu, F. X. Jiang, Y. Z. Li, and Z. Zhang, "Thermoelectric Performances of Free-Standing Polythiophene and Poly(3-Methylthiophene) Nanofilms," *Chinese Physics Letters*, vol. 27, p. 4, May.

2011 International Conference on Mechanical, Industrial, and Manufacturing Engineering
Lecture Notes in Information Technology Vols. 1-2

Dynamic Response Analysis of Temporarily Installed Suspended Access Equipment

Xijian Zheng, Zhen Lu, Zeguang Han, Xingliang Gao
School of transportation & Mechanical Engineering
Shenyang Jianzhu University,
Shenyang, 110168, CHINA
xijianzheng@sina.com, luzhen1983@126.com,
hanzeguang1@163.com, xinglianggao@163.com

***Abstract* - This paper analyzes the dynamic response of temporarily installed suspended access equipment at two special conditions as sudden loading and mobile loads, calculates out the impact load at different heights under the condition of sudden loading and establishes structure simplified mechanical model and analysis plan under the condition of mobile loads. Finite element method is adopt to obtain dynamic response of the whole structure, and the stress and displacement response curves of key points. With the analysis of above results, measure to reduce hoisting impact load is put forward, which provides certain basis for the further standardization of operation of temporarily installed suspended access equipment and the improvement of structure design.**

Index Terms* - *Temporarily installed suspended access equipment; Sudden loading; Moving load; Finite element method(FEM)

I. INTRODUCTION

Temporarily installed suspended access equipment is a kind of special aerial equipment, which is more and more widely used in decoration, cleaning, maintenance and construction of high-rise buildings wall. Putting weight into aerial platform, especially by free falling, will lead to impact effect when platform is at aerial working condition. The impact load reduces quickly, but the dynamic response caused by is very remarkable in short time and can not be ignored [1]. As a result, the dynamic response is usually taken as criterion to check structure strength. Transient vibration effect is accordingly becoming the most important aspect of dynamics research of temporarily installed suspended access equipment. In this paper, two special working conditions of temporarily installed suspended access equipment are taken into consideration, adding weight suddenly and taking mobile loads. Finite element method is adopt to get strength and stiffness results, dynamic stress and displacement response curves of the whole structure under dynamic load, and measures to reduce the effect of impact load.

A. Impact load calculation for adding weight suddenly

In actual construction process, temporarily installed suspended access equipment is often added loads in the air. It will be have a large dynamic impact load to the suspended platform, if the weight drop-in it with a certain height, and the load transferred from hoist to rope, then to the suspended equipment. This series of reaction would cause damage to the structure of parts under certain conditions, such as the broken of wire rope, suspended equipment deformation and overturn, etc. So, it is necessary to calculate dynamic load in this kind of condition [2].

By the law of conservation of energy, the reduced kinetic energy T and potential energy V during the process that the weight fell into suspension platform should be equal to the increased deformation energy U_d in suspended platform, that is:

$$T+V=U_d \tag{1}$$

Both starting speed and termination speed are zero of the falling weights, so the kinetic energy T is zero, when the displacement of bottom of the suspension platform reaches the maximum δ_d , the potential energy reduced is:

$$V = P\ (\ h + \delta_d) \tag{2}$$

The increased deformation energy of suspension platform is :

$$U_d = \frac{1}{2}\frac{P_d}{\delta_d} = \frac{1}{2}\frac{P}{\delta_j}\delta_d^2 \tag{3}$$

So δ_d can be described by (2) and (3) as:

$$\delta_d = \delta_j + \sqrt{\delta_j^2 + 2\delta_j h} = \delta_j(1+\sqrt{1+\frac{2h}{\delta_j}}) \tag{4}$$

If the quality of suspension platform is considered, so:

$$\delta_d = \delta_j(1+\sqrt{1+\frac{2h}{\delta_j}\frac{P_1}{P_1+P_2}}) \tag{5}$$

Both of them, P_1 is the weight of the object; P_2 is the weight of suspended platform (suspended platform's no-load net weight is 6370N).

By the hooker law knowledge:

$$C = \frac{P}{\delta_j} = \frac{P_d}{\delta_d} \tag{6}$$

So the impact load can be got:

$$P_d = P_j(1+\sqrt{1+\frac{2h}{\delta_j}\frac{P_1}{P_1+P_2}}) \tag{7}$$

When different mass of load was added to the suspended platform, the impact load could be calculated by formula (7), when the object fell from different height. The results were listed in table I.

TABLE I
THE IMPACT LOAD VALUE FOR FALLING FROM DIFFERENT HEIGHT OF THE OBJECT

Object mass(kg)	Impact load of 0.2m height (N)	Impact load of 0.5m height (N)	Impact load of 0.8m height (N)
20	762	1058	1276
50	2294	3279	3997
100	5008	7234	8855
150	7690	11138	13646

B. FEM solving and analysis for the whole structure

As can be seen in fig. 1, it is the object of study - ZLP800 temporarily installed suspended access equipment, its finite element model is established [3]. It has been divided into two conditions for the process of adding load to the suspended platform: (1) Adding weight slowly, (2) Adding weight suddenly. The first kind of conditions， add weight to suspended platform without height, this situation can be considered that there is no impact load of the object to the suspended platform, and can be analyzed by the static. The second, added loads suddenly, this condition becomes free falling movement when the object falls into the suspended platform at a certain height, which produces a certain impact load, this process should be analyzed by the method of transient dynamics [4-5]. In this paper, the finite element analysis software ANSYS which is used widely is applied for solving above two conditions for the structural displacement and stress. The results were listed in table 2, 3.

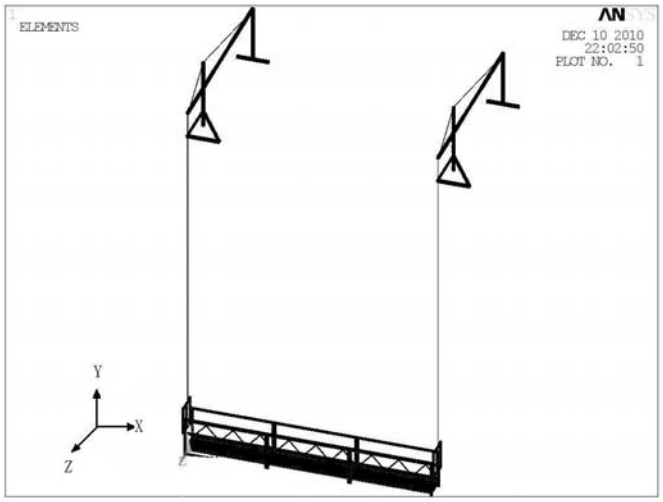

Fig. 1 Finite element model of temporarily installed suspended access equipment

TABLE II
THE STATIC ANALYSIS RESULTS FOR ADDING WEIGH SLOWLY
（DUE TO THE SYMMETRY OF THE STRUCTURE, SO IT CONSIDERED ONLY ONE SIDE OFFSET LOAD）

Object mass (kg)	Dynamic load corresponding (N)	Platform midpoint		Left offset load	
		Max displacement (mm)	Max stress (MPa)	Max displacement (mm)	Max stress (MPa)
20	196	-1.627	20.761	-1.619	21.262
50	490	-2.275	22.098	-2.275	23.353
100	980	-3.356	24.328	-3.453	26.836
150	1470	-4.437	28.218	-4.781	30.32

TABLE III
THE TRANSIENT DYNAMIC ANALYSIS RESULT FOR 0.5m HEIGHT ADDING LOAD SUDDENLY

Object mass (kg)	platform midpoint		Left offset load	
	Max displacement (mm)	Max stress (MPa)	Max displacement (mm)	Max stress (MPa)
20	-2.558	22.549	-1.961	37.934
50	-7.62	60.243	-1.684	71.234
100	-8.89	155.81	-13.003	157.15
150	-17.904	239.90	-24.06	241.97

From the results of table II, table III, it can be known that the influence to structure when adding weights to suspended platform suddenly is more large than adding weights slowly. Take adding loads to the platform suddenly from 0.5m height as the example, when the mass of object increases gradually, the max displacement and max stress of whole machine increases obviously. If the mass of object increases to 150kg, the impact stress coming from sudden loading is 8.5 times larger than slow loading. Its value has also exceeded material's allowable stress (This machine uses the Q235 structural steel, if the safety factor is 2, the allowable stress is 117.5MPa), it is easy for destroying the structure, causes the dangerous accident.

C. Structure FEM analysis under the mobile loads

When the temporarily installed suspended access equipment works in the sky, there are mobile loads on the suspended platform. Mobile loads are a kind of load that the value and the direction hold the line, but the position of load varies continuously. Such as the operating staffs walked in the suspended platform, or carried the stuffs and tools, all of what will cause mobile loads to the suspended platform. There are few persons to research the influence causing by the mobile loads to the whole structure at the present time. There are broad prospects for the structure transient dynamics analysis under the mobile loads in engineering application. The bridges bear the load of the trains, cars, and the walking people, and the crane beams bear the load of goods, all of these were the mobile loads.

Model simplifying and plan building

1) When the mass of mobile things is smaller than that of the platform, the inertia of mobile mass could be ignored, the problem could be simplified to a dynamic response analysis of suspended platform under the mobile loads;

2) To the problem of constant speed mobile loads, impact equivalent load plan was built. As the fig 2, it could be equal to multi-points impact load, force to the finite element model of ZLP800 temporarily installed suspended access equipment, and dynamic response analysis was done to the machine.

3) According to the surroundings of job location, it should be slow when moving in the suspended platform. The setting value of move velocity in this paper is v=0.5m/s, the length of the suspended platform is L=7.5m, and think about the influence of mass change of mobile objects, transient dynamics solving was done to this working condition. The solution results are listed in table IV.

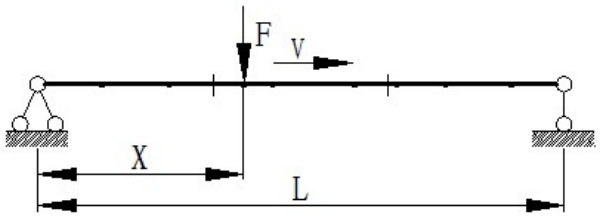

Fig. 2 Simplified model of suspended platform under the mobile loads

TABLE IV
TRANSIENT SOLVING RESULT UNDER DIFFERENT MOBILE LOADS

Different mobile loads(kg)	Max displacement of left suspended point (mm)	Max displacement of right suspended point (mm)	Max stress of left cantilever root segment (MPa)	Max stress of right cantilever root segment (MPa)
65	7.7151	8.1352	16.928	13.61
100	6.4639	6.7195	13.168	19.155
180	6.2016	6.6637	11.348	15.128

It could be known form TABLE IV:

The different mass objects move in the platform at a velocity of 0.5m/s, the displacement and stress of two suspended access equipments changed less, this explains that it has less influence to the structure when objects move in the suspended platform at lower velocity. When move velocity increases, the displacement and stress of suspended access equipment increase too. At the same time, friction force along the opposite direction of velocity on platform comes into being by the mobile objects, the more large velocity, the more large friction force, a stated horizontal force is caught by the friction force, and the suspended platform swings horizontally, what made horizontal load come into being of suspended access equipment. It has gained by calculation: when the velocity of move object in the platform is not more than 2m/s, the whole structure would be safe, and run steadily.

D. Dynamics response graphs of key structure

According to the statics and transient dynamics solving and analysis to the whole machine, the area that load is the largest mainly concentrates the following positions: point of objects falling, suspended point of suspended access equipment, and cantilever root segment. Therefore, node displacement and dynamic stress response graphs of above-mentioned several positions were extracted. As fig.3, fig.4.

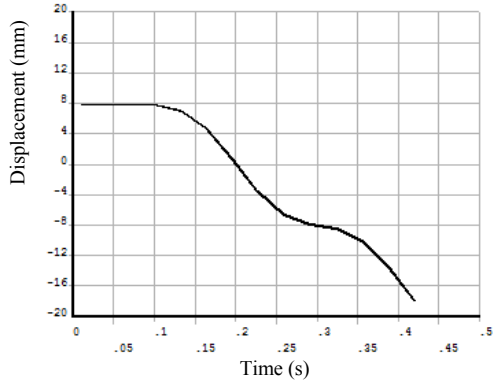

Fig. 3 displacement response graph of 150kg object at the middle of platform

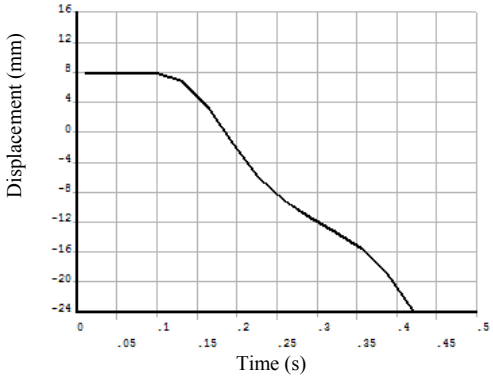

Fig. 4 displacement response graph of 150kg object at the position of left offset load

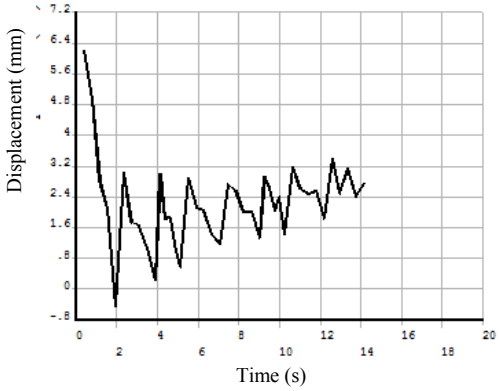

Fig. 5 Displacement response graph of left suspended point under mobile loads

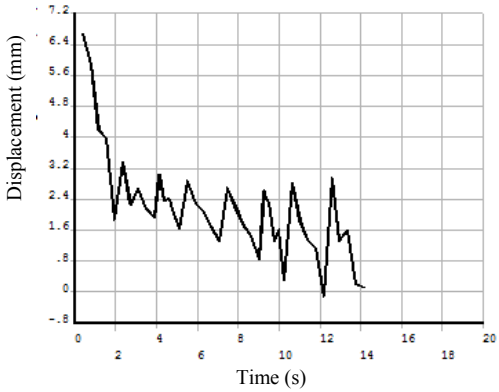

Fig. 6 Displacement response graph of right suspended point under mobile loads

As can be seen from fig.3 and fig.4, with the change of time, the displacement of loading point increased gradually. The max displacement has achieved 24.06mm, the rule of suspended platform maximum distortion in GB19155-2003 could not exceed 1/300 of overall length, which is 25mm [6]. Therefore, the condition of heavy object with a difference in height fell into suspended platform should be avoided. Fig.5 and fig.6 were the displacement response graphs of two suspended points on the suspended access equipment, when suspended platform bore mobile loads with a speed of 0.5m/s. With the move of load point, the displacement of left suspended point decreases gradually, and the displacement of right suspended point increases gradually, as a whole, the

impact to the structure of suspended access equipment is small, the structure would not be destroyed generally.

E. Conclusion

The paper chooses ZLP800 temporarily installed suspended access equipment as the object of study, and the dynamic response of structure in two working conditions was analyzed, the following conclusions were gained:

1) At the time of adding load suddenly to the suspended platform, larger impact load would cause by the object, the value of impact load depended on the mass of object and falling height.

2) The displacement and stress of the structure increases significantly when adding load suddenly, the stress value would exceed allowable stress value of the material under certain conditions, and lead to structure destroy. Therefore, the difference in height of object and platform must be controlled strictly in the process of operation. It is calculated that the difference in height for adding load should not exceed 0.3m, when the mass of object did not exceed 100kg.

3) The mobile loads on the suspended platform mainly influence the suspended access equipment. Knowing from analysis, the influence on suspended access equipment is small with the small move velocity. The influence on the structure could be ignored when the move velocity does not exceed 2m/s.

ACKNOWLEDGMENT

The research in this paper has been supported by National "Eleventh Five-Year" Key Scientific and Technological Plan, 2008BAJ09B02-2. Liaoning Province's Natural Science Funds，20102184.

REFERENCES

[1] Xiaoyan Jiang. Dynamic Analysis of Wire Rope Breaking Accidents in Tower Crane and Hoisting Basket. Petroleum Engineering Construction. Vol. 34 (2008), p. 59-61. In Chinese

[2] Peiwen Huang. Dynamic Load Calculation Method of Mechanical System Vibration[M]. Wuhan: Huazhong Industrial College Press, 1987.5

[3] Zhenfei Xu. Project Application example course of ANSYS Finite Element Method Analysis [M]. Beijing: China Architecture & Building Press,2010.8

[4] Heroyuki Sogo，Dynamic Load Factor of Crowler Crane with a Lifted During Publ[J]. Propelling(1st Report) Proc .Int .Conf. on ATEMH'94 by China Machine Press,1994

[5] Rao S S · The Finite Element Method in Structural Mechanics, Academic Press 1982

[6] GB19155-2003, Suspended Access Equipment. In Chinese

2011 International Conference on Mechanical, Industrial, and Manufacturing Engineering
Lecture Notes in Information Technology Vols. 1-2

Study on classification and application of applicable safety mining conditions of coal seams on the high-risk outburst water*

LIU Yu-de
College of Safety Engineering
North China Institute of Science & Technology
Beijing 101601, China
lydcumt@126.com

YAN Shou-feng
Department of basic courses
North China Institute of Science & Technology
Beijing 101601, China
yansf@ncist.edu.cn

***Abstract*： Safety mining of coal seam on confined water is an urgent problem. We describe briefly current conditions abroad and in China. Based on an Ordovician limestone aquifer with high-risk water outburst seams in the Feicheng coal field, we analyzed the moving law of underlying atrata and the water-resistant characteristics of coal floor aquifuge and the guide-rise rule of press-water synthetically by means of many methods & measures, such as theoretical analyse, physical simulation, numerical calculation etc., and analyzed the rationale and key of coal floor water-inrush. We brought forward the main influence factors and the corresponding formulae, and breakdown-analyzed the mining condition of coal seam above water with "multi-index synthetic analysis method". Consequently, we formed a preliminary classification system of mining condition of coal seam on press-water and took it into the application of engineering practice successfully.**

Index Terms: multi-index synthetic analysis method; physical simulation; FLAC^{3D}; with-pressure coefficient; water-inrush coefficient; "nether Three-Zones" of Floor

Ⅰ. INTRODUCTION

Underground mining will cause redistribution of underground rock stress and cracks in rock masses and will also change the permeability of the surrounding rock. Underground water threatens bottom coal seams in the course of mining and can lead to water invasion of coal floors and mining accidents. About 60 percen of Chinese coal mines in different degrees were affected by pressure water. The damage, from the high pressure water of Ordovician limestone of coal seam bottom, will cause around 40 percent of the coal mining cannot normally. Therefore, it is important to emphasize the value of research in safe mining technology to prevent accidents associated with water outburst in high-risk coal seams.

Foreign scientists have proposed relative coefficients, but many problems are still at the stage of investigation due to the complexity of safe coal mining above confined aquifers [1-5]. Chinese scientists have put forward the concept of a coefficient of water inrush, to represent an assessment criterion of floor stability. Meanwhile, they found the rise of confined aquifers in overlying strata, and several water inrush criteria and theories have been proposed: the water inrush coefficient method, a water inrush critical exponent, the "Down Three Zone" theory, a theory of tension fissure and failure at zero position, a floor strata model theory, a key strata theory, a catastrophe theory, a water-inrush preferred plane theory, etc [6-12]. However, in the aspect of applicable condition classification of aquifer-protective mining there is still much to be done.

We used the coal field of Feicheng as our research object on the water-resistant characteristics or guide-rise characteristics or penetration characteristics of a coal floor and distortion or moving rules of underlying strata, established initially a classification criterion system of emphasizing value in order to prepare for safe mining in water inrush seams.

Ⅱ. GENERAL CONDITIONS OF MINING AREA

The hydrogeological conditions of the Feicheng coal field are very complex. This field is one of the largest water containing mining areas.

The 18 coal seams of Feicheng are permo-carboniferous and are, in total, 14.55 m thick. The primary mineable coal bed is the $3_1^{\#}$ in the Shanxi group and the $7^{\#}$, $8^{\#}$, $9^{\#}$ and $10_2^{\#}$ seams in the Taiyuan group. Fig. 1 shows a coal seam column.

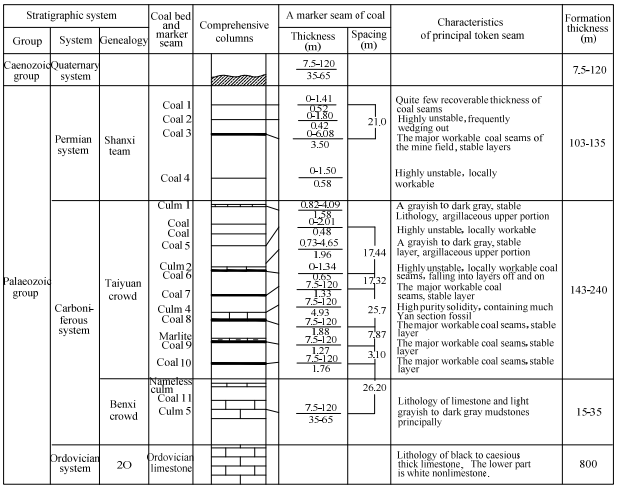

Fig. 1 Hydrogeological column of the Feicheng mining area

The sedimentary stratigraphy in Feicheng is steady and has a monoclinal structure with symphitic sedimentary fractures. The sedimentary fractures cut the stratum with crisscross faults and form a waffle tectonic framework; they also damage the integrity of the batholith, which provides a passageway for the fifth limestone aquifer and the Ordovician water.

* This work is partially supported by Research Fund of North China Institute of Science and Technology (No.A09002).

III. WATER-RESISTING CHARACTERISTICS OF FLOOR STRATA AND MOVING OR DISTORTION RULES

A. Physical experimental analysis of the water-resisting characteristics of floor strata

1) *Experimental equipment* [11-13]: the experimental equipment consists of a model lab, a pressurization and compression-stability system, a device to add water and a data acquisition system, as shown in Fig. 2.

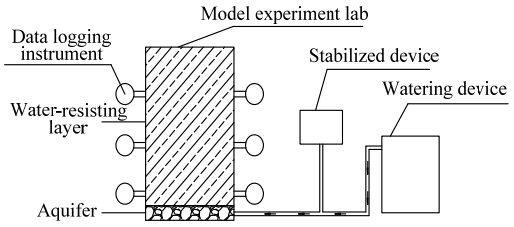

Fig. 2 Frame of experimental devices

2) *Experimental process:* the experimental material consisted mainly of sand, $CaCO_3$ powder and cement, mixed in different proportions. We designed three different schemes, shown in Table 1. Under various levels of water pressures, the experiment was conducted given the three proportions of the ingredients.

Table 1 Experimental schemes

Scheme	Material proportion	Original water pressure (MPa)
I	Sand:$CaCO_3$ powder=3:1	0.0565, 0.059, 0.1, 0.15…
II	Sand:$CaCO_3$ powders=1:1	0.021, 0.036, 0.049, 0.06…
III	Sand:$CaCO_3$ powder:cement=3:3:1	0.1, 0.105, 0.1211, 0.1244…

3) *Analysis*: we obtained the following results:

(a) When the highly confined water rises through the floor aquifuge, the water head loss is related to the characteristics of the rock. The smaller the permeability of the coal seam, the stronger its ability to weaken the water head pressure, as seen in Fig. 3.

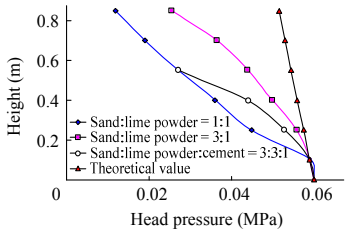

Fig. 3 Relations between rock permeability and water head loss

(b) In the course of the rise in the floor confined water, at the same height, the energy loss of the water head is related to the permeability of the rock. Weak permeability releases more energy from the water head. The following is the equation of the water head loss as a function of the permeability coefficient:

$$\eta = 0.0906e^{-14.969K}$$

Where η stands for rate of water head loss, MPa/m; and K is the permeability coefficient of the rock stratum, m/d.

(c) In the course of the rise in the highly confined water of the coal floor, the loss of the water head pressure, via the zones of dissolution cracks, primary fractures and extended fractures in the water flowing crevices, is caused by the water head loss in the water-resistant floor. When the pressure has declined to a specific value, ththe water can no longer rise and causes the pressure in the water remnant. The height of the rise in the confined water equals the thickness of the water flowing crevice zone. Following is the equation of the water inrush coefficient:

$$T = \frac{P_0 - \eta \times M_{III}}{M \cdot \sum_{i=1}^{n} M_i \xi_i - M_I - M_{III}} \quad \text{(Formula-1)}$$

Where P_0 the floor water pressure, MPa; η the rate of water head loss, MPa/m; ξ_i the intensity factor of water-resisting pressure in various types of rock; M the thickness of aquifuge, m; M_I the thickness of the zone destroyed by underground pressure, m; and M_{III} the thickness of primary water flowing crevice zone, m.

(d) The water-resistant property of the protective seam of the coal floor can be shown by the parameter of groundwater pressure, "D", calculated as follows:

$$D = \frac{H_0}{h_{dy}} \div 100 \quad \text{(Formula-2)}$$

Where D is the parameter of groundwater pressure, MPa/m; H_0.is the top water pressure of guide-rise zone of floor (water elevation), m; h_{dy} is the length of resistance pressure zone (water- display zone), m.

B. numerical analysis of mining deformation rule

We analyzed the mining deformation rules of strata between main coal seam and Ordovician limestone aquifer of Feicheng Mining area by $FLAC^{3D}$ simulation. Model was shown in figure 4. We chose waterproof pillar 20 m and 40 m for simulation respectively. See figure 5 shows.

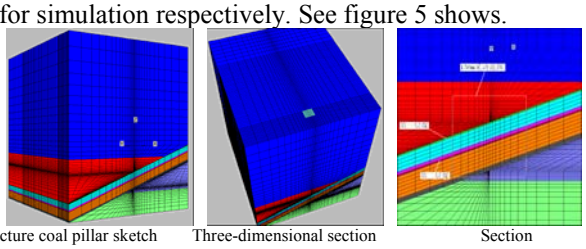

Figure 4 numerical calculation model

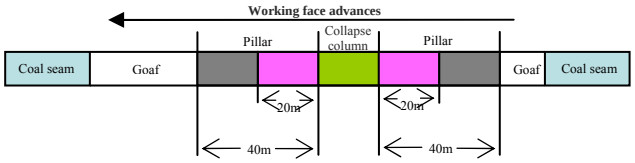

Figure 5 Set sketch of waterproof pillar

It revealed by simulation results that:

(a) Three-Zone range of coal floor underlying strata was roughly that depth of scathe-zone is 60 m above, and height of conduction-water fracture-zone is about 35 m and height of damage-zone is about 8 m.

(b) In a certain period, the pillar size has a bigger influence on stress distribution and displacement of floor. Floor failure depths decreases with pillar size increases, but as the distances of advances increases, the influence of coal pillar decrease gradually until influence disappear.

C. Water-bursting mechanism and safety mining key under mining conditions

In mining conditions, ground stresses not only control the water-hearing capability, penetration ability of strata, and decide the water-blocking ability of coal floor [12-13].

1) *The water-inrush mechanism under normal conditions:* the situation of "Nether-Three-Zones" of coal seam was shown in figure 6 below.

(a) When the protective thinner or protective intensity is lower, coal mining makes the mutual connection between the floor damage-zone and guide-rise zone.

(b) When there is no protective-zone, coal mining makes the mutual connection between the floor damage-zone and guide-rise zone or connects the aquifer directly [15].

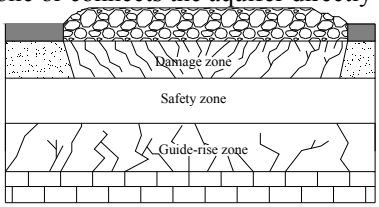

Figure 6 distribution sketches of "Nether-Three-Zones" of coal floor

2) *Water-bursting mechanism of structure*:

(a) Water-bursting mechanism of faulting:

In regional faulting nearby, the natural guide-rise zone of press-water is larger increase than the others (is normal strata of 1 times or so), and the mining damage-zone is greater decrease than other regions. The result will connect damage-zone and guide-rise zone along the fracture, and make press-water influx into working face or goaf along the fracture, and cause the water-bursting accidents.

(b) Water-bursting mechanism of collapse column

According to principle of hydraulic crack, when collapse column exists and groundwater guide-conduction to a certain height, cracks under the action of the water pressure outspread along the direction of least resistance, and effective water-resisting layer thickness decreases, and local stress concentration strengthenes. The result makes the geological environment near collapse column is more advantageous to interaction and promotes each other between water seepage softening and fracturing expansion of press-water. Once the pressure of press-water is greater than the minimum principal stress of underlying key strata, it occurs rock water-fracturing phenomenon and the piping formation, then occurs water-bursting accidents, as shown in figure 7.

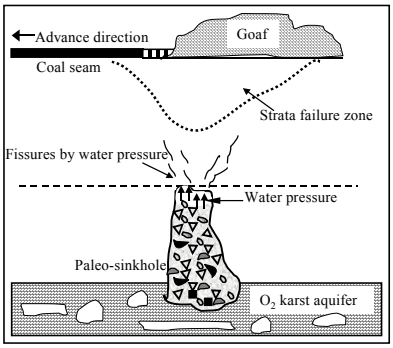

Fig.7 Cause of emergent water from collapsing pulse

3) *Key to safety mining of coal seam on press-water*: before broken, terrane has the property of approximate continuum; after broken it takes the property of non-continuum. The vertical fractures across layers of underlying strata of coal seam are important fractures leading water in the aquifer to the stope. Therefore, the key point in safety mining is to ensure that the damaged zone does not break over the aquifer or the guide-rise zone by controlling the controllable factors under different natural conditions.

Ⅳ. THE CLASSIFICATION OF APPLICABLE SAFETY MINING CONDITION OF COAL SEAM ON PRESS-WATER

A. The main influence factors of water-inrush from coal floor

1) *The resistiong ability of water-resisting layer of floor*: the resistiong ability of water-resisting depends on the thickness, strength and fracture degree of water-resisting layer.

2) *Water and water pressure of confined aquifers*: in other conditions being simultaneously, the probability of floor water-irruption is larger with the water pressure is greater. While, the harm is more serious with the water is more abundant.

3) *Geological structure*: about 80 percent of working face floor water-bursting accidents occurred near the structures.

4) *Ground pressure*: support pressure is a predisposing factor of floor water-irruption which destroyes the integrity of coal floor, develops and expands the original structural-fissure of water-resisting layer.

B. classification method and indices

According to the key point of coal floor water-bursting, there are a lot of factors influencing safety mining of coal seam on water, and it is hard to use one physical quantity as the only classifying index. So, the multi-index synthetic analysis method is used to classify the applicable conditions of safety mining of coal seam on press-water. We take the damage-zone depth, with-pressure coefficient, water-inrush coefficient, rock integrity, and mining influence for relevant classification indices.

1) *Damage depth of coal seam floor:* we take the plane stress state to analyze the maximum damage depth of floor (numerical simulation results show that the floor damage depth in plane stress state calculation is bigger than the one in plane strain state calculation), h_{damage} is calculated by the following formula:

$$h_{damage} = \frac{1.57\gamma^2 H^2 L_x}{4\sigma_c^2} \quad (\textit{During the first broken})$$

$$h_1 = \frac{x_a \cos\varphi_0}{2\cos\left(\frac{\pi}{4}+\frac{\varphi_0}{2}\right)} e^{\left(\frac{\pi}{4}+\frac{\varphi_0}{2}\right)\operatorname{tg}\varphi_0} \quad (\textit{During periodic broken})$$

$$h_m = \frac{100M}{3.3n+3.8} + 5.1 \quad (\textit{Statistical formula})$$

Where γ is the rock density, kg/m^3; H is the depth of working face, m; L_x is the breadth of working face, m; σ_c is the compressive strength of strata, MPa. x_α is the coal edge plastic zone width, m; φ_0 is the weight average internal friction Angle of floor rock; M is the total thickness of coal seam, m; N is the number of coal seam stratified layers.

2) *Water-inrush coefficient*: water-inrush coefficient is calculated with mentionged Formula-1.

3) *With-pressure coefficient*: resisting capability of floor protective-zone is reflected by with-pressure coefficient. And the average with-pressure coefficient is calculated with mentionged Formula-2.

C. To classify of the applicable safety mining condition of coal seam on press-water

According to experimental results, calculation analysis conclusion and water-filling characteristics of coal floor water-resisting layer we present the classification system of mining conditions of coal seam on press-water, see table 2.

Ⅴ. PRACTICE APPLICATION

We classify the mining conditions of coal seam on press-water in the middle-3 mining area of the Taoyang Coal Mine in the Feicheng coal field by the classification system, and take corresponding measures.

Implementation situation is shown in Table 3.

Practice showed that this classification provided good effects which secured safety in mining of coal seam on press-water.

Ⅵ. CONCLUSIONS

We use multi-index synthetic analysis method, and select the with-pressure coefficient, water bursting coefficient, “nether three-zone” thickness of floor, mining influence and rock integrity as classification indices, and form the classification s ystem of applicable mining condition of coal seam on press-water.

The applicable mining condition is divided into four categories, i.e. structure water bursting dangerous class, sirect type water bursting class, obstructing type water bursting dangerous class, and closed type relative safety class. Index is easy to determine, is simple to Contrast. The classification system is used conveniently, and provides satisfactory results.It provides a technology for safety in mining of coal seams above high pressure aquifers and should be emphasized for practical purposes.

Experimental results are consistent with actual situation which determine the scope Nether-three-zones of floor. It shows that the depth of scathe-zone is 60.0 m above, and height of conduction-water fracture-zone is about 35.0 m and height of damage-zone is about 8.0 m.

Table 2 the classification system of mining conditions of coal seam on press-water

No.	Type		Classification indices			Characteristics	Secutity	Mining measure
Ⅰ	Structure water bursting dangerous class					Guide-rise zone height near fracture abnormal place close or cut through coal seam	Very dangerous	Change coal mining method, keep protective pillar enough, and reinforce the rupture.
Ⅱ	Direct type water bursting class	one zone direct sort	H_s=0	H_r＝0		Difficult to measure the water inrush. Damage zone direct conducts press-water.	Dander, easy bursting	Change coal mining method, reduce floor failure depths, drain and depressurization, transformat floor, and increase the covering thickness.
		two zones direct sort		H_r>0		Difficult to measure the water inrush. Damage zone direct conducts press-water throng guide-rise zone.	Insecurity	
Ⅲ	Obstructing type water bursting dangerous class	Strong water permeability sort	H_s>0	H_d≥H_t	D>T	Permeability water yielding, more water means more dangerous	Safe not enough	Narrow working face length, reduce damage depth, increase covering thickness
		High permeability sort			D＝T			
		Permeability sort			D＜T			
Ⅳ	Closed type relative safety class	Micro-bursting		H_d<H_t	D>T	No water inrush danger	relative safety	Normal mining
		No-bursting			D＝T	No water inrush		
		Completely without bursting			D＜T	There is no water inrush		

Note: H_{safe} is the effective thickness of protective-zone; H_{damage} is the thickness of floor damage-zone; H_{rise} is the thickness of guide-rise-zone; H_{tip} is the distance between the coal seam and the top interface of original guide-rise zone

Table 3 Practice application of classification system

Item	Hole number	
	D_1 (-550 m)	D_3 (-350 m)
Floor thichness	34.80 m	34.00 m
H_t	31.70m-18.467m	<19.582 m
H_s	34.80-(31.70m-18.467)=(3.1-16.333) m >0	34.00-19.582=14.418 m >0
H_d	9.88 m	20.153 m
Test result	D>T	D<T
Class	Ⅳ-Closed type relative safety class	Ⅲ- Obstructing type water bursting dangerous class
Sort	$Ⅳ_1$- Micro-bursting	$Ⅲ_3$- Permeability sort
Secutity	relative safety	Safe not enough
Mining measure	Normal mining	Narrow working face length, reduce damage depth, increase covering thickness
effect	Mining passes through safely.	The total injection cement of this area is 14.35 t. Mining passes through safely.

REFERENCES

[1] Sidle R C, Kamil I, Sharma A, Yamashita S. Stream response to subsidence from underground coal mining in central Utah. *Environmental Geology*, 2000, 39(3/4): 279-291.

[2] Booth C J, Bertsch L P. Groundwater geochemistry in shallow aquifers above longwall mines in Illinois, USA. *Hydrogeology Journal*, 1999, 7(6): 561-575.

[3] Booth C J. Groundwater as an environmental constraint of longwall coal mining. *Environmental Geology*, 2006, 49(6): 796-803.

[4] Karaman A, Carpenter P J, Booth C J. Type-curve analysis of water-level changes induced by a longwall mine. *Environmental Geology*, 2001, 40(7): 897-901.

[5] Roberto S, Ira D S. Development of collapse sinkholes in areas of groundwater discharge. *Journal of Hydrology*, 2002, 264(1/4): 1-11.

[6] Zhong Y P. *Comprehensive Research of Water Control Technology in Kailuan Coal Mine*. Beijing: Coal Industry Press, 2001.

[7] Zhang J C, Zhang Y Z, Liu T Q. *Rock Mass Seepage and Coal Floor* Water Bursting. Beijing: Geology Press, 1997.

[8] Peng S P, Wang J A. The Safety Mining of the Coal Seams above Pressure Aquifers. Beijing: Coal Industry Press, 2001.

[9] Xu X H, Wang J. Research on Water Bursting of Coal Mine. Beijing: Geology Press, 1991

[10] Li L J. Research on Mechanism and Evaluation of Coal Seam Bottom Water Bursting [Ph.D. dissertation]. Beijing: China University of Mining & Technology, 1995.

[11] Wang Z Y, Liu H Q. Mining above Confined Water Floor. Beijing: Coal Industry Press, 1992.

[12] Yin S X. Simulation and Application of Water Inrush System in Coal Mines [Ph.D. dissertation]. Beijing: China University of Mining & Technology, 2002.

[13] Yin S X, Hu W Y, Liu Q S, Li K K. Assessment research on mining danger in the confined aquifer. Journal of China University of Mining & Technology, 2008, 37(3): 311-315. (In Chinese)

[14] Wang L G, Miao X X, Wu Y, Sun J, Yang H B. Discrimination conditions and process of water-resistant key strata. Mining Science and Technology, 2010, 20(2): 224-229.

[15] Wang C, Wang E Y, Xu J K, Liu X F, Ling L. Bayesian discriminant analysis for prediction of coal and gas outbursts and application. Mining Science and Technology, 2010, 20(4): 520-523.

2011 International Conference on Mechanical, Industrial, and Manufacturing Engineering
Lecture Notes in Information Technology Vols. 1-2

The Simulation Research of Cascade Control System in the Control of Motor

Tang Yonghong
Department of Marine
Yantai Vocation Institute
Yantai,264001,China

Gao Yanli, and Liu Di
Department Control of engineering
Naval Aeronautical and Astronautical University
Yantai,264001,China
gaoyanli2003@163.com

***Abstract* - For the situation that factories require more stringent for control technology and the regulating quality of motor, but traditional single-loop control system is unable to meet the control requirements of the motors better, cascade control system is applied to the control of motor. Cascade control system is a double-loop system, the object inertia of Vice-loop is small, the frequency of work is high, but the inertia of main circuit is large, frequency of work is law. As the control system increases a Vice-loop, when the interference falls in the Vice-loop, the capability of anti-jamming has more improved than the single-loop control system in the same conditions. The simulation found that this system can reduce the amount of overshoot by 5%, shorten regulation time by 7% through changing the parameters of PI regulator PID regulator, the superiority of cascade control system is reflected in the control of motor.**

Index Terms – Motor. Single-loop Control system. Simulation. Regulator. Overshoot.

I. SUMMARY

The last two decades, motor control technology to obtain the amazing achievements in industrial production and scientific development plays a key role. At present, the motor has become a important part of a large number of devices. It can be said, if you do not configure the appropriate automatic control system, large-scale production process is simply not run. In fact, the degree of the motor automatic control has become an important symbol of industrial enterprises modernization.

Designing an automatic control system, we must first understand the composition and characteristics of the control system. In the early industrial production, the main motor control system is single-loop controller which refers to an object by adjusting a regulator to maintain a constant parameter, while the regulator will only accept a measurement signal, the output control of an executive body only. We can say that it is a basic control system of the most widely used, but it only solves the production problem of adjusting the constant value. With the development of modern industry and technology innovation, quality requirements for regulation have become more sophisticated. In some cases, single-loop control system will do nothing. So we find another control system is multi-loop system which is on the basis of a single loop to take other measures to form a complex system. In this system, or by multiple measurements, multiple regulators, or by a number of measurements, a regulator, a compensation, or a decoupler compose the multi-loop control system.

Among the many complex control systems, cascade control system is more common in motor control. Cascade control system is a double-loop system, the output of a controller to control the settings of another controller. Cascade control system connects the two regulators, through their coordination, to make a precise amount to be adjusted to maintain the set value. Typically, Deputy Central Cascade System has inertia object, high frequency, and while the main ring inertia, the operating frequency is low[1].

II. ADVANTAGES OF CASCADE CONTROL SYSTEM

A.Cascade Control System Response

The effect of cascade control is illustrated in Figure 1. The tasks of main regulator are to overcome the disturbance falls outside the vice ring, and to maintain the accuracy for a given value of amount adjusted. Because of the presence of Vice-loop, compared with the single-loop systems, in addition to it overcomes the disturbance falls within the Vice-ring, but also it improves the system operating frequency and speeds up the transition process. Vice-loop controller is mainly used to overcome the disturbance falls within the closed loop. These disturbances can be reflected in the intermediate variables and soon offset by Vice-regulator. Compared with the single-loop system, the amount of interference on the impact to be transferred many times can be reduced.

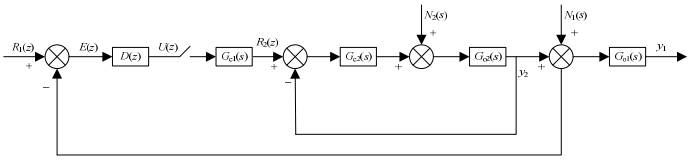

Fig 1 Cascade control system structure

In this figure, the objects of regulators are two first-order inertia and regulators are proportional control law. Their transfer functions are

$$\left.\begin{aligned} G_{01}(s)=\frac{K_{01}}{T_1 s+1},\ \ G_{02}(s)=\frac{K_{02}}{T_2 s+1} \\ G_{c1}(s)=K_{c1},\ \ G_{c2}=K_{c2} \end{aligned}\right\} \tag{1}$$

The closed-loop sub-circuit equivalent objects is looked as $G_{c2}(s)$, so its transfer function is:

$$G_{02}^{'}(s)=\frac{Y_2(s)}{L(R_2(z))}=\frac{G_{c2}(s)G_{02}(s)}{1+G_{c2}(s)G_{02}(s)}=$$
$$\frac{K_{c2}\dfrac{K_{02}}{T_2s+1}}{1+K_{c2}\dfrac{K_{02}}{T_2s+1}}=\frac{\dfrac{K_2}{T_2s+1}}{1+\dfrac{K_2}{T_2s+1}}=\frac{\dfrac{K_2}{1+K_2}}{\dfrac{T_2s}{1+K_2}}=\frac{K_{02}^{'}}{T_2^{'}s+1} \quad (2)$$

If $K_2=K_{c2}K_{02}$,

$$\left.\begin{aligned}K_{02}^{'}&=\frac{K_2}{1+K_2}\\ T_2^{'}&=\frac{T_2}{1+K_2}\end{aligned}\right\} \quad (3)$$

We can see that with the use of cascade regulation, the time constant T_2 decrease $1+K_2$ times. Vice-ring adjustment object is first-order inertia, so it can obtain the amplification factor K_2 great vice ring and make constant value be reduced to very small time. Therefore, in the cascade control system, under the same conditions the main regulator of the amplification factor to adjust is larger than single-loop system, which improve the control system for anti-interference ability is also good[2].

B. Cascade Control System Frequency of The Transition Process

In cascade system, when the main feedback loop is broken, open-loop transfer function is G(s).

$$G(s)=G_{c1}(s)\frac{G_{c2}(s)G_{01}(s)}{1+G_{c2}(s)G_{02}(s)}G_{02}(s) \quad (4)$$

Closed-loop system characteristic equation is

$$1+G(s)=0 \quad (5)$$

Putting (4) into (5), we can find

$$1+G_{c2}(s)G_{02}(s)+G_{c1}(s)G_{c2}(s)G_{01}(s)G_{02}(s)=0 \quad (6)$$

Putting the transfer functions of (1) into (6), we can simplified (6) and find

$$T_1T_2s^2+(T_1+T_2+K_{c2}K_{02}T_1)s+(1+K_{c2}K_{02}+K_{c1}K_{c2}K_{01}K_{02})=0 \quad (7)$$

if

$$\left.\begin{aligned}2\varsigma\omega_0&=\frac{T_0+T_2+K_{c2}K_{02}T_1}{T_1T_2}\\ \omega_0^2&=\frac{1+K_{c2}K_{02}+K_{c1}K_{c2}K_{01}K_{02}}{T_1T_2}\end{aligned}\right\} \quad (8)$$

We rewrite the characteristic equation above to the following standard form.

$$s^2+2\varsigma\omega_0s+\omega_0^2=0 \quad (9)$$

ς —Cascade control system attenuation coefficient;

ω_0 ——Cascade control system's natural frequency.

From (9), we find the solution is

$$s_{1,2}=\frac{-2\varsigma\omega_0\pm\sqrt{4\varsigma^2\omega_0^2-4\omega_0^2}}{2}=-\varsigma\omega_0\pm\omega_0\sqrt{\varsigma^2-1} \quad (10)$$

Only when $0<\varsigma<1$, the system oscillation will appear. Oscillation frequency is the cascade control system frequency[3].

$$\omega=\omega_0\sqrt{1-\varsigma^2}=\frac{\sqrt{1-\varsigma^2}}{2\varsigma}\frac{T_1+T_2+K_{c2}K_{02}T_1}{T_1T_2} \quad (11)$$

Because Vice-loop control system improves dynamic characteristics of the object in cascade regulation, the whole system has increased the frequency of the transition process. When the object properties are certain, the amplification factor of Deputy Controller is larger and frequency of work is higher.

III. CASCADE CONTROL SYSTEM SETTING PRINCIPLE

Cascade control system tuning than single-loop system is more complicated because the two regulators are more or less of each other in a system to work. In operation, the fluctuation frequency is different between main ring and vice ring, vice ring has high frequency, and the main ring frequency is low. The frequency is mainly determined by adjusting the dynamic characteristics of the object, but also with the main and secondary regulator tuning status. The vice regulator and the frequency of vice ring gain should be increased, when the system is tuning. The purpose is to enable the main and vice ring frequency staggered, preferably a difference of more than three times in order to reduce the impact of each other to improve the quality of regulation.

1. Under normal circumstances, the objects of the vice ring time constant are smaller, but other than that part of the vice ring object properties and lag time constants are larger. There are more differences between main ring and vice ring in the frequency, fluctuations can be set through the following methods.

Renovated the main regulator and make the main ring in the case of breaking before tuning. Then into vice regulator, the Vice-ring is as a part of the equivalent second-order weak damping the object, along with some object outside the vice ring.

In the run-time, sometimes the main regulator is from "automatic" to "manual". Then disconnect the main ring, only the deputy controller work independently. In this case, vice ring should have a certain stability, not the vice regulator amplification factor over the whole set so large that the vice ring in the oscillation state.

2. The two parts which is divided by Vice-loop have the approximately equal time constant and delay, when the frequency of ring main is closer, the interaction between them is on the big. In this case, you need to repeat testing between main ring and vice ring, in order to achieve optimal tuning. However, this repeated testing is a very troublesome. General cascade control system of quality indicators for sub-loop is

not strict requirements, and the main ring demands quality indicators. At this time, there are interaction between the main ring and the vice ring, as long as quality indicators meet the requirements, the regulation of the quality of vice ring is allowed reducing a little[4].

IV. DESIGN CASCADE CONTROL SYSTEM

A. Cascade control system example

We give a concrete example to better understand the theory of cascade control system composition. Figure 2 is a single-loop control system for surface, Degree of motor control switch on the valve is an important parameter of the system, requiring more stringent. To ensure a constant water level inside the tank, we use a regulator which is in Figure 2 to regulate valve, Opening the valve sensor can measure the actual height of water level, when injected into the pool water occurs disruptions, regulator 1 begins to move, to control the flow of water in the pool, but it takes some time lag before they can act on the water injected into the pool, in this way, early detection can not be disturbed, they can not adjust in time reflect the effects of dynamic deviation occurring, and they reflect the safe operation of the system[5].

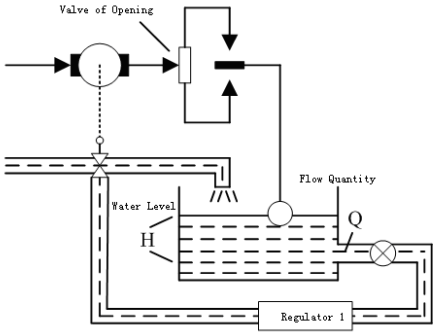

Fig 2 Liquid single-loop control system

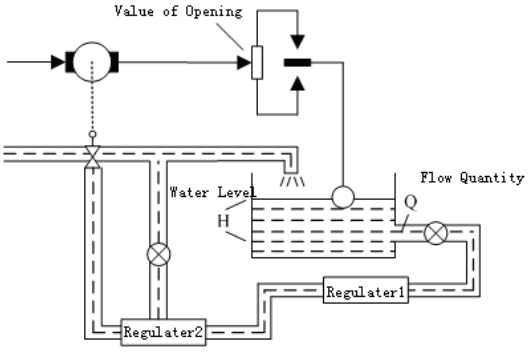

Fig 3 Liquid level cascade control system

To solve this problem, we add a controller 2 in a cascade control system of liquid level in Figure 3, it constitutes a cascade regulation system. Once the water which is injected into the pool occurs disturbance, at the first, regulator 2 reflects the changes in water flow regulation, and the output of regulator 1 regulator is used to change the reference value of regulator 2, playing a role in the last correction, so the impact of disturbance on the water flow is greatly reduced and the quality of regulation is improved. Through the analysis of the above example, we can be summarized as a cascade control system block diagram shown in Figure 4.

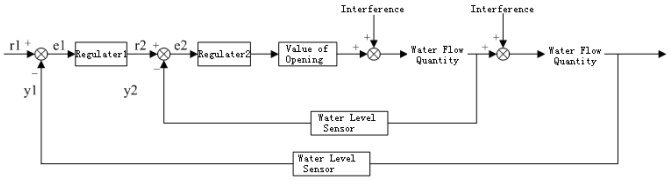

Fig 4 Cascade control system block diagram

The figure shows, the Deputy loop in the control process plays the "coarse" role, the main circuit is used to perform "fine tune" to ensure that the final adjusted amount meet the system requirements. Regulator 1 and regulator 2 do not interact. Regulator 1 has an independent to set the and its output as a setting value of regulator 2 which output signal is used to control the further opening the valve to control the flow of water. In the cascade control system, the tasks of two regulators are different. The task of regulator 2 is to quickly fall off the disturbance which are in the vice ring, while the intermediate variables do not require non-poor, and it is generally used PID regulator. The mission of Regulator 1 is to accurately maintain the transferred amount meeting the production requirements. Therefore, a regulator must have integral action, and it is generally adjusted by PI[6].

B. Introduction of simulation

According to the above description, we can abstract the above mentioned actual example to a mathematical model. We has given the system transfer function $G(s)=\frac{10}{(s+3)(s+7)}$ and the vice loop plays a "coarse" role in the control process, the main circuit is used to perform "fine tune" ,anglicizing of the transfer function, that it is composed of two series consisting of inertia. Main circuit control object is $G(s)=10/s+7$, vice-loop control object is $G(s)=1/(s+3)$. Based on the principle regulator, vice loop is selected PI controller and the main loop is selected PID regulator. The main regulator is in the entire set, and vice regulator is in the fine-tuning until we get the more satisfactory control effect. The entire process is implemented in the SIMULINK environment. The function of the first regulator transfer is $G(s)=\frac{10}{(s+7)}$, the tuning parameters of PI controller are P = 4, I = 2; the transfer function of the main object is $G(s)=\frac{1}{(s+3)}$:,the tuning parameters of PID controller are P = 5, I = 3, D = 2. Cascade control system model simulation is shown in Figure 5.

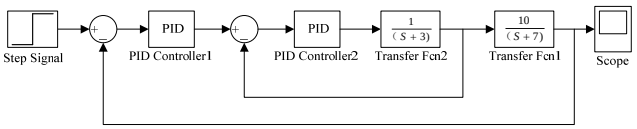

Fig 5 SIMULINK model of cascade control system diagram

The inputting of Cascade control system is input a step signal, the oscilloscope to get the simulation is shown in Figure 6. It is clear to see, the use of cascade control system has been the simulation curve, the transition process is very smooth, no overshoot, small fluctuations in the curve, good stability.

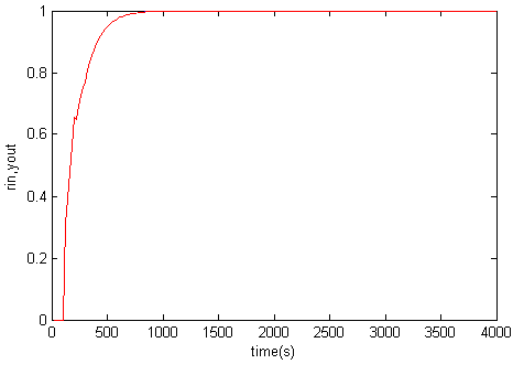

Fig 6 Cascade control system simulation diagram

CONCLUSIONS

Cascade control system is a double-loop system, in essence, it connects the two controllers, through their coordination, and cascade control system makes a precise amount to be adjusted to maintain the set value. Typically, vice loop has small inertia and high frequency, while the main has big inertia, low frequency. This structure, it has its own characteristics, in a cascade control system, because the controller determines the amplification factor values the system sensitivity of the error signal, therefore, it reflects the system's interference capacity on some extent. It can be proved, in the cascade control system, because the system has more than a deputy circuit, when the disturbance down at the vice ring, the disturbance under the same conditions than the single-loop control system has improved. The simulation shows that we can change the PI controller and PID controller parameters to achieve reduced overshoot or decrease the purpose of settling time, which you can demonstrate the advantages of cascade control system.

REFERENCES:

[1] Shi wen, Liu wen-jiang. Instrumentation and Process Control Automation. Electronic Industry Press, 2003

[2] Zhang guang-yi, Hui yi. SCR cascade control system engineering. Electric Transmission ,1985

[3] Wang li-tao. High internal feedback cascade speed motor and control device in Waterworks. China Water & Wastewater, 1999,15

[4] Qin xiao-ping,Wang ke-cheng. Double-fed induction motor speed control and cascade control. Machinery Industry Press,1990

[5] Wang ji-wei, Chen yi-xin, Wu zhen-shun. Modern control theory and engineering. Higher Education Press,2003

Tu Zhi-ying,Zhu Lin-zhang. Process Control System. Machinery Industry Press,1998

2011 International Conference on Mechanical, Industrial, and Manufacturing Engineering
Lecture Notes in Information Technology Vols. 1-2

Online Monitoring System of HVDC Breaker based on PAC Data Acquisition Technique

Jun Wang
Hubei Electric Testing Research Institute
Wuhan, Hubei Province, China
baozi572@163.com

Zhihua Li , Tao Ning, Wei Chen
School of Electrical Engineering
Wuhan University
Wuhan, Hubei Province, China
lizhihua_87@163.com

***Abstract* - In order to get the real-time operating state of the oscillation circuit of HVDC breaker, and calculate the RLC parameters of the oscillation circuit, there put forward a online monitoring system of HVDC breaker's oscillation circuit based on PAC (Programmable Automation Controller) Data Acquisition Technique. The hard ware and software were designed to achieve this goal. In this system, a Hall sensor was used to linearly transform the oscillation current into voltage signal, then the voltage was gathered by PAC Data Acquisition system, after stored on local disk of PAC, the data was transmitted to the data processing center. After these, the RLC parameters of the oscillation circuit could be calculated automatically. With this online monitoring system of DC breaker's oscillation circuit, we have done experiments in our lab and in Gezhou Dam convertor station. The experimental data proved that this system do not have any impact on the electric power system, the most important is that it can accurately gather the oscillation current signal at high definition, and calculate the RLC parameters quickly and exactly. We can master the state of the breaker whether it can interrupt the current normally with these parameters.**

Index Terms - DC breaker; PAC data Acquisition system; oscillation current; RLC parameters; online monitoring system.

I. INTRODUCTION

With the DC Transmission technology developing so much, HVDC breakers are being used more and more. It can change the run mode of DC Transmission System and clear the fault of DC Transmission System. However there is no zero crossing point in the direct current interruption, presently almost all the HVDC have a shunt circuit with an inductance and a capacitance in series which can generate an oscillatory current[1][2]. When the HVDC breaker starts to interrupt the current, there will be superposition of the arc current and the oscillatory current, and then the HVDC breaker's arc current has zero crossing point. So it becomes easier to interrupt the current. Whether the breaker interrupts the current successfully or not depends on the oscillatory current a lot. So RLC parameters matter a lot for the HVDC breakers interrupting the current. So the online monitoring of the oscillation circuit is very important. In this test, a new method for calculating the RLC parameters was introduced. All this method needs is the oscillatory current of the oscillation circuit. So it's very important to gather the oscillatory current accurately.

At present, the most common method of data acquisition technology are Analog-to-Digital Converter, MCU, Data acquisition card and PLC. However, when use the Analog-to-Digital Converter to acquire data, the sampling rate is not so fast and precision is low. For MCU, its anti-interference ability is not good, and the sampling rate is low which can't meet the high speed acquisition, when construct a system, it is very huge. For Data acquisition card, it's not very reliable, and it's quite costly, what's more, the Data acquisition card must work with the computer, in other words, it can't work independently, which limit it's usage. For PLC, its data processing ability is poor, and it's not good at network communication, so it's not real time [3]. Knowing all of these, and considering the oscillation circuit is under ±500KV circumstance, with strong electromagnetic interference, and the signal must be sent to data processing centre quickly and reliably, PAC (Programmable Automation Controller) Data acquisition technology is chose. First of all, a Hall sensor is used to transform the oscillation current into voltage signal linearly, then the PAC Data acquisition system gathers the voltage signal accurately and at high-precision. After this the data is sent to the data processing centre at once, now the data processing centre can calculate the RLC parameters of the oscillation circuit automatically and quickly. Using PAC technology, the current can be got accurately and quickly, which ensure that the RLC parameters calculation is accurate.

II. PAC DATA ACQUISITION TECHNOLOGY AND ITS ADVANTAGE

The PAC data acquisition technology combines the strong network data processing ability and the complex programming algorithm of computer and the strong stability and reliability of PLC. The flow control engine of PAC has nothing to do with the hardware, which makes the system more flexible and more open when used in data acquisition. Except for small volume, professional design of hardware and software, simple programming language, rich instructions, strong anti-interference ability, easy to use, easy to communicate with computer, the PAC's most important advantage are shown below[4]:

1. The strong openness of PAC make it easier to hardware expanding, it's more convenient for constructing s system.
2. Its strong network data processing ability can process the data quickly and communicate with remote control centre quickly.
3. The advanced programming language makes it easy to program, debug and optimize the programs.

4. The hardware of PAC is small, and its strong anti-interference ability which can meet the harsh data acquisition circumstance.

The frequency of the oscillation current is about 4.000Hz, and under ±500KV circumstance, with strong electromagnetic interference, so it claim that the data acquisition system have enough data sampling frequency and strong anti-interference ability. What's more, the data processing centre is remote, how to transform the data? It must be wireless, so the data acquisition system must be good at transform data wirelessly. The PAC data acquisition system can meet all of these requirements, the PAC data acquisition system have strong anti-interference ability meets EN61000-6-2/EN 61000-6-4 standard, and this system can get the data between 0 and 30.000 Hz sampling frequency which involve 4.000 Hz, for the sampling theorem tells us the sampling frequency is at least two times of the data frequency. So the PAC system can accurately gather the oscillation current at high fidelity. The PAC data acquisition system have strong data processing ability and data throughput ability which make it can communicate with the other communication equipments, and send the data to the remote centre quickly and accurately.

III. WORKING PRINCIPLE OF HVDC BREAKER

The structure of HVDC breaker is showed below. There are three loops: interruption loop; oscillation loop; MOV loop.

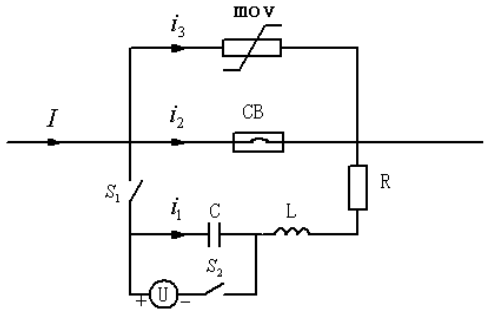

Fig. 1 Structural drawing of HVDC breaker

When the breaker starts to interrupt current, the CB opens, and there comes arc. At the same time, S_1 closes, leading the RLC loop generate oscillatory current for the C is charged well. Now the current i_2 is superposition of the oscillatory current and the arc current. So the current i_2 has zero crossing point, arc-extinguishing medium restores, and the arc can be crushed out. At this moment, the recovery voltage is very high, it could reach the reference voltage of the MOA, and the MOA can release the huge energy during the interruption course[5][6]. Then the HVDC breaker interrupts the current successfully.

IV. ONLINE MONITORING SYSTEM BASED ON PAC

A. The Extensional Organization Of Online Monitoring System

The online monitoring system is made up of signal transformation, data acquisition, data transformation and data process. The structural drawing of the system is showed below:

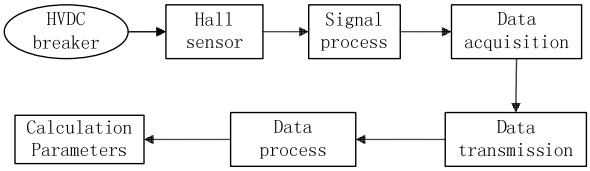

Fig. 2 The structural drawing of the online monitoring system

The Hall sensor can transform the oscillation current to voltage signal linearly. When transform the current, there exist shield reducing electromagnetic interference which can improve the precision. The PAC module is in charge of gathering the voltage signal. This is the most important part in the online monitoring system, because all the calculation is based on this data. When the voltage signal is gathered, some essential processes are done, for example, data filtering[7][8]. After this, the data is transformed to the data processing centre by GPRS equipments. The data processing centre will calculate the RLC parameters automatically.

The solar panels and accumulators are in charge of all the online monitoring system's power supply. They can ensure the power supply is reliable and stable. It's green, environmental protective and pollution-free. When the system is installed, it can work 24 hours a day and there is few maintenance.

The space which we can make use of beside the MRTB (Metal Return Transfer Breaker) is small, and the whole system is small enough to be installed beside the MRTB. Besides, we use Hall sensor to transform the current, the Hall sensor is non-contacting instrument, so it has no impact on the power system. What's more, the data transmission is wireless avoiding the insulation problem when lineate way used. The PAC data acquisition system has high accuracy, high precision and strong anti-interference ability which suit the requirement of data acquisition at the electromagnetic circumstance. At last, the whole system's power supply is self-sufficient.

B. How Does Online Monitoring System Access To The HVDC Breaker

This online monitoring system is related to the oscillation circuit of HVDC breakers, so we only pay attention to the oscillation circuit. For the converter station is very important in the power system, so the online monitoring system cannot have any impact on the power system. The Hall sensor is contactless instrument, using this instrument to transform the current have no impact on the power system[9]. The PAC data acquisition system can gather the voltage signal instead. What's more, the Hall sensor is split. The wire of the oscillation can go through Hall's centre as long as open the Hall sensor, which avoids demolishing the wire. The figure below shows us how this system joins up the DC breaker:

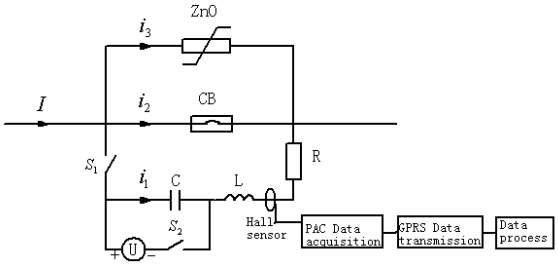

Fig. 3 The online monitoring system access to the HVDC breaker

C. Realization Of Gathering Oscillatory Current

The PAC data acquisition system has high precision, high resolution and real time characteristic. The sampling terminal is EL3702 used to process voltage from -10V to +10V, its sampling frequency is between 0 and 30K Hz including 4K Hz of the oscillation current. After the voltage signal is digitized, its resolution ratio is 16, and sent to the upper automation equipment with electrical isolation, which reduces the electromagnetic interference. The El3702's sampling error is less than 0.3%. When the data gathering is done, the PAC asks for communication task immediately, sending the data to the remote data processing centre.

As to software, a triggered program is designed. It can detect the current of the oscillation circuit all the time[10]. When the current is heavy enough to trigger the set point, the program starts to gather the signal for 40ms, which can ensure that the every oscillatory current will be got accurately and analyzed by the data processing centre[11]. However when the communication fault occurs, the data will lose. The program is designed to prevent the data losing, when the whole voltage data is got by the EL3702, the PAC module will store it on the local disk of PAC. So each oscillatory current data will be got, and we can check this data by remote desktop[12]. All of these can improve the reliability of data acquisition. The logic diagram below shows how program works:

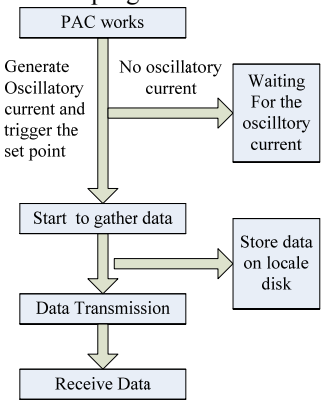

Fig. 4 The logical diagram of data acquisition

V. TEST

After the whole online monitoring system fixed, it's very important to test it. We have done many experiments to test it, like in our laboratory and Gezhou Dam converter. The experiments data showed us that this system can calculate the RLC parameters accurately and reliably.

A. Experiments In The Laboratory

The oscillation circuit could be looked as a LC second order circuit. As long as the RLC parameters meet $R < 2\sqrt{\frac{L}{C}}$ there comes oscillatory current. So we can simulate the course of the HVDC breaker interrupt current when oscillatory current generated in our laboratory. Then we can test the online monitoring system. We have fixed a LC second order circuit in our laboratory. The circuit diagram is showed below:

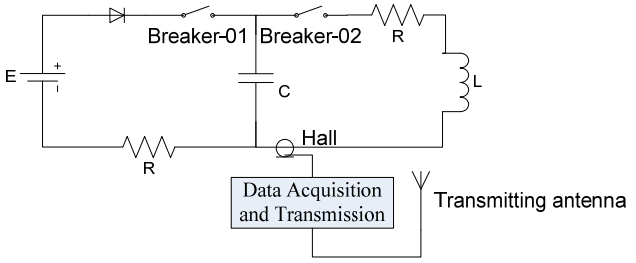

Fig. 5 Schematic diagram of the experiment in the Lab

In Fig. 5, at first open breaker-02, close breaker-01. When the voltage of the C is stable, write down this voltage value, open the breaker-01 and closes the breaker-02 quickly, then oscillatory current occurs. Unless the voltage is high enough, or the online system do not get the oscillatory current. When the transformed voltage triggers the set point, the online monitoring system will gather and send the data, the data processing centre will calculate the RLC parameters. In the course of experiments, the capacitance had been charged at different level, and the experiments data is showed below:

TABLE I
DATA ANALYSIS OF THE EXPERIMENT IN THE LAB

U_c(V)		75.4	42	44	57.6	62.4
L(μH)	Calculated value	38.7	38.9	41.2	38.1	41.5
	Real value	39.7	39.7	39.7	39.7	39.7
	Error	2.51%	2.01%	3.77%	4.03%	4.53%
C(μF)	Calculated value	32.50	31.63	14.97	16.04	14.98
	Real value	31.74	31.08	15.70	15.70	15.70
	Error	2.39%	1.73%	4.60%	2.16%	4.58%
R (Ω)		0.28	0.26	0.26	0.31	0.29

From table I, we know that the error of inductance is less than 4.55%, while the capacitance is 4.6%. The average error of inductance is 3.37% while the capacitance is 3.09%, and the resistance is about 0.3Ω. The error sources are: ① the measurement tools are not so accurate that the error is amplified in the calculation. ② the wire has its own inductance. The error is small enough, so we can consider these data are accurate. It proved that the online monitoring system is feasible and reliable under laboratory circumstance.

B. Gezhou Dam On-scene Experiment

We had done an experiment with the MRTB (Metal Return Transfer Breaker) in Gezhou Dam converter during its overhaul period. The experiment principle is same as in the laboratory. First of all, install the online monitoring system on the Metal return transfer breaker of Gezhou Dam converter.

Then charge the capacitance, let the oscillation circuit works generating oscillatory current. And the online monitoring system can gather the oscillatory signal and send it to the remote data processing centre, and the data processing centre calculates the RLC parameters of the circuit automatically and quickly.

After the data received, the data processing centre can draw its oscillogram by the received discrete data. And we can see the calculated RLC value at the right side of the oscillogram, which is showed below:

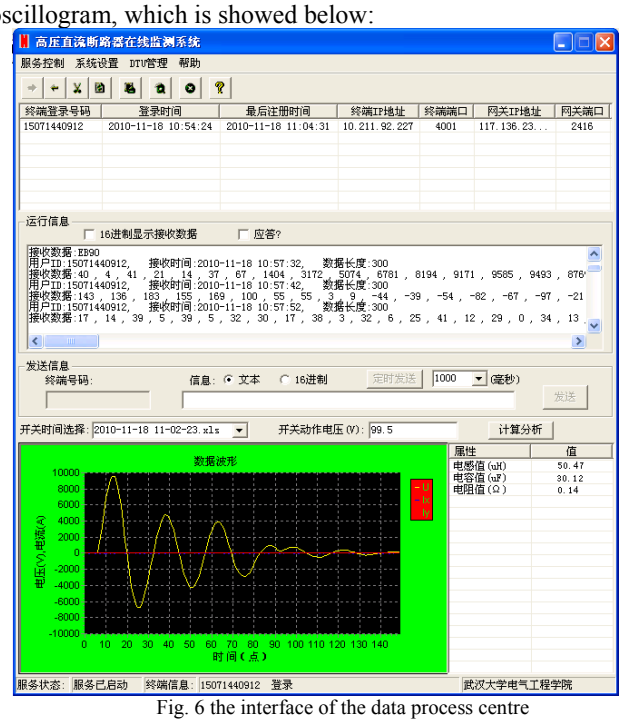

Fig. 6 the interface of the data process centre

After the experiment, we analyze the data, the result is showed below:

TABLE Ⅱ

DATA ANALYSIS OF THE EXPERIMENT IN GEZHOU DAM CONVERTER

U_c(V)	R(Ω)	L(μF)	Error	C(μH)	Error
99.2	0.16	52.66	5.32%	30.66	2.22%
99.5	0.20	49.46	1.07%	30.11	0.38%
116.4	0.13	51.88	3.76%	28.74	4.17%
146.8	0.12	49.08	1.82%	31.39	4.66%
147.1	0.17	51.19	2.38%	28.85	3.83%
147.4	0.14	50.47	0.95%	30.12	0.40%

In the calculation above, the standard value of inductance and capacitance are 50uH and 30uF, for some reason we can only get these value form the station office. From the we know that the error of inductance is between 0.95% and 5.32%,the average error is 2.55%,while the capacitance is between 0.38% to 4.66%, and the average error is 2.61. Both of the average errors are less than 2.7%. The R is about 0.2Ω.The error sources are: ①The measurement tool is not so accurate that the error is amplified in the calculation. ②There exist the stray capacitance which affects the capacitance of the oscillation circuit. ③After the capacitance is charged, the oscillation circuit starts to discharge so slowly that the voltage of capacitance is changed, not the same as measured before. ④The values of inductance and capacitance are changed, their values are not the same as values got from the station office because of years of running. ⑤The temperature impacts on Hall sensor when it is transform the current, leading the voltage is disturbed.

Considering all these influence factors, the calculated RLC parameters are very close to the real value, we can consider these data is accurate. So the online monitoring system of oscillation circuit is reliable and accurate.

VI. CONCLUSION

The online monitoring system of oscillation circuit can calculate the RLC parameters accurately and reliably only with the oscillatory current signal, which had been demonstrated by the experiments, the error is low. By these parameters we can master the real-time state of the HVDC breaker. And it has these Advantages:

1. Compared with traditional off-line maintenance, this system can do online-maintenance of HVDC breakers. It's convenient, and there is no need to dismount the HVDC breakers.
2. It gather the current signal by non-contacting way, it has no impact on the power system. And the online monitoring system's power supply are solar panel and storage battery, which is green, environmental protective and pollution-free.
3. The PAC data acquisition system has high precision and high precision. And the wireless data transmission at 500KV circumstance is its advantage.
4. Based on the RLC parameters, we can know the HVDC breaker's working state conveniently, which contributes much to the HVDC breaker's safe and steady operation.

REFERENCE

[1] Tseng, K. Development of a Dynamic Model of Electric Arc for Power Electronics Simulations[C].IEEE Conference on industry Applications. 1996,2173-2180.

[2] Zhen, Zhanfeng; Dong, Enyuan. Direct Current Interruption And Direct Current Breaker [J]. High-Voltage Electrical Appliances. Dce, 2008.

[3] Kulkarni Rahul1, Saxe Walter and Misra Ranganath. PACs making inroads into automation: 20 Reasons to choose a PAC over a PLC[J]. Robotics World, September, 2004.

[4] Walter, Todd. Welcome PAC [J]. In Tech, Jan, 2005.

[5] Dag Anderson and Anders Henriksson. Passive and Active DC Breakers in the Three Gorges-Changzhou HVDC Project[C].ICPS 2001 Conference, Wuhan, China,2001.

[6] Nakao, H; Nakagoshi, Y; DC Current Interruption in HVDC SF6 Gas MRTB by Means of Self-excited Oscillation Superimposition [J].IEEE Transactions on Power Delivery, Oct,2001.

[7] Black, Garth. Tips for choosing a data acquisition platform [J]. Plant Engineering. Sep, 2003.

[8] Zhang, Junjie; Zhang, Fenglin. Design of High Speed Data Acquisition System[J]. Computer Engineering. Jan, 2009.

[9] Yu, Shuhai and Chen, Hanxiang. The Application of Hall Current Sensor in Series Active Power Filter[J].The application of electrical devices and components, Oct, 2008.

[10]Li, Han and Zhou, Wenjun. Online Monitoring System of Lighting in Power System [J]. Power automation equipment, Aug, 2010.

[11]Chen, Minzhong and Sun, Yukun. Realization of Detecting System of DC Breaker by Using Bluetooth Technique [J]. High Voltage Technology, Jun, 2008.

[12]Zhao, Hanbiao; Lin,Hui. Online Monitoring System of Insulator's Leakage Current [J]. Automation of Electric Power Systems, Nov, 2004.

2011 International Conference on Mechanical, Industrial, and Manufacturing Engineering
Lecture Notes in Information Technology Vols. 1-2

The Simulation and Experimental Research of a Novel Three Phase UPFC

Jiaxin Yuan, Junbo Liu, Baichao Chen, Yongsheng Zeng, S.A.K.SJafri
High Voltage And Insulation Technology Institute
University of Wuhan
Wuhan, Hubei Province, China
Whu.42ljb@yahoo.com.cn

***Abstract* - The high cost hampers the widely use of traditional unified power flow controller (UPFC) in the power system. Contrary to that, Sen Transformer has the advantage of high capacity as well as low cost, although its flexibility and action speed cannot satisfy the required accurate regulation. The hybrid power flow controller (HPFC) is constituted by traditional UPFC and "Sen Transformer" (S.T.) in series and it has the advantages of high capacity and low cost. This text firstly introduces the basic theory of HPFC, and then realizes the function of voltage and power control through the simulation of MATLAB/Simulink, at last, realizes that function through hardware experiment.**

Index Terms - HPFC, S.T., Simulation, Experiment

I. INTRODUCTION

With the speedy development of modern power electronic technology, Flexible AC Transmission System technology is widely used nowadays.

After 2 decades of its development, FACTS family has experienced three generations: the most basic thyristor-capacitor set, the Static Synchronous Series Compensator[1], and finally the latest unified power flow controller (UPFC).

UPFC integrates all previous FACTS devices' regulation performance, but its expensive cost and power limitation restrict it in real system.

Hybrid Power Flow Controller (HPFC) is the reasonable unification of Unified Power Flow Controller and Sen Transformer[2,3]. A HPFC has the large capacity and good stability of S.T., and rapidly adjusted performance of UPFC, which has the innovative theoretical meaning and great value of engineering application. But at present the research work is limited to partial characteristic of HPFC, which has not involve any hardware experiments. This article will provide the theory analysis, simulation and experimental verification related to the regulation performance of HPFC.

II. HYBRID POWER FLOW CONTROLLER

A. The Theory of UPFC

The main circuit of UPFC device is composed of series converter and parallel converter. The two converters are connected back to back to share the same capacitor. Its structure is shown in figure 1 .

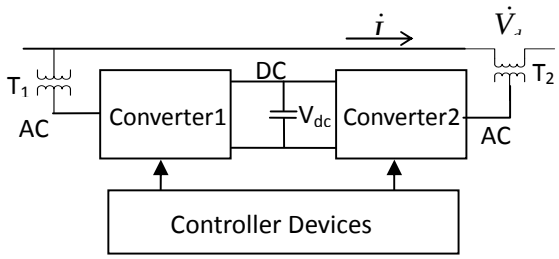

Fig. 1 The model of UPFC

Parallel converter access the system through transformer T_1, and performs the functions of injecting inductive or capacitive reactive power, provide UPFC active power, stabilize accessing point voltage. The Series converters access system by transformer T_2, mainly responsible for voltage compensation, phase adjuster, and power control functions [4].

The control of system voltage and power flow provides by UPFC relies mainly on the series converters, and the parallel converter provides the required power supply. UPFC can inject a voltage called $\dot{V}_d$ to system , whose amplitude and phase can be controlled independently. Its control range is a circle whose radius has a positive relationship with capacity, so as to achieve flexible and effective control to system[5].

B. The Theory of S.T.

S.T. is also series and parallel hybrid FACTS components. It is a kind of improved phase shifting transformer based on the transformer and thyristor control tap technology[6]. As figure 2 shows, S.T. access system send end by star connection, parallel, and constitutes excitation unit. Each phase of the secondary edge is constitued by three tapped windings.

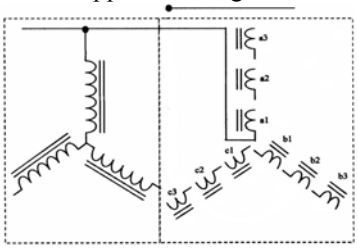

Fig. 2 The structure of S.T.

This work is supported by The national natural science funds (Grant No.50807041), National key basic research development planning (973 planning) (2009CB724506)

The a1, a2, a3 are the secondary edge taps, and a1, b1, c1 constitude the compensation voltage of phase A. $\dot{V}_{dA}$ is constituted by $\dot{V}_{a1}$、 $\dot{V}_{b1}$ 、$\dot{V}_{c1}$ in series, and make the send end voltage of phase A into $\dot{V}_A'$. $\dot{V}_{a1}$, $\dot{V}_{b1}$,$\dot{V}_{c1}$ have the phase difference of 120 degrees between each two. Through the control of tap, the three voltage vector combination is changed, so as to change $\dot{V}_{dA}$.

Ideally， the range of $\dot{V}_A'$ is a hexagon area, whose center is the terminal point of $\dot{V}_A$. The voltage vector diagram shows in fig.3.

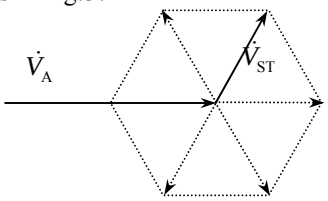

Fig. 3 The control extent of S.T.

C. Hybrid Power Flow Controller

UPFC and S.T. can be equivalent to the series-parallel power supply. The part in series is used to control the system voltage. UPFC's 360 degrees phase-modulation and flexibility make its cost greatly high, which limits its regulation capacity; S.T.'s adjusting flexibility is limited by thyristor switch movement speed and tap number, that is to say the voltage injected to system is only limited points within the hexagon, but S.T. has the advantages of large capacity and low cost, so S.T. can undertake the main regulating task in power control[7]. Hybrid power flow controller will connect UPFC and S.T. in series, using the advantages of both, to control system power.

HPFC integrates large extent of the point control ability of S.T. with small extent of the surface control ability of UPFC. The coordination control of the two can be the equivalent of large capacity UPFC. In these conditions, compared to UPFC, HPFC has the following advantages:

1) Low Cost: The main cost of UPFC lies in large capacity electronic devices. Under the equal capacity, the cost of electromagnetic devices is far less than that of power electronic devices. Therefore, HPFC has a vast advantage of cost control.

2) Reasonable Response Time: S.T.'s response time is 100 ms level, which deals with large capacity power control. At the same time, UPFC's response time is 1 ms level, which deals with the accurate control. The cooperation can satisfy the power system in most of the application.

3) Better Stability: Except for the high cost, the stability of large capacity UPFC is also difficult to guarantee in the corresponding complex power flow change. Through mature on-load changer technology in S.T., HPFC can be assured reponding instructions rapidly and stably.

4) Good Electromagnetic Environment: Compared with the traditional UPFC, HPFC greatly reduces the application of power electronic devices, which make switch loss and electromagnetic interference greatly reduced.The harmonic produced by voltage inverter drops accordingly, which ensure the quality of power transmission and distribution.

III. THE SIMULATION OF HPFC

Figure 4 shows the simple power system simulation diagram established by Matlab/Simulink. The simulation proves the function of adjusting systems voltage amplitude and phase angle of HPFC.

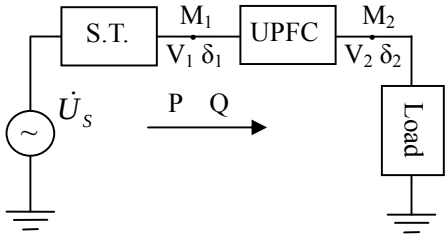

Fig.4 Simulation diagram

In the simulation, the phase of UPFC output voltage and S.T. output voltage are the same to system voltage. Fig. 5 shows the waveform of simulation. The first waveform in (a) is the output voltage of UPFC; the second is the voltage of M_1 point; the third is the voltage of M_2 point, and so forth.

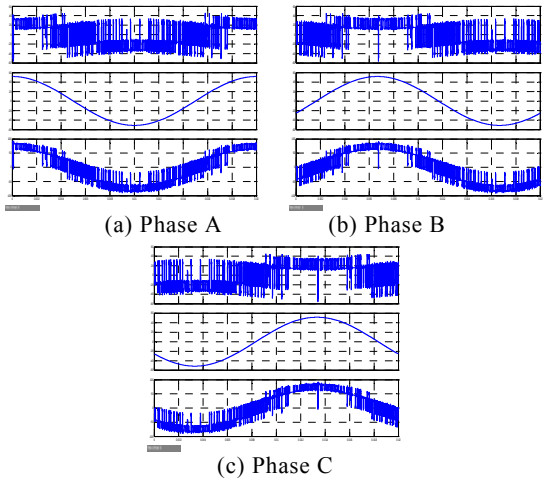

(a) Phase A (b) Phase B

(c) Phase C

Fig. 5 HPFC simulation waveform

By changing the UPFC injection system voltage phase angle, the system voltage amplitude and phase are changed.

The simulation data shows in table 1.

TABLE I
SIMULATION VALUE AND THEORY VALUE

Phase	M_1 voltage	$\dot{V}_d$	M_2 voltage (experiment)	M_2 voltage (theory)
A	38∠0°	40∠0°	78.3∠0°	78∠0°
B	38∠-120°	40∠-120°	78.2∠-120°	78∠-120°
C	38∠120°	40∠120°	78.0∠120°	78∠120°
A	38∠0°	40∠90°	55.2∠46.4°	55.2∠46.5°
B	38∠-120°	40∠-30°	55.1∠-73.3°	55.2∠-73.5°
C	38∠120°	40∠-150°	55.2∠166.6°	55.2∠166.5°

IV. THE EXPERIMENT OF HPFC

Figure 6 is three phase diagram of the system hardware experiment. $\dot{U}_S$ is system power supply. Load is three-phase star connected inductance.

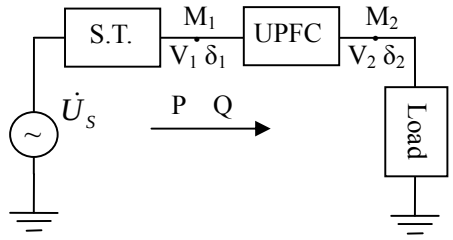

Fig. 6 Hardware experiment diagram

The load end voltage adjustment is controlled through open loop. S.T. is controlled by relay. UPFC consists mainly of power electronic devices, including converter 1, which is working in rectifying state, and converter 2, which is working in inverter state. The converter 2 is a three-phase full bridge controllable inverter, which is controlled by DSP2812 and drive amplification device. The optimal three-phase control sequences used in DSP2812 are calculated by genetic algorithm.

In order to determine the phase of the output voltage of UPFC, a synchronous circuit is designed which can monitor system phase real-time and send the synchronous signal to DSP. When the system voltage get to the zero point from the negative, synchronous circuit output rising edge, when the system voltage get to the zero point from positive, synchronous circuit output falling edge. Only when the DSP detected synchronous circuit input of the rising edge, the pulse is began to send out, on which way to control the UPFC output voltage phase.

In the experiment, system phase voltage value is 20V; S.T. output voltage is 18V; UPFC output voltage is 40V; take system phase angle for 0 degree, being same with S.T. and UPFC phase angle. Fig. 7 shows UPFC output voltage and the voltage of M_2 point, and the experimental data is shown in table 2.

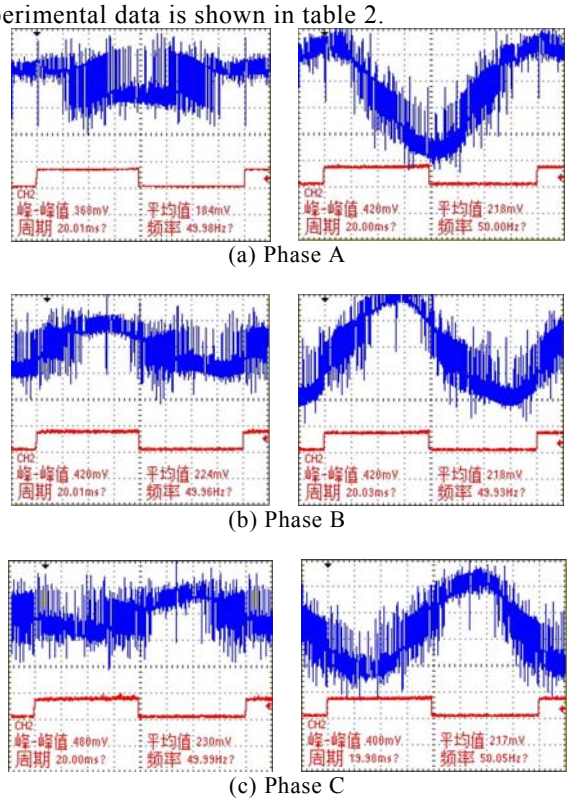

Fig. 7 UPFC output voltage and the voltage of M2 point

V. CONCLUSION

This article realized the function of control system voltage amplitude and phase angle by three aspects of theory analysis, simulation and experiment. The simulation voltage waveform and experimental waveform is consistent, and experimental data errors are within the acceptable range.

TABLE II
EXPERIMENT VALUE AND THEORY VALUE

Phase	System	S.T. voltage	$\dot{V}_d$	M_1 voltage	M_2 voltage (experiment)	M_2 voltage (theory)
A	20∠0°	17.7∠0°	42.1∠0°	37.7∠0°	75.9∠0°	79.8∠0°
B	20∠-120°	16.2∠-120°	37.8∠-120°	36.2∠-120°	72.0∠-120°	74.0∠-120°
C	20∠120°	19.6∠120°	39.6∠120°	39.6∠120°	72.4∠120°	74.9∠120°
A	20∠0°	17.5∠0°	41.1∠90°	37.5∠0°	52.5∠45°	55.6∠47.6°
B	20∠-120°	16.2∠-120°	38.5∠-30°	36.2∠-120°	53.1∠-75°	52.8∠-73.2°
C	20∠120°	19.3∠120°	39.8∠-150°	39.3∠120°	54.1∠160°	55.9∠165.4°

ACKNOWLEDGEMENT

This work is supported by The national natural science funds (Grant No.50807041), National key basic research development planning (973 planning) (2009CB724506).

REFERENCES

[1] Shahab Mehraeen, S. Jagannathan, Mariesal L. Crow. Novel Dynamic Representation and Control of Power Systems With FACTS Devices. IEEE Transactions on Power systems, 2010,25(3):1542-1554.

[2] Chen Baichao, Tian Cuihua. Ultra-high Voltage Unified Power Flow Controller of Electromagnetic Type. High Voltage Engineering, 2006,32(12):96-98.

[3] Yao Yao, Qiu Hao, Chen Baichao, Tian Cuihua. A Novel Unified Power Flow Controller. Automation of Electric Power Systems, 2008,32（16）：78-82.

[4] Mahyar Zarghami, Mariesa L. Crow, Jagannathan Sarangapani, Yilu Liu. A Novel Approach to Interarea Oscillation Damping by Unified Power Flow Controllers Utilizing Ultracapacitors. IEEE Transactions on Power systems, 2010,25(1):404-412.

[5] Kalyan K.Sen, Eric J. Stacey. UPFC-Unified Power Flow Controller: Theory, Modeling, and Applications. IEEE Transactions on Power Delivery, 1998,13(4):1453-1460.

[6] Kalyan K. Sen, Mey Ling Sen. Introducing the Family of "Sen" Transformers: A Set of Power Flow Controlling Transformers. IEEE Transactions on Power Delivery, 2003,18(1):149-157.

[7] Kalyan K. Sen, Mey Ling Sen. Comparison of the "Sen" Transformer with the Unified Power Flow Controller. IEEE Transactions on Power Delivery, 2003,18(3):1523-1533.

[8] Papic I, Zunko P. Comparison of the "Sen" Transformer with the Unified Power Flow Controller IEEE Transactions on Power System, 1997,12(11):1734-1739.

[9] Saurabh Chanana, Ashwani Kumar. Comparison of Sen Transformer and Unified Power Flow Controller on Spot Price Variation of Real and Reactive Power under Maximum Loadability Condition[J]. Electric Power Components and system, 2008, 36:1369-1387.

[10] Gyugui L, Sen K K, Schauder C D. The interline power flow controller concept: a new approach to power flow management in transmission system[J]. IEEE Trans on Power Delivery, 1999,14(3):1115-1123.

[11] Gyugui L, Rietman T R. The unified power flow controller: A new approach to power transmission control[J]. IEEE Transactions on Power Delivery, 1995,10(4):1085-1093.

2011 International Conference on Mechanical, Industrial, and Manufacturing Engineering
Lecture Notes in Information Technology Vols. 1-2

Force Analysis and Strength Check for Gear Trains of the Loader Transmission Gearbox

Yi Zou , Liang Hou
Department of Mechanical and Electrical Engineering
University of Xiamen
Xiamen Fujian 361005, China
flyzouyi@sina.com

***Abstract* - Gearbox is the key component of Loader transmission system. This paper introduces the force analysis and strength check for gear trains of Loader Transmission Gearbox in different kinds of speed conditions. The model for Transmission Gearbox is set up in software Romaxdesigner to simulate and analyze the gear trains of Transmission Gearbox. Both of these results are compared, and the consistency is confirmed. This paper supplies certain reference value for the research and development of Transmission Gearbox.**

Index Terms - Transmission Gearbox; Gear trains; Force Analysis; Strength check; Romaxdesigner.

I. INTRODUCTION

Transmission gearbox has direct influence on Loader's characteristics, such as power performance, fuel economics, operating reliability and portability, transmission stability and efficiency. Gears are the critical components of Transmission Gearbox, whether gears' intensity in different working conditions is sufficient or not, has important significance for the properties of the Transmission Gearbox. This paper discusses two methods, Theoretically calculation and Romaxdesigner software modeling analysis, to analyze the force status and check the contact fatigue strength and bending fatigue strength of gear trains in seven kinds of speed conditions.

I I. CALCULATION THEORY OF GEAR STRENGTH CHECK

The first step of gear meshing analysis is to check contact fatigue strength and bending fatigue strength, to avoid spot corrosion of tooth surface and break of gear tooth. The calculation of contact fatigue strength and bending fatigue strength is the basic work for gear's design.

A. Gear tooth surface contact fatigue strength check

1) Calculated Contact stress σ_H (Mpa):

$$\sigma_H = Z_H Z_E Z_{\varepsilon\beta}\sqrt{\frac{F_t}{bd_1}\frac{u+1}{u}}\sqrt{K_A K_V K_{H\beta} K_{H\alpha}} \quad (1)$$

In this formula, Z_H, Z_E, $Z_{\varepsilon\beta}$—Zone Factor, Elasticity Factor, Contact Ratio Factor and Helix Angle Factor; F_t—Tangential force in Reference pitch circle diameter of gear, N; d_1—Reference pitch circle diameter of driving gear, mm; b—gear tooth width, mm; u—gear ratio of driven and driving gears; K_A, K_V, $K_{H\beta}$, $K_{H\alpha}$—Application Factor、Dynamic Factor、Longitudinal Load Distribution Factor, Transverse Load Distribution Factor.

2) *Permissible contact stress, σ_{HP} (Mpa):*

$$\sigma_{HP} = \frac{\sigma_{H\lim}}{S_{H\min}} Z_{NT} Z_{LVR} Z_W Z_X \quad (2)$$

In this formula, σ_{Hlim}—Contact fatigue limit stress, Mpa; S_{Hmin}—The Minimum Safety Factor; Z_{NT}、Z_{LVR}、Z_W、Z_X—Life Factor of the Contact strength calculation, Lubrication Factor, Work Hardening Factor, Size Factor.

B. Gear tooth root bending fatigue strength check

1) Calculated bending stress σ_F (Mpa):

$$\sigma_F = \frac{F_t}{bm_n} K_A K_V K_{F\beta} F_{F\alpha} Y_{FS} Y_{\varepsilon\beta} \quad (3)$$

In this formula: m_n—Normal module; K_A、K_V、$K_{F\beta}$、$K_{F\alpha}$—Application Factor, Dynamic Factor, Longitudinal Load Distribution Factor, Transverse Load Distribution Factor; Y_{FS} —Form Factor; $Y_{\varepsilon\beta}$—Contact Ratio Factor and Helix Angle Factor for bending.

2) Permissible bending stress,σ_{HP} (Mpa):

$$\sigma_{FP} = \frac{\sigma_{FE}}{S_{F\min}} Y_{NT} Y_X Y_{\delta relT} Y_{RrelT} \quad (4)$$

In this formula: σ_{FE}—The bending fatigue strength basic values of gear materials, Mpa; S_{Fmin}—The minimum safety factor; Y_{NT}、Y_X—Life Factor of the Bending strength calculation, Size Factor; $Y_{\delta relT}$、Y_{RrelT}—Relative Sensitivity Coefficient of Tooth root fillet, Relative Coefficient of the tooth root surface status.

C. Strength conditions:

The tooth surface contact fatigue strength condition:

$\sigma_H \le \sigma_{HP}$ (5)

The tooth root bending fatigue strength conditions:

$\sigma_F \le \sigma_{FP}$ (6)

III. GEAR FORCES ANALYSIS AND CALCULATION

The loader Transmission Gearbox is of seven-speeds and five-shafts structure, four forward speeds and three reverse speeds ("Forward" is abbreviated as "F" and "Reverse" is

abbreviated as " R" later). Speed ratios are i_1=4.166(F), i_2=2.594(F), i_3=1.178(F), i_4=0.672(F); i_1=4.166(R), i_2=2.594(R), i_3=1.178(R). Fig.1 is the transmission diagram.

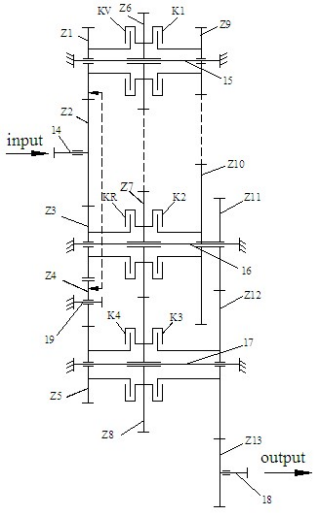

Fig.1 the Transmission diagram.

In Fig.1，z1、z2、…、z13—gears；KV、KR、K1、K2、K3、K4—clutches; 14、15、16、17、18、19—shafts. The transfer route of all speeds of Transmission Gearbox is showed as Table I.

TABLE I
The transfer route of all speeds of transmission gearbox

1st speed(F)	z2→z1→kv→z6→k1→z9→z10→z11→z12→z13
2nd speed(F)	z2→z1→kv→z6→z7→k2→z11→z12→z13
3rd speed(F)	z2→z1→kv→z6→z7→z8→k3→z12→z13
4th speed(F)	z2→z1→z4→z5→k4→z8→k3→z12→z13
1st speed(R)	z2→z3→kr→z7→z6→k1→z9→z10→z11→z12→z13
2nd speed(R)	z2→z3→kr→z7→k2→z10→z11→z12→z13
3rd speed(R)	z2→z3→kr→z7→z8→k3→z12→z13

The Transmission Gearbox is of spur gear trains, cite 1st speed(F) as a example, the transmission process of this speed can be divided into three parts, due to the limited space, only list the force diagram of final drive gear set of 1st speed(F), as showed in Fig.2.

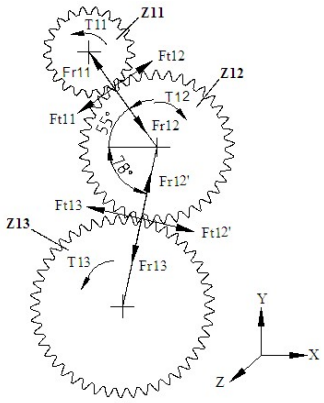

Fig.2 The force diagram of final drive gear set of 1st speed (F)

In Fig.2, T_{11}、T_{12}、T_{13}—torque transferred by gear z11、z12、z13，F_{r12}、F_{r12}、F_{r12}'、F_{r13}—Radial forces of gears.

Input torque: $T=T_2=9549P/n=9549\times190/2600=697.8$ N·m

$T_{10}= T_2z_1z_{10}/(z_2\ z_9)=697.8\times46\times53/(38\times33)=1356.6$ N·m

gear z_{10}、z_{11} are duplex gears, so

$T_{11}=T_{10}=1356.6$ N·m

$T_{12}= T_{11}\times z_{12}/z_{11}=1356.6\times37/21=2390$ N·m

$T_{13}= T_{12}\times z_{13}/z_{12}=2390\times45/37=2907$ N·m

$F_{t11}=2T_{11}/d_{11}=2000\times1356.6/126=21533$ N

$F_{t11}'=2T_{11}/d_{11}'=2000\times1356.6/129.4=20968$ N

$F_{r11}= F_{t11}'\tan\alpha'_{11}=20968\times\tan27.2°=10776$ N

$F_{t12}= F_{t12}'= F_{t13}= F_{t11}=21533$ N

$F_{r12}= F_{r12}'= F_{r13}= F_{r11}=10776$ N

Note: d_{11}'—the pitch circle diameter of gear z_{11}; α'_{11}—the meshing angle of pair of gears z_{11}、z_{12}.

so we can get: $F_{t12\Sigma}=0$

Project F_{r12}、F_{r12}' to the x-axis direction and y-axis direction of the coordinate：

$F_{r12x}= F_{r12}\times\cos55°=10776\times\cos55°=6181$ N

$F_{r12y}= -F_{r12}\times\sin55°=-10776\times\sin55°=-8827$ N

$F_{r12x}'= F_{r12}'\times\cos78°=10776\times\cos78°=2240$ N

$F_{r12y}'= F_{r12}'\times\sin78°=10776\times\sin78°=10540$ N

so we can get:

$F_{r12x\Sigma}= F_{r12x} + F_{r12x}'=8421$N

$F_{r12y\Sigma}= F_{r12y} + F_{r12y}'=1713$N

$F_{r12\Sigma}=\sqrt{(F_{r12x\Sigma})^2+(F_{r12y\Sigma})^2}=8593$N

Gear forces analysis and calculation of other speeds are similar, summary results of all speeds are showed in Table II. Due to the limited space, we only list the tangential force of gears in all kinds of speeds, as showed in Table II.

Table II
The tangential force of gears in all kinds of speeds

Units: N

mode	Z_1	Z_2	Z_3	Z_4	Z_5	Z_6	Z_7	Z_8	Z_9	Z_{10}	Z_{11}	Z_{12}	Z_{13}
1st (F)	9182	9182	—	—	—	—	—	—	11376	11376	21533	0	21533
2nd (F)	9182	9182	—	—	—	8664	8664	—	—	—	13408	0	13408
3rd (F)	9182	9182	—	—	—	8664	0	8664	—	—	—	6088	6088
4th (F)	0	9182	—	0	9182	—	—	—	—	—	—	3474	3474
1st (R)	—	9182	9182	—	—	8664	8664	—	11376	11376	21533	0	21533
2nd (R)	—	9182	9182	—	—	—	—	—	—	—	13408	0	13408
3rd (R)	—	9182	9182	—	—	—	8664	8664	—	—	—	6088	6088

Note:"—" means the gear does not participate in the movement and power transmission of that speed, the same below.

IV. GEAR STRENGTH CHECK

The material of gears is carburized hardened steel, 20CrMnTi, according to The medium quality of gear materials and medium Heat Treatment Quality, we can find σ_{Hlim} =1500 Mpa, σ_{FE}=920 Mpa.

A. The selection of strength check coefficients.

The selection of coefficients of tooth surface contact fatigue strength check and tooth root bending fatigue strength check refers to Ref.[2]. Due to the limited space, we only list the coefficients of the final pair of gears of 1st speed (F), as showed in Table III and Table IV.

Table III
The coefficients of contact fatigue strength check of 1st speed (F)

mode	gear	K_A	K_V	$K_{H\beta}$	$K_{H\alpha}$	Z_H	Z_E	$Z_{\varepsilon\beta}$	Z_{NT}	Z_{LVR}	Z_W	Z_X	S_{Hmin}
1st(F)	12/13	1	1.14	1.06	1.1	2.22	189.8	0.92	1.14/ 1.145	0.95	1	1	1.05

Table IV
The coefficients of bending fatigue strength check of 1st speed (F)

mode	gear	K_A	K_V	$K_{F\beta}$	$K_{F\alpha}$	Y_{FS}	$Y_{\varepsilon\beta}$	Y_{NT}	Y_X	$Y_{\delta relT}$	Y_{RrelT}	S_{Fmin}
1st(F)	12/13	1	1.14	1.06	1.1	3.96/ 3.9	0.77	0.99/ 0.9	1	1	1	1.05

B. The tooth surface contact stress calculation

Refer to (1)、(2), we can get the calculated contact stress and permissible contact stress of gears in every speed, as showed in Table V.

Table V
The calculated contact stress and permissible contact stress of gears
Units: Mpa

mode	Stress	Z_1	Z_2	Z_3	Z_4	Z_5	Z_6	Z_7	Z_8	Z_9	Z_{10}	Z_{11}	Z_{12}	Z_{13}
1st (F)	σ_H	1223	1223	—	—	—	—	—	—	1402	1402	1334	1334	1105
	σ_{HP}	1546	1542	—	—	—	—	—	—	1546	1549	1550	1547	1554
2nd (F)	σ_H	1223	1223	—	—	—	1195	1195	—	—	—	1105	1105	936
	σ_{HP}	1546	1542	—	—	—	1546	1546	—	—	—	1546	1543	1553
3rd (F)	σ_H	1223	1223	—	—	—	1195	1195	1294	—	—	—	837	837
	σ_{HP}	1546	1542	—	—	—	1546	1546	1534	—	—	—	1534	1544
4th (F)	σ_H	1223	1223	—	1220	1287	—	—	—	—	—	—	911	911
	σ_{HP}	1546	1542	—	1450	1513	—	—	—	—	—	—	1513	1527
1st (R)	σ_H	—	1223	1223	—	—	1195	1195	—	1402	1402	1334	1334	1106
	σ_{HP}	—	1542	1546	—	—	1546	1546	—	1546	1550	1550	1547	1554
2nd (R)	σ_H	—	1223	1223	—	—	—	—	—	—	—	1334	1334	1106
	σ_{HP}	—	1542	1546	—	—	—	—	—	—	—	1550	1547	1554
3rd (R)	σ_H	—	1223	1223	—	—	—	1294	1294	—	—	—	837	837
	σ_{HP}	—	1542	1546	—	—	—	1546	1534	—	—	—	1534	1544

C. The tooth root bending stress calculation

Refer to (3)、(4), we can get the calculated bending stress and permissible bending stress of gears in every speed, as showed in Table VI.

D. Strength check conclusion

Table V and Table VI show that the contact fatigue stress and permissible contact stress satisfy (5), Tooth root bending fatigue stress and permissible bending stress satisfy (6), so the contact fatigue strength and bending fatigue strength are enough theoretically speaking.

Table VI
The calculated bending stress and permissible bending stress of gears
Units: Mpa

mode	Stress	Z_1	Z_2	Z_3	Z_4	Z_5	Z_6	Z_7	Z_8	Z_9	Z_{10}	Z_{11}	Z_{12}	Z_{13}
1st (F)	σ_F	477	582	—	—	—	—	—	—	676	843	435	515	500
	σ_{FP}	865	859	—	—	—	—	—	—	865	859	869	867	874
2nd (F)	σ_F	477	582	—	—	—	831	831	—	—	—	298	353	359
	σ_{FP}	865	859	—	—	—	865	865	—	—	—	865	860	871
3rd (F)	σ_F	477	582	—	—	—	831	831	871	—	—	—	287	287
	σ_{FP}	865	859	—	—	—	865	865	872	—	—	—	815	832
4th (F)	σ_F	477	582	—	394	482	—	—	—	—	—	—	340	340
	σ_{FP}	865	859	—	863	866	—	—	—	—	—	—	865	869
1st (R)	σ_F	—	582	477	—	—	830	830	—	672	843	435	515	500
	σ_{FP}	—	859	865	—	—	865	865	—	865	869	869	867	874
2nd (R)	σ_F	—	582	477	—	—	—	—	—	—	—	298	353	359
	σ_{FP}	—	859	865	—	—	—	—	—	—	—	865	860	871
3rd (R)	σ_F	—	582	477	—	—	—	678	862	—	—	—	281	283
	σ_{FP}	—	859	865	—	—	—	865	863	—	—	—	863	867

V. *STRENGTH CHECK BASED ON ROMAXDESIGNER SOFTWARE*

A. The simulation model of Transmission Gearbox

Romaxdesigner software is mainly used for the design of Gear Transmission and the Analysis of Virtual Prototype. We build the simulation model of Transmission Gearbox by Romaxdesigner software, as showed in Fig.3.

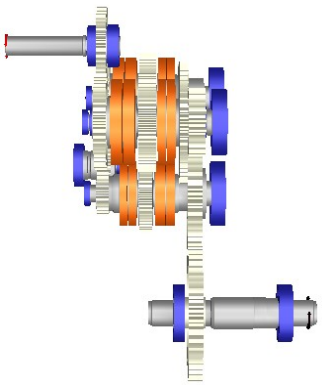

Fig.3 The simulation model of Transmission Gearbox.

B. Applied loads of the simulation model of Transmission Gearbox

The applied loads of the simulation model of Transmission Gearbox is showed as Table VII.

Table VII
The applied loads of the simulation model

mode	Input speed(rpm)	Input power (kW)	T (°C)	duration (hrs)
1st (F)	2600	190	80	500
2nd (F)	2600	190	80	1000
3rd (F)	2600	190	80	1000
4th (F)	2600	190	80	1000
1st (R)	2600	190	80	500
2nd (R)	2600	190	80	1000
3rd (R)	2600	190	80	1000

Note: "T" means Temperature.

C. strength check based on Romaxdesigner

Run all duty cycle analyses on all components in the gearbox, we can get results calculated by Romaxdesigner.

1) Tooth surface contact fatigue strength check.

The contact stress and permissible contact stress calculated by Romaxdesigner are showed in Table VIII.

Table VIII

The contact stress and permissible contact stress by Romaxdesigner

Units: Mpa

mode	Stress	Z_1	Z_2	Z_3	Z_4	Z_5	Z_6	Z_7	Z_8	Z_9	Z_{10}	Z_{11}	Z_{12}	Z_{13}
1st (F)	σ_H	1328	1360	—	—	—	—	—	—	1515	1464	1586	1452	1222
	σ_{HP}	1297	1290	—	—	—	—	—	—	1295	1314	1286	1314	1350
2nd (F)	σ_H	1328	1360	—	—	—	1235	1235	—	—	—	1309	1199	1029
	σ_{HP}	1297	1290	—	—	—	1305	1305	—	—	—	1284	1307	1331
3rd (F)	σ_H	1328	1360	—	—	—	1235	1235	1370	—	—	—	937	903
	σ_{HP}	1297	1290	—	—	—	1305	1305	1292	—	—	—	1322	1330
4th (F)	σ_H	1328	1360	—	1422	1645	—	—	—	—	—	—	1006	970
	σ_{HP}	1297	1297	—	1267	1247	—	—	—	—	—	—	1318	1326
1st (R)	σ_H	—	1361	1328	—	—	1235	1235	—	1515	1464	1586	1452	1222
	σ_{HP}	—	1290	1297	—	—	1305	1305	—	1295	1314	1286	1314	1350
2nd (R)	σ_H	—	1361	1328	—	—	—	—	—	—	—	1309	1199	1029
	σ_{HP}	—	1290	1297	—	—	—	—	—	—	—	1284	1307	1331
3rd (R)	σ_H	—	1361	1328	—	—	—	1343	1370	—	—	—	937	1330
	σ_{HP}	—	1290	1297	—	—	—	1370	1292	—	—	—	1322	903

2) Tooth root bending fatigue strength check.

The tooth root bending stress and permissible bending stress calculated by Romaxdesigner are showed in Table VIIII.

Table VIIII

The bending stress and permissible bending stress by Romaxdesigner

Units: Mpa

mode	Stress	Z_1	Z_2	Z_3	Z_4	Z_5	Z_6	Z_7	Z_8	Z_9	Z_{10}	Z_{11}	Z_{12}	Z_{13}
1st (F)	σ_F	417	514	—	—	—	—	—	—	566	656	393	434	478
	σ_{FP}	568	807	—	—	—	—	—	—	809	817	809	575	831
2nd (F)	σ_F	417	514	—	—	—	703	703	—	—	—	268	296	339
	σ_{FP}	568	807	—	—	—	812	569	—	—	—	801	569	823
3rd (F)	σ_F	417	514	—	—	—	703	703	736	—	—	—	275	261
	σ_{FP}	568	807	—	—	—	812	569	807	—	—	—	801	810
4th (F)	σ_F	417	514	—	361	418	—	—	—	—	—	—	317	301
	σ_{FP}	568	807	—	559	794	—	—	—	—	—	—	792	801
1st (R)	σ_F	—	515	418	—	—	703	703	—	566	656	393	434	478
	σ_{FP}	—	807	811	—	—	812	812	—	809	817	809	575	831
2nd (R)	σ_F	—	515	418	—	—	—	—	—	—	—	268	296	339
	σ_{FP}	—	807	811	—	—	—	—	—	—	—	801	569	823
3rd (R)	σ_F	—	515	418	—	—	—	657	763	—	—	—	275	261
	σ_{FP}	—	807	811	—	—	—	812	807	—	—	—	801	810

3) The maximum contact stress and bending stress of gears.

The maximum contact stress and bending stress of gears are showed in Fig.4 and Fig.5.

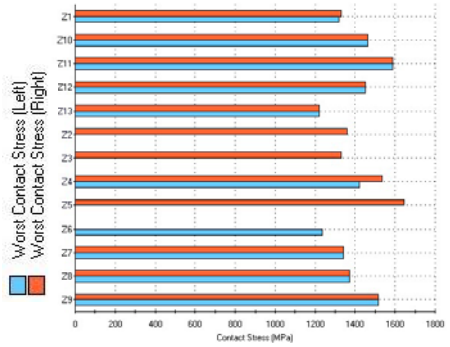

Fig.4 The maximum contact stress of gears.

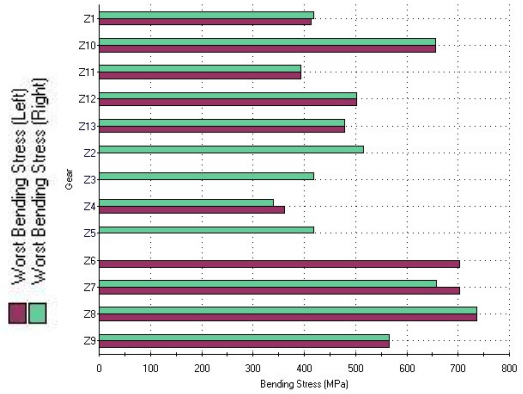

Fig.5 The maximum bending stress of gears.

4) Results Comparison

Comparing results in Table VI and Table VIIII, we can find that the bending stress and permissible bending stress of gears theoretically calculated have consistent trend with results from Romaxdesigner, and the values are close to each other.

Comparing results in Table V and Table VIII, the contact stress and permissible contact stress of gears have the same similar situation with the bending strength check. We can also see that the contact strength calculated by Romaxdesigner partly is a little insufficient, this is related to the limit load cycles of Fatigue life curve (SN curve), and so on. Considering practical application, the bending strength is the one have to be guaranteed first, on the other hand, it can be solved by increasing lubrication.

VI. CONCLUSION

This paper introduces the forces analysis and the process of contact strength and bending strength check of Loader Transmission Gearbox in seven kinds of speed conditions, theoretically. These results are consistent with those ones from Romaxdesigner software. It has certain reference value for force calculation and strength check of the multi-gears meshing system.

This paper only analyze the macro forces of gear trains of Transmission Gearbox, doesn't implement the micro-stress analysis, it is further to be studied.

REFERENCES

[1] G.-Y. Zhang, C. –X. Xu, Construction equipment chassis design, Beijing: Machinery Industry Press, 2004, pp. 130-135.

[2] Editorial Board of Machine Design Handbook, Mechanical Design Handbook, 3rd ed., Beijing: Machinery Industry Press, 2004, pp. 16-43～16-56.

[3] Jilin gong da, Wheel loader design, Beijing: China Building Industry Press, 1982.

[4] RomaxDesigner User Manual, Romax Technology Ltd, Nottingham,UK, 2003.

[5] L.-G.Pu, M.–G,Ji, Mechanical Design, 8thed., Beijing: Machinery Industry Press, 2006.

[6] Yi-shih Lin, Kristina Shea, A Method and Software Tool for Automated Gearbox Synthesis[C], IDETC/CIE 2009-86935.

[7] X.-L Zhu, Handbook of gear design, Chemical Industry Press, 2005.

2011 International Conference on Mechanical, Industrial, and Manufacturing Engineering
Lecture Notes in Information Technology Vols. 1-2

Study on Fixation mechanism of CuAz preservatives in Moso bamboo *

Wang Ya-mei and Wang Xi-ming
College of Material Science and Art Design
University of Inner Mongolia Agricultural
Hohhot, ZhaoWuDa Road 306,China
wangym80@126.com

Liu Jun-liang
Research Institute of Wood Industry
Chinese Academy of Forestry
Beijing, China
liujunliang@caf.ac.cn

***Abstract* - This research studies the fixation mechanism of CuAz preservatives in bamboo with ATR-FTIR. FTIR spectra analysis of bamboo powder, bamboo lignin and bamboo holocellulouse through chemicals around showed that interaction between CuAz preservatives and bamboo occurred in hemi-cellulose and lignin. Adsorption of copper is the main location of the carboxyl hemi-celluloses and lignin, products by interaction, which are mainly copper-oxygen and copper–carboxylate complexes bondings.**

Index Terms – Fixation, CuAz preservatives, Bamboo

I. INTRODUCTION

Fixation preservative is key factors to achieve long-term protection of bamboo, especially in the case of outside contact with soil and related to environmental safety. Copper-based preservatives fixation in the wood has conducted extensive research, especially for CCA, has published many reports on soil test of the CCA-treated wood and durability [1-9]. In recent years, fixation of other water-borne preservatives also begins to study, such as CCA, ACZA, Cu-N, CC, CuAz etc. [10]

Compared with wood, there were fewer studies on preservative fixation of bamboo. The researchers are in China, India, Bangladesh and pharmaceutical research is mainly CCA and CCB, etc. But fixation performance of CuAz preservatives on Moso bamboo is not been reported. In order to study the fixation mechanism of copper-azole preservatives, with bamboo as experimental materials, confer the chemical combination between preservatives and bamboo components with ATR Fourier transform infrared spectroscopy (ATR-FTIR).

II. EXPERIMENTAL MATERIALS AND METHODS

2.1 Experimental materials

Prepare the bamboo powder, bamboo lignin and bamboo holocellulose from 4 years Moso bamboo. Preservative is CuAz (Active ingredients：Cu, EA, TEB, BAC; Remark: $CuSO_4 \cdot 5H_2O$).

2.2 Experimental methods

Treat bamboo powder, bamboo lignin and bamboo holocellulose with CuAz, concentration0.4%. Specific ways: take about 2.5g into about 50g formula in 100ml flask, sealed and oscillate 24 h, filter with glass sand funnel, and then rinse with distilled water, until the eluate colorless far, specimens air-dry two weeks and oven dry 8h, analyze the infrared absorption of sample, confer the chemical combination between preservatives and bamboo components with ATR Fourier transform infrared spectroscopy (ATR-FTIR).

The fixation mechanism test used Nexus®670 IR spectrometer of the International Bamboo and Rattan Network center. The machine was made by THERMO NICOLET company in USA and its test range was 400～4000cm^{-1}. The research used reflect measure method with 50μm × 50μm range and 8 cm^{-1} distinguish rate.

III. RESULTS AND DISCUSS

Use CuAz treat bamboo powder, bamboo lignin and holocellulose, use ART-FTIR analysis and compare the bands change before and after treating, to speculate chemical combination of preservatives and bamboo components, and then analyze the fixation mechanism of preservatives in bamboo.

3.1 FTIR analysis of bamboo powder

Fig.1 is the infrared spectra of moso bamboo powder treated with CuAz and untreated.

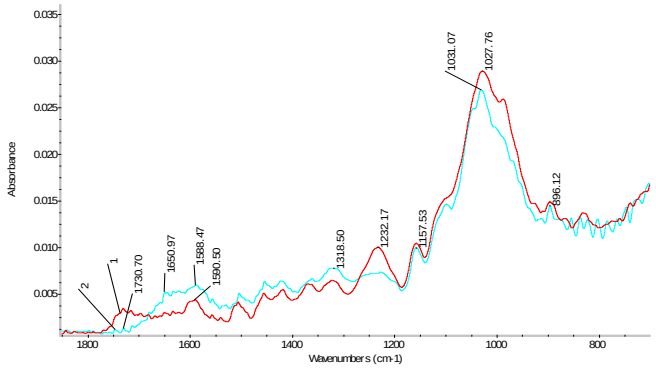

Fig.1 FTIR spectra of Moso bamboo powder treated with low content CuAz and untreated
(1.untreated Moso bamboo powder, 2. treated powder with CuAz)

In infrared spectra of low concentrations treated bamboo powder, 1740cm^{-1} absorption peak disappeared, near 1657cm^{-1}

* This work is partially supported by CNSF Grant #30860222 to W. Yamei.

and 1600cm^{-1} the peak intensity increased and near 1230cm^{-1} the peak weakened.

The disappearance of the 1740cm^{-1} absorption peaks, means that the carboxyl hemicellulose changed [11-12]. This is because the ligand exchange between CuAz and wood hemicellulose, caused the carboxylate anions increase of wood surface. In this reaction, a copper ammonia complexes ligand was replaced by carboxyl or carbonyl of bamboo components, and CuAz formed complexes with hemicellulose the carboxyl. At the same time, weak alkaline (pH 8 ~ 9) conditions, the lignin ester hydrolysis to become aromatic acid groups, and then form copper acid, would lead to near 1740 cm^{-1} absorption peaks weaken even disappeared. Near 1657cm^{-1} and 1600cm^{-1} peak increased, showed chain-substituted aromatic ketone and quinone carbonyl vibration and aromatic group skeleton vibration increased. 1600 cm^{-1} peak showed a sharp increase because carboxylates C=O stretching vibration increased, carboxyl in 1740 cm^{-1} absorption in the vicinity of the carboxyl group into carboxylates would transfer to 1600 cm^{-1}, this made 1600 cm^{-1} intensity increased.

Near 1230cm^{-1} is the absorption band of bamboo lignin Guaiacyl benzene ring and hemicellulose-oxygen bond (CO-O) stretching vibration, from the above analysis, 1230cm^{-1} peak significantly decreased may be the complexation of Cu with benzene ring lignin and hemicellulose carboxyl. From the spectra, we can see that the characteristics of cellulose 1425cm^{-1}, 1370cm^{-1}, and 895cm^{-1} were not significant form and intensity difference before and after treatment.

3.2 FTIR analysis of bamboo lignin

In order to analyze further the interaction between CuAz preservatives and bamboo, treated bamboo lignin and holocellulose, and studied the chemical combination between various components and preservatives. Fig.2 is FTIR spectra of *Moso* bamboo lignin treated with low content CuAz and untreated.

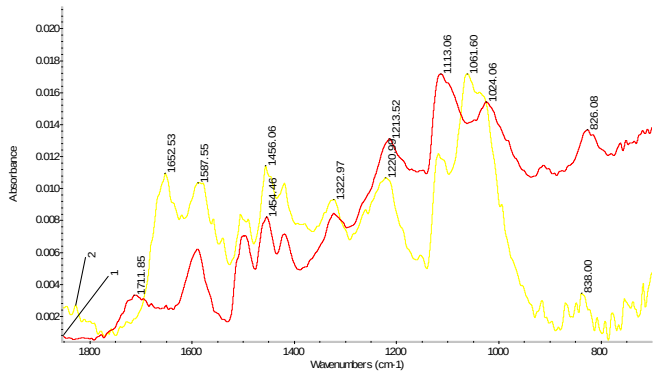

Fig.2 FTIR spectra of Moso bamboo lignin treated with low content CuAz and untreated
(1.untreated Moso bamboo lignin, 2. treated lignin with CuAz)

Bamboo lignin treated witn low concentration CuAz in 1712cm-1 the absorption peak weakened, because the region is non-conjugated ketone (carbonyl), the conjugate acid and their esters have absorption [13-14]. It is reported that the lignin acid in 1700~1715cm-1 has stretching absorption vibration of a feature carbon atom, lignin Guaiacyl propane, p-propane, lilac propane in 1705cm-1, 1709cm-1, 1710cm-1 have absorption [15].

This shows that in 1712cm^{-1} absorption is non-conjugated carbonyl.

1712cm^{-1} absorption peaks weakened after treatment, 1650cm^{-1} peak intensity increased. It is reported that the carboxyl content of lignin is very low. In alkaline solution, the ester group (1712cm-1) will become the carboxyl hydrolysis [16], the carboxyl and copper can further react to form acid copper, this led the 1712cm^{-1} absorption peaks weakened, 1650cm^{-1} increased. At 1220 cm^{-1} absorption is the reason of phenol, peak weakening showed the phenolic hydroxyl took part in lignin-copper complex formation. 1610cm^{-1} formed a new absorption peak, this can be considered phenol copper C-O stretching vibrations. Cu-O stretching vibrations of the 660cm^{-1} peak markedly enhanced showed Cu-O structure existed in treated bamboo.

FTIR spectra of *Moso* bamboo lignin treated with high content CuAz and untreated see figure 6, still 1712cm^{-1} absorption peaks weakened after treatment, 1650cm^{-1} peak intensity increased after high concentration treatment. Cu-O stretching vibrations of the 660cm^{-1} peak markedly enhanced, near 1510cm^{-1} absorption peak of the aromatic framework vibration weakened this is the characteristic peak of lignin.

3.3 FTIR analysis of bamboo holocellulose

From the spectra 4 we can see that the spectra change is not very clear. In spectra, 1740cm^{-1} absorption peak moved to 1730cm^{-1} and absorption peak intensity significantly weakened, it is the characteristic peaks of hemicellulose, means that the hemicellulose carboxyl changed and CuAz formed complex with the carboxyl of hemicellulose, 1600cm^{-1} absorption intensity increased, some people think that the majority of carboxyl of wood is from hemicellulose like uronic acid[17], copper absorption is ralated to these carboxyl component. In holocellouse spectra, 1510cm^{-1} has weaker absorption peak, may be a small amount of lignin caused. Another 1240cm^{-1} peak is the hemicellulose-oxygen bond (CO-O) stretching vibration absorption bands, significantly decreased peak showed the complexation of hemicellulose carboxyl and Cu.

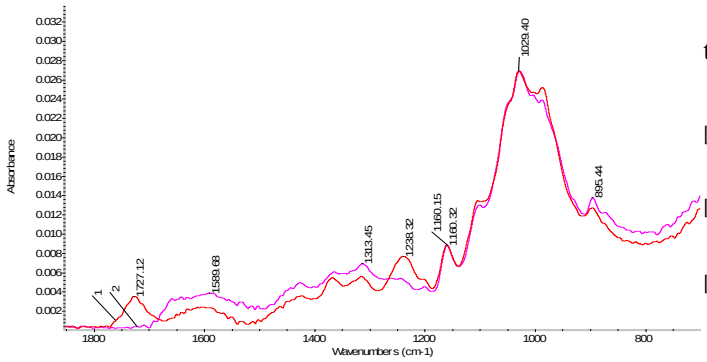

Fig.3 FTIR spectra of bamboo holocellulose treated with low content CuAz and untreated

(1.untreated Moso bamboo holocellulose, 2. treated holocellulose with CuAz)

Holocellouse is the mixtures of cellulose and hemicellulose, from the spectra can analyze, the form and intensity difference of cellulose characteristic peaks 1425cm^{-1}, 1370cm^{-1} and 895cm^{-1} before and after treatment was not significant, Cellulose studies show only a small part of the copper absorption, is likely to be the physical adsorption between copper and cellulose between, like van der waals' force, the results showed that copper absorption of cellulose was very limited, and in treatment conditions, aliphatic carboxylic acid to copper is not lively. In holocellouse, copper adsorption is the main location of hemicellulose-carboxylic acid and CO-O.

Ⅳ. Conclusions

This research studies the fixation mechanism of CuAz preservatives in bamboo through analyzing the FTIR spectra of bamboo powder, bamboo lignin and holocellulose before and after treatment with ART-FTIR to speculate chemical combination of preservatives and bamboo components, the results show:

（1）FTIR spectra analysis of bamboo powder before and after treatment shows this is because the ligand exchange between CuAz and wood hemicellulose, caused the carboxylate anions increase of wood surface. The absorption band of bamboo lignin Guaiacyl benzene ring and hemicellulose-oxygen bond (CO-O) stretching vibration significantly decreased is caused by the complexation of Cu with benzene ring lignin and hemicellulose carboxyl.

（2）In order to analyse further the interaction between CuAz preservatives and bamboo, treated bamboo lignin and holocellulose. The results shows: the infrared spectra of lignin after treatment have been a significant change, Lignin characteristic peaks (1510cm^{-1}) changes obviously. Lignin phenolic hydroxyl is involved in the lignin-copper complex formation. Holocellouse spectra after treatment changed little, it is just the hemicellulose carboxyl and hemicellulose acyl-oxygen bond (CO-O) stretching vibration changed.

Acknowledgment

This work was supported by the grant (30860222) from the National Natural Science Foundation of China.

References

[1] Permad, i P., DeGroot, R. C., Woodward, B. Alternative Wood Preservatives for Use in Indonesia[J]. Forest Prod. J,1998,48(11/12): 98-101.

[2] Lebow, S. Leaching of Wood Preservative Components and Their Mobility in the Environment[R]. USDA, Forest products laboratory，General Technical Report, 1993, FPL-GTR-93, 1-36.

[3] Venkatasamy R. The effects of pH on leaching of copper-chrome-arsenate (CCA) from pressure-treated Kenyan-grown Eucalyptus saligna and Acacia mearnsii: Initial findings[C]. International Research Group on Wood Preservation, International Research Group on Wood Preservation, 2002, IRG/WP 02-30298B. Simpson, et al, “Title of paper goes here if known,” unpublished.

[4] Venkatasamy R. The influence of age on retention and fixation of CCA in pressure-treated Kenyan-grown Eycalyptus saligna: Summary of findings[C]. International Research Group on Wood Preservation, 2002, IRG/WP 02-30296.

[5] Crawford D et al. Laboratory studies of CCA-C-leaching: Influence of Wood and Soil Properties on Extent of As and Cu Depletion[C]. International Research Group on Wood Preservation, 2002, IRG/WP 02-50186.

[6] Rao, M.V., Kuppusamy, V., Rao, K. S., Santhakumaran, L.N. Leaching of CCA preservative from treated timber in marine environment[C]. International Research Group on Wood Preservation, 2001, IRG/WP 01-30254.

[7] Willeitner, H, brandt, K. Problems of fixation of CCA-preservatives in palm-wood[C]. International Research Group on Wood Preservation, 1985, IRG/WP 3338.

[8] Cooper P A, D Jeremic, Y T Ung. Cooper Effectiveness of CCA fixation to avoid hexavalent chromium leaching[C]. International Research Group on Wood Preservation, 2002, IRG/WP 02-50187

[9] Kennedy M J. Leaching of preservative components from pine decking treated with CCA and copper azole,and interactions of leachates with soils[C]. International Research Group on Wood Preservation, 2001, IRG/WP 01-50171.

[10]Miao jiancai.Harbin:Northeast forestry university press, 1995:17-18.

[11]Bolker NI，Somerville NG. Infrared spectroscopy of lignins. Part II. Lignins in unbleached pulp[J]. Pulp and paper Canada, 1963, (4):187-193.

[12]Michell AJ, Wetson AJ, Higgins HG. An infrared spectroscopic study of delignification of Eucalyptus regnans[J]. Tappi, 1965, (48):520-532.

[13]Miha HUMAR, Marko PETRIÈ. Determination of ethanolamine in impregnated wood[C]. International Research Group on Wood Preservation, 2000, IRG/WP 00-20198.

[14]Petriè M, Pohleven F, Turel I, egedin P, White AJP, Williams DJ. Complexes ofcopper(II) carboxylates with 2-aminoethanol syntheses, characterization and fungicidal activity; crystal structure of Cu(O2CC8H17)2 (NH2C2H4OH)2[J]. Polyhedron, 1997, (17):255-260.

[15]Hughes AS. Studies on the fixation mechanisms, distribution and biological performance of copper-based timber preservatives[D]. Ph. D. thesis, Imperial College of Science, Technologyand Medicine, London, 1999, 313.

[16]Rodrigues J. Determination of lignin content of eucalyptus globulus wood using FTIR spectroscopy[J]. Holzforschung, 1998, (42):46-50.

[17]L.Jin&K Archer. Copper Based Wood Preservatives:Observation on Fixation,Distribution and Performance[R]. preprints for American Wood-Preservers' Association Apr, meeting, 1991.

2011 International Conference on Mechanical, Industrial, and Manufacturing Engineering
Lecture Notes in Information Technology Vols. 1-2

Research on the Formation Mechanism of the Innovative Enterprises Growth Path

Tao Guo and Xiaomeng Niu
School of Economics and Management
Harbin Engineering University
Harbin, Heilongjiang Province, China
solesunnie@126.com

***Abstract* – Defined the innovative enterprises growth path, explained the growth process of the innovative enterprises that the innovative enterprises achieve the developing goals through interaction between the quality growth and the quantity growth of the innovative enterprises. thoroughly analyzed the formation of the innovative enterprises growth path by means of the complexity theory, revealed the innovative enterprise growth path including gradual path, mutant path, and hybrid path.**

Index Terms - formation mechanism, innovative enterprises, growth path.

I. INTRODUCTION

With the advent of post-crisis era, the world economic "recovery" is facing many uncertainties, grasping the initiative after the economy bottomed to accelerate economic recovery has become the subject of a new round of competition. It is important for change in China's economic development to face the reality of conditions according to China's development status, and keep a correct understanding of the growth path of innovative enterprises to explore the right route to sustainable growth, no matter from innovative enterprises their own point of view to survive and develop, or the innovative long-term strategic goal of nation-building.

II. DEFINATION OF INNOVATIVE ENTERPRISES GROWTH PATH

Innovative enterprises with the innovation capability as core competencies, is the new enterprises that rational allocate the resources and the ability of the organization, create business value to gain the sustainable survival and development of the enterprises. For study on the formation mechanism of the innovative enterprises growth path, the first task is to accurately define the growth path of innovative enterprises meaning. The interpretation of the path, it is the route to the destination.

So explain the innovative enterprises growth path, can be defined as that line or means of an innovative enterprises to achieve business goals. Although this definition can be initially defined the meaning of corporate growth path, but for the management of corporate real meaningful guidance, so we need a more practical effect definition. The definition of innovative enterprises growth path should be combined with innovative enterprises to see their own characteristics, so as to obtain more accurate and more specific definition. Innovative enterprises growth path can be so defined, that is a series of methods, ways and means to achieve the business objectives of corporate survival and sustainable development, through the rational allocation of enterprise resources and capabilities, with its core ability base for the operation of the innovation enterprises.

III. INNOVATIVE ENTERPRISES GROWTH PATH UNDER THE INERACTION BETWEEN THE QUALITY GROWTH AND THE QUANTITY GROWTH

A. Interaction between the Quality Growth and the Quantity Growth

The growth of innovative enterprises refers to the enterprises from small to large and from weak to strong in the development process. It includes two aspects: the amount increase and quality improvement. Amount increase, the quantity growth, refers to the expansion of enterprise scale. you can use the scale of production, capital size, market share, product output, employees number, and other indicators to measure it. Quality improvement, the quality growth, means improving the quality of the enterprise, which is the better essence meaning of the business growth, reflected in the production process technology and product technology from immature to mature technology innovation, but also in business organizational innovation & change, and other aspects.

The growth of innovative enterprises is the unity of the quality and quantity, also the interaction of quality and quantity. Quality improvement of the enterprises promote the growth of quantity, that because the quality improvement increase the enterprise the overall system efficiency, so that enterprises put into production with less but get more output; Quality improvement make changes in the enterprise's products performance, so as to promote products sales, increase in corporate profits, and improving the scale of output; Product Innovation provides room for the quantity growth, to enable enterprises to market a certain amount of new products; organizational functions change to make business organization and management more efficient. Although this change is through the influence on the interaction and contact of information & value main activities

of the subsystem or unit to achieve, that improve the overall efficiency of the enterprise, promote the effectiveness of technological innovation activities. Meanwhile, the quantity growth also contributed to the qualitative improvement, and the quality improvement in any terms all need the enterprise quantity accumulation. For example: if enterprises conduct technical innovation, we must get a certain amount of production factors and resources. the quantity growth provides a solid foundation and broad space for the quality Improvement. Without the support of quantitative , qualitative improvement just like the river without water, or forest without trees, they will lay as the tall buildings with no foundation, crumbling and eventually collapse. Therefore, the quality improvement and quantity growth are the two unified aspects in the process of the firm growth, that is interaction of quality and quantity.

B. Enterprise Growth Path for Stage Objectives

Reflected in the growth path of innovative enterprises, business development goals can be decomposed into the growth stage business objectives, its growth path can be described as the following figure (Figure 1).

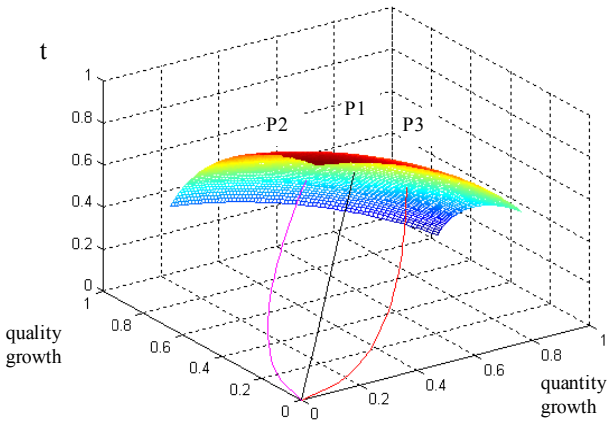

Fig. 1 the Enterprise Growth Path for Stage Objectives

If we take the stage enterprises growth objectives as the short-term growth targets, it is reflected in the diagram can be described as a spherical surface. The enterprise growth path begin with the origin 0, the initial state of business growth, through a variety of enterprise rational allocation of resources and capabilities so as to achieve the target surface, that is to say the enterprises will complete the stage target. In this process, a variety of configuration methods, ways and means of resources and capabilities is that enterprises meet milestones in the growth path.

In the business growth process, when the quantity growth and quality growth were close to each other or reach a state of relative equilibrium, we obtained the P1 path, then the enterprise relative balance between quality and quantity; if companies pay more attention to the quality of the actual operation growth, available resources and capabilities in the enterprise under this conditions is fixed, and the amount of investment for quantity growth is bound to reduce, its growth path as P2, in the quality, quantity and time of the three-dimensional space, will be biased in favor of the quality growth side; if companies more likely to break quantity indicators, the relative qualitative input reduce, then its growth path will tend to grow in quantity side.

It should be noted that the growth process in the enterprise, the quality growth and the quantity growth are inextricably linked, and interactive in relevancy. Qulity grow, while quantity grow; Quantity growth also will increase the quality., but different degree and growth proportion of investment will lead to different final results. Whether emphasis on quality growth, or the quantity growth, or a combination of the two, in ideal conditions, the inevitable result of its growth is to achieve the setting stage business objectives, so its growth path of the side bias regardless, or what the specific track show does not affect it reach the predetermined target surface, complete the milestones.The only difference between the quality growth and quantity growth is on the different superimposed effects in the timeline, the different lengths of time used. For business growth and development, this time minimum means optimum of it? The answer is no.

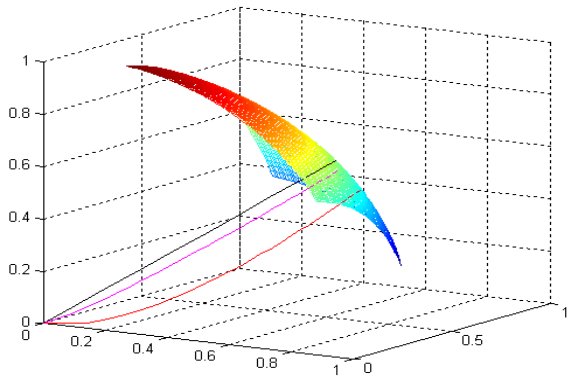

Fig. 2 the Enterprise Growth Path for Stage Objectives 2

Figure 1 for the rotation, rotated in Figure2, you can obviously see different growth path trajectories reach the target in the face, that did not set at the same point, but on different points scattered in a sphere, which means that enterprises in different growth path, its growth had the same total degree, but not the same as the state reached. In other words, the same allocation of available resources and capacity issues, the business focus is not just about the time of reaching the different milestones, but also affect the enterprises state after the completion of thetarget, such as the remaining resources and excess capacity situation, thereby affecting the enterprse's next strategic plan, and even affect the long-term development.

In business growth process, one or two decision-making is insufficient to support the sustainable and healthy development of enterprises, the "setting goals - targets achievement- stage growth," decision-making process continued in cycles, will enable enterprises to achieve the purpose of growing .

Ⅳ. FORMATION OF COMPLEX SYSTEM EVOLUTION PATH OF INNOVATIVE ENTERPRISES GROWTH

Complexity theory suggests that the evolution of complex systems are mostly carried out through three ways: First, the system self-organization. Self-organization allows the system to change the internal structure to better adapt to the environment, to make the system to change its internal structure a little bit in the learning process, this process is a gradual style. Second, the dissipation of the system.

With the interaction between the system and one or more other organizations, the internal organization will be able to continue, if the fluctuation within the system maintain a certain extent. If the fluctuation exceeds a certain limit, the system will lose stability, then the system will face two states: collapse, which is the degradation of the system, or jumped to a new level, the emergence of new functions, the system occurred new qualitative change, which is the evolution of the system, this process is abrupt for. Third, the system self-organized criticality. Complex system have the ability to keep the balance between random change and stagnation, so that a system to reach a critical point, do not take any action on the system can be rendered at the brink of collapse.That complex systems far from equilibrium in the critical state, does not follow a gentle, gradual evolutionary approach as usually, but by the intermittency and chaos evolution way similar to avalanche. And this process is abrupt.

The theoretical study shows that, whether natural or human society, The development and evolution process of objective material is widespread, which process typically consists of two paths - gradual and mutant. This paper argues that enterprise as a man-made complex organic system, its growth follows the law, so that business growth also has two paths - gradual and mutant.

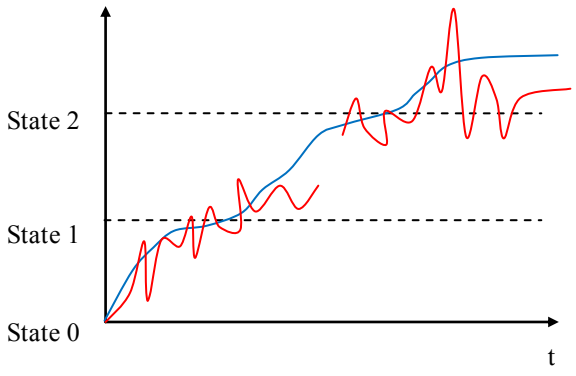

Fig. 3 gradual growth and mutant growth

From this, the gradual growth, means the enterprises showing a slow, steady and continuous evolution, the elements of the enterprise systems and the relation among them do not change much in a period of business existence. Enterprises growth process is gradual, with no obvious inflection point. Enterprise system is in relatively stable (equilibrium) state, slowly changing from one steady state to another.(blue line in the fig3)

Mutant growth of the enterprise, is enterprises showing a fast, unstable, discontinuous evolution, the enterprise itself and the elements of the system and between the various elements have larger changes, in a period of business existence. Business growth process is intense, mutation, and have a clear inflection point or a breakpoint. Enterprise system is relatively unstable, non-equilibrium state, will rapidly change from one stable state to another stable state.(red line in the fig3)

And because of the complexity and dynamic of the growth of innovative enterprises , we can integrated use of two paths according to the actual situation to guide the enterprises growth strategy formulation and operational decision-making. We call it the hybrid growth path. Therefore, the growth path of innovative enterprises can be divided into three types.

Ⅴ. THREE INNOVATIVE ENTERPRISES GROWTH PATHS

According to the foregoing analysis, in the dynamic and complex business conditions and business environment, there are three growth paths for the innovative enterprises. enterprises can select the appropriate path according to the actual situation.

A. Innovative Enterprises Gradual Path

Refers to that the innovative companies use their own core competencies or core competitiveness to reach a relatively stable and continuous growth of the enterprises with the accumulation of management resources and capabilities.

B. Innovative Enterprises Mutant Path

Mutant growth path is that, innovative companies jumped off the original business direction or the direction of corporate strategy, relying on the business opportunities and uncertainties, facing the changes in response and control, reasonable planning, so as to realize incontinuous, rapid growth.

C. Innovative Enterprises Hybrid Path

Innovative enterprises synthetically use two kinds growth paths in the process of business growth, rationally manage and operate the available resources and capabilities in the enterprise and achieve the growth effect both of the gradual way and the matant way.

Business growth the process of interaction and wheeled with three elements, the internal factors, external environment and the subjective efforts. Accurately determine the situation of the enterprise is situated, at the right time to choose the right growth path, enterprises will achieve sustained and rapid development route.

ACKNOWLEDGMENT

The finance supported by the fund of China Ministry of Education for Humanities and Social Sciences project is acknowledged. This work was developed within the project ‘ Research on Growth Path of Underdeveloped Areas Innovative Enterprises’(Fund No.:10YJC630064). This paper also developed from the ‘Social Science Fund of Heilongjiang Province’ (Fund No.:08D002)

REFERENCES

[1] Amit R, Schoemaker P J H. Strategy assets and organizational rent. Strategic Management Journal, 14(1), 1993 ·

[2] Jianjun Wang. Research on Enterprise Growth Model and the Influence Factors. An Academic Edition of ManaMag, March,2010

[3] Yuli Zhang. The Dissymmetry of Firm Growth Law to be the Draft of National Capital Law. Journal of Capital University of Economics and Business, June, 2004

[4] Haijian Liu, Songtao Chen, Chuanming Chen. The Rigidity and Its Exceed for the Corporations' Core Competence. China Industrial Economy, 2003

[5] Tao Guo, Yu Lou, Xianglin Teng. Research on Knowledge Innovation System of Enterprise Based on Complexity Theory. , Journal of Information, Apirl, 2008

2011 International Conference on Mechanical, Industrial, and Manufacturing Engineering
Lecture Notes in Information Technology Vols. 1-2

Effect of Polypropylene Grafted Maleic Anhydride on Properties of Flame Retarded Polypropylene Composite

Zhou-qiao Lei, You-ming Cao, Fei Xie, Hui Ren
Faculty of Polymer Materials and Engineering
Guangdong University of Technology
Guangzhou Higher Education Mega Center, Guangzhou City 510006, P. R. China
Leizq8677@yahoo.cn

***Abstract* - The flame retarded PP composite was prepared by torque rheometer. The mechanical properties of PP composite was examined, the flammability characterization was studied by thermogravimetric analysis (TGA), limiting oxygen index (LOI), differential scanning calorimetry (DSC),** and the **microcosmic structure of the composites was researched by scanning electron microscope (SEM). The results showed that PP-g-MAH could enhance the affinity between flame retardant and PP, and with the increasing of the content of PP-g-MAH, the tensile strength, elongation at break of composite increased at first, then decreased a little; when the content of PP-g-MAH was 5wt%, the flexural strength was a maximum, but the notched impact strength decreased and the flame retardant properties were a little alteration with increasing of the amount of PP-g-MAH. The initial decomposition temperatures were fall with increasing of the amount of PP-g-MAH; but the maximum endothermic temperatures were increase.**

***Index Terms* – polypropylene, PP-g-MAH, IFR, compatibility, thermal property**

1. Introduction

Polypropylene (PP) as one of the five common plastics, with excellent mechanical properties, chemical resistance and electrical insulation, is widely used in automobile, insulation, building materials, etc [1-2]. However, PP has many drawbacks; the most deadly shortcoming is easy to burning, which limits its application. Flame retardant added into Polypropylene is a good way to improve the combustion properties of polypropylene [3-4]. Such as, the environmentally friendly intumescent fire retardant (IFR) added into plastic for fire retardant treatment has been obtained more and more researcher's interest. The intumescent fire retardant (IFR), while burning, gave a swollen multicellular char which protects the underlying material from the action of the fire. The mechanism of the IFR is assumed that the multicellular char as a physical barrier against heat transmission and oxygen diffusion, thus preventing pyrolysis of polymer to volatile combustible products. But the dominant intumescent flame retardant has polarity, so the compatibility between intumescent flame retardant and non-polar PP is poor. The mechanical properties of composite materials are seriously decreased with increasing of flame retardant, which seriously limites the range of its applying fields. Therefore, it is important to improve the compatibility of flame retardants and PP in order to improve the composite mechanical properties, rheological behavior and widening the scope of application of PP [5-6]. Many researches have reported that the polypropylene grafted maleic anhydride (PP-g-MAH) as a compatibilizer has obvious effect.

In this paper, the intumescent flame retardant (IFR) system is composed of ammonium polyphosphate (APP) and pentaerythritol (PER), and the PP-g-MAH is selected as compatibilizer to research various compatibilizer contents how affect the mechanical properties, flame retardant properties, thermal properties and microstructure morphology of composite materials.

2. Experimental

2.1 Materials

PP (T30S) with a melt flow index (MFI) of 3.0 g/10 min (230℃/2.16 kg) was provided by Da Qing Petroleum Chemical Company. APP with average degree of polymerization n>1,000 was kindly supplied by Hangzhou JLS Flame Retardants Chemical Corporation.

Pentaerythritol (PER) was provided by Tianjin kermel chemical reagents development centre. PP-g-MAH was purchased from Huangpu district Guangzhou paoji plastic factory.

2.2 Preparation of Flame Retarded PP Composites

Samples were mixed at 50 revolutions per minute screw speed at 180℃ for 10min. At first; polypropylene and PP-g-MAH were melted at 180℃ in the torque rheometer (shanghai P.R. China) for 2min, and then APP and PER was added to the molten PP.

Mixed materials were hot-pressed at 180℃ under 10MPa for 10min into sheets after mixing; the samples were hot-pressed at 180℃ under 10MPa for 10min into the sheets with dimensions of 160×160×3mm.The formulation were given in Table 1.

TABLE. 1 Formulation of PP/IFR/PP-MAH composites

Sample code	a	b	c	d	e
PP-g-MAH (wt %)	0	3	5	7	9
PP (wt %)	70	70	70	70	70
APP (wt %)	22.5	22.5	22.5	22.5	22.5
PER (wt %)	7.5	7.5	7.5	7.5	7.5

3. MEZSUREMENTS

3.1 Mechanical testing

The dimensions of the samples with 100×10×4mm were prepared by injection moulding. The tensile strength and elongation at break were measured with a CMT4204 Universal Testing Machine (Shenzhen, P.R. China) at 50mm/min according to GB/T9341-2000, the flexural strength were measured using a CMT4204 Universal Testing Machine (Shenzhen, P.R. China) with a speed of 2mm/min according to GB/T1040-92, the notched impact strength was measured with a XJU-22(Chengde, P.R. China) according to GB/T 1834-1996.

3.2 TG-DSC

TG-DSC was carried out using TA Instruments STD 2960, US. The samples were heated from room temperature to 700℃ at heating rate 10℃/min under nitrogen with a flowing rate of 10ml/min.

3.3 Limiting oxygen index (LOI)

LOI was measured according to ASTM D4863-77. The apparatus was an HC-2 oxygen index meter (Jiangning Analysis Instrument Company, P.R. China).The specimens used for the test was of dimensions 100×6.5×3mm according to ASTM D 2863

3.4 UL-94 testing

UL-94 vertical burning tests were carried out on an AG5100A instrument (AnGui Analysis Instrument Company, P.R. China). The specimens used for the test were of dimensions 130×13×3mm according to UL-94 test standard.

3.5 Scanning electron microscopy (SEM)

The SEM micrographs of the sections of PP composites after being gold-sputtered were obtained by a Hitachi X-650 scanning electron microscope (Japan).

4. RESULTS AND DISCUSSION

4.1 Mechanical properties

The effect of the PP-g-MAH addition on the mechanical properties of composite materials was showed in Fig 1and Fig.2.

Fig.1 indicated that the tensile strength, elongation at break increased with increasing the amount of PP-g-MAH additive at first. However, when the PP-g-MAH addition was more than 5wt%, the tensile strength, elongation at break declined slightly. The tensile strength, elongation at break reached a maximum value at addition of 5wt% of the PP-g-MAH. The tensile strength had obvious increase when the content of PP-g-MAH added less than 3wt%, but then the change was not too obvious when the content of PP-g-MAH added more than 3wt%.

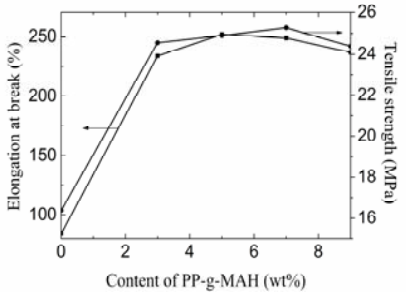

Fig.1 Effect of PP-g-MAH addition on tensile strength and elongation at break of PP/IFR/PP-MAH

The notched impact strength and the flexural strength

were showed in Fig.2.

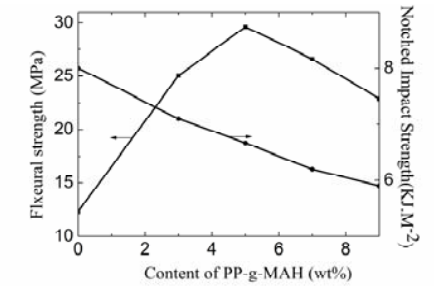

Fig.2 Effect of PP-g-MAH addition on notched impact strength and flexural strength of PP/IFR/PP-MAH

From Fig.2, it can be seen that the notched impact strength declined with increasing the amount of PP-g-MAH additive. The flexural strength increased with increasing the amount of PP-g-MAH additive at first, but when the PP-g-MAH addition was more than 5wt%, the flexural strength declined.

The improvement of the mechanical properties can be attributed to the increase in the adhesion between IFR and PP substrate by means of the compatiblizer. The grafted maleate groups increased the polarity of the grafted polymer. The polar carboxyle groups in the side chains of the grafted PP had good compatibility with IFR, thus improved the adhesion between IFR and PP. However, the content of PP-g-MAH is above a numerical value, the mechanical properties of composite materials decreased for increasing of the low molecular chain scission of the blends. With increasing of the PP-g-MAH content, the notched impact strength of composite materials became worse, mainly due to PP-g-MAH molecular chain was relatively short, crisp and poor deformation ability can not effectively absorb impact energy, thus resulting in poor the notched impact strength of composite materials.

4.2 Thermal and flame retardant properties

The LOI value and UL-94 tests of composite materials were listed in the table 2. Table 2 indicated that the LOI value and UL-94 tests hardly changed. These results can be explained that the PP-g-MAH didn't have flame retardant synergistic effect.

TABLE.2 LOI value and UL-94 results of PP/IFR/PP-g-MAH bends

Sample code	a	b	c	d	e
UL94 Rating	V-0	V-0	V-0	V-0	V-0
LOI value	27	28	29	29	28

Fig.3 and Fig.4 showed the TGA and DSC curves respectively. For pure PP, the temperature began to decompose at about 288℃. The maximum endothermic temperature (T_{maxen}) was 446℃. The residual weight of PP was 0.8% at 680℃. Compared with pure PP, the temperature beginning to decompose of the PP/IFR(a) at about 210℃, because the thermal stability of IFR system was poor, and ammonium polyphosphate was easy to emit ammonia to form polyphosphoric acid, which can easily react with PER. However, the T_{maxen} occured about 460℃ as it can be seen from the DSC curve. These results can be explained that the IFR gives a swollen multicellular char at high temperature which protects the underlying material from the action of the fire. For the PP/IFR/PP-MAH(C) composite, its initial decomposition temperature was 200℃, the T_{maxen} was 471℃, and the residue at 680℃ reached to 16.7%. The results showed that PP/IFR/PP-MAH (C) composite materials can form a more stable multicellular char compared to PP/APP/PER (a).

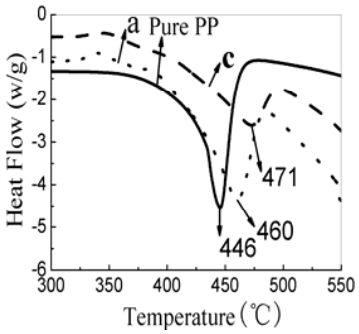

Fig.3 DSC curve of pure PP, PP/IFR (a) and PP/IFR/ PP-g-MAH(c)

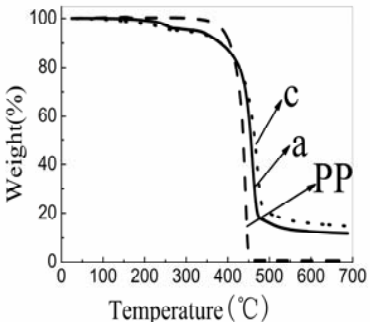

Fig.4 TG curve of pure PP, PP/IFR (a) and PP/IFR/ PP-g-MAH(c)

4.3 The SEM of PP composites

The 1,000 times SEM of PP/IFR and PP/IFR/PP-g-MAH were showed in Fig.5 and Fig.6, it can be clearly seen that there was bigger gab between APP particles and PP for PP/IFR and there is almost no gap between APP and PP for PP/IFR system containing compatibilizer PP-g-MAH. Because APP had polar groups $—NH_4$ whose polarity was different from PP, the no-match of the polarity make the compatibility between APP and PP was poor. However, for PP/IFR/PP-g-MAH composite, carboxyle groups in the side chains of the grafted PP were compatible with IFR. Whereas the main chain of the grafted polymer has good compatibility with PP, and thus improved the adhesion between IFR and PP.

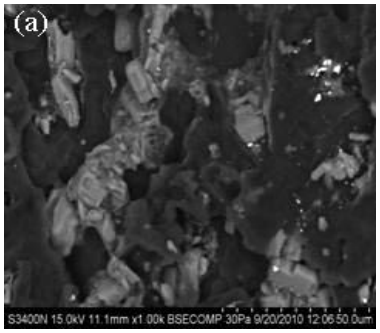

Fig.5 The SEM picture of PP/IFR(a)

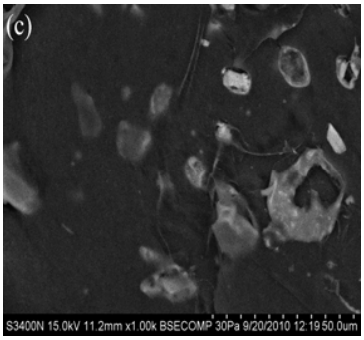

Fig.6 The SEM picture of PP/IFR/PP-g-MAH(c)

5. CONCLUSIONS

1) With increasing the amount of PP-g-MAH, the tensile strength, the elongation at break and the flexural strength of PP/IFR/PP-g-MAH composites increased at first and then decreased, but the notched impact strength decreased with increasing the amount of PP-g-MAH additive. The flame retardancy of the composites had little effect with increasing the contend of PP-g-MAH. The composite system had the best properties when the contend of PP-g-MAH is 5wt%.

2) The initial decomposition temperatures of composite materials were fall with adding of PP-g-MAH, but the T_{maxen} increased, when PP-g-MAH was added into PP/IFR system. The ultimate residue at 680℃ was 0.8% for pure PP and 16.7% for the PP/IFR/PP-MAH (C).

3) The PP-g-MAH was obvious improvement the compatibility between IFR and PP.

REFERENCES

[1] X. Almeras, F. Dabrowski, M. Le Bras, R. Delobel, S. Bourbigot, G. Marosi, et al., "Using polyamide-6 as charring agent in intumescent polypropylene formulations II. Thermal degradation,"Polymer Degradation and Stability, Vol. 2, pp. 315-323, Aug 2002.

[2] K. Wu, L. Song, Z. Wang, Y. Hu, "Preparation and characterization of double shell microencapsulated ammonium polyphosphate and its flame retardance in polypropylene,"Journal of Polymer Research, Vol. 3, pp. 283-294, 2009.

[3] X. Almeras, F. Dabrowski, M. Le Bras, F. Poutch, S. Bourbigot, G. Marosi, et al., "Using polyamide-6 as charring agent in intumescent polypropylene formulations I. Effect of the compatibilising agent on the fire retardancy performance,"Polymer Degradation and Stability, Vol. 2, pp. 305-313, Aug 2002.

[4] S. H. Chiu, W. K. Wang, "Dynamic flame retardancy of polypropylene filled with ammonium polyphosphate, pentaerythritol and melamine additives,"Polymer, Vol. 10, pp. 1951-1955, May 1998.

[5] C. Y. Sun, Q. B. Zhang, B. Li, "The water resistance of surface-modified APP with melamine-TDI in LLDPE,"Journal of Polymer Research, Vol. 6, pp. 505-509, Dec 2007.

[6] K. Wu, Z. Z. Wang, H. J. Liang, "Microencapsulation of ammonium polyphosphate: Preparation, characterization, and its flame retardance in polypropylene,"Polymer Composites, Vol. 8, pp. 854-860, Aug 2008.

2011 International Conference on Mechanical, Industrial, and Manufacturing Engineering
Lecture Notes in Information Technology Vols. 1-2

Study on Polyvinyl Chloride blends modified by Powdered Nitrile Butadiene Rubber

Hao Wu, Youming Cao, Xinghao Sun

Faculty of Materials and Energy
Guangdong University of Technology
Guangzhou, Guangdong Province, China

wu.hao_happy@163.com

***Abstract* - In this paper, the polyvinyl chloride blends modified by powdered nitrile butadiene rubber were prepared by melt blending method, and the mechanical properties of the blends were measured using microcomputer control electronic universal testing machine, thermal properties were tested by differential scanning calorimetry-differential thermal analysis and macrostructure was observed by scanning electron microscopy. While the content of NBR was increased, the elongation at break of PVC composites greatly enhanced, tear strength and tensile yield stress slightly decreased, the tensile strength was almost not changed. When rare earth calcium-zinc stabilizer was added in 2phr, the PVC blends have good thermal stability. The NBR improved the interfacial adhesion between PVC and $CaCO_3$.**

Index Terms - PVC, NBR, rare earth calcium-zinc stabilizer.

I. Introduction

Polyvinyl chloride (PVC) is the second largest general-purpose resin in the world. The consumption of PVC is just less than the consumption of polyethylene. For a long time, PVC was used to manufacture doors and windows of profile shapes, drainage pipes, preservative films, agricultural films, wood grain film and so on, but the poor toughness and thermal stability limited the application of PVC in areas of higher requirements for performance.

Nitrile butadiene rubber (NBR) has good compatibility with PVC. Low addition of NBR can improve the toughness of PVC significantly. Rare earth calcium-zinc stabilizer has non toxic, high efficiency, and widely prospect for application as a non-toxic and environmentally friendly stabilizer. In recent years, many scholars carried out relevant studies. In Ref. [1], Deng Yueyi blended PVC with NBR and nano-$CaCO_3$. The notched impact strength was 24MPa and elongation at break was 140% for PVC/NBR/ nano-$CaCO_3$ at a weight ratio of 100/0/8. The notched impact strength increased to 30MPa and elongation at break reached 260% for PVC/NBR/nano-$CaCO_3$ at a weight ratio of 100/12/8. The SEM photograph indicated that NBR could enhance the dispersive degree of nano-$CaCO_3$ and the plastically fibrous deformation arose on the fracture surface of the PVC blends，which was associated with the improvement of impact strength. In Ref. [2,3], Wang Qingguo prepared the composites composed of PVC and ultrafine vulcanized powdered nitrile butadiene rubber(NBR-UFPR). The results indicated that NBR-UFPR particles of different size could increase the toughness and thermal stability of rigid PVC simultaneously. The mechanical performance increased with the particle size decreased. In Ref. [4], Liu Wenjing studied the properties of PVC soft products modified by liquid NBR. The tensile strength and elongation at break rose to peak and then followed by a gradual reduction with the increased addition of NBR. The elongation at break of PVC products improved obviously and tensile strength improved slightly with the addition of NBR at 10-20phr. In Ref. [5], Gong Yaohua tested the thermal stability of PVC at 180℃. When added in a single calcium-zinc stabilizer, the steady flow time of PVC was only 15.1min. When added in calcium-zinc stabilizer and 3.5phr rare earth stabilizer, the steady flow time of PVC reached 114.6min, which indicated that rare earth/ calcium-zinc complex stabilization system had good synergistic effects.

Our work was improving the toughness and thermal stability of PVC. In this paper, PVC was modified by blending NBR to improve the toughness and adding rare earth calcium-zinc stabilizer to improve the thermal stability. The work was the basic study for multi-layer composite home appliance membrane.

Ⅱ. Experiental section

2.1 Materials and equipments

The materials used in this paper listed in Table 1.

TABLE 1 MATERIALS USED IN THIS PAPER

Materials	*Content(phr)*	*Name*	*Manufacture*
PVC	100	S-60	Formosa plastics corporation, Taiwan
NBR	0-41	Chemigum P83	Eliokem company,France
rare earth calcium-zinc stabilizer	0-6	GS-21A	Guangyang hi-tech Co.Ltd, P.R.China
barium-zinc stabilizer	0-2	Industrial	
DINP	20	Industrial	
epoxy soybean oil	2	Industrial	
$CaCO_3$	20	Industrial	

Two-roll open mill for plastics, SK-160B, Shanghai sinan rubber machinery Co.Ltd. Plate vulcanizing machine(for hot pressing), QLB-D, Shanghai rubber machinery works No.1 Co.Ltd. Plate vulcanizing machine(for cold pressing), ST92-70,Guangzhou leather machinery company. Microcomputer control electronic universal testing machine, CMT4204, Shenzhen xinsansi materials testing Co.Ltd. Scanning electron microscopy, S3400N, Hitachi company, Japan.

Differential scanning calorimetry-differential thermal analysis(DSC-TGA), SDT 2960, Ta instruments of America.

2.2 sample preparation

Mixed powder PVC and thermal stabilizer, then added in DINP, epoxy soybean oil, $CaCO_3$ during stirring. The mixture was blended in a two-roll open mill for plastics at 160-165℃ for 2min. Added in NBR and then blended for 8min.The materials was pressed in plate vulcanizing machine at 180℃ for 6min and at room temperature for 5min.Then the PVC sample was obtained.

2.3 Experimental measurements

Tensile sample was made into dumbbell shaped of 1mm thick, 25mm wide and 115mm long. Tear test was according to universal standard of tear test. Tensile test and tear test were carried out at room temperature by using microcomputer control electronic universal testing machine with a tensile speed of 100mm/min.Test of thermal stability was carried out under the atmosphere of N_2 from room temperature to 600℃ at a rate of 10℃/min by using DSC-TGA. The macrostructure was observed by using SEM after spraying treatment.

III. Result And Discussion

3.1 Mechanical properties

The elongation at break of PVC blends were showed in Fig. 1. The elongation at break improved greatly with the addition of NBR increasing. When NBR was added in 0phr, elongation at break was 272.69%. When NBR was added in 11phr, elongation at break reached 452.11%. When NBR was added in 41phr, elongation at break reached 763.09%. The reason to the results was that NBR dispersed in the PVC matrix. Once under the external tensile force, the elastomeric NBR induced to produce craze and shear band, which could absorb the tensile energy and improve the elongation at break of PVC composites.

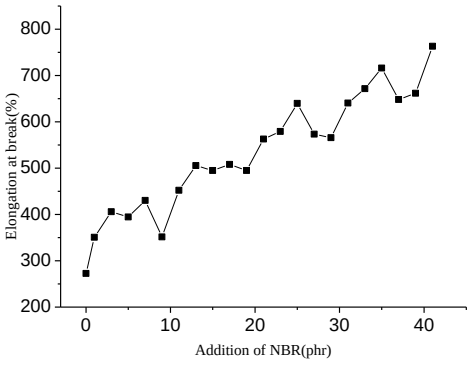

Fig. 1 Elongation at break of PVC blended with different content NBR

The relationship between the addition of NBR and the tensile yield stress, tensile strength, tear strength was showed in Fig. 2. Fig. 2 indicated that the tensile strength was almost no changed. The tensile yield stress and tear strength declined slightly with the increased addition of NBR. It due to that the addition of flexible NBR molecules could increase the distance of PVC molecular chain and reduce the intermolecular interactions, which lead to the reduction of tensile yield stress and tear strength.

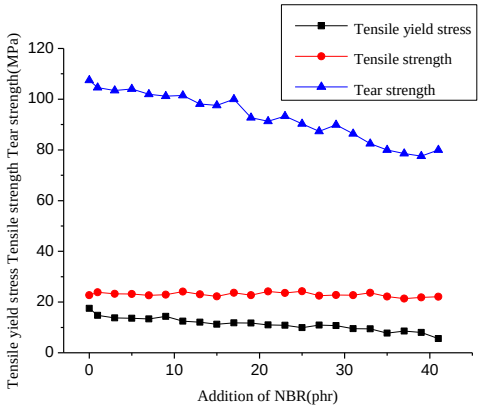

Fig. 2 Mechanical Properties of PVC blended with different content NBR

3.2 Thermal stability

The thermal property of PVC blends were showed in Fig. 3. The Thermo Gravimetric(TG) in the fig. 3(a) indicated that the thermal decomposition of PVC blends had two stages. Stage one between 190-380℃ was thermal decomposition of PVC molecular chain which released HCl. Stage two between 380-540℃ was the C-C bond cracking.

In fig. 3(b), Temperature of endothermic peak had the trend of moving to higher temperature with the increased addition of rare earth calcium-zinc stabilizer. When rare earth calcium-zinc stabilizer was added in 0phr, the intensity of endothermic peak was 111.3J/g. When rare earth calcium-zinc stabilizer was added in 2phr, the intensity of endothermic peak was 72.18J/g. When rare earth calcium-zinc stabilizer was added in 6phr, the intensity of endothermic peak reached 53.68J/g. The results indicated that 2phr stabilizer was able to significantly improve the thermal stability of PVC composites, and continue to add in stabilizer had few effect on thermal stability.

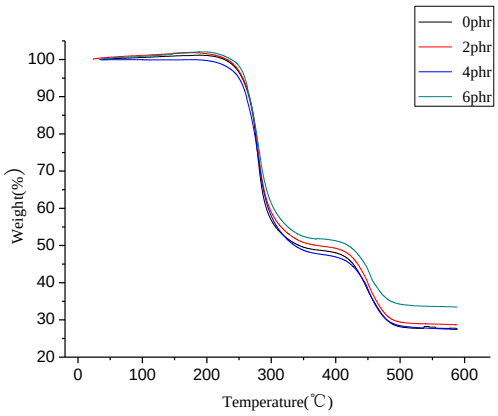

(a)

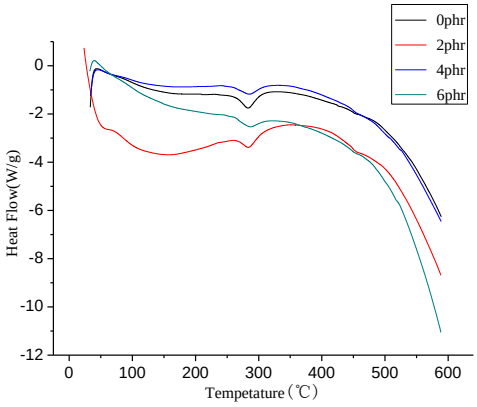

(b)

Fig. 3 DSC and TGA curves of PVC blended with different content of rare earth calcium-zinc stabilizer

The thermal data of DSC-TGA curves was listed in Table 2. The mass remains and Final decomposition temperature had the trend to increase with the increasing of rare earth calcium-zinc stabilizer used in PVC, which indicated that rare earth calcium-zinc stabilizer could form complex structure to improve the thermal stability of PVC.

TABLE 2 EXPLANATION OF DSC-TGA CURVES

Content of rare earth calcium-zinc stabilizer（phr）	0	2	4	6
Temperature of endothermic peak（℃）	260.56	265.33	255.39	262.46
Intensity of endothermic peak（J/g）	111.3	72.18	68.86	53.68
Initial decomposition temperature（℃）	197.46	193.67	194.43	193.67
Mass remains of stage one（%）	48.63	49.84	47.45	51.74
Initial decomposition temperature of stage two（℃）	380.60	377.57	384.38	382.11
Final mass（%）	27.83	29.07	27.78	33.66
Final decomposition temperature（℃）	516.06	519.85	544.06	544.82

3.3 Macrostructures

SEM photograph of different content of NBR showed in Fig. 4. $CaCO_3$ particles were white and PVC matrix was gray. When NBR was added in 0phr, there are many cavities between PVC and $CaCO_3$. Interface bonding was poor. When NBR was added in 9phr, the amount of cavity reduced and $CaCO_3$ particles partly embedded in PVC matrix. The result indicated that a few NBR improved the interface bonding between PVC and $CaCO_3$ and reduced defects in system. When NBR was added in 39phr, part of $CaCO_3$ particles divorced from PVC. This phenomenon explained why tensile yield stress and tear strength decline.

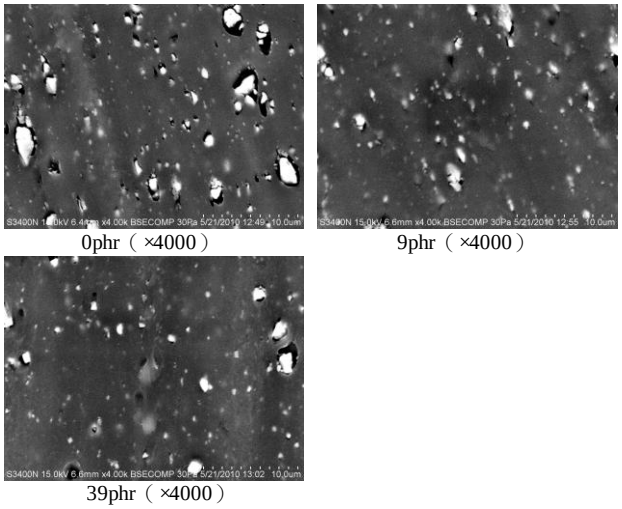

0phr（×4000） 9phr（×4000）

39phr（×4000）

Fig. 4 SEM photograph of different content of NBR

Ⅳ. CONCLUSIONS

(1)Blending PVC with NBR, elongation at break of composites greatly increased. Tensile strength almost not changed. Tensile yield stress and tear strength slightly decreased.

(2)When rare earth calcium-zinc stabilizer was added in 2phr, thermal stability of composites improved obviously. While the content of stabilizer was increased, thermal stability improved slightly.

REFERENCES

[1] Deng Yueyi, Dai Yunshui, Kuang Bo, Zhao Shugao, "NBR modified PVC/nano-$CaCO_3$ composites," *Plastics*, vol. 36, no. 5, pp. 84-87.15, 2007.

[2] Wang Qingguo, Zhang Xiaohong, Liu Shanyuan, et al, "Ultrafine full-vulcanized powdered rubbers/PVC compounds with higher toughness and higher heat resistance," *Polymer*, no. 46, pp. 10614-10617, September 2005.

[3] Wang Qingguo, Zhang Xiaohong, Gui Hua, et al, "Effect of ultrafine vulcanized powdered nitrile rubber on the properties of PVC," *Acta Polymerica Sinica*, no. 4, pp. 332-336, April 2007.

[4] Liu Wenjing, Xu Weiqing, Wang Xingyuan, "Influences of LNBR on the properties of PVC Paste and soft PVC products," *Plastics Additives*, no. 3, pp. 40-42, 2010.

[5] Gong Yaohua, Wu Jianjun, Luo Zhu, et al, "Effects of Ca-Zn/rare-earth compound stabilizer on the thermal stability of PVC," *Polyvinyl Chloride*, vol. 37, no. 5, pp. 33-34.44, May 2009.

2011 International Conference on Mechanical, Industrial, and Manufacturing Engineering
Lecture Notes in Information Technology Vols. 1-2

Study on the characterization of ultrafine zinc phosphate powder by hydrothermal synthesis

Xie Fei , Youming Cao, Zhouqiao Lei, Xinqi Zhou, Minjuan Lei
Faculty of Polymer Materials and Engineering
University of Guangdong Technology
Guangzhou City 510006, P. R. China
xflmj2008@163.com

***Abstract*-Ultrafine Zinc phosphate powder was synthesized by $Na_2HPO_4 \cdot 12H_2O$ and $ZnSO_4 \cdot H_2O$ in a Teflon-lined steel autoclave. The structure of zinc phosphate was identified by XRD, FT-IR and TG/DTG, the size distribution and morphology of zinc phosphate were investigated by dynamic light scattering (DLS) and scanning electron microscopy (SEM). The results showed that there were four crystal water in zinc phosphate, $Zn_3(PO_4)_2 \cdot 4H_2O$ decomposed to $Zn_3(PO_4)_2$ by three dehydration reactions. The surface active agent had great effect on the size distribution and morphology of zinc phosphate, and the size distribution of zinc phosphate modified by OP-10 was uniform, the average particle diameter was about 1μm.**

Index Terms - hydrothermal, ultrafine zinc phosphate, structure, size distribution, morphology.

I. INTRODUCTION

Zinc phosphate, as a new type of non-toxic, ecological anticorrosive pigment with excellent properties, had been applied in a wide variety of fields [1-5]. For example, corrosion preventive pigment, paint, steel and other metal surface phosphating agents and medical, dental adhesives, Chlorinated rubber and flame retardant, et al. The production and demand of zinc phosphate increase year by year, which provides a vast space for the development and application [6-7].

However, owing to its low activity resulting from weaker solubility and hydrolysis, it could not completely replace traditional toxic anticorrosive pigment. To improve its properties and enlarge its application [8-10], the main method is to reduce its particle size. In this paper, high active ultrafine zinc phosphate powder was prepared by the hydrothermal method.

The hydrothermal method can be described that high-temperature and high-pressure aqueous solution is used to enable the dissolution and recrystallization of an ordinarily insoluble material. It has been extensively applied to material synthesis, chemical reaction, and wasteful material treatment [11-12]. Zinc phosphate synthesized by this method was small diameters, narrow size distributions and high surface activity, which overcame many deficiencies in the application.

II. EXPERIMENTAL SECTION

2.1. Materials

All reagents such as $ZnSO_4 \cdot H_2O$ (99%, Tianjin BaiShi Chemical and Industry Ltd. P. R. China), $Na_2HPO_4 \cdot 12H_2O$ (99%,Tianjin Bodi Chemical and Industry Ltd. P. R. China), OP-10 (99%, Tianjin Regent Chemical Co、Ltd. P. R. China), ammonia(99%,Tianjin Damao Chemical Reatent Factory. P. R. China) are used at analytical grade. Distilled water was used throughout all the experiments.

2.2. Preparation of ultrafine zinc phosphate powder

Ultrafine zinc phosphate powder was synthesized by hydrothermal method under autogenous pressure. Firstly, ground $Na_2HPO_4 \cdot 12H_2O$ and $ZnSO_4 \cdot H_2O$ were mixed together with some molar ratio. The mixture was ground by addition of approximate surface active agent (OP-10) and ammonia, 30ml of distilled water stirred at 1000 rpm, the precursor of hydrothermal reaction was achieved, then was sealed in a Teflon-lined steel autoclave, and heated in 100℃ for 12 hours and then cooled to room temperature. The resulting product

was washed with water until no SO_4^{2-}. Then, zinc phosphate was washed again for several times with ethanol and dried at 80℃for 10 hours for use. The reaction could be expressed as (1):

$$Na_2HPO_4 \longrightarrow 2Na^+ + 2HPO_4^{2-}$$

$$3Zn + 2HPO_4^{2-} + 4H_2O \longrightarrow Zn_3(PO_4)_2 \cdot 4H_2O \quad (1)$$

III. MEASUREMENTS

3.1. Structure identification of ultrafine Zinc phosphate

The structures and crystallite sizes of the prepared sample and its dehydration product were identified by a D/max-ⅢA automatic X-ray diffractometer (Japanese) powder, and X-ray diffraction (XRD) used Cu-Kα radiation (λ =0.1546 nm). The Scherrer method was used to evaluate the crystallite size D as follows (2):

$$D = K\lambda/\beta\cos\theta \quad (2)$$

where λ is the wavelength of X-ray radiation, K is a constant taken as 0.89, θ is the diffraction angle, and β is the full width at half-maximum.

Fourier transform infrared (FTIR) spectra were recorded using a Nicolet MAGNA-IR 750 spectrophotometer (American), powders were mixed with KBr powders, and the mixture was pressed into a tablet.

Thermogravimetric analysis (TG) was carried out using TA Instruments STD 2960(US). The samples were heated from room temperature to 800℃ at heating rate 10℃/min under nitrogen with a flowing rate of 10ml/min in order to measure the heat transition temperature.

3.2. Dynamic light scattering (DLS)

The particles size and distribution of all sample solutions were conducted using a Microtrac Nanotra^{TM} 150 Instrument. The microtrac Nanotra^{TM} 150 DLS instrument can detect particles range 0.8~6500 nanometers, and DLS data were attained by a Cumulant method. The testing methods and process of zinc phosphate diameter: First of all, zinc phosphate modified the different surface active agent and ethanol was confected into 0.01g/L, then librating of half an hour by the ultrasonic. The influence of experimental conditions on radius and dispersion of ultrafine particles were studied by light scattering technique.

3.3. Scanning electron microscopy (SEM)

The SEM micrographs of ultrafine Zinc phosphate powders after being gold-sputtered were obtained by a Hitachi X-650(Hitachi, Ltd) scanning electron microscope.

Ⅳ. RESULTS AND DISCUSSION

4.1. Identification of zinc phosphate

The X-ray diffraction pattern of zinc phosphate was showed in Fig. 1. The seven strong peaks (2θdata) were at 19.36°, 20.08°, 25.67°, 26.25°, 31.30°, 39.321°and 46.76°, respectively. The pattern matches the standard XRD data for $Zn_3(PO_4)_2 \cdot 4H_2O$ (PDF no. 37-0465). No characteristic peaks of impurities could be found in Fig. 1. So pure $Zn_3(PO_4)_2 \cdot 4H_2O$ was obtained under the present experimental conditions. The Scherrer line width analysis of the [220] reflection gives an estimate of the primary crystallite size in the range of 83 nm .

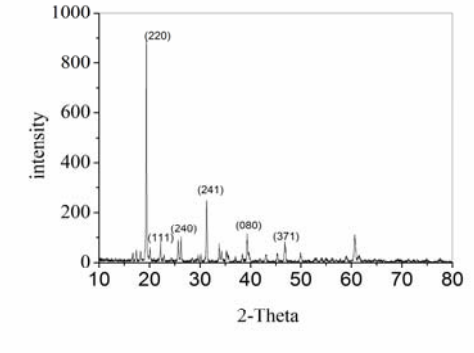

Fig.1. XRD patterns for $Zn_3(PO_4)_2 \cdot 4H_2O$

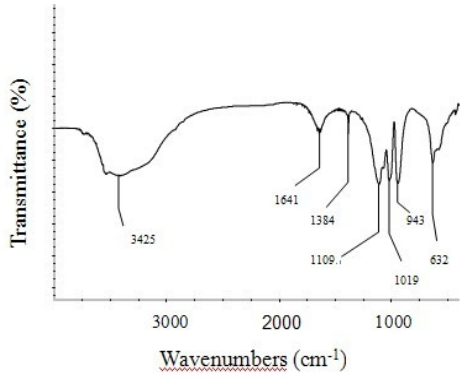

Fig. 2. FTIR spectra of synthesized $Zn_3(PO_4)_2 \cdot 4H_2O$

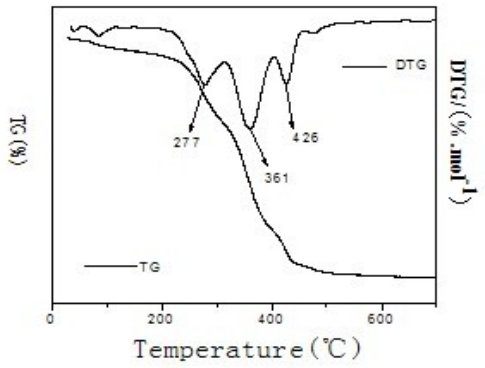

Fig. 3. TG/DTG curves of synthesized $Zn_3(PO_4)_2 \cdot 4H_2O$

The FT–IR spectrum of zinc phosphate hydrate was shown in Fig. 2. Fig. 2 demonstrated that the characteristic bands related to H_2O and PO_4^{3-}. The broad band centered at 3425 cm^{-1} was attributed to the O-H stretching vibration, and the strong vibrational band at 1641 cm^{-1} was attributed to H_2O bonding. The broad bands shown at 900-1250 cm^{-1} and 400-700 cm^{-1} were attributed to the complex stretching and bending vibrations of the PO_4^{3-} group, Vibrational bands of the PO_4^{3-} anion were observed in the regions of 370-400, 450-600, 900-1000, and 1000-1200 cm^{-1}. These bands were assigned to the $\nu_2(PO_4^{3-})$, $\nu_4(PO_4^{3-})$, $\nu_1(PO_4^{3-})$ and $\nu_3(PO_4^{3-})$ vibrations, respectively. Therefore, the FT–IR spectrum indicated that the synthesized product had the structure of $Zn_3(PO_4)_2 \cdot 4H_2O$.

The thermogravimetry(TG) and DTG curves of $Zn_3(PO_4)_2 \cdot 4H_2O$ were shown in Fig. 3. The TG curve relating to the elimination of water molecules in the crystal hydrate showed three stages of mass loss between 0 and 800℃. The onset temperatures were 277, 361and 426℃, respectively, and the total mass loss is 15.55% in the range of 35-512℃. Based on theoretical analysis, the thermal dehydration period involved that dehydration of the coordinated water was 4 mol H_2O molecules. The stage of dehydration process was described as (3):

$$Zn_3(PO_4)_2 \cdot 4H_2O \xrightarrow{-2H_2O} Zn_3(PO_4)_2 \cdot 2H_2O \xrightarrow{-H_2O} Zn_3(PO_4)_2 \cdot H_2O \xrightarrow{-H_2O} Zn_3(PO_4)_2 \quad (3)$$

So, From above XRD, FT-IR and TG/DTG analysis, zinc phosphate with 4mol H_2O was synthesized under the current hydrothermal method.

4.2. Size distribution and morphology analysis

The particle size distribution of zinc phosphate prepared with no surface active agent and OP-10 were showed as Fig.4.

The zinc phosphate prepared with no surface active agent was showed in the curve A of Fig.4. The curve A displayed two size distribution peaks around 1.6μm and 4.6μm, respectively. In other word, the particle diameter distribution of zinc phosphate was non-uniform. The zinc phosphate prepared with surface active agent OP-10 was showed in the curve B of Fig.4. The curve B indicated that the zinc phosphate had the morphology of narrow size distribution, and the particles with diameters ranging from 0.28μm to 1.1μm were about 96 wt%. The distribution of zinc phosphate is uniform, and the average particle diameter was about 0.8μm.

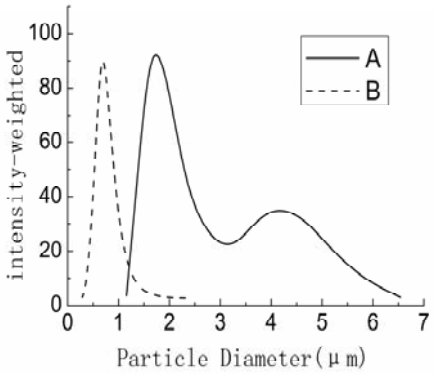

Fig. 4. The size distribution curves of zinc phosphate prepared with no surface active agent (A) and OP-10(B).

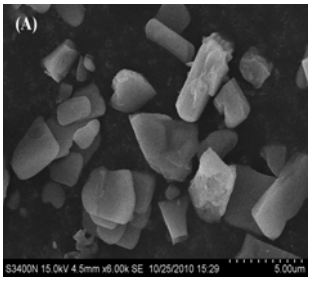

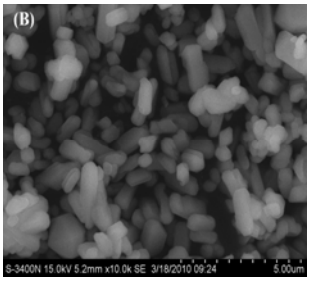

Fig.5. SEM images of zinc phosphate prepared with no surface active agent (A) and OP-10(B).

Furthermore, the SEM image of as-synthesized zinc phosphate sample was shown in Fig. 5. It could clearly be seen that zinc phosphate prepared with no surface active agent appeared as blocks, and the particles were non-uniform. Large particle diameter was about 5μm, while small particle diameter was about 1.5μm. In contrast, a different scenario was observed in Fig.5B. The distribution of zinc phosphate modified by OP-10 was uniform, and the average particle diameter was about 1μm. Moreover, the zinc phosphate particle was easily dispersed and little reunited.

So, nonionic surfactant OP-10 had an effect on the particle diameter and particle distribution of zinc phosphate. Because the nonionic surfactant OP-10 had surface adsorption effect on the surface of zinc phosphate particles, the formation of zinc phosphate crystal was arrested by stereo-hindrance effect, which made the particle size of zinc phosphate particle decreased.

Ⅴ. CONCLUSIONS

In this study, the characterization of ultrafine Zinc phosphate powder synthesized by the hydrothermal method in the presence of surfactant active agent OP-10 was studied. The conclusions are as follows:

(1) The zinc phosphate with 4mol H_2O was synthesized under the current hydrothermal method, and the distance of zinc phosphate crystal cell was the range of 83 nm.

(2) $Zn_3(PO_4)_2{\cdot}4H_2O$ decomposed to $Zn_3(PO_4)_2$ by three dehydration reactions, the onset temperatures were 277, 361and 426℃.

(3) The size distribution of zinc phosphate prepared by nonionic surfactant OP-10 was uniform, and the average particle diameter was about 1μm.

REFERENCES

[1] B. delamo, R. Romagnoli, C. Deyá,J. A. González, "High performance water-based paints with non-toxic anticorrosive pigments,"Progress in Organic Coatings, Vol. 4, pp. 389-397, 2002.

[2] S. H. Jung, E. Oh, D. Shim, D. H. Park, S. Cho, B. R. Lee, et al. "Sonochemical Synthesis of Amorphous Zinc Phosphate Nanospheres,"Bulletin of the Korean Chemical Society, Vol. 10, pp. 2280-2282, 2009.

[3] B. Boonchom, R. Baitahe, S. Kongtaweelert,N. Vittayakorn, "Kinetics and Thermodynamics of Zinc Phosphate Hydrate Synthesized by a Simple Route in Aqueous and Acetone Media,"Ind. Eng. Chem. Res., Vol. 8, pp. 3571-3576,Apr 2010.

[4] S. Yawei, J. Cao, M. Guozhe, Z. Tao,W. Fuhui, "The role of a zinc phosphate pigment in the corrosion of scratched epoxy-coated steel,"Corrosion Science, Vol. pp. 371-9, 2009.

[5] Y. J. Zhong, Y. M. Chen, Y. Q. Sun,G. Y. Yang, "Synthesis and characterization of a two-dimensional zinc phosphite, Zn-3(tren)(HPO_3)$_3$ center dot xH_2O (x approximate to 0.5; tren = tris(2-aminoethyl)amine),"Zeitschrift Fur Anorganische Und Allgemeine Chemie, Vol. 10, pp. 1957-1960, 2005.

[6] D. He, A. Zhou, Y. Liu, L. Nie,S. Yao, "A study of the viscoelasticity of zinc phosphate coatings using a quartz crystal impedance system,"Surface and Coatings Technology, Vol. 2-3, pp. 225-231, 2000.

[7] A. A. Ayi, S. Neeraj, A. Choudhury, S. Natarajan,C. N. R. Rao, "One-dimensional zinc phosphates with linear chain structure,"Journal of Physics and Chemistry of Solids, Vol. 8, pp. 1481-1491, 2001.

[8] S. Ding,M. Wang, "Studies on synthesis and mechanism of nano-$CaZn_2(PO_4)_2$ by chemical precipitation,"Dyes and Pigments, Vol. 1, pp. 94-96, 2008.

[9] M. Mahdavian,M. M. Attar, "Evaluation of zinc phosphate and zinc chromate effectiveness via AC and DC methods,"Progress in Organic Coatings, Vol. 3, pp. 191-194, 2005.

[10] W. He, S. Yan, Y. Wang, X. Zhang, W. Zhou, X. Tian, et al. "Biomimetic synthesis of mesoporous zinc phosphate nanoparticles,"Journal of Alloys and Compounds, Vol. 1-2, pp. 657-660, 2009.

[11] W. Q. Qin, C. R. Yang, R. Yi,G. H. Gao, "Hydrothermal Synthesis and Characterization of Single-Crystalline alpha-Fe_2O_3 Nanocubes,"J. Nanomater., Vol.7, pp. 321-329, 2011.

[12] S. Dikmen, P. Shuk, M. Greenblatt,H. Gocmez, "Hydrothermal synthesis and properties of Ce1-xGdxO_2-[delta] solid solutions,"Solid State Sciences, Vol. 5, pp. 585-590, 2002.

2011 International Conference on Mechanical, Industrial, and Manufacturing Engineering
Lecture Notes in Information Technology Vols. 1-2

Study on the QQ Instant Communication Activities in Artificial Intelligence

Yong-Min Liu[1, 2], Wu-Yi Lu[2], Xin-Hua Jiang[2]

1. College of Computer and Information Engineering
Central South University of Forestry and Technology
ChangSha, China
lym37212004@126.com

2. School of Information Science and Engineering
Central South University
ChangSha, China
lym37212002@yahoo.com.cn

***Abstract*—Nowadays, QQ Instant Message has become one of the most popular and widely used forms of electronic instant communication way. The social interactions or contacts patterns between people by QQ Instant Message can be analysis using social network mode. Tracking the user' data activities is always known as significant source of information, allowing the Network Managements to be aware of the activities that the user carried through, along with their outputs. At the same time, it can be considered a privileged element, exploited by the researchers and the developers to improve the communication environments. In this paper, we present the latest results of our research works, regarding the approach adopted for efficiently tracking the QQ user's activities.**

Keywords-Artificial Intelligence; Instant Message; QQ; Communication Activities

I. INTRODUCTION

One of most common forms of electronic communication in use today is QQ Instant Message. The use of QQ has made a large impact on society in the way people communicate with each other, because it is easy to write, quick to send, and allows a single message to be sent to large groups of people. The result of these features of QQ Instant Message has made it a popular and wide-spread form of electronic communication that people use to communicate with each other. This has provided a suitable environment for researchers to study the social interactions of individuals over QQ Instant Message, part of a field of study called social network analysis [1, 2].

Our research works are particularly involved in keeping track of the user's activities through the QQ platforms and exploiting the tracking data in different learning contexts. The main objective of the project is to use the tracking data, collected during the user's communication activities on discussion forums, to assist both user and peers in their distance communication activities. Tracking data are too called "traces", generally generated by tracking system in accordance with its defined trace format or model [1]. The collected traces are used to depict the activities of the users or the events occurred during the usage of the systems in a specific context.

In Web-based communication situations, the trace of user' activities is a significant source of information that reveals not only the activities themselves, but also their outputs, which the results of the activities that the user carried through the communication process. Furthermore, by analyzing the traces in collaborative communication environments, the Network Managements could evaluate social and cognitive aspects of user [4].

Figure 1. Two QQ Instant communication Message gragh interface.

As shown in Figure 1. The observation of QQ Instant Message communication social networks can be represented as a type of complex network, where each QQ graph interface represents a person or individual represents the interaction or contact between people, displaying a type of graph. A simple diagram of QQ communications involving the authors of this paper, shown in Figure 2, provides an example of how the QQ communication social network could be represented. In the diagram, weights can be assigned to the graph edges to indicate the strength of the communication link, which in this case is used to describe the frequency of QQ transmissions between particular

individuals in the QQ Instant Message communication social network.

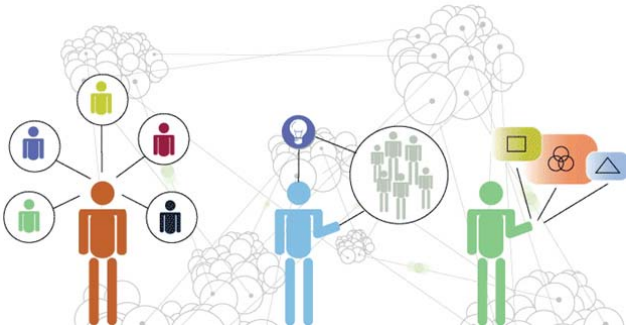

Figure 2. Common QQ Instant communication Message network.

The focus of this research will be to monitor the QQ Instant Message communication links between individuals or groups of people for any changes in the social network. The types of changes that are to be considered, which are changes in the communication activity between particular individuals and predicting the additions of new links to the QQ Instant Message communication social network.

There are several applications where our research could be useful. Firstly, for the homeland security and intelligence gathering community, the techniques of monitoring for changes in QQ communication activities could be useful for tracking the electronic communication of terrorist suspects for any clues of an upcoming terrorist attack. The detection of increased QQ Instant Message traffic between particular parts of the terrorist social network over a particular period of time can be helpful in determining when and where an upcoming event is likely to take place. At the same time, it can be used for law enforcement agencies.

Another third application is for tracking and monitoring the spread of QQ viruses through QQ Instant Message social networks. The detection of unusual variations in QQ communication activities can be used to locate individuals in the social network who are currently affected by QQ virus. This can then be used to determine how quickly the QQ Instant Message virus will spread via the social contacts of the infected individual and how many ***hops*** it will take for the QQ virus to spread globally via QQ Instant Message social networks.

II. COMPLEX NETOWORKS

The study of social networks focuses on finding patterns in the way people interact or contact with each other. This is just one of the many types of networks being studied under the broad field of complex networks [1]. To examine the complex networks' statistical large-scale properties of networks, we can found it contain millions or billions of vertexes. Although this field is primarily in the area of physics, its applications are interdisciplinary in that they can be applied to any discipline that requires the understanding of complex interactions or processes. The various complex networks disciplines can be applied to include computer science, electrical engineering, geology, or biology, just to name a few disciplines.

A. Statistical Properties

There are several statistical properties of complex networks described by [1]. Similar to complex network, the common QQ instant Message communications activity has the following properties:

1) Transitivity or clustering:

The network property of transitivity or clustering, describes the ratio of connectedness between sets of vertices, described as triples, in a complex network [1]. Essentially the property describes that if vertex A is connected to vertex B, there is an increased probability that vertex A will be connected to vertex C. In terms of a social network, it describes the probability that a friend of your friend is likely to be also your friend. Studies have been conducted by [3] and [4] that investigate the clustering effect in several real-world networks, such as the autonomous system level Internet, the router level Internet and power grid.

2) Community structure:

The community structure network property seeks to describe how vertices in a network are clustered together into groups of vertices with a high density of edges between them [1]. In the context of a social network, this property describes how people naturally divide into social groups based on shared attributes such as for example: common interests, age or occupation. This network property is useful for analyzing QQ Instant Message social networks in that it allows one to examine where various individuals in the network form social groups and to determine the likely paths for messages to pass between individuals.

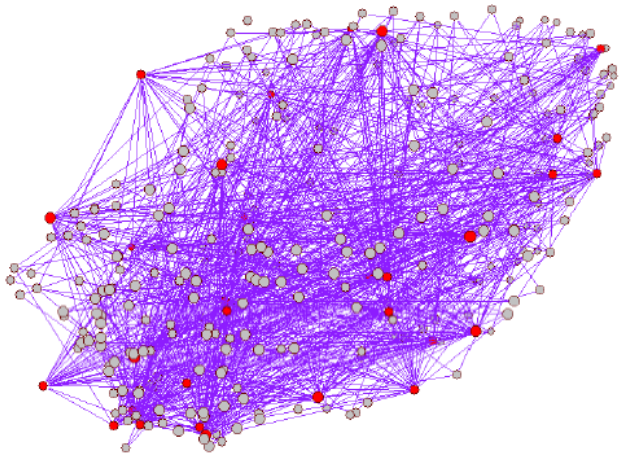

Figure 3. A complex network topology with hundreds randomly vertexes.

B. Models of Complex Networks

Building proper network models is important (e.g. Figure 3), which we study on the complex network. We can compare the simulated statistical properties of the model to those found in real-world networks (e.g. Internet, World Wide Web). Two main approaches for modeling complex networks are:

1) Static modelling:

The static modeling of complex networks aims to create models of networks with particular structural properties such

as the clustering and community structure [1]. There are several models that are useful for comparisons with empirical studies of QQ Instant Message social networks [5], scale-free model [6] and community structures model [7]. Static modeling is useful in that one can easily build a complex network, containing more than a thousand vertices, without having to collect large amounts of experimental data in order to observe particular properties of complex networks.

2) Dynamic modelling:

A disadvantage with the static modeling approach is that it is unable to provide information on how the network topology has evolved over time to obtain a particular network structure. Dynamic modeling or growth modeling techniques take into account the influence that network topology evolution has on the structure of the network [1]. There have been many techniques developed for modeling evolving network topology, some of which includes the growth of transitivity and clustering by increasing links between existing vertices [8].

III. USER BEHAVIOUR ANALYSIS

User behavior analysis examines the on-line actions of an individual or group of users on a computer network. It belongs to the field anomaly detection, which forms part of intrusion detection systems [9]. Anomaly detection analyses computer network traffic for network activity that is considered different from ***normal*** network activity. The difference in activity is determined by building a profile of ***normal*** activity from historical data collected over a period of ***normal*** operation, then comparing the profile of current network activity to the ***normal*** profile.

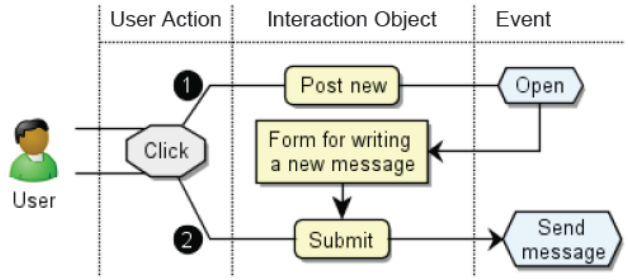

Figure 4. An example of a usage model for an activity.

As shown in figure 4, a usage model for an activity called P***ost a new message***. The interaction objects in the context of this activity could be a ***Post new*** button, a ***Form for a new messag***e, and a ***Submit*** button, by which users employ to post a new message. The arrow (1) represents a sequence of event that happens when the user clicks on the ***Post new*** button to open the ***Form for a new message*** in order to write a new message. When the user clicks on the ***Submit*** button (arrow 2), there is another event called ***Send message***, representing the action that the user's message is being submitted to the server.

There have been a variety of methods used to monitor the on-line activities of users. One approach has been to monitor the command line sequences or keystrokes of users to determine the presence of masqueraders, who are computer users that use another person's computer account [8, 9].

Another approach for monitoring the on-line activities of users has been to examine QQ Instant Message traffic data for changes in traffic activity. The studies by [9, 10] use methods for differentiating ***normal*** traffic generated by computer users from traffic generated by QQ viruses. The study by [9] simulates the behavior of QQ users and computer viruses using the ***specification-based anomaly detection*** technique [11], which combines state-machine specifications of network protocols with statistical machine learning. In their specification-based model, they simulate the protocol interactions between QQ clients and QQ servers belonging to the same organization, by manually mapping the interactions onto a state-machine model consisting of three states: INIT, RCVD and DONE. The anomaly detector then uses statistical machine learning to monitor the statistical properties of the state-machine transitions for any variations from the ***normal*** statistical properties. Detection of significant variations indicates that QQ viruses are causing changes to the QQ traffic activity.

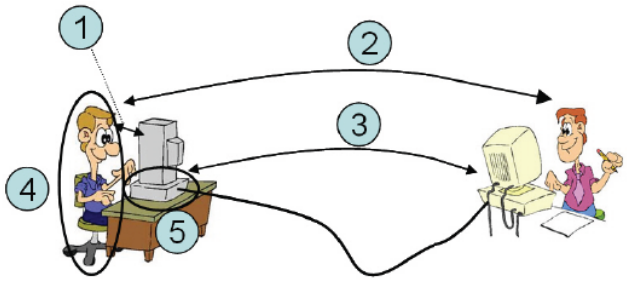

Figure 5. Different monitor levels to users' activities on-line.

The identification of the interaction objects and the successive events to be observed let the tracking system take into account every user's interactions with those objects, and to produce simultaneously the tracking data of user's activities in accordance with its defined usage model. In this way, each usage model indicates how to observe, when to capture the user's actions and User-Machine interactions, and what to generate as tracking data.

IV. SOME ARTIFICIAL INTELLIGENCE APPLICATION

A. Artificial Intelligence in Complex Networks

There are some applications for the use of AI (Artificial Intelligence) in complex networks in the areas of dynamic modeling and link prediction. In dynamic modeling, the current approaches lack the mechanism for incorporating the intuitive reasoning used by individuals when forming new links in social networks. This is an area where fuzzy systems or neural networks could be applied [12], to account for some of the intuition mechanisms missing in current dynamic modeling approaches. Neural networks have already been applied for growth modeling by [7], where they use it to more precisely model the growth of real-world networks, such as the World Wide Web. They achieved this by allowing their neural network to learn from the changing

topology of real World Wide Web data, in order to more closely model the changes in network topology.

B. AI in User Behaviour Analysis

The approaches for anomaly detection described by [9-11] only use mathematical techniques to detect ***abnormal*** variations in the behavior of users. The problem with using mathematical techniques is that they impose strict boundaries around the profiles of what is considered ***normal*** and ***abnormal*** behavior. The slightest deviation from the ***normal*** profile while the actual network activity is still operating normally will cause the anomaly detector to give off a false alarm. Incorrect identification can also occur if the actual network activity is operating abnormally, but does not have the profile that the anomaly detector considers to strictly match an ***abnormal*** profile, resulting in missed detection. These problems with imposing strict boundaries on the ***normal*** and ***abnormal*** profiles can be seen from the results of the false alarm and miss rates of [10], where a summary of their best results are shown in Table 1.

TABLE I. THE BEST FALSE ALARM AND MISS RATES OF ANOMALY DETECTORS USING MATHEMATICAL TECHNIQUES .

Technique	False Alarm	Miss Rate
Uniqueness [16]	1.4%	60.6%
Naive Bayes [17]	1.3%	38.5%
Histogram/Statistical [19]	4%	41%

Because of the uncertainty in defining the boundaries between what is ***normal*** and ***abnormal*** user behavior when analyzing command sequences or QQ Instant Message traffic behavior of users, this is an ideal area for fuzzy systems to be applied [12]. Some studies have already been conducted using fuzzy systems for anomaly detection, such as in [13]. In [13], they applied fuzzy logic and data mining techniques for anomaly detection of TCP-level network traffic.

The advantage of using neural networks in anomaly detection is that features of ***normal*** and ***abnormal*** behavior can easily be learned by the neural network, as opposed to applying mathematics to describe the features of the data to the anomaly detector. The applications of either fuzzy systems or neural networks will be ideal for analyzing QQ Instant Message communication traffic activity.

V. CONCLUSION AND FURTURE WORK

We have shown that the analysis of QQ Instant Message communications is also suitable for applying artificial intelligence techniques in this paper. It provided a brief review about some of the work done in complex networks and user behavior analysis, related to the analysis of QQ communications. We pointed out the key issues related to the problems in tracking user's activities on CMC (Computer Mediated Communication) tools.

Our principal contribution to this research challenge is an approach for efficiently tracking the user's communication activities on different types of communication ways. The suggested approach is for building Web-based tracking system, which takes into account different levels of Human and Machine Interactions, where the observation must be carried out in order to collect as rigorously as possible the necessary information about the CMC activities, including the content of the exchanged communications. The tracking data at each level contain different indicators that will be served by different users, especially the participants in the communication process as well as the researchers and the developers of Web-based communication tools.

Our future work is to make the approach become general so that we can provide an explicit framework to support the tracking system of different CMC tools. It will involve the use of artificial neural networks or fuzzy systems for anomaly detection of user behavior and link prediction in QQ Instant Message communication social networks.

REFERENCES

[1] M. E. J. Newman, "The structure and function of complex networks," *Siam Review*, vol. 45, no. 2, pp. 167–256, 2003.

[2] M. E. J. Newman and P. Juyong, "Why social networks are different from other types of networks," *Physical Review E (Statistical, Nonlinear, and Soft Matter Physics)*, vol. 68, no. 3, pp. 36122–1–8, 2009.

[3] E. Ravasz and A. L. Barabasi, "Hierarchical organization in complex networks," *Physical Review E*, vol. 67, no. 2, pp. 26112–1–7, 2010.

[4] May M., George S., Prévôt P., "A Web-based System for Observing and Analyzing Computer Mediated Communications", *Proceeding of the IEEE/WIC/ACM International Conference on Web Intelligence*, Hong Kong, 18-22 December 2006, pp. 983-986.

[5] Y. J. Tsai, C. C. Lin, and P. N. Hsiao, "Modeling Instant Message communications," *Ieice Transactions on Information and Systems*, vol. E87D, no. 6, pp. 1438–1445, 2008.

[6] A. L. Barabasi and R. Albert, "Emergence of scaling in random networks," *Science*, vol. 286, no. 5439, pp. 509–512, 1999.

[7] M. Kimura, K. Saito, and N. Ueda, "Modeling of growing networks with directional attachment and communities," *Neural Networks*, vol. 17, no. 7, pp. 975–988, 2004.

[8] De Wever, B., T. Schellens, M. Valcke, and H. Van Keer. "Content Analysis Schemes to Analyze Transcripts of Online Asynchronous Discussion Groups: A Review.", *Computers & Education* 46, no. 1, 2006, pp. 6-28.

[9] R. A. Maxion and T. N. Townsend, "Masquerade detection augmented with error analysis," *IEEE Transactions on Reliability*, vol. 53, no. 1, pp. 124–147, 2004.

[10] S. J. Stolfo, S. Hershkop, K. Wang, O. Nimeskern, and C. W. Hu, "A behaviorbased approach to securing Instant Message systems," in Computer Network Security, vol. 2776, *Lecture Notes in Computer Science*, pp. 57–81. SPRINGER-VERLAG BERLIN, Berlin, 2003.

[11] Pozzi F., Manca S., Persico D.,Sarti L., "A general framework for tracking and analysing learning processes in computer-supported collaborative learning environments", *Innovations in Education and Teaching International*, Volume 44, Issue 2, May 2007 , pp. 169-179.

[12] M. Negnevitsky, *Artificial Intelligence: A Guide to Intelligent Systems*, 3rd edition, Addison Wesley, Essex, 2009.

[13] J. Guan, D. X. Liu, and T. Wang, "Applications of fuzzy data mining methods for intrusion detection systems," in Computational Science and Its Applications - Iccsa 2004, Pt 3, vol. 3045, *Lecture Notes in Computer Science*, pp. 706–714. SPRINGER-VERLAG BERLIN, Berlin, 2004

2011 International Conference on Mechanical, Industrial, and Manufacturing Engineering
Lecture Notes in Information Technology Vols. 1-2

Vibration Analysis of FGM Timoshenko Beam Based on Gradient Mode of Exponential Function*

Lulu Yang, Wei Liang and Naibin Yang
School of Aeronautics Science and Engineering
Beihang University
Beijing 100191, P.R.China
liangwei@buaa.edu.cn

***Abstract* - This paper analyses the vibration of FGM Timoshenko beam based on graded mode of exponential function. The material properties are assumed to vary as an exponent form of thickness coordinate variable. The free vibration equations of FGM beam are derived by Hamilton principle, and the equations of natural frequencies for a simply supported FGM beam are presented. The influences of functionally graded index difference and different metal material and span-depth ratio that influence vibration frequencies are finally discussed.**

Index Terms* - *Functionally graded material; Timoshenko beam; Vibration; Exponential function

I. INTRODUCTION

Functionally graded material (FGM) refers to a kind of new material whose constitution (composition, structure) varies continuously gradient in the thickness direction from one side to the others so that the material properties and functions are also shown gradient change[1]. Since the concept of FGM was first proposed in 1984 by a Japanese scholar Toshio Hirai[2], it has been used in a wide range due to its excellent properties. Reference [3] discussed three different graded models of physical parameters along the thickness direction. The hypothesis of graded exponential function of physical parameters facilitates solutions because of its relatively simple mathematical form and to some extent reflects the characteristics of FGM. Reference [4] studied the vibration of symmetry composite beam with fiber volume fraction variable along the thickness. Currently for FGM beam, research of shear effect is still rare, therefore in this paper, nonlinear distribution of physical parameters of FGM beam along the thickness direction is simulated with graded model of exponential function based on the previous work considered shear effect. FGM free vibration equation of the shear beam is derived using Hamilton principle. The expression of natural frequencies with both ends simply supported is gained. Finally the influence on vibration frequency of FGM beam including vibration orders, different metal materials and span-depth ratio is discussed.

II. DESCRIPTION AND EXPRESSION OF PHYSICAL PARAMETERS

Consider an FGM beam with the thickness of *h*, the coordinate system is established shown in Figure 1. The FGM beam is composed of metal and ceramic based on gradient mode of exponential function.

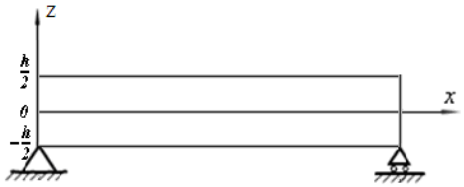

Fig.1 Geometric illustration and coordinate system of FGM beams

According to the actual situation of the material properties, metal and ceramic Poisson's ratio is the same, Poisson's ratio within the FGM beam, therefore, is the same. Physical properties of arbitrary parameters are given by:

$$K(z)=\frac{K_m-e^k K_c}{1-e^k}+\frac{K_c-K_m}{1-e^k}e^{k\left(\frac{z}{h}+\frac{1}{2}\right)} \tag{1}$$

K(*z*) is the material density and elastic modulus in any depth, *k* is the gradient index, *m* and *c* separately represent metal and ceramics.

III. THEORETICAL ANALYSIS

A. Geometric Equations

For the FGM beam as shown in Figure 1, assuming the deformation agrees with the small deformation theory, then the displacement field of FGM shear beam is as follows:

$$U_x=U=-z\Psi,\ U_z=V \tag{2}$$

where U_x and U_z is the displacement components in *x* and *z* directions, Ψ is the profile angle, *V* is the deflection in the mid-plane.

According to the small deformation theory, FEM shear beam strain - displacement relations are as follows:

$$\varepsilon_x=\frac{\partial U}{\partial x}=-z\frac{\partial \Psi}{\partial x},\quad \varepsilon_z=0,\ \gamma_{xz}=\gamma=\frac{\partial V}{\partial x}-\Psi \tag{3}$$

B. Constitutive Equations

According to Hooke's law, stress within the FGM beam at any point is:

$$\sigma_X=E(z)\varepsilon_X,\sigma_Z=0,\tau_{XZ}=kG(z)\gamma \tag{4}$$

C. Free Vibration Equation

By the generalized Hamilton principle[3], that is:

$$\int_{t_1}^{t_2}\delta L dt=0 \tag{5}$$

* This work is partially supported by the National Natural Science Foundation of China through the grant 10972021.

where $L=T-U-W$, T, U and W are respectively kinetic energy, potential energy and external work of the system.

Brought the kinetic energy, potential energy, external work, respectively, into (5), then (5) can be expressed as:

$$\int_{t_1}^{t_2} dt\delta \iint_{\Omega} \{\int_{-\frac{h}{2}}^{\frac{h}{2}} \tfrac{1}{2}[\rho(z)\left(\dot{U}_x{}^2+\dot{U}_z{}^2\right)-\sigma_x\varepsilon_x-\sigma_z\varepsilon_z-\tau_{xz}\gamma_{xz}]dz\}d\Omega \quad (6)$$
$$+\int_{t_1}^{t_2} dt \iint_{\Omega}\left[q(x,y,t)\delta U_z\right]d\Omega=0$$

where $\dot{U}_x, \dot{U}_z$ are separately velocity component of the beam in x and z direction, $q(x,y,t)$ is transverse distributed load.

By variational calculations and taking into account the boundary conditions, then (6) can be translated into the following form:

$$\int_{t_1}^{t_2} dt \iint_{\Omega}\left\{\left[-\bar{m}\frac{\partial^2 V}{\partial t^2}+k'\bar{G}\left(\frac{\partial^2 V}{\partial x^2}-\frac{\partial \Psi}{\partial x}\right)\right]\delta V\right.$$
$$\left.+\left[-\bar{A}\frac{\partial^2 \Psi}{\partial t^2}+\bar{D}\frac{\partial^2 \Psi}{\partial x^2}+k'\bar{G}\left(\frac{\partial V}{\partial x}-\Psi\right)\right]\delta\Psi\right\}dxdy \quad (7)$$
$$+\int_{t_1}^{t_2} dt \iint_{\Omega} q(x,y,t)\delta V dxdy=0$$

where

$$\left\{\bar{m},\bar{G}\right\}=\int_{-\frac{h}{2}}^{\frac{h}{2}}\left\{\rho(z),G(z)\right\}dz\ ,\ \left\{\bar{A},\bar{D}\right\}=\int_{-\frac{h}{2}}^{\frac{h}{2}}\left\{\rho(z),E(z)\right\}z^2dz$$

It can be calculated into:

$$\bar{m}=\frac{h}{1-e^k}\left[\rho_m-e^k\rho_c-\frac{\rho_{mc}}{k}\left(e^k-1\right)\right]$$
$$\bar{G}=\frac{h}{2\left(1+\nu_0\right)\left(1-e^k\right)}\left[E_m-e^kE_c-\frac{E_{mc}}{k}\left(e^k-1\right)\right]$$
$$\bar{A}=\frac{h^3}{12\left(1-e^k\right)}\left\{E_m-e^kE_c-E_{mc}\left[\left(\frac{3}{k}-\frac{12}{k^2}+\frac{24}{k^3}\right)e^k-\left(\frac{3}{k}+\frac{12}{k^2}+\frac{24}{k^3}\right)\right]\right\}$$
$$\bar{D}=\frac{h^3}{12\left(1-\nu_0^{\,2}\right)\left(1-e^k\right)}\left\{E_m-e^kE_c-E_{mc}\left[\left(\frac{3}{k}-\frac{12}{k^2}+\frac{24}{k^3}\right)e^k-\left(\frac{3}{k}+\frac{12}{k^2}+\frac{24}{k^3}\right)\right]\right\}$$

Owing to the arbitrariness $\delta\Psi$ and δV, it can be obtained as:

$$\begin{cases}\bar{m}\dfrac{\partial^2 V}{\partial t^2}=k'\bar{G}\left(\dfrac{\partial^2 V}{\partial x^2}-\dfrac{\partial \Psi}{\partial x}\right)+q(x,y,t)\\ \bar{A}\dfrac{\partial^2 \Psi}{\partial t^2}=\bar{D}\dfrac{\partial^2 \Psi}{\partial x^2}+k'\bar{G}\left(\dfrac{\partial V}{\partial x}-\Psi\right)\end{cases} \quad (8)$$

Free vibration is considered, that means

$$q(x,y,t)=0 \quad (9)$$

The free vibration equation of beam is therefore obtained:

$$\begin{cases}\bar{m}\dfrac{\partial^2 V}{\partial t^2}=k'\bar{G}\left(\dfrac{\partial^2 V}{\partial x^2}-\dfrac{\partial \Psi}{\partial x}\right)\\ \bar{A}\dfrac{\partial^2 \Psi}{\partial t^2}=\bar{D}\dfrac{\partial^2 \Psi}{\partial x^2}+k'\bar{G}\left(\dfrac{\partial V}{\partial x}-\Psi\right)\end{cases} \quad (10)$$

Eliminating variables Ψ, we can get the differential equation with V as the variable:

$$\bar{D}\frac{\partial^4 V}{\partial x^4}+\bar{m}\frac{\partial^2 V}{\partial t^2}-\left(\frac{\bar{m}\bar{D}}{k'\bar{G}}+\bar{A}\right)\frac{\partial^4 V}{\partial x^2\partial t^2}+\frac{\bar{m}\bar{A}}{k'\bar{G}}\frac{\partial^4 V}{\partial t^4}=0 \quad (11)$$

D. Natural Frequency Expression of FGM Beam

Taking a simply supported FGM beam with thickness of h as the example, the size is $l\times h$. The boundary conditions are:

$$V\left(0,t\right)=\frac{d\psi}{dx}\left(0,t\right)=V\left(l,t\right)=\frac{d\psi}{dx}\left(l,t\right)=0 \quad (12)$$

The transverse displacement of beam V is assumed as follows, according to the separation of variables:

$$V(x,t)=v(x)e^{i\omega_n t} \quad (13)$$

where ω_n is the *n-th* order natural frequency of beam.

To take (13) into (11) where, and using the boundary conditions (12), the equation of the form can be obtained as:

$$v^{(4)}+\left(\frac{\bar{m}}{k'\bar{G}}+\frac{\bar{A}}{\bar{D}}\right)\omega_n{}^2v''+\frac{\bar{m}}{\bar{D}}\omega_n{}^2(\frac{\bar{A}}{k'\bar{G}}\omega_n{}^2-1)v=0 \quad (14)$$

Assuming that $a^2=\frac{\bar{m}}{\bar{D}}\omega_n{}^2$, $b^2=\frac{\bar{D}}{k'\bar{G}}$, $c^2=\frac{\bar{A}}{\bar{D}}\omega_n{}^2$ and $v(x)=e^{\lambda x}$ to be brought into the above equation, algebraic function is gained as:

$$\lambda^4+\left(a^2b^2+c^2\right)\lambda^2+a^2(b^2c^2-1)=0 \quad (15)$$

Then the function is solved with the results that:

$$\lambda_1{}^2=-\frac{1}{2}\left[\left(a^2b^2+c^2\right)+\sqrt{\left(a^2b^2+c^2\right)^2-4a^2(b^2c^2-1)}\right]$$
$$\lambda_2{}^2=-\frac{1}{2}\left[\left(a^2b^2+c^2\right)-\sqrt{\left(a^2b^2+c^2\right)^2-4a^2(b^2c^2-1)}\right]$$

Mode shape function of the beam can be expressed as:

$$v(x)=C_1\sin(\lambda_1x)+C_2\cos(\lambda_1x)+C_3\sinh(\lambda_2x)+C_4\cosh(\lambda_2x) \quad (16)$$

where

$$\lambda_1=\sqrt{\frac{1}{2}\left[\left(a^2b^2+c^2\right)+\sqrt{\left(a^2b^2+c^2\right)^2-4a^2(b^2c^2-1)}\right]}$$
$$\lambda_2=\sqrt{\frac{1}{2}\left[\left(a^2b^2+c^2\right)-\sqrt{\left(a^2b^2+c^2\right)^2-4a^2(b^2c^2-1)}\right]} \quad (17)$$

For the simply supported beam, $\sin(\delta l)=0,(\delta l)_n=n\pi$,the natural frequencies can be obtained from $\lambda_1=n\pi/l$.

$$\frac{n^4\pi^4}{l^4}-\frac{\bar{m}}{\bar{D}}\omega_n{}^2-\left(\frac{n^2\pi^2\bar{m}}{l^2k'\bar{G}}+\frac{n^2\pi^2\bar{A}}{l^2\bar{D}}\right)\omega_n{}^2+\frac{\bar{m}\bar{A}}{\bar{D}k'\bar{G}}\omega_n{}^4=0 \qquad (18)$$

where the first two terms can be regarded as the frequency of simply supported Euler beam $\omega_n=\left(n\pi/l\right)^2\Big/\sqrt{\bar{m}/\bar{D}}$ and the third term shows the main effects of moment inertia and shear deformation. Solving (18) with only one positive real root needed, so the vibration natural frequency of FGM shear beam is expressed as:

$$\omega_n=\sqrt{\frac{1}{2}\frac{\bar{D}k'\bar{G}}{\bar{m}\bar{A}}}\cdot\sqrt{\sqrt{\beta^2-\frac{4n^4\pi^4\bar{m}\bar{A}}{l^4\bar{D}k'\bar{G}}}-\beta} \qquad (19)$$

where

$$\beta=\frac{l^{-2}}{\bar{D}}\left(\bar{m}+\frac{n^2\pi^2\bar{m}}{k'\bar{G}/\bar{D}}+n^2\pi^2\bar{A}\right) \qquad (20)$$

$\bar{m},\bar{D},\bar{G},\bar{A}$ is given above. Then the natural frequencies corresponding to the order can be obtained with n equated different integer values.

IV. Numerical Examples

The simply supported FGM beam is shown in Figure 1, and we assume ν_0=0.3, l=1m. Two different metals are chosen: titanium and aluminium, to compose of FEM with ceramic. The following table shows physical parameters of titanium, aluminium and ceramic:

TABLE I
PHYSICAL PARAMETERS OF TITANIUM, ALUMINUM AND CERAMICS

	Titanium	Aluminum	Ceramics
$E(Pa)$	1.057×10^{11}	0.71×10^{11}	1.51×10^{11}
ν_0	0.3	0.3	0.3
$\rho(kg/m^3)$	4429	2700	3000

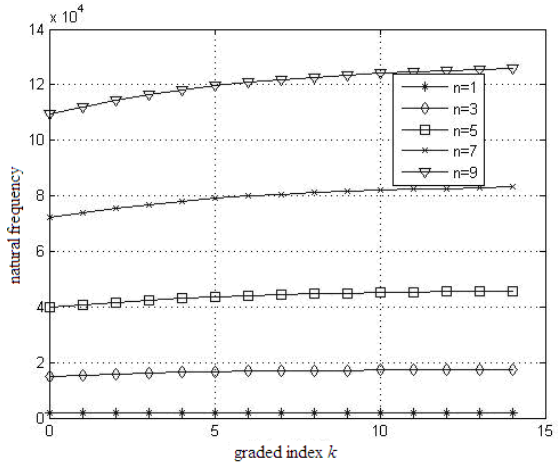

Fig.2 The change of FGM beams with graded index in different orders

Figure 2 illustrates the natural frequency of FGM beams changes with graded index in different orders. Some simple cases are taken to analyze with h=0.1m and n=1,3,5,7,9. It can be seen that the natural frequencies increases with n value and also increases with the gradient index, but the rate of change decreases with the increase of k. And the value ω of FEM beam tends to the constant value when $k\to\infty$, and the value is similar to the natural frequency of homogeneous and isotropic ceramic material beam.

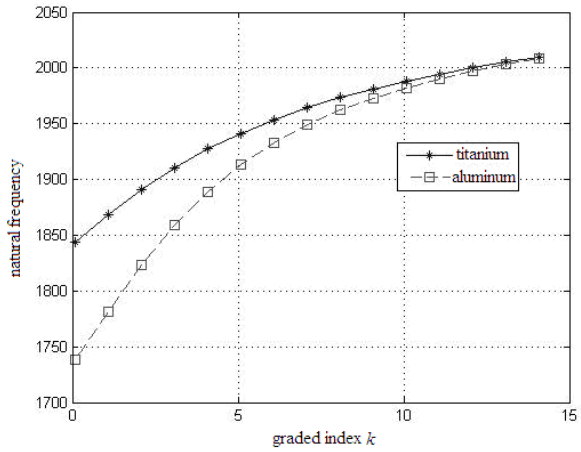

Fig.3 The change of FGM beams with graded index used different metals

Figure 3 shows the natural frequency of FGM beams changes with graded index used the different metal materials. The titanium and aluminium is selected to analyse. It can be seen that he natural frequency of FGM beam composed by both of the two materials increases with the gradient index, and the natural frequency of titanium FGM beam is larger but the change of the natural frequency of titanium FGM is faster when $k\to\infty$. Finally both of two natural frequencies tend to the same value, namely, ceramic natural frequency of homogeneous isotropic beam.

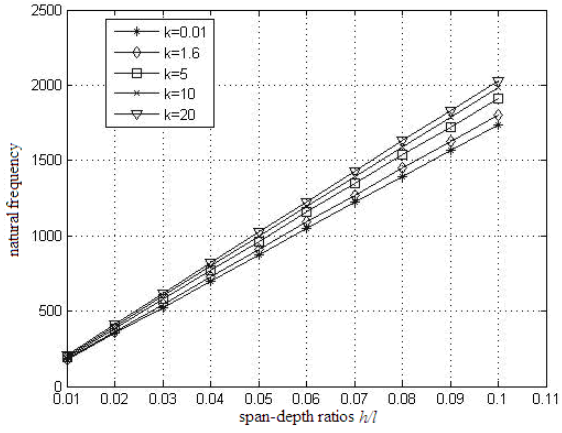

Fig.4 The change of FGM beams with graded index in different span-depth ratios

Figure 4 demonstrates the natural frequency of FGM beams changes with graded index in different span-depth ratios when n=1. It illustrates that the first order natural

frequency linearly increases with span-depth ratio. The first order natural frequency deceases as gradient index increases and the natural frequency gets its maximum when k=0.

V. Conclusion

This paper has researched FGM shear beam based on exponential function. The free vibration equation of FGM beam has been derived applying Hamilton principle. The natural frequency expression of simply supported beam has been gained. Finally the effects of the vibration order, the metal material type and the span-depth ratios to the vibration frequency of the FGM beam have been discussed. The results illustrate that:

The natural frequency of FGM beam increases with the gradient index k when taking different values of n, but eventually tends to the natural frequency of homogeneous isotropic ceramic. Therefore, changing the value of the order n can render the natural frequency vary in a specific range. In general, FGM the rate of natural frequency change with graded index is not the same when the metals which compose of FEM with ceramic are different. Therefore, in actual production, we can select the appropriate metal with ceramic to make up FGM that satisfies the requirements and furthermore to control rate of change of the natural vibration frequency. For the beams that span-depth ratio > 30, the Timoshenko beam can be converted into simple Euler beam for simple analysis and calculation. Significantly higher frequencies of the beam are affected by shear deformation and rotary inertia, therefore using elementary beam theory to calculate high frequency of shallow beam may also lead to considerable error.

Acknowledgment

This work is partially supported by the National Natural Science Foundation of China through the grant 10972021.

References

[1] L. Yin, and Y. Shen, “Mechanical Behavior and Engineering Applications of Piezo-intelligent Structures,” *Advances in Mechanics*, vol. 28, no. 2, pp. 163-172, 1998.(in Chinese)

[2] M. Koizumi, “FGM activities in Japan,” *Composites*, vol. 28, no. 1-2, pp.1-4, 1997.

[3] W. Liu, L. Ding, and H. Luo, “Analyses of In-plane Stress and Out-of-plane Displacement of Piezoelectric Functionally Graded Plates Base on Different Gradient Models,” *Journal of Jilin University (Science Edition)*, vol. 43, no. 5, pp. 589-593, 2005. (in Chinese)

[4] Y. Bedjilili, A. Tounsi, H.M. Berrabah, and et al. “Natural Frequencies of Composite Beams Having Variable Fiber Volume Fraction Including Rotary Inertia and Shear Deformation,” *Applied Mathematics and Mechanics*, vol. 30, no. 6, pp. 667-676, 2009.

2011 International Conference on Mechanical, Industrial, and Manufacturing Engineering
Lecture Notes in Information Technology Vols. 1-2

Experimental investigation of non-linearity critical strain energy release rate of frozen soil

Yuedong Wang*, Chunge Nie
School of traffic and transportation
Dalian JiaoTong University
Dalian, China 116028
wydstar@163.com

Hongsheng Li
Department of engineering mechanics
Dalian university of technology
Dalian, China 116024
lihs@dlut.edu.cn

Abstract- This paper describes an experimental study on the non-linearity critical strain energy release rate for frozen soil. Single edge straight-through cracked specimens and single edge chevron-notched specimens in three-point bending were used in the test under mode I loading. The measured technique and principle of non-linearity critical strain energy release rate are discussed. Some preliminary results are given.

Keywords- frozen soil; nonlinearity; critical strain energy release rate

I. Introduction

The fracture toughness of metal, concrete, ceramic, rack and ice, etc. has been studied many years, and there is great deal of literature available in these fields (e.g., Hertzberg 1983, Atkin and Mai 1985, Shen et al 1988, Dempsey et al 1989, Gdoutos 1990, Ayoub and Brown 1991, Dempsey 1991, Whittaker et al 1992, Qiuhua et al 2003). In recent years, some progress has also been made in the field of frozen soil fracture toughness (e.g., Li and Zhang 1995, Li and Yang 2000, Li and Yang et al 2000, Li and Zhu 2002).

For many practical applications in frozen soil engineering the nondistrubed soil type may be dominant and greater significance. However, studies of the fracture behaviour under mode I and mode II loading in nondistrubed frozen soil have received little attention, and fracture toughness data from these modes of loading are scarcer.

In this paper, an experimental study on the non-linearity strain energy release rate of nondistrubed frozen soil is described. Both single edge straight-throught cracked specimens and single edge chevron-notched specimens were used in the test in three-point bending under mode I loading. The measured technique and principle of non-linearity critical strain energy rate are discussed. The methods of specimen preparation and measured crack length are presented. Some preliminary results had been obtained.

II. Experimental principle and method

Considering a specimen with single edge straight-through crack loading in three-point bending, in which the specimen thickness as B, Crack length as a, external force as P as shown in Figure 1.

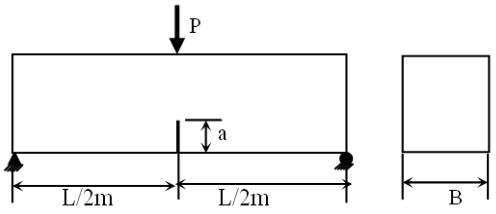

Fig. 1 The specimen with single edge crack

Based on the energy balance principle (We are neglecting any losses of energy), the formula for the non-linear strain energy release rate G has been derived by Liebowitz and is expressed as follows (Wang 1982)

$$\frac{\partial W}{\partial A}-(\frac{\partial U_e}{\partial A}+\frac{\partial U_p}{\partial A})=\frac{\partial \Gamma}{\partial A}=\tilde{G} \tag{1}$$

When critical condition occurs, equation (1) is rewritten as follows:

$$(\frac{\partial W}{\partial A}-\frac{\partial U_e}{\partial A}-\frac{\partial U_p}{\partial A})_{crit}=\frac{\partial \Gamma}{\partial A}=\tilde{G}_C \tag{2}$$

* This work is partially supported by LiaoNing Province doctor research Foundation (No. 20101009), Scientific research plan projects of LiaoNing Education (No. L2010087) of P. R. China

Where ： W is Work done by the load P under loading point displacement △, U_e is Strain energy of elastic, U_p is Strain energy of plastic, Γ is Consumed energy of the crack grown, A is Area of crack face (i.e. $A = Ba$), $\tilde{G}_C$ is Non-linearity critical strain energy release rate.

The non-linearity curve of $P-\Delta$ is obtained as shown in Figure 2, and can be adequately described by a three parameters equation:

$$\Delta = \frac{P}{M_0} + k(\frac{P}{M_0})^n \tag{3}$$

Where, M_0 is The slope of linear part of the $P-\Delta$ curve, $M_0 = \tan\theta(a_0) = M(a_0)$, k is Constant of the frozen soil materials, k >0, n is Constant of the frozen soil materials, n >1.

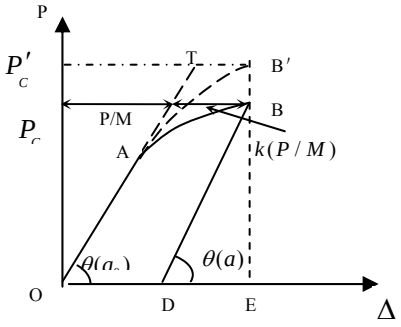

Fig. 2 The curve of $P-\Delta$

The general expression of strain energy U ($U = U_e + U_p$) can be obtained as follows:

$$U = P\Delta - \int_0^P \Delta dP \tag{4}$$

Substituting equation (3) into equation (4), after integrated yield:

$$U = \frac{1}{2}\frac{P^2}{M} + \frac{nk}{n+1}P^{n+1}(\frac{1}{M})^n \tag{5}$$

In the critical case, the load P is approach to P_c, so that load P and displacement Δ with increase are small amount, therefore, the work done by the P is approximate to zero. After taken derivative to the equation (5) and substituting it into equation (2) can be expressed as follows:

$$\begin{aligned}(\frac{\partial W}{B\partial a} - \frac{\partial U}{B\partial a})_{crit} &= \frac{\partial}{B\partial a}(-U_e - U_p)_{crit} \\ &= \frac{1}{B}[1 + \frac{2nk}{n+1}(\frac{P_c}{M_0})^{n-1}] \times \frac{1}{2}P_c^2\frac{d}{da}(\frac{1}{M})_{a_0}\end{aligned} \tag{6}$$

The above equation can be farther simplified as:

$$\tilde{G}_C = \frac{1}{B}[1 + \frac{2nk}{n+1}(\frac{P_c}{M_0})^{n-1}] \times \frac{1}{2}P_c^2\frac{d}{da}(\frac{1}{M})_{a_0} \tag{7}$$

In which, $1/M$ is the compliance for system and can be measured from the ASTM-E399 standard method used to determine the stress intensity factors.

When crack extension contains not only the plasticity deformation, but also crack propagation in which is very obvious, an expression for $\tilde{G}_C^*$ to amount for the effects of the crack propagation as follows:

$$\tilde{G}_C^* = \frac{1}{B}[1 + \frac{2nk}{n+1}(\frac{P_c}{M(a)})^{n-1}] \times \frac{1}{2}P_c^2\frac{d}{da}(\frac{1}{M})_a \tag{8}$$

Where, $1/M$ is the compliance of the crack length as a.

III. Testing requirements

A. Specimens

The non-linearity critical strain energy release rate $\tilde{G}_C$ or $\tilde{G}_C^*$ was measured by using the experimental arrangement in which the specimens included straight-through cracked and chevron notch were subjected to 3-point bending as shown in Fig.3 and Fig.4. The nonstandard specimens were adopted, the dimensions of frozen soil specimen were taken as B×H×L=(0.1×0.1×0.4)m and B×H×L=(0.1×0.07×0.4)m，a≤0.04m~0.05m, respectively.

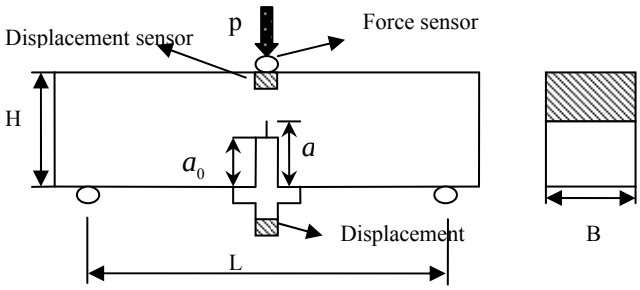

Fig. 3 The specimens of straight-through crack

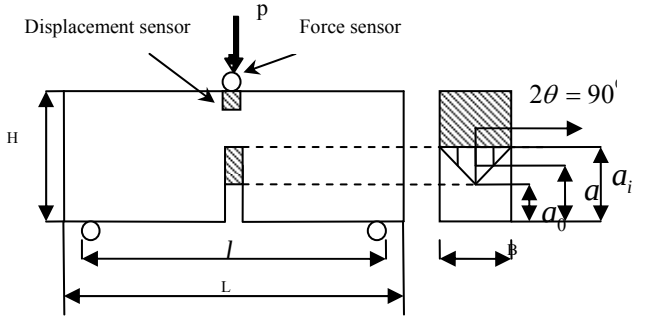

Fig. 4 The specimens of chevron-notch

B. Experimental set-up

In order to obtain valid crack length values which the both the critical crack length and the creek length at failure, the experimental set-up which the photos as shown in Fig.5 is reformed on the traditional set-up. After the reformed set-up loading was from bottom up wards, the crack growth was from top downwards. The dye penetrant technique (Schmidt.1997) is also applied in this paper. Daring testing, using dye in the crack of frozen soil which penetrates into mew crack tip as the crack grows is more easily to implement. Test system is built in the field. An automatic controlling system and a microcomputer-aided data-collecting system are built too. Both the load p and the loading point displacement Δ can be recorded automatically, and are plotted in the form of $P-\Delta$ curve.

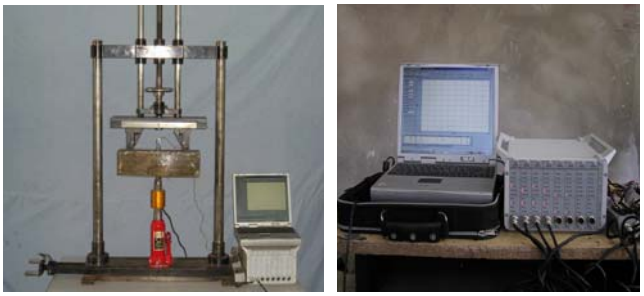

Fig. 5 The photos of experiment

IV. Experimental results

1) The specimen soil is the lower liquid clay of Shen Yang province, in the northeast part of China. It basically consists by different grain sizes and the physical properties are shown in Table 1.

Table 1 ingredient of soil grain and the physical properties

Soil specimen	size（mm）					Character index			
	5~2	2~0.5	0.5~0.2	0.2~0.07	<0.07	ω_L	I_P	ω_P	ω_0
1	8.0%	17.5%	14.5%	20.0%	40%	25.0%	9.4	15.6%	10.6%
2						22.3%	6.7	15.6%	10.6%

2) The values of freezing-depth at nondistrubed soil layers, the temperature and water content at depth as 60cm in freezing layer are shown in Tab. 2.

3) The typical curves of the load P and loading point displacement Δ for both specimens of straight-through crack and chevron-notch at depth as 60cm in freezing layers is shown in Fig. 6 and Fig. 7.

Tab. 2 Values of frost depth, frost heaving amount, soil temperature and water content

date	frost depth (mm)	frost heaving amount (mm)	Temperature(℃) (in 60cm)	water content (%)
2005-1-1	75	3.9	-2.3	17.5
2005-1-15	106	5.2	-4.4	17.2
2005-2-1	110	8	-4.5	17.0
2005-1-15	76	8	-3.8	17.1
2005-3-1	42	4	-3.2	17.4

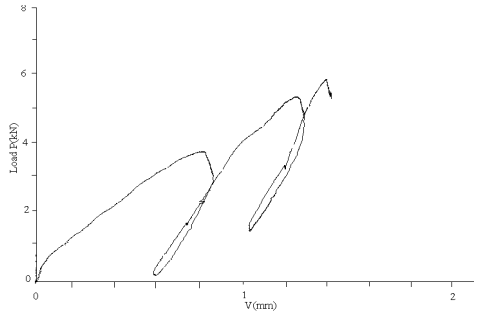

Fig. 6 The typical curves of P - Δ for the straight-through crack specimens

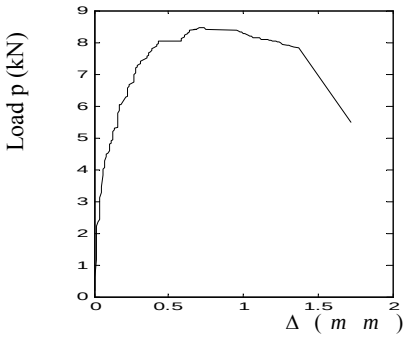

Fig. 7 The typical curves of P - Δ for the chevron-notch crack specimens

4) The three parameters of the n , k and $\frac{d}{da}(\frac{1}{M})_a$ can be obtained as shown in the Tab. 3.

Tab. 3 The parameters of the n , k and $\frac{d}{da}(\frac{1}{M})_a$

Parameter	single edge straight cracked specimens			chevron-notched specimens	
n	4.278			3.848	
k	6.749			2.87	
$\frac{d}{da}(\frac{1}{M})$	a =4.15cm	a =4.25cm	a =4.30cm	a =1.0cm	a =2.0cm
	0.009	0.013	0.017	0.003	0.007

5) The $\tilde{G}_c$ and $\tilde{G}_c^*$ for single edge straight cracked specimens at a water content W=17.2% and temperature θ =-4.4℃, with the freezing history as 2005-1-15, a number of specimens were tested. The results are shown in Table 4, in which is linear elastic critical strain energy release rate for parameters n =1, k =0.

6) The G_C and $\tilde{G}_C^*$ for chevron-notched specimens at a water content W=17.2% and temperature θ=-4.4℃, with the freezing history as 2005-1-15. The results are shown in table 5. In which G_C is also linear elastic critical strain energy release rate.

Tab.4 The $\tilde{G}_C$ and $\tilde{G}_C^*$ for single edge straight cracked specimens

No	a (cm)	B (cm)	P_C (KN)	G_C (N/m)	$\tilde{G}_C$ (N/m)	$\tilde{G}_C^*$ (N/m)
1	4.26	11.8	3.22	395	474	764
2	4.28	11.4	3.81	430	495	798
3	4.25	11.6	3.47	363	435	674
4	4.25	11.8	3.25	334	401	620
5	4.3	11.6	3.33	336	403	624
6	4.33	11.8	4.18	518	596	962
7	4.33	11.3	3.24	418	481	789
8	4.25	12.8	3.24	369	443	697
Average	4.28	11.76	3.47	395	466	741

Tab. 5 The G_C and $\tilde{G}_C^*$ for chevron-notched specimens

No.	B (cm)	P_C (KN)	G_C (N/m)	$\tilde{G}_C$ (N/m)
1	11.6	6.18	493	801
2	12.5	6.24	467	766
3	10.9	5.54	422	617
4	10.6	4.58	445	563
5	11	3.35	408	451
6	11	6.04	497	788
7	10.3	6.23	565	926
8	11	6.3	541	898
9	10.3	5.6	457	673
Average	11.0	5.6	477	720

V. Discussion

From the study for the critical strain energy release rate of nondistrubed frozen soil (or original stale frozen soil), the authors attempt to discuss the following problems with some specialists of this region:

1) Duo to many practical applications in frozen engineering the nondistrubed soil type may be dominate and nonlinearity $\tilde{G}_C$ or $\tilde{G}_C^*$ index values may be greater significance. However, studies of nonlinearity $\tilde{G}_C$ or $\tilde{G}_C^*$ for nondistrubed frozen soil in comparison with the linear elastic G_C of frozen soil have not received same amount of attention. The main reason for this may be duo to lack of sufficient experimental data.

2) there exist obvious differences of the critical strain energy release rate G_C between the straight-through cracked specimens and the chevron-notched specimens although the samples are tested under the same condition of initial water content, dry density and temperature. The main reason for this may be due to differences of the specimen types. In order to obtain valid G_C values, the crack of specimen precrack is sufficiently sharp must be satisfied. But, non-linearity $\tilde{G}_C^*$ of the straight-through cracked specimens and $\tilde{G}_C$ of the chevron-notched specimens are accord well, which are not so strongly dependent on specimen types and crack preparation.

REFERENCES

[1]Atkins, A.G. and Mai, Y.W., "Elastic and plastic fracture: metals, polymers, ceramics, composites, biological materials". Ellis Horwood, chichesler, U.K. 1985.

[2]Ayoub, A.S., and Brow, T.G., (1991). "Fracture analysis of ice force". Joundal of ColdRegion Engineering. ASCE, vol. 5(4), pp. 158-173.

[3]B.N.whittaker, R.N.singh and G.Sun, "Rock fracture mechanics principle, design and applications". ELSEVIER Science Publisher B.V. 1992.

[4]Dempsey, J.P., et al.. "Fracture toughness of S_2 columnar freshwater ice: crack length and specimen size effect", part I, Proc. 8th Int. POAC conf., The Hague, The Netherlands, 1989, vol. 4, pp. 83-89.

[5]Dempsey, J.P., et al. "Fracture toughness of ice", Ice-structure interaction ,Springer-Verlag, Berlin, 1991, pp. 109-145.

[6]Gdoutos, E.E.. "Fracture analysis of ice force". Joundal of ColdRegion Engineering. ASCE, 1990, vol. 5(4), pp. 158-173.

[7]Hertzberg,R.W., "Deformation and fracture mechanics of engineering materials". Wiley, New York, 1983.

[8]Li H.S., Yang H.T. and Liu Z.L.. "Experimental Investigation of Fracture Toughness K_{IIC} of Frozen Soil". Canadian Geotechnical Journal, 2000, vol. 37, pp. 253-258.

[9]Li H.S. and Yang H.T. "Experimental investigation of fracture toughness of frozen soil". ASCE, J. Cold Region Engineering", 2000, vol. 14(1), pp. 43-49.

[10]Li, H.S. and Zhu, Y.L. "Fracture mechanics of frozen soil and its application". Chinese, Beijing, China Ocean Press. 2002

[11]Li H.S., Zhang X.P., and Zhu Y.L., "Experimental studies of fracture toughness K_{IC} for frozen soil", Chinese J. Glaciology and Geocryology, 1995, vol. 17 (4), pp. 328-333.

[12]Qiuhua, R, et al., "Shear fracture (mode II) of brittle rock", Int, J. Rock. Mech. Min. Sci, 2003, vol. 40, pp. 355-375.

[13]Shen, W., et al., "A new concept of compact compression test specimen to study of K_I and K_{IC} for BoHai See ice".the OMAE Proc, 1988, vol. 4: pp. 25-29.

[14]Wang F. "Fracture mechanics". NanNing: GuangXi Press. 1982.

2011 International Conference on Mechanical, Industrial, and Manufacturing Engineering
Lecture Notes in Information Technology Vols. 1-2

Discussion on the Application of Stone Bank Terrace in Zhoujiahe River Valley Treatment*

Song Guohui and Li Yunfeng
school of environmental science and engineering
Chang'an University
No.126 Yanta South Road, Xi'an 710054, China
Songguohui_sophia@yahoo.cn

Xu Yanjuan
Shaanxi Institute of Engineering Survey
Liu Linian
Soil and Water Conservation Bureau in Shaanxi Province
He Ming and Liao Changchun
Zhenba County Soil and Water Conservation Station

Abstract: **Stone bank terrace which is marked by its functions of dispersing slope runoff, changing continuous slope into discontinuous slope, reducing slope length, conserving water and soil, preventing flood and improving water conservation and drought resistance of crops, has been widely used in small watershed comprehensive management. With the use of GIS and linear programming, the slope, rainfall and water requirement of crops in Zhoujiahe river valley of Zhenba County were analyzed, and existing water and soil of the slope and population resources in this area were studied. Then, the optimal arrangement scheme of stone bank terrace which could produce maximum economic benefit was determined. The conclusion was arrived at as follows: 1. under the precondition that of average per capita farmland was one Mu, according to the optimal scheme, there should be 279 Mu of irrigated stone bank terrace, 0 Mu of dry stone bank terrace, 1644.62 Mu of fish-scale pits and 1652.67 Mu of water catchment forest-grass land. The increment of target function was 801272.00 Yuan, which was a considerable benefit. 2. The transformation of all appropriate slopes into stone bank terrace was not quite reasonable with the increment of target function of 698313.40 Yuan compared with that of 102958.6 Yuan in plan 1.**

Index Terms : **Stone bank terrace; Zhoujiahe river valley; linear programming; slope runoff**

I THE NECESSITY OF STUDY ON STONE BANK TERRACE IN ZHOUJIAHE RIVER VALLEY

Stone bank terrace, the major measure for slope cropland rebuilding and water and soil conservation, which could disperse slope runoff, change continuous slope into discontinuous slope, reduce slope length, conserve water and soil, prevent flood, improve water conservation of drought resistance of crops and increase crop yield, has been widely used in small watershed comprehensive management, and it is the basic guarantee for the high-yield farmland in mountainous area. It could be known from relevant literature that the previous studies of terrace application were mainly focused on loess regions, while less attention was paid to the mountainous area. Especially, the reasonable arrangement of stone bank terrace in small watershed comprehensive management required careful research. Therefore, the achievement of a rational deployment of stone bank terrace, fish-scale pit and water catchment forest-grass land in the small watershed comprehensive management of Zhenba County in south Shaanxi was of high urgency.

II. INTRODUCTION OF STONE BANK

Terrace is the stepped or wave-like farmland constructed along the contour line in hilly land [1] (Wang Lixian etc.). According to its profile, terraces fall into two types, stepped or wave-like. Wave-like terrace is also called broad-base terrace. The types of stepped consist of level terrace, sloping terrace, reverse-sloped terrace and separate-sloped terrace, or the types of terraces can be classified into earth bank terrace, stone bank terrace, grass bank terrace and earth-stone bank terrace in terms of the construction materials of terrace bank. In the loess region of north Shaanxi of China, the terraces are mostly the earth bank terrace; and those in the mountainous area of south Shaanxi, are stone bank terraces.

Ⅲ APPLICATION OF STONE BANK TERRACE IN SOUTH SHAANXI OF CHINA

Zhenba County is situated in the southeast of Hanzhong city in Shaanxi Province, which is the typical mountainous area in south Shaanxi and also the rainfall center of the entire Shaanxi Province. Zhenba County, the state poverty county of China, was listed as the major water and soil conservation area in upper and middle reach of Yangtze River in 1989. In order to solve the food and clothing problems for people in Zhenba County, "Yangtze River Regulation Project" was implemented. By adjusting the measures to local conditions, stone bank terraces were built in hilly area slanting 5°-25° with the local materials, which had made significant contribution to the small watershed comprehensive management. According to the records of water conservation station of Zhenba County, 60109.00 Mu of stone bank terraces were built from 1989 to 1998, with the total economic benefit reaching 73576000.00 Yuan in these 10 years and 385620400.00 Yuan to be expected in the next 30 years.

Since the construction of stone bank terrace is highly demanding of human resources and material resources, the

* This paper is sponsored by the item of Shaanxi Province Soil and Water Conservation Bureau: 'The study of slope runoff utilization in the south of Shaanxi Province in China'

rationality of transforming all the appropriate slopes into stone bank terraces has to be evaluated. The key to the incorporation of environmental, social and economic benefits into the small watershed comprehensive management is the reasonable arrangement of stone bank terraces, which involves many factors. In this study, the major aspects of consideration were population, water and soil resource on slopes. The precondition that the average per capita farmland was one Mu was met as much as possible. In drought seasons, the method of gathering slope runoff for irrigation could be used to ensure the crop yield. There are two kinds of stone bank terrace, the irrigated type and dry type. Stone bank terrace was located in area 1, namely rainfall catchment area with slope gradient less than 25°. Fish-scale pit was located in area 2, namely rainfall catchment area with slope gradient between 25°-35°. Natural forest-grass land was located in area 3, namely rainfall catchment area with slope gradient more than 35°.

The efforts were made in the maximization of economic benefits with the satisfaction of the above conditions.

The slope gradient, rainfall and water requirement of crops was studied to obtain the reasonable arrangement of stone bank terraces in Zhoujiahe river valley of Zhenba County by adopting linear programming in the following chapters.

Ⅳ Analysis of Slope Gradient of Soil Resources in Zhoujiahe River Valley

A. Analysis of Slope Gradient of Soil Resources and Distribution of Water Catchment in Zhoujiahe River Valley

Zhoujiahe river valley is a complete branch gorge and the whole topography is inclined from northeast to southwest. The slope is steep on the northeast where the terrain undulates roughly, while on the southwest slope is gentle and the terrain is smooth. The overall topography features a gorge wedged between two hills and the mouth of the gorge is linked to the valley of the main gorge. Slopes and water catchment area is generated with the use of software ARCGIS. The area with slope gradient less than 5° accounts for 11.5% of the whole region. The area with slope gradient between 5° and 15°, accounts for 1.5% of the whole region. The area with slope gradient between 15° and 25° accounts for 15.2% of the whole region. The area with slope gradient between 25° and 35° accounted for 32.7% of the whole region. The area with slope gradient more than 35° accounts for 39.4% of the whole region. Water catchment areas can be divided into H2 high water catchment area and H1 low water catchment area.

B. *Distribution and Measurement of Water Catchment Area in Zhoujiahe River Valley*

The analysis of slope types and water catchment characteristics in Zhoujiahe river valley revealed that there were two types of slopes where high-standard stone bank terraces (irrigated croplands) could be built. One was low sloping field (code $p25_1$) with slope gradient less than or equal to 25 °, which was mainly irrigated by the water in H1 or the remaining water of H2. The other was high sloping field (code $p25_2$) with slope gradient more than or equal to 25 °, which could only be irrigated by water from H2.

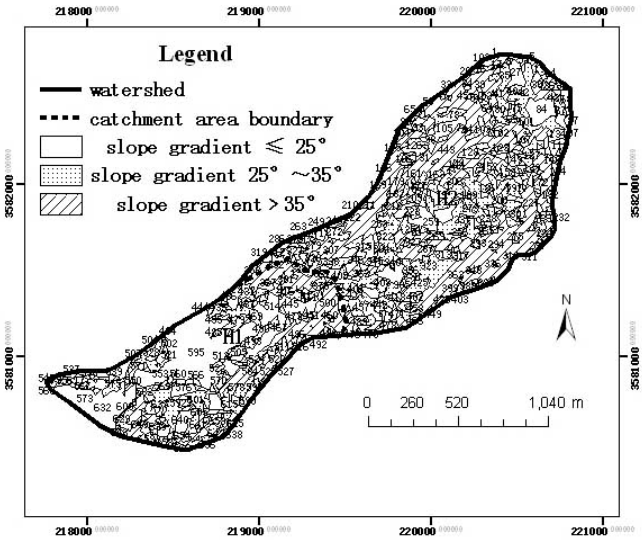

Figure 1 polygons for different field in Zhoujiahe river valley

The main part of $p25_1$ was at the bottom of gorge, namely polygon 632, 595, 514, 539, 640, 591 and 576 and part of polygon 457, 436 and 361 (see Figure 1.).

Polygon 259, 84, 408, 134, 105, 346, 27 and part of polygon 457, 436 and 361 was distributed in $p25_2$, the high sloping field.

Besides the above two kinds of fields, there were second-class steep sloping fields with slop gradient between 25 °-35 ° and third-class steeper sloping field with slop gradient of more than 35 °.

The 569.8 Mu of low sloping fields (code $p25_1$) among sloping fields with slope gradient less than or equal to 25°, were the most suitable for the construction of high-standard level terraces.

Ⅴ Analysis of Rainfall Resource in Zhoujiahe River Valley

A. Calculation of Slope Runoff Resources and Irrigation Volume Required in Zhoujiahe River Valley

1) Experiential Frequency for Rainfall Calculation

According to the rainfall data measured from 1959 to 1972 by weather station of Zhenba County, the average annual rainfall was 1251.8mm, while the maximum was 1782mm (1964) and the minimum was 789mm (1966). The results of experiential frequency calculation showed that the annual rainfall in 1966 could be used in 95% frequency year; the annual rainfall in 1972 could be used in 75% frequency year; the annual rainfall in 1963 could be used in 50% frequency year.

The proportion of average monthly rainfall from 1959 to 1972 was used to determine the beginning and ending month of rainy season and droughty season. (If the monthly rainfall was more than 10% of annual rainfall, this month was

considered to be rainy month.The month with proportion of less than 15% was considered to be a drought month). Therefore, the drought season lasted for 9 months, beginning in October and ending in June of the following year.

2) The Prediction of Each Month's Rainfall and Runoff

According to hydrology calculation code of China, Pearson-Ⅲ was adopted for the calculation of theoretical frequency distribution of hydrology variable.

The proportions of annual rainfall with different frequencies were calculated using theoretical frequency of 93.33%, 73.33% and 53.33%, respectively, in each month. The distribution of theoretical annual rainfall calculated using theoretical frequency of 95%, 75% and 50%, respectively, in each month (See Table 1).

TABLE 1 DISTRIBUTION OF THEORETICAL RAINFALL CALCULATED USING THREE THEORETICAL FREQUENCIES IN EACH MONTH

Freq	Year	Theo annual rainfall (mm)	Distribution of theoretical rainfall calculated by three theoretical frequencies in each month					
			Jan	Feb	Mar	Apr	May	Jun
95%	1966	785.560	1.892	23.696	24.194	109.023	127.442	44.306
75%	1972	979.060	21.924	2.803	64.570	72.579	203.821	68.674
50%	1963	1138.270	0.000	2.693	35.183	138.212	234.204	110.587
Freq	Year	Theo annual rainfall (mm)	Distribution of theoretical rainfall calculated using three theoretical frequencies in each month					
			Jul	Aug	Sep	Oct	Nov	Dec
95%	1966	785.56	110.616	97.374	128.935	91.201	25.688	1.195
75%	1972	979.06	212.430	74.180	152.765	65.971	37.140	2.202
50%	1963	1138.3	103.898	172.091	247.235	32.490	50.385	11.293

B. Calculation of Runoff Volume in Each Water Catchment

Except the transformation of sloping croplands into high-quality stone bank terraces, the other sloping fields should be reserved as natural forest-grass land in Zhoujiahe river valley.

TABLE 2 RAINFALL AND SLOPE RUNOFF DEPTH WITH DIFFERENT FREQUENCIES IN ZHENBA COUNTY

Theo freq (%)	Theo annual rainfall (mm)	slope runoff depth		Theo freq (%)	Theo annual rainfall (mm)	slope runoff depth	
		E	D			E	D
0.001	2679.48	35	937.82	30	1276.87	35	446.9
0.01	2426.91	35	849.42	40	1203.58	35	421.25
0.0333	2288.53	35	800.99	50	1138.27	35	398.39
0.05	2240.52	35	784.18	60	1076	35	376.6
0.1	2156.93	35	754.93	70	1012.68	35	354.44
0.2	2070.85	35	724.8	75	979.06	20	195.81
0.3333	2005.57	35	701.95	80	942.81	20	188.56
0.5	1952.42	35	683.35	85	902.12	20	180.42
1	1858.44	35	650.45	90	853.27	20	170.65
2	1759.59	35	615.86	95	785.56	20	157.11
3.3333	1682.76	35	588.97	97	744.5	20	148.9
5	1618.72	35	566.55	99	673	20	134.6
10	1500.88	35	525.31	99.9	567.78	20	113.56
20	1367.23	35	478.53	99.99	496.35	10.5	52.12
25	1319	35	461.65	99.999	444.4	10.5	46.66

Note: E-Rain-Water collection efficiency of slope runoff (%)
D-Annual runoff depth (mm)

The area of stone bank terraces should not be taken into account of the calculation of runoff volume for both low water catchment and high water catchment after the construction of stone bank terraces, for the rainfall was intercepted by the stone bank terraces with no slope runoff produced. For the calculation of runoff volume of fish-scale pit to be built, 20% of slope runoff could be taken into account. For that of natural slope in forest-grass land, all the slope runoff could be taken into account. The cost for the construction of water catchment slope of forest-grass land was 0 and the average runoff yield could be obtained by checking *Technical Code of Practice for Rainwater Collection and Storage Utilization SL267-2001*, The theoretical annual rainfall in Table 2 is the annual rainfall calculated using theoretical frequency distribution model of Pearson-Ⅲ hydrology variable (P-Ⅲ), according to hydrology calculation code in China.

Ⅵ WATER REQUIREMENT OF CROP IN STONE BANK TERRACE OF ZHOUJIAHE RIVER VALLEY

A. Acquirement of calculation parameters for required water volume of crop in Zhoujiahe River Valley

In this study, corn and winter wheat were chosen as the representatives of crops in Zhenba County. Then, water requirement value of crop ET_0 and crop efficient of winter wheat Kc provided by *water Requirement of Crop and Divisional Irrigation Model of Shaanxi Province* are substituted in the formula:$ET=ET_0 \times Kc$.

After water requirement value of winter wheat ET and that of corn in Zhenba County was obtained, respectively (water requirement periods of the two were head and tail connected), water requirement value of crops ET of each month from January to December in Zhenba County was thus acquired.

The sum of ET of the whole year was 740.2747mm/a, i.e. water requirement of crops, which were represented by corn and winter wheat in Zhenba County, was 740.2747mm/a.

B. Calculation of Water Requirement of Irrigation of Stone Bank Terrace Crop in Zhoujiahe River Valley

The calculation of the water requirement of crop was conducted according to exi.FOR program:

1) For 50% frequency year, water requirement of crop irrigation in Zhoujiahe river valley was 164.43m^3/year•Mu and runoff yield per Mu in water catchment area was 265.61m^3/year•Mu.

2) For 75% frequency year, water requirement of crop irrigation in Zhoujiahe river valley was 172.11m3/year•Mu and runoff yield per Mu in water catchment area was 130.55m^3/year•Mu.

3) For 95% frequency year, water requirement of crop irrigation in Zhoujiahe river valley was 177.08m^3/year•Mu and runoff yield per Mu in water catchment area was 104.75m^3/year•Mu.

Ⅶ ARRANGEMENT OPTIMIZATION OF STONE BANK TERRACE IN STUDY REGION

Target function for various kinds of arrangement schemes for stone bank terraces in Zhoujiahe river valley was expressed as Max $Z=c_1x_1+c_2x_2+c_3x_3+c_4x_4$.

The general objective of arrangement optimization of soil and water of stone bank terrace was to maximize economic benefits. Economic benefit was calculated according to target function Z.

Value coefficient of each decision variable could be calculated according to either of the following two computational methods.

(1) In terms of net profit per Mu·year, namely, c_i=income/ (Mu·year)-payout/(Mu·year).

(2) In terms of increment of net profit per Mu·year before and after the transformation of sloping fields, namely, c_i=net profit increment/ (Mu·year).

A. Determination of Decision Variables in Zhoujiahe River Valley

Based on the actual conditions of Zhoujiahe river valley and mathematical model of arrangement optimization of stone bank terraces, four variables were involved:

x_1-first-class stone bank terrace, namely irrigable stone bank terrace, whose value coefficient was represented as c_1.

x_2-second-class stone bank terrace, namely dry stone bank terrace, whose value coefficient was represented as c_2.

x_3-fish-scale pit with forests (economic forest, fruit trees, timber production forest etc.), whose value coefficient was represented as c_3.

x_4-natural forest-grass land in water catchment area, whose value coefficient was represented as c_4.

B. Determination of Value Coefficient of Target Function in Zhoujiahe River Valley

The calculation of value coefficients was conducted based on *Economic Survey of Small Watershed Comprehensive Management in Zhenba County*.

(1) Value coefficient of irrigable stone bank terrace, c_1

The calculation results were as follows:

c_1= 420-157.99=262.01Yuan/ (year·Mu) in plan 1.

c_1= 420-160.95=259.05Yuan/ (year·Mu) in plan 2.

(2) Value coefficient of dry stone bank terrace, c_2

c_2=160kg/(Mu·year)×1.5Yuan/kg-152Yuan/(Mu·year)
=88Yuan

(3) Value coefficient of -fish-scale pit with forests, c_3

c_3=500Yuan/ (Mu·year)-90 Yuan/ (Mu·year)
=410 Yuan/ (Mu·year)

(4) Value coefficient of natural forest-grass land, c_4

c_4=37.6Yuan/ (Mu·year)-5Yuan/ (Mu·year)
=32.6Yuan/ (Mu·year).

95% frequency year was taken as an example. Parameters could be substituted into mathematical models of each arrangement optimization scheme in 95% frequency year, and then the results were calculated.

C. Establishment and calculation of mathematical models of plan 1 in 95% frequency year in Zhoujiahe river valley

The mathematical model of linear programming of plan 1 was as follows:

$$(\text{I})\begin{cases} \text{Max } Z=262.01x_1+88x_2+410x_3+32.6x_4 \\ \text{St}: x_1+x_2+x_3+x_4 \leqslant 3576.29 \quad \cdots\cdots (1) \\ 177.08x_1-20.95x_3-104.75x_4 \leqslant 0 \quad \cdots\cdots (2) \\ x_4 \geqslant 1652.67 \quad \cdots\cdots (3) \\ x_1 = 279 \quad \cdots\cdots (4) \\ x_1+x_2+x_3 \leqslant 1923.62 \cdots\cdots (5) \\ x_i \geqslant 0 \quad (i=1\cdots 4) \end{cases}$$

It was shown from the calculation results of plan 1 that irrigable stone bank terraces covered 279 Mu; dry stone bank terraces covered 0 Mu; fish-scale pits covered 1644.620 Mu; water catchment grasslands covered 1652.670 Mu and the increment of target function was 801272.00 Yuan.

D. Establishment and calculation of Mathematical Model of plan 2 in 95% Frequency Year in Zhoujiahe River valley

The mathematical model of linear programming was established under the assumption that 955.6 Mu of high and low sloping fields in $p25_1$and $p25_2$ with slope gradient less than or equal to 25° were transformed into stone bank terraces:

$$(\text{II})\begin{cases} \text{Max } Z=259.05x_1+88x_2+410x_3+32.6x_4 \\ \text{St}: x_1+x_2+x_3+x_4 \leqslant 3576.29 \quad \cdots\cdots (1) \\ 177.08x_1-20.95x_3-104.75x \leqslant 0 \quad \cdots\cdots (2) \\ x_4 \geqslant 1652.67 \quad \cdots\cdots (3) \\ x_1+x_2 \leqslant 955.6 \quad \cdots\cdots (4) \\ x_1+x_2+x_3 \leqslant 1923.62 \quad \cdots\cdots (5) \\ x_i \geqslant 0 \quad (i=1\cdots 4) \end{cases}$$

The calculation shows that the irrigated stone bank terrace is 955.60 Mu, dry stone bank terrace is 0 Mu, fish-scale pits is 968.02 Mu and water catchment forest-grass land is 1652.67 Mu. The increase of target function is 698313.40 Yuan.

The comparison of plan 2 and plan 1 indicates that the transformation of all the appropriate sloping fields into stone bank terraces was not the best option, as the increment of target function of plan 2 would be only 698313.40 Yuan, which was less than that of plan 1, which was 801272.00 Yuan, with a difference of 102958.60 Yuan.

CONCLUSION

The following conclusion could be drawn from the research on the application of stone bank terraces in Zhoujiahe river valley, Zhenba County.

(1)Under the precondition that the average per capita farmland was 1 Mu, the increment of target function was calculated to be 801272.00 Yuan according to linear programming, which indicated the effectiveness of stone bank terrace in the improvement of agriculture production and water and soil conservation.

(2)The comparison of plan 2 and plan 1 indicated that the transformation of all the appropriate sloping fields into stone bank terrace was not the optimal scheme, as the increment of target function was only 698313.40 Yuan, compared with that of 102958.60 Yuan in Plan 1.

REFERENCES

[1] Wang Lixian etc.Water and Soil Conservation Engineering, China Forestry Publishing House 2000

[2] Jia Hengyi, Discussion on China Terrace, Agriculture Archeology, January, 2003,1 pp.157

[3] Technical Code of Practice for Rainwater Collection and Storage Utilization SL267-2001, pp.1

[4] Soil and Water Conservation Bureau of Shaanxi Province, Northwest Agriculture University Crop Water Demand and Divisional Irrigation Model of Shaanxi Province, Beijing Waterpower Press, 1992,pp.71

[5] Li Yunfeng, Song Guohui, Liu Linian, Wang Jiangxia etc. Study on Runoff Condition in Slope of Mountainous Area-Case Study of Mountainous Area of Shaanxi, pp.112-119, Collected Papers of Seminar of Soil and Water Conservation and Ecological Restoration, July 20-22, 2007, Urumchi, Sinkiang

[6] Jiang Jifa etc. Bring Forth New Ideas in Management Pattern of Rainfall Collection and Storage Utilization Project in Bazhong City, Sichuan Water Conservancy, 2004

[7] Weather Station of Shaanxi Revolutionary Committee Weather Bureau, Daily Rainfall Data of Shaanxi (1951-1972), 1973

[8] Work Station of Soil and Water Conservation of Zhenba County，Comprehensive Introduction of Scheme Implementation for Soil and Water Conservation in Ecological Construction Demonstration Area in Zhenba County, pp2-4, 2004

2011 International Conference on Mechanical, Industrial, and Manufacturing Engineering
Lecture Notes in Information Technology Vols. 1-2

Research on Monitoring Technique of Intelligent Vehicle Based on Laser Scanner

Shao-Bin Wu, Xue-Wei Wang, Ruo-Nan Geng , Li Gao
School of Mechanical and Vehicular Engineering
Beijing Institute of Technology
Beijing, China
wu.shaobin0@gmail.com

***Abstract*—Monitoring technique of intelligent vehicles for intelligent vehicle competition was studied to achieve the objective evaluation of intelligent vehicles. The method for measuring the position of intelligent vehicles was designed through integrating the sensors such as laser scanner, GPS receiver, and electronic compass equipped on the monitoring vehicle following intelligent vehicles. The algorithm of object detection and tracking using a laser scanner was developed with scan segmentation, object detection based on the shape and contour characteristics of vehicles and object tracking using a Kalman filter. The indirect localization algorithm of intelligent vehicles was proposed based on multi-sensor data fusion, realizing the monitoring of intelligent vehicles. Vehicle tracking and monitoring experiments were conducted, and experiment results show that the monitoring technique of intelligent vehicles is feasible.**

Keywords- intelligent vehicle; monitoring; laser scanner; object recognition; multi-sensor data fusion

I. INTRODUCTION

During recent decades intelligent vehicle research has been of great interest all over the world and has been listed as one of the major research projects in many countries [1-3]. Intelligent vehicle integrates multi-disciplinary, multi-field research results, and the key technologies of intelligent vehicle include real-time vision processing, environment perception based on multi-sensor data fusion, positioning technology, motion planning, navigation, control of vehicle and system architecture etc. Intelligent vehicle research results will make important contribution to ensure national security and public safety, and promote the development of information and automobile industries. To accelerate research and development in intelligent vehicles, many competitions have been held in many countries [4-8], including the Grand Challenge and Urban Challenge held by DARPA in 2004, 2005 and 2007, a series of European Land-Robot Trial (ELROB) race held in Europe since 2006, the Future Challenge held by National Natural Science Funds Commission of China in 2009 and 2010. Meanwhile, the testing of intelligent vehicles has been conducted by the third party independent of the intelligent vehicle research groups. Through the establishment of a comprehensive evaluation system and the research of testing methods and techniques, the third-party testing motivates the research group's enthusiasm on some key technologies for intelligent vehicles, makes the indicators of the relevant technologies clearer, and guides the development of intelligent vehicle technologies.

The running poses of intelligent vehicles in intelligent vehicle competitions are the embodiment of the ability of environment perception and intelligence decision-making, and the monitoring of running poses of intelligent vehicle is the base of evaluating the key technologies and research level of intelligent vehicles. This paper described the monitoring technique of the running poses of intelligent vehicle, through detecting and tracking intelligent vehicles by laser scanner, integrating the sensors such as laser scanner, GPS receiver, and electronic compass equipped on the monitoring vehicle following intelligent vehicles to localization, and realizing the real-time monitoring without disturbing intelligent vehicles.

II. MONITORING REQUIREMENTS OF INTELLIGENT VEHICLES AND OPERATION PRINCIPLE

A. Monitoring requirements of intelligent vehicles

The intelligent vehicle research is in the state of high level abroad. The different stages for intelligent vehicle competitions were designed according to the testing goals and the relevant evaluation system is very simple. For example, DARPA Grand Challenges were conducted in the cross-country environment in 2004、2005 and Urban Challenge in an urban environment in 2007. Whether the competing vehicles completed the tasks and the finishing time are the primary target of the evaluation system, meanwhile violation of rules and dangerous actions would be the supplementary evaluation index. In that case, the testing requirements of intelligent vehicles for these competitions are very simple, and finishing time is the only parameter to be tested. The simple evaluation system may lead to such situation that the teams tried to avoid the difficult tasks to finish the competition [9]. For example, in the 2007 Urban Challenge, many teams applied some conservative methods so that their vehicles chose stopping and waiting maneuvers to avoid high density of traffic flow instead of having an interaction with the environment through meeting, overtaking and changing lane just like human driving.

The evaluation of intelligent vehicles according to the completion of tasks or the finishing time is not sufficient, and

the whole competition progress should be monitored in real-time. The information and data of the progress of conducting different tasks and the performances of intelligent vehicles should be recorded accurately to provide support for evaluating intelligent vehicles objectively and equitably. To avoid disturbing intelligent vehicles in the competition, the external sensors without contacting with intelligent vehicles should be used to monitor the running poses of intelligent vehicles.

B. Operation principle of intelligent vehicle monitoring

The position and velocity of intelligent vehicle could be measured by using fixed sensors mounted on the side of roads in small areas, but the method dose not work effectively in large areas because numbers of sensors should be required to be mounted on the whole competition field. The real-time monitoring requirements can be achieved by using the sensors mounted on the monitoring vehicle following the competing intelligent vehicles. The operation principle of intelligent vehicle monitoring is illustrated as Fig. 1. The position coordinates and speed of the monitoring vehicle can be acquired by using GPS receiver and electronic compass mounted on the monitoring vehicle, the competing intelligent vehicle is detected and tracked through laser scanner and the relative position between the monitoring vehicle and the intelligent vehicle can also be collected, and the state of the competing intelligent vehicle can be indirectly monitored through integrating the above information. Meanwhile the position of the competing intelligent vehicle would be located in the field map based on GIS.

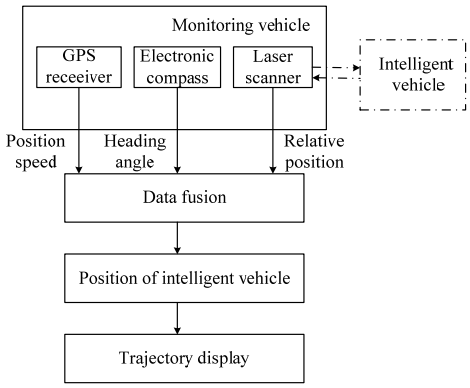

Figure 1. Operation principle of intelligent vehicle monitoring

III. VEHICLE IDENTIFICATION METHOD BASED ON LASER SCANNER

Laser scanner can measure the distances and azimuths between laser scanner and the neighbour objects, but the measuring data contain some noise signal due to measuring principle limits. In the real monitoring environment the measured data may represent the same object or the different objects. The exact real-time identification of the competing intelligent vehicle is necessary for monitoring the intelligent vehicle. The raw measuring data should be processed to draw the useful information and to eliminate the noise signal. The competing intelligent vehicle should be identified from the raw measuring data and the identification of other objects can be ignored.

A. Variable threshold clustering

The angular resolution of 2D laser scanner is 0.25°, of which the scan range is from 0° to 180°, and there are 721 points in each scan. According to the environmental features of monitoring system for intelligent vehicle, the contours of the objects in the scan region are considered as rectangle. The scan segmentation is to look for segments defined by several lines, fitting the points that represent each object. All the measure points of each scan are to be grouped into several clusters, according to the distances between consecutive measure points. Taking into account that the distance between each two consecutive points of the same object is shorter than the one of the different object, the distance thresholds are determined to process clustering. The larger the distance r_k, r_{k+1} between two consecutive points and the laser scanner, the greater the distance between consecutive points is. The greater the angle β_k, β_{k+1} between the contour line of the objects and the laser scan line, the greater the distance between the consecutive points is (illustrated as Fig. 2).

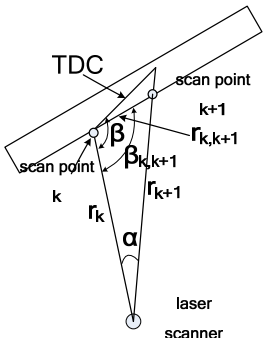

Figure 2. Schematic of clustering method

Considering that the monitoring vehicle follows the intelligent vehicles, the following distance is closely related to the speed of the intelligent vehicles. The higher the speed is, the greater the following distance is. Therefore, the value of distance threshold is not fixed, which is calculated as follow.

$$TDC = \begin{cases} 0.5; & \min(r_k, r_{k+1}) < 3 \\ \dfrac{r_{\max} \sin\phi}{\sin\beta}; & \min(r_k, r_{k+1}) > 3 \end{cases} \quad (1)$$

where r_k and r_{k+1} are the distances between scanning point and laser scanner, $r_{max}=max(r_k, r_{k+1})$, ϕ is the angular resolution of laser scanner, β is the angle for the recognition, which is associated with the distance r_k, r_{k+1} and is determined as follow.

$$\beta = \begin{cases} 170; & \max(r_k, r_{k+1}) < 15 \\ 185 - \max(r_k, r_{k+1}); & 15 < \max(r_k, r_{k+1}) < 30 \\ 150; & \max(r_k, r_{k+1}) > 30 \end{cases} \quad (2)$$

The scan data of each scan are clustered based on the principle of variable distance threshold, and the process is as follow.

a) $C_1 = \{z_1\}, Num = 1, Z = \{z_2, ..., z_n\}$

b) Select point z_i, z_{i+1} consecutively, and calculate the distance between the two points.

if $(d(z_i, z_{i+1}) > TDC)$

{ *Create a new cluster*, *Num=Num+1,* $C_{Num}=\{z_{i+1}\}$ }

else { Put z_{i+1} into C_i , $C_i=C_i \cup \{Z_{i+1}\}$ }

When the above clustering process finish, a collection of clusters are obtained, in which each cluster represents the characteristics of objects in the environment, the other points which have not been clustered will be considered as scattered points and be neglected. In addition, the clusters which contain no more than two points are not taken into account.

After the above clustering analysis, a collection C of clusters is obtained. In intelligent vehicle competition, the monitoring vehicle follows the intelligent vehicle and maintains an appropriate distance to ensure that the laser scanner can capture the target of the intelligent vehicle, no matter the intelligent vehicle driving in a straight line or curve. Therefore, the cluster data contain the cluster set of the rear or side of the monitored intelligent vehicle. The core of monitoring intelligent vehicle is to extract the cluster sets of the rear or side of the intelligent vehicle from the cluster collection C. Such cluster sets of the intelligent vehicle are represented as two classes of cluster, including straight line class and perpendicular line class.

B. Cluster extracting and merging

1) Finding breakpoints

The least square method is used to fit line segments for each cluster in the cluster set C, and a set L of line segments is defined as [10,11]:

$$L = \{l_i = [P_{ini}, P_{end}, r_{ini}, r_{end}, m, b]; 0 \le i < n\} \quad (3)$$

where, l_i is the line segment corresponding to cluster i, P_{ini} and r_{ini} are the index and scan distance of the initial point in cluster i, P_{end} and r_{end} are the index and scan distance of the end point in cluster i, m and b are the parameters of the line segment. The error may be too large to fit one cluster into a line segment, for example the cluster of the rear and side of intelligent vehicle may be perpendicular line class. The breakpoint should be searched to fit one cluster into two or more line segments. The search process is as follow.

a) Compute the perpendicular distance to the line for all points in the cluster.

$$d_{i,j} = \frac{|x_j k_i - y_j + b_i|}{\sqrt{k_i^2 + 1}} \quad (4)$$

where, x_j and y_j are the coordinates of point j in cluster i, k_i and b_i are the parameters of the line segment of cluster i.

b) If the maximum of these distances satisfies the following conditions.

$$d_{i,b} = max(d_{i,j}) > TH \quad (5)$$

where, TH is the threshold value, which is 0.5m.

Then, cluster i is split into two clusters i_1 and i_2 in the point b, and point b is respectively the initial point and end point of clusters i_1 and i_2. Afterward, clusters i_1 and i_2 are fit into line segments again.

c) Repeat steps a) and find breakpoints in cluster i_1 , i_2 and other clusters.

2) Merging cluster

Taking into account that small objects such as trees, people which may block the large objects and divide the large objects into two adjacent or nearby clusters, the separated clusters are merged by analyzing the distance and angle of line segments of adjacent or nearby clusters. The process is as follows:

a) Calculate the distance d between the end point of last cluster and the initial point of the next cluster and the angle α between the line segments of adjacent or nearby clusters;

b) if $d<d_0$ (d_0=0.5m), and $\alpha < \alpha_0$(α_0=10°), then the adjacent or nearby clusters are related and may be the same object in the environment. Such clusters are merged and a new cluster set C ' is formed.

C. Object detection and tracking

1) Object detection

The line segments of cluster C' are identified to determine which lines are the rear or side of the intelligent vehicle. Considering that the dimensions of vehicles should meet certain specifications, the maximum width of the vehicle does not exceed 2.5m, the width of passenger car is about 1.5m~1.8m, of which the length is about 3.6m~5.2m. The intelligent vehicles are usually modified from passenger car, thus the length of the rear and side of the intelligent vehicle ranges between 1.3m~1.8m and 3.3m~5.2m. The line segments in the cluster set C' of which the length exceeds the above range are eliminated. If the length of line segments is about 1.3m~1.8m, it may represent the rear of the intelligent vehicle, and if the length is about 3.3m~5.2m, it may represent the side of intelligent vehicle. If two adjacent line segments meet the above condition and the end point of one line segment is the initial point of another line segment, and the angle between two line segments is between [85°, 95°], then the two adjacent line segments may be the rear and side of intelligent vehicle.

The object detection at each scan can not assure assigning the line segments to every object after the above process since the shape of a same object may look like a small line, two perpendicular lines or even other set of geometric features. An effective way to surpass this problem is to take into account as many features as possible from previous object detections in particular dimensions and dynamics. The line segments should have the similar length for the same object at consecutive scan. If some line segment represents the rear of the vehicle, the midpoint of the line segment is considered as the midpoint of the rear of the intelligent vehicle. According to the distance and angle of the midpoint at each scan, the relative location information between intelligent vehicle and monitoring vehicle can be obtained.

2) Object tracking

The core of object tracking is to determine the relation of the objects in consecutive scans which can be processed based on the similar shape and contour characteristics of the same object. Object tracking is performed by a Kalman filter, assuming an object model with constant velocity and white

noise acceleration, considering different maximum accelerations for each object type.

IV. INDIRECT LOCALIZATION ALGORITHM BASED ON MULTI-SENSOR DATA FUSION

In order to acquire the position coordinates of intelligent vehicle, the fixed latitude and longitude coordinates system is establish firstly. As the distances between intelligent vehicle and test vehicles in actual monitoring process are relative close, the latitude and longitude coordinates are assumed to plane coordinate, and the dynamic coordinate system solid connected with the monitoring vehicle only moves in the first quadrant of latitude and longitude coordinates (illustrated as Fig. 3).

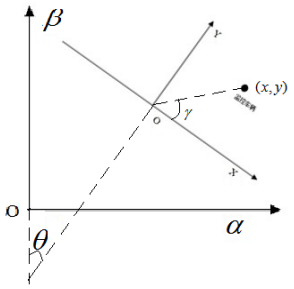

Figure 3. latitude and longitude coordinate and dynamic coordinate

The origin point of dynamic coordinates is the center of mass of monitoring vehicle, which is obtained by GPS receiver mounted on the monitoring vehicle. The angle θ is heading angle of the monitoring vehicle, the coordinates (x, y) represents the relative position between the monitoring vehicle and intelligent vehicle, and γ represents the relative angle of the intelligent vehicle and monitoring vehicle. While Δx and Δy respectively represent axial increment distance of the intelligent vehicle relative to the monitoring vehicle in α and β axial direction.

The different range of heading angle θ corresponds to different distance increment model. The distance increment model corresponding to θ ranging from 0° to 90° is as follow.

$$\text{if } 0^o \le \theta < 90^o,\ \theta' = \theta,$$

$$\begin{cases} \left.\begin{aligned} \Delta x &= -[\cos\theta'(|x| - y\tan\theta')] \\ \Delta y &= \sin\theta'(|x| - y\tan\theta') + \frac{y}{\cos\theta'} \end{aligned}\right\}, \gamma \in [0^o, 90^o - \theta') \\ \left.\begin{aligned} \Delta x &= \sin\theta'(y - |x|\cot\theta') \\ \Delta y &= \cos\theta'(y - |x|\cot\theta') + \frac{|x|}{\sin\theta'} \end{aligned}\right\}, \gamma \in [90^o - \theta', 90^o) \\ \left.\begin{aligned} \Delta x &= \sin\theta'(y - x\tan\theta') + \frac{x}{\cos\theta'} \\ \Delta y &= \cos\theta'(y - x\tan\theta') \end{aligned}\right\}, \gamma \in [90^o, 180^o - \theta') \\ \left.\begin{aligned} \Delta x &= \cos\theta'(x - y\cot\theta') + \frac{y}{\sin\theta'} \\ \Delta y &= -[\sin\theta'(x - y\cot\theta')] \end{aligned}\right\}, \gamma \in [180^o - \theta', 180^o) \end{cases} \tag{6}$$

The other distance increment models in other angle ranges have the similar forms as (6).

The transformation model between distance increment and latitude/longitude increment is computed as follow.

$$\begin{cases} \Delta\alpha = F(\Delta x) = k \bullet \frac{1}{r_{\text{latitude}}} \bullet \Delta x \\ \Delta\beta = F(\Delta y) = k \bullet \frac{1}{r_{\text{longitude}}} \bullet \Delta y \end{cases} \tag{7}$$

where, $\Delta\alpha$ is longitude increment, $\Delta\beta$ is latitude increment, k is transform coefficient, which is 57.29578, $r_{latitude}$ is latitude circle radius, $r_{longitude}$ is longitude circle radius.

According to (6), (7) and integrating other data such as the latitude and longitude coordinate of the monitoring vehicle, the position coordinate of the monitored intelligent vehicle can be obtained.

V. EXPERIMENTS AND RESULT ANALYSIS

The monitoring experiments of vehicle were conducted in the straight road and simple environment. The leading vehicle which GPS receiver was mounted on to acquire the position and speed of the vehicle was driven by a tester, and the monitoring vehicle which laser scanner, GPS receiver and electronic compass were mounted on followed the leading vehicle. The data acquired by laser scanner was processed to determine the relative position between the leading vehicle and monitoring vehicle, Fig. 4 shows the processing result of scan data from laser scanner, in which the green lines represent the back of vehicle. Fig. 4 shows that identification algorithm for laser scanner was effective to cluster the scan data, and the vehicle object were detected and tracked exactly in the experiments. Fig. 5 shows the results of vehicle localization which are gained from the GPS receiver on the leading vehicle and through integrating the multi sensors on the monitoring vehicle. In Fig. 5, the red points represent the acquired data of the leading vehicle position coordinates directly from the GPS receiver, the black points represent the computing data from the monitoring vehicle, and the computing data keep in with the acquired data, thus indirect localization algorithm of intelligent vehicle integrating multi sensors data can be effective to obtain the driving position information of the monitored intelligent vehicles accurately.

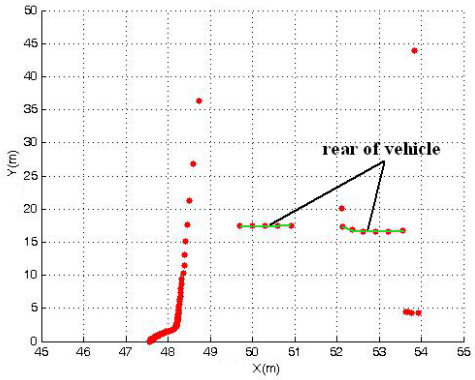

Figure 4. Result of laser scanner data processing

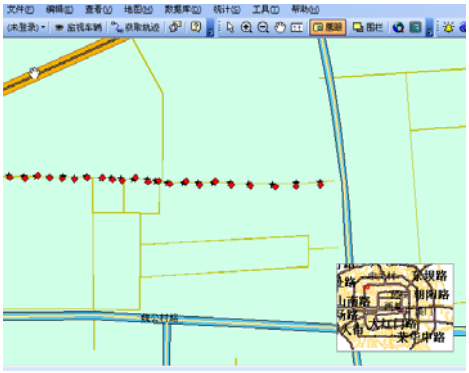

Figure 5. Result of vehicle localization

VI. CONCLUSION

In this paper the monitoring technique of intelligent vehicles was studied based on the analyses of monitoring requirements for intelligent vehicle competitions. The algorithm of object detection and tracking using a laser scanner and indirect localization algorithm of intelligent vehicle through integrating laser scanner, GPS receiver, and electronic compass multi-sensor data fusion were developed, and the algorithms have been verified in field experiments. The tests were only conducted in straight roads and simple environment, and further research will be conducted to test detecting and tracking vehicles in curve roads and complex environment.

ACKNOWLEDGMENT

This work was partially supported by National Natural Science Funds Commission of China (No. 90920304), “Design of integrated detection environment and research on detection and evaluation infrastructure of an unmanned vehicle intelligent action”.

REFERENCES

[1] B. Ulmer, ”‘VITA - An Autonomous Road Vehicle(ARV) for Collision Avoidance in Traffic”’, in IEEE Proceedings of the Intelligent Vehicle Symposium, Detroit, MI, pp. 36-41, 1992.

[2] C. Thorpe, M. Hebert, T. Kanade, and S. Shafer, ”‘Vision and Navigation for the Carnegie-Mellon Navlab”’, IEEE Transactions on Pattern Analysis and Machine Intelligence, Vol. 10, No. 3, pp. 362-373, 1988.

[3] A. Hattori, A. Hosaka, and M. Taniguchi, ”‘Driving Control System for an Autonomous Vehicle Using Multiple Observed Point Information”’, in IEEE Proceedings of the Intelligent Vehicle Symposium, Detroit, MI, pp. 207-212, 1992.

[4] http://www.darpa.mil/grandchallenge04/

[5] http://www.darpa.mil/grandchallenge05/

[6] http://www.darpa.mil/grandchallenge/index.asp

[7] http://www.elrob.org/objectives.html

[8] http://ccvai.xjtu.edu.cn/

[9] Junqing Wei; Dolan, J.M. A robust autonomous freeway driving algorithm. 2009 IEEE Intelligent Vehicles Symposium , Xi’an, Shaanxi, China , June,2009.

[10] Mendes, A., U. Nunes. Situation-based multi-target detection and tracking with laserscanner in outdoor semi-structured environment. Intelligent Robots and Systems, 2004.(IROS 2004). Proceedings. 2004 IEEE/RSJ International Conference on. 1.

[11] Santos, S., J. Faria, F. Soares. Tracking of multi-obstacles with laser range data for autonomous vehicles. Proceedings of ROBOTICA 3 Festival Nacional de Robotica, Lisboa. 2003.

2011 International Conference on Mechanical, Industrial, and Manufacturing Engineering
Lecture Notes in Information Technology Vols. 1-2

RCPL: A new task scheduling algorithm by Reduction of Critical Path Length in Grid Computing

Elnaz Rashid Hossein Zadeh
Department of Computer Engineering,
Islamic Azad University - Tabriz Branch
Tabriz, Iran
El.rashidi@Yahoo.com

***Abstract*- In this paper, we propose a new algorithm for restructuring task graphs for suitable scheduling in grid computing. This algorithm obtains the critical path length in task graph and then start to reduce the length of this path. For optimize the length of critical path To do this. this algorithm reduces communication costs by merging tasks from task graph who are pertained to this path and their communication costs exceed their execution time. Task duplication techniques are applied when the task merging operation on critical path change at least the length of one of other paths and its length is greater than the updated critical path length .Afterward, these operations apply to the new critical path, if it exists .this algorithm changing critical path to optimized path example is shown to improve performance.**

Keywords-Task graph- critical path- merging- duplication-scheduling

I. INTRODUCTION

Grid is a large geographical distribution resources system that is collection of heterogeneous resources. Grid scheduling is explained as the process of making scheduling decisions involving resources over multiple managerial domains .The purpose of this paper is task graphs restructuring such that when applying any task scheduling algorithm to the restructured task graph, the minimum possible completion is achieved .Task merging and clustering are techniques to restructure task graphs for benefit scheduling [1-5].

When merging a task node in its parent nodes, other children of parent in the task graph, could be delayed. To find a solution the difficulty, it is proposed to duplicate the parent nodes before the merge, under the condition that their execution times is less than the maximum time needed to communicate with their successors [2]. On the other hand, above condition does not always necessitate the merge. In the approach presented in [5], a node is merged in a subset of its parents on the condition that the merge operation reduces its earliest time to start. If the merge retards the execution of the other children of the parent node, the parent node is duplicated.

In this paper we propose the approach that applies the merge and duplication techniques by considering length of critical path and other paths from start task to end task. In this approach, task duplication techniques are applied when sum of delays caused by task merging cause the length of other path be longer than critical path length. If after the duplication, the number of independent tasks gets above the number of available processors, the duplication is considered as a contrary factor.

The rest of this paper organized as follows: In Section 2, our proposed algorithm is presented. In Section 2.1, a relation for computing the earliest start time of tasks within a task graph is presented. In Section 2.2 a relation to compute the benefits of merging a task node with any subset of its parents is offered. Section 3 explores the evaluation results. Final section contains the conclusion and future works.

II. OUR ALGORITHM

In this section our proposed algorithm: a new task scheduling algorithm by reduction of critical path length in grid computing (RCPL) is presented. When combining a node v which is on the critical path with one of its parents, p, the start time of the siblings of v that is in other path may be increased. Sometimes it is may be that sum of these delays cause increasing the length of it path so that be greater than updated critical path length. To resolve the difficulty, the parent node, p, could be duplicated before the merge. However, if there are not enough processors to execute the duplicated tasks in parallel, the merge may not be beneficial. Thus, in the task merging quality function, Q, is shown in section 2.2, the number of available processors, the total execution time of the tasks to be duplicated and the amount of reduction in earliest start time are considered as main factors in deciding whether to merge a task v with a subset, P_k, of its parents. Our new task merging algorithm is presented in Fig. 1.

A. The RCPL Algorithm

Our purposed algorithm, RCPL, is shown in Fig. 1. The algorithm tries to increase parallelism in the execution of a definite task graph by reducing the earliest start time of tasks in the task graph. As shown in relation (1) [5], to compute the earliest start time, EST_v, of a task, v, the earliest start time and the execution time of its parent nodes and the time that takes to receive the results from its parent, $\tau(pi)$, the size of the data to be received by the task nodes, $c(pi, v)$, the latency, L, and the bandwidth, B, of the communication lines are needed.

$$EST_v = \begin{cases} 0 & Parent(v) = \emptyset \\ MAX_{p_i \in Parents_{(v)}} \left(EST(p_i) + \tau(p_i) + L + \frac{c(p_i,v)}{B} \right) & Parent(v) \neq \emptyset \end{cases} \quad (1)$$

A node v is merged in the subset of its parents, which reduce its earliest start time generally , $EST_{v,}$. To obtain this, the time, $R_{pi,v}$, at which the outputs of each parent node, p_i, can be aggregated by the child, v, is computed .As shown in relation (2) [5]:

$$R_{p_i,v} = EST(p_i) + \tau(p_i) + L + \frac{c(p_i, v)}{B} \quad (2)$$

Since $R_{pi,v}$ are computed, the parents are sorted in decreasing order of $R_{pi,v}$. Starting of the node with the highest value of $R_{pi,v}$, the benefit of merging v in of the parents, p_i, on the earliest start time of v is calculated. The node v is then merged with the subset of its parents, that reduce its earliest start time, then their number does not exceed complete of available pro

```
Step1
  1.  Algorithm RCPL
  2.  Input: a task graph G (V, E, τ, c) where:
  3.        V: Set of tasks, E: set of task inter-connection lines
  4.        τ: A function to compute the execution cost of each task
  5.        c: A function to compute the communication costs
  6.  Output: G'(V', E', τ', c') = the modified task graph
  7.  Method:
  8.    For each v in V do apply relation (1) to compute EST (v); End For;
Step2
  9.    For each p_i in parents (ET) do // ET: End Task.
  10.     Apply relation (2), below, to compute the earliest time, R_pi,ET,
  11.       to collect data from parent, p_i, on ET;
  12.     Sort the PLs on the value of R_pi,ET, descendingly,
  13.       Giving the sequence PL = (PL_1, PL_2, ..., PL_k);
  14.   End For; //PL: Path Length from Start Task to End Task.
  15.   i := 1;
Step3
  16. L1: For each v (start from ST to ET) in V which is pertain to PL_i do // ST: Start Task.
  17.     For each p_i in parents (v) do
  18.       Apply relation (2), below, to compute the earliest time, R_pi,v, to collect data
  19.         From parent, p_i, on v;
  20.       Sort the parents, p_i, on the value of R_pi,v, descendingly,
  21.         Giving the sequence P = (P_1, P_2, ..., P_k);
  22.   End For;
  23.   Apply relation (3) to compute the benefit Q_v,k, of merging v with its parents
  24.                 p_1 to p_k in P for 1 ≤ k ≤ n;
  25.   If there are no Q_v,k > 0 then it is not possible to merge v with any subset of its
  26.   go to L1; End if;
  27.   Find the subsequence P_k = {(p_1, p_2, ..., p_k) in P, 1 ≤ k ≤ n} such that Q_v,k is maximum;
  28. End For;
Step4
  29. Let Ψ_v,Pk be the set of siblings of v whose earliest start time increases
  30. Let D_v,Pk be the set of parent nodes p_i in P_k with at least one child in Ψ_v,Pk
  31. For j from 1 to n do
  32.   If PL_j is increased to its previous value and is greater than PL_i then
  33.     For each node p in D_v,pk which pertain to PL_j do
  34.       Let p' be a copy of p
  35.         Remove any edges from p to nodes in Ψ_v,Pk ;
  36.         Remove any edges from p' to nodes that not in Ψ_v,Pk ;
  37.       End For;
  38.   End If;
  39. End For;
Step5
  40.     Sort the PLs on the value of R_pi,ET, descendingly,
  41.       Giving the sequence PL = (PL_j, PL_j+1, ..., PL_j+n);
  42.   If j is not equal i then i is equal to the j; go to L1; End If;
  43. End;
```

Fig. 1. The RCPL Algorithm

Step1 presents the input and output parameters. First, this algorithm computes the earliest start time of each node v in V, EST_v, .The result of step2 is sorting the paths discerningly on the value of their lengths and discovering the critical path. The critical path is a path that value of its length from start task to end task is more than length of other paths which exist between start task and end task. In step3, proposed algorithm starts the merging of each node v in V which is pertain to critical path with its parents in a top to down manner, from start task to end task. Step4 duplicates the nodes of critical path that merging of them with their child caused that length of other

path is increased to its previous value and is greater than critical path. Step5 discovers the new critical path if exists and repeat these operations for it.

B. Task Merging Benefits

We used checking utility of merging node from[5] that used follow relating:

(3)

$$Q = \alpha \times \Delta T$$

In the above relation ΔT demonstrated the amount of reduction in the earliest start time of the node v, ΔE is the total of the execution time of the duplicated parents of v and α is a parameter. The amount of the parameter α depends on the number of available processors and the maximum number of tasks to be executed in parallel.

III. EVALUATION OF PROPOSED ALGORITHM

In this section, because RTM algorithm[5] is close to our work ,we use it for evaluating .we evaluate the RCPL Algorithm in comparison to RTM algorithm. To this evaluation, we assume that task graph is same Fig.2 with RCPL execution on this task graph, the task graph shown in Fig.2 (e) is reached. The operations are described below.

In Fig. 2, at first the critical path (the path from start task to end task) is distinguished as shown in Fig. 2 (a). The path is selected as a critical path which $R_{pi,ET}$ of the parent of end task pertain to this path is maximum. Then this algorithm begins from start task with applying the relation (3) to merge node v which is pertaining to critical path with set of its parents.

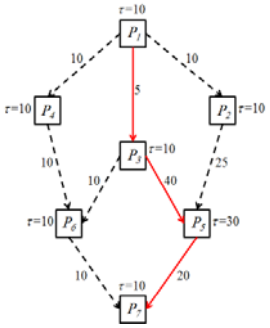

(a) critical path discovering

PL_1:P_1,P_4, P_6 PL_1=60
PL_2:P_1,P_3,P_6 PL_2=55
PL_3:P_1,P_3,P_5 PL_3=115
PL_4:P_1,P_2,P_5 PL_4=105
CP=PL_3=115

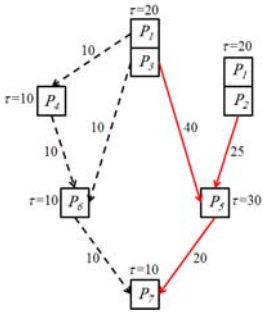

(b) merging P_3 and P_2 with P_1

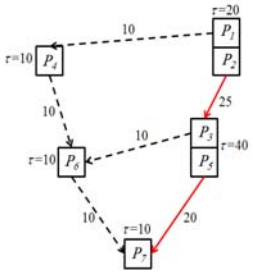

(c) merging P_5 with P_3

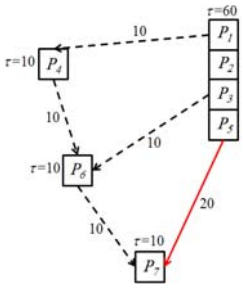

(d) merging P_3 with P_2

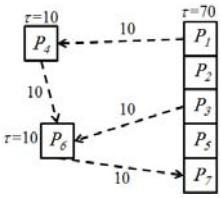

(e) merging P_7 with P_5
CP_{after}: P_1,P_2, P_3 ,P_5
CP_{after} =60

Fig. 2. Decreasing the Critical Path Length by RCPL Algorithm

But the RTM execution on this task graph is resulted the more duplication of task. For example with RTM execution on task graph Fig. 2 (b), the task graph shown in Fig. 3 is obtained.

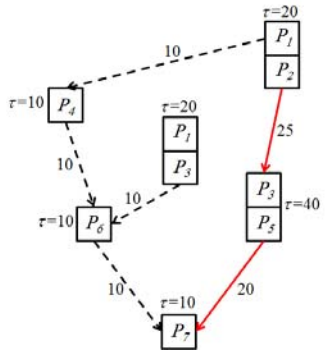

Fig 3. Execution of RTM algorithm on task graph Fig. 2 (b)

As shown in Fig. 3, RTM algorithm decides to merge the node P_5 with its parent P_3 and also decides to duplicate P_3 to avoid of increasing the earliest start time of node P_6, EST_{P6}. While the duplication of node P_3 is inappropriate from the viewpoint of RCPL, because this duplication has no efficacy in decreasing of critical path length. Furthermore, the RTM spends a lot of time for merging and duplication of the task which might not be effect in reducing the critical path length.

IV. CONCLUSION AND FUTURE WORK

This work proposes a pre-scheduling algorithm that can restructure the task graph before applying any scheduling algorithm to it. The tasks could be merged with their parents by applying the RCPL algorithm in order to take advantage of parallelism inherent in the execution of tasks in a task graph. The algorithm attempts to exploit the inherent parallelism by minimizing the earliest start time of each task which is pertained to critical path within the task graph. Task duplication techniques are applied when the task merging operation on critical path change at least the length of one of other paths and its length is greater than the updated critical path length. Our research group is going to uses the standard task graphs and famous scheduling algorithms for simulation and evaluation of RCPL and other pre-scheduling algorithms in future work.

References

[1]. Aronsson, P., Fritzson, P, "A Task Merging Technique for Parallelization of Modelica Models" In: 4th International Modelica Conference, Hamburg (2005)

[2]. Aronsson, P., Fritzson, P, "Task Merging and Replication using Graph Rewriting ," In: 2nd International Modelica Conference, Germany 2003

[3]. Ayed, M., Gaudiot, J.: An efficient heuristic for code partitioning. Parallel Computing 26(4), 399–426 (2000)

[4]. Kwok, Y., Ahmad, I , "Static scheduling algorithms for allocating directed task graphs to multiprocessors, " ACM Computing Surveys (CSUR) 31(4), 406–471 1999

[5]. Parsa, S., Soltani, N., Shariati, S. , " Task Merging for Better Scheduling," Lecture Notes in Computer Science, Springer, 311-316 2010

2011 International Conference on Mechanical, Industrial, and Manufacturing Engineering
Lecture Notes in Information Technology Vols. 1-2

Research on the Testing about Anchoring Forces of Screw-Thread Steel Bolt Based on Variable Diameters Drills

Liang Cui, Nianjie Ma and Chong Li
Faculty of Resources and Safety Engineering,
China University of Mining and Technology (Beijing),
D-11, Xueyuan Road, Haidian District, Beijing, China
lcck07@126.com

Chao Zhang
Faculty of Geoscience and Surveying Engineering,
China University of Mining and Technology (Beijing)
D-11, Xueyuan Road, Haidian District, Beijing, China
zcgeology@126.com

***Abstract* - In order to make a accurate evaluation about the anchoring forces of different anchorage lengths of the sinistrogyration screw-thread steel bolts, this paper designed a approach of variable diameters drilling to the same drill to control the anchoring length accurately. What we did was the destructive drawing experiments about twelve bolts which were different anchorage lengths. With the value of different anchoring types and anchorage lengths bolts anchoring, we can make supports about the collection of bolt and anchoring types for different mines.**

***Index Terms* - variable diameter drills, screw-thread steel bolt, anchoring forces, anchorage lengths**

I. INTRODUCTION

Because of the uncontrolled length of anchorage lengths, so it is popular that the anchoring forces can not correspond to the theoretical calculation anchorage lengths when we test the anchoring forces of different anchoring types. Because of the point, the test designed destructive drawing experiments of variable diameter drills to the drilling which could control the anchorage lengths. So we can make supports about the collection of bolt and anchoring types for different mines.

II. DESIGN OF EXPERIMENT

In order to satisfy the roadway support requirement, which need the anchoring forces of screw-thread steel bolt must be five tons above. The experiment collected three types bolts to the destructive drawing. The experiment held in Shangwan coal mine, and the detailed design as followed:

A. Collecting of Bolts and Anchor Agenttypes

Ø18×1800mm deformed steel bars, 6, anchor agenttypes : CK2335

B. The Drill Types:

1) Group 1: hole depth 1800mm, divided to two sections, forepart1400mm, diameter32mm; back end 400mm, diameter 27mm,four drill holes. Rock bolt installed as formal after the accomplishment of the drill holes, the exposure length is 5cm approximately. The schematic diagram is as followed in figure 1;

2) Group 2: hole depth 1800mm, divided to two sections, forepart 1300mm, diameter 32mm; back end 500mm, diameter 27mm, four drill holes. Rock bolt installed as formal after the accomplishment of the drill holes, the exposure length is 5cm approximately. The schematic diagram is as followed in figure 1;

3) Group 3: hole depth 1800mm, divided to two sections, forepart 1200mm, diameter 32mm; back end 600mm, diameter 27mm, four drill holes. Rock bolt installed as formal after the accomplishment of the drill holes, the exposure length is 5cm approximately. The schematic diagram is as followed in figure 1;

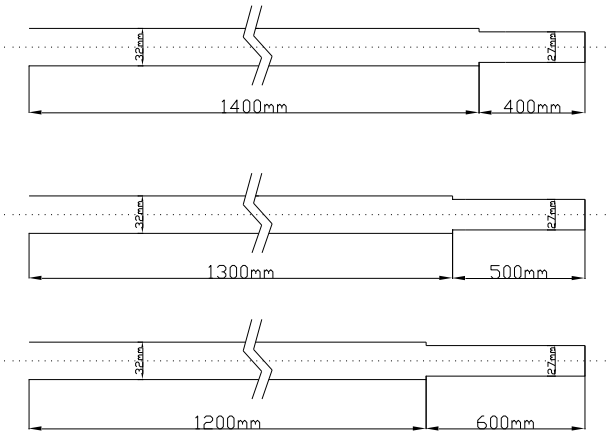

Fig. 1 The designed plan of variable diameters drills

C. Design of Anchorage Length and Theoretical Calculation of Anchorage agent:

Based on the cubature formula:

$$\pi R_K{}^2 L_K = \pi R_Y{}^2 L_Y. \quad (1)$$

Type:

R_K: the radius of anchoring section/mm

L_K: the length of anchoring section/mm

R_Y: the radius of anchor agent/mm

L_Y: the designed anchor agent/mm

the designed anchor agent:

$$L_K = \frac{R_Y{}^2 L_Y}{R_K{}^2}. \quad (2)$$

The designed anchor agent are as followed due to the calculations:

TABLE I

DISING OF LENGTH OF ANCHORING SECTION AND AGENT

Types \ Group No.	Groud 1	Groud 2	Groud 3
Length of anchoring section /mm	400	500	600
Length of anchor agent/mm	774	968	1161

D. The Research of Roof Strata According to the Experiment Area

The experiment area lays on 66、67、68 transport roadway join-roadway position of Wanli mine aero in inner Mongolia, assigning as followed in figure 2.

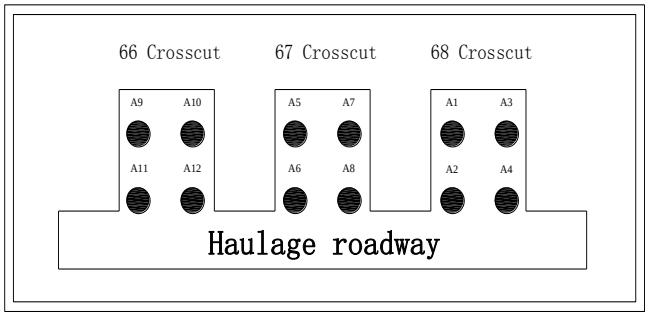

Fig. 2 The experiment place diagram of anchoring forces testing

The roof strata of anchoring section are researched by Roof Detecting Instrument, most of which is fine sandstone. The strata are stable. The histogram and lithology result diagram are as followed in figure 3.

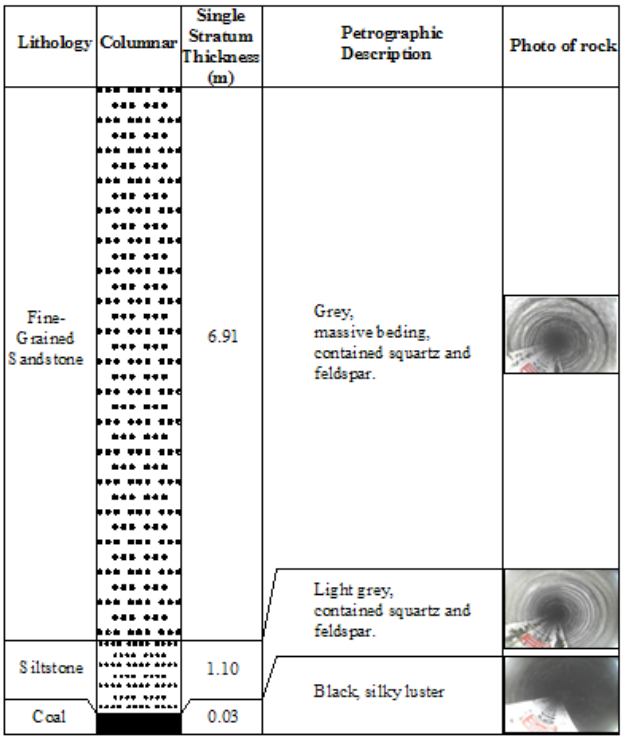

Fig. 3 Geologic column in experiment area

E. Experimental Apparatus

The range of the drawing machine is 2000Mpa. When doing the rock bolt experiment, putting the hydraulic jack between layer and nut, screw down the nuts and throw some prestressing force. After that give pressure using the hydraulic pump, and then record the values about the hydraulic pressure gauge and displacement. Pull the experiment bolts out in order to be sure the accuracy of the experiment.

Fig. 4 The drawing bolt machine

F. Test Result

Through the twelve bolts of anchoring force testing, the results are as followed in table II:

TABLE II

ANCHORING FORCE TESTING RESULT DIAGRAM

No.	Anchoring Length /mm	Anchor Agent Diameter / mm	Drawing Force/T	Length Tray to the Roof / cm
1	400	774	11.35	5
2	400	774	11.25	5

3	400	774	10.55	5
4	400	774	11.15	5
5	500	968	12.45	5
6	500	968	12.68	5
7	500	968	12.55	5
8	500	968	12.38	5
9	600	1161	12.95	5
10	600	1161	13.55	5
11	600	1161	12.85	5
12	600	1161	13.75	5

The experiment bolts are all sinistrogyration screw-thread steel bolt, anchor agent is CK2335, resin drug. The first experiment anchorage length is 400mm，the range of the anchoring force is 10.55～11.35T; The second experiment anchorage length is 500mm，the range of the anchoring force is 12.38～12.68T; The third experiment anchorage length is 500mm，the range of the anchoring force is 12.38～12.68T.

III. CONCLUSION

1、Have designed the variable diameters drills, the forepart radius of the drill hole is Ø32, the segmenta posterius radius of the drill hole is Ø27,so we can control the anchoring length more accurately.

2、The anchoring force increases as the anchoring section adding, but which is controlled by many points, the relationship of which is nonlinearity.

3、In the process of designed anchoring length, it can satisfy the requirement of roadway support if the anchoring force are above 10.55T.

REFERENCES

[1] Nianjie Ma, Lianjun Wu and Hongyan Liu, "The Key Technology and Development Tendency of Roadway Sopport[J]," Coal Science and Technology,2006 (5), pp. 77-79

[2] Nianjie Ma and Chaojiong Hou, "The Application and Theory of Underground Pressure in Preparatory Workings," China Coal Industry Publishing House, 1995.

[3] Guanyi Wei and Changjun Zhang, "Petrologyconcise tutorial," Geology Press, 2006, pp. 136-137.

[4]

[5] Zaixing Jiang, "Sedimentology," Petroleum Industry Press, 2003, pp. 375-379.

[6] Meifeng Jiang, Manchao He and Dongyan Liu, "Rock mechanics and engineering," Science Press, 2002, pp. 14.

2011 International Conference on Mechanical, Industrial, and Manufacturing Engineering
Lecture Notes in Information Technology Vols. 1-2

Design of Step Motor and RS-485 based Yarn Feeding Control System for Carpet Tufting Machine*

Chen Guangfeng, Sun Haochun, Wang Weibin, Li Qingqing
College of Mechanical Engineering,
Donghua University
Shanghai 201620, China
chengf@dhu.edu.cn, sunvhao@163.com, weibinqdu@126.com, ruguoabc@163.com

***Abstract* - This paper design a RS-485 based yarn feeding control system for tufting carpet machine. To provide more flexibility, the yarn feeding control systems adopt step motors instead of clutches to drive the rollers to delivery yarns. Base on requirement of control of yarn feeding of tufting carpet production, design the hardware of control system. The control systems adopt the Industrial computer(IPC) as the master platform and user interface. The lower computer consists of yarn feed controller, synchronization controller and yarn guiding controller. Design the communication protocol and construct the RS-485 net to communicate between modules. According to the requirements of process control, devise the control logic for IPC and lower controller in detail.**

Index Terms - yarn feeding, RS-485, step motor, carpet tufting machine, pattern

I. INTRODUCTION

Carpet is manufactured in various ways, and at present more than 90 percent of the produced carpet is tufted carpet [1-4]. Most domestic manufacturers tufted carpet manufacturing machinery in the past to rely on imported technology and equipment. In recent years, domestic carpet tufting machine jacquard technology research and development yielded some results[5-13], reference [10] adopt fuzzy control strategy to drive servo motor to achieve the constant tension of backing fabric, the literature[11,12] adopt industrial computer(IPC) to control servo motors through the dynamic control of yarn feeding to improve the quality of loop pile carpet surface appearance.

This study is conducted to control the corresponding step motor to replace the clutch groups to drive the roller delivery the yarn. Cooperate with tufting process to form different height loop pile, eventually form various pattern on carpet surface.

II. YARN FEEDING MECHANISM AND PRINCIPLE

Fig.1 is a schematic diagram illustrating the typical yarn feed mechanism of carpet tufting machine assembled with jacquard mechanism of clutches. A tuft cycle start from top dead center (TDC), the needle threaded with yarn is pushed down through a backing fabric. As the needle approaches bottom dead center (BDC), a looper advances and passes between the needle and the yarn. The needle retracts, to leave a loop of yarn around the looper. This loop of yarn is released intact to produce a loop-pile fabric. In the carpet tufting art to utilize a yarn feed roller attachment for producing variations in pile height of loop pile products. The yarn feed rollers act either to feed the full amount of yarn to adequately accommodate the yarn requirements of the particular needle or to feed less than that adequate amount of yarn so as to back draw yarn from the previous stitch. During this process different pile heights can be formed on carpet surface depend on the condition of yarn feeding length and tension control. Despite the tension affection, the yarn delivery in each tufting cycle is the key factor to affect the pile height of loop pile. So the process staff could control the each pile height and produce various patterns on the carpet.

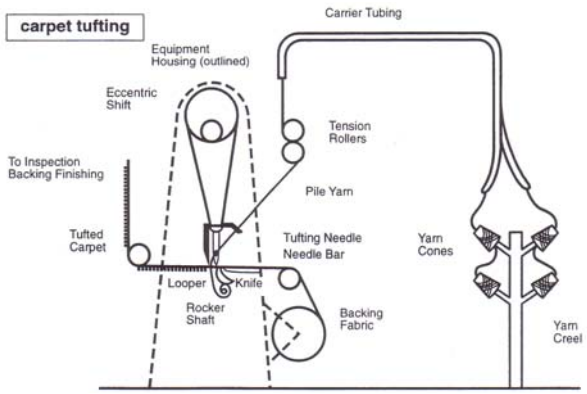

Fig.1 Yarn feed mechanism of carpet tufting machine

III. SYSTEM REQUIREMENT ANALYZE

In the developed tufting machine, the gauge is 1/10 inch, and the width is 4m. The yarn-delivery mechanism is composed of stepping motor and tension roller, the stepping motor direct drive a group of tension rollers through synchronous belt. There are 120 groups of tension rollers altogether. That mean the pattern cycle width of tufted carpet will be 120 needles.

The system's main function is translate digital design information from PC to lower controller, and control the step

* This work is supported by Shanghai Natural Science Foundation Grant #10ZR1401500 to Chen Guangfeng and Fundamental Research Funds for the Central Universities Grant #9D10307 to Chen Guangfeng.

motor rotation to delivery desired length of yarn for each tufting stitch. This requires controlling the stepping motor rotate certain angle in a tufting cycle.

Main shaft rotate 360 degrees is a loop pile forming cycle. Due to spindle speed has obvious deceleration or acceleration process in start-stop stage, the others states running speed also have certain degree of fluctuation. So we cannot suppose the man shaft has a constant speed. As Fig.1 shown, suppose between $[t_i, t_{i+1}]$, the main shaft rotate exactly 360 degrees, from (1) we could get the rotated angle θ. If we drive the step motor to rotate at angle speed $k\omega$, then we could get the rotation angle of stepping motor during $[t_i, t_{i+1}]$ is $k \times \theta$.

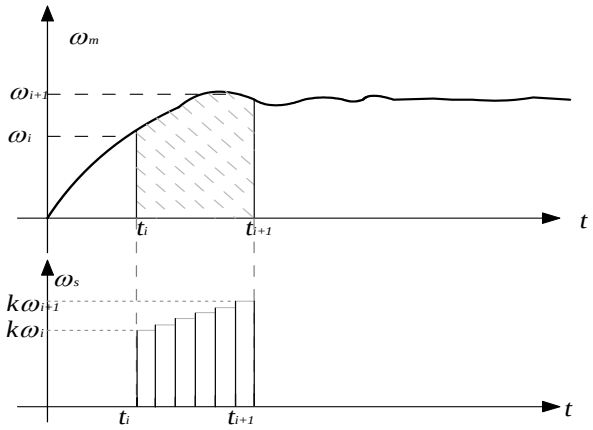

Fig.2 Yarn feed mechanism of carpet tufting machine

$$\theta = \int_{t_i}^{t_{i+1}} \omega \, dt \tag{1}$$

$$\beta = \int_{t_i}^{t_{i+1}} k\omega \, dt = k\int_{t_i}^{t_{i+1}} \omega \, dt = k \times \theta \tag{2}$$

Ignore the yarn skid case, suppose the motor rotate one turn will feed L_d yarn. Then we could get (3).

$$L = \int_{t_i}^{t_{i+1}} k\omega \frac{L_d}{2\pi} dt = k\int_{t_i}^{t_{i+1}} \omega \frac{L_d}{2\pi} dt = k \times \theta \times \frac{L_d}{2\pi} \tag{3}$$

Since during $[t_i, t_{i+1}]$ the main shaft rotate exactly one turn $\theta = 2\pi$, then get (4).

$$L = k \times L_d \tag{4}$$

From (4), the length of yarn feed is relying on the parameter k, we name it speed ratio. This is the basic idea of yarn feed control system for carpet tufting machine. Base on this principle we design the control system structure.

IV. System Structure Design

The system consists of industrial computer(IPC), RS232-485 converter, yarn feed controller, yarn guide controller, synchronization controller, encoder, proximity switch and stepper motors. The system structure is as Fig.3 shown. The industrial computer acts as the master platform together with user interface. The IPC communicate with sub-controller through RS232-485 converter. After the IPC download the control data to sub-controller, the synchrony controller at regular time gather the main shaft position and speed information, and dispatch them to other substation in RS485 network. Other controllers received the signal and drive the step motor to change state and run at a new calculated speed.

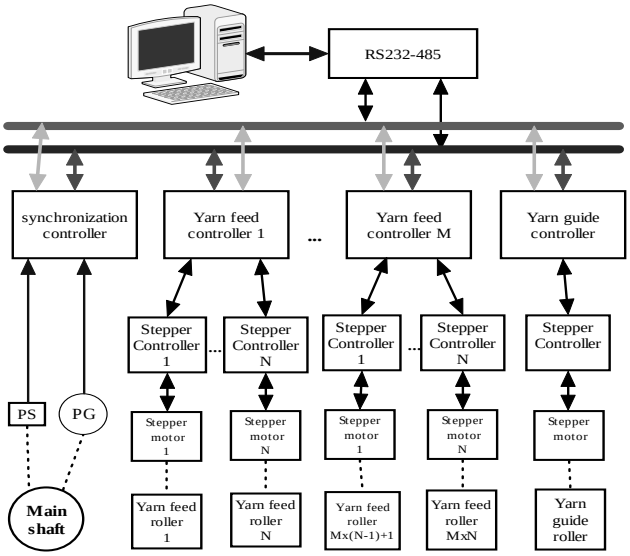

Fig.3 Yarn delivery control system structure

V. Control Logic Design

According to the provided hardware and jacquard process of carpet tufting process, devise the flowchart of the control system. The flowchart is shown as Fig 4.

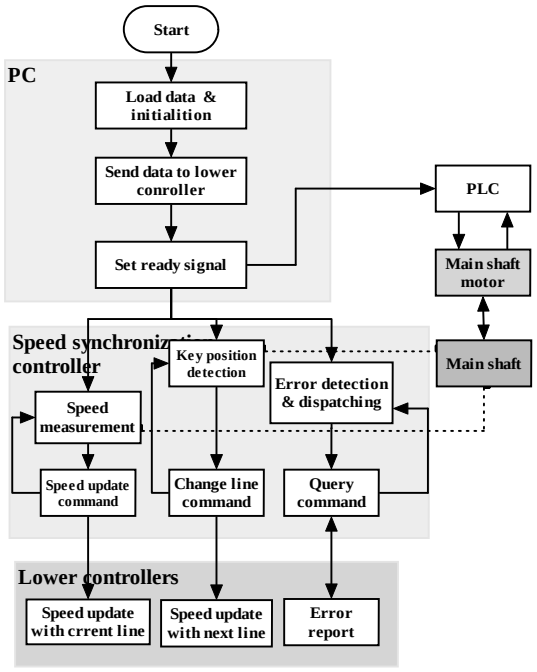

Fig.4 Control logic of system

The system start from loading and setting parameter, and then download the control data to lower controllers, and set the ready signal to enable the lower controller to start speed

tracing. Once synchronization controller received ready signal, the controller automatic change itself into 485 network hosts, begin measuring the main shaft rotation speed and key position, and according to the measured speeds and key position send corresponding command to other controller. While the 485 bus is idle, the controller sends error check instructions. Besides IPC, the other controllers node receiving signal, according to the instructions execution corresponding actions.

VI. RS-485 Communication Protocol Design

The RS485 communication process as follows: when a host site communicate with a slave site, first host sends the address frames including the slave address on the bus, at that moment, lower computer are in receiving address frame status, and receive only address state frame. If the slave with the same address were online, this slave will change its state to receive data frames, and send its address as answering to host site. While host received the response codes, the handshake establish, and host and slave can communicate through 485. Shaking hands process, host sent complete address frame, should be in a certain time keep receiving state (this time should be more than address frame from the host sent to add response from machine code from machine to host the time), namely host inside this paragraph of time cannot send data to avoid bus conflict.

In the system, the RS-485 communication using standard frame, such as shown in table 1, one of the start bit, 8 bits of data bits, 1 bit stop bits.

TABLE I
DATA FRAME FORMAT

Start bit	Data								Stop bit
0	0	0	1	0	1	0	0	0	1

During the control process, there are some data need translate on the bus, they are pattern and process information, main shaft speed information, change line command, update speed command, stop command, and status check command etc.

The pattern and process information is defined as Table II shown.

TABLE II
PATTERN DATA FORMAT DEFINITIONS FOR DOWNLOAD

Data	Data length	Comment
Pattern Lines	16bits	Pattern
Pile height levels	8 bits	Pattern
Ratio 0	16 bits	Pattern
…		Pattern
Ratio n	16 bits	Pattern
Pattern data	8 bits	Pattern
…		Pattern
Pattern data	8 bits	Pattern
CRC data	8 bits	Pattern

Other command and data are defined as Table III shown.

TABLE III
OTHER COMMAND DEFINITIONS

Data	Data length	Comment	
Ready signal	8 bits	Command	
Change line	8 bits	Command	‘c’
Update speed	8 bits	Command	‘u’
Speed data	16 bits	Data	
Stop	8 bits	Command	‘s’
Status check	8 bits	Command	‘e’
sampling interval	8 bits	Data	

VII. Hardware Design for Lower Controller

The lower controllers consist of yarn feed controller, yarn guider controller and speed synchronization controller.

Yarn feed controllers hardware adopts a master MCU plus four slave MCU. The hardware structure is shown as Fig.5. The yarn feed controller adopt the I2C bus to communication and transfer data between master and slave MCU. Master MCU is responsible for communication with PC and synchronous through RS485, and dispatch the data and command to slave MCU. The slave MCU is responsible for receive the data and command and generate the PWM signal to drive certain stepper motor. The PWM signal is generate with the 16 bit timer, which could provide the 65536 various PWM period. Different PWM period is corresponding to different speed of stepper motor. The yarn guider controller takes the same structure as yarn feeding controller.

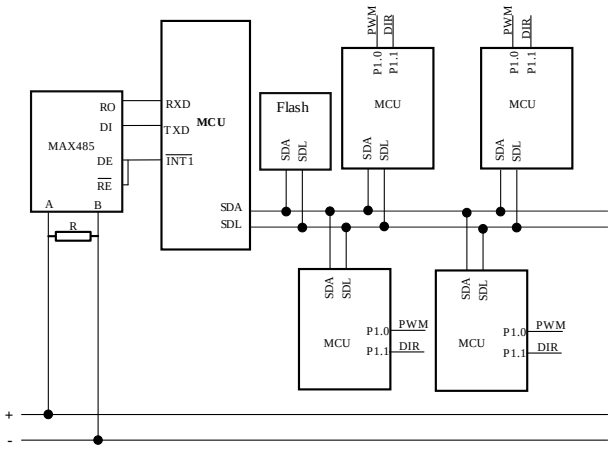

Fig.5 Hardware scheme of yarn feed controller

The main function of speed synchronization controller is to detect the main shaft speed and key position, and send change line command and speed to other controllers. Another function is regular inquires the state of other controller and feed back error status to IPC. The synchronization controller adopt a MCU to connect and count the encoder pulse at predefined time span, and get the speed information of main shaft. And the other INT0 pin connects with to the spindle of proximity switch. When the main shaft rotate to its scheduled position, the proximity switch trigger a pulse and the pulse falling edge trigger an interrupt, and the MCU send the change line command through RS485.

VIII. Lower Computer Control Logic Design

The yarn feed controller MCU received the control data from IPC, and then drive the stepper motors to trace the main shaft at different the speed ratio as design pattern required. The detail flowchart is as Fig.7 shown.

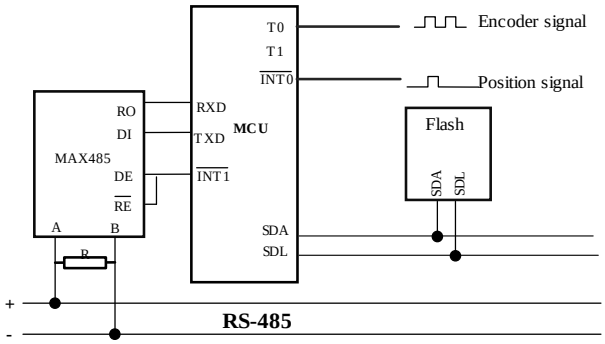

Fig.6 Hardware of synchronization controller

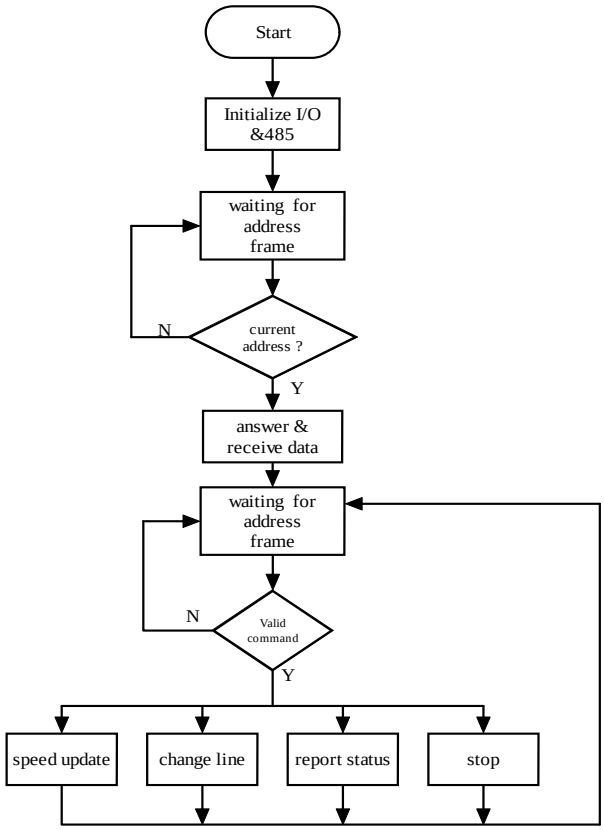

Fig.7 Flowchart of yarn feed controller

While speed synchrony controller received the data of time span of speed measurement, and ready signal, the speed synchrony controller change its status into host site on RS485 bus and measure the speed and send the change line and update speed command. While the bus is unoccupied send the command check the status of other controller and send the status to IPC.

IX. CONCLUSIONS

This article designs the carpet tufting machine yarn feeding control system, employ the computer to act as a master platform and user interface, design the sub modules including yarn feeding controller, yarn guide controller and synchronization controller. Through industrial analysis, design the control logic for the control system. And expatiated discusses the hardware design of Lower controller modules and its internal control program logic design. Construct the communication network base on RS-485 and devise the communication protocol, develop the control system and realize the yarn feeding amount control of each yarn in a tufting cycle. Cooperate with tufting needle and hook action could produce various patterns on tufted carpet surface.

ACKNOWLEDGMENT

This work was supported by the Fundamental Research Funds for the Central Universities (9D10307), Shanghai Natural Science Foundation (No. 10ZR1401500).

REFERENCES

[1] Xue Shi-xin. Machine-made carpet. Chemical industry publishing company ,2004

[2] Lee, Hsi-Lung Stephen. “Study of the industrial through-air drying process for tufted carpet”. Georgia Institute of Technology. 2000,pp.7-10

[3] Sherrill, Sarah B., Carpets and Rugs of Europe and America, Abbeville Press., New York, 1996.

[4] Zhao Yue, Dai Hui-liang. “Advanced tufted carpet patterning technology”. Journal of Zhejiang University-Science A. 2006, vol 7,pp.374-377.

[5] Chen Guangfeng and Yang Yanzhu. Electromagnetic Clutch Based High-Low Carpet Jacquard Control System. Proceedings of IITA 2008 Workshop, pp.176-179

[6] Chen Guangfeng, Zhang Yawei, Jin Zhilei, Sun Zhijun, Sun Yize. Research on Jacquard Control System for Three-pile-height Carpet Tufting Machine. Proceedings of International Conference on Control, Automation and Systems Engineering, 2009,pp.367-370

[7] Chen Guangfeng, Zhang Yawei, Jin Zhilei, Xu Yang, and Meng Zhuo. Study on Pattern Preparing System for Three-Level Loop Tufting Carpet. Proceedings of International Conference on Control, Automation and Systems Engineering, 2009,pp.363-366

[8] Zhou Tingzhe. Study on computer jacquard control system for carpet tufting machine. Dong Hua University. 2006.

[9] Wang Zhiping, Meng zhuo, Yang Yanzhu. Fuzzy Control on Background-material Tension of Carpet Tufting Machine. Mechanical Engineering & Automation, 2007(6),pp.96-99.

[10] Yang Yanzhu, Zhao Binliang, Sun Jingjing. Transversing Bucking-Out System of Carpet Tufting Machine Based on Servocontrol. Journal of Donghua University:Natural Science Edition, 2008, 34 (2) ,pp.208-212.

[11] Zhao Binliang, Chen Guangfeng, Sun Yize. Designing and Implementation of Software Based on Delphi for Transversing Bucking-out System of Tufting Carpet Machine. Journal of Donghua University： Natural Science Edition, 2008, 34 (1) ,pp.93-97.

[12] Ding Caihong, Zhang Shaoping, Sun Yize. Kinematical analysis of the needle's driving mechanism within a carpet tufting machine. Journal of Textile Research, 2006, 27(5) ,pp.37-40

[13] Guo Feng, Cai Zongping. Research and design of the compound control system of an AC servo system. Microcomputer Information 2008,24(2-1) ,pp.25,26,40.

[14] Su Kui-feng, Lu Qiang, Geng Qingfeng, et al. TMS320F2812 principles and development. Beijing: Publishing House of Electronics Industry, 2005,4,pp.11-13,156-275.

[15] Chen Feng, Zhu Deming, Zhu Guangbin,et al. Permanent Magnet AC Servo system speed control and precise line detection. Micromotor, 2008,41(11),pp.40-43

2011 International Conference on Mechanical, Industrial, and Manufacturing Engineering
Lecture Notes in Information Technology Vols. 1-2

Open Inventor based 3D Modeling of Loop-Pile Tufted Carpet*

Chen Guangfeng, Li Qingqing, Sun Haochun, Wang Weibin
College of Mechanical Engineering,
Donghua University
Shanghai 201620, China
chengf@dhu.edu.cn, ruguoabc@163.com, sunvhao@163.com, weibinqdu@126.com

***Abstract* - This paper proposes 3D modeling for simulation of tufted carpet's appearance based on Open Inventor. By analyzing the space structure and the influence factors of appearance of tufted carpet, present a 3D simulation method for tufted carpet in Open inventor environment. According to the structure characteristic, use NURBS curve to create a mass of fibers in loop pile, through control the key points of NURBS to determine the pile height, cross section, trajectory and deformation of loop pile. According to design pattern and process parameters, dynamically assembly loop pile models on backing cloth model and form the 3D model of tufted carpet.**

Index Terms* - *Open inventor; simulation; tufted carpet; yarn modeling; design pattern

I. INTRODUCTION

Together with the progress three-dimensional (3D) graphics technology, the structure of the fabric and appearance of the three-dimensional simulation as a research focus in recent years. Considering light model and material of fabric, researchers build 3D models with DirectX and OpenGL to get the three-dimensional simulation of textile visual appearance[1-2]. The complexity of design pattern and 3D space of carpet increase the difficulty of tufted carpet appearance simulation. It is hard to simulate tufted carpet based on planner image technology. Some foreign textile CAD, such as the Nedgraphics provides the carpet simulation module. However, to the author's knowledge, there is no literature available about tufted carpet appearance simulation [3]. The authors try to use Direct 3D, and color block to simulate the tufted carpet[4][5][6], and get some certain effect, but the simulation results a bit stiff, not lively.

Based on above issues, this article analyses appearance characteristics and influence of multi-level tufted carpet, and studied the method to simulate the visual appearance simulation of loop pile tufted carpet made up of single no twist yarn based on TGS Open Inventor.

II. SIMULATION SCHEME FOR TUFTED CARPET

A. 3D Structure of Tufted Carpets

Tufted carpet is constructed by using needles to force yarns through the primary backing. And a secondary backing fabric is applied and bonded by latex for greater stability and strength. As mention above tufted carpet is consist of loop pile, primary backing and secondary backing fabric. As Fig. 1 shown is process variable of loop pile carpet. The process variables of tufted carpet including gauge, stitch and pile height. In a carpet, the stitch and gauge decides the loop pile arrangement density in horizontal and vertical direction. And with the change in pile height will form raised empaistic texture on the carpet. The primary backing and second backing is just act like a rigid body, but the loop pile is composed by soft yarns, is a typical soft objects, which is easier to deform by external forces. So the simulation of tufted carpet need to consider the deformation of loop piles.

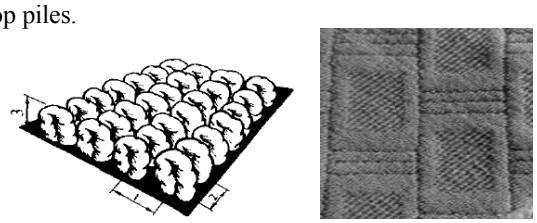

1-gauge; 2-stitch length; 3-pile height
Fig.1 Tufted carpet structure Figure 1. Sampled tufted carpet

As Fig.2 is a schematic cross-section diagram of tufted carpet along the stitch length direction. In the picture all loop piles is connected with same yarn.

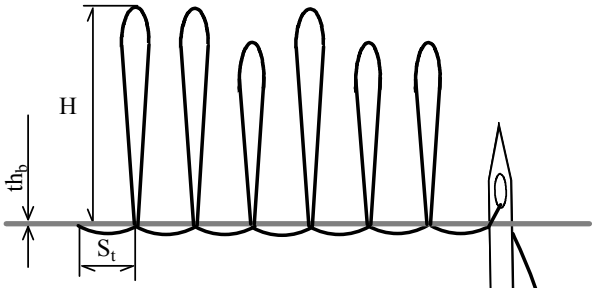

Fig.2 Pile height and yarn usage

B. Analyze of Tufted Carpet Appearance

To take two level loop pile tufted carpet with Gray color as an example to analyze its appearance characteristics, the carpet scanned picture as Fig. 1 shown. Tufted carpet is consisting of loop piles, latex and backing cloth. Because of

* This work is supported by Shanghai Natural Science Foundation Grant #10ZR1401500 to Chen Guangfeng and Fundamental Research Funds for the Central Universities Grant #9D10307 to Chen Guangfeng.

shelter from loop pile, latex and backcloth almost have no influence on appearance in front view. The loop piles with different pile heights which form the pattern on the carpet. As Fig. 1 shown is a scanned image of two level single color tufted carpet. Traditional two-dimensional simulation for this kind of carpet always got a single color block, the carpet pattern information would lose. Due to tufted carpet appearance characteristic, the simulation should be on basis of three-dimensional simulation technology. Appearance influence factors are list as Fig.3.

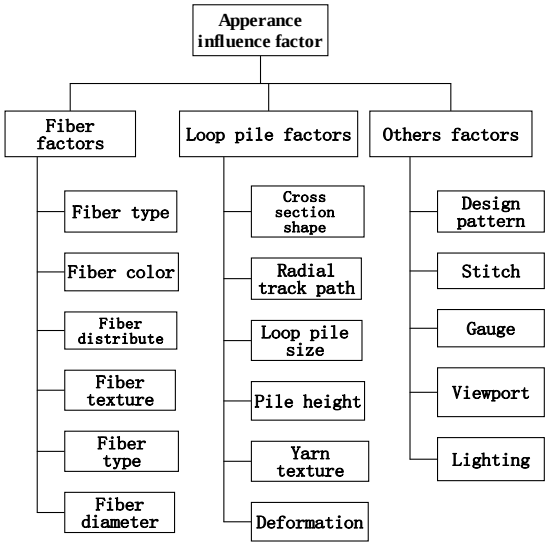

Fig.3 Influencing factors in appearance of tufted carpet

To get better simulation effect, the key lies in whether we can reflect the geometric structure of the carpet and carpet surface gloss and texture. Carpet texture is consist of different types, different colours of the optical properties of yarns, including various diffuse reflectivity, specular reflectivity and refractive index, transparency, etc. These optical characteristics have a greater impact on the carpet appearance.

For tufted carpet manufacturing, process variable including yarn type, gauge, and stitch and pile height. Pile height has great impact on simulation result. As a result of the extrusion around the loop pile, each loop pile will have different degrees of compression deformation. From the view of microscopic, fibre distribution in loop pile will affect the lustrousness of loop pile. In this paper, we focus on the 3D modelling of tufted carpet in Open Inventor.

III. Open Inventor Based Simulation Process

Open Inventor is an object-oriented, cross-platform 3D graphics toolkit for the development of industrial-strength, interactive applications using C++, .NET or Java. Its easy-to-use API, its extensible architecture, and its large set of advanced components provide developers with a high-level platform for rapid prototyping and development of 3D graphics applications[14].

Open Inventor adopt the hierarchical structure to keep it sub models and prosperities. All object information such as position, shape, size, color, texture and light source are store in scene database. In this study, in order to simplify the simulation process, we separate a carpet into several different parts, such as back cloth, loop piles and light models, and assembly these part into one scene in Open Inventor.

Tufted carpet simulation flowchart is shown as Fig.2. Firstly, the operator inputs the design pattern, then set the process parameter, and then creates the Open Inventor scene window. First create the backcloth model and add to the scene. Then through dynamic construct the loop pile according to the pattern and process parameters and arrange these piles on the backcloth. After this, adding the light model and interactive adjust the viewport, at last render the scene and output the simulation image. The key process will discuss in detail.

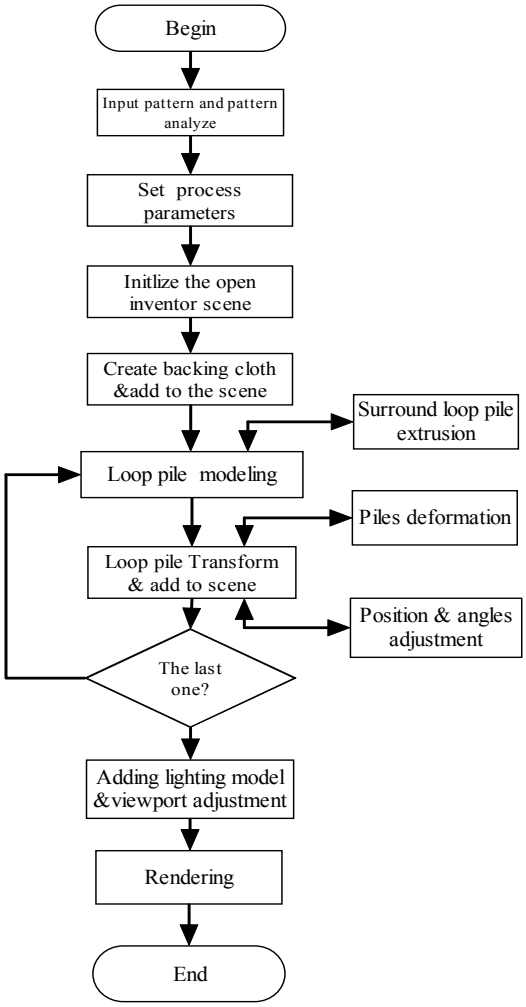

Fig.4 Simulation process of tufted carpet

IV. 3D Modeling of Tufted Carpet

A. *Pattern Input and Analyze*

In carpet production, bitmap is wildly used as the pattern carrier to keep the pile height level information. In generally each pixel in the pattern represent a loop pile on the carpet, Fig.5 is a design pattern of two level tufted carpet. Black pixel represent loop pile with pile height 4.2 mm, white pixel represent pile height 2.8 mm.

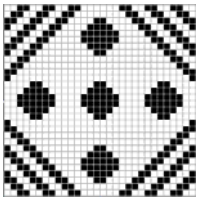

Fig.5 A sample of design pattern

Design pattern is converting to two dimension matrix to describe the loop piles height level of each loop.

$$A=\begin{bmatrix} a_{1,1} & a_{1,2} & a_{1,3} & \cdots & a_{1,m} \\ a_{2,1} & a_{2,2} & a_{2,3} & \cdots & a_{2,m} \\ a_{3,1} & a_{2,2} & a_{2,3} & \cdots & a_{2,m} \\ \vdots & \vdots & \vdots & \vdots & \vdots \\ a_{n,1} & a_{n,2} & a_{n,3} & \cdots & a_{n,m} \end{bmatrix}_{n\times m} \quad (1)$$

$a_{n,m}$ is the RGB value in design pattern represent the level of pile height. Each RGB value represents a certain pile height as parameters assignment. To convert the pattern as pile level information through Look-up table mapping.

$$P=\begin{bmatrix} p_{1,1} & p_{1,2} & p_{1,3} & \cdots & p_{1,m} \\ p_{2,1} & p_{2,2} & p_{2,3} & \cdots & p_{2,m} \\ p_{3,1} & p_{3,2} & p_{3,3} & \cdots & p_{2,m} \\ \vdots & \vdots & \vdots & \vdots & \vdots \\ p_{n,1} & p_{n,2} & p_{n,3} & \cdots & p_{n,m} \end{bmatrix}_{n\times m} \quad (2)$$

$p_{n,m}$ is the pile height level value. For example Black represent pile height level 2, pile height 5.5mm, Gray represent pile height level 1, pile height is 4 mm, and White represent pile height level 0, pile height is 3 mm.

The sample pattern matrix P is as (3) shown.

$$P=\begin{bmatrix} 0 & 0 & 2 & \cdots & 0 \\ 0 & 2 & 2 & \cdots & 0 \\ 2 & 2 & 0 & \cdots & 2 \\ \vdots & \vdots & \vdots & \vdots & \vdots \\ 0 & 0 & 2 & \cdots & 0 \end{bmatrix}_{30\times 30} \quad (3)$$

B. Back Cloth Modeling

This study establishes a cube flattened entity to represent back cloth.

The back cloth is construct with a size of $W\times H\times T$, and their value is take as (4).

$$\begin{aligned} W &= m\times g \\ H &= \sum_{j=0}^{n-1} s_j \\ T &= 0.5 \end{aligned} \quad (4)$$

C. Loop Pile Modeling

The modeling of loop pile is one of key problems in tufted carpet simulation. There are a various expression models of loop piles. In our previous study, we try to use a 3D solid to represent a loop pile. In reference[7], Fredrick Thomas Pierce simplify yarn cross section in woven fabric to circular, ellipse, convex and raceway and other shape.

In this study, to get better performance, simplified the yarn cross-section as circle while modeling the loop pile. In our study, we construct a NURBS curve to represent a fiber in a loop pile. To form certain cross section, the fiber should uniformly fill the cross section. In the modeling of loop pile, using NURBS curves to simulate fibres in loop pile, through control the control points of NURBS to form circle cross section.

Loop pile bending status is determined by internal stress and external stress between loop piles. Fig. 6 shows the stress act on a single loop. Reference [9] mentioned simplified yarn model with external stress, splines curve of yarn can be described by the cubic polynomial, and parameter *a*, *b*, *c* and *d* are constant polynomial coefficients.

$$y(x)=ax^3+bx^2+cx+d \quad (5)$$

As B-spline curve has a better geometric features and high flexibility, and could simulate the central axis of loop pile. This paper adopts B-spline curve to describe the spatial structure of loop pile. NURBS curve is a B-spline curve of the general form of the expression as (6).

$$C(u)=\frac{\sum_{i=0}^{n} W_i P_i N_{i,k}(u)}{\sum_{i=0}^{n} W_i N_{i,k}(u)}=\sum_{i=0}^{n} P_i N_{i,k}(u) \quad (6)$$

In (2) P_i is characteristic polygon vertex position vector, $N_{i,k}(u)$ is k B-spline basis function, W_i is the weight coefficient of $k+1$ control point P_i. The number of nodes in the node vector $m=n+k+1$, $n+1$ is the number of control points, k is times of B-spline function.

To construct a fibre in a loop pile, we first need to get the size value of loop pile. For example height, width, and cross section diameter. The height is determined by the process parameter and the pile height setting. The width is determined by current loop pile and the surrounding loop piles. The cross section of yarn is a const value depends on the yarn used.

For example, to use seven control points to construct a fibre curve, the points set as follow list. And take all W_i take the value as 1.0. Then we could get a fibre curve.

P[7][3] = { { 0.0, 0.0, -1.0}, {1.0, 0.0, 3.0},{3, 0, 7.0},

{0.0, 0.0, 10.0},{ -3, 0, 7.0}, { -1.0, 0.0, 3.0},
{0.0, 0.0, -1.0}};

Through construct a mass of fibres curve with a little deviation in each control points, we could get the loop pile model.

D. Pile Arrangement

All loop pile is dynamic constructed base on its pile height and colour, Here is to discuss the arrangement of loop pile on the carpet. Setup the three-dimensional coordinates, along needle bar is x, y is direction along backing cloth feeding direction, z is point to pile height direction.

Suppose the pattern data is store in matrix A ($n \times m$). Axis z is the pile height direction, axis x is the transverse direction, and y is along the back fabric feeding direction.

Suppose the first loop pile is in (0, 0, 0). According to the process parameters and pattern data, we could get the base position of each loop pile in the pattern. For example, suppose a loop pile in design pattern, row number is N_x , column number is N_y , and its pile height is 5.4 mm, according to (7) calculate their space position.

$$\begin{aligned} P_x &= \sum_{i=1}^{N_x-1} g + \Delta g \\ P_y &= \sum_{j=1}^{N_y-1} s_j + \Delta s \\ P_z &= \Delta z \end{aligned} \tag{7}$$

Point $P(P_x, P_y, P_z)$ represents spatial location of loop pile in carpet respectively. g usually is a const value represents gauge between i loop pile and $i-1$ loop pile, s_j represent distance between j loop pile and $j-1$ loop pile along backing cloth feeding direction, and Δs is the deviation form its exact value. Δz represents a random float number in $[min, max]$.

$$\Delta z = \text{rand}(min, max) \tag{8}$$

As Fig.6 is a snapshot of 3D modelling test of tufted carpet. In the test all loop pile is constructed with twenty fibres which consist of three different colours.

V. SUMMARY

This paper presents a scheme for 3D modelling base on Open Inventor for multi-level loop pile tufted carpet appearance simulation. In the modelling of loop pile, using NURBS curves to simulate fibre in loop pile, through control the control points of NURBS to form elliptical cross section. By assembly backcloth and loop piles into scene window, set up the total 3D model for tufted carpet appearance simulation. The further study will discuss the simulation of tufted carpet base on the 3D model.

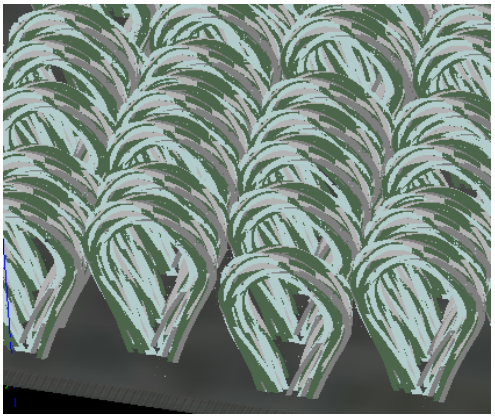

Fig.6 Snapshot of 3D modeling of tufted carpet

ACKNOWLEDGMENT

This work was supported by Shanghai Natural Science Foundation (No. 10ZR1401500) and Fundamental Research Funds for the Central Universities(No. 9D10307).

REFERENCES

[1] Zhang Ruiyun, Huang Xinlin, LI Ruqin. 3D computer simulation of woven fabric. Journal of Textile Research, 2005, 26(1):62-69.

[2] Yuan Jie, Zhang Hui. Three-dimensional simulation of fabric based on DirectX 3D technology. Progress in Textile Science & Technology, 2008(1):17-19.

[3] Chiristiane Szczesny, Klaus Hardt and Brigitte Scheuffele. Simulation of fancy yarns on the screen. ITB, 1997,(2):3-9.

[4] Chen Guangfeng, Sun Haochun, Li Qingqing. Color Appearance Simulation Method for Multilevel Loop Tufed Carpet Produced by Single Needle Bar Machine. Procceedings of 2010 2nd Interational Conference on Industrial and Information Systems.2010,pp44-47

[5] Chen Guangfeng, Wang Weibin, Jin, Zhilei. Spatial structure analysis and simulation of multi-level tufted Carpet. Procceedings of 2009 Pacific-Asia Conference on Knowledge Engineering and Software Engineering,2009,pp143-146

[6] Chen Guangdfeng, Li Qingqing, Sun Haochun and Wang Weibin. Study on 2D Simulation Algorithm and Implementation for Loop Pile Tufted Carpet Advanced Materials Research 2011, 179-180:651-656

[7] Xue Shixin. Machine made carpet. Beijing: Chemical industry press, 2004:320-330.

[8] Wang Decai, Yang Guansheng, SUN Yuping. Master in DirectX 3D & Animation Programming. Beijing: Posts & Telecom Press, 2007:14-17, 25-29.

[9] Wang Dongfeng. The study on 3D yarn model. Donghua university master dissertation, 2006.

[10] Zheng Tianyong. Textile CAD/CAM. Beijing: Chemical industry press, 2007:134-139.

[11] WANG Meizhen. Studies on the incorporate integration system of fabric design and dummy scene. Donghua University doctor dissertation,2004:54-58.

[12] Zheng Tianyong. Research on 3D imitation for displaying structure and pattern of woven fabric. Tianjin Polytechnic university doctor dissertation. 2000:47-50.

[13] Teng J G, CHEN S F, HU J L. A finite-volume method for deformation analysis of woven fabrics. International Kournal for Numerical Methods in Engineering, 1999, 46(12):2061-2098

[14] http://www.vsg3d.com/open-inventor/sdk

[15] Frederick Thomas Peirce. The Geometry of Cloth Structure. Journal of Textile Institute, 1937(3): 45-96

2011 International Conference on Mechanical, Industrial, and Manufacturing Engineering
Lecture Notes in Information Technology Vols. 1-2

Study on Multi-Units Synchronous Control System for Carpet Tufting Machine*

Chen Guangfeng, Wang Weibin, Li Qingqing, Sun Haochun
College of Mechanical Engineering,
Donghua University
Shanghai 201620, China
chengf@dhu.edu.cn, weibinqdu@126.com, ruguoabc@163.com, sunvhao@163.com

***Abstract* --To get greater control flexibility of tufting carpet machine, this paper conducted the study to integrate several function units include jacquard unit, transverse shifting unit, backing fabric feeding unit on one carpet tufting machine. Through analyze of previous developed function units, merged similar sub-module, established hardware framework of integration system. Adopt to use CAN-bus to establish communication network to connect control units and devised the communication protocol realize communication between modules. Reference existing control software constructed the software framework and design the control logic according to the integrated system. Developed the prototype system and verify the proposed system.**

Index Terms -carpet tufting machine; system integration; function unit; CAN bus, Synchronous control

I. INTRODUCTION

Carpet is manufactured in various ways [1-4], and at present more than 90 percent of the produced carpet is tufted carpet. The basic tufted carpet is constructed by using needles to force yarns through a backing cloth [1]. The yarn delivery is the key factor to affect the pile height of loop pile. During the tufting process, the tension rollers rotate with different speeds to pull yarn from yarn cones; the needle carries the pile yarn penetrates the primary backing; a looper moves between the yarn and the needle, and the needle withdraws to leave a loop of pile yarn around the looper on backing cloth.

Besides the control of yarn delivery quantity, needlebar transverse shifting, backing fabric(or backing cloth) feed rate and the yarn guide roller control also effect the carpet pattern and quality. In producing tufted carpet, distinct patterns, such as various zigzag patterns have been formed in backing fabrics by transversely shifting the needle bar or backing cloth[]. Needle bar transversely shifting mechanism could be driven in many actuators, such as the mechanical cam, hydraulic, pneumatic or servo motor etc [5][9]. In our previous developed tufting machines, both mechanical cam and servo based transversely shifting mechanisms are adopted to produce such carpets [10][12]. The feed rate of backing fabric will affect the stitch ratio of tufted carpet. Traditional backing fabric is feed with the spindle drive. New developed carpet tufting machines adopt a servo motor-driven mechanism for moving a backing fabric longitudinally through the machine in a feeding direction.

As mentioned above, our previous research develop the several jacquard function units, such as back cloth feeding unit, needle bar transverse unit, yarn feed unit [10][12]. But each of these function units was develop and testified separately in different carpet machine.

Based on above issues, for more control flexibility, this paper conducts the study attempt to ingrate multi function units on a single tufted machine.

II. PREVIOUS DEVELOPED FUNCTION UNITS

Our previous study developed servel function unit for carpet tufting machine, sucha as yarn feeding mechnasim, yarn puller mechansim, needle bar shifting mechnasim and back fabric feeding system. This study aim to integrate these three function units into one carpet tufting machine.

A. Yarn Feed Control Unit

Yarn feed control is the basic requirement of jacquard mechanism for carpet tufting machine. In our previous studies, we developed servel kind of yarn feed mechansin,such as clutch based yarn feed mechanisim, servos roller and clutch based yarn feed mechanism, stepper motor drived yarn feed mechanisim. These three types of has its own characteristic, the mechanism driven by stepper has more flexibility, its control structure as Fig.1 shown.

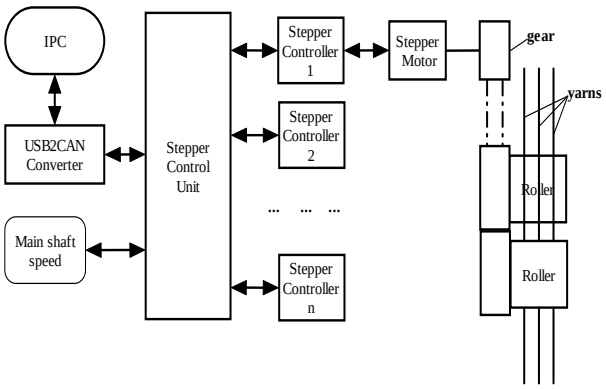

Fig.1 Step motor drive yarn feed unit

* This work is supported by Shanghai Natural Science Foundation Grant #10ZR1401500 to Chen Guangfeng and Fundamental Research Funds for the Central Universities Grant #9D10307 to Chen Guangfeng.

IPC send pattern data to stepper control unit through CAN bus, the stepper control unit drive the stepper motor to rotate the yarn feed roller base on the pattern data, so to control the yarn delivery of each tuft cycle.

Yarn puller mechanism has the similar structure as stepper based yarn feeder unit. Only use a high-power step motor instead of low power step motor.

B. Needlebar Transverse Shifting Unit

In previous art, a mechanical cam has been used for many years as means for converting rotating motions of main shaft of tufting carpet machine into cyclic linear motion of needle bar. However, use the mechnasim cam to drive the needle bar has many shortage. We developed an electronic cam deveice directtly drive the needle bar by a servomotor on the basis of preset cam data. The control system consists USBCAN converter, DSP based controller, servomotor and its controller, photoelectric encoder and a proximity switch. The system download the cam data through USBCAN converter to DSP base controller.

C. Backing Cloth Feed Control Unit

During loop pile tufted carpet production process, need to control the feeding amount of yarn and backing cloth in each tufting cycle. The backing cloth feeding amount will affect the stitch ratio of tufted carpet. The backing fabric feed mechanism adopt the servo motor to drive the back fabric feed roller. The mechanism of back fabric feeder is similar to the mechanism of needle bar shifting.

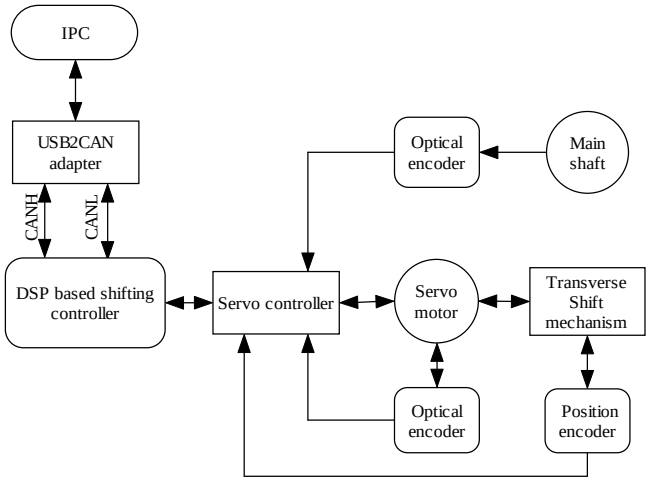

Fig.2 Control system of needle bar shifting mechanism

III. MULTI-FUNCTION INTEGRATION SCHEME

A. Control Framework Design

Functional units list above adopt control structure of industrial computer(IPC) monitor plus a of lower computer model, Integrated systems continue to adopt this control structure.

In communications, continue to use of the existing CAN bus communication, but the unification of several communication protocols and integrated into one communication module. The communication protocal is

The integration system structure is as Fig. 3 shown.

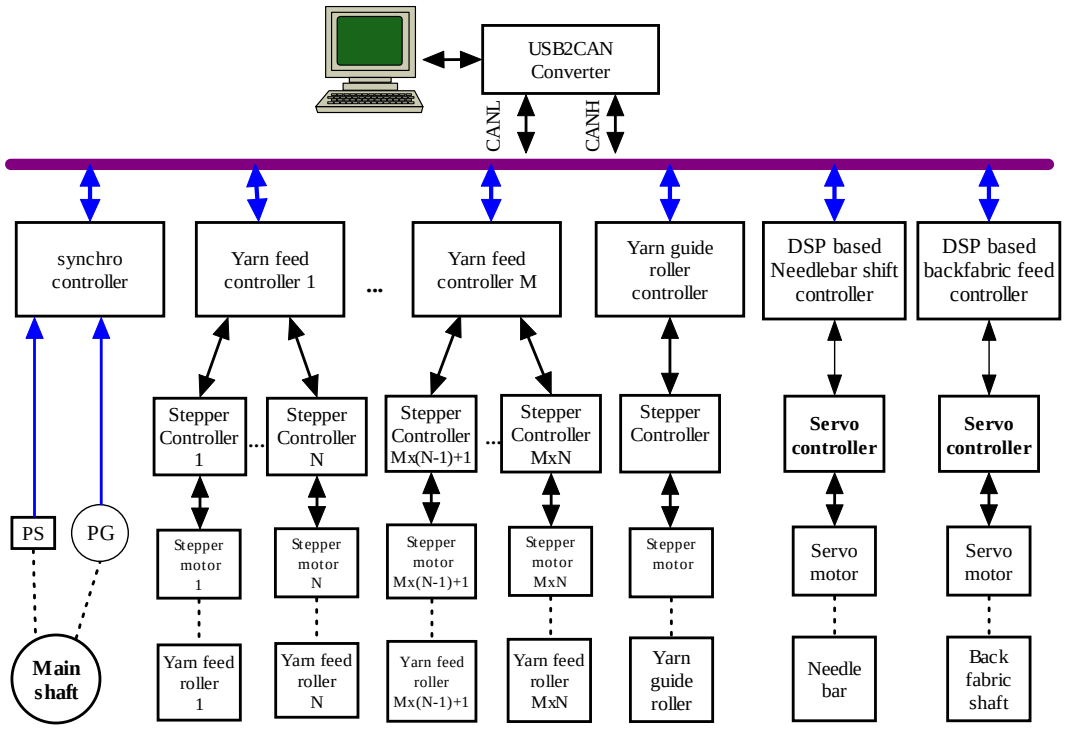

Fig.3 Hardware structure of Integration system

B. Software Framework of IPC

Through analyse of control software of previous developed function units, construct the final structure of integration system as Fig.4 shown.

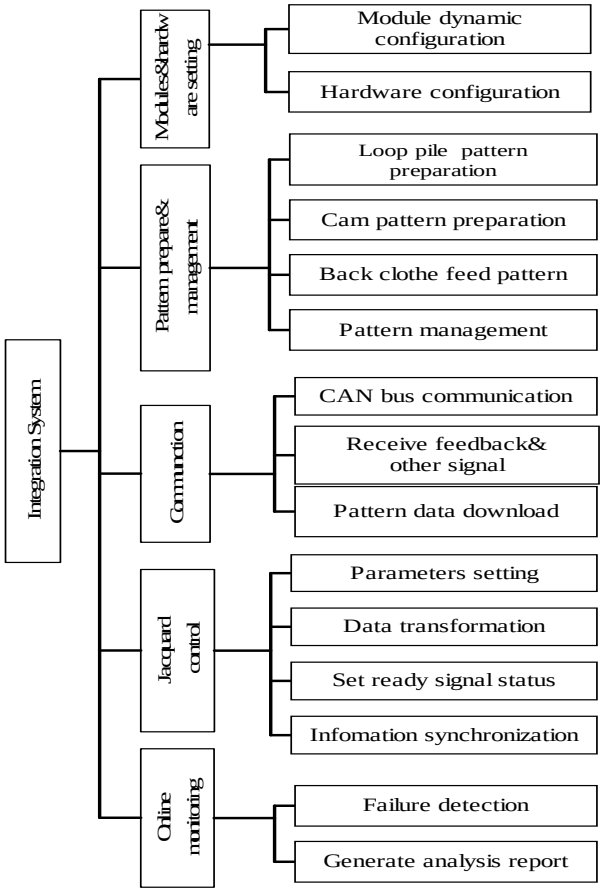

Fig.4 Software structure of integrate system

The software includes four sub-modules. The modules& hardware setting is responsible for modules dynamic configuration and hardware configuration. The pattern prepare &management module is responsible for control preparation and data management. The communication module is responsible for CAN bus communication, control data download, feedback receiving. The jacquard control is take charge of parameters setting, data transformation, information synchronization and ready signal. The last module is to detect the error status and generate the analyst report and log into files

.

C. Control Logic Design

As the system integrate several function unit, timing sequence is critical for carpet tufting machine control. Base on the analyze of production process of tufted carpet, constructed the control logic for the integration system. The control logic is shown as Fig.5.

D. CAN-Bus Communication Protocol Design

From flow we know, the communication through CAN-Bus mainly includes pattern data download process, updated speed, change line instructions, error query, error reports, start command and stop command.

The CAN-Bus communications have two different frame formats, the difference in lengths of identifier, the frame with 11 bits identifier is name standard frame, and frame of identifiers containing 29 bits named expansion frame. In this design, we design a communication protocol based on extended frame of CAN-Bus. The detail communication protocol is devised as Table I shown.

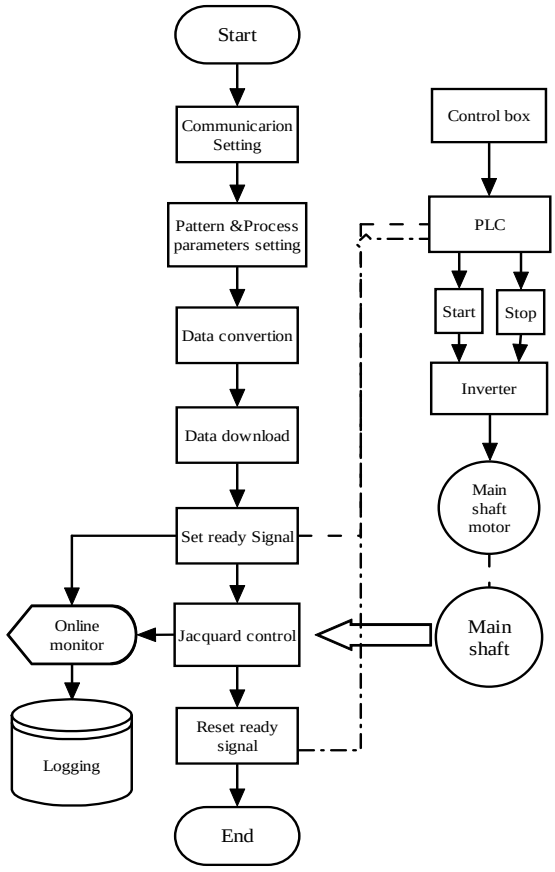

Fig.5 Flowchart of integrated control system

TABLE I
COMMUNICATION PROTOCOL OF CONTROL SYSTEM

Function	Arbitration bits			Data field
	Function code 5 bits	Site ID 8 bits	Data address 16 bits	8 bytes
Start	00000	0x08	0x0000	-
Stop	00001	0x08	0x0000	-
Write data	01110	Site address	Store address	8 bytes data
Read data	01111	Site address	Store address	-
Speed update	00101	0x08	0x0000	Speed data
Change line	00110	0x08	0x0000	Line number
Error detect	00111	0x08	0x0000	-
Error report	00111	0x08	0x0001	Error code or 0

The address of lower controller site IDs are designated as follow: synchronous controller is 0x10, yarn guider controller is 0x20, other stepping motor controller node is 0x30 ~ 0x4D respectively.

IV. Prototype Implementation

Base on the control logic list above, developed the prototype control system with C++ builder. The user interfaces are shown as Fig.6 and Fig.7.

Fig.6 User interface of communication operation

Fig.7 User interface of jacquard control system

V. Conclusion

This paper conducts the study to integrate serval function units into one carpet tufting machine. Through analysis the hardware structure and control logic of each function unit, construct the final hardware structure of integration system. Devise the final control logic and communication protocols. Integrate the control software of each function unit and developed control software of the system.

Acknowledgment

This work was supported by the Fundamental Research Funds for the Central Universities (9D103107), Shanghai Natural Science Foundation (No. 10ZR1401500).

References

[1] Lee, Hsi-Lung Stephen. “Study of the industrial through-air drying process for tufted carpet”. Georgia Institute of Technology. 2000:pp.7-10

[2] Sherrill, Sarah B., Carpets and Rugs of Europe and America, Abbeville Press., New York, 1996.

[3] Xue Shi-xin. Machine-made carpet. Chemical industry publishing company,2004

[4] Morgante M R, Bishop M, Stanfield R E, et al. Servo Motor Driven Scroll Pattern Attachment for Tufting Machine and Computerized Design System for Tufting Carpet, US Patent 6877449. 2005.04.12.

[5] Gary L. Ingram, Jimmie D. Scott, Randel P. Smith Chattanooga; Shiftable needle plate. US Patent 3964407,June 22, 1976

[6] James A. Cobbel SR, James A. Cobbel JR. Backing fabric lateral shifting arrangement for tufting and like machines, US. Pat. No. 33265, Nov. 14, 1967

[7] Michael R. Morgante, Buffalo , Greogory J. Guzewich. Control system for hydraulic needle bar positioning apparatus for a tufting machine. U.S. Pat. No. 4829917, May 16,1989

[8] Henry A. Schmidt, Elma. Electrohydraulic needle bar positioning appratus for tufting machines, U.S. Pat. No. 4173192, Nov. 6, 1979

[9] Ikuo Nagamatsu, Shigenori Ohkubo. Electronic cam device and method of preparing cam data in electronic device. US Patent No. 7,228,294 B2, Jun. 5, 2007

[10] Chen Guangfeng,Yang Yanzhu and Zou kun. Electromagnetic Clutch Based High-Low Carpet Jacquard Control System. Proceedings of IITA 2008 Workshop, pp.176-179

[11] Chen Guangfeng, Zhang Yawei, Jin Zhilei. Study on Pattern Preparing System for Three-Level Loop Tufting Carpet. Proceeding of CASE 2009,pp:363-366

[12] Chen Guangfeng, Zhang Yawei, Jin Zhilei. Research on Jacquard Control System for Three-Pile-Height Carpet Tufting Machine. Proceeding of CASE 2009,pp:367-370

[13] Lee, Hsi-Lung Stephen. Study of the industrial through-air drying process for tufted carpet. Georgia Institute of Technology. 2000:pp.7-10

[14] D.T.Ward. Introduction to tufting production. Pekin:Textile publishing company,1987:9

[15] Morgante MR, Bishop M, and Stanfield RE. Single end servo motor driven scroll pattern attachment for tufting machine and computerized design system for tufting carpet. US- Patent Number: US 6508185. 2003.

[16] Slattery, Ian. Tufting machine yarn feed pattern control. Patent Number: US6213036. 2001.

[17] Christman W M. Precision drive system for tufting machines. US Patent: EP867553-A.

[18] Zhao Yue, Dai Hui-liang. “Advanced tufted carpet patterning technology”. Journal of Zhejiang University- Science A. 2006,7(3):374-377

2011 International Conference on Mechanical, Industrial, and Manufacturing Engineering
Lecture Notes in Information Technology Vols. 1-2

Oxidation Kinetics of Sodium Sulfite with Five Catalysts*

Wendi Zhang and Lidong Wang
Department of Environment Science and Engineering
North China Electric Power University
Baoding, Hebei Province, China
{zwd8611@126.com} wld@tsinghua.edu.cn

Yongliang Ma
Department of Environmental Science and Engineering
Tsinghua University
Beijing, China
liang@tsinghua.edu.cn

***Abstract* - Under the fixed experimental conditions, effects of five additives, such as cobalt sulfate, manganese sulfate, copper sulfate, nickel sulfate, and ferrous sulfate on the oxidation rate were compared. The results show that cobalt sulfate is the most effective catalyst, and the reaction order with respect of cobalt sulfate concentration is 0.214. Under the condition of high concentration, the catalytic effect of ferrous sulfate is more obvious than that of manganese sulfate. The comparison of kinetics of oxidation catalyzed by cobalt sulfate with ferrous sulfate, indicates that the intrinsic reaction rate is supposed to be the control step of sodium sulfite oxidation.**

Index Terms – Kinetics, oxidation, sodium sulfite, catalyst.

I. INTRODUCTION

At present different kinds of transition metal ions are used as catalyst in the research on sulfite catalytic oxidation, and the comparison of different catalyst in catalytic effect on sulfite oxidation reaction, as well as the discussion of oxidation kinetics are reported in some researches. The experiment of Bronikowska in Ref. [1] used two types of reactors indicated that, cobalt sulfate could enhance sulfite dissolved ability, and the catalytic effect of cobalt sulfate in weakly alkaline condition was better than manganese sulfate in acidic condition.

Ref. [2] conducted a sulfite oxidation reaction in a falling-film absorption column, the result showed there would be catalytic effect only when Fe^{2+} and Mn^{2+} were added simultaneously, and Mn^{2+} was the main reason for the catalytic effect, well the catalytic effect of Fe^{2+} was limited by mass transfer of oxygen. Although in Ref. [3] Ermakov agreed that the catalytic effect with both ferrous ion and manganese ion would be best, but he indicated that the participating in the chain reaction of ferrous ion induced the catalytic effect of manganese ion on the oxidation, which is different with that of Vorbach.

Ref. [4, 5] showed that the catalytic effect of ferrous sulfate was more significant than manganese sulfate and copper ion in calcium hydrosulfite oxidation reaction, the mass transfer theory was used to analyze the experimental results.

Obviously some differences are found in these conclusions of current researches on catalytic sulfite oxidation, and the differences of reaction apparatus and experimental conditions would bring difficulties to the comparison and analysis.

According to these difficulties, experiments in this paper were conducted in the same reactor and a fixed condition, the catalytic effect on the sodium sulfite oxidation with cobalt sulfate, manganese sulfate, nickel sulfate, copper sulfate and ferrous sulfate was studied respectively.

II. EXPERIMENTS

A. Facility and Process

A bubbling apparatus is shown in Fig. 1, When 200 ml de-ionized water was added, and catalyst with known concentration was supplied into the reactor. The pure nitrogen, oxygen and air controlled by flow meter were blended in the buffer reactor, and then were injected into the reactor. Then reaction was started, and a known amount of sodium sulfite was added to the reactor at the same time.

* This work is partially supported by the National High Technology Research and Development Program of China (No. 2007AA061703) and the Key Project of Chinese Ministry of Education (No. 109157) and the Fundamental Research Funds for the Central Universities (No. 10MG35).

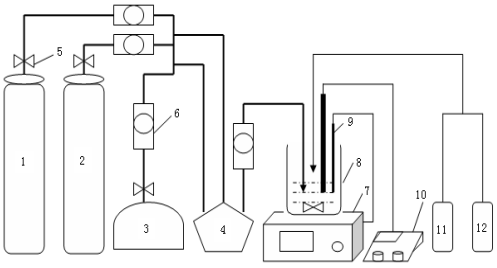

Fig. 1 The bubbling reaction facility

1-Nitrogen, 2-Oxygen, 3-air compressor, 4-buffer reactor,

5-pressure-reducing valve, 6-flowmeter, 7-magnetic stirrer, 8-reactor,

9-thermoelectric couple, 10-acidometer, 11-HCl, 12-NaOH

Hydrochloric acid and sodium hydroxide were used to adjust pH. Some trace amount of reaction solution taken out at intervals was dissolved by hydrochloric acid and diluted to a desired volume then. The concentration of sulfate at different point of time was determined by barium sulfate spectrophotometry. Under the given conditions, the results indicate that the sulfate concentration increases linearly with the rise of reaction time. Thus the slop is the oxidation rate of sodium sulfite that reflects the relationship between sulfate concentration and reaction time.

B. Comparison of the Effect of Five Kinds of Catalysts

The initial amount of sodium sulfite was 2.1g, the oxygen particle pressure, flow of air, pH, temperature and stirred rate was 0.21 atm, 60 L/h, 7, 45 ℃, 860 rpm respectively, and the initial concentration of cobalt sulfate was 0.89 mmol·L^{-1}, as well as that of manganese sulfate, nickel sulfate, copper sulfate and ferrous sulfate. The result was shown in Fig. 2, the catalytic effect of cobalt sulfate was most significant compared with other catalyst,

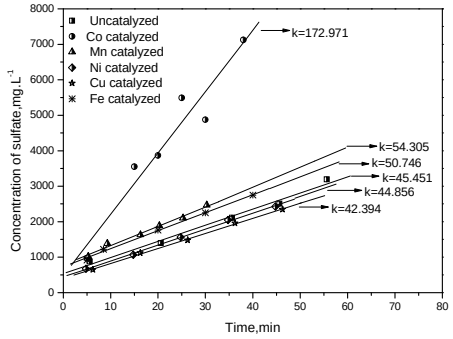

Fig. 2 Comparison of the effect on oxidation rate with five kinds of catalyst

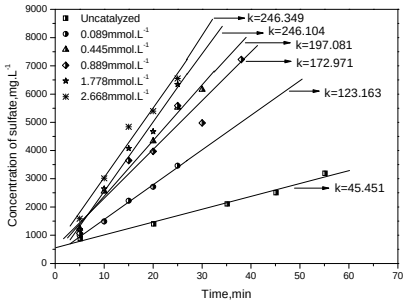

Fig. 3 Effect of cobalt sulfate concentration

manganese sulfate and ferrous sulfate had little effect on the oxidation rate, and copper sulfate, nickel sulfate had no catalytic effect. The order of catalytic ability with metal ions was: Co (Ⅱ) > Mn (Ⅱ) > Fe (Ⅱ) > Ni (Ⅱ) > Cu (Ⅱ).

C. *Effect of Cobalt Sulfate Concentration*

Under the same condition as that in section B, the initial concentration of cobalt sulfate was 0.089, 0.445, 0.889, 1.778, 2.668 mmol·L^{-1} respectively, results were showed in Fig. 3.

The results showed that, when the concentration was larger than 0.089 mmol·L^{-1}, the oxidation rate increased greatly with the rise of concentration. The oxidation rate of 0.889 mmol·L^{-1} was 4 times lager than uncatalyzed oxidation rate, and the increase of rate was not obvious any more when the concentration was larger than 0.889 mmol·L^{-1}. So it indicated that there was a catalytic limited concentration around 0.889 mmol·L^{-1}, and the rate increase of the concentration lager than this limited one was not obvious any more, this inference was similar with ammonium sulfite oxidation research of Ref. [6]. The reaction order was got from the effect of cobalt sulfate

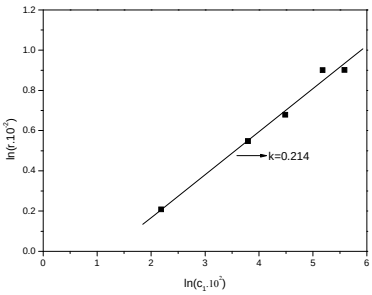

Fig. 4 Reaction order in cobalt sulfate concentration

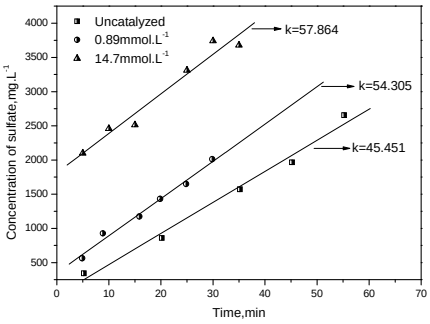

Fig. 5 Effect of manganese sulfate concentration

concentration on the oxidation rate, as showed in Fig. 4 the reaction order of cobalt sulfate was 0.214.

D. Effect of Manganese Sulfate Concentration

Under the same condition as that in section B, the concentration of manganese sulfate was 0.089, 14.7 mmol·L^{-1} respectively, and the comparison of oxidation rate catalyzed by manganese sulfate with uncatalyzed rate was shown in Fig. 5.

The result indicated, when the concentration increased from 0.0089 mmol·L^{-1} to 14.7 mmol·L^{-1}, which was almost 200 times lager than 0.0089 mmol·L^{-1}, the oxidation rate just increased 3.5 mg·L^{-1}·min^{-1}, and the rate of 14.7 mmol·L^{-1} was just 127% of uncatalyzed rate. So the catalytic effect of manganese sulfate was not obvious.

E. Effect of Nickel Sulfate Concentration

Under the same condition as that in section B, the initial concentration of nickel sulfate was 0.0089, 8.9 mmol·L^{-1} respectively. The comparison of uncatalyzed rate with the oxidation rate catalyzed by nickel sulfate was showed in Fig. 6.

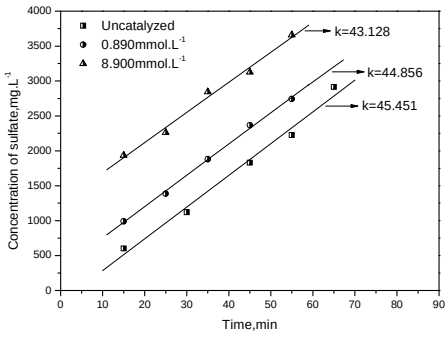

Fig. 6 Effect of nickel sulfate concentration

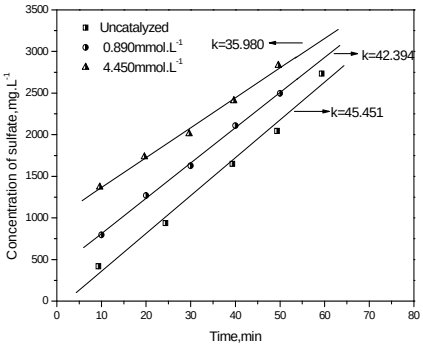

Fig. 7 Effect of copper sulfate concentration

The result indicated that, the effect of initial concentration of nickel sulfate on oxidation rate was little, both of the oxidation rate of 0.89 and 8.9 mmol·L^{-1} was similar with uncatalyzed rate. Therefore nickel sulfate had no catalytic effect on sodium sulfite oxidation reaction.

F. Effect of Copper Sulfate Concentration

Under the same condition as that in section B, the initial concentration of copper sulfate was 0.089, 4.45 mmol·L^{-1} respectively. The comparison of uncatalyzed rate with the oxidation rate catalyzed by copper sulfate was shown in Fig. 7.

The results in Fig. 7 indicated, copper sulfate had no catalytic effect on the oxidation rate, and the oxidation rate even decreased a little with the increase of copper ion concentration, which was identical with the results of Charles H. Barron.

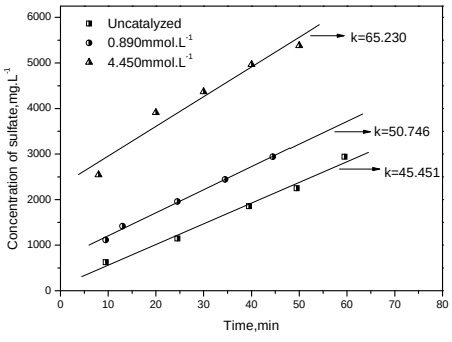

Fig. 8 Effect of ferrous sulfate concentration

G. Effect of Ferrous Sulfate Concentration

Under the same condition as that in section B, the initial concentration of ferrous sulfate was 0.089, 4.45 mmol·L^{-1} respectively. The comparison of uncatalyzed rate with the oxidation rate catalyzed by ferrous sulfate was shown in Fig. 8.

As Fig. 8 showed, the oxidation rate increased slowly with the increase of ferrous sulfate concentration, the oxidation rate of 4.45 mmol·L^{-1} was about 143.5% of uncatalyzed rate, the catalytic effect was not obvious. The comparison of Fig. 5 with Fig. 8 showed that the oxidation rate of 4.45 mmol·L^{-1} ferrous sulfate was larger than that of 14.7 mmol·L^{-1} manganese sulfate, which indicated that the catalytic effect of ferrous sulfate under high concentration conditions was more obvious than that of manganese sulfate.

III. ANALYSIS AND DISCUSSION

In sulfite oxidation reaction, the rate of oxidation was controlled by solubility, oxygen mass transfer, and intrinsic reaction rate. Because the solubility of sodium sulfite and sodium sulfate was 37.2, 48.8 g/100g water, so the effect of solubility on the oxidation rate was little, which indicates the general reaction of sodium sulfite oxidation is controlled by oxygen mass transfer or intrinsic oxidation reaction.

As in Fig. 4, the reaction order was 0.21, then the catalytic effect of cobalt sulfate combines with chain reaction mechanism of Backstrom, indicate that cobalt sulfate participated the chain reaction, which induced generating of free radical, and caused the enhancement of reaction rate. So the intrinsic reaction rate is supposed to control the catalytic oxidation rate of sodium sulfite in presence of cobalt sulfate.

In Fig. 8, the enhancement of oxygen mass transfer was inferred to be the main reason for the catalytic effect of ferrous sulfate. However the catalytic effect of cobalt ion was more obvious compared with that of ferrous ion, which indicated that the effect on the total reaction rate of intrinsic reaction was more significant than that of oxygen mass transfer in sodium sulfite oxidation reaction. So the key step of controlling sodium sulfite oxidation rate was the control of intrinsic reaction rate.

IV. CONCLUSIONS

The research on the sodium sulfite oxidation reaction under the same condition shows that the catalytic effect on the oxidation reaction varies much with different kinds of sulfate, and cobalt sulfate is selected to be the most effective catalyst. The kinetics of catalytic oxidation of cobalt sulfate and ferrous sulfate have been studied respectively, the analysis indicates that intrinsic reaction rate is supposed to be the control step of sodium sulfite oxidation rate. Because of the strictly same reaction condition, it is more convenient and reliable to compare with different catalyst.

ACKNOWLEDGMENT

The present work is supported by the National High Technology Research and Development Program of China (No. 2007AA061703) and the Key Project of Chinese Ministry of Education (No. 109157) and the Fundamental Research Funds for the Central Universities(No. 10MG35).

REFERENCES

[1] W. P. Bronikowska, T. Bronikowski, M. Ulejczyk, "Mechanism and kinetics of autoxidation of calcium sulfite slurries," *Environ. Sci. Technol*, vol. 26, no. 10, pp. 1976-1981, 1992.

[2] M. Vorbach, "Catalytic oxidation of sulfite/bisulfite in a falling-film absorption column," *Studies in Surface Science and Catalysis*, vol.133, pp. 575-580, 2001.

[3] A. N. Ermakov, A. P. Purmal, "Catalysis of HSO_3^-/SO_3^{2-} oxidation by manganese ions," *Kinetics and Catalysis*, vol.43, no. 2, pp. 249-260, 2002.

[4] D. Karatzaa, M. Prisciandaro, A. Lancia, D. Musmarra, "Reaction rate of sulfite oxidation catalyzed by cuprous ions," *Chemical Engineering Journal*, vol. 145, pp. 285-289, 2008.

[5] D. Karatza, M. Prisciandaro, A. Lancia, D. Musmarra, "Kinetic and reaction mechanisms of calcium bisulfite catalytic oxidation," *Chemical Engineering Science*, vol. 60, pp. 1497-1502, 2005.

[6] X. –L. Long, W. Li, W. –D. Xiao, W. -K. Yuan, "Novel homogeneous catalyst system for the oxidation of concentrated ammonium sulfite," *Journal of Hazardous Materials*, vol. 129, pp. 260-265, 2006.

2011 International Conference on Mechanical, Industrial, and Manufacturing Engineering
Lecture Notes in Information Technology Vols. 1-2

Positioning System GPS and RTK VRS type, using the Internet as a base, a network of multiple stations

Rodica Bădescu, Gabriel Bădescu, Ovidiu Ştefan,
Department Geodesy of Mines
The North University of Baia Mare
Baia Mare,Victor Babeş Nr. 62/A, ROMÂNIA
badescu_rodica@yahoo.com; gabrielbadescu@yahoo.com; o.stefan@ymail.com

Caius Didulescu, Gheorghe Badea, Ana Cornelia Badea
Department Geodesy
Tehnical University of Civil Engineering
Bucureşti,District 2, Bld Lacul Tei No.122-124 , ROMÂNIA
caiusdidulescu@yahoo.com; badeacadastru@gmail.com

Abstract

Multiple reference station networks using GNSS navigation have been established for high precision applications in many countries around the world and in Romania. Nevertheless, real-time application is still a task which is difficult to put into practice. The concept of virtual reference station (VRS) is an efficient means of transmitting corrections to network users for a RTK positioning. Nowadays, the challenge regarding VRS with RTK positioning resides in communication technologies with wireless adaptation feeder for real-time corrections. Using GPRS technology, a system based on VRS Internet RTK with GPRS positioning infrastructure was developed and tested. This paper talks about the VRS data transmission mechanism, and offers an overall image over VRS with generated RTK positioning data. The results of the tests are presented in order to be able to evaluate the performance of the above mentioned system. The results show that based on VRS Internet and RTK positioning, one can achieve a little over 2-3 centimeters accuracy in horizontal position.

Precision when it comes to height is found in the interval 2-5 centimeters, depending on the precision of the quasi-geoid, for transformation in the national altitude system (normal altitude system Black Sea 1975).

Keywords: GNSS, GPS, Precision, VRS, RTK, Networks, Errors.

1. INTRODUCTION

GPS Real Time Kinematics (RTK) positioning becomes ever more important for many GPS precision applications – high-precision photogrammetry, topography, constructions, agriculture, and precision, like: the Geographical Information System (GIS).

Basically, a mobile receiver needs a field reference station at approximately 8-12 km, in order to insure the centimeter precision level. Recently, more networks which use the reference stations have been installed in many countries around the world and they surpass the limits of the standard RTK systems.

Over the years, different approaches have been tested in order to take advantage of the existing multitude of reference stations, mentioning here the doctorate thesis entitled "Some contributions regarding the use of GPS technology in cadastre surveys" – Gabriel Bădescu-2005. A great part of the research involved the spatial modeling of distance errors – base station receiver (errors mainly regarding the ionosphere and, on the side, of the troposphere). Nevertheless, the research was made on a distribution of these corrections for the potential GPS users located inside and around the GPS RTK positioning system and must be appropriately handled before the effective construction of the multiple reference station network and application (Fotopoulos et al, 2001).

Recently, using the VRS (Virtual Reference Station) as a concept was suggested by many research groups as a more reliable approach for transmitting and correcting inside the information network for the RTK network users (see Wanninger, 1997; Vollath et al,. 2000;). This approach does not require a reference station from a physical point of view. On the other hand, it allows the user to have access to data coming from a non-existing reference station, but virtual in any location in the permanent station network's cover area. Among other facilities, the VRS approach is more flexible in what concerns allowing the users to use their current receivers and software without involving any special software in order to simultaneously administrate the corrections in a series of reference stations(G.R. Hu et al, 2002). With regards to the Virtual Reference Stations (VRS), the users in the reference station network can operate constantly at great distances, while precision only slightly changes (a couple of centimeters). However, there must be a communication connection for transmitting reliable VRS data from a control centre to a receiver which is being used as a mobile receiver (rover) by the user.

There are more ways to transfer GPS data for RTK positioning.

For certain wireless transmission services there are frequency and power restrictions, which regulate the use of such data transmission devices. GSM is a widely available public service and can be used as a distribution channel for VRS data (Vollath et al, 2000.). Using GSM as a communication link is, unfortunately, relatively expensive, because GSM data transmission services are very expensive and the cover areas differ from one GSM carrier to another (G.R. Hu et al, 2002).

From an operational point of view, cost is a very important aspect especially in the context we are in, meaning a crisis, especially in Romania. This cost can be reduced by using the GPRS technique (General Packet Radio Service).

Each wireless communication module has pro and against arguments related to it, but must, generally, support the VRS and RTK data transmission connection with small data latency, good performance in moving the mobile receivers,

cheap user equipment and national service cover. The main objective of this paper is to demonstrate once more that the new method mentioned below based on Internet and GPRS positioning using RTK and VRS. The transmission of VRS data based on the Internet is a communication method which is being tested and discussed, regarding the results of the field tests made using the Romanian Positioning System, GNSS system named ROMPOS, in order to evaluate the performance of the suggested system.

2. GENERAL PRESENTATION OF THE VIRTUAL REFERENCE STATIONS (VRS) USED IN ROMÂNIA

This paper will present the VRS used in Romania and of the NTRIP utilitarian together with the Internet, when transmitting data.

In order to create data at a virtual reference station from the observations in the Real Reference Stations National Network, there are a number of processing steps which must be taken in order to reach the data. The first step is to solve the double-difference phase ambiguities between the network's stations.

One can observe that the double-difference phase ambiguities between the network's stations must be known, together with the precise coordinates for the reference stations.

The reference stations' coordinates can be provided by the Geodesy Department, through the National Geodesy Fund service, in the case of a permanent national and regional reference network for the National Network of Permanent Stations. Alternatively, these coordinates can be obtained through a static measurement on every station over long periods of time, using also the traditional long-area effect procedure for static positioning. However, even with a precision of the known coordinates, it is not easy to establish ambiguities between reference stations for the real-time network, because time is short and the stations are at approximately 60-70 km away from each other.

In order to support the RTK positioning method, the whole ambiguities of the double-differences between the reference stations of the network must be solved in real-time, because these ambiguities should be instantly recalculated in case the satellite constellation changes and new satellites appear, or the connection with the ones located in the receiving area is lost or the delay is longer for the received data. At this point, an adjusted residual Kalman filter is suggested, to solve the double-difference phase ambiguities between the stations of the observed network, filter which has the ability to be used in real-time. This method, using the Kalman filter, is based on data which was received at previous dates and not only in current ones.

So as to help in solving the ambiguities in the network process, the error caused by orbits can be reduced or eliminated using type IGS orbits, ultra-fast predictable Orbit (IGU), instead of emissive orbits. Exact ephemeredes can be obtained from GPS International Service (IGS), ephemeredes centers, which include a day of predicted orbits.

After the double-difference ambiguities associated with reference stations have been established at their correct values, the terms for the so-called correction for atmospheric deviations regarding the troposphere and ionosphere and other errors can be generated as residual in the L1 and L2 phase measurements from satellite to satellite and from one date to another(G.R. Hu et al, 2002). The purpose of these corrections is to reduce the influence of spatially correlated errors. This means that, when the user applies corrections to the code and the phase observations, the influence in the atmospheric errors and other errors shall be reduced or eliminated. This leads to improving the positioning performance in the network in which it is calculated and the measurements are made. There are numerous methods to set corrections for the user paper mentioned above showed that performance, regardless of the method used, is the same.

In the following step, the VRS data for user receivers are generated because it is necessary. In order to generate VRS data if there were no reference station at the user's location, the approximate position of the user and the position of the user related to this VRS, in relation to the transport carrier and the pseudo-range observations at the master reference station must be geometrically moved and improved, by applying corrections to the network according to the approximate position of the user, namely the VRS position. The approximate position of the user can be obtained through absolute GPS positioning or positioning code.

The approximate position of the user can be obtained through absolute GPS positioning or by using the codes.

After this, the VRS data are generated as a RTCM or CMR format and are then transmitted to the users. In order to generate VRS data we need to fulfill three steps. The first step is to solve the double-difference ambiguities for phase measurements in real-time, between the stations in the network inside of which the work occurs. The second step is to generate correlations for a satellite used as a base satellite, date by date for the users of the network in which the measurements are made, according to the user's approximate position. The third step is to transform the VRS data into RTCM format or CMR messages, by applying correlations to the master reference station data and by then sending them to the location requested by the users as VRS data. VRS data are then transmitted to the user as unique RTK correlations of the reference station for the receiver. The receiver can then use these correlations as if there were a unique approach of the reference station for RTK.

3.THE VIRTUAL REFERENCE STATIONS (VRS) HAVE MORE WAYS OF TRANSMITTING THE DATA FOR A VERY ACCURATE POSITIONING.

An efficient communication connection is essential for Virtual Reference Station (VRS) and for RTK positioning, because the transfer in due time (real time) of the VRS data is necessary for such a system. The communication connection

must insure reliability in transferring the data and should not cause any significant delay in the transmission time. It is expected that, also, the links are to be without restrictions, so as to cover a wide range of users. Up to now, there are a number of practical manners of distributing the VRS data to users in real time, like GSM and the Internet (Hada et al, 1999;. Vollath et al, 2000;. Liu şi Gao, 2001; Ko et al , 2001).
In the case of a developed mobile telephone network, the easiest transmission mechanism is GPS technology, because it holds the lowers risk of data loss. A mobile phone allows the bi-directional communication between a user and the data control center of the VRS, so, the user can transmit his approximate position to the control center.

Other advantages include the fact that there is no need to apply radio frequencies which are limited to the maximum power of 1 wat, and the low cost of installing this system. One of the disadvantages of GSM is the limited number of users at the same time dictated by the control center, because each GSM line can only support a single user, but there is some software which simulates more users (the Trimble Company). Another important disadvantage of GSM is its high price, because the user must be constantly logged while the RTK system with VRS is being used.

There is, also, the possibility to use the Internet as a data connection between the control center and the user. The Internet is the worldwide network system which is, and will become, the most important means of common communication, mostly viewed from the point of view of its fast data transmission rhythm, and the opening to an unlimited number of users. The Internet uses bi-directional communication and, because of this, the user can also send his approximate position and his requests to the control center, and then the control center can provide data to the Virtual Reference Station (VRS) for the request of each user according to his approximate position.

With the Internet's increased capacity and recent developments in communications technology, especially in what concerns GPRS technology, the Internet is a trustworthy choice for transmitting GPS data of the VRS type for RTK positioning, through a GPRS. Using the GPRS technology we can send and receive information directly from the Internet, the media for transferring the VRS data through the Internet being favorable, and much cheaper than the GSM telephone media. As a result, a GNSS system with Virtual Reference Stations (VRS) and Real Time Kinematic (RTK) through the Internet is being used in Romania and it is a NTRIP type (the system was developed by a specialized university in Germany). This system uses GPRS technology as a communication connection between the control center which is coordinated by the ANCPI and administrated by ROMPOS and the stations which are made use of by the users.

Fig.1. Setup of Internet-based VRS RTK positioning via GPRS (G.R. Hu et al, 2002).

Consequently, a GNSS system with Virtual Reference Stations (VRS) and Real Time Kinematic (RTK) through the Internet is being used in Romania and it is a NTRIP type (the system was developed by a specialized university in Germany). This system uses GPRS technology as a communication connection between the control center which is coordinated by the ANCPI and administrated by ROMPOS and the stations which are made use of by the users.

The observation files for each reference station are transmitted to a control center (ANCPI-ROMPOS), using the Internet. The user is equipped with a RTK receiver and a pocket PC with GPRS or a mobile phone, as shown in Illustration no. 1. This user uses the client software to connect to the control center server (ANCPI-ROMPOS) through GPRS Internet, and his approximate position is transmitted to the control center. The control center software (ANCPI-ROMPOS) automatically receives the user's approximate position and selects the closest reference station for the user as a master reference station (the permanent stations in the A class GNSS Network or the A class EUREF stations). The raw data from the reference station are then corrected as a geometrical position and improved by applying network corrections according to the user's approximate position. This is in a VRS data format, which is then transmitted as RTCM or CMR messages to the user's receiver through the GPRS Pocket PC serial port, at a rate of 9,600 bps or greater.

The receiver can then use these messages as is the case with the unique reference RTK stations.

Six testing points in the North and North-West part of Romania (Class A stations), with different distances from the master reference station have been used in order to test the new communication method, as shown in fig.2. Using the Internet and GPRS are of good omen and they bring a level of novelty and at the same time a saving in what concerns the price of data transmissions.

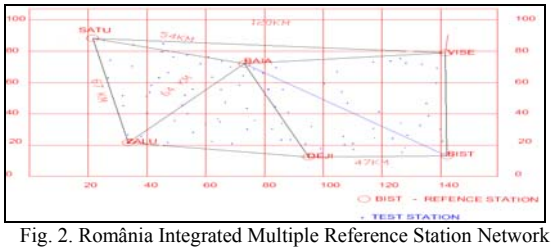

Fig. 2. România Integrated Multiple Reference Station Network (ROMPOS) and Internet-based VRS RTK test stations

The test site of the testing center identified as ȚAPU is considered to be the first example, 17,3 km away from the BAIA master reference station. A Leica 1200 with a dual receiver frequency was used together with a GX1230 antenna. This test was carried out in the time interval 10:23-15:45 UTC (12:23-17:45 local time), on July 25st 2010.

The real-time positions during the test have been continuously recorded in the receiver's memory. As a result, the real base position could be calculated before, if the connection to raw data is made.

The standard deviations (interior precision) of East path and North, and the height elements are 0.015m, 0.012m and 0.024m. As it was expected, the standard deviation in the horizontal position is a factor with 1,5-2 better than in height. The reason for the significant compensation in the height element is caused by the troposphere residual delay, which has a much greater effect than the horizontal coordinates.

One can observe that 99% horizontal (2D) position precision is smaller than 2 cm and 99% vertical position precision is smaller than 4 cm.

Besides precision, a crucial factor in using the operational usage of the RTK GPS is the speed with which it can initiate (e.g. to solve complete ambiguities). This is expressed as TTF (Time To Fix) or TTFA (Time To Fix Ambiguities) value (Edwards et al, 1999; Wübbena et al 2001). TTF of RTK refers to the observation moment which is required in order to solve complete ambiguities in real-time, after re-initiation.

Six seconds after each successful fix – or 2 minutes at the most, if the fix did not take place – the RTK receiver engine is totally reset. In consequence, a TTF analysis was possible. For the ȚAPU radio station, the time of the test series TTF for RTK vs. the number of satellites and a HDOP value.

The initiation time and the precision were analyzed on all testing stations which were used. In this section, the six trial stations were compared in order to evaluate performance based on Internet VRS with RTK positioning in different locations in Romania, and the results are presented in Table no.1.

Test Station	Distance from Master Reference Station (km)	Standard Deviation (m)		
		Northing	Easting	Height
ȚAPU	17.3	0.015	0.012	0.024
SEINI	20.3	0.015	0.024	0.040
TURȚ	20.7	0.016	0.017	0.038
FELDRU	12.3	0.013	0.015	0.039
ODOREU	4.2	0.012	0.005	0.021
JIBOU	25.3	0.011	0.016	0.046

Initiation is much more difficult when there is a greater PDOP value and fewer satellites. The reason for greater dispersion at certain times is the weak satellite geometry, which leads to a higher PDOP value. It is responsible on many occasions, because ambiguities have to be set each time.

4. CONCLUSIONS AND SUGGESTIONS

The precise RTK positioning on longer distances requires a GNSS reference stations network, which presently has an average density of 60-70 km between them. In Romania, the Romanian Positioning System named ROMPOS has been used for almost 2 years. It is based on Internet with the use of VRS and RTK technology, GPRS positioning infrastructure and NTRIP which was developed and is used in Romania. The active operation of the multiple reference stations network in Romania and the various field tests in different locations in Romania confirmed the fact that horizontal precision is much better, roughly 2-3 cm, and the vertical one still depends on an exact determination of the quasi-geoid with 2-5 cm precision, which can occur with an initiation time of less than 1-2 minutes.

Based on the Internet, the system which uses VRS and RTK real-time positioning technology has a precision of centimeters and is used at the level of services in constructions, fast topography and GIS. With a better communication through the wireless technologies and RTK positioning using multiple VRS reference stations if used, we will be able to see it being used, very soon, in different domains across the world and especially in Romania.

REFERENCES

[1] Chen X.M., Han S.W., Rizos C., Goh P.C. (2000) *Improving real-time positioning efficiency using the Singapore Integrated Multiple Reference Station Network (SIMRSN)*, Proc 13th Int. Tech. Meeting of the Satellite Division of the U.S. Inst. of Navigation, ION GPS-2000, Salt Lake City, September 19-22, 9-16.

[2] Fotopoulos G., Cannon M.E. (2001) *An overview of multi-reference station methods for cm-level positioning*, GPS Solutions 4(3): 1-10.

[3] Han S.W. (1997) *Carrier phase-based long-range GPS kinematic positioning*, Ph.D. dissertation, rep. UNISURV S-49, School of Geomatic Engineering, The University of New South Wales, Sydney, Australia.

[4] Hu G.R., Khoo H.S., Goh P.C., Law C.L. (2002) *Testing of Singapore Integrated Multiple Reference Station Network (SIMRSN) for precise fast static positioning*, Proceedings of the European Navigation Conference-GNSS2002, 27-30 May, Copenhagen, Denmark, CD-ROM.

[5] Muellerschoen, R., W. Bertiger, M. Lough (2000) *Results of an Internet-Based dual-frequency Global Differential GPS System*, Proceedings of IAIN World Congress in Association with the U.S. ION 56th Annual Meeting, San Diego, California, June 26-28, 2000.

[6] Teunissen P.J.G., Kleusberg A. (eds) (1998) *GPS for Geodesy*. 2nd enlarged edn. Springer, Berlin Heidelberg New York.

[7] Vollath U., Buecherl A., Landau H., Pagels C., Wager B. (2000) *Multi-base RTK positioning using virtual reference stations*, Proc 13th Int. Tech. Meeting of the Satellite Division of the U.S. Inst. of Navigation, ION GPS-2000, Salt Lake City, September 19-22, 123-131.

[8] Wanninger L. (1997) *Real-Time differential GPS-error modeling in regional reference station networks*, Proc. of the IAG Scientific Assembly, Rio de Janeiro, Sep. 1997, IAG-Symposia 118, Springer Verlag, 86-92.

[9] Wübbena G., Bagge A., Schmitz M. (2001) *RTK network based on Geo++@ GNSMART-concepts, implementation, results*, Proc 14th International Technical Meeting of the Satellite Division of the Institute of Navigation, Salt Lake City, USA, ION GPS-2001, September, 368-378.

2011 International Conference on Mechanical, Industrial, and Manufacturing Engineering
Lecture Notes in Information Technology Vols. 1-2

RENEWABLE ENERGY AND COMPOSITES.DESIGN OF BICONVEX REFRACTIVE SOLAR CONCENTRATORS.

José Ignacio Pérez Calero

Mechanics of Continuous Media Department, ETS of Architecture at University of Seville.
Avenida de Reina Mercedes, nº 2. Sevilla. 41.012. Spain.
perezcalero@us.es

***Abstract* - The present work tries to study the important role which they carry out the Composites, in the complex process of the design of solar refractive concentrators, that would be unthinkable and unrealizable without their employment, when having necessary the technical characteristics that they make them viable. It contributes, also, the methodologies followed for the accomplishment of optimal prototypes, by means of Numeric Methods of simulation (Finite Elements), experimental on models and of characterization of composite laminates.**

Keywords: Composites, Composites Characterization, Numerical and Extensometric Methods, Optimal Structural Designs, Solar Energy.

I. INTRODUCTION

For the design of Refractive Solar Concentrators (RSC) we need a sophisticated methodology, which has multiple and important applications. Its construction is inconceivable without the use of composites, so that it is necessary to take into consideration their specific technical characteristics so that they will be viable. For that reason, to solve this question, we shall find a general methodology for their design and study based on refractive phenomenon. We will search for simple and light designs, mass-produced, in most cases, using generally fluids as refractive element, especially water. In this article we will deal with biconvex designs, thing or thick, working on paraxial zone or not, and with multiple apertures. We will consider any captive plane, focal or not. The choice of of biconvex models is based on the optimization for real prototypes

This investigation deals with theoretical analysis of every Refractive Solar Concentrators' biconvex model, by optical-informatic simulation of the solar rays. The conclusion obtained is that we find optimal design based on fundamental definition parameters [1].

On the other hand, this investigation line is intrinsically related, as we showed in our works [2], to the design and construction of real models of fluids storage deposits on plastic materials with spherical surfaces. Those designs entail additional problems because it is necessary to store big amounts of liquids in deposits with very thing walls (in order to reach correct refractive interphases) and almost transparent, essential for practical applications. The analysis is made by numerical and experimental process. To solve the technical requirements it is necessary the use of composites with a matrix of polycarbonates reinforced with E glass fibers, which guarantee resistance, economy and transparency requirements. We need to know the mechanical-resistant behaviour of the models' membrane, in order to design the surfaces to be reinforced with fibers, taking into account the small stress and strainth tolerance compatibles with the optimal prototypes to be built state of service. We will study the models designed just with the matrix, we will analyze their behaviour and deduce the quantity, volumetric relation and interphase with the matrix and distribution of reinforcing fibers, for a later study once placed, making an strict characterization of laminated materials to be use with the verification of their proper work, in the second supposition, with the solicitations needed in each situation and according to International Standards.

II. THEORETICAL ANALYSIS METHODOLOGIES.

The methodology used takes us to a multiple analysis for each studied part of the work. For the analysis of general models, we use a mixed one. In one hand, an analytical-theoretical study in the optical-mathematical field of the three-dimensional solar rays beam, incidents to the system in any position relative to them, until their intersection with desired captive planes. In the other hand, a computer simulation, on the basis of different parameters, geometrical and physical that allows us to know the general behaviour of any prototype makes the study. Figures 1 and 2 show the diagrams obtained by this methodology [3], they allow us to optimize the theoretical design of the desired refractive concentrate for its construction.

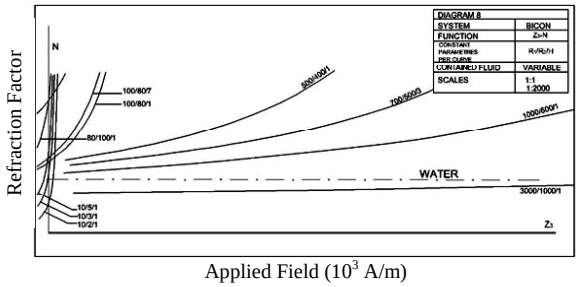

Fig. 1 Focal Plan Situation and Main Concentration Factor (η) -R2 diagrams.

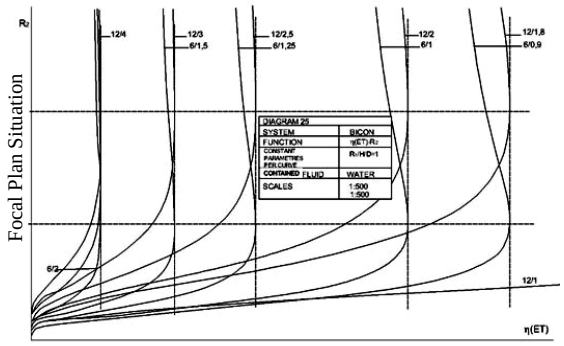

Fig. 2 Focal Plan Situation and Main Concentration Factor (η) -R2 diagrams.

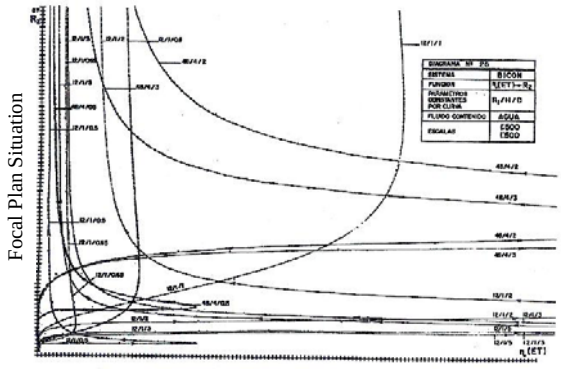

Fig. 3 Focal Plan Situation and Main Concentration Factor (η) -R2 diagrams.

For the important problem of the study of the mechanical behaviours of refractive concentrate simple models, it can be made in different ways, usually with a big mathematical complexity, so that we think that there are two clear methods for that research. First, the experimental process on reduced scale models, if necessary, of polycarbonate prototypes, with extensiometric gages fixed in different points in order to know the global behaviour of the prototypes. Furthermore, we have the informatic simulation based on F.E.M., consisting of discretising the model to analyze and the actions working on it [4].

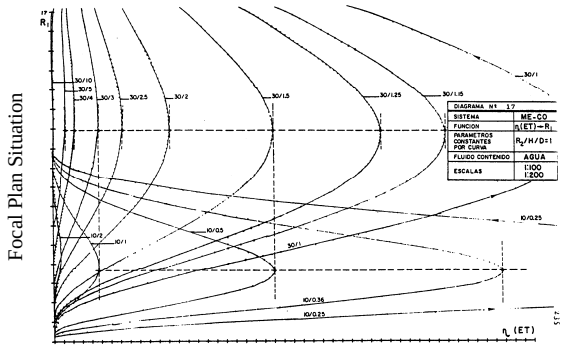

Fig. 4 Focal Plan Situation and Main Concentration Factor (η) -R2 diagrams.

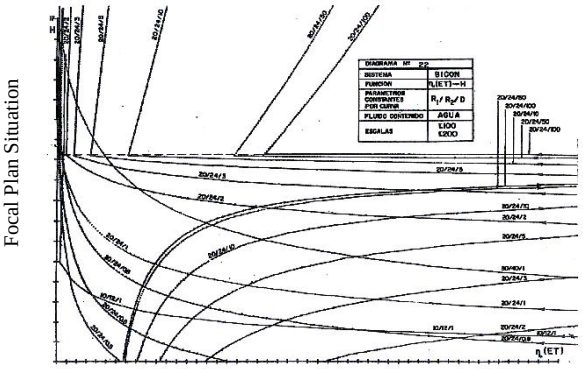

Fig. 5 Focal Plan Situation and Main Concentration Factor (η) -R2 diagrams.

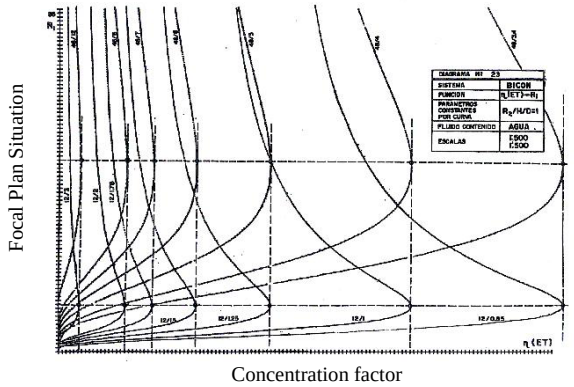

Fig. 6 Focal Plan Situation and Main Concentration Factor (η) -R2 diagrams.

Regarding the preceding, it is based on the theory that the conventional methods to calculate membranes and sheets, even Laplace formulation, are not able to be applied because of the studied problem considerations, so that to determine the orthogonal stress (usually called circumpherencial and meridional tensions on each shell) is necessary the indicated process. Both investigation ways are independent between them, although they can be complementary in order to reaffirm and to test the results obtained. In this work we will follow both methods for the objectives that we want to reach [5].

III. Service Considerations for the Models to be Design.

We will use prototypes with optimal designs, as shown, and we will choose those with diameters 59/79, being the first one the hemispheric surface. Obviously the methodology is universal, even if we analyze this special case. The fundamental service angle (horizontal in relation with the maximum common circle) shall be 45º, coincident with the standard working angle in our latitudes for Refractive Solar Concentrators, although the method is totally universal. The nodes will be placed in every 10º meridian and every 15º parallel, for the numerical process and every 30º meridians and parallels for experimental process.

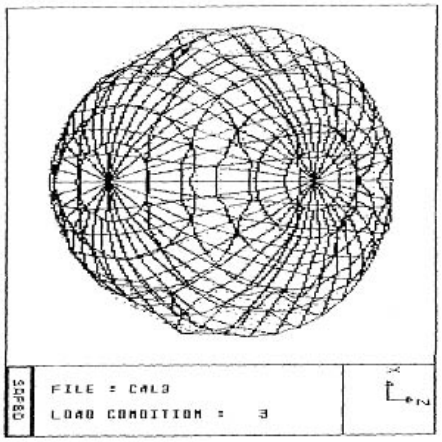

Fig. 7 Undeformed model

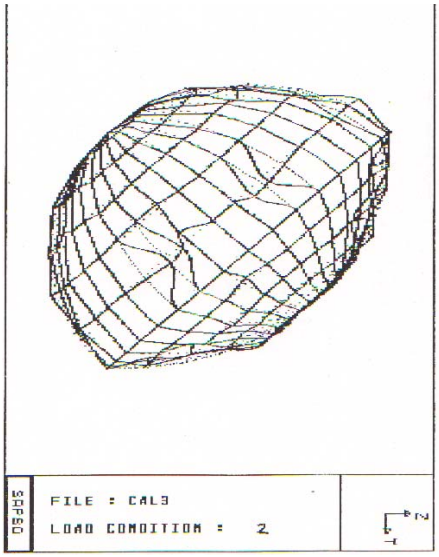

Fig. 8 Deformed model

In the prototype there are a perimetral closing belt and fixed supports connected to three points delimited in each case. Storage-models are defined with three-dimensional shell elements that contain 4 nodes, able to assume a membrane behaviour (in most cases) or sheet.

Analyzing the results obtained by informatic process we can generate discretized diagrams of efforts and deformations that are a guide, in every parameter, as detailed as desired, for the areas to be reinforced by E glass fibers. (Fig 7 and 8)

IV. Design by Numeric Process

We use the module SAP-2000, combination of programs linked by internal files that constitute a data base, every one of them operating upon one or more blocks of data entry, and providing different exit blocks.

The process of data entry is analyzed through ASCII files, with 13 blocks of which 6 have been used (Title, System, Joints, Restraints, Quad and Solid) that indicate the nodes and their possibilities of displacement or rotation in tree directions, the three-dimensional shells of four nodes and the three-dimensional solids of charge of 8 nodes. The exit files analyse and calculate the system for the different hypotheses of supposed load. The program incorporates a modulus called Saplot that makes it possible to visualize the deformations produced in the elements studied, which has been done for a better understanding with a rebound coefficient of 500 units [6].

The analysis of the results from the computer allows us to generate discretized efforts and deformation diagrams, that are the guide, as in detail as we need, for the zones to be reinforced with E glass fibers in a anisotropic behaviour of composite with the polycarbonate matrix in the model.

V. Treatment by Experimental Process

We have used a Strainmeter KYOWA SM-60-D and a Switching and Balancing Box SS-24-R, with possibilities for 60,120,350 and 500 Ohms and for 1,2 and 4 extensometric gages, which levelled to zero and tared with a piece of the same material allows to proceed to the measurement with everyone of the models (Fig 9).

In the case of the bi-convex models (that give the more interesting and useful results regarding the technological applications) we include the map of gages on both sides. In order to analyse the results of the most characteristic points, we tried first the model in a position of service with upper side A. Experimenting with the opposite position, the sudden breaking of the model is produced, which confirms the unavoidable need of its reinforcement, Fig. 5.2 showing the breaking lines that were produced, according to the previsions of the non-experimental methodology (Fig 10) [7].

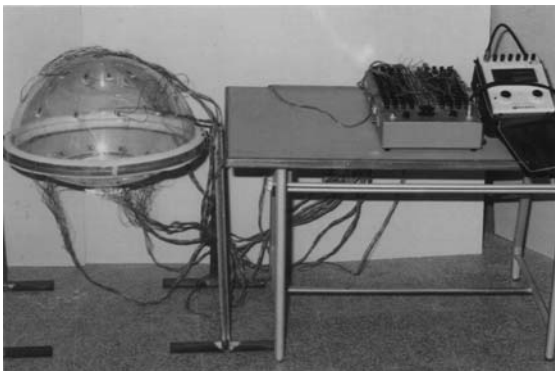

Fig. 9 Experimental process equipment

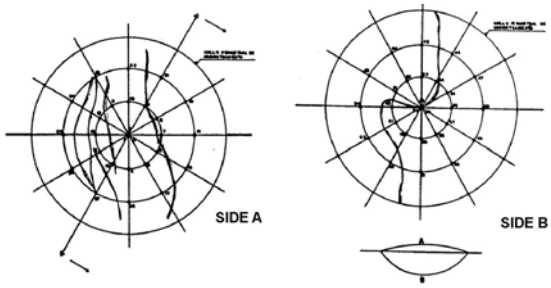

Fig. 10. Breaking Lines with upper side B.

VI. Composites characterization by tests

The reinforcements to make will materialize for the configuration of laminates bi or trhee-layers with short fibers, or exceptionally with random fibers. Since there are referenced, it is necessary to make a rigorous characterization of the final laminates to verify his perfect supposed operation of models in the last reinforced. They are had to make tests of flat traction, by means of a universal machine of tests. Also test of interlaminar traction (Daniel and Ishai, 1994) [8] with semicircular tube test, the Celanese load breakage test (although it would be possible also to be made by the Iitri method).

In general, it is not necessary to go to the interlaminar fracture tests, in order to verify the dislamination process in these composites. In extraordinary models, sufficient tools for the determination of the fracture tenacity exist, in the three possible ways of fissure extension, before arriving at the torn one. In all the cases is obligatory, the strict fulfilment of the International Standards, especially ASTM, ISO and UNE.

VII. Results and Conclusions.

In sum, we can assure the design and analysis of the biconvex Refractive Solar Concentrators (RSC) of spherical surfaces built into composites (generally made of polycarbonate with reinforcement of E glass fibers), allowing us to deduce the quantity, volumetric relation and ideal interphase [9], counting with strong methodologies of simulation and experimentation to meet Optimum Designs. In the same way, we can attain the construction of real prototypes with a powerful tool, the Finite Elements Method (FEM) and a powerful way of experimental support, by extensometric gages, that allows us to reach a three-dimensional "map" in detail (with a configuration and scale of ranges as tight and adjusted as we need) under the various hypothesis considered, either simple or combined, changeable according to our will. Thus, we can configurate the prototypes of the different systems that we wish to study and use in any case to respond to the technological needs that arise in this area, with enormous possibilities in various fields, specially in architectonic models for solar energy applications [10], as well as desalinisation process [11] and [12]

References

[1] Pérez Calero, J. I. Contribution to the study of solar concentrators by refraction static: application for Cuenca Baja del Guadalquivir. Th.D.. Madrid Politechnic University. Spain 1988.Pubications Secretariat at Seville University. ISBN 84-7405-550-4.1.991.

[2] Pérez Calero, J. I. Analysis and calculation of the composite refracted solar concentrators: prototyping. ISBN-84-920374-6-6. 2.006.

[3] Pérez Calero, J. I. Analysis and design of solar Refracted solar concentrators spherical configuration. Twin Edit. ISBN-920374-3-1, Sevilla, Spain; 1995.

[4] Pérez Calero, J. I. European Conference on Composites Materials ECCM-8. “Composites and Construction: Design of Solar Refractive-Concentrators Prototipes” Náples (Italy). Proceedings pp. 347-354. 1998.

[5] Miravete A. et al. Composite Materials II. Ino Reprod. Zaragoza. Spain. 2000.

[6] Pérez Calero, J.I. Numerical and extensometric methods for design of Refractive Solar Concentrators. International Journal of Renevable Energy. ISSN 0960-1481.. Vol 3. pp 1828-1831. USA.1996.

[7] Pérez Calero, J.I Design and calculation of optimal prototypes made composite refracted solar concentrators biconvex and analysis of the mechanical behavior, structural and functional. Proceedings XIV Iberian Congress y IX Iberoamerican Congress Energy Solar.pp 521-526.ISBN 978-84-612-4470-6. Vigo, Spain; 2008.

[8] Daniel, I. y Ishai, O. “Engineering mechanics of Composites materials” Oxford University Press. 1991.

[9] Wilson, D. W. and Carlsson, L. A., Physical methods of chemistry, 2nd edn. Vol.7, Determination of Elastic and Mechanical Propieties. Ed. John Wiley & Sons Inc..1991.

[10]Pérez Calero, J. I. Refracted solar concentrators: Proposals for Architecture and Urbanism. Magazine Era Solar nº 65: pp. 13-18.ISSN 0212-4157. Madrid, Spain. 1995.

[11]Pérez Calero, J.I. Composites in the Design and Calculation of Solar Refractive Concentrators Prototypes. Proceedings CCC 2001 Composites in Construction Internacional Conference, pp 777-781, Porto, Portugal; 2001.

[12]Pérez Calero, J.I. Composites in the design optimization of Biconvex Refractive Solar Concentrators. Study and calculation of prototypes. Congress "Energy and Enviroment Engineering and Management".Portalegre.Portugal 20009. Publications "Advanced Materials Research".Vol 107 pp. 71-75 .2010.Switzerland.

2011 International Conference on Mechanical, Industrial, and Manufacturing Engineering
Lecture Notes in Information Technology Vols. 1-2

Launch Bar Load Investigation during Off-center Catapult Launch of Carrier-based Aircraft

Hao Yu, Hong Nie, Xiaohui Wei and Ming Zhang
College of Aerospace of Engineering
Nanjing University of Aeronautics and Astronautics
Nanjing 210016, CHINA
yuhao@nuaa.edu.cn

***Abstract* - Considering the off-center position of carrier-based aircraft, a six-degree-of-freedom dynamics model of catapult launch is established. The launch bar load during off-center catapult launch is calculated. The effects of initial off-center distance and take-off weight on these launch bar load is analysed,while the kinetic reason of this phenomenon is also discussed detailed. From the catapult launch calculation, three important conclusions are obtained: the roll movement of the aircraft is the primarily reason of the bending moment and the torsion which act on the launch bar; the bending moment and the torsion are increased sharply with the increase of initial off-center distance, while the axle load is affected slightly; in the prophase of catapult launch, the launch bar load, including axle load, bending moment and torsion are all increased with the decrease of the take-off weight, but in the anaphase of catapult launch, these load are decreased with the decrease of the take-off weight.**

Index Terms* - *carrier-based aircraft; catapult launching; off-center distance; launch bar.

I. INTRODUCTION

The launch bar of carrier-based aircraft is an important bearing part which passes the catapult load and stabilizes the aircraft direction during the catapult launch process. When taxing along the midline of the steam-powered catapult, the plane moves in the vertical plane with only 3DOF, and the launch bar just bears axial pull load. But in fact, there is usually an initial angle between steam-powered catapult midline and aircraft at the very beginning of launch. The initial yaw angle leads to an off-center distance which makes the aircraft moving with 6DOF and the launch bar bearing very complex load during catapult launch process. The definition of off-center distance[1] is shown in Fig. 1, and (1) gives the relationship between initial yaw angle and initial off-center distance.

Where, A: nose landing gear location; B,C: main landing gear locations; d_y: initial off-center distance; L_1: horizontal distance between aircraft center of gravity(CG) and midpoint of two main landing gears; L_2: horizontal distance between aircraft CG and nose landing gear location; L_3: horizontal distance between nose and main landing gear; L_4: half of the horizontal distance between two main landing gears; ψ_0 : initial yaw angle of aircraft.

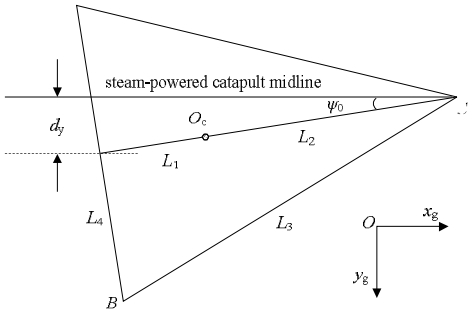

Fig. 1 Definition of initial off-center distance

$$\sin\psi_0 = d_y / (L_1 + L_2) \tag{1}$$

This article deals with the launch bar load during off-center catapult launch process. To achieve this goal, a 6DOF dynamics model is developed. With this model, the launch bar load is investigated, and its dynamics reason is also analyzed.

II. MODELING OF OFF-CENTER CATAPULT LAUNCH

During the off-center distance catapult launch, the launch bar bears not only the axial load but also bending moment and torsion. To calculate these load, 6DOF dynamics model of off-center distance catapult launch is essential.

From the consideration of the forces acting on the aircraft, the forces analysis is shown in Fig.2.

Where, F_{cx}, F_{cy}, F_{cz}: components of catapult force in geodetic coordinate; F_{mf1}, F_{mf2}: friction force between deck and main landing gear tires; F_{nf}: friction force between deck and nose landing gear tires; g : gravity acceleration; m :mass of aircraft; N_{m1}, N_{m2} :vertical force act on main landing gear tires; N_n: vertical force act on nose landing gear tires; O_c: CG of aircraft; O_c' : O_c projection in plane $Ox_g y_g$ of geodetic coordinate; Q: drag force act on aircraft; S_{m1}, S_{m2}: side force act on main landing gear tires; T: engine thrust; T_c: couple act on the launch bar along x_g axis of geodetic coordinate; Y: lift force act on aircraft; Z: side force act on aircraft; z_c : height of aircraft CG ; θ_{s1}, θ_{s2}: yaw angle of main landing gear tires.

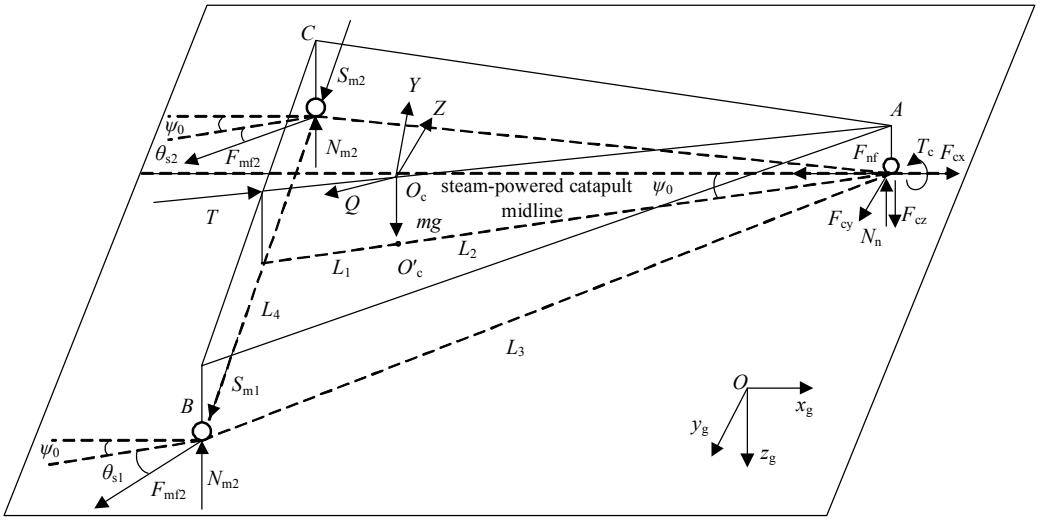

Fig. 2 Analysis of the force act on the aircraft during off-center catapult launch

According to Fig.2, the equations of motion based on Newton law Ⅲ and the theorem of angular momentum are shown in (2)～(7):

$$\begin{aligned} ma_{xg} &= F_{cx} - F_{nf} + (S_{m1} + S_{m2})\sin\psi_0 \\ &\quad - F_{mf1}\cos(\theta_{s1} + \psi_0) - F_{mf2}\cos(\theta_{s2} + \psi_0) \\ &\quad + (1 \quad 0 \quad 0)\mathbf{A}^{gb}(T \quad 0 \quad 0)^T \\ &\quad + (1 \quad 0 \quad 0)\mathbf{A}^{gq}(-Q \quad Z \quad -Y)^T \end{aligned} \tag{2}$$

$$\begin{aligned} ma_{yg} &= F_{cy} + (S_{m1} + S_{m2})\cos\psi_0 \\ &\quad + F_{mf1}\sin(\theta_{s1} + \psi_0) + F_{mf2}\sin(\theta_{s2} + \psi_0) \\ &\quad + (0 \quad 1 \quad 0)\boldsymbol{A}^{gb}(T \quad 0 \quad 0)^T \\ &\quad + (0 \quad 1 \quad 0)\mathbf{A}^{gq}(-Q \quad Z \quad -Y)^T \end{aligned} \tag{3}$$

$$\begin{aligned} ma_{zg} &= -N_n - N_{m1} - N_{m2} + F_{cz} + mg \\ &\quad + (0 \quad 0 \quad 1)\boldsymbol{A}^{gb}(T \quad 0 \quad 0)^T \\ &\quad + (0 \quad 0 \quad 1)\boldsymbol{A}^{gq}(-Q \quad Z \quad -Y)^T \end{aligned} \tag{4}$$

$$\begin{aligned} I_{xg}\dot{\omega}_{xg} &= -F_{cy}z_c - F_{cz}L_2\sin\psi_0 + N_nL_2\sin\psi_0 \\ &\quad - N_{m1}(L_1\sin\psi_0 + L_4\cos\psi_0) - S_{m1}z_c\cos\psi_0 \\ &\quad + N_{m2}(L_4\cos\psi_0 - L_1\sin\psi_0) - S_{m2}z_c\cos\psi_0 \\ &\quad - [F_{mf1}\sin(\theta_{s1} + \psi_0) + F_{mf2}\sin(\theta_{s2} + \psi_0)]z_c \\ &\quad + T_c + (1 \quad 0 \quad 0)\boldsymbol{A}^{gq}(M_x \quad M_y \quad M_z)^T \end{aligned} \tag{5}$$

$$\begin{aligned} I_{yg}\dot{\omega}_{yg} &= F_{cx}z_c - F_{cz}L_2\cos\psi_0 - F_{nf}z_c + N_nL_2\cos\psi_0 \\ &\quad - [F_{mf1}\cos(\theta_{s1} + \psi_0) + F_{mf2}\cos(\theta_{s2} + \psi_0)]z_c \\ &\quad + S_{m1}z_c\sin\psi_0 - N_{m1}(L_1\cos\psi_0 - L_4\sin\psi_0) \\ &\quad + S_{m2}z_c\sin\psi_0 - N_{m2}(L_1\cos\psi_0 + L_4\sin\psi_0) \\ &\quad + (0 \quad 1 \quad 0)\boldsymbol{A}^{gq}(M_x \quad M_y \quad M_z)^T \end{aligned} \tag{6}$$

$$\begin{aligned} I_{zg}\dot{\omega}_{zg} &= (F_{cx} - F_{nf})L_2\sin\psi_0 + F_{cy}L_2\cos\psi_0 \\ &\quad + F_{mf1}(L_4\cos\theta_{s1} - L_1\sin\theta_{s1}) - S_{m1}L_1 \\ &\quad - F_{mf2}(L_1\sin\theta_{s2} + L_4\cos\theta_{s2}) - S_{m2}L_1 \\ &\quad + (0 \quad 0 \quad 1)\boldsymbol{A}^{gq}(M_x \quad M_y \quad M_z)^T \end{aligned} \tag{7}$$

Where, a_{xg}, a_{yg}, a_{zg} : components of *CG* acceleration in geodetic coordinate; $\dot{\omega}_{xg}, \dot{\omega}_{yg}, \dot{\omega}_{zg}$: components of angular acceleration of aircraft in geodetic coordinate; I_{xg}, I_{yg}, I_{zg} : moment of inertia of aircraft in geodetic coordinate; M_x, M_y, M_z : rolling, yawing and pitching moment act on aircraft; $\boldsymbol{A}^{gb}$: conversion matrix from body-fixed coordinate to geodetic coordinate; $\boldsymbol{A}^{gq}$: conversion matrix from aerodynamics coordinate to geodetic coordinate.

The launch bar connect the nose landing gear through a gimbal, as shown in Fig.3.

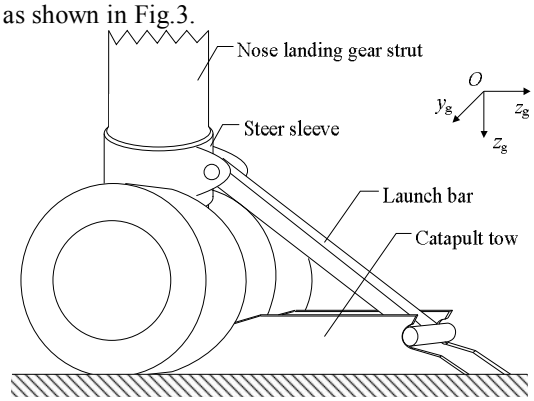

Fig. 3 Engagement systems of nose landing gear, launch bar and catapult tow fitting

This kind of connection restricts the rolling movement of aircraft around axis x_g , so (5) should be rewritten into a balance equation:

$$I_{xg}\dot{\omega}_{xg} = 0 \tag{8}$$

Conversion (5)～(8) from geodetic coordinate into body-fixed coordinate:

$$\begin{pmatrix} I_x\dot{\omega}_{xb} \\ I_y\dot{\omega}_{yb} \\ I_z\dot{\omega}_{zb} \end{pmatrix} = \boldsymbol{A}^{bg} \begin{pmatrix} 0 \\ I_{yg}\dot{\omega}_{yg} \\ I_{zg}\dot{\omega}_{zg} \end{pmatrix} \tag{9}$$

Where, $\dot{\omega}_{xb}, \dot{\omega}_{yb}, \dot{\omega}_{zb}$: components of angular acceleration of aircraft in body-fixed coordinate; I_x, I_y, I_z : moment of inertia of aircraft in body-fixed coordinate.

Launch bar connects the catapult tow with a rotation joint, the force act on the launch bar in launch bar coordinate $Ox_cy_cz_c$ is shown in Fig.4.

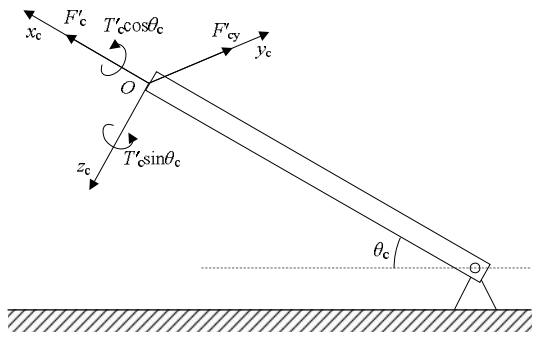

Fig. 4 Analysis of the load acting on the aircraft

Where, θ_c : catapult angle; F'_c : launch bar axial load; F'_{cy} : side force act on launch bar; T'_c ：couple act on launch bar.

$$F'_c = -F_c = -F_{cx}/\cos\theta_c \tag{10}$$

$$T'_c = -T_c \tag{11}$$

III. Solution of Equations of Motion

To solving the dynamics model, the landing gear load and the attitude of aircraft are essential.

A. Vertical force act on the landing gear tires:

The equations of motion of unsprung mass are:

$$N(s_t) - F_a(u) + F_h(\dot{u}) = m_{us}\ddot{s}_t \tag{12}$$

Where, $N(s_t)$: vertical force act on the landing gear tires; $F_a(u), F_h(\dot{u})$: pneumatic and hydraulic force of the landing gear; m_{us} : unsprung mass of landing gear; s_t : vertical tire deflection; u : landing gear stroke.

The relationship between the stroke of landing gears and aircraft attitude are given by:

$$\begin{cases} u_n = u_{n0} + d_z - L_2(\theta - \theta_0) - s_{nt} \\ u_{m1} = u_{m0} + d_z + L_1(\theta - \theta_0) + L_4(\gamma - \gamma_0) - s_{m1t} \\ u_{m2} = u_{m0} + d_z + L_1(\theta - \theta_0) - L_4(\gamma - \gamma_0) - s_{m2t} \end{cases} \tag{13}$$

Derivative of (13) are:

$$\begin{cases} \dot{u}_n = \dot{d}_z - L_2\dot{\theta} - \dot{s}_{nt} \\ \dot{u}_{m1} = \dot{d}_z + L_1\dot{\theta} + L_4\dot{\gamma} - \dot{s}_{m1t} \\ \dot{u}_{m2} = \dot{d}_z + L_1\dot{\theta} - L_4\dot{\gamma} - \dot{s}_{m2t} \end{cases} \tag{14}$$

Where, θ_0 : initial pitch angle of aircraft; $\dot{\theta}$: pitch angular velocity of aircraft; γ_0 : initial roll angle of aircraft; $\dot{\gamma}$: roll angular velocity of aircraft; u_{n0}, u_{m0} : initial stroke of nose and main landing gears; d_z : vertical displacement of aircraft CG in geodetic coordinate; u_n, u_{m1}, u_{m2} : nose and main landing gears stroke; s_{nt}, s_{m1t}, s_{m2t} : vertical tire deflection of landing gear tires.

B. lateral friction of tires:

$$\begin{cases} F_{nf} = N_n\mu_1 \\ F_{mf1} = N_{m1}\mu_2 \\ F_{mf2} = N_{m2}\mu_2 \end{cases} \tag{15}$$

Where, μ_1 : friction coefficient between nose landing gear tires; μ_2 : friction coefficient between main landing gear tires.

C. side force act on tires

According to the test investigation of pneumatic tire[2], side force and tire yaw angle could be written as follows:

$$S = \begin{cases} \left[1.2(s_t/D) - 8.8(s_t/D)^2\right] C_c\left(p + 0.44p_R\right)W^2\theta_s \\ \qquad\qquad s_t/D \le 0.0875 \\ \left[0.0764 - 0.34(s_t/D)\right] C_c\left(p + 0.44p_R\right)W^2\theta_s \\ \qquad\qquad s_t/D > 0.0875 \end{cases} \tag{16}$$

Where, S : side force act on tire; D : tire diameter; W : tire width; p : actual tire pressure; p_R :rated tire pressure; θ_s : tire yaw angle; C_c : tire yawing coefficient, which depends on tire type.

Relationship between tire yaw angle and tire velocity is shown in Fig.(5).

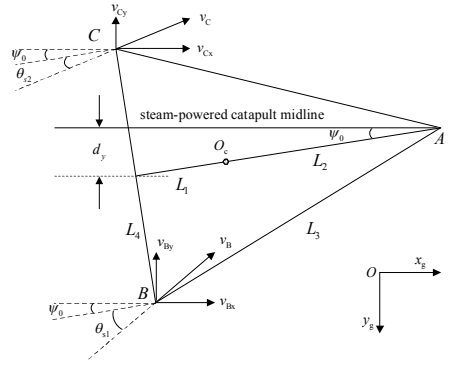

Fig. 5 Relationship between slip angle and tire speed

$$\theta_{s1} = \arctan\frac{v_{By}}{v_{Bx}} - \psi_0 \tag{17}$$

$$\theta_{s2} = \arctan\frac{v_{Cy}}{v_{Cx}} - \psi_0 \tag{18}$$

Where, v_B : velocity of tire B ; v_{Bx}, v_{By} : components of velocity of tire B in geodetic coordinate; v_C : velocity of tire C ; v_{Cx}, v_{Cy} : components of velocity of tire B in geodetic coordinate.

D. aircraft attitude calculation

The relationship between rotating angular velocity of aircraft around body-fixed coordinate and the aircraft attitude could be written as follows:

$$\begin{pmatrix}\dot{\phi}\\ \dot{\theta}\\ \dot{\psi}\end{pmatrix} = \begin{pmatrix}1 & \sin\phi\tan\theta & \cos\phi\tan\theta\\ 0 & \cos\phi & -\sin\phi\\ 0 & \dfrac{\sin\phi}{\cos\theta} & \dfrac{\cos\phi}{\cos\theta}\end{pmatrix}\boldsymbol{\omega} \tag{19}$$

The attack angle and sideslip angle are necessary for calculating the aerodynamic force act on the aircraft.

When $-\frac{\pi}{2} < \alpha < \frac{\pi}{2}$, there is:

$$\begin{pmatrix}\dot{\alpha}\\ \dot{\beta}\end{pmatrix} = \begin{pmatrix}\omega_y\\ \dfrac{\omega_z}{\cos\alpha}\end{pmatrix} \tag{20}$$

The aircraft attitude angle could be easily derived from (19) and (20).

The 6DOF dynamics model of off-center distance catapult launch could be solved from simultaneous (1)～(20).

IV. Parameter Studies

In the calculation of this model, the catapult force is shown in Fig.6:

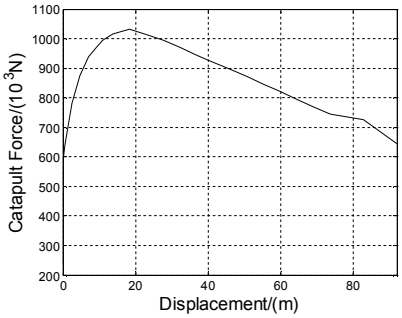

Fig. 6 Catapult force vs. launch stroke

A launch bar load analysis

Refer to Fig.3, launch bar torsion and bending moment are composed by the couple T_c' and the side force F_{cy}':

$$T_{bar} = T_c' \cos\theta_c \tag{21}$$

$$M_{bar} = T_c' \sin\theta_c + F_{cy}' L_{lbar} \tag{22}$$

Supposing the initial off-center distance $d_y = 0.61\text{m}$, gross weight $m = 30,000\text{kg}$, the two components of (22) are shown in Fig.7 :

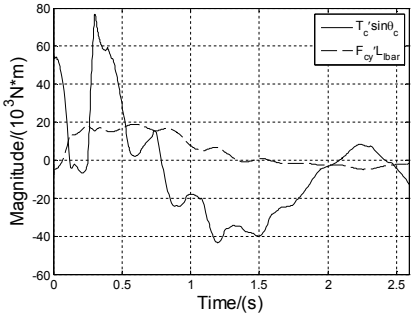

Fig. 7 Time histories of components of bending moment

Where, $T_c' \sin\theta_c$: bending moment produced by couple T_c'; $F_{cy}' L_{lbar}$: bending moment produced by side force F_{cy}'.

In the whole catapult process, bending moment produced by side force F_{cy}' is just $1/3 \sim 1/4$ the bending moment which produced by couple T_c' at most. So the most part of the bending moment acting on launch bar is caused by the component of couple T_c'.

It can be readily seen from the connection between nose landing gear and launch bar in Fig.3 that the couple T_c' along axis x_g is caused by the aircraft rolling movement, while the yawing movement causes the side force F_{cy}' along axis y_g. So, the rolling movement of aircraft which caused by the initial off-center distance is the main reason which caused the launch bar bending moment and torsion during the off-center catapult launch.

B effect of the initial off-center distance

According to Ref.[1], $d_y \le 24\text{inch}$. So, in this part, assuming the initial off-center distance to be 0m , 0.3m , 0.61m , 1.04m, gross weight $m = 30,000\text{kg}$.

According to the theory in 3A, the rolling movement of aircraft is the main reason which caused the launch bar bending moment and torsion. The effects of the initial off-center distance on the rolling movement of aircraft is shown in Fig.8:

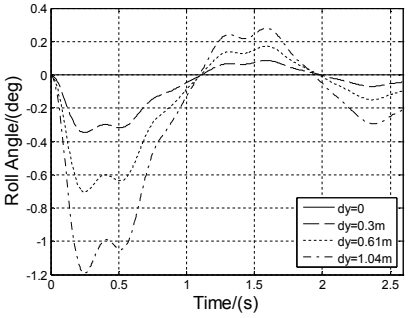

Fig. 8 Time histories of aircraft roll angle

The rolling angle increases with the increasing of d_y, while the launch bar bending moment and torsion have the similar trend in Fig.9, Fig.10.

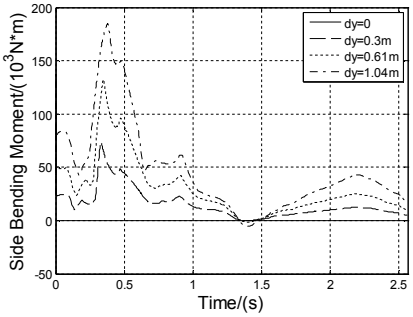

Fig. 9 Time histories of launch bar bending moment

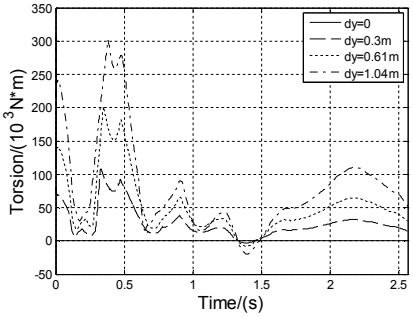

Fig. 10 Time histories of launch bar torsion

With the increasing of off-center distance, the launch bar bending moment and torsion increases sharply. When d_y is assumed to be equal to 0.61m which mentioned in Ref.[1], the bending moment and torsion are $90.2\text{kN}\cdot\text{m}$, $130.4\text{kN}\cdot\text{m}$. When d_y exceeds that value to be 1.04m, these load increase to be $144.7\text{kN}\cdot\text{m}$ and $210.7\text{kN}\cdot\text{m}$, both of the amplitude of these load exceed 50%.

The initial off-center distance has slight effect on the pitching movement of aircraft and the catapult angle θ_c, as shown in Fig.11, Fig.12. With the same catapult force, it can be readily seen from (10) that the initial off-center distance almost has no effect on the launch bar axial load as shown in Fig.13.

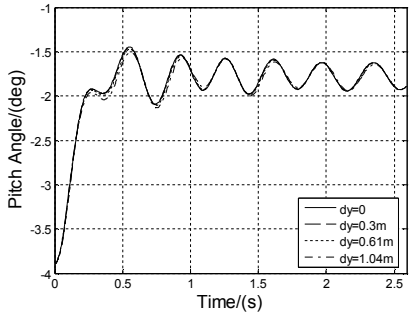

Fig. 11 Time histories of aircraft pitch angle

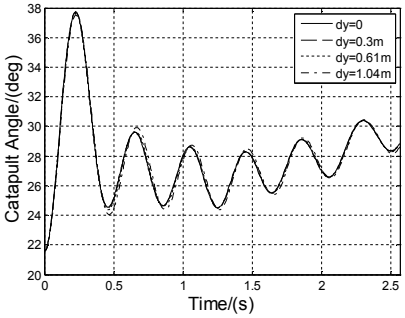

Fig. 12 Time histories of catapult angle

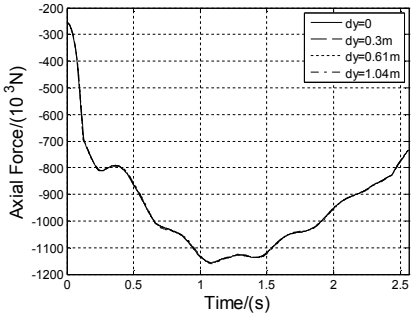

Fig. 13 Time histories of launch bar axial load

C effect of the gross weight of aircraft

The gross weight of aircraft is one of the most important factor of catapult launch. Assuming the gross weight to be $25,000\text{kg}$, $30,000\text{kg}$, $33,000\text{kg}$, d_y to be 0.61m in this part. The histories of rolling movement of aircraft, launch bar bending moment and torsion are shown in Fig.14～Fig.16.

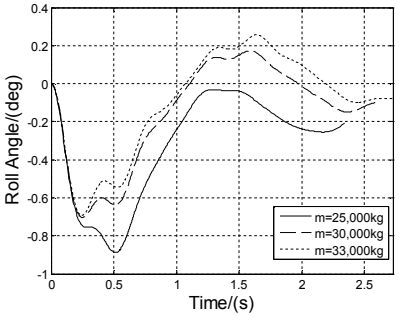

Fig. 14 Time histories of aircraft roll angle

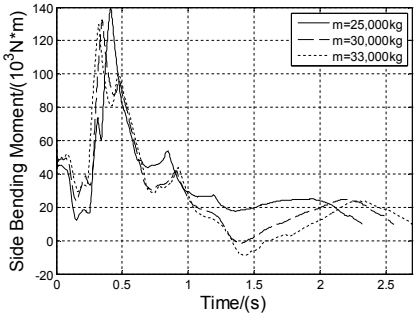

Fig. 15 Time histories of launch bar bending moment

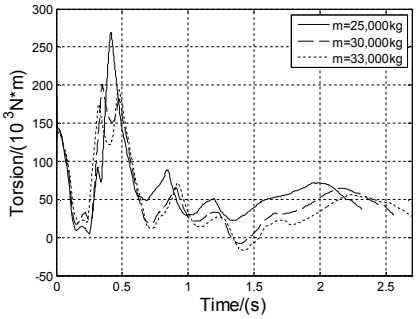

Fig. 16 Time histories of launch bar torsion

From the definition of moment of inertia, the magnitude of moment of inertia represents the stability of the rotating state of object. So it is more difficult to change the rotating state of object with larger magnitude of moment of inertia. In the initial stage of catapult(before 1s～1.5s), lesser gross weight caused biggish rolling movement. The launch bar bending moment and torsion are decreasing with the increasing of gross weight, and achieve the peak value of the whole process. After the initial stage, the rolling movement of smaller gross weight aircraft attenuates rapidly, while the bending moment and torsion are both decreasing with the decreasing of gross weight.

The launch bar axial load has the similar trend with bending moment and torsion, as shown in Fig.17.

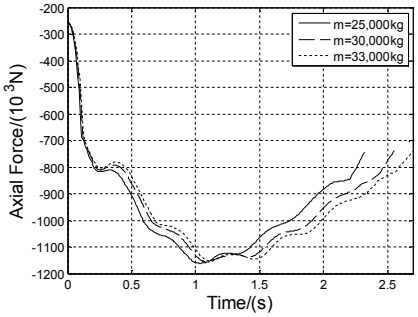

Fig. 17 Time histories of launch bar axle load

In the initial stage of catapult, launch bar axial load decreasing with the increasing of gross weight, while the load decreasing with the decreasing of gross weight after the initial stage.

V. CONCLUSION

In this paper, a 6DOF dynamics model of catapult launch is established with the considering of the off-center position of carrier-based aircraft. From analysis of the model, we obtain conclusions that:

(1) The roll movement of the aircraft is the primarily reason of the bending moment and the torsion which act on the launch bar;

(2) The launch bar bending moment and torsion increase sharply with the increasing of initial off-center distance, while the initial off-center distance has almost no effects on launch bar axial load;

(3) The gross weight has different effects on the launch bar load(launch bar axial load, bending moment and torsion) in different catapult stage: during the initial stage of catapult, all of the launch bar load decrease with the increasing of gross weight, while after the initial stage, these load decrease with the decreasing of gross weight.

ACKNOWLEDGMENT

The authors acknowledge research support under the National Natural Science Foundation of China under grant number 51075203 and NUAA Research Funding, NO. NS2010023.

REFERENCES

[1] "Launching System, Nose Gear Type," Aircraft[S]. MIL-L-22589D(AS). 1991, 10: 3, 16.

[2] Robert F.Smiley, Walter B.Horne, "Mechanical properties of Pneumatic Tires with Special Reference to Modern Aircraft Tires," Langley Research Center, pp. 33-35.

2011 International Conference on Mechanical, Industrial, and Manufacturing Engineering
Lecture Notes in Information Technology Vols. 1-2

Experimental Investigation in Strength Properties of Prestressed Steel Wires under High Temperatures*

Qingxiang Fu and Wei Hao
Department of Environmental Engineering
Shandong Water Polytechnic
Xueyuan Road No.677, Rizhao, Shandong Provice, P.C. China
Fu-qx@126.com.cn

Sha Sheng and Kesen Chen
Department of Civil Engineering
Changyi Bureau of Communications
Beihai Road No.671, Changyi, Shandong Provice, P.C. China
cks111@126.com

Abstract: **This paper aims at conducting research on the strength variation of prestressed steel wires (f_{ptk} = 1570Mpa) under high temperatures commonly used in the prestressed structural engineering. We obtained the ultimate strength and the yield strength of prestressed steel wires under different stresses—at different temperatures using the self-designed high-temperature trial furnace testing steel wires and the deformation measuring device to perform the experiment, and meanwhile obtained the theoretical fitting comparison expression through the theoretical regression. The achievement can be applied in the correlation calculation of the prestressed concrete structure under high-temperature conditions, and it also provides some references for further study on high-temperature resistance properties of the reinforced concrete structure and its damage assessment.**

Keywords: prestressing force; steel wires; high-temperature; strength

Ⅰ. INTRODUCTION

No matter whether in terms of the legend of Prometheus stealing fire from heaven, or the story of Suiren discovering fire by drilling into wood, they have described a significant relationship between fire and humans. Fire can't be separated from human life and productions, however, the incontrollable fire may result in disasters. In addition to substantial losses to human life and property, the fire hazard may cause a serious damage on the building structure. Therefore, we have necessities in figuring out changes in carrying capacity of buildings during and after the fire, as well as the high-temperature effects on structural reliability. The previous experimental study data have drawn some regularity conclusions on properties of prestressed steel wires[1] [2] [3] [4] [5]under high temperatures, however, there is a marked difference among research results due to dissimilarity existing in testing methods, materials and types. Moreover, as the emphatic points of tests are different, no final conclusion has yet been reached on properties of prestressed steel wires, and researches on strength variation of prestressed steel wires (f_{ptk} = 1570Mpa) under high-temperature conditions is especially more scarce. Therefore, it is necessary to develop the systematic study on properties of carbon steel wires commonly used in prestressed architectural structure under high temperatures. Its significance will contribute to figuring out the basic mechanical characteristics of prestressed steel wires and analyzing properties and safety degrees of architectural structures under high temperatures.

Ⅱ. EXPERIMENTAL OVERVIEW

This experiment mainly studied high-temperature strength properties of prestressed steel wires in the ways of thermostatic loading. Experiment apparatus consists of three parts including loading system, heating and control systems, and measurement recording system. Among them, loading system used 100KN punching jacking apparatus; heating and control systems used the self-developed electric furnace for heating and the controllable transformer to control temperatures in the thermoelectric furnace.

This experiment adopted 7 groups of prestressed steel wires Φ5 (f_{ptk} =1570Mpa) altogether and each group in threes. We placed steel wire specimens into the furnace with both ends held tightly by clamping apparatus in testing machine, put a little tension in advance in order to fasten the steel wire, then fixed the dynamic displacement sensor plug well, and finally sealed the furnace mouth to start heating. There were 6 temperature stages including 200℃, 300℃, 400℃, 500℃, 600℃, 800℃. When the temperature was increased to a fixed one and maintained constant, we took continuous loads until specimens were damaged so that we could test their strength.

Ⅲ. EXPERIMENTAL RESULTS AND ANALYSIS

A. Apparent characteristics of steel wire specimens under different experimental temperatures

The surface color of prestressed steel wire specimens was similar to that at normal temperatures when the temperature was less than 300℃. In close proximity to destruction, there was no necking phenomenon. The surface color of specimens began to deepen and peel off, and generated the necking phenomenon at 400℃. The phenomenon of peeling off became more serious at 500℃, and the necking section

*This work is supported by SWP Grant #2008-10
978-0-9831693-1-4/10/$25.00 ©2011 IERI

began to become longer with plastic deformability decreasing. When the temperature reached 600℃, the surface of specimens became reddish with the necking section extending to the entire heated area, while partial necking phenomenon was no longer obvious, and the plastic deformation further decreased with both aciform and sharp cross-sections. The surface of specimens with hardly any carrying capacity appeared to be reddish black at 800℃, while plastic deformation was greatly increased. This phenomenon was mainly due to the recrystallization process performed by steel wires at the temperature with the result of keeping wires in a mesomeric and rheologic state[6] [7] [8].

B. Changes in strength index of prestressed steel wires under high temperatures

1) Ultimate strength

The ultimate strength value of prestressed steel wires under different temperatures should be taken as the maximum stress of the stress-strain curve[9] [10]. Graph 1 shows the curve of ultimate strength varying with temperatures. As the temperature increased, the ultimate strength of prestressed steel wires took on the tendency of descension. When the temperature ranged from the normal to 300℃, the strength of prestressed steel wire 1570 also increased slightly; however, in the range of 300 ℃ to 600 ℃, the ultimate strength reduced dramatically; when the temperature exceeded 600℃, the reduction extent began to slow down, while ultimate strength of prestressed steel wires became very low.

When the temperature reached 800℃, steel wires possessed hardly any carrying capacity, while its plastic deformation increased greatly. Seeing that the analysis of test results accomplished by Southeast University and Tongji University all considered temperatures within 600 ℃[2] [6] [7], this experimental result only analyzed the situation within 600 ℃ for the convenience of comparison.

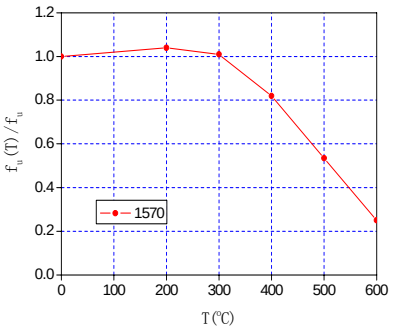

Fig.1 Variation curve of ultimate strength under different temperatures

2) Yield strength

The experimental result showed that f_y / f_u value of the prestressed steel wire（f_{ptk} =1570Mpa） reduced slightly at T=300℃; it was somewhat higher at T = 400 ℃; it reduced gradually at T> 400℃, with minimum value being basically about 0.7. In the fire-resistant structural design for the prestressed reinforced concrete, we used the yield strength of this calculation as the strength design index, and it should be multiplied by the coefficient as 1.2 for safety[9] [10]. Fig.2 shows the curve of yield strength varying with temperatures. As seen from the graph, the yield strength of reinforcing steel bar gradually reduced with the increase of temperatures.

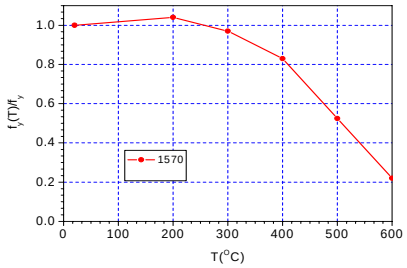

Fig.2 Variation curve of yield strength under different temperatures

3) Comparison of test results

By means of contrast between this experimental data and pertinent literatures[2] [6] [7], we have obtained results indicating: the yield strength of prestressed steel wires（f_{ptk} =1570Mpa） increased slightly due to " blue brittleness phenomenon" at 200℃, while that of other steel products all reduced with a smaller decline, which showed there being a little change in the mechanical property of steel wires within 200℃; the yield strength further reduced at a slightly higher rate at 200℃ ~ 300 ℃; the strength reduced at a accelerated rate with temperature increasing when it exceeded 300℃, and there appeared to be a roughly linear relationship. The variation trend of experimental data was consistent with that of regression curve drawn through the prestressed steel wire test executed by Tongji University[2] [10]（Fig.3）.

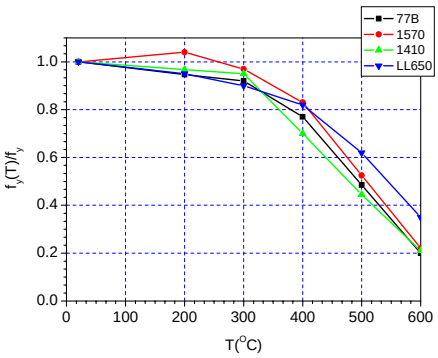

Fig.3 comparison of strength change of the reinforcing steel material under high temperatures

Ⅳ. STRENGTH EXPRESSION OF PRESTRESSED STEEL WIRES

Based on the experimental data results, we obtained the expressions of ultimate strength and yield strength of prestressed steel wires（f_{ptk} =1570Mpa） under high temperature through regression analysis.

1）Ultimate strength

$$f_{ptk,T} = 〔1.01+6.94\times10\text{-}5\ (T\text{-}20)〕\ f_{ptk}$$
$$20℃ \leqslant T \leqslant 300℃ \qquad (1)$$

$$f_{ptk,T} = 〔1.77\text{-}2.59\times10\text{-}3\ (T\text{-}20)〕\ f_{ptk}$$
$$300℃ < T \leqslant 600℃ \qquad (2)$$

Where:

$f_{ptk,T}$ is ultimate strength of prestressed steel wires under different temperatures;

f_{ptk} is ultimate strength of prestressed steel wires under the normal temperatures;

T is the temperature of steel wire specimens.

2) Yield strength

$$f_{0.2,T} = 〔1.01\text{-}6.42\times10\text{-}5\ (T\text{-}20)〕\ f_{0.2}$$
$$20℃ \leqslant T \leqslant 300℃ \qquad (3)$$

$$f_{0.2,T} = 〔1.73\text{-}2.56\times10\text{-}3\ (T\text{-}20)〕\ f_{0.2}$$
$$300℃ < T \leqslant 600℃ \qquad (4)$$

where:

$f_{0.2,T}$ is yield strength of prestressed steel wires under different temperatures;

$f_{0.2}$ is yield strength of prestressed steel wire under the normal temperature;

T is the temperature of steel wire specimens.

V. CONCLUSION

(Ⅰ)The yield strength of prestressed steel wires increased slightly due to “blue brittleness phenomenon” at 200℃, which showed that there was a little change in the mechanical property of steel wires within 200℃; the yield strength and ultimate strength increased as temperatures increased in general.

(Ⅱ) The strength induced at an accelerated rate with the temperature increasing and appeared to be a roughly linear relationship when temperature exceeded 300℃.

(Ⅲ) We established the theoretical curve expression of high-temperature yield strength and ultimate strength of prestressed steel wires heated after being constantly loaded.

REFERENCES

[1] Xiong Xiangjun, Current Status and Prospect of Study on Structural Fire Resistance Performance of Reinforced Concrete, Sichuan Building Science, 1999

[2] Hua Yijie, Study of Fire Response and Fire Resistance of Prestressed Concrete Structures, PhD Thesis of Tongji University, 2000

[3] Li Ming, Zhu Yongjiang, Wang Zhenglin, Mechanical Properties of prestressed reinforcement and nonprestressed reinforcement under high temperatures, Journal of Chongqing Jianzhu University, 1998

[4] Lie T T, Celikkol B., Method to Calculate the Fire Resistance of Circular R. C. columns, ACI Material Journal, 1991

[5] Yan Huiqun, Wang Qingyuan, Yan Ning, On the Performances of Reinforced Concrete Structure under and after Elevated Temperature, Journal of Chongqing Jianzhu University, 2003

[6] Lue Tongguang, Experimental Investigation of Material Properties and Deformation of Steel Bars After High Temperatures, Master's Thesis of Tsinghua University, 1996

[7] Guo Zhenhai, Shi Xudong, Elevated Temperature Performance and Calculation of Reinforced Concrete,Tsinghua University Press, 2002

[8] Guo Zhenhai, Li Wei, Experimental Investigation on Deformation Test and Constitutive Relation of Concretes at Different Stresses - Elevated Temperatures, China Civil Engineering Journal, 1993

[9] Lu Chunsen,Qu Lijun, Xue Wuping etc., Fire-resistant Design of Construction Structures, China Building Materials Industry Press, 1995

[10] Cai Yue, Study on Calculation Theory and Fire-resistant Design of Prestressed Concrete Structure Subjected to Fires, PhD Thesis of Tongji University, 2003

2011 International Conference on Mechanical, Industrial, and Manufacturing Engineering
Lecture Notes in Information Technology Vols. 1-2

A Hybrid Genetic &Ant-colony Algorithm for Fuzzy Petri Net Parameter Optimization Problems*

Bo Shi
Department of Computer Science
Jining University
Xingtan Road No.1, Qufu Shandong Provice, P.C. China
Smith1220@163.com

Li Liu, Jun Cao and Kesen Chen
Department of Environmental Engineering
Shandong Water Polytechnic
Xueyuan Road No.677, Rizhao Shandong Provice, P.C. China
cks111@126.com

***Abstract*：In the process of establishing fuzzy Petri net, how to determine the parameters of fuzzy production rules is a hot issue which is yet to be resolved. This paper proposes a HAGA algorithm which combines ant colony algorithm with genetic algorithm. Simulation results show that this algorithm has strong generalization ability and adaptive capability which can achieve the purpose of parameter optimization.**

Key words*：*fuzzy Petri net*；*ant colony algorithm*；*genetic algorithm*；*parameter optimization

1. INTRODUCTION

Fuzzy Petri net(Fuzzy Petri Net, FPN) is a good model tool based on fuzzy production rules and knowledge base system, it has obvious advantage for knowledge representation and reasoning . Currently use methods for its parameter optimization research work has obtained the certain result [1-3], but in generalization ability on unsatisfactory. This paper will ant colony algorithm and genetic algorithm is proposed, which combines fuzzy Petri nets parameter optimization HAGA method, simulation experiment shows that the algorithm is suitable for various FPN model, through the learning and training FPN model has a strong generalization ability and adaptive function, and can achieve the parameters optimization targets.

2. FUZZY PETRI NET AND FUZZY REASONING FUNCAITON

2.1The formal definition of fuzzy Petri net

Defining 1:A misty Petri net can be defined as follows with the 7 dollars set formalization: FPN=(P,T, I(p, t), O(t,p), τ (t), f(t), S0(p))

Among them:

The P is a limited set of fuzzy place crunode ;

The T is a limited set of fuzzy transition crunode ;

The I(p,t) is a fuzzy relation with marked on P x T (sum settle importation quantity ik, conjunction strength α k ,importation strength calculation function S), namely: I(p,t):P x T →(ik,αk), among them: αk∈ [0,1];

The O(t, p) is a fuzzy relation of marking on T x P (the sum certainly outputs quantity oj, conjunction strength βj, output strength calculation function R), namely: O(t,p):T x P->(oj,βj), among them: βJ∈[0,1];The τ(t) is a real amount function From T to[0,∞),in order to describe the worth τ on each change crunode ;

The f(t) is a nonnegative function, as well be called the change crunode T appearance to transfer control function;S0(p) is a real amount function from P to [0, ∞), which used in token of each place crunode the Initial marking state at the beginning of misty Petri net circulates.

2.2 fuzzy production rules

The fuzzy production rules is used to describe each the fuzzy relation between propositions, generally can described for:

if di then dk (CF = u,τ,w)

among them

dj =< dj1,dj2,…,djm > is precondition of "and" conjunction and "or" conjunction;

dk =< dk1,dk2,…,dkn > is Conclusion proposition.

u is rule sure degrees, τ is rule threshold, w is rule weights.

For multi-input multi-output fuzzy rules can be divided into many input and single output of fuzzy rules. Here only giving and rules and or rules FPN model, as shown in figure 1.

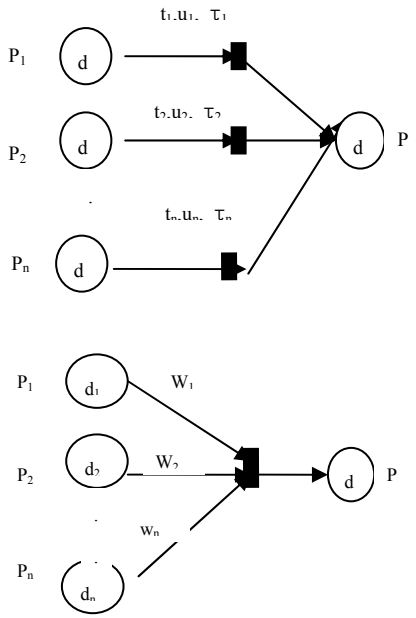

Figure 1 and rules & OR rules 's FPN model

*This work is partially supported by JNXYJXF Grant #2009jx16 and JNXYKYF Grant #2010ky21

Definition 2 : if transition t meet the following formula, says transition t is enabled.

$$\sum_{i=1}^{n} M(p_{ij}) \times w_{ij} \geq \tau(t)$$

t ∈ T, if pij ∈ I(t),

Transition enabled can ignite. When Transition t ignited for fuzzy reasoning, all marking values in t unchanged, to transmit new marker value $u \times \sum_{i=1}^{n} M(p_{ij}) \times w_{ij}$ to the output place. To "and" rules and "or" rule, transfer marker value to output place results in different. Following definition computation or rules teleport to output place's token values.

Definition 3: if place is the output place of more transition ti (i=1, 2,…n),the marked value M (p)obtained by the place p is the biggest one in n values transmitted.

$$M(p) = \max(u_1 \times \sum_{i=1}^{n} M(p_{1j}) \times w_{1j}, u_2 \times \sum_{i=1}^{n} M(p_{2j}) \times w_{2j}, \ldots\ldots, u_n \times \sum_{i=1}^{n} M(p_{nj}) \times w_{nj}$$

Judge transition enabled problem is transformed into a continuous function, whether meet some requirements independent variable and makes fuzzy reasoning result is a handy first-order derivation of continuous function Sigmoid function, establish the change of continuous functions and maximum operation lit continuous functions.

2.3 fuzzy reasoning funcaiton

Set y (x) is a Sigmoid type function, b is a constant, y (x) expression for:

$$y(x) = \frac{1}{1+e^{-b(x-k)}}$$

When b is big enough,then have the following two situations:

When x>k, $e^{-b(x-k)} \approx 0$,then have y(x)≈1;

When x<k, $e^{-b(x-k)} -> \infty$,then have y(x) ≈0

Therefore, binary value of continuous function y (x) is used as flag of whether transition can be enabled.

2.3.1 Change lit continuous function is established

From the above ,have $x = \sum_{i=1}^{n} M(p_{ij}) \times w_{ij}, k = \tau(t)$, then the function established judge of transition enabled:

When b is big enough,then have the following :

When x>k, y(x)≈1;shows the transtion t enabled; transmit the marked value $y(x) \times u \times \sum_{i=1}^{n} M(p_{ij}) \times w_{ij}$ to output place.

When x<k,y(x) ≈0;shows the transition t not enabled; transmit the marked value 0 to output place, that is ,the transition t is not ignited. On or rules, similarly you can establish the following maximum operation continuous function.

2.3.2 establish maximum operation of continuous functions

Use front y (x) function, set x1,x2,x3 for three output values when transition enabled. when b enough big, obviously the following deducing process was established .

$$g = \max(x_1, x_2) \approx \frac{x_1}{1+e^{-b(x_1-x_2)}} + \frac{x_2}{1+e^{-b(x_2-x_1)}}$$

$$h = \max(x_1, x_2, x_3) \approx \max(\max(x_1, x_2), x_3)$$

$$\approx \max(g, x_3) \approx \frac{g}{1+e^{-b(g-x_3)}} + \frac{x_3}{1+e^{-b(x_3-g)}}$$

By analogy, when more than one change can, corresponding to the output of the database p total can get a continuous biggest function values. Establish fuzzy reasoning function, can of fuzzy Petri nets and parameters of the learning and fixed

3. FUZZY PETRI NET PARAMETER OPTIMIZATION ALGORITHMS BASED ON ANT-COLONY& GENETIC ALGORITHM

3.1 establish fpn model

Using literature [2] the FPN model, specific described below:

Known place:p1, p2,p3,p4,p5,p6,p7,p8 respectively corresponds to the relevant proposition d1, d2,d3,d4,d5,d6,d7,d8 in an expert system, each proposition exists between the fuzzy production rules are as follows:

R1:if d1 then d2(u2,τ2)

R2:if d1 or d2 then d3(u1,τ1 ,u3,τ3)

R3:if d3 and d4 and d5 then d6(w1,w2 ,w3,u4, τ4)

R4:if d6 and d7 then d8(w4, w5 ,u5, τ5)

According to the fuzzy production rules, the establishment of FPN model shown in figure 2.

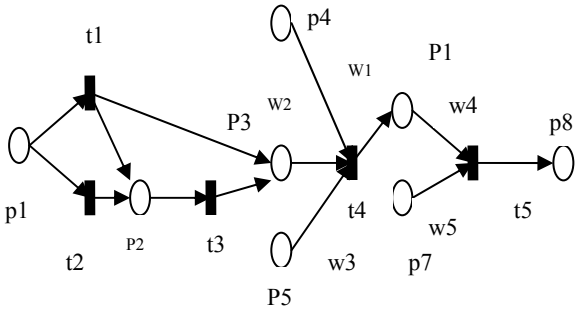

Figure 2 the establishment of FPN model

3.2 HAGA algorithm framework and principle

The genetic and ant colony algorithm combining, puts forward HAGA algorithm. The specific algorithm modules figure 3 shows.

Genetic algorithm (GA) by simulating natural selection and the survival of the fittest competitive strategies to solve the optimization problems. Its genetic operators include: selection, crossover and mutation, Genetic algorithm is the core content of the criterion by parameters of the code, initial group Settings, fitness function design, genetic operation design and the control parameters set constitutes. GA performance of global searching predominance, but in actual application is easy to produce premature convergence, later evolution search efficiency low defects.

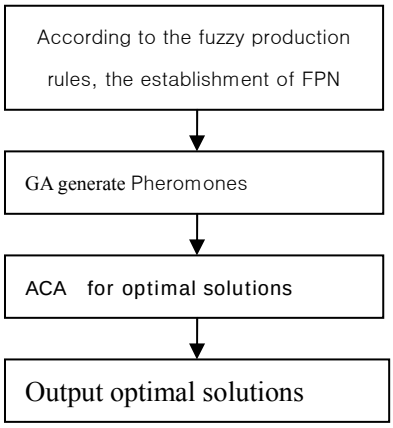

Figure 3 HAGA algorithm framework

Ant colony algorithm (ACA) simulation is the ant through the release of pheromone for looking for ant nest with food of the shortest path between this for a fact. Advance process, ants leave volatile pheromone, subsequent ants choose this path of probability and then this path is proportional to the pheromone strength. Ant colony algorithm in early operation period due to lack of pheromone, limiting the algorithm of the search efficiency, studies show that: the ant colony algorithm in the whole operation process accounted for about 65% of time, be used to form the optimal solution of information intensity.

Based on fuzzy Petri nets parameters optimization process HAGA algorithm is introduced, the combination of fusion reflect: using genetic algorithm generated pheromone distribution, reusing the ant colony algorithm for the optimal solution. The solving process combines the advantages of two kinds of overall algorithm. Better to overcome the defects of the respective algorithm, achieves the parameters optimization purposes.

3.3 HAGA algorithm implenment

3.3.1 Codeing

To accelerate the convergence of GA. In each of the transformation weights and sure degree and threshold by binary coding.

3.3.2 Fitness funcation

Set the initial population $\pi(0)$, chromosome ck,its fragment mark fk, then fitness function of the chromosome ck

Fitness(ck)= $k_1 \sum_{s=1}^{\lambda} f_{ks} + k_2(C_{\max} - time(c_k))$

Among them,fks represents the s-bit code values of fragment fk in chromosome ck ;| λ | represents the codeing length of fragment mark fk in chromosome ck,Cmax is a certain maximum of the selected,time(ck) represents delay sum for all the transition of the chromosome ck;k1,k2 is two constants and 0< k1,k2<1.

3.3.3 Selection operator

Proportional selection method is used as selection operator, namely in the t'st generation calculation process, the probability of chromosome ck selected in groups is proportional to its relative fitness $F(c_k)/\sum_{k=1}^{N} F(c_k)$, $\sum_{k=1}^{N} F(c_k)$ is the sum of individual fitness for population in the generation t.

3.3.4 Crossover operator

Crossover operator adopt partial matching crossover method, namely first according to evenly distributed generates two a string of intersection, choose this zone between two points for matching cross sections, and use position exchange operations cross sections of text exchange matching. One crossover probability PC = 0.6

3.3.5 Mutation operator

Selected individuals take reverse with mutation probability PM, including a PM = 0.2

3.3.6 Genetic algorithm termination conditions

In this algorithm, genetic algorithm and termination conditions is actually judgment fusion opportunity of genetic algorithm and the ant colony algorithm. Evolution in consecutive Genedie generation, if the daughter evolution rate are less than Genemin - improv - ratio ,then the algorithm terminates. Among them, Genedie = 3,Genemin-improv-ratio = 3% [4].

3.3.7 Ant colony algorithm for fusion

Pheromones initial value setting:In MMAS algorithm,each path pheromone initial set for maximum τMax. Here by genetic algorithm got certain path pheromone, so the pheromone initial set for: $\tau_{ij}^{S} = \tau_{ij}^{c} + \tau_{ij}^{G}$

Among them, τ_{ij}^{c} is pheromones constant for path (i,j), equal to the τmin of MMAS algorithm,set τ_{ij}^{c} =τmin = 60, τ_{ij}^{c} is the pheromone values for path (i,j) from genetic algorithm results converted, the initial value is zero. According to the result of the termination of genetic algorithm, calculate the fitness F (ck) of the chromosome ck (k = 1,2,…, m), if chromosome ck is composed by a sequence t1,t2,…, ti,tj,…,ts-1,ts,then the path (I,j) (i = 1, 2,…,s-1,j = i+1), add pheromone values τ_{ij}^{c} =F(ck)

Pheromones update model: in the pheromone update stage adopts the optimal - the worst ant colony algorithm thoughts, only to have the shortest path ants pheromone modify its increase. And all the path of trajectory update equations are used:

$$\tau_{ij}(t+1) = \begin{cases} (1-\rho)*\tau_{ij}(t) + \sum \Delta\tau_{ij}^{k}(t) \\ \tau_{ij}(t)_{\max}, if \tau_{ij}(t) > \tau_{ij}(t)_{\max} \\ \tau_{ij}(t)_{\min}, if \tau_{ij}(t) < \tau_{ij}(t)_{\min} \end{cases}$$

Among them, τij (t) Max and τ ij (t) min represents respectively path (i,j) pheromone's maximum and minimum; $\Delta\tau_{ij}^{k}$ (t) = Q/Zk, Zk is the path lengths for the ant k walked in this cycle,Q for a constant.

The ant transition probability: setting η ij for path (i,j) visibility, generally take for 1 /dij, here dij for path (i,j) in length, β (β >=0) for the relative importance of the path visibility, α (α >=0) for the relative importance of path trajectory,U for viable vertex set,

p_{ij}^{k} (t) for ants k in moment t of transition probability,then p_{ij}^{k} (t) can be defined as follows :

$$p_{ij}^{k}(t)=\begin{cases}\dfrac{\tau_{ij}(t)^{\partial}\eta_{ij}{}^{\beta}}{\sum_{l\in U}\tau_{il}(t)^{\partial}\eta_{il}{}^{\beta}}, j\in U\\ 0\end{cases}$$

4. THE SIMULATION RESULTS

According to the figure 2 FPN model to 15 parameters expectations hypothesis is as follows:
w1 =0.2，w2 =0.5，w3 =0.3，w4 =0.4，w5 =0.6，u1 =0.7，u2 =0.9，u3 =0.6，u4 =0.8，u5 =0.7，τ1 =0.3，τ2 =0.4，τ3 =0.2，τ4 =0.5，τ5 =0.4 .

ACA-BP algorithm for the performance of the same model for comparison, respectively, the ant colony algorithm, BP algorithm parameter optimization experiment. Among them, the ant colony algorithm optimal results parameters adapted in reference [2]

4.1 parameter optimization results comparison

The above three kinds of optimization algorithm run 10 times, take its average, using the mean square error (MSE) and to calculate the parameters obtained, sorting chart 1.

chart 1 Optimization of various parameters of optimization results comparison table

		1	2	3	4	5	MSE (10-3)
A	w	0.222	0.506	0.273	0.379	0.594	0.339
C	u	0.686	0.813	0.645	0.844	0.710	2.361
A	τ	0.379	0.441	0.300	0.481	0.424	2.655
G	w	0.305	0.433	0.427	0.471	0.493	9.669
A	u	0.777	0.763	0.767	0.793	0.737	13.10
	τ	0.295	0.337	0.310	0.356	0.313	8.866
H	w	0.194	0.441	0.376	0.398	0.514	0.178
A	u	0.865	0.767	0.658	0.788	0.658	0.337
G	τ	0.319	0.313	0.296	0.405	0.346	0.151
A							

4.2 generalization ability of testing

With single ant colony algorithm and genetic algorithm HAGA algorithm in comparison, weights, threshold and sure degrees were superior to separate the result of ant colony, genetic algorithm. So he parameters optimization algorithm for terms HAGA FPN parameter optimization get a satisfactory result.

With 5 groups of FeiYangben input data, to pass HAGA algorithm learning and trained FPN models for fuzzy reasoning, the results as shown in chart 2.

Chart 2 generalization ability of testing

no	Expect output	actual output
1	0.652 400	0.576 271
2	0.876 400	0.778 082
3	0.409 192	0.356 784
4	1.103 200	1.020 514
5	0.756 560	0.668 654
MSE(10-3)	0.181 007	

Reasoning results such as actual output shown in chart 2, reflects membership value of the M (p8) results proposition, the output value of mean square error and for 4.035 4 * 10-3, and the result is satisfactory.

5.SUMMARY AND PROSPECT

Combined with the existing literatures, the research idea based on ant colony and genetic algorithm is proposed.This fuzzy Petri nets parameter optimization algorithm respectively avoids the defects of the genetic & ant colony algorithm, and gives them a good combination together.The algorithm can be learning and training directly without strict layered by virtual place and virtual transtion for FPN which genarated by fuzzy production rules system. Simulation results show that this algorithm has strong generalization ability and adaptive capability which can achieve the purpose of parameter optimization.

REFERENCES

[1]. Bao Pei Ming. Petri nets learning ability fuzzy based on BP neural network [J].Chinese journal of Computer 94 (5) : 696-702.

[2].LiYang, LeXiao Bo. Ant colony algorithm Petri nets in fuzzy parameter optimization application [J]. Journal of Computer applications, 2007, 27 (3) : 638 -641.

[3].Zhou Kai Qing, Le Xiao Bo, TangMing. Ant colony and BP combined fuzzy Petri nets parameter optimization [J].Journal of system simulation , 2009,20 (s1) : 20-24.

[4].Zhang Wen,Xiu Liang Yi. the mathematical basis of Genetic algorithm [j].concrete: xi 'an jiaotong university press, 2006:10-57.

[5].Li Shi Yong.Ant colony algorithm and its application [M].Harbin:Harbin industrial university press, 2004:41-52.

[6]. Wu Zhe Hui. Introduction to Petri nets [M].Beijing: mechanical industry press, 2006:264-26.

[7].Yuan Chong yi,Petri nets Princple [M].Beijing:Electric industry press,1998.

[8]. Looney C G. Fuzzy Petri nets for rule2based decision mak2ing[J] . IEEE Trans Syst ,Man , Cybern , 1988 , 18 (1) :178～183.

[9].Chen SM,KeJS ,Chang JF. Knowledge representation using fuzzy Petri nets [J] . IEEE Trans Knowledge and Data Engineering ,1990 ,2 (3) : 311～319.

2011 International Conference on Mechanical, Industrial, and Manufacturing Engineering
Lecture Notes in Information Technology Vols. 1-2

Quality Control on the Making and Installation of Flat Slab Steel Gate*

Kesen Chen[1] and Yanxun Liu[2]
1.Department of Environmental Engineering
Shandong Water Polytechnic
Xueyuan Road No.677, Rizhao Shandong
Provice, P.C. China
cks111@126.com

Maosen Chen[2] and Shanshan Xu[1]
2. Shandong Provice Second Water
Conservancy Bureau
Jianshexi Road No.55, Yanzhou Shandong
Provice, P.C. China
106625586@qq.com

Abstract: **In this paper, we carried out a study on quality control in the process of making and installing flat slab steel gate. And a set of quality control standard for the key segments in the process, such as blanking, structural parts manufacturing, etc, was put forward. At the same time, the reasons for disqualification were also found by investigating 72 disqualified welding joints, and the main factors affecting the weld quality of CO_2 gas shielded arc welding were analyzed either, thus we proposed the welding technical parameter for all kinds of welding methods. Finally, after studying the quality control methods when installing steel gate, we brought forward the installation quality standard for both gate slot and steel gate.**

Keywords: **flat slab steel gate; making; installment; quality control standard**

1. INTRODUCTION

Nowadays, flat slab steel gate has been widely used in floodgate project for the purpose of water shielding. Flat slab steel gate is generally composed of deck, girder, and secondary beam, boundary beam, lifting lug, water seal devices and mobile equipment, etc, and they are usually connected by welding. Therefore, its making and installation are the important metal structural part in the whole construction process. Meanwhile, a higher degree of accuracy in making must be required, and the degree of permitted deviation should also be under strict supervision, mainly due to the need for shielding water and raising gate. Besides, the flatness of the deck can not easily meet the quality requirements even after finishing the whole making, as the gate deck is very thin [1-5]. In addition, the distance between gate girders is long, thus resulting in the unevenness on the deck surface and distortion of the central longitudinal baffle, as well as the uneven whole contraction in the parts of gate leaf, after entire welding. No wonder the welding deviation control has become the technical difficulty in gate making. In this case, we brought forward related technical measures after studying the flat slab steel gate production and its quality control of installation in industrial practice.

*This work is supported by SWP Grant #2008-06

2. QUALITY CONTROL OF STEEL GATE

Making steel gate should be operated in specialized metal workshop. We usually make steel gate section by section for the sake of convenient transportation (small gate may not be separated when making). And the whole assembling will be carried out in construction site after the transportation. The process for making steel gate is as follows: blanking→ making single component→assembling gate leaf →welding gate leaf→form regulation of gate leaf→ assembling attachment→ antisepsis. The overall welding of the gate will be operated after putting all the deck, secondary beam, girder, carling and boundary beam.

2.1 Blanking

1) Automatic incision machine will finish blanking if it is accurate in size after inspection, and stainless steel is incised by plasmon incision machine.

2) Those components that are incised by steel plate or section steel must meet the requirements listed in table 1 if there is no limit deviation of allowance size noted in construction drawings.

Table 1. Limit deviation value of dimensional tolerances

Fundamental dimensions/mm	Permitted deviation/mm	
	Incision	Edge of plane（mill）
≤1000	±2.0	±0.5
≥1000`2000	±2.5	±1.0
＞2000~3150	±2.5	±1.5
＞3150	±3.0	±2.0

3) The requirements of geometric tolerance for the surface incised when cutting steel plate or section steel are as follows: ① the deviation of straight line in lateral direction should be bigger than the length of arris by 0.5/1000, and should be bigger than 1.5mm;② the vertical deviation

in lengthwise direction should follow such rules as: If the thickness $\delta \leqslant 24$mm, then the vertical deviation is no more than 0.5mm. And if there is few and deeper cutting mark (deeper than 2mm), then welding is allowed. Welding should be operated on established welding standard, and welding slot must be planished after repair welding.

4) The lines set out when finishing assembling flat slab should keep the margin big enough for anther two incisions (50 mm should be left for the same side). And the requirements for blanking are: ① the deviation for either length and width is 0~2.0mm; ② the deviation for diagonal is 0~3.0mm.

2.2 The production of structural units

1) The points of Girder will be fixed on established working platform, and Automatic submerged arc welding machine will finish the job of welding if it is qualified after inspection. As for the form regulation, we use I beam form regulator to do that. If the distortion occurred in regional area, water and fire can be used to revise. And examination is also necessary after the revise. The requirements are as follows: the error for girder straight should be $<$ 3mm, distortion below should be $<$ 3mm, lateral distortion should be $<$3mm, distortion should be $<$2mm, regional unevenness of connection board should be $<$2mm/m, and the width of the connection board should be±2.0 mm. As for the flange slab, the width should be ±1.0mm, the verticality between the flange slab and the plate should be no more than 1.0mm margin. And the requirements for making clapboard are as the same as making girder.

2) Plane plate should be put together and then be butt joint on the platform.

3) When assembling and welding each component, we must weld each other in a stagger way with short welding slot at first; and next comes the long welding slot by welding each other exactly in straight line. And if there is more than one level; there will be correspondent levels of welding. In this way, the concentrated deviation caused by welding stress can be prevented.

4) If the distortion is severer than the permitted deviation after welding each parts, mechanical method or blaze method can be adopted for regulating.

5) Strict inspection for all the sizes must be carried out after the assembling. And all the qualified components should put in the area of "passed" for assembling sectioned gates. Automatic submerged arc welding machine will be used for further welding into certain form, and the welding slot belong to the second level. And the welding slot must be qualified under the examination of ultrasonic or ray crack detector. The welding slot must not be overlapped with other slots when assembling gate leaf, and should leave the distance between each other for at least 300mm.

2.3 The assembling of gate leaf

1) Assembling gate leaf should be operated on pre-set platform, and done section by section. Firstly, we must regulate the deck, and the concave convex degree should be kept within the extend of $\leqslant$3.0mm/m.

2) According to the requirements of the construction drawing, lines will be set out centered on cross shape to locate the accurate position of girder, secondary beam, boundary beam and clapboard for the convenience of overall assembling.

3) Put the pre-set girder, secondary beam, boundary beam and clapboard into pair based on the lines drawn on the deck, and the size should be kept within such extent as follows: the distance between girder and center is ±3.0mm, the dislocation for clapboard in lengthwise direction should be $<$ 2.0mm. All the pair should be made from the center to sides, and each position will be fixed when sizes are set within permitted area.

4) All components should be assembled in free state to prevent distortion caused by strong stress and welding. Under the smallest stress, the paired components should be put together as close as possible, and the gap between the pair should be less than 1.0mm (those parts requiring welding will be excluded).

5) The size will be inspected after assembling. The permitted deviation of thickness in gate leaf should be kept within ±3.0mm, and for the outside height of gate leaf, the permitted deviation should be kept within ±5.0mm, width ±5.0mm, diagonal should be $\leqslant$3.0mm, and gate leaf distortion should be $\leqslant$3.0mm.

6) If all the sizes inspected are accurate and precise, then welding will be followed. In the process of welding, we must weld each other in a stagger way with short welding slot at first; and next comes the long welding slot by welding each other exactly in straight line. And if there is more than one level; there will be correspondent levels of welding. In this way, the overall welding stress and distortion can be lessened.

7) Shape will be checked after welding gate leaf. If all the sizes are suitable, we will carry out the line setting to the flat slab plate for the second time centered on the original cross shape.

8) Inspection. The limit deviation for the final height of the gate leaf should be ±5.0mm, width ±5.0mm, diagonal $\leqslant$3.0mm, gate leaf distortion

⩽3.0mm (the one at the joint of girder and boundary beam), and gate leaf thickness ± 3.0mm, the regional flatness of the plane plate should be ⩽3.0mm per meter, lateral straight line of gate leaf should be no more than 3.5mm, lengthwise straight line should be no more than 2.0mm.

3. QUALITY CONTROL OF WELDING STEEL GATE

Welding is the key part of the whole process of making steel gate; therefore, the welding quality decides the quality of steel gate. When utilizing CO_2 gas shielded arc welding in the process, little stretch is desired, resulting in simplifying the operation of rectifying. At the same time, this method requires no slag crust cleaning, and has low sensitivity to oil and rust, enjoys high production efficiency. But the defect lies in the instability of welding line quality and poor forming of welding line. Thus we analyzed 72 disqualified welding lines and made a conclusion about the disqualifying reasons. We found that air hole and welding appearance quality is the main factors affecting welding quality in gas shielded arc welding (table 2). While the reasons causing air hole and influencing welding appearance mainly due to the poor welding technique, material quality and the technical level of operators. In addition, environment, machines should also be put into consideration.

Table 2 Classifications and statistics of the disqualification reasons from disqualified welding

Serial NO.	Types of effecting factors	frequency	Cumulative frequencies	Summation of percentage
1	Air hole	36	36	50%
2	Weld appearance	18	54	75%
3	Poor hot melting in Root of welding	8	62	86%
4	slag inclusion	6	68	94%
5	others	4	72	100%
		N=72		

Table 4 Technical parameter for the ship-sized fillet welding of submerged arc welding

Height of welds fillet （mm）	Welding Wire diameter (mm)	Welding current (A)	Welding voltage (V)	Welding speed (cm/min)
6	2	450~475	34~36	67
8	3	550~600	34~36	50
	4	575~625	34~36	50
10	3	600~650	34~36	38
	4	650~700	34~36	38
12	3	600~650	34~36	25
	4	725~775	34~38	33

Table 3 Technical parameter for CO_2 gas shielding welding

Slab thickness	Connector types	Level number	Welding condition			feed rate of welding wire （m/h）	Gas flow L/min
			Welding Wire diameter	current（A）	voltage（V）		
5~8	T type	1	1.2	280~320	25~30	210	8~10
	Butt joint	1		300~340	26~31	236	8~10
8~12	T type	The 1st level	1.2	220~280	22~26	190	8~10
	Butt joint	The 2nd level		300~340	26~31	236	8~10
10~16	T type	The 1st level	1.2	400~450	28~32	337	12~14
		The 2nd level		370~420	27~32	298	10~12
		After the 1st level		370~420	27~32	298	10~12
				350~400	26~31	265	10~12
14~20	Butt joint T type	The 1st level	1,2	220~280	22~26	190	8~10
		After the 1st level		300~340	26~30	236	8~10
				370~420	27~32	298	10~12
				400~450	28~32	337	12~14

Table 5 Technical parameter for submerged arc welding beveling double-welded butt joint

Slab thickness	Wire diameter (mm)	Welding sequence	Bevel size			Welding current (A)	Welding voltage (V)	Welding speed (cm/min)
			α(°)	h(mm)	g(mm)			
14	φ4	Front	70	3	3	830~850	36~38	42
		Back				600~620	36~38	75
16	φ4	Front	70	3	3	830~850	36~38	33
		Back				600~620	36~38	75
18	φ4	Front	70	3	3	830~860	36~38	33
		Back				600~620	36~38	75
22	φ4	Front	70	3	3	1050~1150	38~40	30
		Back				600~620	36~38	75
24	φ4	Front	70	3	3	1100	38~40	40
		Back				600~620	36~38	75

4. QUALITY CONTROL OF THE INSTALLMENT IN STEEL GATE

In order to stop the water with gate in the best way, we must keep the size of the gate slot within strict extend. AND the width of the gate slot can be smaller than the designed size by 1~2 mm, the gate opening can be larger than the designed one by 2~3mm. When installing the gate, we can regulate the verticality of the gate with the help of the straight line in gate slot. When gate is lowered to the bottom of gate slot, water will be poured for water blocking to prevent any damage to water block caused by overheat or scorch. As for those gates requiring two-side

water seal, the flatness of the water block deck in gate slot must be strictly supervised (the flatness should be within the extent of 1mm), in this way, the distortion occurred to the water block surface can be prevented, and the distance between two-side water block should also be kept within 1mm, thus effective water seal in the gate sides can sure be reached.

According to the study, we proposed the quality standard for installing gate slot which is shown in table 6, and the quality standard for installing gate is listed in table 7.

Table 7 quality standards for installing gate

Serial No.	Inspection items	Permitted deviation
1	Water seal rubber top flatness	2
2	Distance between water seal rubber and wheel or slipway	±1
3	Distance from reverse slide block to slipway or wheel （reverse slide block is in free state）	+2，-1
4	Distance from either side to water seal center and the distance from top water seal to bottom water seal	±3

Table 6 Quality control for installing gate slot

Serial No.	Name of embedded parts		Bottom sill	Do-or lint-el	Main track		Siding track	Oppose -d track	Sidin-g water seal base plate	Doubling with corner protect-or and rail
					Machinin g	Non-machinin g				
1	Central line between opposing gate slots a	Within the operation area	±5	+2 -1	+2 -1	+2 -1	±5	+3 -1	+2 -1	±5
		Out of the operating area	/	/	+3 -1	+5 -2	±5	+5 -2	/	±5
2	Central line between Opposing gate openings b	Within the operation area	±5	/	±3	±3	±5	±3	±3	±5
		Out of the operating area	/	/	±4	±4	±5	±5	/	±5
3	Elevation △		±5	/	/	/	/	/	/	±5
4	Distance from door lintel to Bottom sill h		/	±3	/	/	/	/	/	/
5	Difference in elevation from one side to another side of the working surface	l≥10000	3	/	/	/	/	/	/	/
		l < 10000	2	/	/	/	/	/	/	/
6	Working surface flatness	Within the operation area	2	2	/	/	/	/	2	/
		Out of the operating area	/	/	/	/	/	/	/	/
7	Deviation in Working surface combination	Within the operation area	1	0．5	0．5	1	1	1	0．5	1
		Out of the operating area	/	/	1	2	2	2	/	2
8	Surface distortio-n		1	1	0．5	1	2	2	1	2

5. CONCLUSION

In this paper, we proposed the quality control standard in the process of making flat slab steel gate and the welding technique parameters for all kinds of welding methods. They are both quite effective in improving the quality of making steel gate and facilitating the production efficiency. At the same time, the proposed installation standards for either gate slot or the gate are of great importance in supervising engineering construction, and have significantly materialized in some floodgate projects of Shandong.

REFERENCES

[1]Li Dian-qing, Wu Shuai-bing. System reliability analysis on main girder of plane gates considering multiple correlated failure modes. *Journal of Hydraulic Engineering, 2009, vol.40, No. 7,870-876.*

[2]Amaya-Roncancio S, Restrepo-Pana E. Finite elements modeling of multiayers of C_r/C_rN [J]. Micoelectronics Journal, 2008, 39(11): 1336-1338.

[3]Bai Run-bo, Cao Ping-zhou, Cao Mao-sen. Determination of surface heat treatment indices of large-scale hydraulic steel-gate wheel and track. *Engineering Mechanics, 2009, vol.26, No. 11,184-189.*

[4]Guo Jian-bin, Su Hao. Research on safety simulation of hydraulic steel gate based on reliability enhancement test. *China Rural Water and Hydropower, 2010, No. 4,91-93.*

[5]Zhao Qiao-liang, Jin Qiao-fang. Control of welding deformation of flat steel gate. *Hot Working Technology, 2009, vol.38, No. 13,163-166.*

2011 International Conference on Mechanical, Industrial, and Manufacturing Engineering
Lecture Notes in Information Technology Vols. 1-2

A Possible Solution to the Conflict between Economic Development and Environmental Protection in China
Environmental Studies Research Project

Yuchen Lorin Gu

Abstract **–Environmental protection and economic development have a complex relationship. Environmental protection projects depend on funds and advanced technologies from economic development, and that development utilizes environmental resources to maintain continuous growth. At the same time, serious conflicts exist between economic development and environmental protection. Economic growth requires an increasing amount of capital, including natural resources. Resource use is properly controlled in many developed countries, but many developing countries seeking exponential economic growth necessarily exploit increasing quantities of natural resources. China, a growing international trading power that has been called the "world's factory," is a prime example of a country that impetuously pursues economic growth while neglecting environmental protection. Many severe environmental issues have emerged due to the prioritization of economic development in China, including accelerated ecological degradation, biodiversity loss, simplification of natural systems, and various types of pollution. Conflicts between economic development and environmental protection are currently peaking in China, and a balanced solution is fervently demanded to address intensifying dissent. This paper argues that NGOs are a possible mechanism for solving China's conflicts between economic development and environmental protection. The subsequent sections closely examine the origin of these conflicts, describe significant events in the evolution of both conflicts and relevant NGOs, analyze the macroeconomic reasons that NGOs are a possible solution to the conflicts, and suggest future actions that may help NGOs to achieve their goals.**

I. Introduction

Environmental change is inevitable during any kind of economic development. Therefore, the intention of environmental protection is not to keep the environment intact or to recreate primitive conditions but to sustain the environment at a reasonably healthy level that can continuously supply natural resources for human development and that does not pose a threat to the survival of the majority of organisms. After World War II, many western countries believed blindly in economic growth and made GDP increase their most important or even sole goal. The incredibly fast pace of economic growth in those countries, particularly the United States and the United Kingdom, caused many severe and negative environmental consequences, notably the emission of toxic chemicals and water pollution. Economic development resulted in a direct exchange of natural resources for GDP. However, when environmental issues threatened to limit further economic growth, many governments initiated environmental protection programs. This policy is known as "pollution first, treatment after" and was widely implemented in western countries in the 20th century. However, this policy is incompatible with both the 21st century and the situation in China. Like many preceding countries, China considers GDP growth to be its most urgent goal because a great number of people need critical improvements in living standards. China has certainly been successful in the sense that the country has maintained an annual GDP increase of 8% for many years. However, behind this miraculous economic development, China has incurred many issues due to over-exploitation of the environment.

Sustainability is necessary for long-term economic development. Because sustainability is achieved through environmental protection, environmental protection is not simply a favor for the environment; it is also a requirement for continuous prosperity. Despite the numerous policies and laws decreed by the government to ameliorate air and land contamination, 70% of the water supply in China is contaminated and no longer potable, 300 million people have no access to clean water, 400 million people suffer from polluted air, and one-third of the land in China is affected by acid rain. The current situation is already dire, but trends suggest that more severe consequences are still forthcoming. Limited land availability for settlement and development by the huge human population in addition to sharp increases in both pollutant discharge and energy consumption due to economic growth and increasing domestic wealth exert enormous pressures on the environment. These pressures threaten to make the land worthless and the air poisonous. Moreover, China now has entered a phase of development in which it must sacrifice a great amount of resources to maintain the same level of GDP growth. For instance, in 2006, China represented about 5.5% of the global GDP but was also responsible for 15% of global coal consumption, 30% of global steel consumption, and as much as 54% of global cement consumption. The costs associated with rapid economic development, industrial expansion are unacceptably high and suggest that production in China is still highly inefficient despite economic growth. Both rapid economic expansion and industrial inefficiency exacerbate environmental problems. Therefore, a suitable solution to the conflicts between economic development and environmental protection for China's domestic situation is urgently needed.

II. Background Information: Conflicts and NGOs

The history of China's conflicts between economic growth and environmental protection can be traced back to 1949, when China was first founded. From 1949 to 1978, China

978-0-9831693-1-4/10/$25.00 ©2011 IERI

experienced the Great Leap Forward and the Cultural Revolution; both events caused severe environmental and ecological damage to the post-war environment. Moreover, soon after the Cultural Revolution, China returned to its economic development track. Because industrial development was largely impeded by the Revolution, the government made economic growth its priority. Due to the tremendous scale of modernization, urban development, infrastructure construction, and development of high-pollution industries to satisfy the needs of both Chinese citizens and foreigners, the scope of environmental pollution broadened and the amount of environmental damage rose significantly. The conflicts between environmental protection and economic development became obvious in the late 1970s; however, most people chose to neglect environmental degradation and concentrate only on GDP growth.

From 1978 to 2000, three phases of industrialization occurred that helped to make China the "world's factory" but that also harmed the fragile domestic environment. From a historical perspective, the rural reform phase occurred from 1978 to 1984, during which the Chinese government focused on agricultural and rural development. At the beginning of this phase, fertilizer and pesticide supplies were still limited, and the environment was not seriously impacted. Increases in production and access to chemicals led to increasing impacts on the rural environment. Poor management and heavy consumption of available resources without pollution prevention methods caused environmental problems to surface. The environmental protection institutions that appeared in this period gained no attention; enthusiasm for economic development made everything else "irrelevant," including environmental issues. The period from 1985 to 1992 saw the development of light industry. To address expanding demands for food, clothing and other necessities, numerous new factories opened in mainland China and deforested and over-exploited many natural resources. Although production increased, concurrent decreases in air and water quality were not recognized and natural resource exploitation made existing environmental issues more severe. At this point, conventional environmental controls were futile and the rate of environmental deterioration accelerated recklessly. Concrete evidence is available for the existence of notable and widespread environmental issues; for example, 436 of 532 monitored rivers were polluted. The government issued new policies like "Decisions on Further Strengthening Environmental Protection Work" to control the situation, but the policies that were intended to enact environmental protection laws on businesses were not effectively implemented. Therefore, the conflicts between environmental protection and economic development continued to worsen.

From 1993 to 2000, China entered a preliminary heavy chemical industry phase and enjoyed significant GDP growth. The amazing economic development experienced during this period was a direct result of profits generated from the heavy chemical industry. Beginning in 1993, heavy chemical industries represented a greater proportion of the Chinese economy than light industries as a result of public demand for convenient transportation and other products such as automobiles and electronics, which made citizens' lives much easier but profoundly harmed the environment. Industrial waste increased sharply along with productivity. Emissions of the poisonous gas SO_2 increased by 31.3% in this phase compared with the previous phases. In addition, as more electronics were produced and used, more electricity was demanded. Uncontrolled energy consumption during this phase initiated another round of environmental deterioration.

Since 2000, mature heavy chemical industry has dominated the Chinese economy. Intensive heavy chemical industrial processes have generated even more environmental issues. At this point, the extent of damage to many rivers and forests necessitates immediate treatment to avoid serious damage to not only China's land and air but also to the bodies of Chinese people.

The economic development in these four phases can be summarized by the following graph, which shows GDP growth.

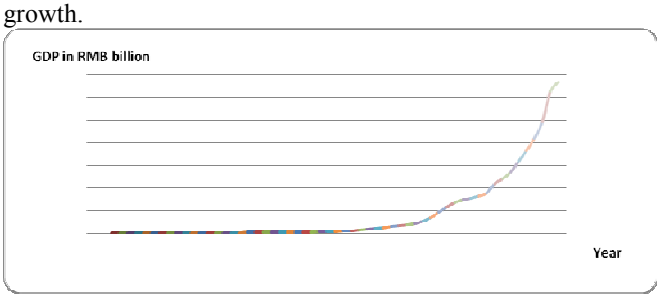

Figure 1: China's GDP and Economic Growth from 1952 to 2009

This graph demonstrates Chinese economic growth due to large-scale industrialization. This graph is accompanied, however, by the following graph, which shows pollution.

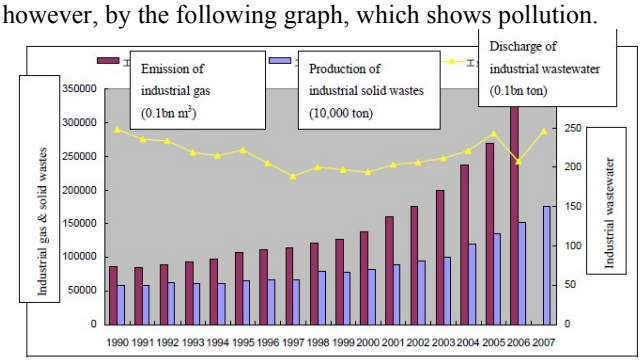

Figure 2: Generation of Industrial Wastes

Figure 2 shows the amounts of pollution accumulated in China over the past two decades. Like economic growth, increases in pollution have been exponential. In the five-year period from 2002 to 2007, for instance, the emission of industrial gas increased by 121% and the production of industrial solid waste increased by 84%. This momentous increase in pollutant discharge reflects the fact that China is not fully prepared for elevated international economic status

and is not proficient at handling the challenging environmental issues incurred by economic development.

The foundations of China's environmental problems were built over four phases of economic development. Because the conflicts between environmental protection and economic development were not addressed for decades, China now faces a predicament: the environmental issues inherited from previous phases of industrialization and mechanization must be addressed along with those associated with ongoing, impressive economic growth.

III. Current Situation and Modern Conflicts

A. *Current Situation*

To solve the conflicts between economic development and environmental protection, a clear and defined model must be created. The relationship between national GDP and various indicators of environmental pollution can be modeled by the Environmental Kuznets Curve, also known as EKC. Although EKC is a controversial theory, it does have merits in the environmental studies field. The "∩" shape of the curve (Figure 3) reveals three stages of the relationship between environmental quality and economic development: (1) the environment degenerates slowly during slow, early economic development; (2) environmental degradation and pollution increase as economic development accelerates and agricultural exploitation and heavy industry production increase; and (3) the environment improves and pollution decreases after the GDP passes a certain threshold due to increased public awareness, advancements in technology, and strict execution of legislation.

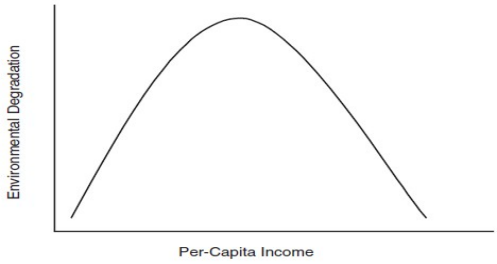

Figure 3: Typical Environmental Kuznets Curve

In China, environmental studies scholars such as Jin Fan and Shuijun Peng have shown that the Environmental Kuznets Curve can appropriately explain the situations of 81 Chinese cities. Several EKC studies have concluded that sulfur dioxide pollution does begin to decline when per-capita income reaches the range of $5,000 to $15,000. A model selected by Yaobin Liu for SO_2 concentration is represented by equation (1).

$$\ln[SO_2]_{it} = a_0 + a_1 \ln\left(\frac{GDP}{p}\right)_{it} + a_2 \ln^2\left(\frac{GDP}{p}\right)_{it} + a_3 \ln(\text{density})_{it} + \varepsilon_{it} \quad (1)$$

In this equation, $[SO_2]$ represents the concentration of SO_2, i represents the i-th sample, t represents time, $\left(\frac{GDP}{p}\right)_{it}$ represents the real GDP per capita of the i-th sample at time t, $(\text{density})_{it}$ represents the population density of the i-th sample at time t, and ε_{it} represents the residual. Based on the available data, the concentration of SO_2 can be calculated for each city and each year.

According to the calculations of Jingming Hao and Litao Wang at Tsinghua University, declining trends in SO_2 concentration have appeared in certain cities with a per-capita income of more than $3,000. The occurrence of the SO_2 pollution peak at $3,000 instead of $5,000 may be due to China's unique economic development model. The following graph (Figure 4) demonstrates the decline in SO_2 over the last decade. As China entered the heavy industry era in the early 1990s, economic development drove up the per-capita income in all cities across the country. According to EKC theory, the environment improves when economic development reaches a certain level; this claim is supported by the trend line on the graph. Since 1992, the SO_2 level in both northern cities and southern cities started to drop. However, the SO_2 level stayed roughly the same from 2002 to 2010. Similar declines are observed for NO_2 and CO. Despite the noteworthy decline, the concentrations of SO_2 and other suspended particles in the ambient remain high and continue to exceed the Grade II standard, China's air quality standard for urban areas, as shown in Figure 5. Therefore, air pollution remains a significant issue.

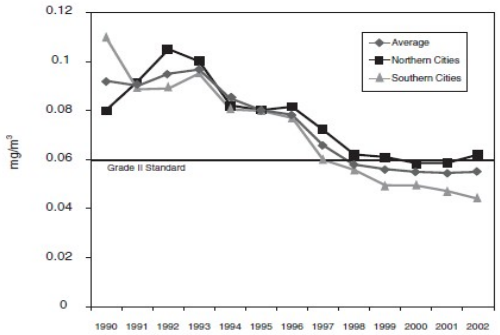

Figure 4: Average Annual SO_2 Levels in Chinese Cities

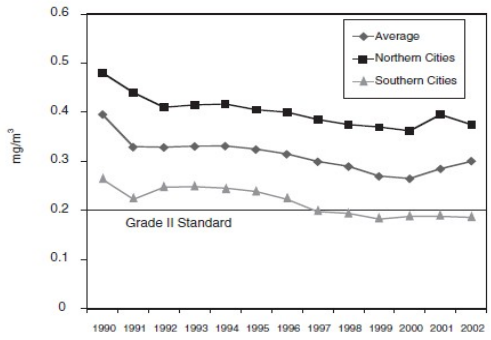

Figure 5: Average Annual Total Suspended Particle Concentrations in Ambient Air

The Environmental Kuznets Curve can also be used to describe other types of environmental damage. COD concentrations and Cr^{6+} discharge also show decreasing trends over the last decade but are still far from reaching acceptable standards. The discrepancy between China's situation and the ECK theory is, again, largely due to the inefficiency of industrial production. Although the concentrations of some chemical wastes decrease, the total areas of polluted land, water, and air continue to increase, and China's pollution level relentlessly rises.

The high consumption of energy and other resources associated with China's economic development mode will always cause environmental issues and be problematic for achieving the current standards. Nevertheless, the current situation is encouraging because there is substantial evidence that repairing the Chinese environment is an achievable goal.

B. Modern Conflicts

Since China entered the era of heavy industry, the conflicts between economic development and environmental protection have only intensified. Consistent increases in economic output are important for China to maintain its newly established status in the international economy. However, although China has become a much more powerful country in the international economy, the "high input, high consumption, high emission, difficult circulation and low efficiency" growth mode continues to govern its industry. The products of heavy industry and industrial facilities also have high energy consumption demands, creating a downward spiral that appears to produce more output but in fact consumes more resources and increases pollutant discharge. The violent protest in Harbin in 2005 represented public anger toward environmental issues. After a chemical spill in the Songhua River, the water supply of this city with 3.8 million people was shut down. This event is one example of how intractable economic development has directly harmed the lives of Chinese citizens.

The question of whether environmental protection should be prioritized over economic development is controversial in some underdeveloped areas in China. Some areas are intact and pristine, especially those that are remote from main industrial cities. However, the living standards in these areas are extremely low compared to those in major cities such as Beijing, Shanghai and Shenzhen. Therefore, it has been suggested that these areas exchange their lands and resources for wealth. Opponents of this idea claim that improper development in these areas could not only permanently damage the land and deplete its natural resources but also lead the residents of these areas into more serious impoverishment. One example of such an unfortunate situation is ShuXian village. Red Pine, a rare kind of slow-growing tree, was briefly popular for making furniture. Villagers in ShuXian razed their valley, harvesting as much Red Pine as possible as well as the fruit trees upon which their livelihood depended, to plant Red Pine. However, the demand for Red Pine faded and the villagers received almost no orders for the lumber. Because they had consumed all of their resources, they became more destitute than before. Those that recommend prioritizing economic development, however, pronounce that the quality of life of human beings is more important than environmental protection. They argue that "environment serves for people. If people are unable to survive or lead the lifestyles they desire because of their lack of wealth, there is no point for environmental protection." The debate between environmental protection and human wealth prevents actions that could help both the environment and poor citizens.

The above examples are only two of the many modern conflicts. The true difficulty in solving the conflicts lies in the fact that no consensus can be reached until a method is found to unify economic development and environmental protection.

C. Southwest Drought: A Current Conflict

The 2010 southwestern drought is a prime example of the consequences of placing economic development ahead of environmental protection. Although many believe the principal cause of the drought to be climate change, long-term environmental issues are also believed to have contributed to this natural disaster. The ecosystem of southwest China has been altered significantly since industrialization. The mass construction of hydroelectric plants and deforestation may both be responsible for the drought in the southwest region.

The Three Gorges hydropower complex project is not only designed to supply electricity but also to boost the local economy. The Three Gorges Reservoir, which was built as part of this project, influences the precipitation and ecosystem of the area for several reasons. First, dam construction increases the surface area of the water, increasing evaporation and reducing local diurnal temperature variations, which in turn changes regional climate. Second, dam construction creates a $20^{\circ}C$ temperature difference between the surface and the bottom of the reservoir, trapping heat and consequently increasing the amount of hot air. The hot air rises and blocks cold air from moving south, preventing precipitation in that region. Therefore, the hydroelectric project may have exacerbated the drought in the southwest.

Deforestation of the southwestern regions, especially Yunnan, has significantly changed the ecosystem and the environment. From 1994 to 2007, the price of rubber and tobacco rose by 900%, motivating local villagers to enter the rubber and

tobacco market. Rubber and tobacco have been planted in Yunnan to meet increasing demands and to drive local economic development, which has caused vast deforestation and reduced biodiversity. Moreover, large-scale rubber cultivation has caused a 0.5 ℃ increase in annual average temperature, which, especially for this dry region, has a dramatic effect on the water supply.

The absence of proper controls on economic development and appropriate solutions to environmental issues exacerbates problems of environmental degradation and could theoretically cause serious disasters like the southwest drought.

D. A Brief History of Chinese Environmental NGOs

It is not surprising to find environmental problems in developing countries that prioritize economic growth and minimize costs to maximize profit; China is no exception. Therefore, advocates are necessary to restrain government policies that neglect potential harms to the environment. These advocates, known as grassroots organizations and non-governmental organizations, have had many achievements but have not yet obtained a powerful role in China. These organizations have raised the awareness of environmental protection among citizens and have spread the view that environmental protection is not only about battling dust storms and deforestation but also about saving natural resources, employing sustainable development, and solving global environmental issues. Moreover, these non-governmental organizations have also been credited with mitigating the deadlock between the environment and the economy in the past decade.

Grassroots organizations in China experienced three main phases: 1978-1994, 1994-2003, and 2003 to the present. Grassroots organizations and NGOs first appeared between 1978 and the early 1990s. The Chinese Society for Environmental Sciences first introduced Chinese citizens to the word "environmental protection." Early activists focused their campaigns on factories and universities, targeting mostly educated adults. Although the notion of environmental protection was still vague, a small group of people began to view the environment as a future concern. During this period, environmental issues were neglected due to overwhelming political and economic changes. The event that marked the inception of environmental protection in China was the formation of China's first grassroots environmental protection organization, Friends of Nature (see below). Although Friends of Nature worked on several projects, including the protection of wild animals, it failed to establish a belief in environmental protection among the public. On the other hand, its promotion of wild animal protection raised public awareness and inspired the formation of several environmental protection organizations. Beginning in 1995, there was a boom in NGOs and grassroots organizations. Another well-known NGO, Global Village China, was established in Beijing in 1996, targeting students and community members. The organization organized workshops in schools, hosted recycling events and provided environmental education to elementary and secondary school students. Volunteers from Global Village China also distributed information to adults, showing daily behaviors and habits that can improve the environment. Although these activities appeared powerless, their increasing popularity caused the government to recognize and value grassroots organizations and NGOs and to make them a factor in policy development.

The third period of Chinese environmentalism began in 2003. The development of the Nujiang River for hydropower involved groundbreaking cooperation among individual grassroots organizations. Subsequent activities like "26℃ air" also provided opportunities for Chinese organizations to interact with international NGOs. Currently, China has more than 3000 grassroots environmental organizations, which hold more than 1000 activities every year. The following chapters will specifically discuss the history and contributions of the three most influential organizations: Friends of Nature, Global Village China, and Society of Entrepreneurs and Ecology.

E. Friends of Nature and Global Village China

China' environmental revolution started with the formation of Friends of Nature and gained enormous momentum from the work of Global Village China. These two major organizations should be closely examined because they served as models for later groups.

Friends of Nature was the first grassroots organization dedicated to the environment in China, and it played a pivotal role in promoting environmental awareness among adults. The founder, Congjie Liang, was inspired by international NGOs and decided to form a team to raise awareness about environmental protection among Chinese citizens. The formation of Friends of Nature is particularly noteworthy. Instead of propagating his notion publicly, Liang shared his vision with elites, i.e., successful and famous people who he believed could have more significant effects on society. In 1994, this organization was officially formed with the aid of Dongping Yang, an environmental scientist, Lixiong Wang, a writer and explorer, and Xiaoyan Liang, the chief editor of the magazine Asia. Although the organization experienced a difficult time in its first few years due to a lack of financial support and a limited audience, it later obtained opportunities to promote its values in universities and governmental departments. Through its campaigns, Friends of Nature raised the environmental awareness of hundreds of thousands of Chinese students, citizens, and government officials. The organization was therefore recognized and financially supported by other national and international charitable foundations. As the organization became more influential, it helped other visionaries to establish grassroots environmental NGOs and chapters in universities at the same time that it achieved major progress in several environmental issues. For instance, Friends of Nature focused on promoting a "green culture" among China's emerging urban middle class. It has organized recycling programs in schools and colleges, formed workshops to teach sustainability, held national energy saving

projects such as "26℃ air," and, most importantly, lobbied government officials to protect the forest and wilderness.

Global Village China, on the other hand, focused on educating children and publicizing contemporary environmental issues. Founded in 1996 by Xiaoyi Liao, the organization originally targeted local residents in Beijing. The first activity by Global Village China was to shoot the weekly TV program "Moment of Environmental Protection." This TV show aired on CCTV, the largest TV channel in China, for five years. In addition, Liao and her fellow supporters also sold DVDs of the program to increase the awareness of environmental protection and, at the same time, alleviate the organization's financial burden. This show made Global Village China widely known across China. In 1998, Global Village China together with the Ministry of Environmental Protection published a guide for students because Liao believed that environmentalism should start with young people. Later, Global Village China organized a series of events specifically for elementary, secondary and high school students that reached over fifty cities nation-wide. In 2000, 83,000 students participated in the "Green Promise" activity, which spread the concept of Green Earth to hundreds of thousands of families. "Green Promise" was one of the most successful events planned by Global Village China.

Both Friends of Nature and Global Village China continue to work toward improving the Chinese environment. Over the next few years, they expect to gain more support from the government and the public.

F. Issues Facing China's Environmental NGOs Today

Despite their successes in the past several decades, NGOs in China have not yet fully matured. This section discusses four major factors deterring the growth of China's environmental NGOs.

First, China's environmental NGOs do not have effective fundraising mechanisms to gain financial support. Because donation is not a part of Chinese culture, members of the public rarely donate to NGOs even though they know that NGOs are charities. In response, NGOs generally organize formal fundraisers or request financial support from companies. These passive fundraising methods are directly responsible for the severe shortage of funding for almost all environmental NGOs, which limits their growth and prevents them from taking major action on serious environmental issues or developing effective recommendations.

Second, the Chinese government does not fully support the work of NGOs and hence restricts their development. The government allocates the majority of the available resources to governmental departments related to the environment rather than to NGOs. Moreover, NGOs have not been fully legalized by the government, which tolerates propaganda and broadcasting activities but does not allow NGOs to register as authorized environmental protection organizations. Due to the lack of official recognition, these organizations not only obtain no financial support from the government but also have difficulty in raising money from companies. This situation directly restricts the expansion and the development of NGOs.

Third, although the public supports environmental protection in theory, controversies arise when environmental protection interferes with economic development. NGOs fought an epic "battle" to restrict the construction of the Nujiang hydroelectric plant. Because the placement of the plant would seriously damage the local environment, NGOs defied the government and repeatedly sent representatives to talk to the government spokesman. In 2004, NGOs celebrated their uneasy success: they temporarily stopped the construction of the hydroelectric plant. However, many people did not appreciate the NGOs' efforts, arguing that the environment serves the people and "no environmental protection is needed if people are starving to death." In other words, environmental protection was considered irrelevant if the opportunity to escape poverty was lost. After another recent review, it was decided that the economic benefits of the Nujiang hydroelectric project outweigh its disadvantages; the government is considering resuming the project in the near future.

Fourth, NGOs do not yet have enough influence to make permanent structural changes in the Chinese environmental protection field. Environmental NGOs in China are not as powerful as their foreign peers; they do not have the right to lobby or to put pressure on decreed policies. Therefore, although NGOs can educate the public in hopes of stimulating people's enthusiasm for environmental protection, they cannot tackle the causes of many problems, especially those caused by the government's indulgent policies. Since these organizations are unable to interfere with major polluting industries and have not gained full support from the government, they cannot make permanent structural progress in China.

Despite the problems facing NGOs, the popularity of environmental protection organizations among the public suggests that NGOs have a bright future. If they find a way to obtain sufficient financial support, they can gain a strong voice in front of both the government and industry and eventually make constructive changes for the country on their own power.

Ⅳ. ANALYSIS

A. Unifying Economic and Environmental Goals in China

Numerous domestic and foreign research institutions have estimated the losses due to environmental pollution and ecological damage in China through 2000. The highest estimate of this loss was 7.7% of annual GDP (World Bank, 1997), and the lowest was 2.1% (U.S. East-West Center, 1990). In 2006, the State Environmental Protection Administration and National Bureau of Statistics accounted for the national economic losses caused by environmental pollution, the cost of treatment, and the economic loss caused by ecological damage for 2004. In that study, the total proportion of economic loss was between 7% and 20% of China's national GDP. For many years, researchers have been

evaluating possible methods to integrate environmental factors into economic development goals through the work of the Chinese government. This concept aims to develop unified objectives for the conflicting goals of environmental damage and economic growth. Unquestionably, there has been some progress along these lines over the past decade; however, the improvement has not yet been sufficient to transform China from a heavily polluted country to a green society. For instance, the goal of reducing the rate of non-renewable resource consumption to below the rate of renewable resource development has not been achieved because the government was unsuccessful in controlling the energy consumption of its citizens and because government-sponsored research into new alternative resources has not achieved its goals. In addition, insufficient funds have been used to rehabilitate rivers, lakes, oceans and forests, not because the government is not supportive of this transformation but because the lack of strict supervision and the large available sums have encouraged the corruption of local officials, who have severely reduced the money intended for purchasing equipment and supporting research projects. Because there is no transparent system to verify the quality of rehabilitation projects for water and forests, it is not possible to know whether rehabilitation has been successful. The Chinese political bureaucracy slows the restoration process and further aggravates conflicts. Therefore, current methods to unify economic development and environmental protection goals in China are well-intentioned but poorly implemented. Simply expecting the government to mitigate China's environmental situation is not leading to the desired success; rather, external forces to the government are needed to help supervise and conduct this transformation.

B. Macroeconomic Analysis of Unified Sustainable Development Goals

Although transforming the relationship between economic development and environmental protection from conflict to unification seems like an arduous task, it is in fact feasible. Based on macroeconomic concepts of aggregate supply and aggregate demand, the transformation can be achieved through a series of fiscal policies, monetary policies, and actions by industries.

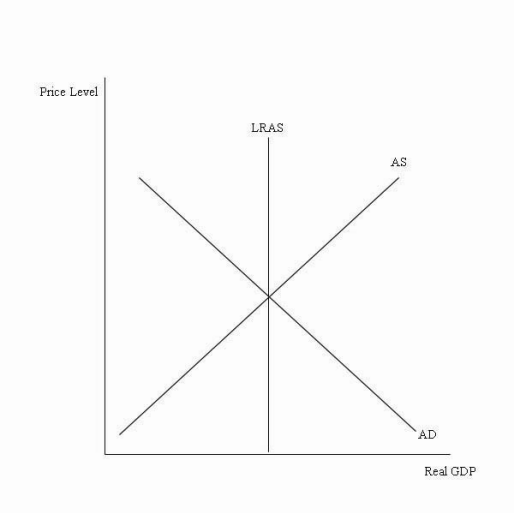

Figure 6: AS/AD Model

Figure 6, above, represents the aggregate demand/aggregate supply model, which is also known as the AS/AD model. This model explains price level and output through the relationship between social aggregate demand and aggregate supply. In this graph, LRAS represents long-term aggregate supply, AS represents short-term aggregate supply, and AD represents aggregate demand.

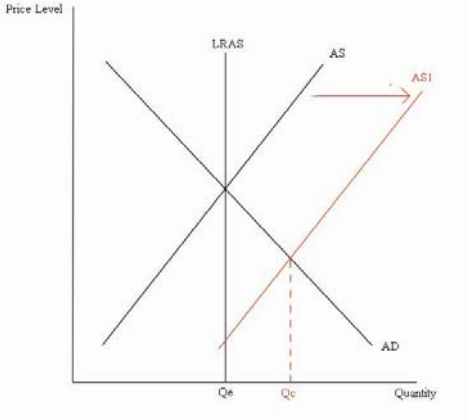

Figure 7: Current Aggregate Supply Situation

Current heavy and light industries in the Chinese economy are shown in Figure 7. In this graph, AS1 represents the current aggregate supply of heavy and light industries in China, AD represents the current aggregate demand for products produced from these industries, and Qc represents the current output. Output is to the right of the long-term social economic equilibrium because China has allowed its industries to grow independently; in other words, Chinese industries can employ the "high input, high consumption, high emission, difficult circulation and low efficiency" economic model without government limitations on their operations. According to the graph, the Chinese economy is in a desirable position because more goods are being supplied than the amount expected at the social economic equilibrium point, which lowers product

prices. However, this aggregate supply curve is also the reason for the increasing pollution in China.

The environment should be considered a natural resource, and the environmental costs should be counted toward the costs of resource use. Because heavy and light industries in China do not have to account for environmental costs, their cost per unit output is lower than for industries in western countries, where governments assess strict pollution fees on waste-producing companies and factories. In addition, because the demand for jobs is much larger than the supply, wages are also low. These two factors together control the cost per unit output for China's heavy and light industries. Because cost per unit output affects aggregate supply, the comparatively low cost per unit output shifts the aggregate supply curve to the right and results in a relatively low price point for Chinese goods compared to similar products from other countries. Because the current price level is lower than the social economic equilibrium, goods produced in China are competitive in both the domestic and international markets. Industries profit from low prices and consequentially have no incentive to seek alternative production methods to increase efficiency and reduce emissions. Industries prefer to continue with their low-efficiency, high-emissions practices than to pay extra to make their operations more environmentally friendly. Moreover, because China does not have strict legislative requirements for managing environmental damages from factories, environmentally irresponsible factories continue to take advantage of the huge profits that can be generated from the "cheap" operations allowed in China. Most of these factories are poorly organized and do not have the financial capacity to mitigate the consequences of their environmental pollution. They contribute a huge proportion of the total pollution released in China each year. Economically, this situation undeniably increases China's output and exports, which in turn achieves the economic growth, increases domestic wealth, shifts the aggregate demand curve to the right (from AD to AD1), and achieves a higher GDP (Figure 8).

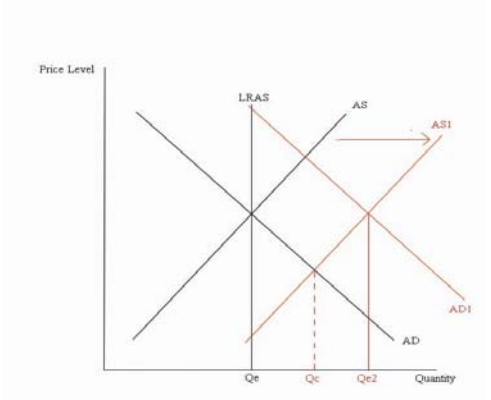

Figure 8: Increased GDP

However, the relationship in Figure 8 neglects environmental damage. To alleviate environmental issues in China, heavy and light industries must accept sacrifices and the country should try to eliminate most, if not all, of the irresponsible polluters. This process will require coordination and collaboration between the government and industries. Real GDP will initially decrease, but, after the establishment of better standards and a better economic environment, GDP will rise again.

Notably, current supply and demand both exceed the best social economic equilibrium; bringing these parameters into the best social-economic equilibrium is the first step in reducing the conflicts between economic development and the environment. The AS curve needs to shift to the left until it reaches the best social-economic equilibrium, as demonstrated in Figure 9. A leftward shift of the AS curve will help the country reduce heavy pollution from factories and will mitigate conflicts.

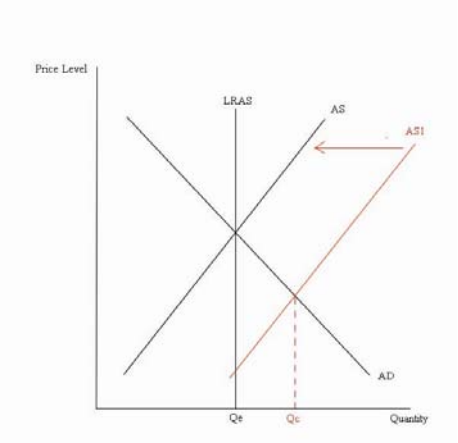

Figure 9: Leftward Shift of AS

Some crucial factors for shifting AS to the left are an increase in wages, an increase in operation prices, and a decrease in future demand for the goods produced. Operational prices increase due to charges for environmental pollution. Both wage and operation price increases need to be supported by the Chinese government. If the government establishes strict orders to protect worker's rights and to allow workers who work in physically harmful factories to obtain more profits, then industries will have an incentive to invent a healthier production system, which will increase the costs of operation. Decreasing future demands, however, is mainly a task for consumers. Although the government has increased taxes on luxury products and the incomes of wealthy people, it is unwilling to make the necessary compromises to shift the AD curve to the left and decrease the future demand for goods. Because most luxury products are imported, the luxury tax does not affect the environmental behavior of domestic factories. To reduce demand, consumers need to consume fewer goods from heavily polluting factories, be aware of environmental issues, and help the economy reach its best social-economic equilibrium. When production is limited, producers reduce their production and release less pollution. If consumers prefer environmental friendly products, producers will seek greener alternatives that release less pollution. As the cost per unit output rises, the AS curve will shift leftward and fewer goods will be produced thereby decreasing environmental pollution and relieving the conflict between

economic development and environmental protection. However, this stage does not represent the final solution to the conflict.

After the establishment of more rigorous legislation for heavy and light industries and the initiation of a trend toward environmentally friendly production, the LRAS (long-run aggregate supply) curve and AD curve will rise again, leading to a higher real GDP and milder conflicts between the economy and the environment. This transformation is illustrated by Figure 10, in which LRAS1 represents the new long-term aggregate supply and AD1 represents the new aggregate demand.

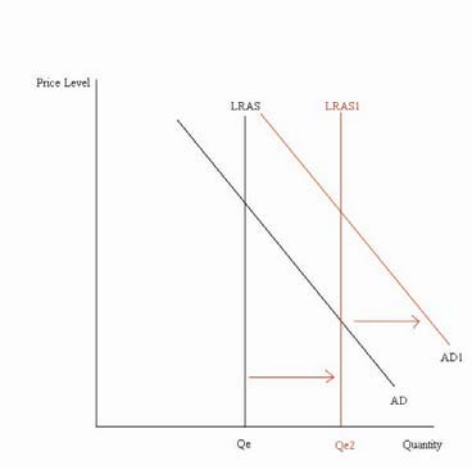

Figure 10: New LRAS and AD

This economic model provides a method for mitigating the conflicts between economic development and environmental protection. However, it also generates additional questions. For example: How can this model be achieved? Is the government willing to reduce GDP for the good of the environment? Is the government willing to strictly enforce its environmental policies for the heavy and light industries, a core section of the national economy? Is the public willing to choose environmentally friendly products?

These questions can be answered in the affirmative if Chinese NGOs play a critical role in advancing solutions to the conflicts between economic development and environmental protection.

Ⅴ. A Possible Solution

A. NGOs as a Solution to the Conflict between Economic Development and Environmental Protection

Environmental NGOs are a possible solution to the conflict between economic development and environmental protection in China because they mediate among the government, the public, and industry. However, as described above, Chinese NGOs are still in the early stages of development and have yet to develop social status and influence. NGOs need to gain a substantial voice in government and industry and must obtain strong support from the public. Although most Chinese citizens are familiar with the concept of environmental protection, they are largely unaware of environmental NGOs. This situation is attributed to the limited finances of these groups. Therefore, the ability of NGOs to mediate unified environmental solutions depends on the acquisition of a firm financial foundation.

Because environmental NGOs in China are not officially recognized, businesses receive no significant benefit for donating to them. At the same time, the public generally does not feel responsible for supporting charity organizations. Therefore, it is difficult for NGOs to raise money for their activities, and Chinese NGOs must develop alternative fundraising methods. For example, NGOs could ally with research centers or form their own research groups to devise feasible production processes for specific industries that cost less and are more efficient than those currently in use. The NGO and research team could partner with businesses and industries, providing beneficial technologies while being financially supported by the business. NGOs would gain a major financial supporter as well as an intimate understanding of the industry and its byproducts. In addition, Chinese NGOs should strengthen their relationships with well-endowed international environmental NGOs. The Chinese government has clearly demonstrated that international organizations will not be allowed to work on China's problems, so the burden of solving environmental issues lies entirely on domestic organizations. NGOs in China need to obtain both financial support and training from experienced international NGOs to become more mature and effective advocates.

After obtaining funding, the second stage of Chinese NGO development is disseminating propaganda. Without financial support, NGOs have been unable to conduct large-scale promotions to convey their message to Chinese citizens. Many Chinese are therefore unfamiliar with NGOs and underestimate or even resent their work. Environmental protection also gains relatively little support because many Chinese people do not see environmental damage as a violation of their human rights. NGOs are needed to help the public understand that they have ownership of the air, water, forest and other elements of the environment and, therefore, that they have the right to protect them from being harmed by others. Public support will help NGOs gain a strong voice with both government and industry, as demonstrated in western countries. In North America and Europe, governments do not unilaterally dictate policies to require sacrifices from businesses that protect the environment; those compromises are made in response to public pressure.

NGOs can use the influence they gain through public support to become both advocates for and lobbyists of the government. Still, NGOs must use a distinct approach that is compatible with the special situation in China. They may modify and limit the decisions made by the government but cannot emphasize the government's faults. This third stage of the development of Chinese NGOs includes the first concrete steps toward solving the conflicts between economic development and environmental protection. Because the communist party is the only legal political party in China, NGOs must not antagonize the government and must obtain support from crucial party officials to survive and successfully

influence policy. At the same time, NGOs will sometimes disagree with the government because they represent a public interest that could differ from governmental policy. To handle this delicate situation, NGOs should work closely with the government and government-sponsored research institutions. They must be allies of the government, helping the country to achieve goals such as a low-carbon economy. The relationships that develop between representatives of environmental NGOs and government officials will further establish the status of non-profit environmental groups. In response to decisions that favor the economy while significantly degrading the environment, NGOs can use their financial foundation and friendships with other international organizations to gain local and international attention. Due to China's international power, international and domestic pressures can be applied to demand the improvement of environmentally destructive policies. The collaborations between the Chinese government and Chinese NGOs and between Chinese NGOs and international organizations will facilitate the resolution of the conflicts caused by governmental policies and will initiate more research projects in this area.

In the fourth stage of Chinese NGO development, NGOs need to work with the government to regulate heavily polluting industries. For instance, companies that financially support the research of NGOs could gain an introduction to government officials. By demonstrating concern for the environment and a willingness to work toward solutions to environmental conflicts, these companies should receive tax benefits from the government. Tax benefits would encourage these environmentally beneficial activities. In the meantime, the government needs to raise taxes on heavy polluters to disincentivize their operations. Aggregate supply will decrease as a result of both the expense of financially supporting NGOs and the increased taxes on environmentally unfriendly companies. However, lost profits will be compensated for by the reduced costs of environmental treatment.

The fifth stage of NGO development involves long-term conflict resolution and achievement of unified, sustainable development goals. NGOs have an invaluable role in supervising the relationship between the governmental and industrial sectors and in promoting the public voice. Corruption is prevalent among Chinese officials, and many companies use bribes to escape regulatory compliance and maximize profits. Therefore, NGOs should regularly monitor the relationships between governmental officials and industry. Because local officials have tolerated violations of environmental laws that seem to threaten economic development, Gregory Chow from Princeton University proposes that the Chinese government issues a fixed number of pollution permits that can be traded at market prices. In this scenario, both the supply of and demand for pollution permits will equilibrate at levels that optimize natural resource use. Chow's idea is both ideal and practical, but it neglects the fact that the prevalent corruption could undermine such a policy and its desired outcomes. Therefore, NGOs must verify the implementation of this policy as a neutral third party.

After these five stages of development, NGOs will have achieved a stable position from which they can manage the relationships among the public, government, and industry. Moreover, the economy should become more efficient and real output should rise. According to the Environmental Kuznets Curve, increases in real output should reduce environmental degradation and improve the environment. Through the process described above, China's economy can become more efficient, pollution can be reduced, and the environment can be protected by the public and public-interest NGOs. A healthy environment can then support sustainable, long-term economic growth. The conflicting goals of economic development and environmental protection can thus be effectively unified.

VI. Summary

There is no objective answer to the question of how to resolve China's conflicts between environmental protection and economic growth. In western countries, governments and the public have spent decades seeking an equilibrium between the economy and the environment. Some countries like Canada have seen substantial growth in and profits from green industries. However, China is still in the early stages of balancing its miraculous economic boom with its devastating environmental degradation. This paper is divided into two major sections: the first section reviews and analyzes the evolution of these conflicts and the reasons for their severity and impact; the second section proposes a solution to these conflicts. Since the early 1980s, China has been moving toward economic prosperity, but overwhelming economic development has neglected sustainability and incurred major environmental costs. Corruption among governmental officials has exacerbated the situation by allowing many businesses to circumvent environmental policies and expand irresponsibly. This paper proposes a series of developmental stages for Chinese NGOs that could solve the long-term conflicts between economic development and environmental protection in China. NGOs have a special role in monitoring both government and industry, and they therefore have the potential to become a main force for achieving sustainable economic growth in China.

References

[1] David I. Stern, the Environmental Kuznets Curve, Department of Economics, Rensselaer Polytechnic Institute: 2003

[2] Steven F. Hayward, the China syndrome and the Environmental Kuznets Curve, American Enterprise Institute for Public Policy Research: 2005

[3] Junyi Shen, Environmental Kuznets Curve on Country Level: Evidence from China, Osaka University: 2004

[4] Guang Xiao, Xiaofei Pei, Xiaoming Yang, China's Economic Growth and Environmental Protection, Environmental and Economic Policy Research Center: 2005

[5]

[6] Guobin Yang, Global Environmentalism Hits China, Yale Global: 2004

[7] Gregory Chow, Policies for Environmental Protection, Princeton University: 2009

[8] Yaobin Liu, Change in Relationships between Economic Growth and Environmental Qualities in Cities of China, Nanjing University: 2007
[9] Lu Hong, Analysis on China's Environmental Issues and Economic Growth, Shanghai University of Finance & Economics: 2000
[10] Yongjiu Xia, Xingpeng Chen, Na Li, Economic Growth and Environmental Pollution in China's Northwestern Cities: 2005
[11] Guanghui Cao, Unification of Environmental Protection and Economic Growth, Chongqing: 2009
[12] Xiaoying Xu, Fight of Nujiang, Yunnan: 2004
[13] Ying Jiang, NGOs in Environmental Protection, Hebei University: 2006
[14] Jianguo Liu, China's Road to Sustainability, Science: 2010
[15] Peiqun Zhang, Climate Change Causing China Drought, Xinhua Pub: 2010

Author Index

Author Index

Author Index

Author Index

Author Index

Author Index

Author Index

Author Index

Author Index